

Volume 4, Number 1

January 2009

ISSN:1559-1948 (PRINT), 1559-1956 (ONLINE)

EUDOXUS PRESS,LLC



JOURNAL OF APPLIED FUNCTIONAL ANALYSIS

SCOPE AND PRICES OF
JOURNAL OF APPLIED FUNCTIONAL ANALYSIS
A quarterly international publication of **EUDOXUS PRESS,LLC**
ISSN:1559-1948(PRINT),1559-1956(ONLINE)

Editor in Chief: George Anastassiou
Department of Mathematical Sciences
The University of Memphis
Memphis, TN 38152,USA
E mail: ganastss@memphis.edu

The purpose of the "Journal of Applied Functional Analysis"(JAFA) is to publish high quality original research articles, survey articles and book reviews from all subareas of Applied Functional Analysis in the broadest form plus from its applications and its connections to other topics of Mathematical Sciences. A sample list of connected mathematical areas with this publication includes but is not restricted to: Approximation Theory, Inequalities, Probability in Analysis, Wavelet Theory, Neural Networks, Fractional Analysis, Applied Functional Analysis and Applications, Signal Theory, Computational Real and Complex Analysis and Measure Theory, Sampling Theory, Semigroups of Operators, Positive Operators, ODEs, PDEs, Difference Equations, Rearrangements, Numerical Functional Analysis, Integral equations, Optimization Theory of all kinds, Operator Theory, Control Theory, Banach Spaces, Evolution Equations, Information Theory, Numerical Analysis, Stochastics, Applied Fourier Analysis, Matrix Theory, Mathematical Physics, Mathematical Geophysics, Fluid Dynamics, Quantum Theory. Interpolation in all forms, Computer Aided Geometric Design, Algorithms, Fuzzyness, Learning Theory, Splines, Mathematical Biology, Nonlinear Functional Analysis, Variational Inequalities, Nonlinear Ergodic Theory, Functional Equations, Function Spaces, Harmonic Analysis, Extrapolation Theory, Fourier Analysis, Inverse Problems, Operator Equations, Image Processing, Nonlinear Operators, Stochastic Processes, Mathematical Finance and Economics, Special Functions, Quadrature, Orthogonal Polynomials, Asymptotics, Symbolic and Umbral Calculus, Integral and Discrete Transforms, Chaos and Bifurcation, Nonlinear Dynamics, Solid Mechanics, Functional Calculus, Chebyshev Systems. Also are included combinations of the above topics.

Working with Applied Functional Analysis Methods has become a main trend in recent years, so we can understand better and deeper and solve important problems of our real and scientific world.

JAFA is a peer-reviewed International Quarterly Journal published by Eudoxus Press,LLC.

We are calling for high quality papers for possible publication. The contributor should send four copies of the contribution to the EDITOR in CHIEF in TEX,LATEX double spaced,in ten point type size. They should be sent BY REGULAR MAIL ONLY, NOT REGISTERED MAIL, AND NO E-MAIL SUBMISSIONS [See: Instructions to Contributors]

Journal of Applied Functional Analysis(JAFA)
is published in January, April, July and October of each year by

EUDOXUS PRESS,LLC,

1424 Beaver Trail Drive,Cordova,TN38016,USA,

Tel.001-901-751-3553

anastassioug@yahoo.com

<http://www.EudoxusPress.com> visit also <http://www.msci.memphis.edu/~ganastss/jafa>.

Webmaster:Ray Clapsadle

Annual Subscription Current Prices:For USA and Canada,Institutional:Print \$280,Electronic \$220,Print and Electronic \$350.Individual:Print \$ 100, Electronic \$60,Print &Electronic \$150.For any other part of the world add \$40 more to the above prices for Print.
Single article PDF file for individual \$10.Single issue in PDF form for individual \$40.

The journal carries page charges \$15 per page of the pdf file of an article, plus \$40 for the electronic publication of all article, both payable upon acceptance of the article within one month and before publication.

No credit card payments.Only certified check,money order or international check in US dollars are acceptable.

Combination orders of any two from JoCAAA,JCAAM,JAFa receive 25% discount,all three receive 30% discount.

Copyright©2009 by Eudoxus Press,LLC all rights reserved.JAFa is printed in USA.

JAFa is reviewed and abstracted by AMS Mathematical Reviews,MATHSCI,and Zentralblatt MATH.

It is strictly prohibited the reproduction and transmission of any part of JAFa and in any form and by any means without the written permission of the publisher.It is only allowed to educators to Xerox articles for educational purposes.The publisher assumes no responsibility for the content of published papers.

JAFa IS A JOURNAL OF RAPID PUBLICATION

Journal of Applied Functional Analysis

Editorial Board

Associate Editors

Editor in-Chief:

George A. Anastassiou
Department of Mathematical Sciences
The University of Memphis
Memphis, TN 38152, USA
901-678-3144 office
901-678-2482 secretary
901-751-3553 home
901-678-2480 Fax
ganastss@memphis.edu
Approximation
Theory, Inequalities, Probability,
Wavelet, Neural Networks, Fractional Calculus

Associate Editors:

1) Francesco Altomare
Dipartimento di Matematica
Universita' di Bari
Via E. Orabona, 4
70125 Bari, ITALY
Tel+39-080-5442690 office
+39-080-3944046 home
+39-080-5963612 Fax
altomare@dm.uniba.it
Approximation Theory, Functional Analysis,
Semigroups and Partial Differential
Equations,
Positive Operators.

2) Angelo Alvino
Dipartimento di Matematica e Applicazioni
"R. Caccioppoli" Complesso
Universitario Monte S. Angelo
Via Cintia
80126 Napoli, ITALY
+39(0)81 675680
angelo.alvino@unina.it,
angelo.alvino@dma.unina.it
Rearrangements, Partial Differential
Equations.

3) Catalin Badea
UFR Mathematiques, Bat. M2,
Universite de Lille1
Cite Scientifique
F-59655 Villeneuve d'Ascq, France

23) Nikolaos B. Karayiannis
Department of Electrical and
Computer Engineering
N308 Engineering Building 1
University of Houston
Houston, Texas 77204-4005
USA
Tel (713) 743-4436
Fax (713) 743-4444
Karayiannis@UH.EDU
Karayiannis@mail.gr
Neural Network Models, Learning
Neuro-Fuzzy Systems.

24) Theodore Kilgore
Department of Mathematics
Auburn University
221 Parker Hall,
Auburn University
Alabama 36849, USA
Tel (334) 844-4620
Fax (334) 844-6555
Kilgota@auburn.edu
Real Analysis, Approximation Theory,
Computational Algorithms.

25) Jong Kyu Kim
Department of Mathematics
Kyungnam University
Masan Kyungnam, 631-701, Korea
Tel 82-(55)-249-2211
Fax 82-(55)-243-8609
jongkyuk@kyungnam.ac.kr
Nonlinear Functional Analysis, Variational
Inequalities, Nonlinear Ergodic Theory,
ODE, PDE, Functional Equations.

26) Miroslav Krbeč
Mathematical Institute
Academy of Sciences of Czech Republic
Žitná 25
CZ-115 67 Praha 1
Czech Republic
Tel +420 222 090 743
Fax +420 222 211 638
krbecm@matsrv.math.cas.cz
Function spaces, Real Analysis, Harmonic

Tel. (+33)(0)3.20.43.42.18
Fax (+33)(0)3.20.43.43.02
Catalin.Badea@math.univ-lille1.fr
Approximation Theory, Functional
Analysis, Operator Theory.

4) Erik J. Balder
Mathematical Institute
Universiteit Utrecht
P.O. Box 80 010
3508 TA UTRECHT
The Netherlands
Tel. +31 30 2531458
Fax +31 30 2518394
balder@math.uu.nl
Control Theory, Optimization,
Convex Analysis, Measure Theory,
Applications to Mathematical
Economics and Decision Theory.

5) Carlo Bardaro
Dipartimento di Matematica e Informatica
Universita di Perugia
Via Vanvitelli 1
06123 Perugia, ITALY
TEL +390755853822
+390755855034
FAX +390755855024
E-mail bardaro@unipg.it
Web site: <http://www.unipg.it/~bardaro/>
Functional Analysis and Approximation
Theory,
Signal Analysis, Measure Theory, Real
Analysis.

6) Heinrich Begehr
Freie Universitaet Berlin
I. Mathematisches Institut, FU Berlin,
Arnimallee 3, D 14195 Berlin
Germany,
Tel. +49-30-83875436, office
+49-30-83875374, Secretary
Fax +49-30-83875403
begehr@math.fu-berlin.de
Complex and Functional Analytic
Methods in PDEs, Complex Analysis,
History of Mathematics.

7) Fernando Bombal
Departamento de Analisis Matematico
Universidad Complutense
Plaza de Ciencias, 3
28040 Madrid, SPAIN
Tel. +34 91 394 5020
Fax +34 91 394 4726
fernando_bombal@mat.ucm.es

Analysis, Interpolation and
Extrapolation Theory, Fourier Analysis.

27) V. Lakshmikantham
Department of Mathematical Sciences
Florida Institute of Technology
Melbourne, FL 32901
e-mail: lakshmik@fit.edu
Ordinary and Partial Differential Equations,
Hybrid Systems, Nonlinear Analysis

28) Peter M. Maass
Center for Industrial Mathematics
Universitaet Bremen
Bibliotheksstr. 1,
MZH 2250,
28359 Bremen
Germany
Tel +49 421 218 9497
Fax +49 421 218 9562
pmaass@math.uni-bremen.de
Inverse problems, Wavelet Analysis and
Operator Equations, Signal and Image
Processing.

29) Julian Musielak
Faculty of Mathematics and Computer Science
Adam Mickiewicz University
Ul. Umultowska 87
61-614 Poznan
Poland
Tel (48-61) 829 54 71
Fax (48-61) 829 53 15
Grzegorz.Musielak@put.poznan.pl
Functional Analysis, Function Spaces,
Approximation Theory, Nonlinear Operators.

30) Vassilis Papanicolaou
Department of Mathematics
National Technical University of Athens
Zografou campus, 157 80
Athens, Greece
tel.: +30(210) 772 1722
Fax +30(210) 772 1775
papanico@math.ntua.gr
Partial Differential Equations,
Probability.

31) Pier Luigi Papini
Dipartimento di Matematica
Piazza di Porta S. Donato 5
40126 Bologna
ITALY
Fax +39(0)51 582528
papini@dm.unibo.it
Functional Analysis, Banach spaces,

Operators on Banach spaces,
Tensor products of Banach spaces,
Polymeasures, Function spaces.

8) Michele Campiti
Department of Mathematics "E.De Giorgi"
University of Lecce
P.O. Box 193
Lecce, ITALY
Tel. +39 0832 297 432
Fax +39 0832 297 594
michele.campiti@unile.it
Approximation Theory,
Semigroup Theory, Evolution problems,
Differential Operators.

9) Domenico Candeloro
Dipartimento di Matematica e Informatica
Universita degli Studi di Perugia
Via Vanvitelli 1
06123 Perugia
ITALY
Tel +39(0)75 5855038
+39(0)75 5853822,
+39(0)744 492936
Fax +39(0)75 5855024
candelor@dipmat.unipg.it
Functional Analysis, Function spaces,
Measure and Integration Theory in
Riesz spaces.

10) Pietro Cerone
School of Computer Science and
Mathematics, Faculty of Science,
Engineering and Technology,
Victoria University
P.O.14428,MCMC
Melbourne,VIC 8001,AUSTRALIA
Tel +613 9688 4689
Fax +613 9688 4050
Pietro.cerone@vu.edu.au
Approximations, Inequalities,
Measure/Information Theory,
Numerical Analysis, Special Functions.

11) Michael Maurice Dodson
Department of Mathematics
University of York,
York YO10 5DD, UK
Tel +44 1904 433098
Fax +44 1904 433071
Mmd1@york.ac.uk
Harmonic Analysis and Applications to
Signal Theory, Number Theory and
Dynamical Systems.

Approximation Theory.

32) Svetlozar T. Rachev
Chair of Econometrics, Statistics
and Mathematical Finance
School of Economics and
Business Engineering
University of Karlsruhe
Kollegium am Schloss, Bau II, 20.12, R210
Postfach 6980, D-76128,
Karlsruhe, GERMANY.
Tel +49-721-608-7535,
+49-721-608-2042(s)
Fax +49-721-608-3811
Zari.Rachev@wiwi.uni-karlsruhe.de
Second Affiliation:
Dept. of Statistics and Applied Probability
University of California at Santa Barbara
rachev@pstat.ucsb.edu
Probability, Stochastic Processes and
Statistics, Financial Mathematics,
Mathematical Economics.

33) Paolo Emilio Ricci
Department of Mathematics
Rome University "La Sapienza"
P.le A.Moro, 2-00185
Rome, ITALY
Tel ++3906-49913201 office
++3906-87136448 home
Fax ++3906-44701007
Paoloemilio.Ricci@uniroma1.it
riccip@uniroma1.it
Special Functions, Integral and Discrete
Transforms, Symbolic and Umbral Calculus,
ODE, PDE, Asymptotics, Quadrature,
Matrix Analysis.

34) Silvia Romanelli
Dipartimento di Matematica
Universita' di Bari
Via E.Orabona 4
70125 Bari, ITALY.
Tel (INT 0039)-080-544-2668 office
080-524-4476 home
340-6644186 mobile
Fax -080-596-3612 Dept.
romans@dm.uniba.it
PDEs and Applications to Biology and
Finance, Semigroups of Operators.

35) Boris Shekhtman
Department of Mathematics
University of South Florida
Tampa, FL 33620, USA
Tel 813-974-9710

12) Sever S.Dragomir
School of Computer Science and
Mathematics, Victoria University,
PO Box 14428,
Melbourne City,
MC 8001,AUSTRALIA
Tel. +61 3 9688 4437
Fax +61 3 9688 4050
sever@csm.vu.edu.au
Inequalities,Functional Analysis,
Numerical Analysis, Approximations,
Information Theory, Stochastics.

13) Paulo J.S.G.Ferreira
Department of Electronica e
Telecomunicacoes/IEETA
Universidade de Aveiro
3810-193 Aveiro
PORTUGAL
Tel +351-234-370-503
Fax +351-234-370-545
pjf@ieeta.pt
Sampling and Signal Theory,
Approximations, Applied Fourier Analysis,
Wavelet, Matrix Theory.

14) Gisele Ruiz Goldstein
Department of Mathematical Sciences
The University of Memphis
Memphis,TN 38152,USA.
Tel 901-678-2513
Fax 901-678-2480
ggoldste@memphis.edu
PDEs, Mathematical Physics,
Mathematical Geophysics.

15) Jerome A.Goldstein
Department of Mathematical Sciences
The University of Memphis
Memphis,TN 38152,USA
Tel 901-678-2484
Fax 901-678-2480
jgoldste@memphis.edu
PDEs,Semigroups of Operators,
Fluid Dynamics,Quantum Theory.

16) Heiner Gonska
Institute of Mathematics
University of Duisburg-Essen
Lotharstrasse 65
D-47048 Duisburg
Germany
Tel +49 203 379 3542
Fax +49 203 379 1845
gonska@math.uni-duisburg.de
Approximation and Interpolation Theory,

boris@math.usf.edu
Approximation Theory, Banach spaces,
Classical Analysis.

36) Panayiotis Siafarikas
Department of Mathematics
University of Patras
26500 Patras
Greece
Tel/Fax +302 610 997169
panos@math.upatras.gr
ODE,Difference Equations, Special
Functions, Orthogonal Polynomials,
Applied Functional Analysis.

37) Rudolf Stens
Lehrstuhl A fur Mathematik
RWTH Aachen
52056 Aachen
Germany
Tel ++49 241 8094532
Fax ++49 241 8092212
stens@mathA.rwth-aachen.de
Approximation Theory, Fourier Analysis,
Harmonic Analysis, Sampling Theory.

38) Juan J.Trujillo
University of La Laguna
Departamento de Analisis Matematico
C/Astr.Fco.Sanchez s/n
38271.LaLaguna.Tenerife.
SPAIN
Tel/Fax 34-922-318209
Juan.Trujillo@ull.es
Fractional: Differential Equations-
Operators-
Fourier Transforms, Special functions,
Approximations,and Applications.

39) Tamaz Vashakmadze
I.Vekua Institute of Applied Mathematics
Tbilisi State University,
2 University St. , 380043,Tbilisi, 43,
GEORGIA.
Tel (+99532) 30 30 40 office
(+99532) 30 47 84 office
(+99532) 23 09 18 home
Vasha@viam.hepi.edu.ge
tamazvashakmadze@yahoo.com
Applied Functional Analysis, Numerical
Analysis, Splines, Solid Mechanics.

40) Ram Verma
International Publications
5066 Jamieson Drive, Suite B-9,
Toledo, Ohio 43613,USA.

Computer Aided Geometric Design,
Algorithms.

17) Karlheinz Groechenig
Institute of Biomathematics and Biometry,
GSF-National Research Center
for Environment and Health
Ingolstaedter Landstrasse 1
D-85764 Neuherberg, Germany.
Tel 49-(0)-89-3187-2333
Fax 49-(0)-89-3187-3369
Karlheinz.groechenig@gsf.de
Time-Frequency Analysis, Sampling Theory,
Banach spaces and Applications,
Frame Theory.

18) Vijay Gupta
School of Applied Sciences
Netaji Subhas Institute of Technology
Sector 3 Dwarka
New Delhi 110075, India
e-mail: vijay@nsit.ac.in;
vijaygupta2001@hotmail.com
Approximation Theory

19) Weimin Han
Department of Mathematics
University of Iowa
Iowa City, IA 52242-1419
319-335-0770
e-mail: whan@math.uiowa.edu
Numerical analysis, Finite element method,
Numerical PDE, Variational inequalities,
Computational mechanics

20) Tian-Xiao He
Department of Mathematics and
Computer Science
P.O.Box 2900, Illinois Wesleyan University
Bloomington, IL 61702-2900, USA
Tel (309)556-3089
Fax (309)556-3864
the@iwu.edu
Approximations, Wavelet, Integration Theory,
Numerical Analysis, Analytic Combinatorics.

21) Don Hong
Department of Mathematical Sciences
Middle Tennessee State University
1301 East Main St.
Room 0269, Bldg KOM
Murfreesboro, TN 37132-0001
Tel (615) 904-8339
dhong@mtsu.edu
Approximation Theory, Splines, Wavelet,
Stochastics, Mathematical Biology Theory.

Verma99@msn.com
rverma@internationalpubls.com
Applied Nonlinear Analysis, Numerical
Analysis, Variational Inequalities,
Optimization Theory, Computational
Mathematics, Operator Theory.

41) Gianluca Vinti
Dipartimento di Matematica e Informatica
Universita di Perugia
Via Vanvitelli 1
06123 Perugia
ITALY
Tel +39(0) 75 585 3822,
+39(0) 75 585 5032
Fax +39 (0) 75 585 3822
mategian@unipg.it
Integral Operators, Function Spaces,
Approximation Theory, Signal Analysis.

42) Ursula Westphal
Institut fuer Mathematik B
Universitaet Hannover
Welfengarten 1
30167 Hannover, GERMANY
Tel (+49) 511 762 3225
Fax (+49) 511 762 3518
westphal@math.uni-hannover.de
Semigroups and Groups of Operators,
Functional Calculus, Fractional Calculus,
Abstract and Classical Approximation
Theory, Interpolation of Normed spaces.

43) Ronald R. Yager
Machine Intelligence Institute
Iona College
New Rochelle, NY 10801, USA
Tel (212) 249-2047
Fax (212) 249-1689
Yager@Panix.Com
ryager@iona.edu
Fuzzy Mathematics, Neural Networks,
Reasoning,
Artificial Intelligence, Computer Science.

44) Richard A. Zalik
Department of Mathematics
Auburn University
Auburn University, AL 36849-5310
USA.
Tel 334-844-6557 office
678-642-8703 home
Fax 334-844-6555
zalik@auburn.edu
Approximation Theory, Chebychev Systems,
Wavelet Theory.

22) Hubertus Th. Jongen
Department of Mathematics
RWTH Aachen
Templergraben 55
52056 Aachen
Germany
Tel +49 241 8094540
Fax +49 241 8092390
jongen@rwth-aachen.de
Parametric Optimization, Nonconvex
Optimization, Global Optimization.

On the Green Function of the $(\diamond_B + m^4)^k$ Operator Related to the Bessel-Helmholtz Operator and the Bessel Klein-Gordon Operator

Chalermpon Bunpog and Amnuay Kananthai

Department of Mathematics, Chiang Mai University, Chiang Mai, 50200 Thailand
malamnka@science.cmu.ac.th

Abstract

In this paper, we study the Green function of the operator $(\diamond_B + m^4)^k$ which is iterated k -times and is defined by

$$(\diamond_B + m^4)^k = \left[\left(\sum_{i=1}^p B_{x_i} \right)^2 - \left(\sum_{j=p+1}^{p+q} B_{x_j} \right)^2 + m^4 \right]^k, \quad (0.1)$$

where m is a positive real number and $p+q = n$ is the dimension of \mathbb{R}_n^+ and k is a nonnegative integer and $B_{x_i} = \frac{\partial^2}{\partial x_i^2} + \frac{2v_i}{x_i} \frac{\partial}{\partial x_i}$, $2v_i = 2\alpha_i + 1$, $\alpha_i > -\frac{1}{2}$, $x_i > 0$. At first we study the Green function of the operator $(\diamond_B + m^4)^k$, we have that such a Green function related to the elementary solutions of the Bessel-Helmholtz operator $(\triangle_B + m^2)^k$ iterated k -times and the Bessel Klein-Gordon operator $(\square_B + m^2)^k$ iterated k -times. We also apply such a Green function to solve the solution of the equation $(\diamond_B + m^4)^k u(x) = f(x)$ where f is a generalized function and $u(x)$ is an unknown function for $x \in \mathbb{R}_n^+$.

Keywords: Green function, Bessel diamond operator, Helmholtz operator, Klein-Gordon operator

1 Introduction

A. Kananthai [1] first introduced the diamond operator \diamond^k iterated k -times, defined by

$$\diamond^k = \left[\left(\sum_{i=1}^p \frac{\partial^2}{\partial x_i^2} \right)^2 - \left(\sum_{j=p+1}^{p+q} \frac{\partial^2}{\partial x_j^2} \right)^2 \right]^k,$$

the equation $\diamond^k u(x) = f(x)$, see [2], has been already studied and the convolution $u(x) = (-1)^k R_{2k}^H(x) * R_{2k}^e * f(x)$ has been obtained as a solution of such an equation.

Later the equation $(\diamond + m^4)^k u(x) = f(x)$, see [3], has been studied and the convolution $u(x) = (W_{2k}^H(u, m) * W_{2k}^e(v, m)) * (s^{*k})^{*-1}(x) * f(x)$ has been obtained a solution of such an equation.

Furthermore, Hüseyin Yildirim, Mzeki Sarikaya and Sermin Öztürk [4] first introduced the Bessel diamond operator \diamond_B^k iterated k -times, defined by

$$\diamond_B^k = \left[\left(\sum_{i=1}^p B_{x_i} \right)^2 - \left(\sum_{j=p+1}^{p+q} B_{x_j} \right)^2 \right]^k \quad (1.1)$$

where $B_{x_i} = \frac{\partial^2}{\partial x_i^2} + \frac{2v_i}{x_i} \frac{\partial}{\partial x_i}$, $2v_i = 2\alpha_i + 1$, $\alpha_i > -\frac{1}{2}$, $x_i > 0$. The operator \diamond_B^k can be expressed by $\diamond_B^k = \Delta_B^k \square_B^k = \square_B^k \Delta_B^k$, where

$$\Delta_B^k = \left(\sum_{i=1}^p B_{x_i} \right)^k. \quad (1.2)$$

and

$$\square_B^k = \left[\sum_{i=1}^p B_{x_i} - \sum_{j=p+1}^{p+q} B_{x_j} \right]^k. \quad (1.3)$$

The equation $\diamond_B^k u(x) = \delta(x)$, see([4], p.382), has been already studied and the convolution $u(x) = (-1)^k S_{2k} * R_{2k}$ has been obtained as a solution of such an equation where the function S_{2k} and R_{2k} are defined by (2.1) and (2.2), respectively, with $\alpha = \beta = 2k$. In this work, we study the equation of the form

$$(\diamond_B + m^4)^k G(x) = \delta(x).$$

We obtain the elementary solution $G(x) = (T_{2k}(x) * W_{2k}(x)) * (C^{*k})^{*-1}(x)$, where the symbol $*k$ denotes the convolution of itself k -times and the symbol $*-1$ is an inverse of the convolution algebra, $T_{2k}(x)$ is the elementary solution of the Bessel-Helmholtz operator $(\Delta_B + m^2)^k$ iterated k -times, that is $T_{2k}(x)$ satisfy the equation

$$(\Delta_B + m^2)^k u(x) = \delta(x)$$

and $W_{2k}(x)$ is the elementary solution of the Bessel Klein-Gordon operator $(\square_B + m^2)^k$ iterated k -times, that is $W_{2k}(x)$ satisfy the equation

$$(\square_B + m^2)^k u(x) = \delta(x)$$

and $C(x)$ is defined by

$$C(x) = \delta(x) - m^2(T_2(x) + W_2(V)) + 2m^4(T_2(x) * W_2(V)).$$

Moreover, we apply such a Green function to obtain the solution of the equation

$$(\diamond_B + m^4)^k u(x) = f(x).$$

where f is a generalized function.

2 Preliminaries

Definition 2.1 Let $x = (x_1, x_2, \dots, x_n), \nu = (\nu_1, \nu_2, \dots, \nu_n) \in \mathbb{R}_n^+$. For any complex number α , we define the function $S_\alpha(x)$ by

$$S_\alpha(x) = \frac{2^{n+2|\nu|-2\alpha} \Gamma\left(\frac{n+2|\nu|-\alpha}{2}\right) |x|^{\alpha-n-2|\nu|}}{\prod_{i=1}^n 2^{\nu_i-\frac{1}{2}} \Gamma(\nu_i + \frac{1}{2})} \quad (2.1)$$

Definition 2.2 Let $x = (x_1, x_2, \dots, x_n), \nu = (\nu_1, \nu_2, \dots, \nu_n) \in \mathbb{R}_n^+$, and denote by $V = x_1^2 + x_2^2 + \dots + x_p^2 - x_{p+1}^2 - x_{p+2}^2 - \dots - x_{p+q}^2$ the nondegenerated quadratic form. Denote the interior of the forward cone by $\Gamma_+ = \{x \in \mathbb{R}_n^+ : x_1 > 0, x_2 > 0, \dots, x_n > 0, V > 0\}$. The function $R_\beta(x)$ is defined by

$$R_\beta(x) = \frac{V^{\frac{\beta-n-2|\nu|}{2}}}{K_n(\beta)}, \quad (2.2)$$

where

$$K_n(\beta) = \frac{\pi^{\frac{n+2|\nu|-1}{2}} \Gamma\left(\frac{2+\beta-n-2|\nu|}{2}\right) \Gamma\left(\frac{1-\beta}{2}\right) \Gamma(\beta)}{\Gamma\left(\frac{2+\beta-p-2|\nu|}{2}\right) \Gamma\left(\frac{p-\beta}{2}\right)},$$

where β is a complex number.

Definition 2.3 Let $x = (x_1, x_2, \dots, x_n) \in \mathbb{R}_n^+$, For any complex number α , we define the function

$$T_\alpha(x) = \sum_{r=0}^{\infty} \frac{(-1)^r \Gamma\left(\frac{\eta}{2} + r\right)}{r! \Gamma\left(\frac{\eta}{2}\right)} (m^2)^r (-1)^{\frac{\alpha}{2}+r} S_{\alpha+2r}(x), \quad (2.3)$$

where η is a complex number and $S_{\alpha+2r}(x)$ is defined in definition 2.1.

Definition 2.4 Let $x = (x_1, x_2, \dots, x_n)$, For any complex number β , we define the function

$$W_\beta(x) = \sum_{r=0}^{\infty} \frac{(-1)^r \Gamma\left(\frac{\eta}{2} + r\right)}{r! \Gamma\left(\frac{\eta}{2}\right)} (m^2)^r R_{\beta+2r}(x), \quad (2.4)$$

where η is a complex number and $R_{\beta+2r}(x)$ is defined in definition 2.2.

Lemma 2.1 *Given the equation $\Delta_B^k u(x) = \delta(x)$ for $x \in \mathbb{R}_n^+$, where Δ_B^k is defined by (1.2). Then*

$$u(x) = (-1)^k S_{2k}(x)$$

where $S_{2k}(x)$ is defined by (2.1), with $\alpha = 2k$.

Proof. See ([4], p.379). □

Lemma 2.2 *Given the equation $\square_B^k u(x) = \delta(x)$ for $x \in \mathbb{R}_n^+$, where \square_B^k is defined by (1.3). Then*

$$u(x) = R_{2k}(x)$$

where $R_{2k}(x)$ is defined by (2.2), with $\beta = 2k$

Proof. See ([4], p.379). □

Lemma 2.3 (The elementary solution of the Bessel-Helmholtz operator).

Given the equation $(\Delta_B + m^2)^k u(x) = \delta(x)$ for $x \in \mathbb{R}_n^+$, where Δ_B is defined by (1.2) with $k = 1$. Then

$$u(x) = T_{2k}(x)$$

where $T_{2k}(x)$ is defined by (2.3), with $\alpha = 2k$.

Proof. At first, the following formula is valid ([5], p.3),

$$\Gamma\left(\frac{\eta}{2} + r\right) = \frac{\eta}{2} \left(\frac{\eta}{2} + 1\right) \cdots \left(\frac{\eta}{2} + r - 1\right) \Gamma\left(\frac{\eta}{2}\right).$$

Equivalently,

$$\begin{aligned} (-1)^r \frac{1}{r!} \Gamma\left(\frac{\eta}{2} + r\right) &= \frac{(-1)^r \frac{\eta}{2} \left(\frac{\eta}{2} + 1\right) \cdots \left(\frac{\eta}{2} + r - 1\right) \Gamma\left(\frac{\eta}{2}\right)}{r!} \\ &= \frac{\left(-\frac{\eta}{2}\right) \left(-\frac{\eta}{2} - 1\right) \cdots \left[-\left(\frac{\eta}{2} + r - 1\right)\right]}{r!} \Gamma\left(\frac{\eta}{2}\right). \end{aligned}$$

We have,

$$(-1)^r \frac{1}{r!} \Gamma\left(\frac{\eta}{2} + r\right) = \binom{-\frac{\eta}{2}}{r} \Gamma\left(\frac{\eta}{2}\right).$$

Then, we obtain the function $T_\alpha(x)$ is defined by Definition 2.3 become

$$T_\alpha(x) = \sum_{r=0}^{\infty} \binom{-\frac{\eta}{2}}{r} (m^2)^r (-1)^{\frac{\alpha}{2}+r} S_{\alpha+2r}(x). \quad (2.5)$$

Putting $\alpha = \eta = 2k$ in (2.5), we have

$$T_{2k}(x) = \sum_{r=0}^{\infty} \binom{-k}{r} (m^2)^r (-1)^{k+r} S_{2k+2r}(x).$$

Since the operator Δ_B is linearly continuous and has 1-1 mapping, then it has inverse, by Lemma 2.1 we obtain

$$\begin{aligned} T_{2k}(x) &= \sum_{r=0}^{\infty} \binom{-k}{r} (m^2)^r \delta(x) * \Delta_B^{-k-r} \\ &= (\Delta_B + m^2)^{-k} \delta(x), \end{aligned} \quad (2.6)$$

where $(\Delta_B + m^2)^{-k}$ is the inverse operator of the operator $(\Delta_B + m^2)^k$. By applying the operator $(\Delta_B + m^2)^k$ to both sides of (2.6), we obtain

$$(\Delta_B + m^2)^k T_{2k}(x) = (\Delta_B + m^2)^k . (\Delta_B + m^2)^{-k} \delta(x).$$

Thus

$$(\Delta_B + m^2)^k T_{2k}(x) = \delta(x).$$

□

Lemma 2.4 (The elementary solution of the Bessel Klein-Gordon operator).

Given the equation $(\square_B + m^2)^k u(x) = \delta(x)$ for $x \in \mathbb{R}_n^+$, where \square_B is defined by (1.3) with $k = 1$. Then

$$u(x) = W_{2k}(x)$$

where $W_{2k}(x)$ is defined by (2.4), with $\alpha = 2k$.

Proof. The proof of lemma 2.4 is similar to the proof of Lemma 2.3. □

Lemma 2.5 *Let $T_{2k}(x)$ and $W_{2k}(x)$ be defined by (2.3) and (2.4) respectively, where $\alpha = \beta = 2k$. Then the convolution $T_{2k}(x) * W_{2k}(x)$ exist and it is lie in \mathcal{S}' , where \mathcal{S}' is a space of tempered distribution.*

Proof. From (2.3) and (2.4) with $\alpha = \beta = 2k$, we have

$$\begin{aligned} T_{2k}(x) * W_{2k}(x) &= \left(\sum_{r=0}^{\infty} \frac{(-1)^r \Gamma(k+r)}{r! \Gamma(k)} (m^2)^r (-1)^{k+r} S_{2k+2r}(x) \right) \\ &\quad * \left(\sum_{r=0}^{\infty} \frac{(-1)^r \Gamma(k+r)}{r! \Gamma(k)} (m^2)^r R_{2k+2r}(x) \right) \\ &= \sum_{r=0}^{\infty} \sum_{s=0}^{\infty} \frac{(-1)^s \Gamma(k+s)}{s! \Gamma(k)} (m^2)^s \cdot \frac{(-1)^r \Gamma(k+r)}{r! \Gamma(k)} (m^2)^r \\ &\quad (-1)^{k+r} S_{2k+2r}(x) * R_{2k+2r}(x). \end{aligned}$$

Hüseyin Yildirim, Mzeki Sarikaya and Sermin Öztürk ([4],p.380) has shown that $S_{2k+2r}(x) * R_{2k+2r}(x)$ exists and is a tempered distribution. It follows that $T_{2k}(x) * W_{2k}(x)$ exists and also is a tempered distribution. □

Lemma 2.6 *Let $T_2(x)$ and $W_2(x)$ be defined by (2.3) and (2.4) respectively, where $\alpha = \beta = 2$. Then*

$$[(\Delta_B + m^2)(\square_B + m^2) - m^2(\Delta_B + \square_B)] (T_2(x) * W_2(x)) = C(x), \quad (2.7)$$

where $C(x) = \delta(x) - m^2(T_2(x) + W_2(x)) + 2m^4(T_2(x) * W_2(x))$

Proof. We have

$$\begin{aligned} & [(\Delta_B + m^2)(\square_B + m^2) - m^2(\Delta_B + \square_B)] (T_2(x) * W_2(x)) = \\ & [(\Delta_B + m^2)(\square_B + m^2) (T_2(x) * W_2(x)) - m^2(\Delta_B + \square_B) (T_2(x) * W_2(x))] = \\ & [(\Delta_B + m^2)T_2(x) * (\square_B + m^2)W_2(x) - m^2(\Delta_B T_2(x) * W_2(x) + T_2(x) * \square_B W_2(x))] . \end{aligned} \quad (2.8)$$

From Lemma 2.3 and Lemma 2.4, for $k = 1$ we have

$$(\Delta_B + m^2)T_2(x) = \delta(x) \quad \text{and} \quad (\square_B + m^2)W_2(x) = \delta(x),$$

respectively. Moreover,

$$\Delta_B T_2(x) = \delta(x) - m^2 T_2(x)$$

and

$$\square_B W_2(x) = \delta(x) - m^2 W_2(x),$$

thus(2.8) become

$$\begin{aligned} & [(\Delta_B + m^2)(\square_B + m^2) - m^2(\Delta_B + \square_B)] (T_2(x) * W_2(x)) = \\ & \delta(x) * \delta(x) - m^2 [(\delta(x) - m^2 T_2(x)) * W_2(x) + T_2(x) * (\delta(x) - m^2 W_2(x))] = \\ & \delta(x) - m^2 [W_2(x) - m^2 T_2(x) * W_2(x) + T_2(x) - m^2 T_2(x) * W_2(x)] = \\ & \delta(x) - m^2 (T_2(x) + W_2(x)) - 2m^4 (T_2(x) * W_2(x)) = C(x). \end{aligned}$$

□

Lemma 2.7 *Let $S_\alpha(x)$ be the function, defined by (2.1). Then*

$$S_\alpha(x) * S_\beta(x) = S_{\alpha+\beta}(x),$$

where α and β are a positive even numbers.

Proof. See([4],p.380)

□

Lemma 2.8 *Let $R_\beta(x)$ be the function, defined by (2.2). Then*

$$R_\beta(x) * R_\alpha(x) = R_{\beta+\alpha}(x),$$

where α and β are a positive even numbers.

Proof. Since $R_\beta(x)$ and $R_\alpha(x)$ are tempered distributions (see [4], p.380). Let $\text{Supp}R_\beta(x) = K \subset \bar{\Gamma}_+$, where K is a compact set and $\bar{\Gamma}_+$ is a closure of Γ_+ appears in Definition 2.2, then $R_\beta(x) * R_\alpha(x)$ exists and is well defined. To show that $R_\beta(x) * R_\alpha(x) = R_{\beta+\alpha}(x)$, by Lemma 2.2 $\square_B^k u(x) = \delta(x)$ Then $u(x) = R_{2k}(x)$. Now, $\square_B^k u(x) = \square_B^r \square_B^{k-r} u(x) = \delta(x)$ for $r < k$, then by Lemma 2.2 $\square_B^{k-r} u(x) = R_{2r}(x)$. Convolving both sides by $R_{2(k-r)}(x)$ we obtain

$$R_{2(k-r)}(x) * \square_B^{k-r} u(x) = R_{2(k-r)}(x) * R_{2r}(x)$$

or,

$$\square_B^{k-r} R_{2(k-r)}(x) * u(x) = R_{2(k-r)}(x) * R_{2r}(x)$$

by Lemma 2.2 again, we have

$$\delta(x) * u(x) = R_{2(k-r)}(x) * R_{2r}(x).$$

It follow that

$$u(x) = R_{2(k-r)}(x) * R_{2r}(x).$$

Since $u(x) = R_{2k}(x)$, thus

$$R_{2(k-r)}(x) * R_{2r}(x) = R_{2k}(x).$$

Let $\beta = 2(k-r)$ and $\alpha = 2r$, actually β and α are positive even numbers. It follows that $R_\beta(x) * R_\alpha(x) = R_{\beta+\alpha}(x)$ as required. \square

3 Main Results

Theorem 3.1 *Given the equation*

$$(\diamond_B + m^4)^k G(x) = \delta(x) \quad (3.1)$$

where $(\diamond_B + m^4)^k$ is the operator iterated k -times defined by (0.1), δ is the Dirac-delta distribution, $x = (x_1, x_2, \dots, x_n) \in \mathbb{R}_n^+$ and k is a nonnegative integer. Then we obtain $G(x) = T_{2k}(x) * W_{2k}(x) * (C^{*k}(x))^{*-1}$ is a Green function for the operator $(\diamond_B + m^4)^k$ iterated k -time where \diamond_B is defined by (1.1) with $k = 1$, m is a nonnegative real number and

$$C(x) = \delta(x) - m^2(T_2(x) + W_2(x)) + 2m^4(T_2(x) * W_2(x)) \quad (3.2)$$

$C^{*k}(x)$ denote the convolution of C it self k -time, $(C^{*k}(x))^{*-1}$ denote the inverse of $C^{*k}(x)$ in the convolution algebra. Moreover $C(x)$ is a tempered distribution.

Proof. Since $(\diamond_B + m^4)^k = ((\Delta_B + m^2)(\square_B + m^2) - m^2(\Delta_B + \square_B))^k$.

$$\begin{aligned} & [(\Delta_B + m^2)(\square_B + m^2) - m^2(\Delta_B + \square_B)] \cdot \\ & [(\Delta_B + m^2)(\square_B + m^2) - m^2(\Delta_B + \square_B)]^{k-1} G(x) = \delta(x) \quad (3.3) \end{aligned}$$

From Lemma 2.5 we have $T_2(x) * W_2(x)$ exists and is a tempered distribution. Convolving both sides of the above equation by $T_2(x) * W_2(x)$, we obtain

$$\begin{aligned} & [(\Delta_B + m^2)(\square_B + m^2) - m^2(\Delta_B + \square_B)] (T_2(x) * W_2(x)) * \\ & [(\Delta_B + m^2)(\square_B + m^2) - m^2(\Delta_B + \square_B)]^{k-1} G(x) = (T_2(x) * W_2(x)) * \delta(x) \end{aligned}$$

by Lemma 2.6, we have

$$C(x) * [(\Delta_B + m^2)(\square_B + m^2) - m^2(\Delta_B + \square_B)]^{k-1} G(x) = (T_2(x) * W_2(x)) * \delta(x).$$

Keeping on convolving both sides of the above equation by $T_2(x) * W_2(x)$ up to $k - 1$ times, we have

$$C^{*k}(x) * G(x) = (T_2(x) * W_2(x))^{*k},$$

where $*k$ denotes the convolution of itself k -times.

By Lemma 2.7, Lemma 2.8 and definitions of $T_\alpha(x)$ and $W_\beta(x)$, we have

$$(T_2(x) * W_2(x))^{*k} = T_{2k}(x) * W_{2k}(x),$$

then

$$C^{*k}(x) * G(x) = T_{2k}(x) * W_{2k}(x).$$

Now, consider the function $C^{*k}(x)$, since $\delta(x)$, $T_2(x)$, $W_2(x)$ and $T_2(x) * W_2(x)$ are lies in \mathcal{S}' where \mathcal{S}' is a space of tempered distribution, then $C(x) \in \mathcal{S}'$, moreover by ([6], p.152) we obtain $C^{*k}(x) \in \mathcal{S}'$. Since $T_{2k}(x) * W_{2k}(x) \in \mathcal{S}'$, choose $\mathcal{S}' \subset \mathcal{D}'_{\mathcal{R}}$ where $\mathcal{D}'_{\mathcal{R}}$ is the right-side distribution which is a subspace of \mathcal{D}' of distribution. Thus $T_{2k}(x) * W_{2k}(x) \in \mathcal{D}'_{\mathcal{R}}$, it follow that $T_{2k}(x) * W_{2k}(x)$ is an element of convolution algebra, thus by ([7], p.150-151), we have that the equation (2.8) has a unique solution

$$G(x) = T_{2k}(x) * W_{2k}(x) * (C^{*k}(x))^{*-1}$$

where $(C^{*k}(x))^{*-1}$ is an inverse of C^{*k} in the convolution algebra, $G(x)$ is called the Green function of the operator $(\diamond_B + m^4)^k$. Since $T_{2k}(x) * W_{2k}(x)$ and $(C^{*k}(x))^{*-1}$ are lies in \mathcal{S}' , then by ([6], p.152) again, we have $T_{2k}(x) * W_{2k}(x) * (C^{*k}(x))^{*-1} \in \mathcal{S}'$. Hence $G(x)$ is a tempered distribution. \square

Theorem 3.2 *Given the equation*

$$(\diamond_B + m^4)^k u(x) = f(x) \quad (3.4)$$

where f is a given generalized function and $u(x)$ is an unknown function, we obtain

$$u(x) = G(x) * f(x)$$

is a unique solution of the equation (3.4) where $G(x)$ is a Green function for $(\diamond_B + m^4)^k$.

Proof. Convolving both sides of (3.4) by $G(x)$ where $G(x)$ is a Green function for $(\diamond_B + m^4)^k$ in theorem 3.1, we obtain

$$G(x) * (\diamond_B + m^4)^k u(x) = G(x) * f(x)$$

or,

$$(\diamond_B + m^4)^k G(x) * u(x) = G(x) * f(x)$$

applying the Theorem 3.1, we have

$$\delta(x) * u(x) = G(x) * f(x).$$

Therefor,

$$u(x) = G(x) * f(x).$$

Sine $G(x)$ is unique. Hence $u(x)$ is a unique solution of the equation (3.4). □

Acknowledgement.

The authors would like to thank The Commission on Higher Education Scholarship and Graduate School, Chiang Mai University, Thailand for financial support.

References

- [1] A. Kananthai, *On the solution of the n -dimensional Diamond operator*, Applied Mathematics and computation, vol. 88, Elsevier Science Inc., New York, 1997, p. 27-37.
- [2] A. Kananthai, *On the Diamond operator related to the wave equation*, Nonlinear Analysis, 2001, 47 (2), p. 1373-1382.
- [3] A. Kananthai, *On the Green function of the Diamond operator related to the Klein-Gordon operator*, Bull. Cal. Math. Soc., 2001, 93 (5), p.353-360.

- [4] Hüseyin Yildirim, Mzeki Sarikaya and Sermin Öztürk, *The solution of the n -dimensional Bessel diamond operator and the Fourier-Bessel transform of their convolution*, Proc. Indian Acad. Sci. (Math. Sci.) Vol. 114, No.4, November 2004, 375–387.
- [5] Bateman, Manuscript Project, *Higher Trascendental Functions*, Vol.I, Mc-Graw Hill, New York, 1953.
- [6] Donoghue, W. F., *Distributions and Fourier transform*, Academic Press, (1969).
- [7] Zemanian, A. H., *Distribution Theory and Transform Analysis*, Mc-Graw Hill, New York, (1964).

Measures of smallness in a Banach space

Chiara Donnini

Dipartimento di Matematica per le Decisioni,

Università degli Studi di Firenze,

Via Lombroso, 6/17

50134 Firenze (Italy)

donnini@dipmat.unipg.it

Abstract

We extend the notion of *measure of smallness*, given for subsets of the real line, to the case of subsets of a Banach space X , introducing two new different notions: the scalar measures of smallness and the strong measure of smallness.

AMS Classification: 28A12, 46B20 (primary) 28A05, 46B25 (secondary).

Key words: Microscopic sets, measure of smallness, Kuratowski measure of non compactness, Lebesgue measure, Banach space.

1 Introduction

Appell proposed a definition of microscopcity for subsets of \mathbb{R} in 2001 [1]:

Definition 1 [1] A subset M of \mathbb{R} is *microscopic* iff for all $\varepsilon \in (0, 1)$ one can find a sequence of intervals $(I_n)_n$ such that $M \subseteq \bigcup_{n=1}^{\infty} I_n$ and, for all n , $\lambda(I_n) \leq \varepsilon^n$, where λ is the Lebesgue measure.

Appell, D’Aniello e Văth, [2], introduced a definition of measure of smallness of subsets of \mathbb{R} .

Definition 2 [2] Given a subset M of \mathbb{R} the *measure of smallness of M* , $\mu_{\mathbb{R}}(M)$, is the number

$$\mu_{\mathbb{R}}(M) = \inf\{\varepsilon > 0 : \exists (I_n)_n \text{ such that } M \subseteq \bigcup_{n=1}^{\infty} I_n \text{ and for all } n, \lambda(I_n) \leq \varepsilon^n\}.$$

Later, in [5], the notion of microscopic sets was extended to the case of subsets of a Banach space X in two different ways.

Definition 3 [5] $M \subseteq X$ is *microscopic* iff for all $\varepsilon > 0$ there exists a sequence $(x_n)_n \in X$ such that $M \subseteq \bigcup_{n=1}^{\infty} (x_n + \varepsilon^n X_1)$, where X_1 is the closed unit ball of X .
 $M \subseteq X$ is *scalarly microscopic* iff for all functional $x^* \in X^*$, $x^*(M)$ is microscopic in \mathbb{R} .

In this paper we extend the notion of measure of smallness in two different ways introducing, for each subset M of a Banach space, the *scalar measure of smallness*, $\mu(M)$, and the *strong measure of smallness* $\nu(M)$. More precisely:

Definition 4 Let $X = (X, \|\cdot\|)$ be a Banach space; then for each of its subsets M we define the *scalar measure of smallness of M* , as the value

$$\mu(M) = \sup_{x^* \in X_1^*} \mu_{x^*}(M),$$

where $\mu_{x^*}(M) = \mu_{\mathbb{R}}(x^*(M))$ and X_1^* is the closed unit ball of X^* .

Definition 5 Given a subset M of X we define the *strong measure of smallness of M* , as

$$\nu(M) = \inf \left\{ \varepsilon > 0 : \exists (x_n)_n \subset X \text{ s.t. } M \subseteq \bigcup_{n=1}^{\infty} (x_n + \varepsilon^n X_1) \right\}.$$

We shall prove that these two smallness parameters satisfy properties analogous to those of $\mu_{\mathbb{R}}$ and of the Kuratowski measure of non compactness α . More precisely μ fulfills the following properties:

- (a') $\mu(M) = 0 \iff M$ is scalarly microscopic.
 - (b') $M \subseteq N \implies \mu(M) \leq \mu(N)$.
 - (c') $|c|\mu(M) \leq \mu(cM) \leq \mu(M)$, for $|c| \leq 1$;
 $\mu(M) \leq \mu(cM) \leq |c|\mu(M)$, for $|c| > 1$.
 - (d') There are cases for which $\mu(M) < \mu(\overline{M})$.
 - (e') There are cases for which $\mu(M) < \mu(\text{co } M)$.
 - (f') $M, N \subseteq X$ segments $\implies \mu(M + N) \leq \mu(M) + \mu(N)$;
 $M, N \subseteq X$ closed balls $\implies \mu(M + N) \leq \mu(M) + \mu(N)$.
 - (g') Let X be reflexive and let $(X_n)_n \subset X$ be a decreasing sequence of weakly closed, bounded, non-empty subsets such that $\lim_{n \rightarrow \infty} \mu(X_n) = 0$, then the intersection of all X_n is scalarly microscopic and non empty.
 - (h') μ does not fulfill the maximum property, but it satisfies the following estimate $\mu\left(\bigcup_{i=1}^n M_i\right) \leq (\max\{\mu(M_1), \dots, \mu(M_n)\})^{\frac{1}{n}}$.
- While ν verifies

- (a'') $\nu(M) = 0 \iff M$ is microscopic.

- (b'') $M \subseteq N \implies \nu(M) \leq \nu(N)$.
- (c'') $|c|\nu(M) \leq \nu(cM) \leq \nu(M)$, for $|c| \leq 1$;
 $\nu(M) \leq \nu(cM) \leq |c|\nu(M)$, for $|c| > 1$.
- (d'') There are cases for which $\nu(M) < \nu(\overline{M})$.
- (e'') There are cases for which $\nu(M) < \nu(\text{co } M)$.
- (f'') There are cases for which $\nu(M + N) > \nu(M) + \nu(N)$;
- (g'') Let X be reflexive and let $(X_n)_n \subseteq X$ be a decreasing sequence of non-empty, bounded and weakly closed subsets with $\lim_{n \rightarrow \infty} \nu(X_n) = 0$. Then the intersection of all X_n is microscopic and non empty.
- (h'') ν does not fulfill the maximum property, but it satisfies the following estimate $\nu\left(\bigcup_{i=1}^n M_i\right) \leq (\max\{\nu(M_1), \dots, \nu(M_n)\})^{\frac{1}{n}}$.

Furthermore we shall compare μ and ν and deduce that in \mathbb{R} microscopic sets are also scalarly microscopic and both definitions coincide with microscopcity in the sense of Definition 1.

Finally we shall consider the strong measure of smallness of the unit ball.

We can observe that when $X = \mathbb{R}$ the notion of strong measure of smallness, introduced in Definition 5, does not coincide with the measure of smallness in \mathbb{R} and that a natural extension of $\mu_{\mathbb{R}}$ in a Banach space might be the following:

Definition 6 Given a subset M of X the *strong measure of smallness* of M , is the number

$$\tilde{\nu}(M) = \inf \left\{ \varepsilon > 0 : \exists (x_n)_n \subset X \text{ s.t. } M \subseteq \bigcup_{n=1}^{\infty} \left(x_n + \frac{\varepsilon^n}{2} X_1 \right) \right\}.$$

Nevertheless, we prefer to use the Definition 5, because it proceeds from the notion of microscopcity in X in the sense of the Definition 3, that makes the class of microscopic sets more easily comparable with another class of “small” sets: the ones with the small ball property introduced and studied in [4].

2 Microscopicity and measure of smallness on \mathbb{R}

In this section we shall remind some results from [2] and [5] that will be needed in the sequel. Moreover we shall give some useful results concerning $\mu_{\mathbb{R}}$ and compare the notions of microscopcity given in Definitions 1 and 3 in the particular case $X = \mathbb{R}$.

For microscopic subsets of \mathbb{R} the following proposition holds:

Proposition 1 ([2], Proposition 1)

- i) Every subset of a microscopic set is microscopic;
- ii) the countable union of microscopic sets is microscopic;
- iii) given a microscopic set M and a point $x \in \mathbb{R}$, the set $x + M$ is microscopic;
- iv) given a microscopic set M and $\alpha \in \mathbb{R}$, the set αM is microscopic;
- v) every microscopic set is a nullset;
- vi) every countable set is microscopic.

Easily one can prove:

Proposition 2 ([5], Proposition 1) *For subsets of X the following properties hold:*

- i) *every subset of a scalarly microscopic set is scalarly microscopic;*
- ii) *countable unions of scalarly microscopic sets are scalarly microscopic;*
- iii) *given a scalarly microscopic set M and $x \in \mathbb{R}$, $x+M$ is scalarly microscopic;*
- iv) *given a scalarly microscopic set M and $\alpha \in \mathbb{R}$, αM is scalarly microscopic;*
- v) *X is not scalarly microscopic;*
- vi) *every countable set is scalarly microscopic.*

For the measure of smallness in \mathbb{R} the following proposition holds:

Proposition 3 ([2], Proposition 6)

- i) *For every subset M of \mathbb{R} , $0 \leq \mu_{\mathbb{R}}(M) \leq 1$, and if M is bounded $\mu_{\mathbb{R}}(M) < 1$;*
- ii) *$\mu_{\mathbb{R}}(M) = 0$ if and only if M is microscopic;*
- iii) *$\mu_{\mathbb{R}}$ is monotone, that is if $M \subseteq N$ then $\mu_{\mathbb{R}}(M) \leq \mu_{\mathbb{R}}(N)$;*
- iv) *given M subset of \mathbb{R} , and $x \in \mathbb{R}$, $\mu_{\mathbb{R}}(x + M) = \mu_{\mathbb{R}}(M)$;*
- v) *defined λ^* the outer Lebesgue measure, for every subset M of \mathbb{R} the following estimate is true: $\mu_{\mathbb{R}}(M) \geq \frac{\lambda^*(M)}{1 + \lambda^*(M)}$. Therefore, if $\lambda^*(M) = \infty$ then $\mu_{\mathbb{R}}(M) = 1$.*

Proposition 4 ([2], Example 8) *If M is a closed and bounded interval, then the following equality holds: $\mu_{\mathbb{R}}(M) = \frac{\lambda(M)}{1 + \lambda(M)}$.*

We can observe that $\mu_{\mathbb{R}}$ is not homogeneous. This is obvious, if the multiplicative constant c is allowed to be larger than 1. Even when we consider $c \in]-1, 1[\setminus \{0\}$ the equality does not hold, as we can see in the following example.

Example 1 If we consider $[a, b] \subseteq \mathbb{R}$, then $\mu_{\mathbb{R}}([a, b]) = \frac{b-a}{1+b-a}$. Now, let c be strictly between 0 and 1. Obviously $c[a, b] = [ca, cb]$ and the measure $\mu_{\mathbb{R}}$ is $\mu_{\mathbb{R}}(c[a, b]) > c\mu_{\mathbb{R}}([a, b])$.

Since the equality $\mu_{\mathbb{R}}(cM) = |c|\mu_{\mathbb{R}}(M)$ is not generally true, we study an estimate of the measure of cM , given $\mu_{\mathbb{R}}(M)$.

Proposition 5 *For every subset M of \mathbb{R} , given a real c such that $|c| < 1$ the following estimates hold:*

$$|c|\mu_{\mathbb{R}}(M) \leq \mu_{\mathbb{R}}(cM) \leq \mu_{\mathbb{R}}(M).$$

Proof. We prove the inequality $\mu_{\mathbb{R}}(cM) \leq \mu_{\mathbb{R}}(M)$. Without loss of generality we suppose that $\mu_{\mathbb{R}}(M) < 1$, if $\mu_{\mathbb{R}}(M) = 1$ the thesis is trivially true. Let ε be positive and such that $\mu_{\mathbb{R}}(M) + \varepsilon < 1$.

Then, setting $\tau = \mu_{\mathbb{R}}(M) + \varepsilon$, by definition, there exists a sequence of intervals $(I_n)_n$ such that the Lebesgue measure of each I_n is less than τ^n , and $M \subseteq \bigcup_{n=1}^{\infty} I_n$.

If we consider $(cI_n)_n$, then $cM \subseteq \bigcup_{n=1}^{\infty} cI_n$ and $\lambda(cI_n) = |c|\lambda(I_n) \leq |c|\tau^n \leq \tau^n$.

So, by definition of $\mu_{\mathbb{R}}$, $\mu_{\mathbb{R}}(cM) \leq \mu_{\mathbb{R}}(M)$.

Now, we prove the inequality $|c|\mu_{\mathbb{R}}(M) \leq \mu_{\mathbb{R}}(cM)$.

Without loss of generality, we suppose $c \neq 0$ and consider only the case $\mu_{\mathbb{R}}(cM) < 1$, otherwise the proof is trivial.

Let ε be positive and such that $\sigma = \mu_{\mathbb{R}}(cM) + \varepsilon$ is strictly less than 1.

Then, by definition, one can find a sequence of intervals $(I_n)_n$ such that $\bigcup_{n=1}^{\infty} I_n \supseteq M$

and $\lambda(I_n) \leq \sigma^n$, for all n .

We consider the sequence $(dI_n)_n$, where $d = \frac{1}{c}$, and then $|d| > 1$.

Then, trivially, $\bigcup_{n=1}^{\infty} dI_n \supseteq M$.

Moreover $\lambda(dI_n) = |d|\lambda(I_n) \leq |d|\sigma^n \leq |d|^n \sigma^n$, for all n .

Then, $\forall \varepsilon > 0$, $\mu_{\mathbb{R}}(M) \leq \frac{\mu_{\mathbb{R}}(cM) + \varepsilon}{|c|}$, so $|c|\mu_{\mathbb{R}}(M) \leq \mu_{\mathbb{R}}(cM)$. \blacksquare

Analogously the following proposition holds:

Proposition 6 *For each subset M of \mathbb{R} , given a real d such that $|d| > 1$ the following estimates hold:*

$$\mu_{\mathbb{R}}(M) \leq \mu_{\mathbb{R}}(dM) \leq |d|\mu_{\mathbb{R}}(M).$$

As anticipated in the introduction, in \mathbb{R} microscopic sets are also scalarly microscopic and both definitions coincide with microscopicity in the sense of Definition 1.

Trivially Definition 1 coincides with the scalar microscopicity. Indeed, since the elements of X^* are the functional $x^*(x) = \alpha x$, with $\alpha \in \mathbb{R}$, if we consider a scalarly microscopic set $M \subseteq \mathbb{R}$ and we consider $\alpha = 1$ we get that M is microscopic. Moreover, if we consider M microscopic (in the sense of Definition 1) it is trivially scalarly microscopic, by *iv*) of Proposition 1.

Now, let us show that if M is microscopic in the sense of Definition 3 then it is microscopic in the sense of Definition 1; the reverse is obviously true.

By definition, for every $\varepsilon > 0$ there exists a sequence $(x_n)_n$ such that

$$M \subseteq \bigcup_{n=1}^{\infty} ([x_n - \varepsilon^n, x_n + \varepsilon^n]).$$

Let be $\sigma > 0$. Then, setting $\varepsilon = \frac{\sigma}{2}$ and applying the definition, there exists a

sequence $(\xi_n)_n$ such that

$$\begin{aligned} M &\subseteq \bigcup_{n=1}^{\infty} ([\xi_n - \varepsilon^n, \xi_n + \varepsilon^n]) \subseteq \bigcup_{n=1}^{\infty} ([\xi_n - 2\varepsilon^n, \xi_n + 2\varepsilon^n]) \subseteq \\ &\subseteq \bigcup_{n=1}^{\infty} ([\xi_n - (2\varepsilon)^n, \xi_n + (2\varepsilon)^n]) \subseteq \bigcup_{n=1}^{\infty} ([\xi_n - \sigma^n, \xi_n + \sigma^n]). \end{aligned}$$

3 Scalar measure of smallness in a Banach space - some properties

Let $X = (X, \|\cdot\|)$ be a Banach space. In this section we shall consider the scalar measure of smallness in X , introduced in Definition 4.

Proposition 7 *Let M be a subset of X . Then*

$$\mu(M) = \sup_{x^* \in S_1^*} \mu_{x^*}(M),$$

where S_1^* is the unit sphere of X^* .

Proof. The inequality $\sup\{\mu_{x^*}(M), x^* \in X_1^*\} \geq \sup\{\mu_{x^*}(M), x^* \in S_1^*\}$ is trivial.

Whereas if $x^* \in X_1^* \setminus S_1^*$, $x^* \neq 0$, defined $u^* = \frac{x^*}{\|x^*\|}$, $x^*(M) = \alpha u^*(M)$, with $\alpha = \|x^*\| < 1$, and then $\mu(x^*(M)) \leq \mu(u^*(M))$, by Proposition 5. This clearly suffices to prove the converse inequality. ■

We can then immediately extend statement *i)* in Proposition 3. First it is clear that $\mu(M) \leq 1$, for each subset M of X . Also, thanks to the previous proposition, we deduce that $\mu(rX_1) = \frac{2r}{1+2r}$, since for each $x^* \in X_1^*$, $x^*(rX_1) = [-r, r]$, and $\mu_{\mathbb{R}}([-r, r]) = \frac{2r}{1+2r}$, and this in turn implies that if B is bounded then $\mu(B) < 1$.

Proposition 8 *Let M be a subset of X . Then $\mu(M) = 0$ if and only if M is scalarly microscopic.*

Proof. Trivially if M is a microscopic subset of X , $\mu(M) = 0$. Whereas, if M is a subset of X such that $\mu(M) = 0$, then $\mu_{x^*}(M) = 0$ for all $x^* \in X_1^*$. We can observe that if $x^* \notin X_1^*$ (then it is non zero) setting $u^* = \frac{x^*}{\|x^*\|}$, we have $x^*(M) = \|x^*\|u^*(M)$, with $u^*(M)$ microscopic by *ii)* of Proposition 3; then by *iv)* of Proposition 1, $x^*(M)$ is microscopic. ■

By *i)*, *iii)* e *iv)* of Proposition 2, statements *iii)* and *iv)* of Proposition 3 can be extended to μ :

Proposition 9 *The following properties hold:*

- i) μ is monotone;
- ii) μ is translation-invariant.

As one can expect, μ is not homogeneous. However, by Propositions 5 and 6 and by definition of μ the following proposition is true:

Proposition 10 *For each subset M of X , given a real c the following estimates hold:*

$$\begin{aligned} |c|\mu(M) &\leq \mu(cM) \leq \mu(M), & \text{if } |c| \leq 1, \\ \mu(M) &\leq \mu(cM) \leq |c|\mu(M), & \text{if } |c| > 1. \end{aligned}$$

Next we shall consider some analogous properties enjoyed by the Kuratowski measure of non compactness α (see [3]). First we list them

- (a) $\alpha(A) = 0 \iff A$ is compact.
- (b) $A \subseteq B \implies \alpha(A) \leq \alpha(B)$.
- (c) $\alpha(cA) = |c|\alpha(A), \quad \forall c \in \mathbb{R}$.
- (d) $\alpha(A) = \alpha(\overline{A})$.
- (e) $\alpha(\text{co}A) = \alpha(A)$.
- (f) $\alpha(A + B) \leq \alpha(A) + \alpha(B)$.
- (g) If $(X_n)_n$ is a decreasing sequence of closed, bounded, non-empty subsets of a Banach space X , such that $\lim_{n \rightarrow \infty} \alpha(X_n) = 0$, then the intersection of all X_n is compact and non empty.
- (h) $\alpha(A \cup B) = \max\{\alpha(A), \alpha(B)\}$.

For what we have already seen, μ satisfies

- (a') $\mu(A) = 0 \iff A$ is microscopic,
- (b') $A \subseteq B \implies \mu(A) \leq \mu(B)$

and we have already considered how to extend (c).

Moreover, by monotonicity, for each $M \subseteq X$ we have $\mu(M) \leq \mu(\overline{M})$. Generally, the equality is not true, as we can see in the following example:

Example 2 Let $X = \mathbb{R}$. Let $A = \mathbb{Q} \cap [0, 1]$. Then A is a countable set, so $\mu_{\mathbb{R}}(A) = 0$. But, clearly, $\mu_{\mathbb{R}}(\overline{A}) = \mu_{\mathbb{R}}([0, 1]) = \frac{1}{2}$.

We can observe that the above example proves also that $\mu(M) \neq \mu(\text{co}M)$. Then in this case the unique relationship between a set and its convex hull is $\mu(A) \leq \mu(\text{co}A)$, because μ is monotone.

We now show that subadditivity can fail.

Example 3 Let $X = \mathbb{R}$, $A = [1, 2]$ and $B = \left\{ \frac{1}{n}, \text{ with } n \in \mathbb{N} \right\} \cup \{0\}$.

Now, $A + B = [1, 3]$, then $\mu_{\mathbb{R}}(A + B) = \frac{2}{3}$, $\mu_{\mathbb{R}}(A) = \frac{1}{2}$, but B is microscopic, so $\mu_{\mathbb{R}}(B) = 0$, then $\mu_{\mathbb{R}}(A + B) > \mu_{\mathbb{R}}(A) + \mu_{\mathbb{R}}(B)$.

However μ is subadditive in some special cases.

Proposition 11 *Given $[a, b]$, $[c, d]$ subsets of \mathbb{R} the following inequality holds:*

$$\mu_{\mathbb{R}}([a, b] + [c, d]) \leq \mu_{\mathbb{R}}([a, b]) + \mu_{\mathbb{R}}([c, d]).$$

The proof is a trivial consequence of Proposition 4.

Analogously if A and B are two balls of X , the inequality $\mu(A + B) \leq \mu(A) + \mu(B)$ is true.

Now we can prove, a kind of Kuratowski Theorem for the measure of smallness:

Proposition 12 *Let $X = (X, \|\cdot\|)$ be a reflexive Banach space. Given a decreasing sequence $(X_n)_n$, of weakly closed, bounded, non-empty subsets of X , with $\mu(X_n)$ convergent to 0, then $\bigcap_{n=1}^{\infty} X_n$ is non empty and scalarly microscopic.*

Proof. We can observe that, for each natural n , X_n is weakly compact and applying the finite intersection property to X_1 we get that $\bigcap_{n=1}^{\infty} X_n$ is non empty.

Moreover, $\bigcap_{n=1}^{\infty} X_n \subseteq X_n$, for all n , so $\mu\left(\bigcap_{n=1}^{\infty} X_n\right) \leq \mu(X_n)$, for all n .

Then $\mu\left(\bigcap_{n=1}^{\infty} X_n\right) = 0$, so $\bigcap_{n=1}^{\infty} X_n$ is scalarly microscopic. \blacksquare

The maximum property (h) is the most delicate. We observe first that μ does not fulfill the *maximum property*, that is given A and B subsets of X the measure of their union is not necessarily the maximum of their measures, as the following example proves.

Example 4 Let $X = \mathbb{R}$ and $M = [a, b]$.

Let c be the middle point of the interval $[a, b]$. Then M can be written as the union of $[a, c]$ and $[c, b]$.

Let L be the width of $[a, b]$, then $\mu_{\mathbb{R}}(M) = \frac{L}{1 + L}$.

But $[a, c]$ and $[c, b]$ have the same width $\frac{L}{2}$, so same measure of smallness $\mu_{\mathbb{R}}$,

$\mu_{\mathbb{R}}([a, c]) = \mu_{\mathbb{R}}([c, b]) = \frac{\frac{L}{2}}{1 + \frac{L}{2}}$, then $\max\{\mu_{\mathbb{R}}([a, c]), \mu_{\mathbb{R}}([c, b])\} < \mu_{\mathbb{R}}([a, b])$.

But it is possible to have the following estimates.

Proposition 13 *Let A and B be subsets of X . Then the measure of their union fulfills the following estimates:*

$$\max\{\mu(A), \mu(B)\} \leq \mu(A \cup B) \leq (\max\{\mu(A), \mu(B)\})^{\frac{1}{2}}.$$

Proof. The thesis is trivially true if either $\max\{\mu(A), \mu(B)\} = 1$, or A and B are microscopic. Then let A and B be bounded, or let both have non unitary measure of smallness, and let at least one be non microscopic. The first inequality follows by the monotonicity of μ .

So we have just to prove that the second inequality holds in \mathbb{R} , then, trivially it holds in X .

For convenience let μ be the measure of smallness in \mathbb{R} , and let A and B be two subsets of \mathbb{R} such that $\mu(A)$ and $\mu(B)$ are less than 1 and non zero.

Without loss of generality we can suppose $\mu(A) = \max\{\mu(A), \mu(B)\}$.

Let ε be positive and such that $\mu(A) + \varepsilon$ is strictly less than 1.

Then by definition there exists a sequence of intervals $(I_n)_n$ that covers A , and such that $\lambda(I_n) \leq (\mu(A) + \varepsilon)^n$.

Because $\mu(B) \leq \mu(A) < \mu(A) + \varepsilon$, there exists a sequence of intervals $(J_k)_k$ that covers B , such that $\lambda(J_k) \leq (\mu(A) + \varepsilon)^k$.

Let $\tau = \mu(A) + \varepsilon$ and $\sigma = \sqrt{\tau}$.

We can construct a sequence $(U_k)_k$ by $(I_n)_n$ and $(J_k)_k$, in the following way:

$$U_k = \begin{cases} I_{\frac{k+1}{2}}, & \text{if } k \text{ is odd} \\ J_{\frac{k}{2}}, & \text{if } k \text{ is even} \end{cases}$$

Then by construction and by definition of σ , $\lambda(U_n) \leq \sigma^n$ for all n and $(U_n)_n$ covers $A \cup B$. So $\mu(A \cup B) \leq (\max\{\mu(A), \mu(B)\})^{\frac{1}{2}}$. ■

More generally

Corollary 1 *Given a finite number of subsets M_1, \dots, M_m with $m \geq 2$, the measure of their union fulfills the following estimates:*

$$\max_{1 \leq i \leq m} \mu(M_i) \leq \mu\left(\bigcup_{i=1}^m M_i\right) \leq \left(\max_{1 \leq i \leq m} \mu(M_i)\right)^{\frac{1}{m}}.$$

4 Strong measure of smallness

Let us consider the strong measure of smallness defined in Definition 5.

We can note that $\mu(M) \leq \sqrt{\nu(M)}$, for every $M \subseteq X$.

In fact let $M \subseteq X$ and let $\varepsilon > \nu(M)$. Then there exists $(x_n)_n$ such that

$$M \subseteq \bigcup_{n=1}^{\infty} (x_n + \varepsilon^n X_1)$$

and so for every $x^* \in S_1^*$

$$x^*(M) \subseteq \bigcup_{n=1}^{\infty} [x^*(x_n) - \varepsilon^n \|x^*\|, x^*(x_n) + \varepsilon^n \|x^*\|]$$

and the length of the n -th interval is $2\varepsilon^n$.

Set $I_n = [x^*(x_n) - \varepsilon^n \|x^*\|, x^*(x_n) + \varepsilon^n \|x^*\|] = [a_n, b_n]$ and consider the intervals $J_n = \left[a_n, \frac{a_n + b_n}{2} \right]$ and $K_n = \left[\frac{a_n + b_n}{2}, b_n \right]$.

Then $x^*(M) \subseteq M_1 \cup M_2$, where $M_1 = \bigcup_{n=1}^{\infty} J_n$ and $M_2 = \bigcup_{n=1}^{\infty} K_n$, and both $\mu_R(M_1) = \mu_R(M_2) < \varepsilon$. So, according to (h') , $\mu_R(M_1 \cup M_2) < \sqrt{\varepsilon}$.

Hence $\mu_R(x^*(M)) \leq \sqrt{\varepsilon}$, $\forall x^* \in S_1^*$, that is $\mu(M) \leq \sqrt{\varepsilon}$. The relationship $\mu(M) \leq \sqrt{\nu(M)}$ then follows by arbitrariness of ε .

We can observe that, since for each $M \subseteq \mathbb{R}$ $\mu(M) \leq \sqrt{\nu(M)}$, every microscopic set is scalarly microscopic. The following example shows that the reverse is not true.

Example 5 Let $(X, \|\cdot\|) = (B([0, 1]), \|\cdot\|_{\infty})$.

Setting $H = \{\chi_{\{x\}} : x \in [0, 1]\}$, we get that H is scalarly microscopic, but not microscopic.

Indeed, let $f_t = \chi_{\{t\}}$, for every $t \in [0, 1]$. Then $\|f_t\|_{\infty} = 1$ and $\|f_t - f_r\|_{\infty} = 1$, for every $t, r \in [0, 1]$.

Now, if H is microscopic then for every ε there exists $(x_n)_n \subset X$ such that $H \subseteq \bigcup_{n=1}^{\infty} (x_n + \varepsilon^n X_1)$. But let $\varepsilon < \frac{1}{2}$ and let us consider the sequence $(\xi_n)_n \subset X$

such that $H \subseteq \bigcup_{n=1}^{\infty} (\xi_n + \varepsilon^n X_1)$.

So for every t in $[0, 1]$ there exists n such that $f_t \in \xi_n + \varepsilon^n X_1$.

Since $\#([0, 1]) > \aleph_0$, there exist t, r in $[0, 1]$, with $t \neq r$, and $\bar{n} \in \mathbb{N}$, such that $f_t, f_r \in \xi_{\bar{n}} + \varepsilon^{\bar{n}} X_1$.

Hence $\|f_t - \xi_{\bar{n}}\|_{\infty} \leq \varepsilon^{\bar{n}} < \frac{1}{2}$ and $\|f_r - \xi_{\bar{n}}\|_{\infty} \leq \varepsilon^{\bar{n}} < \frac{1}{2}$ that imply $\|f_t - f_r\|_{\infty} < 1$, then a contradiction.

On the other hand, every $x^* \in X^*$ is represented by a finitely additive and bounded signed measure m . So, fixed m , the set $m(H) = \{m(\{x\}) : x \in [0, 1]\}$ either is finite or is countable, since m and its total variation are bounded and the singletons are pairwise disjoint. Hence, by arbitrariness of m , H is scalarly microscopic.

We shall now extend some of the properties of μ to ν .

It is immediate to note that ν satisfies

$$(a'') \quad \nu(M) = 0 \iff M \text{ is microscopic}$$

and it is monotone, i.e.

$$(b'') \quad M \subseteq N \implies \nu(M) \leq \nu(N).$$

Moreover ν is translation invariant and it fulfills the following proposition:

Proposition 14 $\nu(X) = 1$.

Proof. Since $\nu(X) \geq \mu^2(X) = 1$, $\nu(X) \geq 1$. But if we consider any $\varepsilon > 0$ it is clear that $X \subseteq \bigcup_{n=1}^{\infty} (0 + (1 + \varepsilon)^n X_1)$. Hence $\nu(X) \leq 1 + \varepsilon$, for every $\varepsilon > 0$, then $\nu(X) = 1$. ■

As announced in the introduction we shall consider the particular case of the unit ball.

Proposition 15 *If $\nu(X_1) = 1$ then $\nu(rX_1) = r$, $\forall r \in [0, 1]$.*

Proof. Without loss of generality we can consider $r \in]0, 1[$, indeed the proposition is trivially verified for $r = 0$ and $r = 1$.

Taking $x_n = 0$, for each n , and $\varepsilon = r$, it is obvious that $rX_1 = \bigcup_{n=1}^{\infty} x_n + \varepsilon^n X_1$ and so $\nu(X_1) \leq r$.

Suppose that $\nu(rX_1) < r$, and let $\sigma \in]\nu(rX_1), r[$. Then $rX_1 = \bigcup_{n=1}^{\infty} x_n + \sigma^n X_1$.

So for each $u \in X_1$, $ru = x_n + \sigma^n v$, for some n and $v \in X_1$.

Hence, $u = \frac{x_n}{r} + \sigma^n \frac{v}{r}$.

But, since $\frac{\sigma^n}{r} \leq \frac{\sigma^n}{r^n}$, $\frac{\sigma^n}{r} v \in \frac{\sigma^n}{r} X_1 \subseteq \frac{\sigma^n}{r^n} X_1$ and so $u = \frac{x}{r} + \left(\frac{\sigma}{r}\right)^n w$, where $w \in X_1$, that means $X_1 \subseteq \bigcup_{n=1}^{\infty} \left(\frac{x}{r} + \left(\frac{\sigma}{r}\right)^n X_1\right)$. Hence we get $\nu(X_1) \leq \frac{\sigma}{r} < 1$, that contradicts the hypothesis. ■

Proposition 15 makes it interesting to verify in which cases $\nu(X_1) = 1$. The next statement provides us with an answer.

Proposition 16 *If X is not separable, then $\nu(X_1) = 1$.*

Proof. Let us suppose that $\nu(X_1) < 1$.

Then we can choose $\varepsilon \in]\nu(X_1), 1[$ and $(x_n)_n$ such that $X_1 \subseteq \bigcup_n (x_n + \varepsilon^n X_1)$.

We shall prove that for each $x \in X$ and for each $\sigma > 0$ there exists y in $\text{span}\{x_n, n \in \mathbb{N}\}$ such that $\|x - y\| < \sigma$.

Let us consider $x \in X_1$. Let $p \in \mathbb{N}$ such that $\varepsilon^p < \sigma$. Since $x \in X_1$, there exists $n_1 \in \mathbb{N}$ such that $x = x_{n_1} + \varepsilon^{n_1} u$, with $u \in X_1$. But u can be written as $u = x_{n_2} + \varepsilon^{n_2} v$ with $v \in X_1$ too. An so,

$$x = x_{n_1} + \varepsilon^{n_1} x_{n_2} + \varepsilon^{n_1+n_2} v.$$

But, again, $v = x_{n_3} + \varepsilon^{n_3} w$, with $w \in X_1$ and hence

$$x = x_{n_1} + \varepsilon^{n_1} x_{n_2} + \varepsilon^{n_1+n_2} x_{n_3} + \varepsilon^{n_1+n_2+n_3} w.$$

Thus continuing we have that x can be represented as

$$x = x_{n_1} + \sum_{i=2}^p \varepsilon^{n_1+\dots+n_{i-1}} x_{n_i} + \varepsilon^{n_1+\dots+n_p} z$$

with $z \in X_1$.

So setting $y = x_{n_1} + \sum_{i=2}^p \varepsilon^{n_1+\dots+n_{i-1}} x_{n_i}$ we get $y \in \text{span}\{x_n, n \in \mathbb{N}\}$ and

$$\|x - y\| = \varepsilon^{n_1+\dots+n_p} \|z\| \leq \varepsilon^{n_1+\dots+n_p}$$

and since $\varepsilon < 1$, $\|x - y\| \leq \varepsilon^{n_1+\dots+n_p} \leq \varepsilon^p < \sigma$.

If $x \notin X_1$, we consider $\xi = \frac{x}{\|x\|} \in X_1$, and $y \in \text{span}\{x_n, n \in \mathbb{N}\}$ such that

$$\|\xi - y\| \leq \frac{\sigma}{\|x\|}; \text{ then}$$

$$\|x - \|x\|y\| = \|x\| \|\xi - y\| < \sigma$$

with $\|x\|y \in \text{span}\{x_n, n \in \mathbb{N}\}$.

Hence

$$X = \overline{\text{span}\{x_n, n \in \mathbb{N}\}}$$

that contradicts the assumption X non separable. \blacksquare

It is not clear whether the previous result is in fact a characterization of non separable Banach spaces.

For example, one can easily check that for $X = \mathbb{R}$, $\nu(X_1) = \frac{1}{2}$.

In fact $X_1 = [-1, 1]$ and $X_1 \subseteq \bigcup_{n=1}^{\infty} (x_n + \varepsilon^n X_1)$ implies $\lambda(X_1) = 2 \leq 2 \sum_{n=1}^{\infty} \varepsilon^n$.

Trivially the previous inequality is satisfied only if $\varepsilon \geq \frac{1}{2}$, so $\nu(X_1) \geq \frac{1}{2}$. On the

other hand, it is easy to find a sequence $(x_n)_n$ such that $X_1 = \bigcup_{n=1}^{\infty} \left(x_n + \left(\frac{1}{2}\right)^n X_1 \right)$,

hence $\nu(X_1) \leq \frac{1}{2}$.

For more general bounded sets, we do not reach complete homogeneity of ν , but the following estimates hold:

Proposition 17 *For every $M \subseteq X$ and given $c \in \mathbb{R}$ there holds*

$$|c|\nu(M) \leq \nu(cM) \leq \nu(M), \quad \text{if } |c| \leq 1,$$

$$\nu(M) \leq \nu(dM) \leq |d|\nu(M), \quad \text{if } |d| > 1.$$

Proof. If $c = 0$ or $c = 1$ the inequality is immediate.

The proof in the case $0 < c < 1$ is analogous to the one of Proposition 15.

Finally, if $-1 < c < 0$, then $cM = |c|(-M)$. It is now immediate to recognize

that $\nu(M) = \nu(-M)$ and thus the first inequality is completely proved. The right inequality can be proved similarly to Proposition 5. As for the second line of estimates, it is enough to consider $c = \frac{1}{d}$ and setting $dM = B$ write $M = cB$ with $|c| < 1$. ■

Also in this case we can only reach

$$\begin{aligned}\nu(M) &\leq \nu(\overline{M}) \\ \nu(M) &\leq \nu(\text{co}M),\end{aligned}$$

as Example 2, with the appropriate computations, shows.

Again Example 3, with the suitable calculations, shows that there are cases where $\nu(A + B) > \nu(A) + \nu(B)$.

Finally the same proofs of Propositions 12, 13 and Corollary 1, apply to ν too, namely the following results hold.

Proposition 18 *Let $X = (X, \|\cdot\|)$ be a reflexive Banach space and let $(X_n)_n$ be a decreasing sequence of non-empty, bounded, and weakly closed sets, with $\nu(X_n)$ convergent to 0, then $\bigcap_{n=1}^{\infty} X_n$ is non empty and microscopic.*

Proposition 19 *Let A and B be subsets of X . Then the measure of their union fulfills the following estimates:*

$$\max\{\nu(A), \nu(B)\} \leq \nu(A \cup B) \leq (\max\{\nu(A), \nu(B)\})^{\frac{1}{2}}.$$

Corollary 2 *Given a finite number of subsets M_1, \dots, M_m with $m \geq 2$, the measure of their union fulfills the following estimates:*

$$\max_{1 \leq i \leq m} \nu(M_i) \leq \nu\left(\bigcup_{i=1}^m M_i\right) \leq \left(\max_{1 \leq i \leq m} \nu(M_i)\right)^{\frac{1}{m}}.$$

References

- [1] J. Appell, Insieme ed operatori “piccoli” in analisi funzionale, *Rend. Sem. Mat. Trieste*, **33**, (2001) 127-199.
- [2] J. Appell, E. D’Aniello, M. Văth, Some remarks on small sets, *Ricerche di Matematica*, **L**, fasc.2°, (2001), 252-274.
- [3] J. Banaś, K. Goebel, *Measure of noncompactness in Banach spaces*, New York (1980).
- [4] E. Behrends, V. M. Kadets, Metric spaces with the small ball property, *Studia Math*, **148**, (2001), 275-287.
- [5] C. Donnini, A. Martellotti, Microscopic Subsets of a Banach Space and Characterizations of the Drop Property, *Scientiae Mathematicae Japonicae (Osaka, Japan)*, **59**, No. 3 (2004), 525-530, :e9, 369-374.

Asymptotic Analysis of a Parabolic Problem with Rapidly Varying Type of Boundary Conditions in a Thick two-level Junction

Tiziana Durante

Dipartimento di Ingegneria dell' Informazione e Matematica Applicata
 Università di Salerno
 via Ponte don Melillo, 84084 Fisciano (SA), Italy
 E-mail: durante@diima.unisa.it¹

We consider a mixed boundary-value problem for the heat equation in a plane two-level junction Ω_ε that is the union of a domain Ω_0 and a large number $2N$ of thin rods with thickness of order $\varepsilon = O(N^{-1})$. The thin rods are divided into two levels depending on their lengths and boundary conditions given on their sides. Inhomogeneous Robin boundary conditions are given on the sides of the thin rods of the first level and homogeneous Dirichlet boundary conditions are given on the sides of the rods of the second level. In addition, the thin rods from each level are ε -periodically alternated between themselves along some part of the boundary of Ω_0 . We investigate the asymptotic behavior of a solution of this problem as $\varepsilon \rightarrow 0$ and prove a convergence theorem.

Key words: homogenization, thick multi-level junction, varying type of boundary conditions, parabolic boundary-value problem, asymptotic behavior of a solution.

A.M.S. Classification: 35B27, 35B40, 74K30, 35C20.

1 Introduction and statement of the problem

In recent years the interest in investigation of boundary-value problems in thick junctions (by a thick junction we mean a domain in \mathbb{R}^n , which consists of some domain Ω_0 and a large number of thin domains that ε -periodically distributed along some manifold on the boundary of Ω_0 ; the number of components of such junctions grows infinitely as the perturbation parameter ε tends to zero) has quickened in connection with the development of technologies of porous, composite and other micro-inhomogeneous materials and biological structures (see [1]-[6], [10]-[12], [16], [19]-[28], [33]).

In this paper we consider initial/boundary-value parabolic problem in new kind of thick junctions, namely, thick multi-level junctions (the thin attached domains are divided into finite number levels depending on their geometrical characteristics and boundary conditions given on their sides). Elliptic boundary-value problems and spectral problems in thick multi-level junctions of different type were investigated in [13, 14], [29]-[31]. As was established in [14] such problems behave as a "two-phase system" in the region filled up with the thin rods from each level in the limit passage. Detail review on these theme is presented in [31].

Here we continue the research made in [15] and investigate the influence boundary conditions on the asymptotic behavior of the solution, namely the inhomogeneous Robin boundary conditions are given on the sides of the thin rods of the first level and the homogeneous Dirichlet boundary conditions are given on the sides of the rods of the second one. In addition, the thin rods from each level are ε -periodically alternated between themselves along some part of the boundary of Ω_0 . It should be noted that the inhomogeneous Robin boundary conditions depend on a parameter $\beta \geq 1$ and we made the asymptotic analysis of this problem for different values of the parameter β . Asymptotic analysis of boundary-value problems with periodic change of boundary conditions (Neumann and Dirichlet conditions) on the boundary of smooth unperturbed domains was carried out in [7]-[9], where it was shown that the first term of the asymptotics is mainly the solution of the corresponding boundary-value problem with the Dirichlet condition. The qualitatively new result of the present paper implies that the first term of asymptotics is a vector function whose components are solution of two independent boundary-value problems (one in the junction body and another in a domain filled up with thin rods of the first level in the limit) with homogeneous Dirichlet conditions in the joint zone in the case $\beta = 1$. Note also that the second problem is a problem for parabolic equation with respect to the value variable x_2 only and with a new right-hand side that "remember" the inhomogeneity in the Neumann boundary conditions of the original problem. The similar results for elliptic problem were obtained in [30]. In the case $\beta > 1$ the first term of asymptotics is only the solution to the boundary-value problem in the junction body.

1.1 Statement of the problem

Let a, d_1, d_2, b_1, b_2 be positive real numbers and let $d_1 \geq d_2, 0 < b_1 < b_2 < 1$. Consider two positive piecewise smooth functions h_1 and h_2 on the segments $[-d_1, 0]$ and $[-d_2, 0]$ respectively. Suppose the functions h_1 and h_2 satisfy the following conditions

$$\begin{aligned} \exists \delta_0 \in (b_1, b_2) \quad \forall x_2 \in [-d_1, 0] : \quad & 0 < b_1 - h_1(x_2)/2, \quad b_1 + h_1(x_2)/2 < \delta_0; \\ \forall x_2 \in [-d_2, 0] : \quad & \delta_0 < b_2 - h_2(x_2)/2, \quad b_2 + h_2(x_2)/2 < 1. \end{aligned}$$

It follows from these assumptions that there exist positive constants m_0, M_0 such that

$$\begin{aligned} 0 < m_0 \leq h_1(x_2) < \delta_0 \quad \text{and} \quad |h'_1(x_2)| \leq M_0 \quad \text{a.e. in } [-d_1, 0]; \\ 0 < m_0 \leq h_2(x_2) < 1 - \delta_0 \quad \text{and} \quad |h'_2(x_2)| \leq M_0 \quad \text{a.e. in } [-d_2, 0]. \end{aligned}$$

Let us divide segment $[0, a]$ on N equal segments $[\varepsilon j, \varepsilon(j+1)]$, $j = 0, \dots, N-1$. Here N is a large integer, therefore, the value $\varepsilon = a/N$ is a small discrete parameter.

A model plane thick two-level junction Ω_ε (see Figure 1) consists of the junction's body

$$\Omega_0 = \{x = (x_1, x_2) \in \mathbb{R}^2 : 0 < x_1 < a, \quad 0 < x_2 < \gamma(x_1)\}$$

where $\gamma \in C^1([0, a])$, $\min_{[0, a]} \gamma > 0$, $\gamma(0) = \gamma(a) = \gamma_0$, and a large number of the thin rods

$$G_j^{(1)}(\varepsilon) = \{x \in \mathbb{R}^2 : |x_1 - \varepsilon(j + b_1)| < \varepsilon h_1(x_2)/2, \quad x_2 \in (-d_1, 0]\},$$

$$G_j^{(2)}(\varepsilon) = \{x \in \mathbb{R}^2 : |x_1 - \varepsilon(j + b_2)| < \varepsilon h_2(x_2)/2, \quad x_2 \in (-d_2, 0]\},$$

$j = 0, 1, \dots, N-1$, i.e., $\Omega_\varepsilon = \Omega_0 \cup G_\varepsilon^{(1)} \cup G_\varepsilon^{(2)}$. Here

$$G_\varepsilon^{(1)} = \bigcup_{j=0}^{N-1} G_j^{(1)}(\varepsilon), \quad G_\varepsilon^{(2)} = \bigcup_{j=0}^{N-1} G_j^{(2)}(\varepsilon).$$

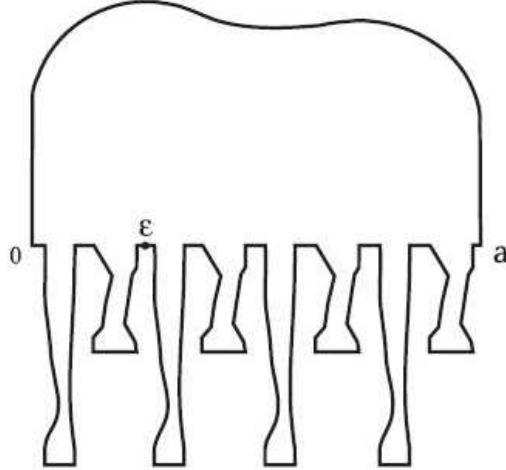


Figure 1: The plane thick two-level junction Ω_ε

We see that the number of the thin rods is equal to $2N$ and they are divided into two levels $G_\varepsilon^{(1)}$ and $G_\varepsilon^{(2)}$ depending on their lengths, namely, d_1 and d_2 . The parameter ε characterizes the distance between the thin neighboring rods and their thickness. The thickness of the rods from the first level is equal to εh_1 and it is equal to εh_2 for the rods from the second level. These thin rods from each level are ε -periodically alternated along the segment

$$I_0 = \{x : x_1 \in [0, a], \quad x_2 = 0\}.$$

Denote by $\Upsilon_j^{(i,\pm)}(\varepsilon)$ the lateral surfaces of the thin rod $G_j^{(i)}(\varepsilon)$; the signs " + " or " - " indicate the right or left surface respectively. The base of $G_j^{(i)}(\varepsilon)$ will be denoted by $\Theta_j^{(i)}(\varepsilon)$. Also we introduce the following notations

$$\Upsilon_\varepsilon^{(i,\pm)} := \cup_{j=0}^{N-1} \Upsilon_j^{(i,\pm)}(\varepsilon), \quad \Theta_\varepsilon^{(i)} := \cup_{j=0}^{N-1} \Theta_j^{(i)}(\varepsilon),$$

$$\Upsilon_\varepsilon^{(i)} := \Upsilon_\varepsilon^{(i,+)} \cup \Upsilon_\varepsilon^{(i,-)} \cup \Theta_\varepsilon^{(i)}, \quad i = 1, 2.$$

In $\Omega_\varepsilon \times (0, T)$ we consider the following initial boundary-value problem

$$\left\{ \begin{array}{ll} \partial_t u_\varepsilon(x, t) = \Delta_x u_\varepsilon + f_0(x, t), & (x, t) \in \Omega_0 \times (0, T); \\ \partial_t u_\varepsilon(x, t) = \Delta_x u_\varepsilon(x, t), & (x, t) \in (G_\varepsilon^{(1)} \cup G_\varepsilon^{(2)}) \times (0, T); \\ \partial_{x_1}^p u_\varepsilon(0, x_2, t) = \partial_{x_1}^p u_\varepsilon(a, x_2, t), & (x_2, t) \in (0, \gamma_0) \times (0, T), \quad p = 0, 1; \\ \partial_\nu u_\varepsilon(x, t) + \varepsilon k_1 u_\varepsilon(x, t) = \varepsilon^\beta g_\varepsilon(x, t), & (x, t) \in \Upsilon_\varepsilon^{(1)} \times (0, T); \\ u_\varepsilon(x, t) = 0 & (x, t) \in \Upsilon_\varepsilon^{(2)} \times (0, T); \\ \partial_\nu u_\varepsilon(x, t) = 0, & (x, t) \in \Gamma_\varepsilon \times (0, T); \\ u_\varepsilon(x, 0) = 0, & x \in \Omega_\varepsilon; \end{array} \right. \quad (1)$$

where $\partial_\nu = \partial/\partial\nu$ is the outward normal derivative; $\partial_{x_1} = \partial/\partial x_1$; the constant k_1 is positive; the parameter β is greater than or equal 1. Thus, we have the inhomogeneous Fourier conditions on the boundaries of the thin rods of the first level, the homogeneous Dirichlet conditions on the boundaries of the rods of the second level, the periodic conditions on the vertical sides of Ω_0 and the homogeneous Neumann condition on $\Gamma_\varepsilon = \partial\Omega_\varepsilon \setminus (\Upsilon_\varepsilon^{(1)} \cup \Upsilon_\varepsilon^{(2)} \cup ((0) \times (0, \gamma_0)) \cup ((a) \times (0, \gamma_0)))$.

At first we assume that for any $T > 0$ the given function f_0 belongs to $L^2(\Omega_0 \times (0, T))$ and for any $t \in [0, T]$ its support with respect to x is strictly located Ω_0 . This is a natural condition since such problems are mathematical models of the heat transfer in radiators (heat radiator, microstrip radiator, tubular radiator, ferrite-filled rod radiator, folded core radiator, waveguide radiator), which have the form of thick multi-structures, and the heat source is usually located in the body of a radiator.

The function g_ε belongs to $L^2(0, T; H^1(D_1))$, where $D_1 = \{x : 0 < x_1 < a, -d_1 < x_2 < 0\}$ is a rectangle that is filled up by the thin rods from the first level in the limit passage as $\varepsilon \rightarrow 0$. In addition,

(i) for any $T > 0$ there exist constants c_0, ε_0 such that for any $\varepsilon \in (0, \varepsilon_0)$

$$\|g_\varepsilon\|_{L^2(0, T; H^1(D_1))} \leq c_0; \quad (2)$$

(ii) moreover if $\beta = 1$, then

$$g_\varepsilon \rightarrow g_0 \quad \text{in } L^2(D_1 \times (0, T)) \quad \text{as } \varepsilon \rightarrow 0. \quad (3)$$

Recall that a function $u_\varepsilon \in L^2(0, T; \mathcal{H}_\varepsilon)$, where

$$\mathcal{H}_\varepsilon = \{u \in H^1(\Omega_\varepsilon) : u|_{\Upsilon_\varepsilon^{(2)}} = 0, \quad u(0, x_2) = u(a, x_2) \quad \text{for } x_2 \in (0, \gamma_0)\},$$

is a weak solution to problem (1) if for any function $\psi \in H^1(\Omega_\varepsilon \times (0, T))$ such that

$$\forall t \in (0, T) \quad \psi(\cdot, t) \in \mathcal{H}_\varepsilon \quad \text{and} \quad \psi(x, T) = 0 \quad x \in \Omega_\varepsilon,$$

the following integral identity

$$\begin{aligned} \int_0^T \left(- \int_{\Omega_\varepsilon} u_\varepsilon \partial_t \psi \, dx + \int_{\Omega_\varepsilon} \nabla_x u_\varepsilon \cdot \nabla_x \psi \, dx + \varepsilon k_1 \int_{\Upsilon_\varepsilon^{(1)}} u_\varepsilon \psi \, dl_x \right) dt = \\ = \int_0^T \left(\int_{\Omega_0} f_0 \psi \, dx + \varepsilon^\beta \int_{\Upsilon_\varepsilon^{(1)}} g_\varepsilon \psi \, dl_x \right) dt \end{aligned} \quad (4)$$

holds. It follows from the theory of boundary value problems (see for instance [18]) that for any fixed value $\varepsilon > 0$ there exists a unique weak solution to problem (1).

The aim of this paper is to study the asymptotic behavior of the weak solution to problem (1) as $\varepsilon \rightarrow 0$, i.e., when the number of the attached thin rods from each level infinitely increases and their thickness tends to zero.

2 Auxiliary uniform estimates

To homogenize boundary-value problems in thick multi-structures with the non-homogeneous Neumann or Fourier conditions on the boundaries of the thin attached domains the method of integral identities was proposed in [26, 27]. For our problem the corresponding identity is as follows

$$\int_{\Upsilon_\varepsilon^{(1, \pm)}} \frac{\varepsilon h_1(x_2) \varphi(x)}{2\sqrt{1 + \varepsilon^2 4^{-1} |h'_1(x_2)|^2}} \, d\sigma_x = \int_{G_\varepsilon^{(1)}} \varphi \, dx - \varepsilon \int_{G_\varepsilon^{(1)}} Y\left(\frac{x_1}{\varepsilon}\right) \partial_{x_1} \varphi \, dx \quad \forall \varphi \in H^1(G_\varepsilon^{(1)}), \quad (5)$$

where $Y(t) = -t + b_1 + [t]$ ($[t]$ is the integer part of t). To prove (5) we have to integrate by parts the last integral in (5) and take into account the view of the outward normal (beside some set of zero measure) to the lateral surfaces $\Upsilon_j^{(1, \pm)}(\varepsilon)$ of the thin rod $G_j^{(1)}(\varepsilon)$:

$$\nu_\pm(\varepsilon) = \frac{1}{\sqrt{1 + \varepsilon^2 4^{-1} |h'_1(x_2)|^2}} \left(\pm 1, -\varepsilon \frac{h'_1(x_2)}{2} \right). \quad (6)$$

By the same arguments as in the proof of Lemma 1 ([14]), it is easy to prove the following fact.

Statement 1. *For sufficiently small ε , the usual norm $\|\cdot\|_{H^1(\Omega_\varepsilon)}$ in the Sobolev space $H^1(\Omega_\varepsilon)$ and the following norm*

$$\|v\|_{\varepsilon,k_1} = \left(\int_{\Omega_\varepsilon} |\nabla v|^2 dx + \varepsilon k_1 \int_{\Upsilon_\varepsilon^{(1)}} v^2 dl_x \right)^{1/2}$$

are uniformly equivalent, i.e., there exist constants $C_1 > 0$, $C_2 > 0$ and $\varepsilon_0 > 0$ such that for all $\varepsilon \in (0, \varepsilon_0)$ and any function $v \in H^1(\Omega_\varepsilon)$ the following inequalities

$$C_1 \|v\|_{H^1(\Omega_\varepsilon)} \leq \|v\|_{\varepsilon,k_1} \leq C_2 \|v\|_{H^1(\Omega_\varepsilon)} \quad (7)$$

are satisfied.

By using the identity (5) and the fact that $\beta \geq 1$, we can prove in a standard way (see for instance [17, Sec. 7] or [18, Sec. 3]) the following *a-priori* estimate for the solution to problem (1):

$$\begin{aligned} & \|u_\varepsilon\|_{L^2(0,T;H^1(\Omega_\varepsilon))} + \max_{t \in [0,T]} \|u_\varepsilon(\cdot, t)\|_{L^2(\Omega_\varepsilon)} \leq \\ & \leq C_1 \left(\|f_0\|_{L^2(\Omega_0 \times (0,T))} + \varepsilon^{\beta-\frac{1}{2}} \|g_\varepsilon\|_{L^2(\Upsilon_\varepsilon^{(1,\pm)} \times (0,T))} + \varepsilon^\beta \|g_\varepsilon\|_{L^2(\Theta_\varepsilon^{(1)} \times (0,T))} \right) \end{aligned} \quad (8)$$

Taking into account (2), with the help of the identity (5) we deduce from (8) the following estimate

$$\begin{aligned} & \|u_\varepsilon\|_{L^2(0,T;H^1(\Omega_\varepsilon))} + \max_{t \in [0,T]} \|u_\varepsilon(\cdot, t)\|_{L^2(\Omega_\varepsilon)} \leq \\ & \leq C_1 \left(\|f_0\|_{L^2(\Omega_0 \times (0,T))} + \varepsilon^{\beta-1} C_2 + \varepsilon^\beta C_3 \right) \leq C_4. \end{aligned} \quad (9)$$

Remark 1. In (8) and (9) and in what follows all constants $\{C_i\}$ and $\{c_i\}$ in asymptotic inequalities are independent of the parameter ε .

3 Convergence theorem

As was showed in [21]-[27] thick multi-structures are not strong or weak connected domains, i.e., there is no any sequence of extension operators $\{\mathbf{P}_\varepsilon : H^1(\Omega_\varepsilon) \mapsto H^1(\mathbb{R}^N)\}_{\varepsilon > 0}$ whose norms are uniformly bounded in ε . This fact creates one of the main difficulties in proofs of convergence theorems for solutions to boundary-value problems in thick junctions.

There are different methods to prove such convergence theorems. The first convergence theorems for solutions to boundary-value problems in thick junctions of

different types were proved in [21, 22, 23], using special extension operators whose H^1 -norms are uniformly bounded in ε only for the solutions. Such approach allows to prove the convergence theorems if the boundaries of the thin domains of thick junctions are not smooth and rectilinear with respect to some variables and in case of different boundary conditions on the boundaries of the thin domains.

Later, in [6], where a homogeneous Neumann boundary-value problem was studied in a thick junction, it was shown that if the boundaries of thin rods are rectilinear, then the solution can be extended by zero. This is explained by the fact that this extension preserves the generalized derivative with respect to x_2 due to the rectilinearity of the boundaries of the rods along the Ox_2 -axis. This approach was used to prove the convergence theorem for non-linear problems in [3, 4]. Also, in [6], the homogeneous Neumann problem was considered in a bounded plane domain whose boundary is waved by the function $x_2 = h(x_1/\varepsilon)$, where h must be a continuously differentiable periodic function and the reciprocal functions of h on some intervals have to exist to construct special extension operators. But this extension does not preserve the space class of the solution and this extension was constructed under the assumption that the right-hand side $f_0 \in H^1$.

In this section we prove the convergence theorem for the solution to problem (1) with minimal conditions for the functions f_0 and g_ε .

In addition to the assumptions made in Section 1 we suppose that for any $T > 0$ there exist positive constants C_1, ε_0 such that for all value $\varepsilon \in (0, \varepsilon_0)$

$$\int_0^T \int_{\Omega_0} \mathbf{f}_\varepsilon^2(x, t) \, dx \, dt \leq C_1, \quad (10)$$

where $\mathbf{f}_\varepsilon(x, t) = \varepsilon^{-1}(f_0(x_1 + \varepsilon, x_2, t) - f_0(x, t))$. In fact, every function in the space $L^2(\Omega_0 \times (0, T))$ is continuous with respect to the L^2 -norm, but we need in (10) a little more (Lipschitz continuous in x_1 with respect to the L^2 -norm). Also without the loss of generality we can regard that f_0 and g_ε are a -periodic with respect to x_1 .

Due to the Dirichlet boundary condition on the sides of the thin rods from the second level we can extend by zero the solution to problem (1):

$$\widetilde{u_\varepsilon(x, t)} = \begin{cases} u_\varepsilon(x, t), & (x, t) \in G_\varepsilon^{(2)} \times (0, T), \\ 0, & (x, t) \in (D_2 \setminus G_\varepsilon^{(2)}) \times (0, T), \end{cases} \quad (11)$$

where $D_2 = (0, a) \times (-d_2, 0)$ is a rectangle that is filled up by the thin rods from the second level in the limit passage. Obviously, $\widetilde{u_\varepsilon} \in L^2(0, T; H^1(D_2))$.

To extend the solution from the thin rods of the first level we use the approach and results of papers [22] and [15, Th. 5.1].

Statement 3.1. *If the conditions (2), (3) and (10) hold, then for any $T > 0$ there*

exists an extension operator

$$\mathbf{P}_\varepsilon : L^2(0, T; H^1(\Omega_0 \cup G_\varepsilon^{(1)})) \mapsto L^2(0, T; H^1(\Omega_1))$$

such that for the solution u_ε to problem (1) we have

$$\|\mathbf{P}_\varepsilon u_\varepsilon\|_{L^2(0, T; H^1(\Omega_1))} \leq C_2, \quad (12)$$

where the constant C_2 is independent of ε ; Ω_1 is the interior of the union $\overline{\Omega_0 \cup D_1}$.

Theorem 3.2 (convergence theorem) *If (10) and assumptions made for functions f_0, g_ε in Section 1 hold, then*

$$u_\varepsilon|_{\Omega_0} \rightarrow v_0^+, \quad (\mathbf{P}_\varepsilon u_\varepsilon)|_{D_1} \rightarrow v_0^-, \quad \tilde{u}_\varepsilon \rightarrow 0, \quad (13)$$

weakly in $L^2(0, T; H^1(\Omega_0))$, $L^2(0, T; H^1(D_1))$, $L^2(0, T; H^1(D_2))$ respectively as $\varepsilon \rightarrow 0$, where v_0^+ is the unique solution to the following problem

$$\left\{ \begin{array}{ll} \partial_t v_0^+(x, t) = \Delta_x v_0^+(x, t) + f_0(x, t), & (x, t) \in \Omega_0 \times (0, T) \\ \partial_{x_1}^p v_0^+(0, x_2) = \partial_{x_1}^p v_0^+(a, x_2), \quad p = 0, 1, & (x_2, t) \in (0, \gamma_0) \times (0, T) \\ \partial_\nu v_0^+(x, t) = 0, & (x, t) \in \Gamma_\gamma \times (0, T) \\ v_0^+(x_1, 0, t) = 0, & (x_1, t) \in (0, a) \times (0, T) \\ v_0^+|_{t=0} = 0, & \end{array} \right. \quad (14)$$

and v_0^- is the unique solution to the problem

$$\left\{ \begin{array}{ll} h_1(x_2) \partial_t v_0^-(x, t) = \partial_{x_2} (h_1(x_2) \partial_{x_2} v_0^-(x, t)) - \\ \quad - 2k_1 v_0^- + 2 \delta_{\beta, 1} g_0(x, t), & (x, t) \in D_1 \times (0, T) \\ \partial_{x_2} v_0^-(x_1, -d_1, t) = 0, & (x_1, t) \in (0, a) \times (0, T) \\ v_0^-(x_1, 0, t) = 0, & (x_1, t) \in (0, a) \times (0, T), \\ v_0^-|_{t=0} = 0. & \end{array} \right. \quad (15)$$

where $\delta_{\beta, 1}$ is the Kronecker symbol.

Proof. Thanks to the Dirichlet conditions on the sides of the rods of the second level, we have

$$\int_{G_\varepsilon^{(2)}} u_\varepsilon^2 dx \leq \varepsilon^2 c_1 \int_{G_\varepsilon^{(2)}} (\partial_{x_1} u_\varepsilon)^2 dx,$$

from which, taking (9) into account, it follows

$$\|\tilde{u}_\varepsilon\|_{L^2(D_2 \times (0, T))}^2 \leq c_2 \varepsilon^2.$$

Therefore, $\tilde{u}_\varepsilon \rightarrow 0$ weakly in $L^2(0, T; H^1(D_2))$ as $\varepsilon \rightarrow 0$ and due to the compactness of the trace operator $T : H^1(D_2) \mapsto L^2(I_0)$ for a.e. $t \in (0, T)$

$$\tilde{u}_\varepsilon|_{I_0} \rightarrow 0 \quad \text{in } L^2(I_0) \quad \text{as } \varepsilon \rightarrow 0. \quad (16)$$

In view of inequalities (9) and (12), we can choose a subsequence $\{\varepsilon'\}$ (we denote it again by $\{\varepsilon\}$) such that

$$u_\varepsilon|_{\Omega_0} \rightarrow v_0^+, \quad (\mathbf{P}_\varepsilon u_\varepsilon)|_{D_1} \rightarrow v_0^-,$$

weakly in $L^2(0, T; H^1(\Omega_0))$, $L^2(0, T; H^1(D_1))$ respectively as $\varepsilon \rightarrow 0$; in addition, due to Lemma 3 in [32, Chap. 6], for any $\theta \in L_2(0, T)$

$$\int_0^T u_\varepsilon(\cdot, t) \theta(t) dt \rightarrow \int_0^T v_0^+(\cdot, t) \theta(t) dt, \quad \int_0^T (\mathbf{P}_\varepsilon u_\varepsilon)|_{D_1} \theta(t) dt \rightarrow \int_0^T v_0^-(\cdot, t) \theta(t) dt, \quad (17)$$

weakly in $H^1(\Omega_0)$, $H^1(D_1)$ and strongly in $L^2(\Omega_0)$, $L^2(D_1)$ respectively and

$$\partial_{x_q} \int_0^T u_\varepsilon(x, t) \theta(t) dt = \int_0^T \partial_{x_q} u_\varepsilon(x, t) \theta(t) dt \rightarrow \partial_{x_q} \int_0^T v_0^+ \theta dt = \int_0^T \partial_{x_q} (v_0^+) \theta dt \quad (18)$$

$$\begin{aligned} \partial_{x_q} \int_0^T (\mathbf{P}_\varepsilon u_\varepsilon)|_{D_1} \theta(t) dt &= \int_0^T \partial_{x_q} (\mathbf{P}_\varepsilon u_\varepsilon)|_{D_1} \theta dt \rightarrow \\ &\rightarrow \partial_{x_q} \int_0^T v_0^- \theta dt = \int_0^T \partial_{x_q} (v_0^-) \theta dt \end{aligned} \quad (19)$$

weakly in $L^2(\Omega_0)$, $L^2(D_1)$ respectively as $\varepsilon \rightarrow 0$, $q = 1, 2$.

Consider the following characteristic functions

$$\chi_\varepsilon^{(i)}(x) := \chi^{(i)}\left(\frac{x_1}{\varepsilon}, x_2\right) = \begin{cases} 1, & x \in \overline{G_\varepsilon^{(i)}}, \\ 0, & x \in D_i \setminus \overline{G_\varepsilon^{(i)}}, \end{cases} \quad (i = 1, 2),$$

which we periodically extend with respect to x_1 . Similarly as in Sec. 4([12]), we can prove that $\chi_\varepsilon^{(i)} \rightarrow h_i$ weakly in $L_2(D_i)$ as $\varepsilon \rightarrow 0$, $i = 1, 2$. Also, it is easy to verify that for any $\varrho \in [-d_i, 0]$ $\chi_\varepsilon^{(i)}|_{x_2=\varrho} \rightarrow h_i(\varrho)$ weakly in $L_2(0, a)$ as $\varepsilon \rightarrow 0$.

From (16) and the following equality

$$\widetilde{u_\varepsilon(x, t)|_{I_0}} = \chi_\varepsilon^{(2)}(x_1, 0) u_\varepsilon(x_1, 0 + 0, t) \quad \text{for a.e. } (x_1, t) \in I_0 \times (0, T),$$

it follows that the trace $v_0^+|_{I_0} = 0$ for a.e. $t \in (0, T)$. Then from the equality

$$(\mathbf{P}_\varepsilon u_\varepsilon)(x_1, 0 - 0, t) = u_\varepsilon(x_1, 0 + 0, t) \quad (x_1, t) \in I_0 \times (0, T),$$

we obtain in the limit passage that $v_0^-(x_1, 0, t) = 0$ for a.e. $(x_1, t) \in I_0 \times (0, T)$. Thus,

$$v_0^+|_{I_0} = v_0^-|_{I_0} = 0 \quad \text{for a.e. } t \in (0, T). \quad (20)$$

Let us define the following sets

$$\begin{aligned} \Lambda_0 &= \{ \varphi_0 \in C^\infty(\overline{\Omega}_0) : \varphi_0(0, x_2) = \varphi_0(0, x_2), \quad x_2 \in (0, \gamma_0), \quad \varphi_0|_{I_0} = 0 \} \\ \Lambda_1 &= \{ \varphi_1 \in C^\infty(\overline{D}_1) : \varphi_1|_{I_0} = 0 \} \end{aligned}$$

and the function

$$\Phi_{\varphi_0, \varphi_1}(x) = \begin{cases} \varphi_0(x) & x \in \overline{\Omega}_0 \\ \varphi_1(x) & x \in \overline{D}_1 \\ 0 & x \in \overline{D}_2 \end{cases}$$

Consider the set of the following test- functions

$$\mathcal{C}_0 = \{ \theta(t) \Phi_{\varphi_0, \varphi_1}(x) : \theta \in C^1([0, T]), \quad \theta(T) = 0, \quad \varphi_0 \in \Lambda_0, \quad \varphi_1 \in \Lambda_1 \}.$$

Obviously, the set of their restrictions $\{ \theta(t) (\varphi_0, \varphi_1|_{G_\varepsilon^{(1)}}, 0) \}$ belongs to $L^2(0, T; \mathcal{H}_\varepsilon)$.

By using the extension operators \mathbf{P}_ε , the functions $\chi_\varepsilon^{(1)}$ and equality (5), we now rewrite identity (4) with any test function from \mathcal{C}_0

$$\begin{aligned} & - \int_{\Omega_0} \left(\int_0^T u_\varepsilon(x, t) \partial_t \theta(t) dt \right) \varphi_0 dx - \int_{D_1} \chi_\varepsilon^{(1)} \left(\int_0^T (\mathbf{P}_\varepsilon u_\varepsilon) \partial_t \theta(t) dt \right) \varphi_1 dx + \\ & + \int_{\Omega_0} \nabla_x \left(\int_0^T u_\varepsilon \theta dt \right) \cdot \nabla_x \varphi_0 dx + \int_{D_1} \chi_\varepsilon^{(1)} \nabla_x \left(\int_0^T (\mathbf{P}_\varepsilon u_\varepsilon) \theta dt \right) \cdot \nabla_x \varphi_1 dx + \\ & + 2k_1 \int_{D_1} \frac{\sqrt{1 + \varepsilon^2 4^{-1} |h_1'(x_2)|^2}}{h_1(x_2)} \chi_\varepsilon^{(1)}(x) \left(\int_0^T (\mathbf{P}_\varepsilon u_\varepsilon)(x, t) \theta(t) dt \right) \varphi_1(x) dx - \\ & - 2\varepsilon k_1 \int_0^T \int_{G_\varepsilon^{(1)}} Y\left(\frac{x_1}{\varepsilon}\right) \frac{\sqrt{1 + \varepsilon^2 4^{-1} |h_1'(x_2)|^2}}{h_1(x_2)} \partial_{x_1} (u_\varepsilon \varphi_1) \theta(t) dx dt + \\ & + \varepsilon k_1 \int_0^a \chi_\varepsilon^{(1)} \int_0^T (\mathbf{P}_\varepsilon u_\varepsilon)|_{x_2=-d_1} \theta dt \varphi_1(x_1, -d_1) dx_1 = \int_0^T \int_{\Omega_0} f_0 \theta \varphi_0 dx dt + \\ & + 2\varepsilon^{\beta-1} \int_0^T \int_{D_1} \frac{\sqrt{1 + \varepsilon^2 4^{-1} |h_1'(x_2)|^2}}{h_1(x_2)} \chi_\varepsilon^{(1)}(x) g_\varepsilon(x, t) \theta(t) \varphi_1(x) dx dt - \\ & - 2\varepsilon^\beta \int_0^T \int_{G_\varepsilon^{(1)}} Y\left(\frac{x_1}{\varepsilon}\right) \frac{\sqrt{1 + \varepsilon^2 4^{-1} |h_1'|^2}}{h_1(x_2)} \partial_{x_1} (g_\varepsilon \varphi_1) \theta(t) dx dt + \varepsilon^\beta \int_0^T \int_{\Theta_\varepsilon^{(1)}} g_\varepsilon \varphi_1 \theta dx_2 dt. \end{aligned} \quad (21)$$

Let us pass to the limit in (21). Because of (12), the sequences

$$\chi_\varepsilon^{(1)} \partial_{x_q} \left(\int_0^T (\mathbf{P}_\varepsilon u_\varepsilon)(x, t) \theta(t) dt \right), \quad q = 1, 2, \quad (22)$$

are bounded in $L_2(D_1)$. Therefore, we can choose a subsequence of $\{\varepsilon\}$ (still denoted by $\{\varepsilon\}$) and find the weak limits σ_1 and σ_2 of these sequences in $L_2(D_1)$ as $\varepsilon \rightarrow 0$.

Taking into account (2) and (12), we see that limits of the last integral in the left-hand side and the integrals in the fourth and last line of (21) are equal to zero. For the other summands, in view of the facts mentioned above, we get in the limit passage the following relation

$$\begin{aligned} & - \int_{\Omega_0} \left(\int_0^T v_0^+(x, t) \partial_t \theta dt \right) \varphi_0(x) dx - \int_{D_1} h_1 \left(\int_0^T v_0^-(x, t) \partial_t \theta dt \right) \varphi_1(x) dx + \\ & + \int_{\Omega_0} \nabla_x \left(\int_0^T v_0^+(x, t) \theta(t) dt \right) \cdot \nabla_x \varphi_0 dx + \int_{D_1} \sum_{q=1}^2 \sigma_q(x) \partial_{x_q} \varphi_1 dx + \\ & + 2k_1 \int_{D_1} \int_0^T v_0^- \theta dt \varphi_1 dx \\ & = \int_0^T \int_{\Omega_0} f_0(x, t) \theta(t) \varphi_0(x) dx dt + 2\delta_{\beta,1} \int_0^T \int_{D_1} g_0(x, t) \theta(t) \varphi_1(x) dx dt, \end{aligned} \quad (23)$$

where $\delta_{\beta,1}$ is the Kronecker symbol.

Next we are going to find σ_q , $q = 1, 2$. In order to determine σ_1 , we consider the integral identity (4) with the following test function :

$$\psi_1(x, t) = \begin{cases} 0, & (x, t) \in \Omega_0 \times [0, T], \\ \varepsilon Y\left(\frac{x_1}{\varepsilon}\right) \phi_1(x) \theta(t), & (x, t) \in G_\varepsilon^{(1)} \times [0, T], \\ 0, & (x, t) \in G_\varepsilon^{(2)} \times [0, T], \end{cases}$$

where ϕ_1 is an arbitrary function from $C_0^\infty(D_1)$ and $\theta \in C^1([0, T])$, $\theta(T) = 0$. It is obvious that ψ_1 belongs to $L^2(0, T; \mathcal{H}_\varepsilon)$. As a result, we get

$$\int_{D_1} \chi_\varepsilon^{(1)} \partial_{x_1} \left(\int_0^T (\mathbf{P}_\varepsilon u_\varepsilon)(x, t) \theta(t) dt \right) dt \phi_1(x) dx = \mathcal{O}(\varepsilon), \quad \varepsilon \rightarrow 0,$$

whence $\sigma_1 \equiv 0$.

By the same arguments as in [15, Th.5.2] we deduce that

$$\sigma_2(x, t) = h_1(x_2) \int_0^T \partial_{x_2} v_0^-(x, t) \theta(t) dt, \quad x \in D_1.$$

As a result we get the integral identity

$$\begin{aligned} \int_0^T \left(- \int_{\Omega_0} v_0^+(x, t) \partial_t \theta(t) \varphi_0(x) dx - \int_{D_1} h_1(x_2) v_0^-(x, t) \varphi_1(x) \partial_t \theta(t) dx + \right. \\ \left. + \int_{\Omega_0} \nabla_x v_0^+(x, t) \cdot \nabla_x \varphi_0(x) \theta(t) dx + \right. \\ \left. + \int_{D_1} (h_1(x_2) \partial_{x_2} v_0^-(x, t) \partial_{x_2} \varphi_1 + 2k_1 v_0^-(x, t) \varphi_1(x)) \theta(t) dx \right) dt = \\ \int_{\Omega_0 \times (0, T)} f_0(x, t) \theta(t) \varphi_0(x) dx dt + 2\delta_{\beta, 1} \int_{D_1 \times (0, T)} g_0(x, t) \theta(t) \varphi_1(x) dx dt \quad (24) \end{aligned}$$

for any test-function from \mathcal{C}_0 .

Due to (22) the identity (24) is equivalent to the following two integral identities

$$\begin{aligned} \int_0^T \left(- \int_{\Omega_0} v_0^+(x, t) \partial_t \psi_0(x, t) dx + \int_{\Omega_0} \nabla_x v_0^+(x, t) \cdot \nabla_x \psi_0(x, t) dx \right) dt = \\ = \int_{\Omega_0 \times (0, T)} f_0(x, t) \psi_0(x, t) dx dt \quad (25) \end{aligned}$$

for any $\psi_0 \in H^1(\Omega_0 \times (0, T))$ such that $\psi_0(0, x_2, t) = \psi_0(a, x_2, t)$ for $(x_2, t) \in (0, \gamma_0) \times (0, T)$, $\psi_0|_{I_0} = 0$, $\psi_0|_{t=T} = 0$;
and

$$\begin{aligned} \int_0^T \left(- \int_{D_1} h_1(x_2) v_0^-(x, t) \partial_t \psi_1(x, t) dx + \right. \\ \left. + \int_{D_1} (h_1(x_2) \partial_{x_2} v_0^-(x, t) \partial_{x_2} \psi_1(x, t) + 2k_1 v_0^-(x, t) \psi_1(x, t)) dx \right) dt = \\ = 2\delta_{\beta, 1} \int_{D_1 \times (0, T)} g_0(x, t) \psi_1(x, t) dx dt \quad (26) \end{aligned}$$

for any $\psi_1 \in L^2(0, T; W^{0,1}(D_1, I_0))$ such that $\partial_t \psi_1 \in L^2(D_1 \times (0, T))$, $\psi_1|_{t=T} = 0$. Here $W^{0,1}(D_1, I_0) = \{v \in L^2(D_1) : \partial_{x_2} v \in L^2(D_1), v|_{I_0} = 0\}$.

It follows from (25) and (22) that v_0^+ is the unique weak solution to problem (14), and relation (26) and (22) imply that v_0^- is the unique weak solution to problem (15). In problem (15) variable x_1 plays the role of a parameter.

Due to the uniqueness of the weak solutions to these limit problems, the above arguments hold for any subsequence of $\{\varepsilon\}$ chosen at the beginning of the proof. Therefore, the theorem is proved. \square

References

- [1] *Y. Amirat, O. Bodart, U. De Maio and A. Gaudiello*, Asymptotic approximation of the solution of the Laplace equation in a domain with highly oscillating boundary. – *SIAM, J. Math. Anal.* vol. 35, pp. 1598–1616, (2004).
- [2] *A. Benkaddour and J. Sanchez-Hubert*, Spectral study of a coupled compact-noncompact problem. – *Model Math. Anal. Numer.* vol. 26, pp. 659–672, (1992).
- [3] *D. Blanchard, L. Carbone, and A. Gaudiello*, Homogenization of a monotone problem in a domain with oscillating boundary. – *Mathematical Modelling and Numerical Analysis.* vol. 33, No. 5, pp. 1057–1070, (1999).
- [4] *D. Blanchard, A. Gaudiello, and J. Mossino*, Highly oscillating boundaries and reduction of dimension: the critical case, *Analysis and Application*, 5, pp. 137–163, (2007).
- [5] *D. Blanchard, A. Gaudiello, and T. A. Mel'nyk*, Boundary homogenization and reduction of dimension in a Kirchhoff-Love plate, Preprint R07018 of the Laboratoire Jacques-Louis Lions, *SIAM Journal on Mathematical Analysis*, to appear, (2007).
- [6] *R. Brizzi and J.P. Chalot*, Boundary homogenization and Neumann boundary value problem. – *Ricerche di Matematica.* (1997), vol. 46, pp. 341–387.
- [7] *G.A. Chechkin* Homogenization of boundary-value problems with singular perturbation of boundary conditions. – *Mat. Sb.*, **184**, no. 6, pp.99-105 (in Russian), (1993).
- [8] *G.A. Chechkin* Asymptotic expansion of a solution of a boundary-value problem with quickly varying type of boundary conditions. – *Tr. Semin. im. I.G. Petrovskogo.*, **19**, pp. 323-338, (1996) .
- [9] *Damlamian A., Li Ta-Tsien.* Boundary homogenization for elliptic problems. – *J. Math. Pures et Appl.*, **66**, pp. 351-361, (1987).
- [10] *C. D'Apice, U. De Maio, and T. A. Mel'nyk*, Asymptotic analysis of a perturbed parabolic problem in a thick junction of type 3:2:2. – *Networks and Heterogeneous Media*, 2, pp. 255–277, (2007).
- [11] *U. De Maio and T. A. Mel'nyk*, Asymptotic analysis of the Neumann problem for the Ukawa equation in a thick multi-structure of type 3:2:2. – In the book "Progress in Nonlinear Differential Equations and Their Applications", Birkhauser Verlag, Basel, 63, pp. 207–215, (2005).

- [12] *U. De Maio and T.A. Mel'nyk*, Homogenization of the Robin problem in a thick multi-structures of type 3:2:2. – *Asymptotic Analysis.*, vol. 41, pp. 161–177, (2005).
- [13] *U. De Maio , T.A. Mel'nyk and C. Perugia*, Homogenization of the Robin problem in a thick multi-level junction. – *Nonlinear oscillations*, vol. 7, No. 3, pp. 336–356, (2004).
- [14] *U. De Maio , T. Durante and T.A. Mel'nyk*, Asymptotic approximation for the solution to the Robin problem in a thick multi-level junction. – *Mathematical Models and Methods in Applied Sciences.*, vol. 15, No. 12, pp. 1897–1921, (2005).
- [15] *T. Durante and T.A. Mel'nyk*, Asymptotic analysis of a parabolic problem in a thick two-level junctions. – *Journal of Math. Physics, Analysis, Geometry.* , vol. 3, No. 3, pp. 318–337, (2007).
- [16] *F. Fleury and E. Sanchez-Palencia*, Asymptotic and spectral properties of the acoustic vibrations of body perforated by narrow channels. – *Bull. Sci. Math.*, vol. 2, No. 110, pp. 149–176, (1986).
- [17] *L.C. Evans*, Partial differential equations. (Graduate studies in Math., Vol. 19). – American Math. Soc., Providence, RI, (1998).
- [18] *O.A. Ladyzhenskaya, V.A. Solonnikov and N.N. Ural'tseva*, Linear and quasi-linear equations of parabolic type. – Moscow, Nauka (1967) [in Russian]; English transl.: American Math. Soc., Providence, RI, (1968).
- [19] *V.A. Marchenko and E.Ya. Khruslov*, Boundary-value problems in domains with finegrained boundary. – Naukova Dumka, Kiev (1974) (in Russian).
- [20] *V.A. Marchenko and E.Ya. Khruslov*, Homogenized models of micro-heterogeneous mediums. – Naukova Dumka, Kiev (2005) (in Russian).
- [21] *T.A. Mel'nyk and S.A. Nazarov*, Asymptotic structure of the spectrum of the Neumann problem in a thin comb-like domain. – *C.R. Acad. Sci.,Paris, Serie 1.*, vol. 319, pp. 1343–1348, (1994).
- [22] *T.A. Mel'nyk and S.A. Nazarov*, Asymptotics of the Neumann spectral problem solution in a domain of "thick comb" // Trudy Seminara imeni I.G. Petrovskogo., vol. 19, p. 138-174 (in Russian); translation in: Journal of Mathematical Sciences. (1997), vol. 85, No. 6, pp. 2326-2346, (1996).
- [23] *T.A. Mel'nyk*, Homogenization of the Poisson equation in a thick periodic junction. – *Zeitschrift für Analysis und ihre Anwendungen.* , vol. 18, No. 4, pp. 953–975, (1999).

- [24] *T.A. Mel'nyk*, Asymptotic analysis of a spectral problem in a periodic thick junction of type 3:2:1. – *Mathematical Methods in the Applied sciences.*, vol. 23, No. 4, pp. 321–346, (2000).
- [25] *T.A. Mel'nyk and S.A. Nazarov*, Asymptotic analysis of the Neumann problem of the junction of a body and thin heavy rods. – *Algebra i Analiz.*, vol. 12, No. 2, p. 188–238 (in Russian); English transl. in *St.Petersburg Math.J.* (2001), vol. 12, No. 2, pp. 317–351, (2000).
- [26] *T.A. Mel'nyk*, Homogenization of a singularly perturbed parabolic problem in a thick periodic junction of type 3:2:1. – *Ukrainian Math. Journal.*, vol. 52, No. 11, pp. 1737–1749, (2000).
- [27] *T.A. Mel'nyk*, Asymptotic behavior of eigenvalues and eigenfunctions of the Fourier problem in a thick periodic junction of type 3:2:1. – *Grouped and Analytical Methods in Math. Physics, Akad. Nauk of Ukraine, Inst. of Mathematics, Kiev.*, vol. 36, pp. 187–196, (2001).
- [28] *S.A. Nazarov*, Junctions of singularly degenerating domains with different limit demension. – *Trudy Seminara imeni I.G. Petrovskogo.* (1995), vol. 18, pp. 1–78 (Part I); *Trudy Seminara imeni I.G. Petrovskogo.*, vol. 20, pp. 155–196 (Part II), (2000). (in Russian)
- [29] *T.A. Mel'nyk*, Asymptotic behavior of eigenvalues and eigenfunctions of the Fourier problem in a thick multi-level junction. – *Ukrainian Math. Journal.*, vol. 58, No. 2. pp. 195–216, (2006).
- [30] *T.A. Mel'nyk and P.S. Vashchuk*, Homogenization of a boundary-value problem with varying type of boundary conditions in a thick two-level junction. – *Nonlinear Oscillations.* , vol. 8, No. 2, pp. 241–257, (2005).
- [31] *T.A. Mel'nyk and P.S. Vashchuk*, Homogenization of the Neumann-Fourier problem in a thick two-level junction of type 3:2:1. – *Journal of Math. Physics, Analysis, Geometry*, vol. 2, No. 3, pp. 318–337, (2006).
- [32] *V.P. Mikhailov*, Partial differential equations. – Nauka, Moscow, (1983) [in Russian].
- [33] *J. Sanchez-Hubert and E. Sanchez-Palencia*, Vibration and Coupling of Continuous Systems. – Springer-Verlag, Berlin, Heidelberg (1989).

Weighted Simultaneous Approximation by Left Gamma Quasi-Interpolants*¹⁾

Hong-biao Jiang¹, Shun-sheng Guo²

1. Department of Mathematics, Lishui University, Lishui, 323000, P.R. China

2. College of Mathematics and Information Science, Hebei Normal University,

Shijiazhuang, 050016, P.R. China

Abstract: Recently Müller introduced the left Gamma quasi-interpolants and obtained an approximation equivalence theorem with $\omega_{\varphi}^{2r}(f, t)_p$. Guo extended the results with $\omega_{\varphi\lambda}^{2r}(f, t)_{\infty}$. In this paper we will improve the previous results and give a weighted simultaneous approximation equivalence theorem with $\omega_{\varphi\lambda}^{2r}(f, t)_{\infty}$ which unified classical modulus and Ditzian-Totick modulus.

Key words and phrases : Gamma operator, quasi-interpolants, weighted simultaneous approximation, modulus of smoothness, equivalent theorem

AMS classification: 41A25, 41A35, 41A28

1. Introduction

Gamma operators are given by

$$G_n(f, x) = \int_0^{\infty} g_n(x, t) f\left(\frac{n}{t}\right) dt, \quad x \in I = [0, \infty), \quad (1.1)$$

with the kernel $g_n(x, t) = \frac{x^{n+1}}{n!} e^{-xt} t^n$. Sometimes, we also use an alternate representation

$$G_n(f, x) = \frac{1}{n!} \int_0^{\infty} e^{-t} t^n f\left(\frac{nx}{t}\right) dt, \quad x \in I \quad (1.2)$$

*Supported by NSF of China(10571040) and NSF of Zhejiang Province(102005)

1)E-mail: hongbiaojiang@yahoo.com.cn, ssguo@hebtu.edu.cn

These operators have been introduced in [6] and investigated in subsequent papers (e.g. [1], [4], [5], [9]) and their references). In order to obtain much faster convergence, quasi-interpolants $G_n^{(k)}$ of G_n in the sense of Sablonnière [8] are considered in [7] and were quite well studied in subsequent paper (e.g. [2], [3], [7]).

We first recall the construction of the left Gamma quasi-interpolants (cf. [7]).

$$G_n^{(k)}(f, x) = \sum_{j=0}^k \alpha_j^n(x) D^j G_n(f, x), 0 \leq k \leq n. \quad (1.3)$$

where $D^j = \frac{d^j}{dx^j}$, $D^0 = id$ and $\alpha_j^n(x) \in \Pi_j$ (the space of algebraic polynomials of degree at most j). In 2001, Müller [7] obtained an approximation equivalence theorem: for $f \in L_p(I)$, $1 \leq p \leq \infty$, $\varphi(x) = x$, $n \geq 4r$, $r \in \mathbb{N}$, and $0 < \alpha < r$, the following statements are equivalent, that is

$$\|G_n^{(2r-1)}f - f\|_p = O(n^{-\alpha}) \Leftrightarrow \omega_\varphi^{2r}(f, t)_p = O(t^{2\alpha}). \quad (1.4)$$

In 2005, Guo [3] gave a weighted approximation equivalence theorem for $G_n^{(2r-1)}(f, x)$ in L_∞ -space: for $f \in L_\infty(I)$, $0 \leq \lambda \leq 1$, $\varphi(x) = x$, $w(x) = x^a(1+x)^b$ ($a \geq 0$, b is arbitrary), $n \geq 4r$, and $0 < \alpha < 2r$, then

$$|w(x)(G_n^{(2r-1)}(f, x) - f(x))| = O((n^{-\frac{1}{2}}\varphi^{1-\lambda}(x))^\alpha) \Leftrightarrow \omega_{\varphi^\lambda}^{2r}(f, t)_w = O(t^\alpha). \quad (1.5)$$

In this paper we will consider weighted simultaneous approximation for $G_n^{(2r-1)}(f, x)$ in L_∞ -space with $\omega_{\varphi^\lambda}^{2r}(f, t)_w$. Our main result is that for $f^{(s)}, wf^{(s)} \in L_\infty(I)$, $0 \leq \lambda \leq 1$, $\varphi(x) = x$, $w(x) = x^a(1+x)^b$, $n - s \geq 4r$, $0 < \alpha - s < 2r$, $s \in \mathbb{N}_0$, $\mathbb{N}_0 = \{0\} \cup \mathbb{N}$, then

$$|w(x)D^s(G_n^{(2r-1)}(f, x) - f(x))| = O((n^{-\frac{1}{2}}\varphi^{1-\lambda}(x))^{\alpha-s}) \Leftrightarrow \omega_{\varphi^\lambda}^{2r}(f^{(s)}, t)_w = O(t^{\alpha-s}). \quad (1.6)$$

In L_∞ -space, when $s = 0$, (1.6) is (1.5); when $s = 0$, $a = b = 0$, $\lambda = 1$, (1.6) is (1.4).

Throughout this paper $\|\cdot\|$ denotes $\|\cdot\|_\infty$, C denotes a positive constant independent of n, x and not necessarily the same at each occurrence.

2. Preliminaries and Lemmas

In this section, we first give some notations. For $0 \leq \lambda \leq 1$, $0 < \alpha - s < 2r$, $s \in \mathbb{N}_0$,

$$\|f\|_0 = \sup_{x \in (0, \infty)} |w(x)\varphi^{(\alpha-s)(\lambda-1)}(x)f(x)|,$$

$$C_{\lambda, w}^0 = \{f | wf \in L_\infty, \|f\|_0 < \infty\},$$

$$\|f\|_{2r} = \sup_{x \in (0, \infty)} |w(x)\varphi^{2r+(\alpha-s)(\lambda-1)}(x)f^{(2r)}(x)|,$$

$$C_{\lambda, w}^{2r} = \{f \in C_{\lambda, w}^0 : f^{(2r-1)} \in A.C_{loc}, \|f\|_{2r} < \infty\}.$$

The modulus of smoothness and K -functional which will be used later is defined as follows (cf. [1]).

$$\omega_{\varphi^\lambda}^r(f, t)_w = \begin{cases} \sup_{0 < h \leq t} \|w \Delta_{h\varphi^\lambda}^r f\|, & a = 0, \\ \sup_{0 < h \leq t} \|w \Delta_{\varphi^\lambda}^r f\|_{[t^*, \infty)} + \sup_{0 < h \leq t^*} \|w \vec{\Delta}_h^r f\|_{[0, 12t^*]}, & a > 0. \end{cases}$$

where

$$t^* = \begin{cases} (rt)^{\frac{1}{1-\lambda}}, & 0 < t < \frac{1}{8r}, 0 \leq \lambda < 1, \\ 0, & \lambda = 1, \end{cases} \quad \varphi(x) = x, w(x) = x^a(1+x)^b (a \geq 0, b \in \mathbb{R}).$$

$$\Omega_{\varphi^\lambda}^r(f, t)_w = \sup_{0 < h \leq t} \|w \Delta_{h\varphi^\lambda}^r f\|_{[t^*, \infty)}, 0 \leq \lambda < 1. \quad (2.1)$$

$$K_{\varphi^\lambda}^r(f, t^r)_w = \inf_g \{ \|w(f - g)\| + t^r \|w\varphi^{r\lambda} g^{(r)}\|, g^{(r-1)} \in A.C_{loc} \}. \quad (2.2)$$

$$K_\lambda^\alpha(f, t^{2r})_w = \inf_{g \in C_{\lambda, w}^{2r}} \{ \|f - g\|_0 + t^{2r} \|g\|_{2r} \}. \quad (2.3)$$

It is known that

$$\omega_{\varphi^\lambda}^r(f, t)_w \sim K_{\varphi^\lambda}^r(f, t^r)_w. \quad (2.4)$$

$$C^{-1} \Omega_{\varphi^\lambda}^r(f, t)_w \leq \omega_{\varphi^\lambda}^r(f, t)_w \leq C \int_0^t \frac{\Omega_{\varphi^\lambda}^r(f, \tau)_w}{\tau} d\tau. \quad (2.5)$$

Some very important properties of $G_n(f, x)$ and $G_n^{(k)}(f, x)$, we briefly recall here, which can be found in [7].

(1) For $j \in N_0, n \geq j$ and $x \in I$

$$\alpha_j^n(x) = \left(\frac{x}{n}\right)^j L_j^{(n-j)}(n), \alpha_0^n(x) = 1, \alpha_1^n(x) = 0, \quad (2.6)$$

where for $\alpha \in \mathbb{R}$

$$L_j^{(\alpha)}(x) = \sum_{r=0}^j (-1)^r \binom{j+\alpha}{j-r} \frac{x^r}{r!} \quad (2.7)$$

is the Laguerre polynomial of degree j .

(2) For $j \in N_0$ and $n \geq j$

$$\left| \frac{1}{n^j} L_j^{(n-j)}(n) \right| \leq C n^{-\frac{j}{2}}. \quad (2.8)$$

(3) If $p \in \Pi_k$, then

$$G_n^{(k)}(p, x) = p(x). \quad (2.9)$$

(4)

$$\frac{\partial^m}{\partial x^m} g_n(x, t) = \frac{m!}{x^m} g_n(x, t) L_m^{(n+1-m)}(xt). \quad (2.10)$$

(5)

$$\begin{aligned} (G_n f)^{(2r)}(x) &= \frac{n^{2r}}{n!} \int_0^\infty e^{-t} t^{n-2r} f^{(2r)}\left(\frac{nx}{t}\right) dt \\ &= \frac{n^{2r}(n-2r)!}{n!} \int_0^\infty g_{n-2r}(x, u) f^{(2r)}\left(\frac{n}{u}\right) du. \end{aligned} \quad (2.11)$$

 (6) For $\alpha > -1$,

$$\int_0^\infty e^{-t} t^\alpha |L_j^{(\alpha)}(t)|^2 dt = \frac{\Gamma(j + \alpha + 1)}{j!}. \quad (2.12)$$

 (7) For $m, n, l \in N_0$

$$\frac{1}{(n+l)!} \int_0^\infty e^{-t} t^{n+l} \left(\frac{nx}{t} - x\right)^m dt \leq C \frac{x^m}{n^{\lfloor \frac{m+1}{2} \rfloor}}. \quad (2.13)$$

For the sake of convenience, utilizing (1.1) and (2.11) we introduce the auxiliary operator for $x \in I$,

$$G_{n,s}^{(k)} f =: \sum_{j=0}^k \alpha_j^n(x) \sum_{i=0}^{\hat{s}} \binom{\hat{s}}{i} (j)_i x^{-i} (G_{n,s} f)^{(j-i)} \quad (2.14)$$

Where $G_{n,s} f^{(s)} =: \int_0^\infty g_{n-s}(x, t) f^{(s)}\left(\frac{n}{t}\right) dt = \frac{n!}{n^s(n-s)!} D^s G_n f$, $\hat{s} = \min\{s, j\}$. Hence, $G_{n,s}^{(k)}(1, x) = 1 + O(\frac{1}{n})$. Moreover, for $f^{(s)} \in L_\infty$, there holds $G_{n,s}^{(k)}(f^{(s)}, x) = \frac{n!}{n^s(n-s)!} D^s G_n^{(k)}(f, x)$.

Next we give three lemmas.

Lemma 2.1 ([3]) (1) Let $w(x) = x^a(1+x)^b$, $a \geq 0, b \in R, x, \mu \in (0, \infty)$, then

$$\frac{w(x)}{w(\mu)} \leq 2^{|b|} \left(\left(\frac{x}{\mu}\right)^a + \left(\frac{x}{\mu}\right)^{a+b} \right). \quad (2.15)$$

 (2) For $\forall \beta \in R$ we have

$$\frac{1}{n!} \int_0^\infty e^{-t} t^n \left(\frac{n}{t}\right)^\beta dt \leq C(\beta). \quad (2.16)$$

Lemma 2.2 For $n - s \geq k, f^{(s)} \in L_\infty(I), s \in N_0$, we have

$$\|w G_{n,s}^{(k)} f^{(s)}\| \leq C \|w f^{(s)}\|. \quad (2.17)$$

Proof. Using (2.14) and (2.6),

$$|w(x) G_{n,s}^{(k)}(f^{(s)}, x)| \leq |w(x) G_{n,s}(f^{(s)}, x)| + |w(x) \sum_{j=2}^k \alpha_j^n(x) \sum_{i=0}^{\hat{s}} \binom{\hat{s}}{i} (j)_i x^{-i} (G_{n,s}(f^{(s)}, x))^{(j-i)}|.$$

By (2.15), (2.16) and [1, p165], we can easily obtain

$$|w(x) G_{n,s}(f^{(s)}, x)| \leq C \|w f^{(s)}\|. \quad (2.18)$$

By (2.10), (2.12), (2.15) and (2.16) we have

$$\begin{aligned}
|w(x)D^{j-i}G_{n,s}(f^{(s)}, x)| &= |w(x) \int_0^\infty \frac{(j-i)!}{x^{j-i}} g_{n-s}(x, t) L_{j-i}^{(n-s+1-j+i)}(xt) f^{(s)}\left(\frac{n}{t}\right) dt| \\
&\leq \left| \frac{w(x)(j-i)!}{(n-s)!x^{j-i}} \int_0^\infty x^{n-s+1} e^{-tx} t^{n-s} \right. \\
&\quad \times \left. L_{j-i}^{(n-s+1-j+i)}(xt) w^{-1}\left(\frac{n}{t}\right) dt \right| \|wf^{(s)}\| \\
&\leq \frac{Cx^{-j+i}}{(n-s)!} \int_0^\infty e^{-\mu} \mu^{n-s} |L_{j-i}^{(n-s+1-j+i)}(\mu)| \frac{w(x)}{w(\frac{n\mu}{x})} d\mu \|wf^{(s)}\| \\
&\leq C \frac{x^{-j+i}}{(n-s)!} \left(\int_0^\infty e^{-\mu} \mu^{n-s+1-j+i} |L_{j-i}^{(n-s+1-j+i)}(\mu)|^2 d\mu \right)^{\frac{1}{2}} \\
&\quad \times \left(\int_0^\infty e^{-\mu} \mu^{n-s-1+j-i} \left(\left(\frac{\mu}{n}\right)^a + \left(\frac{\mu}{n}\right)^{a+b} \right)^2 d\mu \right)^{\frac{1}{2}} \|wf^{(s)}\| \\
&\leq Cx^{-j+i} \left(\frac{(n-s+1)!}{(j-i)!(n-s)!} \right)^{\frac{1}{2}} \left(\frac{(n-s-1+j-i)!}{(n-s)!} \right)^{\frac{1}{2}} \|wf^{(s)}\| \\
&\leq Cx^{-j+i} (n-s)^{\frac{j-i}{2}} \|wf^{(s)}\| \\
&\leq Cx^{-j+i} n^{\frac{j}{2}} \|wf^{(s)}\|.
\end{aligned}$$

Notice that $|\alpha_j^n(x)| \leq Cn^{-\frac{j}{2}}x^j$, we get

$$\begin{aligned}
&|w(x) \sum_{j=2}^k \alpha_j^n(x) \sum_{i=0}^{\hat{s}} \binom{\hat{s}}{i} (j)_i x^{-i} (G_{n,s}(f^{(s)}, x))^{(j-i)}| \\
&\leq C \sum_{j=2}^k n^{-\frac{j}{2}} x^j \sum_{i=0}^{\hat{s}} x^{-i} x^{-j+i} n^{\frac{j}{2}} \|wf^{(s)}\| \\
&\leq C \sum_{j=2}^k \sum_{i=0}^{\hat{s}} \|wf^{(s)}\| \\
&\leq C \|wf^{(s)}\|.
\end{aligned} \tag{2.19}$$

By (2.18) and (2.19), we can prove (2.17). The proof of Lemma 2.2 is complete.

Lemma 2.3 For $n-s \geq 4r$, $s \in N_0$, we have

$$\|G_{n,s}^{(2r-1)} f^{(s)}\|_{2r} \leq Cn^r \|f^{(s)}\|_0, f^{(s)} \in C_{\lambda,w}^0. \tag{2.20}$$

$$\|G_{n,s}^{(2r-1)} f^{(s)}\|_{2r} \leq C \|f^{(s)}\|_{2r}, f^{(s)} \in C_{\lambda,w}^{2r}. \tag{2.21}$$

Proof. At fist we prove (2.20). By [7, (32)], we have

$$\begin{aligned}
& |w(x)\varphi^{2r+(\alpha-s)(\lambda-1)}(x)(G_{n,s}^{(2r-1)}(f^{(s)}, x))^{(2r)}| \\
&= |w(x)\varphi^{2r+(\alpha-s)(\lambda-1)}(x)((G_{n,s}f^{(s)})^{(2r)}(x) \\
&+ (\sum_{j=2}^{2r-1} \frac{1}{n^j} L_j^{(n-j)}(n)\varphi^j(x) \sum_{i=0}^{\hat{s}} \binom{\hat{s}}{i} (j)_i x^{-i} D^{2r+j-i} G_{n,s}(f^{(s)}, x))^{(2r)}| \\
&\leq |w(x)\varphi^{2r+(\alpha-s)(\lambda-1)}(x)(G_{n,s}f^{(s)}, x)^{(2r)} \\
&+ Cw(x)\varphi^{2r+(\alpha-s)(\lambda-1)} \sum_{j=2}^{2r-1} n^{-\frac{j}{2}} \sum_{i=0}^{\hat{s}} \sum_{k=0}^{j-i} \varphi^{j-i-k}(x)(G_{n,s}f^{(s)})^{(2r+j-i-k)}| \\
&=: I_1 + I_2.
\end{aligned}$$

By (2.10) we have

$$\begin{aligned}
(G_{n,s}f^{(s)})^{(2r+j-i-k)}(x) &= \int_0^\infty \frac{\partial^{2r+j-i-k}}{\partial x^{2r+j-i-k}} g_{n-s}(x, t) f^{(s)}\left(\frac{n}{t}\right) dt \\
&= \frac{(2r+j-i-k)!}{x^{2r+j-i-k}} \frac{1}{(n-s)!} \int_0^\infty x^{n-s+1} e^{-tx} t^{n-s} L_{2r+j-i-k}^{(n-s+1-2r-j+i+k)}(xt) f^{(s)}\left(\frac{n}{t}\right) dt.
\end{aligned}$$

Thus

$$\begin{aligned}
I_2 &\leq C \sum_{j=2}^{2r-1} n^{-\frac{j}{2}} w(x) \varphi^{(\alpha-s)(\lambda-1)}(x) \sum_{i=0}^{\hat{s}} \sum_{k=0}^{j-i} \frac{(2r+j-i-k)!}{(n-s)!} \\
&\times \int_0^\infty e^{-\mu} \mu^{n-s} |L_{2r+j-i-k}^{(n-s+1-2r-j+i+k)}(\mu)| w^{-1}\left(\frac{nx}{\mu}\right) \varphi^{(\alpha-s)(1-\lambda)}\left(\frac{nx}{\mu}\right) d\mu \|f^{(s)}\|_0 \\
&\leq C \|f^{(s)}\|_0 \sum_{j=2}^{2r-1} \sum_{i=0}^{\hat{s}} \sum_{k=0}^{j-i} \frac{n^{-\frac{j}{2}}}{(n-s)!} \left(\frac{(n-s+1)!}{(2r+j-i-k)!}\right)^{\frac{1}{2}} \\
&\times \left(\int_0^\infty e^{-\mu} \mu^{n-s+1+2r+j-i-k} \frac{w^2(x) \varphi^{2(\alpha-s)(\lambda-1)}(x)}{w^2\left(\frac{nx}{\mu}\right) \varphi^{2(\alpha-s)(\lambda-1)}\left(\frac{nx}{\mu}\right)} d\mu\right)^{\frac{1}{2}} \\
&\leq C \|f^{(s)}\|_0 \sum_{j=2}^{2r-1} \sum_{i=0}^{\hat{s}} \sum_{k=0}^{j-i} n^{-\frac{j}{2}} \left(\frac{(n-s+1)!}{(n-s)!}\right)^{\frac{1}{2}} \left(\frac{(n-s-1+2r+j-k)!}{(n-s)!}\right)^{\frac{1}{2}} \\
&\leq C n^r \|f^{(s)}\|_0 \sum_{j=2}^{2r-1} \sum_{i=0}^{\hat{s}} \sum_{k=0}^{j-i} (n-s)^{-\frac{j}{2}-\frac{k}{2}} \\
&\leq C n^r \|f^{(s)}\|_0.
\end{aligned}$$

Analogously we also have

$$I_1 \leq C n^r \|f^{(s)}\|_0.$$

Hence, (2.20) is valid. Now we prove (2.21).

In the same way, by (2.10) and (2.11) we can get

$$\begin{aligned}
& (G_{n,s}f^{(s)})^{(2r+j-i-k)} \\
&= \frac{(n-s)^{2r}(n-s-2r)!}{(n-s)!} \int_0^\infty \frac{(j-i-k)!}{x^{j-i-k}} g_{n-s-2r}(x, \mu) L_{j-i-k}^{(n-s-2r+1-j+i+k)}(\mu) f^{(s+2r)}\left(\frac{n}{\mu}\right) d\mu \\
&= \frac{(n-s)^{2r}(n-s-2r)!}{(n-s)!(n-s-2r)!} \frac{(j-i-k)!}{x^{j-i-k}} \int_0^\infty e^{-t} t^{n-s-2r} L_{j-i-k}^{(n-s-2r+1-j+i+k)}(t) f^{(s+2r)}\left(\frac{nx}{t}\right) dt
\end{aligned} \tag{2.22}$$

By (2.10), (2.11) and (2.22), in the similarly way from above procedure we can obtain

$$I_2 \leq C \|f^{(s)}\|_{2r},$$

$$I_1 \leq C \|f^{(s)}\|_{2r}.$$

Thus, (2.21) is valid. The proof of lemma 2.3 is complete.

3. The Main Results

In this section we will show the simultaneous approximation direct inverse theorem for $G_{n,s}^{(2r-1)}f^{(s)}$ with the 2r-th Ditzian-Totick weighted modulus of smoothness.

Theorem 3.1 Let $n-s \geq 4r$, $s \in N_0$, then for $wf^{(s)} \in L_\infty$, we have

$$|w(x)(G_{n,s}^{(2r-1)}(f^{(s)}, x) - f^{(s)}(x))| \leq C \omega_{\varphi^\lambda}^{2r}(f^{(s)}, n^{-\frac{1}{2}}\varphi^{1-\lambda}(x))_w. \tag{3.1}$$

Proof. For any $g \in w_\infty^{2r} =: \{g : g^{(2r-1)} \in A.C._{loc}, w\varphi^{2r\lambda}g^{(2r)} \in L_\infty\}$, Using the Taylor formula

$$g(t) = \sum_{j=0}^{2r-1} \frac{1}{j!} (t-x)^j g^{(j)}(x) + R_{2r}(g, t, x).$$

Where the integral remainder $R_{2r}(g, t, x) = \frac{1}{(2r-1)!} \int_x^t (t-\mu)^{2r-1} g^{(2r)}(\mu) d\mu$. As $G_{n,s}^{(2r)}(f, x)$ is exact on Π_{2r-1} and $\alpha_0^n(x) = 1, \alpha_1^n(x) = 0$, we have

$$\begin{aligned}
& |w(x)(G_{n,s}^{(2r-1)}(g, x) - g(x))| \leq |w(x) \sum_{j=0}^{2r-1} \alpha_j^n(x) D^j(G_{n,s}(g, x) - g(x))| \\
& \leq |w(x)G_{n,s}(R_{2r}(g, \cdot, x), x)| + C \left| \sum_{j=2}^{2r-1} \sum_{i=0}^{\hat{s}} n^{-\frac{j}{2}} \varphi^j(x) w(x) \binom{\hat{s}}{i} (j)_i x^{-i} D^{j-i} G_{n,s}(R_{2r}(g, \cdot, x), x) \right| \\
& =: I_1 + I_2.
\end{aligned} \tag{3.2}$$

For μ between x and t , by (cf. [1, Lemma 9.6.1]), we have

$$\frac{|\mu - x|}{\varphi^\lambda(\mu)} \leq \frac{|x - t|}{\varphi^\lambda(x)}, \quad \frac{1}{\varphi^\lambda(\mu)} \leq \frac{1}{\varphi^\lambda(x)} + \frac{1}{\varphi^\lambda(t)}$$

Hence

$$|w(x)R_{2r}(g, t, x)| \leq C \frac{|t-x|^{2r-1}}{\varphi^{(2r-1)\lambda}(x)} \left(\frac{1}{x^\lambda} + \frac{1}{t^\lambda} \right) \|w\varphi^{2r\lambda}g^{(2r)}\| \left| \int_x^t w^{-1}(\mu) d\mu \right|. \quad (3.3)$$

By (2.10) and (3.3), we can get

$$\begin{aligned} & |w(x)|D^{j-i}G_{n,s}(R_{2r}(g, \cdot, x), x)| = |w(x) \int_0^\infty \frac{\partial^{j-i}}{\partial x^{j-i}} g_{n-s}(x, t) R_{2r}(g, \frac{n}{t}, x) dt| \\ & = |w(x) \frac{(j-i)!}{x^{j-i}} \int_0^\infty \frac{x^{n-s+1}}{(n-s)!} e^{-xt} t^{n-s} L_{j-i}^{(n-s+1-j+i)}(xt) R_{2r}(g, \frac{n}{t}, x) dt| \\ & \leq C \|w\varphi^{2r\lambda}g^{(2r)}\| \frac{x^{i-j}}{(n-s)!} \int_0^\infty e^{-\mu} \mu^{n-s} |L_{j-i}^{(n-s+1-j+i)}(\mu)| \frac{|nx-x|^{2r-1}}{\varphi^{(2r-1)\lambda}(x)} \left(\frac{1}{x^\lambda} + \left(\frac{\mu}{nx}\right)^\lambda \right) \left| \int_x^{\frac{nx}{\mu}} \frac{w(x)}{w(\tau)} d\tau \right| d\mu \end{aligned}$$

Utilizing (2.15) we have

$$\left| \int_x^{\frac{nx}{\mu}} \frac{w(x)}{w(\tau)} d\tau \right| \leq C \left| \int_x^{\frac{nx}{\mu}} \left(\left(\frac{x}{\tau}\right)^a + \left(\frac{x}{\tau}\right)^{a+b} \right) d\tau \right| \leq C \left(1 + \left(\frac{\mu}{n}\right)^a + \left(\frac{\mu}{n}\right)^{a+b} \right) \left| \frac{nx}{\mu} - x \right|.$$

Hence

$$\begin{aligned} & |w(x)|D^{j-i}G_{n,s}(R_{2r}(g, \cdot, x), x)| \\ & \leq C \|w\varphi^{2r\lambda}g^{(2r)}\| \frac{x^{i-j-2r\lambda}}{(n-s)!} \int_0^\infty e^{-\mu} \mu^{n-s} |L_{j-i}^{(n-s+1-j+i)}(\mu)| \left(\frac{nx}{\mu} - x \right)^{2r} \\ & \quad \times \left(1 + \left(\frac{\mu}{n}\right)^\lambda + \left(\frac{\mu}{n}\right)^a + \left(\frac{\mu}{n}\right)^{\lambda+a} + \left(\frac{\mu}{n}\right)^{a+b} + \left(\frac{\mu}{n}\right)^{\lambda+a+b} \right) d\mu. \end{aligned} \quad (3.4)$$

Using (2.12), (2.13) and (2.16), for $\forall \beta \in R$

$$\begin{aligned} & \int_0^\infty e^{-\mu} \mu^{n-s} |L_{j-i}^{(n-s+1-j+i)}(\mu)| \left(\frac{nx}{\mu} - x \right)^{2r} \left(\frac{\mu}{n} \right)^\beta d\mu \\ & \leq \left(\int_0^\infty e^{-\mu} \mu^{n-s+1-j+i} |L_{j-i}^{(n-s+1-j+i)}(\mu)|^2 d\mu \right)^{\frac{1}{2}} \left(\int_0^\infty e^{-\mu} \mu^{n-s-1+j-i} \left(\frac{nx}{\mu} - x \right)^{4r} \left(\frac{\mu}{n} \right)^{2\beta} d\mu \right)^{\frac{1}{2}} \\ & \leq C \left(\frac{(n-s+1)!}{(j-i)!} \right)^{\frac{1}{2}} \left(\int_0^\infty e^{-\mu} \mu^{n-s-1+j-i} \left(\frac{nx}{\mu} - x \right)^{8r} d\mu \right)^{\frac{1}{4}} \left(\int_0^\infty e^{-\mu} \mu^{n-s-1+j-i} \left(\frac{\mu}{\mu+j-1} \right)^{4\beta} d\mu \right)^{\frac{1}{4}} \\ & \leq C ((n-s+1)!)^{\frac{1}{2}} ((n-s-1+j-i)! \frac{x^{8r}}{n^{4r}})^{\frac{1}{4}} ((n-s-1+j-i)!)^{\frac{1}{4}} \\ & \leq C ((n-s+1)!)^{\frac{1}{2}} ((n-s-1+j-i)!)^{\frac{1}{2}} n^{-r} x^{2r}. \end{aligned} \quad (3.5)$$

By (3.4) and (3.5) we have

$$\begin{aligned} I_2 & \leq C \sum_{j=2}^{2r-1} \sum_{i=0}^{\hat{s}} n^{-\frac{j}{2}} \frac{x^{2r(1-\lambda)} n^{-r}}{(n-s)!} ((n-s+1)!)^{\frac{1}{2}} ((n-s-1+j-i)!)^{\frac{1}{2}} \|w\varphi^{2r\lambda}g^{(2r)}\| \\ & \leq C n^{-r} x^{2r(1-\lambda)} \|w\varphi^{2r\lambda}g^{(2r)}\| \sum_{j=2}^{2r-1} \sum_{i=0}^{\hat{s}} n^{-\frac{j}{2}} \left(1 + \frac{1}{n-s} \right)^{\frac{1}{2}} (n-s)^{\frac{j-i}{2}} \\ & \leq C n^{-r} x^{2r(1-\lambda)} \|w\varphi^{2r\lambda}g^{(2r)}\| \sum_{j=2}^{2r-1} \sum_{i=0}^{\hat{s}} n^{-\frac{j}{2}} \\ & \leq C n^{-r} x^{2r(1-\lambda)} \|w\varphi^{2r\lambda}g^{(2r)}\|. \end{aligned} \quad (3.6)$$

From the procedure of proof of (3.6), analogously we can deduce that

$$I_1 \leq Cn^{-r}x^{2r(1-\lambda)}\|w\varphi^{2r\lambda}g^{(2r)}\|. \quad (3.7)$$

Combining (3.2), (3.6) and (3.7), for $g \in w_\infty^{2r}$ we have

$$|w(x)(G_{n,s}^{(2r-1)}(g, x) - g(x))| \leq Cn^{-r}\varphi^{2r(1-\lambda)}\|w\varphi^{2r\lambda}g^{(2r)}\|. \quad (3.8)$$

By the definition of $K_{\varphi^\lambda}^r(f, t)_w$, for $wf^{(s)} \in L_\infty$ we can choose $g = g_{n,x,\lambda} \in w_\infty^{2r}$, such that

$$\|w(f^{(s)} - g)\| + n^{-r}\varphi^{2r(1-\lambda)}(x)\|w\varphi^{2r\lambda}g^{(2r)}\| \leq C\omega_{\varphi^\lambda}^{2r}(f^{(s)}, n^{-\frac{1}{2}}\varphi^{1-\lambda}(x))_w. \quad (3.9)$$

By (3.8) and (3.9) we have

$$\begin{aligned} |w(x)(G_{n,s}^{(2r-1)}(f^{(s)}, x) - f^{(s)}(x))| &\leq C(\|w(f^{(s)} - g)\| + |w(G_{n,s}^{(2r-1)}(g, x) - g(x))|) \\ &\leq C(\|w(f^{(s)} - g)\| + n^{-r}\varphi^{2r(1-\lambda)}(x)\|w\varphi^{2r\lambda}g^{(2r)}\|) \\ &\leq C\omega_{\varphi^\lambda}^{2r}(f^{(s)}, n^{-\frac{1}{2}}\varphi^{1-\lambda}(x))_w. \end{aligned}$$

Therefore, (3.1) is valid.

Theorem 3.2 For $wf^{(s)} \in L_\infty$, $0 \leq \lambda \leq 1$, $0 < \alpha - s < 2r$, $n - s \geq 4r$, $s \in N_0$, then

$$|w(x)(G_{n,s}^{(2r-1)}(f^{(s)}, x) - f^{(s)}(x))| \leq O((n^{-\frac{1}{2}}\varphi^{1-\lambda}(x))^{\alpha-s}), \quad (3.10)$$

implies $\omega_{\varphi^\lambda}^{2r}(f^{(s)}, t)_w = O(t^{\alpha-s})$.

Proof. By the definition of $K_\lambda^\alpha(f, t^{2r})_w$, for a fixed x and λ we can choose $g \in C_{\lambda,w}^{2r}$, such that

$$\|f^{(s)} - g\|_0 + n^{-r}\|g\|_{2r} \leq 2K_\lambda^\alpha(f^{(s)}, n^{-r})_w.$$

Using (3.10) we have

$$|w(x)\varphi^{(\alpha-s)(\lambda-1)}(x)(G_{n,s}^{(2r-1)}(f^{(s)}, x) - f^{(s)}(x))| \leq Cn^{-\frac{\alpha-s}{2}}. \quad (3.11)$$

Combining (2.3), (2.20), (2.21) and (3.11), we can obtain

$$\begin{aligned} K_\lambda^\alpha(f^{(s)}, t^{2r})_w &\leq \|f^{(s)} - G_{n,s}^{(2r-1)}f^{(s)}\|_0 + t^{2r}\|G_{n,s}^{(2r-1)}f^{(s)}\|_{2r} \\ &\leq Cn^{-\frac{\alpha-s}{2}} + t^{2r}(\|G_{n,s}^{(2r-1)}(f^{(s)} - g)\|_{2r} + \|G_{n,s}^{(2r-1)}g\|_{2r}) \\ &\leq C(n^{-\frac{\alpha-s}{2}} + t^{2r}(n^r\|f^{(s)} - g\|_0 + \|g\|_{2r})) \\ &\leq C(n^{-\frac{\alpha-s}{2}} + t^{2r}n^rK_\lambda^\alpha(f^{(s)}, n^{-r})_w). \end{aligned}$$

By Berens-Lorentz lemma, we have

$$K_\lambda^\alpha(f^{(s)}, t^{2r})_w = O(t^{\alpha-s}).$$

When $\lambda = 1$, $K_1^r(f^{(s)}, t^{2r})_w = K_\varphi^{2r}(f^{(s)}, t^{2r})_w = O(t)^{\alpha-s}$. So that $\omega_\varphi^{2r}(f^{(s)}, t)_w = O(t)^{\alpha-s}$. When $1 \leq \lambda < 1$, the proof is similar to [3, p79], we omit the details. The proof of Theorem 3.2 is complete.

References

1. Z. Ditzian and V. Totik, *Moduli of Smoothness*. Springer-Verlag, New York, 1987.
2. S. Guo, L. Liu, Q. QI and G. Zhang, A strong converse inequality for left Gamma quasi-interpolants in L_p space. *Acta Math. Hungar.* 105, 17-26 (2004).
3. S. Guo, G. Zhang, Q. QI and L. Liu, Pointwise weight approximation by left Gamma quasi-interpolants. *J. Comput. and Appl.*, 2, 71-80 (2005).
4. A. Lupas, D. H. Mach, V. Maier and M. W. Müller, Linear combination of Gamma operators in L_p space. *Results Math.*, 34, 156-168 (1998).
5. A. Lupas, D. H. Mach, V. Maier and M. W. Müller, *Certain results involving Gamma operators*, in: New Developments in Approximation Theory (International Series of Numerical Mathematics, Vol. 132), (M. W. Müller, M. Buhmann D. H. Mach, and M. Felten, eds) Birkhäuser-Verlag (Basel, 1999), pp. 199-214.
6. A. Lupas and M. W. Müller, Approximationseigenschaften der Gammaoperatoren. *Math. Z.*, 98, 208-226 (1967).
7. M. W. Müller, The central approximation theorems for the method of left Gamma quasi-interpolants in L_p space. *J. Comput. and Appl.*, 3, 207-222 (2001).
8. P. Sablonnière, A family of Bernstein quasi-interpolants on $[0, 1]$. *Approx. Theory and its Appl.*, 8:3, 62-76 (1992)
9. V. Totik, The Gamma operators in L_p space. *Publ. Math. Debrecen*, 32, 43-55 (1985).

Non-uniform sampling problem

S.H. Kulkarni, R. Radha and S. Sivananthan

Department of Mathematics, Indian Institute of Technology Madras,
Chennai - 600 036, India.

e-mail: shk@iitm.ac.in, radharam@iitm.ac.in, ssiva_math@yahoo.co.in

Abstract

If φ is a continuous function satisfying certain decay properties, then it is shown that any f belongs to the shift invariant space $V(\varphi)$ can be reconstructed uniquely and stably from its sample points which are perturbed version of integers. The reconstruction procedure is discussed based on the convergence of the projection method of Laurent operators and the computation of the solutions of finite dimensional truncated matrix equations recursively. The implementation is carried out using MatLab. Some illustrations are given.

1 Introduction

A sampling problem involves the reconstruction of a function f from its samples $f(x_j), j \in \mathbb{Z}$. Unless apriori some conditions are assumed on f , the problem is not meaningful. In fact, one has to obtain some conditions on a sampling set $X = \{x_j \in \mathbb{R} / j \in J\}$, J a countable set, to recover a certain class of functions f from the sample set X in a stable and unique manner. Since sampling problem deals with real world applications, it is also important to find a stable numerical algorithm to obtain a reconstruction procedure.

The classical Shannon sampling theorem states that if $f \in L^2(\mathbb{R}) \cap B_{[-\frac{1}{2}, \frac{1}{2}]}$, then f can be reconstructed from its samples $\{f(k)/k \in \mathbb{Z}\}$ by the formula

$$f(x) = \sum_{k \in \mathbb{Z}} f(k) \operatorname{sinc}(x - k),$$

where $\operatorname{sinc}(y) = \frac{\sin \pi y}{\pi y}$ and $B_{[-\frac{1}{2}, \frac{1}{2}]}$ denotes the class of functions in $L^1(\mathbb{R})$ whose Fourier transforms have support in $[-\frac{1}{2}, \frac{1}{2}]$. Kadec in [10] proved that if $X = \{x_k \in \mathbb{R} : |x_k - k| \leq L < \frac{1}{4}, k \in \mathbb{Z}\}$ then any $f \in L^2(\mathbb{R}) \cap B_{[-\frac{1}{2}, \frac{1}{2}]}$ can be completely recovered from the sample points in X . Another important result in this direction is stated in terms of Berling density. Let

$$D(X) = \liminf_{r \rightarrow \infty} \inf_{y \in \mathbb{R}} \frac{\# [X \cap (y + [0, r])]}{r}.$$

If $D(X) > 1$, then any $f \in L^2 \cap B_{[-\frac{1}{2}, \frac{1}{2}]}$ can be reconstructed from its samples $\{f(x_j)/x_j \in X\}$ stably and uniquely. Conversely, if every $f \in L^2 \cap B_{[-\frac{1}{2}, \frac{1}{2}]}$ can be uniquely and stably

reconstructed from its samples then $D(X) \geq 1$ (see [11]). Notice that in all these cases f is assumed to be a band limited function, that is, its Fourier transform has a compact support.

The problem of nonuniform sampling in general shift invariant spaces was studied by Aldroubi and Gröchenig in [1]. In this paper they proved that if f belongs to a shift invariant space $V(\varphi)$, where φ is an n th order B-spline function, then f can be reconstructed stably and uniquely from a non-uniform sampled data. They have also obtained equivalent conditions for the stable set of sampling for $V(\varphi)$ for certain φ (see proposition 1 in [1]). A more detailed study of shift invariant spaces can be found in [2].

In this paper, we prove that if φ belongs to a more general class namely $\varphi \in \mathcal{F}_1$ given in definition 3.3, and if X is a non-uniform sample consisting of perturbed version of integers, then $f \in V(\varphi)$ can be reconstructed uniquely and stably.

Before stating other main results of this paper, we recall the following definitions.

Definition 1.1. *The Wiener amalgam space $W(L^p)$ ($1 \leq p < \infty$) is defined to be the class of measurable functions f satisfying*

$$\|f\|_{W(L^p)}^p := \sum_{k \in \mathbb{Z}} \text{ess sup}\{|f(x+k)|^p / x \in [0, 1]\} < \infty.$$

For the importance of these spaces and further details, we refer to [6] and [7]. Let $W_c(L^p)$ denote the class of functions in $W(L^p)$ which are continuous.

Definition 1.2. *A sampling set $X = \{x_j \in \mathbb{R} / j \in J\}$ is said to be a stable set of sampling for a class of functions in $V \subseteq L^2(\mathbb{R})$ if there exists $A, B > 0$ such that*

$$A\|f\|_2^2 \leq \sum_{x_j \in X} |f(x_j)|^2 \leq B\|f\|_2^2 \quad \forall f \in V. \quad (1.1)$$

Definition 1.3. *Shift-invariant space $V(\varphi)$: Let φ be a continuous real valued function on \mathbb{R} . Assume that $\exists A', B' > 0$ satisfying*

$$A'\|c\|_{\ell^2(\mathbb{Z})} \leq \left\| \sum_{k \in \mathbb{Z}} c_k \varphi(\cdot - k) \right\|_2 \leq B'\|c\|_{\ell^2(\mathbb{Z})}, \quad \forall c = (c_k) \in \ell^2(\mathbb{Z}) \quad (1.2)$$

Let $\tau_k \varphi$ be defined by $\tau_k \varphi(x) = \varphi(x - k)$, where $k \in \mathbb{Z}$ and

$$V(\varphi) := \left\{ f = \sum_{k \in \mathbb{Z}} c_k \tau_k \varphi / (c_k) \in \ell^2(\mathbb{Z}) \right\}.$$

Notice that $V(\varphi)$ is (integer)shift invariant, this means that if $f \in V(\varphi)$, then $\tau_k f \in V(\varphi)$, $\forall k \in \mathbb{Z}$.

The following theorem is proved in [1].

Theorem 1.4. *Let $\varphi \in W_c(L^1)$ and φ satisfy (1.2). Then $V(\varphi) \subseteq W_c(L^2)$ and the following conditions are equivalent:*

- (a) *X is a stable set of sampling for $V(\varphi)$*
- (b) *There exists constants $A_1, A_2 > 0$ such that*

$$A_1 \|c\|_{\ell^2(\mathbb{Z})} \leq \|Uc\|_{\ell^2(\mathbb{Z})} \leq A_2 \|c\|_{\ell^2(\mathbb{Z})}, \quad \forall c \in \ell^2(\mathbb{Z})$$

where U is an infinite matrix with entries $U_{jk} = \varphi(x_j - k)$, $j, k \in \mathbb{Z}$.

The condition (1.1) shows that the reconstruction is unique. The inequalities in theorem 1.4(b) show that the operator U is bounded and is also bounded below.

Obviously U satisfies these conditions if we take $\varphi(x) = \frac{\sin \pi x}{\pi x}$ and X is the class of integers or the perturbed version of integers. In fact this is the reformulation of the statements of Shannon's theorem and Kadec's theorem. To the best of our knowledge, it has been shown that U is bounded and is also bounded below only when $\varphi = \frac{\sin \pi x}{\pi x}$ or an n th order B-spline. In this paper, we show that if $\varphi \in \mathcal{F}_1$ and X is the perturbed version of integers, it turns out that U is invertible. This leads to the stable and unique reconstruction for all $f \in V(\varphi)$. We then give a reconstruction procedure and illustrate it with some examples using Matlab. The invertibility and projection method of Laurent operator along with recurrence relation between the solutions of the matrix equation of the finite dimensional truncations of an operator help us to obtain an iterative reconstruction procedure. The questions of speed, storage, complexity of the algorithms are not investigated and hence no claims are made in this regard.

We organize our paper as follows. In section 2, we discuss the invertibility of a Laurent operator and convergence of projection method for a Laurent operator. In section 3, we prove our main results. In section 4, we prove a recurrence relation between the solutions of the matrix equation of the finite dimensional truncations of an operator and discuss the reconstruction procedure. In section 5, we provide algorithm along with illustration.

2 Laurent Operators

In this section we briefly review some properties of Laurent operators and projection method applied to operator equation involving Laurent operators. A detailed treatment of these topics including proofs of theorems 2.2, 2.3, 2.4, 2.5 can be found in [9].

Definition 2.1. *A bounded operator A on $\ell^2(\mathbb{Z})$ is a Laurent operator if $\langle Ae_k, e_j \rangle$ depends on the difference $j - k$ only, where $\{e_n\}_{n=-\infty}^{\infty}$ is the standard orthonormal basis of $\ell^2(\mathbb{Z})$.*

Let 'a' be a bounded complex valued function on $[0, 1]$. Then

$$a_{mn} = \int_0^1 a(t) e^{2\pi i(m-n)t} dt = a_{m-n}, \quad \forall m, n \in \mathbb{Z}$$

which defines a Laurent operator A on $\ell^2(\mathbb{Z})$. In this case we say that A is the Laurent operator defined by 'a'. The function 'a' is called the symbol of A . The properties of the Laurent operator A and its symbol 'a' are closely related as shown by the following theorem.

Theorem 2.2. *Let A be the Laurent operator defined by the continuous function 'a'. Then A is invertible iff $a(t) \neq 0$ for each $0 \leq t \leq 1$.*

Theorem 2.3. *Let T be a bounded and invertible operator on $\ell^2(\mathbb{Z})$. If S is a bounded operator on $\ell^2(\mathbb{Z})$ and $\|S\| < \frac{1}{\|T^{-1}\|}$ then $T + S$ is invertible.*

Let $\{P_n\}$ denote a sequence of projection in $\mathcal{B}(H)$ (the class of bounded operators on a separable Hilbert space H) such that $P_n \rightarrow I$ in the strong operator topology. Given $T \in \mathcal{B}(H)$, consider $T_n = P_n T P_n$. The method of obtaining solution x of the operator equation $Tx = y$ as a limit (in the norm topology) of x^n satisfying $T_n x^n = P_n(y)$ is called a projection method. The projection method for T is said to converge if there exists an integer N_0 such that for each $y \in H$ and $n \geq N_0$, there exists a unique solution x^n satisfying $T_n x^n = P_n(y)$ and in addition the sequence $\{x^n\}$ converges to $T^{-1}y$. Let $\Pi(P_n)$ denote the class of invertible operators for which the projection method converges.

Let H denote the separable Hilbert space having an orthonormal basis $\{..., e_{-n}, e_{-n-1}, ..., e_{-1}, e_0, e_1, ..., e_{n-1}, e_n, ...\}$. Let H_n denote the closed subspace of H generated by $\{e_{-n}, ..., e_0, ..., e_n\}$. We shall need the following known theorems for proving the main results in the next section.

Theorem 2.4. *Suppose $T \in \Pi(P_n)$ and $M = \sup_{n \geq N} (\|(P_n T P_n)^{-1}\| + \|P_n\|)$. If $S \in \mathcal{B}(H)$ such that $\|S\| < \min\{\frac{1}{\|T^{-1}\|}, \frac{1}{M^2}\}$, then $T + S \in \Pi(P_n)$.*

Theorem 2.5. *Let T be an invertible Laurent operator with continuous symbol ω . Then the projection method converges for T iff the winding number of ω relative to zero is equal to zero.*

3 The Main Results

Definition 3.1. *Let \mathcal{F} denote the class of all complex valued continuous functions φ defined on \mathbb{R} satisfying the following conditions*

(i) $\exists c_1, c_2 > 0$ and $\alpha > 1$ such that

$$|\varphi(x)| \leq \frac{c_1}{1 + |x|^\alpha}, \quad |\hat{\varphi}(x)| \leq \frac{c_2}{1 + |x|^\alpha}, \quad \forall x \in \mathbb{R},$$

where $\hat{\varphi}$ denotes the Fourier transform of φ .

(ii) $\hat{\varphi}(x) \neq 0$ on some unit interval $[b, b+1]$, for some $b \in \mathbb{R}$.

Example 3.2. It is easy to show that

- the class of Hermite functions h_n where $h_n(x) = (-1)^n e^{\frac{x^2}{2}} \frac{d^n}{dx^n}(e^{-x^2})$, $n = 0, 1, \dots$ with $h_0 = e^{-\frac{x^2}{2}}$
- the function $\varphi_{2n} = \chi_{[a, a+1]} * \chi_{[a, a+1]} * \dots * \chi_{[a, a+1]}$, $2n-1$ fold convolution of a characteristic function on $[a, a+1]$, where $a \in \frac{\mathbb{Z}}{2}$ and $n \geq 1$

are contained in \mathcal{F} .

Proposition 3.3. Let $\varphi \in \mathcal{F}$. Then $V(\varphi)$ is a closed subspace of $L^2(\mathbb{R})$, $\{\tau_k \varphi / k \in \mathbb{Z}\}$ is a Riesz basis for $V(\varphi)$ and $V(\varphi) \subseteq W_c(L^2)$.

Proof. Since $\hat{\varphi}$ satisfies $|\hat{\varphi}(x)| \leq \frac{c_2}{1+|x|^\alpha}$, $\forall x \in \mathbb{R}$, it is easy to show that $\sum_{k \in \mathbb{Z}} |\hat{\varphi}(x+k)|^2 \leq M$, for some positive constant M . On the other hand as $\hat{\varphi}(x) \neq 0$ on the interval $[b, b+1]$ which is compact and $\hat{\varphi}$ is continuous, hence there exists a real number $m > 0$ such that $|\hat{\varphi}(x)|^2 \geq m$, $\forall x \in [b, b+1]$. Thus, we get

$$0 < m \leq \sum_{k \in \mathbb{Z}} |\hat{\varphi}(x+k)|^2 \leq M < \infty \quad \forall x \in \mathbb{R}.$$

But this is equivalent to the condition

$$A \|c\|_{\ell^2(\mathbb{Z})} \leq \left\| \sum_{k \in \mathbb{Z}} c_k \varphi(\cdot - k) \right\|_2 \leq B \|c\|_{\ell^2(\mathbb{Z})}, \quad \forall c = (c_k) \in \ell^2(\mathbb{Z})$$

for some $A > 0$ and $B < \infty$, which means that $V(\varphi)$ is closed and $\{\varphi(\cdot - k)\}$ forms a Riesz basis for $V(\varphi)$ (see [12] and [5] section 5.3).

Let $k \in \mathbb{Z}$ and $x \in [0, 1]$. Then we have

$$|\varphi(x+k)| \leq \frac{c_1}{1+|x+k|^\alpha} \leq \begin{cases} \frac{c_1}{1+|k+1|^\alpha}, & \text{for } k < 0 \\ \frac{c_1}{1+|k|^\alpha}, & \text{for } k \geq 0 \end{cases}$$

which implies that

$$\sum_{k \in \mathbb{Z}} \text{ess sup}\{|\varphi(x+k)| / x \in [0, 1]\} < \infty.$$

Hence $\varphi \in \mathcal{F} \subseteq W_c(L^1)$ and using theorem 1.4, $V(\varphi) \subseteq W_c(L^2)$. □

Theorem 3.4. Suppose $\varphi \in \mathcal{F}$ also satisfies an additional condition namely

$$\sum_{k \in \mathbb{Z}} \hat{\tilde{\varphi}}(t+k) \neq 0, \quad \forall t \in [0, 1] \tag{3.1}$$

where $\tilde{\varphi}(x) = \varphi(-x)$. Let T_φ be the infinite matrix defined by $(T_\varphi)_{jk} = \varphi(j-k)$ for $j, k \in \mathbb{Z}$. Then T_φ defines an invertible, Laurent operator on $\ell^2(\mathbb{Z})$.

Proof. Let $\varphi \in \mathcal{F}$. Consider the series

$$a(t) = \sum_{k \in \mathbb{Z}} \hat{\varphi}(t + k).$$

This series converges uniformly on $[0, 1]$ by Weierstrass M-test. Further $\tau_k \hat{\varphi}$ is continuous for each $k \in \mathbb{Z}$. Then it follows that $a = \sum_{k \in \mathbb{Z}} \tau_k \hat{\varphi}$ is convergent to a continuous function on $[0, 1]$ which also satisfies $a(0) = a(1)$. Corresponding to this function a , we can define a Laurent operator T_φ by

$$(T_\varphi)_{jk} = \int_0^1 a(t) e^{-2\pi i(j-k)t} dt = \varphi(j - k), \quad j, k \in \mathbb{Z}.$$

As φ is a continuous function satisfying 3.1 (b), the Poisson summation formula holds for $\hat{\varphi}$ viz

$$a(t) = \sum_{k \in \mathbb{Z}} \hat{\varphi}(t + k) = \sum_{k \in \mathbb{Z}} \varphi(k) e^{2\pi i k t}, \quad \forall t \in [0, 1].$$

In other words, ‘ a ’ is a symbol of T_φ . Since $a(t) \neq 0, \forall t \in [0, 1]$ and a is continuous which defines T_φ . By theorem 2.2, T_φ is invertible. \square

Definition 3.5. Let \mathcal{F}_1 denote the class of functions in \mathcal{F} satisfying (3.1).

Example 3.6. The functions φ_{2n} defined in Example 3.2 and $h_0 = e^{-\frac{x^2}{2}}$ belong to \mathcal{F}_1 .

Let $x_j = j, j \in \mathbb{Z}$. Then the following result can be proved in a straight forward manner using theorem 1.4 and 3.4.

Corollary 3.7. If $\varphi \in \mathcal{F}_1$, then \mathbb{Z} is a stable set of sampling for $V(\varphi)$.

Notation: Let $\varphi \in \mathcal{F}_1$ and $X = \{x_j \in \mathbb{R}/j \in \mathbb{Z}\}$. Let U_X denote the operator on $\ell^2(\mathbb{Z})$ given by the matrix $\alpha_{jk} = \varphi(x_j - k)$.

Definition 3.8. Let $\delta > 0$. Then a set $Y = \{y_j \in \mathbb{R}/j \in \mathbb{Z}\}$ is said to be in a δ -neighbourhood of X if $|x_j - y_j| < \delta, \forall j \in \mathbb{Z}$.

Next we prove the following theorem.

Theorem 3.9. Suppose φ is a continuous function on \mathbb{R} such that $|\varphi(x)| \leq \frac{c_1}{1+|x|^\alpha}$ for all $x \in \mathbb{R}$, for some $c_1 > 0, \alpha > 1$. Then $\forall \epsilon > 0, \exists \delta > 0$ such that whenever Y is in a δ -neighbourhood of X , $\|U_X - U_Y\| < \epsilon$.

Proof. Let φ be a function satisfying all the hypotheses. Then, $\exists M > 0$ such that

$$\sum_{k \in \mathbb{Z}} |\varphi(x + k)| \leq M < \infty, \quad \forall x \in \mathbb{R}.$$

Therefore, for given $\epsilon > 0$, there exists $N \in \mathbb{N}$ such that

$$\sum_{|k|>N} |\varphi(x+k)| < \frac{\epsilon}{4}, \quad \forall x \in \mathbb{R}.$$

Now, consider

$$\begin{aligned} \sum_{k \in \mathbb{Z}} |\varphi(x_j - k) - \varphi(y_j - k)| &= \sum_{|k| \leq N} |\varphi(x_j - k) - \varphi(y_j - k)| \\ &\quad + \sum_{|k| > N} |\varphi(x_j - k) - \varphi(y_j - k)| \\ &< \sum_{|k| \leq N} |\varphi(x_j - k) - \varphi(y_j - k)| + \frac{\epsilon}{2} \end{aligned}$$

where, $y_j \in \mathbb{R}$ and $j \in \mathbb{Z}$. By the given assumption on φ it can be easily shown that φ is uniformly continuous. Let $r = \frac{\epsilon}{2(2N+1)}$. Then $\exists \delta > 0$ such that whenever $|x - y| < \delta$, $x, y \in \mathbb{R} \Rightarrow |\varphi(x) - \varphi(y)| < r$. Take any set Y such that it is a δ -neighbourhood of X which implies that

$$\sum_{|k| \leq N} |\varphi(x_j - k) - \varphi(y_j - k)| \leq \frac{\epsilon}{2}, \quad \forall j \in \mathbb{N}$$

Now, we have

$$\sum_{k \in \mathbb{Z}} |\varphi(x_j - k) - \varphi(y_j - k)| < \epsilon, \quad \forall j \in \mathbb{N}. \quad (3.2)$$

Notice that $\sum_{k \in \mathbb{Z}} |\varphi(x+k)|$ is uniformly bounded in x and $|x_j - y_j| < \delta$, for $j \in \mathbb{Z}$. Instead of considering the sum over k , we shall consider the sum over j and proceed as before, we shall show that

$$\sum_{j \in \mathbb{Z}} |\varphi(x_j - k) - \varphi(y_j - k)| < \epsilon, \quad \forall k \in \mathbb{N}. \quad (3.3)$$

And we know that $\|A\| \leq \sqrt{\alpha\beta}$, where A is a bounded operator on $\ell^2(\mathbb{Z})$, $\alpha = \max_{j \in \mathbb{Z}} \sum_{k \in \mathbb{Z}} |A_{jk}|$ and $\beta = \max_{k \in \mathbb{Z}} \sum_{j \in \mathbb{Z}} |A_{jk}|$. Thus, using (3.2) and (3.3), we get

$$\|U_X - U_Y\| < \epsilon.$$

□

Corollary 3.10. *Let $\varphi \in \mathcal{F}_1$ and X be a stable set of sampling for $V(\varphi)$ such that U_X is invertible. Then $\exists \delta > 0$ such that whenever Y is in a δ -neighbourhood of X , U_Y is also invertible and Y is a stable set of sampling for $V(\varphi)$.*

Proof. Let Take $\epsilon = \frac{1}{\|U_X^{-1}\|}$. Then by theorem 3.9 and 2.3, U_Y is invertible. Thus the required result follows from theorem 1.4. \square

Corollary 3.11. *Let $\varphi \in \mathcal{F}_1$. Then $\exists \delta > 0$ such that if X is in a δ -neighbourhood of \mathbb{Z} , then X is a stable set of sampling for $V(\varphi)$ and U_X is invertible.*

Proof. By theorem 3.4, $T = U_{\mathbb{Z}}$ is invertible. Now applying Corollary 3.10, we get the required result. \square

Corollary 3.12. *Suppose $\varphi \in \mathcal{F}_1$ and $U_X \in \Pi(P_n)$. Then $\exists \delta > 0$ such that whenever Y is in a δ -neighbourhood of X , $U_Y \in \Pi(P_n)$.*

Proof. Let $M = \sup_{n \geq N} (\|(P_n U_X P_n)^{-1}\| + \|P_n\|)$. Take $\epsilon < \min\{\frac{1}{\|U_X^{-1}\|}, \frac{1}{M^2}\}$. Then the result follows from the theorem 3.9 and 2.4. \square

Theorem 3.13. *Let $\varphi \in \mathcal{F}_1$. Define*

$$a(t) = \omega(e^{2\pi it}) = \sum_{n \in \mathbb{Z}} \varphi(n) e^{2\pi i n t}.$$

Suppose φ satisfies one of the following conditions:

$$(i) \sum_{n \neq 0} |\varphi(n)| \leq |\varphi(0)|$$

or

$$(ii) \omega(e^{2\pi it}) \text{ is a (complex) constant multiple of a real valued function.}$$

Then the projection method converges for the operator T where $T_{jk} = \varphi(j - k)$, $j, k \in \mathbb{Z}$, that is $T = U_{\mathbb{Z}}$.

Proof. Since $\varphi \in \mathcal{F}_1$, it follows from theorem 3.4, that T is an invertible Laurent operator. Also $\omega(e^{2\pi it}) = a(t) = \sum_{k \in \mathbb{Z}} \hat{\varphi}(t + k)$ is a continuous symbol of T . Further if (i) holds, then

$$\begin{aligned} |\omega(e^{2\pi it}) - \varphi(0)| &= \left| \sum_{n \neq 0} \varphi(n) e^{2\pi i n t} \right| \\ &\leq \sum_{n \neq 0} |\varphi(n)| \\ &\leq |\varphi(0)|. \end{aligned}$$

Thus the curve ω lies inside the disc with centre $\varphi(0)$ and radius of $|\varphi(0)|$. Notice that the circle passes through the origin and $\omega(e^{2\pi it}) \neq 0$, $\forall t \in [0, 1]$, which means the curve

ω can not pass through the origin. Thus the winding number of ω relative to zero equals to zero. Hence the projection method for T converges.

If we assume (ii), then $\omega(e^{2\pi it}) = kg(t) \neq 0$, for all $t \in [0, 1]$ for some $k \in \mathbb{C}$. It is easy to see geometrically that ω is contained in as line segment not passing through the origin and hence the winding number of ω relative to zero is equal to zero. Hence the projection method for T converges in this case also. \square

Examples 3.14.

- The Gaussian function $g(x) = \frac{e^{-\alpha x^2}}{\sqrt{\pi\alpha}}$, $\alpha > 0$ satisfies both the conditions.
- We can choose φ to be the inverse Fourier transform of g where $g(\xi) = kp_n(\xi)e^{-\xi^2}$ where k is constant and $p_n(\xi) = a_0 + a_2\xi^2 + \dots + a_{2n}\xi^{2n}$, $a_{2m} \geq 0$ or even more generally we can choose p_n such that $p_n(\xi) \geq 0$, $\forall \xi \in \mathbb{R}$.
- $\varphi = \chi_{[-\frac{1}{2}, \frac{1}{2}]} * \chi_{[-\frac{1}{2}, \frac{1}{2}]} * \chi_{[-\frac{1}{2}, \frac{1}{2}]}$
- The projection method does not converge when $\varphi = \chi_{[a, a+1]} * \chi_{[a, a+1]}$, where $a \in \frac{\mathbb{Z}}{2} \setminus \{-\frac{1}{2}\}$. In fact, it is easy to show that $\varphi \in \mathcal{F}$, $\text{supp}(\varphi) \subseteq [2a, 2a+2]$ and $\omega(e^{2\pi it}) = \varphi(2a+1)e^{2\pi i(2a+1)t}$, which in turn implies that the winding number of ω relative to zero is nonzero.

4 A Reconstruction Procedure

In this section, we wish to present an iterative reconstruction algorithm for reconstructing function $f \in V(\varphi)$, $\varphi \in \mathcal{F}_1$. In order to do this, we prove a theorem which is useful in computing the solution of a finite matrix equation recursively. First, we introduce the notations. Consider an $(n+2) \times (n+2)$ real matrix equation given by

$$\begin{pmatrix} a_{11} & a_{12} & \cdots & a_{1,n+2} \\ a_{21} & a_{22} & \cdots & a_{2,n+2} \\ & & \cdots & \\ a_{n+2,1} & a_{n+2,2} & \cdots & a_{n+2,n+2} \end{pmatrix} \begin{pmatrix} x_1 \\ x_2 \\ \cdot \\ \cdot \\ x_{n+2} \end{pmatrix} = \begin{pmatrix} y_1 \\ y_2 \\ \cdot \\ \cdot \\ y_{n+2} \end{pmatrix} \quad (4.1)$$

We first write this in terms of block matrices. Let $R_i = (a_{i2} \ a_{i3} \ \dots \ a_{i,n+1})$, $C_i^T = (a_{2i} \ a_{3i} \ \dots \ a_{n+1,i})$, $i = 1, \dots, n+2$. Let $X_n^T = (x_2 \ x_3 \ \dots \ x_{n+1})$ and $Y_n^T = (y_2 \ y_3 \ \dots \ y_{n+1})$. Let T_{n+1} be the given matrix $T_{n+1} = (a_{ij})_{(n+2) \times (n+2)}$.

Let T_n be the matrix $\begin{pmatrix} a_{22} & \cdots & a_{2,n+1} \\ & \cdots & \\ a_{n+1,2} & \cdots & a_{n+1,n+1} \end{pmatrix}$. Then the matrix equation (4.1) becomes $T_{n+1}X = Y$. Now, we prove the following theorem.

Theorem 4.1. Suppose T_n and T_{n+1} are invertible. Then the solution X of matrix equation $T_{n+1}X = Y$ is given by $X^T = (x_1, X_n^T, x_{n+2})$ where

$$\begin{aligned} x_1 &= \frac{(y_1 - R_1 T_n^{-1} Y_n) \alpha - (y_{n+2} - R_{n+2} T_n^{-1} Y_n) \beta}{(a_{11} - R_1 T_n^{-1} C_1) \alpha - \beta (a_{n+2,1} - R_{n+2} T_n^{-1} C_1)} \\ x_{n+2} &= \frac{(a_{11} - R_1 T_n^{-1} C_1) (y_{n+2} - R_{n+2} T_n^{-1} Y_n) - (y_1 - R_1 T_n^{-1} Y_n) (a_{n+2,1} - R_{n+2} T_n^{-1} C_1)}{(a_{11} - R_1 T_n^{-1} C_1) \alpha - \beta (a_{n+2,1} - R_{n+2} T_n^{-1} C_1)} \\ X_n &= T_n^{-1} Y_n - T_n^{-1} C_1 x_1 - T_n^{-1} C_{n+2} x_{n+2} \\ \alpha &= (a_{n+2,n+2} - R_{n+2} T_n^{-1} C_{n+2}) \text{ and } \beta = (a_{1,n+2} - R_1 T_n^{-1} C_{n+2}). \end{aligned}$$

Proof. The equation $T_{n+1}X = Y$ can be written as a system of equations in the following manner

$$a_{11}x_1 + R_1X_n + a_{1,n+2}x_{n+2} = y_1 \quad (4.2)$$

$$C_1x_1 + T_nX_n + C_{n+2}x_{n+2} = Y_n \quad (4.3)$$

$$a_{n+2,1}x_1 + R_{n+2}X_n + a_{n+2,n+2}x_{n+2} = y_{n+2} \quad (4.4)$$

Since T_n is invertible, (4.3) can be solved to obtain X_n

$$X_n = T_n^{-1}Y_n - T_n^{-1}C_1x_1 - T_n^{-1}C_{n+2}x_{n+2} \quad (4.5)$$

Substitute (4.5) in (4.2) and (4.4), we get

$$a^{(n)}x_1 + b^{(n)}x_{n+2} = u^{(n)} \quad (4.6)$$

$$c^{(n)}x_1 + d^{(n)}x_{n+2} = v^{(n)} \quad (4.7)$$

where $a^{(n)} = a_{11} - R_1 T_n^{-1} C_1$, $b^{(n)} = a_{1,n+2} - R_1 T_n^{-1} C_{n+2}$, $c^{(n)} = a_{n+2,1} - R_{n+2} T_n^{-1} C_1$, $d^{(n)} = a_{n+2,n+2} - R_{n+2} T_n^{-1} C_{n+2}$, $u^{(n)} = y_1 - R_1 T_n^{-1} Y_n$, and $v^{(n)} = y_{n+2} - R_{n+2} T_n^{-1} Y_n$.

The above set of equations has a unique solution provided $a^{(n)}d^{(n)} - b^{(n)}c^{(n)} \neq 0$, we show that $a^{(n)}d^{(n)} - b^{(n)}c^{(n)} = \frac{\det T_{n+1}}{\det T_n}$, which in turn will give required result.

Now consider, T_{n+1} . This can be written as a product of two matrices A and B , where

$$A = \begin{pmatrix} a_{11} & R_1 T_n^{-1} & a_{1,n+2} \\ C_1 & I & C_{n+2} \\ a_{n+2,1} & R_{n+2} T_n^{-1} & a_{n+2,n+2} \end{pmatrix}, \quad B = \begin{pmatrix} 1 & 0 & 0 \\ 0 & T_n & 0 \\ 0 & 0 & 1 \end{pmatrix}$$

$\det A = \frac{\det T_{n+1}}{\det B} = \frac{\det T_{n+1}}{\det T_n}$, it is enough to show that $a^{(n)}d^{(n)} - b^{(n)}c^{(n)} = \det A$.

If $U^{(n)}$ denotes a column vector of row ' n ' and $V^{(n)}$ denote a row vector of column ' n ' and I_n denotes the identity matrix of order ' n ', then we have

$$\begin{vmatrix} I_n & U^{(n)} \\ V^{(n)} & d \end{vmatrix} = d - V^{(n)}U^{(n)} \quad (4.8)$$

$$\text{and } \begin{vmatrix} U^{(n)} & I_n \\ d & V^{(n)} \end{vmatrix} = (-1)^n (d - V^{(n)}U^{(n)}). \quad (4.9)$$

Let $R_1 T_n^{-1} = (b_{12} \dots b_{1,n+1})$ and $R_{n+2} T_n^{-1} = (b_{n+2,2} \dots b_{n+2,n+1})$. Expand determinant of A with respect to first row. The following coefficients are calculated using (4.8) and (4.9). Coefficient of a_{11} in $\det A$ is $a_{n+2,n+2} - R_{n+2} T_n^{-1} C_{n+2}$, coefficient of $a_{1,n+2}$ in $\det A$ is $(-1)^{n+1} [(-1)^n (a_{n+2,1} - R_{n+2} T_n^{-1} C_1)]$ which is equal to $R_{n+2} T_n^{-1} C_1 - a_{n+2,1}$ and coefficient of b_{1j} , $j = 2, \dots, n+1$ in $\det A$ is given by $(-1) a_{j1} [a_{n+2,n+2} - b_{n+2,n+1} a_{n+1,n+2} - \dots - b_{n+2,j+1} a_{j+1,n+2} - b_{n+2,j-1} a_{j-1,n+2} - \dots - b_{n+2,2} a_{2,n+2}] - a_{j,n+2} [a_{21} b_{n+2,2} + \dots + a_{j-1,1} b_{n+2,j-1} + a_{j+1,1} b_{n+2,j+1} + \dots + a_{n+1,1} b_{n+2,n+1} - a_{n+2,1}]$.

Now, $a^{(n)} d^{(n)} - b^{(n)} c^{(n)} = a_{11} (a_{n+2,n+2} - R_{n+2} T_n^{-1} C_{n+2}) - R_1 T_n^{-1} C_1 (a_{n+2,n+2} - R_{n+2} T_n^{-1} C_{n+2}) + R_1 T_n^{-1} C_{n+2} (a_{n+2,1} - R_{n+2} T_n^{-1} C_1) - a_{1,n+2} (a_{n+2,1} - R_{n+2} T_n^{-1} C_1)$
By expressing $a^{(n)} d^{(n)} - b^{(n)} c^{(n)}$ interms of $a_{11}, b_{12}, \dots, b_{1,n+1}, a_{1,n+2}$ and we can show by direct calculation that

$$a^{(n)} d^{(n)} - b^{(n)} c^{(n)} = \det A.$$

Thus the conclusion follows. \square

Now, assume that $\varphi \in \mathcal{F}_1$ and it satisfies the hypothesis of theorem 3.13. Then, by corollary 3.11 the infinite matrix U , given by $U_{jk} = \varphi(x_j - k)$, is invertible. By corollary 3.12, $U \in \Pi(P_n)$. Thus the solutions of $Ux = y$ can be obtained from its finite dimensional truncation $U_n x^n = y_n = y|_{R(P_n)}$. In order to provide the reconstruction algorithm, we know that $f \in V(\varphi)$ and $f = \sum_{k \in \mathbb{Z}} c_k \varphi(\cdot - k)$. Thus reconstructing f is equivalent to determining the sequence $c = \{c_n\} \in \ell^2(\mathbb{Z})$. We know the values of $\varphi(x_j - k)$ and we need to reconstruct ' f ' from these samples $f(x_j)$.

Now, $U_n x^n = y_n$ can be written as

$$\begin{pmatrix} a_{-n,-n} & R_{-n} & a_{-n,n} \\ C_{-n} & U_{n-1} & C_n \\ a_{n,-n} & R_n & a_{n,n} \end{pmatrix} \begin{pmatrix} x_{-n} \\ X_{n-1} \\ x_n \end{pmatrix} = \begin{pmatrix} y_{-n} \\ Y_{n-1} \\ y_n \end{pmatrix}$$

where $a_{jk} = \varphi(x_j - k)$. Thus we obtain the following algorithm using theorem 4.1.

5 Algorithm

Let $Z_n = U_n^{-1} Y_n$, $D_n = U_n^{-1} C_{-(n+1)}$, $E_n = U_n^{-1} C_{n+1}$, $U_{00} = a_{00}$ and e_i denote the vector whose i th element is one and other entries are zero. We further assume that every U_n is invertible and define $W_i^{(n)} = U_n^{-1} e_i$, $i = -n, \dots, n$. Let N be a large positive integer.

Step-1 Input the sample set $X = \{x_j / j = -N, \dots, N\}$ and $Y = (f(x_j))_{j=-N}^N$.

Step-2 Define $U_{jk} = \varphi(x_j - k)$, $j, k = -N, \dots, N$

$$Z_0 = \frac{f(x_0)}{U_{00}}; D_0 = \frac{C_{-1}}{U_{00}}; E_0 = \frac{C_1}{U_{00}}; W_0^{(0)} = \frac{e_0}{U_{00}};$$

Step-3 For $n = 1, \dots, N$ do the following

Step-3.1 To calculate $U^{-1}e_i$, for $i = -n, \dots, n$. Take $a^{(n)} = a_{-n,-n} - R_{-n}D_{n-1}$, $b^{(n)} = a_{-n,n} - R_{-n}E_{n-1}$, $c^{(n)} = a_{n,-n} - R_nD_{n-1}$, $d^{(n)} = a_{n,n} - R_nE_{n-1}$.

Step-3.2 For $i = -n, \dots, n$. Let

$$\begin{aligned} x_{-n} &= \frac{(e_i(-n) - R_{-n}W_i^{(n-1)})d^{(n)} - (e_i(n) - R_nW_i^{(n-1)})b^{(n)}}{a^{(n)}d^{(n)} - b^{(n)}c^{(n)}} \\ x_n &= \frac{(e_i(n) - R_nW_i^{(n-1)})a^{(n)} - (e_i(-n) - R_{-n}W_i^{(n-1)})c^{(n)}}{a^{(n)}d^{(n)} - b^{(n)}c^{(n)}} \\ X_{n-1} &= W_i^{(n-1)} - D_{n-1}x_{-n} - E_{n-1}x_n \\ W_i^{(n)} &= (x_{-n} \ X_{n-1}^T \ x_n)^T \end{aligned}$$

Step-3.3 Define

$$\begin{aligned} Z_n &= \sum_{i=-n}^n y_i W_i^{(n)} \\ D_n &= \sum_{i=-n}^n C_{-(n+1)}(i) W_i^{(n)} \\ E_n &= \sum_{i=-n}^n C_{n+1}(i) W_i^{(n)} \end{aligned}$$

Step-4 Let $d_k^N = Z_N(k)$, $k = -n, \dots, n$.

Reconstruct

$$f_r^N(x) = \sum_{k=-N}^N d_k^N \varphi(x - k)$$

and plot f_r^N .

Let $f(x) := \sum_{k \in \mathbb{Z}} c_k \varphi(x - k)$, $x \in \mathbb{R}$ be the function to be reconstructed and $f_r^N(x) := \sum_{k=-N}^N d_k^N \varphi(x - k)$, $x \in \mathbb{R}$ be the function reconstructed using the above algorithm with $2N + 1$ sample values $\{f(x_j) : |j| \leq N\}$.

Let $c = (c_k)_{k \in \mathbb{Z}}$, $d^N = \begin{cases} d_k^N & |k| \leq N \\ 0 & \text{otherwise} \end{cases}$

Then $c, d^N \in \ell^2(\mathbb{Z})$ and

$$f(x) - f_r^N(x) = \sum_{k \in \mathbb{Z}} (c_k - d_k^N) \varphi(x - k), \quad x \in \mathbb{R}.$$

Thus $f - f_r^N \in V(\varphi)$. The error in reconstruction can be defined as $E_N = \|f - f_r^N\|_2$ and relative error by $\frac{\|f - f_r^N\|_2}{\|f\|_2}$.

In practice, it may be difficult to estimate E_N directly. Hence we make use of the following observations:

1. Since φ satisfies the conditions of Definition 1.3 and $f - f_r^N \in V(\varphi)$, we have

$$A' \|c - d^N\|_{\ell^2(\mathbb{Z})} \leq \|f - f_r^N\|_2 \leq B' \|c - d^N\|_{\ell^2(\mathbb{Z})}.$$

2. Since X is a stable set of sampling for $V(\varphi)$ (see Definition 1.2),

$$A \|f - f_r^N\|_2^2 \leq \sum_{x_j \in X} |f(x_j) - f_r^N(x_j)|^2 \leq B \|f - f_r^N\|_2^2.$$

Hence in place of $\|f - f_r^N\|_2$, we can use any one of the following estimates:

$$\begin{aligned} E'_N &= \|c - d^N\|_{\ell^2(\mathbb{Z})} := \left(\sum_{k \in \mathbb{Z}} |c_k - d_k^N|^2 \right)^{\frac{1}{2}} \\ E''_N &= \left(\sum_{x_j \in X} |f(x_j) - f_r^N(x_j)|^2 \right)^{\frac{1}{2}} \end{aligned}$$

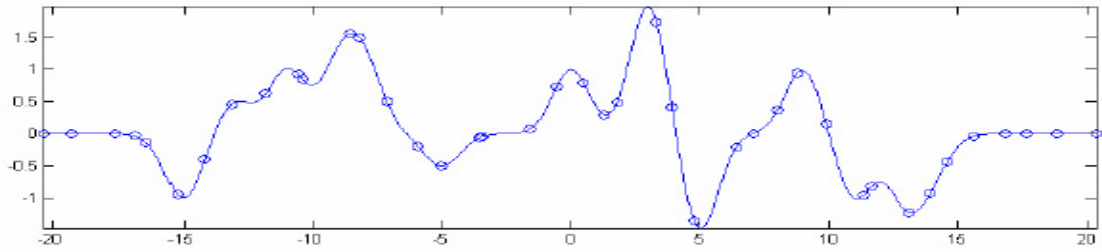
Again, in practice, we have to replace the infinite series in the above expressions by suitable finite(partial) sums.

The above algorithm is implemented using Matlab and results are shown in figure 1, 2 and figure 3. We plot the original function f and the corresponding reconstructed function f_r^N in the following figures. In figure 1, we take $\varphi(x) = e^{-x^2}$, $f(x) = \sum_{k=-15}^{k=15} c_k \varphi(x - k)$, where $c_0 = 1$, $c_3 = 2$, $c_5 = -\frac{3}{2}$, $c_9 = 1$, $c_{11} = -1$, $c_{13} = -1$, $c_{14} = -\frac{1}{2}$, $c_{-5} = -\frac{1}{2}$, $c_{-8} = 1$, $c_{-9} = 1$, $c_{-11} = 1$, $c_{-13} = \frac{1}{2}$, $c_{-15} = -1$ and remaining $c_i = 0$ with $\delta = 0.45$. We also tabulate E'_N and E''_N for various values of N in table 1.

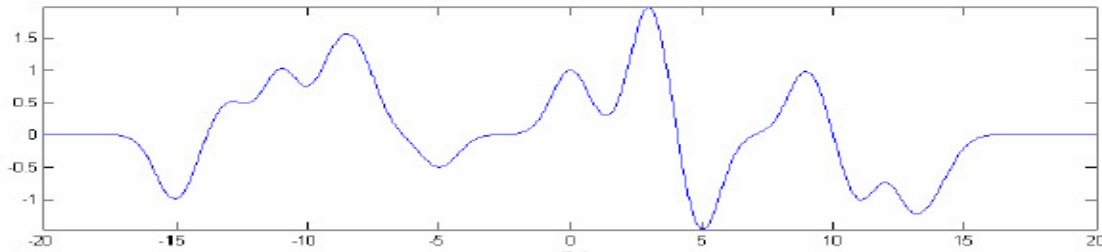
In figure 2, we take $\varphi(x) = (4x^2 - 2)e^{-x^2}$, $f(x) = \sum_{k=-15}^{k=15} c_k \varphi(x - k)$, where $c_0 = 1$, $c_3 = \frac{3}{2}$, $c_5 = -\frac{1}{2}$, $c_9 = \frac{3}{2}$, $c_{11} = -1$, $c_{13} = -1$, $c_{14} = 1\frac{1}{2}$, $c_{-5} = -\frac{1}{2}$, $c_{-8} = 1$, $c_{-9} = 1$, $c_{-11} = 1$, $c_{-13} = \frac{1}{2}$, $c_{-15} = -2$ and remaining $c_i = 0$ with $\delta = 0.1$. We also tabulate E'_N and E''_N for various values of N in table 2.

In figure 3, we take $\varphi = \chi_{[-\frac{1}{2}, \frac{1}{2}]} * \chi_{[-\frac{1}{2}, \frac{1}{2}]} * \chi_{[-\frac{1}{2}, \frac{1}{2}]}$, $f(x) = \sum_{k=-15}^{k=15} c_k \varphi(x - k)$, where $c_0 = 1$, $c_1 = \frac{1}{2}$, $c_2 = -\frac{1}{2}$, $c_3 = 2$, $c_5 = -\frac{3}{2}$, $c_6 = 1$, $c_8 = 3$, $c_9 = 1$, $c_{11} = -1$, $c_{13} = -1$, $c_{14} = -\frac{1}{2}$, $c_{-1} = -1$, $c_{-3} = 3$, $c_{-5} = -\frac{1}{2}$, $c_{-7} = -1$, $c_{-8} = 1$, $c_{-9} = 1$, $c_{-11} = 1$, $c_{-13} = \frac{1}{2}$, $c_{-15} = -1$ and remaining $c_i = 0$ with $\delta = 0.47$. We also tabulate E'_N and E''_N for various values of N in table 3.

In the following figures (a) denotes the original function and (b) denotes the reconstructed function.

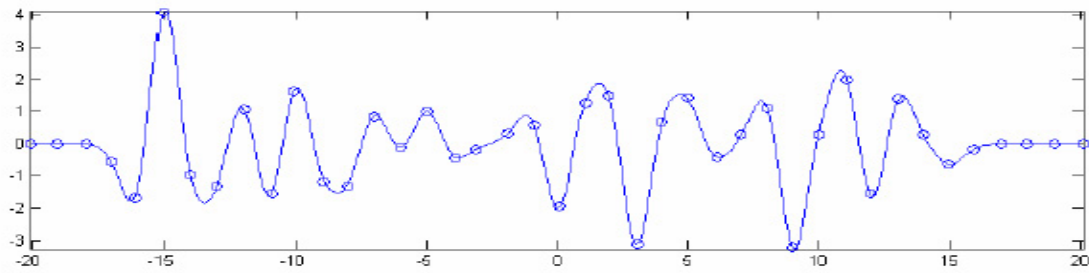


(a)

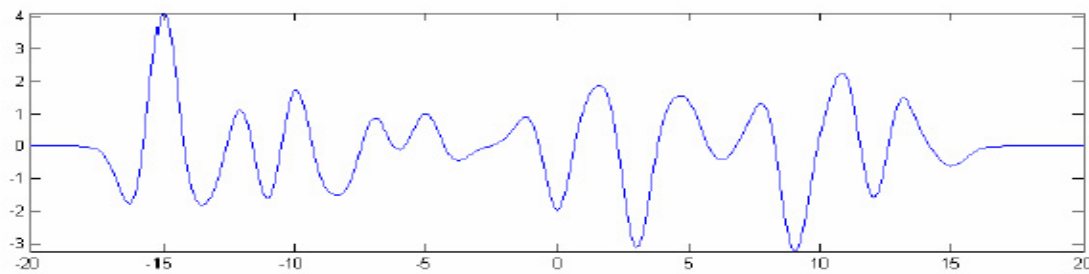


(b)

Figure 1



(a)



(b)

Figure 2

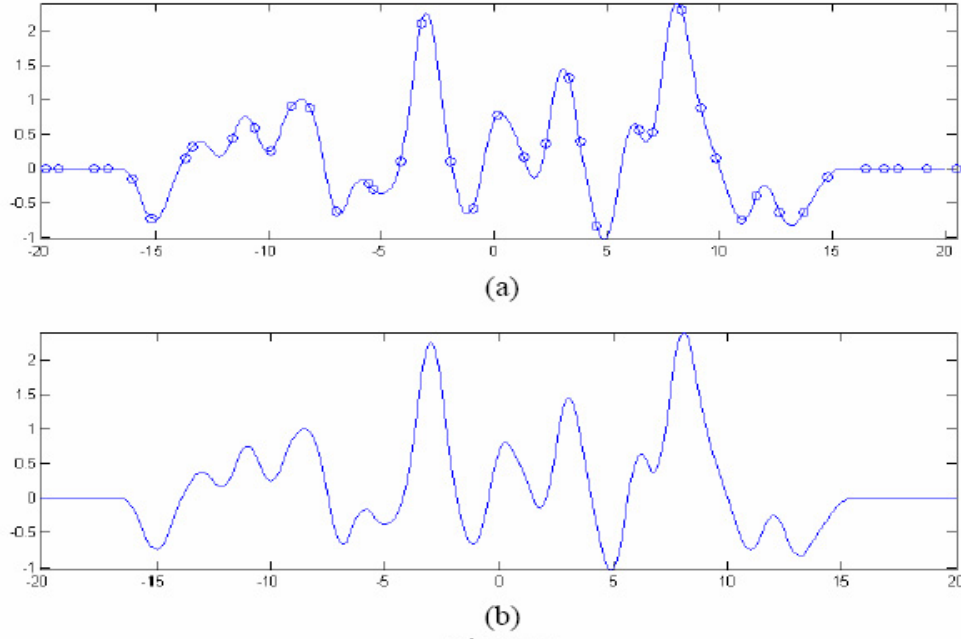


Figure 3

In all the above illustrations, we have taken $|j| \leq 1000$ to calculate E''_N .

N	E'_N	E''_N
5	2.7386	3.6458
10	2.3251	2.3823
15	2.2365×10^{-15}	2.5428×10^{-15}
20	2.9205×10^{-15}	3.7155×10^{-15}
30	2.8164×10^{-15}	2.5112×10^{-15}
50	2.9645×10^{-15}	2.1153×10^{-15}
100	2.9645×10^{-15}	2.1331×10^{-15}
300	2.9645×10^{-15}	2.1331×10^{-15}
600	2.9645×10^{-15}	2.1331×10^{-15}

Table 1

N	E'_N	E''_N
5	4.3045	3.7464
10	2.2617	1.6811
15	2.4863×10^{-15}	1.1985×10^{-15}
20	2.4918×10^{-15}	1.4652×10^{-15}
30	2.4216×10^{-15}	1.4530×10^{-15}
50	2.4698×10^{-15}	1.4180×10^{-15}
100	2.4698×10^{-15}	1.4180×10^{-15}
300	2.4698×10^{-15}	1.4180×10^{-15}
600	2.4698×10^{-15}	1.4180×10^{-15}

Table 3

N	E'_N	E''_N
5	3.4278	7.3028
10	3.3352	5.6506
15	1.1132×10^{-14}	2.2548×10^{-14}
20	1.9185×10^{-14}	4.2904×10^{-14}
30	3.5195×10^{-14}	8.0473×10^{-14}
50	6.6224×10^{-14}	1.4812×10^{-13}
100	9.9978×10^{-14}	2.2335×10^{-13}
300	1.4992×10^{-13}	3.0936×10^{-13}
500	1.4919×10^{-13}	3.1109×10^{-13}
700	1.4919×10^{-13}	3.1109×10^{-13}
900	1.4919×10^{-13}	3.1109×10^{-13}

Table 2

Remark 5.1. *In this paper, we have shown that if U is invertible and if the projection method converges for U , then it is possible to obtain a stable reconstruction of a function $f \in V(\varphi)$ from its samples. This again leads naturally to a question: “Which operators U have these properties?”. Sufficient conditions for this have been studied when U is a Toeplitz, block Toeplitz, Laurent, block Laurent operators in [4], [9] and tridiagonal operators in [3]. In future, if the above problem is solved for other class of operators, one can obtain reconstruction procedure for large class of functions.*

Acknowledgement

The authors thank National Board for Higher Mathematics, Department of Atomic Energy No: 48/4/2004/R & D-II/2119 for the financial grant.

References

- [1] A. Aldroubi and K. Gröchenig, Beurling-Landau-Type Theorems for Non-Uniform Sampling in Shift Invariant Spline Spaces, *J. Fourier Anal. and Appl.*, 6 (1):93 - 103 (2000).
- [2] A. Aldroubi and K. Gröchenig, Non-Uniform Sampling and Reconstruction in Shift-Invariant Spaces, *SIAM Rev.*, 43 (4):585 - 620 (2001).
- [3] R. Balasubramanian, S.H. Kulkarni and R. Radha, Solution of a tridiagonal operator equation, *Linear Algebra and its Applications*, 414(1):389 - 405 (2006).
- [4] A. Bottcher and B. Silberman, *Introduction to large truncated Toeplitz matrices*, Springer, New York (1998).
- [5] I. Daubechies, *Ten Lectures on Wavelets*, Society for Industrial and Applied Mathematics (SIAM), Philadelphia, PA (1992).

- [6] H.G. Feichtinger, New results on regular and irregular sampling based on Wiener amalgams, *Proc. Conf. Function Spaces* (K. Jarosz, Ed.), Lecture Notes in Mathematics, No. 136:107 - 121, Springer-Verlag, New York (1991).
- [7] H.G. Feichtinger, Wiener amalgams over Euclidean spaces and some of their applications, *Proc. Conf. Function Spaces* (K. Jarosz, Ed.), Lecture Notes in Mathematics, No. 136:123 - 137, Springer-Verlag, New York (1991).
- [8] K. Gröchenig and H. Schwab, Fast local reconstruction methods for nonuniform sampling in shift-invariant spaces, *SIAM J. Matrix Anal. and Appl.*, 24 (4):899 - 913 (2003).
- [9] I. Gohberg, S. Goldberg and M.A. Kaashoek, *Basic classes of linear operators*, Birkhauser Verlag (2003).
- [10] M.I. Kadec, The exact value of Paley-Wiener constants, *Soviet Math. Dokl.*, 5:559 - 561 (1964).
- [11] H. Landau, Necessary density conditions for sampling and interpolation of certain entire functions, *Acta Math.*, 117 : 37 - 52 (1967).
- [12] S.G. Mallat, Multiresolution approximations and wavelet orthonormal bases of $L^2(\mathbb{R})$, *Trans. Amer. Math. Soc.*, 315: 69 - 97 (1989).
- [13] C.E. Shannon, Communication in the presence of noise, *Proc. IRE*, 37(1):10-21 (1949).
- [14] L. Schumaker, *Spline Functions: Basic Theory*, Wiley-Interscience, Boston (1981).
- [15] E.M. Stein and G. Weiss, *Introduction to Fourier Analysis on Euclidean spaces*, Princeton University Press, Princeton, NJ (1971).

Common Fixed Point Theorems in IF-Metric Spaces

Servet Kutukcu

Department of Mathematics, Faculty of Science and Arts
Ondokuz Mayıs University, 55139 Kurupelit, Samsun, Turkey
E-mail: skutukcu@yahoo.com

September 7, 2007

Abstract

The purpose of this paper is to obtain common fixed point theorems for asymptotically commuting mappings in intuitionistic fuzzy metric spaces. This gives a generalization of the results by Mishra et al. [7]. Our results extend, generalize and fuzzify several fixed point theorems on metric spaces, Menger spaces and uniform spaces.

Keywords: Contraction, asymptotically commuting maps, compatible maps, intuitionistic fuzzy metric space

AMS Subject Classifications: 47H10, 54H25, 54A40

1 Introduction

After the pioneering work of Zadeh [12], one of the most important problems in fuzzy topology is to obtain an appropriate concept of (fuzzy) metric space and there has been a great effort to obtain (fuzzy) analogues of classical theories [1,2,5,10]. Recently, many authors have proved fixed point theorems [3,4,6-9,11].

The purpose of this paper is to obtain common fixed point theorems for asymptotically commuting mappings in intuitionistic fuzzy metric spaces. This gives a generalization of the results by Mishra et al. [7]. Also our results extend, generalize and fuzzify several fixed point theorems on metric spaces, Menger spaces and uniform spaces.

2 Preliminaries

Throughout this section, we use all symbols and basic definitions of Park [10].

DEFINITION 2.1. A 5-tuple $(X, M, N, *, \diamond)$ is said to be an intuitionistic fuzzy metric space (shortly IF-metric space) if X is an arbitrary set, $*$ is a continuous t -norm, \diamond is a continuous t -conorm and M, N are fuzzy sets on $X^2 \times (0, \infty)$ satisfying the following conditions: for all $x, y, z \in X$, $s, t > 0$,

(IFM-1) $M(x, y, t) + N(x, y, t) \leq 1$,

(IFM-2) $M(x, y, t) > 0$,

(IFM-3) $M(x, y, t) = 1$ if and only if $x = y$,

(IFM-4) $M(x, y, t) = M(y, x, t)$,

(IFM-5) $M(x, y, t) * M(y, z, s) \leq M(x, z, t + s)$,

(IFM-6) $M(x, y, \cdot) : (0, \infty) \rightarrow (0, 1]$ is continuous,

(IFM-7) $N(x, y, t) = 0$ if and only if $x = y$,

(IFM-8) $N(x, y, t) = N(y, x, t)$,

(IFM-9) $N(x, y, t) \diamond N(y, z, s) \geq N(x, z, t + s)$,

(IFM-10) $N(x, y, \cdot) : (0, \infty) \rightarrow [0, 1]$ is continuous.

Then (M, N) is called an intuitionistic fuzzy metric on X . The functions $M(x, y, t)$ and $N(x, y, t)$ denote the degree of nearness and the degree of non-nearness between x and y with respect to t , respectively.

DEFINITION 2.2. Let $(X, M, N, *, \diamond)$ be an IF-metric space. Then

- (a) a sequence $\{x_n\}$ in X is said to be convergent x in X if for each $\epsilon > 0$ and each $t > 0$, there exists $n_0 \in \mathbf{N}$ such that $M(x_n, x, t) > 1 - \epsilon$ and $N(x_n, x, t) < \epsilon$ for all $n \geq n_0$,
- (b) a sequence $\{x_n\}$ in X is said to be Cauchy if for each $\epsilon > 0$ and each $t > 0$, there exists $n_0 \in \mathbf{N}$ such that $M(x_n, x_m, t) > 1 - \epsilon$ and $N(x_n, x_m, t) < \epsilon$ for all $n, m \geq n_0$,
- (c) an IF-metric space in which every Cauchy sequence is convergent is said to be complete.

Throughout this paper, $(X, M, N, *, \diamond)$ will denote the IF-metric space with $\lim_{t \rightarrow \infty} M(x, y, t) = 1$ and $\lim_{t \rightarrow \infty} N(x, y, t) = 0$ for all $x, y \in X$.

LEMMA 2.1 ([6]). Let $\{y_n\}$ be a sequence in an IF-metric space $(X, M, N, *, \diamond)$. If there exists a constant $k \in (0, 1)$ such that $M(y_{n+2}, y_{n+1}, kt) \geq M(y_{n+1}, y_n, t)$ and $N(y_{n+2}, y_{n+1}, kt) \leq N(y_{n+1}, y_n, t)$ for all $t > 0$ and $n = 1, 2, 3, \dots$ then $\{y_n\}$ is a Cauchy sequence in X .

LEMMA 2.2 ([6]). Let $(X, M, N, *, \diamond)$ be an IF-metric space. If there exists $k \in (0, 1)$ such that $M(x, y, kt) \geq M(x, y, t)$ and $N(x, y, kt) \leq N(x, y, t)$ for $x, y \in X$. Then $x = y$.

3 Asymptotically Commuting Mappings and Common Fixed Points

DEFINITION 3.1. Two self mappings A and S of an IF-metric space $(X, M, N, *, \diamond)$ will be called z -asymptotically commuting (shortly asymptotically commuting) iff for all $t > 0$, $\lim_{n \rightarrow \infty} M(ASx_n, SAx_n, t) = 1$ and $\lim_{n \rightarrow \infty} N(ASx_n, SAx_n, t) = 0$ whenever $\{x_n\}$ is a sequence in X such that $\lim_{n \rightarrow \infty} Ax_n = \lim_{n \rightarrow \infty} Sx_n = z$ for some z in X .

An equivalent formulation of Definition 5 in a metric space is refer to Jungck [3,4]. Asymptotically commuting mappings may also be called compatible mappings. Such maps are more general than commuting and weakly commuting mappings.

Example. Let $X = [2, 20]$ with the usual metric d and define $M(x, y, t) = t/t + |x - y|$ and $N(x, y, t) = |x - y|/t + |x - y|$ for all $x, y \in X$ and $t > 0$. Clearly $(X, M, N, *, \diamond)$ is a complete IF-metric space where $*$ and \diamond are defined by $a * b = ab$ and $a \diamond b = \min \{1, a + b\}$ for all $a, b \in [0, 1]$. Let A and S be self mappings of X defined as

$$Ax = \begin{cases} 2, & x = 2 \text{ or } x > 5 \\ 8, & 2 < x \leq 5 \end{cases} \quad \text{and} \quad Bx = \begin{cases} 2, & x = 2 \\ 12 + x, & 2 < x \leq 5 \\ x - 3, & x > 5 \end{cases}$$

It can be easily verified that A and S are commuting and weakly commuting mappings but not asymptotically commuting mappings.

LEMMA 3.1. Let A and S are asymptotically commuting mappings on an IF-metric space $(X, M, N, *, \diamond)$ with $t * t \geq t$ and $(1 - t) \diamond (1 - t) \leq (1 - t)$ for all $t \in [0, 1]$. If $\{y_n\}$ is a sequence in X such that $Ay_n, Sy_n \rightarrow z$ for some z in X then $ASy_n \rightarrow Sy_n$ provided S is continuous at z .

Proof. By the continuity of S at z , $SAy_n \rightarrow Sz$ and $SSy_n \rightarrow Sz$. By the asymptotic commutativity of $\{A, S\}$, we have

$$M(ASy_n, SAy_n, t) \rightarrow 1 \text{ and } N(ASy_n, SAy_n, t) \rightarrow 0$$

as $n \rightarrow \infty$. Therefore

$$\begin{aligned} M(Sz, ASy_n, t) &\geq M(Sz, SAy_n, t/2) * M(SAy_n, ASy_n, t/2) \rightarrow 1, \\ N(Sz, ASy_n, t) &\leq N(Sz, SAy_n, t/2) \Diamond N(SAy_n, ASy_n, t/2) \rightarrow 0 \end{aligned}$$

as $n \rightarrow \infty$. This completes the proof.

THEOREM 3.1. *Let $(X, M, N, *, \Diamond)$ be a complete IF-metric space with $t * t \geq t$ and $(1 - t) \Diamond (1 - t) \leq (1 - t)$ for all $t \in [0, 1]$, and P, Q be self mappings of X . If there exist continuous self mappings S, T of X and a constant $k \in (0, 1)$ satisfying*

- (i) $PT(X) \subset ST(X)$ and $QS(X) \subset ST(X)$,
- (ii) $\{P, S\}$ and $\{Q, T\}$ are z -asymptotically commuting pairs,
- (iii) $ST = TS$,
- (iv)

$$\begin{aligned} M(Px, Qy, kt) &\geq M(Sx, Ty, t) * M(Px, Sx, t) * M(Qy, Ty, t) \\ &\quad * M(Px, Ty, \alpha t) * M(Qy, Sx, (2 - \alpha)t), \\ N(Px, Qy, kt) &\leq N(Sx, Ty, t) \Diamond N(Px, Sx, t) \Diamond N(Qy, Ty, t) \\ &\quad \Diamond N(Px, Ty, \alpha t) \Diamond N(Qy, Sx, (2 - \alpha)t) \end{aligned}$$

for all $x, y \in X, t > 0$ and $\alpha \in (0, 2)$. Then P, Q, S and T have a unique common fixed point.

Proof. Let x_0 be an arbitrary point of X . By (i), we can construct a sequence $\{x_n\}$ in X as follows:

$$PTx_{2n} = STx_{2n+1}, QSx_{2n+1} = STx_{2n+2}, n = 0, 1, 2, \dots$$

Indeed, such a sequence was first introduced in [7]. Now, let $z_n = STx_n$. Then, using (iii) and taking $x = Tx_{2n}, y = Sx_{2n+1}, \alpha = 1 - q, q \in (0, 1)$ in (iv), we have

$$\begin{aligned} M(PTx_{2n}, QSx_{2n+1}, kt) &\geq M(STx_{2n}, TSx_{2n+1}, t) * M(PTx_{2n}, STx_{2n}, t) \\ &\quad * M(QSx_{2n+1}, TSx_{2n+1}, t) * M(PTx_{2n}, TSx_{2n+1}, t) \\ &\quad * M(QSx_{2n+1}, STx_{2n}, (2 - \alpha)t), \\ N(PTx_{2n}, QSx_{2n+1}, kt) &\leq N(STx_{2n}, TSx_{2n+1}, t) \Diamond N(PTx_{2n}, STx_{2n}, t) \\ &\quad \Diamond N(QSx_{2n+1}, TSx_{2n+1}, t) \Diamond N(PTx_{2n}, TSx_{2n+1}, \alpha t) \\ &\quad \Diamond N(QSx_{2n+1}, STx_{2n}, (2 - \alpha)t). \end{aligned}$$

It follows that

$$\begin{aligned} M(z_{2n+1}, z_{2n+2}, kt) &\geq M(z_{2n}, z_{2n+1}, t) * M(z_{2n+1}, z_{2n}, t) * M(z_{2n+2}, z_{2n+1}, t) \\ &\quad * M(z_{2n+1}, z_{2n+1}, \alpha t) * M(z_{2n+2}, z_{2n}, (2 - \alpha)t) \\ &\geq M(z_{2n}, z_{2n+1}, t) * M(z_{2n+1}, z_{2n+2}, t) \\ &\quad * M(z_{2n+1}, z_{2n+1}, (1 - q)t) * M(z_{2n}, z_{2n+2}, (1 + q)t) \\ &\geq M(z_{2n}, z_{2n+1}, t) * M(z_{2n+1}, z_{2n+2}, t) * M(z_{2n}, z_{2n+1}, qt), \end{aligned}$$

$$\begin{aligned}
N(z_{2n+1}, z_{2n+2}, kt) &\leq N(z_{2n}, z_{2n+1}, t) \diamond N(z_{2n+1}, z_{2n}, t) \diamond N(z_{2n+2}, z_{2n+1}, t) \\
&\quad \diamond N(z_{2n+1}, z_{2n+1}, \alpha t) \diamond N(z_{2n+2}, z_{2n}, (2 - \alpha)t) \\
&\leq N(z_{2n}, z_{2n+1}, t) \diamond N(z_{2n+1}, z_{2n+2}, t) \\
&\quad \diamond N(z_{2n+1}, z_{2n+1}, (1 - q)t) \diamond N(z_{2n}, z_{2n+2}, (1 + q)t) \\
&\leq N(z_{2n}, z_{2n+1}, t) \diamond N(z_{2n+1}, z_{2n+2}, t) \diamond N(z_{2n}, z_{2n+1}, qt).
\end{aligned}$$

Since t-norm $*$ and t-conorm \diamond are continuous, letting $q \rightarrow 1$, we have

$$\begin{aligned}
M(z_{2n+1}, z_{2n+2}, kt) &\geq M(z_{2n}, z_{2n+1}, t) * M(z_{2n+1}, z_{2n+2}, t), \\
N(z_{2n+1}, z_{2n+2}, kt) &\leq N(z_{2n}, z_{2n+1}, t) \diamond N(z_{2n+1}, z_{2n+2}, t).
\end{aligned}$$

Similarly, using (iii) and taking $x = Tx_{2n+1}, y = Sx_{2n+2}, \alpha = 1 - q, q \in (0, 1)$ in (iv), we have

$$\begin{aligned}
M(z_{2n+2}, z_{2n+3}, kt) &\geq M(z_{2n+1}, z_{2n+2}, t) * M(z_{2n+2}, z_{2n+3}, t), \\
N(z_{2n+2}, z_{2n+3}, kt) &\leq N(z_{2n+1}, z_{2n+2}, t) \diamond N(z_{2n+2}, z_{2n+3}, t).
\end{aligned}$$

So, in general

$$\begin{aligned}
M(z_{m+1}, z_{m+2}, kt) &\geq M(z_m, z_{m+1}, t) * M(z_{m+1}, z_{m+2}, t), \\
N(z_{m+1}, z_{m+2}, kt) &\leq N(z_m, z_{m+1}, t) \diamond N(z_{m+1}, z_{m+2}, t)
\end{aligned}$$

for $m \in \mathbb{N}$. Consequently,

$$\begin{aligned}
M(z_{m+1}, z_{m+2}, kt) &\geq M(z_m, z_{m+1}, t) * M(z_{m+1}, z_{m+2}, tk^{-p}), \\
N(z_{m+1}, z_{m+2}, kt) &\leq N(z_m, z_{m+1}, t) \diamond N(z_{m+1}, z_{m+2}, tk^{-p})
\end{aligned}$$

for $m, p \in \mathbb{N}$. Since $M(z_{m+1}, z_{m+2}, tk^{-p}) \rightarrow 1$ and $N(z_{m+1}, z_{m+2}, tk^{-p}) \rightarrow 0$ as $p \rightarrow \infty$, we have $M(z_{m+1}, z_{m+2}, kt) \geq M(z_m, z_{m+1}, t)$ and $N(z_{m+1}, z_{m+2}, kt) \leq N(z_m, z_{m+1}, t)$ for $m \in \mathbb{N}$. Hence, by Lemma 2.1, $\{z_n\}$ is a Cauchy sequence in X . Since IF-metric space is complete, it converges to a point z in X . Since $\{PTx_{2n}\}$ and $\{QSw_{2n+1}\}$ are subsequences of $\{z_n\}$, $PTx_{2n} \rightarrow z$ and $QSw_{2n+1} \rightarrow z$ as $n \rightarrow \infty$. Let $y_n = Tx_n$ and $w_n = Sx_n$ for $n = 1, 2, \dots$. Then, we have $Py_{2n} \rightarrow z, Sy_{2n} \rightarrow z, Tw_{2n+1} \rightarrow z$ and $Qw_{2n+1} \rightarrow z$,

$$\begin{aligned}
M(PSy_{2n}, SPy_{2n}, t) &\rightarrow 1 \text{ and } N(PSy_{2n}, SPy_{2n}, t) \rightarrow 0 \\
M(QTw_{2n+1}, TQw_{2n+1}, t) &\rightarrow 1 \text{ and } N(QTw_{2n+1}, TQw_{2n+1}, t) \rightarrow 0
\end{aligned}$$

as $n \rightarrow \infty$. Moreover, by the continuity of T and Lemma 3.1, we have

$$TTw_{2n+1} \rightarrow Tz, QTw_{2n+1} \rightarrow Tz \text{ and } TQw_{2n+1} \rightarrow Tz$$

as $n \rightarrow \infty$. Now, taking $x = y_{2n}$ and $y = Tw_{2n+1}$ in (2) with $\alpha = 1$, we have

$$\begin{aligned}
M(Py_{2n}, QTw_{2n+1}, kt) &\geq M(Sy_{2n}, TTw_{2n+1}, t) * M(Py_{2n}, Sy_{2n}, t) \\
&\quad * M(QTw_{2n+1}, TTw_{2n+1}, t) * M(Py_{2n}, TTw_{2n+1}, t) \\
&\quad * M(QTw_{2n+1}, Sy_{2n}, t), \\
N(Py_{2n}, QTw_{2n+1}, kt) &\leq N(Sy_{2n}, TTw_{2n+1}, t) \diamond N(Py_{2n}, Sy_{2n}, t) \\
&\quad \diamond N(QTw_{2n+1}, TTw_{2n+1}, t) \diamond N(Py_{2n}, TTw_{2n+1}, t) \\
&\quad \diamond N(QTw_{2n+1}, Sy_{2n}, t).
\end{aligned}$$

Hence, these yield

$$\begin{aligned} M(z, Tz, kt) &\geq M(z, Tz, t) * 1 * 1 * M(z, Tz, t) * M(z, Tz, t) \geq M(z, Tz, t), \\ N(z, Tz, kt) &\leq N(z, Tz, t) \diamond 0 \diamond 0 \diamond N(z, Tz, t) \diamond N(z, Tz, t) \leq N(z, Tz, t). \end{aligned}$$

Thus, by Lemma 2.2, $z = Tz$. Similarly $z = Sz$. Now, taking $x = y_{2n}$ and $y = z$ in (2) with $\alpha = 1$, we have

$$\begin{aligned} M(Py_{2n}, Qz, kt) &\geq M(Sy_{2n}, Tz, t) * M(Py_{2n}, Sy_{2n}, t) * M(Qz, Tz, t) \\ &\quad * M(Py_{2n}, Tz, t) * M(Qz, Sy_{2n}, t), \\ N(Py_{2n}, Qz, kt) &\leq N(Sy_{2n}, Tz, t) \diamond N(Py_{2n}, Sy_{2n}, t) \diamond N(Qz, Tz, t) \\ &\quad \diamond N(Py_{2n}, Tz, t) \diamond N(Qz, Sy_{2n}, t). \end{aligned}$$

Hence, these yield

$$\begin{aligned} M(z, Qz, kt) &\geq 1 * 1 * M(Qz, z, t) * 1 * M(Qz, z, t) \geq M(z, Qz, t), \\ N(z, Tz, kt) &\leq 0 \diamond 0 \diamond N(Qz, z, t) \diamond 0 \diamond N(Qz, z, t) \leq N(z, Qz, t). \end{aligned}$$

Thus, by Lemma 2.2, $z = Qz$. Similarly $z = Pz$. So, z is a common fixed point of P, Q, S and T . Let v be another ($v \neq z$) common fixed point of P, Q, S and T . Then, taking $x = z, y = v$ in (iv) with $\alpha = 1$, we have

$$\begin{aligned} M(z, v, kt) &= M(Pz, Qv, kt) \geq M(Sz, Tv, t) * M(Pz, Sz, t) * M(Qv, Tv, t) \\ &\quad * M(Pz, Tv, t) * M(Qv, Sz, t) \\ &\geq M(z, v, t) * 1 * 1 * M(z, v, t) * M(z, v, t) \geq M(z, v, t), \\ N(z, v, kt) &= N(Pz, Qv, kt) \leq N(Sz, Tv, t) \diamond N(Pz, Sz, t) \diamond N(Qv, Tv, t) \\ &\quad \diamond N(Pz, Tv, t) \diamond N(Qv, Sz, t) \\ &\leq N(z, v, t) \diamond 0 \diamond 0 \diamond N(z, v, t) \diamond N(z, v, t) \leq N(z, v, t) \end{aligned}$$

Thus, by Lemma 2.2, $z = v$. Hence P, Q, S and T have a unique common fixed point.

If we take $S = T = I^X$ (the identity mapping of X), we have:

COROLLARY 3.1. *Let $(X, M, N, *, \diamond)$ be a complete IF-metric space with $t * t \geq t$ and $(1 - t) \diamond (1 - t) \leq (1 - t)$ for all $t \in [0, 1]$, and P, Q be self mappings of X . If there exists a constant $k \in (0, 1)$ satisfying*

$$\begin{aligned} M(Px, Qy, kt) &\geq M(x, y, t) * M(Px, x, t) * M(Qy, y, t) \\ &\quad * M(Px, y, \alpha t) * M(Qy, x, (2 - \alpha)t), \\ N(Px, Qy, kt) &\leq N(x, y, t) \diamond N(Px, x, t) \diamond N(Qy, y, t) \\ &\quad \diamond N(Px, y, \alpha t) \diamond N(Qy, x, (2 - \alpha)t) \end{aligned}$$

for all $x, y \in X, t > 0$ and $\alpha \in (0, 2)$. Then P and Q have a unique common fixed point.

If we take $P = Q$ and $S = T$, we have:

COROLLARY 3.2. *Let $(X, M, N, *, \diamond)$ be a complete IF-metric space with $t * t \geq t$ and $(1 - t) \diamond (1 - t) \leq (1 - t)$ for all $t \in [0, 1]$, and P be self mapping of X . If S is continuous and there exists a constant $k \in (0, 1)$ satisfying*

$$\begin{aligned} M(Px, Py, kt) &\geq M(Sx, Sy, t) * M(Px, Sx, t) * M(Py, Sy, t) \\ &\quad * M(Px, Sy, \alpha t) * M(Py, Sx, (2 - \alpha)t), \\ N(Px, Py, kt) &\leq N(Sx, Sy, t) \diamond N(Px, Sx, t) \diamond N(Py, Sy, t) \\ &\quad \diamond N(Px, Sy, \alpha t) \diamond N(Py, Sx, (2 - \alpha)t) \end{aligned}$$

for all $x, y \in X, t > 0$ and $\alpha \in (0, 2)$. Then P and S have a unique common fixed point.

Now, we prove the projection of Theorem 3.1 from complete IF-metric space to complete metric space:

THEOREM 3.2. *Let P, Q, S and T be self mappings on a complete metric space (X, d) satisfying (i)-(iii) of Theorem 2. If there exists $k \in (0, 1)$ such that*

$$d(Px, Qy) \leq k \max \left\{ \begin{array}{l} d(Sx, Px), d(Ty, Qy), d(Sx, Ty), \\ [d(Ty, Px) + d(Sx, Qy)] / 2 \end{array} \right\}$$

for all $x, y \in X$, then P, Q, S and T have a unique common fixed point in X .

Proof. The proof follows from Theorem 3.1 considering the induced IF-metric space $(X, M, N, *, \diamond)$ (see [10]), where $a * b = ab$, $a \diamond b = \min \{1, a + b\}$, $M(x, y, t) = t/t + d(x, y)$ and $N(x, y, t) = d(x, y)/t + d(x, y)$.

References

- [1] K. Atanassov, Intuitionistic fuzzy sets, *Fuzzy Sets and Systems* **20** (1986), 87-96.
- [2] A. George, P. Veeramani, On some results in fuzzy metric spaces, *Fuzzy Sets and Systems* **64** (1994), 395-399.
- [3] G. Jungck, Compatible mappings and common fixed points, *Internat. J. Math. & Math. Sci.* **9** (1986), 771-779.
- [4] G. Jungck, Common fixed points for commuting and compatible maps on compacta, *Proc. Amer. Math. Soc.* **103** (1988), 977-983.
- [5] O. Kramosil and J. Michalek, Fuzzy metric and statistical metric spaces, *Kybernetika* **11** (1975), 326-334.
- [6] S. Kutukcu, S. Sharma, Some properties of intuitionistic fuzzy metric spaces, *J. Appl. Func. Anal.*, in press.
- [7] S.N. Mishra, N. Sharma, S.L. Singh, Common fixed points of maps on fuzzy metric spaces, *Internat. J. Math. & Math. Sci.* **17** (1994), 253-258.
- [8] R.P. Pant, Common fixed points of four mappings, *Bull. Cal. Math. Soc.* **90** (1998), 281-286.
- [9] R.P. Pant, Common fixed point theorems for contractive maps, *J. Math. Anal. Appl.* **226** (1998), 251-258.
- [10] J.H. Park, Intuitionistic fuzzy metric spaces, *Chaos, Solitons & Fractals* **22** (2004), 1039-1046.
- [11] R. Vasuki, Common fixed points for R-weakly commuting maps in fuzzy metric spaces, *Indian J. Pure Appl. Math.* **30** (1999), 419-423.
- [12] L.A. Zadeh, Fuzzy sets, *Inform. and Control* **8** (1965), 338-353.

Analysis of the Factors Influencing Momentum Profits

Almira Biglova

Department of Econometrics, Statistics
and Mathematical Finance
School of Economics and Business Engineering
University of Karlsruhe
Kollegium am Schloss, Bau II, 20.12, R210
Postfach 6980, D-76128, Karlsruhe, Germany
E-mail: biglovaalmira@mail.ru

Svetlozar Rachev *

Chair of Econometrics, Statistics
and Mathematical Finance
School of Economics and Business Engineering
University of Karlsruhe and Karlsruhe Institute of Technology (KIT)
Postfach 6980, 76128 Karlsruhe, Germany and
Department of Statistics and Applied Probability
University of California, Santa Barbara
CA 93106-3110, USA
E-mail: rachev@statistik.uni-karlsruhe.de

Stoyan Stoyanov

Finanalytica Inc., Seattle, USA, and
Department of Econometrics, Statistics
and Mathematical Finance
School of Economics and Business Engineering
University of Karlsruhe and Karlsruhe Institute of Technology (KIT)
Kollegium am Schloss, Bau II, 20.12, R210
Postfach 6980, D-76128, Karlsruhe, Germany
E-mail: stoyan.stoyanov@finanalytica.com

Sergio Ortobelli

Department MSIA
University of Bergamo,
Via dei Caniana, 2 - 24127-Bergamo- Italy
E-mail: sergio.ortobelli@unibg.it

Abstract: In this paper, we provide further insight into the stock return momentum phenomena by investigating the sources of momentum profits. Applying statistical factor analysis, we identify the most important variables significantly affecting momentum profits: volatility and changes in the currency component of M1. We also document the periodic dynamics of momentum returns that is their inflation at quarter-, month- and year- ends and their deflation at quarter-, month- and year - beginnings.

Key words: momentum strategies, momentum effect, risk-adjusted criteria, factor models.

* Contact Author.

1 Introduction

This paper analyzes and discusses the motivations of the profitability of momentum strategies in US market. In particular, we investigate and examine the factors that influence momentum profits. Doing so, we distinguish the main fundamental, macroeconomic and statistical variables which have an impact on momentum strategies based on optimal performance ratios (see Biglova, et al (2004b)).

Several empirical studies have shown that stocks with high returns over the past three to twelve months continue to perform well in future periods. Any momentum strategy is based on a mechanistic decision criterion for evaluating and ranking the stock performance. For example, Jagadeesh and Titman (1993) and Grundy and Martin (2001), use the cumulative return as criterion for ranking stocks into winner and loser portfolios. Alternatively to these analyses we apply performance ratios in the ranking process as shown by Biglova et al. (2004b). Since abnormal returns can be considered only if we assume that return distributions present heavy tails, the ranking criteria should consider the possibility that the return could have infinite variance. Therefore, our strategies use the performance ratios introduced in Biglova, et al (2004a), that are also applicable in the case of stable distributed returns (with finite mean) as criteria for constructing winner and loser portfolios. On the other hand, the existence of momentum strategies, based on the Rachev performance ratio have been empirically proved (see Biglova et al. (2004b)).

The contrasting interpretations of the possible causes of momentum effect have generated a heated debate in the recent literature (see Jagadeesh and Titman (1993), Rouwenhorst (1998) Griffin, et al. (2003)). A first justification given by Kahneman and Tversky (1982) and De Bondt and Thaler (1985) was based on market participants overreaction to information. However, Jagadeesh and Titman (1993) and others have shown that this motivation is insufficient to justify properly the higher returns achieved in momentum strategies. Moreover neither Fama and French (1996) or Chordia and Shivakumar (2002) multi-factor models (used to mimic portfolio returns), or the conditional CAPM (see Lewellen and Nagel (2004)) could explain the abnormal momentum returns.

In this paper, we investigate the major sources of momentum profits. Therefore first we determine the momentum profits with the Rachev ratio performance criterion applied at the components of the S&P500. To test which factors influence momentum profits, we examine the factors of the spread of the winner and loser portfolios. In particular we try to identify how momentum returns are related to fundamental, country-specific macroeconomic, and statistic factors. Finally we interpret those factors that better explain abnormal returns.

The remainder of the paper is organized as follows: Section 2 provides a brief description of the data and methodology and examines the profitability of momentum strategies. Section 3 provides an analysis of factors, that have an influence on momentum profits and Section 4 concludes the paper.

2 Algorithm of Momentum Strategies

In momentum strategies, there are the following three main decision steps (1) the length of the ranking or formation period, (2) the length of the holding or investment period, and (3) the ranking criterion. The strategy consists in selling losers and buying winners assets at the end of the ranking period and assessing their performance over the holding period. Biglova et al. (2004b) have shown that we obtain optimal length of the ranking period and holding period with “6-month/6-month” momentum strategy (also defined 6/6 strategy). This strategy involves evaluating returns over the past 6-months and holding the position for the next 6 months. Thus we first determine winners and losers based on prior returns in the ranking period, then the zero-investment, self-financing strategy generates momentum profits in the holding period. In particular, Bris et al. (2004) have shown that such zero-investment strategy is applicable in international equity investment management practice.

2.1 Description of the Data and Methodology

Usually in the momentum strategies literature, the stocks are ranked in ascending order. “Winners” are those stocks with the top 10% ranking-period returns and “losers” are those stocks with the lowest 10% ranking-period returns. Optimal winner and loser portfolios at formation are constructed and held for 6 months (the holding period). During the holding period, these portfolios are not rebalanced.

We consider all the stocks included in the S&P500 index over the 12-year time period from January 1992 to December 2003. Over that time period, there were more than 800 companies included in the index. However, we apply momentum strategies only on those companies that had a complete return history (3,026 observations). Therefore we have not included many of the components of the S&P500 index since they have shorter historical series with unequal histories. For the risk-free asset, we use daily observations of the one-month London interbank offered rate (US\$ Libor). We use daily log returns $r_t^i = \ln((S_t^i + D_{[t-1,t]}^i)/S_{t-1}^i)$ $i=0, \dots, N$; $t=1, \dots, T$ where S_t^i is the i -th stock price at time t , $D_{[t-1,t]}^i$ is the dividend on i -th asset during the period $[t-1, t]$, and r_t^0 is the risk-free log return valued at time t . Our procedure for implementation of momentum strategy is briefly summarized here below.

Step 1. Consider the matrix of excess returns $ER = [a_{i,j}]$ where $a_{i,j} = r_t^j - r_t^0$ is the i -th observation of the excess return ($i=1, \dots, T$ observations) on the j -th asset ($j=1, \dots, N$ assets)

Step 2. Divide the data into sub-periods equal to the length of the formation period. Compute the ranking ratio for each stock based on observations in this period and rank the stocks. The 10% of stocks with the highest ratio values will constitute winner portfolio, and the 10% stocks with the lowest ratio will form the loser portfolio.

Step 3. Form the zero-investment portfolios of winners and losers at the end of each formation period of 6-months (taking a long position in the winner top

decile portfolio and a short position in the bottom loser decile portfolio).

Step 4. Evaluate the performance of the winner and loser portfolios and of the zero-cost strategy at the end of each holding period taking into account the transaction costs.

2.2 Risk-Adjusted Criteria for Stock Ranking

In constructing a momentum portfolio, first we have to specify the criteria for forming a winner and loser portfolios. In previous studies the winners were those stocks with the highest past cumulative monthly returns over some ranking period (e.g., six-month monthly return for the six-month ranking period). Clearly this selection criterion does not consider the riskiness and the distributional behavior of the stock in the ranking period. Since abnormal returns can be considered only assuming heavy tailed return distributions, it would be more appropriate to develop a selection criterion applicable to non-Gaussian distributed asset returns. For example, stable non Gaussian distributions are fat-tailed and they do not admit finite variance even if they satisfy many of the properties of a Gaussian law. Moreover, stable distributions have been used to model both the unconditional and conditional returns, as well as theoretical framework of portfolio theory and market equilibrium models (see Rachev (2003)).

2.2.1 Alternative Risk Measures and Risk-Return Ratios

In the last years, several alternative measures have been proposed and used in portfolio theory to capture non-normality of asset returns (see Rachev et al (2008a) and the reference therein). Among these we recall a coherent risk measure, called Expected Tail Loss (ETL), also known as Total Value at Risk, Expected Shortfall, Conditional Value-at-Risk (CVaR) , is defined as

$$ETL_{\alpha}(X) = \frac{1}{\alpha} \int_0^{\alpha} VaR_q(X) dq,$$

where $VaR_q(X) = -F_X^{-1}(q) = -\inf \{x | P(X \leq x) > q\}$ is the Value-at-Risk (VaR) of the random return X . If we assume a continuous distribution for the probability law of X , then $ETL_{\alpha}(X) = -E(X | X \leq -VaR_{\alpha}(X))$ and thus, ETL can be interpreted as the average loss beyond VaR, see Rachev et al. (2008a). Expected tail loss conveys the information about the expected size of a loss exceeding VaR. For example, suppose that a portfolio's risk is calculated through the simulation. For 1,000 simulations and $\alpha = 0.95$, the portfolio's VaR would be the smallest of the 50 largest losses. The corresponding expected shortfall would be then estimated by the numerical average of these 50 largest losses.

These alternative risk-return performance measures can be used as criterion in forming momentum portfolios. One of these ratios is the Rachev ratio (denoted by R- ratio). This ratio with parameters α and β is defined as:

$$RR(\alpha, \beta) := RR_{(\alpha, \beta)}(r) := \frac{ETL_{\alpha 100\%}(r_f - r)}{ETL_{\beta 100\%}(r - r_f)},$$

where α and β are in $[0,1]$. Here, r denotes the return of a portfolio or asset over the given time horizon. The R-ratio is applied for different parameters α and β . The parameters α and β cover different significance levels of the right and left tail distribution, respectively. As observed by Rachev et al. (2008) investors that maximize the R-ratio prefer more than less and they are neither risk averse nor risk lover investors. The use of the R-ratio is largely justified by the investors behavior. As a matter of fact several empirical analyses have shown that investors who maximize this ratio increase their final wealth much more than using other performance ratios (see Biglova, et al (2004a)).

Biglova, et al (2004a) analyzed and compared the traditional Sharpe ratio (Sharpe (1994)) with alternative R-ratios for various parameter values that define different level of coverage of the tail of the distribution, demonstrating that statistical arbitrage approach based on alternative criterion generates more profitable momentum strategies than those based on the conventional cumulative or total return criterion. Results of that study are robust to transaction costs for both equal-weighted and optimized-weighted strategies. In particular, they find that empirically alternative R ratios outperform the cumulative return and the Sharpe ratio across all momentum strategies that they investigated, and measured by total realized return and independent performance measures over the observed period.

2.3 Optimization of Winner and Loser Portfolios Based on Risk-Return Criteria

Let us summarize our risk-adjusted criteria for construction of momentum strategies. First we identify winners and losers among the extreme deciles of stocks in S&P500 ordered with respect to the risk-return ratio measure. At any rebalancing time point, we solve two optimization problems where we still use the R-ratio as an objective function in the optimization. In particular, we maximize among the winners the R-ratio with α and β both equal to 0.05 and we minimize among the losers the same R-ratio. We choose these α and β since the empirical evidence has shown the possibility of momentum strategies for these values (see Biglova et al. (2004b)). Therefore, for any risk-return criterion, we can compute the optimal winner portfolio from the following optimization problem:

$$\begin{aligned} & \max_x RR_{(0.05, 0.05)}(x'r) \\ & \text{subject to} \\ & \sum_{i=1}^n x_i = 1; x_i \geq 0; i = 1, \dots, n \end{aligned} \tag{1}$$

and the following optimization problem to determine the loser portfolio:

$$\begin{aligned} \min_x & RR_{(0.05,0.05)}(x'r) \\ \text{subject to} & \\ \sum_{i=1}^n x_i &= 1; x_i \geq 0; i = 1, \dots, n \end{aligned} \quad (2)$$

where $x = (x_1, \dots, x_n)'$ represents portfolio weights in the winner and loser portfolios, respectively, and n is the number of stocks in winner or loser portfolio. Note that the constraint on positive weights is necessary since within the winner portfolio further short-selling is not plausible. The same holds for the loser portfolio.

By solving the two optimization problems above, we adjust the proportion of stocks in the winner and loser portfolio according to the obtained weights. We calculate the profits and the spread values between the winner portfolio and the loser portfolio for an optimized-weighted 6/6 strategy over the holding periods. We also take into account that the investor pays proportional transaction costs of 0.485% on the absolute difference of the changes of portfolio compositions (see Biglova et al. (2004b)). The sequence of the spread values (total 2865 observations: starting from observation on day 162 till observation on day 3026) is used as independent variable, which we intend to explain, in factor models described in Section 3.

3 Types of Factors influencing Momentum Profits and Their Estimation

Let us recall some basic facts on factor models (for more detailed information see Rachev et al (2008b)). In financial econometrics, the factors used in factor models can be divided into three categories: fundamental factors, macroeconomic factors, and statistical factors.

Macroeconomic factors are economic variables that would affect asset returns. In particular, macroeconomic variables are exogenous factors that influence the model variables but are not influenced by them. Among the macroeconomic variables we tested the following U.S. potential factors: exports, imports, inflation rate, currency component of M1, Industrial Production Index, S&P 500 dividend yield, corporate spread. Fundamental factors are variables that are derived from financial analysis and characterize the momentum strategy. As fundamental factors we used variables proxying for the effect of timing, the influence of volatility, and the influence of the market state. In contrast, the statistical factors are endogenous factors that should derive from the mathematical process. In particular, the statistical factors should be determined either with principal component analysis or with a factor analysis. These factors are hidden variables that can be seen as a linear combinations of all the variables and they often permit some important economic interpretations. Next, we describe how the various factors, that we obtain from an estimated factor model, influence momentum profits.

3.1 Fundamental factors: Influence of the effect of “timing” on momentum profits

In this subsection we employ a factor model to assess the effect of “timing” in momentum strategies.

It’s well documented (see Haugen and Lakonishok (1988), Harris (1989), Musto (1997) Carhart et al. (2002) and the reference therein) that the “timing” could have an important influence on the amount of portfolio momentum strategy, in particular at year-end. The reasons are: the tax year change (see among other Roll (1983), Ritter (1983)), liquidity demands for the year end gifts and bonuses, capital requirements applied to year end portfolios (see Keim (1983), Roll (1983)). In particular, Harris (1989) finds that transactions prices systematically rise at the close and the effect is stronger for low-priced firms at month-ends. In order to identify the main fundamental “timing” factors that influence the momentum profits, we primarily analyze returns’ behaviour over calendar years. The second target is investigating returns’ behaviour over quarters, given their prominence in the press (e.g., the Wall Street Journal’s quarterly pull-out section), in shareholder reports (e.g., the quarterly mailings to pension-plan participants), and elsewhere.

We test the year-end, quarter-end, and month-end patterns with simple dummy variable regressions. If momentum returns are inflated at quarter- and year- ends, we should observe abnormally high returns on the last day of each quarter and year, and abnormally low returns on the first day.

Let R_t be daily return of the spread. We run the following OLS-indicator-variable regression:

$$R_t = b_0 + b_1 YEND_t + b_2 YBEG_t + b_3 QEND_t + b_4 QBEG_t + b_5 MEND_t + b_6 MBEG_t + b_7 WEND_t + b_8 WBEG_t + e_t \quad (3)$$

where YEND is 1 when t is the last day of a year, and zero otherwise, YBEG is 1 when t is the first trading day of the year, and zero otherwise, QEND is 1 when t is the last of a calendar quarter other than the fourth, and zero otherwise, QBEG_t is 1 when t is the first of a calendar quarter other than the first, and zero otherwise, MEND is 1 when t is the last of a month but not the last of quarter, and zero otherwise, MBEG is 1 when t is the first of a month but not the first of a quarter, and zero otherwise, WEND takes value of one when t is the last of a week but not the last of month, and zero otherwise, WBEG takes value of one when t is the first of a week but not the first of a month, and zero otherwise.

From the Table I it follows that the results indicate a strong two-day return reversal pattern across month-end, quarter-end, and year-end periods. The results are statistically significant at the 5% percent level.

The results are strongest for quarter- and year- ends: the coefficient b_1 has the largest estimated value of the coefficients while b_2 has the smallest estimated value. This suggests that investors should buy stocks on the second-to-last day of each year and sell the next day. If we use the strategy for a one-year holding

**Table I Winner minus Loser Momentum Returns around
year-, quarter-, month-, week- ends**

Coefficients of the Model 3.1								
beta0	beta1	beta2	beta3	beta4	beta5	beta6	beta7	beta8
0.0005	0.0160	-0.0089	-0.0026	0.0021	0.0010	-0.0005	0.0001	0.0005
Additional Statistics								
R-square statistic			F statistic		p value for the full model		Variance error	
0.0057			2.0628		0.0361		0.0003	

This Table reports coefficients (factor loadings), obtained by running OLS-indicator-variable regression, described above. Additional statistics, indicating model's statistical significance are also presented: the R-square statistic (the R-square value is one minus the ratio of the error sum of squares to the total sum of squares), the F-statistic (Fisher criterion for the hypothesis test that all the regression coefficients are zero), p value for the full model, and an estimate of the error variance.

period, these results suggest that investors should rebalance their portfolios at the end of the year. The same situation is for the strategy with one month-holding period. Coefficient b5 the great value compared to other betas, and the coefficient b6 has the small value compared to other betas. It seems that they must be buying at the end of the month and selling soon after. The R-Square is 0.0057 indicating the model accounts for over 95% of the variability in the observations. The F statistic of about 2.06 and its p-value of 0.0361 indicate that it is highly unlikely that all of the regression coefficients are zero, and therefore the model is statistically significant.

To test whether the reversal pattern is significantly more intense at quarter-ends than at other month-ends, we rerun the nine regressions with the variables regrouped so that the second and third coefficients pick the marginal effect of being a quarter-end (including year end) in addition to being a month-end:

$$R_t = b_0 + b_1(YEND_t + QEND_t) + b_2(YBEG_t + QBEG_t) + b_3(YEND_t + QEND_t + MEND_t) + b_4(YBEG_t + QBEG_t + MBEG_t) + e_t \quad (4)$$

The results, in Table II, are statistically insignificant; therefore we don't analyze this model in detail. For our purpose, it is clear that year-, quarter-end momentum profits are inflated in that rebalancing of the portfolio at these periods delivers profits.

Table II Vector B of regression coefficients in the linear model $Y = X*B$

Coefficients of the Model 3.2				
beta0	beta1	beta2	beta3	beta4
0.0006	0.0012	-0.00008	0.0009	-0.0005
Additional Statistics				
R-square statistic		F statistic	p value for the full model	Variance error
0.0004		0.3178	0.8661	0.00027

This Table reports coefficients (factor loadings), obtained by running OLS-indicator-variable regression, described above. Additional statistics, indicating model's statistical significance are also presented: the R-square statistic (coefficient of Multiple Determination is one minus the ratio of the error sum of squares to the total sum of squares), the F-statistic (Fisher criterion for the hypothesis test that all the regression coefficients are zero), p value for the full model, and an estimate of the error variance. According to F statistic and p value, this model is statistically insignificant.

3.2 Fundamental factors: Influence of the volatility on momentum profits

Financial markets sometimes appear quite calm and at other times highly volatile. Describing how this volatility changes over time is important and it can also influence momentum profits.

In this section we value with a factor model the influence of the volatility and statistical measures on "momentum effect". We consider here two cases. In Case 1 we compute the risk measures based on spread Data. In Case 2 we calculate the statistical measures for equally weighted portfolio (EVP) of all stocks, included in S&P500 index.

Let us denote the spread (winner-loser). As independent variables here we use the R-Ratio, Standard deviation and MAD (Mean-Absolute-Deviation).

OLS-indicator-variable regressions, we use, have the following forms:

$$R_t = \lambda_0 + \lambda_1(nominator_of_R_Ratio)_t + \lambda_2(denominator_of_R_Ratio)_t + e_t$$

$$R_t = \alpha_0 + \alpha_1(STD)_t + e_t$$

$$R_t = \gamma_0 + \gamma_1(MAD)_t + e_t$$

where $MAD(r - r_f) = E|r - r_f - E(r - r_f)|$ and STD is the standard deviation of momentum profits. Moreover, $((de)nominator_of_R_Ratio)_t$, $(STD)_t$, and

$(MAD)_t$ are calculated based on previous month's observations (22 observations) of momentum profits and for different values of the α and β R-Ratio parameters.

In Table III we check the hypothesis that all regression coefficients are zero. p value is very low for all of the cases, it means that the chance to have all coefficients zero is insignificant. The R-square value is one minus the ratio of the error sum of squares to the total sum of squares and very low for all of the cases. It means that the model explains the main part of the momentum returns' variance. Moreover, we can give the right interpretation of the statistical measures on the spread (case 1). As a matter of fact, volatility of the spread tends to decline the as momentum profits rises and it tends to increase as the stock market falls.

3.3 Fundamental factors: Influence of the state of economy on momentum profits

In this section we value the influence of the state of economy on "momentum effect". We first assume that the market follows a two states Markov Chain. Then we test the dependence of the momentum profits with being in a bull/bear market.

We consider two cases. In case 1 we use equally weighted portfolio (EWP) of all stocks components of the S&P500 to define the state of the market. In case 2 we use the spread between the winner and loser returns to define the state of the market.

Case 1: If the difference of returns of the equally weighted portfolio $r_t - r_{t-1}$ takes positive value, it means that there is bull-market at time t , if it takes negative value, we are in bear-market at time t . We analyze a total of 2864 equally weighted portfolio returns, except the data of the first ranking period.

Case 2: If the difference between the spread at time t and the spread at time $(t-1)$ $r_t - r_{t-1}$ takes positive value, it means that there is bull-market at time t , if it takes negative value, we are in bear-market at time t . We analyze a total of 2864 values of spread except the first ranking period.

Markov Chain: Assume, furthermore, that, at time t , the market is in state $s_t = j$ with probability $\lambda_{t,j}$, i.e.,

$$\Pr(s_t = j) = \lambda_{t,j}.$$

We assume that there are 2 states of the market (e.g., bull and bear). Thus, assume that the states of the market are generated by a Markov chain with 2 dimensional state space and transition matrix, where an element (i,j) is the probability of transition from state i to state j):

$$\begin{bmatrix} p & 1-p \\ 1-q & q \end{bmatrix}$$

Table III Coefficients and statistics of the model
Influence of volatility on momentum profits of the next day

Risk measures	Case 1 (spread)			Case 2(Equally weighted)		
R-Ratio(0.3,0.4)	<i>coefficients</i>	<i>Intervals of coefficients</i>		<i>coefficients</i>	<i>Intervals of coefficients</i>	
Lambda0	0,0012	-0,0002	0,0027	0,0000	-0,0009	0,0009
Lambda1	-0,0156	-0,0955	0,0644	-0,0017	-0,0881	0,0846
Lambda2	-0,0252	-0,1215	0,0711	0,0961	0,0018	0,1904
R-square statistic	0,0003			0,0022		
variance error	0,0003			0,0001		
R-Ratio(0.5,0.5)	<i>coefficients</i>	<i>Intervals of coefficients</i>		<i>coefficients</i>	<i>Intervals of coefficients</i>	
Lambda0	0,0013	-0,0002	0,0027	0,0000	-0,0009	0,0008
Lambda1	-0,0341	-0,1404	0,0721	0,0091	-0,1027	0,1208
Lambda2	-0,0224	-0,1279	0,0832	0,1092	0,0126	0,2058
R-square statistic	0,0003			0,0024		
variance error	0,0003			0,0001		
R-Ratio(0.1,0.1)	<i>coefficients</i>	<i>Intervals of coefficients</i>		<i>coefficients</i>	<i>Intervals of coefficients</i>	
Lambda0	0,0011	-0,0002	0,0024	0,0000	-0,0009	0,0008
Lambda1	0,0107	-0,0378	0,0591	0,0081	-0,0508	0,0670
Lambda2	-0,0325	-0,0877	0,0226	0,0446	-0,0153	0,1046
R-square statistic	0,0005			0,0016		
variance error	0,0003			0,0001		
STD	<i>coefficients</i>	<i>Intervals of coefficients</i>		<i>coefficients</i>	<i>Intervals of coefficients</i>	
Alpha0	0,0011	-0,0003	0,0024	0,0009	0,0002	0,0017
Alpha1	-0,0269	-0,1061	0,0523	0,0000	0,0000	0,0000
R-square statistic	0,0002			0,0001		
variance error	0,0003			0,0001		
MAD	<i>coefficients</i>	<i>Intervals of coefficients</i>		<i>coefficients</i>	<i>Intervals of coefficients</i>	
Gamma0	0,0012	-0,0002	0,0026	-0,0002	-0,0010	0,0007
Gamma1	-0,0494	-0,1662	0,0674	0,1266	0,0202	0,2330
R-square statistic	0,0002			0,0019		
variance error	0,0003			0,0001		

Table III reports coefficients (factor loadings), obtained by running OLS-indicator-variable regression, described above. For each coefficient we give the confidence interval. Additional Statistics, indicating model's statistical significance are also presented: the R-square statistic (coefficient of Multiple Determination), and an estimate of the error variance.

where

$p = \Pr(\text{bull market next period} / \text{bull market today}) = \Pr(s_{t+1} = 1 | s_t = 1)$;

and, similarly,

$q = \Pr(\text{bear market next period} / \text{bear market today}) = \Pr(s_{t+1} = 2 | s_t = 2)$.

Table IV reports the transition matrix. According to the results, for *case 1*:

$p = \Pr(\text{bull market next period} / \text{bull market today}) = \Pr(s_{t+1} = 1 | s_t = 1) = 0,38706$;

and, similarly,

$q = \Pr(\text{bear market next period} / \text{bear market today}) = \Pr(s_{t+1} = 2 | s_t = 2) = 0,33218$.

For *case 2*:

$p = \Pr(\text{bull market next period} / \text{bull market today}) = \Pr(s_{t+1} = 1 | s_t = 1) = 0,33823$;

and, similarly,

$q = \Pr(\text{bear market next period} / \text{bear market today}) = \Pr(s_{t+1} = 2 | s_t = 2) = 0,33799$.

From Table IV we can't say that the state of the market in the next period(s) were predictable from current and past observations as the hypothesis of effective market consider. For example, the probability of being in a bull market next period may depend on the current state of the market. It is usually higher when we are currently in a bull market also. But our results show that the probability of being in a bull market next period is higher when we are currently in a bear market.

Fundamental factor analysis for bull market: In order to test the dependence of momentum profits on the hypothesis of being in a bull market (for both cases), we use OLS-indicator-variable regressions, with the following form:

$$R_t = \lambda_0 + \lambda_1(Var1)_t + e_t$$

Daily returns on each portfolio (winner and loser portfolios) are calculated and the dependent variable is the winner return minus loser return (total 2864 observations excepting the first ranking period). As independent variables we use a variable $(Var1)_t$ that takes value of 1 if we have the bull-market at time t , and zero otherwise. (We could also consider another variable Var2 that takes value of 1 if we have the bear-market at time t , and zero otherwise, but clearly this variable is linear dependent with Var1, since $Var2 = 1 - Var1$). Therefore we test here, whether the state of the market has an explanatory power for the momentum profit on the next day and the results are reported in Table IV.

The hypothesis that regression coefficients are zero is rejected for the one factor model in the case we use equally weighted portfolio of all stocks components of the S&P500 to define the bull state of the market. We do not get analogous result when we use the spread to identify the bull market. As a matter of fact, the p-value in case 2 is more than 14% and also statistic F is much lower than the value obtained with case 1. The R-square value is one minus the ratio of the error sum of squares to the total sum of squares and equal to 0.0013 and 0.0007.

Table IV Vector of regression coefficients in the linear model, estimated transition matrices and an additional statistics

	Case 1 (Equally weighted)	Case2 (Spread)
λ_0	0.0001	0.0011
λ_1	0.0012	-0.0009
Estimated transition matrices	$\begin{pmatrix} 0.3870 & 0.6129 \\ 0.6678 & 0.3321 \end{pmatrix}$	$\begin{pmatrix} 0.3382 & 0.6617 \\ 0.6620 & 0.3379 \end{pmatrix}$
R-square statistic	0.0013	0.0007
F-statistic	3.7291	2.1423
P value for the full model	0.0536	0.1434
an estimate of the error variance	0.0003	0.0003

Table IV reports coefficients (factor loadings), obtained by running OLS-indicator-variable regression, described in Section 3.3. The estimated transition matrices and an additional Statistics, indicating Model's statistical significance is also presented: the R-square statistic (coefficient of Multiple Determination), the F-statistic (Fisher criterion for the hypothesis test that all the regression coefficients are zero), p value for the full model, and an estimate of the error variance.

It means that the model explains the most part of the momentum returns' variance, and therefore the influence of the other factors, which we didn't consider in this model is insignificant. Therefore the model is statistically significant for case 1.

3.4 Macroeconomic factors: Impact of Macroeconomic Variables on momentum profits

It's well known that macroeconomic variables affect security prices. The fundamental work of Fama (1986) has sparked considerable interest in studying the relation between stock markets and economic variables (see, among others, .Chen et.al. (1986)). In this section we investigate how momentum returns are related to country-specific macroeconomic factors for a sample of S&P500 data. We assume that momentum returns are described by a factor model and test, whether they can be predicted by independent. macroeconomic variables.

The macroeconomic data were obtained from COMPUSTAT over the 1992-2006 period. The set of macroeconomic variables includes exports, imports, inflation, Currency Component of M1, Industrial Production Index, Dividend yield of S&P 500 COMP LTD, corporate spread. We use returns series of macroeconomic data calculated using the following formula:

$$return_t = \ln(S_t/S_{t-1})$$

All macroeconomic data are obtained at the daily frequency since we analyze the data of momentum returns at this frequency. However we have monthly values of

Table V Summary statistics for macroeconomic variables

Variable	Mean	Standard Deviation	Minimum	Maximum
corporate spread	-0.0004	0.0050	-2.3269	2.3735
exports	0.0050	0.0004	-0.0591	0.0863
imports	0.0075	0.0003	-0.0497	0.0747
CPI (inflation)	0.0022	0.000007	-0.0080	0.0121
Currency Component of M1	0.0059	0.00003	-0.0120	0.0325
Industrial Production Index	0.0028	0.00002	-0.0132	0.0213
DIV (S&P 500 COMP-LTD)	0.0041	0.0948	-0.8713	0.8179
S&P 500 returns	0.0003	0.0055	-2.3747	2.3489

Table V summarizes statistics for returns of shares included in S&P 500, and for macroeconomic variables, the influence of which on momentum returns we analyze. The sample of shares includes total of 382 stocks traded on the American Stock Exchange during the period of January 1992 and December 2003. The sample of macroeconomic data covers the same period.

exports, imports, inflation, Currency Component of M1, Industrial Production Index, Dividend yield of S&P 500 COMP LTD from Federal Reserve Bank of St. Louis (Economic Research). Table V summarizes statistics for macroeconomic variables.

Since daily data are not available for the entire sample period, we interpolate monthly data into daily observations using simulating procedures based on estimated parameters of stable distribution for monthly returns.

Simulating of macroeconomic variables daily returns is based on three steps:

1. Estimation of the symmetric stable parameters of monthly returns, assuming that they are iid and symmetric.
2. Estimation of the symmetric stable parameters of daily returns α_{daily} , c_{daily} , $mean_{daily}$ using estimated parameters $\alpha_{monthly}$, $c_{monthly}$, $mean_{monthly}$ from the first step. We consider here 21 working days in a month and set:

$$\alpha_{daily} = \alpha_{monthly}; mean_{daily} = \frac{1}{n} mean_{monthly};$$

$$c_{daily} = n^{\frac{-1}{\alpha}} c_{monthly}$$

where α represents the index of stability for daily and monthly sequences of observations, c is the scale parameter, $mean$ is the location parameter for daily and monthly sequences of observations, and $n=21$ is the number of monthly observations.

3. Simulating 21 daily returns from symmetric alpha stable distribution with estimated parameters $(\alpha, c, mean)$ $x_1, \dots, x_{21}, x_{22}, \dots, x_{42}, \dots$, etc. We consider here two possible cases: the additive and the scale transformations, for rescaling the distribution to become for daily returns.

In the case of scale transformation we calculate first the sum $x_1 + \dots + x_{21}$ which will not be exactly the observed monthly value $m(1)$, but $x_1 + \dots + x_{21} = m(1)d_1 = D_1$. Then set $d_1 = \frac{D_1}{m(1)}$. In this case we use as daily returns the scaled values replacing x_i with x_i/d_1 . Important here is that for every monthly return $m(i)$ the normalizing constant d will be different, that is $d = d(m(i))$. In the case of additive transformation we calculate d_1 using the formula: $d_1 = \frac{m(1)-D_1}{21}$, and then replace x_i with $x_i + d_1$. Now the sum of the new shifted will sum to $m(1)$, but we will not change the extreme values so the index α of the new sequence of daily returns stay the same as the index α of the sequence of monthly returns. We have chosen the additive transformation to receive daily returns having monthly returns as in this case we received that parameter α is above 1 for daily returns and the mean is so small that it does not play role in the estimation process, even if it is slightly modified. In each period of time, t , the investor considers a set of 7 macroeconomic variables that may be useful for making a one-period-ahead forecast of momentum returns. In order to conduct this search over a large number of forecasting models in an efficient and timely manner, we used the ordinary least squares technique to estimate, in each period of time t , linear regression models of the following format:

$$R_t = \lambda_0 + \lambda_1 (exports)_t + \lambda_2 (imports)_t + \lambda_3 (inflation)_t + \lambda_4 (M1)_t + \lambda_5 (Ind_Prod_Index)_t + \lambda_6 (DIV)_t + \lambda_7 (Corp_spread)_t + e_t \quad (5)$$

where R_t denotes the variable of spread determined as the difference between winner and loser portfolios, and representing momentum returns, λ_i are factor loadings, indicating, how sensitive momentum returns are to its corresponding explanatory power, denoted in parenthesis, and e_{t+1} is the error term. Table VI represents vector of regression coefficients of the model.

Let us examine each of the variables in our regression. We have prior beliefs about the signs of the coefficients for some, but not all, of these variables.

Exports and imports : We expect that exports will have a positive coefficient, and imports will have a negative coefficient in our regression model. That is, when country's values of exports increase, there is a propensity for it's a stock prices increase in the world market. Similarly, when country's values of imports increase, the country may face with the bear tendency of its fond-market. In Table VI, we find, as expected, that momentum returns are significantly positive related to exports and significantly negative related to imports. Thus we can conclude that exports (imports) are associated with more (less) positive momentum profits.

Inflation: Inflation is defined as

Table VI Regression coefficients of the linear model and additional statistics

lambda 0	lambda 1	lambda 2	lambda 3	lambda 4	lambda 5	lambda 6	lambda 7
0.00057	0.44086	-0.2111	0.12556	0.43346	-0.52426	-0.00137	0.0003
R-square statistic				p value for the full model		an estimate of the error variance	
0.003				0.2749		0.00027	

Table VI reports coefficients (factor loadings), obtained by running OLS-indicator-variable regression, described above. The additional statistics, indicating model's statistical significance is also presented: the R-square statistic (coefficient of Multiple Determination), p value for the full model, and an estimate of the error variance. We check the hypothesis that all regression coefficients are zero. p value is low, it means that the chance to have all coefficients zero is insignificant.

$$Inflation_t = \ln(CPI_t/CPI_{t-1}),$$

where CPI is a Consumption Price Index. According to the Fisher theory, if stocks provide a hedge against inflation, the relation between stock returns and inflation should be positive. Therefore, returns of optimal momentum strategies should be also positively correlated with Inflation rate. We find in Table VI, as it was expected, that inflation is positively related to momentum profits.

Currency Component of M1: We expect that M1 will have a positive coefficient in our regression model, as the growth of M1 means also the growth of inflation, which is positively correlated with the stock prices. We find in Table VI, as it was expected, that Currency Component M1 is positively related to momentum profits.

Industrial Production Index: We find in Table VI, that Industrial Production Index is negatively correlated with momentum returns.

Dividend yield of S&P 500 COMP LTD: This variable indicates the average dividend payments of S&P. We analyze momentum returns, constructed from the winner and loser portfolios of S&P shares. Our winner portfolio consists of the shares, which we have to buy, and our loser portfolio consists of the shares, which we have to sell at the moments of portfolio rebalancing. Therefore, it's very difficult to predict, whether dividend yield will have positive or negative correlation with momentum returns. We find in Table VI, that it's negatively correlated with momentum returns, but the coefficient of the regression is small enough to be treated as the noise.

Corporate spread: The corporate spread is the spread between the default able and default-free interest rate. Having series of 2-Year Treasury Constant Maturity Rate, 5-Year Treasury Constant Maturity Rate, 3-Year Treasury Constant Maturity Rate, and 3-Month Treasury Constant Maturity Rate we perform the PCA on them and find one factor, which explains most of them. We get one curve that represents most of the movements of the treasuries using Principal

Components Analysis. It is the first principal component. Then as corporate spread variable we use the difference between S&P 500 returns and this factor (the first principal component) indicating the behavior of Treasury Rates. On the other hand, Estrella and Mishkin (1998) find that the term spread (the long-term interest rate minus the short-term interest rate) is a good out-of-sample as well as in-sample predictor of recessions. In particular, they have shown there is a correspondence between a more positive term spread and a lower probability of recession, while a more negative term spread indicates a higher probability of recession. Thus we expect to see the same tendency for corporate spread also, and the positive correlation between the corporate spread and momentum profits.

As we can see from the coefficients of linear regression in Table VI, momentum returns inflate, if values of exports, inflation, currency component of M1, and corporate spread inflate and deflate, if value of imports, industrial production index, and dividends of S&P 500 COMP LTD inflate. These macroeconomic variables significantly affect momentum profits, and thus may be useful as predictors of momentum profits.

3.5 Fundamental and Macroeconomic factors: Impact of Fundamental and Macroeconomic Variables on momentum profits

In this Section we describe the model considering as the explanatory variables all fundamental and macroeconomic variables, described in previous Sections.

Let R_t be daily return of the spread, and run the following OLS-indicator-variable regression:

$$\begin{aligned} R_t = & b_0 + b_1 YEND_t + b_2 YBEG_t + b_3 QEND_t + b_4 QBEG_t + b_5 MEND_t + \\ & + b_6 MBEG_t + b_7 WEND_t + b_8 WBEG_t + b_9 (nominator_of_R_Ratio)_t + \\ & + b_{10} (denominator_of_R_Ratio)_t + b_{11} (STD)_t + b_{12} (MAD)_t + b_{13} (Var1)_t + \\ & + b_{14} (exports)_t + b_{15} (imports)_t + b_{16} (inflation)_t + b_{17} (M1)_t + \\ & + b_{18} (Ind_Prod_Index)_t + b_{19} (DIV)_t + b_{20} (Corp_spread)_t + e_t \end{aligned} \quad (6)$$

Table VII represents vector of regression coefficients of the model and an additional statistics indicating Model's statistical significance. Obtained results confirm the results of previous Sections.

The hypothesis that all regression coefficients are zero is rejected, as follows from the value of the F statistic for 2841 and 20 factors. The p value is equal to 0.0149, and it means that the chance to have all coefficients zero is only 1.49%. The R-square value is one minus the ratio of the error sum of squares to the total sum of squares and equal to 0.0126. It means that the model doesn't explain only 1.26% of the momentum returns' variance, and therefore the influence of the other factors, which we didn't consider in this model is insignificant.

Table VII Regression coefficients of the linear model and additional statistics

beta 0	beta 1	beta 2	beta 3	beta 4	beta 5	beta 6	beta 7
0.0013	0.0187	-0.0088	-0.0031	0.0018	0.0012	-0.0006	0.00003
beta 8	beta 9	beta 10	beta 11	beta 12	beta 13	beta 14	beta 15
0.0003	-1.7557	-1.6811	3.1981	0.0779	0.0001	0.4833	-0.1726
beta 16	beta 17	beta 18	beta 19	beta 20			
0.0795	0.4922	-0.6311	-0.0012	-0.00012			
Additional Statistics							
R-square statistic		F statistic		p value for the full model		an estimate of the error variance	
0.0126		1.8112		0.0149		0.0002	

Table VII reports coefficients (factor loadings), obtained by running OLS-indicator-variable regression, described above. The additional statistics, indicating model's statistical significance are also presented: the R-square statistic (coefficient of Multiple Determination), the F-statistic (Fisher criterion for the hypothesis test that all the regression coefficients are zero), p value for the full model, and an estimate of the error variance.

3.6 Statistical Factors: Principal Components Analysis

In this section we investigate statistical factors, which are endogenous to the system and determined by principal component or factor analyses. We suppose that combinations of macroeconomic and fundamental variables, described in previous sections, form the statistical factors and estimate their influence on momentum profits. In such way we reduce the number of variables to analyze. For more detailed information according to the method of Principal Components (PCA) and Factor Analysis (FA) see Rachev et al.(2008b).

3.6.1 PCA for macroeconomic and fundamental factors

As independent variables (factors) we use here the following variables: variables, capturing effect of timing: YEND, YBEG, QEND, QBEG, MEND, MBEG, WEND, WBEG, variables, capturing the influence of volatility: nominator of R-RATIO denominator of R-RATIO, MAD STD, which are calculated based on previous month's observations (22 observations) of momentum profits, variables, capturing the influence of the market state: VAR1, macroeconomic variables: EXPORTS, IMPORTS, INFLATION, CURRENCY COMPONENT OF M1, INDUSTRIAL PRODUCTION INDEX, DIVIDEND YIELD OF S&P 500 COMP LTD, CORPORATE SPREAD.

Let's now proceed to perform PCA using the covariance matrix of variables. We have to compute the eigenvalues and the eigenvectors of the covariance matrix. The corresponding eigenvalue of eigenvectors is shown in Table VIII. Eigenvalues are listed in descending order; the corresponding eigenvectors go from left to right in the matrix of eigenvectors. Thus, the leftmost eigenvector

corresponds to the largest eigenvalue. The eigenvectors are normalized in the sense that the sum of the squares of each component is equal to 1. The sum of the squares of the elements in each column is equal to 1. If we form portfolios whose weights are the eigenvectors, we can form 20 portfolios that are orthogonal (i.e., uncorrelated). These orthogonal portfolios are called principal components. The variance of each principal component will be equal to the corresponding eigenvalue. Thus the first principal component (i.e., the portfolio corresponding to the first eigenvalue), will have the maximum possible variance and the last principal component (i.e., the portfolio corresponding to the last eigenvalue) will have the smallest variance. The 20 principal components thus obtained are linear combinations of the original series, $X = (X_1, \dots, X_N)'$ that is, they are obtained by multiplying X by the matrix of the eigenvectors. If the eigenvalues and the corresponding eigenvectors are all distinct, as it is the case in our illustration, we can apply the inverse transformation and recover the X as linear combinations of the principal components.

Table VIII shows also the total variance explained by a growing number of components. Thus, the first component explains 37.81% of the total variance, the first two components explain 64.31% of the total variance, 4 components explain 86% of the total variance, 8 components explain 98% of total variance, and so on. Now we can regress the dependent variable (the spread) with respect to the PCA factors with all 20 components, and receive the residuals processes for principal components. Then we fit PCA for residuals to see what is left from the systematic risk. Our results show, that we can use 10 principal components (9 of them were received in the first PCA analysis, one of them was received in the PCA analysis of residuals) to regress momentum profits.

3.7 Statistical Factors: Factor Analysis

Through principal components analysis we determined factors that explain most of the variance. In this section, we consider a factor analysis to determine the main statistical factors. See Rachev et al (2008b) for more detailed information.

Description of the algorithms and results: Consider the 20 time series and their 2865 observations, which were described in previous section. At first we have to compute the positive definite covariance matrix of initial data.

We have covariance matrix $C1$ (20x20) of our independent variables, which is strictly positive definite. Having calculated matrix $C1$ and supposing 8 factors we obtain maximum likelihood estimates of the factor loadings, $LAMBDA$, model with 8 factors. The (i,j)-th element of the 20-by-8 factor loadings matrix $LAMBDA$ is the estimated coefficient, or loading, of the jth factor for the ith variable. We calculate also maximum likelihood estimates of the specific variances in the 21-by-1 vector.

Table IX shows the factor loadings. Each row represents the loadings of the eight factors corresponding to each independent variable. The last column of the table shows the idiosyncratic variances.

The idiosyncratic variances are numbers between 0 and 1, where 0 means that the variance is completely explained by common factors and 1 that common

Table VIII Eigenvalues of the Covariance Matrix, and Percentage of the Total Variance Explained by a growing number of components based on the covariance matrix

Principal component	Eigenvalues of the Covariance Matrix	Percentage of variance explained	Percentage of total variance explained
P1	0.2497766256	37.8101294615	37.8101294615
P2	0.1750390363	26.4966692159	64.3067986775
P3	0.1143015042	17.3024784112	81.6092770887
P4	0.0315509332	4.7760468615	86.3853239502
P5	0.0291775816	4.4167789343	90.8021028844
P6	0.0240844090	3.6457959959	94.4478988803
P7	0.0119535440	1.8094769415	96.2573758219
P8	0.0115705633	1.7515029443	98.0088787662
P9	0.0052848687	0.8000010741	98.8088798403
P10	0.0038713418	0.5860273560	99.3949071962
P11	0.0038258707	0.5791441245	99.9740513207
P12	0.0001376654	0.0208392035	99.9948905243
P13	0.0000246788	0.0037357650	99.9986262893
P14	0.0000034206	0.0005177952	99.9991440845
P15	0.0000026583	0.0004023999	99.9995464844
P16	0.0000024769	0.0003749418	99.9999214262
P17	0.0000002326	0.0000352135	99.9999566397
P18	0.0000001852	0.0000280309	99.9999846706
P20	0.0000000302	0.0000045728	100.0000000000

Table IX A Factor Loadings and Idiosyncratic Variances

	Factor 1	Factor 2	Factor 3	Factor 4	Factor 5	Factor 6	Factor 7	Factor 8	Variance
<i>YEND</i>	-0.009338	-0.020519	-0.033579	-0.013775	-0.008253	-0.075705	-0.026133	0.019284	0.991151
<i>YBEG</i>	0.024226	-0.033802	-0.018359	-0.009530	-0.066951	-0.126668	0.030058	0.068763	0.977418
<i>QEND</i>	0.011794	-0.010967	-0.055297	-0.024185	-0.041929	0.039196	0.001103	0.025244	0.994308
<i>QBEG</i>	0.026761	-0.059329	-0.040552	-0.025478	-0.054331	0.034196	-0.062461	0.036916	0.989653
<i>MEND</i>	0.001823	-0.005822	-0.004831	0.996914	-0.001176	0.002759	-0.002901	0.001907	0.005000
<i>MBEG</i>	-0.029266	-0.091821	-0.038701	-0.038522	0.061959	0.026572	0.051729	-0.039145	0.985442
<i>WEND</i>	-0.000369	-0.009247	0.996714	-0.004940	-0.002410	0.001502	0.000069	0.033976	0.005000
<i>WBEG</i>	-0.000849	1.003606	-0.009228	-0.005728	0.002382	-0.000023	-0.000278	-0.108909	0.005000
<i>nominator of R-Ratio</i>	1.052038	0.000814	-0.002905	-0.000032	-0.230983	-0.010828	0.004321	-0.050045	0.005000
<i>denominator of R-Ratio</i>	0.243487	0.002200	-0.002159	-0.001081	0.866431	-0.005826	-0.003386	0.016695	0.005000
<i>MAD</i>	0.791471	0.001433	-0.002769	-0.001002	0.370343	-0.008415	0.001079	0.001113	0.005000
<i>STD</i>	0.947840	-0.003487	0.005621	0.003096	0.030727	0.018897	0.008682	0.358888	0.005000
<i>VarI</i>	-0.003698	-0.003178	0.000454	-0.008962	-0.021620	-0.034607	-0.021862	-0.003384	0.997909
<i>exports</i>	0.047187	0.022003	0.019950	-0.010567	-0.045633	0.009849	0.311761	0.030198	0.897241
<i>imports</i>	0.020750	-0.020497	-0.013330	-0.005991	0.042740	0.014218	0.332831	-0.020024	0.885416
<i>inflation</i>	-0.026972	0.000937	0.009580	0.017878	0.018976	-0.150489	0.086934	-0.041945	0.971634
<i>M1 Currency Component</i>	-0.001434	-0.000750	0.001260	0.003223	-0.007393	0.790914	0.018139	0.079633	0.396793
<i>Industrial Production Index</i>	-0.058963	0.003274	-0.006017	0.015474	-0.025372	0.030086	0.278309	0.011978	0.918047
<i>Dividend yield of S&P 500</i>									
<i>COMP LTD</i>	0.002918	-0.031758	0.001785	0.008777	0.018138	0.008910	-0.029552	-0.012870	0.997590
<i>corporate spread</i>	-0.010645	-0.010940	-0.039793	-0.005784	0.010896	-0.002456	0.044110	-0.001422	0.996488

Table IX presents the factor loadings. In bold we remark the highest absolute values for each factor.

factors fail explain variance.

From Table IX we can see that different factors influence momentum profits. Factors 1, 5 and 8 are associated with the influence of volatility, because loadings of MAD, STD, and R-Ratio are large for them, Factor 2, 3 and 4 indicate the influence of the “effect of timing”, factors 6 and 7 indicate the influence of the macroeconomic variables, mainly the influence of currency component M1 (factor 6) and the influence of the import, exports and industrial production (factor 7).

Let’s run the regression model for R_{t+1} - momentum returns, we intend to explain.

OLS-indicator-variable regression, has the following form:

$$R_{t+1} = b_0 + b_1(Variable1)_t + b_2(Variable2)_t + b_3(Variable3)_t + b_4(Variable4)_t +$$

Table X Vector B of regression coefficients in the linear model $Y = X*B$

beta0	beta1	beta2	beta3	beta4	beta5	beta6	beta7	beta8
0.001089	0.001394	-0.00269	0.001482	-0.00071	-0.03468	0.044082	-0.01072	-0.03387
R-square statistic					p value for the full model	an estimate of the error variance		
0.002260208					0.600857	0.000278		

Table X reports coefficients (factor loadings), obtained by running OLS-indicator-variable regression, described above. The additional statistics, indicating model's statistical significance is also presented: the R-square statistic (coefficient of Multiple Determination), p value for the full model, and an estimate of the error variance. p value is equal to 0.60085, it means that the chance to have all coefficients zero is 60%. The R-square value is one minus the ratio of the error sum of squares to the total sum of squares and equal to 0.0023. It means that the Model explains the most part of the momentum returns' variance, and therefore the influence of the other factors, which we didn't consider in this Model is insignificant.

$$+b_5(Factor5)_t + b_6(Factor6)_t + b_7(Factor7)_t + b_8(Factor8)_t + e_{t+1}. \quad (7)$$

Table X shows that the most important influence on momentum profits have the factors 5, 6, 7 and 8. Factors 5 and 8 indicate the influence of volatility: momentum profits deflate, when volatility inflates and conversely. Factor 7 is linked with the macroeconomic factors: import, exports and industrial production. Factor 6 is associated with the influence of currency component M1: momentum profits deflate, when currency component M1 rises.

In order to improve the obtained results on this factor analysis we tested two methods of the stepwise regression: backward removal method and forward entry method, which provided the same results. Testing backward removal method we started with the whole model that includes all the 8 factors. At each step, after the initial step the removal criteria (p-value and R-square statistics) were computed for each factor to be removed from the model. Testing forward entry method, we started with the model included the regression intercept and one factor. At each step after the initial step the removal criteria were computed for each factor for entry in the model.

Results of the applications of this stepwise regression methodology are presented in Table XI.

Presented results confirm the most important influence of the volatility, "effect of timing" and the currency component's M1 changing on momentum returns.

Additional Statistics indicates model's statistical significance: p value is improved with respect to the previous factor analysis. The R-square value is one minus the ratio of the error sum of squares to the total sum of squares and equal to 0.002. It means that the model explains the most part of the momentum returns' variance, and therefore the influence of the other factors, which we didn't consider in this model is insignificant.

Table XI Vector B of regression coefficients in the linear model $Y = X*B$

beta0	beta1	beta2	beta3	beta4	beta5	beta6	beta7	beta8
0.001238	-0.01064	0.000906	0.000435	0	-0.015	0.038706	-0.01802	0
R-square statistic					p value for the full model	an estimate of the error variance		
0.002038					0.447587	0.000278		

Table XI reports coefficients (factor loadings), obtained by running OLS-indicator-variable regression, described above. These coefficients are obtained applying stepwise regression methodology. The additional statistics, indicating model's statistical significance is also presented: the R-square statistic (coefficient of Multiple Determination), p value for the full model, and an estimate of the error variance.

4 Conclusions

In this paper, we extend the momentum trading methodology and we analyze the main motivations of momentum effects. In particular, we use ratios based on the coherent risk measure of the expected shortfall to rank the risk-return profile of the individual stocks. These risk-return ratio criterion capture the distributional properties of stock returns at different threshold levels of the tail distribution. Furthermore, using the ratio criterion as the objective function in the portfolio optimization we propose an alternative methodology that optimizes weights in the winner and loser portfolios of momentum strategies. In order to analyze the source of momentum profits, we first tested the influence of several factors on momentum profits with the help of separate models. Then, we combined all factors in one model to see the “marginal” effect of a given explanatory variable.

We found that a set of fundamental, macroeconomic, and statistic variables significantly influence the momentum returns. We documented long-term yearly periodicity and intermediate-term quarterly and monthly periodicities of momentum returns, which inflate at quarter-, month- and year- ends and deflate at quarter-, month- and year - beginnings. From the analysis of volatility, it follows that as volatility rises, there is a propensity for the momentum profits to experience losses. Volatility tends to decline as the momentum profits rises and it tends to increase as the stock market falls. Analysis of the market state influence shows that momentum returns inflate, if the state of the market is bull and deflate, if the market is bear.

Our contribution to the literature on the macroeconomic determinants is twofold. First, we have found that several variables including exports, inflation, currency component of M1, corporate spread, imports, industrial production index, and dividends of S&P 500 COMP LTD, significantly influence on momentum returns.

Second, we employed a modeling approach to simulate daily data based on monthly sequences of initial returns. Such daily data set is not usually available

to an investor in real time. In the earlier literature, it has been common practice to use the monthly and year data set, but using daily data, in our opinion, can give us much more precise estimates.

To reduce a set of analyzed factors we used the Principal Component Analysis. PCA is interesting if in using only a small number of principal components, we nevertheless obtain a good approximation. That is, we used PCA to determine principal components but we used only those principal components that have a large variance as factors. Stated otherwise, we regressed the original series of spread data onto a small number of principal components. In this way, PCA implements a dimensionality reduction because it allows one to retain only a small number of components. By choosing as factors the components with the largest variance, we could explain a large portion of the total variance of spread data. We received that using 10 principal components allows to explain more than 99% of momentum returns.

To give an explanation in terms what factors explain what processes, we applied Statistical Factor Analysis, which concludes our work. Factor analysis, in contrast to the Principal Component Analysis, tends to reveal the exact factor structure of the data. We marked out the factors, which have the significant influence on momentum profits: In particular we observe the associated influence on volatility, on “effect of timing” and on macroeconomic variables.

On one hand, the results of this paper should help investors to be more profitable in optimal portfolio selection. In particular, the proposed analysis should force investors to more efficiently monitor and manage financial risks associated with a momentum strategy. On the other hand, the above discussion should be useful for politicians, central bankers and macroeconomists, to develop a better understanding of macroeconomic determinants of the source of momentum profits.

Acknowledgement: We thank Frank Fabozzi and Teo Jasic for helpful comments. Rachev’s research was supported by grants from the Division of Mathematical, Life and Physical Science, College of Letters and Science, University of California, Santa Barbara, and the Deutschen Forschungsgemeinschaft. Sergio Ortobelli was partially supported by grants from ex-murst 60% 2007, 2008.

References

- [1] P. Artzner, F. Delbaen, J-M.Eber, and D. Heath, Coherent measures of risk, *Mathematical Finance*, 3, 203-228 (1999).
- [2] A. Biglova, S. Ortobelli, S. Rachev, and S. Stoyanov. Comparison among different approaches for risk estimation in portfolio theory, *Journal of Portfolio Management*, Fall, 103-112 (2004a).
- [3] A. Biglova, T. Jasic, S. Rachev, and F.J. Fabozzi Profitability of momentum strategies: Application of novel risk/return Ratio stock selection criteria, *Investment Management and Financial Innovations*, 4 issue, pages 48-62 (2004b).

- [4] A. Bris, W. N. Goetzmann, and N. Zhu. Short sales in global perspective, Chapter 13, *Short-Selling: Strategies, Risks and Rewards* (Ed. F. J. Fabozzi), Hoboken, New Jersey, 2004, pp. 323-343.
- [5] M.M. Carhart, R. Kaniel, K. D. Musto, and V.A. Reed. Learning for the Tape: Evidence of Gaming Behaviour in Equity Mutual Funds, *Journal of Finance*, 57(2), April (2002).
- [6] N.-F.Chen, R. Roll, and S.A. Ross Economic Forces and the Stock Market. *Journal of Business*, 59, 383-403 (1986).
- [7] T. Chordia, and L. Shivakumar. Momentum, business cycles and time varying expected returns, *Journal of Finance* 57, 985-1019 (2002).
- [8] W. F.M. De Bondt, and R. Thaler. Does the stock market overreact?, *Journal of Finance*, 40, 793-805 (1985).
- [9] Estrella A. and F. Mishkin. Predicting U.S. recessions: financial variables as leading indicators, *Review of Economics and Statistics*, 80, 45-61 (1998).
- [10] E. F. Fama Stock returns, real activity, inflation, and money, *American Economic Review*, 71, 545-65 (1981).
- [11] E. F. Fama, and K.R. French. Multifactor explanations of asset pricing anomalies, *Journal of Finance*, 51, 55-84 (1996).
- [12] J.M.Griffin, X. Ji, and J.S. Martin. Momentum investing and business cycle risk: evidence from pole to pole, *Journal of Finance* 58, 2515-2547 (2003).
- [13] B.D. Grundy, and J.S. Martin Understanding the nature of risks and the sources of rewards to momentum investing, *Review of Financial Studies* 14, 29-78 (2001).
- [14] L. Harris. A day-end transaction price anomaly, *Journal of Finance and Quantitative Analysis* 24, 29-45 (1989).
- [15] R. Haugen, and J. Lakonishok *The Incredible January Effect: The Stock Market's Unsolved Mystery*. Homewood, Ill.: Dow Jones Irwin Publishers 1988.
- [16] N. Jegadeesh, and S. Titman, Returns to buying winners and selling losers: implications for stock market efficiency, *Journal of Finance*, 48, 65-91 (1993).
- [17] D. Kahneman, and A. Tversky *Intuitive prediction: Biases and corrective procedures*, Cambridge University Press, London, 1982.
- [18] D. Keim, Size-related anomalies and stock return seasonality: Further empirical evidence, *Journal of Financial Economics*, 12, 13-32 (1983).

- [19] R. Lewellen, and S. Nagel. The conditional CAPM does not explain asset pricing anomalies, *Working Paper*, MIT (2004).
- [20] D. Musto. Portfolio disclosures and year-end price shifts, *Journal of Finance* 52, 1563-1588, (1997).
- [21] S.T. Rachev *Handbook of Heavy Tailed Distributions in Finance*, Elsevier: New York (2003) .
- [22] S. T. Rachev, S. Ortobelli , S. Stoyanov, F. Fabozzi, A. Biglova Desirable Properties of an Ideal Risk Measure in Portfolio Theory, *International Journal of Theoretical and Applied Finance* 11(1), 19-54 (2008a).
- [23] S.T. Rachev, J. Hsu, B. Bagasheva, F. Fabozzi *Bayesian methods in finance*, Hoboken: Wiley and Son (2008b)
- [24] J. Ritter. The buying and selling behaviour of individual investors at the turn of the year, *Journal of Finance* 43, 701-717 (1988).
- [25] R. W. Roll. Was ist das? The turn of the year effect and the return premium of small firms, *Journal of Portfolio Management* 9, 18-28 (1983).
- [26] K. G. Rouwenhorst International momentum strategies, *Journal of Finance* 53, 267-284 (1998).
- [27] W. F. Sharpe The Sharpe ratio, *Journal of Portfolio Management*, Fall, 45-58 (1994).

Existence and Uniqueness of Solutions to a diffusive Predator-Prey Model

By

Marwan S. Abualrub

Department of Mathematics / University of Jordan / P.O.Box 11942 / Amman - Jordan

E-mail: abualrubms@yahoo.com

2000 Mathematics Subject Classification code: **92B99**

Keywords : diffusion, predator, prey.

Abstract

A model for predator-prey has been considered, existence and uniqueness to the diffusion of such model has been shown.

Introduction

Predator-prey models and competing species relations have been initiated by Lotka in [6], [7], and Volterra [8], in a classical way, to represent the interaction between populations in terms of simultaneous nonlinear differential equations.

Predator-prey systems have been described properly using mathematical models. Such models describe the interaction between multi-species, particularly two species for which the growth rate of one of the species is increased but decreased for the other.

In this paper, we include diffusion to a model that describes the interaction between the prey and the predator; and we use a time-continuous model rather than discrete, even though the problem is inherently discrete, since we expect a continuous overlap of generations in the population of such models. Therefore, continuous models might be a reasonable approximation.

In this paper, we consider the more realistic case; namely a diffusion model in the (x_1, x_2) plane instead of the one dimensional case. In such model, we consider two coupled nonlinear parabolic partial differential equations (PDEs) including diffusion; for more details see [4].

In this paper, we talk about the existence and uniqueness of solutions to our model.

In [1], a model which is close to our model here has been considered and a traveling wave solution has been obtained to that model.

1. The Predator- Prey Model

The model we are going to consider here is a modification to the planktonic patchiness model, a kind of predator-prey models, which was originally considered by Levin and Segel in 1976 [5]; in which they considered some biological hypotheses concerning the origin of planktonic patchiness that led to their model in [5].

We used the model in [5] and assumed that the species specific diffusion coefficients be constants to come up with the predator-prey model:

$$u_t - \Delta u = au + ku^2 - buv \quad (1.1)$$

and

$$v_t - \Delta v = cuv - dv^2 \quad (1.2)$$

; where $u = u(x, t)$ is the prey density, $v = v(x, t)$ is the predator density, $x = (x_1, x_2)$,

$$u_t = \frac{\partial u}{\partial t}, \text{ and } v_t = \frac{\partial v}{\partial t}.$$

We shall assume that a, b, c, d , and k are constants however, a may assumed to be compact supported and bounded function of x (i.e., $a = a(x)$; $a(x) = 0$ for $|x| > N$; where N is a constant) not a constant. The reason for this assumption is that the birth (or death) rate may depend on the environment, which is assumed to be bounded. Another reason for assuming that a, b, c, d , and k are constants, is due to the fact that the birth (or death) rate could just depend on the interaction between the male and the female (sexual interaction as in terms ku^2 and $-dv^2$), or just on the binary interaction (sexual, birth or death like in the term uv).

Here $\Delta = \frac{\partial^2}{\partial x_1^2} + \frac{\partial^2}{\partial x_2^2}$ represents the diffusion (dispersal).

uv represents the binary interaction which result in either growth or decay.

au represents the birth or death of the prey.

u^2, v^2 represent the sexual interaction between the males and the females of the prey and the predator, respectively.

Finally, we shall assume that the initial data are in the same L^p space for some $p > 1$. The initial values for equations (1.1) and (1.2) will be given by $u(x, 0) = g(x)$ and $v(x, 0) = h(x)$, respectively, where both $g(x)$ and $h(x) \in L^p(R^2)$.

In addition, we will consider small values of time t , since we are looking for local solutions in the usual diffusion; but for large values of time one should talk about long range diffusion as done in [2].

2. Usual diffusion with $p = q$ in the $L^{p,q}$ norms

To ease solving (1.1) and (1.2) we shall make the term au disappear from (1.1); to do so let $u(x, t) = e^{at}w(x, t)$. Therefore (1.1) and (1.2) together with the initial conditions become as follows:

$$w_t - \Delta w = ke^{at}w^2 - bwv, \quad (2.1)$$

$$w(x, 0) = g(x) \quad (2.2)$$

and

$$v_t - \Delta v = ce^{at}wv - dv^2, \quad (2.3)$$

$$v(x, 0) = h(x) \quad (2.4)$$

Since we have the heat operator $\frac{\partial}{\partial t} - \Delta$ in the left hand sides of (2.1) and (2.3), therefore w

and v can be obtained by solving the following integral equations:

$$w = \int_0^t \int_{R^n} K(x-y, t-\tau)[ke^{a\tau}w^2 - bwv]dyd\tau + \int_{R^n} K(x-y, t)g(y)dy \quad (2.5)$$

and

$$v = \int_0^t \int_{R^n} K(x-y, t-\tau)[ce^{a\tau}wv - dv^2]dyd\tau + \int_{R^n} K(x-y, t)h(y)dy; \quad (2.6)$$

where K is the fundamental solution to the heat equation with $n = 2$

$$; \text{thus } K(x, t) = \frac{1}{2\pi t} e^{-\frac{|x|^2}{2t}} \text{ and } |x| = (x_1^2 + x_2^2)^{1/2} \quad (2.7)$$

Using the symbol \otimes to represent the convolution in space and time while the symbol $*$ to represent the convolution in space only; we can rewrite (2.5) and (2.6) in a simpler way as follows:

$$w = K \otimes [ke^{\alpha\tau} w^2 - bwv] + K * g \quad (2.8)$$

$$v = K \otimes [ce^{\alpha\tau} wv - dv^2] + K * h; \quad (2.9)$$

where w and v are weak solutions of (2.1), (2.2), (2.3), and (2.4) respectively..

We will now introduce the function φ as follows:

$$\varphi(\tau) = 0 \text{ if } \tau > T^i \text{ and } \varphi(\tau) = e^{\alpha\tau} \text{ if } \tau \leq T^i; \quad (2.10)$$

where $0 < \tau < T^i$ and T^i is small.

Let us now consider $T(w)$ and $T(v)$ to be the images of w and v respectively.. Thus, if $\tau \leq T^i$, then equations (2.8) and (2.9) become:

$$T(w) = K \otimes [k\varphi(\tau) w^2 - bwv] + K * g \quad (2.11)$$

$$T(v) = K \otimes [c\varphi(\tau) wv - dv^2] + K * h \quad (2.12)$$

We are assuming small values of t in order to show the existence and uniqueness of local solutions to (2.11), (2.12).

Lemma(2.1.1)

If $w(x, t), v(x, t) \in L^{(\frac{4}{2-\epsilon}, \frac{4}{2-\epsilon})}(R^2 \times [0, T^i])$; and $g(x), h(x) \in L^{\frac{8}{3(2-\epsilon)}}(R^2)$,

then for $\epsilon > 0$, we have

$$\|T(w)\|_{\frac{4}{2-\epsilon}, \frac{4}{2-\epsilon}} \leq C'_{\frac{4}{2-\epsilon}} \|w\|_{\frac{4}{2-\epsilon}, \frac{4}{2-\epsilon}}^2 + C''_{\frac{4}{2-\epsilon}} \|w\|_{\frac{4}{2-\epsilon}, \frac{4}{2-\epsilon}} \|v\|_{\frac{4}{2-\epsilon}, \frac{4}{2-\epsilon}} + C_{\frac{8}{3(2-\epsilon)}} \|g\|_{\frac{8}{3(2-\epsilon)}}$$

and

$$\|T(v)\|_{\frac{4}{2-\epsilon}, \frac{4}{2-\epsilon}} \leq D'_{\frac{4}{2-\epsilon}} \|w\|_{\frac{4}{2-\epsilon}, \frac{4}{2-\epsilon}} \|v\|_{\frac{4}{2-\epsilon}, \frac{4}{2-\epsilon}} + D''_{\frac{4}{2-\epsilon}} \|v\|_{\frac{4}{2-\epsilon}, \frac{4}{2-\epsilon}}^2 + D_{\frac{8}{3(2-\epsilon)}} \|h\|_{\frac{8}{3(2-\epsilon)}}.$$

Proof:

It is obvious from (2.7) that

$$0 \leq |K(x, t)| \leq \frac{c_0}{(|x| + t^{1/2})^2}; \quad (2.13)$$

where c_0 is some positive constant.

Observe that

$$(|x| + t^{1/2})^2 = (|x| + t^{1/2})^{2-\theta} (|x| + t^{1/2})^\theta \geq |x|^{2-\theta} t^{\frac{\theta}{2}}$$

for $t > 0$ and $0 < \theta < 2$.

Thus

$$|K(x, t)| \leq c_0 \frac{1}{|x|^{2-\theta}} \frac{1}{t^{\frac{\theta}{2}}} \quad (2.14)$$

Now, for very small positive $\epsilon > 0$, we may rewrite (2.14) as

$$|K(x, t)| \leq c_0 \frac{1}{|x|^{2-\theta}} \frac{1}{t^{\frac{\theta}{2}}} \frac{t^{\frac{\epsilon}{2}}}{t^{\frac{\epsilon}{2}}} \quad (2.15)$$

Using the assumption that $0 < t < T^i$ and T^i is very small, (2.15) may be expressed as

$$|K(x, t)| \leq \frac{c_0 T^{i \frac{\epsilon}{2}}}{|x|^{2-\theta} t^{\frac{\theta+\epsilon}{2}}} \quad (2.16)$$

Observe that

$$\frac{\theta+\epsilon}{2} = 1 - \frac{2-(\theta+\epsilon)}{2}$$

The very small value of $\epsilon > 0$ is chosen to satisfy $0 < \theta + \epsilon < 2$; thus (2.16) may be written as:

$$|K(x, t)| \leq c_0 \frac{1}{|x|^{2-\theta}} \frac{T^{i \frac{\epsilon}{2}}}{t^{1-\frac{2-(\theta+\epsilon)}{2}}} \quad (2.17)$$

By (2.11), (2.17), and (2.10) we obtain:

$$|T(w(x, t))| \leq kc_0 e^a T^{\frac{\epsilon}{2}} \int_0^{T'} \int_{R^2} \frac{|w(y, \tau)|^2 dy d\tau}{|x-y|^{2-\theta} |\tau-\tau'|^{1-\frac{2-(\theta+\epsilon)}{2}}} + bc_0 T^{\frac{\epsilon}{2}} \int_0^{T'} \int_{R^2} \frac{|w(y, \tau)| |v(y, \tau)| dy d\tau}{|x-y|^{2-\theta} |\tau-\tau'|^{1-\frac{2-(\theta+\epsilon)}{2}}} + |K * g| \quad (2.18)$$

Let us now assume that $g \in L^p(R^2)$, $wv \in L^{\frac{p}{2}}(R^2)$, and $w^2 = w \cdot w \in L^{\frac{p}{2}}(R^2)$. Let $r > 1$ be chosen so that:

$$\frac{1}{r} = \frac{2}{p} - \frac{\theta}{2}, \quad 2 < p < \frac{4}{\theta} \quad (2.19)$$

Now, by taking the $L^r(R^2)$ norm of both sides and using the same idea as in Benedek-Panzone Potential Theorem, see [3] page 321, theorem 1, the first and second terms of the right hand side of (2.18) become:

$$\|T(w(\cdot, t))\|_r \leq kc_0 c_p T^{\frac{\epsilon}{2}} \int_0^{T'} \frac{\|w(\cdot, \tau)\|_p^2 d\tau}{|\tau-\tau'|^{1-\frac{2-(\theta+\epsilon)}{2}}} + bc_0 c_p T^{\frac{\epsilon}{2}} \int_0^{T'} \frac{\|w(\cdot, \tau)\|_p \|v(\cdot, \tau)\|_p d\tau}{|\tau-\tau'|^{1-\frac{2-(\theta+\epsilon)}{2}}} + \|K * g(\cdot, t)\|_r \quad (2.20)$$

Now, if we let $\|w(\cdot, \tau)\|_p^2 \in L^{\frac{q}{2}}(R^+)$, $\|w(\cdot, \tau)\|_p \cdot \|v(\cdot, \tau)\|_p \in L^{\frac{q}{2}}(R^+)$, and $s > 1$ so that

$$\frac{1}{s} = \frac{2}{q} - \frac{2-(\theta+\epsilon)}{2}, \quad 2 < q < \frac{4}{2-(\theta+\epsilon)} \quad (2.21)$$

Again, by applying the Benedek-Panzone Potential Theorem to the first and second terms of the right hand side of (2.20), and upon taking the $L^s(R^+)$ norm of both sides, we obtain:

$$\|T(w)\|_{r,s} \leq kc_0 c_p c_q \|w\|_{p,q}^2 + bc_0 c_p c_q \|w\|_{p,q} \cdot \|v\|_{p,q} + \|K * g\|_{r,s} \quad (2.22)$$

We shall now take $p = r = \frac{2}{\theta}$, and $q = s = \frac{2}{2-(\theta+\epsilon)}$, $0 < \theta < 2$ and $\epsilon > 0$.

In addition, we shall require that $p = q$. Therefore $\theta = \frac{2-\epsilon}{2}$; which implies that $p = q = r = s = \frac{4}{2-\epsilon}$, ($\epsilon > 0$).

By selecting $C_{\frac{4}{2-\epsilon}} = kc_0 c_p c_q = kc_0 c_{\frac{4}{2-\epsilon}} c_{\frac{4}{2-\epsilon}}$ and $C''_{\frac{4}{2-\epsilon}} = bc_0 c_p c_q = bc_0 c_{\frac{4}{2-\epsilon}} c_{\frac{4}{2-\epsilon}}$; and since

$\|K * g\|_{\frac{4}{2-\epsilon}, \frac{4}{2-\epsilon}} \leq C_{\frac{8}{3(2-\epsilon)}} \|g\|_{\frac{8}{3(2-\epsilon)}}$ follows directly from the following imbedding lemma (namely Lemma(2.1.2)) for the initial data; this in turns will conclude our Lemma(2.1.1).

Lemma(2.1.2)

Let $F(x, t) = K * g$. Assume that $g \in L^r(R^2)$; $1 < r < \infty$.

If for $p > 1$ and $q > 1$ with $\frac{1}{p} + \frac{1}{q} = \frac{1}{r}$, then $F(x, t) \in L^{p,q}(R^2 \times R^+)$ and $\|F\|_{p,q} \leq c(r) \|g\|_r$; where $c(r)$ is some constant depending on r and the dimension.

Proof:

Using (2.13) we have

$$|F(x, t)| \leq c_0 \int_{R^2} \frac{|g(x-y)| dy}{(|y|+t^{1/2})^2}$$

By taking the $L^q(R^+)$ norm of both sides, we obtain

$$\left(\int_{R^+} |F(x, t)|^q dt \right)^{1/q} \leq c_0 \left[\int_{R^+} \left\{ \int_{R^2} \frac{|g(x-y)| dy}{(|y|+t^{1/2})^2} \right\}^q dt \right]^{1/q}$$

Applying the integral inequality of Minkowski on the right hand side to get

$$\|F(x, \cdot)\|_q \leq c_0 \int_{R^2} |g(x-y)| \left[\int_{R^+} \frac{dt}{(|y|+t^{1/2})^{2q}} \right]^{1/q}$$

from which we obtain

$$\|F(x, \cdot)\|_q \leq c_0 d \int_{R^2} \frac{|g(y)| dy}{|x-y|^{2-\frac{1}{q}}} \text{ for some constant } d \text{ that does not exceed } \int_0^\infty \frac{dt}{(1+t^{1/2})^{2q}}.$$

Since $g \in L^r(R^2)$ and $1 < p < \infty$, we get for $\frac{1}{p} = \frac{1}{r} - \frac{1}{2q}$ the necessary conditions to apply the Benedek-Panzone theorem to reach

$$\|F\|_{p,q} \leq c(r) \|g\|_r;$$

where $c(r) = C(c_0, d, r)$.

This concludes the proof of Lemma (2.1.2).

REFERENCES

- [1] Abualrub, M.S.: Vaccination in a model of an epidemic. *The International Journal of Mathematics and Mathematical Sciences (IJMMS)*, Vol.23, No.6, pp.425-429, 2000.
<http://ijmms.hindawi.com/volume-23/issue-6.html>
- [2] Abualrub, M.S.: Long range diffusion-reaction model on population dynamics. *Documenta Mathematica* (J. of German Mathematician Union). Vol. 3, pp.331-340, Dec. 1998.
<http://www.math.uiuc.edu/documenta/vol-03/vol-03-eng.html>
- [3] Benedek, A. and Panzone, R.: The space L^p with mixed norm. *Duke Math. J.*, 28: pp.302-324, 1961.
- [4] Calderon, C.P.: Diffusion and nonlinear population theory. *Rev. U. Mat.*, Argentina, 35, pp.283-288, 1990.
- [5] Levin, S.A., and Segel, L.A.: Hypothesis for the origin of planktonic patchiness. *Nature*, 259: 659.
- [6] Lotka, A.J.: Elements of physical biology. Baltimore: *Williams and Wilkins Co., Inc.*, 1924.
- [7] Lotka, A.J.: Elements of mathematical biology. New York: *Dover Pub.*, 1956.
- [8] Volterra, V.: Variazioni e fluttuazioni del numero d individui in specie animali conviventi. *Memor. Accad. Lincei, Ser. 6*, 2, 31-113, 1926 (translated as: Variations and fluctuations of the number of individuals in animal species living together. *J. du Cons. int. Explor. Mer.* 3, 1-51, 1928).

Simultaneous Approximation In Operator And Tensor Product Spaces

By

Eyad Abu-Sirhan

Al-Hussain University-Tafeela-Jordan

Abu-Sirhan_74@yahoo.com

and

Roshdi Khalil

University of Jordan-Amman-Jordan

roshdi@ju.edu.jo

Abstract

Let X and Y be Banach spaces, $L(X, Y)$ the space of bounded linear operators from X into Y , and $X \overset{\alpha}{\otimes} Y$ be the tensor product of X and Y with a uniform cross norm α . A subspace G is called 2-simultaneously proximal if for every $x_1, x_2 \in X$ there exists $y \in G$ such that $\|x_1 - y\| + \|x_2 - y\| \leq \|x_1 - z\| + \|x_2 - z\|$ for all $z \in G$. n -simultaneously proximality is defined similarly. In this paper, we discuss simultaneous approximation in $L(X, Y)$ and $X \overset{\alpha}{\otimes} Y$.

Key Words: Simultaneous approximation.

Classification Numbers: Primary: 41A28, secondary: 41A65

I. **Introduction.** Let X be a Banach space and G be a closed subspace of X . For a finite set $E \subset X$, we write

$$d_p(E, G) = \inf \left\{ \left(\sum_{e \in E} \|e - y\|^p \right)^{\frac{1}{p}} : y \in G \right\}, 1 \leq p < \infty, \text{ and } d_\infty(E, G) = \inf \left\{ \sup_{e \in E} \|e - y\| : y \in G \right\}.$$
 Such infimum need not be attained. In case the infimum is attained for any subset $E \subset X$, we say that G is $|E|$ -simultaneously proximal in X , where $|E|$ is the cardinality of E . We say G is n -simultaneously

proximal in X for d_1 , if for any set E in X , with $|E| = n$, there exists $y \in G$ such that $d_1(E, G) = \sum_{e \in E} \|e - y\|$. In case $|E| = 1$, then 1-simultaneous proximality is just proximality. The first result on 2-simultaneous approximation in $C(I, R)$, the space of continuous real valued functions on some compact interval I , is due to Dunham [4]. Many good results had appeared since then. We refer to [2], [7], [10], [11], [8], [9], and [12]. However, all these results except for [8], dealt with the space of continuous functions with d_∞ instead of d_1 . No results on simultaneous approximation has been cited in spaces of operators. It is the object of this paper to study such problem in certain operator spaces. We prove that the space of compact operators on a Hilbert space H is 2-simultaneously proximal in $L(H)$, the space of bounded linear operators on H . Proximality in tensor product spaces is also discussed. We only discuss 2-simultaneous proximality. The proofs work for n -simultaneous proximality for any n .

Through out this paper, if X and Y are Banach spaces, then $L(X, Y)$ denotes the space of all bounded linear operator from X into Y , and $K(X, Y)$ the subspace of compact operators. $X \overset{\vee}{\otimes} Y$ and $X \overset{\wedge}{\otimes} Y$ are the injective and the projective tensor products of X and Y respectively. The closed unit ball of a Banach space X will be denoted by $B[X]$, and $S[X]$ denotes the unit sphere of X .

II. Simultaneous Approximation in Tensor Product Spaces.

Let X and Y be Banach spaces and $X \overset{\vee}{\otimes} Y$ and $X \overset{\wedge}{\otimes} Y$ be the injective and the projective tensor products of X and Y respectively. In general $X \overset{\vee}{\otimes} Y \subseteq K(X^*, Y)$, and $X \overset{\wedge}{\otimes} Y$ is a subspace of the space of the nuclear operators from X^* into Y , [3]. For any Banach space Y and closed subspace F of Y , we set: $J(Y) = Y \oplus_1 Y$ with $\|x + y\| = \|x\| + \|y\|$, and $D(F) = \{(z, z) : z \in F\}$, with $\|(z, z)\| = \|z\| + \|z\|$.

Clearly, $D(F)$ is a closed subspace of $J(Y)$. Further, F is 2-simultaneously proximal in Y if and only if $D(F)$ is proximal in $J(Y)$.

We start with the following simple but interesting result.

Theorem 2.1. Let G be a closed subspace of the Banach space Y . If $X \overset{\vee}{\otimes} G$ is 2-simultaneously proximal in $X \overset{\vee}{\otimes} Y$, then G is 2-simultaneously proximal in Y .

Proof. Let $y_1, y_2 \in Y$. Let $x \in S[X]$. Choose $x^* \in S[X^*]$ such that $\langle x, x^* \rangle = 1$. The elements $x \otimes y_1$ and $x \otimes y_2$ are in $X \overset{\vee}{\otimes} Y$. Since $X \overset{\vee}{\otimes} G$ is 2-simultaneously proximal in $X \overset{\vee}{\otimes} Y$, there exists $z_0 \in X \overset{\vee}{\otimes} G$ such that $\|x \otimes y_1 - z_0\| + \|x \otimes y_2 - z_0\| \leq \|x \otimes y_1 - z\| + \|x \otimes y_2 - z\|$ for all $z \in X \overset{\vee}{\otimes} G$. In particular this inequality is valid if we choose $z = x \otimes g$, for some $g \in G$.

So $\|x \otimes y_1 - z_0\| + \|x \otimes y_2 - z_0\| \leq \|x \otimes y_1 - x \otimes g\| + \|x \otimes y_2 - x \otimes g\|$
 $\leq \|x\| (\|y_1 - g\| + \|y_2 - g\|) = \|y_1 - g\| + \|y_2 - g\|$.

Hence, for any $v^* \in S[X^*]$, we have

$\|(x \otimes y_1)(v^*) - z_0(v^*)\| + \|(x \otimes y_2)(v^*) - z_0(v^*)\| \leq \|y_1 - g\| + \|y_2 - g\|$.
 Choose v^* to equal x^* . However, $(x \otimes y_1)(x^*) = y_1$ and $(x \otimes y_2)(x^*) = y_2$.
 Thus $\|y_1 - z_0(x^*)\| + \|y_2 - z_0(x^*)\| \leq \|y_1 - g\| + \|y_2 - g\|$ for all $g \in G$.
 Consequently, $z_0(x^*)$ is a best 2-simultaneous approximation of $y_1, y_2 \in Y$.
 Hence G is 2-simultaneously proximal in Y with respect to d_1 .

Notice that Theorem 2.1 is true for n-simultaneous proximality, and the proof is exactly the same. We should remark that when we don't mention the distance, it is meant d_1 .

Corollary 2.2. If $C(I, G)$ is 2-simultaneously proximal in $C(I, X)$, then G is 2-simultaneously proximal in X .

Proof. The proof follows from Theorem 2.1 and the fact that $C(I, X) = C(I) \overset{\vee}{\otimes} X$, [3].

As for the projective tensor product spaces, we have:

Theorem 2.3. Let X be a reflexive Banach space with the approximation property, and G be a reflexive subspace of a Banach space Y . Then $X \overset{\wedge}{\otimes} G$ is 2-simultaneously proximal in $X \overset{\wedge}{\otimes} Y$.

Proof. Since X is reflexive, then X has the Radon Nikodym property, [3].
 Hence by assumption on X , $X \overset{\wedge}{\otimes} Y^{**} = (X^* \overset{\vee}{\otimes} Y^*)^*$ [6]. We claim that $D(X \overset{\wedge}{\otimes} G)$ is proximal in $X \overset{\wedge}{\otimes} Y^{**} \oplus_1 X \overset{\wedge}{\otimes} Y^{**}$. To Prove our claim, it is sufficient to prove that $D(X \overset{\wedge}{\otimes} G)$ is w^* -closed in $X \overset{\wedge}{\otimes} Y^{**} \oplus_1 X \overset{\wedge}{\otimes} Y^{**} = ((X^* \overset{\vee}{\otimes} Y^*) \oplus_\infty (X^* \overset{\vee}{\otimes} Y^*))^*$.
 So, let (S, T) be a w^* -limit point of $D(X \overset{\wedge}{\otimes} G)$ in $X \overset{\wedge}{\otimes} Y^{**} \oplus_1 X \overset{\wedge}{\otimes} Y^{**}$. Then,

we can assume the existence of a sequence $(A_n, A_n) \in D(X \overset{\wedge}{\otimes} G)$ such that $(A_n, A_n) \longrightarrow (S, T)$ in the w^* -topology. Hence,
 $\lim_{n \rightarrow \infty} (S_n, S_n)(x_1^* \otimes y_1^*, x_2^* \otimes y_2^*) = \lim_{n \rightarrow \infty} (< S_n x_1^*, y_1^* > + < S_n x_2^*, y_2^* >)$. But this is equal to $< S x_1^*, y_1^* > + < T x_2^*, y_2^* >$.

Further, this is true for all x_i^* and y_i^* in X^* and Y^* respectively. In particular, choose $y_2^* = 0$. Then

$\lim_{n \rightarrow \infty} < S_n x_1^*, y_1^* > = < S x_1^*, y_1^* >$ for all x_i^* and y_i^* in X^* and Y^* respectively. So (S_n) is a sequence of operators that converges in the weak operator topology. By the Uniform Boundedness Principle, the sequence is uniformly bounded, say $\sup \|S_n\| \leq M$.

Now, for non zero $x^* \in X^*$, we have $\frac{S_n(x^*)}{M\|x^*\|} \in B_1(G)$ for all n . Since $B_1[G]$ is closed and bounded in a reflexive Banach space, we get $B_1(G)$ is compact in the w^* - topology. But $(\frac{S_n(x^*)}{M\|x^*\|})$ converges to $\frac{S(x^*)}{M\|x^*\|}$ in the w^* - topology. Consequently, $S(x^*) \in G$ for all $x^* \in X$. Hence $S \in X \hat{\otimes} G$. Further, one can easily see that $S = T$. So, $(S, T) = (S, S) \in D(X \hat{\otimes} G)$. Hence $D(X \hat{\otimes} G)$ is w^* -closed, and hence proximal in $X \hat{\otimes} Y^{**} \oplus_1 X \hat{\otimes} Y^{**}$. Consequently, $D(X \hat{\otimes} G)$ is proximal in $X \hat{\otimes} Y \oplus_1 X \hat{\otimes} Y$, Hence, $X \hat{\otimes} G$ is 2- simultaneously proximal in $X \hat{\otimes} Y$.

As a corollary to Theorem 2.3. one can easily prove that for any closed subspace $G \subseteq L^p(I)$, we have $L^p(I) \hat{\otimes} G$ is 2-simultaneously proximal in $L^p(I) \hat{\otimes} L^p(I)$.

We should remark that if G is any closed subspace of any Hilbert space, then G is 2-simultaneously proximal in H for d_2 . This follows from the fact that $H \oplus_2 H$, is a Hilbert space, and $D(G)$ is a closed subspace of $H \oplus_2 H$, so proximal.

Theorem 2.4. Let G be a closed subspace of a Banach space X . The following are equivalent:

- (i) G is 2-simultaneously proximal in X for d_1 .
- (ii) $\ell^1(G)$ is 2-simultaneously proximal in $\ell^1(X)$ for d_1 .

Proof. (i) \longrightarrow (ii). Let $J = \ell^1(X) \oplus_1 \ell^1(X)$, $M = D(\ell^1(G)) = \{(g, g) : g \in \ell^1(G), \|g, g\| = \|g\| + \|g\|\}$. Assume (f, h) be any element in J . Then, $\|(f, h) - (g, g)\| = \|f - g\| + \|h - g\|$. So, if $f = (x_n)$, $h = (y_n)$ and $g = (z_n)$, then $\|(f, h) - (g, g)\| = \sum (\|x_n - z_n\| + \|y_n - z_n\|)$. So if we choose z_n to be the best 2-simultaneous approximant of x_n and y_n , we get $\|x_n - z_n\| + \|y_n - z_n\| \leq \|x_n - w_n\| + \|y_n - w_n\|$ for any $w_n \in G$. In particular, if we take $w_n = 0$, then using the triangular inequality we get $\|z_n\| \leq \|x_n\| + \|y_n\|$.

Consequently, $(z_n) \in \ell^1(G)$. This implies that (z_n) is a best 2-simultaneous approximant of (x_n) and (y_n) , and $\ell^1(G)$ is 2-simultaneously proximal in $\ell^1(X)$ for d_1 .

Conversely. (ii) \longrightarrow (i). Let $\ell^1(G)$ be 2-simultaneously proximal in $\ell^1(X)$ for d_1 . Let $x, y \in \ell^1(X)$. Set $\hat{x} = (x, 0, 0, 0, \dots)$ and $\hat{y} = (y, 0, 0, 0, \dots)$. Then \hat{x} and \hat{y} are both in $\ell^1(X)$. By assumption, there exists $z = (z_n) \in \ell^1(G)$ such that $\|\hat{x} - z\| + \|\hat{y} - z\| \leq \|\hat{x} - w\| + \|\hat{y} - w\|$ for all $w \in \ell^1(G)$. Take $w = (z_1, 0, 0, 0, \dots)$. So,

$$\|x - z_1\| + \sum_{k=2} \|z_k\| + \|y - z_1\| + \sum_{k=2} \|z_k\| \leq \|x - z_1\| + \|y - z_1\|.$$
 Hence,

$z_k = 0$ for all $k \geq 2$. So $\|x - z_1\| + \|y - z_1\| + \leq \|x - g\| + \|y - g\|$ for all $g \in G$, and G is 2-simultaneously proximal in X for d_1 .

As a consequence of Theorem 2.4, we get

Corollary 2.5. If G is a reflexive subspace of the Banach space X , then $\ell^1(G)$ be 2-simultaneously proximal in $\ell^1(X)$ for d_1 .

Definition 2.6. A subspace G of the Banach space X is called p -summand, $1 \leq p < \infty$, if there exists a closed subspace $W \subset X$, such that $X = G \oplus W$, and for $x = g + w$, one has $\|x\| = (\|g\|^p + \|w\|^p)^{\frac{1}{p}}$. We write $X = G \oplus_p W$. If G is 1-summand in X , then the projection $P : X \rightarrow G$, $P(g + w) = g$, is called an L^1 - projection of X onto G , and G is called 1-complemented in X . In case $\|x\| = \max\{\|g\|, \|w\|\}$, in this case we call G an ∞ -summand. We refer to [1] for more on contractive projections.

Proposition 2.7. If G is 1-summand of the Banach space Y , then $X \hat{\otimes} G$ is 1-summand in $X \hat{\otimes} Y$ for any Banach space X .

Proof. Since G is 1-complemented, $X \hat{\otimes} G$ is closed in $X \hat{\otimes} Y$, [5]. Let P be the L^1 - projection associated with G . For $A \in X \hat{\otimes} Y$, set $A_1 = PA$ and $A_2 = (I - P)A$. Clearly both A_1 and A_2 are in $X \hat{\otimes} Y$. Choose $\epsilon > 0$ and a representation of A , $A = \sum x_i \otimes y_i$ such that $\|A\| \leq \sum \|x_i\| \|y_i\| \leq \|A\| + \epsilon$, [3]. Then $A_1 = \sum x_i \otimes Py_i$ and $A_2 = \sum x_i \otimes (I - P)y_i$. Now, $A = A_1 + A_2$, and $\|A_1\| + \|A_2\| \leq \sum \|x_i\| (\|Py_i\| + \|(I - P)y_i\|) = \sum \|x_i\| \|y_i\|$, since G is 1-summand. Thus $\|A\| \leq \|A_1\| + \|A_2\| \leq \sum \|x_i\| \|y_i\| \leq \|A\| + \epsilon$. Since ϵ was arbitrary, the result follows.

Theorem 2.8. If G is a 1-summand subspace of the Banach space Y , then $X \hat{\otimes} G$ is 2-simultaneously proximal in $X \hat{\otimes} Y$ for the d_1 .

Proof. By Proposition 2.7, it follows that $X \hat{\otimes} G$ is 1-summand of $X \hat{\otimes} Y$. Theorem 3.1 of [5] now gives the result.

III. Simultaneous Approximation in Operator Spaces.

Let X and Y be Banach spaces, and $L(X, Y)$ be the Banach space of all bounded linear operators from X into Y . In this section we present some results on simultaneous proximality in $L(X, Y)$. We start with the following:

Lemma 3.1. Let G be a reflexive subspace of the Banach space X . Then $L(X, G)$ is 2-simultaneously proximal in $L(X, X)$ in d_1 .

Proof. Let $D = \{(A, A) : A \in L(X, G)\}$. Then
 $D \subseteq L(X, X) \oplus_1 L(X, X) \subseteq L(X, X^*) \oplus_1 L(X, X^*)$

$$= (X \hat{\otimes} X^*)^* \oplus_1 (X \hat{\otimes} X^*)^* = ((X \hat{\otimes} X^*) \oplus_\infty (X \hat{\otimes} X^*))^*.$$

Since G is reflexive, then D is w^* -closed in $((X \hat{\otimes} X^*) \oplus_\infty (X \hat{\otimes} X^*))^*$.

Hence D is proximal in $L(X, X) \oplus_1 L(X, X) \subseteq ((X \hat{\otimes} X^*) \oplus_\infty (X \hat{\otimes} X^*))^*$.

Consequently, $L(X, G)$ is simultaneous 2-proximal in $L(X, X)$ in d_1 .

It should be remarked that Lemma 3.1 implies that for any closed subspace $G \subseteq \ell^2$, $L(\ell^2, G)$ is 2-simultaneously proximal in $L(\ell^2, \ell^2)$ in d_1 .

Lemma 3.2. Let G be 1-summand subspace of the Banach space Y . Then $L(X, G)$ is an ∞ -summand subspace in $L(X, Y)$ for any Banach space X .

Proof. Let $T \in L(X, Y)$. With no loss of generality we assume $\|T\| = 1$. Since G is 1-summand, then for any $x \in X$, $Tx = y + z \in Y = G \oplus W$, with $\|Tx\| = \|y\| + \|z\|$. Define $T_1x = y$, and $T_2x = z$. So $T_1x = PTx$, and $T_2x = (I - P)Tx$. Since $\sup\{\|Tx\| : x \in S[X]\} = 1$, and $\max\{\|P\|, \|I - P\|\} = \|P + (I - P)\|$, the result follows.

The following result is needed in consequent results.

Lemma 3.3. Let X and Y be Banach spaces such that $(X \overset{\vee}{\otimes} Y)^* = X^* \hat{\otimes} Y^*$. Then $(X \overset{\vee}{\otimes} G)^\perp = X^* \hat{\otimes} G^\perp$ for any closed subspace $G \subseteq Y$.

Proof. That $X^* \hat{\otimes} G^\perp \subseteq (X \overset{\vee}{\otimes} G)^\perp$ is simple. To prove the other inclusion:

Let $F \in (X \overset{\vee}{\otimes} G)^\perp \subseteq X^* \hat{\otimes} Y^*$ such that $F = \sum_{n=1}^k x_n^* \otimes y_n^*$, where $\{x_1^*, \dots, x_k^*\}$

are chosen to be independent.

We claim that $y_i^* \in G^\perp$. Indeed; let $g \in G$, and $M = [x_2^*, \dots, x_k^*]$. By the Hahn Banach Theorem, there exists $z_1 \in X^{**}$ such $z_1(m) = 0$ for all $m \in M$ and $z_1(x_1^*) \neq 0$. Then, since $G \subseteq G^{**}$, it follows $z_1 \otimes g \in (X \overset{\vee}{\otimes} G)^{**}$. Since G is w^* -dense in G^{**} , and $F \in X^* \hat{\otimes} Y^*$, it follows that $\langle z_1, x_1^* \rangle \langle y_1^*, g \rangle = 0$. Since $\langle z_1, x_1^* \rangle \neq 0$, then $\langle y_1^*, g \rangle = 0$. In a similar way, $\langle y_i^*, g \rangle = 0$ for all i . Hence $y_i^* \in G^\perp$ for all i . So $F \in X^* \hat{\otimes} G^\perp$. Since elements F of the given form are dense in $(X \overset{\vee}{\otimes} G)^\perp$, the result follows.

As a consequence, we get:

Lemma 3.4. Let Y be a Banach space that satisfies the Radon Nikodym property and the approximation property. If G is an M -ideal of Y , then $X \overset{\vee}{\otimes} G$ is an M -ideal in $X \overset{\vee}{\otimes} Y$.

Proof. Since G is an M -ideal in Y , then G^\perp is a 1-summand in Y^* . By Proposition 2.7, $X \hat{\otimes} G^\perp$ is a 1-summand $X^* \hat{\otimes} Y^*$. So, by Lemma 3.2 $(X \overset{\vee}{\otimes} G)^\perp$ is a 1-summand in $(X \overset{\vee}{\otimes} Y)^* = X^* \hat{\otimes} Y^*$. This gives the result.

Proposition 3.5. If G is an M -ideal of the Banach space X , then G is 2-simultaneously proximal in d_∞ .

Proof. Let $Y = X \oplus_\infty X$, and $W = \{(g, g) : g \in G\}$. It is sufficient to show W is proximal in Y . Now, since G is an M -ideal in X , then $X^* = G^\perp \oplus_1 Q$. Consequently, $Y^* = X^* \oplus_1 X^* = G^\perp \oplus_1 (Q \oplus_1 Q \oplus_1 G^\perp)$.

But in Y , the spaces G and W are isometrically isomorphic. Hence, G^\perp and W^\perp are isometrically isomorphic. Thus we can write $Y^* = W^\perp \oplus_1 L$, where $L = Q \oplus_1 Q \oplus_1 G^\perp$. Hence, W is an M -ideal of Y , and consequently W is proximal in Y . This ends the proof.

As a nice consequence of Proposition 3.5 is:

Theorem 3.6. $K(\ell^2)$ is 2-simultaneously proximal in $L(\ell^2)$ in d_∞ .

Proof. It is known that $K(\ell^2)$ is an M -ideal of $L(\ell^2)$. Proposition 3.5 now gives the result.

Another consequence of proposition 3.5 we have:

Proposition 3.7. Let X and Y be two Banach spaces such that Y^* has the approximation and the Radon-Nikodym properties. If G is an M -ideal of Y , the $X \overset{\vee}{\otimes} G$ is 2-simultaneously proximal in $X \overset{\vee}{\otimes} Y$ in d_∞ .

The proof follows from proposition 3.4 and Lemma 3.3.

Proposition 3.8. $K(\ell^p)$ is simultaneously proximal in $L(\ell^p)$ in d_∞ .

The proof follows from the fact [1], that $K(\ell^p)$ is an M -ideal in $L(\ell^p)$ and proposition 3.5.

As for proximality in the space of compact operators, we do have the following result.

Let $C(I, X)$ be the space of continuous functions on the compact interval I with values in X , and $C_0(I, X)$ be the subspace of $C(I, X)$ that vanish at infinity. It is known [10], that $C(I, X) = C(I) \overset{\vee}{\otimes} X$, and $C_0(I, X) = C_0(I) \overset{\vee}{\otimes} X$. Further, [1], $C_0(I, X)$ is an M -ideal in $C(I, X)$. Consequently:

Proposition 3.7. Let X be a Banach space with the approximation and the Radon Nikodym properties. Then $C_0(I, X)$ is simultaneously proximal in $C(I, X)$ in d_∞ .

Lemma 3.7. Let X be a Banach space and G be any closed subspace of X . Then under the N -norm we have: $D(L(X, G)) = L(X, D(G))$.

Proof. Let $T \in L(X, D(G))$, then $Tx = (z, z)$. Define $A(x) = z$. Then A is well defined linear operator.

Moreover $\|T(x)\| = \|(A(x), A(x))\| = 2\|A(x)\|$. Then, A is bounded and hence $A \in L(X, G)$. Now define

$\Phi : L(X, D(G)) \rightarrow D(L(X, G))$ by $\Phi(T) = 2A$. Clearly Φ is onto isometry.

Lemma 3.8. Let X be a Banach space, then $L\left(X, X \oplus_\infty X\right) = L(X, X) \oplus_\infty L(X, X)$.

Proof. Let $T \in L\left(X, X \oplus_{\infty} X\right)$, $T(x) = (z_1, z_2)$. Define $A(x) = z_1$ and $B(x) = z_2$. Then $A, B \in L(X, X)$. For any $x \in X$ with $\|x\| = 1$, we have

$$\begin{aligned} \|A(x)\| &\leq \max\{\|A(x)\|, \|B(x)\|\} \leq \max\{\|A\|, \|B\|\}, \\ \|A\| &\leq \sup_{\|x\|=1} \max\{\|A(x)\|, \|B(x)\|\} \leq \max\{\|A\|, \|B\|\}. \end{aligned} \quad (1)$$

Similarly we have

$$\|B\| \leq \sup_{\|x\|=1} \max\{\|A(x)\|, \|B(x)\|\} \leq \max\{\|A\|, \|B\|\}. \quad (2)$$

From (1) and (2) we have

$$\max\{\|A\|, \|B\|\} \leq \sup_{\|x\|=1} \max\{\|A(x)\|, \|B(x)\|\} \leq \max\{\|A\|, \|B\|\}.$$

Thus

$$\max\{\|A\|, \|B\|\} = \sup_{\|x\|=1} \max\{\|A(x)\|, \|B(x)\|\}.$$

So, if we define $\Phi : L\left(X, X \oplus_{\infty} X\right) \rightarrow L(X, X) \oplus_{\infty} L(X, X)$ by $\Phi(T) = (A, B)$.

Then one can easily checked that Φ is onto isometry.

Theorem 3.9. For any closed subspace G of X . The following are equivalent :

- (i) $L(X, D(G))$ is proximal in $L\left(X, X \oplus_{\infty} X\right)$.
- (ii) $L(X, G)$ is ∞ -simultaneously proximal in $L(X, X)$.

Proof. By Lemma 3.7, $D(L(X, G))$ is proximal in $L\left(X, X \oplus_{\infty} X\right)$ and by Lemma 3.8 $D(L(X, G))$ is proximal in $L(X, X) \oplus_{\infty} L(X, X)$. But $D(L(X, G))$ is proximal in $L(X, X) \oplus_{\infty} L(X, X)$ if and only if $L(X, G)$ is ∞ -simultaneously proximal in $L(X, X)$. The result follows.

Theorem 3.10. Let G be w^* -closed subspace of a dual space X . Then $\ell^{\infty}(G)$ is simultaneously proximal in $\ell^{\infty}(X)$.

Proof. It is sufficient to show that $D = \{(h, h) : h \in \ell^{\infty}(G)\}$ is proximal in $\ell^{\infty}(X) \oplus_1 \ell^{\infty}(X)$. So we will prove that D is w^* -closed in $\ell^{\infty}(X) \oplus_1 \ell^{\infty}(X)$. Let

$((x_n), (y_n)) \in \ell^{\infty}(X) \oplus_1 \ell^{\infty}(X) \subset \left(\ell^{\infty}(X^*) \oplus_{\infty} \ell^{\infty}(X^*)\right)^*$ be a w^* -limit point of D . Then there exists $\{(h_n, h_n)\}_{n=1}^{\infty}$ a sequence in D such that $(h_m, h_m) \xrightarrow{w^*}$

$((x_n), (y_n))$; where $h_m = \left(h_n^{(m)}\right)_{n=1}^{\infty}$. Then for all $((s_n^*), (t_n^*)) \in \ell^\infty(X^*) \oplus \ell^\infty(X^*)$ we have

$$\begin{aligned} \lim_{m \rightarrow \infty} \langle ((s_n^*), (t_n^*)), (h_m, h_m) \rangle &= \langle ((s_n^*), (t_n^*)), ((x_n), (y_n)) \rangle, \\ \lim_{m \rightarrow \infty} \left(\sum_{n=1}^{\infty} \langle h_n^m, s_n^* \rangle, \sum_{n=1}^{\infty} \langle h_n^m, t_n^* \rangle \right) &= \lim_{m \rightarrow \infty} \left(\sum_{n=1}^{\infty} \langle h_n^m, x_n \rangle, \sum_{n=1}^{\infty} \langle h_n^m, y_n \rangle \right) \end{aligned}$$

take $(t_n^*) = 0$ and $(s_n^*) = (0, 0, \dots, x_{n^*}^*, 0, \dots)$, then $\lim_{m \rightarrow \infty} x^*(h_n^m) = x^*(x_n)$ and this is true for all $x^* \in X^*$. Thus $h_n^m \xrightarrow{w^*} x_n$ for all n. Since G is w^* -closed, then $x_n \in G$ for all n. So $(x_n) \in \ell^\infty(G)$. Similarly $(y_n) \in \ell^\infty(G)$. Since $\lim_{m \rightarrow \infty} x^*(h_n^m) = x^*(x_n) = x^*(y_n)$ for all $x^* \in X^*$ and for all n, then $x_n = y_n$ for all n. Thus $((x_n), (y_n)) \in D$ and D is w^* -closed. This ends the proof.

Theorem 3.11. Let H be a Hilbert space and $P : H \rightarrow G$ be the orthogonal projection from H into a closed subspace G of H . Then for any $x, y \in H$, $z = \frac{P(x) + P(y)}{2}$ is a best simultaneous approximant of x, y in H from G in d_2 .

Proof. If possible, assume that there exists $z_1 \in G$ such that

$$\left(\|x - z_1\|^2 + \|y - z_1\|^2 \right)^{\frac{1}{2}} < \left(\|x - z\|^2 + \|y - z\|^2 \right)^{\frac{1}{2}}. \quad (*)$$

Let $w_x = x - z_1$ and $w_y = y - z_1$. Then $w_x = P(w_x) + w_x^\perp$ and $w_y = P(w_y) + w_y^\perp$; where $w_x^\perp, w_y^\perp \in G^\perp$. Then $x = P(w_x) + z_1 + w_x^\perp$ and $y = P(w_y) + z_1 + w_y^\perp$. Further $x = P(x) + (I - P)(x)$ and $y = P(y) + (I - P)(y)$. Since the representation of x in $H = G + G^\perp$ is unique, it follows that

$P(y) = P(w_y) + z_1$ and $w_y^\perp = y - P(y)$. Similarly $P(x) = P(w_x) + z_1$ and $w_x^\perp = x - P(x)$. Now from (*) we have

$$\|w_x\|^2 + \|w_y\|^2 < \|x - z\|^2 + \|y - z\|^2.$$

So

$$\|w_x^\perp + P(w_x)\|^2 + \|w_y^\perp + P(w_y)\|^2 < \|x - P(x)\|^2 + \frac{1}{2} \|P(x - y)\|^2 + \|y - P(y)\|^2.$$

Hence

$$\|w_x^\perp\|^2 + \|w_y^\perp\|^2 + \|P(w_x)\|^2 + \|P(w_y)\|^2 < \|w_x^\perp\|^2 + \frac{1}{2} \|P(x - y)\|^2 + \|w_y^\perp\|^2.$$

Consequently

$$2 \|P(w_x)\|^2 + 2 \|P(w_y)\|^2 < \|P(x - y)\|^2.$$

But $x - y = w_x - w_y$. So by Parallelogram identity we get

$$\|P(w_x - w_y)\|^2 + \|P(w_x + w_y)\|^2 < \|P(w_x - w_y)\|^2.$$

Thus $\|P(w_x + w_y)\|^2 < 0$, which is a contradiction.

References

1. Alfsen, E. M. and E. Effros, E. M. Structure in Real Banach Spaces. Ann. of Math. 96(1972) 98-173.
2. Chong, Li. and Watson, G. A. On best simultaneous approximation. J. Approx. Theory. 91(1997)332-348.
3. Diestel, J., and Uhl, J. J. Vector measures. The American Mathematical Society, Providence, R. I. 1977
4. Dunham, C.B. Simultaneous Chebyshev approximation of functions on an interval. Proc. Amer. Math. Soc. 18(1967), 472-477.
5. Khalil, R. Best approximation in $L^p(I, X)$. Math. Proc. Camb. Phil. Soc. 94(1983)177-279.
6. Light, W. A., and Cheney. Approximation Theory in Tensor Product spaces. Lecture Notes in Mathematics. 1169, Singer-Verlag, New York. 1985.
7. Mach, J. Best simultaneous approximation of bounded functions with values in certain Banach spaces. Math. Ann. 240(1979)157-164.
8. Saidi, F. Hussein, D. and Khalil, R. Best simultaneous approximation in $L^p(I, X)$. J. Approx. Theory. 116(2002)369-379.
9. Shany, B. N. and Singh, S. P. On best simultaneous approximation in Banach spaces. J. Approx. Theory. 35(1982)222-224.
10. Tanimoto, S. Characterization of best simultaneous approximation. J. Approx. Theory. 59(1989)359-361.
11. Tanimoto, S. On best simultaneous approximation. Math. Jap. 48(1998)275-279.
12. Watson, G. A. A characterization of best simultaneous approximations. J. Approx. Theory. 75(1993)175-182.

WEAK COMPATIBILITY AND FIXED POINT THEOREMS IN FUZZY METRIC SPACE USING IMPLICIT RELATION.

By

Sushil Sharma* and Goldi Tiwari**

* Department of Mathematics

Madhav Science College, Vikram University, Ujjain M.P., India

Sksharma2005@yahoo.com

** Department of Mathematics

Laxmi Narain Institute of Technology

Sanver Road, Indore, M.P., India

Ayushitiwari8@yahoo.com

Abstract : In this paper we prove common fixed point theorems for weak compatible mappings satisfying implicit relations. We extend some earlier results.

1.Introduction : The concept of fuzzy sets was introduced initially by Zadeh [10] in 1965 since then ,to use this concept in topology and analysis many authors have expansively developed the theory of fuzzy sets and application, Especially, Deng [26], Erceg [12], Kaleva and Seikkala [13], Kramosil and Michalek [9] have introduced the concept of fuzzy metric spaces in different ways. Recently many authors have also studied the fixed point theory in these fuzzy metric spaces ([1],[2],[3],[7],[8],[11],[14],[16-21],[23],[24],[25]) .

Grabiec [11] followed Kramosil and Michalek [9] and obtained the fuzzy version of Banach's fixed point theorem.

In 1976, Jungck [4] established common fixed point theorems for commuting maps generalizing the Banach's fixed point theorem. Sessa [15] defined a generalization of commutativity, which is called weak compatibility. Further Jungck [5] introduced more generalized commutativity, so called compatibility.

Mishra, Sharma and Singh [14] introduced the concept of compatibility in fuzzy metric spaces. In 1998, Jungck and Rhoades [6] introduced the notion of weakly compatible maps and showed that compatible maps are weakly compatible but converse need not true. Sharma and Deshpande [21] improved the result of Mishra, Sharma and Singh

[14], Cho [23], Cho, Pathak, Kang and Jung [25], Sharma [16] Sharma and Deshpande [20]. They proved common fixed point theorems for weakly compatible maps in fuzzy metric spaces without taking any mapping continuous.

AMS (2000) Subject Classification : 47H10, 54H25.

Key Words : Common fixed point, weak compatible mappings, implicit relations,...

In this paper, we prove common fixed point theorem, for four mappings under the condition of weak compatible mappings in non-complete fuzzy metric spaces, without taking any function continuous. We improve result of Singh and Jain [2],[3], Sharma and Deshpande [19] [21], Sharma [18].

2. Preliminaries

Definition 2.1. A binary operation $*$: $[0,1] \times [0,1] \rightarrow [0,1]$ is called a continuous t-norm if $([0,1], *)$ is an abelian topological monoid with unit 1 such that $a*b \leq c*d$ whenever $a \leq c$ and $b \leq d$ for all a, b, c and d in $[0,1]$.

Definition 2.2 (Kramosil and Michalek [9]). The 3-tuple $(X, M, *)$ is called a fuzzy metric space if X is an arbitrary set, $*$ is a continuous t-norm, and M is a fuzzy set in $X^2 \times [0, \infty)$ satisfying the following conditions for all $x, y, z \in X$ and $s, t > 0$:

(FM-1) $M(x, y, 0) = 0$;

(FM-2) $M(x, y, t) = 1$, for all $t > 0$ if and only if $x = y$;

(FM-3) $M(x, y, t) = M(y, x, t)$;

(FM-4) $M(x, y, t) * M(y, z, s) \geq M(x, z, t+s)$;

(FM-5) $M(x, y, \cdot) : [0, \infty) \rightarrow [0, 1]$ is left continuous.

Note that $M(x, y, t)$ can be thought of as the degree of nearness between x and y with respect to t . we identify $x = y$ with $M(x, y, t) = 1$ for all $t > 0$. The following example shows that every metric space induces a fuzzy metric space.

Example 2.1 (George and Veeramani [1]). Let (X, d) be a metric space. Define $a \cdot b = \min \{a, b\}$ and for all $a, b \in X$,

$$M(x, y, t) = \frac{t}{t + d(x, y)} \quad \forall t > 0;$$

$$M(x, y, 0) = 0$$

Then $(X, M, *)$ is a fuzzy metric space. It is called the fuzzy metric space induced by metric d .

Lemma 2.1 (Grabiec [11]). For all $x, y \in X$, $M(x, y, \cdot)$ is a non decreasing function.

Remark 2.1. Since $*$ is continuous, it follows from (FM-4) that the limit of a sequence in a fuzzy metric space is a unique.

In this paper, $(X, M, *)$ is considered to be non-complete fuzzy metric space with the condition (FM-6)

$$\lim_{t \rightarrow \infty} M(x, y, t) = 1, \text{ for all } x, y \in X.$$

Lemma 2.2 (Cho [23]). Let $\{y_n\}$ be a sequence in a fuzzy metric space $(X, M, *)$ with the condition (FM-6). If there exist a number $k \in (0, 1)$ such that

$$M(y_{n+2}, Y_{n+1}, kt) \geq M(y_{n+1}, Y_n, t)$$

for all $t > 0$, then $\{y_n\}$ is a Cauchy sequence in X .

Let Ψ is the set of all real continuous functions $\varphi : (R^+)^4 \rightarrow R$, non-decreasing and satisfying the following conditions.

For $u, v \geq 0$,

$$(i) \quad \varphi(u, v, v, u) \geq 0 \quad \text{or} \quad \varphi(u, v, u, v) \geq 0,$$

implies that $u \geq v$.

$$(ii) \quad \varphi(u, u, 1, 1) \geq 0 \quad \text{or} \quad \varphi(u, 1, u, 1) \geq 0 \quad \text{or} \quad \varphi(u, 1, 1, u)$$

Implies that $u \geq 1$.

Example 2.2 : Define $\varphi(t_1, t_2, t_3, t_4) = 15 t_1 - 13 t_2 + 5 t_3 - 7 t_4$. Then $\varphi \in \Psi$.

3. Main Results

Theorem 3.1. Let A, B, S and T be self-mappings of a fuzzy metric space $(X, M, *)$ satisfying that ;

$$(3.1) \quad A(X) \subseteq T(X), B(X) \subseteq S(X);$$

$$(3.2) \quad \text{the pair } (A, S) \text{ and } (B, T) \text{ is weak compatible};$$

$$(3.3) \quad \text{for some } \varphi \in \Psi, \text{ there exist } k \in (0, 1) \text{ such that for all } x, y \in X \text{ and } t > 0$$

$$\varphi \left(\begin{array}{c} M(Ax, By, kt), M(Sx, Ty, t), M(Ax, Sx, t), M(By, Ty, kt) \\ M(Ax, By, kt), M(Sx, Ty, t), M(Ax, Sx, kt), M(By, Ty, t) \end{array} \right) \geq 0$$

(3.4) One of $A(X)$, $B(X)$, $S(X)$, or $T(X)$ are complete subspace of X . Then

A, B, S and T have a unique common fixed point in X .

Proof. Let $x_0 \in X$ be any arbitrary point as $A(X) \subseteq T(X)$ and $B(X) \subseteq S(X)$ exists

$x_1, x_2 \in X$ such that $Y_{2n+1} = Ax_{2n} = Tx_{2n+1}$, $Y_{2n+2} = Bx_{2n+1} = Sx_{2n+2}$, for $n = 0, 1, 2, \dots$

now using (3.3) with $x = x_{2n}$, $y = x_{2n+1}$ we get

$$\varphi \left(\begin{array}{c} M(Ax_{2n}, Bx_{2n+1}, kt), M(Sx_{2n}, Tx_{2n+1}, t), M(Ax_{2n}, Sx_{2n}, t), M(Bx_{2n+1}, Tx_{2n+1}, kt) \\ M(Ax_{2n}, Bx_{2n+1}, kt), M(Sx_{2n}, Tx_{2n+1}, t), M(Ax_{2n}, Sx_{2n}, kt), M(Bx_{2n+1}, Tx_{2n+1}, t) \end{array} \right) \geq 0$$

that is

$$\varphi \left(\begin{array}{c} M(y_{2n+1}, y_{2n+2}, kt), M(y_{2n}, y_{2n+1}, t), M(y_{2n+1}, y_{2n}, t), M(y_{2n+2}, y_{2n+1}, kt) \\ M(y_{2n+1}, y_{2n+2}, kt), M(y_{2n}, y_{2n+1}, t), M(y_{2n+1}, y_{2n}, kt), M(y_{2n+2}, y_{2n+1}, t) \end{array} \right) \geq 0$$

Using (i), we get

$$M(y_{2n+1}, y_{2n+2}, kt) \geq M(y_{2n}, y_{2n+1}, t).$$

Similarly, by putting $x = x_{2n+2}$ and $y = x_{2n+3}$ in (3.3), We have

$$\varphi \left(\begin{array}{c} M(y_{2n+2}, y_{2n+3}, kt), M(y_{2n+1}, y_{2n+2}, t), M(y_{2n+2}, y_{2n+1}, t), M(y_{2n+3}, y_{2n+2}, kt) \\ M(y_{2n+2}, y_{2n+3}, kt), M(y_{2n+1}, y_{2n+2}, t), M(y_{2n+2}, y_{2n+1}, kt), M(y_{2n+3}, y_{2n+2}, t) \end{array} \right) \geq 0$$

using (i), we get

$$M(y_{2n+3}, y_{2n+2}, kt) \geq M(y_{2n+1}, y_{2n+2}, t)$$

Thus for any n and t , we have

$$M(y_n, y_{n+1}, kt) \geq M(y_{n-1}, y_n, t)$$

Hence by Lemma 2.2, $\{y_{2n}\}$ is a Cauchy sequence in X .

Suppose $S(X)$ is complete subspace of X there exist a point $u = (S)^{-1}z$ i.e. $Su = z$, we have

by (3.3)

$$\varphi \left(\begin{array}{c} M(Au, Bx_{2n+1}, kt), M(Su, Tx_{2n+1}, t), M(Au, Su, t), M(Bx_{2n+1}, Tx_{2n+1}, kt) \\ M(Au, Bx_{2n+1}, kt), M(Su, Tx_{2n+1}, t), M(Au, Su, kt), M(Bx_{2n+1}, Tx_{2n+1}, t) \end{array} \right) \geq 0$$

taking the limit $n \rightarrow \infty$, we get

$$\varphi \left(\begin{array}{c} M(Au, z, kt), 1, M(Au, z, t), 1 \\ M(Au, z, kt), 1, M(Au, z, kt), 1 \end{array} \right) \geq 0$$

Using (ii), we get

$M(Au, z, kt) \geq 1$ for all $t > 0$, which gives $M(Au, z, kt) = 1$ i.e. $Au = z$, therefore $Au = Su = z$.

Now suppose $T(X)$ is complete subspace of X , there exist a point $v = (T)^{-1}z$ i.e. $Tv = z$,

By (3.3), we have

$$\varphi \left(\begin{array}{c} M(Au, Bv, kt), M(Su, Tv, t), M(Au, Su, t), M(Bv, Tv, kt) \\ M(Au, Bv, kt), M(Su, Tv, t), M(Au, Su, kt), M(Bv, Tv, t) \end{array} \right) \geq 0$$

This gives

$$\varphi \left(\begin{array}{c} M(z, Bv, kt), M(z, z, t), M(z, z, t), M(Bv, z, kt) \\ M(z, Bv, kt), M(z, z, t), M(z, z, kt), M(Bv, z, t) \end{array} \right) \geq 0$$

Therefore by using (ii), we have

$M(Bv, z, kt) \geq 1$ for all $t > 0$, which gives $M(Bv, z, kt) = 1$ i.e. $Bv = z$, therefore $Bv = TV = z$.

Hence $Su = Au = Bv = TV = z$.

Again since the pair $\{A, S\}$ is weakly compatible, therefore A and S commute at their coincidence point i.e. $ASu = SAu$ or $Az = Sz$. By (3.3), we have

$$\varphi \left(\begin{array}{c} M(Az, Bv, kt), M(Sz, Tv, t), M(Az, Sz, t), M(Bv, Tv, kt) \\ M(Az, Bv, kt), M(Sz, Tv, t), M(Az, Sz, kt), M(Bv, Tv, t) \end{array} \right) \geq 0$$

As φ is non-decreasing, we have

$$\varphi \left(\begin{array}{c} M(Az, z, kt), M(Sz, z, t), 1, 1 \\ M(Az, z, kt), M(Sz, z, t), 1, 1 \end{array} \right) \geq 0$$

Using (ii), we have

$M(Az, z, kt) \geq 1$ for all $t > 0$, which gives $M(Az, z, kt) = 1$ i.e. $Az = z$, therefore $Az = Sz = z$.

Similarly, we can prove that

$Bz = Tz = z$

Hence $Az = Bz = Sz = Tz = z$

i.e. z is a common fixed point of A, B, S and T

For uniqueness let w ($w \neq z$) be another common fixed point of A, B, S and T by (3.3), we have

$$\varphi \left(\begin{array}{c} M(Az, Bw, kt), M(Sz, Tw, t), M(Az, Sz, t), M(Bw, Tw, kt) \\ M(Az, Bw, kt), M(Sz, Tw, t), M(Az, Sz, kt), M(Bw, Tw, t) \end{array} \right) \geq 0$$

$$\varphi \left(\begin{array}{c} M(z, w, kt), M(z, w, t), 1, 1 \\ M(z, w, kt), M(z, w, kt), 1, 1 \end{array} \right) \geq 0$$

Therefore, by (ii), we have

$M(z, w, kt) \geq 1$ for all $t > 0$, which gives $M(z, w, kt) = 1$ i.e. $z = w$.

This completes the proof.

If we take the space to be complete then we have the following

Corollary 3.1: Let A, B, S and T be self mappings of complete fuzzy metric space $(X, M, *)$

satisfying that

$$(3.1) \quad A(X) \subseteq T(X), B(X) \subseteq S(X);$$

$$(3.2) \quad \text{the pair } (A, S) \text{ and } (B, T) \text{ is weak compatible};$$

$$(3.3) \quad \text{for some } \varphi \in \Psi, \text{ there exist } k \in (0, 1) \text{ such that for all } x, y \in X \text{ and } t > 0$$

$$\varphi \left(\begin{array}{c} M(Ax, By, kt), M(Sx, Ty, t), M(Ax, Sx, t), M(By, Ty, kt) \\ M(Ax, By, kt), M(Sx, Ty, t), M(Ax, Sx, kt), M(By, Ty, t) \end{array} \right) \geq 0$$

Then A, B, S and T have a unique common fixed point in X .

References

- [1] A. George and P. Veeramani, On some results in fuzzy metric spaces, Fuzzy set and Systems 64 (1994), no.3, 395-399.
- [2] B. Singh and S. Jain, Semi-compatibility, compatibility and fixed point theorems in fuzzy metric space, J. Chungcheong Math. Soc. 18 (2005), no.1, 1-23
- [3] B. Singh, and S. Jain, Semi-compatibility, and fixed point theorems in fuzzy -metric

space using implicit-relation, *Int. J. Math. Math. Soc.* 16 (2005), no. 2617-2629.

- [4] G. Jungck, Commuting mappings and fixed points, *Amer. Math. Monthly*, 83(1976), 261-263.
- [5] G. Jungck, Compatible mappings and common fixed points, *Internat. J. Math. Math. Sci.*, 9(1986), 771-779.
- [6] G. Jungck and B. E. Rhoades, Fixed points for set valued functions without continuity, *Indian J. pure appl. Math.* 29(1998), no 3, 227-238.
- [7] I. Kubiacyk and Sushil Sharma, Common coincidence point in fuzzy metric space, *J. Fuzzy Math.* 11 No.1(2003), 1-5.
- [8] I. Kubiacyk and Sushil Sharma, Common fixed point, multimaps in fuzzy metric space, *East Asian Math. J.*, Vol. 18, No. 2 (2002), 175-182.
- [9] I. Kramosil and J. Michalek, Fuzzy metrics and statistical metric spaces, *Kybernetika (Prague)* 11(1975), no. 5, 336-344.
- [10] L.A. Zadeh, Fuzzy sets. *Information and control* 8(1965), 338-353.
- [11] M Grabiec, Fixed point in fuzzy metric spaces, *Fuzzy sets and Systems* 27, No.3 (1998), 85-389.
- [12] M.A. Erceg, Metric spaces in fuzzy set theory, *J. Math. Anal. Appl.*, 69(1979), 205-230.
- [13] O. Kaleva and S. Seikkala, On fuzzy metric spaces, *Fuzzy Sets and Systems*, 12(1984), 215-229.
- [14] S.N. Mishra, N. Sharma and S.L. Singh, Common fixed point of maps on in fuzzy metric space. *Internat. J Math. Math. Sci.* 17 (1994), no. 2, 253-258.
- [15] S. Sessa : On a weak commutative condition of mappings fixed point considerations, *Pub. Inst. Math.* 32(46) (1982), no. 149-155.
- [16] S. Sharma : On fuzzy metric spaces, *South East Asian Bulletin of Maths.* 26, No. 1 (2002), 145-157.
- [17] S. Sharma, common fixed point of maps on in fuzzy metric space, *Fuzzy Sets and Systems* 127 (2002), no. 3, 345-352.
- [18] S. Sharma : Fixed point theorems for fuzzy mappings satisfying an implicit relation, *East Asian Math. J.*, Vol. 18, No. 2 (2002), 225-233.
- [19] S. Sharma and B. Deshpande, Common fixed point of compatible maps of type (β) on fuzzy metric space. *Demonstration Math.* 35(2002). No 1. 165-174.
- [20] S. Sharma and B. Deshpande, Common fixed point theorem for weakly compatible mappings without continuity in Menger space, *J. Korea Soc. Math. Educ. Ser. B Pure. Appl. Math.* 10 (2003), no. 2, 133-144.

- [21] S. Sharma and B. Deshpande, Discontinuity and weak compatibility in fixed point consideration on noncomplete fuzzy metric spaces, J Fuzzy Math. 11(2003).no.3, 671-686.
- [22] V.Popa, Fixed points for non –surjective expansion mappings satisfying an implicit relation, Bul.Stiinj. Univ. Baia Mare Ser. B Fasc. Mat- Inform. 18(2002),no.1,105-108.
- [23] Y.J.Cho, Fixed points in fuzzy metric space, J. Fuzzy math. 5(1997), no. 4,949-962
- [24] Y.J.Cho,B.K.Sharma and D.R. Sahu, Semi-compatibility and fixed point, Math. Japon.42(1995),no. 1,91-98.
- [25] Y.J. Cho , H.K Pathak.,S.M Kang and J.S. Jung, Common fixed points of compatible maps of type (b) on fuzzy metric spaces, Fuzzy Sets and Systems, 93(1998),99-111.
- [26] Z.K. Deng, Fuzzy pseudo metric spaces , J. Math. Anal. Appl., 86(1982), 74-95.

Controllability Of Nonlinear Infinite Neutral Functional Differential Systems

R. A. Umana

Department of Mathematics and Computer Science,
Federal University of Technology, Owerri, Imo State, Nigeria.

E-mail: reubenandy@yahoo.com

Abstract

In this paper controllability of nonlinear infinite neutral systems is considered. Using Schauder's fixed point theorem sufficient conditions for controllability in a given finite interval are formulated and proven.

Keywords: Controllability, infinite neutral system, Schauder fixed point theorem.

1. Introduction

Controllability is one of the fundamental concepts in modern mathematical theory [9]. The concept of controllability plays a major role in finite dimensional control theory so it is natural to try to generalize this to infinite dimensions. Roughly speaking, controllability means that it is possible to steer a dynamical system from an arbitrary initial state to an arbitrary final state using a set of admissible controls.

Neutral differential equations arise in many areas of applied mathematics and such equations have received much attention in recent years. Moreover, the study of integrodifferential equations with infinite delay has emerged in recent years as an independent branch of modern research due to its connection with many fields such as continuum mechanics, population dynamics, ecology, system theory, viscoelasticity, biology epidemics and chemical oscillations [2].

In recent years various controllability problems for different types of nonlinear infinite delay systems have been considered by several authors [3,6]. However, it should be stressed that the most literature in this direction has been mainly concerned with either null controllability of

nonlinear infinite delay systems in the Euclidean space [2,8,10,11,12] or controllability of nonlinear infinite delay systems in Banach spaces [1,5,7,4].

In this paper, we shall consider controllability problems for nonlinear infinite neutral systems. More precisely, we shall formulate and prove sufficient conditions for the controllability in a prescribed time interval for nonlinear infinite neutral systems. Proof of the main results is mainly based on the Schauder fixed point theorem.

2. Preliminaries

Suppose $h > 0$ is a given real number, $R = (-\infty, \infty)$, R^n is an n -dimensional linear vector space over the reals with norm $|\cdot|$, $C([a, b], R^n)$ is the Banach space of continuous functions mapping the interval $[a, b]$ into R^n with the topology of uniform convergence. If $[a, b] = [-h, 0]$ we let $C = C([-h, 0], R^n)$ and designate the norm of an element ϕ in C by $\|\phi\| = \sup_{-h \leq s \leq 0} |\phi(s)|$. If $\tau \in R$, $a > 0$ and $x \in C([a, b], R^n)$ for any $a \leq b$, then for each fixed $t \in [a, b]$, we let $x_t \in C$ be defined by $x_t(s) = x(t+s)$, $-h \leq s \leq 0$.

Suppose $L, D: [\tau, \infty) \times C \rightarrow R^n$ are continuous functions. We say that a relation of the type

$$\frac{d}{dt} D(t, x_t) = L(t, x_t) \quad (2.1)$$

is a functional differential equation of neutral type.

A function x is said to be a solution of (2.1) if there exist $\sigma \in R$, $a > 0$, such that $x \in C([\sigma-h, \sigma+a], R^n)$, $t \in [\sigma, \sigma+a]$, $D(t, x_t)$ is continuously differentiable and satisfies (2.1) on $[\sigma, \sigma+a]$. For a given $\sigma \in R$, $\phi \in C$, we say $x(\sigma, \phi)$ is a solution of (2.1) with initial value ϕ at σ or simply a solution through (σ, ϕ) if there exists $a > 0$ such that $x(\sigma, \phi)$ is a solution of (2.1) on $[\sigma-h, \sigma+a]$ and $x_\sigma(\sigma, \phi) = \phi$.

Our objective is to study the controllability of perturbed neutral systems with infinite delay described by

$$\frac{d}{dt}D(t, x_t) = L(t, x_t) + B(t)u(t) + \int_{-\infty}^0 A(s)x(t+s)ds + f(t, x_t, u(t)) \quad (2.2)$$

$$x(t) = \phi(t), \quad t \in (-\infty, 0]$$

where $L(t, \phi)$ is continuous in t , linear in ϕ and is given by

$$L(t, \phi) = \sum_{k=0}^{\infty} A_k(t)\phi(-t_k) + \int_{-\tau}^0 A(t, s)\phi(s)ds \equiv \int_{-\tau}^0 d_s \eta(t, s)\phi(s)$$

and where each A_k , $A(t, s)$ is a continuous $n \times n$ matrix function for $-\infty < t$, $s < \infty$, $0 \leq t_k$, $\tau \leq h$ for $0 \leq t_k \leq \tau$, and $A(t, s)$ is an $n \times n$ matrix whose elements are square integrable on $(-\infty, 0]$.

In system (2.2), B is a continuous $n \times m$ matrix function, $A(s)$ is an $n \times n$ matrix whose elements are square integrable on $(-\infty, 0]$, $x \in R^n$ and $u \in R^m$. Also, $D(t, \phi) = \phi(0) - g(t, \phi)$, where

$$g(t, \phi) = \sum_{n=1}^{\infty} A_n(t)\phi(-w_n(t)) + \int_{-\tau}^0 A(t, s)\phi(s)ds \equiv \int_{-\tau}^0 d_s \mu(t, s)\phi(s)$$

and where $0 < w_n(t) \leq \tau$ and $A_n(t)$ and $A(t, s)$ are $n \times n$ matrix functions.

The operators $g(t, \phi)$ and $L(t, \phi)$ are bounded linear operators from C into R^n for each fixed

$$t \in [0, \infty), \quad g(t, \phi) \text{ is continuous for } (t, \phi) \in [0, \infty) \times C, \quad g(t, \phi) = \int_{-\tau}^0 d_s \mu(t, s)\phi(s),$$

$$L(t, \phi) = \int_{-\tau}^0 d_s \eta(t, s)\phi(s),$$

$$|g(t, \phi)| \leq k \|\phi\|, \quad |L(t, \phi)| \leq L(t) \|\phi\|, \quad (t, \phi) \in [0, \infty) \times C,$$

for some nonnegative constant k , continuous nonnegative l and $\mu(t, s)$, $\eta(t, s)$ are $n \times n$ matrix functions of bounded variation on $[-h, 0]$. We also assume that g is uniformly nonatomic at zero, that is, there exists a continuous, nonnegative, nondecreasing function $l(s)$ for $s \in [0, h]$ such that $l(0) = 0$,

$$\left| \int_{-s}^0 d_{\tau} \mu(t, \tau) \phi(\tau) \right| \leq l(s) \|\phi\|.$$

With the conditions on (2.2) solutions of (2.1) exist and are unique and depend continuously on initial conditions. Furthermore, if the solution $x_t(\sigma, \phi, 0)$ of (2.1) is designated by $T(t, \sigma)\phi$ the variation of constants formula yields the existence of an $n \times n$ function $X(t, s)$ defined for $0 \leq s \leq t + h$, $t \in [0, \infty)$, continuous in s from the right, of bounded variation in s , $X(t, s) = 0$, $t < s \leq t + h$, such that the solution $x(\sigma, \phi, u, f)$ of (2.2) is given by $x_{\sigma}(\sigma, \phi, u, f) = \phi$ and

$$\begin{aligned} x(t, \sigma, \phi, u, f) &= T(t, \sigma)\phi(0) + \int_{\sigma}^t X(t, s)B(s)u(s)ds \\ &\quad + \int_{\sigma}^t X(t, s) \left(\int_{-\infty}^0 A(s)x(t+s)ds \right) ds \\ &\quad + \int_{\sigma}^t X(t, s)f(s, x_s, u(s))ds, \quad t \geq \sigma, \end{aligned} \quad (2.3)$$

where $x(t, \sigma, \phi, 0) = T(t, \sigma)\phi(0)$ is the solution of (2.1) at time t . Observe that if we define the

$n \times n$ matrix X_0 as

$$X_0(s) = \begin{cases} 0 & \text{if } s < 0 \\ I & \text{if } s = 0 \end{cases}$$

we can set

$$T(t, s)X_0(\theta) = X_t(\cdot, s)\theta = X(t + \theta, s)$$

so that

$$X(t, s) = T(t, s)X_0(0) = T(t, s)I = T(t, s).$$

In (2.3), set $Y(t, s) = X(t, s)B(s)$. Then the controllability matrix of (2.2) at time t is defined by

$$W(\sigma, t) = \int_{\sigma}^t Y(t, s)Y^*(t, s)ds$$

where $*$ denotes the matrix transpose.

Definition 2.1: The system (2.2) is said to be controllable on $[\sigma, t_1]$ if for any function $\phi \in C$, and any vector $x_1 \in R^n$, there exists a control $u \in C = C([\sigma, t_1], R^m)$ such that the solution $x(t) = x(t, \sigma, \phi, u, f)$ of (2.2) satisfies

$$x_{\sigma}(\cdot, \sigma, \phi, u, f) = \phi, \quad x(t_1, \sigma, \phi, u, f) = x_1.$$

3. Main Result

In this section, using Schauder's fixed point theorem, sufficient conditions for the controllability of nonlinear neutral system (2.2) in a given time interval are formulated and proven. For simplicity and compactness of notation, we will take

$$p = (x, u) \in R^n \times R^m$$

and let

$$|p| = |x| + |u|,$$

where $|\cdot|$ denotes the standard norm in the finite dimensional Euclidean space.

Theorem 3.1: Let the continuous function f satisfy the so called growth condition

$$\lim_{|p| \rightarrow \infty} \frac{|f(t, p)|}{|p|} = 0 \tag{3.1}$$

uniformly in $t \in [\sigma, t_1]$, and suppose that the function g is continuous and uniformly nonatomic

at zero. Moreover, let us assume that there exists a positive constant d such that for each pair of functions $\{x, u\} \in C([\sigma, t_1], R^n) \times C([\sigma, t_1], R^m)$

$$\det W(\sigma, t_1) \geq d.$$

Then the nonlinear neutral system (2.2) is controllable on $[\sigma, t_1]$.

Proof: Let $Q = C_n[\sigma, t_1] \times C_m[\sigma, t_1]$, where $C_n[\sigma, t_1]$ is the Banach space of continuous R^n -valued functions defined on $[\sigma, t_1]$ with the supremum norm. Define the nonlinear continuous operator

$$T : Q \rightarrow Q \quad \text{by} \quad T(x, u) = (y, v)$$

where

$$v(t) = Y^*(t_1, t)W^{-1}(\sigma, t_1) \left[x_1 - T(t_1, \sigma)\phi(0) - \int_{\sigma}^{t_1} X(t_1, s) \left(\int_{-\infty}^0 A(s)x(t+s)ds \right) ds \right. \\ \left. - \int_{\sigma}^{t_1} X(t_1, s)f(s, x_s, u(s))ds \right]$$

and

$$y(t) = T(t, \sigma)\phi(0) + \int_{\sigma}^t Y(t, s)v(s)ds + \int_{\sigma}^t X(t, s) \left(\int_{-\infty}^0 A(s)x(t+s)ds \right) ds \\ + \int_{\sigma}^t X(t, s)f(s, x_s, u(s))ds.$$

Let us introduce the following notations:

$$a_1 = \sup |Y(t, s)|, \quad 0 \leq s \leq t \leq t_1$$

$$a_2 = \sup |W^{-1}(\sigma, t_1)|$$

$$a_3 = \sup \left| T(t, \sigma)\phi(0) + \int_{\sigma}^t X(t, s) \left(\int_{-\infty}^0 A(s)x(t+s)ds \right) ds \right| + |x_1|$$

$$a_4 = \sup |X(t, s)|, \quad (t, s) \in [\sigma, t_1] \times [\sigma, t_1]$$

$$a_5 = \sup \left\{ \left| f(s, x_s, u(s)) \right| : s \in [\sigma, t_1] \right\}$$

$$b = \max \{ (t_1 - \sigma)a_1, 1 \}$$

$$c_1 = 4ba_1a_2a_4(t_1 - \sigma)$$

$$c_2 = 4a_4(t_1 - \sigma)$$

$$d_1 = 4a_1a_2a_3b$$

$$d_2 = 4a_3$$

$$c = \max \{ c_1, c_2 \}$$

$$d = \max \{ d_1, d_2 \}.$$

Then

$$|v(t)| \leq a_1a_2[a_3 + a_4a_5(t_1 - \sigma)]$$

$$= \frac{d_1}{4b} + \frac{c_1}{4b}a_5$$

$$\leq \frac{d + ca_5}{4b}$$

and

$$|y(t)| \leq a_3 + (t_1 - \sigma)a_1\|v\| + (t_1 - \sigma)a_4a_5$$

$$= b\|v\| + \frac{d_2}{4} + \frac{c_2a_5}{4}$$

$$\leq b\|v\| + \frac{d + ca_5}{4}.$$

It follows from the growth condition (3.1) that for each pair of positive constants c and d , there

exists a positive constant r such that if $|p| \leq r$ then

$$d + c|f(t, p)| \leq r, \quad \text{for all } t \in [\sigma, t_1]. \quad (3.2)$$

Now, take c and d as given above, and let r be chosen so that (3.2) is satisfied.

Therefore, if we take $\|x\| \leq r/2$ and $\|u\| \leq r/2$, then $\|(x, u)\| \leq r$. It follows that $d + ca_s \leq r$.

Therefore,

$$|v(t)| \leq \frac{r}{4b} \quad \text{for all } t \in [\sigma, t_1],$$

and hence $\|v\| \leq r/4b$. It follows that

$$|y(t)| \leq \frac{r}{4} + \frac{r}{4} = \frac{r}{2} \quad \text{for all } t \in [\sigma, t_1],$$

and hence $\|y\| \leq r/2$. Thus we have proved that if

$$H = \left\{ (x, u) \in Q : \|x\| \leq r/2 \text{ and } \|u\| \leq r/2 \right\},$$

then T maps H into itself. Since all the functions involved in the definition of the operator T are continuous, it follows that T is continuous and hence it is completely continuous by the application of Arzela-Ascoli theorem. Since the set H is closed, bounded, and convex, then by Schauder's fixed point theorem there exists at least one fixed point $(x, u) \in H$ such that $T(x, u) = (x, u)$. Hence, for $(y, v) = (x, u)$ we have

$$\begin{aligned} x(t) = & T(t, \sigma)\phi(0) + \int_{\sigma}^t Y(t, s)u(s)ds + \int_{\sigma}^t X(t, s) \left(\int_{-\infty}^0 A(s)x(t+s)ds \right) ds \\ & + \int_{\sigma}^t X(t, s)f(s, x_s, u(s))ds. \end{aligned}$$

Thus $x(t)$ is a solution of the system (2.2) and

$$\begin{aligned} x(t_1) = & T(t_1, \sigma)\phi(0) + \int_{\sigma}^{t_1} X(t_1, s) \left(\int_{-\infty}^0 A(s)x(t_1+s)ds \right) ds \\ & + \int_{\sigma}^{t_1} Y(t_1, s)Y^*(t_1, s)W^{-1}(\sigma, t_1)[x_1 - T(t_1, \sigma)\phi(0) \end{aligned}$$

$$\begin{aligned}
& - \int_{\sigma}^{t_1} X(t_1, s) \left(\int_{-\infty}^0 A(s) x(t+s) ds \right) ds - \int_{\sigma}^{t_1} X(t_1, s) f(s, x_s, u(s)) ds \Big] ds \\
& + \int_{\sigma}^{t_1} X(t_1, s) f(s, x_s, u(s)) ds = x_1.
\end{aligned}$$

Hence (2.2) is controllable on $[\sigma, t_1]$.

Conclusion

The paper contains sufficient conditions for the controllability in a given finite time interval of a certain special class of nonlinear infinite neutral systems. In the proof of the main result, the well known Schauder fixed point theorem has been used. Our result extends most results on general nonlinear finite-dimensional neutral systems to nonlinear infinite-dimensional neutral systems.

References

- [1] K. Balachandran and E. A. Anandhi, Controllability of neutral functional integrodifferential infinite delay systems in Banach spaces, *Taiwanese J. Math.*, 8, 689 – 702 (2004).
- [2] K. Balachandran and J. P. Dauer, Null controllability of nonlinear infinite delay systems with time varying multiple delays in control, *Appl. Math. Lett.*, 9, 115 – 121 (1996).
- [3] K. Balachandran and J. P. Dauer, Controllability of nonlinear systems in Banach spaces: a survey, *J. Optim. Theory Appl.*, 115, 7 -28 (2002).
- [4] P. Balasubramaniam and C. Loganathan, Controllability of functional differential equations with unbounded delay in Banach Space, *J. Indian Math. Soc.*, 68, 191 – 203 (2001).
- [5] H. Bouzahir, On controllability of neutral functional differential equations with infinite delay, *Monografias del Seminario Matematico Garcia de Galdeano*, 33, 75 – 81 (2006).
- [6] E. N. Chukwu, *Differential Models and Neutral Systems for Controlling the Wealth of Nations*, Series on Advances in Mathematics for Applied Sciences, vol.54, World Scientific, New Jersey, 2001.

- [7] X. L. Fu, Controllability of abstract neutral functional differential systems with unbounded delay, *Appl. Math. Comp.*, 151, 299 – 314 (2004).
- [8] D. Iyai, Euclidean null controllability of infinite neutral differential systems, *ANZIAM J.*, 48, 285 – 293 (2006).
- [9] J. Klamka, Controllability of nonlinear discrete systems, *Int. J. Appl. Math. Comput. Sci.*, 12, 173 – 180 (2002).
- [10] J. U. Onwuatu, Null controllability of nonlinear infinite neutral systems, *Kybernetika*, 29, 325 – 336 (1993).
- [11] A. S. C. Sinha, Null controllability of nonlinear infinite delay systems with restrained controls, *Int. J. Control*, 42, 735 – 741 (1985).
- [12] R. A. Umana, Null controllability of nonlinear infinite neutral systems with multiple delays in control, *J. Comp. Anal. Appl.*, (To Appear).

On Infinite Order K-dV Hierarchies

Luca Zampogni

Dipartimento di Matematica, Università di Perugia, Italy

e-mail: zampogni@dipmat.unipg.it

Abstract

We use a zero-curvature method together with an approximation process to find solutions $u(x, t)$ of all equations in a commuting hierarchy containing the Korteweg-de Vries (K-dV) equation, when the initial condition $u(x, 0)$ satisfies the “infinite order stationary K-dV equation” and determines a Schrödinger potential lying in the class of “reflectionless” Sturm-Liouville potentials.

Keywords: Korteweg-de Vries equation, Sturm-Liouville equation, zero-curvature method.

2000 AMS Mathematics Subject Classification: 34A55: 34B24: 35Q53: 37K10.

1 Introduction

In the last 40 years, the Korteweg-de Vries (K-dV) equation

$$u_t = u_{xxx} - 6uu_x \quad (1)$$

describing the shallow water waves, has received a considerable attention. It was a discovery in [8] that solutions $u(x, t)$ of the K-dV equation which are real-valued, $C^\infty(\mathbb{R})$ and rapidly decreasing as $x \rightarrow \pm\infty$ determine, for every $t \in \mathbb{R}$, potentials $x \mapsto q_t(x) := u(x, t)$ of a Schrödinger operator

$$L_t = -\frac{d^2}{dx^2} + q_t(x) \quad (2)$$

which are all lying in the same isospectral class. In particular, a consequence of this result is that the eigenvalues of (2) are conserved quantities for the K-dV flow. This idea was successfully used by Dubrovin, Matveev and Novikov [5] and brought to the discovery of the relation between the finite-gap Schrödinger potentials and the solutions of the K-dV equation. They described the nature of the solution by using techniques of the theory of algebraic curves (in particular, the theory of the compact hyperelliptic Riemann surfaces).

A natural step further after these results was to find solutions of the K-dV equation which determine potentials of the Schrödinger operators of the type in (2) whose spectra are not of finite-gap type, but more generally of infinite-gap type (a particularly important class of these potentials in that of “reflectionless” potentials, which we will describe below). Among the large number of papers devoted to this subject, it is worth mentioning the papers [18, 20, 21, 6, 23]. In those papers, strong assumptions on the decay of the spectral gaps of the Schrödinger operator, whose potential is determined by the initial condition $q_0(x) := u(x, t_0)$ for which the K-dV

equation is solved, must be taken in order to formulate and solve the problem in a satisfactory manner. In particular, in [20, 21], it is proved the almost periodicity of the finite-gap and of the infinite-gap solutions $u(x, t)$ of the K-dV equation under the condition that the spectrum Σ_0 of the related Schrödinger operator (2) with potential $q_0(x) := u(x, t_0)$ has, for some $t_0 \in \mathbb{R}$, the following form:

$$\Sigma_0 = [\lambda_0, \lambda_1] \cup \dots \cup [\lambda_{2g}, \lambda_{2g+1}] \cup \dots$$

where the sequence $\{\lambda_i\} \subset \mathbb{R}$ satisfies the following assumptions:

- (i) there exists a number $p > 1$ such that $\sum_{i \in \mathbb{N}} \lambda_{2i-1}^p (\lambda_{2i} - \lambda_{2i-1}) < \infty$;
- (ii) there are constants $C, \alpha > 0$ for which $(\lambda_{2i} - \lambda_{2i-1}) > Ci^\alpha$ ($i \in \mathbb{N}$).

These hypotheses were necessary to obtain a well-defined algebro-geometric structure where to study the recurrence properties of the solutions, which are found to be almost periodic uniformly with respect to the x and t variables. Concerning the almost periodicity with respect to the variable x , it is possible to substitute (i) and (ii) above with a more general property of “homogeneity” of the spectrum [29]. As far as I know, however, potentials of (2) having a homogenous spectrum need not give rise to well-defined K-dV flows: moreover, even if they do, it is not clear neither what happens to the t -motion, nor if the uniformity is conserved.

Commuting hierarchies of evolution equations containing the K-dV equation have been obtained by means of the Lax pair method [17, 18]. This method allows to solve the so called “ n -th order K-dV equation” for every $n \in \mathbb{N}$, when, however, initial data has a fast decay as $x \rightarrow \pm\infty$. In this paper we use a zero-curvature method to determine a hierarchy of commuting equations containing the K-dV equation. These equations will be the compatibility conditions for an overdetermined system. First of all, we will find useful to find solutions of the r -th order K-dV equation when the initial data $u(x, 0)$ determines a Schrödinger potential of algebro geometric-type, i.e., it is a finite-gap potential having $n > r$ spectral gaps. This case will be studied by the introduction of a hierarchy made of complex polynomials whose coefficients will in turn determine the equations in the hierarchy. The same method was applied to the Camassa-Holm equation in [9] and [30]. Then we will focus our attention on the determination of a hierarchy of commuting equations containing the K-dV equation when the initial data $u(x, 0)$ determines a Schrödinger potential of reflectionless type, in particular when its spectrum is an infinite union of closed intervals clustering at ∞ and when the spectral gaps satisfy certain assumption, which, however, are weaker than those mentioned above. The construction of this hierarchy will be carried out by the usage of entire functions instead of polynomials, and those entire functions will be in part determined by an “algebro-geometric” approximation, i.e., they will be the uniform limit on compact subsets of the complex unit disc of a sequence of polynomials giving rise to hierarchies for which the corresponding solution of the K-dV equation is of algebro-geometric type. We mention that we are able to solve the K-dV equation of any arbitrary order $n \in \mathbb{N}$.

The paper is organized as follows: in Section 2 we will give the necessary background material concerning the spectral theory for the Sturm-Liouville operator. We will state some of the results in [14, 16], and we will observe how to construct Sturm-Liouville potentials having an assigned spectrum. In Section 3, we will start by introducing the so-called stationary zero-curvature condition of finite order $n \in \mathbb{N}$, which will be used to determine the suitable initial conditions to solve the time-dependent r -th order K-dV equation ($r < n$). The determination of the solution of the r -th order K-dV equation will be the matter of Section 4. In

this section, we will also describe briefly the application of the theory of algebraic curves to the study of the solutions of the K-dV hierarchy. We will observe how the almost-periodicity of the solution of the r -th order K-dV equation can be obtained by means of the Abel map and the Riemann Θ -function. In the final Section 5, we will construct a hierarchy of commuting equations and solve the K-dV equation of any arbitrary order $r \in \mathbb{N}$ when the initial data determines a particular subclass of the family of the Schrödinger reflectionless potentials. The theory of entire functions will be used, and some result of approximation presented in [16] will reveal to be very useful.

We finish this introductory part by observing that it is possible to solve the K-dV equation even when the initial data lies in other classes of the family of the reflectionless potentials; for example, there are certain solutions of the K-dV equation which are called of Sato-Segal-Wilson type (see [26, 27, 12]), whose initial data determine potentials having a Cantor part in the spectrum. See [12] and [11] for further information concerning this topic.

2 Preliminaries

In this section we review some of the material in [14] and [16] which will be useful for our purposes. First of all, we describe a procedure to construct algebro-geometric Sturm-Liouville potentials. Then, we will move our attention on a special class of reflectionless potentials, by briefly illustrating a limit procedure which will enable us to construct them as well.

Let us assume that we are given g disjoint closed intervals $I_1 = [\lambda_1, \lambda_2], \dots, I_g = [\lambda_{2g-1}, \lambda_{2g}]$, where $I_k \subset \mathbb{R}$ and $\lambda_1 < \lambda_2 < \dots < \lambda_{2g}$. Let $\mathcal{E}_m = \{a : \mathbb{R} \rightarrow \mathbb{R}^m \mid a \text{ is uniformly bounded and uniformly continuous}\}$. We put the compact-open topology on \mathcal{E}_m . We consider the Bebutov flow on \mathcal{E}_m , i.e., $\tau_x(a)(\cdot) = a(\cdot + x)$ ($a \in \mathcal{E}_m$, $x \in \mathbb{R}$). This flow is indeed a topological flow on \mathcal{E}_m . Let us write $a = (p, q, y) \in \mathcal{E}_3$ where $p, q, y : \mathbb{R} \rightarrow \mathbb{R}$, and let us assume that \mathcal{A} be the subset of \mathcal{E}_3 consisting of those $a = (p, q, y) \in \mathcal{E}_3$ such that there exists a number $\delta > 0$ with $p(x) \geq \delta$, $y(x) \geq \delta$ for every $x \in \mathbb{R}$ and the derivative $\frac{dp}{dx}$ is uniformly bounded and continuous. Every $a \in \mathcal{E}_3$ gives rise to a Sturm-Liouville equation

$$-\frac{d}{dx} \left(p(x) \frac{d\varphi}{dx} \right) + (q(x) - \lambda y(x)) \varphi = 0. \quad (3)$$

This equation is equivalent to the differential system

$$\begin{pmatrix} \varphi \\ \psi \end{pmatrix}' = \begin{pmatrix} 0 & 1/p(x) \\ q(x) - \lambda y(x) & 0 \end{pmatrix} \begin{pmatrix} \varphi \\ \psi \end{pmatrix}. \quad (4)$$

For every $a \in \mathcal{A}$, the correspondence

$$L_a : L^2(\mathbb{R}, ydx) \rightarrow L^2(\mathbb{R}, ydx) : \varphi \mapsto \frac{1}{y(x)} \left[-\frac{d}{dx} \left(p(x) \frac{d\varphi}{dx} \right) + q(x) \varphi \right]$$

defines a self-adjoint operator. For every $a \in \mathcal{A}$, the operator L_a has a spectrum $\Sigma_a \subset \mathbb{R}$ which is bounded below and unbounded above. Next, we will define the Weyl m -functions. For $a \in \mathcal{A}$, let us consider the operators L_a^\pm which are the restrictions of L_a to $L^2(\mathbb{R}^\pm, ydx)$, where the Dirichlet boundary condition $\varphi(0) = 0$ is fixed. For $\lambda \in \mathbb{C}$ with $\Im \lambda \neq 0$, the equation (3) admits nontrivial solutions $\varphi_\pm \in L^2(\mathbb{R}^\pm, ydx)$. Moreover, since L_a^\pm are of limit-point type, these solutions are

unique up to constant multiples. It follows that the quantities

$$m_{\pm}(a, \lambda) = p(0) \frac{\varphi'_{\pm}(0)}{\varphi_{\pm}(0)}$$

are well-defined. They are called the Weyl m -functions. Both m_+ and m_- are holomorphic in $\mathbb{C} \setminus \mathbb{R}$ and have nonzero imaginary parts there. Moreover $\text{sgn}(\Im m_{\pm} \cdot \Im \lambda) = \pm 1$ if $\Im \lambda \neq 0$. When $\Im \lambda \neq 0$, then $\lambda \notin \Sigma_a$, hence L_a is invertible. The Green's function is now defined as the integral kernel of the resolvent operator $(L_a - \lambda I)^{-1}$, i.e., the Green's function $G_a(x, s, \lambda)$ can be defined as to satisfy

$$(L_a - \lambda I)^{-1}(f)(x) = \int_{\mathbb{R}} G_a(x, s, \lambda) f(s) ds.$$

The Green's function has a very nice expression in terms of the solutions $\varphi_{\pm}(x)$, and, in particular, the diagonal Green's function $G_a(\lambda) = G_a(0, 0, \lambda)$ assumes the form

$$G_a(\lambda) = \frac{y(0)}{m_-(a, \lambda) - m_+(a, \lambda)}.$$

Let us now fix $a \in \mathcal{A}$, and let us consider the triples $\tau_x(a) \in \mathcal{A}$ (where x varies over \mathbb{R}). Then one has a family of self-adjoint operators $L_{\tau_x(a)}$. One can check that the Weyl m functions corresponding to $L_{\tau_x(a)}$ are exactly given by

$$m_{\pm}(\tau_x(a), \lambda) = p(x) \frac{\varphi'_{\pm}(x)}{\varphi_{\pm}(x)}.$$

It turns out that clearly the diagonal Green's function is

$$G_{\tau_x(a)}(\lambda) = G_a(x, x, \lambda) = \frac{y(x)}{m_-(\tau_x(a), \lambda) - m_+(\tau_x(a), \lambda)}. \quad (5)$$

It can be proved (see [7]) that, if $a \in \mathcal{A}$, then $\Sigma_{\tau_x(a)} = \Sigma_a$ for every $x \in \mathbb{N}$ and that in turn Σ_a can be characterized as the non-dichotomy set of a family of Sturm-Liouville differential systems of the form (3).

Definition 2.1 *A potential $a \in \mathcal{A}$ is called “algebro-geometric” if:*

- (i) *the spectrum of the associated operator L_a has the form $\Sigma_a = [\lambda_0, \lambda_1] \cup \dots \cup [\lambda_{2g}, \infty)$;*
- (ii) *the upper Lyapunov exponent $\beta(\lambda)$ vanishes a.e. in Σ_a .*

The upper Lyapunov exponent is defined as follows: let $\Phi_a(x)$ be the fundamental matrix solution of (4) with $\Phi_a(0) = I$. Then

$$\beta(\lambda) = \lim_{x \rightarrow \pm\infty} \frac{1}{x} \ln |\Phi_a(x)|.$$

It turns out that $\beta(\lambda)$ is well defined for every $a \in \mathcal{A}$ (but, a priori, it can depend on the choice of $a \in \mathcal{A}$). See [13, 14, 7, 15, 30] for further information concerning the Lyapunov exponent and its invariance with respect to “ergodic families” of Sturm-Liouville potentials in \mathcal{E}_3 .

Our aim now is to explain how to construct algebro-geometric Sturm-Liouville potentials $a = (p, q, y) \in \mathcal{A}$. Let $b = (p, \mathcal{M}) \in \mathcal{E}_2$ be such that $\mathcal{M}(x) \geq \delta$ for every $x \in \mathbb{R}$ and $p'(x), \mathcal{M}'(x), \mathcal{M}''(x)$ exist and are bounded and uniformly continuous. Let $0 < \lambda_0 < \lambda_1 \dots, \lambda_{2g}$ be real numbers, set $\Sigma_g = [\lambda_0, \lambda_1] \cup \dots \cup [\lambda_{2g}, \infty)$, $I_k = [\lambda_{2k-1}, \lambda_{2k}]$ ($k = 1, \dots, g$) and $\mathcal{I}_g = I_1 \times I_2 \times \dots \times I_g$. Let $(P_1^0, \dots, P_g^0) \in \mathcal{I}_g$,

and let $k_g : (-\infty, \lambda_0] \times \mathcal{I}_g \rightarrow \mathbb{R} : \lambda \mapsto \sqrt{-(\lambda - \lambda_0)(\lambda - \lambda_1) \dots (\lambda - \lambda_{2g})}$. Let $(P_1(x), \dots, P_g(x))$ be the solution of the differential system

$$P'_r(x) = \frac{(-1)^g k(P_r(x)) \mathcal{M}(x) \prod_{i=1}^g P_i(x)}{p(x) k_g(0) \prod_{s \neq r} (P_r(x) - P_s(x))}, \quad r = 1, \dots, g \quad (6)$$

satisfying $P_r(0) = P_r^0$ ($r = 1, \dots, g$). Define

$$y(x) = \left(\frac{\mathcal{M}(x) \prod_{i=1}^g P_i(x)}{2k_g(0) \sqrt{p(x)}} \right)^2, \quad (7)$$

$$q(x) = y(x) \left[\lambda_0 + \sum_{i=1}^g (\lambda_{2i-1} + \lambda_{2i} - 2P_i(x)) \right] + q'_g(x) + \frac{q_g(x)^2}{p(x)}, \quad (8)$$

where $q_g(x) = -\frac{(p(x)y(x))'}{4y(x)} = -\frac{p(x)}{2} \frac{d}{dx} \left[\ln \left(\mathcal{M}(x) \prod_{i=1}^g P_i(x) \right) \right]$. It turns out that

the triple $a = (p, q, y) \in \mathcal{A}$, where p is the first component of $b = (p, \mathcal{M}) \in \mathcal{E}_2$ and q, y are defined in (8) and (7) respectively, is an algebro-geometric Sturm-Liouville potential whose spectrum equals the set Σ_g . If $a = (p, q, y)$ is defined as above, one can see that the Weyl m -functions $m_{\pm}(a, \lambda)$ corresponding to the operators L_a^{\pm} satisfy $\mathcal{M}(x) = m_{-}(\tau_x(a), 0) - m_{+}(\tau_x(a), 0)$. Moreover, the solution $(P_1(x), \dots, P_g(x))$ of the system (6) equals the set of the zeros of the diagonal Green's function $G_a(x, x, \lambda) = G_{\tau_x(a)}(\lambda)$: by using the relation (5), one can see that, equivalently, the set $(P_1(x), \dots, P_g(x))$ equals the set of the poles of the function $m_{-}(\tau_x(a), \lambda) - m_{+}(\tau_x(a), \lambda)$. One can show (see [7]) that each $P_i(x)$ ($i = 1, \dots, g$) is a pole either of m_{-} or of m_{+} . However, see [7, 14, 15] for further detailed information concerning algebro-geometric Sturm-Liouville potentials.

Next, we describe a procedure based on a so-called “algebro-geometric approximation” to construct reflectionless Sturm-Liouville potentials. First we define what we mean by the term reflectionless [16].

Definition 2.2 A triple $a = (p, q, y) \in \mathcal{A}$ is called a “reflectionless Sturm-Liouville potential” if the following relations hold:

- (i) the spectrum Σ_a of the operator L_a has locally positive measure, i.e., if $\lambda \in \Sigma_a$ and I is any open interval containing λ , then $I \cap \Sigma_a$ has positive Lebesgue measure;
- (ii) $\Re G_a(\lambda + i0) = 0$ for Lebesgue a.e. $\lambda \in \Sigma_a$.

For instance, algebro-geometric potentials and periodic potentials are reflectionless. Many other well-known classes of Sturm-Liouville potentials are reflectionless as well. For example, a large family of Sato-Segal-Wilson potentials are reflectionless [26, 27, 12, 16]. We will need the following result (see [16]).

Proposition 2.3 Let $\{a_n\} = \{(p_n, q_n, y_n)\} \subset \mathcal{A}$ be a sequence of reflectionless potentials. Suppose that $\lim_{n \rightarrow \infty} a_n = a = (p, q, y) \in \mathcal{E}_3$ uniformly on compact subsets of \mathbb{R} . Assume that $\Sigma_{a_n} \supset \Sigma_{a_{n+1}}$ for every $n \in \mathbb{N}$ and that $\Sigma := \bigcap_{n \in \mathbb{N}} \Sigma_{a_n}$ has locally positive Lebesgue measure. Then a is reflectionless and $\Sigma_a = \Sigma$.

Proposition 2.3 is the key to construct reflectionless potentials having an assigned spectrum. We briefly describe how this can be done and address the reader to [16] for details. Some of the techniques exploited in that paper will be used in Section 5. Let $\{\lambda_k\} \subset \mathbb{R}$ be such that

- $\lambda_k > \lambda_0$ for all $k \geq 1$,
- $\lambda_{2k} > \lambda_{2k-1}$ for all $k \geq 1$,
- no λ_j lies in $(\lambda_{2k-1}, \lambda_{2k})$ ($j \neq 2k-1, j \neq 2k, k \geq 1$).

Let $I_k = [\lambda_{2k-1}, \lambda_{2k}]$, $d_k = |\lambda_{2k} - \lambda_{2k-1}|$, $h_{jk} = \text{dist}(I_k, I_j)$ and let $h_{0k} = |\lambda_{2k-1} - \lambda_0|$ ($k \in \mathbb{N}$). We impose further fundamental conditions on the sequence $\{\lambda_k\}$, i.e.,

Hypotheses 2.4 *Let $\{\lambda_k\}_{k=0,1,\dots}$ be a sequence of distinct real numbers with the properties listed above. We assume that*

$$(a) \sup_{k \in \mathbb{N}} \sqrt{d_k h_{0k}} < \infty.$$

$$(b) \sup_{j \in \mathbb{N}} \sum_{k \neq j} \frac{\sqrt{d_k}}{h_{jk}} = D_1 < \infty$$

Let $b = (p, \mathcal{M}) \in \mathcal{E}_2$ be as above. Let $\mathcal{I} = I_1 \times I_2 \times \dots \times I_k \times \dots$. Choose $(P_1^0, \dots, P_k^0, \dots) \in \mathcal{I}$, and consider the following differential system made up of infinite differential equations

$$P_r(x)' = \pm \frac{\mathcal{M}(x) k_\infty(P_r(x)) \prod_{j \in \mathbb{N}} P_j(x)}{p(x) k_\infty(0) \prod_{r \neq j \in \mathbb{N}} [P_r(x) - P_j(x)]}, \quad (9)$$

where $k_\infty(\lambda)$ is formally defined for $\lambda \in (-\infty, \lambda_0] \times \mathcal{I}$ as $k_\infty(\lambda) = \sqrt{\prod_{n=0}^{\infty} (\lambda - \lambda_n)}$.

Next, use Hypotheses (2.4) to show that actually the right-hand side of (9) is well defined for every $r \in \mathbb{R}$. One can show the uniqueness of a solution $\{P_r(x) : \mathbb{R} \rightarrow \mathcal{I}$ of (9) by using a Gronwall-like technique (see [16]). To prove the existence of a solution of the system (9), one constructs a sequence $\{a_n\} = \{(p, q_n, y_n)\}$ of algebro-

geometric potentials whose spectra Σ_{a_n} equal the sets $\Sigma_{a_n} = \mathbb{R} \setminus \left((-\infty, \lambda_0) \bigcup_{k=1}^n \overset{\circ}{I}_k \right)$ (note that p is kept fixed in the sequence). Then it can be shown that the sequence $\{a_n\}$ converges to a triple $a = (p, q, y) \in \mathcal{A}$ uniformly on compact subsets of \mathbb{R} , and hence the sequence $\{a_n\}$ satisfies the assumptions of Proposition 2.3. It follows that the triple $a = (p, q, y)$ is reflectionless and has a spectrum $\Sigma_a = \bigcap_{n \in \mathbb{N}} \Sigma_{a_n} =$

$\mathbb{R} \setminus \left((-\infty, \lambda_0) \bigcup_{k \in \mathbb{N}} \overset{\circ}{I}_k \right)$. Moreover, one can find an expression for $y(x)$ by means of the trace formula

$$y(x) = \left(\frac{\mathcal{M}(x) \prod_{i \in \mathbb{N}} P_i(x)}{2k_\infty(0) \sqrt{p(x)}} \right)^2. \quad (10)$$

In order to have a trace formula for $q(x)$ (which, however exists anyway, because it reveals to depend only on the choice of $b = (p, \mathcal{M}) \in \mathcal{E}_2$) we have to assume that

$$\sum_{k \in \mathbb{N}} d_k < \infty.$$

It follows that

$$q(x) = y(x) \left(\lambda_0 + \sum_{k \in \mathbb{N}} [\lambda_{2k-1} + \lambda_{2k} - 2P_k(x)] \right) + \text{other terms}. \quad (11)$$

The other terms in (11) are quantities analogous to those in the formula (8) characterizing the algebro-geometric potentials. For details and an ample discussion concerning this topic, see [16]. The general theory of the Sturm-Liouville operator sketched above includes the Schrödinger operator as a special case. Indeed, it can be shown that, if we choose $p(x) \equiv 1$, then for every initial condition $\{P_k^0\} \in \mathcal{I}$, one can define a function $\mathcal{M}(x)$ in such a way that the corresponding triple $a = (1, q, y) \in \mathcal{E}_3$ satisfies $y(x) \equiv 1$. In this case, however, the differential systems (6) and (9) (according to if we deal with algebro-geometric or general reflectionless potentials) must be slightly modified as to satisfy the well-known Dubrovin equations for the Schrödinger operator [5], and in fact the trace formulas (10) and (11) translate to

$$1 = \left(\frac{\mathcal{M}(x) \prod_{i \in \mathbb{N}} P_i(x)}{2k_\infty(0)} \right)^2$$

and

$$q(x) = \lambda_0 + \sum_{k \in \mathbb{N}} [\lambda_{2k-1} + \lambda_{2k} - 2P_k(x)].$$

The matrix formulation of the Schrödinger equation is clearly given by

$$\begin{pmatrix} \varphi \\ \psi \end{pmatrix}' = \begin{pmatrix} 0 & 1 \\ q(x) - \lambda & 0 \end{pmatrix} \begin{pmatrix} \varphi \\ \psi \end{pmatrix}. \quad (12)$$

We finish this section by spending a word concerning the notation. Throughout all the paper, if $f : \mathbb{R}^2 \rightarrow \mathbb{R}$, we will sometimes use the symbols f_x, f_t, f_{xt} , etc. to

denote the partial derivatives $\frac{\partial f}{\partial x}, \frac{\partial f}{\partial t}, \frac{\partial^2 f}{\partial x \partial t}$, etc.

3 The Initial Condition: the Stationary K-dV Hierarchy

As far as we know, a K-dV hierarchy of commuting equations has been obtained by means of the well-known Lax-pairs method [17]. Now we use a zero-curvature method to obtain a commuting hierarchy of K-dV type. Our formalism is analogous to those exposed in [30] and [9] which, however, deal with a Camassa-Holm hierarchy. We find convenient to fix ideas by giving first a complex polynomial-type zero-curvature hierarchy. Then we will extend our method to a kind of hierarchy which depends on entire functions.

Let A denote the matrix $\begin{pmatrix} 0 & 1 \\ q(x) - \lambda & 0 \end{pmatrix}$ (see (12) above). We now determine the form of the initial conditions $u_0(x)$ for which we will solve the K-dV hierarchy.

Let

$$B_g(x, \lambda) = \begin{pmatrix} -U_x/2 & U \\ (1-\lambda)V & U_x/2 \end{pmatrix}$$

be a matrix whose entries U, V (and U_x) are complex polynomials of degree g in the variable $\lambda \in \mathbb{C}$ and with coefficients $u_i(x), v_i(x) : \mathbb{R} \rightarrow \mathbb{R}$ ($i = 0, \dots, g$). We require that u_i, v_i be continuously differentiable on all \mathbb{R} ($i = 0, \dots, g$). Note that, for the moment, no time dependence is considered. We define the stationary zero-curvature condition between A and B_g the following equation

$$-B_{g,x} + [A, B_g] = 0, \quad (13)$$

where $[A, B_g] = AB_g - B_gA$ is the commutator of A and B_g . The equation (13) is equivalent to the following system

$$\begin{cases} U_{xxx} + 4(1-\lambda)V_x - 2q_x U = 0 \\ U_{xxx} - 4(q-\lambda)U_x - 2q_x U = 0 \end{cases} \quad (14)$$

The second equation in (14) determines the recursion formulas for the coefficients $u_i(x)$ of the polynomial U : these coefficients, in turn, determine those of the polynomial V by using the first equation in (14). We have:

$$\begin{aligned} u_{0,xxx}(x) - 4q(x)u_{0,x}(x) - 2q_x(x)u_0(x) &= 0 \\ u_{1,xxx}(x) - 4q(x)u_{1,x}(x) + 4u_0(x) - 2q_x(x)u_1(x) &= 0 \\ \vdots \\ u_{n,xxx}(x) - 4q(x)u_{n,x}(x) + 4u_{n-1}(x) - 2q_x(x)u_n(x) &= 0 \\ \vdots \\ u_{g,x}(x) &= 0. \end{aligned} \quad (15)$$

The coefficients $v_i(x)$ are determined by

$$\begin{aligned} 4v_{0,x}(x) &= 2q_x(x)u_0(x) - u_{0,xxx}(x) \\ 4v_{1,x}(x) &= 2q_x(x)u_1(x) - u_{1,xxx}(x) + 2q_x(x)u_0(x) - u_{0,xxx}(x) \\ \vdots \\ 4v_{n,x}(x) &= 2q_x(x)u_n(x) + 4v_{n-1,x}(x) - u_{n,xxx}(x) \\ \vdots \\ v_{g,x}(x) &= 0. \end{aligned} \quad (16)$$

Note that we can “read” the recursion formulas for the coefficients $u_i(x)$ ($i = 1, \dots, g$) in the opposite direction, as follows: first, for simplicity, we normalize both U and V as to have $u_g = v_g = 1$. For the moment, we use the notation $\tilde{u}_i(x), \tilde{v}_i(x)$ to denote the normalized coefficients. Then we use (15) to obtain

$$\begin{aligned} \tilde{u}_g(x) &= 1 \\ \tilde{u}_{g-1,x}(x) &= \frac{q_x(x)}{2} \\ 4\tilde{u}_{g-2,x}(x) &= q_x^2(x) - 4q(x) \left(\frac{q(x)}{2} + c_{g-2} \right) - \frac{q_{xxx}(x)}{2} \\ \vdots \\ \tilde{u}_{0,xxx}(x) - 4q(x)\tilde{u}_{0,x}(x) - 2q_x(x)\tilde{u}_0(x) &= 0. \end{aligned} \quad (17)$$

The quantity c_{g-2} in (17) is a constant of integration.

The equation

$$u_{0,xxx}(x) - 4q(x)u_{0,x}(x) - 2q_x(x)u_0(x) = 0 \quad (18)$$

which appears in (15) and (17) is called “the stationary g -th order K-dV equation”. Note that, if $g = 1$, then the recursion formula (15) translates to

$$(i) \quad u_1(x) = c_1$$

$$(ii) \quad u_{0,x}(x) = c_1 \frac{q_x(x)}{2},$$

$$(iii) \quad q_{xxx}(x) - 6q(x)q_x(x) + c_0q_x(x) = 0$$

where c_0 and c_1 are constants. If we set $c_0 = 0$, then (iii) is the standard “stationary K-dV equation”.

We will need the following fundamental

Lemma 3.1 *Let $A(x) = \begin{pmatrix} 0 & 1 \\ q(x) - \lambda & 0 \end{pmatrix}$ be a matrix of Schrödinger type, with $\lambda \in \mathbb{C}$ and $q \in \mathcal{E}_1$. Let $B(x)$ be a zero-trace matrix whose entries are arbitrarily chosen differentiable functions of the variable $x \in \mathbb{R}$. If A and B satisfy the zero-curvature relation (13), then*

$$\frac{d}{dx} \det B(x) = 0. \quad (19)$$

Proof. Write $B(x) = \begin{pmatrix} -a(x) & b(x) \\ c(x) & a(x) \end{pmatrix}$, where $a(x), b(x)$ and $c(x)$ are differentiable functions. Then the zero-curvature relation (13) tell us that

$$\begin{cases} a_x(x) = (q(x) - \lambda)b(x) - c(x) \\ b_x(x) = 2a(x) \\ c_x(x) = -2(q(x) - \lambda)a(x). \end{cases} \quad (20)$$

Now, write down the expression (19) explicitly and use (20): a simple computation concludes the proof. \blacksquare

Note that the matrix B_g has zero trace and satisfies the zero-curvature relation for every $\lambda \in \mathbb{C}$ and $x \in \mathbb{R}$. We can then write

$$-\det B_g(x, \lambda) = \frac{U_x^2}{4} + (1 - \lambda)UV = k^2(\lambda) = -c^2 \prod_{i=0}^{2g} (\lambda - \lambda_i), \quad (21)$$

where $\lambda_0, \lambda_1, \dots, \lambda_{2g}$ are distinct positive real numbers and $c = u_g = v_g$ is a constant as well (see (15) and (16)).

We want now to find an expression for the solution $q(x)$ of the stationary K-dV equation (18). Such expression will be closely related to the spectral parameters of the equation (12), in the sense that it will be completely determined by the values λ_i ($i = 0, \dots, 2g$) and the moving poles $P_i(x)$ ($i = 1, \dots, g$). We point out that the expression we will find is nothing but the well known one appearing in the beautiful papers [17, 18, 5]. We begin by normalizing the polynomials U and V in such a way that $u_g = v_g = 1$. We will denote the normalized polynomials by \tilde{U} and \tilde{V} . We have

$$\begin{aligned} \tilde{U}(x) &= \lambda^g + \tilde{u}_{g-1}(x)\lambda^{g-1} + \dots + \tilde{u}_1(x)\lambda + \tilde{u}_0(x) \\ \tilde{V}(x) &= \lambda^g + \tilde{v}_{g-1}(x)\lambda^{g-1} + \dots + \tilde{v}_1(x)\lambda + \tilde{v}_0(x). \end{aligned} \quad (22)$$

Next, we set

$$\tilde{U}(x, \lambda) = \prod_{i=1}^g (\lambda - s_i(x)), \quad (23)$$

where $s_i : \mathbb{R} \rightarrow \mathbb{R}$ ($i = 1, \dots, g$) are bounded continuously differentiable functions. We will now prove the existence of the functions $s_i(x)$ characterizing the expression (23), and we will observe the surprising relation occurring between the points $s_i(x)$ and the zeroes $P_i(x)$ of the diagonal Green's function $G(x, \lambda)$ (or, equivalently, the poles of the function $\mathcal{M}(x, \lambda)$). Inserting (23) into (21) and computing the resulting expression at $\lambda = s_j(x)$, we obtain

$$s_{j,x}(x) = -\frac{2k(s_j(x))}{c \prod_{j \neq i} (s_j(x) - s_i(x))} =: F_j(x), \quad j = 1, \dots, g \quad (24)$$

The expressions on the right-hand side of (24) are well defined mappings $F_j : \mathbb{R} \rightarrow \mathbb{R} : x \mapsto F_j(x)$ ($j = 1, \dots, g$), and in fact (24) are exactly the Dubrovin equations [5] for the K-dV flow. This allows us to draw the following conclusions:

- (i) A unique solution $\{s_i(x)\}_{i=1, \dots, g}$ for the system (24) exists for every fixed initial condition $s_i(0) \in [\lambda_{2i-1}, \lambda_{2i}]$, it is defined on all \mathbb{R} and is of class C^∞ (to see this, begin differentiating the expression (24) with respect to $x \in \mathbb{R}$, and observe that the singularities at the points λ_k cancel out).
- (ii) One has $\lambda_{2i-1} \leq s_i(x) \leq \lambda_{2i}$ for every $i = 1, \dots, g$. Each $s_i(x)$ reaches the values λ_{2i-1} and λ_{2i} exactly at those points $x \in \mathbb{R}$ where $s_{i,x}(x) = 0$. When a certain $s_i(x)$ reaches this value, it starts moving backwards to the opposite extreme point in the gap containing it.
- (iii) For every fixed initial condition $s_i(0) \in [\lambda_{2i-1}, \lambda_{2i}]$, the solution $\{s_i(x)\}_{i=1, \dots, g}$ of the system (24) equals the set $\{P_1(x), \dots, P_g(x)\}$ of the zeroes of the Green's function $G(x, \lambda)$.

We can now write

Theorem 3.2 *Let $\tilde{U}(x, \lambda)$ be as in (23), let $s_1^0 \in I_1, \dots, s_g^0 \in I_g$, and let $\{s_i(x)\}$ be the unique solution of the system (24) satisfying $s_i(0) = s_i^0$ for every $i = 1, \dots, g$. Then the set $\{s_1(x), \dots, s_g(x)\}$ coincides with the set $\{P_1(x), \dots, P_g(x)\}$ consisting of the zeroes of the diagonal Green's function $G(x, \lambda)$ corresponding to the Schrödinger equation (12). In particular, for every choice of $0 < \lambda_0 < \lambda_1 < \dots < \lambda_{2g} \in \mathbb{R}$ and s_1^0, \dots, s_g^0 as above, there exists an algebro-geometric Schrödinger potential $q(x) \in \mathcal{E}_1$ whose spectrum equals the set $\Sigma = [\lambda_0, \lambda_1] \cup \dots \cup [\lambda_{2g}, \infty)$. Moreover one has the trace formula (8), i.e.,*

$$q(x) = \sum_{k=1}^g (\lambda_{2k} - \lambda_{2k-1} - 2P_k(x)).$$

The trace formula (8) is well known (see [5, 25]). However, it is worth noting that one can obtain it simply by means of the recursion formulas (17) and (21): it suffices to see that the (normalized) coefficient $\tilde{u}_{g-1}(x)$ satisfies $q(x) = 2\tilde{u}_{g-1}(x) + \alpha$, where

α is a constant of integration, then to write $\tilde{u}_{g-1}(x) = -\sum_{i=1}^g s_i(x)$, and finally to

compute the constant α from (21), obtaining $\alpha = \sum_{i=0}^{2g} \lambda_i$.

We finish this section by expressing the Weyl m -functions for the Schrödinger equation (12) in terms of the entries of the matrix B_g . To this aim, it is convenient to introduce the Riemann surface \mathcal{R} of genus g of the algebraic relation

$$w^2 = -c^2(\lambda - \lambda_0)(\lambda - \lambda_1) \dots (\lambda - \lambda_{2g}) = k^2(\lambda). \quad (25)$$

Then \mathcal{R} can be viewed as two copies of the Riemann sphere $\hat{\mathbb{C}} = \mathbb{C} \cup \{\infty\}$ glued together in a standard way at the points λ_i ($i = 0, \dots, 2g$). Let us consider the pairs $(\lambda, w) \in \mathbb{C}^2$ which satisfy (25). It is clear then that two values of w correspond to each $\lambda \in \hat{\mathbb{C}} \setminus \{\lambda_0, \lambda_1, \dots, \lambda_{2g}, \infty\}$. If $\lambda \in \{\lambda_0, \lambda_1, \dots, \lambda_{2g}\}$, then w takes the value 0, while if $\lambda = \infty$, then $w = \infty$ as well. Next, let $\pi : \mathcal{R} \rightarrow \hat{\mathbb{C}}$ be the projection on the first factor. Then π is 2-to-1 except at $\{\lambda_0, \lambda_1, \dots, \lambda_{2g}, \infty\}$ where it is 1-to-1. Points in \mathcal{R} will be denoted by P and, when necessary, we will write P^+ for $(\lambda, c\sqrt{-(\lambda - \lambda_0)(\lambda - \lambda_1) \dots (\lambda - \lambda_{2g})}) \in \mathcal{R}$ and P^- for the point

$$(\lambda, -c\sqrt{-(\lambda - \lambda_0)(\lambda - \lambda_1) \dots (\lambda - \lambda_{2g})}) \in \mathcal{R}. \text{ So, for instance, } 0^\pm = \left(0, \pm c\sqrt{\prod_{i=0}^{2g} \lambda_i}\right).$$

Note that \mathcal{R} ramifies at the inverse images under π of the points $\lambda_0, \lambda_1, \dots, \lambda_{2g}, \infty$. We abuse notation slightly and write $\lambda_0, \lambda_1, \dots, \lambda_{2g}, \infty \in \mathcal{R}$. After these observations, it becomes clear that the map $k : P \mapsto k(\lambda)$ ($\lambda = \pi(P)$) is meromorphic on \mathcal{R} . Let $\sigma : \mathcal{R} \rightarrow \mathcal{R}$ denote the hyperelliptic involution, i.e., $\sigma(P^\pm) = P^\mp$ for every $P^\pm \in \mathcal{R}$. For every $x \in \mathbb{R}$, we define functions $\tilde{m}_\pm^x : \mathcal{R} \rightarrow \mathbb{C}$ as follows

$$\tilde{m}_+^x(P) = \frac{U_x/2 + k(\lambda)}{U}, \quad \tilde{m}_-^x(P) = (\tilde{m}_+^x \circ \sigma)(P) = \frac{U_x/2 - k(\lambda)}{U}, \quad \lambda = \pi(P).$$

Note that for every fixed $\lambda \in \mathbb{C}$, one can consider the maps $x \mapsto \tilde{m}_\pm^x(\lambda) = m_\pm(x, \lambda) : \mathbb{R} \rightarrow \mathbb{C}$. We denote by $\tilde{m}_{\pm,x}$ the x -derivatives of these maps. We have:

Proposition 3.3 *Let \mathcal{R} and let $\tilde{m}_\pm : \mathcal{R} \rightarrow \mathbb{C}$ be defined as above. Then, for fixed λ the maps $x \mapsto \tilde{m}_\pm(x, \lambda)$ satisfy the following Riccati equation*

$$M_x + M^2 = q - \lambda. \quad (26)$$

In particular, \tilde{m}_\pm are the “meromorphic extensions” to \mathcal{R} of the Weyl m -functions m_\pm associated to the Schrödinger equation (12).

Proof. The proof is an easy computation. We have, using (14),

$$U^2(\tilde{m}_{\pm,x} + \tilde{m}_\pm^2) = \frac{U_{xx}}{2}U - \frac{1}{2}U_x^2 + k^2(\lambda) = (q - \lambda)U^2.$$

■

4 The r -th Order K-dV Equation: the K-dV Hierarchy

In this section we will solve the r -th order K-dV equation arising from a time-dependent zero-curvature relation, when the initial data is the solution of the stationary g -th order K-dV equation (18) (here and below, we will always assume that $r < g$).

Assume that we have developed the procedure described in the previous section: we have a stationary K-dV equation of order $g \in \mathbb{N}$

$$u_{0,xxx}(x) - 4q(x)u_{0,x}(x) - 2q_x(x)u_0(x) = 0$$

together with the solution $q(x)$ we have determined satisfying a certain initial data

$$q(0) = \sum_{k=1}^g (\lambda_{2k} - \lambda_{2k-1} - 2P_k^0).$$

We know that $q(x)$ determines a Schrödinger potential in \mathcal{E}_1 (see the discussion in Section 2). Now we introduce the time dependence. Imagine that in the previous section we have fixed an initial time t_0 . Then $U = U(x, t_0, \lambda)$, $V = V(x, t_0, \lambda)$, $P_i^0 = P_i^0(t_0)$, $P_i(x) = P_i(x, t_0)$ ($i = 1, \dots, g$) and $q(x) = q(x, t_0)$. It is understood that also (18) translates to

$$u_{0,xxx}(x, t_0) - 4q(x, t_0)u_{0,x}(x, t_0) - 2q_x(x, t_0)u_0(x, t_0) = 0.$$

Let us fix a number $r \in \mathbb{N}$ with $r \leq g$. We introduce a time-dependent zero-curvature relation as follows: let $A(x, t) = \begin{pmatrix} 0 & 1 \\ q(x, t) - \lambda & 0 \end{pmatrix}$ be a matrix of Schrödinger type where the potential q depends on t as well, and let

$$B_r(x, t) = \begin{pmatrix} -U_{r,x}(x, t)/2 & U_r(x, t) \\ (1 - \lambda)V_r(x, t) & U_{r,x}(x, t)/2 \end{pmatrix}$$

where U_r and V_r are polynomials of order r in the complex variable $\lambda \in \mathbb{C}$ and whose coefficients $u_i^{(r)}$ and $v_i^{(r)}$ depend continuously on $x, t \in \mathbb{R}$. We require that the following zero-curvature relation holds:

$$A_t(x, t) - B_{r,x}(x, t) + [A, B_r] = 0, \quad (r < g). \quad (27)$$

We argue as in the previous section and observe that (27) is equivalent to the system

$$\begin{cases} 2q_t - U_{r,xxx} - 4(1 - \lambda)V_{r,x} + 2q_x U = 0 \\ 2q_t + U_{r,xxx} - 4(q - \lambda)U_{r,x} - 2q_x U = 0 \end{cases} \quad (28)$$

As before, from the second equation in (28) we determine the recursion formulas for the coefficients $u_i^{(r)}(x)$ of the polynomial U_r and then we find those of the polynomial V_r by using the first equation in (28). We have:

$$\begin{aligned} 2q_t(x, t) + u_{0,xxx}^{(r)}(x, t) - 4q(x, t)u_{0,x}^{(r)}(x, t) - 2q_x(x, t)u_0^{(r)}(x, t) &= 0 \\ u_{1,xxx}^{(r)}(x, t) - 4q(x, t)u_{1,x}^{(r)}(x, t) + 4u_0(x, t) - 2q_x(x, t)u_1^{(r)}(x, t) &= 0 \\ \vdots & \\ u_{n,xxx}^{(r)}(x, t) - 4q(x, t)u_{n,x}^{(r)}(x, t) + 4u_{n-1}^{(r)}(x, t) - 2q_x(x, t)u_n^{(r)}(x, t) &= 0 \\ \vdots & \\ u_{r,x}^{(r)}(x, t) &= 0. \end{aligned} \quad (29)$$

The coefficients $v_i^{(r)}(x, t)$ are determined analogously.

The equation

$$2q_t(x, t) + u_{0,xxx}^{(r)}(x, t) - 4q(x, t)u_{0,x}^{(r)}(x, t) - 2q_x(x, t)u_0^{(r)}(x, t) = 0 \quad (30)$$

which appears in (29) is the “ r -th order K-dV equation”. Note that, if $r = 1$, then the recursion formula (29) translates to

- (i) $u_1^{(1)}(x, t) = c_1$
- (ii) $u_{0,x}^{(1)}(x, t) = c_1 \frac{q_x(x, t)}{2},$
- (iii) $q_t(x, t) + q_{xxx}(x) - 6q(x)q_x(x) + c_0q_x(x) = 0$

where c_0 and c_1 are constants. If we set $c_0 = 0$, then (iii) is the well-known “K-dV equation”. As an example, we write below the expression of the the 2nd order K-dV equation:

$$q_t + \frac{3}{4}q_{xxx}^2 - \frac{c_2}{2}q_{xxx} - \frac{1}{2}q_{xxxx} - \frac{9}{4}q^2q_x + \frac{c_2}{2}qq_x + \frac{1}{4}qq_{xxx} + \frac{1}{8}q_xq_{xx} - c_3q_x = 0,$$

where c_2 and c_3 are constants.

We look for a solution $q(x, t)$ of the r -th order K-dV equation as the evolution with respect to $t \in \mathbb{R}$ of the initial data $q(x, t_0)$, hence we require that the initial data varies with t : this means that the the following stationary zero-curvature relation

$$-B_{g,x}(x, t) + [A, B_g] = 0 \quad (31)$$

holds for every $x, t \in \mathbb{R}$. The idea now is to find a function $q(x, t)$ together with complex polynomials $U(x, t), V(x, t), U_r(x, t), V_r(x, t)$ which satisfy (27) and (31). Note that we assume that for every $t \in \mathbb{R}$, the potential $q(x, t)$ and the matrix $B_g(x, t)$ are defined in such a way as to satisfy the relation (21), i.e., for every fixed $t \in \mathbb{R}$, the maps $x \mapsto q(x, t)$ and $x \mapsto B_g(x, t)$ define an initial condition for the K-dV flow at time t . After these observations, it follows that we must have

$$\frac{d}{dt} \det B_g(x, t) = 0, \quad (32)$$

or, equivalently,

$$\frac{U_x^2(x, t)}{4} + (1 - \lambda)U(x, t)V(x, t) = -k^2(\lambda).$$

Next, we proceed to find the relations occurring between the entries U, V, U_r, V_r . As before, for every fixed $(x, t) \in \mathbb{R}^2$, we define functions $P \mapsto \tilde{m}_\pm(x, t, \pi(P)) : \mathcal{R} \rightarrow \mathbb{C}$ as follows:

$$\tilde{m}_\pm(x, t, \lambda) = \frac{U_x/2 \pm k(\lambda)}{U}.$$

Note again that for every fixed $P \in \mathcal{R}$, the maps $(x, t) \mapsto \tilde{m}_\pm(x, t, \lambda)$ are well defined. The following relations occur between the functions \tilde{m}_\pm :

$$\tilde{m}_+ + \tilde{m}_- = \frac{U_x}{U} \quad (33)$$

$$\tilde{m}_+ - \tilde{m}_- = \frac{2k(\lambda)}{U} \quad (34)$$

$$\tilde{m}_+\tilde{m}_- = -(1 - \lambda)\frac{V}{U} \quad (35)$$

$$\tilde{m}_{\pm,x,t} + 2\tilde{m}_\pm\tilde{m}_{\pm,t} = q_t. \quad (36)$$

These trivial relations allow us to find a Riccati equation for the t -motion of \tilde{m}_\pm

Theorem 4.1 *For every fixed $x \in \mathbb{R}$ and $\lambda \in \mathbb{C}$, the functions $t \mapsto \tilde{m}_\pm(x, t, \lambda)$ satisfy the following Riccati equation*

$$M_t = U_{r,x}M - U_rM^2 + (1 - \lambda)V_r. \quad (37)$$

Proof. We adapt a computation from [9, 30]. Write M for both \tilde{m}_\pm . We have, using (13), (27) and (26)

$$\begin{aligned} & \left(\frac{\partial}{\partial x} + 2M \right) (M_t + U_r M^2 - U_{r,x} M - (1 - \lambda) V_r) = \\ & = q_t + 2(q - \lambda) U_r M - (q - \lambda) - U_{r,x} - U_{r,xx} M - (1 - \lambda) V_{r,x} - 2(1 - \lambda) V_r M = 0. \end{aligned}$$

This relation implies that

$$M_t + U_r M^2 - U_{r,x} M - (1 - \lambda) V_r = C e^{\int_0^x 2M(s) ds}, \quad (38)$$

where C is a constant. Now, the left hand side of (38) is meromorphic at ∞ , while the right-hand side is not, hence we must have $C = 0$. This concludes the proof. \blacksquare

The equation (37) is the Riccati equation associated to the Schrodinger equation $-\frac{d^2}{dx^2} \varphi(x, t) + q(x, t) \varphi(x, t) = \lambda \varphi(x, t)$. The t -dependence is due to the presence of a potential $q(x, t)$ which varies with t as well. While the Riccati equation for the x -motion is an intrinsic fact of the Schrödinger equation, it seems that the one related to the t -motion exists only in correspondence with the K-dV flow. In fact, a Riccati equation for the t -motion does not exist when we consider a generic t -dependent potential $q(x, t)$. However, once we have the relations (33)–(37), we can determine the relations occurring between the polynomials U_r, V_r, U and V .

Proposition 4.2 *Let the matrices B_g and B_r satisfy the zero-curvature (13) and (27) respectively. Then they satisfy the following zero-curvature relation*

$$B_{g,t} = [B_r, B_g]. \quad (39)$$

Proof. Note that (39) means that

$$\frac{1}{2} U_{xt} = (1 - \lambda) [U V_r - U_r V] \quad (40)$$

$$U_t = U_r U_x - U_{r,x} U \quad (41)$$

$$V_t = U_{r,x} V - U_x V_r \quad (42)$$

hold simultaneously. To prove (41), we differentiate (34) with respect to t , obtaining

$$[\tilde{m}_+ - \tilde{m}_-]_t = -\frac{2k(\lambda) U_t}{U^2}$$

Since (37) holds both for \tilde{m}_+ and \tilde{m}_- , we can write

$$[\tilde{m}_+ - \tilde{m}_-]_t = 2k(\lambda) \left(\frac{U_{r,x} U - U_r U_x}{U^2} \right).$$

Putting together these formulas we obtain (41). For (40), we differentiate (33) with respect to t , obtaining

$$[\tilde{m}_+ + \tilde{m}_-]_t = \frac{U_{xt} U - U_x U_t}{U^2}.$$

Again, from (37) we get

$$[\tilde{m}_+ + \tilde{m}_-]_t = U_{r,x} \frac{U_x}{U} - U_r \frac{U_x^2}{U^2} - 2(1 - \lambda) \left[\frac{V U_r}{U} - V_r \right].$$

Again, we put these formula together, and (40) follows using (41) as well. It remains to prove (42): we use (35) together with (37), and write

$$\begin{aligned} -(1-\lambda)V_t &= [U\tilde{m}_+\tilde{m}_-]_t = -(1-\lambda)U\frac{V}{U} + \\ &+ (1-\lambda)\left[\frac{U_r V U_x}{U} + V_r U_x - 2U_{r,x}V\right]. \end{aligned}$$

The relation (42) now follows easily by using (41). \blacksquare

Write

$$U(x, t) = c \prod_{i=1}^g (\lambda - s_i(x, t)),$$

where c is a constant (see (22) and (23)). We want to determine the functions $s_i(x, t)$ ($i = 1, \dots, g$). The importance of Proposition 4.2 lies in the fact that the relations (40)–(42) allow us to determine the equations of the t -motion of the functions $s_i(x, t)$ ($i = 1, \dots, g$). It is clear that the x -motion is determined by the system (24) as well, because it depends only on the stationary conditions. We then have

Theorem 4.3 *Assume that (31) and (27) are valid for the matrices $B_g(x, t)$ and $B_r(x, t)$. Let $U(x, t) = c \prod_{i=1}^g (\lambda - s_i(x, t))$. Then for every initial condition $P_1^0 = P_1(0, t_0), \dots, P_g^0 = P_g(0, t_0)$, the functions $s_i(x, t)$ ($i = 1, \dots, g$) are uniquely determined as the solution of the following differential systems*

$$s_{j,x}(x, t) = -\frac{2k(s_j(x, t))}{c \prod_{j \neq i} (s_j(x, t) - s_i(x, t))}, \quad j = 1, \dots, g \quad (43)$$

$$\begin{aligned} s_{j,t}(x, t) &= -\frac{2k(s_j(x, t))}{c \prod_{j \neq i} (s_j(x, t) - s_i(x, t))} U_r(s_j(x, t)) = \\ &= U_r(s_j(x, t)) s_{j,x}(x, t), \quad j = 1, \dots, g \end{aligned} \quad (44)$$

Proof. We only have to prove (44). We compute (41) at $s_j(x, t)$, obtaining

$$U_t(s_j(x, t)) = U_r(s_j(x, t)) U_x(s_j(x, t)).$$

Then we use (32) to find that $U_x(s_j(x, t)) = 2k(s_j(x, t))$. Next we compute the derivative of $U(x, t)$ with respect to t at $s_j(x, t)$, obtaining

$$U_t(x, t) = -cs_j(x, t) \prod_{i \neq j} (s_j(x, t) - s_i(x, t)).$$

Putting all this information together, we obtain the desired result (44). \blacksquare

Apparently, the factor $k(s_j(x, t))$ in both (43) and (44) would imply that the functions $s_j(x, t)$ are only of class $C^1(\mathbb{R}^2)$. Actually, a direct computation shows that $s_j(x, t) \in C^\infty(\mathbb{R}^2)$ (because of the canceling out of the singularities at $\lambda_0, \lambda_1, \dots, \lambda_{2g}$ after the differentiation). For every fixed initial condition $P_1^0 = P_1(0, t_0), \dots, P_g^0 = P_g(0, t_0)$, the systems (43) and (44) admit a unique solution $\{s_j(x, t)\}$ which is globally defined on all \mathbb{R}^2 . Note that we have the bounds $s_j(x, t) \in [\lambda_{2j-1}, \lambda_{2j}]$ for every $j = 1, \dots, g$, that is, the motion of $s_j(x, t)$ stays confined in the spectral gaps $[\lambda_{2j-1}, \lambda_{2j}]$. This observation is of fundamental importance: imagine that we have

fixed a value $t \in \mathbb{R}$. Then one can look at the values $P_1(0, t), \dots, P_g(0, t)$ as an initial condition to solve the system (43). In this case the solution $\{s_j(x, t)\}$ equals the set $\{P_i(x, t)\}$ consisting on the zeroes of the diagonal Green's function $G_t(x, \lambda)$ associated to the Schrödinger equation $-\frac{d^2}{dx^2}\varphi + q(x, t)\varphi = \lambda\varphi$. The potential $q(x, t)$ of Schrödinger type whose related spectrum is $\Sigma = [\lambda_0, \lambda_1] \cup \dots \cup [\lambda_{2g}, \infty)$ can be thus obtained by means of the trace formula

$$q(x, t) = \lambda_0 + \sum_{i=1}^g [\lambda_{2i-1} + \lambda_{2i} - 2P_i(x, t)].$$

Theorem 4.4 *Let B_g and B_r satisfy (27) and (31). Let $\{s_j(x, t)\}_{j=1, \dots, g}$ be the unique solution of (43) and (44) subject to the initial condition $P_1^0, \dots, P_g^0 \in I_1 \times \dots \times I_g$. Then for every $t \in \mathbb{R}$ the functions $x \mapsto s_j(x, t)$ equals the zeros of the diagonal Green's function $G_t(x, \lambda)$ associated to a Schrödinger equation with potential $q_t(x) := q(x, t) = \lambda_0 + \sum_{i=1}^g [\lambda_{2i-1} + \lambda_{2i} - 2P_i(x, t)]$. The family of potentials $\{x \mapsto q_t(x) \mid t \in \mathbb{R}\}$ lies all the same isospectral class $\mathcal{I}(\Sigma) := \{f \in \mathcal{E}_1 \mid \text{the spectrum of the associated Schrödinger equation equals } \Sigma\}$. The function $q(x, t)$ is a solution of the r -th order K-dV equation (30)*

$$2q_t(x, t) + u_{0,xxx}^{(r)}(x, t) - 4q(x, t)u_{0,x}^{(r)}(x, t) - 2q_x(x)u_0^{(r)}(x, t) = 0,$$

where the initial data $q(x, t_0)$ solves the stationary g -th order K-dV equation (actually, $q(x, t)$ solves the stationary g -th order relation for every $t \in \mathbb{R}$).

We finish this section by determining the form of the polynomial $U_r(x, t)$. Let

$$U(x, t) = c \prod_{i=1}^g (\lambda - s_i(x, t))$$

be determined as above. Next, we write down explicitly the polynomials U and U_r and use (41): it follows that $U_r U_x - U_{r,x} U$ must be a polynomial of degree g in λ , and hence all the coefficients of the expression $U_r U_x - U_{r,x} U$ of order higher than g in λ must vanish identically. It is easy to verify that

$$U_r(x, t) = \left[\frac{1}{\lambda^{g-r}} U(x, t) \right]_p, \quad (45)$$

where the symbol $[\cdot]_p$ denotes the polynomial part. Equivalently, one can write

$$u_r^{(r)}(x, t) = u_g(x, t), \quad u_{r-1}^{(r)}(x, t) = u_{g-1}(x, t), \dots, u_0^{(r)}(x, t) = u_{g-r}(x, t).$$

We recall now how the coefficients $u_i(x, t)$ ($i = 1, \dots, g$) of the polynomial $U(x, t)$ can be written in terms of its roots $s_i(x, t)$ ($i = 1, \dots, g$). Let $\mathcal{A} = (a_1, \dots, a_g) \in \mathbb{C}^g$, set $\Lambda_i = \{\ell \in \mathbb{N}^i \mid 1 \leq \ell_1 < \dots < \ell_i \leq g\}$, and define

$$\varsigma_i(\mathcal{A}) = (-1)^i \sum_{\ell \in \Lambda_i} a_{\ell_1} a_{\ell_2} \cdot \dots \cdot a_{\ell_i}, \quad 1 \leq i \leq g. \quad (46)$$

Then $\varsigma_i(\mathcal{A})$ is, up to the sign, the i -th symmetric function of the g -tuple $(a_1, a_2, \dots, a_g) \in \mathbb{C}^g$. We set $\mathcal{S}(x, t) = (s_1(x, t), \dots, s_g(x, t))$. It follows that

$$U(x, t) = c \left(\lambda^g + \sum_{i=1}^g \varsigma_i(\mathcal{S}(x, t)) \lambda^{g-i} \right)$$

and

$$U_r(x, t) = c \left(\lambda^r + \sum_{i=1}^r \varsigma_i(\mathcal{S}(x, t)) \lambda^{r-i} \right).$$

The case of the standard K-dV equation

$$q_t(x, t) + q_{xxx}(x) - 6q(x)q_x(x) = 0$$

is obtained by letting $r = 1$, hence we have $U_1(x, t) = c\lambda - c \left(\sum_{i=1}^g s_i(x, t) \right)$, and (44) translates to

$$s_{j,t}(x, t) = \frac{2k(s_j(x, t))}{\prod_{j \neq i} (s_j(x, t) - s_i(x, t))} \left(\sum_{k \neq j} s_k(x, t) \right) = cs_{j,x}(x, t) (\varsigma_1(\mathcal{S}) - s_j(x, t)).$$

We want now to study the nature of the solution $q(x, t)$ of the r -th order K-dV equation ($r \leq g$). We will see that $q(x, t)$ is quasi-periodic both in x and in t . To distinguish the order r of the K-dV equation, we will denote the corresponding t variable with t_r , so, for instance $q(x, t_r)$ will be the solution of the r -th order K-dV equation, while $P_i(x, t_r)$ will be the roots of the polynomial $U(x, t_r)$. The result stated here, although expressed in a different form, are very well known when $r = 1$, and we will not pause too much in the details. To study $q(x, t_r)$, we move our attention to the Riemann surface \mathcal{R} defined in the previous section. Let $\alpha_1, \dots, \alpha_g, \beta_1, \dots, \beta_g$ be a homology basis of the surface \mathcal{R} consisting of simple closed curves. We require that the following intersection conditions are satisfied:

$$\alpha_i \cdot \alpha_j = 0, \quad \beta_i \cdot \beta_j = 0, \quad \alpha_i \cdot \beta_j = \delta_{ij} \quad (1 \leq i, j \leq g)$$

Define the following differential forms on \mathcal{R} :

$$\omega_n = \frac{\lambda^{n-1}}{k(P)} d\lambda, \quad n = 1, \dots, g.$$

Then $\{\omega_1, \dots, \omega_g\}$ form a basis for the set of holomorphic 1-forms on \mathcal{R} . Let Γ_g be the \mathbb{Z} -lattice spanned by all the vectors in \mathbb{C}^g of the form

$$\int_{\alpha_i} (\omega_1, \dots, \omega_g), \int_{\beta_i} (\omega_1, \dots, \omega_g), \quad (i = 1, \dots, g).$$

Then Γ_g has rank $2g$ in \mathbb{C}^g . Define

$$J(\mathcal{R}) = \mathbb{C}^g / \Gamma_g.$$

$J(\mathcal{R})$ is called the Jacobi variety associated to \mathcal{R} . It is easy to show that $J(\mathcal{R})$ is isomorphic to a complex analytic g -torus. The reader which is not familiar with these topics can be addressed to texts as [28, 24, 7], or to the papers [1, 2, 5, 14, 15, 30]. The Jacobi variety $J(\mathcal{R})$ can be constructed starting from the set \mathcal{D} of the divisors of degree g in \mathcal{R} . Given a divisor $\mathfrak{D} = (P_1, \dots, P_g) \in \mathcal{D}$, we define the Abel map

$$I : \mathcal{D} \rightarrow J(\mathcal{R}) : \mathfrak{D} = (P_1, \dots, P_g) \mapsto \sum_{i=1}^g \int_{P_*}^{P_i} (\omega_1, \dots, \omega_g) \mod \Gamma_g,$$

where $P_* \in \mathcal{R}$ is a base point different from the ramification points $\lambda_0, \lambda_1, \dots, \lambda_{2g}$. It turns out that the Abel map is a birational isomorphism. Now, let us consider the

set $\mathcal{I} = I_1 \times I_2 \times \dots \times I_g$. The inverse image $\pi^{-1}(\mathcal{I})$ is a real g -torus on \mathcal{R} , which we will denote by \mathcal{T} . It follows that the restriction of I to \mathcal{T} is a diffeomorphism onto its image $I(\mathcal{T}) \subset J(\mathcal{R})$. The g -tuple $\mathcal{S}(x, t_r) = (s_1(x, t_r), \dots, s_g(x, t_r))$ determined by the roots of the polynomial $U(x, t_r)$ lies in \mathcal{I} for every $(x, t_r) \in \mathbb{R}^2$. It is natural to ask which is the image under I of this g -tuple and especially which kind of motion $(x, t_r) \mapsto I(\mathcal{S}(x, t_r))$ is determined on $J(\mathcal{R})$. To this aim, given $\mathcal{A} = (a_1, \dots, a_g) \in \mathbb{C}^g$, we first recall some properties of the symmetric functions of \mathcal{A} . Let $\Lambda_i^{(j)} = \{\ell \in \mathbb{N}^i \mid 1 \leq \ell_1 < \dots < \ell_i \leq g, \ell_k \neq j\}$, then define

$$\sigma_i^{(j)}(\mathcal{A}) = (-1)^i \sum_{\ell \in \Lambda_i^{(j)}} a_{\ell_1} \dots a_{\ell_i}, \quad \ell = (\ell_1, \dots, \ell_i), 1 \leq i \leq g-1. \quad (47)$$

The following formulas will be very important

$$\sum_{j=1}^g \frac{a_j^{k-1}}{\prod_{s \neq j} (a_j - a_s)} \sigma_i^{(j)}(\mathcal{A}) = \delta_{k,g-i} - \varsigma_{i+1}(\mathcal{A}) \delta_{k,g+1}. \quad (48)$$

$$\sum_{i=0}^r \varsigma_i(\mathcal{A}) a_j^{r-i} = \sigma_r^{(j)}(\mathcal{A}), \quad r = 0, \dots, g, \quad j = 1, \dots, g \quad (49)$$

where $\varsigma_0(\mathcal{A}) = \sigma_r^{(j)}(\mathcal{A}) = 1$.

For $i = 0$, the relation (48) reads

$$\sum_{j=1}^g \frac{a_j^{k-1}}{\prod_{s \neq j} (a_j - a_s)} = \delta_{k,g}, \quad k = 1, \dots, g.$$

Let us consider the maps

$$\omega_n : \mathbb{R}^2 \rightarrow \mathbb{C} : (x, t_r) \mapsto \omega_n(x, t_r) = \sum_{i=1}^g \int_{P_*}^{P_i(x, t_r)} \omega_n, \quad n = 1, \dots, g$$

Differentiation with respect to x of the functions $\omega_n(x, t_r)$ yields

$$\frac{\partial}{\partial x} \omega_n(x, t_r) = -2 \sum_{i=1}^g \frac{P_i^{n-1}(x, t_r)}{\prod_{i \neq j} (P_i(x, t_r) - P_j(x, t_r))} = -2\delta_{n,g}, \quad n = 1, \dots, g. \quad (50)$$

The relations (50) determine the x -motion on $J(\mathcal{R})$, as follows:

$$\begin{cases} \omega_1(x, t_r) = c_1(t_r) \mod \Gamma_g \\ \vdots \\ \omega_{g-1}(x, t_r) = c_{g-1}(t_r) \mod \Gamma_g \\ \omega_g(x, t_r) = (-2x + c_g(t_r)) \mod \Gamma_g \end{cases} \quad (51)$$

For every fixed $t_r \in \mathbb{R}$, the linearity of the motion $(x, t_r) \mapsto (\omega_1(x, t_r), \dots, \omega_g(x, t_r))$ has as consequence the periodicity with respect to the variable x on $J(\mathcal{R})$. It is easy to study the t_r -motion as well. We have, using (44), (48) and (49)

$$\frac{\partial}{\partial t_r} \omega_n(x, t_r) = -2 \sum_{i=1}^g \frac{P_i^{n-1}(x, t_r) \sigma_r^{(i)}(\mathcal{S}(x, t_r))}{\prod_{i \neq j} (P_i(x, t_r) - P_j(x, t_r))} = -2\delta_{n,g-r}, \quad n, r = 1, \dots, g. \quad (52)$$

The motion $(x, t_r) \mapsto (\omega_1(x, t_r), \dots, \omega_g(x, t_r))$ is completely determined, and in fact we obtain

$$\begin{cases} \omega_1(x, t_r) = c_1 \mod \Gamma_g \\ \vdots \\ \omega_{g-r}(x, t_r) = (-2t_r + c_{g-r}) \mod \Gamma_g \\ \vdots \\ \omega_g(x, t_r) = (-2x + c_g) \mod \Gamma_g. \end{cases} \quad (53)$$

Again, the relations (53) tell us that the motion $(x, t_r) \mapsto (\omega_1(x, t_r), \dots, \omega_g(x, t_r))$, when viewed on $J(\mathcal{R})$, is periodic both in x and in t_r . We will not pause to much now to explain the reason why from the periodicity of such a motion follows the quasi-periodicity of the solution of the r -th order K-dV equation $q(x, t_r)$; however, this is a well-known fact which depends on the possibility to express $q(x, t_r)$ by means of a so-called Θ -quotient. To be a little bit more rigorous, let $Symm^g(\mathcal{R})$ be the set of unordered g -tuples of distinct points in \mathcal{R} . A general theory [28] explains that every symmetric functions $f : Symm^g(\mathcal{R}) \rightarrow \mathbb{C}$ can be written as a function defined on $J(\mathcal{R})$ by means of the Abel map and the Riemann Θ -function. Note that $q(x, t_r)$ is a symmetric function of the points $P_1(x, t_r), \dots, P_g(x, t_r) \in \mathcal{R}$: since the motion $(x, t_r) \mapsto (P_1(x, t_r), \dots, P_g(x, t_r))$ is transformed into a periodic motion $(x, t_r) \mapsto (\omega_1(x, t_r), \dots, \omega_g(x, t_r))$ on $J(\mathcal{R})$, it follows that $q(x, t_r)$ is quasi-periodic in x and t_r , because its expression in terms of the Riemann Θ -function depends on normalized differentials w_1, \dots, w_g of the first kind on \mathcal{R} which can be obtained from $\omega_1, \dots, \omega_g$ and a normalizing $g \times g$ matrix D , as follows: $(w_1, \dots, w_g) = D(\omega_1, \dots, \omega_g)^t$. The matrix D transforms the periodicity of $(\omega_1(x, t_r), \dots, \omega_g(x, t_r))$ into a quasi-periodicity of $(w_1(x, t_r), \dots, w_g(x, t_r))$. For a detailed treatment of the topics discussed in these last few lines, see [28, 24, 5, 20, 21, 14, 15, 30]. It is worth mentioning that, as far as I know, the result of quasi-periodicity of the solution of the K-dV equation $q(x, t_r)$ when $\{x \mapsto q(x, t_r) \mid t_r \in \mathbb{R}\}$ is a family of finite gap potentials in $\mathcal{I}(\Sigma)$ was known only in the case $r = 1$.

5 A Hierarchy Based on Entire Functions

We have seen in the previous section that the solution $q(x, t_r)$ of the r -th order K-dV equation are quasi periodic as soon as for every $t_r \in \mathbb{R}$ the potential $x \mapsto q(x, t_r)$ is of finite-gap type, i.e. it determines a spectrum $\Sigma_t = [\lambda_0, \lambda_1] \cup \dots \cup [\lambda_{2g}, \infty)$ which does not vary with $t_r \in \mathbb{R}$ and such that the upper Lyapunov exponent $\beta(\lambda)$ vanishes a.e. in Σ . The question which naturally arises is the following: can we find solutions which need not be quasi periodic? A first answer to this question was given by McKean and Trubovich [23] and Levitan [20, 21], where the almost periodicity of the solution of the first order K-dV equation was investigated. In those papers it was proved that the solution of the first order K-dV equation is almost periodic with respect to x and t if the map $x \mapsto q(x, t)$ is a reflectionless Schrödinger potential for which the spectral gaps $I_k = [\lambda_{2k-1}, \lambda_{2k}]$ form an infinite (increasing) sequence $\{I_k\}_k$ such that the lengths $|I_k|$ have a fast decay as $k \rightarrow \infty$ and $\lambda_j \rightarrow \infty$ as $j \rightarrow \infty$. Another assumption is made to ensure the solvability of the Riemann inversion problem in a Riemann surface of infinite genus (which was necessary to prove almost periodicity of the solution of the K-dV equation), i.e. it was assumed that the gap be “sufficiently far” each other (see the discussion in Section 1).

We will solve the r -th order K-dV equation when the initial data $q(x, t_0)$ deter-

mines a Schrödinger operator whose spectrum Σ has the form

$$\Sigma = \mathbb{R} \setminus \left((-\infty, \lambda_0) \bigcup_{k=1}^{\infty} I_k^{\circ} \right).$$

The sets I_k are intervals $[\lambda_{2k-1}, \lambda_{2k}]$ and they are called, as usual, spectral gaps. Let $d_k = |\lambda_{2k} - \lambda_{2k-1}|$ denote the length of the spectral gap I_k , $h_{jk} = \text{dist}(I_j, I_k)$ and $h_{0k} = |\lambda_{2k-1} - \lambda_0|$. Throughout this section we will assume we are given an increasing sequence of positive real numbers $\lambda_0, \dots, \lambda_n \dots$ such that:

Hypothesis 5.1 *The set $\{\lambda_0, \lambda_1, \dots, \lambda_n, \dots\}$ has the following properties:*

$$(5.1a) \quad \lambda_0 < \lambda_1 < \dots < \lambda_n < \dots;$$

$$(5.1b) \quad \sum_{i=0}^{\infty} \frac{1}{\lambda_i} < \infty$$

$$(5.1c) \quad \sum_{j=1}^{\infty} d_j < \infty$$

$$(5.1d) \quad \sup_{j \in \mathbb{N}} d_j h_{0j} < \infty$$

$$(5.1e) \quad \sup_{j \in \mathbb{N}} \sum_{k \neq j} \frac{\sqrt{d_k}}{h_{jk}} = D_1 < \infty.$$

Hypotheses 5.1 are weaker than those of Levitan [20, 21], and are sufficient to guarantee the existence of a Schrödinger potentials $q(x) \in \mathcal{E}_1$ which is reflectionless and such that the corresponding spectrum Σ equals the set $\Sigma = \mathbb{R} \setminus \left((-\infty, \lambda_0) \bigcup_{k=1}^n I_k^{\circ} \right)$. This is because Hypotheses 5.1 imply Hypotheses 2.4. See the discussion in Section 2. A simple technical reason for which Hypothesis (5.1) is assumed is that (5.1b) and (5.1c) imply that the infinite products

$$\prod_{j=0}^{\infty} \left(1 - \frac{\lambda}{\lambda_j} \right), \quad \prod_{j=1}^{\infty} \left(1 - \frac{\lambda}{x_j} \right), \quad (x_j \in I_j)$$

converge. Next, we introduce a stationary zero-curvature relation as before, where, however, the entries of the matrix $B = \begin{pmatrix} -U_x/2 & U \\ (1-\lambda)V & U_x/2 \end{pmatrix}$ are made of entire functions. So U, V are now entire functions of the variable $\lambda \in \mathbb{C}$. Clearly the relations (14) and (21) retain validity. To obtain recursion formulas analogous to (15) and (16), one can argue as follows: we develop both U and V in Taylor series at $\lambda = 0$, obtaining

$$U = \sum_{j=0}^{\infty} u_j(x) \lambda^j, \quad V = \sum_{j=0}^{\infty} v_j(x) \lambda^j. \quad (54)$$

Then we put these expressions in (14), and obtain again recursion formulas which are analogous to (15) and (16). We rewrite down these recursion formulas again:

$$\begin{aligned}
u_{0,xxx}(x) - 4q(x)u_{0,x}(x) - 2q_x(x)u_0(x) &= 0 \\
u_{1,xxx}(x) - 4q(x)u_{1,x}(x) + 4u_0(x) - 2q_x(x)u_1(x) &= 0 \\
\vdots \\
u_{n,xxx}(x) - 4q(x)u_{n,x}(x) + 4u_{n-1}(x) - 2q_x(x)u_n(x) &= 0 \\
\vdots
\end{aligned}$$

and

$$\begin{aligned}
4v_{0,x}(x) &= 2q_x(x)u_0(x) - u_{0,xxx}(x) \\
4v_{1,x}(x) &= 2q_x(x)u_1(x) - u_{1,xxx}(x) + 2q_x(x)u_0(x) - u_{0,xxx}(x) \\
\vdots \\
4v_{n,x}(x) &= 2q_x(x)u_n(x) + 4v_{n-1,x}(x) - u_{n,xxx}(x) \\
\vdots
\end{aligned}$$

As before, the relation $u_{0,xxx}(x) - 4q(x)u_{0,x}(x) - 2q_x(x)u_0(x) = 0$ is the “infinite-order” stationary K-dV equation. It is clear that (19) holds, but instead of (21), we require now that

$$\frac{U_x^2}{4} + (1 - \lambda)UV = \prod_{j=0}^{\infty} \left(1 - \frac{\lambda}{\lambda_j}\right). \quad (55)$$

We observe again that the right-hand side of (55) is well defined. We slightly modify the expression given in (23), and assume that the entire function $U(x, \lambda)$ can be written as

$$U(x, \lambda) = \frac{1}{\sqrt{\lambda_0}} \prod_{j=1}^{\infty} \frac{s_j(x)}{\sqrt{\lambda_{2j-1}\lambda_{2j}}} \prod_{i=1}^{\infty} \left(1 - \frac{\lambda}{s_i(x)}\right). \quad (56)$$

Note that $U(x, \lambda)$ is well defined, because $\prod_{i=1}^{\infty} \left(1 - \frac{\lambda}{s_i(x)}\right)$ converges, and

$$\prod_{j=1}^{\infty} \frac{s_j(x)}{\sqrt{\lambda_{2j-1}\lambda_{2j}}} \leq \prod_{j=1}^{\infty} \left(1 + \frac{s_j(x) - \lambda_{2j-1}}{\lambda_{2j-1}}\right) \leq \prod_{j=1}^{\infty} \left(1 + \frac{d_j}{h_{0j}}\right)$$

converges as well. We want to determine the functions $s_j(x)$ which appear in (56) and a function $q(x)$ for which the zero-curvature relation is valid. To this aim, we compute (55) at $\lambda = s_j(x)$ ($j = 1 \in \mathbb{N}$), obtaining

$$\frac{U_x^2(x, s_j(x))}{4} = \prod_{i=0}^{\infty} \left(1 - \frac{s_j(x)}{\lambda_i}\right).$$

Set

$$k_{\infty}(0) = \prod_{n=0}^{\infty} \lambda_n.$$

We have

$$U_x(x, \lambda) = \frac{1}{k_{\infty}(0)} \sum_{i=1}^{\infty} \left(s_{i,x}(x) \prod_{r \neq i} (s_r - \lambda) \right),$$

and hence

$$U_x(x, s_j(x)) = \frac{1}{k_\infty(0)} s_{j,x}(x) \prod_{r \neq j} (s_r - s_j).$$

Putting these relations together, we obtain the following formal system determining the motion of the functions $s_j(x)$ ($j \in \mathbb{N}$):

$$s_{j,x}(x) = \frac{2 \sqrt{\prod_{i=0}^{\infty} (s_j(x) - \lambda_i)}}{\prod_{r \neq j} (s_r(x) - s_j(x))} = F_j(x), \quad (j \in \mathbb{N}). \quad (57)$$

The relation (57) is a system of infinite differential equations. First of all we have to determine whether its right-hand side $F_j(x)$ is well defined, then we will determine a solution by using methods similar to those in [16]. We will prove more than the simple existence of a solution, in fact we will prove that for every fixed initial condition $s_1(0) \in I_1, \dots, s_n(0) \in I_n, \dots$ the system (57) admits a unique solution defined globally on all \mathbb{R} . Note further that if a solution $\{s_j(x)\}$ of the system (57) exists, then one has $s_j(x) \in [\lambda_{2j-1}, \lambda_{2j}]$ for every $j \in \mathbb{N}$.

First of all, we show that the right-hand side $F_j(x)$ of (57) is well defined for every $j \in \mathbb{N}$. Set

$$k_\infty(\lambda) = \sqrt{\lambda - \lambda_0} \prod_{n=1}^{\infty} \sqrt{(\lambda - \lambda_{2i-1})(\lambda_{2i} - \lambda)}.$$

Let us consider the set $\mathcal{I} = I_1 \times I_2 \times \dots \times I_k \times \dots$. Denote points in \mathcal{I} by $\{X\}$. It is clear that a point $\{X\} \in \mathcal{I}$ consists of a sequence of positive real numbers $X_k \in I_k$. We equip \mathcal{I} with the following metric

$$\|\{X\} - \{Y\}\|_{\mathcal{I}} = \sup_{k \in \mathbb{N}} |X_k - Y_k| \sqrt{d_k}.$$

Since $|X_k - Y_k| \leq d_k$, it follows that the metric $\|\cdot\|_{\mathcal{I}}$ is well defined. Fix arbitrarily a point $\{\tilde{s}(0)\} = \{\tilde{s}_1(0), \dots, \tilde{s}_n(0), \dots\} \in \mathcal{I}$. For every $j \in \mathbb{N}$, we define a function $F_j : \mathcal{I} \rightarrow \mathbb{R}$ as follows

$$F_j(\{X\}) = \frac{2k_\infty(X_j)}{\prod_{k \neq j} (X_j - X_k)}.$$

Lemma 5.2 *Let the sequence $\{\lambda_0, \lambda_1, \dots, \lambda_n, \dots\}$ satisfy Hypotheses 5.1. Then the maps $F_j(\{X\})$ defined above are well defined for every $j \in \mathbb{N}$.*

Proof. We show that $|F_j(\{X\})|$ is bounded, uniformly with respect to $j \in \mathbb{N}$. Set $D = \sup_{k \in \mathbb{N}} d_k$. We have

$$\begin{aligned} \frac{|F_j(\{X\})|^2}{4} &\leq |(\lambda_{2j} - X_j)(X_j - \lambda_{2j-1})|(X_j - \lambda_0)| \times \\ &\times \prod_{k \neq j \in \mathbb{N}} \left| \frac{(\lambda_{2k} - X_j)(\lambda_{2k-1} - X_j)}{(X_j - X_k)^2} \right| \leq \\ &\leq d_r^2(h_{0r} + d_r) \prod_{s \in \mathbb{N}} \exp \left(\sum_{k \neq j \in \mathbb{N}} \ln \left(1 + \frac{d_k}{h_{jk}} \right) \right), \end{aligned}$$

and the proof follows by using Hypotheses (5.1). ■

Let

$$D_2 = \sup_{j \in \mathbb{N}} \sup_{\{X\} \in \mathcal{I}} |F_j(\{X\})|.$$

Next, we want to obtain some estimates for the derivatives $\frac{\partial F_j}{\partial X_k}$. Unfortunately, it seems that F_j is not differentiable with respect to the variable X_j . To solve this problem, we introduce a change of variables [20],

$$X_k = \lambda_{2k-1} + d_k \sin^2 \theta_k \quad \theta_k \in [0, \pi/2], \quad (k \in \mathbb{N}).$$

With this change of variables, one obtains functions $F_j(\{\theta\}) = F_j(\{X(\theta)\})$ which assume the simpler form

$$F_j(\{\theta\}) = 2\sqrt{X_j(\theta_j) - \lambda_0} \prod_{s \neq j} \frac{\sqrt{(X_j(\theta_j) - \lambda_{2s-1})(X_j(\theta_j) - \lambda_{2s})}}{X_j(\theta_j) - X_s(\theta_s)}.$$

For every $j \in \mathbb{N}$, denote by \tilde{F}_j the map

$$\tilde{F}_j : \mathcal{I} \rightarrow \mathbb{R} : \{X\} \mapsto 2\sqrt{X_j - \lambda_0} \prod_{s \neq j} \frac{\sqrt{(X_j - \lambda_{2s-1})(X_j - \lambda_{2s})}}{X_j - X_s}.$$

Let us consider the functions $s_k(x)$ ($k \in \mathbb{N}$). Then $s_k \in I_k$ for every $k \in \mathbb{N}$, and the change of variables transforms the functions $s_k(x)$ into functions $\theta_k(x)$ ($k \in \mathbb{N}$). The system (57) translates to

$$\theta_{k,x}(x) = F_j(\{\theta(x)\}), \quad k \in \mathbb{N} \quad (58)$$

We have

Proposition 5.3 *Let $r, k \in \mathbb{N}$. Then*

$$\left| \frac{\partial F_r}{\partial \theta_k}(\{\theta\}) \right| \leq \sup_{\{X\} \in \mathcal{H}} \left| 2d_k \tilde{F}_r(\{X\}) \left(\frac{1}{X_k} + \frac{1}{X_r - X_k} \right) \right|, \quad r \neq k \in \mathbb{N} \quad (59)$$

$$\begin{aligned} \left| \frac{\partial F_r}{\partial \theta_r}(\{\theta\}) \right| &\leq \sup_{\{X\} \in \mathcal{H}} \left| 2d_r \tilde{F}_r(\{X\}) \right| \left| \frac{1}{X_r} + \frac{1}{2(X_r - \lambda_0)} + \right. \\ &\quad \left. + \frac{1}{2} \sum_{r \neq s \in \mathbb{N}} \left(\frac{1}{(X_r - \lambda_{2s})} + \frac{1}{(X_r - \lambda_{2s-1})} - \frac{2}{(X_r - X_s)} \right) \right|. \end{aligned} \quad (60)$$

A proof of Proposition 5.3 can be found in [16]. Actually, more can be said concerning the derivatives of the maps $\{\theta\} \mapsto F_r(\{\theta\})$ ($r \in \mathbb{N}$): further computations show that these maps are differentiable infinitely many times with respect to the variables θ_k ($k \in \mathbb{N}$). Next, we find convenient to show first the uniqueness of the solution of (57) for every fixed initial condition $\{s(0)\} = \{s_1(0), \dots, s_n(0), \dots\} \in \mathcal{I}$.

Theorem 5.4 *Suppose that Hypotheses 5.1 are valid. Let $\{\tilde{s}(0)\} \in \mathcal{H}$. Suppose that a continuous solution $x \mapsto \{s(x)\} \in \mathcal{H}$ of the differential system (57) exists and satisfies $\{s(0)\} = \{\tilde{s}(0)\}$. Then the solution is unique.*

Proof. We adapt to the Schrödinger case the proof in [16]. See also [4]. We will prove the uniqueness of a solution $x \mapsto \{\theta(x)\}$ satisfying the initial condition $\{\theta(0)\}$ which is due to the change of variable. This in turn will imply the uniqueness of a

solution $x \mapsto \{s(x)\}$. Suppose that $\{\theta(x)\}$ and $\{\rho(x)\}$ solve the system (58) with the same initial condition $\{\theta(0)\}$. We have

$$\begin{aligned}
& \sqrt{d_r} |F_r(\{\theta(x)\}) - F_r(\{\rho(x)\})| \leq \\
& \leq \sum_{k \in \mathbb{N}} \sqrt{d_r} \sup_{\{X\} \in \mathcal{I}} \left| \frac{\partial \tilde{F}_r(\{X\})}{\partial \theta_k} \right| |\theta_k(x) - \rho_k(x)| \leq \\
& \leq \sum_{k \in \mathbb{N}} \frac{\sqrt{d_r}}{\sqrt{d_k}} \sup_{\{X\} \in \mathcal{I}} \left| \frac{\partial \tilde{F}_r(\{X\})}{\partial \theta_k} \right| |\theta_k(x) - \rho_k(x)| \sqrt{d_k} \leq \\
& \leq \sum_{k \in \mathbb{N}} \frac{\sqrt{d_r}}{\sqrt{d_k}} \sup_{\{X\} \in \mathcal{I}} \left| \frac{\partial \tilde{F}_r(\{X\})}{\partial \theta_k} \right| \|\{\theta(x)\} - \{\rho(x)\}\|_{\mathcal{I}}
\end{aligned} \tag{61}$$

Now we divide the remaining sum into two terms, namely

$$\begin{aligned}
& \sum_{r \neq k \in \mathbb{N}} \frac{\sqrt{d_r}}{\sqrt{d_k}} \sup_{\{X\} \in \mathcal{I}} \left| \frac{\partial \tilde{F}_r(\{X\})}{\partial \theta_k} \right| \leq \\
& \leq 2 \sup_{\{X\} \in \mathcal{I}} |\sqrt{d_r} \tilde{F}_r(\{X\})| \sum_{r \neq k \in \mathbb{N}} \left| \frac{\sqrt{d_k}}{h_{0k}} + \frac{\sqrt{d_k}}{h_{jk}} \right| \leq \\
& \leq 2D_1 \sup_{\{X\} \in \mathcal{I}} |\sqrt{d_r} \tilde{F}_j(\{X\})|
\end{aligned} \tag{62}$$

and

$$\begin{aligned}
& \sup_{\{X\} \in \mathcal{I}} \left| \frac{\partial \tilde{F}_r(\{X\})}{\partial \theta_r} \right| \leq \sup_{\{X\} \in \mathcal{I}} \left| 2d_r \tilde{F}_r(\{X\}) \right| \left| \frac{1}{\lambda_{2r-1}} + \frac{1}{2h_{0r}} + \right. \\
& \left. + \frac{1}{2} \sum_{r \neq s \in \mathbb{N}} \left(\frac{1}{(X_r - \lambda_{2s})} + \frac{1}{(X_r - \lambda_{2s-1})} - \frac{2}{(X_r - X_s)} \right) \right| \leq \\
& \leq 2 \sup_{\{X\} \in \mathcal{I}} |\sqrt{d_r} \tilde{F}_r(\{X\})| \left| \frac{\sqrt{d_r}}{h_{0r}} + \frac{\sqrt{d_r}}{2h_{0r}} + \frac{\sqrt{d_r}}{2} \sum_{r \neq s \in \mathbb{R}} \frac{d_s}{h_{rs}^2} \right| \leq \\
& \leq \sup_{\{X\} \in \mathcal{I}} |2\sqrt{d_r} \tilde{F}_r(\{X\})| (2D_1 + \sqrt{D}D_1^2),
\end{aligned} \tag{63}$$

where we used the estimates of Proposition 5.3. From equations (62) and (63) it is easily seen that

$$\begin{aligned}
& \sup_{r \in \mathbb{N}} |F_r(\{\theta(x)\}) - F_r(\{\rho(x)\})| \sqrt{d_r} \leq \\
& \leq D_2 (2D_1 + \sqrt{D}D_1^2) \|\{\theta\} - \{\rho\}\|_{\mathcal{I}} \leq \\
& \leq C \|\{\theta\} - \{\rho\}\|_{\mathcal{I}}.
\end{aligned} \tag{64}$$

Now consider the map $U : x \mapsto \|\{\theta(x)\} - \{\rho(x)\}\|_{\mathcal{I}}$. Then $U(x)$ is a continuous function on \mathbb{R} because $|U(x)| \leq D^{3/2}$ and $\sqrt{d_r} \rightarrow 0$ as $r \rightarrow \infty$. Using (64), we have

$$U(x) \leq \int_0^x \sup_{r \in \mathbb{N}} \sqrt{d_r} |F_r(\{\theta(s)\}) - F_r(\{\rho(s)\})| ds \leq C \int_0^x U(s) ds.$$

Using standard arguments, we have $U(x) \equiv \text{const}$, and $U(0) = 0$ implies that $\theta_r(x) = \rho_r(x)$ ($x \in \mathbb{R}$, $r \in \mathbb{N}$). This completes the proof of Theorem 5.4. ■

Now we turn to the question of the existence of a solution for the system (57) (or, equivalently, for the system (58)). We sketch the proof of this fact. For a detailed proof, the interested reader can be addressed to [16], where the more general case of the Sturm-Liouville operator is discussed. The proof of the existence of a

solution for (57) is carried out by a so-called “algebro-geometric approximation”. We explain this in a little bit more detail. Fix $n \in \mathbb{N}$. Let us consider the set $\Sigma_n = [\lambda_0, \lambda_1] \cup \dots \cup [\lambda_{2n}, \infty)$. There exists an algebro-geometric Schrödinger potential $q_n(x)$ such that the spectrum of the operator

$$L_n := -\frac{d^2}{dx^2} + q_n(x)$$

equals the set Σ_n (see [14, 15, 16] and the discussion in Section 2). For every fixed choice of initial data $(P_1^{(n)}(0), \dots, P_n^{(n)}(0)) \in I_1 \times \dots \times I_n$, there holds the trace formula (8)

$$q_n(x) = \lambda_0 + \left(\sum_{i=1}^n \lambda_{2i} + \lambda_{2i-1} - 2P_i^{(n)}(x) \right).$$

The functions $P_1^{(n)}(x), \dots, P_n^{(n)}(x)$ are determined as the solution of the differential system (6)

$$P_{j,x}^{(n)}(x) = F_j^{(n)}(P_1^{(n)}(x), \dots, P_n^{(n)}(x)) = \frac{-2k_n(P_j^{(n)}(x))}{\prod_{k \neq j} (P_j^{(n)}(x) - P_k^{(n)}(x))},$$

where $k_n(\lambda) = \sqrt{-\prod_{i=0}^{2n} (\lambda - \lambda_i)}$.

Now, fix $k \in \mathbb{N}$: as n runs over \mathbb{N} , one has a sequence $\{P_k^{(n)}(x)\}_n$. We use the Ascoli-Arzelà theorem to show that there is a subsequence of $\{P_k^{(n)}(x)\}_n$ (which we still denote in the same way) which converges uniformly on compact subsets of \mathbb{R} to $s_k(x)$. Moreover, the same holds for the sequence of the derivatives $\{P_{k,x}^{(n)}(x)\}_n$, i.e., such a sequence has a subsequence which converges uniformly on compact subsets of \mathbb{R} . Putting these information together, we observe that the limits $\lim_{n \rightarrow \infty} P_k^{(n)}(x) = s_k(x)$ ($k \in \mathbb{N}$) provide a solution for the system (57) (see again [16]). Again, one can show that the resulting set $\{s_k(x)\}$ equals the set $\{P_k(x)\}$ of the zeros of the diagonal Green function $G(\lambda)$ corresponding to the Schrödinger equation whose potential is given by

$$q(x) = \lim_{n \rightarrow \infty} q_n(x) = \lambda_0 + \sum_{k=1}^{\infty} (\lambda_{2k} + \lambda_{2k-1} - 2P_k(x)). \quad (65)$$

Note that the right-hand side of (65) converges (use Hypothesis 5.1). The potential $q(x)$ defined in (65) is reflectionless and its spectrum has the form

$$\Sigma = \bigcap_{n \in \mathbb{N}} \Sigma_n.$$

See the discussion in Section 2 and Proposition 2.3.

At this point, an observation falls naturally. It is known (see [13]) that if a sequence of Schrödinger potentials $\{q_n(x)\}$ converges on compact subsets to a potential $q(x)$, then the sequence consisting of the Weyl m functions $\{m_{\pm}^{(n)}(\lambda)\}$ (associated to the potential $q_n(x)$) converges to the Weyl m functions $m_{\pm}(\lambda)$ (associated to the potential $q(x)$) uniformly on compact subsets of \mathbb{C}^+ and \mathbb{C}^- . This follows from the Weyl’s decreasing-disc characterization of the functions m_{\pm} (see,

for instance [3]). An interesting consequence of this fact concerns the quantity $\frac{1}{\sqrt{\lambda_0}} \prod_{i=1}^{\infty} \frac{s_i(x)}{\sqrt{\lambda_{2i-1}\lambda_{2i}}}$. Writing $[m_+ - m_-](x, \lambda) = \frac{2k_{\infty}(\lambda)}{U}$, one observes that

$$[m_+ - m_-](x, 0) = \mathcal{M}(x) = \frac{2k_{\infty}(0)}{\prod_{i \in \mathbb{N}} s_i(x)}. \quad (66)$$

In general, the quantity in (66) is hidden in the relations of the Dubrovin flow (57). One of the interesting consequences of the results in [14, 16] is that, in the Schrödinger case, such a quantity does not appear in the Dubrovin equations because it acts in such a way that the triple $(1, q, y) \in \mathcal{E}_3(\mathbb{R})$ resulting from the inverse construction has $y \equiv 1$, that is, $\mathcal{M}(x)$ is invisible in the Schrödinger case because one must have $y \equiv 1$. This interesting fact allows us to make some comments on the existence of reflectionless Schrödinger potentials when the spectral gaps satisfy the hypotheses of Craig [4]. This is not, however, the suitable place where to discuss this matter: we only argue that Craig's hypotheses are not sufficient to guarantee the existence of a corresponding Schrödinger potential because the quantity in (66) need not be the uniform limit on compact subsets of \mathbb{C}^+ and \mathbb{C}^- of the sequence $\{\mathcal{M}_n(x)\} := \{m_+^{(n)} - m_-^{(n)}\}$ (see [16] for details on the inverse Sturm-Liouville problem and further observation concerning these facts).

Once we have proved the existence and the uniqueness of a solution of (57), we have uniquely determined the existence of the entire function $U(x, \lambda)$ defined as in (56). The next step is to prove that actually the function $U(x, \lambda)$ is the normal limit on the unit λ -circle of a sequence of polynomials $U_n(x, \lambda)$ whose roots are exactly the poles $P_j^{(n)}(x)$ ($j = 1, \dots, n$, $n \in \mathbb{N}$). To this aim, let us define

$$U_n(x, \lambda) = \frac{1}{k_n(0)} \prod_{i=1}^n (P_i^{(n)}(x) - \lambda).$$

Let \mathbb{D} denote the unit disc. We show that $\{U_n(x, \lambda)\}_n$ is a normal family (and it converges to $U(x, \lambda)$ in \mathbb{D}).

This is a simple computation: set $\mathcal{S}_n(x) = (P_1^{(n)}(x), \dots, P_n^{(n)}(x))$. We have

$$U_n(x, \lambda) = \frac{(-1)^n}{k_n(0)} \left(\sum_{i=0}^n \varsigma_i(\mathcal{S}_n(x)) \lambda^{n-i} \right),$$

and it follows easily that

$$\frac{|\varsigma_i(\mathcal{S}_n(x))|}{k_n(0)} \leq \begin{cases} \sum_{j \in \mathbb{N}} \frac{1}{h_{0j}} \prod_{k \in \mathbb{N}} \left(1 + \frac{d_k}{h_{0k}} \right), & i \neq n \\ \prod_{k \in \mathbb{N}} \left(1 + \frac{d_k}{h_{0k}} \right), & i = n \end{cases}.$$

This shows that the polynomials $U_n(x, \lambda)$ are equi-bounded in every compact subset of \mathbb{D} , and hence the family $\{U_n(x, \lambda)\}_n$ is normal in \mathbb{D} . We use now Montel's theorem to show that $U(x, \lambda)$ is the normal limit in \mathbb{D} of a subsequence of $\{U_n(x, \lambda)\}_n$.

We now claim that for every $i \in \mathbb{N}$, the sequence $\{\varsigma_i(\mathcal{S}_n(x))\}_n$ converges to the coefficients $u_i(x)$ of the Taylor series (54) ($i \in \mathbb{N}$) uniformly on compact subsets of \mathbb{R} . The equiboundedness of the sequences $\{\varsigma_i(\mathcal{S}_n(x))\}_n$ ($i \in \mathbb{N}$) has been shown

just above. To prove the equicontinuity, we consider the sequences $\left\{ \frac{d}{dx} \varsigma_i(\mathcal{S}_n(x)) \right\}_n$ ($i \in \mathbb{N}$): for every $i \in \mathbb{N}$, we have

$$\begin{aligned} \left| \frac{d}{dx} \varsigma_i(\mathcal{S}_n(x)) \right| &\leq \sum_{j \in \mathbb{N}} \frac{1}{h_{0j}} \sup_{\{X\} \in \mathcal{I}} |F_j(\{X\})| \frac{|\sigma_{i-1}^{(j)}(\mathcal{S}_n(x)) P_j(x)|}{k_n(0)} \leq \\ &\leq C \sum_{j \in \mathbb{N}} \frac{1}{h_{0j}} \frac{2|\varsigma_i(\mathcal{S}_n(x))|}{k_n(0)}. \end{aligned}$$

This shows that for every $i \in \mathbb{N}$, the sequence $\left\{ \frac{d}{dx} \varsigma_i(\mathcal{S}_n(x)) \right\}_n$ is equibounded on compact subsets of \mathbb{R} , and this in turn implies that the sequence $\{\varsigma_i(\mathcal{S}_n(x))\}_n$ is equicontinuous on compact subsets of \mathbb{R} . The claim is now proved by applying the Ascoli-Arzelà theorem and the fact that the sequence $\{U_n\}$ converges to U uniformly on compact subsets of \mathbb{D} . The same result can be proved for the sequences of the derivatives of the coefficients $u_i(x)$ of Taylor expansion at $\lambda = 0$ of the entire function $U(x, \lambda)$, that is, for every $i \in \mathbb{N}$, the sequence (or, if necessary, a subsequence of) $\{\varsigma_{i,x}(\mathcal{S}_n(x))\}_n$ converges to the coefficient $u_{i,x}(x)$ uniformly on compact subsets of \mathbb{R} .

Now, to each matrix $B_n(x, \lambda) = \begin{pmatrix} -U_{n,x}/2 & U \\ (1-\lambda)V_n & U_{n,x} \end{pmatrix}$ ($n \in \mathbb{N}$) there corresponds a stationary K-dV hierarchy analogous to that discussed in the previous section: the limit matrix $B = \begin{pmatrix} -U_x/2 & U \\ (1-\lambda)V & U_x/2 \end{pmatrix}$ (in each compact subset of \mathbb{D}) solves the corresponding infinite order K-dV hierarchy. Note now that the finite-gap potentials $q_n(x) = \lambda_0 + \left(\sum_{i=1}^n \lambda_{2i} + \lambda_{2i-1} - 2P_i^{(n)}(x) \right)$ converge to $q(x) = \lambda_0 + \left(\sum_{i \in \mathbb{N}} \lambda_{2i} + \lambda_{2i-1} - 2P_i(x) \right)$ uniformly on compact subsets of \mathbb{R} . Such $q(x)$ is a reflectionless Schrödinger potential and together with the entire functions (uniquely) determined by the above procedure solves the stationary infinite order K-dV hierarchy. It follows that $q(x)$ is the solution of the infinite order K-dV equation

$$u_{0,xxx}(x) - 4q(x)u_{0,x}(x) - 2q_x(x)u_0(x) = 0.$$

We summarize these results in the following

Theorem 5.5 *Let $\{P_i(x)\}$ denote the unique solution of the system (57) satisfying the initial condition $\{P_i(0)\}$. Then the function*

$$q(x) = \lambda_0 + \left(\sum_{i \in \mathbb{N}} \lambda_{2i} + \lambda_{2i-1} - 2P_i(x) \right)$$

is the uniform limit on compact subsets of \mathbb{R} of a sequence of finite gap potentials. Moreover, $q(x)$ solves the infinite order K-dV hierarchy and hence provides the solution of the infinite order stationary K-dV equation.

As before, we now introduce a time dependent hierarchy of equations. Let $B_r(x, t, \lambda)$ be as in the previous section. Let us assume that now the matrix B of the stationary hierarchy depends on $t \in \mathbb{R}$ in such a way that the zero-curvature conditions (31), (27) and the relation (32) are valid. Recall that $U_r(x, t, \lambda)$ is a complex polynomial of degree r in λ whose coefficients depend on $(x, t) \in \mathbb{R}^2$. All the relations (37), (40)–(42) retain validity because they depend only on the matrix

formulation of our problem. The differential systems expressing the (x, t) -motion of the roots $s_i(x, t)$ ($i \in \mathbb{N}$) of the polynomial $U(x, t)$ translate to

$$s_{j,x}(x, t) = \frac{2 \sqrt{\prod_{i=0}^{\infty} (s_j(x, t) - \lambda_i)}}{\prod_{r \neq j} (s_r(x, t) - s_j(x, t))}, \quad (j \in \mathbb{N}). \quad (67)$$

and

$$\begin{aligned} s_{j,t}(x, t) &= - \frac{2k_{\infty}(s_j(x, t))}{\prod_{r \neq j} (s_r(x, t) - s_j(x, t))} U_r(s_j(x, t)) = \\ &= U_r(s_j(x, t)) s_{j,x}(x, t), \quad (j \in \mathbb{N}) \end{aligned} \quad (68)$$

We already know that for every fixed initial condition $\{s_i(x, t_0)\}$ a unique solution of (67) exists. Now we will prove the same for the system (68). First of all, we need a suitable expression for the polynomials U_r . To this aim, let fix $r \in \mathbb{N}$, and let us define

$$\tilde{U}_r^{(n)}(x, t, \lambda) = \frac{1}{k_n(0)} \left(\sum_{i=1}^r s_i(\mathcal{S}_n(x, t)) \lambda^{r-i} \right), \quad n \geq r,$$

where $\mathcal{S}_n(x, t) = (s_1^{(n)}(x, t), \dots, s_n^{(n)}(x, t))$ are the roots of the polynomial $U_n(x, t)$ corresponding to the n -th order K-dV hierarchy discussed in the previous section. It is easy to show that for every fixed $r \in \mathbb{N}$, $\{\tilde{U}_r^{(n)}(x, t, \lambda)\}_n$ is a normal family in \mathbb{D} (use the same methods as before) and converges to $U_r(x, t, \lambda)$ uniformly on compact subsets of \mathbb{D} . Up to the factor $1/k_n(0)$ the polynomials $\tilde{U}_r^{(n)}(x, t, \lambda)$ solve the time-dependent n -th order K-dV hierarchies for every $n \in \mathbb{N}$. Let us assume for the moment that a solution of the system (68) exists: arguing as before, we see that the matrix

$$B_r = \begin{pmatrix} -U_{r,x}/2 & U_r \\ (1-\lambda)V_r & U_{r,x} \end{pmatrix}$$

where U_r is the limit function above and V_r is determined by the recursion formulas solves r -th order K-dV hierarchy when the initial data is the solution of the infinite order stationary K-dV equation. We have determined a solution of our problem: in fact, once the motion $(x, t) \mapsto s_i(x, t)$ ($i \in \mathbb{N}$) is determined, the function

$$q(x, t) = \lambda_0 + \left(\sum_{i \in \mathbb{N}} \lambda_{2i-1} + \lambda_{2i} - 2s_i(x, t) \right)$$

is well defined. Moreover, it turns out that for every $t \in \mathbb{R}$, the map $x \mapsto q(x, t)$ is a reflectionless Schrödinger potential whose spectrum Σ equals the set $\mathbb{R} \setminus \bigcup_{k \in \mathbb{N}} \overset{\circ}{I}_k$.

It remains to show the existence of a solution of the system (68). This is, however, quite simple. We can use methods similar to those used in the proof of Theorem 5.4 to prove uniqueness (use the fact that the quantities $U_r(s_j(x, t))$ are bounded on all \mathbb{R} for every $j \in \mathbb{N}$, uniformly with respect to $r \in \mathbb{N}$), then we use methods similar to those in [16] to prove that for every $j \in \mathbb{N}$ the sequences $\{s_j^{(n)}(x, t)\}$ and $\{s_{j,t}^{(n)}(x, t)\}$ converge uniformly on compact subsets of \mathbb{R} as $n \rightarrow \infty$. This is sufficient to guarantee the existence of a solution of the system (68). We have found the solution of the r -th order K-dV equation when the initial data satisfies the infinite order stationary K-dV equation ($r \in \mathbb{N}$). Write t_r instead of t to put in evidence the order of the solution of the K-dV equation. We summarize what we have obtained as follows:

Theorem 5.6 *for every $r \in \mathbb{N}$, the solution of the r -th order K-dV equation having as initial condition the solution of the infinite order stationary K-dV equation, can be written as*

$$q(x, t_r) = \lambda_0 + \left(\sum_{i \in \mathbb{N}} \lambda_{2i-1} + \lambda_{2i} - 2s_i(x, t_r) \right).$$

The functions $s_j(x, t_r)$ are completely determined as the solution of the systems (57) and (68). Moreover, for every fixed $t_r \in \mathbb{R}$, the set $\{s_j(x, t_r)\}$ equals the set $\{P_j(x, t_r)\}$ of the zeros of the diagonal Green function $G(x, t_r, \lambda)$ associated to the Schrödinger equation

$$-\frac{d^2}{dx^2} \varphi + q(x, t_r) \varphi = \lambda \varphi.$$

For every fixed $t_r \in \mathbb{R}$, the map $x \mapsto q(x, t_r)$ is a reflectionless Schrödinger potential whose spectrum Σ equals the set $\mathbb{R} \setminus \left((-\infty, \lambda_0) \bigcup_{k=1}^{\infty} \overset{\circ}{I}_k \right)$, and hence the family of Schrödinger potentials $\{x \mapsto q(x, t_r) \mid t_r \in \mathbb{R}\}$ lies in the same isospectral class.

We finish this section by observing that our class of solutions extends those found by Levitan [20, 21], Egorova [6] and Marchenko [22]. Moreover, we are able to find an explicit solution for the K-dV equation of any arbitrary order $r \in \mathbb{N}$. We will not pause here to discuss the almost-periodicity of the solution $q(x, t_r)$ of the r -th order K-dV equation. For every $t_r \in \mathbb{R}$ the almost-periodicity with respect to x can be proved, however, by using a beautiful result appearing in [29] and [10]: in particular, in those papers it is proved that the homogeneity of the spectrum of the Schrödinger operator implies the almost-periodicity with respect to x of the map $x \mapsto q(x, t_r)$ for every $t_r \in \mathbb{R}$. It remains to answer the questions if the motion is t_r -almost periodic (for every $x \in \mathbb{R}$ and for every r) and if so, if the almost periodicity with respect to x and t_r is uniform for every $r \in \mathbb{R}$. We plan to answer these questions in another place.

References

- [1] M. Alber, Y. Fedorov, *Algebraic geometrical solutions for certain evolution equations and Hamiltonian flows on nonlinear subvarieties of generalized Jacobians*, Inverse Problems **17** (2001), 1017–1042.
- [2] M. Alber, Y. Fedorov, *Wave solutions of evolution equations and Hamiltonian flows on nonlinear subvarieties of generalized Jacobians*, J. Phys. A: Math. Gen **33** (2000), 8409–8425.
- [3] E. Coddington, N. Levinson, *Theory of Ordinary Differential Equations*, McGraw-Hill, 1955.
- [4] W. Craig, *The trace formula for Schrödinger operators on the line*, Comm. Math. Phys. **126** (1989), 379–407.
- [5] B. Dubrovin, V. Matveev, S. Novikov, *Nonlinear equations of Korteweg-de Vries type, finite-zone linear operators and Abelian varieties*, Russian Math. Surveys **31** (1976), 59–146.
- [6] I. Egorova, *The Cauchy problem for the KdV equation with almost periodic initial data whose spectrum is nowhere dense*, in Spectral Operator Theory and Related Topics, Vol **19**, 181–208, Adv. Soviet Math., Amer. Math. Soc., Providence USA, 1994.

- [7] R. Fabbri, R. Johnson, L. Zampogni, *Nonautonomous differential systems in two dimensions*, to appear in Handbook of Differential Equations: Ordinary Differential Equations, Vol. 4, F. Battelli/M. Fečkan eds., Elsevier, Amsterdam, 2008.
- [8] Gardner, C., Greene, J., Kruskal, M. and Miura, R., *Methods for Solving the Korteweg-de Vries Equation*, Phys. Rev. Letters, **19** (1967), 1095–1097.
- [9] F. Gesztesy, H. Holden, *Algebro-geometric solutions of the Camassa-Holm hierarchy*, Rev. Math. Iberoamericana **19** (2003), 73–142.
- [10] F. Gesztesy, P. Yuditskii, *Spectral properties of a class of reflectionless Schrödinger operators*, Jour. Func. Anal. **241** (2006), 486–527.
- [11] S. Kotani, *Construction of K-dV flow on generalized reflectionless potentials*, preprint, Osaka Univ., 2003.
- [12] R. Johnson, *On the Sato-Segal-Wilson solutions of the K-dV equation*, Pac. Jour. Math. **132** (1988), 343–355.
- [13] R. Johnson, J. Moser, *The rotation number for almost periodic potentials*, Comm. Math. Phys. **84** (1982), 403–438; correction in Comm. Math. Phys. **90** (1983), 317–318.
- [14] R. Johnson, L. Zampogni, *On the inverse Sturm-Liouville problem*, Discr. Cont. Dyn. Sys. **18** (2007), 405–428.
- [15] R. Johnson, L. Zampogni, *Description of the algebro-geometric Sturm-Liouville coefficients*, Jour. Diff. Eqns. **244** (2008), 716–740.
- [16] R. Johnson, L. Zampogni, *Some remarks concerning reflectionless Sturm-Liouville potentials*, to appear on Stochastic and Dynamics.
- [17] P. Lax, *Integrals of nonlinear equations of evolution and solitary waves*, Comm. Pure Appl. Math. **21** (1968), 467–490.
- [18] P. Lax, *Periodic solutions of the KdV equation*, Comm. Pure Appl. Math. **28** (1975), 141–188.
- [19] P. Lax, *Almost periodic solutions of the KdV equation*, Siam Review **18** (1976), 351–375.
- [20] B. Levitan, *Almost periodicity of infinite-zone potentials*, Math. USSR Izvestija **18** (1982), 249–273.
- [21] B. Levitan, *Approximation of infinite-zone potentials by finite-zone potentials*, Math. USSR Izvestija **20** (1983), 55–87.
- [22] V. A. Marchenko, I. V. Ostrovsky, *Approximation of periodic by finite-zone potentials*, Selecta Mathematica Sovietica **6** (1987), 101–136.
- [23] H. McKean, E. Trubowitz, *Hill's operator and hyperelliptic function theory in the presence of infinitely many branch points*, Comm. Pure Appl. Math. **29** (1976), 143–226.
- [24] D. Mumford, *Tata Lectures on Theta* Vol. 1,2,3, Birkhäuser, 1983.
- [25] S. Novikov, *A periodic problem for the Korteweg-de Vries equation. I*, Functional Anal. Appl. **8** (1974).

- [26] M. Sato, *Soliton equations as dynamical systems on infinite-dimensional Grassmann manifold*, Publ. Res. Inst. Math. Sci., Kokyuroku, **439** (1982), 30.
- [27] G. Segal, G. Wilson, *Loop groups and equations of K-dV type*, Publ. IHES **61** (1985), 5–65.
- [28] C. L. Siegel, *Topics in Complex Function Theory* Vol. 1,2,3, Wiley-Interscience, 1969.
- [29] M. Sodin, P. Yuditskii, *Almost periodic Jacobi matrices with homogeneous spectrum, infinite-dimensional Jacobi inversion, and Hardy spaces of character-automorphic functions*, J. Geom. Anal **7** (1997), 387–435.
- [30] L. Zampogni, *On algebro-geometric solutions of the Camassa-Holm hierarchy*, Adv. Nonlin. Studies **7** (2007), 345–380.

Topological Sequence Entropy of Operators on Function Spaces*

Gengrong Zhang^{1†} Fanping Zeng², and Kesong Yan²

1. Institute of Mathematics, Guangxi University, Nanning, 530004, China

2. Department of Mathematics, Liuzhou Teachers College, Liuzhou, 545004, China

Abstract

We study sequence entropy of actions on function spaces with the focus on Markov operators on Compact spaces. We defined the natural definition of topological sequence entropy for Markov operators on $C(X)$. Firstly, we prove that the three are equal. Secondly, It is proved that $h_A(T) = h_A(S)$ If $Tf = f \circ S$ is an operate generated by a continuous map: $S : X \rightarrow X$ and A is an increasing integer sequence. Finally, It is proved that If for every continuous f there exists an invariant function φ_f such that $\lim_{n \rightarrow \infty} \sup_{x \in X} |T^n f(x) - \varphi_f(x)| = 0$ then $h_A(T) = 0$ for every increasing integer sequence A .

Keyword: k -Warsaw circle; Pointwise recurrent; Equicontinuity;

AMS(2000) Subject Classification: 58F10, 54H20

1 Introduction

Let $C_1(X)$ denote the set of all continuous functions $f : X \rightarrow [0, 1]$. In this paper, X is a compact Hausdorff space and T denotes a Markov operators actin on $C(X)$.

For a continuous f let us define

$$U_{<f}^\varepsilon = \{(x, t) \in X \times [0, 1] : t < f(x) + \varepsilon\}.$$

$$U_{>f}^\varepsilon = \{(x, t) \in X \times [0, 1] : t > f(x) + \varepsilon\}.$$

$$U_f^\varepsilon = U_{<f}^\varepsilon \cap U_{>f}^\varepsilon.$$

Given a finite collection $\mathcal{F} \subset C_1(X)$ we obtain a finite open cover of $X \times [0, 1]$ by the formula

$$\mathcal{U}_{\mathcal{F}}^\varepsilon = \bigvee_{f \in \mathcal{F}} \mathcal{U}_f^\varepsilon$$

If \mathcal{V} is a finite open cover of the unit interval then we let

$$\mathcal{F}^{-1}\mathcal{V} = \bigvee_{f \in \mathcal{F}} f^{-1}(\mathcal{V}).$$

*Project supported by NSFC(10661001), NSF of Guangxi (0649002), NSF of Guangdong(7301276) and NSF of Guangxi University(X061022)

[†]zgr.keyan@yahoo.com.cn; zgrzaw@gxu.edu.cn

If $Tf = f \circ S$, where $S : X \rightarrow X$ is a continuous transformation and $A = \{0 = a_0 < a_1 < a_2 < \dots\}$ is a integer sequence, we denote $\mathcal{F}_A^n = \bigcup_{k=0}^{n-1} T^{a_k} f$.

It is easy to prove the following Lemma 1, in which (i) and (ii) can be found in [2].

Lemma 1 *Let \mathcal{F}, \mathcal{G} be finite subsets of $C_1(X)$, \mathcal{V} a finite open cover of the unit interval and ε a positive number. Then*

- (i) $\mathcal{U}_{\mathcal{F} \cup \mathcal{G}}^\varepsilon = \mathcal{U}_{\mathcal{F}}^\varepsilon \vee \mathcal{U}_{\mathcal{G}}^\varepsilon$
- (ii) $(\mathcal{F} \cup \mathcal{G})^{-1}(\mathcal{V}) = \mathcal{F}^{-1}(\mathcal{V}) \vee \mathcal{G}^{-1}(\mathcal{V})$; (iii) if $Tf = f \circ S$, where $S : X \rightarrow X$ is a continuous transformation then $\mathcal{U}_{\mathcal{F}_A^n}^\varepsilon = \bigvee_{i=0}^{n-1} (S \times Id)^{-a_i}(\mathcal{U}_{\mathcal{F}}^\varepsilon)$ and $(\mathcal{F}_A^n)^{-1}(\mathcal{V}) = \bigvee_{i=0}^{n-1} S^{-a_i}(\mathcal{F}^{-1}(\mathcal{V}))$.

Recall that, for any open cover \mathcal{U} , the symbol $N(\mathcal{U})$ denotes the minimal cardinality of a subcover chosen from \mathcal{U} .

Definition 1 Let $\mathcal{F} \subset C_1(X)$ be a finite collection of functions, $A = \{0 = a_0 < a_1 < a_2 < \dots\}$ be a integer sequence and $\varepsilon > 0$. We define

- (i) $H_1(\mathcal{F}, \varepsilon) = \log N(\mathcal{U}_{\mathcal{F}}^\varepsilon)$,
- (ii) $h_1(T, \mathcal{F}, A, \varepsilon) = \limsup_{n \rightarrow \infty} \frac{1}{n} H_1(\mathcal{F}_A^n, \varepsilon)$,
- (iii) $h_1(T, A) = \sup_{\mathcal{F}} \sup_{\varepsilon} h_1(T, \mathcal{F}, A, \varepsilon)$.

Definition 2 Let $\mathcal{F} \subset C_1(X)$ be a finite collection of functions, $A = \{0 = a_0 < a_1 < a_2 < \dots\}$ be a integer sequence and \mathcal{V} be a cover of interval $[0, 1]$. We define

- (i) $H_2(\mathcal{F}, \mathcal{V}) = \log N(\mathcal{F}^{-1}\mathcal{V})$,
- (ii) $h_2(T, \mathcal{F}, A, \mathcal{V}) = \limsup_{n \rightarrow \infty} \frac{1}{n} H_2(\mathcal{F}_A^n, \mathcal{V})$,
- (iii) $h_2(T, A) = \sup_{\mathcal{F}} \sup_{\mathcal{V}} h_2(T, \mathcal{F}, A, \mathcal{V})$.

Let $d_{\mathcal{F}}$ and $s(d_{\mathcal{F}}, \varepsilon)$ be the same as in [Tomasz]

Definition 3 Let $\mathcal{F} \subset C_1(X)$ be a finite collection of functions, $A = \{0 = a_0 < a_1 < a_2 < \dots\}$ be a integer sequence and $\varepsilon > 0$. We define

- (i) $H_3(\mathcal{F}, \varepsilon) = \log s(d_{\mathcal{F}}, \varepsilon)$,
- (ii) $h_3(T, \mathcal{F}, A, \varepsilon) = \limsup_{n \rightarrow \infty} \frac{1}{n} H_3(\mathcal{F}_A^n, \varepsilon)$,
- (iii) $h_3(T, A) = \sup_{\mathcal{F}} \sup_{\varepsilon} h_3(T, \mathcal{F}, A, \varepsilon)$.

In [2], the authors proved the following Theorems A and B:

Theorem A *For every Markov operate T holds $h_1(T) = h_2(T) = h_3(T)$.*

Theorem B *If $Tf = f \circ S$ is an operate generated by a continuous map: $S : X \rightarrow X$, then $h_1(T)$ is equal to the classic topological entropy of S .*

In this paper, we defined the topological sequence entropy of a Markov operator T and proved the following Theorems 1, 2 and 3:

Theorem 1 *For every Markov operate T and integer sequence $A = \{0 = a_0 < a_1 < a_2 < \dots\}$ hold $h_1(T, A) = h_2(T, A) = h_3(T, A)$.*

Theorem 2 If $Tf = f \circ S$ is an operate generated by a continuous map: $S : X \rightarrow X$ and $A = \{0 = a_0 < a_1 < a_2 < \dots\}$ is a integer sequence, then $h_A(T)$ is equal to the classic topological entropy $h_A(S)$ of S .

Theorem 3. If for every continuous f there exists an invariant function φ_f such that $\lim_{n \rightarrow \infty} \sup_{x \in X} |T^n f(x) - \varphi_f(x)| = 0$ then $h_A(T) = 0$ for every integer sequence $A = \{0 = a_0 < a_1 < a_2 < \dots\}$.

2 Proofs of Theorems 1, 2 and 3

Theorem 1 For every Markov operate T and integer sequence $A = \{0 = a_0 < a_1 < a_2 < \dots\}$ hold $h_1(T, A) = h_2(T, A) = h_3(T, A)$.

Proof. Firstly, we prove that $h_1(T, A) \leq h_2(T, A)$. Choose $\varepsilon > 0$ and let \mathcal{V} be a finite open cover of interval $[0, 1]$ of sets with diameters not greater than ε . Let $\mathcal{W}_n^A = \{U \times V : U \in (\mathcal{F}_A^n)^{-1}(\mathcal{V}), v \in \mathcal{V}\}$.

For each $U \times V \in \mathcal{W}_n^A$, let $\mathcal{F}'_A = \{f \in \mathcal{F}_A^n : f(x) \geq \inf V \text{ for each } x \in U\}$. It is not difficult to see that $U \times V \subset \bigcap_{f \in \mathcal{F}'_A} U_{<f}^\varepsilon \cap \bigcap_{f \in \mathcal{F}_A^n - \mathcal{F}'_A} U_{>f}^\varepsilon \in \mathcal{U}_{\mathcal{F}_A^n}^\varepsilon$. It follows that \mathcal{W}_n^A is inscribed in $\mathcal{U}_{\mathcal{F}_A^n}^\varepsilon$. Thus, $N(\mathcal{U}_{\mathcal{F}_A^n}^\varepsilon) \leq N(\mathcal{W}_n^A) \leq N((\mathcal{F}_A^n)^{-1}(\mathcal{V})) \cdot N(\mathcal{V})$. Since $N(\mathcal{V})$ is independent of n . It follows that $h_1(T, \mathcal{F}, A, \varepsilon) \leq h_2(T, \mathcal{F}, A, \mathcal{V})$. Thus, $h_1(T, A) \leq h_2(T, A)$.

Secondly, we will prove that $h_2(T, A) \leq h_3(T, A)$. Let \mathcal{V} be a finite open cover of interval $[0, 1]$. Denote its Lebesgue number by δ and let E be a maximal $(d_{\mathcal{F}_A^n}, \varepsilon)$ -separated set in X . It follows from the maximality of E that the collection $\{B(x, \frac{\delta}{2}) : x \in E\}$ of balls constitutes a finite open cover of X . For every $f \in \mathcal{F}_A^n$ and $x \in E$, the interval $(f(x) - \frac{\delta}{2}, f(x) + \frac{\delta}{2})$ is contained in some element $V(f, x)$ of \mathcal{V} . Hence $B(x, \frac{\delta}{2}) = \bigcup_{f \in \mathcal{F}_A^n} f^{-1}(f(x) - \frac{\delta}{2}, f(x) + \frac{\delta}{2}) \subset \bigcup_{f \in \mathcal{F}_A^n} f^{-1}(V(f, x)) \in (\mathcal{F}_A^n)^{-1}(\mathcal{V})$ and $N((\mathcal{F}_A^n)^{-1}(\mathcal{V})) \leq N\{B(x, \frac{\delta}{2}) : x \in E\} = N(E) = s(d_{\mathcal{F}_A^n}, \frac{\delta}{2})$. It follows that $h_2(T, A) \leq h_3(T, A)$.

Now we will show that $h_3(T, A) \leq h_1(T, A)$.

Let $D \subset X$ be a $(d_{\mathcal{F}}, \varepsilon)$ -separated set of maximal cardinality. Put $\gamma = \frac{\varepsilon}{6}$ and define $\tilde{\mathcal{F}} = \{\frac{1}{2}f + i\gamma : f \in \mathcal{F}, i \in \mathbf{Z}, 0 \leq i \leq \frac{1}{2\gamma}\}$. Then, by the proof of Theorem 4.2 in [2], we have $s(d_{\mathcal{F}}, \varepsilon) \leq N(\mathcal{U}_{\mathcal{F}}^\gamma)$. Recall that T , as a Markov operator, is linear and preserves constants. This implies that $\tilde{\mathcal{F}}_A^n = \tilde{\mathcal{F}}_A^n$. So we can replace \mathcal{F} with \mathcal{F}_A^n and obtain $s(d_{\mathcal{F}_A^n}, \varepsilon) \leq N(\mathcal{U}_{\mathcal{F}_A^n}^\gamma)$. $h_3(T, A) \leq h_1(T, A)$ holds by taking upper limits and suprema.

The proof of Theorem 1 is completed.

In the following we will use the symbol $h_A(T)$ to denote the common value of $h_1(T, A)$, $h_2(T, A)$ and $h_3(T, A)$.

Theorem 2 If $Tf = f \circ S$ is an operate generated by a continuous map: $S : X \rightarrow X$ and $A = \{0 = a_0 < a_1 < a_2 < \dots\}$ is a integer sequence, then $h_A(T)$ is equal to the classic topological entropy $h_A(S)$ of S .

Proof. Firstly, by Lemma 1(iii), we have $(\mathcal{F}_A^n)^{-1}(\mathcal{V}) = \bigvee_{i=0}^{n-1} S^{-a_i}(\mathcal{F}^{-1}(\mathcal{V}))$. Denote $\mathcal{B}_{\mathcal{V}} = \mathcal{F}^{-1}(\mathcal{V})$.

Then, $(\mathcal{F}_A^n)^{-1}(\mathcal{V}) = \bigvee_{i=0}^{n-1} S^{-a_i}(\mathcal{B})$. Therefore,

$$h_2(T, \mathcal{F}, A, \mathcal{V}) = \limsup_{n \rightarrow \infty} \frac{1}{n} H_2(\mathcal{F}_A^n, \mathcal{V}) = \limsup_{n \rightarrow \infty} \frac{1}{n} \log N((\mathcal{F}_A^n)^{-1} \mathcal{V}) = \limsup_{n \rightarrow \infty} \frac{1}{n} \log N(\mathcal{B}_\mathcal{V}).$$

It follows that

$$h_2(T, A) = \sup_{\mathcal{F}} \sup_{\mathcal{V}} \frac{1}{n} h_2(T, \mathcal{F}, A, \mathcal{V}) = \sup_{\mathcal{F}} \sup_{\mathcal{V}} \limsup_{n \rightarrow \infty} \frac{1}{n} \log N(\mathcal{B}_\mathcal{V}) = \sup_{\mathcal{V}} \limsup_{n \rightarrow \infty} \frac{1}{n} \log N(\mathcal{B}_\mathcal{V}) \leq h_A(S).$$

Let \mathcal{W} be a finite open cover of X . Choose a minimal subcover $\{W_1, W_2, \dots, W_r\} \subset \mathcal{W}$. Using the Tietze–Urysohn Theorem (see [4], Theorem 2.1.8), we can construct $\mathcal{F} = \{f_1, f_2, \dots, f_r\}$ consisting of continuous functions on X such that if $x \in W_i^c$ then $f_i(x) = 0$. Consequently, if $x \in \bigcap_{j \neq i} (W_j^c)$, i.e. x is covered exclusively by W_i , then $f_i(x) = 1$ ($i = 1, \dots, r$). Fix $0 < \varepsilon < \frac{1}{2r}$. Every member of $\mathcal{U}_{\mathcal{F}_A^n}^\varepsilon$ is of the form $\bigcap_{g \in \mathcal{F}_A^n} U_g = \bigcap_{k=0}^{n-1} \bigcap_{g \in T^{a_k} \mathcal{F}} U_g$, where $U_g \in \mathcal{U}_g^\varepsilon$. We will prove that each subcover \mathcal{U}' chosen from $\mathcal{U}_{\mathcal{F}_A^n}^\varepsilon$ determines a subcover of \mathcal{W}_A^n of the same or smaller cardinality, where $\mathcal{W}_A^n = \bigvee_{i=0}^{n-1} S^{-a_i}(\mathcal{W})$. Suppose that an element of \mathcal{U}' satisfies the following condition

$$\text{For each } k < n, \text{ there exists } g_k \in T^{a_k} \mathcal{F} \text{ such that } U_{g_k} = U_{<g_k}^\varepsilon \quad (1)$$

Denote by \widetilde{W}_k the element of $T^{-a_k} \mathcal{W}$ such that $g_k = 1$ on the set covered exclusively by \widetilde{W}_k and vanishes on \widetilde{W}_k . The set $\bigcap_{k=0}^{n-1} \widetilde{W}_k$ belongs to \mathcal{W}_A^n . Pick any $x \in X$. The point $(x, \frac{1}{2r})$ does not belong to $\bigcap_{g \in T^{a_k} \mathcal{F}} U_{>g}^\varepsilon$ for any $k = 0, 1, \dots, n-1$, since one can always find $g_k \in T^{a_k} \mathcal{F}$ such that $g_k(x) \geq \frac{1}{r}$. Thus,

if an element of \mathcal{U}' contains $(x, \frac{1}{2r})$, it satisfies the condition (1) and determines some set $\bigcap_{k=0}^{n-1} \widetilde{W}_k \in \mathcal{W}_A^n$.

This set contains x , because $g_k(x) \geq \frac{1}{r}$ for each $k = 0, 1, \dots, n-1$. Since x is arbitrary, the sets of form $\bigcap_{k=0}^{n-1} \widetilde{W}_k$ constitute a cover of X and hence $N(\mathcal{W}_A^n) \leq N((U)_{\mathcal{F}_A^n}^\varepsilon)$. It follows that

$$\begin{aligned} h_A(S) &= \sup_{\mathcal{W}} \limsup_{n \rightarrow \infty} \frac{1}{n} \log N(\mathcal{W}_A^n) \\ &\leq \sup_{\mathcal{W}} \limsup_{n \rightarrow \infty} \frac{1}{n} \log N((U)_{\mathcal{F}_A^n}^\varepsilon) = \sup_{\mathcal{W}} h_1(T, \mathcal{F}, A, \varepsilon) \\ &\leq \sup_{\mathcal{F}} \sup_{\varepsilon} h_1(T, \mathcal{F}, A, \varepsilon) \\ &= h_1(T, A) \\ &= h_A(T). \end{aligned}$$

The proof of Theorem 2 is completed.

Corollary 1. *If $Tf = f \circ S$ is an operator generated by a continuous map: $S : X \rightarrow X$, where $X = [0, 1]$, then S is chaotic in the sense of Li-York if and only if there is some integer sequence $A = \{0 = a_0 < a_1 < a_2 < \dots\}$ such that $h_A(T) > 0$.*

Theorem 3. *If for every continuous f there exists an invariant function φ_f such that $\lim_{n \rightarrow \infty} \sup_{x \in X} |T^n f(x) - \varphi_f(x)| = 0$ then $h_A(T) = 0$ for every integer sequence $A = \{0 = a_0 < a_1 < a_2 < \dots\}$.*

Proof. The proof of Theorem 3 is analogous to the proof of Theorem 4.7 in [2], so we omitted it.

It is clear that Theorem 3 is a promotion of Theorem 4.7 in [2].

References

- [1] Block, L. and Coppel, W. A. *Dynamics in One Dimension*. Lecture Notes in Math., 1513, Springer, Berlin, 1991.
- [2] D., Tomasz; F., Bartosz *Measure-theoretic and topological entropy of operators on function spaces*. Ergodic Theory Dynam. Systems 25 (2005), no. 2, 455–481.
- [3] F. Blanchard, B. Host, and A. Maass, *Topological complexity*, Ergodic Theory Dynamical Systems, 20 (2000), 641–662.
- [4] R. Engelking, *General Topology*, PWN, Warsaw, 1977.
- [5] D. Kwietniak, P. Oprocha, *Topological entropy and chaos for maps induced on hyperspaces* Chaos Solitons Fractals 33 (2007), no 1, 76–86.
- [6] J. Canovas, *Topological sequence entropy and topological dynamics of interval maps*. Dynamics of Cont. Disct. Impuls. Sys.-Series(A), 14 (2007) no 1, 47–54.

Instructions to Contributors

Journal of Applied Functional Analysis

A quarterly international publication of Eudoxus Press, LLC of TN.

Editor in Chief: George Anastassiou

Department of Mathematical Sciences
University of Memphis
Memphis, TN 38152-3240, U.S.A.

1. Manuscripts, hard copies in quadruplicate and in English, should be submitted by regular, unregistered mail, to the Editor in Chief.

Authors may want to recommend an associate editor most related to the submission to possibly handle it. In addition, to assist the Editor and speed the decision process, authors may include a PDF file of the paper on disk with the submitted copies of the manuscript.

Also authors may want to submit a list of six possible referees, to be used in case we cannot find related referees by ourselves.

2. Manuscripts should be typed using any of TEX, LaTeX, AMS-TEX, or AMS-LaTeX and according to EUDOXUS PRESS, LLC. LATEX STYLE FILE. (Click [HERE](#) to save a copy of the style file.) They should be carefully prepared in all respects. Submitted copies should be brightly printed (not dot-matrix), double spaced, in ten point type size, on one side high quality paper 8(1/2)x11 inch. Manuscripts should have generous margins on all sides and should not exceed 24 pages.

3. Submission is a representation that the manuscript has not been published previously in this or any other similar form and is not currently under consideration for publication elsewhere. A statement transferring from the authors (or their employers, if they hold the copyright) to Eudoxus Press, LLC, will be required before the manuscript can be accepted for publication. The Editor-in-Chief will supply the necessary forms for this transfer. Such a written transfer of copyright, which previously was assumed to be implicit in the act of submitting a manuscript, is necessary under the U.S. Copyright Law in order for the publisher to carry through the dissemination of research results and reviews as widely and effectively as possible.

4. The paper starts with the title of the article, author's name(s) (no titles or degrees), author's affiliation(s) and e-mail addresses. The affiliation should comprise the department, institution (usually university or company), city, state (and/or nation) and mail code.

The following items, 5 and 6, should be on page no. 1 of the paper.

5. An abstract is to be provided, preferably no longer than 150 words.
6. A list of 5 key words is to be provided directly below the abstract. Key words should express the precise content of the manuscript, as they are used for indexing purposes.

The main body of the paper should begin on page no. 1, if possible.

7. All sections should be numbered with Arabic numerals (such as: 1. INTRODUCTION) .

Subsections should be identified with section and subsection numbers (such as 6.1. Second-Value Subheading).

If applicable, an independent single-number system (one for each category) should be used to label all theorems, lemmas, propositions, corollaries, definitions, remarks, examples, etc. The label (such as Lemma 7) should be typed with paragraph indentation, followed by a period and the lemma itself.

8. Mathematical notation must be typeset. Equations should be numbered consecutively with Arabic numerals in parentheses placed flush right, and should be thusly referred to in the text [such as Eqs.(2) and (5)]. The running title must be placed at the top of even numbered pages and the first author's name, et al., must be placed at the top of the odd numbered pages.

9. Illustrations (photographs, drawings, diagrams, and charts) are to be numbered in one consecutive series of Arabic numerals. The captions for illustrations should be typed double space. All illustrations, charts, tables, etc., must be embedded in the body of the manuscript in proper, final, print position. In particular, manuscript, source, and PDF file version must be at camera ready stage for publication or they cannot be considered.

Tables are to be numbered (with Roman numerals) and referred to by number in the text. Center the title above the table, and type explanatory footnotes (indicated by superscript lowercase letters) below the table.

10. List references alphabetically at the end of the paper and number them consecutively. Each must be cited in the text by the appropriate Arabic numeral in square brackets on the baseline.

References should include (in the following order):
 initials of first and middle name, last name of author(s)
 title of article,
 name of publication, volume number, inclusive pages, and year of publication.

Authors should follow these examples:

Journal Article

1. H.H.Gonska, Degree of simultaneous approximation of bivariate functions by Gordon operators, (journal name in italics) *J. Approx. Theory*, 62,170-191(1990).

Book

2. G.G.Lorentz, (title of book in italics) *Bernstein Polynomials* (2nd ed.), Chelsea, New York, 1986.

Contribution to a Book

3. M.K.Khan, Approximation properties of beta operators, in (title of book in italics) *Progress in Approximation Theory* (P.Nevai and A.Pinkus, eds.), Academic Press, New York, 1991, pp.483-495.

11. All acknowledgements (including those for a grant and financial support) should occur in one paragraph that directly precedes the References section.

12. Footnotes should be avoided. When their use is absolutely necessary, footnotes should be numbered consecutively using Arabic numerals and should be typed at the bottom of the page to which they refer. Place a line above the footnote, so that it is set off from the text. Use the appropriate superscript numeral for citation in the text.

13. After each revision is made please again submit four hard copies of the revised manuscript. And after a manuscript has been accepted for publication submit four hard copies of the final revised manuscript. Additionally, two copies of the final version of the TEX/LaTeX source file and a PDF file, are to be submitted to the Editor's Office on personal 3.5 inch computer disks. Label the disks individually with clearly written identifying information, e.g. :

Your name, title of article, kind of computer used, kind of software and version number, disk format and files names of article, as well as abbreviated journal name.

Package the disks in a disk mailer or protective cardboard. Make sure contents of disks are identical with the ones of final hard copies submitted!

Note: The Editor's Office cannot accept the disks without the accompanying matching hard copies of manuscript. No e-mail final submissions are allowed! File submission on disk must be used.

14. Effective 1 Jan. 2009 the journal's page charges are \$15.00 per PDF file page, plus \$40.00 for electronic publication of each article. Upon acceptance of the paper an invoice will be sent to the contact author. The fee payment will be due one month from the invoice date. The article will proceed to publication only after the fee is paid. The charges are to be sent, by money order or certified check, in US dollars, payable to Eudoxus Press, LLC, to the address shown on the Eudoxus [homepage](#).

No galleys will be sent and the contact author will receive one(1) electronic copy of the journal issue in which the article appears.

15. This journal will consider for publication only papers that contain proofs for their listed results.

**TABLE OF CONTENTS, JOURNAL OF APPLIED FUNCTIONAL ANALYSIS,
VOLUME 4, NO.1, 2009**

ON THE GREEN FUNCTION OF THE OPERATOR RELATED TO THE BESSEL- HELMHOLTZ OPERATOR AND THE BESSEL KLEIN-GORDON OPERATOR, C. BUNPOG, A. KANANTHAI,.....	10
MEASURES OF SMALLNESS IN A BANACH SPACE, C.DONNINI,.....	20
ASYMPTOTIC ANALYSIS OF A PARABOLIC PROBLEM WITH RAPIDLY VARYING TYPE OF BOUNDARY CONDITIONS IN A THICK TWO-LEVEL JUNCTION, T. DURANTE,.....	33
WEIGHTED SIMULTANEOUS APPROXIMATION BY LEFT GAMMA QUASI- INTERPOLANTS, H. JIANG, S. GUO,.....	48
NON-UNIFORM SAMPLING PROBLEM, S. KULKARNI, R. RADHA, S. SIVANANTHAN,.....	58
COMMON FIXED POINT THEOREMS IN IF-METRIC SPACES, S.KUTUKCU,.....	75

**TABLE OF CONTENTS, JOURNAL OF APPLIED FUNCTIONAL ANALYSIS,
VOLUME 4, NO.1, 2009, continued from inside back cover**

**ANALYSIS OF THE FACTORS INFLUENCING MOMENTUM PROFITS, A.BIGLOVA,
S.RACHEV, S.STOYANOV, S. ORTOBELLI,.....81**

**EXISTENCE AND UNIQUENESS OF SOLUTIONS TO A DIFFUSIVE PREDATOR-PREY
MODEL, M. ABUALRUB,.....107**

**SIMULTANEOUS APPROXIMATION IN OPERATOR AND TENSOR PRODUCT
SPACES, E. ABU-SIRHAN, R. KHALIL,.....112**

**WEAK COMPATIBILITY AND FIXED POINT THEOREMS IN FUZZY METRIC SPACE
USING IMPLICIT RELATION, S. SHARMA, G. TIWARI,.....122**

**CONTROLLABILITY OF NONLINEAR INFINITE NEUTRAL FUNCTIONAL
DIFFERENTIAL SYSTEMS, R. UMANA,130**

ON INFINITE ORDER K-DV HIERARCHIES, L. ZAMPOGNI,.....140

**TOPOLOGICAL SEQUENCE ENTROPY OF OPERATORS ON FUNCTION
SPACES,G.ZHANG, F.ZENG, K.YAN,.....171**

Volume 4, Number 2

April 2009

ISSN:1559-1948 (PRINT), 1559-1956 (ONLINE)

EUDOXUS PRESS,LLC



JOURNAL OF APPLIED FUNCTIONAL ANALYSIS

GUEST EDITORS: HIKMET CAGLAR and MEHMET OZER

SPECIAL ISSUE I: "CHAOS and COMPLEX SYSTEMS 2008"

SCOPE AND PRICES OF
JOURNAL OF APPLIED FUNCTIONAL ANALYSIS
A quarterly international publication of **EUDOXUS PRESS,LLC**
ISSN:1559-1948(PRINT),1559-1956(ONLINE)

Editor in Chief: George Anastassiou
Department of Mathematical Sciences
The University of Memphis
Memphis, TN 38152,USA
E mail: ganastss@memphis.edu

The purpose of the "Journal of Applied Functional Analysis"(JAFA) is to publish high quality original research articles, survey articles and book reviews from all subareas of Applied Functional Analysis in the broadest form plus from its applications and its connections to other topics of Mathematical Sciences. A sample list of connected mathematical areas with this publication includes but is not restricted to: Approximation Theory, Inequalities, Probability in Analysis, Wavelet Theory, Neural Networks, Fractional Analysis, Applied Functional Analysis and Applications, Signal Theory, Computational Real and Complex Analysis and Measure Theory, Sampling Theory, Semigroups of Operators, Positive Operators, ODEs, PDEs, Difference Equations, Rearrangements, Numerical Functional Analysis, Integral equations, Optimization Theory of all kinds, Operator Theory, Control Theory, Banach Spaces, Evolution Equations, Information Theory, Numerical Analysis, Stochastics, Applied Fourier Analysis, Matrix Theory, Mathematical Physics, Mathematical Geophysics, Fluid Dynamics, Quantum Theory. Interpolation in all forms, Computer Aided Geometric Design, Algorithms, Fuzzyness, Learning Theory, Splines, Mathematical Biology, Nonlinear Functional Analysis, Variational Inequalities, Nonlinear Ergodic Theory, Functional Equations, Function Spaces, Harmonic Analysis, Extrapolation Theory, Fourier Analysis, Inverse Problems, Operator Equations, Image Processing, Nonlinear Operators, Stochastic Processes, Mathematical Finance and Economics, Special Functions, Quadrature, Orthogonal Polynomials, Asymptotics, Symbolic and Umbral Calculus, Integral and Discrete Transforms, Chaos and Bifurcation, Nonlinear Dynamics, Solid Mechanics, Functional Calculus, Chebyshev Systems. Also are included combinations of the above topics.

Working with Applied Functional Analysis Methods has become a main trend in recent years, so we can understand better and deeper and solve important problems of our real and scientific world.

JAFA is a peer-reviewed International Quarterly Journal published by Eudoxus Press,LLC.

We are calling for high quality papers for possible publication. The contributor should send four copies of the contribution to the EDITOR in CHIEF in TEX,LATEX double spaced,in ten point type size. They should be sent BY REGULAR MAIL ONLY, NOT REGISTERED MAIL, AND NO E-MAIL SUBMISSIONS [See: Instructions to Contributors]

Journal of Applied Functional Analysis(JAFA)
is published in January, April, July and October of each year by

EUDOXUS PRESS,LLC,

1424 Beaver Trail Drive,Cordova,TN38016,USA,

Tel.001-901-751-3553

anastassioug@yahoo.com

<http://www.EudoxusPress.com> visit also <http://www.msci.memphis.edu/~ganastss/jafa>.

Webmaster:Ray Clapsadle

Annual Subscription Current Prices:For USA and Canada,Institutional:Print \$280,Electronic \$220,Print and Electronic \$350.Individual:Print \$ 100, Electronic \$60,Print &Electronic \$150.For any other part of the world add \$40 more to the above prices for Print.
Single article PDF file for individual \$10.Single issue in PDF form for individual \$40.

The journal carries page charges \$15 per page of the pdf file of an article, plus \$40 for the electronic publication of all article, both payable upon acceptance of the article within one month and before publication.

No credit card payments.Only certified check,money order or international check in US dollars are acceptable.

Combination orders of any two from JoCAAA,JCAAM,JAFa receive 25% discount,all three receive 30% discount.

Copyright©2009 by Eudoxus Press,LLC all rights reserved.JAFa is printed in USA.

JAFa is reviewed and abstracted by AMS Mathematical Reviews,MATHSCI,and Zentralblatt MATH.

It is strictly prohibited the reproduction and transmission of any part of JAFa and in any form and by any means without the written permission of the publisher.It is only allowed to educators to Xerox articles for educational purposes.The publisher assumes no responsibility for the content of published papers.

JAFa IS A JOURNAL OF RAPID PUBLICATION

Journal of Applied Functional Analysis

Editorial Board

Associate Editors

Editor in-Chief:

George A. Anastassiou
Department of Mathematical Sciences
The University of Memphis
Memphis, TN 38152, USA
901-678-3144 office
901-678-2482 secretary
901-751-3553 home
901-678-2480 Fax
ganastss@memphis.edu
Approximation
Theory, Inequalities, Probability,
Wavelet, Neural Networks, Fractional Calculus

Associate Editors:

1) Francesco Altomare
Dipartimento di Matematica
Universita' di Bari
Via E. Orabona, 4
70125 Bari, ITALY
Tel+39-080-5442690 office
+39-080-3944046 home
+39-080-5963612 Fax
altomare@dm.uniba.it
Approximation Theory, Functional Analysis,
Semigroups and Partial Differential
Equations,
Positive Operators.

2) Angelo Alvino
Dipartimento di Matematica e Applicazioni
"R. Caccioppoli" Complesso
Universitario Monte S. Angelo
Via Cintia
80126 Napoli, ITALY
+39(0)81 675680
angelo.alvino@unina.it,
angelo.alvino@dma.unina.it
Rearrangements, Partial Differential
Equations.

3) Catalin Badea
UFR Mathematiques, Bat. M2,
Universite de Lille1
Cite Scientifique
F-59655 Villeneuve d'Ascq, France

23) Nikolaos B. Karayiannis
Department of Electrical and
Computer Engineering
N308 Engineering Building 1
University of Houston
Houston, Texas 77204-4005
USA
Tel (713) 743-4436
Fax (713) 743-4444
Karayiannis@UH.EDU
Karayiannis@mail.gr
Neural Network Models, Learning
Neuro-Fuzzy Systems.

24) Theodore Kilgore
Department of Mathematics
Auburn University
221 Parker Hall,
Auburn University
Alabama 36849, USA
Tel (334) 844-4620
Fax (334) 844-6555
Kilgota@auburn.edu
Real Analysis, Approximation Theory,
Computational Algorithms.

25) Jong Kyu Kim
Department of Mathematics
Kyungnam University
Masan Kyungnam, 631-701, Korea
Tel 82-(55)-249-2211
Fax 82-(55)-243-8609
jongkyuk@kyungnam.ac.kr
Nonlinear Functional Analysis, Variational
Inequalities, Nonlinear Ergodic Theory,
ODE, PDE, Functional Equations.

26) Miroslav Krbeč
Mathematical Institute
Academy of Sciences of Czech Republic
Žitná 25
CZ-115 67 Praha 1
Czech Republic
Tel +420 222 090 743
Fax +420 222 211 638
krbecm@matsrv.math.cas.cz
Function spaces, Real Analysis, Harmonic

Tel. (+33)(0)3.20.43.42.18
Fax (+33)(0)3.20.43.43.02
Catalin.Badea@math.univ-lille1.fr
Approximation Theory, Functional
Analysis, Operator Theory.

4) Erik J. Balder
Mathematical Institute
Universiteit Utrecht
P.O. Box 80 010
3508 TA UTRECHT
The Netherlands
Tel. +31 30 2531458
Fax +31 30 2518394
balder@math.uu.nl
Control Theory, Optimization,
Convex Analysis, Measure Theory,
Applications to Mathematical
Economics and Decision Theory.

5) Carlo Bardaro
Dipartimento di Matematica e Informatica
Universita di Perugia
Via Vanvitelli 1
06123 Perugia, ITALY
TEL +390755853822
+390755855034
FAX +390755855024
E-mail bardaro@unipg.it
Web site: <http://www.unipg.it/~bardaro/>
Functional Analysis and Approximation
Theory,
Signal Analysis, Measure Theory, Real
Analysis.

6) Heinrich Begehr
Freie Universitaet Berlin
I. Mathematisches Institut, FU Berlin,
Arnimallee 3, D 14195 Berlin
Germany,
Tel. +49-30-83875436, office
+49-30-83875374, Secretary
Fax +49-30-83875403
begehr@math.fu-berlin.de
Complex and Functional Analytic
Methods in PDEs, Complex Analysis,
History of Mathematics.

7) Fernando Bombal
Departamento de Analisis Matematico
Universidad Complutense
Plaza de Ciencias, 3
28040 Madrid, SPAIN
Tel. +34 91 394 5020
Fax +34 91 394 4726
fernando_bombal@mat.ucm.es

Analysis, Interpolation and
Extrapolation Theory, Fourier Analysis.

27) V. Lakshmikantham
Department of Mathematical Sciences
Florida Institute of Technology
Melbourne, FL 32901
e-mail: lakshmik@fit.edu
Ordinary and Partial Differential Equations,
Hybrid Systems, Nonlinear Analysis

28) Peter M. Maass
Center for Industrial Mathematics
Universitaet Bremen
Bibliotheksstr. 1,
MZH 2250,
28359 Bremen
Germany
Tel +49 421 218 9497
Fax +49 421 218 9562
pmaass@math.uni-bremen.de
Inverse problems, Wavelet Analysis and
Operator Equations, Signal and Image
Processing.

29) Julian Musielak
Faculty of Mathematics and Computer Science
Adam Mickiewicz University
Ul. Umultowska 87
61-614 Poznan
Poland
Tel (48-61) 829 54 71
Fax (48-61) 829 53 15
Grzegorz.Musielak@put.poznan.pl
Functional Analysis, Function Spaces,
Approximation Theory, Nonlinear Operators.

30) Vassilis Papanicolaou
Department of Mathematics
National Technical University of Athens
Zografou campus, 157 80
Athens, Greece
tel.: +30(210) 772 1722
Fax +30(210) 772 1775
papanico@math.ntua.gr
Partial Differential Equations,
Probability.

31) Pier Luigi Papini
Dipartimento di Matematica
Piazza di Porta S. Donato 5
40126 Bologna
ITALY
Fax +39(0)51 582528
papini@dm.unibo.it
Functional Analysis, Banach spaces,

Operators on Banach spaces,
Tensor products of Banach spaces,
Polymeasures, Function spaces.

8) Michele Campiti
Department of Mathematics "E.De Giorgi"
University of Lecce
P.O. Box 193
Lecce, ITALY
Tel. +39 0832 297 432
Fax +39 0832 297 594
michele.campiti@unile.it
Approximation Theory,
Semigroup Theory, Evolution problems,
Differential Operators.

9) Domenico Candeloro
Dipartimento di Matematica e Informatica
Universita degli Studi di Perugia
Via Vanvitelli 1
06123 Perugia
ITALY
Tel +39(0)75 5855038
+39(0)75 5853822,
+39(0)744 492936
Fax +39(0)75 5855024
candelor@dipmat.unipg.it
Functional Analysis, Function spaces,
Measure and Integration Theory in
Riesz spaces.

10) Pietro Cerone
School of Computer Science and
Mathematics, Faculty of Science,
Engineering and Technology,
Victoria University
P.O.14428,MCMC
Melbourne,VIC 8001,AUSTRALIA
Tel +613 9688 4689
Fax +613 9688 4050
Pietro.cerone@vu.edu.au
Approximations, Inequalities,
Measure/Information Theory,
Numerical Analysis, Special Functions.

11) Michael Maurice Dodson
Department of Mathematics
University of York,
York YO10 5DD, UK
Tel +44 1904 433098
Fax +44 1904 433071
Mmd1@york.ac.uk
Harmonic Analysis and Applications to
Signal Theory, Number Theory and
Dynamical Systems.

Approximation Theory.

32) Svetlozar T. Rachev
Chair of Econometrics, Statistics
and Mathematical Finance
School of Economics and
Business Engineering
University of Karlsruhe
Kollegium am Schloss, Bau II, 20.12, R210
Postfach 6980, D-76128,
Karlsruhe, GERMANY.
Tel +49-721-608-7535,
+49-721-608-2042(s)
Fax +49-721-608-3811
Zari.Rachev@wiwi.uni-karlsruhe.de
Second Affiliation:
Dept. of Statistics and Applied Probability
University of California at Santa Barbara
rachev@pstat.ucsb.edu
Probability, Stochastic Processes and
Statistics, Financial Mathematics,
Mathematical Economics.

33) Paolo Emilio Ricci
Department of Mathematics
Rome University "La Sapienza"
P.le A.Moro, 2-00185
Rome, ITALY
Tel ++3906-49913201 office
++3906-87136448 home
Fax ++3906-44701007
Paoloemilio.Ricci@uniroma1.it
riccip@uniroma1.it
Special Functions, Integral and Discrete
Transforms, Symbolic and Umbral Calculus,
ODE, PDE, Asymptotics, Quadrature,
Matrix Analysis.

34) Silvia Romanelli
Dipartimento di Matematica
Universita' di Bari
Via E.Orabona 4
70125 Bari, ITALY.
Tel (INT 0039)-080-544-2668 office
080-524-4476 home
340-6644186 mobile
Fax -080-596-3612 Dept.
romans@dm.uniba.it
PDEs and Applications to Biology and
Finance, Semigroups of Operators.

35) Boris Shekhtman
Department of Mathematics
University of South Florida
Tampa, FL 33620, USA
Tel 813-974-9710

12) Sever S.Dragomir
School of Computer Science and
Mathematics, Victoria University,
PO Box 14428,
Melbourne City,
MC 8001,AUSTRALIA
Tel. +61 3 9688 4437
Fax +61 3 9688 4050
sever@csm.vu.edu.au
Inequalities,Functional Analysis,
Numerical Analysis, Approximations,
Information Theory, Stochastics.

13) Paulo J.S.G.Ferreira
Department of Electronica e
Telecomunicacoes/IEETA
Universidade de Aveiro
3810-193 Aveiro
PORTUGAL
Tel +351-234-370-503
Fax +351-234-370-545
pjf@ieeta.pt
Sampling and Signal Theory,
Approximations, Applied Fourier Analysis,
Wavelet, Matrix Theory.

14) Gisele Ruiz Goldstein
Department of Mathematical Sciences
The University of Memphis
Memphis,TN 38152,USA.
Tel 901-678-2513
Fax 901-678-2480
ggoldste@memphis.edu
PDEs, Mathematical Physics,
Mathematical Geophysics.

15) Jerome A.Goldstein
Department of Mathematical Sciences
The University of Memphis
Memphis,TN 38152,USA
Tel 901-678-2484
Fax 901-678-2480
jgoldste@memphis.edu
PDEs,Semigroups of Operators,
Fluid Dynamics,Quantum Theory.

16) Heiner Gonska
Institute of Mathematics
University of Duisburg-Essen
Lotharstrasse 65
D-47048 Duisburg
Germany
Tel +49 203 379 3542
Fax +49 203 379 1845
gonska@math.uni-duisburg.de
Approximation and Interpolation Theory,

boris@math.usf.edu
Approximation Theory, Banach spaces,
Classical Analysis.

36) Panayiotis Siafarikas
Department of Mathematics
University of Patras
26500 Patras
Greece
Tel/Fax +302 610 997169
panos@math.upatras.gr
ODE,Difference Equations, Special
Functions, Orthogonal Polynomials,
Applied Functional Analysis.

37) Rudolf Stens
Lehrstuhl A fur Mathematik
RWTH Aachen
52056 Aachen
Germany
Tel ++49 241 8094532
Fax ++49 241 8092212
stens@mathA.rwth-aachen.de
Approximation Theory, Fourier Analysis,
Harmonic Analysis, Sampling Theory.

38) Juan J.Trujillo
University of La Laguna
Departamento de Analisis Matematico
C/Astr.Fco.Sanchez s/n
38271.LaLaguna.Tenerife.
SPAIN
Tel/Fax 34-922-318209
Juan.Trujillo@ull.es
Fractional: Differential Equations-
Operators-
Fourier Transforms, Special functions,
Approximations,and Applications.

39) Tamaz Vashakmadze
I.Vekua Institute of Applied Mathematics
Tbilisi State University,
2 University St. , 380043,Tbilisi, 43,
GEORGIA.
Tel (+99532) 30 30 40 office
(+99532) 30 47 84 office
(+99532) 23 09 18 home
Vasha@viam.hepi.edu.ge
tamazvashakmadze@yahoo.com
Applied Functional Analysis, Numerical
Analysis, Splines, Solid Mechanics.

40) Ram Verma
International Publications
5066 Jamieson Drive, Suite B-9,
Toledo, Ohio 43613,USA.

Computer Aided Geometric Design,
Algorithms.

17) Karlheinz Groechenig
Institute of Biomathematics and Biometry,
GSF-National Research Center
for Environment and Health
Ingolstaedter Landstrasse 1
D-85764 Neuherberg, Germany.
Tel 49-(0)-89-3187-2333
Fax 49-(0)-89-3187-3369
Karlheinz.groechenig@gsf.de
Time-Frequency Analysis, Sampling Theory,
Banach spaces and Applications,
Frame Theory.

18) Vijay Gupta
School of Applied Sciences
Netaji Subhas Institute of Technology
Sector 3 Dwarka
New Delhi 110075, India
e-mail: vijay@nsit.ac.in;
vijaygupta2001@hotmail.com
Approximation Theory

19) Weimin Han
Department of Mathematics
University of Iowa
Iowa City, IA 52242-1419
319-335-0770
e-mail: whan@math.uiowa.edu
Numerical analysis, Finite element method,
Numerical PDE, Variational inequalities,
Computational mechanics

20) Tian-Xiao He
Department of Mathematics and
Computer Science
P.O.Box 2900, Illinois Wesleyan University
Bloomington, IL 61702-2900, USA
Tel (309)556-3089
Fax (309)556-3864
the@iwu.edu
Approximations, Wavelet, Integration Theory,
Numerical Analysis, Analytic Combinatorics.

21) Don Hong
Department of Mathematical Sciences
Middle Tennessee State University
1301 East Main St.
Room 0269, Bldg KOM
Murfreesboro, TN 37132-0001
Tel (615) 904-8339
dhong@mtsu.edu
Approximation Theory, Splines, Wavelet,
Stochastics, Mathematical Biology Theory.

Verma99@msn.com
rverma@internationalpubls.com
Applied Nonlinear Analysis, Numerical
Analysis, Variational Inequalities,
Optimization Theory, Computational
Mathematics, Operator Theory.

41) Gianluca Vinti
Dipartimento di Matematica e Informatica
Universita di Perugia
Via Vanvitelli 1
06123 Perugia
ITALY
Tel +39(0) 75 585 3822,
+39(0) 75 585 5032
Fax +39 (0) 75 585 3822
mategian@unipg.it
Integral Operators, Function Spaces,
Approximation Theory, Signal Analysis.

42) Ursula Westphal
Institut fuer Mathematik B
Universitaet Hannover
Welfengarten 1
30167 Hannover, GERMANY
Tel (+49) 511 762 3225
Fax (+49) 511 762 3518
westphal@math.uni-hannover.de
Semigroups and Groups of Operators,
Functional Calculus, Fractional Calculus,
Abstract and Classical Approximation
Theory, Interpolation of Normed spaces.

43) Ronald R. Yager
Machine Intelligence Institute
Iona College
New Rochelle, NY 10801, USA
Tel (212) 249-2047
Fax (212) 249-1689
Yager@Panix.Com
ryager@iona.edu
Fuzzy Mathematics, Neural Networks,
Reasoning,
Artificial Intelligence, Computer Science.

44) Richard A. Zalik
Department of Mathematics
Auburn University
Auburn University, AL 36849-5310
USA.
Tel 334-844-6557 office
678-642-8703 home
Fax 334-844-6555
zalik@auburn.edu
Approximation Theory, Chebychev Systems,
Wavelet Theory.

22) Hubertus Th. Jongen
Department of Mathematics
RWTH Aachen
Templergraben 55
52056 Aachen
Germany
Tel +49 241 8094540
Fax +49 241 8092390
jongen@rwth-aachen.de
Parametric Optimization, Nonconvex
Optimization, Global Optimization.

Preface

These three special issues, which constitute the proceedings of the symposium CCS2008 – Second International Interdisciplinary Chaos Symposium on “CHAOS and COMPLEX SYSTEMS”, have tried to create a forum for the exchange of information and experience in the exciting interdisciplinary field of Chaos. However the conference was more in the Applied Mathematics direction centered.

The expectation of the organizers concerning international resonance of the conference has been fulfilled: 150 scientists from 15 different countries (China, France, Greece, Iran, Japan, Kazakhstan, Lebanon, Lithuania, Malaysia, Mexico, Pakistan, Romania, Russia, Turkey, and Uzbekistan) have participated. Good relations to research institutes of these countries might be of great importance for science and applications.

On behalf of the Organizing Committee we would like to express our thanks to the Scientific Committee, the Program Committee and to all who have contributed to this conference for their support and advice. We are also grateful to the invited lecturers Prof. George A. Anastassiou, Prof. Amir Atiya, Prof. Mohamed Saladin El Naschie, Prof. Ramazan Gencay, Prof. Ji-Huan He, Prof. Robert Kozma, Prof. V. Lakshmikantham, and Prof. Paul Refenes.

Special thanks are due to Rector Prof. Tamer Kocel, Vice Rector Prof. Cetin Bolcal and Dean Prof. Dursun Kocer for their support, advice and encouragement.

Our thanks are also due to the Istanbul Kultur University, which was hosting this symposium and provided all of its facilities.

We are grateful to the Editor-in-Chief, Prof. George A. Anastassiou for accepting this volume for publication in Journal of Applied Functional Analysis.

Hikmet Caglar

On behalf of the Organizing Committee

Istanbul Kultur University, Department of Mathematics-Computer, Istanbul, Turkey

Tel.: +90-212-4984367; Fax: +90-212-4658310; E-mail: s.caglar@iku.edu.tr

Mehmet Ozer

On behalf of the Organizing Committee

Istanbul Kultur University, Department of Physics, Istanbul, Turkey

Tel.: +90-212-4984317; Fax: +90-212-4658310; E-mail: m.ozel@iku.edu.tr

Application of homotopy perturbation method to nonlinear oscillator differential equations

A. Barari*, F. Farrokhzad, A. Janalizadeh, D.D. Ganji

Departments of Civil and Mechanical Engineering, University of Mazandaran,
Babol, Mazandaran, Iran

Abstract

In this paper, homotopy perturbation method (HPM) is applied to solve nonlinear oscillator differential equations. We illustrate that this method is very effective and convenient and does not require linearization or small perturbation. Comparison is made between the exact solutions and the results of the homotopy perturbation method.

Keywords: homotopy perturbation method (HPM); nonlinear oscillators; exact solution; Van Der Pol Oscillator problem

1. Introduction

This paper considers two examples of a general oscillator differential equation of the form:

$$u'' + f(t, u, u') = 0, \quad (1)$$

Subject to $u(0) = a$ and $u'(0) = b$, where t is time, u is the displacement, and the prime denotes differentiation with respect to t .

The first example is an oscillator which the voltage i.e. the voltage go through a cycle and repeat their values after some time called the period of oscillation. One may think of these states as stable in the sense that slight changes in the voltage will still lead us back to the same place in the

*Corresponding author. Tel: +981113234205; fax: +981113234205

E-mail address: amin78404@yahoo.com

circuit operation. A prototype of this circuit is the van der pol circuit [1]. Another example is a nonlinear oscillator differential equation.

Balthazar Van Der Pol was a Dutch electrical engineer who initiated modern experimental dynamics in the laboratory during the 1920s and 1930s. Van Der Pol investigated electrical circuits employing vacuum tubes and found that they have stable oscillations, now called limit cycles.

The Van Der Pol equation is:

$$\frac{d^2u}{dt^2} - k(1-u^2)\frac{du}{dt} + u = 0, \quad (2)$$

Where k controls the way in which voltage flows through the system.

The Van Der Pol oscillator is one of the systems whose damping forces are nonlinear. These nonlinear damping forces have a very important property: the damping force will tend to increase the amplitude for small velocities but to decrease it for large velocities.

It follows that the state of rest is not stable and that an oscillation will be built up from rest even in the absence of external forces, this accounts for the description of these oscillations as self-excited or self-sustained oscillations.

In general, the limit cycle system appears in various problems in nonlinear dynamics, particularly in the analysis of relaxation oscillation, as the Van Der Pol Eq. (2), limit cycle oscillators are also useful as phenomenological models for studies of the low-dimensional dynamics of the heart, In chemical kinetics and in electronics, there are certain negative-resistance oscillators [2].

A question that has been addressed in many of these investigations refers to the behavior of limit cycle system under an external, periodic force. If the phase space of the unforced system is two-dimensional, a time dependent external force can lead to different responses, like periodic, quasi-periodic and chaotic motion.

The Van Der Pol oscillator under an external periodic force is:

$$\frac{d^2u}{dt^2} - k(1-u^2)\frac{du}{dt} + u = k\beta\lambda \cos \lambda t, \quad (3)$$

Where λ and $k\beta\lambda$ are the frequency and the amplitude of the external force, respectively [2].

Over the last decades several analytical/approximate methods have been developed to solve nonlinear ordinary and partial differential equations. Some of these techniques include variational

iteration method (VIM) [3-8], decomposition method [9-11], homotopy perturbation method (HPM) [12-19] etc.

Linear and Nonlinear phenomena are of fundamental importance in various fields of science and engineering. Most models of real – life problems are still very difficult to solve. Therefore, approximate analytical solutions such as homotopy-perturbation method [12- 19] were introduced.

This method is the most effective and convenient ones for both linear and nonlinear equations.

Perturbation method is based on assuming a small parameter. The majority of nonlinear problems, especially those having strong nonlinearity, have no small parameters at all and the approximate solutions obtained by the perturbation methods, in most cases, are valid only for small values of the small parameter.

Generally, the perturbation solutions are uniformly valid as long as a scientific system parameter is small. However, we cannot rely fully on the approximations, because there is no criterion on which the small parameter should exists. Thus, it is essential to check the validity of the approximations numerically and/or experimentally. To overcome these difficulties, HPM have been proposed recently.

In this paper we will apply the homotopy perturbation method to the nonlinear oscillator differential equations.

2. Basic idea of homotopy-perturbation method

To explain this method, let us consider the following function:

$$A(u) - f(r) = 0, \quad r \in \Omega \quad (4)$$

With the boundary conditions of:

$$B(u, \frac{\partial u}{\partial n}) = 0, \quad r \in \Gamma, \quad (5)$$

Where A , B , $f(r)$ and Γ are a general differential operator, a boundary operator, a known analytical function and the boundary of the domain Ω , respectively.

Generally speaking the operator A can be divided in to a linear part L and a nonlinear part $N(u)$. Eq. (4) can therefore, be written as:

$$L(u) + N(u) - f(r) = 0, \quad (6)$$

By the homotopy technique, we construct a homotopy

$v(r, p) : \Omega \times [0, 1] \rightarrow R$ Which satisfies

$$H(v, p) = (1 - p)[L(v) - L(u_0)] + p[A(v) - f(r)] = 0, \quad (7)$$

$$p \in [0, 1], r \in \Omega,$$

Or

$$H(v, p) = L(v) - L(u_0) + pL(u_0) + p[N(v) - f(r)] = 0, \quad (8)$$

Where $p \in [0, 1]$ is an embedding parameter, while u_0 is an initial approximation of Eq. (4), which satisfies the boundary conditions. Obviously, from Eqs. (7) and (8) we will have:

$$H(v, 0) = L(v) - L(u_0) = 0, \quad (9)$$

$$H(v, 1) = A(v) - f(r) = 0, \quad (10)$$

The changing process of p from zero to unity is just that of $v(r, p)$ from u_0 to $u(r)$. In topology, this is called deformation, while $L(v) - L(u_0)$ and $A(v) - f(r)$ are called homotopy.

According to the HPM, we can first use the embedding parameter p as a “small parameter”, and assume that the solutions of Eqs. (7) and (8) can be written as a power series in p :

$$v = v_0 + pv_1 + p^2v_2 + \dots, \quad (11)$$

Setting $p = 1$ yields in the approximate solution of Eq. (4) to:

$$u = \lim_{p \rightarrow 1} v = v_0 + v_1 + v_2 + \dots, \quad (12)$$

The combination of the perturbation method and the homotopy method is called the HPM, which eliminates the drawbacks of the traditional perturbation methods while keeping all its advantage.

The series (12) is convergent for most cases. However, the convergent rate depends on the nonlinear operator $A(v)$. Moreover, He made the following suggestions [14]:

- The second derivative of $N(v)$ with respect to v must be small because the parameter may be relatively large, i.e. $p \rightarrow 1$.
- The norm of $L^{-1} \frac{\partial N}{\partial v}$ must be smaller than one so that the series converges.

3. Example 1

Consider the Van Der Pol Oscillator problem [20]:

$$\frac{d^2 u}{dt^2} + \frac{du}{dt} + u + u^2 \frac{du}{dt} = 2 \cos t - \cos^3 t \quad (13)$$

With the boundary conditions:

$$\begin{aligned} u(0) &= 0, \\ u'(0) &= 1. \end{aligned} \quad (14)$$

The exact solution of the above differential system is:

$$u(t) = \sin(t), \quad (15)$$

3.1. Application of Homotopy-perturbation method

To solve Eq. (13) by means of HPM, we consider the following process after separating the linear and nonlinear parts of the equation.

A homotopy can be constructed as follows:

$$\begin{aligned} H(v, p) &= (1-p) \left(\left(\frac{d^2 v(t)}{dt^2} + \frac{dv(t)}{dt} + v(t) \right) - 1 \right) + \\ &+ p \left(\frac{d^2 v(t)}{dt^2} + \left(\frac{d}{dt} v(t) \right) + v(t) + v(t)^2 \left(\frac{d}{dt} v(t) \right) - 2 \cos(t) + \cos(t)^3 \right), \end{aligned} \quad (16)$$

Substituting $v = v_0 + pv_1 + \dots$ in to Eq. (16) and rearranging the resultant equation based on powers of p -terms, one has:

$$p^0 : -1 + \left(\frac{d^2}{dt^2} v_0(t)\right) + v_0(t) + \left(\frac{d}{dt} v_0(t)\right) = 0, \quad (17)$$

$$p^1 : \left(\frac{dv_1(t)}{dt}\right) + 1 + \cos^3(t) + v_1(t) + \left(\frac{d^2 v_1(t)}{dt^2}\right) - 2 \cos(t) + v_0^2(t) \left(\frac{dv_0(t)}{dt}\right) = 0, \quad (18)$$

With the following conditions:

$$\begin{aligned} v_0(0) &= 0, \quad \frac{d}{dt} v_0(0) = 1 \\ v_i(0) &= 0, \quad \frac{d}{dt} v_i(0) = 0 \quad i = 1, 2, \dots \end{aligned} \quad (19)$$

With the effective initial approximation for v_0 from the conditions (19) and solutions of Eqs. (17), (18) may be written as follows:

$$v_0(t) = \frac{1}{3} e^{(-0.5t)} \sin(0.5\sqrt{3}t) \sqrt{3} - e^{(-0.5t)} \cos(0.5\sqrt{3}t) + 1, \quad (20)$$

$$\begin{aligned} v_1(t) = & -\frac{46961}{119574} e^{(-0.5t)} \sin(0.5\sqrt{3}t) \sqrt{3} + \frac{45263}{39858} e^{(-0.5t)} \cos(0.5\sqrt{3}t) \\ & - \frac{4}{21} e^{(-2.5t)} \left(\begin{aligned} & \left(\left(\frac{7}{4} - \frac{7}{4}t \right) (e^t)^2 + \frac{7}{8} e^t \cos(0.5\sqrt{3}t) + \frac{7}{4} \sqrt{3} (-0.5 + (\frac{1}{3} + x) e^t) \right. \\ & e^t \sin(0.5\sqrt{3}t) - \frac{7}{156} \sqrt{3} \sin(1.5\sqrt{3}t) e^t - \frac{7}{26} \cos(1.5\sqrt{3}t) e^t + \\ & \left(-\frac{105}{16} \sin t + \frac{21}{4} - \frac{21}{146} \cos(3t) + \frac{63}{1168} \sin(3t) \right) e^{(2.5t)} + (\sqrt{3} \sin(\sqrt{3}t)) \\ & \left. - \frac{7}{2} + 2 \cos(\sqrt{3}t) e^{(1.5t)} \right) \end{aligned} \right), \end{aligned} \quad (21)$$

In the same manner, the rest of components were obtained using the Maple package.

According to the HPM, we can conclude that:

$$u(t) = \lim_{p \rightarrow 1} v(t) = v_0(t) + v_1(t) + \dots, \quad (22)$$

Therefore, substituting the values of $v_0(t)$, $v_1(t)$ from Equations. (20), (21) in to Eq. (22) yields:

$$u(t) = \frac{1}{3} e^{(-0.5t)} \sin(0.5\sqrt{3}t) \sqrt{3} - e^{(-0.5t)} \cos(0.5\sqrt{3}t) + 1 - \frac{46961}{119574} e^{(-0.5t)} \sin(0.5\sqrt{3}t) \sqrt{3} + \frac{45263}{39858} e^{(-0.5t)} \cos(0.5\sqrt{3}t) - \frac{4}{21} e^{(-2.5t)} \left(\begin{aligned} & \left(\left(\frac{7}{4} - \frac{7}{4}t \right) (e^t)^2 + \frac{7}{8} e^t \cos(0.5\sqrt{3}t) + \frac{7}{4} \sqrt{3} \left(-0.5 + \left(\frac{1}{3} + x \right) e^t \right) \right. \\ & e^t \sin(0.5\sqrt{3}t) - \frac{7}{156} \sqrt{3} \sin(1.5\sqrt{3}t) e^t - \frac{7}{26} \cos(1.5\sqrt{3}t) e^t + \\ & \left(-\frac{105}{16} \sin t + \frac{21}{4} - \frac{21}{146} \cos(3t) + \frac{63}{1168} \sin(3t) \right) e^{(2.5t)} + (\sqrt{3} \sin(\sqrt{3}t)) \\ & \left. - \frac{7}{2} + 2 \cos(\sqrt{3}t) e^{(1.5t)} \right) \end{aligned} \right), \quad (23)$$

As it can be seen, using HPM in solving this equation leads to the exact solution (Table 1).

Table 1. Comparison of the approximate solution with exact solution

t	Exact solution	HPM	Error of HPM
0.0	0.0000000000	0.0000000000	0.00000000E+0
0.1	0.0998334166	0.0998334161	5.5000000E-10
0.2	0.1986693308	0.1986692604	7.0400000E-8
0.3	0.2955202067	0.2955190492	1.1575000E-6
0.4	0.3894183423	0.3894101010	8.2413000E-6
0.5	0.4794255386	0.4793884172	3.7121400E-5
0.6	0.5646424734	0.5645175388	1.2493460E-4
0.7	0.6442176872	0.6438744431	3.4324410E-4
0.8	0.7173560909	0.7165444751	8.1161580E-4
0.9	0.7833269096	0.7816179472	1.7089624E-3
1.0	0.8414709848	0.8381911175	3.27986730E-3

4. Example 2

Consider the nonlinear oscillator differential equation [21]:

$$\frac{d^2 u}{dt^2} - u + u^2 + \left(\frac{du}{dt}\right)^2 - 1 = 0, \quad (24)$$

With the boundary conditions:

$$\begin{aligned} u(0) &= 2, \\ u'(0) &= 0, \end{aligned} \quad (25)$$

The exact solution of the above differential system is:

$$u(t) = 1 + \cos(t), \quad (26)$$

4.1. Application of homotopy perturbation method

To solve Eq. (24) by means of HPM, we consider the following process after separating the linear and nonlinear parts of the equation.

A homotopy can be constructed as follows:

$$H(v, p) = (1-p)\left(\frac{d^2 v(t)}{dt^2} - \frac{d^2 v_0(t)}{dt^2}\right) + p\left(\frac{d^2 v(t)}{dt^2} + \left(\frac{d}{dt} v(t)\right)^2 + v(t)^2 - v(t) - 1\right) = 0, \quad (27)$$

Substituting $v = v_0 + pv_1 + \dots$ in to Eq. (27) and rearranging the resultant equation based on powers of p-terms, one has:

$$p^0 : \frac{d^2}{dt^2} v_0 = 0, \quad (28)$$

$$p^1 : -1 + \left(\frac{d^2}{dt^2} v_1(t)\right) - v_0(t) + \left(\frac{d}{dt} v_0(t)\right)^2 + v_0(t)^2 = 0, \quad (29)$$

$$p^2 : 2\left(\frac{d}{dt} y_0(t)\right)\left(\frac{d}{dt} y_1(t)\right) + \left(\frac{d^2}{dt^2} y_2(t)\right) - y_1(t) + 2y_0(t)y_1(t) = 0, \quad (30)$$

With the following conditions:

$$v_0(0) = 2, \quad \frac{d}{dt} v_0(0) = 0 \quad (31)$$

$$v_i(0) = 0, \quad \frac{d}{dt} v_i(0) = 0 \quad i = 1, 2, \dots$$

With the effective initial approximation for v_0 from the conditions (31) and solutions of Eqs. (28), (29) and (30) may be written as follows:

$$v_0(t) = 2, \quad (32)$$

$$v_1(t) = -0.5t^2, \quad (33)$$

$$v_2(t) = \frac{1}{8}t^4, \quad (34)$$

In the same manner, the rest of components were obtained using the Maple package.

According to the HPM, we can conclude that:

$$u(t) = \lim_{p \rightarrow 1} v(t) = v_0(t) + v_1(t) + \dots, \quad (35)$$

Therefore, substituting the values of $v_0(t)$, $v_1(t)$ and $v_2(t)$ from Eqs. (32), (33) and (34) in to Eq. (35) yields:

$$u(t) = 2 - 0.5t^2 + \frac{1}{8}t^4 \quad (36)$$

As it can be seen, using HPM in solving this equation leads to the exact solution (Table 2).

Table 2. Comparison of the approximate solution with exact solution

t	Exact solution	HPM	Error of HPM
0.0	2.000000000	2.000000000	0.0000000E+0
0.1	1.995004165	1.995012500	8.3350000E-6
0.2	1.980066578	1.980200000	1.3342200E-4
0.3	1.955336489	1.956012500	6.7601100E-4
0.4	1.921060994	1.923200000	2.1390060E-3
0.5	1.877582562	1.882812500	5.2299380E-3
0.6	1.825335615	1.836200000	1.0864385E-2
0.7	1.764842187	1.785012500	2.0170313E-2
0.8	1.696706709	1.731200000	3.4493291E-2
0.9	1.621609968	1.677012500	5.5402532E-2
1.0	1.540302306	1.625000000	8.4697694E-2

5. Conclusions

Homotopy perturbation method is employed successfully to study nonlinear oscillator differential equations. In conclusion, HPM provides highly accurate numerical solutions for nonlinear problems in comparison with other methods. As it is mentioned, this method avoids linearization and physically unrealistic assumptions.

Finally, Comparison with exact solution reveals that homotopy perturbation method is remarkably effective for solving boundary value problems. For Computations and plots, Maple Package has been used.

References

- [1] J. Guckenheimer, Nonlinear oscillations, dynamical systems, and bifurcations of vector field, New York. Springer. Verlag. 1983.
- [2] E.M. Elabbay, M.M. El-Dessoky, Synchronization of van der Pol oscillator and Chen Chaotic dynamical system, Chaos. Soltons & Fractals, in press, 2008.
- [3] Ji-H. He, A new approach to nonlinear partial differential equations, Commun. Nonlinear Sci. Numer. Simul. 2 (1997) 230–235.
- [4] Ji-H. He, Variational iteration method – a kind of non-linear analytical technique: some examples, Int. J. Non-Linear Mech. 34 (1999) 699–708.
- [5] Ji-H. He, Some asymptotic methods for strongly nonlinear equations, Int. J. Modern

- Phys. 20 (2006) 1141–1199.
- [6] Ganji, D.D., M. Jannatabadi., E. Mohseni, Application of He's variational iteration method to nonlinear Jaulent–Miodek equations and comparing it with ADM, J. Comput. Appl. Math. 207 (2007) 35–45.
- [7] Ganji, D.D., A. Sadighi, Application of homotopy–perturbation and variational iteration methods to nonlinear heat transfer and porous media equations, J. Comput. Appl. Math. 207 (2007) 24–34.
- [8] S. Momani, Z. Odibat, Comparison between the homotopy perturbation method and the variational iteration method for linear fractional partial differential equations, Comput. & Math. Appl. 54 (2007) 910–919.
- [9] G. Adomian, Stochastic Systems, Academic Press Inc., New York, 1983.
- [10] G. Adomian, Nonlinear Stochastic Operator Equations, Academic Press Inc., New York, 1986.
- [11] G. Adomian, Solving Frontier Problems of Physics: The Decomposition Method, Kluwer, Boston, 1994.
- [12] Ji-H. He, Homotopy perturbation method: a new nonlinear analytical technique, Appl. Math. Comput. 135 (2003) 73–79.
- [13] Ji-H. He, Addendum: new interpretation of homotopy perturbation method, Int. J. Modern Phys. 20 (2006) 2561–2568.
- [14] Ji-H. He, Homotopy perturbation technique, Comput. Meth. Appl. Mech. Eng. 178 (1999) 257–262.
- [15] M. Rafei, D. D. Ganji, Explicit Solutions of Helmholtz Equation and Fifth–order Kdv Equation using Homotopy–perturbation Method, Int. J. Nonlinear Sci. Numer. Simul. 7 (2006) 321–328 .
- [16] D. D. Ganji, A. Sadighi, Application of He's Homotopy–perturbation Method to Nonlinear Coupled Systems of Reaction–diffusion Equations, Int. J. Nonlinear Sci. and Num. Simu, 7 (2006) 411–418
- [17] A. Janalizadeh, A. Barari, D.D. Ganji, Application of homotopy perturbation method for solving second order nonlinear wave equation, Journal of Physics, in press, 2007.
- [18] A. Barari, A. Janalizadeh, D.D. Ganji, Application of homotopy perturbation method to Zakharov- Kuznetsov equation, Journal of Physics, in press, 2007.
- [19] J. Biazar, H. Ghazvini and M. Eslami, He's homotopy perturbation method for

- systems of integro-differential equations, *Chaos, Solitons & Fractals*, in press, 2007.
- [20] S.H.Behiry, H.Hashish, I.L. El-Kalla, A. Elsaid, A new algorithm for the decomposition solution of nonlinear differential equations, *Comput. & Math. Appl.* 54 (2007) 459-466.
- [21] H.P.W.Gottlieb, Velocity-dependent conservative nonlinear oscillators with exact harmonic solutions, *Journal of sound and vibration*. 230 (2000) 323-333.

ESTIMATING FRACTAL DIMENSION OF FINANCIAL RETURNS USING STABLE DISTRIBUTIONS

Nesrin ALPTEKİN*

Abstract

It is argued that determination of the correct specification of return distributions has attractive implications. This paper estimates α -stable distributions of financial return series. These distributions are fractal and the analysis and estimation of α -stable distributions provide a way to test for fractal structure. Characteristic exponent α of these distributions measures the fractal dimension of the probability space and there is a relationship between the fractal dimensions of time series. This relationship is expressed by Hurst exponent. In this paper, fractal dimension of some financial returns is estimated by stable distributions.

Keywords: Financial returns, Fractal dimension, Hurst exponent, Stable distributions, Time series.

1. Introduction

Financial theory, including the classical portfolio theory, the Black-Scholes-Merton option pricing model and CAPM (Capital asset pricing model) rests heavily on the normality assumption that asset returns follow a normal distribution. However it is well known that the normal distribution frequently fails to represent the distribution of financial returns properly. Rather, the empirical observations exhibit fat tails.

It is often argued that financial returns are the cumulative outcome of a vast number of pieces of information and individual decisions arriving almost continuously in time. According to the Central Limit Theorem, if the sum of a large number of independent, identically distributed random variables has a limiting distribution after appropriate shifting, and scaling, the limiting distribution must be a member of the stable class.

Stable distributions are a rich class of probability distributions that allow skewness and heavy tails and have many intriguing mathematical properties. In his study, Paul Lévy characterized this class in the 1920's. It is therefore natural to assume that financial returns are at least approximately governed by a stable distribution if the accumulation is additive, or by a log-stable distribution if the accumulation is multiplicative.

The Gaussian is the most familiar and tractable stable distribution so either it or the log-normal has routinely been postulated to govern financial returns. However, financial returns are often much more leptokurtic than is consistent with normality. This naturally leads one to

⁷ *Business Department, Anadolu University, Eskişehir, TÜRKİYE.*

consider also the non-Gaussian stable distributions as a model of financial returns, as first proposed by Benoit Mandelbrot.

Stable distributions have been proposed as a model for many types of physical and economic systems. The reasons for using a stable distribution to describe a system can be listed in order as follows:

1. There are solid theoretical reasons for expecting a non-Gaussian stable model, e.g. the gravitational field of stars yielding the Holtsmark distribution, hitting times for a Brownian motion yielding a Lévy distribution.
2. The Generalized Central Limit theorem which states that the only possible non-trivial limit of normalized sums of independent identically distributed terms is stable. Because, some observed quantities are the sum of many small terms like the price of a stock, the noise in a communication system etc., and therefore a stable model should be used to describe such systems.
3. The third reason is empirical. Many large data sets exhibit heavy tails and skewness.

Stable family distributions are parameterized by stable (Levy) index α , $0 < \alpha \leq 2$, and include the normal distribution as a special case, $\alpha = 2$. The stable index, α , is the fractal dimension of the probability space. The unique feature of α -stable family distributions is the existence of a relationship between the fractal dimension of the probability space and the fractal dimension of the time series. This relationship is simply expressed in terms of Hurst exponent (H), i.e. $\alpha = 1/H$. Thus, the estimates of α imply that knowledge of one characteristic parameter of a stable distribution gives us information about another classical exponent developed by Hurst, Hurst exponent. The values of the Hurst exponent range between 0 and 1.

A Hurst Exponent value H close to 0.5 indicates a random walk (a Brownian time series). In a random walk there is no correlation between any element and a future element and there is a 50% probability that future return values will go either up or down. Series of this type are hard to predict.

A Hurst Exponent value H between 0 and 0.5 exists for time series with "anti-persistent behavior". This means that an increase will tend to be followed by a decrease (or a decrease will be followed by an increase). This behavior is sometimes called "mean reversion" which means future values will have a tendency to return to a longer term mean value. The strength of this mean reversion increases as H approaches 0.

A Hurst Exponent value H between 0.5 and 1 indicates "persistent behavior", that is the time series is trending. If there is an increase from time step $[t-1]$ to $[t]$ there will probably be an increase from $[t]$ to $[t+1]$. The same is true of decreases, where a decrease will tend to follow a decrease. The larger the H value is, the stronger the trend. Series of this type are easier to predict than series falling in the other two categories.

The main purpose of this paper is to present the estimates of the Hurst exponent, by estimating the stable distribution. This, in turn, will allow us description of the distribution of financial returns and fractal dimensionality of the underlying process.

The structure of this paper is as follows. Section II describes the properties of stable distributions. Section III contains the empirical results and the final section contains summary and conclusions.

2. Basic Properties of Stable Distributions

An important property of stable random variable is that the sum of two of them is itself a stable random variable. A random variable X is stable or stable in the broad sense if for X_1 and X_2 independent copies of X and positive constants a and b ,

$$aX_1 + bX_2 \stackrel{d}{=} cX + d, \quad (1)$$

for some positive c and some $d \in \mathbb{R}$. (The symbol $\stackrel{d}{=}$ means equality in distribution, i.e. both expressions have the same probability law.) The random variable is strictly stable or stable in the narrow sense if (1) holds with $d = 0$ for all choices of a and b .

Stable distributions have four parameters α, β, γ and δ , and these parameters correspond to first four moments of the distribution. An index of stability $\alpha \in (0, 2]$ also called the tail index, tail exponent or characteristic exponent, a skewness parameter $\beta \in [-1, 1]$, a scale parameter $\sigma > 0$ and a location parameter $\mu \in \mathbb{R}$. A sum of two independent random variables having an α -stable distribution with index α is again α -stable with the same index α . This invariance property, however, does not hold for different α 's.

The α -stable distributions have slowly decaying tails and infinite second moments. These distributions have a much higher degree of variability, which make them useful for modeling the empirical characteristics of log returns. Most stable probability density distributions do not have closed analytical mathematical form. They are simply expressed in terms of their characteristic function which is the Fourier transform of the probability density function.

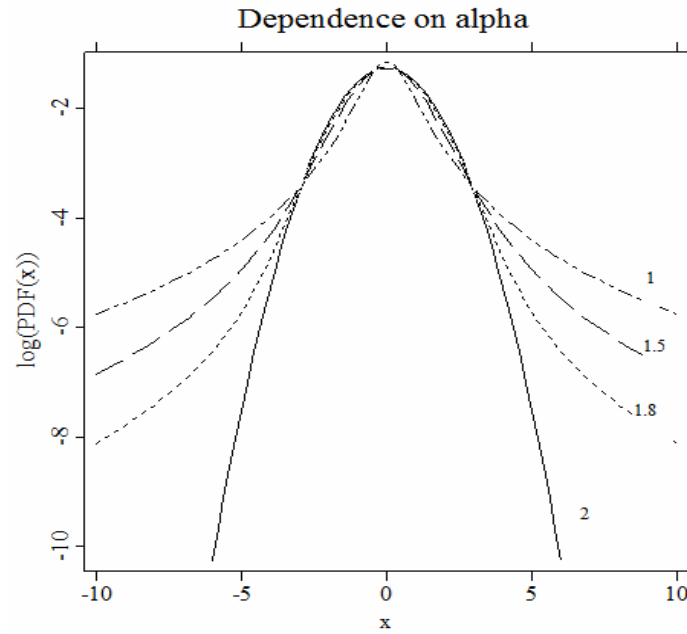


Figure 1. Symmetric ($\beta = \mu = 0$) α -stable probability density functions (pdfs), for $\alpha = 2$, 1.8, 1.5 and 1.

The logarithm of the characteristic function of a stable random variable X is given by:

$$\phi(t) = E(\exp(itX)) = \int_{-\infty}^{\infty} \exp(itx) dF(x) \quad (2)$$

where $i^2 = -1$. The α -stable distributions include the normal distribution as a special case ($\alpha = 2$). For the other possible values of stable index α , the stable distributions have slowly decaying tails and infinite second moments.

2.1 Estimation of Stable Parameters

Since most α -stable distributions do not have simple mathematical expressions, the main difficulty lies with the estimation of the parameters of α -stable distributions. Thus parameter estimation technique has to be based on a different characteristic of stable distributions. Parameter estimation techniques are tail exponent estimation, quantile estimation, maximum likelihood method and characteristic function approaches.

2.1.1 Tail exponent estimation

It is the earliest and the simplest method of estimating stable index α . Tail exponent estimation is to plot the right tail of the empirical distribution function on a log-log scale. The slope of the linear regression for large values of x yields the estimate of the tail index α ,

through the relation $\alpha = -\text{slope}$. This method is highly sensitive to the size of the sample and the choice of the number of observations used in the regression. Generally, the choice of the observations used in the regression is subjective and can yield large estimation errors.

Hill estimator which is a well known method for estimating stable index α , also tends to overestimate the tail exponent of the stable distribution if α is close to two and the sample size is not very large. Thus, the true tail behavior of α -stable laws is visible only for extremely large data sets.

2.1.2 Quantile estimation

This method is based on quantiles of stable distributions. Fama and Roll (1971) provided very simple estimates of symmetric ($\beta = 0, \mu = 0$) stable distributions when $\alpha > 1$. The statistical properties, however, Fama-Roll method are not known.

McCulloch (1986) extended and improved their method. He eliminated bias and obtained consistent estimators for all four stable parameters in terms of five sample quantiles (the 5th, 25th, 50th, 75th and 95th percentiles). If the data set is stable and if the sample set is large, this method gives reliable estimates of stable distributions.

2.1.3 Maximum likelihood method

The maximum likelihood (ML) estimation method for α -stable distributions does not differ from the other methods in theory. For a vector of observations $x = (x_1, \dots, x_n)$ the ML estimate of the parameter vector $\theta = (\alpha, \sigma, \beta, \mu)$ is obtained by maximizing the log-likelihood function:

$$L_{\theta}(x) = \sum_{i=1}^n \ln \tilde{f}(x_i; \theta) \quad (3)$$

where $\tilde{f}(\cdot; \theta)$ is the stable pdf. The tilde means that it is not known the explicit form of the density and has to approximate it numerically.

2.1.4 Characteristic function approaches

Given an independent and identically distributed (i.i.d.) random sample x_1, \dots, x_n of size n , define the sample characteristic function by:

$$\hat{\phi}(t) = \frac{1}{n} \sum_{j=1}^n \exp(itx_j). \quad (4)$$

Since $|\hat{\phi}(t)|$ is bounded by unity all moments of $\hat{\phi}(t)$ are finite and, for any fixed t , it is the sample average of i.i.d. random variables $\exp(itx_j)$. Hence, by the law of large numbers, $\hat{\phi}(t)$ is a consistent estimator of the characteristic function $\phi(t)$.

Press (1972) proposed a simple estimation method, called the method of moments, based on transformations of the characteristic function. The obtained estimates for this method are of poor quality and the method is not recommended for more than preliminary estimation.

Koutrouvelis (1980) presented a regression-type method which is based on characteristic function approaches. It starts with an initial estimate of the parameters and proceeds iteratively until some prespecified convergence criterion is satisfied. Each iteration consists of two weighted regression runs. The number of points to be used in these regressions depends on the sample size and starting values of α . Typically no more than two or three iterations are needed. The speed of the convergence, however, depends on the initial estimates and the convergence criterion.

This method is based on the following observations concerning the characteristic function $\phi(t)$. Firstly, from (2) it can be easily derived

$$\log(-\log|\phi(t)|^2) = \log(2\sigma^\alpha) + \alpha \log|t|. \quad (3)$$

The real and imaginary parts of $\phi(t)$ are for $\alpha \neq 1$ given by

$$\operatorname{Re} \phi(t) = \exp(-|\sigma t|^\alpha) \cos \left[\mu t + |\sigma t|^\alpha \beta \operatorname{sign}(t) \tan \frac{\pi\alpha}{2} \right],$$

and

$$\operatorname{Im} \phi(t) = \exp(-|\sigma t|^\alpha) \sin \left[\mu t + |\sigma t|^\alpha \beta \operatorname{sign}(t) \tan \frac{\pi\alpha}{2} \right].$$

Apart from considerations of principal values, the last two equations lead to

$$\arctan \left(\frac{\operatorname{Im} \phi(t)}{\operatorname{Re} \phi(t)} \right) = \mu t + \beta \sigma^\alpha \tan \frac{\pi\alpha}{2} \operatorname{sign}(t) |t|^\alpha. \quad (4)$$

Equation (2) relies only on α and σ suggest that it is estimated these parameters by regressing $y = \log(-\log|\phi_n(t)|^2)$ on $\omega = \log|t|$ in the model

$$y_k = m + \alpha \omega_k + e_k, \quad k = 1, 2, \dots, K, \quad (5)$$

where (t_k) is an appropriate set of real numbers, $m = \log(2\sigma^\alpha)$, and e_k denotes an error term. Koutrouvelis (1980) proposes to use $t_k = \frac{\pi k}{25}$, $k = 1, 2, \dots, K$; K ranging between 9 and 134 for different estimates of the parameter α and sample sizes.

Once $\hat{\alpha}$ and $\hat{\sigma}$ have been obtained, α and σ have been fixed at these values. Estimates of β and μ can be obtained by using (4).

3. Empirical Results

The data set covers daily returns of Turkish stock exchange indexes, gold series and stocks. The data consist of daily closing prices of these indicators, covering the period 2 January 2003 to 25 March 2008; i.e. 1311 trading days. In this study the behavior of these series will be examined using the continuously compound rates of return calculated by $R_t = \ln(p_t / p_{t-1})$ where p_t is the closing price at time t . Descriptive statistics of return series are reported in Table 1. As evidenced in Table 1, the distributions of six daily log price relatives are positive and all log price changes are leptokurtic, i.e., the actual kurtosis is higher than the kurtosis of the normal distribution. The Jarque-Bera (JB) statistic is used to investigate the normality of log price relatives. According to the JB statistics in Table 1, it is concluded that empirical distributions of all log price relatives of financial series are drawn from an underlying normal distribution is rejected.

Table 1. Descriptive Statistics of Financial Returns

FINANCIAL SERIES	SKEWNESS	KURTOSIS	JARQUE-BERA
ISE100	-0.436330*	7.612850*	1203.012*
ISE30	-0.230331*	6.642210*	736.2305*
GOLD	-0.282840*	6.240756*	595.2370*
AFYON	0.374230*	9.261259*	2167.114*
NETAS	-0.004289	6.170096*	548.5396*
BEKO	0.021895	7.330574*	1023.753*
TCELL	0.224369*	4.894773*	206.3223*
PIMAS	0.382705*	7.424181*	1100.358*
HURGZ	-0.153096	5.527770*	353.8841*
LOGO	0.681988*	7.518404*	1215.920*
KORDS	0.227375*	9.419559*	2260.707*
KOCH	-0.074591	5.503177*	341.6563*

Note: Asterisks denote rejection of the null hypothesis.

The findings of leptokurtosis and the significant deviation of the log price relatives from normality can be a symptom of nonlinear dynamics. Because of the normality is rejected, it is appropriate to use Stable distributions. In Table 2, Stable and Gaussian (normal) distribution fits and Hurst exponent (H) values of log price relatives of financial returns are given.

To make statistical analysis more sound, it is also compared both fits through Anderson-Darling and Kolmogorov test statistics (D'Agostino and Stephens, 1986). Since Anderson-Darling (A-D) and Kolmogorov test statistics for goodness-of-fit of distributions for stable distributions are all smaller than the Gaussian ones, financial returns are better fitted by stable distributions than the Gaussian distribution.

Table 2. Stable and Gaussian Fit of Financial Returns

	STABLE FIT						GAUSSIAN (NORMAL) FIT			
	Parameters				Test Statistics		Parameters		Test Statistics	
	α	σ	β	μ	A-D	K	Mean	Std.	A-D	K
ISE100	1.84	0.011	-0.385	0.010	0.2222	0.4235	0.012	0.0189	5.2965	1.6199
ISE30	1.86	0.013	-0.185	0.001	0.1813	0.5379	0.0012	0.0209	3.8331	1.4801
GOLD	1.78	0.006	0.172	0.001	0.6380	0.7018	0.0007	0.0109	6.8940	1.7882
AFYON	1.38	0.013	0.230	0.003	1.5096	2.4372	0.0021	0.0315	35.6294	4.2614
NETAS	1.78	0.015	0.432	0.000	2.9419	2.9040	0.0000	0.0247	9.5655	3.2816
BEKO	1.71	0.013	0.210	0.000	1.4705	2.5276	-0.0003	0.0240	12.8921	3.0291
TCELL	1.76	0.015	0.543	0.002	2.0735	2.6885	0.0016	0.0254	9.1673	3.2818
PIMAS	1.61	0.014	0.311	0.001	1.8579	2.5724	0.0012	0.0276	20.2504	3.3121
HURGZ	1.85	0.017	0.346	0.001	0.8919	2.3378	0.0007	0.0271	4.3793	2.4968
LOGO	1.58	0.015	0.378	0.002	2.4072	2.9263	0.0017	0.0310	27.0001	4.3479
KORDS	1.64	0.013	0.331	0.001	2.4351	2.9545	0.0008	0.0246	20.4571	3.2048
KOCH	1.88	0.016	0.735	0.001	1.7809	2.9124	0.0007	0.0256	4.4544	3.2248

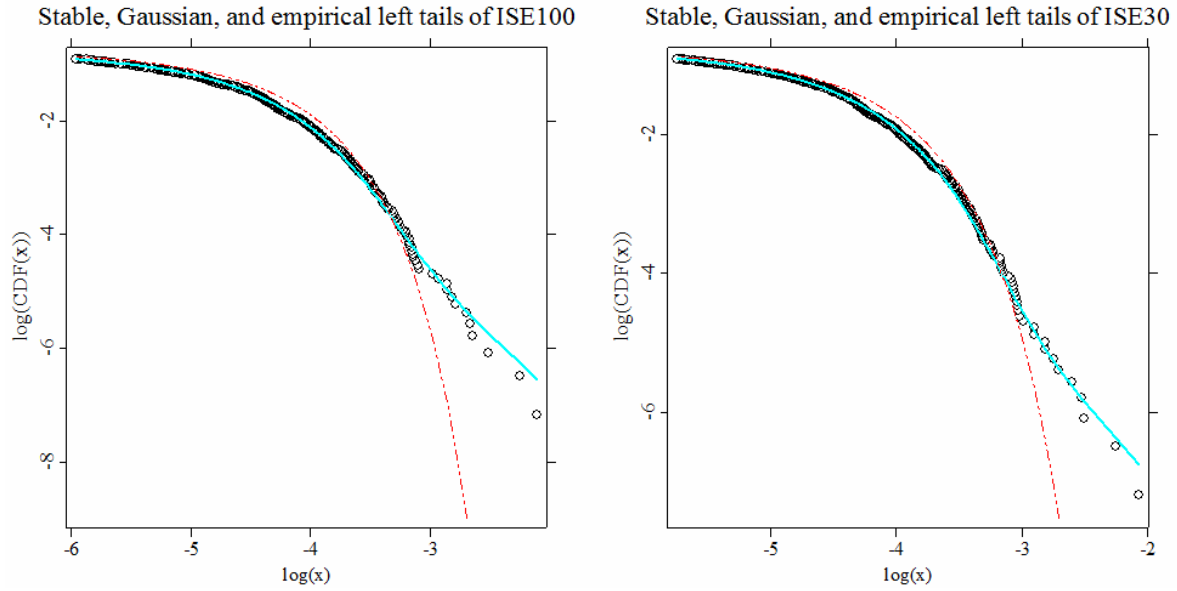


Figure 2. Magnification of the left tails fit of ISE100 and ISE30 returns on a double logarithmic scale clearly showing the superiority of the 1.84 and 1.86-stable law, respectively.

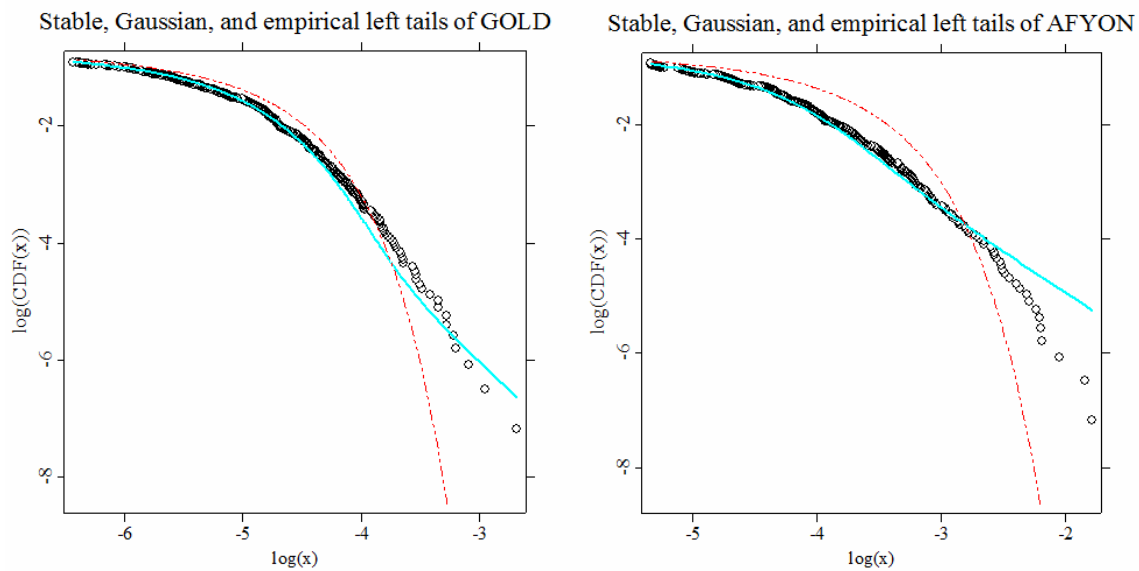


Figure 3. Magnification of the left tails fit of GOLD and AFYON returns on a double logarithmic scale clearly showing the superiority of the 1.78-stable law of GOLD series on the left panel and extreme returns are largely overestimated by the 1.38-stable law of AFYON series on the right panel.

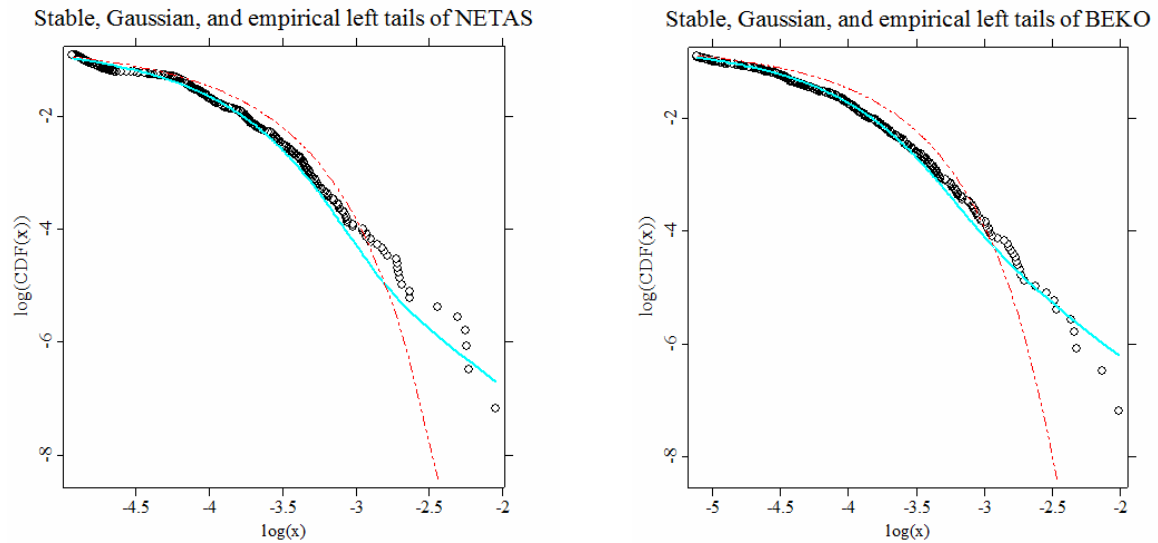


Figure 4. Magnification of the left tails fit of NETAS and BEKO returns on a double logarithmic scale. Extreme returns are largely underestimated by the 1.78-stable law of NETAS series on the left panel. On the right panel, it can be clearly seen the superiority of the 1.71-stable law of BEKO series.

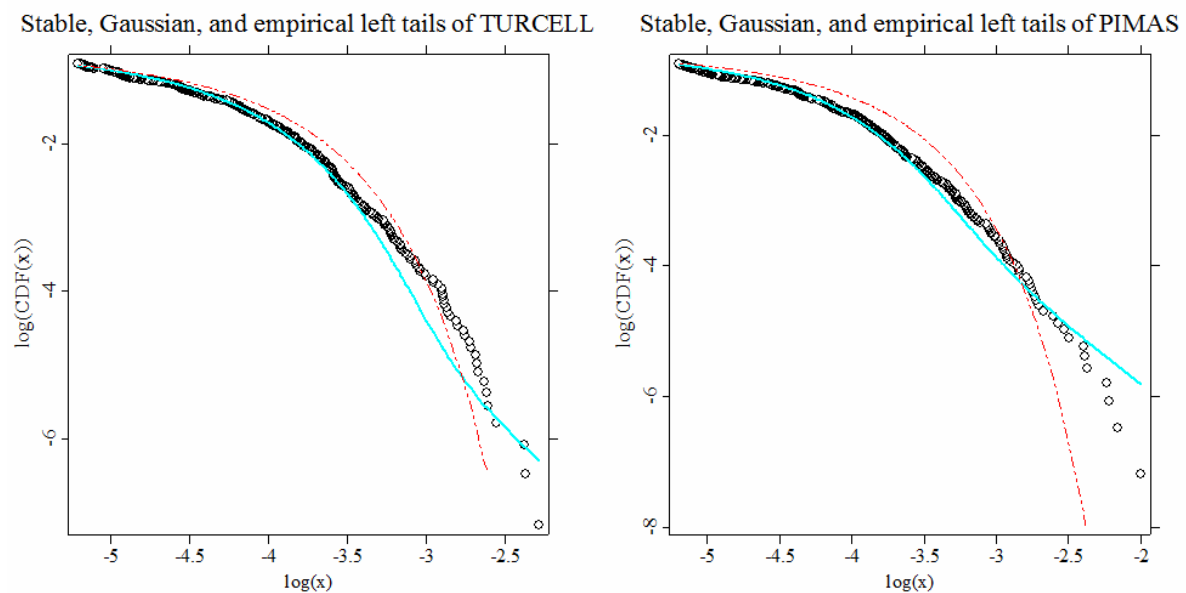


Figure 5. Magnification of the left tails fit of TURCELL and PIMAS returns on a double logarithmic scale. Extreme returns are largely underestimated by the 1.76-stable law of TURCELL series on the left panel. On the right panel, it can be clearly seen the superiority of the 1.61-stable law of PIMAS series.

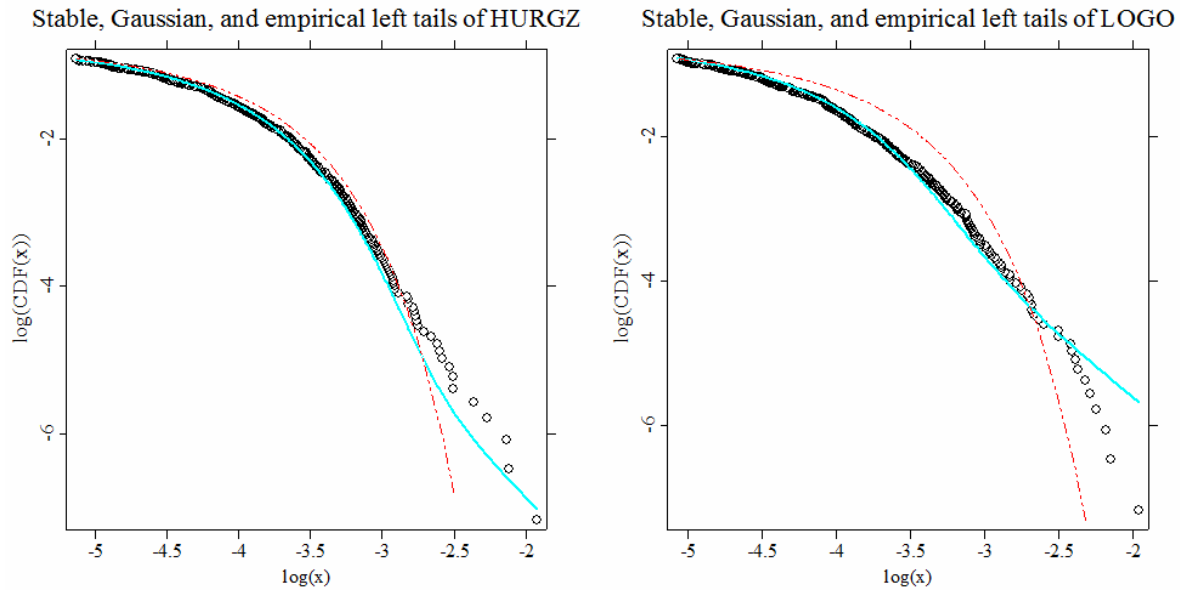


Figure 6. Magnification of the left tails fit of HURGZ and LOGO returns on a double logarithmic scale. Extreme returns are largely underestimated by the 1.85-stable law of HURGZ series on the left panel. On the right panel, it can be clearly seen the superiority of the 1.58-stable law of LOGO series.

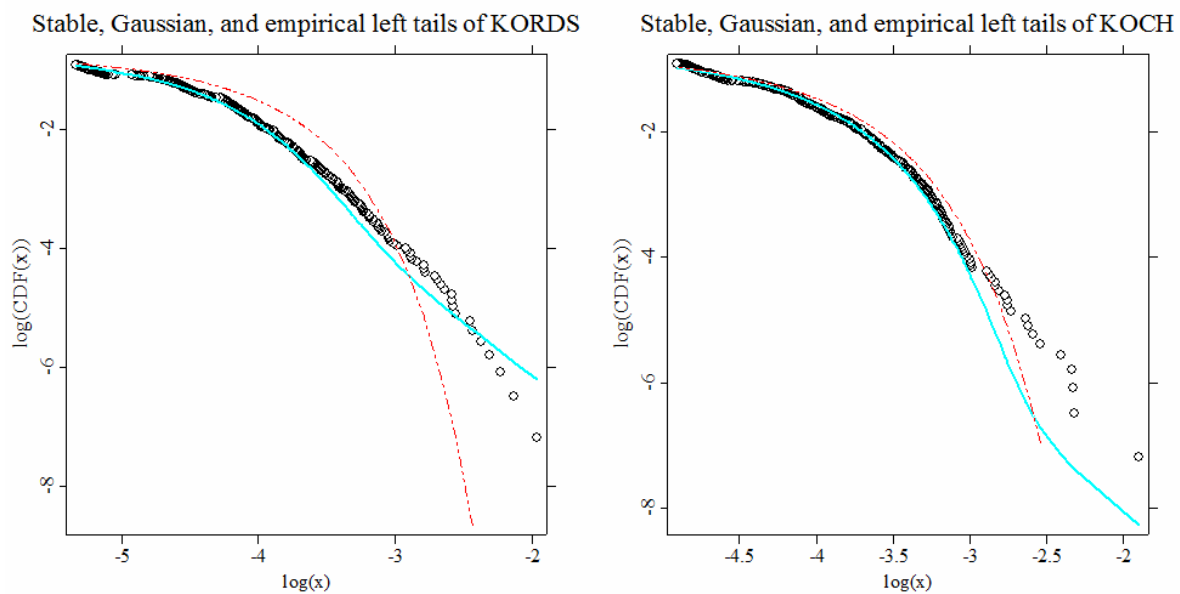


Figure 7. Magnification of the left tails fit of KORDS and KOCH returns on a double logarithmic scale. On the left panel, it can be clearly seen the superiority of the 1.64-stable law of KORDS series. Extreme returns are largely underestimated by the 1.88-stable law of KOCH series on the right panel.

Hurts exponents of financial series as discussed above are listed in Table 3.

Table3. Estimates of Stable Index and Hurst Exponent

FINANCIAL SERIES	STABLE INDEX(α)	HURST EXPONENT(H)
ISE100	1.84	0.54
ISE30	1.86	0.53
GOLD	1.78	0.56
AFYON	1.38	0.72
NETAS	1.78	0.56
BEKO	1.71	0.58
TCELL	1.76	0.56
PIMAS	1.61	0.62
HURGZ	1.85	0.54
LOGO	1.58	0.63
KORDS	1.64	0.60
KOCH	1.88	0.53

4. Conclusions

In this paper, Hurst exponent is estimated by α -stable distributions. Hurst exponent for all return series is greater than 0.5, this means that there is evidence of long memory behavior or persistence dependence in Turkish Stock Exchange and gold market. In left tails fits of financial returns, seven of them are fitted by stable distribution while the others are underestimated by stable distributions.

This kind of analysis can be valuable in examining a long memory process through the Hurst exponent. Once the stable index is estimated, Hurst exponent is fully computed. Given the estimates of the stable index, the Hurst exponent was evaluated which provides evidence of long memory behavior in Turkish financial returns.

For further analysis, these findings must be compared with the results of estimation degree of long memory process techniques, like ARFIMA (AutoRegressive Fractionally Moving Average) and GPH(Geweke, Porter-Hudak).

References

- [1] Akgiray, V., Booth, G.G., (1988), "The Stable-law Model of Stock Returns", *Journal of Business & Economic Statistics*, 6, 51-57.
- [2] Akgiray, V., Lamoureux C. G., (1989), "Estimation of Stable-Law Parameters: A Comparative Study", *Journal of Business and Economic Statistics*, 7, 85-93.
- [3] Arad, R. W., (1980), "Parameter Estimation for Symmetric Stable Distributions", *International Economic Review*, 21(1), 209-220.

- [4] D'Agostino, R. B. and Stephens, M. A. (1986), *Goodness-of-Fit Techniques*, Marcel Dekker, New York.
- [5] DuMouchel, W. H., (1973), "On the Asymptotic of the Maximum-Likelihood Estimate When Sampling From a Stable Distribution" , *The Annals of Statistics*, 1(5), 948-957.
- [6] Fama, E. , Roll, R. , (1968), "Some Properties of Symmetric Stable Distributions", *Journal of the American Statistical Association*, 63, 1968, 817-836.
- [7] Fama, E., Roll, R., (1971), "Parameter Estimates for Symmetric Stable Distributions", *Journal of the American Statistical Association*, 66, 331-338.
- [8] Koutrouvelis, I.A., (1980), "Regression-type Estimation of the Parameters of Stable Laws", *Journal of the American Statistical Association*, 75, 918-928.
- [9] McCulloch, J. H., (1986), "Simple consistent estimators of stable distribution parameters", *Communications in Statistics-Simulations*, 15, 74-81.
- [10] McCulloch, J.H., (1997), "Financial Applications of Stable Distributions", eds. Maddala, G. and Rao, C., *Handbook of Statistics*, 14, Elsevier Science.
- [11] Mitnik, S., Rachev, S. T., (1993), "Modelling Asset Returns with Alternative Stable Distributions", *Econometric Reviews*, 12, 261-330.
- [12] Panas, E., (2001), "Estimating fractal dimension using stable distributions and exploring long memory through ARFIMA models in Athens Stock Exchange", *Applied Financial Economics*, 11, 395-402.
- [13] Peters, E. E., (1989), "Fractal Structure in the Capital Markets", *Financial Analysts Journal*, July-August, 32-37.
- [14] Peters, E. E., (1992), "R/S Analysis Using Logarithmic Returns", *Financial Analysts Journal*, Nov.-Dec., 81-82.
- [15] Peters, E. E., (1996), *Chaos and order in the capital markets : a new view of cycles, prices, and market volatility*, 2nd Edition – New York : J. Wiley.
- [16] Stephens ,M.A., (1974), "EDF Statistics for Goodness of Fit and Some Comparisons", *Journal of the American Statistical Association*, 69(347), 730-737.
- [17] Watkins, T., (2002), "Pareto-Levy Stable Distributions", <http://www.sjsu.edu/faculty/watkins/stable.htm>

Caputo Fractional Ostrowski Type Inequalities

George A. Anastassiou
 Department of Mathematical Sciences
 University of Memphis
 Memphis, TN 38152 U.S.A.
 ganastss@memphis.edu

Abstract

Optimal upper bounds are given to the deviation of a value of a univariate or multivariate function of a Caputo fractional derivative related space from its average, over convex and compact subsets of \mathbb{R}^N , $N \geq 1$. In particular we work over closed intervals, rectangles, balls and spherical shells. These bounds involve the supremum and L_∞ norms of related univariate or multivariate Caputo fractional derivatives of the involved functions. The derived inequalities are sharp, namely they are attained by simple functions. This work has been motivated by the works of Ostrowski [1], 1938, and of the author's Anastassiou [2], 2003 and [3], 2007.

2000 AMS Mathematics Subject Classification: 26A33, 26D10, 26D15.

Key Words and Phrases: Ostrowski inequality, fractional inequality, Caputo fractional derivative, sharp inequality, fractional radial derivative.

1 Background

We start with

Definition 1. ([4]) Let $\nu \geq 0$, the operator J_a^ν , defined on $L_1(a, b)$ by

$$J_a^\nu f(x) := \frac{1}{\Gamma(\nu)} \int_a^x (x-t)^{\nu-1} f(t) dt \quad (1)$$

for $a \leq x \leq b$, is called the Riemann-Liouville fractional integral operator of order ν . For $\nu = 0$, we set $J_a^0 := I$, the identity operator. Here Γ stands for the gamma function. By Theorem 2.1 of [4], p. 13, $J_a^\nu f(x)$, $\nu > 0$, exists for almost all $x \in [a, b]$ and $J_a^\nu f \in L_1(a, b)$, where $f \in L_1(a, b)$.

Here $AC^n([a, b])$ is the space of functions with absolutely continuous $(n-1)$ -st derivative.

We need to mention

Definition 2. ([4], [5]) Let $\nu \geq 0$, $n := \lceil \nu \rceil$, $\lceil \cdot \rceil$ is the ceiling of the number, $f \in AC^n([a, b])$. We call Caputo fractional derivative

$$D_{*a}^\nu f(x) := \frac{1}{\Gamma(n-\nu)} \int_a^x (x-t)^{n-\nu-1} f^{(n)}(t) dt, \quad (2)$$

$\forall x \in [a, b]$.

The above function $D_{*a}^\nu f(x)$ exists almost everywhere for $x \in [a, b]$. If $\nu \in \mathbb{N}$, then $D_{*a}^\nu f = f^{(\nu)}$ the ordinary derivative, also it is $D_{*a}^0 f = f$.

We need

Theorem 3. (Taylor expansion for Caputo derivatives, [4], p. 40)

Assume $\nu \geq 0$, $n := \lceil \nu \rceil$, and $f \in AC^n([a, b])$. Then

$$f(x) = \sum_{k=0}^{n-1} \frac{f^{(k)}(a)}{k!} (x-a)^k + \frac{1}{\Gamma(\nu)} \int_a^x (x-t)^{\nu-1} D_{*a}^\nu f(t) dt, \quad (3)$$

$\forall x \in [a, b]$.

Additionally assume

$$f^{(k)}(a) = 0, \quad k = 1, \dots, n-1,$$

then

$$f(x) - f(a) = \frac{1}{\Gamma(\nu)} \int_a^x (x-t)^{\nu-1} D_{*a}^\nu f(t) dt. \quad (4)$$

Next we mention the multivariate analog of (3) and (4) (see [6])

Remark 4. Let Q be a compact and convex subset of \mathbb{R}^k , $k \geq 2$; $z := (z_1, \dots, z_k)$, $x_0 := (x_{01}, \dots, x_{0k}) \in Q$. Let $f \in C^n(Q)$, $n \in \mathbb{N}$.

Set

$$\begin{aligned} g_z(t) &:= f(x_0 + t(z - x_0)), \\ 0 \leq t \leq 1; \quad g_z(0) &= f(x_0), \quad g_z(1) = f(z). \end{aligned} \quad (5)$$

Then

$$g_z^{(j)}(t) = \left[\left(\sum_{i=1}^k (z_i - x_{0i}) \frac{\partial}{\partial x_i} \right)^j f \right] (x_0 + t(z - x_0)), \quad (6)$$

$j = 0, 1, 2, \dots, n$, and

$$g_z^{(n)}(0) = \left[\left(\sum_{i=1}^k (z_i - x_{0i}) \frac{\partial}{\partial x_i} \right)^n f \right] (x_0). \quad (7)$$

If all

$$f_\alpha(x_0) := \frac{\partial^\alpha f}{\partial x^\alpha}(x_0) = 0, \quad \alpha := (\alpha_1, \dots, \alpha_k),$$

$$\alpha_i \in \mathbb{Z}^+, i = 1, \dots, k; \quad |\alpha| := \sum_{i=1}^k \alpha_i =: l,$$

then

$$g_z^{(l)}(0) = 0, \text{ where } l \in \{0, 1, \dots, n\}.$$

We quote that

$$g'_z(t) = \sum_{i=1}^k (z_i - x_{0i}) \frac{\partial f}{\partial x_i}(x_0 + t(z - x_0)). \quad (8)$$

when $f \in C^2(Q)$, $Q \subseteq \mathbb{R}^2$, we have

$$\begin{aligned} g''_z(t) &= (z_1 - x_{01})^2 \frac{\partial^2 f}{\partial x_1^2}(x_0 + t(z - x_0)) + 2(z_1 - x_{01}) \\ &\quad (z_2 - x_{02}) \frac{\partial^2 f}{\partial x_1 \partial x_2}(x_0 + t(z - x_0)) \\ &\quad + (z_2 - x_{02})^2 \frac{\partial^2 f}{\partial x_2^2}(x_0 + t(z - x_0)), \end{aligned} \quad (9)$$

etc.

Clearly here $g_z \in C^n([0, 1])$, hence $g_z \in AC^n([0, 1])$.

In [6] we proved the following general multivariate fractional Taylor formula.

Theorem 5. ([6]) *Let $\nu > 0$, $n = \lceil \nu \rceil$, $f \in C^n(Q)$, where Q is a compact and convex subset of \mathbb{R}^k , $k \geq 2$; $z := (z_1, \dots, z_k)$, $x_0 := (x_{01}, \dots, x_{0k}) \in Q$. Then*

$$\begin{aligned} 1) \quad f(z) &= f(x_0) + \sum_{i=1}^k (z_i - x_{0i}) \frac{\partial f(x_0)}{\partial x_i} \\ &\quad + \sum_{l=2}^{n-1} \frac{\left[\left(\sum_{i=1}^k (z_i - x_{0i}) \frac{\partial}{\partial x_i} \right)^l f \right](x_0)}{l!} + \\ &\quad \frac{1}{\Gamma(\nu)} \int_0^1 (1-t)^{\nu-1} \left[J_0^{n-\nu} \left\{ \left[\left(\sum_{i=1}^k (z_i - x_{0i}) \frac{\partial}{\partial x_i} \right)^n \right. \right. \right. \\ &\quad \left. \left. \left. f \right](x_0 + t(z - x_0)) \right\} \right] dt. \end{aligned} \quad (10)$$

Additionally assume that

$$f_\alpha(x_0) = 0, \quad \alpha := (\alpha_1, \dots, \alpha_k), \quad \alpha_i \in \mathbb{Z}^+, \quad i = 1, \dots, k;$$

$$|\alpha| := \sum_{i=1}^k \alpha_i =: r, \quad r = 1, \dots, n-1, \text{ then}$$

$$\begin{aligned}
2) \quad f(z) - f(x_0) &= \frac{1}{\Gamma(\nu)} \int_0^1 (1-t)^{\nu-1} [J_0^{n-\nu} \\
&\quad \left\{ \left[\left(\sum_{i=1}^k (z_i - x_{0i}) \frac{\partial}{\partial x_i} \right)^n f \right] \right. \\
&\quad \left. (x_0 + t(z - x_0)) \right\}] dt =: R_\nu.
\end{aligned} \tag{11}$$

Remark 6. ([6]) (on Theorem 5)

Set

$$\begin{aligned}
G_\nu(t) &:= J_0^{n-\nu} \left\{ \left[\left(\sum_{i=1}^k (z_i - x_{0i}) \frac{\partial}{\partial x_i} \right)^n f \right] \right. \\
&\quad \left. (x_0 + t(z - x_0)) \right\}, \quad t \in [0, 1],
\end{aligned} \tag{12}$$

which shows up in R_ν and is continuous, see Proposition 114 of [7] and $R_\nu \in \mathbb{R}$.

So we can rewrite

$$R_\nu = \frac{1}{\Gamma(\nu)} \int_0^1 (1-t)^{\nu-1} G_\nu(t) dt, \quad \nu > 0. \tag{13}$$

We mention

Theorem 7. ([6]) *All as in Theorem 5. Let R_ν be the remainder in (10) (same as in (11)), and $G_\nu(t)$, $t \in [0, 1]$ as in (12), $\nu \geq 1$. Then*

$$\begin{aligned}
|R_\nu| &\leq \min \left\{ \frac{\|G_\nu\|_{L_1([0,1])}}{\Gamma(\nu)}, \frac{\|G_\nu\|_{L_q([0,1])}}{\Gamma(\nu)(p(\nu-1)+1)^{1/p}} \right. \\
&\quad \left. , \frac{\|G_\nu\|_{L_2([0,1])}}{\Gamma(\nu)\sqrt{2\nu-1}}, \frac{\|G_\nu\|_{\infty,[0,1]}}{\Gamma(\nu+1)} \right\} =: \Lambda_\nu,
\end{aligned} \tag{14}$$

where $p, q > 1 : \frac{1}{p} + \frac{1}{q} = 1$.

2 Univariate Results

We present our first Ostrowski type result

Theorem 8. *Let $\nu \geq 0$, $n = \lceil \nu \rceil$, and $f \in AC^n([a, b])$. Assume that*

$$f^{(k)}(a) = 0, \quad k = 1, \dots, n-1, \quad \text{and } D_{*a}^\nu f \in L_\infty([a, b]).$$

Then

$$\left| \frac{1}{b-a} \int_a^b f(x) dx - f(a) \right| \leq \frac{\|D_{*a}^\nu f\|_{\infty,[a,b]}}{\Gamma(\nu+2)} (b-a)^\nu. \tag{15}$$

Proof. By (4) we get

$$\begin{aligned} |f(x) - f(a)| &\leq \frac{1}{\Gamma(\nu)} \int_a^x (x-t)^{\nu-1} |D_{*a}^\nu f(t)| dt \\ &\leq \frac{1}{\Gamma(\nu)} \left(\int_a^x (x-t)^{\nu-1} dt \right) \|D_{*a}^\nu f\|_{\infty, [a, b]} \\ &= \frac{(x-a)^\nu}{\Gamma(\nu+1)} \|D_{*a}^\nu f\|_{\infty, [a, b]}. \end{aligned}$$

I.e. we have

$$|f(x) - f(a)| \leq \frac{\|D_{*a}^\nu f\|_{\infty, [a, b]}}{\Gamma(\nu+1)} (x-a)^\nu, \quad (16)$$

$\forall x \in [a, b]$.

Therefore we get

$$\begin{aligned} \left| \frac{1}{b-a} \int_a^b f(x) dx - f(a) \right| &= \left| \frac{1}{b-a} \int_a^b (f(x) - f(a)) dx \right| \\ &\leq \frac{1}{b-a} \int_a^b |f(x) - f(a)| dx \stackrel{(16)}{\leq} \frac{\|D_{*a}^\nu f\|_{\infty, [a, b]}}{\Gamma(\nu+1)} \frac{(b-a)^\nu}{(b-a)} \\ &= \frac{\|D_{*a}^\nu f\|_{\infty, [a, b]}}{\Gamma(\nu+1)} (b-a)^\nu. \end{aligned}$$

This proves (15). \square

We continue with

Theorem 9. Let $\nu \geq 1$, $n = \lceil \nu \rceil$, and $f \in AC^n([a, b])$. Assume that

$$f^{(k)}(a) = 0, \quad k = 1, \dots, n-1, \quad \text{and } D_{*a}^\nu f \in L_1([a, b]).$$

Then

$$\left| \frac{1}{b-a} \int_a^b f(x) dx - f(a) \right| \leq \frac{\|D_{*a}^\nu f\|_{L_1([a, b])}}{\Gamma(\nu+1)} (b-a)^{\nu-1}. \quad (17)$$

Proof. Again by (4) we get

$$\begin{aligned} |f(x) - f(a)| &\leq \frac{1}{\Gamma(\nu)} \int_a^x (x-t)^{\nu-1} |D_{*a}^\nu f(t)| dt \\ &\leq \frac{1}{\Gamma(\nu)} (x-a)^{\nu-1} \int_a^x |D_{*a}^\nu f(t)| dt \leq \\ &\quad \frac{1}{\Gamma(\nu)} (x-a)^{\nu-1} \|D_{*a}^\nu f\|_{L_1([a, b])}. \end{aligned}$$

I.e. we have

$$|f(x) - f(a)| \leq \frac{\|D_{*a}^\nu f\|_{L_1([a,b])}}{\Gamma(\nu)} (x-a)^{\nu-1}, \quad (18)$$

$\forall x \in [a, b]$.

Therefore we get

$$\begin{aligned} \left| \frac{1}{b-a} \int_a^b f(x) dx - f(a) \right| &\leq \frac{1}{b-a} \int_a^b |f(x) - f(a)| dx \stackrel{(18)}{\leq} \\ &\frac{\|D_{*a}^\nu f\|_{L_1([a,b])}}{\Gamma(\nu)(b-a)} \int_a^b (x-a)^{\nu-1} dx = \\ &\frac{\|D_{*a}^\nu f\|_{L_1([a,b])}}{\Gamma(\nu+1)} (b-a)^{\nu-1}. \end{aligned}$$

This proves (17). \square

We also give

Theorem 10. Let $p, q > 1 : \frac{1}{p} + \frac{1}{q} = 1$, and $\nu > 1 - \frac{1}{p}$, $n = \lceil \nu \rceil$, and $f \in AC^n([a, b])$. Assume that

$$f^{(k)}(a) = 0, \quad k = 1, \dots, n-1, \quad \text{and } D_{*a}^\nu f \in L_q([a, b]).$$

Then

$$\begin{aligned} \left| \frac{1}{b-a} \int_a^b f(x) dx - f(a) \right| &\leq \\ &\frac{\|D_{*a}^\nu f\|_{L_q([a,b])}}{\Gamma(\nu)(p(\nu-1)+1)^{1/p} \left(\nu + \frac{1}{p}\right)} (b-a)^{\nu-1+\frac{1}{p}}. \end{aligned} \quad (19)$$

Proof. Again by (4) we obtain

$$\begin{aligned} |f(x) - f(a)| &\leq \frac{1}{\Gamma(\nu)} \int_a^x (x-t)^{\nu-1} |D_{*a}^\nu f(t)| dt \\ &\leq \frac{1}{\Gamma(\nu)} \left(\int_a^x (x-t)^{p(\nu-1)} dt \right)^{1/p} \left(\int_a^x |D_{*a}^\nu f(t)|^q dt \right)^{1/q} \leq \\ &\frac{1}{\Gamma(\nu)} \frac{(x-a)^{\nu-1+\frac{1}{p}}}{(p(\nu-1)+1)^{1/p}} \|D_{*a}^\nu f\|_{L_q([a,b])}. \end{aligned}$$

I.e. we have

$$|f(x) - f(a)| \leq \frac{\|D_{*a}^\nu f\|_{L_q([a,b])}}{\Gamma(\nu)(p(\nu-1)+1)^{1/p}} (x-a)^{\nu-1+\frac{1}{p}}, \quad (20)$$

$\forall x \in [a, b]$.

Consequently we get

$$\begin{aligned} \left| \frac{1}{b-a} \int_a^b f(x) dx - f(a) \right| &\leq \frac{1}{b-a} \int_a^b |f(x) - f(a)| dx \stackrel{(20)}{\leq} \\ &\frac{\|D_{*a}^\nu f\|_{L_q([a,b])}}{\Gamma(\nu)(p(\nu-1)+1)^{1/p}(b-a)} \int_a^b (x-a)^{\nu-1+\frac{1}{p}} dx \\ &= \frac{\|D_{*a}^\nu f\|_{L_q([a,b])}}{\Gamma(\nu)(p(\nu-1)+1)^{1/p}\left(\nu+\frac{1}{p}\right)} (b-a)^{\nu-1+\frac{1}{p}}. \end{aligned}$$

This proves (19). \square

Corollary 11. (to Theorem 10; $p = q = 2$ case) Let $\nu > \frac{1}{2}$, $n = \lceil \nu \rceil$, and $f \in AC^n([a, b])$. Assume that

$$f^{(k)}(a) = 0, \quad k = 1, \dots, n-1, \quad \text{and } D_{*a}^\nu f \in L_2([a, b]).$$

Then

$$\begin{aligned} \left| \frac{1}{b-a} \int_a^b f(x) dx - f(a) \right| &\leq \\ &\frac{\|D_{*a}^\nu f\|_{L_2([a,b])}}{\Gamma(\nu)(\sqrt{2\nu-1})(\nu+\frac{1}{2})} (b-a)^{\nu-\frac{1}{2}}. \end{aligned} \quad (21)$$

Proof. Apply (19). \square

We finish this section with

Proposition 12. Inequality (15) is sharp, namely it is attained by

$$f(x) = (x-a)^\nu, \quad \nu > 0, \quad \nu \notin \mathbb{N}, \quad x \in [a, b].$$

Proof. Here the function

$$f(x) = (x-a)^\nu, \quad \nu > 0, \quad \nu \notin \mathbb{N}, \quad x \in [a, b],$$

belongs to $AC^n([a, b])$, $n = \lceil \nu \rceil$. We observe that

$$\begin{aligned} f'(x) &= \nu(x-a)^{\nu-1}, \quad f''(x) = \nu(\nu-1)(x-a)^{\nu-2}, \dots, \\ f^{(n-1)}(x) &= \nu(\nu-1)(\nu-2)\dots(\nu-n+2)(x-a)^{\nu-n+1} \\ f^{(n)}(x) &= \nu(\nu-1)\dots(\nu-n+1)(x-a)^{\nu-n}. \end{aligned}$$

Thus

$$D_{*a}^\nu f(x) \stackrel{(2)}{=} \frac{1}{\Gamma(n-\nu)} \int_a^x (x-t)^{(n-\nu)-1}$$

$$\begin{aligned}
& \nu(\nu-1)\dots(\nu-n+1)(t-a)^{\nu-n} dt \\
&= \frac{\nu(\nu-1)\dots(\nu-n+1)}{\Gamma(n-\nu)} \int_a^x (x-t)^{(n-\nu)-1} (t-a)^{(\nu-n+1)-1} dt \\
&\quad (\text{by Whittaker and Watson [8], p. 256; notice that } n-\nu, \nu-n+1 > 0) \\
&= \frac{\nu(\nu-1)\dots(\nu-n+1)}{\Gamma(n-\nu)} \frac{\Gamma(n-\nu)\Gamma(\nu-n+1)}{\Gamma(1)} \\
&= \nu(\nu-1)\dots(\nu-n+1)\Gamma(\nu-n+1) = \Gamma(\nu+1).
\end{aligned}$$

I.e.

$$D_{*a}^\nu f(x) = \Gamma(\nu+1), \quad \forall x \in [a, b]. \quad (22)$$

Also we see that

$$f^{(k)}(a) = 0, \quad k = 0, 1, \dots, n-1, \quad \text{and } D_{*a}^\nu f \in L_\infty([a, b]).$$

So f fulfills all the assumptions of Theorem 8.

Next we find

$$R.H.S \text{ (15)} = \frac{\Gamma(\nu+1)}{\Gamma(\nu+2)} (b-a)^\nu = \frac{(b-a)^\nu}{(\nu+1)}. \quad (23)$$

Furthermore we have

$$\begin{aligned}
L.H.S \text{ (15)} &= \left| \frac{1}{b-a} \int_a^b (x-a)^\nu dx \right| \\
&= \frac{1}{(b-a)} \frac{(b-a)^{\nu+1}}{(\nu+1)} = \frac{(b-a)^\nu}{(\nu+1)}.
\end{aligned} \quad (24)$$

Clearly $R.H.S \text{ (15)} = L.H.S \text{ (15)}$, proving the claim. \square

3 Multivariate Results

We present our first multivariate Ostrowski type fractional inequality in the Caputo sense.

Theorem 13. Let $\nu > 0$, $n = \lceil \nu \rceil$, $f \in C^n(Q)$, where Q is a non-empty compact and convex subset of \mathbb{R}^k , $k \geq 2$; $z := (z_1, \dots, z_k)$, $x_0 := (x_{01}, \dots, x_{0k}) \in Q$. Further assume that

$$f_\alpha(x_0) = 0, \quad \alpha := (\alpha_1, \dots, \alpha_k), \quad \alpha_i \in \mathbb{Z}^+, \quad i = 1, \dots, k;$$

$$|\alpha| := \sum_{i=1}^k \alpha_i =: r, \quad r = 1, \dots, n-1;$$

where $x_0 \in Q$ is fixed.

Then

$$\left| \frac{\int_Q f(z) dz}{Vol(Q)} - f(x_0) \right| \leq \left(\frac{\max_{|\alpha|=n} \|J_0^{n-\nu} f_\alpha(x_0 + t(z-x_0))\|_{\infty, (t,z) \in [0,1] \times Q}}{\Gamma(\nu+1) Vol(Q)} \right) \int_Q \|z - x_0\|_{l_1}^n dz. \quad (25)$$

Proof. Notice that (see (12))

$$\begin{aligned} |G_\nu(t)| &= \left| \left[\left(\sum_{i=1}^k (z_i - x_{0i}) J_0^{n-\nu} \frac{\partial}{\partial x_i} \right)^n f \right] \right. \\ &\quad \left. (x_0 + t(z - x_0)) \right| \leq (\|z - x_0\|_{l_1})^n \\ \max_{|\alpha|=n} \|J_0^{n-\nu} f_\alpha(x_0 + t(z - x_0))\|_{\infty, (t,z) \in [0,1] \times Q}, \\ &\quad \forall z \in Q, x_0 \in Q \text{ being fixed, } 0 \leq t \leq 1. \end{aligned} \quad (26)$$

Hence

$$\begin{aligned} \|G_\nu\|_{\infty, t \in [0,1]} &\leq (\|z - x_0\|_{l_1})^n \\ \max_{|\alpha|=n} \|J_0^{n-\nu} f_\alpha(x_0 + t(z - x_0))\|_{\infty, (t,z) \in [0,1] \times Q}, \end{aligned} \quad (27)$$

and by (11) and (14) we get

$$\begin{aligned} |f(z) - f(x_0)| &\leq \Lambda_\nu \leq \frac{\|G_\nu\|_{\infty, t \in [0,1]}}{\Gamma(\nu+1)} \stackrel{(27)}{\leq} \frac{(\|z - x_0\|_{l_1})^n}{\Gamma(\nu+1)} \\ \max_{|\alpha|=n} \|J_0^{n-\nu} f_\alpha(x_0 + t(z - x_0))\|_{\infty, (t,z) \in [0,1] \times Q}, \end{aligned} \quad (28)$$

$\forall z \in Q$.

Consequently we obtain

$$\begin{aligned} \left| \frac{\int_Q f(z) dz}{Vol(Q)} - f(x_0) \right| &= \left| \frac{\int_Q (f(z) - f(x_0)) dz}{Vol(Q)} \right| \leq \\ &\frac{1}{Vol(Q)} \int_Q |f(z) - f(x_0)| dz \leq \\ &\left(\frac{\max_{|\alpha|=n} \|J_0^{n-\nu} f_\alpha(x_0 + t(z - x_0))\|_{\infty, (t,z) \in [0,1] \times Q}}{\Gamma(\nu+1) Vol(Q)} \right) \int_Q \|z - x_0\|_{l_1}^n dz, \end{aligned} \quad (29)$$

proving the claim. \square

We further have

Theorem 14. Let $f : [a, b] \times [c, d] \rightarrow \mathbb{R}$ be Lebesgue integrable, also $f(a, \cdot)$ integrable on $[c, d]$ and $f(\cdot, y) \in AC^n([a, b])$, $\forall y \in [c, d]$, where $n = \lceil \nu \rceil$, $\nu \geq 0$, and $\frac{\partial^k}{\partial x^k} f(a, y) = 0$, $k = 1, \dots, n-1$, $\forall y \in [c, d]$. Here $\|\cdot\|_{\infty, [a, b] \times [c, d]}$ is the supremum norm.

Further suppose that $\frac{\partial_{*a}^\nu f(x, y)}{\partial x^\nu} \in B([a, b] \times [c, d])$ bounded functions, $(x, y) \in [a, b] \times [c, d]$.

Then

$$\left| \frac{1}{(b-a)(d-c)} \int_{[a, b] \times [c, d]} f(x, y) dx dy - f(a, c) \right| \leq \frac{1}{(d-c)} \int_{[c, d]} |f(a, y) - f(a, c)| dy + \frac{(b-a)^\nu}{\Gamma(\nu+2)} \left\| \frac{\partial_{*a}^\nu f}{\partial x^\nu} \right\|_{\infty, [a, b] \times [c, d]}. \quad (30)$$

Proof. Since $f(\cdot, y) \in AC^n([a, b])$, $\forall y \in [c, d]$ and $\frac{\partial^k}{\partial x^k} f(a, y) = 0$, $k = 1, \dots, n-1$, $\forall y \in [c, d]$, by (4) we have

$$f(x, y) - f(a, y) = \frac{1}{\Gamma(\nu)} \int_a^x (x-t)^{\nu-1} \frac{\partial_{*a}^\nu f}{\partial x^\nu}(t, y) dt, \quad (31)$$

$\forall x \in [a, b]$, $\forall y \in [c, d]$.

Since

$$\frac{\partial_{*a}^\nu f}{\partial x^\nu}(x, y) \in B([a, b] \times [c, d]),$$

we obtain

$$|f(x, y) - f(a, y)| \leq \frac{(x-a)^\nu}{\Gamma(\nu+1)} \left\| \frac{\partial_{*a}^\nu f}{\partial x^\nu} \right\|_{\infty, [a, b] \times [c, d]}, \quad (32)$$

$\forall x \in [a, b]$, $\forall y \in [c, d]$.

But it holds

$$\begin{aligned} |f(x, y) - f(a, c)| &\leq |f(x, y) - f(a, y)| \\ &+ |f(a, y) - f(a, c)| \leq |f(a, y) - f(a, c)| + \\ &\frac{(x-a)^\nu}{\Gamma(\nu+1)} \left\| \frac{\partial_{*a}^\nu f}{\partial x^\nu} \right\|_{\infty, [a, b] \times [c, d]}, \end{aligned} \quad (33)$$

$\forall x \in [a, b]$, $\forall y \in [c, d]$.

Consequently we have

$$\begin{aligned} \left| \frac{1}{(b-a)(d-c)} \int_{[a, b] \times [c, d]} f(x, y) dx dy - f(a, c) \right| &= \\ \frac{1}{(b-a)(d-c)} \left| \int_{[a, b] \times [c, d]} (f(x, y) - f(a, c)) dx dy \right| &\leq \end{aligned} \quad (34)$$

$$\begin{aligned}
& \frac{1}{(b-a)(d-c)} \int_{[a,b] \times [c,d]} |f(x, y) - f(a, c)| dx dy \stackrel{(33)}{\leq} \\
& \frac{1}{(b-a)(d-c)} \int_{[a,b] \times [c,d]} |f(a, y) - f(a, c)| dx dy + \\
& \frac{1}{(b-a)(d-c)} \frac{1}{\Gamma(\nu+1)} \left\| \frac{\partial_{*a}^\nu f}{\partial x^\nu} \right\|_{\infty, [a,b] \times [c,d]} \\
& \int_{[a,b] \times [c,d]} (x-a)^\nu dx dy = \frac{1}{(d-c)} \int_{[c,d]} |f(a, y) - f(a, c)| dy \\
& + \frac{(b-a)^\nu}{\Gamma(\nu+2)} \left\| \frac{\partial_{*a}^\nu f}{\partial x^\nu} \right\|_{\infty, [a,b] \times [c,d]}, \tag{36}
\end{aligned}$$

proving the claim. \square

One can prove similar to (30) inequalities in more than two variables.

Next we study fractional Ostrowski type inequalities over balls and spherical shells. For that we need to make

Remark 15. We define the ball

$$B(0, R) := \{x \in \mathbb{R}^N : |x| < R\} \subseteq \mathbb{R}^N, \quad N \geq 2, \quad R > 0,$$

and the sphere

$$S^{N-1} := \{x \in \mathbb{R}^N : |x| = 1\},$$

where $|\cdot|$ is the euclidean norm.

Let $d\omega$ be the element of surface measure on S^{N-1} and let

$$\omega_N = \int_{S^{N-1}} d\omega = \frac{2\pi^{N/2}}{\Gamma(N/2)}.$$

For $x \in \mathbb{R}^N - \{0\}$ we can write uniquely $x = r\omega$, where $r = |x| > 0$ and $\omega = \frac{x}{r} \in S^{N-1}$, $|\omega| = 1$. Note that

$$\int_{B(0,R)} dy = \frac{\omega_N R^N}{N}$$

is the Lebesgue measure of the ball. Following [9], pp. 149-150, exercise 6 and [10], pp. 87-88, Theorem 5.2.2 we can write for $F : \overline{B(0, R)} \rightarrow \mathbb{R}$ Lebesgue integrable function that

$$\int_{B(0,R)} F(x) dx = \int_{S^{N-1}} \left(\int_0^R F(r\omega) r^{N-1} dr \right) d\omega, \tag{37}$$

we use a lot this formula.

Initially the function $f : \overline{B(0, R)} \rightarrow \mathbb{R}$ is radial, i.e. there exists a function g such that $f(x) = g(r)$, where $r = |x|$, $r \in [0, R]$, $\forall x \in \overline{B(0, R)}$. Here we assume that $g \in AC^n([0, R])$, $n = \lceil \nu \rceil$, $\nu \geq 0$, and $g^{(k)}(0) = 0$, $k = 1, \dots, n-1$.

By (4) we get

$$g(s) - g(0) = \frac{1}{\Gamma(\nu)} \int_0^s (s-t)^{\nu-1} D_{*0}^\nu g(t) dt, \quad (38)$$

$\forall s \in [0, R]$.

Further assume that $D_{*0}^\nu g \in L_\infty([0, R])$.

By (38) we obtain

$$|g(s) - g(0)| \leq \frac{s^\nu}{\Gamma(\nu+1)} \|D_{*0}^\nu g\|_{\infty, [0, R]}, \quad (39)$$

$\forall s \in [0, R]$.

Next we observe that

$$\begin{aligned} & \left| f(0) - \frac{\int_{B(0, R)} f(y) dy}{\text{Vol}(B(0, R))} \right| = \\ & \left| g(0) - \frac{\int_{S^{N-1}} \left(\int_0^R g(s) s^{N-1} ds \right) d\omega}{\int_{S^{N-1}} \left(\int_0^R s^{N-1} ds \right) d\omega} \right| = \end{aligned} \quad (40)$$

$$\begin{aligned} & \left| g(0) - \frac{N}{R^N} \int_0^R g(s) s^{N-1} ds \right| = \frac{N}{R^N} \\ & \left| \int_0^R s^{N-1} (g(0) - g(s)) ds \right| \leq \end{aligned} \quad (41)$$

$$\begin{aligned} & \frac{N}{R^N} \int_0^R s^{N-1} |g(0) - g(s)| ds \stackrel{(39)}{\leq} \\ & \frac{N}{R^N} \frac{\|D_{*0}^\nu g\|_{\infty, [0, R]}}{\Gamma(\nu+1)} \int_0^R s^{N-1} s^\nu ds = \end{aligned} \quad (42)$$

$$\frac{N}{R^N} \frac{\|D_{*0}^\nu g\|_{\infty, [0, R]}}{\Gamma(\nu+1)} \frac{R^{\nu+N}}{(\nu+N)} = \frac{\left(\|D_{*0}^\nu g\|_{\infty, [0, R]} \right) N R^\nu}{\Gamma(\nu+1)(\nu+N)} \quad (43)$$

I.e., we have proved that

$$\begin{aligned} & \left| f(0) - \frac{\int_{B(0, R)} f(y) dy}{\text{Vol}(B(0, R))} \right| = \\ & \left| g(0) - \frac{N}{R^N} \int_0^R g(s) s^{N-1} ds \right| \leq \frac{\left(\|D_{*0}^\nu g\|_{\infty, [0, R]} \right) N R^\nu}{\Gamma(\nu+1)(\nu+N)}. \end{aligned} \quad (44)$$

The last inequality (44) is sharp, namely it is attained by $\bar{g}(r) = r^\nu$, $\nu > 0$, $r \in [0, R]$. Indeed by (2) we get

$$D_{*0}^\nu \bar{g}(r) = \Gamma(\nu+1),$$

and

$$\|D_{*0}^\nu \bar{g}\|_{\infty, [0, R]} = \Gamma(\nu + 1).$$

So that in that case

$$R.H.S \text{ (44)} = \frac{NR^\nu}{\nu + N}. \quad (45)$$

But

$$\begin{aligned} L.H.S \text{ (44)} &= \frac{N}{R^N} \int_0^R s^{\nu+N-1} ds \\ &= \frac{N}{R^N} \frac{R^{\nu+N}}{(\nu + N)} = \frac{NR^\nu}{\nu + N}, \end{aligned} \quad (46)$$

proving equality in (44).

We have established.

Theorem 16. Let $f : \overline{B(0, R)} \rightarrow \mathbb{R}$ that is radial, i.e. there exists g such that $f(x) = g(r)$, $r = |x|$, $\forall x \in \overline{B(0, R)}$. Assume that $g \in AC^n([0, R])$, $n = \lceil \nu \rceil$, $\nu \geq 0$, and

$$g^{(k)}(0) = 0, \quad k = 1, \dots, n-1, \quad \text{and } D_{*0}^\nu g \in L_\infty([0, R]).$$

Then

$$\begin{aligned} \left| f(0) - \frac{\int_{B(0, R)} f(y) dy}{Vol(B(0, R))} \right| &= \\ \left| g(0) - \frac{N}{R^N} \int_0^R g(s) s^{N-1} ds \right| &\leq \frac{(\|D_{*0}^\nu g\|_{\infty, [0, R]}) NR^\nu}{\Gamma(\nu + 1)(\nu + N)}. \end{aligned} \quad (47)$$

Inequality (47) is sharp, it is attained by $g(r) = r^\nu$, $\nu > 0$.

We make

Remark 17. Let the spherical shell $A := B(0, R_2) - \overline{B(0, R_1)}$, $0 < R_1 < R_2$, $A \subseteq \mathbb{R}^N$, $N \geq 2$, $x \in \overline{A}$. Consider again that $f : \overline{A} \rightarrow \mathbb{R}$ be radial, i.e. there exists g such that $f(x) = g(r)$, $r = |x|$, $r \in [R_1, R_2]$, $\forall x \in \overline{A}$. Here again x can be written uniquely as $x = r\omega$, where $r = |x| > 0$, and $\omega = \frac{x}{r} \in S^{N-1}$, $|\omega| = 1$.

Following [9], pp. 149-150, exercise 6 and [10], pp. 87-88, Theorem 5.2.2 we can write for $F : \overline{A} \rightarrow \mathbb{R}$ Lebesgue integrable function that

$$\int_A F(x) dx = \int_{S^{N-1}} \left(\int_{R_1}^{R_2} F(r\omega) r^{N-1} dr \right) d\omega. \quad (48)$$

Here

$$Vol(A) = \frac{\omega_N (R_2^N - R_1^N)}{N},$$

and we assume that $g \in AC^n([R_1, R_2])$, $n = \lceil \nu \rceil$, $\nu \geq 0$, and $g^{(k)}(R_1) = 0$, $k = 1, \dots, n-1$.

By (4) we get

$$g(s) - g(R_1) = \frac{1}{\Gamma(\nu)} \int_{R_1}^s (s-t)^{\nu-1} D_{*R_1}^\nu g(t) dt, \quad (49)$$

$\forall s \in [R_1, R_2]$.

Further assume that $D_{*R_1}^\nu g \in L_\infty([R_1, R_2])$.

By (49) we obtain

$$|g(s) - g(R_1)| \leq \frac{(s-R_1)^\nu}{\Gamma(\nu+1)} \|D_{*R_1}^\nu g\|_{\infty, [R_1, R_2]}, \quad (50)$$

$\forall s \in [R_1, R_2]$.

Next we observe that

$$\left| f(R_1\omega) - \frac{\int_A f(y) dy}{Vol(A)} \right| = \left| g(R_1) - \left(\frac{N}{R_2^N - R_1^N} \right) \int_{R_1}^{R_2} g(s) s^{N-1} ds \right| = \quad (51)$$

$$\left(\frac{N}{R_2^N - R_1^N} \right) \left| \int_{R_1}^{R_2} (g(R_1) - g(s)) s^{N-1} ds \right| \leq \quad (52)$$

$$\left(\frac{N}{R_2^N - R_1^N} \right) \int_{R_1}^{R_2} |g(R_1) - g(s)| s^{N-1} ds \stackrel{(50)}{\leq}$$

$$\left(\frac{N}{R_2^N - R_1^N} \right) \left(\frac{\|D_{*R_1}^\nu g\|_{\infty, [R_1, R_2]}}{\Gamma(\nu+1)} \right) \int_{R_1}^{R_2} (s-R_1)^\nu s^{N-1} ds \quad (53)$$

(by [3], there (2.41))

$$= \left(\frac{N}{R_2^N - R_1^N} \right) \left(\frac{\|D_{*R_1}^\nu g\|_{\infty, [R_1, R_2]}}{\Gamma(\nu+1)} \right) (\Gamma(\nu+1) (N-1)! \sum_{k=0}^{N-1} \frac{(-1)^k}{(N-k-1)!} R_2^{N-k-1} \frac{(R_2 - R_1)^{k+\nu+1}}{\Gamma(k+\nu+2)}) \quad (54)$$

$$= \left(\frac{N! \left(\|D_{*R_1}^\nu g\|_{\infty, [R_1, R_2]} \right)}{R_2^N - R_1^N} \right)$$

$$\left(\sum_{k=0}^{N-1} \frac{(-1)^k}{(N-k-1)!} R_2^{N-k-1} \frac{(R_2 - R_1)^{k+\nu+1}}{\Gamma(k+\nu+2)} \right). \quad (55)$$

Hence in the radial case we proved

$$\left| f(R_1\omega) - \frac{\int_A f(y) dy}{Vol(A)} \right| =$$

$$\left| g(R_1) - \left(\frac{N}{R_2^N - R_1^N} \right) \int_{R_1}^{R_2} g(s) s^{N-1} ds \right| \leq \left(\frac{N! \left(\|D_{*R_1}^\nu g\|_{\infty, [R_1, R_2]} \right)}{R_2^N - R_1^N} \right) \left(\sum_{k=0}^{N-1} \frac{(-1)^k}{(N-k-1)!} R_2^{N-k-1} \frac{(R_2 - R_1)^{k+\nu+1}}{\Gamma(k+\nu+2)} \right). \quad (56)$$

Inequality (56) is attained by

$$g(s) := (s - R_1)^\nu, \quad \nu > 0, \quad s \in [R_1, R_2].$$

Indeed we observe that

$$\begin{aligned} L.H.S \ (56) &= \left(\frac{N}{R_2^N - R_1^N} \right) \int_{R_1}^{R_2} (s - R_1)^\nu s^{N-1} ds = \\ &= \frac{\Gamma(\nu+1) N!}{(R_2^N - R_1^N)} \left(\sum_{k=0}^{N-1} \frac{(-1)^k}{(N-k-1)!} R_2^{N-k-1} \frac{(R_2 - R_1)^{k+\nu+1}}{\Gamma(k+\nu+2)} \right). \end{aligned} \quad (57)$$

But by (22) we get

$$D_{*R_1}^\nu g(s) = \Gamma(\nu+1), \quad \forall s \in [R_1, R_2]. \quad (58)$$

I.e.

$$\|D_{*R_1}^\nu g\|_{\infty, [R_1, R_2]} = \Gamma(\nu+1). \quad (59)$$

The last implies that

$$\begin{aligned} R.H.S \ (56) &= \left(\frac{\Gamma(\nu+1) N!}{R_2^N - R_1^N} \right) \\ &= \left(\sum_{k=0}^{N-1} \frac{(-1)^k}{(N-k-1)!} R_2^{N-k-1} \frac{(R_2 - R_1)^{k+\nu+1}}{\Gamma(k+\nu+2)} \right). \end{aligned} \quad (60)$$

So by (57) and (60) we get

$$L.H.S \ (56) = R.H.S \ (56), \quad (61)$$

proving sharpness of (56).

So putting the above together we derive

Theorem 18. *Let $f : \overline{A} \rightarrow \mathbb{R}$ be radial, i.e. there exists g such that $f(x) = g(r)$, $r = |x|$, $\forall x \in \overline{A}$; $\omega \in S^{N-1}$. Assume that $g \in AC^n([R_1, R_2])$, $n = \lceil \nu \rceil$, $\nu \geq 0$, and*

$$g^{(k)}(R_1) = 0, \quad k = 1, \dots, n-1, \quad \text{and} \quad D_{*R_1}^\nu g \in L_\infty([R_1, R_2]).$$

Then

$$\begin{aligned} & \left| f(R_1\omega) - \frac{\int_A f(y) dy}{Vol(A)} \right| = \\ & \left| g(R_1) - \left(\frac{N}{R_2^N - R_1^N} \right) \int_{R_1}^{R_2} g(s) s^{N-1} ds \right| \leq \\ & \left(\frac{N! \|D_{*R_1}^\nu g\|_{\infty, [R_1, R_2]}}{R_2^N - R_1^N} \right) \\ & \left(\sum_{k=0}^{N-1} \frac{(-1)^k}{(N-k-1)!} R_2^{N-k-1} \frac{(R_2 - R_1)^{k+\nu+1}}{\Gamma(k+\nu+2)} \right). \end{aligned} \quad (62)$$

Inequality (62) is sharp, namely attained by

$$g(s) := (s - R_1)^\nu, \quad \nu > 0, \quad s \in [R_1, R_2]. \quad (63)$$

We need

Definition 19. (see [5]) Let $F : \bar{A} \rightarrow \mathbb{R}$, $\nu \geq 0$, $n := \lceil \nu \rceil$ such that $F(\cdot\omega) \in AC^n([R_1, R_2])$, for all $\omega \in S^{N-1}$. We call the Caputo radial fractional derivative the following function

$$\frac{\partial_{*R_1}^\nu F(x)}{\partial r^\nu} := \frac{1}{\Gamma(n-\nu)} \int_{R_1}^r (r-t)^{n-\nu-1} \frac{\partial^n F(t\omega)}{\partial r^n} dt, \quad (64)$$

where $x \in \bar{A}$, i.e. $x = r\omega$, $r \in [R_1, R_2]$, $\omega \in S^{N-1}$.

Clearly

$$\begin{aligned} & \frac{\partial_{*R_1}^0 F(x)}{\partial r^0} = F(x), \\ & \frac{\partial_{*R_1}^\nu F(x)}{\partial r^\nu} = \frac{\partial^\nu F(x)}{\partial r^\nu}, \quad \text{if } \nu \in \mathbb{N}. \end{aligned} \quad (65)$$

Above function (64) exists almost everywhere for $x \in \bar{A}$ (see [5]).

We continue on Remark 17, we make

Remark 20. We treat here the general, not necessarily radial case of f . We apply (62) to $f(r\omega)$, ω fixed, $r \in [R_1, R_2]$, under the following assumptions: $f(\cdot\omega) \in AC^n([R_1, R_2])$, for all $\omega \in S^{N-1}$, $\nu \geq 0$, $n := \lceil \nu \rceil$, where $f : \bar{A} \rightarrow \mathbb{R}$ Lebesgue integrable;

$$\frac{\partial^k f}{\partial r^k}, \quad k = 1, \dots, n-1 \quad \text{vanish on } \partial B(0, R_1);$$

and

$$\frac{\partial_{*R_1}^\nu f}{\partial r^\nu} \in B(\bar{A}), \quad \text{along with}$$

$$D_{*R_1}^\nu f(\cdot\omega) \in L_\infty([R_1, R_2]), \quad \forall \omega \in S^{N-1}.$$

So we have

$$\begin{aligned} & \left| f(R_1\omega) - \left(\frac{N}{R_2^N - R_1^N} \right) \int_{R_1}^{R_2} f(s\omega) s^{N-1} ds \right| \leq \\ & \left(\frac{N! \left\| \frac{\partial_{*R_1}^\nu f}{\partial r^\nu} \right\|_{\infty, \bar{A}}}{R_2^N - R_1^N} \right) \left(\sum_{k=0}^{N-1} \frac{(-1)^k}{(N-k-1)!} \frac{R_2^{N-k-1} (R_2 - R_1)^{k+\nu+1}}{\Gamma(k+\nu+2)} \right) \\ & =: \lambda_1 \end{aligned} \quad (66)$$

Consequently it holds

$$\begin{aligned} & \left| \frac{\int_{S^{N-1}} f(R_1\omega) d\omega}{\omega_N} - \frac{N}{(R_2^N - R_1^N) \omega_N} \int_{S^{N-1}} \left(\int_{R_1}^{R_2} f(s\omega) s^{N-1} ds \right) d\omega \right| \leq \lambda_1. \end{aligned} \quad (67)$$

That is

$$\left| \frac{\Gamma(N/2)}{2\pi^{N/2}} \int_{S^{N-1}} f(R_1\omega) d\omega - \frac{\int_A f(x) dx}{Vol(A)} \right| \leq \lambda_1. \quad (68)$$

Therefore it holds for $x \in \bar{A}$ that

$$\left| f(x) - \frac{\int_A f(x) dx}{Vol(A)} \right| \leq \left| f(x) - \frac{\Gamma(N/2)}{2\pi^{N/2}} \int_{S^{N-1}} f(R_1\omega) d\omega \right| + \lambda_1. \quad (69)$$

We have established the next result.

Theorem 21. Let $f : \bar{A} \rightarrow \mathbb{R}$ be Lebesgue integrable with $f(\cdot\omega) \in AC^n([R_1, R_2])$, $\nu \geq 0$, $n := \lceil \nu \rceil$, $\forall \omega \in S^{N-1}$; $\frac{\partial^k f}{\partial r^k}$, $k = 1, \dots, n-1$ vanish on $\partial B(0, R_1)$; $D_{*R_1}^\nu f(\cdot\omega) \in L_\infty([R_1, R_2])$, $\forall \omega \in S^{N-1}$; and $\frac{\partial_{*R_1}^\nu f}{\partial r^\nu} \in B(\bar{A})$ (bounded functions on \bar{A}). Then for $x \in \bar{A}$ we have

$$\begin{aligned} & \left| f(x) - \frac{\int_A f(x) dx}{Vol(A)} \right| \leq \left| f(x) - \frac{\Gamma(N/2)}{2\pi^{N/2}} \int_{S^{N-1}} f(R_1\omega) d\omega \right| \\ & + \left(\frac{N! \left\| \frac{\partial_{*R_1}^\nu f}{\partial r^\nu} \right\|_{\infty, \bar{A}}}{R_2^N - R_1^N} \right) \left(\sum_{k=0}^{N-1} \frac{(-1)^k}{(N-k-1)!} \frac{R_2^{N-k-1} (R_2 - R_1)^{k+\nu+1}}{\Gamma(k+\nu+2)} \right). \end{aligned} \quad (70)$$

We make

Remark 22. Let $f : \overline{B(0, R)} \rightarrow \mathbb{R}$ be a Lebesgue integrable function, that is not necessarily a radial function. Assume $f(\cdot\omega) \in AC^1([0, R])$, $\forall \omega \in S^{N-1}$; $0 \leq \nu < 1$, and $D_{*0}^\nu f(\cdot\omega) \in L_\infty([0, R])$, $\forall \omega \in S^{N-1}$.

Clearly here by (3) we obtain

$$f(s\omega) - f(0) = \frac{1}{\Gamma(\nu)} \int_0^s (s-t)^{\nu-1} D_{*0}^\nu f(t\omega) dt, \quad (71)$$

$\forall \omega \in S^{N-1}$, $\forall s \in [0, R]$.

We further assume that

$$\|D_{*0}^\nu f(t\omega)\|_{\infty, (t \in [0, R])} \leq K, \quad \forall \omega \in S^{N-1}, \quad (72)$$

where $K > 0$.

So we apply (47) for $f(\cdot\omega)$, $\forall \omega \in S^{N-1}$.

We obtain

$$\begin{aligned} \left| f(0) - \frac{N}{R^N} \int_0^R f(s\omega) s^{N-1} ds \right| &\leq \\ &\frac{\left(\|D_{*0}^\nu f(t\omega)\|_{\infty, (t \in [0, R])} \right) NR^\nu}{\Gamma(\nu+1)(\nu+N)} \stackrel{(72)}{\leq} \\ &\frac{KNR^\nu}{\Gamma(\nu+1)(\nu+N)}. \end{aligned} \quad (73)$$

Consequently we find

$$\begin{aligned} \left| f(0) - \frac{N}{\omega_N R^N} \int_{S^{N-1}} \left(\int_0^R f(s\omega) s^{N-1} ds \right) d\omega \right| &\leq \\ &\leq \frac{KNR^\nu}{\Gamma(\nu+1)(\nu+N)}. \end{aligned} \quad (74)$$

That is proving

$$\left| f(0) - \frac{\int_{B(0, R)} f(x) dx}{Vol(B(0, R))} \right| \leq \frac{KNR^\nu}{\Gamma(\nu+1)(\nu+N)}. \quad (75)$$

We have established our last result.

Theorem 23. Let $f : \overline{B(0, R)} \rightarrow \mathbb{R}$ be a Lebesgue integrable function, not necessarily radial. Assume $f(\cdot\omega) \in AC^1([0, R])$, $R > 0$, $\forall \omega \in S^{N-1}$; $0 \leq \nu < 1$, and $D_{*0}^\nu f(\cdot\omega) \in L_\infty([0, R])$, $\forall \omega \in S^{N-1}$.

Suppose also that

$$\|D_{*0}^\nu f(t\omega)\|_{\infty, (t \in [0, R])} \leq K, \quad (76)$$

$\forall \omega \in S^{N-1}$, where $K > 0$.

Then

$$\left| f(0) - \frac{\int_{B(0, R)} f(x) dx}{Vol(B(0, R))} \right| \leq \frac{KNR^\nu}{\Gamma(\nu+1)(\nu+N)}. \quad (77)$$

References

- [1] A. Ostrowski, *Über die Absolutabweichung einer differentiabaren Function von ihrem Integralmittelwert*, Comment. Math. Helv., 10 (1938), 226-227.
- [2] G. A. Anastassiou, *Fractional Ostrowski type inequalities*, Communications in Applied Analysis, 7 (2003), no. 2, 203-208.
- [3] G. A. Anastassiou, *Multivariate Fractional Ostrowski type inequalities*, Computers and Mathematics with Applications, 54 (2007), 434-447.
- [4] Kai Diethelm, *Fractional Differential Equations*, on line: <http://www.tu-bs.de/~diethelm/lehre/f-dgl02/fde-skript.ps.gz>
- [5] G. Anastassiou, *Caputo fractional multivariate Opial type inequalities on spherical shells*, submitted, 2007.
- [6] G. Anastassiou, *Multivariate fractional Taylor's formula revisited*, submitted, 2008.
- [7] G. Anastassiou, *Riemann-Liouville Fractional Multivariate Opial type inequalities on spherical shells*, accepted for publication, Bulletin of Allahabad Math. Soc., India, 2007.
- [8] E. T. Whittaker and G. N. Watson, *A Course in Modern Analysis*, Cambridge University Press, 1927.
- [9] W. Rudin, *Real and Complex Analysis*, International Student Edition, McGraw Hill 1970, London, New York.
- [10] D. Stroock, *A Concise Introduction to the Theory of Integration*, 3rd Edition, Birkhäuser, Boston, Basel, Berlin, 1999.

A Chaotic Communication System with Enhanced Security Features

Ioannis P. ANTONIADES¹, Amalia N. MILIOU^{*1}, Stavros G. STAVRINIDES², and
Antonios N. ANAGNOSTOPOULOS²

Abstract— In this work we present the implementation of a chaotic communication system with enhanced security features. The enhancement in the security of the system at hand is achieved neither by increasing chaos dimensionality nor by making synchronization of transmitter and receiver more sensitive to system parameters but by introducing a set of parameters used in the encoding and decoding of the message signal. We also introduce a time delay parameter in the dynamical system which on the one hand improves the chaotic behavior of the system and on the other, adds further security in the encoding-decoding scheme.

In our work, we modify the non-autonomous 2nd order non-linear oscillator system presented by G. Mycolaitis, *et al* in Proc. of 7th Int. Workshop on Non-linear Dynamics of Electronic Systems, which is particularly suitable for digital communications.

Index Terms — Chaos, nonlinear circuits, synchronization, communication system security.

I. INTRODUCTION

The significance of private and secure communications is very clear in a world, which increasingly relies on rapid transmission of large amounts of information. The current solutions for secure communications are the public key cryptosystems using

^{*} ¹A.N. Miliou and I. P. Antoniadis are with the Department of Informatics, Aristotle University of Thessaloniki, Thessaloniki, GR-54124, (corresponding author' phone: +30-2310-998407; fax: +30-2310-998419; e-mail: amiliou@csd.auth.gr).

² S. Stavriniides and A. N. Anagnostopoulos are with the Department of Physics, Aristotle University of Thessaloniki, Thessaloniki, GR-54124.

software techniques to achieve computational complexity while quantum cryptography has the potential to render such techniques obsolete. However, another method of increasing security in communications is to use hardware complexity to hide or mask the message on a chaotic carrier [1-8].

Chaotic communication systems are simpler, from the point of view of the circuit engineering implementation, as compared to the traditional spread spectrum systems. Two key features of chaos are a noise-like time series and sensitive dependence on initial conditions, which cause chaotic transmissions to have low probability of detection as an information-bearing signal and low probability of intercept, respectively.

With chaos-based communication systems, the key fact is that the procedure used by the transmitter to generate the chaotic waveform is deterministic; the knowledge of this procedure by an authorized receiver allows him to replicate, or synchronize, the chaotic waveform, and then to recover the message by subtracting the chaotic carrier [3-9]. The confidentiality of the encryption technique is based on the difficulty to reproduce the chaotic carrier signal if an intruder does not know the particular dynamical system used.

In this paper, we propose a more sophisticated approach combining the simplicity in the implementation of a chaotic system with an enhanced encoding scheme that will overall increase security. The paper is organized as follows: the equations and the synchronization properties of the system are presented in section II. The simulation results obtained are shown and discussed in section III. Finally, concluding remarks are given in section IV.

II. DESCRIPTION OF THE CHAOTIC SYSTEM

The general set-up for the communication system is presented in Fig. 1. The transmitter and the receiver are identical circuits. The circuits include an integrator based 2nd order RC resonance loop, a digital circuitry that performs consecutive comparisons of U_2 and U_o , an exclusive OR gate (and a buffer to avoid overloading), with an input M for the external source of square pulses $M(t)$ of period $T=2\pi/\omega$ or a more complex signal if one wants to encode an arbitrary message. Moreover, a latch is used which introduces a

time delay, t_d , according to a clock frequency. The principle of operation is demonstrated below. Here the chaotic pulses $U^*(t-t_d) \propto F(y_I(t-t_d), t; a_1, a_2, \dots, a_{N_a}, k)$ drive both the resonance loop of the transmitter and the resonance loop of the receiver.

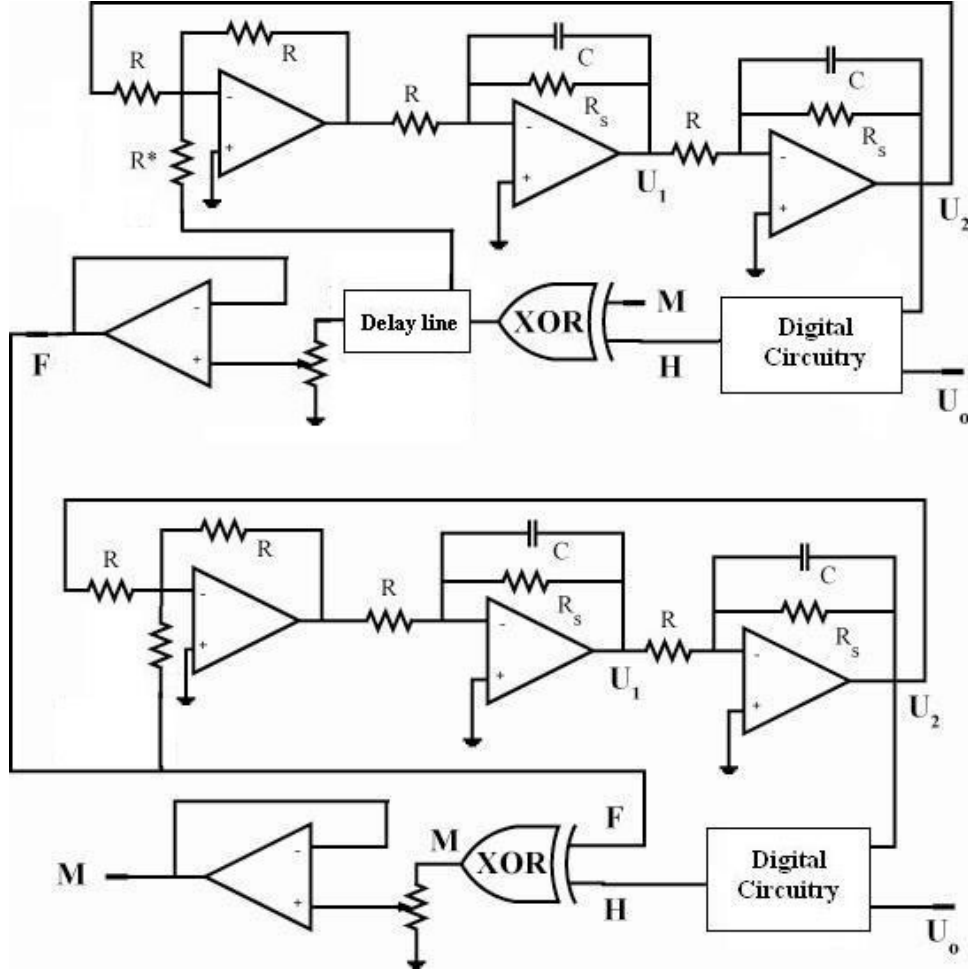


Fig. 1. Schematic diagram of the transmitter-receiver system.

The transmitter-receiver system is governed by the following set of equations:

$$\dot{x}_1 = aF(y_I(t-t_d), t; a_1, a_2, \dots, a_{N_a}, k) - bx_1 + y_1$$

$$\dot{y}_1 = -x_1 - by_1$$

$$F(y_I(t-t_d), t; a_1, a_2, \dots, a_{N_a}, k) = H(y_I(t-t_d); a_1, a_2, \dots, a_{N_a}, k) \oplus M(t)$$

(1)

$$\dot{x}_2 = aF(y_I(t-t_d), t; a_1, a_2, \dots, a_{N_a}, k) - bx_2 + y_2$$

$$\dot{y}_2 = -x_2 - by_2$$

The subscripts ‘1’ and ‘2’ at the state variables specify the transmitter and the receiver, respectively.

The same driving term $F(y_I(t-t_d), t; a_1, a_2, \dots, a_{N_a}, k)$ is used in the equations for the transmitter and the receiver. The following substitutions have been used in the previous system of equations since the parameters are usually written in a dimensionless form:

$$\begin{aligned} x &= \frac{U_1}{U_o}, \quad y = \frac{U_2}{U_o}, \quad t = \frac{t}{RC} \\ \alpha &= \frac{U^* \cdot R}{U_o \cdot R^*}, \quad b = \frac{R}{R_s} \\ \omega &= \omega_M RC \end{aligned} \quad (2)$$

The digital circuitry, implements the newly introduced function $H(y; a_1, a_2, \dots, a_{N_a}, k)$, which is shown in Fig.2. This function replaces the shifted Heaviside function of Ref. [9]. The a_j 's ($j=1, 2, \dots, N_a$ and $a_o = -\infty, a_{N_a+1} = \infty$) are fixed parameters and k is a set of $N_a + 1$ bits, where bit j indicates the binary value (0 or 1) of the function H in the interval $a_j < y < a_{j+1}$. The values of these bits are predetermined by legitimate users of the systems and act as a “soft encryption key” which could be altered at will. The symbol \oplus denotes the exclusive-OR operation and $M(t)$ is the transmitted digitally encoded message. According to the analysis presented in [4] each bit, “0”, and “1”, is encoded by a single period of a square pulse of frequency ω_1 and ω_2 respectively.

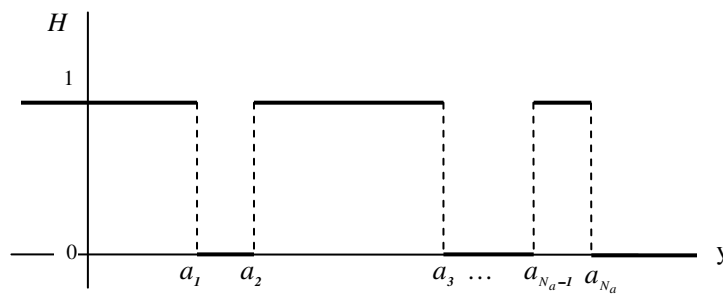


Fig. 2. The implementation of function $H(y; a_1, a_2, \dots, a_{N_a}, k)$.

The message, $M(t)$, is XORed with the value of the function $H(y(t-t_d))$ yielding the

transmitted *digital* signal F which drives the dynamical system of the receiver. If the system of the transmitter and the receiver are identical, the dynamic variables are synchronized enabling the decoding of the message.

As shown in [3, 9] the synchronization is globally asymptotically stable. Thus the corresponding state variables are robustly synchronized ($x_2 \rightarrow x_1$ and $y_2 \rightarrow y_1$). Consequently, the non-linear functions behave in a synchronous way ($H(y_2; a_1, a_2, \dots, a_{N_a}, k) \rightarrow H(y_1; a_1, a_2, \dots, a_{N_a}, k)$) as well. This result suggests an extremely simple technique for recovering the signal $M(t)$ at the receiver end. The received signal $F(y_1(t-t_d), t; a_1, a_2, \dots, a_{N_a}, k) \propto U^*(t-t_d)$ is applied to the XOR unit of the receiver. Due to the sum mod2 property, the signal $M(t)$ can be recovered from the chaotic one $F(y_1(t-t_d), t; a_1, a_2, \dots, a_{N_a}, k)$ without any errors, according to:

$$\begin{aligned} F(y_1(t-t_d), t; a_1, a_2, \dots, a_{N_a}, k) \oplus H(y_2(t-t_d); a_1, a_2, \dots, a_{N_a}, k) = \\ H(y_1(t-t_d); a_1, a_2, \dots, a_{N_a}, k) \oplus M(t) \oplus H(y_2(t-t_d); a_1, a_2, \dots, a_{N_a}, k) \rightarrow \\ \rightarrow H(y_1(t-t_d); a_1, a_2, \dots, a_{N_a}, k) \oplus M(t) \oplus H(y_1(t-t_d); a_1, a_2, \dots, a_{N_a}, k) = M(t) \end{aligned} \quad (3)$$

III. SIMULATION RESULTS AND DISCUSSION

In this work, we present the implementation of a chaotic communication system with enhanced security features.

The division of the y range in many regions, instead of only two presented in [3, 9] and the fact that there is the encryption key, k , determining the value of H in the corresponding region (either 0 or 1) introduces an uncertainty as to how well the intruder could predict the values of $H(y)$ even if he manages to perfectly synchronize his system with the transmitter. The intruder must know the values of *all* the limits of the regions (a_j) as well as all bits of the key k in order to accurately retrieve the message. The larger the number of a_j s and the longer the key, the hardest it is to break the system by brute force.

Moreover, the introduction of a time delay parameter, t_d , in the system improves the chaotic nature of the dynamical system. For example, Ref [10] has shown that the introduction of a time delay in a dissipative system with a non-linear driving term increases

the attractor dimension and yields a probability density function which tends asymptotically to a Gaussian. The high degree of complexity thus obtained makes such systems good candidates for signal encryption; an intruder that is able to intercept the transmitted signal without possessing an identical dynamical system will have a much greater difficulty in separating the message from the chaotic carrier. Even if he possesses an identical dynamical system and manages to synchronize with the transmitter, he will not be able to decode the message if he does not know the exact value of the time delay t_d .

Equations (1) have been numerically integrated. Chaotic oscillations are observed at different frequency windows, i.e. between $\omega=0.7-0.8$ and $\omega=1.05-1.16$ and $\alpha=2.65$ while the damping parameter b should not be too large and in our simulation $b=0.02$. The chaotic behavior of the system depends also on the value of the time delay parameter, the position of the a_j and the key k . Strong chaotic signals were obtained for time delay values ranging from $t_d=20$ to 50.

In order to test the security of the newly proposed encoding scheme, we first assumed that an intruder knows the exact value of the key k and the values of the a_j with some uncertainty. By varying the uncertainty in the values of a_j we investigated its effect on the Bit Error Rate (BER) suffered by the intruder at the decoding stage. We define two measures of the BER; the Raw BER (RBER) which is the average mismatch between the actual message $M(t)$ and the decoded message $M_d(t)$

$$RBER = \frac{1}{t} \int_0^t |M(t) - M_d(t)| dt, \quad (4)$$

and the Relative BER (RelBER) which is RBER divided by the fractional difference of the two encoding frequencies ω_1 and ω_2

$$RelBER = \frac{RBER}{Z}, \quad \text{where} \quad Z = \frac{|\omega_1 - \omega_2|}{\frac{1}{2}(\omega_1 + \omega_2)} \quad (5)$$

The rationale for the second definition is that the smaller the difference between the encoding frequencies, the larger the uncertainty in distinguishing between values “0” and “1” when there is a mismatch between the decoded signal M_d and the actual M . In all our simulations we used the values $\omega_1=0.75$ and $\omega_2=1.15$ (in RC units).

In Fig. 3, we plot the RelBER versus Δa , the fractional mismatch between the values of each respective a_j of the transmitter and the receiver (intruder).

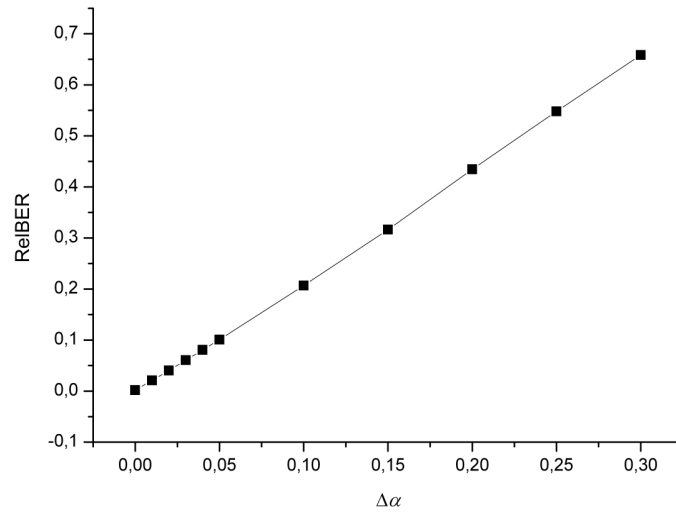


Fig. 3. Relative BER vs fractional mismatch Δa .

We notice that RelBER rises linearly with Δa and for a relative low mismatch of $\Delta a \sim 22\%$ the intruder has a RelBER of about 0.5 which means almost 100% uncertainty in the knowledge of M . This is because a Bit Error Rate of 50% means that for each bit there is a probability of $\sim 50\%$ to get the correct value, which is essentially as good as a guess. In the present simulation we used only 5 a 's ($N_a = 5$).

Next we assumed that the intruder knows the exact values of all the a 's and all the bits of the key k except of one. This means that the decoded signal will be incorrect for all values of y that lie between the a 's corresponding to the unknown bit. Thus, we expect that the BER will be proportional to the size, y_{mis} , of the interval in y where the key mismatch occurs.

In Fig. 4, we plot the dependence of the *Bit Uncertainty* versus the total mismatch y_{mis} for different positions of the incorrect bit in the key k , where Bit Uncertainty is defined as

$$\text{Bit Uncertainty} = 2 \cdot \text{RBER} \quad (6)$$

As expected by the ergodicity of the system in y the BER depends linearly on the size of the mismatch.

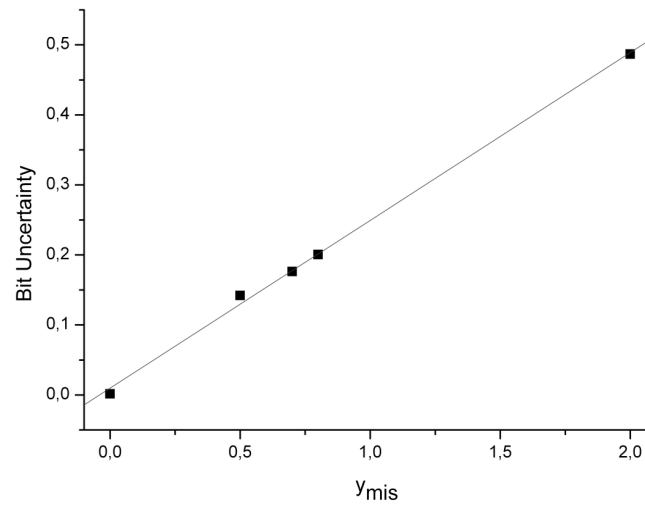


Fig. 4. Bit Uncertainty vs y_{mis} for different positions of the incorrect bit in the key k . The line corresponds to a linear least squares fit.

The above result is further demonstrated in Fig. 5 where we plot the Bit Uncertainty versus y_{mis} for three different values of N_a (5, 9 and 11) and assuming that the intruder knows all bits of the key k in each case. The fractional mismatch Δa in each a_j is the same for all three cases and equal to 0.05. By increasing the N_a , the total y_{mis} increases.

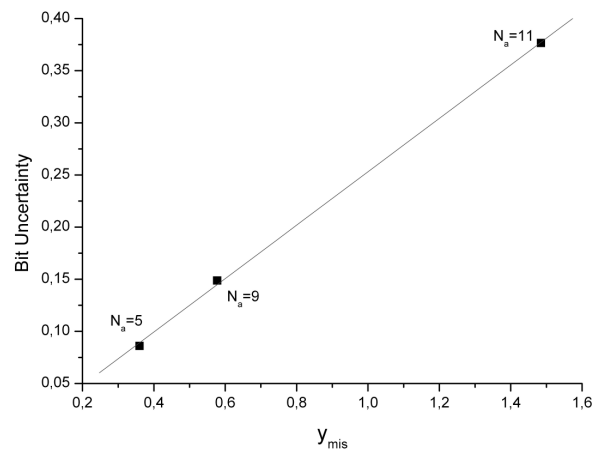


Fig. 5. Bit Uncertainty vs y_{mis} for three different values of N_a . The line corresponds to a linear least squares fit.

In all the above results we presume that the intruder is able to synchronize perfectly with the transmitter, i.e. he knows exactly the system dynamic parameters. Also, that he knows all the a_j to a good precision and all or almost all the bits of the key k . In actuality, the intruder is much more disadvantaged as the N_a increases and the quality of the synchronization is not perfect (he doesn't possess an identical system to the transmitter).

Thirdly, we investigated the dependence of Bit Uncertainty on the mismatch in the time delay between the receiver and the transmitter. We assume that the intruder perfectly matches all system parameters (including the a_j and the key k), except for the time delay. The time delay t_d of the transmitter is 50 (RC)^{-1} .

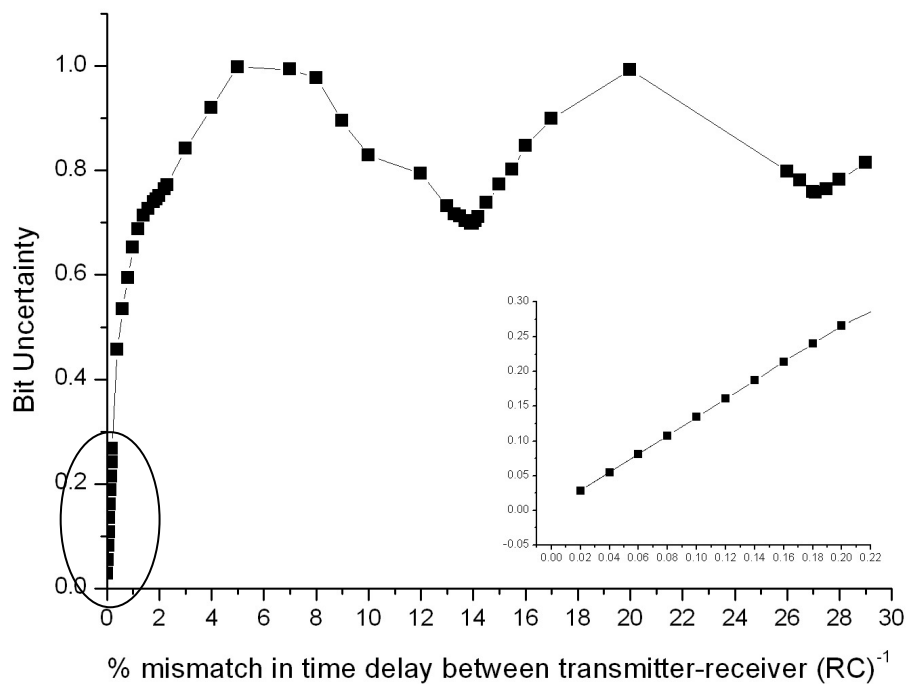


Fig. 5. Bit Uncertainty vs mismatch in time delay between the receiver and the transmitter. The inset figure is a blow-up of circled region.

In Fig. 6 we plot the Bit Uncertainty versus the mismatch in time delay between the receiver (intruder) and the transmitter. We notice that Bit Uncertainty is very sensitive to the time delay mismatch; for a mismatch of only 0.1 (RC)^{-1} ($=0.2\%$) the Bit

Uncertainty is as high as $\sim 27\%$. The Bit Uncertainty grows linearly for small values of mismatch while it reaches its maximum value of ~ 1 for a mismatch of $\sim 2.5 (RC)^{-1}$ ($=5\%$). For larger values of mismatch the Bit Uncertainty oscillates with a period of $\sim 6.85 (RC)^{-1}$. The rise and fall of the Bit Uncertainty is probably attributed to the relation of the delay mismatch with the encoding frequencies ω_1 and ω_2 .

IV. CONCLUDING REMARKS

In this paper (i) we proposed a new encryption scheme for the chaotic communication system already presented in [3,9] based on a more sophisticated process, (ii) we added a time delay parameter at the non-linear driving term in order to improve the chaotic nature of the dynamical system.

We investigated how the new system behaves under attack by an intruder with partial knowledge of system parameters. There is a linear dependence between the size of the uncertainty in the encryption parameters (a_j, k) and the resulting Bit Uncertainty at the decoding phase. However, small uncertainties in the encryption parameters lead to high Bit Uncertainties.

Furthermore, the Bit Uncertainty is very sensitive to time delay mismatch between the transmitter and the receiver a fact that produces an extra disadvantage for the potential intruder.

Weak points of the proposed system are: (i) the fact that by changing the values and the number of the encryption parameters one often has to retune the other system parameters (time delay, encoding frequencies, etc) in order to achieve a good chaotic signal, (ii) the encryption scheme is vulnerable under a known-message attack in the case of that an intruder knows all parameters of the dynamical system but not the encryption parameters and he possesses both the encrypted and decrypted versions on unknown message. This is because he could easily XOR the encrypted signal with the known message and restores the encrypting function H which could be used to decode all subsequent communications. Therefore, the valid users must alter the encryption key k at each communication.

The great advantage of the system still remains the fact that it transmits a digital signal which gives all the advantages of digital technology (for example filtering of channel noise, etc).

REFERENCES

- [1] G. Chen. Control and Synchronization of chaotic systems, [Online]. Available: <ftp.egr.uh.edu/pub/TeX/chaos.tex>.
- [2] G. Kolumban, M. P. Kennedy, L. O. Chua, "The role of synchronization in digital communications using chaos – part II: chaotic modulation and chaotic synchronization", *IEEE Trans. On Circuits and Systems I*, vol. 45, no. 11, pp. 1129-1140, November 1998.
- [3] G. Mycolaitis, A. Tamaševičius, A. Čenys, A. Namajunas, K. Navionis, A. N. Anagnostopoulos, "Globally synchronizable non-autonomous chaotic oscillator", in *Proc. of 7th International Workshop on Nonlinear Dynamics of Electronic Systems*, Denmark, pp. 277-280, July 1999.
- [4] A. Pikovsky, M. Rosenblum, J. Kurths, "*Synchronization: A universal concept in nonlinear sciences*", 1st paperback edition, vol.12, *The Cambridge nonlinear science series*, Cambridge University Press, 2003.
- [5] T. L. Carroll, L. M. Pecora, "Synchronizing nonautonomous chaotic circuits", *IEEE Trans. On Circuits and Systems II*, vol. 40, no. 10, pp. 646-650, October 1993.
- [6] L. M. Pecora, T. L. Carroll, "Synchronization in chaotic systems", *Phys. Rev. Lett.*, vol. 64, no. 8, pp.821-823, February 1990.
- [7] K. M. Cuomo, A. V. Oppenheim, "Circuit implementation of synchronized chaos with applications to communications", *Phys. Rev. Lett.*, vol. 71, no. 1, pp. 65-68, July 1993.
- [8] G. Kolumban, M. P. Kennedy, L. O. Chua, "The role of synchronization in digital communications using chaos – part I: fundamentals of digital communications", *IEEE Trans. On Circuits and Systems I*, vol. 44, no. 10, pp. 927-936, October 1997.
- [9] A.N. Miliou, I.P. Antoniadis, S.G. Stavrinos, A.N. Anagnostopoulos "Secure Communication by Chaotic Synchronization: Robustness under Noisy Conditions",

Journal of Non-linear analysis: Real world applications, Vol.8, No.3, pp. 1003-1012, 2007.

- [10] B. Dorizzi, B. Grammaticos, M. Le Berre, Y. Pomeau, E. Ressayre, A. Taller, "Statistics and dimension of chaos in differential delay systems", *Phys. Rev. A*, vol. 35, no. 1, pp. 328-339, January 1987.

ESTIMATING CHAOS AND COMPLEX DYNAMICS IN AN AUTONOMOUS FOUR-DIMENSIONAL CIRCUIT

Maria S. PAPADOPOULOU¹, Ioannis N. STOUBOULOS¹, Ioannis M. KYPRIANIDIS¹,
Antonios N. ANAGNOSTOPOULOS¹

Abstract

In this paper we have studied the complex dynamics of an autonomous, nonlinear circuit. The system consists of a nonlinear element, with a double-break, piecewise-linear and symmetrical v-i characteristic, a negative conductance, two capacitances, two inductances and two resistances. Using the capacitances C_1 and C_2 as the control parameters, we have observed various types of behaviour, such as periodic and chaotic attractors, period-doubling route to chaos, reverse period doubling, antimonotonicity et.al. The phase portraits, Lyapunov exponents and spectrum diagrams are presented for various values of the control parameters, concluding about circuit's dynamic behaviour.

Keywords: *Autonomous circuit, Control parameter, Chaotic attractor, Lyapunov exponent, Complex dynamics.*

1. Introduction

During the last decade there has been tremendous development in research on the dynamics of nonlinear electric and electronic circuits [1-6]. This was mainly happened due to two reasons. Firstly, electric and electronic circuits constitute a group of real physical systems in which observations and measurements are relatively easy to be done. Secondly, the development of integrated circuits (ICs) has provided the capability of setting up inexpensive laboratory experiments. Consequently, experiments that are not available in any other field of science, such as economics, geology, biology, medicine etc., were become possible. A universal research system is Chua's circuit [7-12], which can produce a large variety of chaotic phenomena. Chua's circuit is a simple electronic circuit which was introduced in 1983 by L. O. Chua, who was a visitor of Waseda University (Japan) at that time [13].

¹Physics Department, Aristotle University of Thessaloniki, Thessaloniki GR-54124, GREECE

In this paper we have studied the dynamic behaviour of a four-dimensional, autonomous circuit with two active elements, one linear negative conductance and one nonlinear resistor. Using the capacitances C_1 and C_2 as the control parameters, we have observed periodic and chaotic attractors, as well as many other interesting chaotic phenomena, such as period-doubling and reverse period-doubling sequences, antimonotonicity and crisis phenomenon, when the spiral attractor suddenly widens to a double-scroll attractor [14].

2. The Four-Dimensional Autonomous System

The circuit, we have studied, is presented in Figure 1. It is a four-dimensional autonomous circuit with two active elements, a nonlinear resistor R_N and a linear negative conductance G_n . The v - i characteristics of the nonlinear element and negative conductance are seen in Figures 2 and 3, respectively.

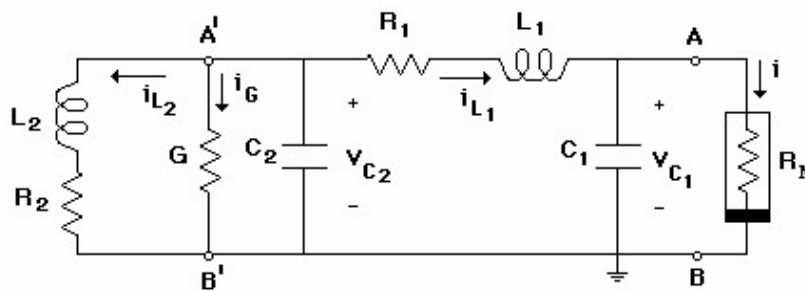


Figure 1. The four-dimensional autonomous electric circuit

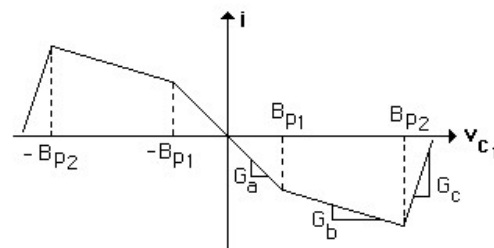


Figure 2. The v - i characteristic of nonlinear element

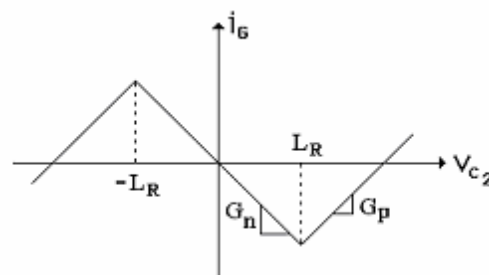


Figure 3. The v - i characteristic of negative conductance

Using Kirchhoff's circuit laws, the following state equations of the system have been derived:

$$\frac{dv_{C1}}{dt} = \frac{1}{C_1} \cdot \{i_{L1} - f(v_{C1})\} \quad (2.1)$$

$$\frac{dv_{C2}}{dt} = -\frac{1}{C_2} \cdot \{G_n \cdot v_{C2} + i_{L1} + i_{L2}\} \quad (2.2)$$

$$\frac{di_{L1}}{dt} = \frac{1}{L_1} \cdot \{v_{C2} - i_{L1}R_1 - v_{C1}\} \quad (2.3)$$

$$\frac{di_{L2}}{dt} = \frac{1}{L_2} \cdot \{v_{C2} - i_{L2}R_2\} \quad (2.4)$$

where:

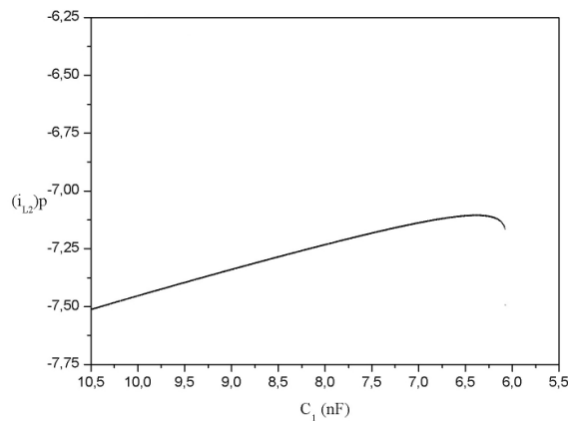
$$i = G_c v_{C1} + 0.5(G_a - G_b) \cdot (|v_{C1} + B_{p1}| - |v_{C1} - B_{p1}|) + 0.5(G_b - G_c) \cdot (|v_{C1} + B_{p2}| - |v_{C1} - B_{p2}|) \quad (2.5)$$

The values of circuit's parameters are: $L_1=10.2\text{mH}$, $L_2=21.5\text{mH}$, $R_1=2.02\text{K}\Omega$, $R_2=190\Omega$, $G_n = -0.5\text{mS} = -G_p$, $G_a = -0.83\text{mS}$, $G_b = -0.51\text{mS}$, $G_c = 2.90\text{mS}$, $B_{p1} = 1.46\text{V}$ and $B_{p2}=10.10\text{V}$, and consider stable during our study.

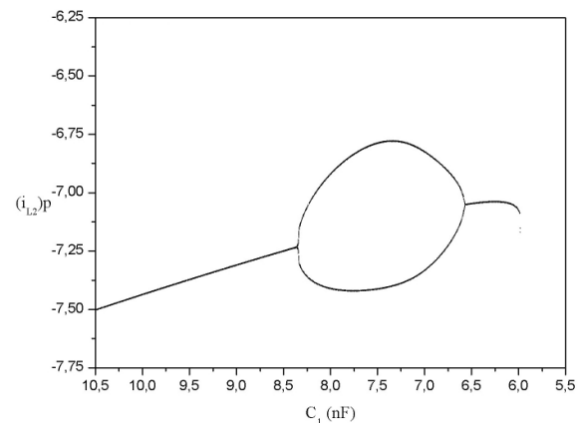
3. Complex Dynamics of the Autonomous Circuit

3.1 Bifurcation Diagrams

In this paragraph, using the capacitances C_1 and C_2 as the control parameters, we have studied the dynamics of the four-dimensional autonomous circuit. In Figures 4 and 5 we can see the bifurcation diagrams $(i_{L2})_p$ vs. C_1 for various values of capacitance C_2 .



(a) $C_2=6.400\text{nF}$



(b) $C_2=6.100\text{nF}$

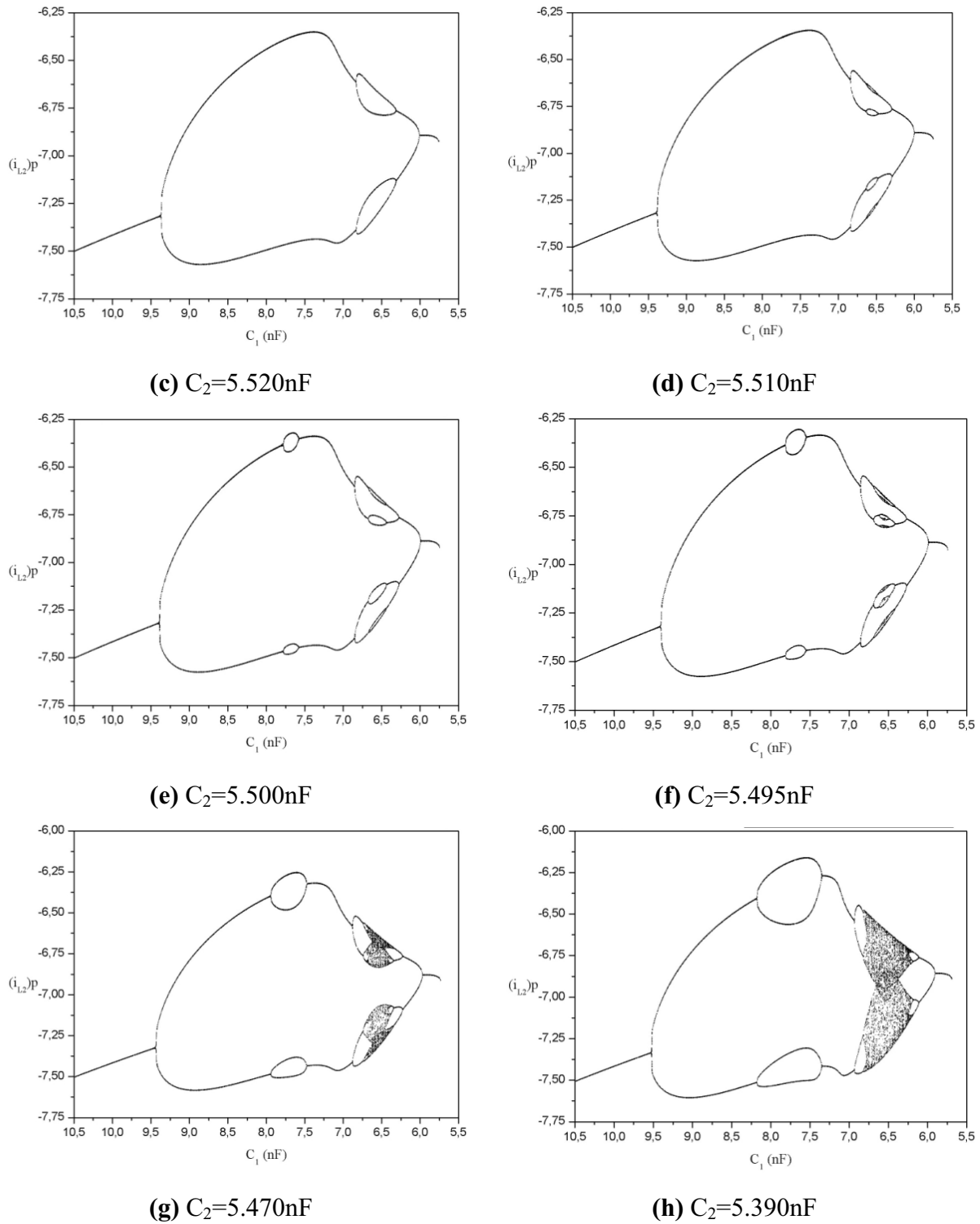


Figure 4. Bifurcation diagrams $(i_{L2})_p$ vs. C_1 for various values of C_2

In the first case (case-1) we examine circuit's behaviour for various values of capacitance C_2 , while capacitance C_1 changes from 7.00nF to 6.00nF. We can see in Figure 4(a) that the system is always in period-1 state for $C_2=6.400\text{nF}$, independently of the capacitance's C_1 value. In Figure 4(b) ($C_2=6.100\text{nF}$) the existence of a period-2 state is appear, while in Figure 4(c) and (d) ($C_2=5.520\text{nF}$ and $C_2=5.510\text{nF}$) the period-4 and period-8

states appear. Following, in Figure 4(e) and (f) the period-16 and period-32 states are presented, while in Figure 4(g) and (h) the system is the chaotic regime.

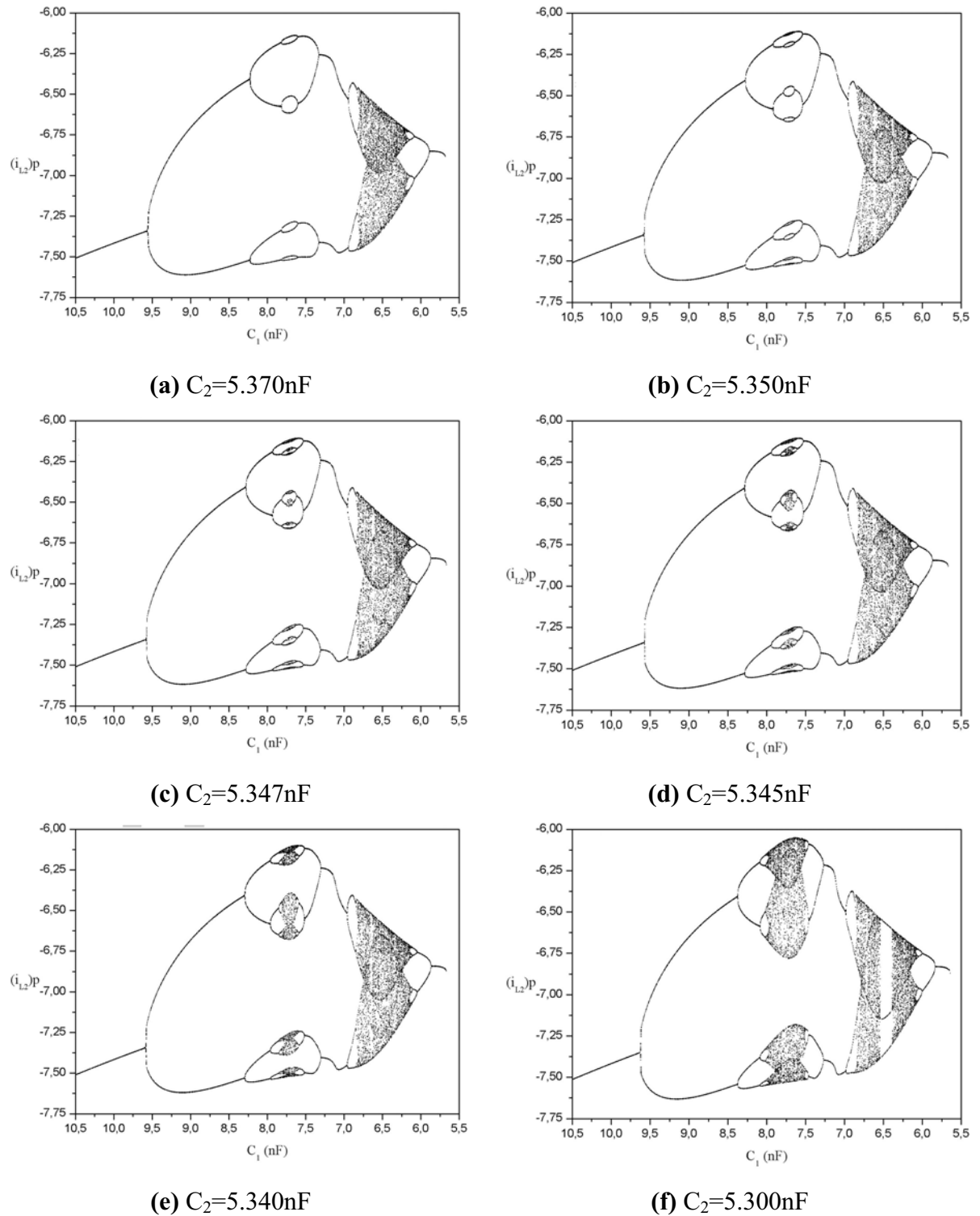
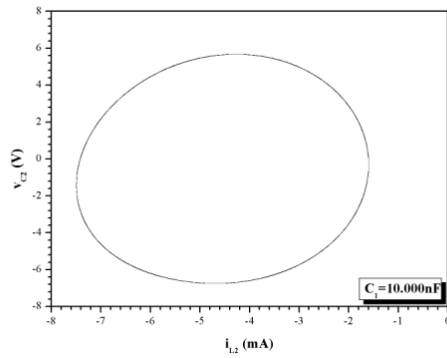


Figure 5. Bifurcation diagrams $(i_{L2})_p$ vs. C_1 for various values of C_2

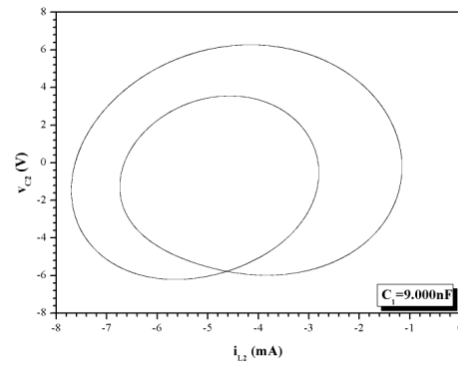
In the second case (case-2) we examine circuit's behaviour for various values of capacitance C_2 , while capacitance C_1 changes from 8.50nF to 7.50nF. The same pattern in states transition is appeared, as before.

3.2 Phase Portraits

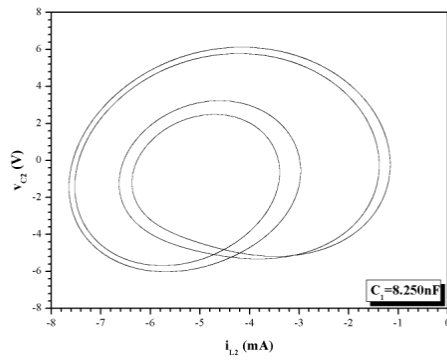
In previous paragraph, we have studied the dynamic behaviour of the circuit for various values of capacitances C_1 and C_2 . Now, we will see the behaviour of the system for $C_2=5.30\text{nF}$ and various values of capacitance C_1 .



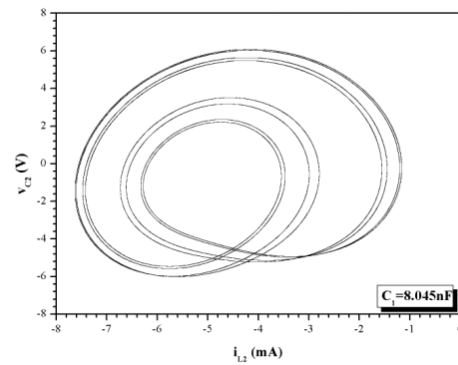
(a) $C_1=10.00\text{nF}$



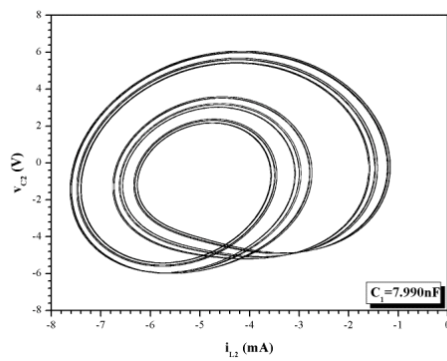
(b) $C_1=9.00\text{nF}$



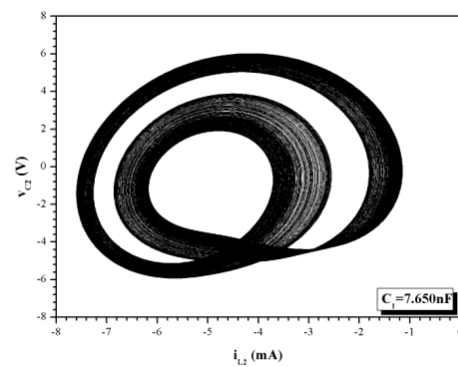
(c) $C_1=8.25\text{nF}$



(d) $C_1=8.05\text{nF}$



(e) $C_1=7.99\text{nF}$



(f) $C_1=7.65\text{nF}$

Figure 6. Lissajous diagrams v_{C2} vs. i_{L2} for $C_2=5.30\text{nF}$ and various values of C_1

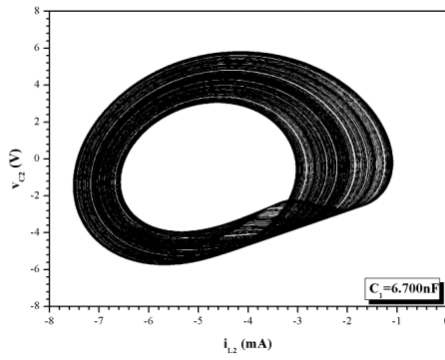
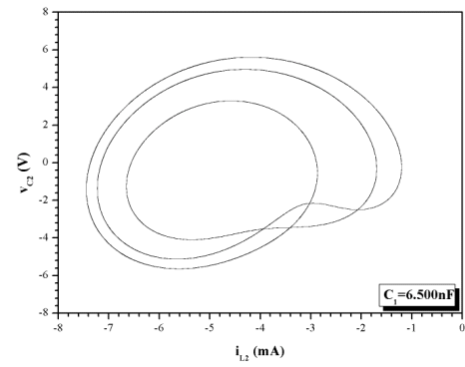
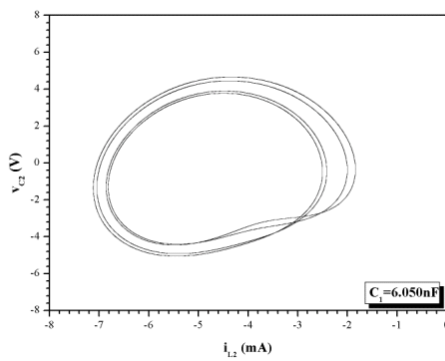
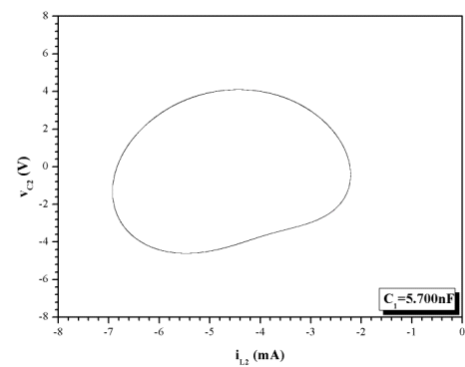
(a) $C_1=6.70\text{nF}$ (b) $C_1=6.50\text{nF}$ (c) $C_1=6.05\text{nF}$ (d) $C_1=5.70\text{nF}$

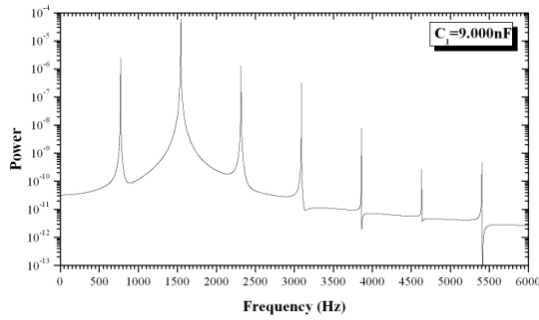
Figure 7. Lissajous diagrams v_{C2} vs. i_{L2} for $C_2=5.30\text{nF}$ and various values of C_1

In Figures 6(a)-(f) we can see the state transition period-1 \rightarrow period-2 \rightarrow period-4 \rightarrow period-8 \rightarrow period-16 \rightarrow chaos, for $C_2=5.30\text{nF}$, as the capacitance C_1 decreases. In Figure 7(a) the chaotic attractor for $C_1=6.70\text{nF}$ and $C_2=5.30\text{nF}$ is presented, while in Figure 7(b) the periodic window p-3 is appeared. Next, in Figures 7(c) and (d) the finally transition to period-1 state is seen.

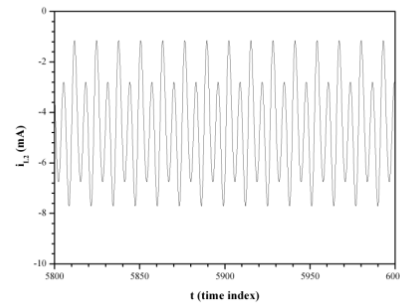
3.3 Spectrum Analysis

In Figure 8 we can see the spectrums and waveforms of a periodic and chaotic attractor. More particularly, in Figure 8(a) and (b) the power spectrum and waveform $i_{L2}(t)$ of a period-2 state are presented. The values of capacitances are $C_1=9.00\text{nF}$ and $C_2=5.30\text{nF}$. In Figure 8(c) and (d) the power spectrum and $i_{L2}(t)$ of an attractor for $C_1=6.70\text{nF}$ and $C_2=5.30\text{nF}$ are displayed. The calculation of Lyapunov exponents and the existence of a

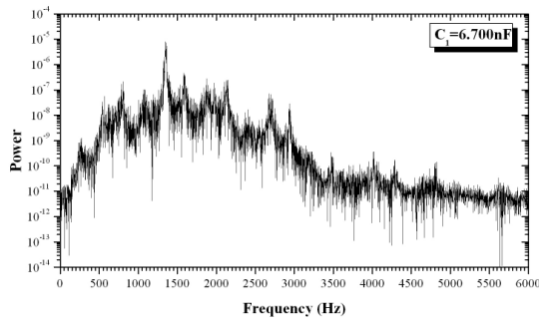
positive number indicate the strong possibility of being a chaotic attractor. More particularly, we have found that $LE1=+0.0665$, $LE2=-0.0005$, $LE3=-1.1472$ and $LE4=-2.9349$.



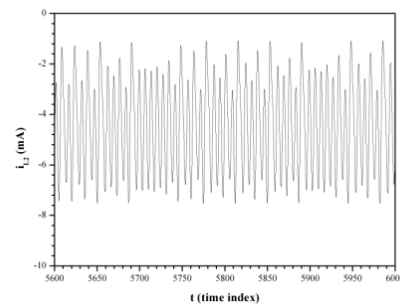
(a) Spectrum for $C_1=9.00\text{nF}$



(b) $i_{L2}(t)$ for $C_1=9.00\text{nF}$



(c) Spectrum for $C_1=6.70\text{nF}$



(d) $i_{L2}(t)$ for $C_1=6.70\text{nF}$

Figure 8. Power Spectrums and Waveforms for $C_2=5.30\text{nF}$

4. Conclusion

In this paper we have studied a four-dimensional autonomous circuit with two active elements, a nonlinear resistance and a negative conductance. Using the capacitances C_1 and C_2 as the control parameters, we have studied the complex dynamics of the system. We have observed the transition from periodic states to chaotic ones and vice versa, as well as period-doubling and reverse period-doubling sequences. The calculation of Lyapunov exponents indicates that the attractor for $C_1=6.70\text{nF}$ and $C_2=5.30\text{nF}$ could be chaotic.

The period-doubling routes to chaos were demonstrated, as well as reverse period-doubling sequences for various values of the control parameters. The state transition period-1 \rightarrow period-2 \rightarrow period-4 $\rightarrow \dots \rightarrow$ chaos $\rightarrow \dots$ period-4 \rightarrow period-2 \rightarrow period-1 is appeared for different values of capacitance C_2 , as the capacitance C_1 decreases from 10.50nF to 5.50nF . The existence of a periodic window in the chaotic region was displayed for $C_1=6.50\text{nF}$ and $C_2=5.30\text{nF}$.

References

- [1] Azzour, A., Duhr, R., and Hasler, M., (1984), "Bifurcation Diagram for a piece-wise-Linear Circuit", *IEEE Transactions on Circuits and Systems*, CAS-31, No.6, pp. 587-588.
- [2] Azzour, A., and Hasler, M., (1987), "Chaos in the RL-Diode Circuit", *Proceedings of the European Conference on Circuit Theory and Design, ECCTD 87*, Vol.1, pp. 295-300.
- [3] Azzour, A., Duhr, R., and Hasler, M., (1983), "Transition to Chaos in a Simple Nonlinear Circuit Driven by a Sinusoidal Voltage Source", *IEEE Transactions on Circuits and Systems*, CAS-30, No.12, pp. 913-914.
- [4] Carroll, T.L., Triandaf, I., Schwartz, I.B., and Pecora, L., (1992), "Tracking Unstable Orbits in an Experiment", *Physical Review A*, Vol.46, pp. 6189-6192.
- [5] Stouboulos, I.N., Kyprianidis, I.M., and Papadopoulou M.S., (2006), "Experimental Study of Antimonotonicity in a 4th Order Nonlinear Autonomous Electric Circuit", *WSEAS Transactions on Circuits and Systems*, Vol.5, Issue 11, pp.1662-1668.
- [6] Stouboulos, I.N., Papadopoulou M.S., Kyprianidis, I.M., (2007), "Genesis and Catastrophe of the Chaotic Double-Bell Attractor", *Proceedings of the 7th WSEAS International Conferences on Systems Theory and Scientific Computation*, pp.139-144.
- [7] Zhong, G.Q., and Ayrom, F., (1985), "Experimental Confirmation of Chaos from Chua's Circuit", *International Journal of Circuit Theory and Applications*, Vol.13, No.1, pp. 93-98.
- [8] Broucke, M.E., (1987), "One Parameter Bifurcation Diagram for Chua's Circuit", *IEEE Transactions on Circuits and Systems*, Vol.CAS-34, No.2, pp. 208-209.
- [9] Kahlert, C., (1988), "The Chaos Producing Mechanism in Chua's Circuit", *International Journal of Circuit Theory and Applications*, Vol.16, No.2, pp. 227-232.
- [10] Chua, L.O., and Lin, G.N., (1990), "Canonical Realization of Chua's Circuit Family", *IEEE Transactions on Circuits and Systems*, Vol.37, No.7, pp. 885-902.
- [11] Chua, L.O., Pivka, L., and Wu, C.W., (1995), "A universal circuit for studying chaotic phenomena", *Philosophical Transactions of the Royal Society of London a Mathematical and Physical Sciences*, Vol.353, No.1701, pp. 65-84.
- [12] Kyprianidis, I.M., Petrani, M.L., Kalomiros, J.A., and Anagnostopoulos, A.N., (1995), "Crisis-induced intermittency in a third-order electrical circuit", *Physical Review E*, Vol.52, No.3, pp. 2268-2273.

- [13] Matsumoto, T., (1984), "A Chaotic Attractor from Chua's Circuit", *IEEE Transactions on Circuits and Systems*, Vol.CAS-31, No.12, pp. 1055-1058.
- [14] Kyprianidis, I. M., Stouboulos, I. N., Haralabidis, P., and Bountis, T., (2000), "Antimonotonicity and chaotic dynamics in a fourth-order autonomous nonlinear electric circuit", *International Journal of Bifurcation and Chaos*, Vol.10, No.8, pp. 1903-1915.

List of Figures:

Figure 1. The four-dimensional autonomous electric circuit.....	2
Figure 2. The v-i characteristic of nonlinear element	2
Figure 3. The v-i characteristic of negative conductance	2
Figure 4. Bifurcation diagrams $(i_{L2})_p$ vs. C_1 for various values of C_2	4
Figure 5. Bifurcation diagrams $(i_{L2})_p$ vs. C_1 for various values of C_2	5
Figure 6. Lissajous diagrams v_{C2} vs. i_{L2} for $C_2=5.30\text{nF}$ and various values of C_1	6
Figure 7. Lissajous diagrams v_{C2} vs. i_{L2} for $C_2=5.30\text{nF}$ and various values of C_1	7
Figure 8. Power Spectrums and Waveforms for $C_2=5.30\text{nF}$	8

NONLINEAR TIME SERIES ANALYSIS OF THE CURRENT THROUGH PEG-Si THIN FILMS UNDER VARYING RELATIVE HUMIDITY

K. Atak[†], Ö. Aybar^{†*}, A. Hacınlıyan^{†*}, G. Şahin^{*}, Y. Skarlatos[†]

July 11, 2008

[†]Boğaziçi University, İstanbul, Turkey

^{*}Yeditepe University, İstanbul, Turkey

1 INTRODUCTION

Hydrophilic polymers attract attention because of their absorption, desorption and swelling behavior under exposure to water vapor and certain chemicals. Depending on environmental conditions (temperature, humidity, the structure of the polymer etc.) diffusion of the penetrants in the polymer networks shows different kinetics. When water molecules penetrate a polymer sample, the macromolecular chains rearrange themselves towards new conformations. The nature of the transport process and polymers' electrical, optical and physical properties are determined by the diffusion rate of the penetrant's molecules and the relaxation process.

Polyethylene glycol (PEG) is one of the mostly examined hydrophilic polymers which is sensitive to the changes in relative humidity and chemicals used as substrate. It is also known that PEG has a problem of stability; when exposed to water vapor, it swells and dissolves easily at high humidity. The instability of the structure and the transport properties in the long term is a general problem of polymer films produced by the physisorption of polymer molecules to the substrate material.

In this study the irregular current characteristic under constant voltage and slowly varying humidity through a thin film of Gamma-isocyanatopropyltriethoxysilane added Polyethylene glycol (PEG-Si) as a function of increasing relative humidity at equal time steps is analyzed for chaoticity. In previous studies it has been suggested that, after reaching a certain relative humidity level, a phase transition occurs from a semi crystalline state to a gel state, fluctuations in the elastic force relaxations and in the number of Hydrogen bonds cause the irregularities in the current [3]. We suggest that the irregular behavior of current

through PEG-Si thin films as a function of increasing relative humidity could be analyzed for chaoticity where the relative humidity is kept as a slowly varying parameter and the data is split into approximately 1% relative humidity bins. The results also indicate that the above mentioned phase transition is signalled by the sudden change in the maximal Lyapunov exponent with changing relative humidity.

2 EXPERIMENT

PEG-Si thin films were prepared either by dip-coating, or by dropping the polymer on the glass substrate. Aluminum electrodes were coated in a coplanar structure on the polymer by vacuum evaporation. The humidity was varied using different salt solutions placed in the chamber with the samples. Both the current and the humidity values were read by computer-controlled ammeters. The relative humidity was increased and the current was measured at uniform time intervals making time series analysis feasible.

The different regimes of conductivity result from the different types of contributions of water molecules to the hosting polymer. As humidity increases water molecules first start to bind to the oxygen atoms in the polymer chain. With increasing humidity, available oxygen atoms become extinct, and water molecules bind to other water molecules. This process results in water clusters among the polymer matrix. These different mechanisms contribute accordingly to the conductivity of the polymer. In Fig.1 the different behavior regimes can be inspected.

3 ANALYSIS

The characteristic and seemingly unstable behavior of the current as a function of increasing relative humidity, suggesting the possibility of chaotic behavior probably by the intermittency route, inspired us to apply non-linear time series analysis on the current measurements. We divide the data set according to observed regimes and kept humidity as a slowly varying parameter. We investigated the delay times using average mutual information; constructed the embedding vectors using embedding dimension values from the method of false nearest neighbors and finally calculated the maximal Lyapunov exponents for these different regimes. The results are shown in Fig.2. A monotonically increasing behavior of Lyapunov exponents with increasing humidity is observed. The chaoticity observed in the sample, as reflected by maximal positive Lyapunov exponents which change their regime around the relative humidity of 70%. This value is consistent with the reported value for the phase transition from the semicrystalline state to the gel state [3, 10]. This is another instance of the well known fact that a significant increase in the maximal positive Lyapunov exponent has been observed for phase transitions in simulated atomic systems interacting with the Lenard Jones potential [13] and of coupled anharmonic

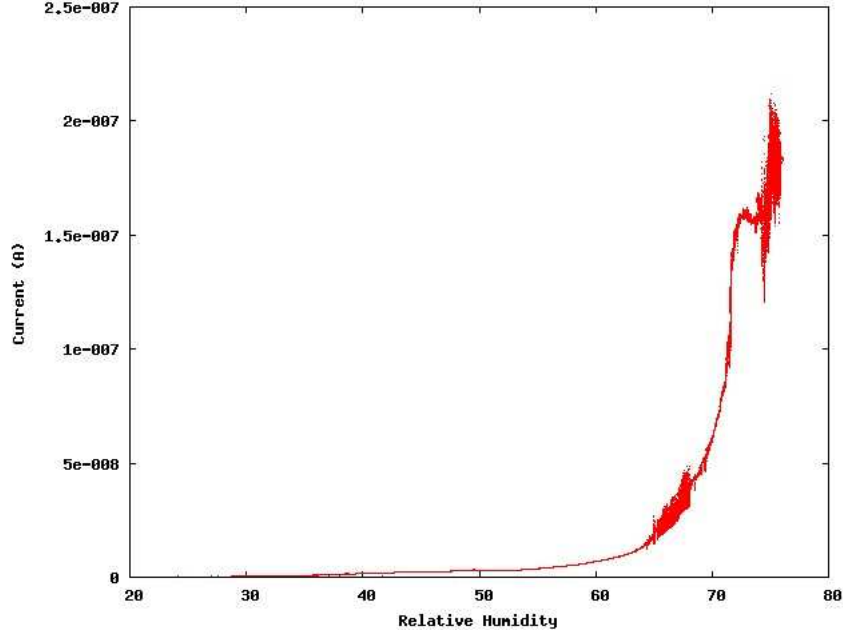


Figure 1: Current vs. Relative Humidity of PEG-Si

oscillator systems [14].

In order to confirm our suggestion of changing regimes due to the different binding modes of the water molecules, we used detrended fluctuation analysis on the data set (Fig.3). We observed two or three different regions where the slope is discontinuous; this points to changing dynamics of the correlations. One of the discontinuities is distinctly different since the slopes are 0.98, 1.03, 1.8.

Detrended fluctuation analysis (DFA) is a scaling analysis method used to estimate long-range power-law correlation exponents[6, 7]. One integrates the time series of length N , then divides the result into boxes of equal length, n . In each box of length n , a least squares line is fit to the data. The y coordinate of the straight line segments is denoted by $y_n(k)$. Next, the integrated time series, $y(k)$, is detrended by subtracting the local trend, $y_n(k)$, in each box. The root-mean-square fluctuation of this integrated and detrended time series is calculated by

$$F(n) = \sqrt{\frac{1}{N} \sum_{k=1}^N [y(k) - y_n(k)]^2}$$

This computation is repeated over all time scales (box sizes) to characterize the relationship between $F(n)$, the average fluctuation, as a function of box size, n . A linear relationship on a log-log plot indicates the presence of power law scaling. Under such conditions, the fluctuations can be characterized by a

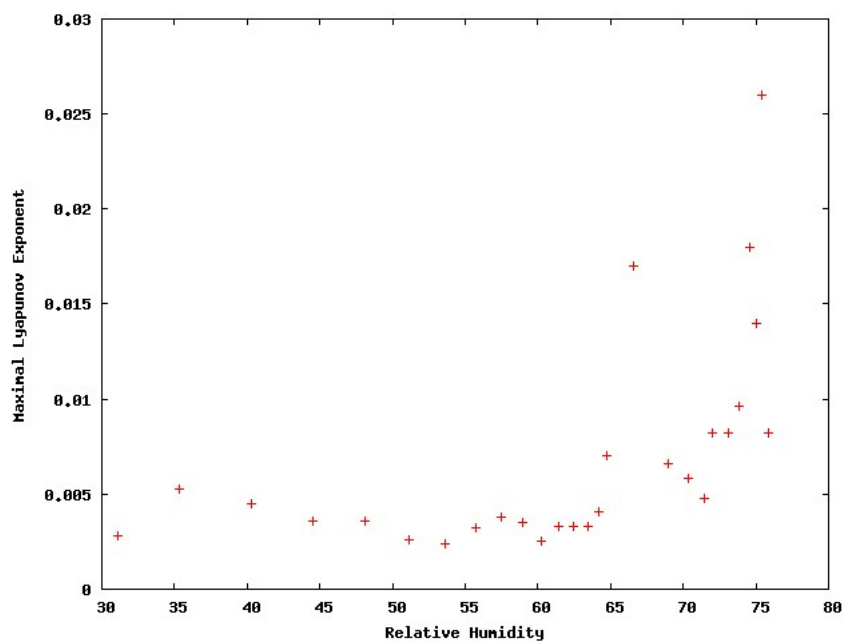


Figure 2: Maximal Lyapunov Exponent vs. Relative Humidity of PEG-Si

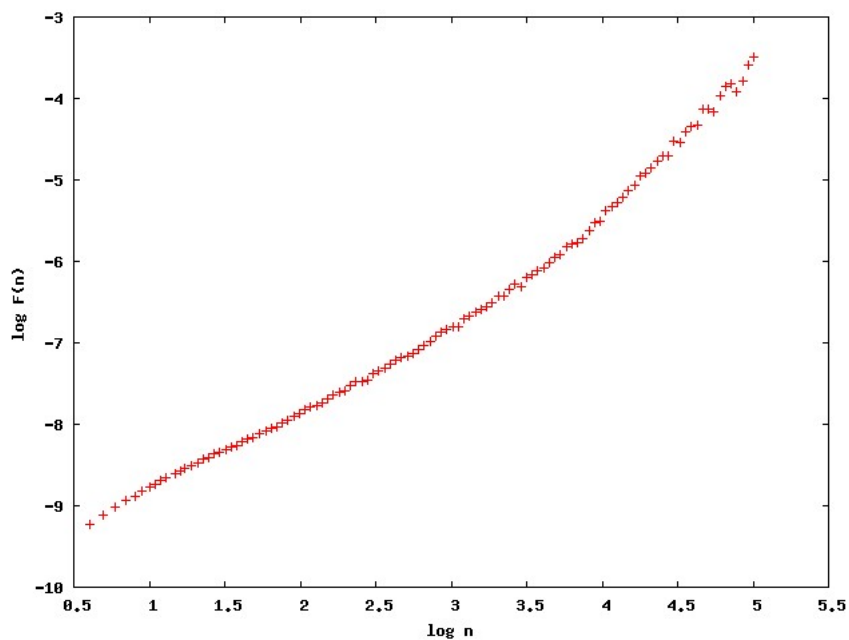


Figure 3: Average fluctuation vs. box size

scaling exponent, α , such that $F(n) : n^\alpha$. A crossover in the scaling exponent, α , indicates a transition from one type to a different type of underlying correlation, due to a transition in the dynamical properties [8, 9].

4 CONCLUSION

The complex structure of polymers (including impurities) implies many degrees of freedom and a multi-fractal structure. The difficulty of obtaining identical results under nearly identical conditions for polymers is well known in the literature [16]. Thus it becomes necessary to analyze the conductivity of polymers by nonlinear considerations such as maximal Lyapunov exponent and the DFA exponent.

The irregular behavior of current through PEG-Si thin films as a function of increasing relative humidity was analyzed using nonlinear time series analysis and detrended fluctuation analysis. Low dimensional chaos with maximal Lyapunov exponents abruptly changing regime at the relative humidity of 70% is observed. Furthermore, the observed chaotic behavior persists for a wide range of values of the humidity. Hence the dynamics underlying the transient current can be understood in terms of chaoticity. Abruptly changing regime of Lyapunov is consistent with the phase transition from semicrystalline state to gel state (for using Lyapunov exponents as an indicator of phase transitions see [14]). The behavior of the system with different regions has also been confirmed via detrended fluctuation analysis. Even though a general relation between Lyapunov exponent and the DFA exponent has not been reported yet, there are case based studies where analogies between the above mentioned exponents are shown [17]. The change in scaling exponent in case of phase transition is also reported [18]. This further supports the detection of phase transition in PEG as well as the necessity of using nonlinear methods in analyzing behavior of current through PEG-Si thin films. Based on the studies of about amorphous materials with irregular behavior, the use of nonlinear methods for analyzing the conductivity mechanisms in such materials seems crucial [4, 5, 19].

References

- [1] H.D.I. Abarbanel, R. Brown, J.J. Sidorowich, L.S. Tsimring, Rev. Mod. Phys. 65 (1993) 1331-1392
- [2] R. Hegger, H.G. Kantz, T. Schreiber, Nonlinear Time Series Analysis, Cambridge University Press, 1997
- [3] O. Erdamar, Y. Skarlatos, G. Aktas, M.N. Inci, Applied Physics A, Vol. 83, 159-162, 2006
- [4] A. Hacinlyan, Y. Skarlatos, G. Sahin, G. Akin, Chaos, Solitons and Fractals 17 (2003) 575-585

- [5] A. Hacinliyan, Y. Skarlatos, H.A. Yildirim, G. Sahin , Phys. Rev. B 73 (2006) 134302 -134307
- [6] C. K. Peng, S. V. Buldyrev, S. Havlin, M. Simons, H. E. Stanley and A. L. Goldberger, Phys Rev E 49, 1685 (1994)
- [7] C.K Peng ,S. Havlin, H.E Stanley, A.L. Goldberger, Chaos 5, 82 (1995)
- [8] K. Hu, P.Ch. Ivanov, Z. Chen, P. Carpena, H.E Stanley, Phys. Rev. E 64, 011114 (2001)
- [9] Z. Chen, P.Ch. Ivanov , K. Hu, H.E Stanley, Phys. Rev. E 65, 041107 (2002)
- [10] J. Crank, G.S. Park (editors), Diffusion in Polymers, Academic Press, London, 1968
- [11] W. Chen, K.R. Shull, Macromolecules, Vol.32, 136-144, 1999
- [12] D. A. Seanor, Electrical Properties of Polymers, 1-58, 1982
- [13] Nayak, S. K., Ramasawamy, R, Chakravarty, C. Physical Review E51, 3376-3380 (1995)
- [14] Barre, J. and Dauxois, T. Europhysics Letters, 55, 164-170 (2001)
- [15] H. Kitano et al., Langmuir, 17, 1889-1895 (2000)
- [16] V. Adamec and J. H. Calderwood, J. Phys. D. 11 (1978) 781-800.
- [17] Sozański,M and Zebrowski, J. Acta Physica Polonica B, 36, 1803-1821,2005.
- [18] G. F. Zebende, M. V. S. da Silva, A. C. P. Rosa, Jr., A. S. Alves, J. C. O. de Jesus and M. A. More,Physica A,342,322-328.
- [19] A. Hacinliyan, Y. Skarlatos, H.A. Yildirim and G. Sahin, Fractals ,14, 125-131,2006.

THE SOLUTIONS OF BRATU-TYPE PROBLEMS BY HE'S HOMOTOPY PERTURBATION METHOD

Ahmet Yıldırım

ahmety@mail.ege.edu.tr

*Department of Mathematics, Science Faculty, Ege University, Campus, 35100 Bornova-İzmir,
Turkey*

Abstract:

A new scheme, deduced from He's homotopy perturbation method, is presented for solving Bratu's problem. Some numerical experiments are made. The scheme is shown to be highly accurate, and only a few terms are required to obtain accurate computable solutions.

Keywords: Bratu-type problems; He's homotopy perturbation technique; Taylor expansion;

1. Introduction

In this paper, we concerned with boundary value and initial value problems which are referred to in the literature [1,2] as Bratu's problem. Bratu's boundary value problem can be given by

$$\begin{aligned} u'' + \lambda e^u &= 0 \\ u(0) &= 0, \quad u(1) = 0 \end{aligned} \quad (1)$$

The exact solution to Eq. (1) is given in [3,6,7] and given by

$$u(x) = -2 \ln \left[\cosh \left(\frac{0.5(x-0.5)\theta}{\cosh(0.25\theta)} \right) \right] \quad (2)$$

where θ satisfies $\theta = \sqrt{2\lambda} \cosh\left(\frac{\theta}{4}\right)$. The Bratu problem has zero, one or two solutions when $\lambda > \lambda_c$, $\lambda = \lambda_c$, $\lambda < \lambda_c$, respectively, where the critical value λ_c satisfies the equation $1 = \frac{1}{4} \sqrt{2\lambda_c} \sinh\left(\frac{\theta_c}{4}\right)$ and its calculated value is $\lambda_c = 3.513830719$.

In higher dimensions, the standard Bratu's problem was used to model a spontaneous combustion in a slab such as the fuel ignition of the thermal combustion theory. Numerical solutions of this problem were obtained by a shooting method [3]. In addition, Boyd [4,5] employed Chebyshev polynomial expansions and the Gegenbauer polynomials as base functions to solve the one and two dimensional Bratu's equations. Deeba *et al* [6] implemented a numerical algorithm, based on the decomposition technique, to standard Bratu's boundary value problem. Recently, Wazwaz [7] has solved Bratu-type boundary value and initial value problems by applying Adomian decomposition method. In addition, Bratu-type initial value problem can also be given by [7]

In addition, Bratu- type initial value problem can also be given by [7]

$$\begin{aligned} u'' - 2e^u &= 0, \quad 0 < x < 1 \\ u(0) &= u'(0) = 0 \end{aligned} \quad (3)$$

where the exact solution of Eq.(3) can be given as

$$u(x) = -2 \ln(\cos x) \quad (4)$$

2. Homotopy Perturbation Method

In recent years, many new analytical approximate methods were suggested to solve two-point boundary-value and initial value problems. Among these, the homotopy method [8], the homotopy analysis method [9-10], the homotopy perturbation method [11-18], Variational methods [19-22] etc. Based on the modified homotopy perturbation technique, we introduce a small parameter and use Taylor expansion to study the problems in hand.

To illustrate the basic concepts of modified homotopy perturbation method, we consider the two special cases of Bratu's problem and we will demonstrate the usefulness and effectiveness of the proposed technique.

Example 1 (*Bratu's boundary value problem*)

The first problem to be considered is Bratu's boundary value problem given in Eq. (1). Now, to apply modified homotopy perturbation method, we re-write Eq.(1) in the form

$$\begin{aligned} u'' + \lambda e^{pu} &= 0 \\ u(0) &= 0, \quad u(1) = 0 \end{aligned} \quad (5)$$

where $p \in [0, 1]$ and is an imbedding parameter. As in He's homotopy perturbation method, it is obvious that when $p = 0$, Eq. (5) becomes a linear equation; when $p = 1$, it becomes the original nonlinear one. Due to the fact that $p \in [0, 1]$, so the imbedding parameter can be considered as a "small parameter". Applying the perturbation technique [20,21], we can assume that the solution of Eq. (5) can be expressed as a power series in p :

$$u = u_0 + pu_1 + p^2u_2 + p^3u_3 + \dots \quad (6)$$

Setting $p = 1$ results in the approximate solution of the problem:

$$u^* = \lim_{p \rightarrow 1} u = u_0 + u_1 + u_2 + u_3 + \dots \quad (7)$$

To obtain its approximate solution of Eq. (5), we expand e^{pu} into Taylor series

$$e^{pu} = 1 + pu + \frac{p^2u^2}{2!} + \frac{p^3u^3}{3!} + \frac{p^4u^4}{4!} + \dots \quad (8)$$

Substituting (6)-(8) into (5) and equating the coefficients of like powers of p , we obtain

$$\begin{aligned} p^0 : & \begin{cases} u_0'' = -\lambda \\ u_0(0) = 0, \quad u_0(1) = 0 \end{cases} \\ p^1 : & \begin{cases} u_1'' = -\lambda u_0 \\ u_1(0) = 0, \quad u_1(1) = 0 \end{cases} \\ p^2 : & \begin{cases} u_2'' = -\lambda u_1 - \frac{\lambda}{2} u_0^2 \\ u_2(0) = 0, \quad u_2(1) = 0 \end{cases} \\ p^3 : & \begin{cases} u_3'' = -\lambda u_2 - \lambda u_0 u_1 - \frac{\lambda}{6} u_0^3 \\ u_3(0) = 0, \quad u_3(1) = 0 \end{cases} \end{aligned} \quad (9)$$

Thus, by solving the equations above, we obtain,

$$u_0 = -\frac{1}{2}\lambda x^2 + \frac{1}{2}x$$

$$u_1 = \frac{1}{24}\lambda^2 x^4 - \frac{1}{12}\lambda^2 x^3 + \frac{1}{24}\lambda^2 x$$

$$u_2 = -\frac{1}{180}\lambda^3 x^6 + \frac{1}{60}\lambda^3 x^5 - \frac{1}{90}\lambda^3 x^4 - \frac{1}{144}\lambda^3 x^3 + \frac{1}{160}\lambda^3 x$$

Hence, we have;

$u_0 = u_0$	with zero-order approximation
$u_1 = u_0 + u_1$	with first-order approximation
$u_2 = u_0 + u_1 + u_2$	with second-order approximation
$u_3 = u_0 + u_1 + u_2 + u_3$	with third-order approximation

Thus, one can recursively determine every term of the series $\sum_{n=0}^{\infty} u_n$ as its shown above.

Therefore, it is easy to compute the approximate solution.

Now, to verify the rapid convergence of the technique, we have conducted some numerical experience for $\lambda = 1$ and $\lambda = 2$, and made the comparison with the exact solution given in Eq.(2). Table 1 shows the comparison obtained by u_2 with exact solution for distinct x values (i.e. 0.1, 0.2, 0.3, ..., 0.9) for $\lambda = 1$. Table 2 shows the comparison obtained by $2u$ with the exact solution for distinct x values (i.e. 0.1, 0.2, 0.3, ..., 0.9) for $\lambda = 2$. As it is seen from the Table 1, the max error is less than 0.06 % and max relative error is less than 1.2 % for $\lambda = 1$. Table 2 gives the max error less than 1.8 % and max relative error less than 5.4 for $\lambda = 2$. Consequently, the numerical results show that the scheme, compared with the exact solution, approximates the exact solution with a high degree of accuracy, using only few terms of the numerical algorithm. And the procedure is simpler to implement.

Table 1: Comparison of the results obtained by HPM, ADM and the exact solution of Bratu's BVP for the case $\lambda = 1$.

x	HPM	Error	ADM	Error	Exact
0.1	0.04970460556	0.000142184	0.0471616875	0.0026851025	0.0498467900
0.2	0.08891497778	0.000274957	0.0871680000	0.0020219350	0.0891899350
0.3	0.11722145000	0.000387646	0.1177614375	0.0001523419	0.1176090956
0.4	0.13431902220	0.000471230	0.1369920000	0.0022017474	0.1347902526
0.5	0.14001736110	0.000521853	0.1435546875	0.0030154733	0.1405392142
0.6	0.13424680000	0.000543452	0.1369920000	0.0022017474	0.1347902526
0.7	0.11706033890	0.000548757	0.1177614375	0.0001523419	0.1176090956
0.8	0.08863164440	0.000558291	0.0871680000	0.0020219350	0.0891899350
0.9	0.04924905000	0.000597740	0.0471616875	0.0026851025	0.0498467900

Table 2: Comparison of the results obtained by HPM, ADM and the exact solution of Bratu's BVP for the case $\lambda = 2$.

x	HPM	Error	ADM	Error	Exact
0.1	0.1112868444	0.012092944	0.1144107440	0.0152172440	0.0991935000
0.2	0.2003864889	0.008642489	0.2064191156	0.0146751156	0.1917440000
0.3	0.2654216000	0.002569900	0.2738793116	0.0058878116	0.2679915000
0.4	0.3049521778	0.013383822	0.3150893646	0.0032466354	0.3183360000
0.5	0.3180555556	0.017881944	0.3289524214	0.0069850786	0.3359375000
0.6	0.3043744000	0.013961600	0.3150893646	0.0032466354	0.3183360000
0.7	0.2641327112	0.003858790	0.2738793116	0.0058878116	0.2679915000
0.8	0.1981198222	0.006375822	0.2064191156	0.0146751156	0.1917440000
0.9	0.1076424000	0.008448900	0.1144107440	0.0152172440	0.0991935000

Example 2 (*Bratu's initial value problem*)

An interesting nonlinear equation is Bratu's initial value problem [7] given by Eq.(3).

Similar to Example 1, we, again, re-write Eq. (3) in the form;

$$\begin{aligned}
 u'' - 2e^{pu} &= 0, \quad 0 < x < 1 \\
 u(0) = u'(0) &= 0
 \end{aligned}
 \tag{10}$$

Substituting, again, (6)-(8) into (10) and equating the coefficients of like powers of p , we obtain

$$p^0 : \begin{cases} u_0'' = 2 \\ u_0(0) = 0, \quad u_0'(0) = 0 \end{cases}$$

$$p^1 : \begin{cases} u_1'' = 2u_0 \\ u_1(0) = 0, \quad u_1'(0) = 0 \end{cases}$$

$$p^2 : \begin{cases} u_2'' = 2u_1 + u_0^2 \\ u_2(0) = 0, \quad u_2'(0) = 0 \end{cases} \quad (11)$$

$$p^3 : \begin{cases} u_3'' = 2u_2 + 2u_0u_1 + \frac{u_0^3}{3} \\ u_3(0) = 0, \quad u_3'(0) = 0 \end{cases}$$

.

.

.

From the above equations, we can obtain

$$u_0 = x^2$$

$$u_1 = \frac{x^4}{6}$$

$$u_2 = \frac{2x^6}{45}$$

$$u_3 = \frac{17x^8}{1260} \quad (12)$$

$$u_4 = \frac{62x^{10}}{14175}$$

$$u_5 = \frac{691x^{12}}{46775}$$

.

.

.

and

$$u(x) = x^2 + \frac{x^4}{6} + \frac{2x^6}{45} + \frac{17x^8}{1260} + \frac{62x^{10}}{14175} + \frac{691x^{12}}{46775} + \dots$$

or equivalently

$$u(x) = -2\left(-\frac{x^2}{2} - \frac{x^4}{12} - \frac{x^6}{45} - \frac{17x^8}{2520} - \frac{31x^{10}}{14175} - \frac{691x^{12}}{935550} + \dots\right) \quad (13)$$

which is the expansion of $-2 \ln(\cos x)$ and is the exact solution of Bratu-type initial value problem given in Eq. (4).

3. Conclusion

In conclusion, the new scheme deduced from He's homotopy perturbation method is powerful and efficient technique in finding the approximate solutions for nonlinear equations using only few terms. The scheme overcomes the difficulty arising in calculating nonlinear intricately terms. The results obtained in this paper can be extended to significantly more general classes of nonlinear problems involving transcendental, trigonometric etc. functions.

4. References

- [1] Aris, R. *The Mathematical Theory of Diffusion and reaction in Premeable Catalyst*, Vol. I, Clarendon Press, Oxford, 1975
- [2] Frank-Kamenetskii, D.A. Calculation of thermal explosion limits, *Acta Phys. Chim. URSS* 10, (1939) 365
- [3] Ascher, U.M. Matheij, R., Russell, R. D., Numerical solution of boundary value problems for ordinary differential equations, SIAM, Philadelphia, PA, 1995.
- [4] Boyd J.P., Chebyshev polynomial expansions for simultaneous approximation of two branches of a function with application to the one-dimensional Bratu equation, *Applied Mathematics and Computation* 142 (2003) 189–200.
- [5] Boyd J.P, An analytical and numerical study of the two-dimensional Bratu equation, *Journal of Scientific Computing* 1 (2) (1986) 183–206.
- [6] Deeba, E., Khuri, S.A. and Xie, S., An algorithm for solving boundary value problems, *Journal of Computational Physics*, 159 (2000) 125–138
- [7] Wazwaz, A-M, adomian decomposition method for a reliable treatment of the Bratu type equations, *Applied Mathematics and Computation*, 166 (2005) 652–663.
- [8] Watson, L.M., Scott, M. R. Solving spline-collocation approximations to nonlinear two-point boundary-value problems by a homotopy method, *Appl. Math. Comput.* 24 (4) (1987) 333–357.
- [9] Liao, S. J. *Beyond Perturbation: Introduction to the Homotopy Analysis Method*, Chapman & Hall/CRC, Boca Raton, 2003.
- [10] Liao, S. J. A challenging nonlinear problem for numerical techniques, *J. Comput. Appl. Math.* 181 (2005) 467–472.
- [11] He, JH, *Non-Perturbative Methods for Strongly nonlinear Problems*, dissertation.de-verlag im Internet GmbH, Berlin, 2006
- [12] He, JH. , Homotopy perturbation technique, *Computer Methods in Applied Mechanics and Engineering*, 178 (3-4): 257-262, 1999
- [13] He, JH. , A coupling method of a homotopy technique and a perturbation technique for non-linear problems, *International Journal of Non-linear Mechanics* 35 (1), 2000, 37-43.

- [14] He, JH., Homotopy perturbation method: a new nonlinear analytical technique, *Applied Mathematics and Computation* , 135 (1): 73-79, 2003
- [15] Öziş, T., Yıldırım, A., A note on He's homotopy perturbation method for van der Pol oscillator with very strong nonlinearity, *Chaos Solitons & Fractals*,34(3),989-991,2007
- [16] Öziş,T., Yıldırım, A., Traveling wave solution of Korteweg-de Vries Equation using He's homotopy perturbation method, *Int. J. Nonlinear Sci. Numer. Simul.*,8(2) (2007) 239-242
- [17] Öziş, T., Yıldırım, A., A comparative study of He's homotopy perturbation method for determining frequency-amplitude relation of a non-linear oscillator with discontinuities, *Int. J. Nonlinear Sci. Numer. Simul.*,8(2) (2007) 243-248
- [18] Ramos, J.I., Series approach to the Lane-Emden equation and comparison with the homotopy perturbation method,*Chaos, Solitons and Fractals*,doi: 10.1016/j.chaos.2006.11.018
- [19] He, JH. Variational iteration method-some recent results and new interpretations, *Journal of Computational and Applied Mathematics*, 207(1),3-17,2007
- [20] He, JH. Variational approach for nonlinear oscillators, *Chaos, Solitons and Fractals*, 34(5),1430-1439,2007
- [21] Momani, S., Abuasad, S., Odibat, Z., Variational iteration method for solving nonlinear boundary value problems, *Applied Mathematics and Computation*, 183(2),1351-1358,2006
- [22] Öziş, T. Yıldırım, A. An application of He's semi-inverse method to the nonlinear Schrödinger(NLS) equation, *Computers and Mathematics with Applications*, 54(7-8),1039-1042,2007

Comparative study between SISCON and MATLAB in pyrolysis reactor identification

MESSAOUDA AZZOUZI*

Abstract

In this work, we have tried to identify a pyrolysis reactor; this type of reactor is widely used in petrochemical plants, especially in oil refineries; the analytical study was suggested to optimize the pyrolysis reactor operation and then to control it, to be as far away as possible so as not to be affected by changes in deliberate operating conditions of the procedure to ensure reactor stability and, certainly, human safety. This is a case study taken from the great oil refinery of Pitesti in Romania, regarded as a major center of oil refining from Eastern Europe. Recorded data were processed by SISCON, the dedicated software to the ACPC laboratory of the Automatic Control Faculty, University "Politehnica" of Bucharest, and the industrial development software MATLAB; the comparison between these two strategies used on pyrolysis reactor identification is deeply studied.

Dans cet article, on a essayé d'identifier un réacteur de pyrolyse, ce type des réacteurs est largement utilisé dans les installations pétrochimiques et précisément les raffineries pétrolières; l'étude analytique a été suggérer en vue d'optimiser le fonctionnement du réacteur de pyrolyse et puis le contrôler, en l'éloignant tant que possible d'être affectée par les variations délibérées des conditions opératoires de la procédure pour garantir la stabilité du réacteur et certainement l'assurance humaine. C'est une étude de cas prise de la grande raffinerie pétrolière de Pitesti en Roumanie, considérée comme un grand pôle du raffinage pétrolier à l'Europe d'Est. Les données enregistrées étaient procédées par le logiciel SISCON dédié au Laboratoire ACPC de la Faculté d'Automatique de l'Université "Politehnica" de Bucarest, et le MATLAB, le logiciel de développement industriel, la comparaison entre ces deux stratégies utilisées à l'identification et l'optimisation du réacteur de pyrolyse est profondément étudiée.

Keywords: *Pyrolysis reactor, Identification, Digital control, Adaptive stochastic control, Stochastic process, Gaussian noise, Optimization, Linearization.*

*Department of Automatic Control and System Engineering, Faculty of Automatic Control and Computer Science, University POLITEHNICA of Bucharest, Str 13 Septembrie, 06003 - Bucharest, Romania.

1. Introduction

Several types of reactors are based on the principle of the fuel especially current reactors, which are exploited in the chemical industry [9] [2]. We want by the combination of a quantity of benzene with water under certain conditions, and under the catalyst effects to produce the optimized quantity of ethylene by assuring the system stability. It is known that the pyrolysis reactor contains two parts:

- **Convection area:** this represents the area where we find the alloy of the primary matter (the benzene and the steam of the water); to produce a chemical reaction, it is necessary that the tank temperature must be equal to 500°C , and the pressure must be equal to 4 atm.
- **Radiation area:** it is the area where we find the reactions under a temperature of $680\text{-}750^{\circ}\text{C}$.



Figure. 1. Pyrolysis reactor example

2. Plant presentation

The pyrolysis reactor is intended to obtain the ethylene, one of its products after its several reactions. Benzene and steam are introduced into the plant by two access routes at a constant debit; the quantity of heat required is obtained from a fire system that uses the right fuel methane gas [4].

To guarantee the desired insurance of pyrolysis reactor operation, it is necessary to create an automation mechanism that controls the primary matter debit, the primary matter compositions analysis and the reactions products alloy analysis [1]; to realize this project we need four controllers:

- 2 debit controllers, one to control the benzene debit then the other to adjust the debit steam introduced into the plant;
- A pressure controller type RST;
- A temperature controller type RST.

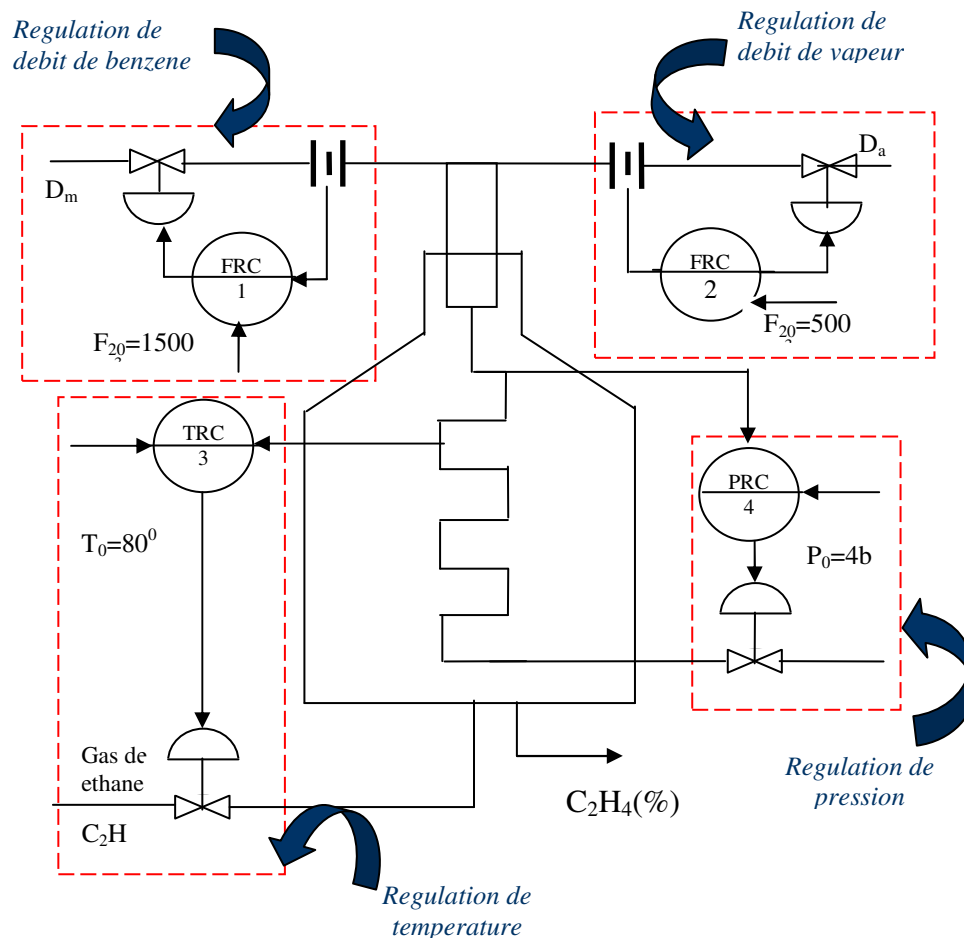


Figure 2. Pyrolysis reactor block scheme

The system variables are limited technologically as follows:

$x_1 = D_{mp}$: benzene debit ($1000-1600 \text{ Nm}^3/\text{h}$)

$x_2 = D_v$: steam debit rate ($430/540 \text{ Nm}^3 / \text{h}$)

x3=T: operation temperature (820-860 °C)

x4=P: operation pressure (3.2-4.5 atm)

X%: the benzene concentration in the reactor (79-99.1%)

Pyrolysis reactors have been used as preparative methods and as means of generating transient intermediates that can be trapped or observed spectroscopically, or quenched by a further reaction. For preparative purposes, reactions in pyrolysis reactor can generally be carried out by a flow process in which the reactant is vaporized with a stream of inert gas through a heated tube, sometimes at reduced pressure; figure (3) demonstrates some of the effectuated reactions in pyrolysis reactor.

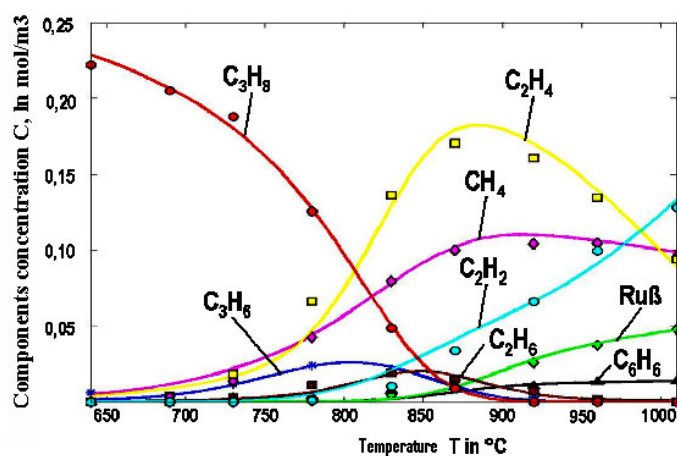


Figure 3. Components concentration depending on the temperature in pyrolysis reactor

3. Data acquisition

About 256 data samples were recorded by using a computer. Because their measurement within the pyrolysis reactor took a long time due to the diversity of sampling period between the input variables, e.g. when we take a temperature sampling period which is equal to 5s, we have to wait for 256 samples during the period of 23 minutes, sufficient duration to record all data, on the contrary in the pressure and the two debits cases the process is not as slow as that in the temperature. See figure (4).

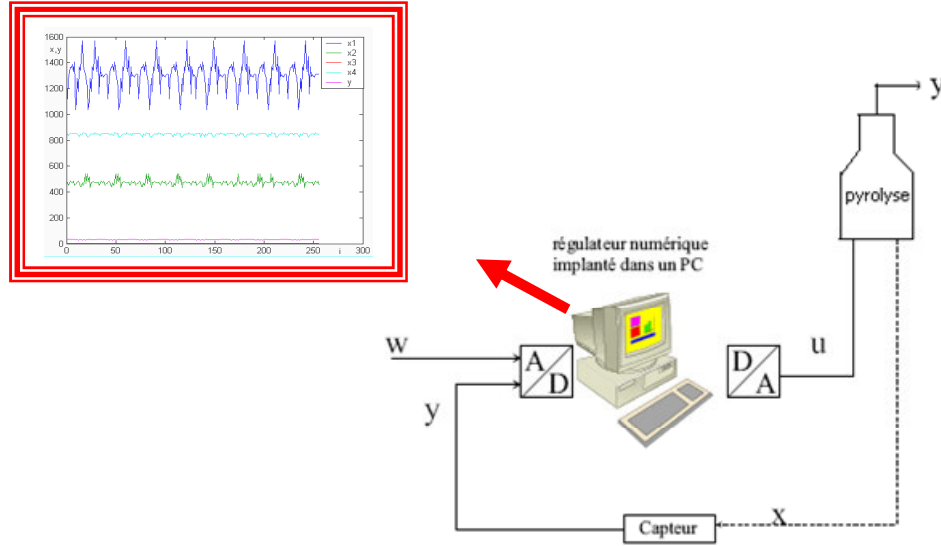


Figure 4. Input/Output data

4. Stochastic adaptive control

The research of Rohrs, Valavani, Athans and Stein pointed out potential instabilities of then existing adaptive control algorithms caused by the presence of unmeasurable output disturbances and high frequency unmodeled dynamics. The publications of Rohrs *et al* were instrumental for defining new research directions in the adaptive control field, and the topic of Stochastic Adaptive Control became a new area for worldwide research [10]. To formulate the adaptive control problem we must specify the model for the process, the admissible control signals, and the specifications (loss function) for the closed loop system. Introduce the following notations:

$y(k)$ is the process output, $u(k)$ is the control signal, $\theta(k)$ is a vector of the unknown parameters of the process, $\hat{\theta}(k)$ is the current estimate of the process parameters, and $P(k)$ is the parameter uncertainty. Inputs up to time $k-1$ and outputs up to time k are collected into the vector

$$\gamma_k = [y(k) \ y(k-1) \ u(k-1) \dots y(0) \ u(0)] \quad (1)$$

It is assumed that the process is described by the discrete time model

$$y(k+1) = f(u(k), \gamma_k, \theta(k), \xi(k)) \quad (2)$$

Where $\xi(k)$ is a stochastic process driving the process and/or the parameters of the process. The probability distribution of ξ is assumed known. This implies that the output at the next sampling

instance, $k+1$ is a, possibly nonlinear, function of the control signal to be determined at time k , some, not necessarily all, of the elements in γ_k , and of the unknown process parameters.

It is assumed that the function $f(\cdot)$ is known. This implies that the structure of the process is known but that there are unknown parameters, $\theta(\cdot)$. The admissible controllers are causal functions $g(\cdot)$ of all information gathered up to time k , i.e. γ_k . If the parameters of the process are known the control signal at time k is also allowed to be a function of $\theta(k)$.

The performance of the closed loop system is measured by a loss function, which should be as small as possible. Assume that the loss function to be minimized is

$$J_N = E \left\{ \frac{1}{N} \sum_{k=1}^N h(y(k), u(k-1), y_r(k), k) \right\} \quad (3)$$

where y is the process output, y_r is the reference signal, $h(\cdot)$ is a positive convex function, and E denotes mathematical expectation taken over the distribution of ξ . This is called an N stage criterion.

The loss function should be minimized with respect to the admissible control signals $u(0)$, $u(1)$, ..., $u(N-1)$. A simple example of the loss function is

$$J_N = E \left\{ \frac{1}{N} \sum_{k=1}^N (y(k) - y_r(k))^2 \right\} \quad (4)$$

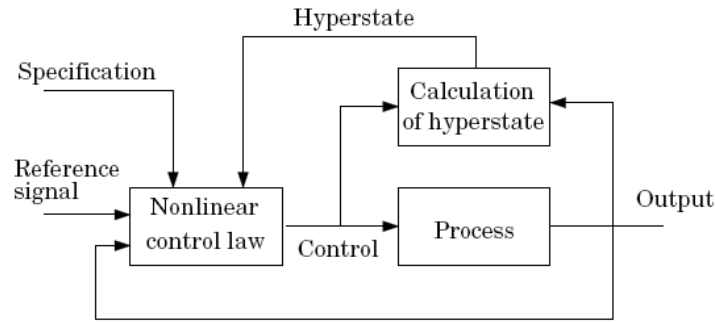


Figure 5. Block diagram of an adaptive controller obtained from stochastic control theory

5. SISCON processing

SISCON is a recent application designed for the systems optimization and efficient control; it is a software that was developed in C++ (Builder), and was installed in computers of the ACPC laboratory Faculty of Automatic Control and Computer Science

of “Politehnica” University of Bucharest [5]. The data are saved in a file named copy265.DNL, which must be uploaded into the software as illustrated in figure (6).

The relation between the output and the four inputs must be constructed from experimental data [8]. The mathematical equation that defines the process operation is given by:

$$y = A_0 + A_1x_1 + A_2x_2 + A_3x_3 + A_4x_4$$

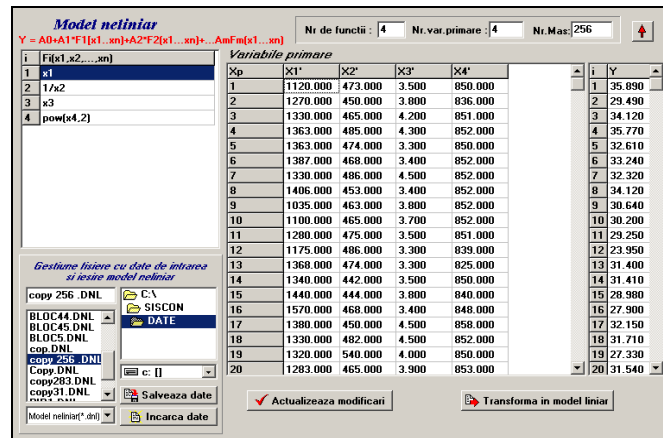


Figure 6. SISCON loading data file

The majority of systems have a non linearity in practice; some of them are described by local linear models in limited scale of operation [6] [7]. The linearization of recorded data in this file is done automatically by clicking to transform into a linear model, after the selection of model parameters.

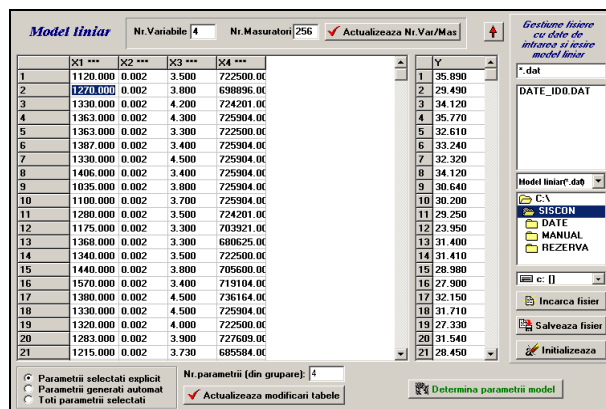


Figure 7. The linear model

Starting from the linearization of the non linear model, we can find the different parameters A_i of the linear model $Y = A_0 + A_1 X_1 + A_2 X_2 + A_3 X_3 + A_4 X_4$; those are well demonstrated in figure (9).

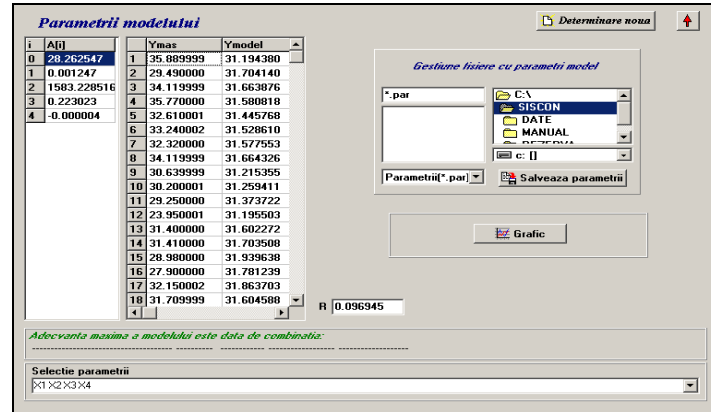


Figure 9. Linear model parameters

The vector parameters A can be displayed directly in the SISCON interface, and they are given by:

$$A = \begin{bmatrix} 28.262547 \\ 0.001247 \\ 1583.228516 \\ 0.223023 \\ -0.000004 \end{bmatrix}$$

The final equation of the linearized system is:

$$Y = (28.262547) + (0.001247) \cdot X_1 + (1583.228516) \cdot X_2 + (0.223023) \cdot X_3 + (-0.000004) \cdot X_4$$

The error and the squared error between the model found and the real output are represented in the figure (10).

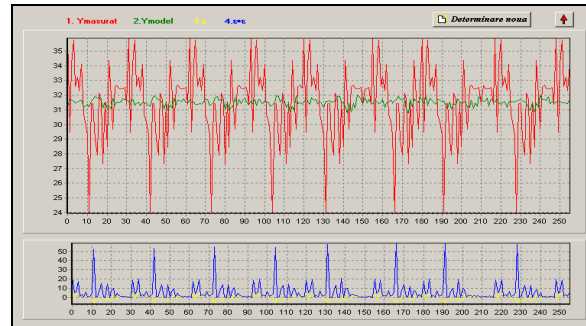


Figure 10. The error and the squared error between the linear model and the real output

Where:

x : is the experimental data matrix

X : is the linearized input matrix

A : is the estimated vector parameters

y : is the process output

$Y=y_{\text{mod}}$: is the model output

6. MATLAB simulation

The use of another method certainly provided other results, in MATLAB simulation we had to use the vector parameters found previously by SISCON software.

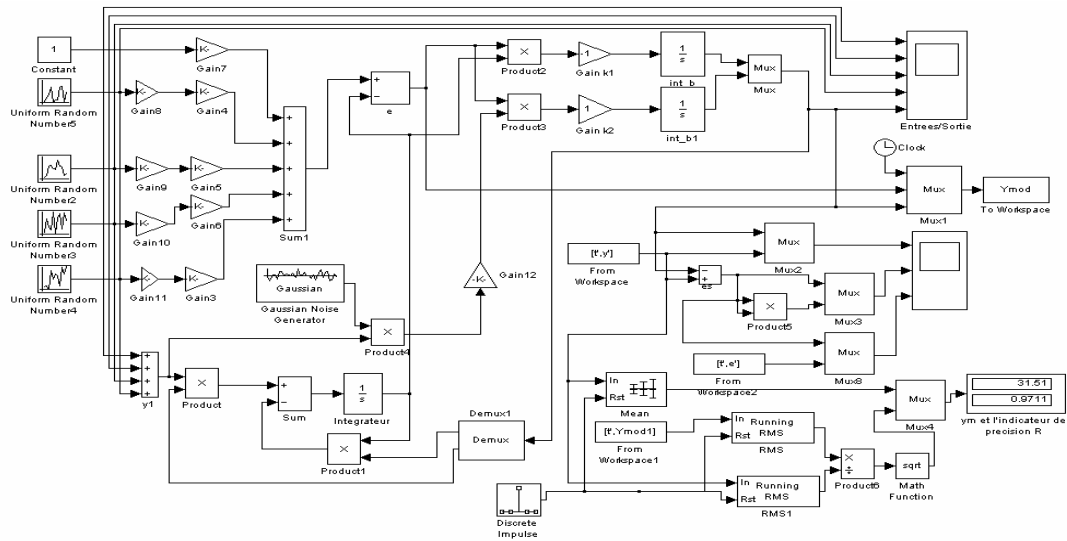
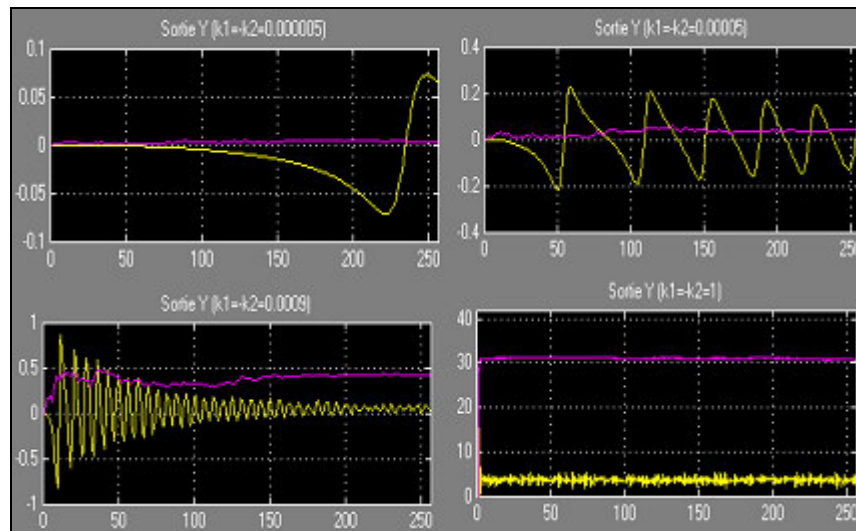


Figure 11. Adaptive stochastic control simulation

We have tested this simulation results in several cases to illustrate the effect of both estimation gains k_1 and k_2 on the efficiency of the adaptive control with Gaussian noise, Figure (12) shows the output y as a function of different gain values.

Figure 12. Model output tuning depending on k_1 and k_2

To know the efficiency of this model we must calculate the error which is given by the relation:

$$e(i) = y(i) - y_{\text{mod}}(i)$$

Where:

$e(i)$: is the error is each step i

$y(i)$: is the real output

$y_{\text{mod}}(i)$: is the model

$y_m(i)$: mean of y

The model with the real output, then the error with the squared error, are presented in figure (13), which demonstrates a small variation in error, by comparing it with the SISCON interface.

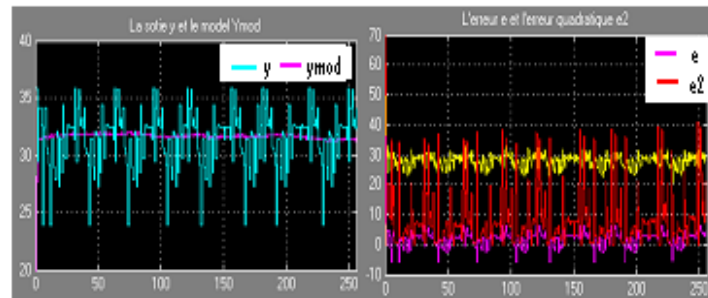


Figure 13. The model with real output and the error with the squared error respectively

5. Comparison between MATLAB SIMULATION and SISCON

The comparison between these two software, in the identification and the control of a non-linear system, gives different results, but there is always the possibility of knowing which of those two software is the most efficient, so it is necessary to calculate the specification indicator in each of the two simulations.

The deviation of the real process to the mean value is given by:

$$S_y = \sum_{k=1}^M (y - y_m)^2$$

The deviation of the found model to the mean value is given by:

$$S_{y_{\text{mod}}} = \sum_{k=1}^M (y_{\text{mod}} - y_m)^2$$

The model specification indicator R is given by the relation

$$R^2 = S_{y \text{ mod}} / S_y$$

Where M=256 is the samples number;

SISCON has the possibility to display directly this specified value in the model parameters determination step when $R=0.097$, then we construct an additional simulink part that calculates directly the specification indicator R, so the specification indicator calculated in MATLAB–Simulation is $R=0.97$ (see figure (11)).

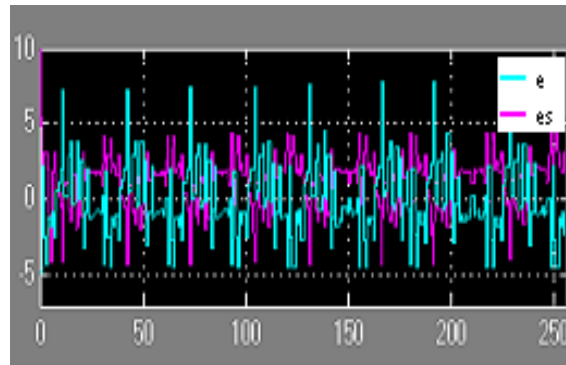


Figure 14. Adaptive stochastic control and SISCON errors

6. Conclusion

From this study we can evaluate these two methods in the identification of the pyrolysis reactor and draw the following conclusions:

- A direct adaptive control framework for stochastic compartmental dynamical systems is applied. In relation to stochastic variations of system coefficients, we presented analysis and adaptive control methodology that guarantees global control of the stochastic systems;
- The application of the SISCON software in the identification of the MISO to confirm its efficiency and the validation of its results by their comparison with MATLAB-Simulation results;
- The validity of any model can be confirmed by the specification indicator which must go toward 1, as verified in the adaptive stochastic control;
- The SISCON makes it easy to treat the data by offering a graphical interface without being necessary to construct a program or a Simulink as in the case of MATLAB, so it is simpler and quicker.

Références

- [1] Koncsag, C., (1998), *Reactoare chimice (note de curs): partea. I*, Conctansa, Editura OVIDIU.
- [2] MATHIEU, L., (2005), "Cycle thorium et réacteurs a sel fondu exploration du champ des paramètres et des contraintes définissant le "thorium molten salt reactor", Ph. D thesis from Institut National Polytechnique de Grenoble.
- [3] Wauquier, J., Leprince, P., Favenec, J., Trambouze, P., (1998), *Le Raffinage Du Pétrole*, Paris, Editions TECHNIP.
- [4] Popescu, D., Lupu, C., Petrescu, C., Matescu, M., (2004), *Sisteme de Conducere a proceselor industriale*, Bucuresti, Editura PRINTECH.
- [5] Popescu, D., Stefanoiu, D., Lupu, C., Petrescu C., Ciubotaru, B., Dimon, C., (2006), *Automatica industrială*, Editura AGIR, Bucuresti.
- [6] Sun, L, Sano, A., (2002), "Identification and predistortion for a class of nonlinear systems", *IFAC papers*, Barcelona.
- [7] Stengel, R., (1994), *Optimal Control and Estimation*, Courier Dover Publications, New York.
- [8] Huang, M, Lin, T., (2008), "An innovative regression model-based searching method for setting the robust injection molding parameters", *journal of materials processing technology*, 198, pp436–444.
- [9] Huijin Fan and S. S., "Adaptive State Feedback Control for a Class of Stochastic Nonlinear Systems", (2001), Huijin, F., Ge, S., *43rd IEEE Conference on Decision and Control*, Atlantis, Paradise Island, Bahamas, ThA 08.1, pp2996-3000.
- [10] Valavani. L, Athan. M., (1988), Final report on robust stochastic adaptive control, massachusetts institute of technology laboratory for information and decision systems cambridge, New York.

EARTHQUAKE HAZARD ASSESSMENT FOR DIFFERENT REGIONS IN AND AROUND TURKEY BASED ON GUTENBERG-RICHTER PARAMETERS BY THE LEAST SQUARE METHOD

Yusuf BAYRAK¹, Serkan ÖZTÜRK², Hakan ÇINAR³, George Ch. KORAVOS⁴ and Theodoros M. TSAPANOS⁵

¹⁻²⁻³ Karadeniz Technical University, Department of Geophysics, 61080 Trabzon, Turkey

⁴⁻⁵ Aristotle University of Thessaloniki, School of Geology, Geophysical Laboratory, Greece

Tel: +90 462 377 2026

e-mail: bayrak@ktu.edu.tr

ABSTRACT

In this study, we made an assessment of earthquake hazard parameters for different 24 source regions in and around Turkey. We used the seismic source zones and the database defined by Bayrak et al. [12] and Bayrak et al. [17], respectively. For the goodness of fit to the Gutenberg-Richter (G-R) frequency-magnitude law, the parameters a and b were calculated from least square (LS) approach for each region. Also, it is estimated the mean return periods, the most probable maximum magnitude in the time period of t -years and the probability for an earthquake occurrence for an earthquake magnitude $\geq M$ during a time span of t -years. We then produced b -value map using G-R with the least square method and the spatial distribution of probabilities and the expected maximum earthquake magnitude in the next 100 years are plotted. The results show that region 21 (central part of NAFZ) is probably the next region for the occurrence of a large earthquake. This conclusion is strongly supported from the probability map in which shows that the largest value (98%) for an earthquake with magnitude greater than or equal to 7.0. The mean return period for such magnitude is the lowest in this region (27-years). It is also determined the most probable earthquake magnitude in the next 100 years. This parameter also supports our conclusion that in the middle of North Anatolian Fault zone the most probable earthquake magnitude in the next 100 years will exceed 7.5. Since it is necessary to have a plenty data in LS, the computed b -values from LS will contain extreme errors for the regions having too few data. So, the computed lower b -value and higher M_{100} value are completely related to small number of data. As a result, the G-R parameters computed from LS for a region having quite little number of data do not reflect tectonics very well.

Keywords: *Earthquake hazard, mean return period, the most probable maximum magnitude*

1. INTRODUCTION

It is a remarkable fact that the evaluation of earthquake hazard parameters is important in seismically active region. Qualitative techniques (epicenter maps, etc) as well as quantitative ones have been applied in order to present the spatial variability of earthquake hazard in different regions of the Earth and Turkey [1,2,3,4]. The maximum observed magnitude M_{max} [5,6], the annual number $N(M)$ or the mean return period T_m of earthquakes [7,8] with magnitudes greater or equal to a given value M are the commonest quantities considered as measures of seismicity. The knowledge of the return period is of great importance in studying and analyzing earthquake hazard and/or seismicity. It contributes with a great importance to the determination of the national seismic code and it conditions the priority of interventions on existing buildings [2]. However, assessment of earthquakes hazard involves the computation of long-term probabilities for the occurrence of earthquakes of a specified size in a given area during a certain time period.

Turkey is located in a very active seismic region, so the earthquake hazard studies in Turkey has been widely made by using a number of different techniques and seismic quantities [9,10,11,12,13]. For this purpose, the seismicity of Turkey is studied through the application of various methods using different parameters. The aim of the present study is to evaluate the earthquake hazard in Turkey in terms of different hazard parameters such as the mean return period for an earthquake occurrence, the most probable maximum magnitude of earthquakes in a certain time interval and the probabilities for the large earthquakes occurrences in the certain times.

2. TECTONIC PROPERTIES and DATA

Turkey is in the Mediterranean part of Alpine-Himalayan orogenic system and this system runs through a mean west-east direction from the Mediterranean to Asia. The tectonic characteristic of Turkey and in the vicinity is controlled by three major plates: African, Eurasian and Arabian, and two generally acknowledged minor plates: Aegean and Anatolian as shown in the neo-tectonic models of McKenzie [14] and Dewey et al. [15]. The most important tectonic characteristics of Turkey are the Aegean Arc, the West Anatolian Graben Complexes (WAGC), the North Anatolian Fault Zone (NAFZ), the East Anatolian Fault Zone (EAFZ), the North East Anatolian Fault Zone (NEAFZ) the Bitlis Thrust Zone (BTZ) and the Caucasus. The African plate is moving to the north, towards Eurasian Plate, pushing the Turkish Plate in a westward motion. NAFZ and EAFZ constitute the northern and southern boundaries, respectively, of this plate, while the southern boundary is not well defined by seismicity. The motion between Africa and Eurasia is not taken up one plate boundary, but is carried by the motion of the Aegean and Turkish plates. The boundary between the Aegean and Turkish plates forms a north-south trending belt of seismicity across western Turkey and the eastern Aegean. The Aegean plate is moving towards the southwest relative to the European plate, producing extension and strike-slip motion along the boundary between the two plates. The southern boundary of the Aegean plate is moving southwest relative to the African plate, and is over thrusting the Mediterranean Sea floor. At the eastern end of the Turkish plate, the motion is taken up by thrust faults associated with the Caucasus. The result of this geometry is a thickening of the continent throughout the active region, which continues to elevate the Caucasus. Thrusting in eastern Turkey and the Caucasus transforms to strike-slip motion between the Turkish and Eurasian plates at the eastern outset of the NAF [10]. McKenzie [14] conjectured that the relative motion between the Black Sea and the Eurasian plate must be in a north-south direction with the Black Sea moving towards Eurasia, though rather slowly, since the seismicity of this boundary has been low for most of this century [10]. The Arabian plate is moving in the north-northwest direction relatively to the Eurasian plate. This motion has resulted in continental collision along the Bitlis fold and the thrust belt which causes high topography in Eastern Turkey and the Caucasus. As a result of compression in the East Anatolia, the Anatolian plate moves to the west and the North Anatolian plate to the east. The major tectonic structures of Turkey adopted from Şaroğlu et al. [16] are shown in Figure 1.

For an ideal delineation of seismic source zones it is necessary a complete comprehension of the historical and instrumental seismicity, tectonics, geology, paleoseismology, and other neotectonic properties of the considering region. But, it is not always possible to compile detailed information in all these fields for the majority of the world. Thus, frequently, seismic source zones are determined with two fundamental tools; a seismicity profile and the tectonic structure of the region under consideration [10]. The seismic source zones used in this study are defined according as Bayrak et al. [12] as shown in Figure 2. Also, epicentral distributions of the earthquakes in Turkey and vicinity are shown in the same figure. The seismic source regions numbered from 1 to 24, all earthquakes with the maximum observed magnitude M_{max}^{obs} , locations and dates are given in Table 1.

The database used in this study is taken from Bayrak et al. [17]. It is compiled from different sources and the seismicity data from different catalogues were provided in different magnitude scales. Turkey earthquake catalogue from 1900 to 1974 come from the International Seismological Centre (ISC) and instrumental catalogue of KOERI. The earthquakes, starting from 1974 until 2005, are taken from the Boğaziçi University, Kandilli

Observatory and Earthquake Research Institute (KOERI). The catalogue contains the origin time, different magnitudes scales (m_b -body wave magnitude, M_S -surface wave magnitude, M_L -local magnitude, M_D -duration magnitude, and M_W -moment magnitude), epicenters and depths information of earthquakes. The earthquake data from different catalogues are given in different scales. An earthquake data set used in the assessment of earthquake hazard must be homogenous in other words it is necessary to use the same magnitude scale. In order to prepare a homogeneous earthquake catalogue, Bayrak et al. [17] are developed some new relationships between the different magnitudes scales (m_b , M_S , M_L , and M_D) for 24 different regions of Turkey shown in Figure 2. Consequently, using the relations given it has been constructed a uniform catalogue of M_S . Thus, the final data catalogue consists of 70876 earthquakes with magnitude 1.0 or greater.

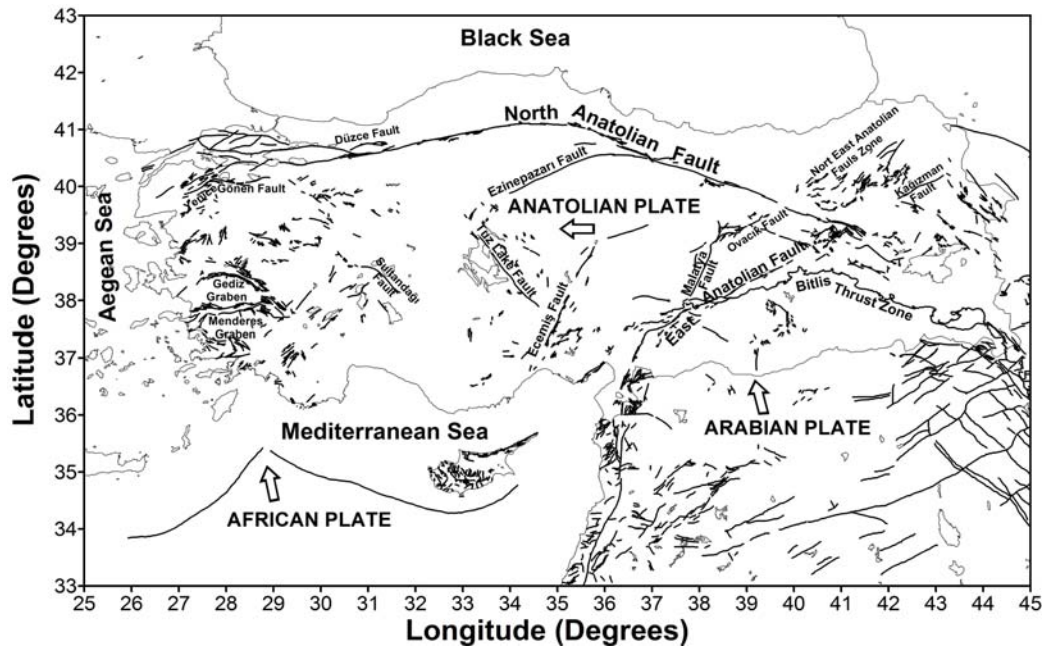


Figure 1. Active tectonics of Turkey. The major tectonic structures are modified from Şaroğlu et al. [16].

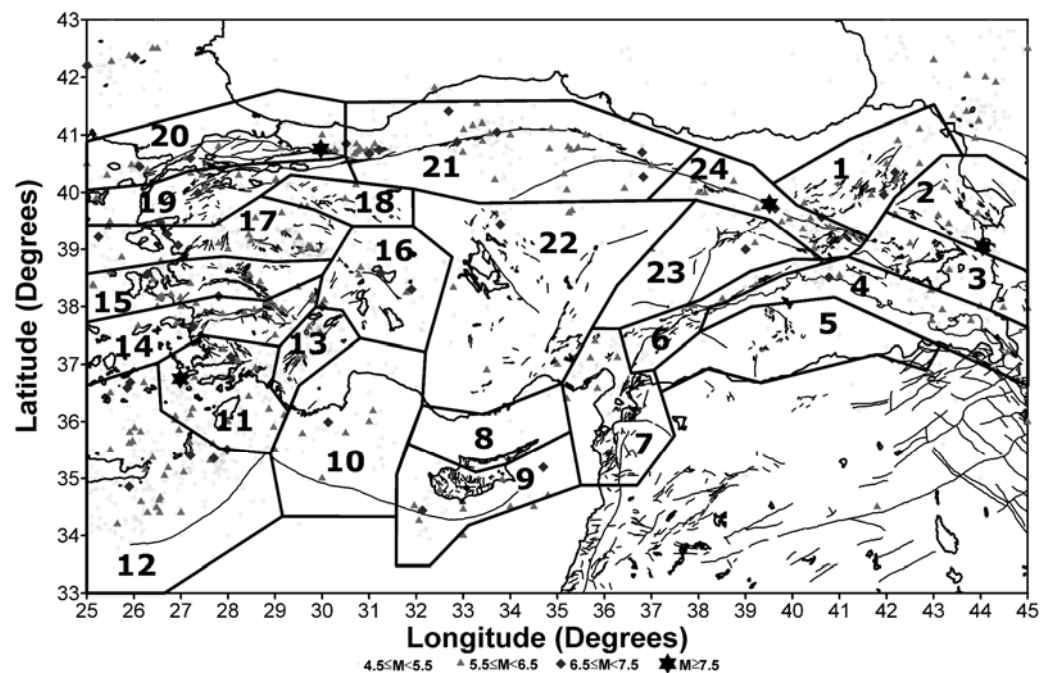


Figure 2. Different seismic zones (Bayrak et al. [12]) and epicenter distribution of earthquakes in Turkey from 1900 to 2005 with major tectonics. Magnitude sizes of earthquakes are shown by different symbol.

Table 1. Different 24 seismic source regions in and around Turkey, maximum observed magnitudes (M_S) in each region, their date and locations.

Region	Maximum observed magnitude (M_S)	Date (m.d.y)	Location	Tectonics
1	6.8 / 6.8	09.13.1924 / 10.30.1983	Pasinler / Horasan	North East Anatolian Fault Zone (NEAFZ)
2	7.5	11.24.1976	Çaldıran-Muradiye	Kağızman, Iğdır, Tutak and Çaldıran faults (KITÇF)
3	6.3	04.28.1903	Patnos	Malazgirt, Erçiş and Süphan faults and Muş Thrust Zone (MESF)
4	6.6	09.06.1975	Lice-Diyarbakır	Bitlis Thrust Zone (BTZ)
5	5.4	05.19.1915	Şanlıurfa	Karadağ Extension Zone (KEZ)
6	5.9	08.11.2004	Elazığ	East Anatolian Fault Zone (EAFZ)
7	6.0 / 6.0	02.17.1908 / 03.20.1945	Adana-Ceyhan / Adana-Ceyhan	A part of Dead Sea Fault
8	5.2	02.14.1995	Cyprus Region	North part of Cyprus
9	6.7	10.09.1996	Cyprus Region	South part of Cyprus, including east part of Cyprus Arc
10	6.8	03.18.1926	Finike	Western part of Cyprus Arc
11	7.7	06.26.1926	Rhodes	Muğla and Rhodes
12	7.4	07.09.1956	Aegean Sea	Aegean Arc
13	6.4	03.01.1926	Burdur	Burdur Fault Zone (BFZ)
14	6.8	07.16.1955	Aydın-Söke	Büyük and Küçük Menderes Grabens
15	6.6	07.23.1949	İzmir-Karaburun	Gediz Graben
16	7.0	04.09.1931	Akşehir	Sultandağı, Beyşehir and Tatar faults (SBTF)
17	7.2	12.19.1981	Aegean Sea	Kütahya, Simav and Zeytindağ-Bergama faults (KSZBF)
18	6.4	02.20.1956	Eskişehir	Eskisehir, İnönü-Dodurga and Kaymaz faults (EİDKF)
19	7.2	03.18.1953	Çanakkale-Yenice	Yenice-Gönen, Manyas, Ulubat and Etili faults (YGMUEF)
20	7.8	08.17.1999	İzmit	Marmara part of North Anatolian Fault Zone (MNAFZ)
21	7.4	11.12.1999	Düzce	Anatolian part of North Anatolian Fault Zone (ANAFZ)
22	6.6	04.19.1938	Kırşehir	Mid Anatolian Fault System (MAFS)
23	6.8	12.04.1905	Çemişgezek	Ovacık fault and Malatya fault (OMF)
24	7.9	12.26.1939	Erzincan	Eastern part of North Anatolian Fault Zone (ENAFZ)

3. METHOD

The commonest description of earthquake occurrence is provided by the Gutenberg-Richter (G-R) law. The parameters currently used for quantitative evaluation of seismicity are the well-known ones, a_t and b , of the magnitude frequency relationship introduced by Gutenberg and Richter [18]:

$$\text{Log}N = a_t - bM \quad (1)$$

The parameter b depends on factors like the mechanical heterogeneity and the density cracks in the medium and on the state of stress in a region [19,20]. The parameter a_t depends on the seismicity of the area, on the time interval for which we have reported events and also on the surface area S outlined by the epicenters. For seismicity study purposes usually a_t is expressed in 1 year by the equation:

$$a_1 = a_t - \text{Log}t \quad (2)$$

where t is the whole time period covered by the data set. Because of Equation (2), relationship (1) transforms to:

$$\text{Log}N = a_1 - bM \quad (3)$$

The expected time interval for the occurrence of an earthquake with magnitude greater than or equal to M is defined as the mean return periods T_m and is given by:

$$T_m = 10^{\text{b}M} / 10^{a_1} \quad (4)$$

This quantity is adopted as a measurement of seismicity. The most probable maximum magnitude of earthquakes in a time period of t years:

$$M_t = (a_1 + \text{log}t)/b \quad (5)$$

The probability P_t for an earthquake occurrence with magnitude $\geq M$ during the time span of t years:

$$P_t = 1 - \exp(-10^{a_1 - \text{b}M} t) \quad (6)$$

In this paper, we aimed to make a quantitative appraisal of earthquake hazard parameters in and around Turkey. Particularly the analysis of the expected time interval for the occurrence of an earthquake, the most probable maximum magnitude of earthquakes in a given time period and the probability for an earthquake occurrence supply information on the earthquake hazard. In order to evaluate the quantitative seismicity for different 24 regions, in which Turkey and the adjacent areas are divided we applied Equations 4, 5 and 6. We used M_S magnitude scale in these equations since our catalogue is uniform of M_S .

4. RESULT and DISCUSSION

An effort is made in this study for evaluation of earthquake hazard parameters of Turkey. The parameters a and b of magnitude-frequency (M-F) relationship is estimated by the least square (LS) method for 24 seismic regions (Figure 2). Then the most probable maximum magnitudes, the mean return periods (in years) and the probabilities for different time periods for a given magnitudes were computed in order to evaluate the seismicity of the 24 seismic regions.

The M-F graphs are shown in Figure 3 and the G-R parameters as well as cut of magnitudes (M_c) for 24 seismic regions of Turkey are given in Table 2. The computed b -values are between 0.52 and 1.27. Minimum b -value is related to North part of Cyprus whereas maximum value is observed in KEZ (abbreviations are given in Table 1). We divided b -values into four groups changing between 0.40 and 0.59, 0.60 and 0.79, 0.80 and 1.00 and larger than 1.00. These four groups drawn with different grey scale are shown in Figure 4. The highest b -values computed in regions 5, 7, 9 and 13, which are related to, KEZ, a part of the Dead Sea fault, South part of Cyprus, including east part of Cyprus Arc and BFZ. The second level b -values changing between 0.80 and 0.99 are obtained in regions of 3, 4, 6, 11, 12, 14, 15, and 17. MESF, BTZ, EAFZ, Aegean Arc, Büyük and Küçük

Menderes Grabens, Gediz Graben and KSZBF are in the borders of these regions. The b -values varying between 0.60 and 0.79 are observed in the regions 1, 2, 10, 16, 18, 19, 20, 21 and 22. These regions are related to NEAFZ, KITÇF, Muğla and Rhodes, SBTF, EİDKF, YGMUEF, Marmara and Anatolian parts of NAF. The values lower than 0.60 are related to regions 8, 23 and 24 covering the North part of Cyprus, Ovacık and Malatya faults and eastern part of North Anatolian Fault zone. Since region 8 includes too few data (Figure 3), we observed very low b values in this region. Fitting a straight line such as that implied by the G-R law through recurrence data in which the mean rate of exceedance of small earthquakes is underestimated will tend to flatten the line. As a result, the actual mean rate of small earthquakes will be underpredicted and the mean rate of large earthquakes will be overpredicted [21]. Since it is necessary to have a plenty data in LS, the computed b values from LS will contain extreme errors for the regions having too few data.

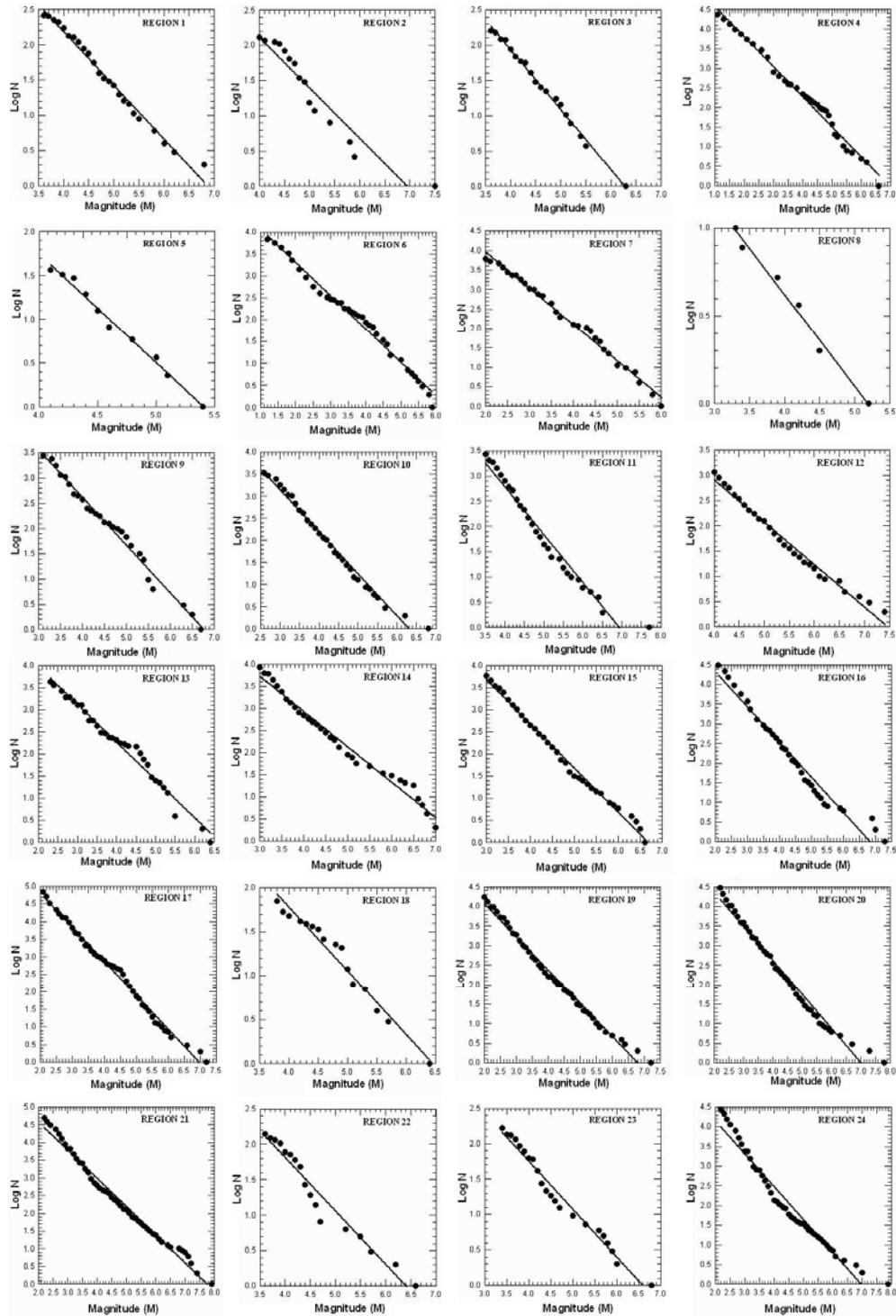


Figure 3. Magnitude-frequency relationships from the least square method in 24 seismic regions of Turkey

Table 2. Gutenberg-Richter parameters, mean return periods for magnitude range between 5.0 and 7.5 and the most probable maximum magnitudes for certain times between 1 and 100 years in the studied regions

		LogN=a-bM			M _S =5.0	M _S =5.5	M _S =6.0	M _S =6.5	M _S =7.0	M _S =7.5	most probable maximum magnitudes				
Region	M _c	a	a ₁	b	T _m	T _m	T _m	T _m	T _m	T _m	M ₁	M ₁₀	M ₂₅	M ₅₀	M ₁₀₀
1	3.6	5.07	3.07	0.73	3.8	8.8	20.4	47.3			4.2	5.6	6.1	6.5	7.0
2	4.0	4.47	2.66	0.65	3.9	8.2	17.4	36.7	77.6	164.1	4.1	5.6	6.2	6.7	7.2
3	3.5	5.39	3.38	0.86	8.3	22.4	60.3				3.9	5.1	5.6	5.9	6.3
4	1.0	6.42	4.43	0.97	2.6	8.0	24.5	75.0			4.6	5.6	6.0	6.4	6.6
5	4.1	6.87	4.92	1.27	26.9						3.9	4.7	5.0	5.2	5.5
6	1.1	5.78	4.03	0.95	5.2	15.7					4.2	5.3	5.7	6.0	6.4
7	2.0	6.63	4.65	1.09	6.3	22.1	77.6				4.3	5.2	5.6	5.8	6.1
8	3.3	2.68	2.07	0.52	3.4						4.0	5.9	6.7	7.3	7.8
9	3.0	6.86	4.92	1.02	1.5	4.9	15.8	51.3			4.8	5.8	6.2	6.5	6.8
10	2.5	4.96	3.07	0.76	5.4	12.9	30.9	74.1			4.0	5.4	5.9	6.3	6.7
11	3.5	6.09	4.15	0.86	1.4	3.8	10.2	27.5	74.1	199.5	4.8	6.0	6.5	6.8	7.2
12	4.0	6.23	4.25	0.85	1.0	2.7	7.1	18.8	50.1		5.0	6.2	6.7	7.0	7.4
13	2.3	6.69	4.79	1.06	3.2	11.0	37.2				4.5	5.5	5.8	6.1	6.4
14	3.0	5.78	3.78	0.86	3.3	8.9	24.0	64.6			4.4	5.6	6.0	6.4	6.7
15	3.0	5.92	3.91	0.86	2.5	6.6	17.8	47.9			4.6	5.7	6.2	6.5	6.9
16	2.0	4.56	2.60	0.64	4.0	8.3	17.4	36.3	75.9		4.0	5.6	6.3	6.7	7.2
17	3.0	6.56	4.55	0.94	1.4	4.2	12.3	36.3	117.2		4.8	5.9	6.3	6.7	7.0
18	3.8	4.89	2.99	0.77	7.2	17.6	42.7				3.9	5.2	5.7	6.1	6.5
19	2.0	5.09	3.09	0.72	3.2	7.4	17.0	38.9	89.1		4.3	5.7	6.2	6.7	7.1
20	2.1	5.07	3.08	0.69	2.3	5.2	11.5	25.4	56.2	124.5	4.5	5.9	6.5	6.9	7.4
21	2.1	4.92	2.91	0.62	1.5	3.2	6.5	13.2	26.9		4.7	6.3	7.0	7.4	7.9
22	3.6	4.52	2.59	0.70	8.1	18.2	40.7	91.2			3.3	5.0	5.7	6.2	6.7
23	3.3	3.90	1.90	0.58	10.0	19.5	38.0	74.1			3.7	5.1	5.7	6.1	6.6
24	2.1	4.26	2.38	0.56	2.6	5.0	9.5	18.2	34.7	66.1	4.3	6.0	6.8	7.3	7.8

The b -value for a region not only reflects the relative proportion of the number of large and small earthquakes in the region, but is also related to the stress condition over the region. Many factors can cause perturbation of the normal b -value. On average, b -value is near unity for most seismically active regions on Earth [22]. However, a detailed mapping of b -value often reveals significant deviations. The spatial variation of b -values is related to the distribution of stress and strain [19,20]. On the other hand, high b -values are reported from areas of increased geological complexity [23] indicating the importance of multifracture area. Thus, the low b -value is related with low degree of heterogeneity, large stress and strain, large velocity of deformation and large faults [24]. We observed the low b values (< 0.70) in regions 20, 21 and 24 which are related the NAFZ. The NAFZ is a large fault zone, has low degree heterogeneity and is a very active structure according to geodesy accommodates 24-30mm/yr of dextral motion [25]. This observation interprets our results, obtained by G-R method (low b -values), and lead us to the conclusion that even after the occurrence of the two recent large earthquake, the NAFZ remains a tectonic structure of high risk. The western Anatolian including regions 11, 13, 14, 15 and 17 is a multifracture area where the seismicity related to graben systems and other faults is high and displays swarm-type activity with remarkable clustering of low-magnitude earthquakes in time and space [26,27]. The high b values (> 0.8) in these regions are consistent with the tectonics.

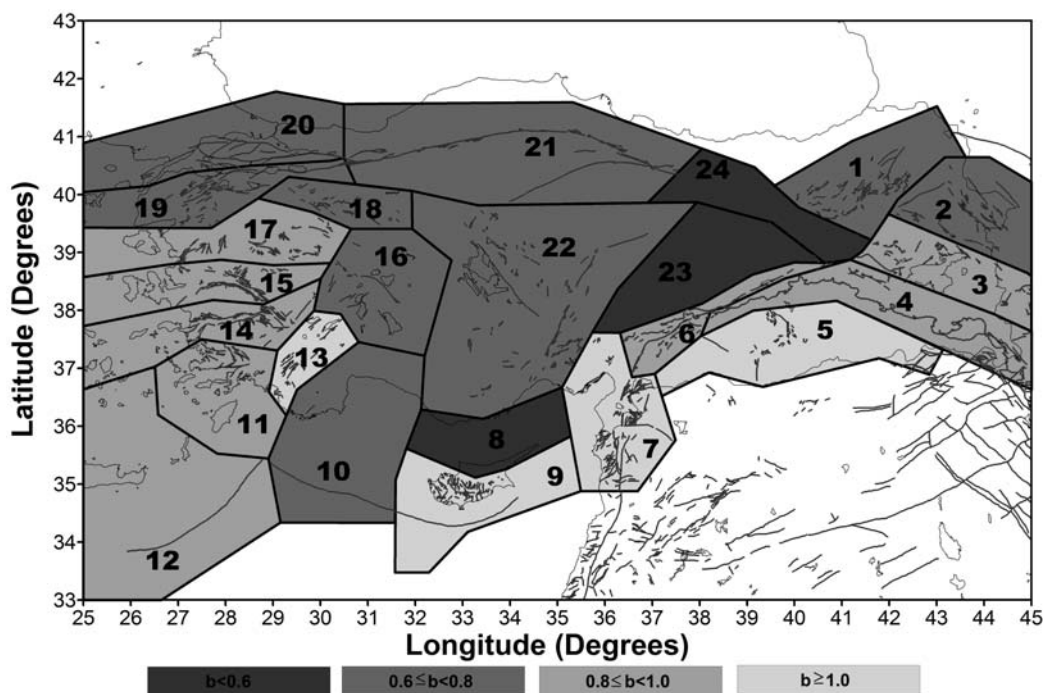


Figure 4. b values of G-R relationships from the least square method in 24 seismic region of Turkey

Earthquake recurrence times (return periods) can be evaluated from paleoseismic observations, patterns of seismicity and strain rates measured from GPS networks. The mean return periods (T_m) computed from G-R parameters during a given time span are listed in table 2. Also, earthquake hazard curves expressed in terms of the mean return period of earthquakes that are expected for the maximum observed magnitudes are shown in Figure 5.

The regions 20, 21 and 24 are covered by NAFZ which is best-known strike slip fault in the world which generates devastating, threatening to human life, earthquakes from time to time. Between 1939 (Erzincan earthquake, $M_S=7.9$) and 1999 (İzmit earthquake, $M_S=7.8$) NAFZ ruptured in a westward migration series of nine moderate-large earthquakes ($M_S>6.7$). The mean return periods estimated indicate that the region 21 (a part of NAFZ) is the most dangerous seismic region, with mean return period ranging between 27 and 48 (the lowest values) years for magnitudes 7.0 and 7.4, respectively. The largest earthquake in region 21 is Düzce earthquake of 1999 with $M_S=7.4$ which is occurred in the western part of this seismic region. This region is a very seismically active one and experienced of a series of large earthquakes (with magnitudes 7.0-7.3) during the years 1942, 1943, 1944 and 1957. In the regions 20 and 24 which are the other parts of NAFZ (Figs.1 and 2) the mean return periods for magnitude $M_S\geq 7.5$ are 124 and 66 years, respectively. The mean return periods for magnitude $M_S\geq 7.0$ are shorter than 100 years as in the regions 11, 12, 16 and 19. The regions 11 and 12 are covered by the subduction zone of the south Aegean area. In this specific area earthquake are known since historic epoch with the very large event of magnitude $M_S=8.0$ occurred in 1303 [28]. Sultandağı fault (normal fault), Beyşehir and Tatar faults (strike-slip faults) are situated in the region 16 where observed maximum

earthquake size is 7.0 (Table 1). The regions 14, 15 and 17 cover E-W trending grabens and their basin-bounding active normal faults generally generate earthquakes with magnitude lower than 7.0. The earthquake ($M_S=7.2$) observed in region 17 is not related to these graben systems and occurred in Aegean Sea. The mean return periods for magnitude $M_S \geq 6.5$ are 65 and 48 and 36 years for the regions 14, 15 and 17, respectively. In the regions 2 and 19 return periods for earthquake of magnitude $M_S=7.0$ are greater than 75 years. The region 2 is covered by Kağızman, Iğdır, Tutak and Çaldıran faults which are active strike-slip faults [29] and experienced of 1976 large Çaldıran earthquake ($M_S=7.5$). Strike-slip faulting mechanism dominates in region 19 where there are Yenice-Gönen, Manyas, Ulubat and Etili Faults and observed largest earthquake is 1953 Çanakkale-Yenice earthquake ($M_S=7.5$). Unlike NAFZ, EAFZ covered by region 6 has been relatively quiescent in the instrumental period when compared to historical epoch [30]. The data used in this study includes only instrumental period earthquakes occurred from 1900 to 2005. Since the very large earthquakes did not occurred in the instrumental period, we could not calculate the mean return periods of the earthquakes greater than 7.0 in this region.

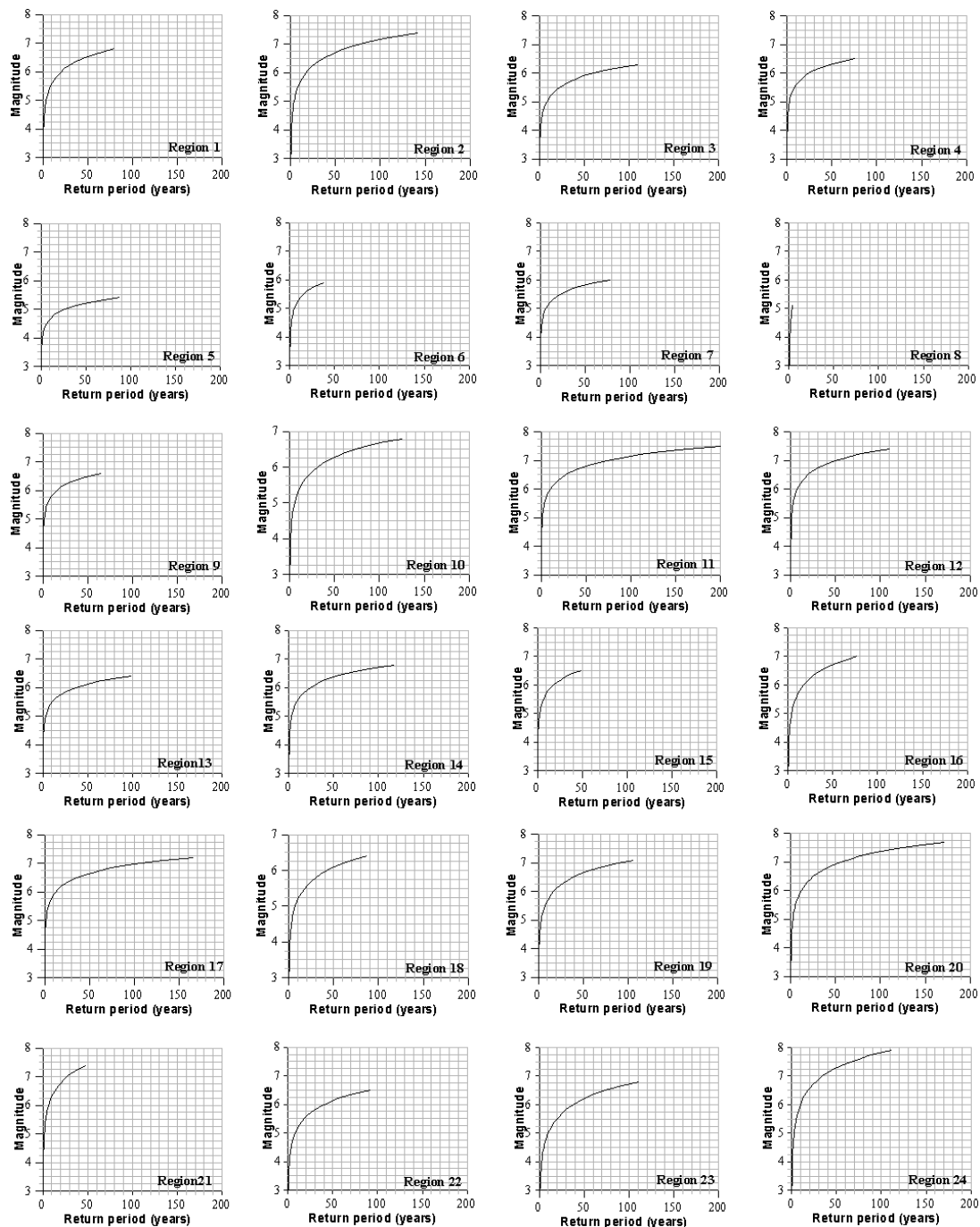


Figure 5. The mean return periods expected for given magnitudes in 24 seismic region of Turkey

Earthquake hazard curves expressed by the probability expected for earthquakes with the maximum observed magnitudes and plotted for magnitudes and during the time span of 25, 50 and 100 are shown in Figure 6. Spatial variability of the probabilities in the next 100 years, P_{100} , with a magnitude ≥ 7.0 in each 24 seismic regions are shown in Figure 7. The P_{100} is divided in four groups of grey scale indicated in this way regions with different probabilities. The probability of occurrence for the earthquakes with $M_S \geq 7.0$ is greater than 75 percent in NAFZ and Aegean subduction zone. Especially, region 21 (central part of NAFZ) has a very high probability value calculated as 98%. The second level probability of occurrence values ranges between 65% and 75% are related to regions 11, 16 and 19. The first level probability of occurrence value smaller than 65% is related to KSZBF and YGMUEF (abbreviations are given in Table 1). In the other regions with white color, we cannot expect an earthquake for magnitude $M_S \geq 7.0$ in the next 100 years.

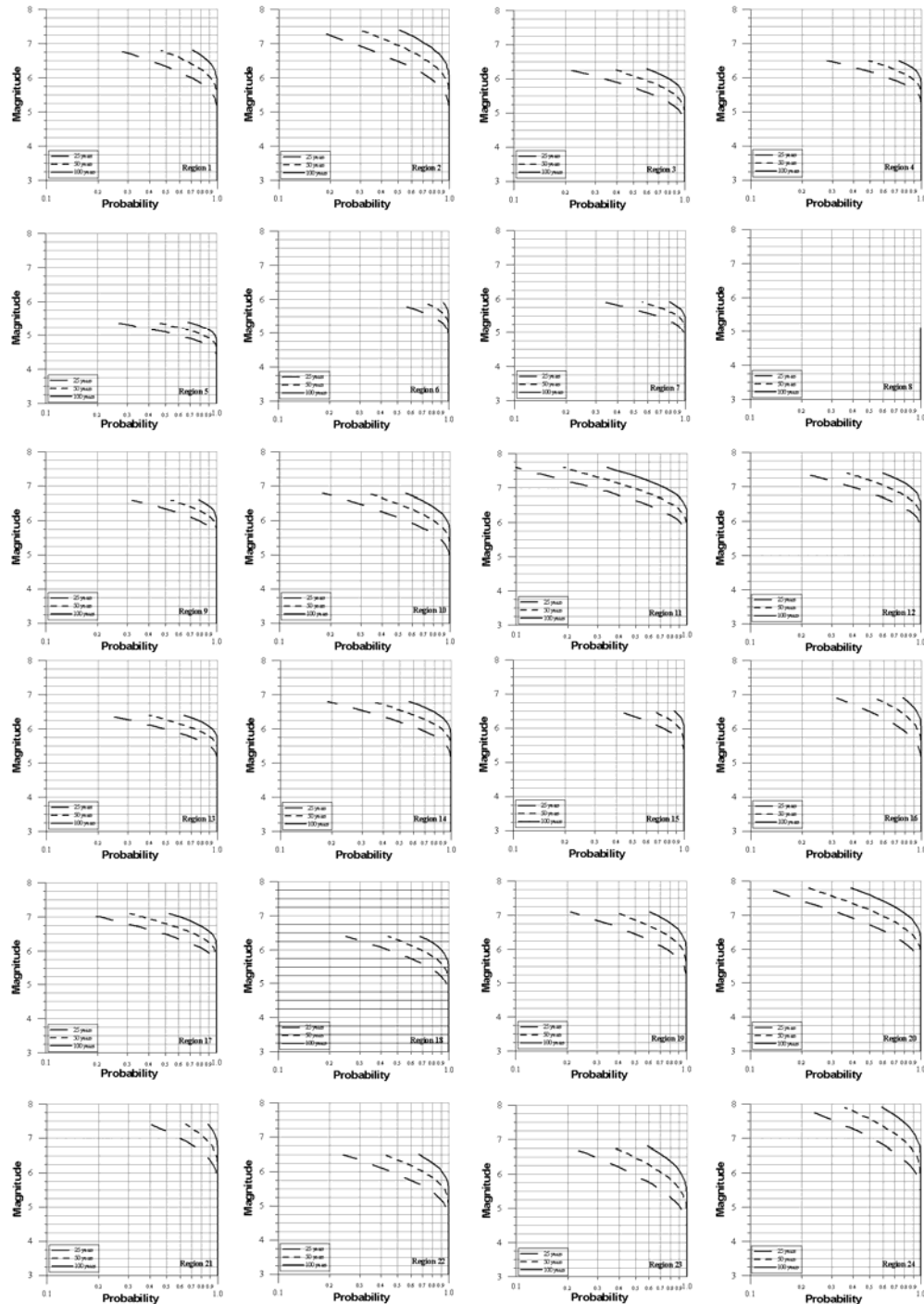


Figure 6. The probability that a given magnitude M will be exceeded in the time period $T=25, 50$ and 100 years, for 24 seismic regions of Turkey

Regional variability of most probable maximum magnitudes to be occurred in the next 100 years for each 24 region is shown in Figure 8. Also, a list of the most probable maximum magnitudes for the certain times is given detailed in Table 2. We divided M_{100} values into four groups as shown by legends with different grey scale in Figure 8.

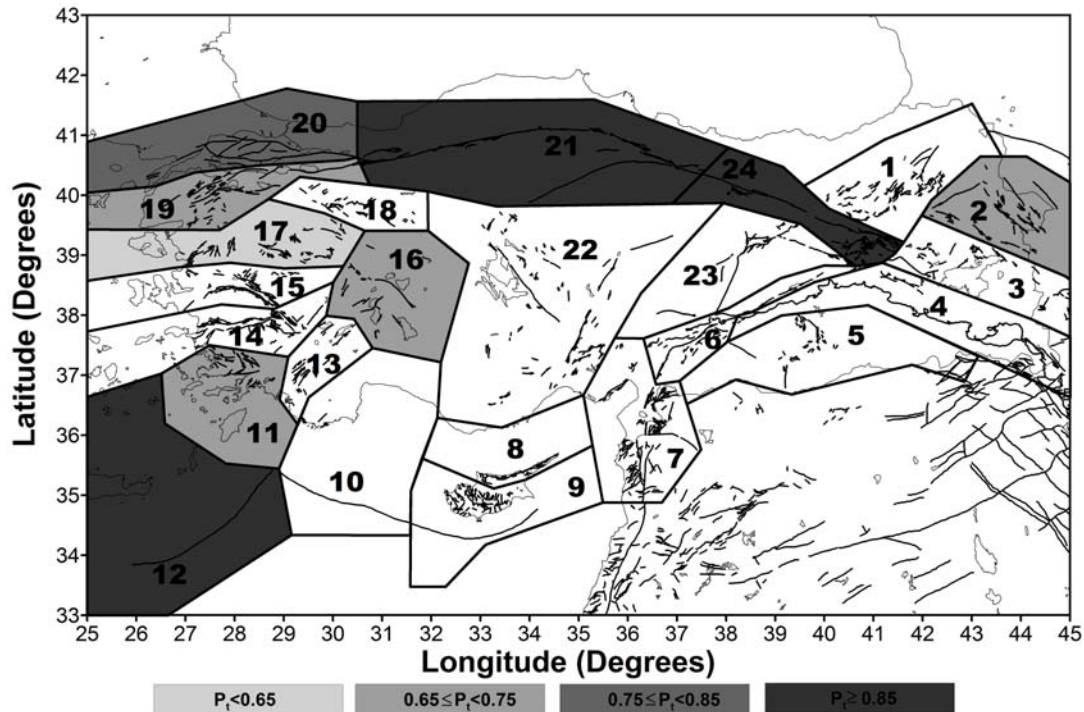


Figure 7. Probabilities in the next 100 years with a magnitude ≥ 7.0 for different 24 seismic source regions in and around Turkey. In regions with white color, there is not an earthquake probability of occurrence for magnitude $M_s \geq 7.0$ in the next 100 years.

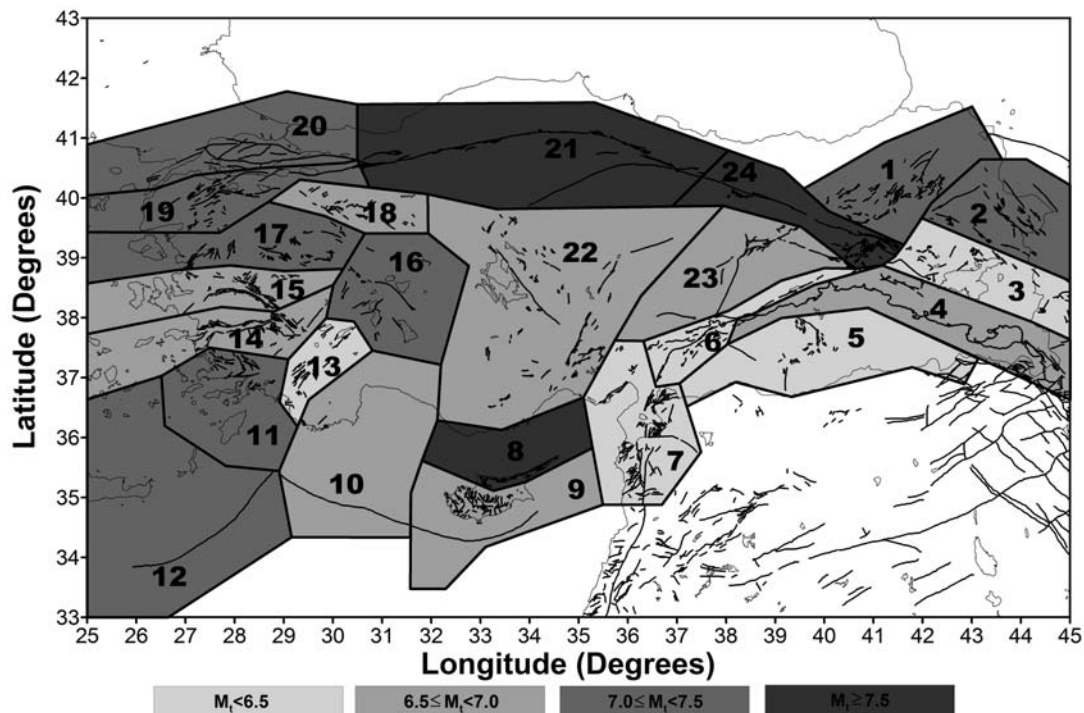


Figure 8. Maximum earthquake size to be occurred in the next 100 years for different 24 seismic source regions in and around Turkey

In the next 100 years, the earthquakes with magnitude $M_S \geq 7.5$ were only estimated in the central and eastern parts of NAFZ and the northern Cyprus (region 8). The most probable maximum magnitudes depend on G-R parameters (Equation 5). Since region 8 includes too few data, we observed very low b value and very high M_{100} value in this region. The central part of NAFZ (region 21) has the maximum earthquake hazard level in and around Turkey according to computed M_{100} value as 7.9. Bayrak et al. [12] calculated the earthquake hazard level for 24 seismic regions of Turkey used in this study from K index, defined as relative earthquake hazard scale. They found that the central part NAFZ between Bolu and Erzincan (particularly region 21) is of very high level because it is unbroken for very large earthquakes ($M_S \geq 7.8$, like those in Erzincan in region 24 and İzmit in region 20). In addition, Bayrak et al. [13] estimated the seismicity in terms of the modal values (a_m/b) for each one of the 24 seismic region and concluded that NAFZ (regions 20, 21 and 24) are ranked to the first position according to their seismicity. We computed M_{100} value of the region 21 in accordance to the results of the studies mentioned above.

5. CONCLUSIONS

In this study, an effort is made in order to assess the earthquake hazard for different regions in and around Turkey. The seismic source zones used in this study are defined according as Bayrak et al. [12]. The database used in this study is taken from Bayrak et al. [17]. Turkey earthquake catalogue from 1900 to 1974 come from the International Seismological Centre and instrumental catalogue of KOERI. The earthquakes, starting from 1974 until 2005, are taken from the Boğaziçi University, Kandilli Observatory and Earthquake Research Institute. The parameters a and b of magnitude-frequency relationship is estimated by the least square method for 24 seismic regions. Also, the hazard parameters such as the mean return periods, the most probable magnitude in a time period of t -years and the probability of earthquake occurrence for a given magnitude during a time span of t -years are estimated. The results lead us to a general conclusion that region 21 (central part of NAFZ) is probably the next region for the occurrence of a large earthquake. This region between Bolu and Erzincan is unbroken since 1943 with magnitude $M_S = 7.2$. This conclusion is strongly supported from the probability map in which shows that the largest value (98%) for an earthquake with magnitude greater than or equal to 7.0. The mean return period for such magnitude is the lowest in the region (27-years). We also estimated the most probable earthquake magnitude in 100 years. This parameter also supports our conclusion that in the specific region the most probable earthquake magnitude in the next 100 years will exceed 7.5. This can be a kind of a proposition to the Turkish authorities to have an open eye to this particular region. The maps of (Figs.5 and 6) provide brief atlas which both depict variations of earthquake hazard throughout Turkey and the adjacent areas. As a result the G-R parameters by LS for a region having quite little number of data do not reflect tectonics because the computed lower b value and higher M_{100} value in the region 8 are almost related to too few data. In order to quantify answers to question how high is the seismicity of a region; numerate methods of earthquake hazard are essential and provide a clear statistical guide. Thus, an attempt is made to form a simple quantitative classification of the studied regions in terms of their earthquake hazard.

6. REFERENCES

- [1] Makropoulos, K. C., 1978, "The statistics of large earthquake magnitude and an evaluation of Greek seismicity", PhD. Thesis, Univ. of Edinburgh, Edinburgh, 193 pp.
- [2] Hamdache, M., Bezzeghoud, M., and Mokrane, A., 1998, "Estimation of seismic hazard parameters in the northern part of Algeria", *Pure Appl. Geophys.* 151, 101-117.
- [3] Tsapanos, T.M., 2003, "Appraisal of seismic hazard parameters for the seismic regions of the east Circum-Pacific belt inferred from a Bayesian approach", *Natural Hazards*, 30, 59-78.
- [4] Bayrak, Y., Yilmaztürk, A., and Öztürk, S., 2005, "Relationships between fundamental seismic hazard parameters for the different source regions in Turkey", *Natural Hazards*, 36, 445-462.
- [5] Yegulalp, T.M., and Kuo, J. T., 1974, "Statistical prediction of occurrence of maximum magnitude earthquakes", *Bull. Seismol. Soc. Am.*, 64, 393-414.
- [6] Koravos, G., Main, I., Tsapanos, T.M., and Musson, R. M. W., 2003, "Maximum earthquake magnitudes in the Aegean area constrained by tectonic moment release rates", *Geophys. J. Int.* 152, 94-112.
- [7] Comninakis, P. E., 1975, "Contribution to the study of the seismicity of Greece", PhD. Thesis, Univ. of Athens, 110pp.
- [8] Tsapanos, T. M., 1988, "The seismicity of Greece in comparison with the seismicity of other seismogenic countries of the world", Proc. 1st Symp. On recent trends in Seismology and Applied Geophysics, Thessaloniki 1-3 July 1988, 186-193.
- [9] Yazar, R., Ergünay, O., Erdik, M., and Gülkan, P., 1980, "A preliminary probabilistic assessment of the seismic hazard in Turkey", Proc. 7th World Conf. Earthquake Eng., Istanbul, 309-316.
- [10] Erdik, M., Alpay, B. Y., Onur, T., Sesetyan, K., and Birgoren, G., 1999, "Assessment of earthquake hazard in Turkey and neighboring regions", *Annali di Geofisica*, 42, 1125-1138.
- [11] Kayabali, K., and Akin, M., 2003, "Seismic hazard map of Turkey using the deterministic approach", *Eng. Geology*, 69, 127-137.
- [12] Bayrak, Y., Öztürk, S., Tsapanos, T. M., Koravos, G. Ch., Leventakis, G-A., and Kalafat, D., 2007a, "An evaluation of earthquake hazard parameters based on the instrumental data for different regions of Turkey and adjacent areas", International Earthquake Symposium Kocaeli 2007, 22-24 October, Kocaeli, Turkey.
- [13] Bayrak, Y., Öztürk, S., Koravos, G. Ch., Leventakis, G-A., and Tsapanos, T.M., 2007b, "A quantitative seismicity analysis for different regions in Turkey and its surroundings from Gumbel first asymptotic distribution and Gutenberg-Richter relationship using instrumental earthquake catalogue", International Earthquake Symposium Kocaeli 2007, 22-24 October, Kocaeli, Turkey.
- [14] McKenzie, D. P., 1972, "Active Tectonics of the Mediterranean region", *Geophys. J. R. Astron. Soc.*, 30, 109-185.
- [15] Dewey, J. F., Pitman, W. C., Ryan, W. B. F., and Bonnin, J., 1973, "Plate tectonics and the evolution of the Alpine system", *Geological Society of America Bulletin*, 84, 3137-3180.
- [16] Şaroğlu, F., Emre, O., and Kuşçu, I., 1992, "Active fault map of Turkey, General Directorate of Mineral Research and Exploration, Ankara, Turkey.
- [17] Bayrak, Y., Öztürk, S., Tsapanos, T. M., Koravos, G. Ch., Leventakis, G-A., and Kalafat, D., 2007c, "Estimation of the Earthquake Hazard Parameters from Instrumental Data for the Different Regions in and around Turkey", *Journal of Geophysical Research*, (Submitted to).
- [18] Gutenberg, B. and Richter, C. F., 1944, "Frequency of earthquakes in California", *Bull. Seism. Soc. Am.* 34, 185-188.
- [19] Mogi, K., 1967, "Regional variation of aftershock activity", *Bull. Earthquake Res. Inst. Univ. Tokyo*, 46, 175-203.
- [20] Scholz, C. H., 1968, "The frequency-magnitude relation of microfracturing in rock and its relation to earthquakes", *Bull. seism. Soc. Am.*, 58, 399-415.
- [21] Slejko, D., 2006, "Basics of Seismology and Seismic Hazard Assessment", European School for Advanced Studies in Reduction of Seismic Risk, Pavia, October 2006.
- [22] Frohlich, C., and Davis, S., 1993, "Teleseismic *b*-values: or, much ado about 1.0", *J. Geophys. Res.*, 98, 631-644.
- [23] Lopez Casado, C., Sanz de Galdeano, C., Delgado, J., and Pienado, M.A., 1995, "The *b* parameter in the Betic Cordillera, Rif and nearby sectors. Relations with the tectonics of the region", *Tectonophysics*, 248, 277-292.
- [24] Manakou, M.V. and Tsapanos, T.M., 2000, Seismicity and seismic hazard parameters evaluation in the island of Crete and surrounding area inferred from mixed files, *Tectonophysics*, 321, 157-178.

- [25] Reilinger, R.E., S., McClusky, Oral, M. B., ,King, R.W. Toksoz, N., Barka, A.A., Kinik, I., Lenk, O., and Sanli, I., 1997, "Global Positioning System measurements of present-day crustal movements in the Arabia-Africa-Eurasia plate collision zone", *J. Geophys. Res.*, 102, 9983-9999.
- [26] Üçer, S. B., Crampin, S., Evabs, R., Miller, A., and Kafadar, N., 1985, "The MARNET radio linked seismometer network spanning the Marmara Sea and the seismicity of western Turkey", *Geophys. J. Royal. Astron. Soc.*, 83, 17-30.
- [27] Eyidoğan, H., 1988, "Rates of crustal deformation in western Turkey as deduced from major earthquakes", *Tectonophysics*, 148, 83-92.
- [28] Papazachos, B.C., 1996, "Large seismic faults, in the Hellenic arc", *Anall. di Geophys.*, 138, 287-308.
- [29] Koçyiğit, A., Yılmaz, B., Adamia, S., and Kuloshvili, S., 2001, "Neotectonics of East Anatolian Plateau (Turkey) and Lesser Caucasus: implication for transition from thrusting to strike-slip faulting", *Geodinamica Acta*, 14, 177-195.
- [30] Nalbant , S. S., McCloskey, J. Steacy, S., and Barka, A. A., 2002, "Stress accumulation and increased seismic risk in eastern Turkey", *Earth and Planetary Science Letters*, 195, 291-298.

Application of homotopy perturbation method and variational iteration method to a nonlinear diffusion equation with a reaction term

A.Barari, A. Janalizadeh, F.Farrokhzad, D.D.Ganji

Departments of Civil and Mechanical Engineering, University of Mazandaran, Babol, Mazandaran, Iran

Abstract

In this paper, variational Iteration method and homotopy perturbation method are applied to solve a nonlinear diffusion equation with a reaction term. This problem used as mathematical models in Geotechnical engineering and fluid mechanics. Comparison is made between the exact solutions and the results of the variational iteration method (VIM) and homotopy perturbation method (HPM). The results reveal that these methods are very effective and simple.

Keywords: homotopy perturbation method (HPM); variational iteration method (VIM); nonlinear diffusion equation; exact solution

1. Introduction

We consider the following diffusion equation with a reaction term:

$$\frac{\partial}{\partial t} u(x, t) = v \frac{\partial^2}{\partial x^2} u(x, t) + p(u), \quad 0 < x < l, \quad t > 0 \quad (1)$$

Where v is the diffusivity constant, with initial condition $u(x, 0) = f(x)$ and dirichlet boundary conditions $u(0, t) = a(t)$, $u(1, t) = b(t)$.

Over the last decades several analytical/approximate methods have been developed to solve nonlinear ordinary and partial differential equations. Some of these techniques include variational iteration method (VIM) [1-6], decomposition method [7-9], homotopy perturbation method (HPM) [10-17] etc.

Linear and Nonlinear phenomena are of fundamental importance in various fields of science and engineering. Most models of real – life problems are still very difficult to solve. Therefore, approximate analytical solutions such as homotopy-perturbation method were introduced.

This method is the most effective and convenient ones for both linear and nonlinear equations.

Perturbation method is based on assuming a small parameter. The majority of nonlinear problems, especially those having strong nonlinearity, have no small parameters at all and the approximate solutions obtained by the perturbation methods, in most cases, are valid only for small values of the small parameter.

Generally, the perturbation solutions are uniformly valid as long as a scientific system parameter is small. However, we cannot rely fully on the approximations, because there is no criterion on which the small parameter should exist. Thus, it is essential to check the validity of the approximations numerically and/or experimentally. To overcome these difficulties, HPM have been proposed recently.

Recently, He [1-3] proposed a variational iteration method based on the use of restricted variations and correction functionals which has found a wide application for the solution of nonlinear ordinary and partial differential equations. This method does not require the presence of small parameters in the differential equation, and provides the solution (or an approximation to it) as a sequence of iterates. The method does not require that the nonlinearities be differentiable with respect to the dependent variable and its derivatives. In this paper we will apply the homotopy perturbation method and variational iteration method to a nonlinear diffusion equation with a reaction term.

2. Basic idea of homotopy-perturbation method

To explain this method, let us consider the following function:

$$A(u) - f(r) = 0, \quad r \in \Omega \quad (2)$$

With the boundary conditions of:

$$B(u, \frac{\partial u}{\partial n}) = 0, \quad r \in \Gamma, \quad (3)$$

Where A , B , $f(r)$ and Γ are a general differential operator, a boundary operator, a known analytical function and the boundary of the domain Ω , respectively.

Generally speaking the operator A can be divided into a linear part L and a nonlinear part $N(u)$. Eq. (2) can therefore, be written as:

$$L(u) + N(u) - f(r) = 0, \quad (4)$$

By the homotopy technique, we construct a homotopy

$v(r, p) : \Omega \times [0, 1] \rightarrow R$ Which satisfies

$$\begin{aligned} H(v, p) &= (1-p)[L(v) - L(u_0)] + p[A(v) - f(r)] = 0, \\ p &\in [0, 1], r \in \Omega, \end{aligned} \quad (5)$$

Or

$$H(v, p) = L(v) - L(u_0) + pL(u_0) + p[N(v) - f(r)] = 0, \quad (6)$$

Where $p \in [0, 1]$ is an embedding parameter, while u_0 is an initial approximation of Eq. (2), which satisfies the boundary conditions. Obviously, from Eqs. (5) and (6) we will have:

$$H(v, 0) = L(v) - L(u_0) = 0, \quad (7)$$

$$H(v, 1) = A(v) - f(r) = 0, \quad (8)$$

The changing process of p from zero to unity is just that of $v(r, p)$ from u_0 to $u(r)$. In topology, this is called deformation, while $L(v) - L(u_0)$ and $A(v) - f(r)$ are called homotopy.

According to the HPM, we can first use the embedding parameter p as a “small parameter”, and assume that the solutions of Eqs. (5) and (6) can be written as a power series in p :

$$v = v_0 + pv_1 + p^2v_2 + \dots, \quad (9)$$

Setting $p = 1$ yields in the approximate solution of Eq. (2) to:

$$u = \lim_{p \rightarrow 1} v = v_0 + v_1 + v_2 + \dots, \quad (10)$$

The combination of the perturbation method and the homotopy method is called the HPM, which eliminates the drawbacks of the traditional perturbation methods while keeping all its advantage.

The series (10) is convergent for most cases. However, the convergent rate depends on the nonlinear operator $A(v)$. Moreover, He made the following suggestions [12]:

- The second derivative of $N(v)$ with respect to v must be small because the parameter may be relatively large, i.e. $p \rightarrow 1$.
- The norm of $L^{-1} \frac{\partial N}{\partial v}$ must be smaller than one so that the series converges.

3. Basic idea of Variational iteration method

To clarify the basic ideas of VIM [1-6], we consider the following differential equation:

$$Lu + Nu = g(t), \quad (11)$$

Where L is a linear operator, N is a nonlinear operator and $g(t)$ is a homogeneous term.

According to VIM, we can write down a correction functional as follows:

$$u_{n+1}(t) = u_n(t) + \int_0^t \lambda (Lu_n(\tau) + N\tilde{u}_n(\tau) - g(\tau)) d\tau \quad (12)$$

Where λ is a general lagrangian multiplier which can be identified optimally via the variational theory. The subscript n indicates the n th approximation and u_n is considered as a restricted variation, i.e. $\delta \tilde{u}_n = 0$.

4. Example

Consider the diffusion equation with a non-linear reaction term:

$$\frac{\partial}{\partial t} u(x, t) = \frac{\partial^2}{\partial x^2} u(x, t) + u(x, t)^2 - u(x, t)^3, \quad 0 < x < 10, t > 0 \quad (13)$$

With the initial and boundary conditions taken from the exact solution given by:

$$u(x, t) = \frac{1}{1 + e^{\sigma(x - \sigma t)}}, \quad \sigma = \frac{1}{\sqrt{2}} \quad (14)$$

4.1. Application of Homotopy-perturbation method

To solve Eq. (13) by means of HPM, we consider the following process after separating the linear and nonlinear parts of the equation.

A homotopy can be constructed as follows:

$$H(v, p) = (1 - p) \left(\frac{\partial}{\partial t} v(x, t) - \frac{\partial}{\partial t} v_0(x, t) \right) + p \left(\frac{\partial}{\partial t} v(x, t) - \frac{\partial^2}{\partial x^2} v(x, t) - v(x, t)^2 + v(x, t)^3 \right), \quad (15)$$

Substituting $v = v_0 + p v_1 + \dots$ in to Eq. (15) and rearranging the resultant equation based on powers of p -terms, one has:

$$p^0 : \frac{\partial}{\partial t} v_0(x, t) = 0, \quad (16)$$

$$p^1 : -v_0(x, t)^2 - \frac{\partial^2}{\partial x^2} v_0(x, t) + \frac{\partial}{\partial t} v_1(x, t) + v_0(x, t)^3 = 0, \quad (17)$$

$$p^2 : -\left(\frac{\partial^2}{\partial x^2} v_1(x, t)\right) + 3v_0(x, t)^2 v_1(x, t) - 2v_0(x, t)v_1(x, t) + \left(\frac{\partial}{\partial t} v_2(x, t)\right) = 0, \quad (18)$$

With the following conditions:

$$v_0(x, 0) = \frac{1}{1 + e^{(0.7071x)}} \quad (19)$$

$$v_i(x, 0) = 0 \quad i = 1, 2, \dots$$

With the effective initial approximation for v_0 from the conditions (19) and solutions of Eqs. (16-18) may be written as follows:

$$v_0(x, t) = \frac{1}{1 + e^{(0.7071x)}}, \quad (20)$$

$$v_1(x, t) = \frac{e^{\left(\frac{7071x}{10000}\right)} \left(49999041 e^{\left(\frac{7071x}{10000}\right)} + 50000959 \right)}{1000000000 \left(1 + e^{\left(\frac{7071x}{10000}\right)} \right)^3}, \quad (21)$$

$$v_2(x, t) = - \frac{\left(t^2 e^{\left(\frac{7071}{10000}x\right)} \left(2500095889883509 e^{\left(\frac{7071}{10000}x\right)} - 2500479489883509 e^{\left(\frac{7071}{10000}x\right)} + \right) \right)}{\left(2 \times 10^{16} \left(1 + 5 e^{\left(\frac{7071}{10000}x\right)} + 10 e^{\left(\frac{7071}{5000}x\right)} + 10 e^{\left(\frac{21213}{10000}x\right)} + 5 e^{\left(\frac{7071}{2500}x\right)} + e^{\left(\frac{7071}{2000}x\right)} \right) \right)}, \quad (22)$$

In the same manner, the rest of components were obtained using the Maple package.

According to the HPM, we can conclude that:

$$u(x, t) = \lim_{p \rightarrow 1} v(x, t) = v_0(x, t) + v_1(x, t) + \dots, \quad (23)$$

Therefore, substituting the values of $v_0(x, t)$, $v_1(x, t)$, $v_2(x, t)$ from Eqs. (20-22) in to Eq. (23) yields:

$$u(x, t) = \frac{1}{1 + e^{(0.7071x)}} + \frac{e^{\left(\frac{7071x}{10000}\right)} \left(49999041 e^{\left(\frac{7071x}{10000}\right)} + 50000959 \right)}{100000000(1 + e^{\left(\frac{7071x}{10000}\right)})^3} - \frac{\left(t^2 e^{\left(\frac{7071}{10000}x\right)} \left(2500095889883509 e^{\left(\frac{7071}{10000}x\right)} - 2500479489883509 e^{\left(\frac{7071}{10000}x\right)} + \right) \right)}{\left(2 \times 10^{16} \left(1 + 5 e^{\left(\frac{7071}{10000}x\right)} + 10 e^{\left(\frac{7071}{5000}x\right)} + 10 e^{\left(\frac{21213}{10000}x\right)} + 5 e^{\left(\frac{7071}{2500}x\right)} + e^{\left(\frac{7071}{2000}x\right)} \right) \right)}, \quad (24)$$

4.2. Application of variational iteration method

To solve the Eq. (13) by means of VIM, one can construct the following correction functional,

$$u_{n+1}(x, t) = u_n(x, t) + \int_0^t \lambda \left(\frac{\partial}{\partial \tau} u_n(x, \tau) - \frac{\partial^2}{\partial x^2} u_n(x, \tau) - u_n(x, \tau)^2 + u_n(x, \tau)^3 \right) d\tau \quad (25)$$

Its stationary conditions can be obtained as follows:

$$\begin{aligned} 1 - \lambda' \Big|_{\tau=t} &= 0 \\ \lambda \Big|_{\tau=t} &= 0 \\ \lambda'' &= 0 \end{aligned} \quad (26)$$

We obtain the lagrangian multiplier:

$$\lambda = -1 \quad (27)$$

As a result, we obtain the following iteration formula:

$$u_{n+1}(x, t) = u_n(x, t) - \int_0^t \left(\frac{\partial}{\partial \tau} u_n(x, \tau) - \frac{\partial^2}{\partial x^2} u_n(x, \tau) - u_n(x, \tau)^2 + u_n(x, \tau)^3 \right) d\tau \quad (28)$$

Now we start with an arbitrary initial approximation that satisfies the initial condition:

$$u_0(x, t) = \frac{1}{1 + e^{(0.7071x)}} \quad (29)$$

Using the above variational formula (28), we have:

$$u_1(x, t) = u_0(x, t) - \int_0^t \left(\frac{\partial}{\partial \tau} u_0(x, \tau) - \frac{\partial^2}{\partial x^2} u_0(x, \tau) - u_0(x, \tau)^2 + u_0(x, \tau)^3 \right) d\tau \quad (30)$$

Substituting Eq. (29) in to Eq. (30) and after simplifications, we have:

$$u_1(x,t) = \frac{1}{1+e^{(0.7071x)^3}} \left(10^{-8}(10^8 + 2 \times 10^8 e^{(0.7071x)} + 10^8 e^{1.4142x} + 4.9999 \times 10^7 e^{(1.4142x)t} + 5 \times 10^7 e^{(0.7071x)t}) \right) \quad (31)$$

and so on. In the same way the rest of the components of the iteration formula can be obtained. The comparison of the results is illustrated in Figs. (1) and (2).

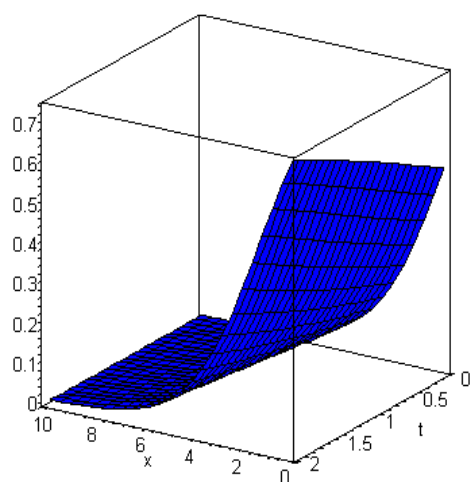


Fig1. Results of exact solution

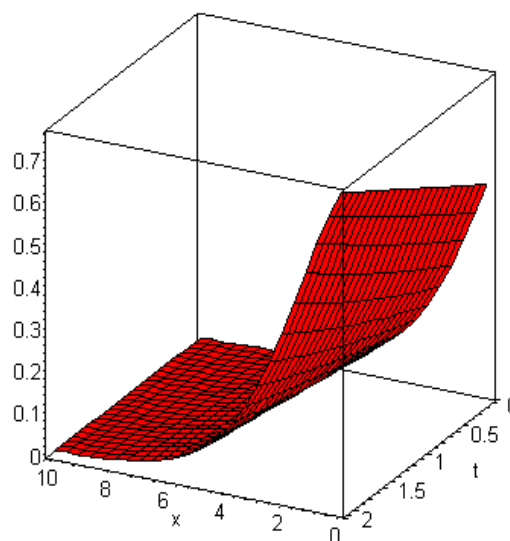


Fig 2. Results of HPM and VIM

5. Conclusions

Homotopy perturbation method and variational iteration method are employed successfully to study a nonlinear diffusion equation with a reaction term. In conclusion, HPM and VIM provide highly accurate numerical solutions for nonlinear problems. As it is mentioned, this method avoids linearization and physically unrealistic assumptions. Finally, Comparison with exact solution reveals that homotopy perturbation method and variational iteration method are remarkably effective for solving nonlinear problems.

References

- [1] Ji-H. He, A new approach to nonlinear partial differential equations, *Commun. Nonlinear Sci. Numer. Simul.* 2 (1997) 230–235.
- [2] Ji-H. He, Variational iteration method – a kind of non-linear analytical technique: some examples, *Int. J. Non-Linear Mech.* 34 (1999) 699–708.
- [3] Ji-H. He, Some asymptotic methods for strongly nonlinear equations, *Int. J. Modern Phys.* 20 (2006) 1141–1199.
- [4] Ganji, D.D., M. Jannatabadi., E. Mohseni, Application of He's variational iteration method to nonlinear Jaulent–Miodek equations and comparing it with ADM, *J. Comput. Appl. Math.* 207 (2007) 35–45.
- [5] Ganji, D.D., A. Sadighi, Application of homotopy–perturbation and variational iteration methods to nonlinear heat transfer and porous media equations, *J. comput. Appl. Math.* 207 (2007) 24–34.
- [6] S. Momani, Z. Odibat, Comparison between the homotopy perturbation method and the variational iteration method for linear fractional partial differential equations, *Comput. & Math. Appl.* 54 (2007) 910–919.
- [7] G. Adomian, *Stochastic Systems*, Academic Press Inc., New York, 1983.
- [8] G. Adomian, *Nonlinear Stochastic Operator Equations*, Academic Press Inc., New York, 1986.
- [9] G. Adomian, *Solving Frontier Problems of Physics: The Decomposition Method*, Kluwer, Boston, 1994.
- [10] Ji-H. He, Homotopy perturbation method: a new nonlinear analytical technique, *Appl. Math. Comput.* 135 (2003) 73–79.
- [11] Ji-H. He, Addendum: new interpretation of homotopy perturbation method, *Int. J. Modern Phys.* 20 (2006) 2561–2568.
- [12] Ji-H. He, Homotopy perturbation technique, *Comput. Meth. Appl. Mech. Eng.* 178 (1999) 257–262.
- [13] M. Rafei, D. D. Ganji, Explicit Solutions of Helmholtz Equation and Fifth–order Kdv Equation using Homotopy–perturbation Method, *Int. J. Nonlinear Sci. Numer. Simul.* 7 (2006) 321–328 .

- [14] D. D. Ganji, A. Sadighi, Application of He's Homotopy-perturbation Method to Nonlinear Coupled Systems of Reaction-diffusion Equations, *Int. J. Nonlinear Sci. and Num. Simu*, 7 (2006) 411–418
- [15] A. Janalizadeh, A. Barari, D.D. Ganji, Application of homotopy perturbation method for solving second order nonlinear wave equation, *Journal of Physics*, in press, 2007.
- [16] A. Barari, A. Janalizadeh, D.D. Ganji, Application of homotopy perturbation method to Zakharov- Kuznetsov equation, *Journal of Physics*, in press, 2007.
- [17] J. Biazar, H. Ghazvini and M. Eslami, He's homotopy perturbation method for systems of integro-differential equations, *Chaos, Solitons & Fractals*, in press, 2007.

Fractional half-tangent of a curve described by Iterated Function Systems

Hicham Bensoudane¹, Christian Gentil¹, and Marc Neveu¹

The University of Burgundy
Laboratory of Electronics, Computer Science and Image(LE2I)
21000, Dijon, France
{hicham.bensoudane,christian.gentil,marc.neveu}@u-bourgogne.fr

Abstract. The deterministic fractal curves and surfaces find many applications in modeling of rough objects. However, these curves and surfaces are nowhere differentiable. Without notion of tangent, we can not determine the relative orientation of two fractal shapes, to join them with a "natural" aspect. Various works proposed a generalization of the concept of derivative by introducing the fractional derivative. In this paper we apply this concept of fractional derivative to the curves described by Iterated Function Systems. We show that if the fractional derivative exists at boundary points of the curve, the direction of the fractional half-tangent is necessarily the eigenvector of the corresponding transformation of the IFS. From the property of self-similarity it is then possible to determine the fractional half tangents for a dense set of points. This concept is illustrated with some classical fractal curves.

Keywords: Iterated Function Systems, fractal, affine space, half- tangent, fractional derivatives.

1 Introduction

Curves and surfaces with irregular structure (i.e. continuous but non differentiable), have been studied from two points of view. The first one is an analysis scheme in order to characterize the structure. The second one is a synthesis scheme in order to simulate and try to predict chaotic phenomena such as the development of an action on a stock exchange or to generate shapes that can be found in nature, such as mountains, terrains, tree... Generally, these methods are based on recursive process, themselves arising from the concept of fractal geometry introduced by Mandelbrot [12].

These methods can be classified according to two categories: deterministic methods and non-deterministic methods. Overall, non-deterministic methods allow obtaining more natural shapes, but because of their non-determinism they remain difficult to control. On the contrary, the deterministic methods will allow easier an control of fractal shapes, but too repetitive aspects may make them appear less "natural" [12, 1, 13].

Taking advantage of the deterministic model, Tosan and all [16] proposed a fractal surface model in order to use fractal structures in architecture. From this Gentil [6, 5] proposed a model to build parametric forms, the aspect of

Bensoudane-Gentil-Neveu

which may vary from smoothness to roughness. This enables to modulate the aspect in a continuous way and to join a fractal structure with an existing classical smooth structure. This allows to built piecewise continuous curves with different roughness properties. Those works insure the C^0 continuity, but what about C^1 continuity on rough piecewise curves? what about joining two rough curves? Figure 1 shows that joining two rough curves with C^1 continuity seems to be "intuitive". In this paper, we deal with the geometry differentiable properties of such a structure.

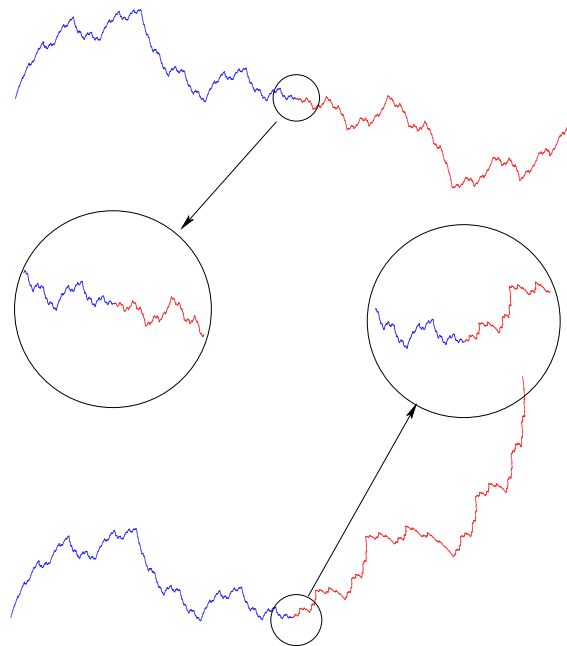


Fig. 1. Joining two curves

Some previous works concern the notion of derivative and tangent. Cochran-Lewis-Hart in [3] show that the integration of a fractal interpolation function (FIF) is a fractal interpolation function. This means that the class of these integrated fractal interpolated functions is derivable and so the tangent exists. But these results are limited on a specific class of functions. Guérin-Tosan-Baskurt in [8][19] discuss the relationship between the curves aspect and the eigenvalues of linear parts associated to the affine transformations of the IFS. LévyVéhel-Daoudi [20] [4] deal with the roughness property of the graph of a continuous function using the Hölder coefficient and propose a method for its estimation. Other works like Kolwankar-Gangal [11] use different gen-

eralizations of the derivative, referred to as fractional derivative, to extend the notion of derivative to nowhere differentiable curves. But generally their results are concerned with the roughness property of the curve and are related to the Hölder coefficient, fractal and Hausdorff dimension, without any relationship to geometric properties such as tangents.

We start from Kolwankar-Gangal's work. They introduced a concept of the local fractional derivative. On the one hand it depends on a generalization of the half-tangent and on the other hand on Hölder's exponent which is related to the irregularity of the curve.

The structure of this document is as follows. In section 2 we present the IFS model. In section 3 we define fractal curves by using the address function and the morphism function. In section 4 we introduce the notion of the fractional derivative. This concept is applied to the continuous but non-derivable curve. In section 5 we present our solutions to apply the concept of fractional derivative to the fractals curves defined by IFS. In section 6 we give an example of application of our approach.

2 Iterated function systems (IFS)

Let (\mathcal{X}, d) be a complete metric space. An IFS is a finite set of contractive operators (in practice affine operators) $\mathbb{T} = \{T_i\}_{i \in \Sigma}$ ($\Sigma = 0, \dots, N-1$) that operates on points of \mathcal{X} . Let \mathcal{H} denote the set of non-empty compact subset of \mathcal{X} and let d_h denote the Hausdorff metric. The metric space (\mathcal{H}, d_h) is complete. Each IFS \mathbb{T} , an operator is associated, called the Hutchinson operator and defined as follows :

$$\begin{aligned} \mathbb{T} : \mathcal{H} &\rightarrow \mathcal{H} \\ K &\mapsto TK = \bigcup_{i=0}^{N-1} T_i(K) \end{aligned} \quad (1)$$

\mathbb{T} is a contraction mapping. Therefore, from the fixed point theorem, there exists a unique compact $\mathcal{A} \in \mathcal{H}$ such that $\mathcal{A} = \mathbb{T}(\mathcal{A})$, called the *attractor* of IFS \mathbb{T} [9, 1] ($\mathcal{A} = \lim_{n \rightarrow \infty} \mathbb{T}^n K$, where K denotes any non empty sub-compact. \mathcal{A} is independent of K (see figure 2)). The attractor \mathcal{A} verifies the following self-similar property :

$$\mathcal{A} = T_0\mathcal{A} \cup \dots \cup T_{N-1}\mathcal{A} \quad (2)$$

3 Parameterized fractal arc

To study the mathematical properties of fractal curves we need to have parametric representation of them. The address function defines a parametrization of the attractor with infinite words of Σ (cf 2). By the introduction of the morphing function (cf 3.2) and additional joining conditions (cf 3.3), it is possible to define a continuous function from a first attractor to a second. By choosing the first attractor equal to $[0, 1]$, the morphing function defines a parametric arc.

Bensoudane-Gentil-Neveu

3.1 Address Function

Let $\mathbb{T} = \{T_i\}_{i \in \Sigma}$ be an IFS indexed by a finite set $\Sigma = \{0, \dots, N-1\}$. The attractor \mathcal{A} associated with \mathbb{T} is provided with an address function [1] defined over Σ^ω (the set of infinite words on Σ). The address function ϕ is defined by :

$$\begin{aligned} \phi : \Sigma^\omega &\rightarrow \mathcal{A} \subset E \\ \sigma &\mapsto \phi(\sigma) = \lim T_{\sigma_1} \dots T_{\sigma_n} \dots p = p_\sigma \end{aligned} \quad (3)$$

where $p \in \mathcal{X}$. It can be shown that $\phi(\sigma)$ is independent of p . We say that $p_\sigma = \phi(\sigma)$ has the address σ .

3.2 Morphism function and parameterized arc

Given two IFS $\mathbb{T} = \{T_i\}_{i \in \Sigma}$ and $\mathbb{T}' = \{T'_i\}_{i \in \Sigma}$ indexed by the same set Σ , Tosan [17] defines the associated morphism function $H : \mathcal{A} \rightarrow \mathcal{A}'$ by :

$$\forall i \in \Sigma, \forall p \in \mathcal{A}, \quad H(T_i p) = T'_i H(p) \quad (4)$$

H is called an morphism function because it transform the substructure of attractor \mathcal{A} to the substructure of attractor \mathcal{A}' : $H(T_i(\mathcal{A})) = T'_i(\mathcal{A}')$.

3.3 Continuity of H and joining conditions

If there exists $p \in \mathcal{A}$ such that $p \in T_i(\mathcal{A}) \cap T_j(\mathcal{A})$, this means that p has two addresses. H is a continuous function if these two addresses represent the same point in \mathcal{A}' . This implies that there exists $p' \in \mathcal{A}'$ such that $p' \in T'_i(\mathcal{A}') \cap T'_j(\mathcal{A}')$ and $H(p) = p'$. This is what Tosan calls the joining condition.

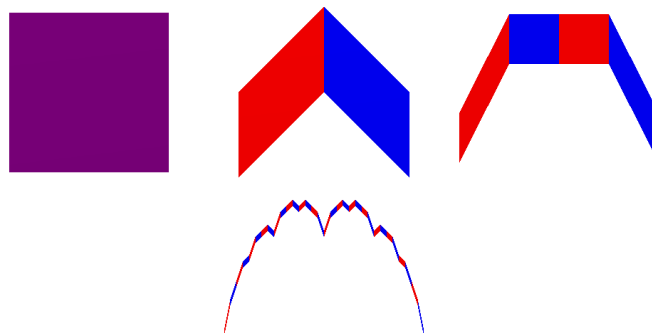


Fig. 2. Takagi curve: iteration 0, 1, 2 and 5

3.4 Parameterized arc

We can choose the first IFS \mathbb{T} such that $\mathcal{A} = [0, 1]$. In practise for $N = 2$ we use $\mathbb{T} = \{\frac{1}{2}x, \frac{1}{2}x + \frac{1}{2}\}$ (standard subdivision of $[0, 1]$ denoted by: $\mathbb{T}^s = \{\tau_0, \tau_1\}$). In this case the joining condition is defined by $\tau_0(c_1) = \tau_1(c_0)$ where $c_0 = 0$ and $c_1 = 1$ designate the boundary points of $[0, 1]$.

Theorem 1. : *For any IFS \mathbb{T}' verifying the same joining conditions $\mathbb{T}'_0(c'_1) = \mathbb{T}'_1(c'_0)$, the associated morphism function H defines a parameterized arc.*

Proof. : see [18]

The first attractor (\mathcal{A}) is considered as a parameterization domain and \mathbb{T} as a subdivision IFS of this domain.

4 Local fractional derivatives

The concept of derivative of non-integer order is by no means new. It was studied by Leibniz (1859), Liouville (1832), Riemann (1853), Holmgren (1864), although Euler (1730), Lagrange (1772), and other made contributions even earlier, as mentioned in [14]. The fractional derivative is interesting to study continuous but nowhere differentiable functions. A continuous function may be sufficiently irregular so that its graph is a fractal and is not derivable, but it is possible to define a fractional derivative. Most of these fractional derivatives are defined from the Riemann-Liouville definition [7, 15, 14, 10].

We begin by recalling the Riemann-Liouville definition of fractional integer of a real function. The fractional derivative, can be introduced from the corresponding fractional integral.

Definition: The Riemann-Liouville definition of the fractional integral of order q is:

$$\frac{d^q f(x)}{[d(x-a)]^q} = \frac{1}{\Gamma(-q)} \int_a^x \frac{f(y)}{(x-y)^{q+1}} dy \quad \text{for } q < 0, \quad (5)$$

where the lower limit a is some real number.

Definition: The Riemann-Liouville definition of fractional derivative of order q is:

$$\frac{d^q f(x)}{[d(x-a)]^q} = \frac{1}{\Gamma(n-q)} \frac{d^n}{dx^n} \int_a^x \frac{f(y)}{(x-y)^{q-n+1}} dy, \quad \text{for } n-1 < q < n \quad (6)$$

Bensoudane-Gentil-Neveu

where Γ is defined by:

$$\Gamma(p) = \int_0^\infty y^{p-1} \exp(-y) dy; \quad p > 0. \quad (7)$$

This definition is a global definition. To access to a local property, Kolwankar and Gangal [11] introduces the notion of local fractional derivative (LFD) of order q .

Definition : Local fractional derivative (LFD) If, for a real function f , the limit

$$D^q f(y) = \lim_{x \rightarrow y} \frac{d^q(f(x) - f(y))}{[d(x - y)]^q} \quad (8)$$

exists and is finite, then we say that the local fractional derivative of order q ($0 < q < 1$), at $x = y$, exists.

Definition The right and left local derivatives are :

$$\begin{aligned} D_+^q f(y) &= \Gamma(1 + q) \lim_{h \rightarrow 0+} \frac{f(y+h) - f(y)}{h^q} \\ D_-^q f(y) &= -\Gamma(1 + q) \lim_{h \rightarrow 0+} \frac{f(y) - f(y-h)}{h^q} \end{aligned} \quad (9)$$

In the LFD notion we are interested by the highest order which corresponds to the critical order.

Definition : Critical order α [11] The critical order α , at y , is defined by :

$$\alpha(y) = \sup\{q \mid \text{all LFDs of order less than } q \text{ exist at } y\}.$$

If $D_+^\alpha f(y) = D_-^\alpha f(y)$, we say, the function f is locally α -differentiable at y and denote the common value by $D^\alpha f(y)$

5 Application to the IFS

Let us consider a parameterized arc defined from $\mathbb{T}^s = \{\tau_0, \tau_1\}$, $\mathbb{T} = \{T_0, T_1\}$ and represented by its morphism H (cf 3.2). Generally, the curve defined by H is nowhere derivable. Nevertheless in some cases H has right and left derivatives (example: Takagi curve). When these derivatives exist we will calculate the associated half-tangents from \mathbb{T} .

So let us suppose that H has right and left derivatives. First we will compute local fractional derivatives of H at boundary points c_0 and c_1 , and we will characterise the half-tangents to the right of c_0 and to the left of c_1 . From self similarity property we will compute right and left half-tangents for a dense set of points of the attractor.

5.1 Locale α -differentiability and half-tangent vector

The right local fractional derivative at 0 of H is given by:

$$D_+^q H(0) = \Gamma(1+q) \lim_{h \rightarrow 0^+} \frac{H(0+h) - H(0)}{h^q} \quad (10)$$

Under the hypothesis that this limit exists, we can compute it with a subsequence.

Let $h_n = \frac{1}{2^n}$ be a sequence in $[0, 1]$ then :

$$D_+^q H(0) = \Gamma(1+q) \lim_{n \rightarrow \infty} \frac{H(0+h_n) - H(0)}{(h_n)^q} \quad (11)$$

The choice of h_n permits to write the local fractional derivative of H at 0 as a function of T_0 :

$$\begin{aligned} H(0) &= H(\phi^s(0^\omega)) = \phi(0^\omega) = c_0 \\ H(0+h_n) &= H(\frac{1}{2^n}) \end{aligned} \quad (12)$$

From the definition of \mathbb{T}^s , $1 = \phi^s(1^\omega)$, $\frac{1}{2} = \phi^s(01^\omega)$ and $(\frac{1}{2})^n = \phi^s(0^n 1^\omega)$ (where ϕ^s is the address function associated with \mathbb{T}^s), and $H(1) = H(\phi^s(1^\omega)) = \phi(1^\omega) = c_1$. Thus

$$H(0+h_n) = H(\phi^s(0^n 1^\omega)) = H(\tau_0^n(1)) = T_0^n H(1) = T_0^n c_1 \quad (13)$$

then

$$D_+^q H(0) = \Gamma(1+q) \lim_{n \rightarrow \infty} \frac{T_0^n c_1 - c_0}{(h_n)^q} \quad (14)$$

T_0 is an affine mapping , then:

$$\forall x \in E, \quad T_0(x) = T_0(a) + \overrightarrow{T_0}(\overrightarrow{ax}) \quad a \in E \quad (15)$$

where $\overrightarrow{T_0}$ is the linear mapping associated to T_0 .

Besides, T_0 is contractive. Applying equation (15) to the fixed point c_0 of T_0 yields:

$$\forall x \in E, \quad T_0(x) = c_0 + \overrightarrow{T_0}(\overrightarrow{c_0 x}) \quad (16)$$

It follows:

$$D_+^q H(0) = \Gamma(1+q) \lim_{n \rightarrow \infty} \frac{\overrightarrow{T_0^n}(\overrightarrow{c_0 c_1})}{(h_n)^q} \quad (17)$$

We notice that the local fractional derivative is expressed as a function of the linear mapping $\overrightarrow{T_0}$. To compute the limit of this expression, we use the power method.

Bensoudane-Gentil-Neveu

The power method Let \vec{T} be a linear mapping and let M be the associated matrix of eigenvalues $\lambda_1 \dots \lambda_r$ and of eigenvectors $\vec{v}_1 \dots \vec{v}_r$.

Consider the series:

$$\begin{cases} \vec{y}_{k+1} = M\vec{y}_k, \forall k \in \mathbb{N} \\ \vec{y}_0 \text{ is an arbitrary vector} \end{cases} \quad (18)$$

If $|\lambda_1| > |\lambda_2| \dots |\lambda_r|$, vectors \vec{y}_k verify:

$$\vec{y}_k = \lambda_1^k (a_1 \vec{v}_1 + \Theta(|\frac{\lambda_2}{\lambda_1}|^k)) \quad (19)$$

(where a_i are the coordinates of \vec{y}_0 in the eigenvectors basis: $\vec{y}_0 = \sum_i a_i \vec{v}_i$).

In other words, $\vec{y}_{k+1} = M^k \vec{y}_0$ (power method) approaches the eigenvector associated to the greatest eigenvalue in absolute value of M .

Applying the power method: the right local fractional derivative of H at 0 is :

$$\begin{aligned} D_+^q H(0) &= \Gamma(1+q) \lim_{n \rightarrow \infty} \frac{\vec{T}_0^n(\vec{c}_0 \vec{c}_1)}{(h_n)^q} = \Gamma(1+q) \lim_{n \rightarrow \infty} \frac{\lambda_1^n (a_1 \vec{v}_1)}{[\frac{1}{2^n}]^q} \\ &= \Gamma(1+q) \lim_{n \rightarrow \infty} (\lambda_1 2^q)^n (a_1 \vec{v}_1) \end{aligned} \quad (20)$$

where \vec{v}_1 is the eigenvector associated to the greatest eigenvalue λ_1 .

It follows that if the eigenvalue is real, the vector tangent to H at 0 is the eigenvector associated to the greatest eigenvalue in absolute value of \vec{T}_0 . By symmetry of the problem, we deduce that the tangent vector to H at 1 is the eigenvector associated to the greatest eigenvalue in absolute value of \vec{T}_1 .

If the greatest eigenvalue λ_1 is complex, then there is no tangent vector. In fact, the operators are characterized by a rotation which generates a spiral at boundary points and from the self-similar property at any point (see figure 3).

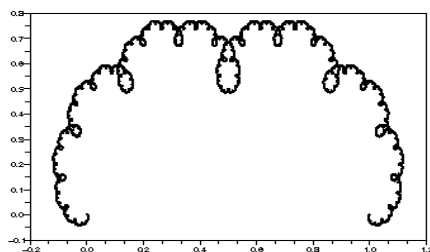


Fig. 3. Spiral fractal curve

Proposition The necessary conditions of local fractional derivatives at boundary points 0 and 1 of the morphism function H are :

- The eigenvalues of the associate linear maps are real and there exists λ_i such that $|\lambda_i| > |\lambda_j| \forall j$
- The existence of critical order α for which the expression $\lim_{n \rightarrow \infty} (\lambda_1 2^\alpha)^n$ converges towards a constant

5.2 Critical order (Hölder exponent)

The critical order α is the greatest value of q such that $D_+^q H(0)$ converges. It follows from (20):

$$\alpha(0) = \frac{\log(\frac{1}{\lambda_1})}{\log(2)} \quad (21)$$

Choosing h_n to determinate the tangent vector is guided by the address system in order to express the limit of local fractional derivative of H at 0 with one transformation (T_0). As a consequence, when computing $D^\alpha H$ the values of h_n depend on the choice of the parameterization (i.e. $\mathbb{T}^s = \{\tau_0, \tau_1\}$). Thus, the values of h_n are deduced from T^s . Another parameterization yields other values for h_n . Thus the norm of the tangent vector and the critical order depend on this parameterization. Indeed :

Proposition [2] Let g be a continuous function in $[a, b]$, and let f be a continuous function in $[g(a), g(b)]$. If $D^\alpha f(g(x))$ and $D^\beta g(x)$ exist for $\alpha, \beta \in [0, 1]$ and $x \in]a, b[$ then:

$$D^{\alpha\beta}(f \circ g)(x) = D^\alpha f(g(x)) \cdot |D^\beta g(x)|^\alpha \quad (22)$$

5.3 Example

Let $\mathbb{T} = \{T_0, T_1\}$ be an IFS composed of two operators, with:

$$T_0 \begin{pmatrix} x \\ y \end{pmatrix} = \begin{pmatrix} a & 0 \\ c & b \end{pmatrix} \begin{pmatrix} x \\ y \end{pmatrix} \quad T_1 \begin{pmatrix} x \\ y \end{pmatrix} = \begin{pmatrix} 1-a & 0 \\ -c & d \end{pmatrix} \begin{pmatrix} x \\ y \end{pmatrix} + \begin{pmatrix} a \\ c \end{pmatrix}$$

The matrices of the linear mappings associated to the operators T_0 and T_1 are:

$$D_0 = \begin{pmatrix} a & 0 \\ c & b \end{pmatrix}, \quad D_1 = \begin{pmatrix} 1-a & 0 \\ -c & d \end{pmatrix}$$

The eigenvalues associated to D_0 (resp. to D_1) are a and b (resp. $1-a$ and d). Let us denote \vec{v}_a, \vec{v}_b (resp. \vec{v}_{1-a}, \vec{v}_d) the eigenvectors associated to the eigenvalues a and b (resp. $1-a$ and d).

if $a = b$:

$$\vec{v}_a = \begin{pmatrix} 0 \\ \delta \end{pmatrix} \quad \text{and} \quad \vec{v}_b = \begin{pmatrix} 0 \\ \delta \end{pmatrix}$$

Bensoudane-Gentil-Neveu

if $a \neq b$:

$$\vec{v}_a = \begin{pmatrix} \delta \\ \frac{-c}{b-a} \times \delta \end{pmatrix} \quad \text{and} \quad \vec{v}_b = \begin{pmatrix} 0 \\ \delta \end{pmatrix}$$

$\forall \delta \neq 0 \in \mathbb{R}$
(same for \vec{v}_{1-a} and \vec{v}_d)

For all examples the critical order in c_0 and c_1 equals to 1, indeed :

$$\alpha(0) = \frac{\log(\frac{1}{\lambda_1})}{\log(2)} = \frac{\log(2)}{\log(2)} = 1$$

where $\lambda_1 = a = \frac{1}{2}$: the greatest eigenvalue in absolute value

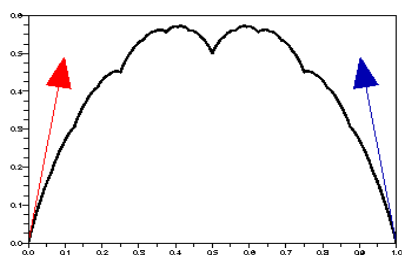


Fig. 4. $a = \frac{1}{2}, b = \frac{2}{5}, c = \frac{1}{2}, d = \frac{2}{5}$

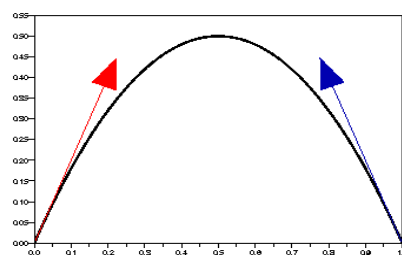


Fig. 5. $a = \frac{1}{2}, b = \frac{1}{4}, c = \frac{1}{2}, d = \frac{1}{4}$

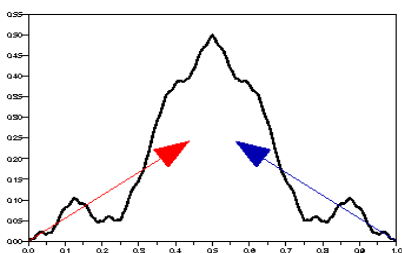


Fig. 6. $a = \frac{1}{2}, b = \frac{-2}{5}, c = \frac{1}{2}, d = \frac{-2}{5}$

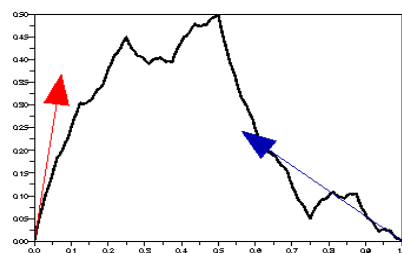


Fig. 7. $a = \frac{1}{2}, b = \frac{2}{5}, c = \frac{1}{2}, d = \frac{-2}{5}$

Example 1 : $a = \frac{1}{2}, b = \frac{2}{5}, c = \frac{1}{2}$ and $d = \frac{2}{5}$.

The curve we get this way is a kind of Takagi curve (see figure 4), continuous

and nowhere derivable, but with right and left half-tangents. The tangent vector at c_0 is the eigenvector $\vec{v}_a = \begin{pmatrix} 1 \\ 5 \end{pmatrix}$ associated to the eigenvalue a .

Example 2 : $a = \frac{1}{2}$, $b = \frac{1}{4}$, $c = \frac{1}{2}$ and $d = \frac{1}{4}$.

The curve we get this way is the quadratic Bézier curve (see figure 5), continuous and derivable. The tangent vector at c_0 is the eigenvector $\vec{v}_a = \begin{pmatrix} 1 \\ 2 \end{pmatrix}$ associated to the eigenvalue a .

Example 3 : $a = \frac{1}{2}$, $b = \frac{-2}{5}$, $c = \frac{1}{2}$ and $d = \frac{-2}{5}$.

In this case, the curve corresponds to figure 6. It is continuous and no where derivable, but also has right and left half-tangents. The tangent vector at c_0 is the eigenvector $\vec{v}_a = \begin{pmatrix} 1 \\ 5 \end{pmatrix}$ associated to the eigenvalue a . Notice that the curve oscillates around \vec{v}_a because the second eigenvalue is negative.

Example 4 : $a = \frac{1}{2}$, $b = \frac{2}{5}$, $c = \frac{1}{2}$ and $d = \frac{-2}{5}$.

In this case, the curve corresponds to figure 7. The tangent vector at c_0 (resp. c_1) is the eigenvector $\vec{v}_a = \begin{pmatrix} 1 \\ 5 \end{pmatrix}$ (resp. $\vec{v}_{1-a} = \begin{pmatrix} 1 \\ -5 \end{pmatrix}$) associated to the eigenvalue a (resp. $1 - a$).

Remark: We have given some examples of curve which are graphs of functions. But our method to calculate fractional half-tangents is applicable to the curves which are not graphs of functions (see figure 8).

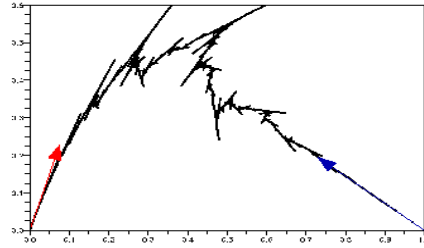


Fig. 8. A fractal curve, which is not a graph of a function

5.4 Half-tangent at a curve point

Joining conditions on curves [17] induce points with a double address. These points constitute a dense set in the attractor \mathcal{A} and for each of them, we will deduce the right (resp. left) half-tangent as a function of the right half-tangent at the point c_0 (resp. left half-tangent at the point c_1).

Bensoudane-Gentil-Neveu

Let us consider the following sets of addresses:

$$\Sigma^{0\omega} = \{\bar{\sigma}10^\omega : \bar{\sigma} \text{ finite word of } \Sigma\}$$

$$\Sigma^{1\omega} = \{\bar{\sigma}01^\omega : \bar{\sigma} \text{ finite word of } \Sigma\}$$

A point that has one address in $\Sigma^{0\omega}$ has also one address in $\Sigma^{1\omega}$ (it is a point with double address).

Indeed: let $\sigma \in \Sigma^{0\omega}$ then $\exists \bar{\sigma}$ such that $\sigma = \bar{\sigma}10^\omega$

By definition of c_0 and c_1 : $\phi(0^\omega) = c_0$ and $\phi(1^\omega) = c_1$. Besides, \mathbb{T} verifies the following joining condition

$$T_0 c_1 = T_1 c_0$$

so

$$\phi(01^\omega) = \phi(10^\omega)$$

Then we deduce:

$$\phi(\bar{\sigma}01^\omega) = \phi(\bar{\sigma}10^\omega)$$

According to the self-similarity properties of curve H , at a point p of address $\sigma = \bar{\sigma}10^\omega$ in $\Sigma^{0\omega}$, the right part of the curve at p corresponds to $T_{\bar{\sigma}_1} \cdots T_{\bar{\sigma}_i} T_1 \mathcal{A}$.

Each T_i ($i = 0, 1$) being an affine transformation, the right tangent vector at p is the transformed of the right tangent vector at c_0 (denoted \vec{t}_0) by $\vec{T}_{\bar{\sigma}_1} \cdots \vec{T}_{\bar{\sigma}_i} \vec{T}_1$.

In a similar way, the left tangent vector at p is equal to $\vec{T}_{\bar{\sigma}_1} \cdots \vec{T}_{\bar{\sigma}_i} \vec{T}_0 \vec{t}_1$ where \vec{t}_1 represents the left tangent vector at c_1 (see figure 9).

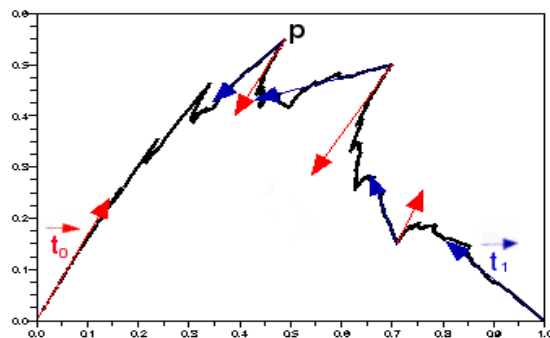


Fig. 9. Right and left half-tangents at points p with addresses 010^ω and 001^ω are respectively $\vec{T}_0 \vec{T}_1 \vec{t}_0$ and $\vec{T}_0 \vec{T}_0 \vec{t}_1$ of the curve

5.5 Generalization

The determination of the half-tangents presented for IFS composed of two transformations is easily generalized to IFS composed of N transformations. Let $\mathbb{T} = \{T_i\}_{i \in \Sigma}$ be an IFS indexed by the set $\Sigma = \{0, \dots, N-1\}$, let $\mathbb{T}^s = \{\tau_i\}_{i \in \Sigma}$ be a subdivision IFS of $[0, 1]$ and let H be the associated IFS morphism.

The curve defined by function H verifies the following joining conditions [17]:

$$T_{i-1}c_{N-1} = T_i c_0, \quad \forall i = 1 \dots N-1$$

with $T_0 c_0 = c_0$ and $T_{N-1} c_{N-1} = c_{N-1}$

Assume that half-tangents at $1(c_0)$ and at $0(c_{N-1})$ to H exist. Let

$$\Sigma^{0\omega} = \{\bar{\sigma}i0^\omega : \bar{\sigma} \text{ finite word of } \Sigma \text{ and } i \neq 0\}$$

$$\Sigma^{(N-1)\omega} = \{\bar{\sigma}i(N-1)^\omega : \bar{\sigma} \text{ finite word of } \Sigma \text{ and } i \neq (N-1)\}$$

be the sets of addresses. In a similar way to the case $N=2$, every point p with a double address has two left and right half-tangents determined by:

$$\overrightarrow{T_{\bar{\sigma}_1}} \dots \overrightarrow{T_{\bar{\sigma}_l} T_i} \overrightarrow{t_0}$$

$$\overrightarrow{T_{\bar{\sigma}_1}} \dots \overrightarrow{T_{\bar{\sigma}_l} T_{i-1}} \overrightarrow{t_{N-1}}$$

where $\overrightarrow{t_0}$ denotes the vector tangent to H at c_0 and $\overrightarrow{t_{N-1}}$ the vector tangent to H at c_{N-1} .

6 Joining curves

Because we can compute the tangent vectors at both ends of a fractal curve, it is then possible to build piecewise fractal curves : joining them requires to align tangent vectors (see figure 10). Notice that this kind of junction ensures the continuity only at the joining points. The fractal nature of fractal curves forbids to spread this continuity when moving away from the joining points. This is due to two facts: on the one hand curves are generally not derivable and on the other hand they have not necessarily the same fractal dimensions. When blending fractal curves with composite (mixed) curves [6], for which the fractal aspect continuously varies along the curve, we get a much more "natural" junction (see figure 11).

Bensoudane-Gentil-Neveu

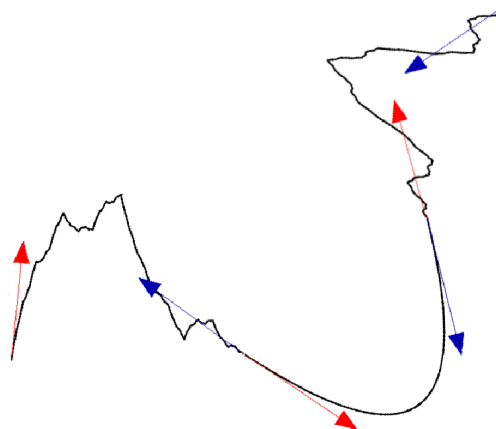


Fig. 10. Piecewise junction between three curves defined by IFS

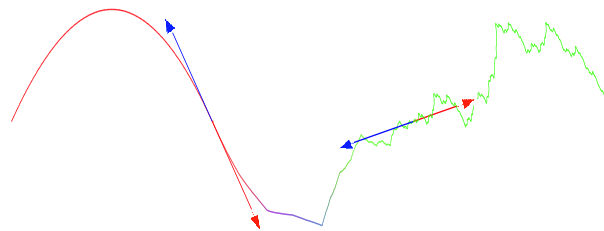


Fig. 11. Piecewise junction between two curves defined by IFS and a mixed intermediate curve

7 Conclusion

From the definition of fractional derivatives we showed that the half tangent vector (if it exists) at the end points of a fractal curve described by an IFS is given by the eigenvector associated to the greatest eigenvalue in absolute value of the corresponding transformation. In this case, we can determine the right and left half-tangents for the set of points with double addresses which is a dense set of \mathcal{A} . Some examples are given for curves which are not graphs of functions. The generalization to any point is not straightforward because of the non-continuity of the derivative. Finally the half tangent vector is used to construct piecewise fractal curves.

As far as the existence conditions are concerned, we know that if the greatest eigenvalue in absolute value is complex, the curve looks like a spiral everywhere without tangent vector but we give only sufficient conditions.

Bibliography

- [1] Michael F Barnsley. *Fractals Everywhere*. ACADEMIC PRESS INC, San Diego, USA, 1988.
- [2] Fayçal BenAdda and Jacky Cresson. About non-differentiable functions. *Mathematical Analysis and Applications*, 263:721–737, 2001.
- [3] Wayne O. Cochran, Robert R. Lewis, and John C. Hart. The normal of a fractal surface. *The Visual Computer*, 17(4):209–218, June 2001.
- [4] Khalid Daoudi, Jacques Lévy Véhel, and Yves Meyer. Construction of continuous functions with prescribed local regularity. *Rapport de Recherche(INRIA)*, December 1995.
- [5] C. Gentil and M. Neveu. Construction de surfaces fractales mixtes quadrangulaires. *GTMG2007*, pages 87–101, Mars 2007.
- [6] Christian Gentil, Eric Tosan, and Marc Neveu. Blended fractal curves. *Fractals*, in revision for publication in 2007.
- [7] Rudolf Goren and Francesco Mainardi. Essentials of fractional calculus. *Submitted to MaPhySto Center*, January 2000.
- [8] Eric Guérin, Eric Tosan, and Attila Baskurt. Description et reconstruction de courbes par une approche fractale. *In Journées AFIG'99*, pages 146–155, Novembre 1999.
- [9] John E Hutchinson. Fractals and self-similarity. *Indiana University Mathematics Journal*, 30(5):713–747, 1981.
- [10] Kiran M. Kolwankar and Anil D. Gangal. Fractional differentiability of nowhere differentiable functions and dimensions. *chao-dyn*, 2, 1996.
- [11] Kiran M. Kolwankar and Anil D. Gangal. Local fractional derivatives and fractal functions of several variables. *chao-dyn*, 1, 1998.
- [12] Benoît B Mandelbrot. *The Fractal Geometry of Nature*. W. H. FREEMAN, San Francisco, USA, 1982.
- [13] Peter R. Massopust. Fractal functions and their applications. *Chaos, Solitons and Fractals*, 8(2):171–190, 197.
- [14] Keith B. Oldham and Jerome Spanier. *The Fractional Calculus*. ACADEMIC PRESS INC, New York, US, 1974.
- [15] Bertram Ross, Stefan G. Samko, and E. Russel Love. Functions that have no first order derivative might have fractional derivatives of all orders less than one. *Real Analysis Exchange*, 20(2):140–157, May 1994.
- [16] E. Tosan, I.Bailly-Salins, I. Stotz, G. Gouaty, and Y. Weinand. Modélisation itérative de courbes et surfaces : aspect multirésolution. *GTMG2007*, pages 55–69, Mars 2007.
- [17] Eric Tosan. Surfaces fractales définies par leurs bords. *in Journées "Courbes, surfaces et algorithmes", Grenoble*, Septembre 1999.
- [18] Eric Tosan. Wire frame fractal topology and ifs morphisms. *in 4th Conference Fractals in Engineering*, (99):67–81, June 1999.

Bensoudane-Gentil-Neveu

- [19] Eric Tosan, Eric Guérin, and Attila Baskurt. Design and reconstruction of fractal surfaces. In *6th International Conference on Information Visualisation IV 2002*, pages 311–316, July 2002.
- [20] Jacques Lévy Véhel and Khalid Daoudi. Generalized ifs for signal processing. *IEEE Digital Signal Processing Workshop*, September 1996.

CONTROL WITH KAPITZA'S AVERAGING FOR CHAOTIC SYSTEMS

SERGEI BORISENOK

ABSTRACT. We generalize Kapitza's averaging procedure for a rapidly oscillating external field to control the chaotic behavior of nonlinear systems. As examples of the method we study the models of thermal convection and Rabinovich – Fabrikant attractor.

Key words: open-loop control, chaos

PACS: 05.45.Gg, 02.30.Yy

1. INTRODUCTION

The set of feedforward (open-loop) control methods is very developed, and it is difficult to systematize it to compare with feedback control [1]. An important part of this set is a sub-set of the methods based on the rapidly changing external forces [2]. Recently we generalized the famous Kapitza's effective potential method [3] to the form of an arbitrary dependency for open-loop control signal on time, it includes the particular cases of a Fourier-expanded periodical modulation [4] and the factorized force [5].

The essence of the Kapitza method is simple. Let's suppose the model of a classical particle with the mass m in two fields: one is a time-independent potential U , and another is rapidly changing open-loop control field $f(x, t)$ with a characteristic time of changing T . For the simplicity we will discuss one-dimensional movement. As it has been shown in [3], the dynamical equations for the particle can be presented as a superposition $x = X + \xi$ of the smooth

*Abdus Salam School of Mathematical Sciences, Government College University,
35-C/2, Gulberg 3, Lahore, Pakistan
E-mail: sebori@mail.ru

** Dept. of Physics, Herzen State Pedagogical University
48 Moika River, 191186 St.Petersburg, Russia .

SERGEI BORISENOK

motion X and the fast changing component ξ :

$$\begin{aligned} m\ddot{X} &= -\frac{dU(X)}{dX} - \xi \frac{d^2U(X)}{dX^2} + \xi \frac{df(X, t)}{dX} ; \\ m\ddot{\xi} &= f(X, t) . \end{aligned} \quad (1)$$

After the application of Kapitza's averaging procedure:

$$\langle A(t) \rangle = \frac{1}{T} \int_0^T A(t) dt$$

the second term in RHS (1a) becomes zero as $\langle \xi \rangle = 0$. Then Eq.(1a) can be presented in the form:

$$m\ddot{X} = -\frac{dU(X)}{dX} + \left\langle \xi \frac{df(X, t)}{dX} \right\rangle .$$

Now let's suppose $\xi(0) = 0$ and $\dot{\xi}(0) = 0$. If the force has the factorized form:

$$f(x, t) = \sum_k F_k(x) G_k(t) , \quad (2)$$

where $F_k(x)$ are the spatial components of the force, and $G_k(t)$ are dimensionless functions of the time, then after the averaging procedure the "smooth" motion with respect to the slow coordinate X can be finally presented in the form:

$$m\ddot{X} = -\frac{dU_{eff}(X)}{dX}$$

with the effective potential [5]:

$$U_{eff}(X) = U(x_0) + \sum_{k,l} G_{k,l} F_k(X) F_l(X) , \quad (3)$$

$$G_{k,l} = \left\langle \int_0^t G_k(t') dt' \int_0^t G_l(t'') dt'' \right\rangle .$$

Eq. (3) includes as particular cases the sin- and cos-shapes for the time dependency [3] and the Fourier expansion presented in [4].

This result is a generalized form of the Kapitza averaging for a system, that can be expressed with Hamiltonian approach via its potential U . Now we want to apply the same ideology to the case of a chaotic dynamical system that doesn't necessary have a Hamiltonian structure. We will illustrate our method by its application to two dynamical system with strange attractors: thermal convection loop model (in fact, that is the modified Lorenz system) in Section 2 and the Rabinovich – Fabricant system in Section 3.

2. THERMAL CONVECTION LOOP MODEL

2.1. The model. So-called thermal convection loop model is given by the system [1]:

$$\begin{aligned}\dot{x} &= \sigma(y - x) ; \\ \dot{y} &= -y - xz ; \\ \dot{z} &= -z + xy - r .\end{aligned}\tag{4}$$

Eq. (4) is a slightly modified Lorenz system. Here σ stands for the Prandtl number, and r is the Raleigh number, both are positive constants.

The system (4) has different structures of its equilibrium points depending mainly on the parameter r . For $r < 1$ the system has only one attracting equilibrium point at $(0, 0, -r)$, for r between 1 and $\sigma(\sigma + 4)/(\sigma - 2)$ we add to equilibria at $(\pm\sqrt{r-1}, \pm\sqrt{r-1}, -1)$ (the phenomenon of steady convection), and at $r = \sigma(\sigma + 4)/(\sigma - 2)$ and above the equilibria lost their stabilities in the Andronov – Hopf bifurcation (for details see [1]).

Recently several authors studied the the controlled case of the system (4):

$$\begin{aligned}\dot{x} &= \sigma(y - x) ; \\ \dot{y} &= -y - xz ; \\ \dot{z} &= -z + xy - r + u ,\end{aligned}\tag{5}$$

where the control signal u came from a fluctuation in the heating rate. In fact, we can include the parameter r into the control signal u , but let's keep it separately to respect the tradition. In [6] the z -dependent closed-loop algorithm for Eq.(5) was proposed:

$$u = -\gamma_1 \cdot \text{sign}(z + 1)$$

with the small positive constant γ_1 . In [7] the adaptive scheme of bifurcation control has been studied. Two loop adaptive control system (the second loop includes the parameter update) is presented in [8], that in the case of the model (5) means the control signal:

$$u = -\sqrt{r-1}(x - \sqrt{r-1}) - \gamma_2 \cdot \text{sign}(z + 1) ,$$

with a constant $\gamma_2 > 0$.

The typical behavior of the system is plotted on Fig.1.

2.2. Re-scaling of parameters by rapidly changing control. We propose here to apply the averaging approach to the system (4) in a rapidly oscillating external field and divide the variable z into two parts, the "slow" one Z and the "fast" one ζ :

$$z = Z + \zeta .$$

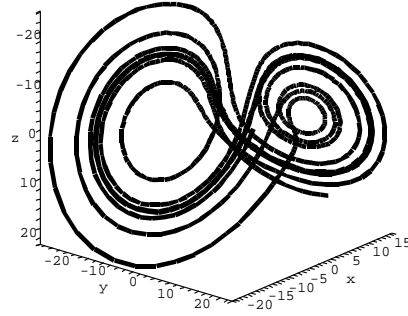


FIGURE 1. The system (4) under the control $u = -\gamma_1 \text{sign}(z + 1)$.

We suppose that the signal $u(z, t)$ consists of two parts: the closed-loop control $F(z)$ and the open-loop part $G(t)$ with the small period of oscillation T . We will discuss several simple cases for u .

Let's start from the signal

$$u(z, t) = F(z) + G(t) . \quad (6)$$

with F in the polynomial form:

$$F(z) = a_0 + a_1 z + a_2 z^2$$

In this case in Eq.(5) the fast component of the dynamical equation for z by definition corresponds to

$$\dot{\zeta} = G(t) .$$

By application of Kapitza's averaging to the third Eq.(5) we get

$$\dot{Z} = -Z + xy - r + F(Z) + a_2 \langle \zeta^2 \rangle ,$$

because $\langle \zeta \rangle = 0$. It means that under the control (6) the addition of the rapidly oscillating field $G(t)$ makes a re-scaling of the parameter r .

If we put

$$u(z, t) = F(z) \cdot G(t) , \quad (7)$$

then

$$\dot{\zeta} = F(Z) \cdot G(t) .$$

After averaging we get:

$$\dot{Z} = -Z + xy - r + b_0 + b_1 Z ,$$

where

$$b_0 = a_1 \langle \zeta G \rangle + a_2 \langle \zeta^2 G \rangle ; \quad b_1 = 2a_2 \langle \zeta G \rangle .$$

Thus, in this case we re-scale two constants (r and the factor of Z) in our initial model. This procedure can be extended for different $F(z)$.

Now we can easily generalize (7) for the factorized force of the type (2):

$$u(z, t) = \sum_k F_k(x, y, z) \cdot G_k(t) . \quad (8)$$

Let's expand F_k in Taylor series:

$$F_k(x, y, Z + \zeta) = \sum_k \sum_{n=0}^{\infty} \frac{1}{n!} \frac{\partial^n F_k(x, y, Z)}{\partial Z^n} \cdot \zeta^n .$$

We define:

$$\dot{\zeta} = \sum_k F_k(x, y, Z) \cdot G_k(t) ,$$

that leads to

$$\dot{Z} = -Z - \zeta + xy - r + \sum_k \left[\sum_{n=0}^{\infty} \frac{\zeta^n}{n!} \frac{\partial^n F_k(x, y, Z)}{\partial Z^n} - F_k(x, y, Z) \right] G_k . \quad (9)$$

Extracting 0-th term in the sum and averaging Eq.(9), we get finally:

$$\dot{Z} = -Z + xy - r + \sum_k \sum_{n=1}^{\infty} \frac{\partial^n F_k(x, y, Z)}{\partial Z^n} \frac{\langle \zeta^n(t) G_k(t) \rangle}{n!} . \quad (10)$$

Choosing different forms of the coefficients F_k , we can re-scale sufficiently the behavior of chaotic system (5).

2.3. System design by rapidly oscillating open-loop control. Nevertheless, our model of Kapitza's type control in the previous subsection is not complete. In fact, we just estimated the rescaling of the constant parameters in the dynamical equations (4). To make a fair job we must include in our model the perturbation from the fast oscillating control signal along other two axes. For simplicity we will limit our investigation by open-loop type of control, when the signal is only time-dependent: $u = u(t)$. Let's put the signal along x -axis and discuss the model:

$$\begin{aligned} \dot{x} &= \sigma(y - x) + u(t) ; \\ \dot{y} &= -y - xz ; \\ \dot{z} &= -z + xy - r . \end{aligned} \quad (11)$$

Now we split all three variables into the slow and fast parts:

$$x = X + \xi ; \quad y = Y + \eta ; \quad z = Z + \zeta$$

with the initial conditions for the fast variables:

$$\xi(0) = \eta(0) = \zeta(0) = 0 .$$

Then (11) becomes:

$$\begin{aligned}\dot{X} + \dot{\xi} &= \sigma(Y + \eta - X - \xi) + u ; \\ \dot{Y} + \dot{\eta} &= -Y - \eta - (X + \xi)(Z + \zeta) ; \\ \dot{Z} + \dot{\zeta} &= -Z\zeta + (X + \xi)(Y + \eta) - r .\end{aligned}\tag{12}$$

The changing of ξ is defined by the fast oscillating signal u , and for $\dot{\eta}$ and $\dot{\zeta}$ in (12) the perturbation comes from ξ , thus:

$$\begin{aligned}\dot{\xi} &= u ; \\ \dot{\eta} &= -Z\xi ; \\ \dot{\zeta} &= Y\xi .\end{aligned}\tag{13}$$

Defining the "fast" subsystem (13) we divide the system (12) into two part, and to the rest, i.e. to the "slow" subsystem we can apply Kapitza's averaging. Of course,

$$\langle \xi \rangle = \langle \eta \rangle = \langle \zeta \rangle = 0$$

and

$$\langle X \rangle = X ; \quad \langle Y \rangle = Y ; \quad \langle Z \rangle = Z .$$

From here all the terms of the kind $\langle X\zeta \rangle$ etc are equal to 0. Then we get:

$$\begin{aligned}\dot{X} &= \sigma(Y - X) ; \\ \dot{Y} &= -Y - XZ - \langle \xi\zeta \rangle ; \\ \dot{Z} &= -Z + XY - r + \langle \xi\eta \rangle .\end{aligned}\tag{14}$$

Let's compare (14) with the initial system (4). Averaging of the control along x gives us, first, re-scaling of r and, second, the addition of a third constant in RHS of the second equation.

The same result will be reproduces by application of the control along y :

$$\begin{aligned}\dot{x} &= \sigma(y - x) ; \\ \dot{y} &= -y - xz + u(t) ; \\ \dot{z} &= -z + xy - r .\end{aligned}\tag{15}$$

We put here:

$$\dot{\xi} = \eta ; \quad \dot{\eta} = u ; \quad \dot{\zeta} = X\eta ,$$

and by the averaging we once again come to (14).

Rapidly oscillating control along z , like in (5), repeats the initial system (4), because z is absent in the first equation, and for this reason $\dot{\xi} = 0$ ($\xi(0) = 0$, then $\xi \equiv 0$).

2.4. Simulations. Let's give several numerical examples of the control system (11). We choose $\sigma = 10$ and $r = 82$, as it was done in [1], and apply

$$u = 10 \sin \omega t . \quad (16)$$

For the initial conditions we plot the Figures 2–5 for different ω .

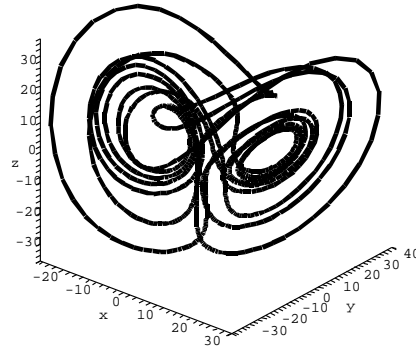


FIGURE 2. The control (16) with $\omega = 1$.

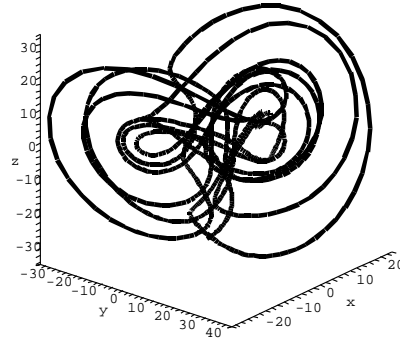
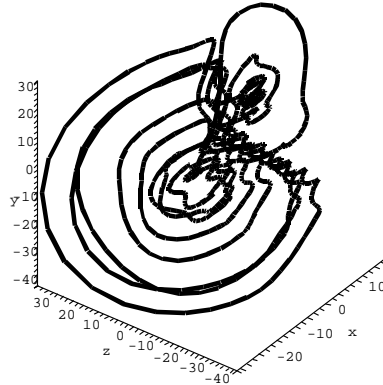
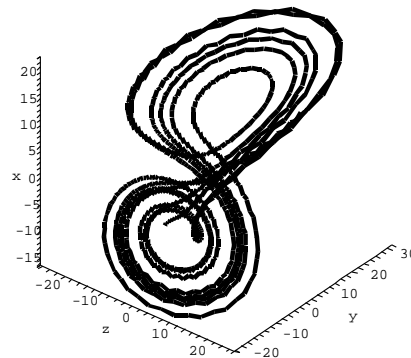


FIGURE 3. The control (16) with $\omega = 10$.

We can easily observe the drastical changes in the attractor design with increasing of ω . This is also a result of rescaling of the constant parameters in the average system (14).

SERGEI BORISENOK

FIGURE 4. The control (16) with $\omega = 10^4$.FIGURE 5. The control (16) with $\omega = 10^7$.

3. RABINOVICH – FABRICANT MODEL

The same procedure can be applied for other famous system [9]:

$$\begin{aligned}\dot{x} &= y(z - 1 + x^2) + ax ; \\ \dot{y} &= x(3z + 1 - x^2) + ay ; \\ \dot{z} &= -2z(b + xy) .\end{aligned}\tag{17}$$

Under the meaning of the parameters $a = 0.87$ and $b = 1.1$ the system (17) has a strange attractor with the correlation dimension 2.19 ± 0.01 [10].

We will study the control along z -axis:

$$\begin{aligned}\dot{x} &= y(z - 1 + x^2) + ax ; \\ \dot{y} &= x(3z + 1 - x^2) + ay ; \\ \dot{z} &= -2z(b + xy) + u(t) .\end{aligned}\tag{18}$$

Dividing the variables into the slow and fast parts, we demand:

$$\begin{aligned}\dot{\xi} &= Y\zeta ; \\ \dot{\eta} &= 3X\zeta ; \\ \dot{\zeta} &= u .\end{aligned}\tag{19}$$

Finally, after the averaging, we get:

$$\begin{aligned}\dot{X} &= Y(Z - 1 + X^2) + aX + \Delta_X ; \\ \dot{Y} &= X(3Z + 1 - X^2) + aY + \Delta_Y ; \\ \dot{Z} &= -2Z(b + XY) + \Delta_Z ,\end{aligned}\tag{20}$$

where

$$\begin{aligned}\Delta_X &= \langle \eta\zeta \rangle + \langle \eta\xi^2 \rangle + 2\langle \xi\eta \rangle X + \langle \xi^2 \rangle Y ; \\ \Delta_Y &= 3\langle \xi\zeta \rangle - \langle \xi^3 \rangle - 3\langle \xi^2 \rangle X ; \\ \Delta_Z &= -2(\langle \xi\eta\zeta \rangle + \langle \eta\zeta \rangle X + \langle \xi\zeta \rangle Y + \langle \xi\eta \rangle Z) .\end{aligned}\tag{21}$$

Thus, we sufficiently designed the initial system (17).

Now let's present the control signal as a Fourier expansion:

$$u = \sum_{k=1}^{\infty} [A_k \cos(k\omega t) + B_k \sin(k\omega t)]\tag{22}$$

with constant coefficients A_k, B_k . Of course, it satisfies the relation $\langle u \rangle = 0$. Then by (19): Let's present the control signal as a Fourier expansion:

$$\begin{aligned}\zeta(t) &= \int_0^t u(t')dt' = \frac{1}{\omega} \sum_{k=1}^{\infty} \left[\frac{A_k}{k} \sin(k\omega t) - \frac{B_k}{k} \cos(k\omega t) \right] ; \\ \xi(t) &= Y \int_0^t \zeta(t')dt' = -\frac{Y}{\omega^2} \sum_{k=1}^{\infty} \left[\frac{A_k}{k^2} \cos(k\omega t) + \frac{B_k}{k^2} \sin(k\omega t) \right] ; \\ \eta(t) &= 3X \int_0^t \zeta(t')dt' = -\frac{3X}{\omega^2} \sum_{k=1}^{\infty} \left[\frac{A_k}{k^2} \cos(k\omega t) + \frac{B_k}{k^2} \sin(k\omega t) \right] .\end{aligned}\tag{23}$$

From (23) we get:

$$\langle \xi\zeta \rangle = 0, \quad \langle \eta\zeta \rangle = 0, \quad \langle \xi^3 \rangle = 0, \quad \langle \xi\eta\zeta \rangle = 0, \quad \langle \eta\xi^2 \rangle = 0,$$

and

$$\langle \xi\eta \rangle = 3\epsilon XY, \quad \langle \eta\zeta \rangle = \epsilon Y^2,$$

SERGEI BORISENOK

where

$$\epsilon = \frac{1}{2\omega^4} \sum_{k=1}^{\infty} \frac{A_k^2 + B_k^2}{k^4} . \quad (24)$$

Thus, finally (21) is presented in the form:

$$\begin{aligned} \Delta_X &= 6\epsilon X^2 Y + \epsilon Y^3 ; \\ \Delta_Y &= -3\epsilon X Y^2 ; \\ \Delta_Z &= -6\epsilon X Y Z . \end{aligned} \quad (25)$$

In the place of (20) we have:

$$\begin{aligned} \dot{X} &= Y (Z - 1 + (1 + 6\epsilon)X^2) + aX + \epsilon Y^3 ; \\ \dot{Y} &= X(3Z + 1 - X^2 - 3\epsilon Y^2) + aY ; \\ \dot{Z} &= -2Z (b + (1 + 3\epsilon)XY) . \end{aligned} \quad (26)$$

We remark here that ϵ is not necessary a small parameter, it is defined by (24) and depend on Fourier coefficients A_k , B_k .

4. CONCLUSION

Kapitza's averaging procedure for a rapidly changing external control field does not necessary demand to present a model in Hamiltonian form. We can apply it also to control by open-loop signal the chaotic behavior of an arbitrary nonlinear dynamical system.

REFERENCES

- [1] Fradkov A., Pogromsky A., (1998), *Introduction to Control of Oscillations and Chaos*, Singapore, World Scientific.
- [2] Blekhman I., (2000), *Vibrational Mechanics - Nonlinear Dynamic Effects, General Approach*, Singapore, World Scientific.
- [3] Landau L., Lifshitz E., (1960), *Mechanics*, NY, Pergamon Press.
- [4] Ahmad B., Borisenok S., (2007), "Stabilization of Kapitza oscillator by periodical kicking pulses", *Preprint No. 46*, School of Mathematical Sciences, Lahore.
- [5] Borisenok S., (2007), "Method of effective potential for the factorized rapidly changing force", *The Journal of Prime Research in Mathematics*, 3, 210-214.
- [6] Singer J., Wang Y., Bau H., (1991), "Controlling a chaotic system", *Phys. Rev. Lett.*, 66, 1123-1125.
- [7] Wang O., Abed E., (1995), "Bifurcation control of a chaotic system", *Automatica*, 31, 1213-1226.
- [8] Pogromsky A., (1995), "Identification based adaptive control of chaotic continuous-time systems", *IFAC Conf. System Structure and Control*, Nantes, France, 629-635.
- [9] Rabinovich M., Fabrikant A., (1979), "Stochastic Self-Modulation of Waves in Nonequilibrium Media", *Sov. Phys. JETP*, 50, 311-317.
- [10] Grassberger P., Procaccia I., (1983), "Measuring the strangeness of strange attractor", *Physica D*, 9, 189-208.

STUDY OF THE BIDIRECTIONAL SYNCHRONIZATION OF TWO IDENTICAL FOUR-DIMENSIONAL NONLINEAR SYSTEMS

Maria S. PAPADOPOULOU¹, Ioannis M. KYPRIANIDIS¹, Ioannis N. STOUBOULOS¹,
Antonios N. ANAGNOSTOPOULOS¹

Abstract

In this paper we have studied the case of hyperchaotic synchronization of two identical, linearly coupled, four-dimensional chaotic systems. Individual system contains one nonlinear element, with a double-break, piecewise-linear and symmetrical v-i characteristic, and one negative conductance. Using the capacitance C_1 as the control parameter, we have observed periodic, chaotic and hyperchaotic attractors. We have established the bidirectional coupling via a variable linear resistance R_C and verified that hyperchaotic synchronization is possible as the coupling coefficient varies.

Keywords: *Hyperchaotic synchronization, Four-dimensional system, Coupling coefficient, Identical circuits, Bidirectional coupling.*

1. Introduction

The idea for chaos synchronization was premised and verified in 1990 by Pecora and Carroll [1, 2]. Over the last decade, chaos synchronization has been widely investigated due to its potential application in many areas such as secure communication, collapse prevention of power systems, secret communication technology, information processing, biomedical applications and chemical reactions [3-6]. Recently, there has been tremendous interest in synchronization of coupled chaotic systems [7-12]. More particularly, the study of coupled identical circuits has received considerable attention [13-15].

In this paper we have studied the case of hyperchaotic synchronization of two identical four-dimensional, autonomous circuits with two active elements, one linear negative conductance and one nonlinear resistor. Using the capacitance C_1 as the control parameter, we have observed periodic, chaotic and hyperchaotic attractors, period-doubling and reverse

¹Physics Department, Aristotle University of Thessaloniki, Thessaloniki GR-54124, GREECE

period-doubling sequences, as well as crisis phenomena, when the spiral attractor suddenly widens to a double-scroll attractor [16]. Furthermore, the bidirectional coupling of two nonlinear systems, when exhibit hyperchaotic behaviour, has been investigated. Both, numerical and experimental results have verified that hyperchaotic synchronization is possible.

2. The Four-Dimensional Nonlinear Circuit

The circuit, we have studied, is shown in Figure 1. It is a four-dimensional autonomous circuit with two active elements, a nonlinear resistor R_N and a linear negative conductance G_n . The v - i characteristics of the nonlinear element and negative conductance are presented in Figures 2 and 3, respectively.

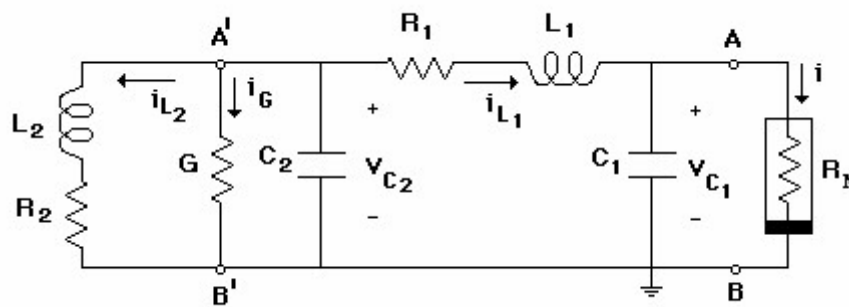


Figure 1. The four-dimensional nonlinear circuit

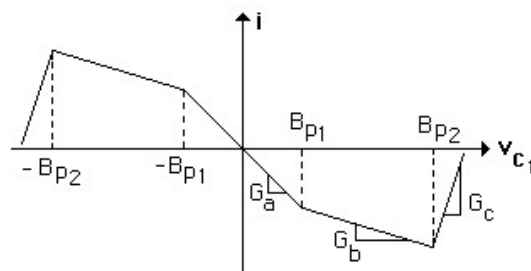


Figure 2. The double-break piece-wise linear v - i characteristic of nonlinear resistor R_N

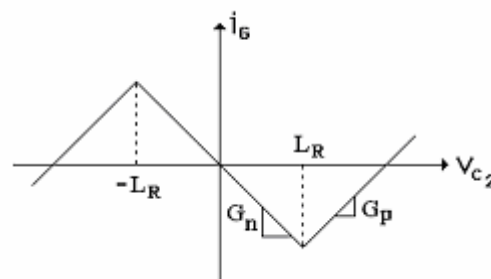


Figure 3. The v - i characteristic of negative conductance G_n

Using Kirchhoff's circuit laws, the following state equations of the system have been derived:

$$\frac{dv_{C1}}{dt} = \frac{1}{C_1} \cdot \{i_{L1} - f(v_{C1})\} \quad (2.1)$$

$$\frac{dv_{C2}}{dt} = -\frac{1}{C_2} \cdot \{G_n \cdot v_{C2} + i_{L1} + i_{L2}\} \quad (2.2)$$

$$\frac{di_{L1}}{dt} = \frac{1}{L_1} \cdot \{v_{C2} - i_{L1}R_1 - v_{C1}\} \quad (2.3)$$

$$\frac{di_{L2}}{dt} = \frac{1}{L_2} \cdot \{v_{C2} - i_{L2}R_2\} \quad (2.4)$$

where:

$$i = G_c v_{C1} + 0.5(G_a - G_b) \cdot (|v_{C1} + B_{p1}| - |v_{C1} - B_{p1}|) + 0.5(G_b - G_c) \cdot (|v_{C1} + B_{p2}| - |v_{C1} - B_{p2}|) \quad (2.5)$$

The values of circuit's parameters are: $L_1=10.2\text{mH}$, $L_2=21.5\text{mH}$, $C_2=5.23\text{nF}$, $R_1=2.02\text{K}\Omega$, $R_2=0.190\text{K}\Omega$, $G_n = -0.5\text{mS} = -G_p$, $L_R=7.50\text{V}$, $G_a = -0.83\text{mS}$, $G_b = -0.51\text{mS}$, $G_c=2.90\text{mS}$, $B_{p1}=1.46\text{V}$ and $B_{p2}=10.10\text{V}$, and consider stable during the numerical and experimental study.

In Figure 4 we observe the bifurcation diagram $(i_{L2})_p$ vs. C_1 for $C_2=5.23\text{nF}$. We can see the sequence p-1, p-2, p-4, p-8, ..., chaos,p-4, p-2, p-1, as the control parameter C_1 varies from 10.50nF to 5.50nF .

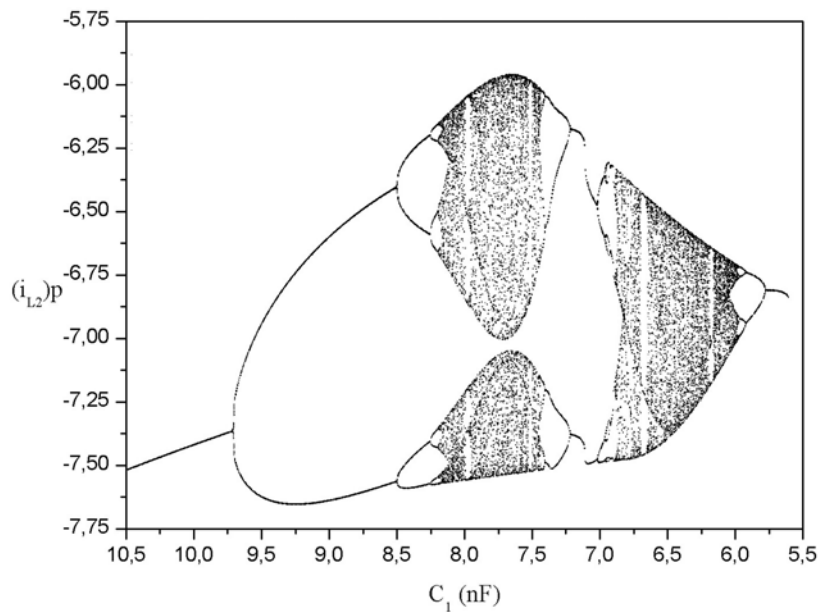


Figure 4. Bifurcation diagram $(i_{L2})_p$ vs. C_1 for $C_2=5.23\text{nF}$

3. Bidirectional Coupling of Two Identical Four-Dimensional Circuits

When two identical circuits are resistively coupled, complex dynamics can be observed, as well as chaotic and hyperchaotic synchronization, as the coupling coefficient is varied. The two circuits can be either v_{C1} -coupled or v_{C2} -coupled. The v_{C1} -coupled system of two identical four-dimensional nonlinear circuits via a linear resistor R_C is shown in Figure 5.

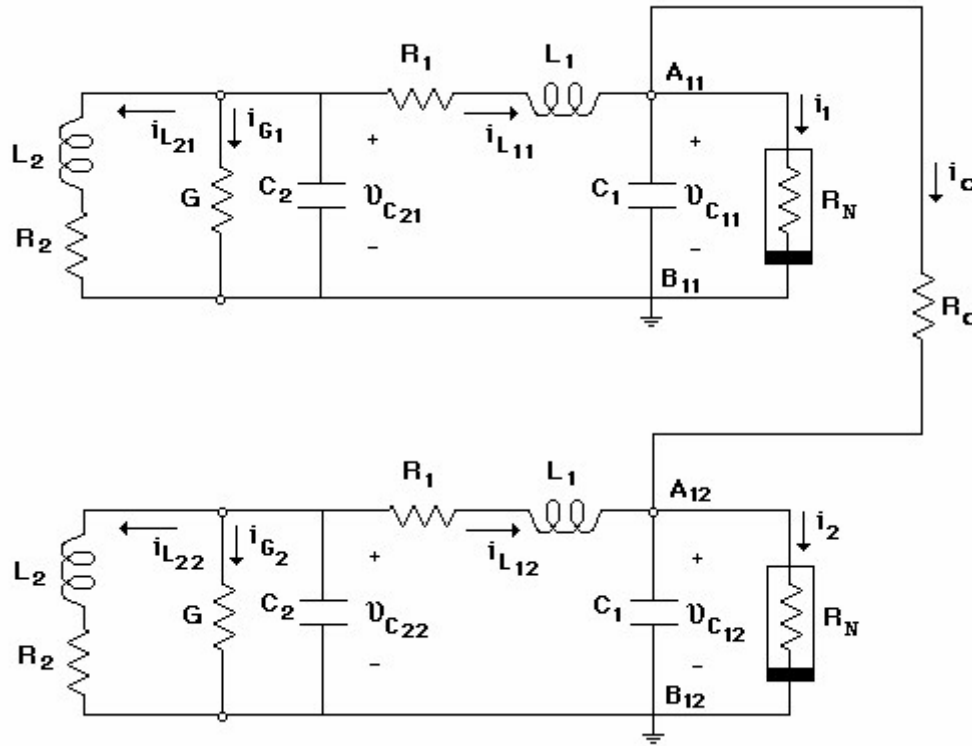


Figure 5. Linear v_{C1} -coupling of the two four-dimensional circuits

The state equations of the coupled system for the case of v_{C1} -coupling are:

$$\frac{dv_{C11}}{dt} = -\frac{1}{C_1} \cdot \left\{ \frac{v_{C11} - v_{C12}}{R_C} - i_{L11} + f(v_{C11}) \right\} \quad (3.1)$$

$$\frac{dv_{C21}}{dt} = -\frac{1}{C_2} \cdot \{ G_n \cdot v_{C21} + i_{L11} + i_{L21} \} \quad (3.2)$$

$$\frac{di_{L11}}{dt} = \frac{1}{L_1} \cdot \{ v_{C21} - i_{L11} R_1 - v_{C11} \} \quad (3.3)$$

$$\frac{di_{L21}}{dt} = \frac{1}{L_2} \cdot \{v_{C21} - i_{L21}R_2\} \quad (3.4)$$

$$\frac{dv_{C12}}{dt} = -\frac{1}{C_1} \cdot \left\{ -\frac{v_{C11} - v_{C12}}{R_C} - i_{L12} + f(v_{C11}) \right\} \quad (3.5)$$

$$\frac{dv_{C22}}{dt} = -\frac{1}{C_2} \cdot \{G_n \cdot v_{C22} + i_{L12} + i_{L22}\} \quad (3.6)$$

$$\frac{di_{L12}}{dt} = \frac{1}{L_1} \cdot \{v_{C22} - i_{L12}R_1 - v_{C12}\} \quad (3.7)$$

$$\frac{di_{L22}}{dt} = \frac{1}{L_2} \cdot \{v_{C22} - i_{L22}R_2\} \quad (3.8)$$

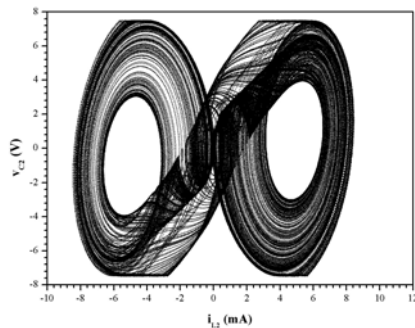
4. Hyperchaotic Synchronization

4.1 Numerical results

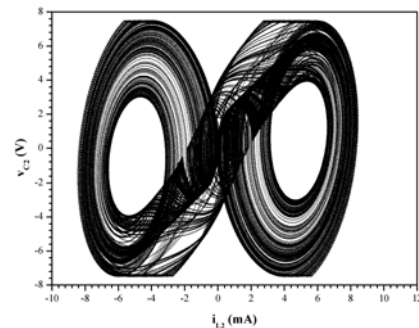
The attractors of the two circuits, when they are uncoupled, are presented in Figure 6. We can see the phase portraits $x-y \rightarrow i_{L2}-v_{C2}$ for $C_1=6.85\text{nF}$, $C_2=5.23\text{nF}$ and different initial conditions (IC). More particularly, in Figure 6(a) we observe the phase portrait of the first circuit and initial conditions I (ICI), while in Figure 6(b) the phase portrait of the second circuit and initial conditions II (ICII) is presented. We have calculated Lyapunov exponents for the double-scroll attractor for each circuit and found:

Lyapunov exponents for ICI: $LE1=+0.1953$, $LE2=+0.0088$, $LE3=-1.0395$, $LE4=-2.7357$

Lyapunov exponents for ICII: $LE1=+0.1936$, $LE2=+0.0106$, $LE3=-1.0270$, $LE4=-2.7223$



(a) phase portrait v_{C2} vs. i_{L2} (ICI)



(b) phase portrait v_{C2} vs. i_{L2} (ICII)

Figure 6. Hyperchaotic attractors for $C_1=6.85\text{nF}$, $C_2=5.23\text{nF}$ and (a) (ICI), (b) (ICII)

The existence of two positive exponents for each circuit is a strong indication that the double-scroll attractors are hyperchaotic. In Figure 7 the waveforms $i_{L2}(t)$ and $v_{C2}(t)$ are presented for the first (Figure 7(a)) and second (Figure 7(b)) circuit, respectively.

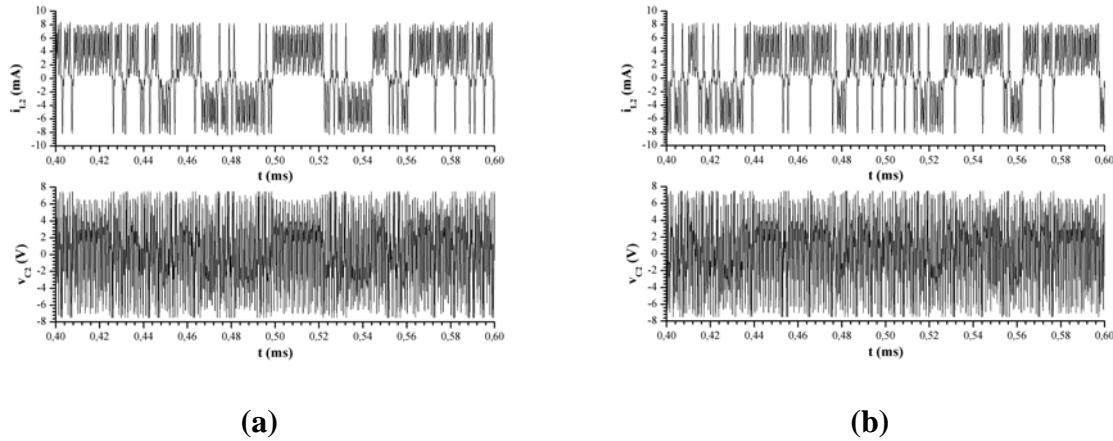


Figure 7. Waveforms $i_{L2}(t)$ & $v_{C2}(t)$ for $C_1=6.85\text{nF}$, $C_2=5.23\text{nF}$ and (a) ICI, (b) ICII

Following, we present the $v_{C22}-v_{C21}$ vs. R_1/R_C diagram. We can see that the two hyperchaotic attractors can be synchronized as the coupling coefficient increases.

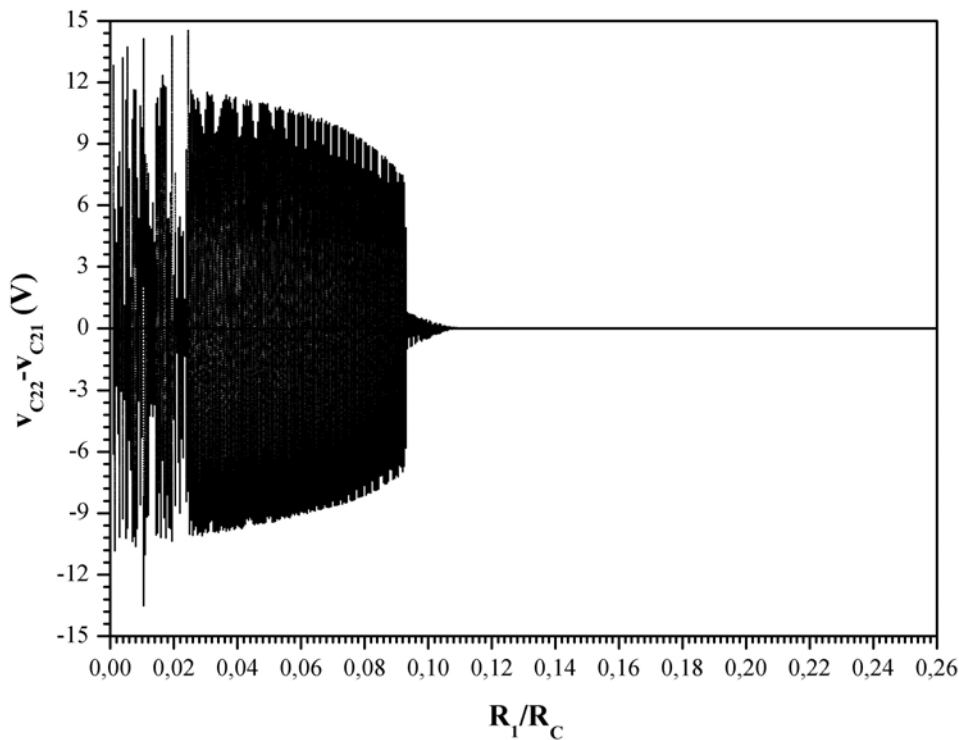


Figure 8. $v_{C22}-v_{C21}$ vs. R_1/R_C diagram

4.2 Experimental results

In previous paragraph we have studied the theoretical possibility of synchronizing two hyperchaotic attractors. Now, we will demonstrate that hyperchaotic synchronization is feasible in the laboratory experiments. In Figures 9 and 10 we can see the experimental phase portraits and waveforms for the two implemented circuits.

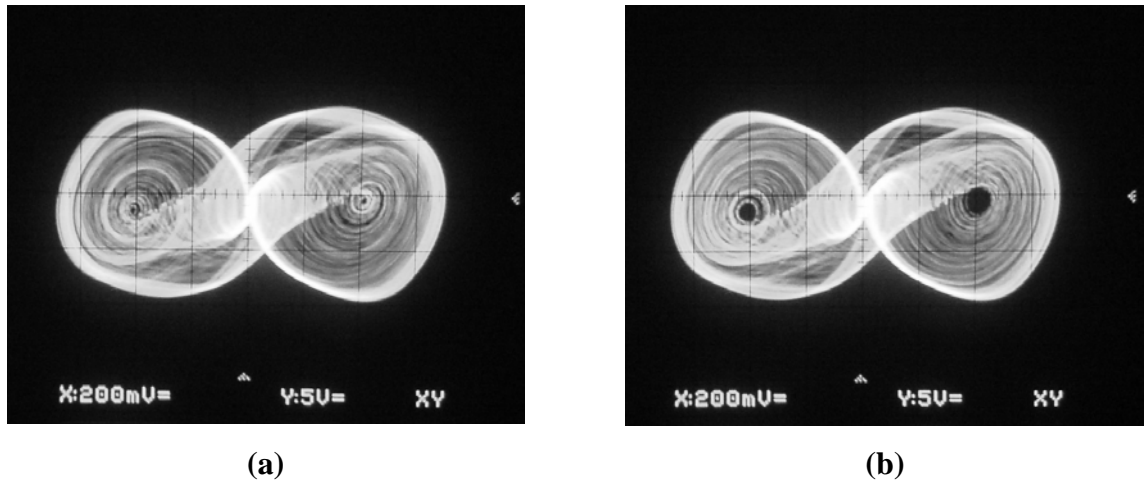


Figure 9. Experimental phase portraits for $C_1=6.85\text{nF}$, $C_2=5.23\text{nF}$ and (a) ICI, (b) ICII

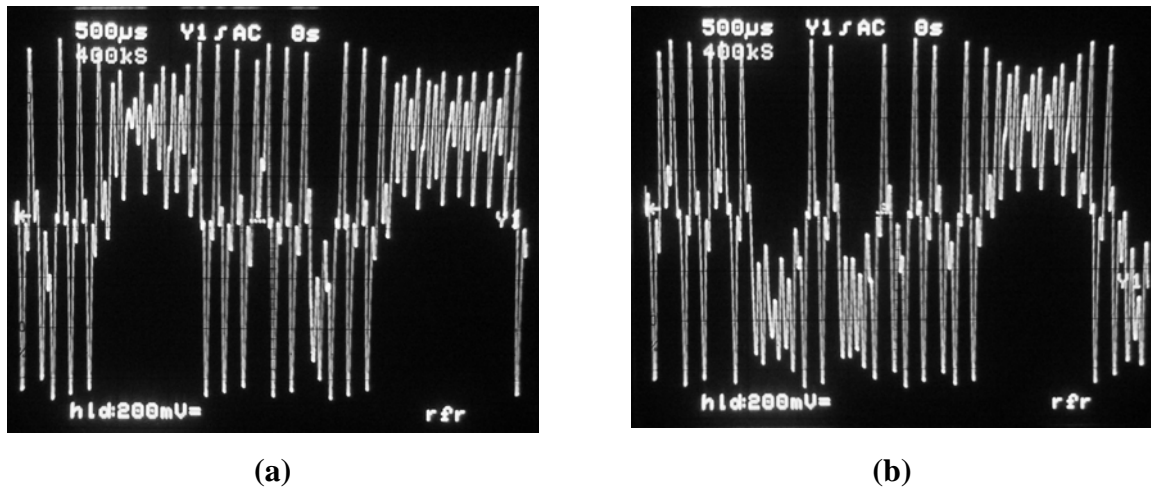


Figure 10. Experimental waveforms $i_{L2}(t)$ for $C_1=6.85\text{nF}$, $C_2=5.23\text{nF}$ and (a) ICI, (b) ICII

In Figure 11 we can see the experimental results (Lissajous diagrams v_{C22} vs. v_{C21}) for the coupled system. More particularly, in Figure 11(a) the v_{C22} vs. v_{C21} diagram is presented when the coupling coefficient approximates zero. In Figure 11(b) we observe the v_{C22} vs. v_{C21} diagram for $R_C=20\text{K}\Omega$, while in Figure 11(c) the same diagram is presented for $R_C=7\text{K}\Omega$. Finally, in Figure 11(d) the case of hyperchaotic synchronization is presented for $R_C=165\Omega$.

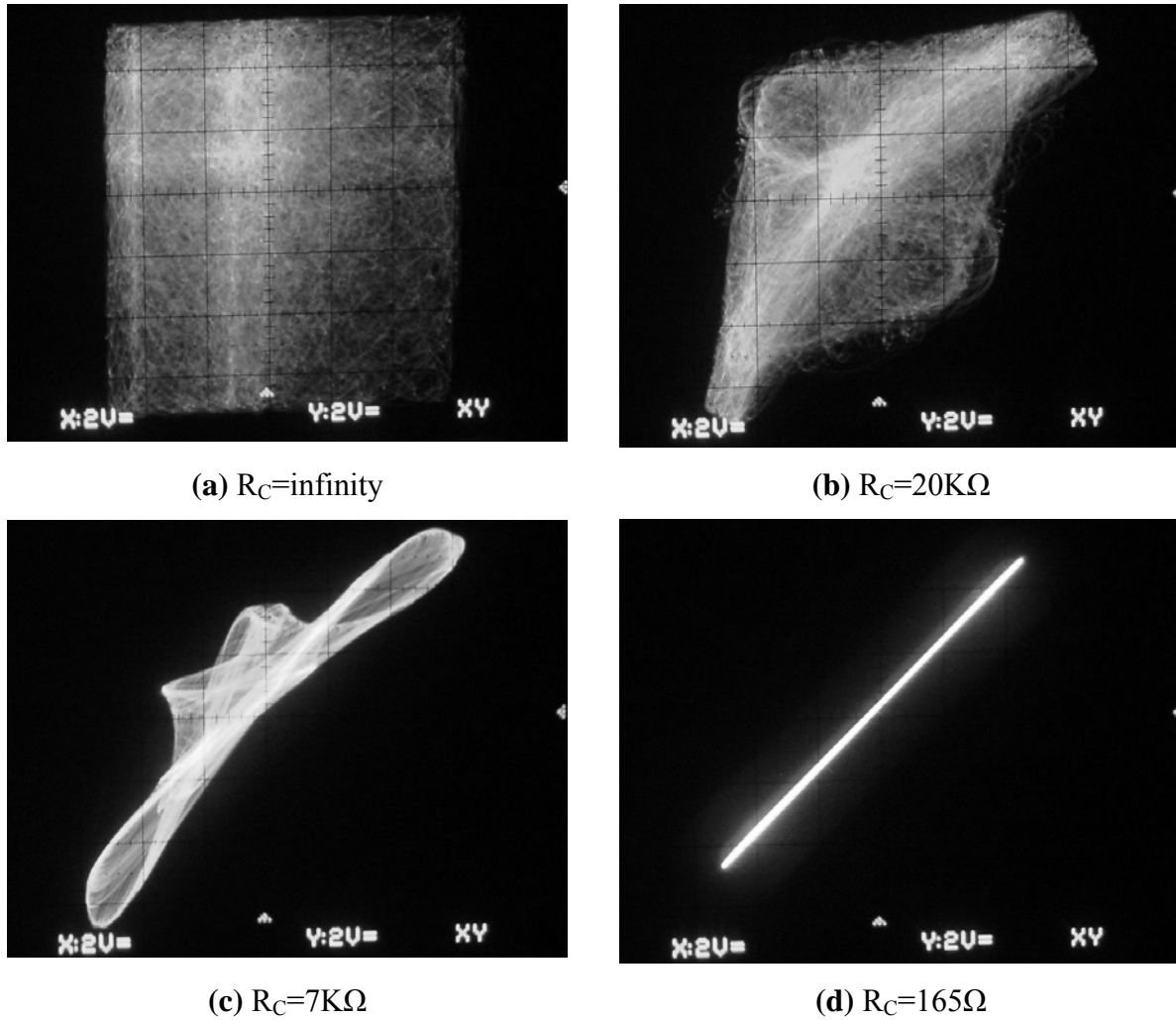


Figure 11. V_{C22} vs. V_{C21} diagrams

5. Conclusion

In this paper we have implemented two identical four-dimensional autonomous circuits. We have seen that synchronization of the bidirectional linear-coupled system, when the two subsystems are in hyperchaotic states, is possible, both numerically and experimentally.

We have studied the dynamics of the individual nonlinear autonomous electric circuit. Using the capacitance C_1 as the control parameter, we have observed the transition from periodic states to chaotic ones and vice versa, as well as hyperchaotic attractors. The existence of two positive Lyapunov exponents bespeaks that double-scroll attractors could be hyperchaotic.

Furthermore, we have seen the synchronization of two identical circuits, which are bidirectionally coupled via a linear resistor R_C . Numerical and experimental results have shown that hyperchaotic synchronization is possible in the case of v_{C2} -coupling. We have observed that for $C_1=6.85\text{nF}$ and $C_2=5.23\text{nF}$ synchronization of hyperchaotic attractors is feasible for coupling parameter $R_C<165\Omega$.

References

- [1] Pecora, L. M., and Carroll, T. L., (1990), "Synchronization in chaotic systems", *Physical Review Letters*, Vol. 64, No.8, pp. 821-824.
- [2] Pecora, L. M., and Carroll, T. L., (1991), "Driving Systems with chaotic signals", *Physical Review A*, Vol. 44, No.4, pp. 2374-2383.
- [3] Chen, G., and Dong, X., (1998), *From chaos to chaos: methodologies, perspectives and applications*, Singapore, World Scientific.
- [4] Lü, J., Lu, J., and Chen, S., (2002), *Chaotic time series analysis and its application*, China, Wuhan University Press.
- [5] Lü, J., Lu, J., and Chen, S., (2002), *Chaotic time series analysis and its application*, China, Wuhan University Press.
- [6] Chen, S., and Lu, J., (1998), *The introduction to chaotic dynamics*, China, Wuhan University Press.
- [7] Wang, X., and Chen, G., "Chaotification via arbitrarily small feedback controls: theory, method, and applications", (2000), *International Journal of Bifurcation and Chaos*, Vol. 10, pp. 549-570.
- [8] Agiza, H.N., and Yassen, M.T., (2001), "Synchronization of Rössler and Chen chaotic systems using active control", *Physics Letters A*, Vol. 278, pp. 191-197.
- [9] Chiu, C., Lin, W., and Peng, C., (2000), "Asymptotic synchronization in lattices of coupled nonlinear Lorenz equations", *International Journal of Bifurcation and Chaos*, Vol. 10, pp. 2717-2728.
- [10] Papadopoulou, M. S., Kyprianidis, I. M., and Stouboulos, I. N., (2006), "Dynamics of two coupled nonlinear autonomous 4th order circuits", *Journal of Istanbul Kültür University*, Vol. 4, pp. 55-64.
- [11] Kyprianidis, I.M., Bogiatzi, A.N., Papadopoulou M.S., Stouboulos, I.N., Bogiatzis, G.N., and Bountis, T., (2006), "Synchronizing Chaotic Attractors of Chua's Canonical

Circuit: The Case of Uncertainty in Chaos Synchronization”, *International Journal of Bifurcation and Chaos*, Vol. 16, pp. 1961-1976.

- [12] Wang, C., Ge, SS, (2001), “Adaptive synchronization of uncertain chaotic systems via backstepping design”, *Chaos, Solitons and Fractals*, Vol. 12, pp. 1199-1206.
- [13] Papadopoulou M. S., Kyprianidis, I. M., Stouboulos, I. N., (2006), “Dynamics of Two Resistively Coupled Electric Circuits of 4th Order”, *Proceedings of the 10th WSEAS International Conferences on CIRCUITS*, pp.191-196.
- [14] Hu, G., Xiao, J., and Zheng, Z., (2000), *Chaos control*, China, Shanghai Scientific and Technological Education Publishing House.
- [15] Papadopoulou, M. S., Kyprianidis, I. M., and Stouboulos, I. N., (2006), “Study of the Behavior of a 4th Order Non Driven Circuit. Chaotic Synchronization of Two Identical Circuits”, *WSEAS Transactions on Circuits and Systems*, Vol. 5, pp. 993-1000.
- [16] Kyprianidis, I. M., Stouboulos, I. N., Haralabidis, P., and Bountis, T., (2000), “Antimonotonicity and chaotic dynamics in a fourth-order autonomous nonlinear electric circuit”, *International Journal of Bifurcation and Chaos*, Vol.10, No.8, pp. 1903-1915.

List of Figures:

Figure 1. The four-dimensional nonlinear circuit	2
Figure 2. The double-break piece-wise linear v-i characteristic of nonlinear resistor R_N	2
Figure 3. The v-i characteristic of negative conductance G_n	2
Figure 4. Bifurcation diagram $(i_{L2})_p$ vs. C_1 for $C_2=5.23\text{nF}$	3
Figure 5. Linear v_{C1} -coupling of the two four-dimensional circuits	4
Figure 6. Hyperchaotic attractors for $C_1=6.85\text{nF}$, $C_2=5.23\text{nF}$ and (a) (ICI), (b) (ICII)	5
Figure 7. Waveforms $i_{L2}(t)$ & $v_{C2}(t)$ for $C_1=6.85\text{nF}$, $C_2=5.23\text{nF}$ and (a) ICI, (b) ICII	6
Figure 8. v_{C22} - v_{C21} vs. R_1/R_C diagram	6
Figure 9. Experimental phase portraits for $C_1=6.85\text{nF}$, $C_2=5.23\text{nF}$ and (a) ICI, (b) ICII	7
Figure 10. Experimental waveforms $i_{L2}(t)$ for $C_1=6.85\text{nF}$, $C_2=5.23\text{nF}$ and (a) ICI, (b) ICII....	7
Figure 11. v_{C22} vs. v_{C21} diagrams	8

A Classical Iteration method solution for nonlinear oscillators with/without discontinuities

Ahmet Yıldırım

ahmety@mail.ege.edu.tr

*Department of Mathematics, Faculty of Science, Ege University, 35100 Bornova- İzmir
TURKEY*

Abstract: A classical iteration method is applied to nonlinear oscillators with/without discontinuities. With the method, the iteration scheme provides excellent approximations to the solutions even though the iteration can only be done to the first stage.

1. Introduction

There are a variety of techniques for constructing analytical approximations to the solutions to the oscillatory systems. The perturbation methods are well established tools to study diverse aspects of nonlinear problems. Surveys of the early literature with numerous references, and useful bibliographies, have been given by Nayfeh [1], Mickens [2], and Jordan and Smith [3]. However, the use of perturbation theory in many important practical problems is invalid, or it simply breaks down for parameters beyond a certain specified range. Also, Lindstedt-Poincaré method [1-3], Multi-time expansions [1-3], harmonic balance method [1-3], and the averaging technique [1-3] are among those of the methods commonly used in nonlinear analysis. But, all these methods apply only to weakly nonlinear cases. The method of harmonic balance is accomplished of producing first order analytical approximation to the nonlinear system, valid even for rather large values of oscillation amplitude. The only negative aspect of harmonic balance is usually rather difficult to apply the method to produce higher-order analytical approximations to the solution because, they require solving sets of equations with very complex non-linearity. To overcome the limitations, many novel techniques have been proposed in recent years. For example, He [4-8] proposed a perturbation technique, so called He's homotopy perturbation method (HPM), which does not require a small parameter in the equation and takes the full advantage of the traditional perturbation methods and the homotopy techniques. In Modified Lindstedt-Poincaré method [9-13], a constant, rather than the nonlinear frequency, is expanded in powers of the expanding parameter to avoid the occurrence of secular terms in the perturbation series solution and the obtained solutions are uniformly valid on the whole solution domain. Moreover, the method is suitable not only for weakly nonlinear systems, but also for strongly nonlinear systems. For example, He contains up-to-date accounts of mathematical developments and of wide-ranging applications of many novel techniques in his comprehensive book and the references therein [14].

There also exists a wide range of literature dealing with the approximate determination of periodic solutions for nonlinear problems by using a mixture of methodologies [15-29]. The main purpose of this paper is the determination of the periodic solutions to nonlinear oscillator equations with/without discontinuities motivated by the methods mainly used in Ref. [30].

2. Solution method

Consider a nonlinear oscillator modeled by the equation

$$x'' + f(x) = 0, \quad x(0) = A, \quad x'(0) = 0 \quad (1)$$

where A is a positive constant and $f(x)$ satisfy the condition

$$f(-x) = -f(x) \quad (2)$$

We, now, suppose that the natural frequency of the system (1) is ω , which is unknown to be further determined. The system (1) can be rewritten as [30-37]

$$x'' + \omega^2 x = \omega^2 x - f(x) =: g(x), \quad x(0) = A, \quad x'(0) = 0 \quad (3)$$

The linearized form of the Eq.(1) is

$$x'' + \omega^2 x = 0, \quad x(0) = A, \quad x'(0) = 0 \quad (4)$$

Comparing Eq.(1) with Eq.(4), easily seen that even though $f(x)$ is not “small”, the function $g(x) = \omega^2 x - f(x)$ is “small”. Then left-hand side of Eq.(3) is linear and the term $g(x)$ on the right-hand side is a “small” function, namely, $g(x)$ does not have for small x a dominant term proportional to x . Hence, we equivalently solve Eq.(3) instead of Eq.(1) for convenience.

Now, following Mickens [31], the subsequent iteration scheme can be formed

$$x''_{k+1} + \omega^2 x_{k+1} = g(x_k), \quad x_k(0) = A, \quad x'_k(0) = 0, \quad k = 0, 1, 2, \dots \quad (5)$$

where the starting function is

$$x_0(t) = A \cos \omega t \quad (6)$$

This iteration can be performed to any k value; however, for most of the cases, the iteration can be stopped at $k = 2$. Because, even termination at $k = 2$ is capable of providing very high accuracy for approximate analytical solution to the exact one [31].

In the next section, the operations of this classical procedure will be illustrated by applying it to two examples with/without discontinuities.

3. Examples

Example: 1 Consider the following oscillation

$$\varepsilon x'' x + 1 = 0, \quad x(0) = A, \quad x'(0) = 0 \quad (7)$$

Now, we re-write Eq.(7) in the form

$$x'' + \varepsilon (x'')^2 x = 0, \quad x(0) = A, \quad x'(0) = 0 \quad (8)$$

For this example, iteration scheme (5) gives

$$x''_{k+1} + \omega^2 x_{k+1} = \omega x_k - \varepsilon (x''_k)^2 x_k, \quad x_k(0) = A, \quad x'_k(0) = 0 \quad (9)$$

The first iteration function (6) leads to

$$x''_1 + \omega^2 x_1 = \omega^2 A \cos \omega t - \varepsilon (-A\omega^2 \cos \omega t)^2 (A \cos \omega t) \quad (10)$$

or

$$x''_1 + \omega^2 x_1 = \left[1 - \frac{3}{4} \varepsilon A^2 \omega^2 \right] A \omega^2 \cos \omega t - \frac{1}{4} \varepsilon A^3 \omega^4 \cos 3\omega t \quad (11)$$

The requirement of no secular terms in $x_1(t)$ implies

$$\omega = \frac{2}{\sqrt{3}} \varepsilon^{-1/2} A^{-1} = 1.1547 \varepsilon^{-1/2} A^{-1} \quad (12)$$

While the exact frequency is $\omega_{ex} = \varepsilon^{-1/2} A^{-1} = 1.2533 \varepsilon^{-1/2} A^{-1}$, the accuracy goes up to 7.8% which is notable good for the first-order approximation. Hence, the first-order approximate solution reads

$$x_1 = A \cos \omega t - \frac{1}{32} \varepsilon A^3 \omega^2 (\cos \omega t - \cos 3\omega t) \quad (13)$$

Example: 2. Second equation to be studied is the following nonlinear oscillators with discontinuities

$$x'' + \text{sign}(x) = 0 \quad (14)$$

with initial conditions $x(0) = A$ and $x'(0) = 0$.

The $\text{sign}(x)$ is defined as

$$\text{sign}(x) = \begin{cases} 1 & x > 0 \\ -1 & x \leq 0 \end{cases} \quad (15)$$

It is worth to note that there is no small parameter in the equation, so the traditional perturbation methods can not be applied. Moreover, the equation involves discontinuities. The Eq.(14), with initial conditions, can be rewritten as

$$x_{k+1}'' + \omega^2 x_{k+1} = \omega^2 x_k - \text{sign}(x_k) \quad (16)$$

$$x_k(0) = A, \quad x_k'(0) = 0 \quad (17)$$

The first iteration function (6) leads to

$$x_1'' + \omega^2 x_1 = \omega^2 \cos \omega t - \text{sign}(A \cos \omega t) \quad (18)$$

The requirement of no secular term in $x_1(t)$, averagingly we set[7]

$$\int_0^T [\omega^2 A \cos \omega t - \text{sign}(A \cos \omega t)] \cos \omega t dt = 0 \quad (19)$$

where $T = 2\pi / \omega$.

Noting that $|\cos \omega t| = \cos \omega t$ when $-\pi/2 \leq \omega t \leq \pi/2$ and $|\cos \omega t| = -\cos \omega t$ when $\pi/2 \leq \omega t \leq 3\pi/2$. Hence, the Eq.(19) can be written as

$$\int_{-\pi/2}^{\pi/2} [\omega^2 A \cos^2 t - \cos t] dt + \int_{\pi/2}^{3\pi/2} [\omega^2 A \cos^2 t + \cos t] dt = 0 \quad (20)$$

From Eq.(20), we can easily find that

$$\omega = \frac{2}{\sqrt{\pi A}} \quad (21)$$

and its approximate period is

$$T = 2\pi / \omega = 5.56\sqrt{A}. \quad (22)$$

$$\text{Its exact period reads } T_{ex} = 4\sqrt{2A} = 5.66\sqrt{A}. \quad (23)$$

Hence, we can see clearly that its first-order approximation is of a high accuracy. It can be easily shown that the maximal relative error is less than 1.76%.

We, now, re-write Eq.(18) in the form

$$x_1'' + \omega^2 x_1 = \begin{cases} A\omega^2 \cos \omega t - 1, & -\pi/2 \leq \omega t \leq \pi/2 \\ A\omega^2 \cos \omega t + 1, & \pi/2 \leq \omega t \leq 3\pi/2 \end{cases} \quad (24)$$

with initial conditions $x_1(0) = A$, $x_1'(0) = 0$.

We, therefore, obtain the solution of Eq.(24) as

$$x_1 = \begin{cases} A \cos \omega t + \frac{1}{2} A \omega t \sin \omega t - \frac{1}{\omega^2} + \frac{1}{\omega^2} \cos \omega t, & -\pi/2 \leq \omega t \leq \pi/2 \\ A \cos \omega t + \frac{1}{2} A \omega t \sin \omega t + \frac{1}{\omega^2} + \frac{1}{\omega^2} \cos \omega t - \frac{2}{\omega^2} \sin \omega t, & \pi/2 \leq \omega t \leq 3\pi/2 \end{cases} \quad (25)$$

which agrees exactly with Liu's solution [10] that is obtained by modified Lindstedt-Poincaré method.

3. Conclusion

In summary, a classical iteration method for calculating analytical approximations to the periodic solutions of nonlinear oscillators with/without discontinuities has been proposed. Its applicability has been demonstrated by means of two examples. The major conclusion is that the iteration scheme provides exceptional approximations to the solutions even though the iteration can only be done to the first stage.

4. References

- [1] Nayfeh, A. H., *Perturbation Methods*, Wiley-Interscience, New York, 1973
- [2] Mickens, R.E., *Oscillations in Planar Dynamics Systems*, World Scientific, Singapore, 1996
- [3] Jordan, D.W. and Smith, P., *Nonlinear Ordinary differential Equations*, Clarendon Press, Oxford, 1987

- [4] He, JH. , Homotopy perturbation technique, *Computer Methods in Applied Mechanics and Engineering*, 178 (3-4): 257-262, 1999
- [5] He, JH. , A coupling method of a homotopy technique and a perturbation technique for non-linear problems, *International Journal of Non-linear Mechanics* 35 (1), 2000, 37-43.
- [6] He, JH., Homotopy perturbation method: a new nonlinear analytical technique, *Applied Mathematics and Computation* , 135 (1): 73-79, 2003
- [7] Öziş, T., Yıldırım, A., A note on He's homotopy perturbation method for van der Pol oscillator with very strong nonlinearity, *Chaos Solitons & Fractals*, 34(3): 989-991, 2007
- [8] He, JH., The homotopy perturbation method for nonlinear oscillators with discontinuities, *Applied Mathematics and Computation*, 151 (2004) 287-292
- [9] He, JH., Modified Lindstedt-Poincaré methods for some strongly non-linear oscillations Part I: expansion of a constant, *International Journal of Non-linear Mechanics*, 37 (2002) 309-314
- [10] Liu, HM., Approximate period of nonlinear oscillators with discontinuities by modified Lindstedt-Poincaré method , *Chaos, Solitons & Fractals*, 23(2005) 577-579
- [11] Öziş, T., Yıldırım, A., Determination of limit cycles by a modified straightforward expansion for nonlinear oscillators, *Chaos Solitons & Fractals*, 32 (2007) 445-448
- [12] Öziş, T., Yıldırım, A., Determination of periodic solution for a $u^{1/3}$ force by He's modified Lindstedt-Poincaré method, *Journal of Sound and Vibration* , 301(1-2), 415-419, 2007
- [13] Cheung, Y. K., Mook, S.H., Lau, S.L., A modified Lindstedt-Poincaré method for certain strongly non-linear oscillators, *International Journal of Non-linear Mechanics*, 26(1991), 367-378

- [14]He, JH, *Non-Perturbative Methods for Strongly nonlinear Problems*, dissertation.de-verlag im Internet GmbH, Berlin, 2006
- [15] Öziş, T., Yıldırım, A., Determination of frequency-amplitude relation for Duffing-Harmonic Oscillator by the Energy Balance Method, *Computers and Mathematics with applications*, 54(7-8),1184-1187,2007
- [16] Wu,B.S., Sun,W.P., Lim, C.W., An analytical approximate technique for a class of strongly non-linear oscillators, *International Journal of Non-Linear Mechanics* ,41(6-7),766-774,2006
- [17]He, JH. , Analytical solution of a nonlinear oscillator by the linearized perturbation technique, *Communication in Nonlinear Science & Numerical Simulation*, 4(2) (1999), 109-113.
- [18]He, JH., Modified straightforward expansion, *Meccanica*, 34 (4),1999, 287-289
- [19]He, JH. , Determination of limit cycles for strongly nonlinear oscillators, *Physical Review Letters*, 90 (17): Art. No. 174301, 2003
- [20]Xiong, Z.G., Hu, H., Tang, Q., A modified eigen-function expansion approximation for nonlinear oscillating equations, *Journal of Sound and Vibration*, 290 (2006) 1315-1321
- [21]Xu, L., He's parameter-expanding methods for strongly nonlinear oscillators, *Journal of Computational and Applied Mathematics*, 207(1),148-154,2007
- [22]D' Acunto, M., Self-excited systems: analytical determination of limit cycles, *Chaos Solitons & Fractals*, 30 (2006) 719-724
- [23]D' Acunto, M., determination of limit cycles for a modified van der Pol oscillator, *Mech. Res. Commun.*, 33 (2006) 93-98
- [24]Hu, H, Tang, J.H., A convolution integral method for certain strongly nonlinear oscillators, *Journal of Sound and Vibration*, 285 (2005) 1235-1241
- [25]He, JH. Bookkeeping parameter in perturbation methods, *International journal of*

- nonlinear Science and numerical Simulation*, 2 (2001) 257-264.
- [26] He, J.H. Variational iteration method-some recent results and new interpretations, *Journal of Computational and applied mathematics*, 207(1),3-17,2007
- [27] Xu, L., Determination of limit cycle by He's parameter-expanding method for strongly nonlinear oscillators, *Journal of Sound and Vibration*, 302(1-2),178-184,2007
- [28] Mickens, R.E., Oscillations in an $x^{4/3}$ potential, *Journal of Sound and Vibration* 246(2) (2001),375-378
- [29] Mickens, R. E., Analysis of non-linear oscillators having non-polynomial elastic terms, *Journal of Sound and Vibration* 255(4) (2002), 789-792
- [30] Timoshenko, S. Yang, D.H., Weaver Jr, W., *Vibration Problems in Engineering*, 4th ed., Wiley, New York, 1974
- [31] Mickens, R. E. Iteration procedure for determining approximate solutions to non-linear oscillator equation, *Journal of Sound and Vibration* 116 (1987) 185-188
- [32] Lim, C.W., Wu, B.S., A modified Micken's procedure for certain non-linear oscillators, *Journal of Sound and Vibration*, 257(1) (2002) 202-206
- [33] Mickens, R. E., A generalized iteration procedure for calculating approximations to periodic solutions of "truly nonlinear oscillators", *Journal of Sound and Vibration*, 287(4-5) (2005) 1045-1051
- [34] Mickens, R. E., Iteration method solutions for conservative and limit-cycle $x^{1/3}$ force oscillators, *Journal of Sound and Vibration* 292(3-5) (2006) 964-968
- [35] Hu, H., Solution of nonlinear oscillators with fractional powers by an iteration procedure, *Journal of Sound and Vibration*, 294 (2006) 608-614
- [36] Hu, H., Solution of the Duffing-harmonic oscillator by an iteration procedure, *Journal of Sound and Vibration*, 298 (2006) 446-452
- [37] Hu, H. Tang, J.H., a classical iteration procedure valid for certain strongly nonlinear

oscillators, *Journal of Sound and Vibration*, 299(1-2),397-402,2007

Instructions to Contributors

Journal of Applied Functional Analysis

A quarterly international publication of Eudoxus Press, LLC of TN.

Editor in Chief: George Anastassiou

Department of Mathematical Sciences
University of Memphis
Memphis, TN 38152-3240, U.S.A.

1. Manuscripts, hard copies in quadruplicate and in English, should be submitted by regular, unregistered mail, to the Editor in Chief.

Authors may want to recommend an associate editor most related to the submission to possibly handle it. In addition, to assist the Editor and speed the decision process, authors may include a PDF file of the paper on disk with the submitted copies of the manuscript.

Also authors may want to submit a list of six possible referees, to be used in case we cannot find related referees by ourselves.

2. Manuscripts should be typed using any of TEX, LaTeX, AMS-TEX, or AMS-LaTeX and according to EUDOXUS PRESS, LLC. LATEX STYLE FILE. (Click [HERE](#) to save a copy of the style file.) They should be carefully prepared in all respects. Submitted copies should be brightly printed (not dot-matrix), double spaced, in ten point type size, on one side high quality paper 8(1/2)x11 inch. Manuscripts should have generous margins on all sides and should not exceed 24 pages.

3. Submission is a representation that the manuscript has not been published previously in this or any other similar form and is not currently under consideration for publication elsewhere. A statement transferring from the authors (or their employers, if they hold the copyright) to Eudoxus Press, LLC, will be required before the manuscript can be accepted for publication. The Editor-in-Chief will supply the necessary forms for this transfer. Such a written transfer of copyright, which previously was assumed to be implicit in the act of submitting a manuscript, is necessary under the U.S. Copyright Law in order for the publisher to carry through the dissemination of research results and reviews as widely and effectively as possible.

4. The paper starts with the title of the article, author's name(s) (no titles or degrees), author's affiliation(s) and e-mail addresses. The affiliation should comprise the department, institution (usually university or company), city, state (and/or nation) and mail code.

The following items, 5 and 6, should be on page no. 1 of the paper.

5. An abstract is to be provided, preferably no longer than 150 words.
6. A list of 5 key words is to be provided directly below the abstract. Key words should express the precise content of the manuscript, as they are used for indexing purposes.

The main body of the paper should begin on page no. 1, if possible.

7. All sections should be numbered with Arabic numerals (such as: 1. INTRODUCTION) .

Subsections should be identified with section and subsection numbers (such as 6.1. Second-Value Subheading).

If applicable, an independent single-number system (one for each category) should be used to label all theorems, lemmas, propositions, corollaries, definitions, remarks, examples, etc. The label (such as Lemma 7) should be typed with paragraph indentation, followed by a period and the lemma itself.

8. Mathematical notation must be typeset. Equations should be numbered consecutively with Arabic numerals in parentheses placed flush right, and should be thusly referred to in the text [such as Eqs.(2) and (5)]. The running title must be placed at the top of even numbered pages and the first author's name, et al., must be placed at the top of the odd numbered pages.

9. Illustrations (photographs, drawings, diagrams, and charts) are to be numbered in one consecutive series of Arabic numerals. The captions for illustrations should be typed double space. All illustrations, charts, tables, etc., must be embedded in the body of the manuscript in proper, final, print position. In particular, manuscript, source, and PDF file version must be at camera ready stage for publication or they cannot be considered.

Tables are to be numbered (with Roman numerals) and referred to by number in the text. Center the title above the table, and type explanatory footnotes (indicated by superscript lowercase letters) below the table.

10. List references alphabetically at the end of the paper and number them consecutively. Each must be cited in the text by the appropriate Arabic numeral in square brackets on the baseline.

References should include (in the following order):
 initials of first and middle name, last name of author(s)
 title of article,
 name of publication, volume number, inclusive pages, and year of publication.

Authors should follow these examples:

Journal Article

1. H.H.Gonska, Degree of simultaneous approximation of bivariate functions by Gordon operators, (journal name in italics) *J. Approx. Theory*, 62,170-191(1990).

Book

2. G.G.Lorentz, (title of book in italics) *Bernstein Polynomials* (2nd ed.), Chelsea, New York, 1986.

Contribution to a Book

3. M.K.Khan, Approximation properties of beta operators, in (title of book in italics) *Progress in Approximation Theory* (P.Nevai and A.Pinkus, eds.), Academic Press, New York, 1991, pp.483-495.

11. All acknowledgements (including those for a grant and financial support) should occur in one paragraph that directly precedes the References section.

12. Footnotes should be avoided. When their use is absolutely necessary, footnotes should be numbered consecutively using Arabic numerals and should be typed at the bottom of the page to which they refer. Place a line above the footnote, so that it is set off from the text. Use the appropriate superscript numeral for citation in the text.

13. After each revision is made please again submit four hard copies of the revised manuscript. And after a manuscript has been accepted for publication submit four hard copies of the final revised manuscript. Additionally, two copies of the final version of the TEX/LaTeX source file and a PDF file, are to be submitted to the Editor's Office on personal 3.5 inch computer disks. Label the disks individually with clearly written identifying information, e.g. :

Your name, title of article, kind of computer used, kind of software and version number, disk format and files names of article, as well as abbreviated journal name.

Package the disks in a disk mailer or protective cardboard. Make sure contents of disks are identical with the ones of final hard copies submitted!

Note: The Editor's Office cannot accept the disks without the accompanying matching hard copies of manuscript. No e-mail final submissions are allowed! File submission on disk must be used.

14. Effective 1 Jan. 2009 the journal's page charges are \$15.00 per PDF file page, plus \$40.00 for electronic publication of each article. Upon acceptance of the paper an invoice will be sent to the contact author. The fee payment will be due one month from the invoice date. The article will proceed to publication only after the fee is paid. The charges are to be sent, by money order or certified check, in US dollars, payable to Eudoxus Press, LLC, to the address shown on the Eudoxus [homepage](#).

No galleys will be sent and the contact author will receive one(1) electronic copy of the journal issue in which the article appears.

15. This journal will consider for publication only papers that contain proofs for their listed results.

TABLE OF CONTENTS, JOURNAL OF APPLIED FUNCTIONAL ANALYSIS,
VOLUME 4, NO.2, 2009

PREFACE,	192
APPLICATION OF HOMOTOPY PERTURBATION METHOD TO NONLINEAR OSCILLATOR DIFFERENTIAL EQUATIONS, A.BARARI, F.FARROKHZAD, A. JANALIZADEH, D.D.GANJI,	193
ESTIMATING FRACTAL DIMENSION OF FINANCIAL RETURNS USING STABLE DISTRIBUTIONS, N.ALPTekin,	205
CAPUTO FRACTIONAL OSTROWSKI TYPE INEQUALITIES, G.A.ANASTASSIOU,	218
A CHAOTIC COMMUNICATION SYSTEM WITH ENHANCED SECURITY FEATURES, I.P.ANTONIADES, A.N.MILIOU, S.G.STAVRINIDES, A.N.ANAGNOSTOPOULOS,	237
ESTIMATING CHAOS AND COMPLEX DYNAMICS IN AN AUTONOMOUS FOUR-DIMENSIONAL CIRCUIT, M. S.PAPADOPOULOU, I.N. STOUBOULOS, I.M. KYPRIANIDIS, A.N.ANAGNOSTOPOULOS,	249
NONLINEAR TIME SERIES ANALYSIS OF THE CURRENT THROUGH PEG-SI THIN FILMS UNDER VARYING RELATIVE HUMIDITY, K.ATAK, O.AYBAR, A.HACINLIYAN, G.SAHIN, Y.SKARLATOS,	259
THE SOLUTIONS OF BRATU-TYPE PROBLEMS BY HE'S HOMOTOPY PERTURBATION METHOD, A.YILDIRIM,	265
COMPARATIVE STUDY BETWEEN SISCON AND MATLAB IN PYROLYSIS REACTOR IDENTIFICATION, M.AZZOUZI,	273
EARTHQUAKE HAZARD ASSESSMENT FOR DIFFERENT REGIONS IN AND AROUND TURKEY BASED ON GUTENBERG-RICHTER PARAMETERS BY THE LEAST SQUARE METHOD, Y.BAYRAK, S.OZTURK, H.CINAR, G.CH.KORAVOS, T.M.TSAPANOS,	286

TABLE OF CONTENTS, JOURNAL OF APPLIED FUNCTIONAL ANALYSIS,
VOLUME 4, NO.2, 2009, continued from inside back cover

APPLICATION OF HOMOTOPY PERTURBATION METHOD AND VARIATIONAL ITERATION METHOD TO A NONLINEAR DIFFUSION EQUATION WITH A REACTION TERM, A.BARARI, A.JANALIZADEH, F.FARROKHZAD, D.D.GANJI,.....	300
FRACTIONAL HALF-TANGENT OF A CURVE DESCRIBED BY ITERATED FUNCTION SYSTEMS, H.BENSOUDANE, C.GENTIL, M.NEVEU,.....	311
CONTROL WITH KAPITZA'S AVERAGING FOR CHAOTIC SYSTEMS, S.BORISENOK,.....	327
STUDY OF THE BIDIRECTIONAL SYNCHRONIZATION OF TWO IDENTICAL FOUR-DIMENSIONAL NONLINEAR SYSTEMS, M.S.PAPADOPOULOU, I. M.KYPRIANIDIS, I.N.STOUBOULOS, A.N.ANAGNOSTOPOULOS,.....	337
A CLASSICAL ITERATION METHOD SOLUTION FOR NONLINEAR OSCILLATORS WITH/WITHOUT DISCONTINUITIES A.YILDIRIM,.....	347

Volume 4, Number 3

July 2009

ISSN:1559-1948 (PRINT), 1559-1956 (ONLINE)

EUDOXUS PRESS, LLC



JOURNAL OF APPLIED FUNCTIONAL ANALYSIS

GUEST EDITORS: HIKMET CAGLAR and MEHMET OZER

SPECIAL ISSUE II: "CHAOS and COMPLEX SYSTEMS 2008"

SCOPE AND PRICES OF
JOURNAL OF APPLIED FUNCTIONAL ANALYSIS
A quarterly international publication of **EUDOXUS PRESS,LLC**
ISSN:1559-1948(PRINT),1559-1956(ONLINE)

Editor in Chief: George Anastassiou
Department of Mathematical Sciences
The University of Memphis
Memphis, TN 38152,USA
E mail: ganastss@memphis.edu

The purpose of the "Journal of Applied Functional Analysis"(JAFA) is to publish high quality original research articles, survey articles and book reviews from all subareas of Applied Functional Analysis in the broadest form plus from its applications and its connections to other topics of Mathematical Sciences. A sample list of connected mathematical areas with this publication includes but is not restricted to: Approximation Theory, Inequalities, Probability in Analysis, Wavelet Theory, Neural Networks, Fractional Analysis, Applied Functional Analysis and Applications, Signal Theory, Computational Real and Complex Analysis and Measure Theory, Sampling Theory, Semigroups of Operators, Positive Operators, ODEs, PDEs, Difference Equations, Rearrangements, Numerical Functional Analysis, Integral equations, Optimization Theory of all kinds, Operator Theory, Control Theory, Banach Spaces, Evolution Equations, Information Theory, Numerical Analysis, Stochastics, Applied Fourier Analysis, Matrix Theory, Mathematical Physics, Mathematical Geophysics, Fluid Dynamics, Quantum Theory. Interpolation in all forms, Computer Aided Geometric Design, Algorithms, Fuzzyness, Learning Theory, Splines, Mathematical Biology, Nonlinear Functional Analysis, Variational Inequalities, Nonlinear Ergodic Theory, Functional Equations, Function Spaces, Harmonic Analysis, Extrapolation Theory, Fourier Analysis, Inverse Problems, Operator Equations, Image Processing, Nonlinear Operators, Stochastic Processes, Mathematical Finance and Economics, Special Functions, Quadrature, Orthogonal Polynomials, Asymptotics, Symbolic and Umbral Calculus, Integral and Discrete Transforms, Chaos and Bifurcation, Nonlinear Dynamics, Solid Mechanics, Functional Calculus, Chebyshev Systems. Also are included combinations of the above topics.

Working with Applied Functional Analysis Methods has become a main trend in recent years, so we can understand better and deeper and solve important problems of our real and scientific world.

JAFA is a peer-reviewed International Quarterly Journal published by Eudoxus Press,LLC.

We are calling for high quality papers for possible publication. The contributor should send four copies of the contribution to the EDITOR in CHIEF in TEX,LATEX double spaced,in ten point type size. They should be sent BY REGULAR MAIL ONLY, NOT REGISTERED MAIL, AND NO E-MAIL SUBMISSIONS [See: Instructions to Contributors]

Journal of Applied Functional Analysis(JAFA)
is published in January, April, July and October of each year by

EUDOXUS PRESS,LLC,

1424 Beaver Trail Drive,Cordova,TN38016,USA,

Tel.001-901-751-3553

anastassioug@yahoo.com

<http://www.EudoxusPress.com> visit also <http://www.msci.memphis.edu/~ganastss/jafa>.

Webmaster:Ray Clapsadle

Annual Subscription Current Prices:For USA and Canada,Institutional:Print \$280,Electronic \$220,Print and Electronic \$350.Individual:Print \$ 100, Electronic \$60,Print &Electronic \$150.For any other part of the world add \$40 more to the above prices for Print.
Single article PDF file for individual \$10.Single issue in PDF form for individual \$40.

The journal carries page charges \$15 per page of the pdf file of an article, plus \$40 for the electronic publication of all article, both payable upon acceptance of the article within one month and before publication.

No credit card payments.Only certified check,money order or international check in US dollars are acceptable.

Combination orders of any two from JoCAAA,JCAAM,JAFa receive 25% discount,all three receive 30% discount.

Copyright©2009 by Eudoxus Press,LLC all rights reserved.JAFa is printed in USA.

JAFa is reviewed and abstracted by AMS Mathematical Reviews,MATHSCI,and Zentralblatt MATH.

It is strictly prohibited the reproduction and transmission of any part of JAFa and in any form and by any means without the written permission of the publisher.It is only allowed to educators to Xerox articles for educational purposes.The publisher assumes no responsibility for the content of published papers.

JAFa IS A JOURNAL OF RAPID PUBLICATION

Journal of Applied Functional Analysis

Editorial Board

Associate Editors

Editor in-Chief:

George A. Anastassiou
Department of Mathematical Sciences
The University of Memphis
Memphis, TN 38152, USA
901-678-3144 office
901-678-2482 secretary
901-751-3553 home
901-678-2480 Fax
ganastss@memphis.edu
Approximation
Theory, Inequalities, Probability,
Wavelet, Neural Networks, Fractional Calculus

Associate Editors:

1) Francesco Altomare
Dipartimento di Matematica
Universita' di Bari
Via E. Orabona, 4
70125 Bari, ITALY
Tel+39-080-5442690 office
+39-080-3944046 home
+39-080-5963612 Fax
altomare@dm.uniba.it
Approximation Theory, Functional Analysis,
Semigroups and Partial Differential
Equations,
Positive Operators.

2) Angelo Alvino
Dipartimento di Matematica e Applicazioni
"R. Caccioppoli" Complesso
Universitario Monte S. Angelo
Via Cintia
80126 Napoli, ITALY
+39(0)81 675680
angelo.alvino@unina.it,
angelo.alvino@dma.unina.it
Rearrangements, Partial Differential
Equations.

3) Catalin Badea
UFR Mathematiques, Bat. M2,
Universite de Lille1
Cite Scientifique
F-59655 Villeneuve d'Ascq, France

23) Nikolaos B. Karayiannis
Department of Electrical and
Computer Engineering
N308 Engineering Building 1
University of Houston
Houston, Texas 77204-4005
USA
Tel (713) 743-4436
Fax (713) 743-4444
Karayiannis@UH.EDU
Karayiannis@mail.gr
Neural Network Models, Learning
Neuro-Fuzzy Systems.

24) Theodore Kilgore
Department of Mathematics
Auburn University
221 Parker Hall,
Auburn University
Alabama 36849, USA
Tel (334) 844-4620
Fax (334) 844-6555
Kilgota@auburn.edu
Real Analysis, Approximation Theory,
Computational Algorithms.

25) Jong Kyu Kim
Department of Mathematics
Kyungnam University
Masan Kyungnam, 631-701, Korea
Tel 82-(55)-249-2211
Fax 82-(55)-243-8609
jongkyuk@kyungnam.ac.kr
Nonlinear Functional Analysis, Variational
Inequalities, Nonlinear Ergodic Theory,
ODE, PDE, Functional Equations.

26) Miroslav Krbeč
Mathematical Institute
Academy of Sciences of Czech Republic
Žitná 25
CZ-115 67 Praha 1
Czech Republic
Tel +420 222 090 743
Fax +420 222 211 638
krbecm@matsrv.math.cas.cz
Function spaces, Real Analysis, Harmonic

Tel. (+33)(0)3.20.43.42.18
Fax (+33)(0)3.20.43.43.02
Catalin.Badea@math.univ-lille1.fr
Approximation Theory, Functional
Analysis, Operator Theory.

4) Erik J. Balder
Mathematical Institute
Universiteit Utrecht
P.O.Box 80 010
3508 TA UTRECHT
The Netherlands
Tel. +31 30 2531458
Fax +31 30 2518394
balder@math.uu.nl
Control Theory, Optimization,
Convex Analysis, Measure Theory,
Applications to Mathematical
Economics and Decision Theory.

5) Carlo Bardaro
Dipartimento di Matematica e Informatica
Universita di Perugia
Via Vanvitelli 1
06123 Perugia, ITALY
TEL +390755853822
+390755855034
FAX +390755855024
E-mail bardaro@unipg.it
Web site: <http://www.unipg.it/~bardaro/>
Functional Analysis and Approximation
Theory,
Signal Analysis, Measure Theory, Real
Analysis.

6) Heinrich Begehr
Freie Universitaet Berlin
I. Mathematisches Institut, FU Berlin,
Arnimallee 3, D 14195 Berlin
Germany,
Tel. +49-30-83875436, office
+49-30-83875374, Secretary
Fax +49-30-83875403
begehr@math.fu-berlin.de
Complex and Functional Analytic
Methods in PDEs, Complex Analysis,
History of Mathematics.

7) Fernando Bombal
Departamento de Analisis Matematico
Universidad Complutense
Plaza de Ciencias, 3
28040 Madrid, SPAIN
Tel. +34 91 394 5020
Fax +34 91 394 4726
fernando_bombal@mat.ucm.es

Analysis, Interpolation and
Extrapolation Theory, Fourier Analysis.

27) V. Lakshmikantham
Department of Mathematical Sciences
Florida Institute of Technology
Melbourne, FL 32901
e-mail: lakshmik@fit.edu
Ordinary and Partial Differential Equations,
Hybrid Systems, Nonlinear Analysis

28) Peter M. Maass
Center for Industrial Mathematics
Universitaet Bremen
Bibliotheksstr. 1,
MZH 2250,
28359 Bremen
Germany
Tel +49 421 218 9497
Fax +49 421 218 9562
pmaass@math.uni-bremen.de
Inverse problems, Wavelet Analysis and
Operator Equations, Signal and Image
Processing.

29) Julian Musielak
Faculty of Mathematics and Computer Science
Adam Mickiewicz University
Ul. Umultowska 87
61-614 Poznan
Poland
Tel (48-61) 829 54 71
Fax (48-61) 829 53 15
Grzegorz.Musielak@put.poznan.pl
Functional Analysis, Function Spaces,
Approximation Theory, Nonlinear Operators.

30) Vassilis Papanicolaou
Department of Mathematics
National Technical University of Athens
Zografou campus, 157 80
Athens, Greece
tel.: +30(210) 772 1722
Fax +30(210) 772 1775
papanico@math.ntua.gr
Partial Differential Equations,
Probability.

31) Pier Luigi Papini
Dipartimento di Matematica
Piazza di Porta S. Donato 5
40126 Bologna
ITALY
Fax +39(0)51 582528
papini@dm.unibo.it
Functional Analysis, Banach spaces,

Operators on Banach spaces,
Tensor products of Banach spaces,
Polymeasures, Function spaces.

8) Michele Campiti
Department of Mathematics "E.De Giorgi"
University of Lecce
P.O. Box 193
Lecce, ITALY
Tel. +39 0832 297 432
Fax +39 0832 297 594
michele.campiti@unile.it
Approximation Theory,
Semigroup Theory, Evolution problems,
Differential Operators.

9) Domenico Candeloro
Dipartimento di Matematica e Informatica
Universita degli Studi di Perugia
Via Vanvitelli 1
06123 Perugia
ITALY
Tel +39(0)75 5855038
+39(0)75 5853822,
+39(0)744 492936
Fax +39(0)75 5855024
candelor@dipmat.unipg.it
Functional Analysis, Function spaces,
Measure and Integration Theory in
Riesz spaces.

10) Pietro Cerone
School of Computer Science and
Mathematics, Faculty of Science,
Engineering and Technology,
Victoria University
P.O.14428,MCMC
Melbourne,VIC 8001,AUSTRALIA
Tel +613 9688 4689
Fax +613 9688 4050
Pietro.cerone@vu.edu.au
Approximations, Inequalities,
Measure/Information Theory,
Numerical Analysis, Special Functions.

11) Michael Maurice Dodson
Department of Mathematics
University of York,
York YO10 5DD, UK
Tel +44 1904 433098
Fax +44 1904 433071
Mmd1@york.ac.uk
Harmonic Analysis and Applications to
Signal Theory, Number Theory and
Dynamical Systems.

Approximation Theory.

32) Svetlozar T. Rachev
Chair of Econometrics, Statistics
and Mathematical Finance
School of Economics and
Business Engineering
University of Karlsruhe
Kollegium am Schloss, Bau II, 20.12, R210
Postfach 6980, D-76128,
Karlsruhe, GERMANY.
Tel +49-721-608-7535,
+49-721-608-2042(s)
Fax +49-721-608-3811
Zari.Rachev@wiwi.uni-karlsruhe.de
Second Affiliation:
Dept. of Statistics and Applied Probability
University of California at Santa Barbara
rachev@pstat.ucsb.edu
Probability, Stochastic Processes and
Statistics, Financial Mathematics,
Mathematical Economics.

33) Paolo Emilio Ricci
Department of Mathematics
Rome University "La Sapienza"
P.le A.Moro, 2-00185
Rome, ITALY
Tel ++3906-49913201 office
++3906-87136448 home
Fax ++3906-44701007
Paoloemilio.Ricci@uniroma1.it
riccip@uniroma1.it
Special Functions, Integral and Discrete
Transforms, Symbolic and Umbral Calculus,
ODE, PDE, Asymptotics, Quadrature,
Matrix Analysis.

34) Silvia Romanelli
Dipartimento di Matematica
Universita' di Bari
Via E.Orabona 4
70125 Bari, ITALY.
Tel (INT 0039)-080-544-2668 office
080-524-4476 home
340-6644186 mobile
Fax -080-596-3612 Dept.
romans@dm.uniba.it
PDEs and Applications to Biology and
Finance, Semigroups of Operators.

35) Boris Shekhtman
Department of Mathematics
University of South Florida
Tampa, FL 33620, USA
Tel 813-974-9710

12) Sever S.Dragomir
School of Computer Science and
Mathematics, Victoria University,
PO Box 14428,
Melbourne City,
MC 8001,AUSTRALIA
Tel. +61 3 9688 4437
Fax +61 3 9688 4050
sever@csm.vu.edu.au
Inequalities,Functional Analysis,
Numerical Analysis, Approximations,
Information Theory, Stochastics.

13) Paulo J.S.G.Ferreira
Department of Electronica e
Telecomunicacoes/IEETA
Universidade de Aveiro
3810-193 Aveiro
PORTUGAL
Tel +351-234-370-503
Fax +351-234-370-545
pjf@ieeta.pt
Sampling and Signal Theory,
Approximations, Applied Fourier Analysis,
Wavelet, Matrix Theory.

14) Gisele Ruiz Goldstein
Department of Mathematical Sciences
The University of Memphis
Memphis,TN 38152,USA.
Tel 901-678-2513
Fax 901-678-2480
ggoldste@memphis.edu
PDEs, Mathematical Physics,
Mathematical Geophysics.

15) Jerome A.Goldstein
Department of Mathematical Sciences
The University of Memphis
Memphis,TN 38152,USA
Tel 901-678-2484
Fax 901-678-2480
jgoldste@memphis.edu
PDEs,Semigroups of Operators,
Fluid Dynamics,Quantum Theory.

16) Heiner Gonska
Institute of Mathematics
University of Duisburg-Essen
Lotharstrasse 65
D-47048 Duisburg
Germany
Tel +49 203 379 3542
Fax +49 203 379 1845
gonska@math.uni-duisburg.de
Approximation and Interpolation Theory,

boris@math.usf.edu
Approximation Theory, Banach spaces,
Classical Analysis.

36) Panayiotis Siafarikas
Department of Mathematics
University of Patras
26500 Patras
Greece
Tel/Fax +302 610 997169
panos@math.upatras.gr
ODE,Difference Equations, Special
Functions, Orthogonal Polynomials,
Applied Functional Analysis.

37) Rudolf Stens
Lehrstuhl A fur Mathematik
RWTH Aachen
52056 Aachen
Germany
Tel ++49 241 8094532
Fax ++49 241 8092212
stens@mathA.rwth-aachen.de
Approximation Theory, Fourier Analysis,
Harmonic Analysis, Sampling Theory.

38) Juan J.Trujillo
University of La Laguna
Departamento de Analisis Matematico
C/Astr.Fco.Sanchez s/n
38271.LaLaguna.Tenerife.
SPAIN
Tel/Fax 34-922-318209
Juan.Trujillo@ull.es
Fractional: Differential Equations-
Operators-
Fourier Transforms, Special functions,
Approximations,and Applications.

39) Tamaz Vashakmadze
I.Vekua Institute of Applied Mathematics
Tbilisi State University,
2 University St. , 380043,Tbilisi, 43,
GEORGIA.
Tel (+99532) 30 30 40 office
(+99532) 30 47 84 office
(+99532) 23 09 18 home
Vasha@viam.hepi.edu.ge
tamazvashakmadze@yahoo.com
Applied Functional Analysis, Numerical
Analysis, Splines, Solid Mechanics.

40) Ram Verma
International Publications
5066 Jamieson Drive, Suite B-9,
Toledo, Ohio 43613,USA.

Computer Aided Geometric Design,
Algorithms.

17) Karlheinz Groechenig
Institute of Biomathematics and Biometry,
GSF-National Research Center
for Environment and Health
Ingolstaedter Landstrasse 1
D-85764 Neuherberg, Germany.
Tel 49-(0)-89-3187-2333
Fax 49-(0)-89-3187-3369
Karlheinz.groechenig@gsf.de
Time-Frequency Analysis, Sampling Theory,
Banach spaces and Applications,
Frame Theory.

18) Vijay Gupta
School of Applied Sciences
Netaji Subhas Institute of Technology
Sector 3 Dwarka
New Delhi 110075, India
e-mail: vijay@nsit.ac.in;
vijaygupta2001@hotmail.com
Approximation Theory

19) Weimin Han
Department of Mathematics
University of Iowa
Iowa City, IA 52242-1419
319-335-0770
e-mail: whan@math.uiowa.edu
Numerical analysis, Finite element method,
Numerical PDE, Variational inequalities,
Computational mechanics

20) Tian-Xiao He
Department of Mathematics and
Computer Science
P.O.Box 2900, Illinois Wesleyan University
Bloomington, IL 61702-2900, USA
Tel (309)556-3089
Fax (309)556-3864
the@iwu.edu
Approximations, Wavelet, Integration Theory,
Numerical Analysis, Analytic Combinatorics.

21) Don Hong
Department of Mathematical Sciences
Middle Tennessee State University
1301 East Main St.
Room 0269, Bldg KOM
Murfreesboro, TN 37132-0001
Tel (615) 904-8339
dhong@mtsu.edu
Approximation Theory, Splines, Wavelet,
Stochastics, Mathematical Biology Theory.

Verma99@msn.com
rverma@internationalpubls.com
Applied Nonlinear Analysis, Numerical
Analysis, Variational Inequalities,
Optimization Theory, Computational
Mathematics, Operator Theory.

41) Gianluca Vinti
Dipartimento di Matematica e Informatica
Universita di Perugia
Via Vanvitelli 1
06123 Perugia
ITALY
Tel +39(0) 75 585 3822,
+39(0) 75 585 5032
Fax +39 (0) 75 585 3822
mategian@unipg.it
Integral Operators, Function Spaces,
Approximation Theory, Signal Analysis.

42) Ursula Westphal
Institut fuer Mathematik B
Universitaet Hannover
Welfengarten 1
30167 Hannover, GERMANY
Tel (+49) 511 762 3225
Fax (+49) 511 762 3518
westphal@math.uni-hannover.de
Semigroups and Groups of Operators,
Functional Calculus, Fractional Calculus,
Abstract and Classical Approximation
Theory, Interpolation of Normed spaces.

43) Ronald R. Yager
Machine Intelligence Institute
Iona College
New Rochelle, NY 10801, USA
Tel (212) 249-2047
Fax (212) 249-1689
Yager@Panix.Com
ryager@iona.edu
Fuzzy Mathematics, Neural Networks,
Reasoning,
Artificial Intelligence, Computer Science.

44) Richard A. Zalik
Department of Mathematics
Auburn University
Auburn University, AL 36849-5310
USA.
Tel 334-844-6557 office
678-642-8703 home
Fax 334-844-6555
zalik@auburn.edu
Approximation Theory, Chebychev Systems,
Wavelet Theory.

22) Hubertus Th. Jongen
Department of Mathematics
RWTH Aachen
Templergraben 55
52056 Aachen
Germany
Tel +49 241 8094540
Fax +49 241 8092390
jongen@rwth-aachen.de
Parametric Optimization, Nonconvex
Optimization, Global Optimization.

Preface

These three special issues, which constitute the proceedings of the symposium CCS2008 – Second International Interdisciplinary Chaos Symposium on “CHAOS and COMPLEX SYSTEMS”, have tried to create a forum for the exchange of information and experience in the exciting interdisciplinary field of Chaos. However the conference was more in the Applied Mathematics direction centered.

The expectation of the organizers concerning international resonance of the conference has been fulfilled: 150 scientists from 15 different countries (China, France, Greece, Iran, Japan, Kazakhstan, Lebanon, Lithuania, Malaysia, Mexico, Pakistan, Romania, Russia, Turkey, and Uzbekistan) have participated. Good relations to research institutes of these countries might be of great importance for science and applications.

On behalf of the Organizing Committee we would like to express our thanks to the Scientific Committee, the Program Committee and to all who have contributed to this conference for their support and advice. We are also grateful to the invited lecturers Prof. George A. Anastassiou, Prof. Amir Atiya, Prof. Mohamed Saladin El Naschie, Prof. Ramazan Gencay, Prof. Ji-Huan He, Prof. Robert Kozma, Prof. V. Lakshmikantham, and Prof. Paul Refenes.

Special thanks are due to Rector Prof. Tamer Kocel, Vice Rector Prof. Cetin Bolcal and Dean Prof. Dursun Kocer for their support, advice and encouragement.

Our thanks are also due to the Istanbul Kultur University, which was hosting this symposium and provided all of its facilities.

We are grateful to the Editor-in-Chief, Prof. George A. Anastassiou for accepting this volume for publication in Journal of Applied Functional Analysis.

Hikmet Caglar

On behalf of the Organizing Committee

Istanbul Kultur University, Department of Mathematics-Computer, Istanbul, Turkey

Tel.: +90-212-4984367; Fax: +90-212-4658310; E-mail: s.caglar@iku.edu.tr

Mehmet Ozer

On behalf of the Organizing Committee

Istanbul Kultur University, Department of Physics, Istanbul, Turkey

Tel.: +90-212-4984317; Fax: +90-212-4658310; E-mail: m.ozel@iku.edu.tr

A Visual Basic software for computing of the one-dimensional heat equation by using B-spline solution

Hikmet Caglar^{a,*}, Levent Cuhaci^a, Nazan Caglar^b, Mehmet Ozer^c

^a *Istanbul Kultur University, Department of Mathematics-Computer, Atakoy Campus, Bakirkoy, 34156 Istanbul, Turkey*

^b *Istanbul Kultur University, Department of Business Administration, Atakoy Campus, Bakirkoy, 34156 Istanbul, Turkey*

^c *Istanbul Kultur University, Department of Physics, Atakoy Campus, Bakirkoy, 34156 Istanbul, Turkey*

*** Corresponding author:**

Tel.: +90 212 4984367 **Fax:** +90 212 4658310 **e-mail:** s.caglar@iku.edu.tr

Abstract

Microsoft Visual Basic[®] has been used for developing a software for the one-dimensional heat equation. We have solved the equation by means of a computer and developed user-friendly software with a graphical user interface. The numerical solution of the equation is visually illustrated. The software does not require familiarity with any new environment and is highly flexible; it can also easily be adapted to other experimental methods.

Keywords: One-dimensional heat equation, B-spline method, Visual Basic software

1. Introduction

Boundary value problems are an important part of computational and mathematical physics. It is usually not so difficult to find a solution of a given differential equation, but the calculation of the solution for a given boundary conditions is not always easy. There are a variety of science and engineering problems that might be modeled by the boundary value problems [1]. One of them is the one-dimensional heat equation. It is a second order linear partial differential equation (PDE) [2-5]. In this equation, the flow of heat in one-dimension (such as in a wire) is insulated everywhere except at the two ends. Solutions of this equation are functions of the position along the rod (x) and time (t).

We consider the one-dimensional heat equation given in [6,7]

$$\frac{\partial u}{\partial t} = \alpha \frac{\partial^2 u}{\partial x^2}, \quad 0 < x < 1, \quad 0 < t \leq T \quad (1)$$

with the initial condition

$$u(x, 0) = f(x) = \sin(\pi x), \quad 0 \leq x \leq 1, \quad (2)$$

and the following boundary conditions

$$u(0, t) = g_0(t), \quad (3)$$

$$u(1, t) = g_1(t). \quad (4)$$

In our previous work, we have examined the similar problem using a family of B-spline methods [7]. Although B-spline curves and surfaces are capable of representing complex curves with a single mathematical formulation, these methods are high level computing tools which require the user to have expert knowledge. So, we have focused on the similar equations and developed user-friendly, easy-to use software by using

Microsoft Visual Basic. Because of their object-oriented feature and the usualness of most of the users with Microsoft Operating Systems, Visual Basic programs are useful.

In this work, we have showed that the developed software is highly flexible and can easily be adapted to other experimental methods.

2. The third-degree B-splines

The third-degree B-splines are used to construct the numerical solutions of the one-dimensional heat equation. A detailed description of B-spline functions generated by subdivision also can be found in [8].

Consider equally-spaced knots of a partition $\pi : a = x_0 < x_1 < \dots < x_n = b$ on $[a, b]$. Let $S_3[\pi]$ be the space of continuously-differentiable, piecewise, third-degree polynomials on π . That is, $S_3[\pi]$ is the space of third-degree splines on π . Consider the B-splines basis in $S_3[\pi]$. The third-degree B-splines are defined as

$$B_{3,i}(x) = \frac{1}{6h^3} \begin{cases} (x - x_i)^3 & \text{where } x \in [x_i, x_{i+1}] \\ h^3 + 3h^2(x - x_{i+1}) + 3h(x - x_{i+1})^2 - 3(x - x_{i+1})^3 & \text{where } x \in [x_{i+1}, x_{i+2}] \\ h^3 + 3h^2(x_{i+3} - x) + 3h(x_{i+3} - x)^2 - 3(x_{i+3} - x)^3 & \text{where } x \in [x_{i+2}, x_{i+3}] \\ (x_{i+4} - x)^3 & \text{where } x \in [x_{i+3}, x_{i+4}] \end{cases} \quad (5)$$

$$B_i(x) = B_0(x - ih), i = -3, -2, -1, \dots$$

To solve the one-dimensional heat problem, B_i , B'_i and B''_i evaluated at the nodal points are needed. Their coefficients are tabulated in Table 1.

Table 1: Values of B_i , B'_i and B''_i .

	x_i	x_{i+1}	x_{i+2}	x_{i+3}	x_{i+4}
B_i	0	1	4	1	0
B'_i	0	3/h	0/h	-3/h	0
B''_i	0	6/h ²	-12/h ²	6/h ²	0

3. B-spline solutions for heat equation

The third-degree B-splines, which are given in previous section, are applied for the solution of the one-dimensional heat equation and the evaluation is based on the collocation approach [9].

Let $S(x)$ to be an approximate solution of equations (1-4) as given

$$S(x) = \sum_{i=1}^{n+2} C_i B_{3,i}(x) \quad (6)$$

where C_i are unknown real coefficients and $B_{3,i}(x)$ are third-degree B-spline functions.

Here x_0, x_1, \dots, x_n are $n+1$ grid points in the interval $[a, b]$ and given as

$$x_i = a + ih, \quad i = 0, 1, \dots, n; \quad x_0 = a, \quad x_n = b, \quad h = (b - a)/n.$$

Difference schemes for the problem are written as following:

$$\frac{u_{i+1} - u_i}{\Delta t} = \alpha \frac{\partial^2 u}{\partial x^2} \quad (7)$$

where $\Delta t = k$. So equation (7) can be re-written as

$$-k \alpha u_{i+1}'' + u_{i+1} = u_i \quad (8)$$

and the initial condition given in equation (2) is now

$$u(x, 0) = f(x) = \sin(\pi x) = u_0. \quad (9)$$

Substituting (9) in (8) yields the followings

$$-k \alpha u_1'' + u_1 = u_0 \quad \rightarrow \quad t = k \quad (10)$$

$$-k \alpha u_2'' + u_2 = u_1 \quad \rightarrow \quad t = 2k \quad (11)$$

$$\vdots \quad \quad \quad \vdots$$

$$-k \alpha u_n'' + u_n = u_{n-1} \quad \rightarrow \quad t = nk \quad (12)$$

The approximate solution of the equations (10)-(12) can be found using B-spline functions $S(x)$:

$$-k \alpha S_1'' + S_1 = u_0 \quad \rightarrow \quad t = k \quad (13)$$

$$-k \alpha S_2'' + S_2 = u_1 \quad \rightarrow \quad t = 2k \quad (14)$$

$$\vdots \quad \quad \quad \vdots$$

$$-k \alpha S_n'' + S_n = u_{n-1} \quad \rightarrow \quad t = nk \quad (15)$$

and the boundary conditions given in equations (3)-(4) are now

$$\sum_{i=-3}^{n-1} C_i B_{3,i}(0) = g_0(t) \quad \text{for} \quad x = 0 \quad (16)$$

$$\sum_{i=-3}^{n-1} C_i B_{3,i}(1) = g_1(t) \quad \text{for} \quad x = 1. \quad (17)$$

The spline solution of equation (13) with the given boundary conditions is obtained by solving to the following matrix equation. The values of spline functions at the knots $\{x_i\}_{i=0}^n$ are determined using Table 1. Then we can write in matrix-vector form as

follows

$$AC = F \quad (18)$$

where

$$C = [C_{-3}, C_{-2}, C_{-1}, \dots, C_{n-3}, C_{n-2}, C_{n-1}]^T \quad (19)$$

and

$$F = [0, f(0), f(h), f(2h), \dots, f((n-1)h), 0]^T \quad (20)$$

Here T denotes transpose.

The matrix A can be written as

$$A = \begin{bmatrix} 1/6 & 4/6 & 1/6 & 0 & 0 & \dots & 0 \\ \varphi_1 & \varphi_2 & \varphi_3 & 0 & 0 & \dots & 0 \\ 0 & \varphi_1 & \varphi_2 & \varphi_3 & 0 & \dots & 0 \\ \vdots & \vdots & \vdots & \vdots & \vdots & \ddots & \vdots \\ 0 & 0 & \dots & \varphi_1 & \varphi_2 & \varphi_3 & 0 \\ 0 & 0 & \dots & 0 & \varphi_1 & \varphi_2 & \varphi_3 \\ 0 & 0 & \dots & 0 & 1/6 & 4/6 & 1/6 \end{bmatrix} \quad (21)$$

where

$$\varphi_1 = -\frac{k\alpha}{h^2} + \frac{1}{6} \quad (22)$$

$$\varphi_2 = \frac{2k\alpha}{h^2} + \frac{4}{6} \quad (23)$$

$$\varphi_3 = -\frac{k\alpha}{h^2} + \frac{1}{6} \quad (24)$$

The same approximation is applied to the other equations (14)-(15).

4. Modeling of the Software

Microsoft's Visual Basic platform is chosen as developing environment for its simplicity and familiar user interface. The flowchart of the developed software is given in Figure 1. It has two main parts namely the initial calculations and the main loop. After the initial calculations, the intermediate results are calculated in the main loop. The loop exits when the final step is reached.

The configuration of form is shown in Fig. 2, which is the main window for data input and output. The general data sheet and the graphic appears on running the software. Among the form controls, there are 4 text boxes for data entry, 6 command buttons for various operations and 4 labels for inspecting step size and parameters given in Eqs. (22)-(24).

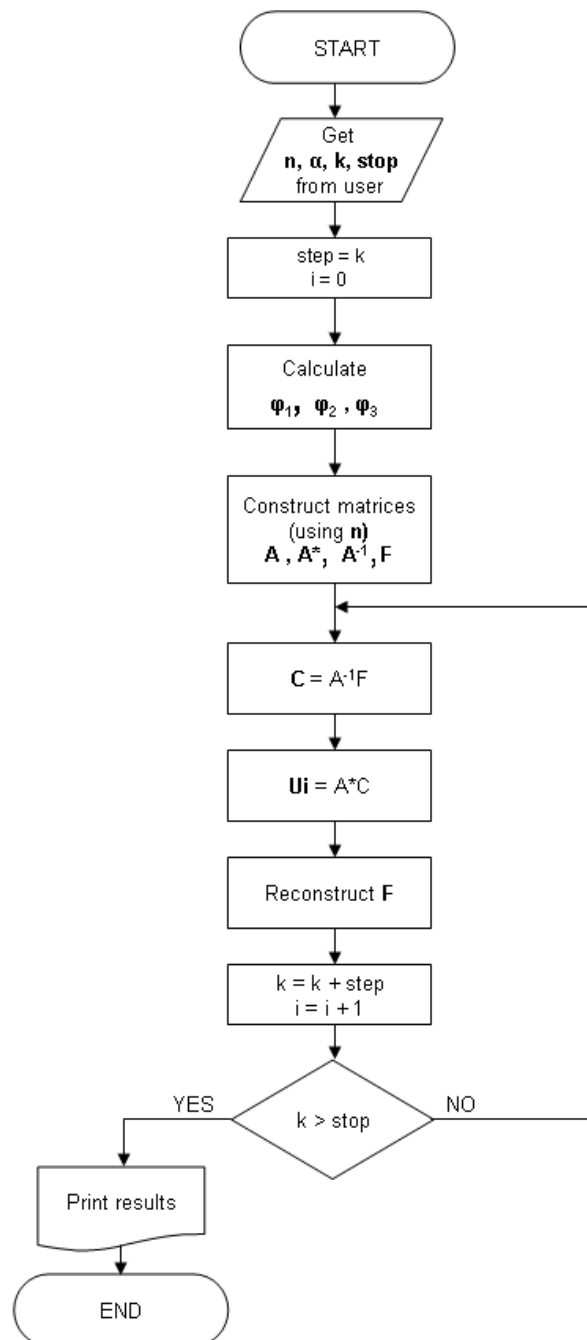


Fig. 1 The flowchart

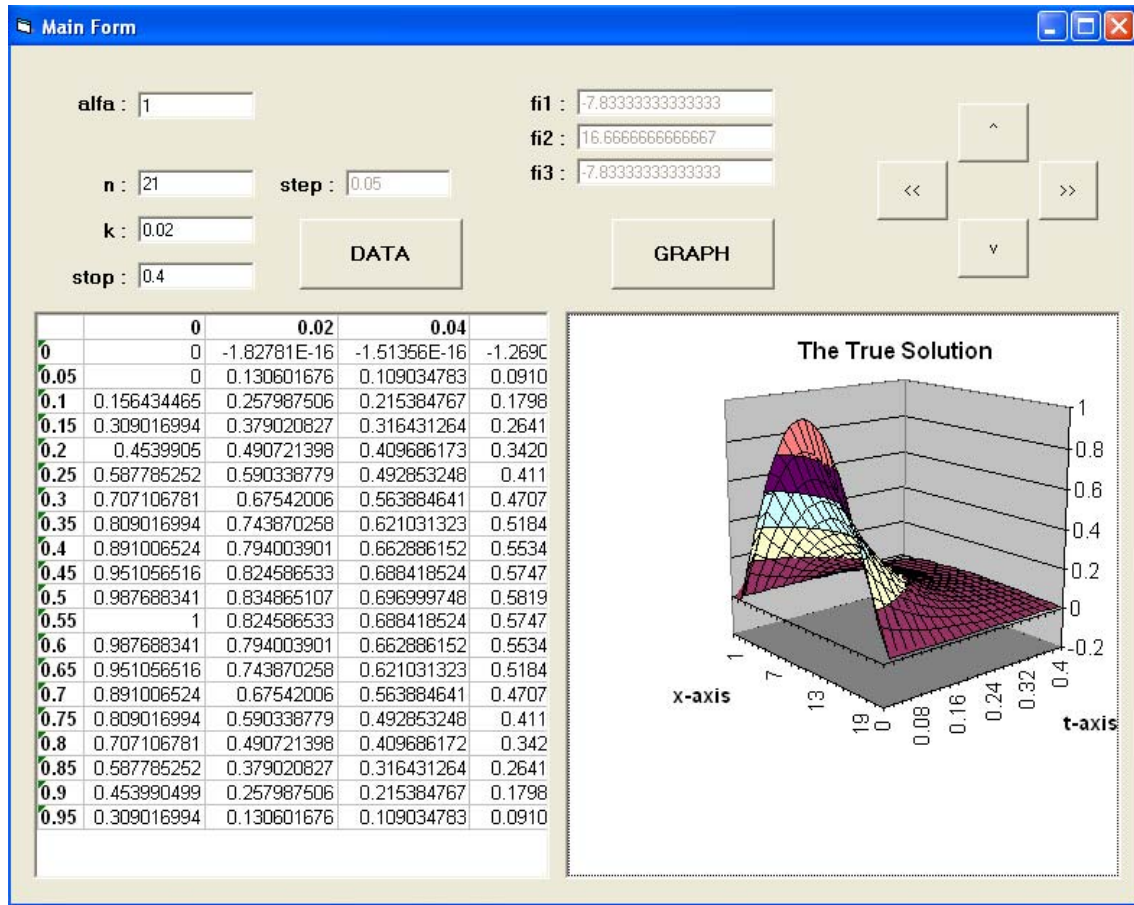


Fig. 2 The main window for data input and output.

All necessary parameters can be given by the user using the text box controls in the form. Since Microsoft Excel is very suitable for representing these kind of numeric data, the software uses two embedded Excel objects in the form: a spreadsheet and a chart. After entering the key parameters to the system, the final matrix is shown on the spreadsheet at the bottom left side of the window by pressing the 'Data' button. All data can be seen by double clicking on the spreadsheet part of the main window. A visual representation of these data can be obtained by pressing the 'Graph' button and the

result graph is shown at the bottom right side of the form. The graph can be rotated with four command buttons above it.

The complete source code of the program is given in Appendix A.

5. Conclusion

In this work, a simulation software in Visual Basic has been developed for solving the one-dimensional heat equation by using B-spline solution. The software is based on dynamic mathematical model of it. The complexity of the equation is simplified by using this program. The numerical solution of the equation is visually illustrated. The software does not require familiarity with any new environment and is highly flexible; it can also easily be adapted to other experimental methods.

Appendix A. Source code

```

Dim oXL As Object      ' Excel application

Dim oBook As Excel.Workbook      ' Excel workbook

Dim oBook2 As Excel.Workbook      ' Excel workbook

Dim oSheet1 As Excel.Worksheet      ' Excel Worksheet

Dim oSheet2 As Excel.Worksheet

Dim oChart As Excel.Chart      ' Excel Chart

Dim n, counter As Integer


Private Sub Command1_Click()

Dim h, k, k2, step, alfa, st, start As Double

Dim fi1, fi2, fi3, pi As Double

Dim i, j, ind, nu As Integer

pi = 3.141592654

n = Val(nField.Text)

k = Val(kField.Text)

start = 0

alfa = Val(alfaField.Text)

st = Val(stopField.Text)

nu = st / k

st = st + 0.0001

If n > 1 And n < 51 Then

    h = 1 / (n - 1)

Else

```

```
MsgBox ("n must be between (2-50)")

Exit Sub

End If

step = k

output.Text = h

Dim A() As Double

Dim invA() As Double

Dim starA() As Double

Dim F() As Double

Dim C() As Double

Dim U() As Double

Dim S() As Double

Dim Header1() As Double

Dim Header2() As String

ReDim A(n + 2, n + 2) As Double

ReDim invA(n + 2, n + 2) As Double

ReDim starA(n, n + 2) As Double

ReDim C(n + 2, 0) As Double

ReDim F(n + 2, 0) As Double

ReDim U(n, 0) As Double

ReDim S(n, nu) As Double

ReDim Header1(nu) As Double

ReDim Header2(n, 0) As String

'Start Excel and create a new workbook
```

```
Set oXL = CreateObject("Excel.application")
```

```
oSheet1.Cells.Clear
```

```
oSheet2.Cells.Clear
```

```
oChart.ChartArea.ClearContents
```

$$fi1 = (((-k) * \alpha) / (h * h)) + 1 / 6$$

$$fi2 = ((k * \alpha * 2) / (h * h)) + 4 / 6$$

$$fi3 = (((-k) * \alpha) / (h * h)) + 1 / 6$$

```
fi1Field.Text = fi1
```

```
fi2Field.Text = fi2
```

```
fi3Field.Text = fi3
```

$$A(0, 0) = 1 / 6$$

$$A(0, 1) = 4 / 6$$

$$A(0, 2) = 1 / 6$$

$$A(n + 1, n - 1) = 1 / 6$$

$$A(n + 1, n) = 4 / 6$$

$$A(n + 1, n + 1) = 1 / 6$$

$$\text{star}A(n - 1, n - 1) = 1 / 6$$

$$\text{star}A(n - 1, n) = 4 / 6$$

$$\text{star}A(n - 1, n + 1) = 1 / 6$$

```
For i = 1 To n
```

$$A(i, i - 1) = fi1$$

$$A(i, i) = fi2$$

$$A(i, i + 1) = fi3$$

```
Next i
```

```

For i = 0 To n

    starA(i, i) = 1 / 6

    starA(i, i + 1) = 4 / 6

    starA(i, i + 2) = 1 / 6

Next i

oSheet2.Range("A1").Resize(n + 2, n + 2).Value = A

oSheet2.Range("A500").Resize(n + 2, n + 2).Value =

oXL.WorksheetFunction.MInverse(oSheet2.Range("A1").Resize(n + 2, n + 2))

' Constructing invA

For i = 0 To n + 1

    For j = 0 To n + 1

        invA(i, j) = oSheet2.Cells(i + 500, j + 1).Value

    Next j

Next i

k2 = 0

F(0, 0) = 0

F(n + 1, 0) = 0

' Constructing F

For i = 1 To n

    F(i, 0) = Sin((pi) * k2)

    S(i, 0) = F(i, 0)

    k2 = k2 + h

Next i

counter = 1

```

Do

For i = 0 To n + 1

$C(i, 0) = 0\#$

Next i

For i = 0 To n - 1

$U(i, 0) = 0\#$

Next i

'Constructing C

For i = 0 To n + 1

For j = 0 To n + 1

$C(i, 0) = C(i, 0) + (\text{invA}(i, j) * F(j, 0))$

Next j

Next i

'Constructing U

For i = 0 To n - 1

For j = 0 To n + 1

$U(i, 0) = U(i, 0) + (\text{starA}(i, j) * C(j, 0))$

Next j

Next i

For i = 0 To n - 1

$F(i + 1, 0) = U(i, 0)$

$S(i, \text{counter}) = U(i, 0)$

Next i

counter = counter + 1

```
k = k + step  
Loop While k <= st  
ind = 0  
For i = start To st Step step  
    Header1(ind) = i  
    ind = ind + 1  
Next i  
For i = 0 To n  
    Header2(i, 0) = i * h  
Next i  
With oSheet1.Range("B1").Resize(1, counter)  
    .Value = Header1  
    .Font.Bold = True  
End With  
With oSheet1.Range("A2").Resize(n, 1)  
    .Value = Header2  
    .Font.Bold = True  
End With  
oSheet1.Range("B2").Resize(n, counter).Value = S  
With oSheet1.Range("A1").Resize(n, n)  
    .EntireColumn.AutoFit  
End With  
oSheet1.Range("A19:C30").Show  
Command2.Enabled = True
```

End Sub

Private Sub Command2_Click()

Dim d As Double

oChart.Activate

oChart.SetSourceData oSheet1.Range("B2").Resize(n, counter), xlColumns

oChart.ChartType = xlSurface

oChart.HasLegend = False

oChart.HasTitle = True

oChart.ChartTitle.Text = "The True Solution"

oChart.Rotation = 60

oChart.PlotArea.Top = 50

oChart.PlotArea.Left = 50

oChart.PlotArea.Height = 600

oChart.PlotArea.Width = 600

oChart.Axes(xlCategory).HasMajorGridlines = False

oChart.Axes(xlSeries).HasTitle = True

oChart.Axes(xlSeries).AxisTitle.Text = "t-axis"

oChart.Axes(xlSeries).AxisTitle.Font.FontStyle = "Bold"

oChart.Axes(xlSeries).AxisTitle.Font.Size = 10

oChart.Axes(xlCategory).HasTitle = True

oChart.Axes(xlCategory).AxisTitle.Text = "x-axis"

oChart.Axes(xlCategory).AxisTitle.Font.FontStyle = "Bold"

oChart.Axes(xlCategory).AxisTitle.Font.Size = 10


```
For x = 1 To oChart.SeriesCollection.Count
```

```
    With oChart.SeriesCollection(x)
```

```
        d = (x - 1) * Val(kField.Text)
```

```
        .Name = Str$(d)
```

```
    End With
```

```
Next x
```

```
End Sub
```

```
Private Sub Command3_Click()
```

```
    oChart.Rotation = (oChart.Rotation + 5) Mod 360
```

```
End Sub
```

```
Private Sub Command4_Click()
```

```
    ang = oChart.Rotation - 5
```

```
    If (ang < 0) Then ang = ang + 360
```

```
    oChart.Rotation = ang
```

```
End Sub
```

```
Private Sub Command5_Click()
```

```
    elv = oChart.Elevation + 5
```

```
    If (elv > 90) Then Exit Sub
```

```
    oChart.Elevation = elv
```

```
End Sub
```

```
Private Sub Command6_Click()
```

```
elv = oChart.Elevation - 5
```

```
If (elv < -90) Then Exit Sub
```

```
oChart.Elevation = elv
```

```
End Sub
```

```
Private Sub Form_Load()
```

```
OLE1.CreateEmbed "", "excel.sheet.8"
```

```
OLE2.CreateEmbed "", "excel.chart"
```

```
Set oBook = OLE1.object
```

```
Set oBook2 = OLE2.object
```

```
Set oSheet1 = oBook.Worksheets(1)
```

```
Set oSheet2 = oBook.Worksheets.Add
```

```
Set oChart = oBook2.Charts(1)
```

```
oChart.ChartArea.ClearContents
```

```
oSheet1.Activate
```

```
End Sub
```

```
Private Sub Form_Terminate()
```

```
Set oXL = Nothing
```

```
Set oBook = Nothing
```

```
Set oBook2 = Nothing
```

```
Set oSheet1 = Nothing
```

```
Set oSheet2 = Nothing
```

```
Set oChart = Nothing
```

```
End Sub
```

References

- [1] Rektorys K., Solving Ordinary and Partial Boundary Value Problems in Science and Engineering, CRC Series in Computational Mechanics and Applied Analysis, 1998.
- [2] Carslaw HS, Jaeger JC. Conduction of heat in solids. Oxford: Oxford University Press, 1959.
- [3] Widder DV. The heat equation. London: Academic Press, 1975.
- [4] Cannon JR. The one-dimensional heat equation. Cambridge: Cambridge University Press, 1984.
- [5] Twizell EH. Computational methods for partial differential equations. Chichester, New York: Ellis Horwood and John Wiley and Sons, 1984.
- [6] Dehghan M., The one-dimensional heat equation subject to a boundary integral specification, *Chaos, Solitons & Fractals* 2007; 32(2): 661–75.
- [7] Caglar H., Ozer M., Caglar N., The numerical solution of the one-dimensional heat equation by using third degree B-spline functions, *Chaos, Solitons & Fractals* (2007), doi:10.1016/j.chaos.2007.01.056
- [8] C. de Boor, A Practical Guide to Splines, New York: Springer Verlag, 1978.
- [9] Golub GH, Ortega JM, Scientific Computing and Differential Equations, New York and London: Academic Press, 1992.

Solution of Beam Deformation Equation Using Perturbation and Homotopy Perturbation Methods

A.J. Choobbasti, F. Farrokhzad*, A.K. Moosavi, A. Barari and D.D. Ganji

Department of Civil & Mechanical Engineering, Technical University of Babol,
Mazandaran, Iran

*FarzadFarrokhzad2003@yahoo.com

Abstract:

One of the responsibilities of the structural design engineer is to devise arrangements and proportions of members that can withstand, economically and efficiently, the conditions anticipated during the lifetime of a structure. A central aspect of this function is the calculation of the beam deformation, which has very wide applications in structural engineering. In this paper, the governing second order differential equation of beam deformation is solved with two approximate methods, namely the Perturbation and Homotopy Perturbation Method (HPM). The comparisons of the results reveal that these two methods are very effective, convenient and quite accurate to systems of non-linear differential equation.

Keywords: Beam, differential equation, Perturbation, homotopy, non-linear.

Introduction

The non-linear differential equation of beam deformation under static load is shown in the following Eq. (1).

$$\frac{\left(\frac{d^2 y}{dx^2}\right)}{\left(1 + \left(\frac{dy}{dx}\right)^2\right)^{\frac{3}{2}}} = \frac{M}{EI}, \quad (1)$$

Note that (E) is the elastic modulus and that (I) is the second moment of area. (I) must be calculated with respect to axis perpendicular to the applied loading. (x) is the length from left support.

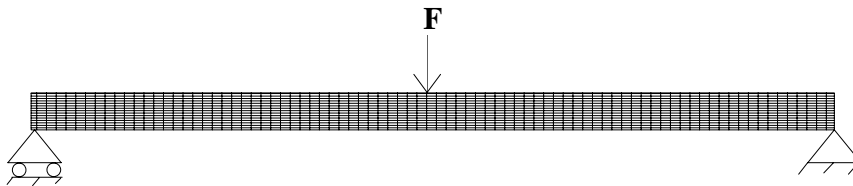


Figure (1): A Simply Supported Beam.

The boundary conditions usually model supports, they can also model point loads, moments, or other effects, as represented by.

$$\begin{aligned} y(x=0) &= 0 \\ \frac{dy}{dx}(x=\frac{l}{2}) &= 0, \end{aligned} \quad (2)$$

Where, (l) represents length of the beam. Here in this paper authors presents approximate methods such as HPM and perturbation methods to solve the above equation and finding the deformation of beam under static loading. Over the last decades several analytical/approximate methods have been developed to solve linear and nonlinear ordinary and partial differential equations. Some of these techniques include Variational Iteration Method (VIM) [1-6], decomposition method [7-9], Homotopy Perturbation Method (HPM) [10-17] etc.

Linear and nonlinear phenomena are of fundamental importance in various fields of science and engineering. Most models of real – life problems are still very difficult to be solved. Therefore, approximate analytical solutions such as homotopy-perturbation method were introduced.

Basic Idea of Perturbation Method

Perturbation method is based on assuming a small parameter. The approximate solution obtained by the perturbation methods, in most cases, are valid only for small value of the small parameter. Generally, the perturbation solutions are uniformly valid as long as a scientific system parameter is small. However, we can not rely fully on approximations, because there is no criterion on which the small parameter should exist. Thus, it is essential to check the validity of approximations numerically and/or experimentally [18,19,20].

For very small ε , let us assume a regular perturbation expansion and calculate the first three terms, thus we assume

$$\theta = \theta_0 + \varepsilon\theta_1 + \varepsilon\theta_2 \quad (3)$$

With substituting Eq. (3) in the Eq. (1) and after expansion and rearranging based on coefficient of ε -term we have:

$$\varepsilon^0: \text{Differential equation in } \theta_0(\tau) = f(u), \quad (4)$$

$$\varepsilon^1: \text{Differential equation in } \theta_1(\tau) \text{ and } \theta_0(\tau) = 0, \quad (5)$$

$$\varepsilon^2: \text{Differential equation in } \theta_2(\tau), \theta_1(\tau) \text{ and } \theta_0(\tau) = 0 \quad (6)$$

And finally with three-term expansion :

$$\theta(\tau) = \varepsilon^0\theta_0(\tau) + \varepsilon^1\theta_1(\tau) + \varepsilon^2\theta_2(\tau) \quad (7)$$

Basic Idea of Homotopy-Perturbation Method

To explain this method, let us consider the following function:

$$A(u) - f(r) = 0, \quad r \in \Omega \quad (8)$$

With the boundary conditions of:

$$B(u, \frac{\partial u}{\partial n}) = 0, \quad r \in \Gamma, \quad (9)$$

Where A , B , $f(r)$ and Γ are a general differential operator, a boundary operator, a known analytical function and the boundary of the domain Ω , respectively. Generally speaking the operator A can be divided in to a linear part L and a nonlinear part $N(u)$. Eq. (8) can therefore, be written as:

$$L(u) + N(u) - f(r) = 0, \quad (10)$$

By the homotopy technique, we construct a homotopy

$v(r, p) : \Omega \times [0, 1] \rightarrow R$ Which satisfies

$$H(v, p) = (1 - p)[L(v) - L(u_0)] + p[A(v) - f(r)] = 0, \quad (11)$$

$$p \in [0, 1], r \in \Omega,$$

Or

$$H(v, p) = L(v) - L(u_0) + pL(u_0) + p[N(v) - f(r)] = 0, \quad (12)$$

Where $p \in [0, 1]$ is an embedding parameter, while u_0 is an initial approximation of Eq. (8), which satisfies the boundary conditions. Obviously, from Eqs. (11) and (12) we will have:

$$H(v, 0) = L(v) - L(u_0) = 0, \quad (13)$$

$$H(v, 1) = A(v) - f(r) = 0, \quad (14)$$

The changing process of p from zero to unity is just that of $v(r, p)$ from u_0 to $u(r)$. In topology, this is called deformation, while $L(v) - L(u_0)$ and $A(v) - f(r)$ are called Homotopy. According to the HPM, we can first use the embedding parameter p as a “small parameter”, and assume that the solutions of Eqs. (11) and (12) can be written as a power series in p :

$$v = v_0 + pv_1 + p^2v_2 + \dots, \quad (15)$$

Setting $p = 1$ yields in the approximate solution of Eq. (11) to:

$$u = \lim_{p \rightarrow 1} v = v_0 + v_1 + v_2 + \dots, \quad (16)$$

The combination of the perturbation method and the homotopy method is called the HPM, which eliminates the drawbacks of the traditional perturbation methods while keeping all its advantage. The series (16) is convergent for most cases. However, the convergent rate depends on the nonlinear operator $A(v)$. Moreover, He made the following suggestions [12]:

- The second derivative of $N(v)$ with respect to v must be small because the parameter may be relatively large, i.e. $p \rightarrow 1$.
- The norm of $L^{-1} \frac{\partial N}{\partial v}$ must be smaller than one so that the series converges.

Application of Perturbation Method

Consider Eq. (1) for beam with conditions as follows:

$$\begin{aligned} E^*I &= 1000 (\text{N.m}^2) \\ L(\text{length of the beam}) &= 1 (\text{m}) \\ F &= 10 (\text{N}) \end{aligned} \quad (17)$$

To solve Eq. (1) by means of Perturbation, we consider the following process. First we change the Eq. (1) to following form:

$$\begin{aligned} \left(\frac{d^2 y}{dx^2}\right)^2 - \left(\frac{M}{EI}\right)^2 \left(1 + \varepsilon \left(\frac{dy}{dx}\right)^2\right)^3 &= 0 \\ M &= \frac{F}{2} x, \end{aligned} \quad (18)$$

Where, x is the length from left support. We assume $\theta(x)$ as Eq. (19)

$$\theta(x) = \theta_0(x) + \varepsilon \theta_1(x) + \varepsilon^2 \theta_2(x) \quad (19)$$

Substituting Eq.(19) in to Eq.(18) and rearranging the resultant equation based on powers of ε -terms, one has:

$$\varepsilon^0 : \left(\frac{d}{dx} \theta_0(x)\right)^2 - \frac{F^2 x^2}{4EI} = 0, \quad (20)$$

$$\varepsilon^1 : 2\left(\frac{d^2}{dx^2} \theta_0(x)\right)\left(\frac{d}{dx} \theta_1(x)\right) - \frac{3F^2 x^2 \left(\frac{d}{dx} \theta_0(x)\right)^2}{4(EI)^2} = 0, \quad (21)$$

$$\begin{aligned} \varepsilon^2 : & -\frac{3F^2 x^2 \left(\frac{d}{dx} \theta_0(x)\right)^4}{4(EI)^2} - \frac{3F^2 x^2 \left(\frac{d}{dx} \theta_0(x)\right)\left(\frac{d}{dx} \theta_1(x)\right)}{2(EI)^2} \\ & + 2\left(\frac{d^2}{dx^2} \theta_0(x)\right)\left(\frac{d^2}{dx^2} \theta_2(x)\right) + \left(\frac{d^2}{dx^2} \theta_1(x)\right)^2 = 0, \end{aligned} \quad (22)$$

$\theta(x)$ may be written as follows by solving the Eqs. (20), (21) and (22):

$$\theta_0(x) = -\frac{Fx^3}{12EI} + \frac{Fl^2x}{16EI}, \quad (23)$$

$$\theta_1(x) = \frac{3F^3(\frac{8}{21}x^7 - \frac{2}{5}l^2x^5 + \frac{1}{6}l^4x^3)}{1024(EI)^3} - \frac{F^3l^6x}{8192(EI)^3} \quad (24)$$

$$\theta_2(x) = \frac{15F^5(\frac{128}{55}x^{11} - \frac{32}{9}l^2x^9 + \frac{16}{7}l^4x^7 - \frac{4}{5}l^6x^5 + \frac{1}{6}l^8x^3)}{1048576(EI)^5} - \frac{3F^5l^{10}x}{8388608(EI)^5}, \quad (25)$$

In the same manner, the rest of components were obtained using the Maple package. According to the Perturbation, we can conclude that:

$$y(x) = \lim_{\varepsilon \rightarrow 1} \theta(x) = \theta_0(x) + \theta_1(x) + \theta_2(x) \dots, \quad (26)$$

Therefore, substituting the values of $\theta_0(x)$, $\theta_1(x)$ and $\theta_2(x)$ from Eqs. (23), (24) and (25) in to Eq. (26) yields:

$$y(x) = -\frac{Fx^3}{12EI} + \frac{Fl^2x}{16EI} + \frac{3F^3(\frac{8}{21}x^7 - \frac{2}{5}l^2x^5 + \frac{1}{6}l^4x^3)}{1024(EI)^3} - \frac{F^3l^6x}{8192(EI)^3} + \frac{15F^5(\frac{128}{55}x^{11} - \frac{32}{9}l^2x^9 + \frac{16}{7}l^4x^7 - \frac{4}{5}l^6x^5 + \frac{1}{6}l^8x^3)}{1048576(EI)^5} - \frac{3F^5l^{10}x}{8388608(EI)^5}, \quad (27)$$

Application of Homotopy-Perturbation Method

To solve Eq. (1) by means of HPM, we consider the following process. First we change the Eq. (1) to following form:

$$\left(\frac{d^2}{dx^2}v(x)\right) - \left(\frac{M}{EI}\right) * \left(1 + \frac{3}{2}\left(\frac{d}{dx}v(x)\right)^2\right) = 0 \quad (28)$$

$$M = \frac{F}{2}x,$$

$$v = v_0 + pv_1 + p^2v_2 + p^3v_3 + \dots, \quad (29)$$

Here it is assumed that $v_2=0$. To solve Eq. (28) by means of HPM, we consider the following process after separating the linear and nonlinear parts of the equation. A Homotopy can be constructed as follows:

$$H(u, p) = (1-p)\left(\frac{\partial^2}{\partial x^2} v(x)\right) + p\left(\left(\frac{d^2 v(x)}{dx^2}\right) - \left(\frac{Fx}{2EI}\right)^* \left(1 + \frac{3}{2}\left(\frac{dv(x)}{dx}\right)^2\right)\right) = 0, \quad (30)$$

Substituting $v = v_0 + pv_1 + \dots$ in to Eq. (30) and rearranging the resultant equation based on powers of p-terms, one has:

$$p^0 : \frac{\partial^2 v_0(x)}{\partial x^2} = 0, \quad (31)$$

$$p^1 : \left(\frac{\partial^2}{\partial x^2} v_1(x)\right) - \frac{Fx}{2EI} - \frac{3Fx\left(\frac{d}{dx} v_0(x)\right)^2}{4EI} = 0, \quad (32)$$

$$p^3 : \left(\frac{d^2}{dx^2} v_1(x)\right) - \frac{3Fx\left(\frac{d}{dx} v_1(x)\right)^2}{4EI} = 0, \quad (33)$$

Where, $V(x)$ may be written as follows by solving the Eqs. (31), (32) and (33):

$$v_0(x) = 0, \quad (34)$$

$$v_1(x) = \frac{Fx^3}{12EI} - \frac{Fl^2x}{16EI}, \quad (35)$$

$$v_3(x) = \frac{3F^3\left(\frac{8}{21}x^7 - \frac{2}{5}l^2x^5 + \frac{1}{6}l^4x^3\right)}{1024(EI)^3} - \frac{F^3l^6x}{8192(EI)^3}, \quad (36)$$

In the same manner, the rest of components were obtained using the maple package. According to the HPM, we can conclude that:

$$y(x) = \lim_{p \rightarrow 1} v(x, t) = v_0(x) + v_1(x) + \dots, \quad (37)$$

Therefore, substituting the values of $v_0(x)$, $v_1(x)$ and $v_2(x)$ from Eqs. (34), (35) and (36) in to Eq. (37) yields:

$$y(x) = \frac{Fx^3}{12EI} - \frac{Fl^2x}{16EI} + \frac{3F^3\left(\frac{8}{21}x^7 - \frac{2}{5}l^2x^5 + \frac{1}{6}l^4x^3\right)}{1024(EI)^3} - \frac{F^3l^6x}{8192(EI)^3}, \quad (38)$$

Result and Discussion

In mechanics of materials for beams with above conditions (supports & loading) the deformation is computed by following formula:

$$y(x) = \frac{F}{48EI} (4x^3 - 3l^2x), \quad (39)$$

In this section the results of perturbation, HPM and formula in mechanics of materials are compared with each other for $0 < l < 0.5$. And for $0.5 < l < 1$ are as same as the previous half.

X(displacement from left support)	Formula in mechanics material	Perturbation Method	HPM
0	0	0	0
0.1	-0.6166666667e-5	-0.6166666678e-5	-0.6166666678e-5
0.2	-0.1183333333e-4	-0.1183333335e-4	-0.1183333335e-4
0.3	-0.1650000000e-4	-0.1650000003e-4	-0.1650000003e-4
0.4	-0.1966666667e-4	-0.1966666670e-4	-0.1966666669e-4
0.5	-0.2083333333e-4	-0.2083333336e-4	-0.2083333336e-4

Conclusion

In this paper, the Homotopy Perturbation Method and Perturbation method have been successfully applied to the governing differential equation of beam deformation with specified boundary conditions. These methods enable to convert a difficult problem into a simple problem which can easily be solved. The comparisons of the results obtained here provide more realistic solutions, reinforcing the conclusions pointed out by many researchers about the efficiency of these two methods. Therefore the HPM and perturbation methods are powerful mathematical tools can be widely applied to structural engineering such as beam problems.

REFERENCES

- [1] Ji-H. He, A new approach to nonlinear partial differential equations, Commun. Nonlinear Sci. Numer. Simul. 2 (1997) 230–235.
- [2] Ji-H. He, Variational iteration method – a kind of non-linear analytical technique: some examples, Int. J. Non-Linear Mech. 34 (1999) 699–708.
- [3] Ji-H. He, Some asymptotic methods for strongly nonlinear equations, Int. J. Modern Phys. 20 (2006) 1141–1199.
- [4] Ganji, D.D., M. Jannatabadi, E. Mohseni, Application of He's variational iteration method to nonlinear Jaulent–Miodek equations and comparing it with ADM, J. Comput. Appl. Math. 207 (2007) 35–45.
- [5] Ganji, D.D., A. Sadighi, Application of homotopy–perturbation and variational iteration methods to nonlinear heat transfer and porous media equations, J. comput. Appl. Math. 207 (2007) 24–34.
- [6] S. Momani, Z. Odibat, Comparison between the homotopy perturbation method and the variational iteration method for linear fractional partial differential equations, Comput. & Math. Appl. 54 (2007) 910–919.
- [7] G. Adomian, Stochastic Systems, Academic Press Inc., New York, 1983.

- [8] G. Adomian, Nonlinear Stochastic Operator Equations, Academic Press Inc., New York, 1986.
- [9] G. Adomian, Solving Frontier Problems of Physics: The Decomposition Method, Kluwer, Boston, 1994.
- [10] Ji-H. He, Homotopy perturbation method: a new nonlinear analytical technique, Appl. Math. Comput. 135 (2003) 73–79.
- [11] Ji-H. He, Addendum: new interpretation of homotopy perturbation method, Int. J. Modern Phys. 20 (2006) 2561–2568.
- [12] Ji-H. He, Homotopy perturbation technique, Comput. Meth. Appl. Mech. Eng. 178 (1999) 257–262.
- [13] M. Rafei, D. D. Ganji, Explicit Solutions of Helmholtz Equation and Fifth-order Kdv Equation using Homotopy-perturbation Method, Int. J. Nonlinear Sci. Numer. Simul. 7 (2006) 321–328 .
- [14] D. D. Ganji, A. Sadighi, Application of He's Homotopy-perturbation Method to Nonlinear Coupled Systems of Reaction-diffusion Equations, Int. J. Nonlinear Sci. and Num. Simu, 7 (2006) 411–418
- [15] A.Janalizadeh, A.Barari, D.D.Ganji, Application of homotopy perturbation method for solving second order nonlinear wave equation, Journal of Physics, in press.
- [16] A.Barari, A.Janalizadeh, D.D.Ganji, Application of homotopy perturbation method to Zakharov- Kuznetsov equation, Journal of Physics, in press.
- [17] J. Biazar, H. Ghazvini and M. Eslami, He's homotopy perturbation method for systems of integro-differential equations, Chaos, Solitons & Fractals, in press, 2007.
- [18] P.aude, C.Beghein, P.Depecher, C. Inard, Perturbation of the input data of models used for prediction of turbulent air flow in an enclosure, nummer. Heat Transf., Part B Fundam (1998) 139-164 .
- [19] J.Fillo, J. Geer, Hybrid perturbation-Galerkin technique for nonlinear heat condition problems 2: partial differential equations, Nummer. Heat Transfer., Part B Fundam. (1996) 75-89
- [20] J.Fillo, J. Geer, Hybrid perturbation-Galerkin technique for nonlinear heat condition problems 1: Steady problem, Nummer. Heat Transfer., Part B Funmdam. (1996) 61-

The ‘Chaosmotic’ and Entropic Situations of Contemporary Art Museums

Deniz Balık*

Abstract

Architecture and art are built upon complexity and inexhaustibility, producing overlapped levels of complex contrasts which make each other perceptible through a network relationship in dialectic way. In this sense, there can be more than one chaos, a composition of chaos, which Deleuze had named as *chaosmos*, neither foreseen nor preconceived.

It becomes problematic that the museum space becomes a chaosmos, where contrasting concepts form an ambiguity like an open work, which opens up to myriad possibilities of perception and experience, leading to the concept of Entropy. Therefore, chaos turns to be a consciously produced and pleasingly approved concept.

Keywords: *entropy, complex contrasts, composed chaos, contemporary art museums, work of art.*

* Dokuz Eylül University Department of Architecture Tınaztepe Campus 35160 Buca / Izmir
e-mail: dbalik@hotmail.com

1. The Unavoidable Complexity

“We are to admit no more causes of natural things than such as are both true and sufficient to explain their appearances.

To this purpose the philosophers say that Nature does nothing in vain, and more is in vain when less will serve; for Nature is pleased with simplicity, and affects not the pomp of superfluous causes.”

Sir Isaac Newton, Principia, Book III, Rule of Reasoning in Philosophy, Rule I [1].

This rule, which is named as *Lex parsimoniae* (the law of parsimony) has been commonly used in scientific methods. Also known as Ockham’s razor, it states that a theory with minimum components is more likely to be correct.

However, there are two cosmic tendencies. One of them is towards geometrical order (in crystals, molecules) and the other one is towards mechanical disorder (Entropy principle) [2]. Leaving the geometrical order aside, this paper investigates the tendency towards mechanical disorder, Entropy, which ends up as chaos.

Looking at the cities, it can be observed that some of them contain nonlinear and complex relationships which have many inputs that make the cities change, transform and grow. For instance, Bilbao in Spain has been known as a developed industrial city in the past. After Guggenheim Bilbao Museum had been built in 1997, the city’s identity had begun to change into a touristic one. While the entire environment had been built according to its industrial needs, in the 21st century, it has unavoidably started to transform into a city of hostels and souvenir shops.

Christopher Alexander has named the cities which have not been deliberately created by designers and planners and have arisen more or less spontaneously over many years, as *natural cities* with semilattice structure [3]. It is much complex because its overlapped components have contrasts and oppositions in the system. However, as Phenomenology approves the thinking way of “both... and...” rather than “either... or...”, the contrasting components of the semilattice structure are able to exist side by side. Insomuch as they

become the elements that make each other visible in dialectic way, like Guggenheim Bilbao Museum makes Bilbao visible and at the same time, cannot be conceived without it.

When the organic components are the parts of a system, as seen in the concept of the city, there can be no certainty and determinism. Because there are some inputs which even the urban planners cannot predict before and these tangible and intangible inputs may cause disorder as a result of the unpredictation and spontaneity. For instance, the creation of pathways or shortcuts other than the urban plan because of the habits of people, a building which has the power to change the city's identity as in the example of Bilbao, or the space – time contraction especially in the metropolises where the concept of time is overlapped in the space as 'now, yesterday and tomorrow'. This is interference without localization. Therefore, observing holistically, both order (planned and predicted parts) and disorder (spontaneous and unpredicted parts) are considered as the parts of a city which eventually form a chaotic structure. However, in a system, these components should not coordinate but fight one another in order to form a chaos.

As Rudolf Arnheim had stated, chaos comes about through the interaction of incompatible forces. Such conflict cannot be grasped as long as one conceives of entities as the mere sum of self-contained wholes; in other words, as long as one uses the method of reductionism to reduce wholeness to an assemblage of elements [4]. Because as Gestalt psychology has approved, in the organization of the whole, the parts that act upon one another cannot be ignored in order to perceive the whole composition or the system. Being side by side, contrasting parts of positive and negative make each other visible with the tension of their existences. Each distinct discipline is, in its own way, in relation with a negative: even science has a relation with a nonscience that echoes its effects or philosophy is prephilosophical insofar as it is considered in itself independently of the concepts that come to occupy it. But nonphilosophy is related to chaos. Philosophy needs a nonphilosophy that comprehends it; it needs a nonphilosophical comprehension just as art needs nonart and science needs nonscience [5]. These contrasting concepts form an ambiguity together. For instance, according to Hermeneutics, the space exists by both an interpreted essence and an interpreting subject. They are not separated, but are against each other, and at the same time expressing one another. These two factors are in interactive relationship by putting forward the concept of productive interpretation, as they make themselves visible again [6]. Forming chaos, both concepts are opposite of each other; however, it is not always an unwanted situation, as in this

paper. For chaos has the ability to produce new perceptions, sensations and aesthetic experiences each time, it turns to be something else– to accidentally or deliberately produced chaos which is unavoidably wanted or needed in architecture or art.

2. Towards Mechanical Disorder

“Nature is pleased with simplicity,” as Newton had quoted in the introduction part of this paper. Now we know that there are complex systems in many parts of our lives, like a storm or our brain, and there are complex reasons behind these systems. Recent experimental studies have led to the conclusion that a distinguishing feature of creative persons is “a cognitive preference for complexity – the rich, dynamic, and asymmetrical – as opposed to simplicity”. Furthermore, most works of art are very complex [7]. Because art is built upon complexity and inexhaustibility where inexhaustibility must be understood in the full sense of ordinality: the complementary relationship of determinateness and indeterminateness; not pure indeterminateness, pure freedom, and unrestrictedness. Besides, complexity must be understood as the conjunctions, unifications, syntheses of contrasts which are dissimilar, opposing constituents of a complex system. The complexity of contrasts also engenders uniqueness and singularity, since there are contrasts in every work that can be shared with no other works or objects. Therefore, aesthetic and artistic values are intense contrasts. Intensity is attained where the opposition is stronger or where the unification is exceptional and the most important feature of contrasts is their capacity to produce level upon level of complex contrasts upon contrasts [8]. In this sense, there can be more than one chaos in order to construct myriad levels of contrasts. Deleuze had very parallel thoughts about this issue. According to him, art is not a chaos but *a composition of chaos* that yields the vision or sensation, so that it constitutes a *chaosmos*, a composed chaos – neither foreseen nor preconceived [9]. In this respect, it becomes problematic that, as the contemporary art museum space has the stratification of the relationships of space and time, we come across myriad levels of meanings and relationships. Therefore, *the museum space becomes a chaosmos* which is interactive and in evolution continuously. Space and time contracts intensely, melting present, past and future in the space until it becomes a knot and the levels of relationships come into being. In such manner, we perceive the museum space through the networks of its visible and invisible dimensions of levels.

A complex system, either a chaos or a chaosmos, which is unstable, unpredictable or uncontrolled, should be either directed by many components which are independent from each

other, or affected by random effects of outer factors [10]. To observe and understand a chaotic structure, first of all, there must be an accurate definition of the terms, order and disorder. The term order is generally a prerequisite of good functioning, in the sense of what works best in our particular environment. However, primarily, it is an objective description of the simplest, most symmetrical, most regular form. The term disorder, when used by physicists, is intended to mean no more than that “the single elements, with which the statistical approach operates, behave in complete independence from one another”. In addition to this, Entropy principle defines order simply as an improbable arrangement of elements, regardless of whether the macro-shape of this arrangement is beautifully structured or most arbitrarily deformed; and it calls disorder the dissolution of such an improbable arrangement [11]. Therefore, it is understood that neither the concept “disorder” nor the paradigm “chaos” have disliked and negative meanings. Although Deleuze had said that we required a little order in our ideas in order to make an opinion and to be protected from chaos, he also had stated that chaos was a concept that poets and artists dealt a bit in their works, not struggle against [12].

In addition to this, as chaotic systems are freed to investigate their own dynamic possibilities, exciting variations and myriad options, possibilities and opportunities are encountered as a result. This understanding is in the same direction with the thoughts of the physicists who believe that chaos is not a science of situation but a science of process, not a science of existence but a science of formation [13]. Because according to this point of view, one can construct multiple meanings when applying this concept to any discipline or field in life and in the end, as mentioned above, chaos becomes a concept that has been produced consciously and willingly.

The concept of process is now genuine for the contemporary art museums, as well, as it is conceived in terms of ‘experience’. Analyzing old museums, we understand that their first mission is displaying the works of art. However, this mission is said to be over, for the display is now not the only solution, but one of the solutions of communication types. Today’s museums mostly aim to give the visitors specific experiences and the works of art are the sites of these experiences. Of course, collecting and displaying of objects continue; however, this old mission is now not the purpose of an art museum; the purpose is to deliver an experience to the visitor. Thinking this way, contemporary art museums are counted as open works, for open work is concerned with the process of making of art rather than a finished work of art.

Open work, which is a concept of Umberto Eco, is a work of art or a text which is not only limited to a single reading, but it forms complexity as a result of a multiplicity of readings. According to Eco, the form of the work of art gains its aesthetic validity precisely in proportion to the number of different perspectives from which it can be viewed and understood. Every performance explains the composition but does not exhaust it. Every performance makes the work an actuality, but is itself only complementary to all possible other performances of the work. In short, we can say that every performance offers us a complete and satisfying version of the work, but at the same time makes it incomplete for us, because it cannot simultaneously give all other artistic solutions which the work may admit. The work remains inexhaustible insofar as it is “open”, because in it an ordered world based on universally acknowledged laws is being replaced by a world based on ambiguity, both in the negative sense that directional centers are missing and in a positive sense, because values and dogma are constantly being placed in question [14]. This ‘chaosmotic’ situation of open work is embodied in the installations which are the works of art “in progress” with specific sites that took away the concepts of “give and take”, and “creating and interpreting” among the artists and visitors of the art museum. The visitors play an active role by contributing to the reinterpretation of the installations, so that in a sense, the works of art are being reconstructed over and over again. During this process, there is always a feedback among the works of art, the visitors and the gallery space of the art museum. In contemporary museums, instead of separating these constituents, there is the understanding of conceiving them as a whole. Because all parts belong to a network system; therefore everything is connected to one another which lead to the conception of the whole. Merleau-Ponty had pointed out the very same thing, stating that passivity and activity were so little distinguishable from each other that who perceived, who was perceived, who painted and who was being painted cannot be known anymore [15]. The forces that act on the system continuously transform into each other while one of them becomes clear, as the others become ambiguous. It makes them inexhaustible as they are ambiguous which opens up to myriad possibilities of perception and experience and leads us to the concept of Entropy, the second law of thermodynamics.

Entropy principle, stated in 1865 by Rudolf Julius Clausius, can be defined as saying that the material world moves from orderly states to ever-increasing disorder and that this process ends up in a state of total disorder. Order is defined here as organized structure, as it is mentioned above. When this structure is gradually destroyed, it gets to be more and more

shapeless, unless it reaches an even distribution of matter [16]. At this point, when it comes to the contemporary art museums, a problematic begins about their architecture: Should the museum be neutral, in other words be a white cube, in order to make the works of art visible and not to compete with them or should the architects be free till the end to express their creativity on this very suitable type of building? As far as I am concerned, in the strong buildings of contemporary art museums; the exhibition galleries, the works of art and the visitors of the museum become constituents with tension which make each other perceptible in dialectic way. They are not separated elements, as they are conceived through the holistic point of view, insisting on that none of these three constituents should be absent. They are the parts of a network system which is conceived through Gestalten, in other words, the relationship of parts with the whole. This conception makes one of the constituents ambiguous due to their entropy-like relationship: They continuously shift one another in the way that when one is perceived, the other one makes it perceptible and meanwhile, tries to take its place.

3. Conclusion - Zeitgeist

Over the last few years, chaos' popularity has gone beyond science. Our period is the time for the chaotic paradigm, whose reflections can be seen in many fields and disciplines, other than physics. Literature about chaotic works of art has been published and curiously followed. Besides, the popular use of the notion of entropy has changed. If during the last century it served to diagnose, explain, and deplore the degradation of culture, it now provides a positive rationale for 'minimal' art and the pleasures of chaos [17].

As far as I am concerned, chaos is a paradigm of architecture, as well, and the purpose of this paper is to explore these relationships. Approaching in phenomenological point of view, which is the conception of 'existing side by side in dialectic way', the concepts in an architectural problem become visible with / by their contrasts. Like the swinging of a pendulum, the balance goes from one end to the other. When it is at an end, the other end becomes ambiguous.

These tense and dynamic relationships of the parts to the whole construct web-like networks. It results as stratified and complex structures, where the *chaosmos* concept of Deleuze intervenes. It causes us to become closer to the notion of 'open work' by Umberto Eco, while

both have common issues like going from order to disorder. It leads us to the concept of Entropy, which provides the limitless aesthetic perceptions and inexhaustible aesthetic experiences.

In my opinion, architecture can be reinterpreted by forming new relationships. This paper explores the chaotic paradigm through the specificity of contemporary art museums in order to clarify the relationships that I have found out. In the architectural academic discourse, the findings of chaotic relationships are very interesting, in the sense of both praxis and theory. From my point of view, as architects, we do not always have to search new concepts and relationships through only architecture itself. Architecture has myriad background disciplines that it interacts with. Therefore, we can transform the notions of other disciplines into architectural context and express them *through the architectural space*. In the end, all the varieties that we attain show us that architecture is made up of complex levels of contrasts; in other words, it is a chaosmos itself.

References

- [1] Newton, I., (1803), *The Principles of Natural Philosophy*, London, H.D. Symonds, 160.
- [2] Arnheim, R., (1971), *Entropy and Art*, USA, University of California Press., 10.
- [3] Alexander, C., (1965), “A City is not a Tree”, *Architectural Forum*, 122/1, 58-62.
- [4] Arnheim, R., (1996), *The Split and the Structure*, USA, University of California Press., 156-157.
- [5] Deleuze, G., Guattari, F., (1991), *What is Philosophy?*, USA, Columbia University Press., 201-204.
- [6] Aydınlı, S., (2002), “Epistemolojik Açıdan Mekan Yorumu”, 41, *Mimarlık ve Felsefe*, ed. Şafak Ural, Ayşe Şentürer, Funda Uz Sönmez, İstanbul, Yapı-Endüstri Merkezi Yayınları.
- [7] Arnheim, R., (1971), *Ibid.*, 46,50.
- [8] Ross, S. D., (1998), “A Theory of Art: Inexhaustibility by Contrast”, 300-303, *Art and Its Significance: An Anthology of Aesthetic Theory*, ed. S. D. Ross, New York, Suny Press.
- [9] Deleuze, G., Guattari, F., (1991), *Ibid.*, 201-204.
- [10] Gleick, J., (1987), *Kaos – Yeni Bir Bilim Teorisi*, Ankara, Tübitak Popüler Bilim Kitapları, 357-358.
- [11] Arnheim, R., (1971), *Ibid.*, 7,15.
- [12] Deleuze, G., Guattari, F., (1991), *Ibid.*, 217-218.
- [13] Gleick, J., (1987), *Ibid.*, VI,362.

- [14] Eco, U., (1989), *The Open Work*, USA, Harvard University Press., 3,9,15.
- [15] Merleau-Ponty, M., (1964), Göz ve Tin, İstanbul, Metis Yayınları, 42.
- [16] Arnheim, R., (1996), Ibid., 157.
- [17] Arnheim, R., (1971), Ibid., 11-12.

GENERATION OF CHAOTIC OSCILLATIONS IN DYNAMICAL SYSTEM WITH FIELD-EFFECT TRANSISTOR AS AN ACTIVE ELEMENT

A.S. Dmitriev*, E.V. Efremova*, L.V. Kuzmin*, A.N. Miliou**, S.G. Stavrinides**

*Institute of RadioEngineering and Electronics of RAS, Russia, Moscow, Mokhovaya St., 11/7

**Aristotle University of Thessaloniki, Greece, GR-54124, Thessaloniki

Chaotic oscillator scheme with field-effect transistor as an active element is considered. Electric scheme of the generator is a variant of capacitive oscillator. Its mathematical model described by three ordinary differential equations along with its circuit model taking into account the internal structure of the transistor and temperature and frequency effects are studied. Scaling relations that make it possible to scale the frequency band of chaotic generation and to use transistors with different steepnesses of the current-voltage characteristic are derived.

Introduction

Application of chaotic signals as information carrier in ultrawideband communication systems makes actual the problem of designing sources of chaotic signals – chaotic generators having preassigned output characteristics such as frequency band, power spectrum form and power of the chaotic signal. Chaotic generators based on solid-state active elements are investigated and applied since the beginning of 80s. Many chaotic generators on bipolar transistor are known and studied rather in detail.

First, they were implemented with a microstrip design and studied experimentally [1-3]; next, low-frequency mathematical models of generators appeared [2-5]; later, methods for computer simulation of chaos generators operating in the radio and microwave ranges were developed [6-7]. Generators calculated via simulations were successfully implemented in experiments [8].

At the same time, FETs have certain advantages in comparison with bipolar transistors. First, they are typical elements of a complementary metal--oxide semiconductor (CMOS) technology. Today it is the most rapidly developing solid-state technology as well as the cheapest one from the point of view of both development and mass production.

In view of the foregoing, the development of chaos generators based on FETs is important. There are virtually no published results on chaos generation in systems with FETs. Study [9] seems to be the only exception. This study contains a description of complex dynamic modes in a self-oscillating system with a high-power FET that were obtained by simulation in the Electronic Workbench package. The system is represented as a Colpitts oscillator. However, it is

not completely clear whether the oscillations are chaotic, since the published results do not contain evidence of chaos and the mathematical model of the system is missing.

This report is devoted to a model of a chaos generator based on a Colpitts oscillator with an FET used as an active element.

Scaling relationships are derived, which allows to scale frequency range of generation and to use transistors with different steepnesses of current-voltage characteristic.

Electric circuit of a chaos generator

We consider the electric circuit of a generator based on a Colpitts oscillator with a CMOS transistor as an active element (Fig. 1).

The main characteristic of a FET is steepness $S = \frac{\partial i_D}{\partial V_{GS}}$, where i_D – is the drain current and V_{GS} – is the gate-source voltage.

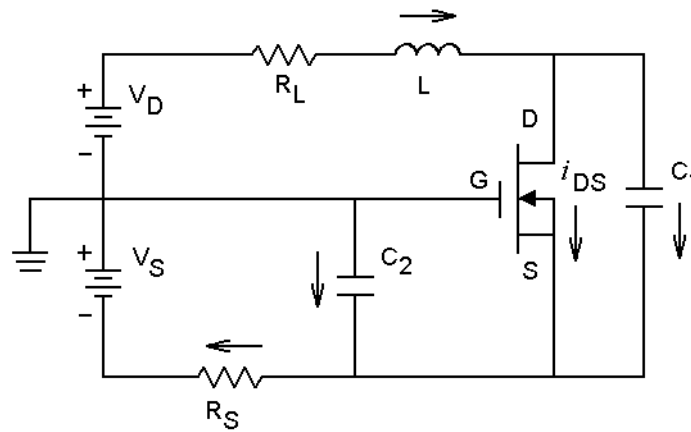


Fig. 1. Circuit of a Colpitts oscillator with an FET as an active element.

Mathematical model and its dynamics

We consider the electric circuit shown in Fig. 1. The static voltage-current characteristic of a FET determines the current passing through the conducting drain-source channel as a function of the gate voltage and can be described with a piecewise linear approximation in the following form:

$$i_{DS}(V_{GS}) = S \cdot (V_{GS} - V_{th}) \cdot \theta(V_{GS} - V_{th}), \quad (1)$$

where $\theta(x)$ is the Heaviside theta function and V_{th} is the minimum (threshold) gate--source voltage under which the conducting channel opens. The larger the current that can pass through a FET, the steeper its characteristic. Therefore, high-power transistors are characterized by a steep current-voltage characteristic. The equations describing the dynamics of the mathematical model

of the circuit shown in Fig. 1 are derived from Ohm's and Kirchhoff's laws and have the following form:

$$\begin{aligned} L\dot{I}_L &= V_C - V_{C1} + V_{C2} - I_L \cdot R_L \\ C_1\dot{V}_{C1} &= I_L - i_{DS}(V_{C2}) \\ C_2\dot{V}_{C2} &= \frac{V_S - V_{C2}}{R_S} - I_L, \end{aligned} \quad (2)$$

where $i_{DS}(V_{C2})$ are determined from expression (1); the signs of the voltages and amperages correspond to the directions indicated in the circuit.

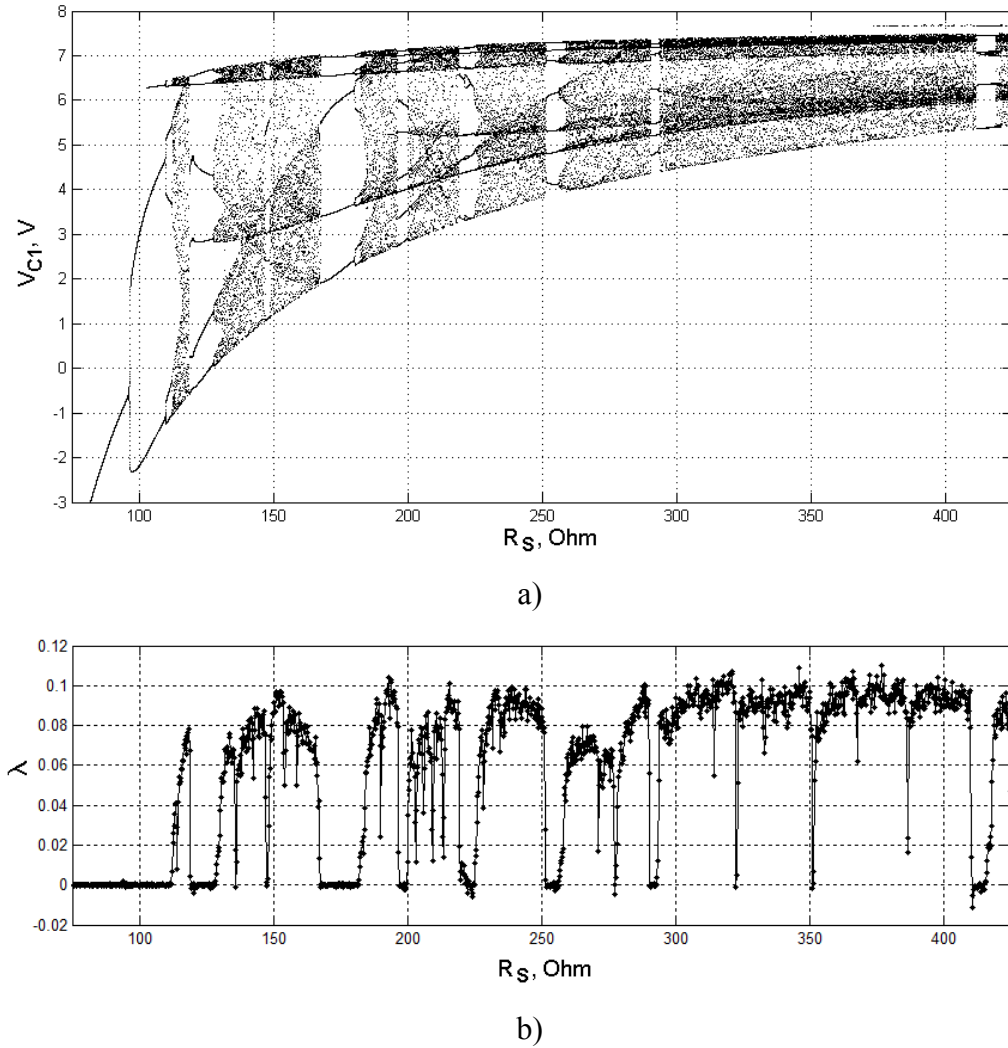


Fig. 2. Dependence of the dynamic modes of the generator on resistance R_S : bifurcation diagram (a) and diagram of Lyapunov exponents (b).

Below, unless stated otherwise, the following set of the parameters is used: $V_D=7$ V, $V_S=2$ V, $L=30$ μ H, $C_1=8$ nF, $C_2=16$ nF, $R_L=40$ Ohm, $R_S=400$ Ohm, $S=1.5$ A/V, $V_{th}=0.75$ V.

Figures 2a and 2b show the bifurcation diagram and the diagram of Lyapunov exponents that illustrate the system's behavior, depending on source resistance R_S . The diagram shows that the chaotic regime appears at the nominal value of resistance $R_S \sim 110$ Ohm after several period-

doubling bifurcations. If the source resistance grows, the zone of chaotic regimes is replaced with the zone of period-six oscillations for $R_S \sim 120 \text{ Ohm}$; if the resistance is increased further, the zones of chaos and regular behavior alternate.

Note that the steepness of the current-voltage characteristic that was used in the calculations corresponds to a FET with a high peak power (tens of watts). The necessity to use such high values of the steepness follows from the inspection of the dependence of the oscillation mode on steepness S . One can see from the diagram that, for the employed values of the electric-circuit parameters, chaotic oscillations appear only for the steepness values $S \geq 0.5 \text{ A/V}$.

Generation of chaos at high frequencies for a given steepness of the transistor characteristic

It has been shown above that chaotic regimes exist in mathematical model (2). The power spectrum of the obtained chaotic oscillations is concentrated in the frequency range $\sim 1 \text{ MHz}$. The steepness of the current-voltage characteristic is $S \sim 1 \text{ A/V}$, a value that corresponds to high-power transistors.

To obtain chaotic oscillations at higher frequencies during use of the steepness value corresponding to a low-power FET, it is necessary to concurrently vary the steepness of both the transistor's characteristic and the frequency and to simultaneously maintain the chaotic generation mode.

To solve this problem, we use a dimensionless mathematical model of the system.

We maintain the numerical values of all coefficients of the dimensionless system when varying different parameters of its elements and the steepness of the current-voltage characteristic. In this way, we maintain the behavior of the system before and after variation of the parameters.

It is assumed that the complete set of circuit parameters L, C_1, C_2, R_S, R_L ; transistor characteristic S ; and the values of S' and f' at which the circuit should be calculated are specified. Here, f' is a characteristic generation frequency. According to the condition that the coefficients before and after (denoted with a prime sign) steepness and frequency scaling remain unchanged, we have expressions for $L', C_1', C_2', R_S', R_L'$:

$$\begin{aligned} L' &= \frac{1}{2\pi f'} \frac{S}{S'} \sqrt{\frac{L(C_1 + C_2)}{C_1 C_2}} \\ C_1' &= \frac{1}{2\pi f'} \frac{S'}{S} \sqrt{\frac{C_1(C_1 + C_2)}{L C_2}} \\ C_2' &= \frac{1}{2\pi f'} \frac{S'}{S} \sqrt{\frac{C_2(C_1 + C_2)}{L C_1}} \end{aligned} \quad \begin{aligned} R_S' &= \frac{S}{S'} R_S \\ R_L' &= \frac{S}{S'} R_L \end{aligned} \quad (3)$$

We assume that the parameters of a generator ensuring the required generation mode are initially specified, but, for some reasons, the employed FET and/or the fundamental generation frequency should be changed.

In this case, if a new model of the transistor (the value of steepness S') and fundamental frequency f' are specified, relations (3) may be used to find new values of L' , C_1' , C_2' , R_S' and R_L' . For the new generation of parameters, the generation mode will possess the property of self-scaling with respect to the generation mode for the initial parameters. The fundamental generation mode will be equal to f' , and the steepness of the transistor employed will be equal to S' .

Circuit simulation

If an actual generator is considered, a simplified mathematical model fails to adequately describe its dynamics. In this case, generator elements are complex dynamic systems that should be described by the models taking into account the internal structure of a transistor and temperature and frequency effects. The generator dynamics, which is close to reality, was simulated with the Advanced Design System (ADS) software package for circuit simulation.

The circuit of the generator used for simulation in the ADS package differed from the circuit considered above (Fig. 1) by the presence of a circuit for outputting signals, that eliminated the effect of the output circuit on the generator and to took into account the output resistance of the actual load.

In the ADS-aided calculations, the SPICE model of a FET was used with the following parameters: the frequency range 0 – 36 GHz, the threshold voltage $V_{th}=0.5$ V and the steepness $S=2.5$ mA/V. The structure of the transistor model may be varied; and, as a result, the steepness value may change with a step of 2.5 mA/V.

In the ADS package, the generator model is a dynamic system described by dozens of differential equations. The structure of these equations is hidden from researchers and, in essence, is a blackbox.

The calculations show that, although the dynamic system describing the generator model seems to be drastically different from the initial mathematical model described by three ordinary differential equations, it exhibits the same types of dynamic behavior as the initial mathematical model. Figure 3 shows as an example the dependence of the dynamic modes of the generator on resistance R_S for $L = 37.2$ uH, $C_1 = 19.2$ nF, $C_2 = 8.7$ nF, $R_L = 36$ Ohm, and $S = 4.85$ A/V. The other circuit parameters here and below are assumed to be invariable. The comparison of the bifurcation diagrams displayed in Figs. 2a and 3 shows that the mathematical and circuit models exhibit not only similar types of dynamic behavior but also a qualitative agreement in the

dynamics of the evolution of the oscillatory modes in the system when the same parameter is varied.

The power spectrum that is characteristic of the region of the chaotic modes for $R_S = 300$ Ohm is shown in Fig. 4a. The majority of the power (up to 95%) of the chaotic signal is concentrated in the frequency band from 100 kHz to 400 kHz. Therefore, this signal can be considered an ultrawideband signal.

To increase the working frequencies of the generator and adapt the circuit to operations with an active element characterized by a lower power, the circuit was simulated in the ADS package via application of the above-described technique for recalculating the parameters of circuit (3).

Figure 4b shows the power spectrum for the circuit with the recalculated parameters of passive elements. For the recalculation procedure, the oscillatory circuit frequency 2.02 MHz (six times the initial value) and an active element with the steepness $S = 0.97$ A/V (one-fifth of the initial value) are chosen.

The analysis of the plots shows that both the mathematical and circuit models exhibit the ultrawideband generation, while the absolute maximum in the spectral power density corresponds to the characteristic frequency of the oscillatory circuit. In addition, the power spectra of the model before and after recalculation of the parameters are qualitatively similar.

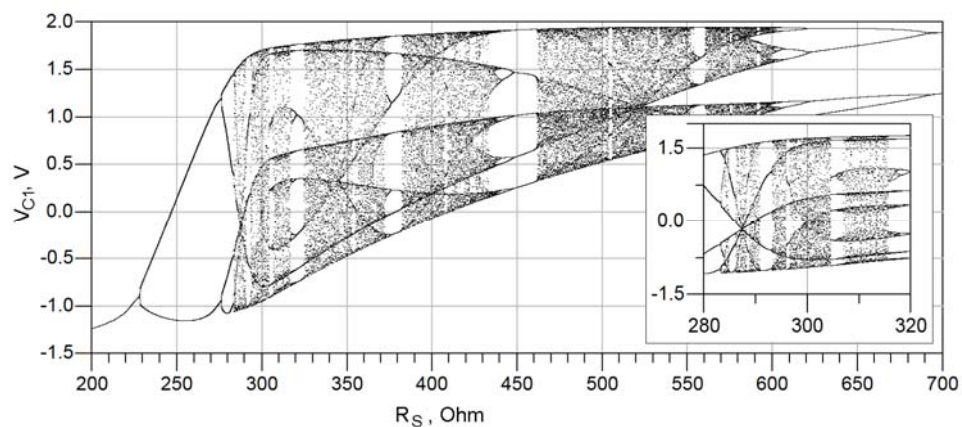
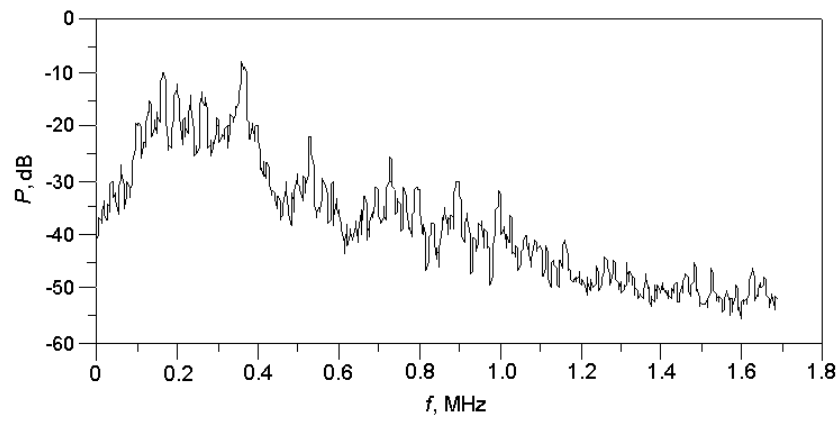
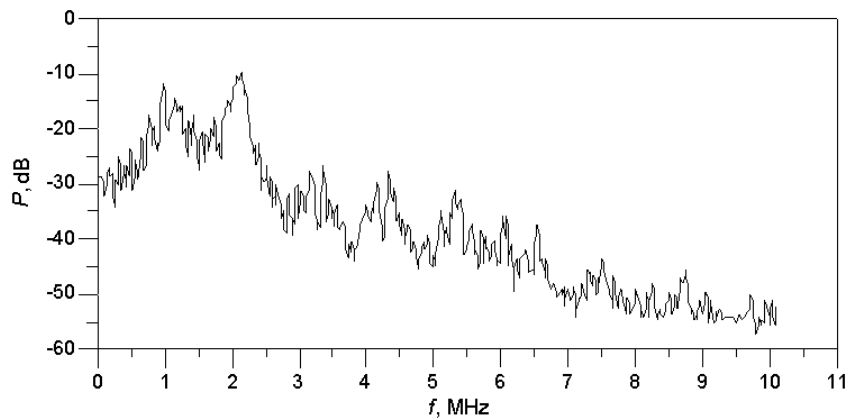


Fig. 3. Dependence of the dynamic modes of a generator on resistance R_S for the circuit model. The insert shows a fragment of the diagram on an enlarged scale for R_S varying from 280 to 320 Ohm.



a)



b)

Рис. 4. Power spectrum obtained in the ADS package for (a) $S = 4.85$ A/V, $f = 0.337$ MHz at $L = 37.2$ uH, $C_1 = 19.2$ nF, $C_2 = 8.7$ nF, $R_S = 300$ Ohm, and $R_L = 36$ Ohm and (b) $S = 0.97$ A/V, $f = 2.02$ MHz at $L = 31.0$ uH, $C_1 = 0.64$ nF, $C_2 = 0.29$ nF, $R_S = 1500$ Ohm, and $R_L = 180$ Ohm.

Conclusions

A generator based on a Colpitts oscillator with an FET has been modeled. A model that exhibits chaotic behavior has been proposed and studied. Similarity relations have been derived that allow scaling of the generation frequency range and usage of transistors with different steepness values of the current-voltage characteristic.

The possibility to apply the derived relations in the mathematical and circuit models has been shown for specific examples.

Acknowledgments

This study was supported in part by the Ministry of Science and Education of the Russian Federation (under the special analytic departmental program Development of the Potential of Institutes of Higher Education (2006--2008)) and by NATO project ICS CLG 981947 .

References

- [1] Kislov V.Ya. (1993) *Radiotekhnika i elektronika*, 38(10), 1783, (in Russian).
- [2] Maximov N., Panas A., Starkov S., (2001) "Chaotic oscillators design with preassigned spectral characteristics", *Proc. Europ. Conf. Circuit Theory and Design (ECCTD '01), Espoo, Finland, August 28-31*, Vol. III, PP. 439-432.
- [3] Maximov N.A., Panas A.I. (2004) "Microwave chaotic oscillators with controlled bandwidth", *Proc. ICCSC'2004*, June 30 - July 2, Moscow, Russia.
- [4] Kennedy M. (1994) "Chaos in Colpitts oscillator," *IEEE Trans. Circuits Syst. I-41*(11), 771-774.
- [5] Feo O., Maggio G. & Kennedy M. (2000) "The Colpitts oscillator: families of periodic solutions and their bifurcations," *Int. J. of Bifurcation and Chaos*, 10(5), 935-958.
- [6] Dmitriev A.S., Efremova E.V, Khilinsky A.D. (2004) "Modeling microwave transistor chaos generators", *Proc. ICCSC'2004*, June 30 - July 2, Moscow, Russia.
- [7] Andreyev Yu.V., Dmitriev A.S., Efremova E.V., Khilinsky A.D., Kuzmin L.V. (2005) "Qualitative theory of dynamical systems, chaos and contemporary communications", *Int. J. Bifurcation and Chaos*, 15(11), 3639-3651.
- [8] Dmitriev A.S., Efremova E.V., Maximov N.A., Grigor'ev E. V. (2007) "Generator of Microwave Chaotic Oscillations Based on a Self-Oscillating System with 2.5 Degrees of Freedom", *J. Commununications Technology and Electronics*, 52(10), 1137-1145.
- [9] A. N. Bulan'kov and B. E. Petrov (2006) "Complex Oscillations in a Double-Circuit Self-Oscillator Built on a Field-Effect Transistor on the Basis of the Inductive Three-Point Circuit", *J. Commununications Technology and Electronics*, 51(11), 1271-1282.

Analysis of Wave Equation in Piles during impact driving using approximate methods

F.Farrokhzad, A. J. Choobasti, A. Barari, D.D.Ganji

Departments of Civil and Mechanical Engineering, University of Mazandaran, Babol,
Mazandaran, Iran

ABSTRACT:

Wave equation is usually used to investigate bearing capacity graph which is a plot of ultimate soil resistance versus set. Giving information about equipment compatibility is another usage of wave equation.

In this paper, Homotopy Perturbation Method (HPM) and Variational Iteration Method (VIM) are applied to solve Wave equation in pile. We illustrate that these methods are very effective and convenient and does not require linearization or small perturbation. Comparison is made between the results of the Homotopy Perturbation Method and Variational Iteration Method and shows same answer for both methods.

KEYWORD: wave equation, pile, Homotopy Perturbation Method (HPM), Variational Iteration Method (VIM).

1. INTRODUCTION

There are many reasons a geotechnical engineer would recommend a deep foundation over a shallow foundation, but some of the common reasons are very large design loads, a poor soil at shallow depth, or site constraints. There are different terms used to describe different types of deep foundations including piles, drilled shafts, caissons, and piers. The naming conventions may vary between engineering disciplines and firms.

Wave mechanics have been employed for the analysis of piles during impact driving for last forty years. Many algorithms have been developed to perform this analysis, starting with [Smith,1960].

Over the last decades several analytical/approximate methods have been developed to solve linear and nonlinear ordinary and partial differential equations. Some of these techniques include variational iteration method (VIM) [1-6], decomposition method [7-9], homotopy perturbation method (HPM) [10-17] etc.

Linear and Nonlinear phenomena are of fundamental importance in various fields of science and engineering. Most models of real – life problems are still very difficult to solve. Therefore, approximate analytical solutions such as homotopy-perturbation method were introduced.

This method is the most effective and convenient ones for both linear and nonlinear equations.

Perturbation method is based on assuming a small parameter. The majority of nonlinear problems, especially those having strong nonlinearity, have no small parameters at all and the approximate solutions obtained by the perturbation methods, in most cases, are valid only for small values of the small parameter.

Generally, the perturbation solutions are uniformly valid as long as a scientific system parameter is small. However, we cannot rely fully on the approximations, because there is no criterion on which the small parameter should exist. Thus, it is essential to check the validity of the approximations numerically and/or experimentally. To overcome these difficulties, HPM have been proposed recently.

Recently, He [1-3] proposed a variational iteration method based on the use of restricted variations and correction functionals which has found a wide application for the solution of nonlinear ordinary and partial differential equations. This method does not require the presence of small parameters in the differential equation, and provides the solution (or an approximation to it) as a sequence of iterates. The method does not require that the nonlinearities be differentiable with respect to the dependent variable and its derivatives.

In this paper we will apply the homotopy perturbation method and variational iteration method to wave equation in piles during impact driving.

2. Basic idea of homotopy-perturbation method

To explain this method, let us consider the following function:

$$A(u) - f(r) = 0, \quad r \in \Omega \quad (1)$$

With the boundary conditions of:

$$B(u, \frac{\partial u}{\partial n}) = 0, \quad r \in \Gamma, \quad (2)$$

Where A , B , $f(r)$ and Γ are a general differential operator, a boundary operator, a known analytical function and the boundary of the domain Ω , respectively.

Generally speaking the operator A can be divided into a linear part L and a nonlinear part $N(u)$. Eq. (1) can therefore, be written as:

$$L(u) + N(u) - f(r) = 0, \quad (3)$$

By the homotopy technique, we construct a homotopy

$v(r, p) : \Omega \times [0, 1] \rightarrow R$ Which satisfies

$$\begin{aligned} H(v, p) &= (1-p)[L(v) - L(u_0)] + p[A(v) - f(r)] = 0, \\ p &\in [0, 1], r \in \Omega, \end{aligned} \quad (4)$$

Or

$$H(v, p) = L(v) - L(u_0) + pL(u_0) + p[N(v) - f(r)] = 0, \quad (5)$$

Where $p \in [0, 1]$ is an embedding parameter, while u_0 is an initial approximation of Eq. (1), which satisfies the boundary conditions. Obviously, from Eqs. (4) and (5) we will have:

$$H(v, 0) = L(v) - L(u_0) = 0, \quad (6)$$

$$H(v, 1) = A(v) - f(r) = 0, \quad (7)$$

The changing process of p from zero to unity is just that of $v(r, p)$ from u_0 to $u(r)$. In topology, this is called deformation, while $L(v) - L(u_0)$ and $A(v) - f(r)$ are called homotopy.

According to the HPM, we can first use the embedding parameter p as a “small parameter”, and assume that the solutions of Eqs. (4) and (5) can be written as a power series in p :

$$v = v_0 + pv_1 + p^2v_2 + \dots, \quad (8)$$

Setting $p = 1$ yields in the approximate solution of Eq. (4) to:

$$u = \lim_{p \rightarrow 1} v = v_0 + v_1 + v_2 + \dots, \quad (9)$$

The combination of the perturbation method and the homotopy method is called the HPM, which eliminates the drawbacks of the traditional perturbation methods while keeping all its advantage.

The series (9) is convergent for most cases. However, the convergent rate depends on the nonlinear operator $A(v)$. Moreover, He made the following suggestions [12]:

- The second derivative of $N(v)$ with respect to v must be small because the parameter may be relatively large, i.e. $p \rightarrow 1$.
- The norm of $L^{-1} \frac{\partial N}{\partial v}$ must be smaller than one so that the series converges.

3. Basic idea of Variational iteration method

To clarify the basic ideas of VIM [1-6], we consider the following differential equation:

$$Lu + Nu = g(t), \quad (10)$$

Where L is a linear operator, N is a nonlinear operator and $g(t)$ is a homogeneous term.

According to VIM, we can write down a correction functional as follows:

$$u_{n+1}(t) = u_n(t) + \int_0^t \lambda (Lu_n(\tau) + N\tilde{u}_n(\tau) - g(\tau)) d\tau \quad (11)$$

Where λ is a general lagrangian multiplier which can be identified optimally via the variational theorem. The subscript n indicates the n th approximation and u_n is considered as a restricted variation, i.e. $\delta \tilde{u}_n = 0$.

4. The Wave Equation in General

The classical one-dimensional wave equation is given by the formula

$$u_{tt}(x,t) = c^2 u_{xx}(x,t) \quad (12)$$

Where c = Acoustic Speed of Pile Material, m/sec

$u(x,t)$ = Displacement of Pile Particle, m

t = Time from Zero Point, seconds

x = Distance from Pile Top, m

For longitudinal vibrations, the constant (c) is the acoustic speed of the material of the bar, given by the equation:

$$c = \sqrt{\frac{E}{\rho}} \quad (13)$$

Where

E = Pile Young's Modulus of Elasticity, Pa

ρ = Pile Density, kg/m^3

Consider Eq. (12), and assume that the bar has but one boundary at ($x=0$). Further assume that the bar begins with no initial displacement or velocity, i.e.,

$$u(x,0) = f(x) = 0 \quad (14)$$

and

$$u_t(x,0) = g(x) = 0 \quad (15)$$

Where $f(x)$ = Initial or Momentary Displacement Distribution in Pile, m

$g(x)$ = Initial or Momentary Velocity Distribution in Pile, $\frac{m}{sec}$

Assume also that the bar is excited at the boundary in such a way that the displacement of the end of the bar can be defined as:

$$u(0,t) = f(t) = 0.0149 - 0.01339e^{-835.176t} - 0.00151e^{-396.154t} \cos(401.6678t) - 0.0293e^{-396.154t} \sin(401.6678t) \quad (16)$$

Where $f(t)$ = Displacement function at Pile Top, m

$$u_x(0,t) = 0 \quad (17)$$

5. Application of Homotopy-perturbation Method

We consider Eq. (12) for steel pile with conditions as follows:

$$E = 200 \times 10^9 \text{ (Pa)} \quad (18)$$

$$\rho = 7850 \text{ (kg/m}^3\text{)} \quad (19)$$

$$c = \sqrt{\frac{E}{\rho}} = 5047.5 \text{ (m/sec)} \quad (20)$$

To solve Eq. (12) by means of HPM, we consider the following process after separating the linear and nonlinear parts of the equation.

A homotopy can be constructed as follows:

$$H(u, p) = (1-p)\left(\frac{\partial^2}{\partial x^2} v(x,t) - \frac{\partial^2}{\partial x^2} v_0(x,t)\right) + p\left(\frac{\partial^2}{\partial t^2} v(x,t) - c \frac{\partial^2}{\partial x^2} v(x,t)\right) = 0, \quad (21)$$

Substituting $v = v_0 + pv_1 + \dots$ in to Eq. (21) and rearranging the resultant equation based on powers of p-terms, one has:

$$p^0 : \frac{\partial^2}{\partial x^2} v_0(x,t) = 0, \quad (22)$$

$$p^1 : \left(\frac{\partial^2}{\partial x^2} v_1(x, t) \right) + \left(\frac{\partial^2}{\partial t^2} v_0(x, t) \right) - \left(\frac{\partial^2}{\partial x^2} v_0(x, t) \right) - c^2 \left(\frac{\partial^2}{\partial x^2} v_0(x, t) \right) = 0, \quad (23)$$

$$p^2 : - \left(\frac{\partial^2}{\partial x^2} v_1(x, t) \right) + \left(\frac{\partial^2}{\partial x^2} v_2(x, t) \right) + \left(\frac{\partial^2}{\partial t^2} v_1(x, t) \right) - c^2 \left(\frac{\partial^2}{\partial x^2} v_1(x, t) \right) = 0, \quad (24)$$

With the following conditions:

$$\begin{aligned} v_0(x, 0) = 0, \quad \frac{\partial}{\partial t} v_0(x, 0) = 0, \quad v_0(0, t) = f(t) = 0.0149 - 0.01339e^{-835.176t} \\ - 0.00151e^{-396.154t} \cos(401.6678t) - 0.0293e^{-396.154t} \sin(401.6678t), \quad \frac{\partial}{\partial x} v_0(0, t) = 0 \end{aligned} \quad (25)$$

$$\begin{aligned} v_i(x, 0) = 0, \quad \frac{\partial}{\partial t} v_i(x, 0) = 0, \\ v_i(0, t) = 0, \quad \frac{\partial}{\partial x} v_i(0, t) = 0 \quad i = 1, 2, \dots \end{aligned}$$

$V(x, t)$ may be written as follows by solving the Eqs. (22), (23) and (24):

$$\begin{aligned} v_0(x, t) = 0.0149 - 0.01339e^{-835.176t} - 0.00151e^{-396.154t} \cos(401.6678t) \\ - 0.0293e^{-396.154t} \sin(401.6678t), \end{aligned} \quad (26)$$

$$\begin{aligned} v_1(x, t) = \frac{1}{2} [9339.8e^{(-835.18t)} - 9331.2e^{(-396.15t)} \cos(401.67t) \\ + 351.66e^{(-396.15t)} \sin(401.67t)] x^2, \end{aligned} \quad (27)$$

$$\begin{aligned}
v_2(x,t) = & 1.6667 * 10^{-15} x^4 \left(\begin{aligned} & -1.62867 * 10^{27} e^{(-835.18t)} \\ & + 1.771610^{21} e^{(-396.15t)} \cos(401.67t) \\ & + 7.427910^{22} e^{(-396.15t)} \sin(401.67t) \end{aligned} \right) \\
& + \frac{1}{2} \left(\begin{aligned} & 9339.8e^{(-835.18t)} - 9331.2e^{(-396.15t)} \cos(401.67t) \\ & + 351.66e^{(-396.15t)} \sin(401.67t) \\ & + 9339.8c^2e^{(-835.18t)} - 9331.2c^2e^{(-396.15t)} \cos(401.67t) \\ & + 351.66c^2e^{(-396.15t)} \sin(401.67t) \end{aligned} \right) x^2, \tag{28}
\end{aligned}$$

In the same manner, the rest of components were obtained using the maple package.

According to the HPM, we can conclude that:

$$\begin{aligned}
u(x,t) = \lim_{p \rightarrow 1} v(x,t) = v_0(x,t) + v_1(x,t) + \dots, \tag{29}
\end{aligned}$$

Therefore, substituting the values of $v_0(x,t)$, $v_1(x,t)$ and $v_2(x,t)$ from Eqs. (26), (27) and (28) in to Eq. (29) yields:

$$\begin{aligned}
u(x,t) = & 0.0149 - 0.01339e^{-835.176t} - 0.00151e^{-396.154t} \cos(401.6678t) \\
& - 0.0293e^{-396.154t} \sin(401.6678t) \\
& + \frac{1}{2} [9339.8e^{(-835.18t)} - 9331.2e^{(-396.15t)} \cos(401.67t) + 351.66e^{(-396.15t)} \sin(401.67t)] x^2 \\
& + 1.6667 * 10^{-15} x^4 \left(\begin{aligned} & -1.62867 * 10^{27} e^{(-835.18t)} \\ & + 1.771610^{21} e^{(-396.15t)} \cos(401.67t) \\ & + 7.427910^{22} e^{(-396.15t)} \sin(401.67t) \end{aligned} \right) \\
& + \frac{1}{2} \left(\begin{aligned} & 9339.8e^{(-835.18t)} - 9331.2e^{(-396.15t)} \cos(401.67t) \\ & + 351.66e^{(-396.15t)} \sin(401.67t) \\ & + 9339.8c^2e^{(-835.18t)} - 9331.2c^2e^{(-396.15t)} \cos(401.67t) \\ & + 351.66c^2e^{(-396.15t)} \sin(401.67t) \end{aligned} \right) x^2, \tag{30}
\end{aligned}$$

Fig. 1 shows result of wave equation in pile after substituting c and plotting for $0 < x < 1$ and $0 < t < 1$.

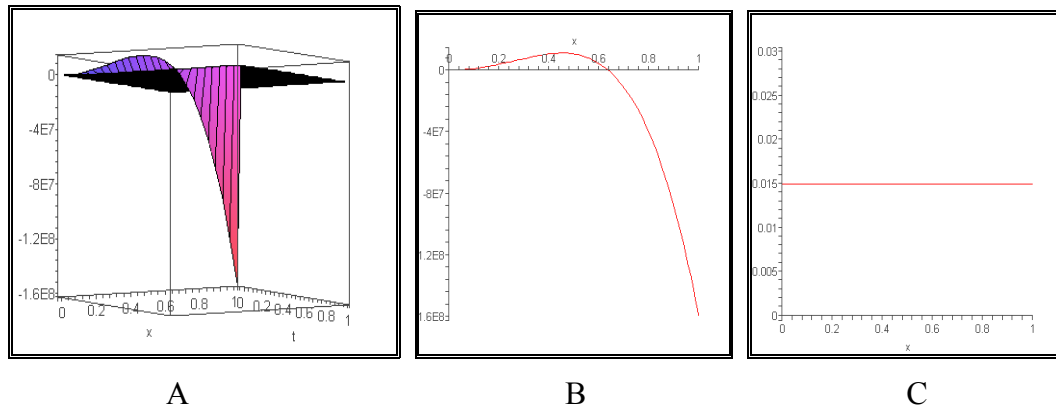


Fig. 1: result of wave equation in pile using (HPM) method [$c=5047.5$ (m/sec) & $0 < x < 1$ & $0 < t < 1$]. (A.....3D , B..... $t=0$, C..... $t=1$) .

6. Application of Variational Iteration Method

In this Section, variational iteration method is developed for solving wave equation in pile.

Consider wave equation in pile (Eq.12).

To solve Eq. (12) via VIM, one has to find the Lagrangian multiplier, which can be identified by substituting Eq. (12) into Eq. (11), upon making it stationary leads to the following:

$$\begin{aligned} 1 - \lambda' \Big|_{\tau=t} &= 0 \\ \lambda \Big|_{\tau=t} &= 0 \\ \lambda'' \Big|_{\tau=t} &= 0 \end{aligned} \quad (31)$$

Solving the system of Eq. (31), yields:

$$\lambda(\tau) = \tau - t, \quad (32)$$

And the variational iteration formula is obtained in the form:

$$u_{n+1}(x,t) = u_n(x,t) + \int_0^t \left\{ (\tau-t) \left(\frac{\partial^2}{\partial \tau^2} u_n(\tau,t) - c^2 \frac{\partial^2}{\partial x^2} u_n(\tau,t) \right) \right\} d\tau, \quad (33)$$

Now, we assume that the initial approximation has the form:

$$u_0(x, t) = 0.0149 - 0.01339e^{-835.176t} - 0.00151e^{-396.154t} \cos(401.6678t) - 0.0293e^{-396.154t} \sin(401.6678t), \quad (34)$$

Using the above variational formula (33), we have:

$$u_1(x, t) = u_0(x, t) + \int_0^t \left\{ (\tau - t) \left(\frac{\partial^2}{\partial t^2} u_0(\tau, t) - c^2 \frac{\partial^2}{\partial x^2} u_0(\tau, t) \right) \right\} dt, \quad (35)$$

Substituting Equation (34) in to Equation (35) and after simplification, we have:

$$\begin{aligned} u_1(x, t) = & 0.0149 - 0.01339e^{-835.176t} - 0.00151e^{-396.154t} \cos(401.6678t) \\ & - 0.0293e^{-396.154t} \sin(401.6678t) + 4669.89x^2e^{-835.176t} \\ & - 4669.89x^2e^{-396.154t} \cos(401.6678t) \\ & + 175.829x^2e^{-396.154t} \sin(401.6678t) \end{aligned} \quad (36)$$

In the same way, we obtain $u_2(x, t)$ as follows:

$$\begin{aligned} u_2(x, t) = & 0.0149 - 0.01339e^{-835.176t} - 0.00151e^{-396.154t} \cos(401.6678t) \\ & - 0.0293e^{-396.154t} \sin(401.6678t) + 1.1897 \cdot 10^{11} x^2 e^{-835.176t} \\ & - 1.1886 \cdot 10^{11} x^2 e^{-396.154t} \cos(401.6678t) \\ & + 4.4796 \cdot 10^9 x^2 e^{-396.154t} \sin(401.6678t) - 2.71444 \cdot 10^8 x^4 e^{-835.176t} \\ & + 2.9527 \cdot 10^6 x^4 e^{-396.154t} \cos(401.6678t) + 1.2379 \cdot 10^8 x^4 e^{-396.154t} \sin(401.6678t), \end{aligned} \quad (37)$$

Fig. 2 shows results of wave equation in pile after substituting c and plotting for $0 < x < 1$ and $0 < t < 1$.

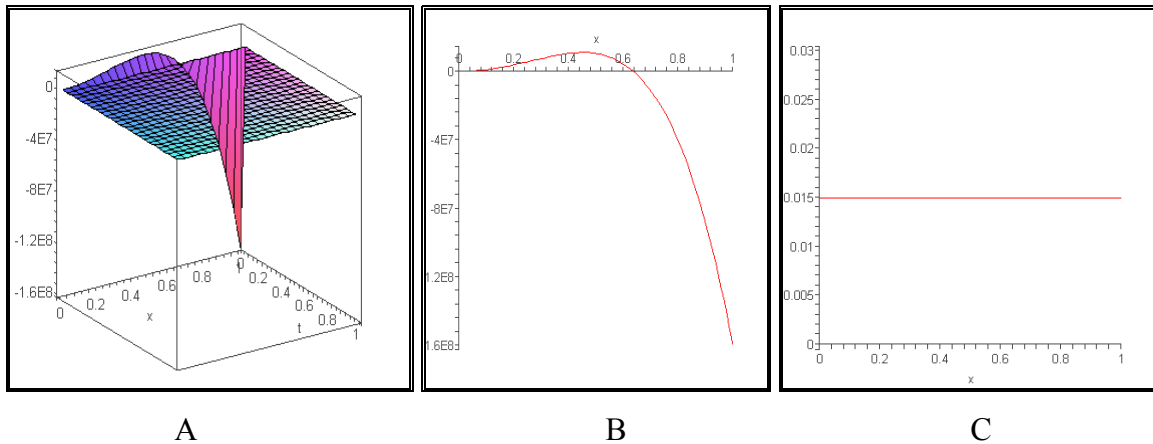


Fig. 2: result of wave equation in pile using (VIM) method [$c=5047.5$ (m/sec) & $0 < x < 1$ & $0 < t < 1$]. (A.....3D , B..... $t=0$, C..... $t=1$) .

CONCLUSION

In this paper, Variational Iteration and Homotopy Perturbation methods have been successfully applied to finding the solution of wave equation in piles during impact driving. Solution of wave equation shows that the results of proposed methods are in agreement with each other. The Homotopy Perturbation method which was used to solve wave equation in piles during impact driving seems to be very easy. There is less computation needed in comparison with other methods (close form solutions and numerical methods). Result clearly shows that Variational Iteration method is capable of solving wave equation in piles during impact driving with a rapid convergent successive approximation without any restrictive assumptions or transformations that may change the physical behavior of the problem.

REFERENCES

- [1] Ji-H. He, A new approach to nonlinear partial differential equations, Commun. Nonlinear Sci. Numer. Simul. 2 (1997) 230–235.
- [2] Ji-H. He, Variational iteration method – a kind of non-linear analytical technique: some examples, Int. J. Non-Linear Mech. 34 (1999) 699–708.

- [3] Ji-H. He, Some asymptotic methods for strongly nonlinear equations, *Int. J. Modern Phys.* 20 (2006) 1141–1199.
- [4] Ganji, D.D., M. Jannatabadi., E. Mohseni, Application of He's variational iteration method to nonlinear Jaulent–Miodek equations and comparing it with ADM, *J. Comput. Appl. Math.* 207 (2007) 35–45.
- [5] Ganji, D.D., A. Sadighi, Application of homotopy–perturbation and variational iteration methods to nonlinear heat transfer and porous media equations, *J. comput. Appl. Math.* 207 (2007) 24–34.
- [6] S. Momani, Z. Odibat, Comparison between the homotopy perturbation method and the variational iteration method for linear fractional partial differential equations, *Comput. & Math. Appl.* 54 (2007) 910–919.
- [7] G. Adomian, *Stochastic Systems*, Academic Press Inc., New York, 1983.
- [8] G. Adomian, *Nonlinear Stochastic Operator Equations*, Academic Press Inc., New York, 1986.
- [9] G. Adomian, *Solving Frontier Problems of Physics: The Decomposition Method*, Kluwer, Boston, 1994.
- [10] Ji-H. He, Homotopy perturbation method: a new nonlinear analytical technique, *Appl. Math. Comput.* 135 (2003) 73–79.
- [11] Ji-H. He, Addendum: new interpretation of homotopy perturbation method, *Int. J. Modern Phys.* 20 (2006) 2561–2568.
- [12] Ji-H. He, Homotopy perturbation technique, *Comput. Meth. Appl. Mech. Eng.* 178 (1999) 257–262.
- [13] M. Rafei, D. D. Ganji, Explicit Solutions of Helmholtz Equation and Fifth–order Kdv Equation using Homotopy–perturbation Method, *Int. J. Nonlinear Sci. Numer. Simul.* 7 (2006) 321–328 .
- [14] D. D. Ganji, A. Sadighi, Application of He's Homotopy–prturbation Method to Nonlinear Coupled Systems of Reaction–diffusion Equations, *Int. J. Nonlinear Sci. and Num. Simu.* 7 (2006) 411–418
- [15] A. Janalizadeh, A. Barari, D.D. Ganji, Application of homotopy perturbation method for solving second order nonlinear wave equation, *Journal of Physics*, in press.
- [16] A. Barari, A. Janalizadeh, D.D. Ganji, Application of homotopy perturbation method to Zakharov- Kuznetsov equation, *Journal of Physics*, in press.

- [17] J. Biazar, H. Ghazvini and M. Eslami, He's homotopy perturbation method for systems of integro-differential equations, *Chaos, Solitons & Fractals*, in press, 2007.

Ergodicity of nonlinear transformations

N. N. Ganikhodjaev ¹

Kulliyyah of Science, International Islamic University Malaysia,
25200 Kuantan, Malaysia and
Institute of Mathematics, Tashkent, 700125, Uzbekistan.

Abstract

We study the asymptotic behavior of nonlinear dynamical system, that has biological significance. The notion of regular direct product of two quadratic stochastic operators is introduced.

1 Introduction

Quadratic stochastic operator was first introduced in [1]. Such operator frequently arises in many models of mathematical genetics [1-3]. Consider a biological population, that is a community of organisms closed with respect to reproduction. Assume that each individual in this population belongs to precisely one species $1, 2, \dots, m$. The scale of species is such that the species of the parents i and j unambiguously determines the probability of every species k for the first generation of direct descendants. We denote this probability, that is to be called the heredity coefficient, by $p_{ij,k}$. It is then obvious that $p_{ij,k} \geq 0$ for all i, j, k and that

$$\sum_{k=1}^m p_{ij,k} = 1, (i, j, k = 1, \dots, m). \quad (1)$$

Assume that the population is so large that frequency fluctuations can be neglected. Then the of the population can be described by the tuple (x_1, x_2, \dots, x_m) of species probabilities, that is x_k is the fraction of the species k in the total population. In the case of panmixia (random interbreeding) the parent pairs i and j arise for a fixed state $\mathbf{x} = (x_1, x_2, \dots, x_m)$ with probability $x_i x_j$. Hence

¹nasirgani@hotmail.com

$$x'_k = \sum_{i,j=1}^m p_{ij,k} x_i x_j, \quad (k = 1, \dots, m), \quad (2)$$

is the total probability of the species k in the first generation of direct descendants.

Let

$$S^{m-1} = \{\mathbf{x} = (x_1, \dots, x_m) \in R^m : x_i \geq 0, \sum_{i=1}^m x_i = 1\} \quad (3)$$

is the $(m-1)$ -dimensional simplex in R^m . The transformation $V : S^{m-1} \rightarrow S^{m-1}$ is called a quadratic stochastic operator(q.s.o.) if

$$V : (V\mathbf{x})_k = \sum_{i,j=1}^m p_{ij,k} x_i x_j, \quad (k = 1, \dots, m), \quad (4)$$

where

$$a) p_{ij,k} \geq 0; b) p_{ij,k} = p_{ji,k}; c) \sum_{k=1}^m p_{ij,k} = 1, \quad (5)$$

for arbitrary $i, j, k = 1, \dots, m$. Note that the condition $p_{ij,k} = p_{ji,k}$ is not overloaded, since otherwise one can determine new heredity coefficient

$$q_{ij,k} = \frac{p_{ij,k} + p_{ji,k}}{2}$$

with preserving operator V .

Let e.g. the q.s.o. V_0 be determined by

$$p_{ij,k} = \begin{cases} 1, & \text{if } i = j = k \\ \frac{1}{2} & \text{if } i \neq j \text{ and } i = k \text{ or } j = k \\ 0, & \text{other cases} \end{cases}$$

It is easy to see that V_0 is the identity mapping on S^{m-1} .

Definition 1 A q.s.o. $V : S^{m-1} \rightarrow S^{m-1}$ is called ergodic if for each initial point $\mathbf{x} \in S^{m-1}$ the limit

$$\lim_{k \rightarrow \infty} \frac{1}{k} \sum_{n=0}^{k-1} V^n(\mathbf{x})$$

exists.

On the basis of numerical calculations Ulam conjectured [5] that any q.s.o. is ergodic transformation. In 1977 Zakharevich [6] showed that this conjecture is false in general. He proved that the q.s.o. V , which is defined on the simplex S^2 by the formula

$$V : (x, y, z) \rightarrow (x^2 + 2xy, y^2 + 2yz, z^2 + 2xz) \quad (6)$$

is non ergodic transformation.

Note that Ulam's conjecture is true for $m = 2$. This fact was proved by D.Zanin and M.Yuldashev [7]

Below we establish a necessary condition to be ergodic for some class q.s.o.'s defined on S^m where $m > 3$ and construct q.s.o which is non ergodic for $m > 3$.

2 Volterra quadratic stochastic operators

In this section we consider special class so-called Volterra q.s.o., which is subset of the border of all q.s.o. set. This subset is commonly believed to contain all the pathological types of behavior, while it's complement's elements to have nice properties of the asymptotic behavior. Thus we presuppose the assumption that any non Volterra q.s.o. is ergodic.

Definition 2 A quadratic stochastic operator is called a Volterra q.s.o. if $p_{ij,k} = 0$ as soon as $k \notin \{i, j\}$.

The biological treatment of such operators is rather clear: the offspring repeats one of its parents.

Proposition 1 A q.s.o. V is a Volterra q.s.o. on S^{m-1} if and only if

$$(V\mathbf{x})_k = x_k(1 + \sum_{i=1}^m a_{ki}x_i)$$

where $A = (a_{ij})_{i,j=1}^m$ is a skew-symmetric matrix, with $a_{ij} = 2p_{ji,j} - 1$ and $|a_{ij}| \leq 1$. If $m = 3$ then arbitrary Volterra q.s.o. can be written as

$$V : (x, y, z) \rightarrow (x(1 + ax - bz), y(1 - ax + cz), z(1 + bx - cy)) \quad (7)$$

In [4] necessary and sufficient conditions were established for the ergodicity of a Volterra q.s.o. on S^2

Theorem 1 The Volterra quadratic stochastic operator (7) is non ergodic if and only if the parameters a, b, c have the same sign and each is non-zero.

If $a = b = c = 1$ we have example (6) considered by Zakharevich [6].

3 A Regular Direct Product of Two Quadratic Stochastic Operators

Let $V_1 : S^{n-1} \rightarrow S^{n-1}$ and $V_2 : S^{m-1} \rightarrow S^{m-1}$ be quadratic stochastic operators.

Let us define an operator $V : S^{n+m-1} \rightarrow S^{n+m-1}$ by

$$V(\mathbf{x}, \mathbf{y}) = (V_1(\mathbf{x}), V_2(\mathbf{y})), \quad (8)$$

where $\mathbf{x} = (x_1, \dots, x_n) \in S^{n-1}$ and $\mathbf{y} = (y_1, \dots, y_m) \in S^{m-1}$.

Evidently the simplices S^{n-1} and S^{m-1} are the sub simplex of the simplex S^{n+m-1} .

It is easy to see that V is not a q.s.o on S^{n+m-1} , as the condition(5) part c) is not satisfied.

To convert V into a q.s.o. it is necessary to add to each component $(V(\mathbf{x}, \mathbf{y}))_k$ a quadratic term α_k such that

$$\sum_{k=1}^{n+m} \alpha_k = 2(x_1 + x_2 + \dots + x_n)(y_1 + y_2 + \dots + y_m).$$

Clearly there are many choices for such quadratic terms. For the purpose of the present paper we make the following choice:

$$(V(\mathbf{x}, \mathbf{y}))_i = (V_1(\mathbf{x}))_i + x_i(y_1 + \cdots + y_m), i = 1, 2, \cdots, n \quad (8)$$

$$(V(\mathbf{x}, \mathbf{y}))_{n+j} = (V_2(\mathbf{y}))_j + y_j(x_1 + \cdots + x_n), j = 1, 2, \cdots, m \quad (9)$$

We say that the operator (8-9) is the regular direct product of V_1 and V_2 . It is denoted by $V_1 \otimes V_2$.

The biological interpretation of the regular direct product of two q.s.o. V_1 and V_2 is as follows: if the V_1 describes a model of heredity for the species $E_1 = \{1, 2, \cdots, n\}$ and if the q.s.o. V_2 describes a model of heredity for the species $E_2 = \{n+1, n+2, \cdots, n+m\}$ then $V_1 \otimes V_2$ describes a model of heredity for the species $E = \{1, 2, \cdots, n+m\}$ where the species $i \in E_1, j \in E_2$ form parent pairs that have the same rights.

Theorem 2. The regular direct product $V_1 \otimes V_2$ is the identity mapping if and only if both components V_1 and V_2 are the identity mapping.

Theorem 3 The regular direct product $V_1 \otimes V_2$ is a Volterra q.s.o. if and only if both components V_1 and V_2 are Volterra q.s.o.

Theorem 4 Let $A = (a_{ij})_{i,j=1}^n$ and $B = (b_{ij})_{i,j=1}^m$ be a skew-symmetric matrices of Volterra q.s.o. V_1 and V_2 respectively. Then a skew-symmetric matrix of regular direct product $V_1 \otimes V_2$ has following form

$$\begin{pmatrix} A & 0 \\ 0 & B \end{pmatrix} \quad (10)$$

Theorem 5 The regular direct product $V_1 \otimes V_2$ of two q.s.o. V_1 and V_2 of Volterra type is ergodic if and only if both components V_1 and V_2 are ergodic.

References

1. S.N. Bernstein, Solution of a mathematical problem connected with the theory of heredity, *Ann. Sci. de l'Ukraine*, 1:83- 114 (1924)
2. Kesten H., Quadratic transformations: a model for population growth. I, II, *Adv. Appl. Prob.*, **2**, 1-82, 179-228 (1970).
3. Lyubich Yu.I., Basic concepts and theorems of the evolution genetics of free populations, *Russian Math. Surveys*, **26**:5, 51-116 (1971).
4. N.N. Ganikhodjaev, D.V. Zanin, On a necessary condition for the ergodicity of quadratic operators defined on the two-dimensional simplex, *Russian Math. Surveys* **59**:3, 571-572, (2004)
5. S. Ulam, *A collection of mathematical problems*, Interscience Publishers, New-York-London 1960.
6. M.I. Zakharevich, On behavior of trajectories and the ergodic hypothesis for quadratic transformations of the simplex, *Russian Math. Surveys* **33**:6, 265-266 (1978)
7. D. Zanin, M. Yuldashev, Master thesis, unpublished, (2002)

IDENTIFICATION OF AN ATTRACTOR IN THE NONLINEAR RESPONSES OF THE HEAD AT SMALL AMPLITUDES

S. Gurses

Department of Engineering Sciences, Middle East Technical University, Ankara 06531,
Turkey, senih@metu.edu.tr

Abstract

It has been previously reported that head-neck neuromechanical system demonstrates nonlinear characteristics in its response to small amplitude perturbations by looking at the sign of the largest Lyapunov exponent of the system dynamics [1]. Twelve healthy young adults seated on a linear sled randomly received anterior-posterior sinusoidal translations with ± 15 mm and ± 25 mm peak displacements at 0.81, 1.76 and 2.25 Hz. Head angular velocity and angular position data were used to construct 3D phase space representation of the system dynamics. In this study, it has been attempted to compute the correlation dimension (D_k) of the chaotic attractor observed at low frequency low amplitude perturbations. An attractor having a correlation dimension of 1.74 ± 0.06 has been diagnosed at Poincaré sections obtained from head responses to small amplitude stimulations. Head responses at 0.81 Hz and 15 mm amplitude perturbation presented lower correlation dimensions with diffused and complex patterns and irregular geometry observed at 3D phase space. Increasing the perturbation frequency and/or the perturbation amplitude increased the dimension of the attractor to a more compact and dense pattern with a more regular and ordered geometry. Computing the correlation dimension of the observed attractor with the Lyapunov exponents will enable us with a better understanding of the nonlinear dynamical characteristics that the head-neck system demonstrates at small amplitude perturbations.

Keywords: Head oscillations, Chaotic attractor, Correlation dimension, Lyapunov exponent

INTRODUCTION

The dynamical behavior of multidimensional musculoskeletal systems such as head-neck neuromechanical system is complex because of forces in different origins arise in dynamic interaction between the segments as well as joint torques may originate from redundant number of muscles contracting of voluntary or reflex origin caused by a structured neural controller [2]. Furthermore, nonlinear properties of tissue and joint response characteristics also with nonlinear frequency dependent properties of the head-neck sensory motor system add to the complexity [3]. There is a surplus amount of data reported in the literature that can not be explained by using linear system approach [4,5,6,7,8,9,10]. Recently, it has been reported that low dimensional chaotic dynamics has been observed at head responses given to small amplitude perturbations by computing the largest Lyapunov exponent of the system dynamics [1]. In this study, it has been attempted to compute the correlation dimension (D_k) of the chaotic attractor observed at the head response to low frequency low amplitude perturbation. Together with the largest Lyapunov exponent of the system, the correlation dimension of the attractor will supply us with a much more complete understanding of nonlinear head-neck dynamics at small amplitude perturbations.

MATERIALS AND METHODS

Data Acquisition

Twelve healthy young adults (7 females and 5 males aged 18–25 yrs) were studied. They had no known musculoskeletal injuries or neurological disorders that might have affected their ability to stabilize their head in space. All subjects gave written consent approved by the Internal Review Board at Northwestern University before undergoing the experimental protocol.

Subjects were seated in a rigid aluminum seat that provided support to the whole body with their legs partially extended and the knees raised. A footrest that could be moved forwards and backwards was positioned so that all subjects had an angle between their thigh and calf of 120 deg. The seatback and seatbase was firm and not supported by any kind of padding. The chair was bolted to a welded steel frame (sled), which was bolted to a high acceleration (2 g maximum), servo-controlled linear motor (Kollmorgan model IC55-100, Hauppauge, NY). A

motion controller board (Galil DMC 1810-16, Rocklin CA) controlled the sled motion. A five-point racing harness secured the subject firmly to the chair and minimized relative movement between the torso and the seat. An individualized bite-bar was made using dental impression material. Attached to the bite-bar with a total mass of 90 grams was a small LED laser that projected a horizontal line, an angular rate sensor oriented to measure angular velocity in pitch (ARS-C141-1ARP, Watson Inc., Eau Claire, WI), and three infrared markers used by the 3-camera motion analysis system (CODAmotion, Charnwood Dynamics, United Kingdom) to record head angular position in space. Additional infra-red markers were attached to the sternum, C7, and the sled. Prior to each experiment, a plumb line and protractor was used to position the head so that the line between the external ear canal and inferior orbital rim was perpendicular to gravity. This angular head position was chosen to offset the angle which the canals make with the gravity vertical and start the subjects from the same initial angular position. Then, head roll position was adjusted by determining that the line projected from the head-mounted laser on to a transversal plane (screen) two and a half meters away from the subject was 0° with the earth horizontal. Once this “horizontal” position was obtained, the position of the projected laser line was marked on the screen so that the head could be realigned by the subject prior to each trial. The laser was automatically turned off when the trial began. Subjects were instructed to hold their head erect while looking ahead with their eyes open. Six 180 sec trials of sinusoidal inputs were randomized for three frequencies (0.81, 1.76, and 2.25 Hz) and two perturbation amplitudes (15 and 25 mm).

Analyses

Linear excursions of the infrared markers were sampled at 100 Hz from which angular displacement of the head in the sagittal plane was calculated. To remove any linear trends in the data, a least-squares fit was performed on the experimentally recorded time series for angular position and angular velocity and the resulting function was subtracted from the data. Phase-plane diagrams for revealing system dynamics were constructed by plotting head angular position against head angular velocity. It is an essential feature to look at the long term evolution of the system trajectories in the phase space representation of the system dynamics in order to understand the characteristics of the dynamical behavior of a nonlinear system. That is because; there appears a subset of the phase points to which the system trajectories eventually evolve, which is known as an attractor [11,12]. An attractor reveals the characteristics of the nonlinear system dynamics by mainly computing two of its basic

properties; i.e., its dimension and associated Lyapunov exponents [13]. There are two general types of dimension definitions for an attractor; those that depend only on metric properties (e.g. capacity dimension), and those that depend on the frequency with which a typical trajectory visits different regions of the attractor; e.g. Lyapunov dimension [13,14]. Nevertheless, it has been shown that these two different types of dimension definitions can be consolidated into a generalized definition of dimension [15]. The dimension of an attractor is a statistical measure in virtue, which gives information about the structure of the attractor and depends on how the phase points on the attractor are spatially correlated [16]. On the other hand, the temporal evolution of the nearby neighboring phase points is characterized by the sign of the largest Lyapunov exponent (LLE) of the attractor, which is a dynamical measure in virtue and refers to the stability of the given phase point [12,14,17].

In this study we use the correlation dimension, D_k for an estimate of the spatial correlations between the pairs of phase points on the given attractor [18,19,20]. Geometrically speaking, an attractor can be a point, a curve, a manifold, or even a complicated set with a fractal structure. Determining the dimension of a geometrically simple attractor is easy. For example, the dimension of a stable fixed point (a stationary time independent equilibrium) has a zero measure, a stable periodic oscillation (limit cycle) has a dimension of one ($D_k=1$), and a double periodic oscillation (2-torus) has a dimension of two ($D_k=2$). For the limit cycle, the phase points are correlated on a curve while, for a 2-torus the phase points are correlated on a plane. Furthermore, the dimensions of these two attractors are integer values because their dynamics fill in the whole phase points on their attractors without leaving any void. This kind of attractor with a regular structure is said to be simple; however, if the nonlinear system demonstrates chaotic dynamics then the distribution of the phase points on the attractor may present complex structural characteristics by leaving voids between the phase points, which is known as a fractal structure [14,16]. In this case the dimension of the attractor (D_k) is no more an integer but, rather it takes a non-integer value.

The phase points either in the full phase space representation of the nonlinear system dynamics or in a Poincaré section from its phase space can be chosen to compute the dimension of the attractor. A Poincaré section is the plane perpendicular to the flow direction of the dynamics represented in the phase plane [12,14,17]. For example; Poincaré section through a stable periodic oscillation maps the limit cycle to a point, while a Poincaré section from a 2-torus maps its dynamics to a circle. Thus, the correlation dimension, D_k of the

attractor computed in the Poincaré section will have a zero measure for the limit cycle and a dimension measure of one for the 2-torus. On the other hand, the spatial distribution of the phase points that the trajectories hit the Poincaré section is an estimate of diverging or converging dynamics generally expressed as Lyapunov exponents [14,17]. Positive Lyapunov exponents are associated with divergence (better known as a chaotic behavior) and negative exponents are a measure of convergence (a stable behavior). A system may be asymptotically stable in the Lyapunov sense, but may demonstrate local instabilities depending on the sign of the largest Lyapunov exponent (LLE>0). Divergence of dynamics observed at a Poincaré section is a sign of local instability related to the given phase point on the identified attractor and causes voids in the structure of the attractor, which is known as a fractal geometry. To quantify system dynamics at the phase-plane we also determined the sign of the largest Lyapunov exponent calculated across the period of the trial [14,21,22,23].

To illustrate the method of computing the dimension of an attractor and its associated largest Lyapunov exponent in the Poincaré section used in this study, a single degree-of-freedom model, an inverted pendulum, was simulated first with a position threshold non-linearity and then with both position and velocity sensor threshold non-linearities. The non-linear equation of motion and the nature of the threshold non-linearity is given below.

$$I\ddot{\theta} + f(\theta, \dot{\theta}) - mgl \sin(\theta) = T$$

$$f(\theta, \dot{\theta}) = \begin{cases} 0 & |\theta| \leq \theta_{th} \text{ and } |\dot{\theta}| \leq \dot{\theta}_{th} \\ k(\theta - \text{sgn}(\theta) \cdot \theta_{th}) & |\theta| > \theta_{th} \text{ and } |\dot{\theta}| \leq \dot{\theta}_{th} \\ b(\dot{\theta} - \text{sgn}(\dot{\theta}) \cdot \dot{\theta}_{th}) & |\theta| \leq \theta_{th} \text{ and } |\dot{\theta}| > \dot{\theta}_{th} \\ k(\theta - \text{sgn}(\theta) \cdot \theta_{th}) + b(\dot{\theta} - \text{sgn}(\dot{\theta}) \cdot \dot{\theta}_{th}) & |\theta| > \theta_{th} \text{ and } |\dot{\theta}| > \dot{\theta}_{th} \end{cases} \quad (1)$$

$$T = A \sin(\omega t)$$

The head-neck system is modeled as an inverted pendulum [24,25,26,27] where m, stands for the mass; g, gravitational acceleration; I, moment of inertia about the joint at C7 (seventh cervical vertebra); T, input torque; k and b are total stiffness and damping around the joint C7, respectively. Simulations performed with the linearized version of Equation (1) about the gravity vertical demonstrate that, for small amplitude perturbations, the system acts in a linear fashion. Thus nonlinear behavior of the system for small amplitude motion is not due to the geometry of the system. Two nonlinear sources of static type were used to model receptor thresholds using a stationary dead-zone, $(\theta_{th} \text{ and } \dot{\theta}_{th})$ that depended upon angular position and angular velocity respectively.

RESULTS

Exemplar model simulations

The system described in Equation 1, was simulated for both a high (2.25 Hz driven by 0.8 Nm) and low (0.81 Hz driven by 0.1 Nm) frequency/velocity pair of input torques with sensor thresholds set only for receptor position. Model parameters were modified to match reported values in the physiological range of the mass and total stiffness of the head-neck complex [27], and the resonance frequency of the system was set near 2 Hz [4]. Simulation results are shown in Figure 1a and b with the system parameters defined in the Figure legend. Figure 1a simulates a case where low frequency and small amplitude perturbation is delivered to the subject. The simulated response of the head demonstrates a complex pattern in 3D phase space. The model outputs; i.e., head angular displacement and head angular velocity fill in the 3D phase space by leaving some voids. Poincaré section (black dots in the figure) made through the complex 3D pattern maps the complex dynamics to a plane perpendicular to the flow direction of the trajectories in the phase space. It is important to notice the existence of the voids also in the plane of Poincaré section, which makes the correlation dimension ($D_k=1.39$) smaller than 2. This kind of complex dynamics with a non-integer correlation dimension points out to a fractal structure of the geometrical pattern in 3D phase space with the sign of the largest Lyapunov exponent being positive ($LLE=0.7 \text{ s}^{-1}$).

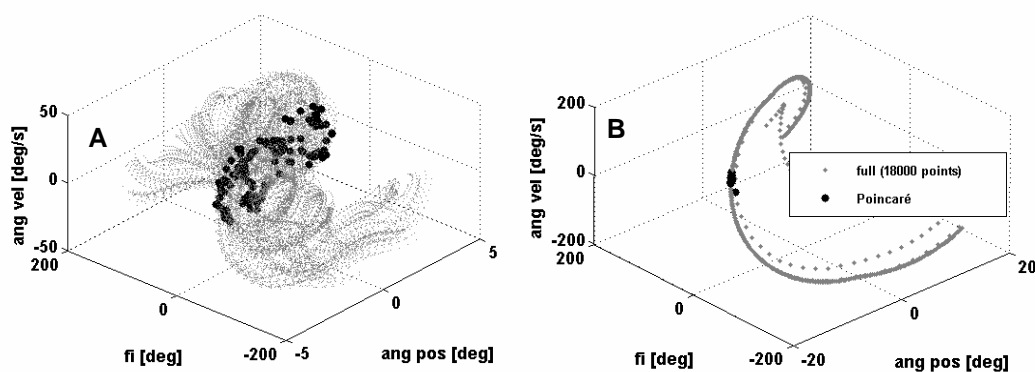


Figure 1 A. Output of the model simulation for low frequency and small amplitude case is presented. Input parameters: driving frequency $\omega_d = 0.81 \text{ Hz}$; input torque $T = 0.1 \text{ Nm}$, $m = 4.5 \text{ kg}$, $k = 10 \text{ Nm/rad}$, $b = 0.01 \text{ Nmsec/rad}$, $\theta_{th} = 1^\circ$, $\dot{\theta}_{th} = 0^\circ/\text{sec}$. Moment of inertia with respect to the center of mass (I) and the length (l) were: 0.0233 kgm^2 and 0.07 m respectively [27]. Time step for numerical integration was 0.01 sec for all simulations and the simulations lasted for 180 sec . Phase points at Poincaré sections are shown as circles filled in black on system trajectories in 3D phase space. The plot (A) is the 3D phase space representation of angular position (θ), phase angle (fi), and angular velocity ($\dot{\theta}$) across the period of the trial. The phase angle, $fi = \omega_d t$; where t denotes for time. Poincaré sections were taken from the phase-plane representation with respect to the initial sled position. Our experimental paradigm was based on holding the peak perturbation

displacement constant so that a positional reference was used in order to ensure that the Poincare section was placed on the first returning phase point ($\dot{\theta}_h=0$). B. Output of the model simulation for high frequency high amplitude case is presented. Plots are the same as in A. Input parameters were: $\omega_d = 2.25$ Hz, $T = 0.8$ Nm, $m = 4.5$ kg, $k = 10$ Nm/rad, $b = 0.2$ Nmsec/rad, $\theta_{th} = 1^\circ$, $\dot{\theta}_{th} = 0^\circ/\text{sec}$.

On the other hand, Figure 1b presents totally different kind of dynamics by using the same model equations (Equation 1) with a different set of system parameters. In this case, the head response to a high frequency and larger amplitude perturbation is simulated. The head-neck system dynamics in its 3D phase space representation eventually converges to a curve (limit cycle), where a Poincare section made through the curve maps the system dynamics to a point ($D_k=0$). The structure of the attractor is very simple in this case compared to Figure 1a and the geometry of the dynamics shows a highly ordered and regular pattern. Accordingly, the largest Lyapunov exponent of the system dynamics is strictly negative for this case ($LLE=-6$ s^{-1}).

Experimental data

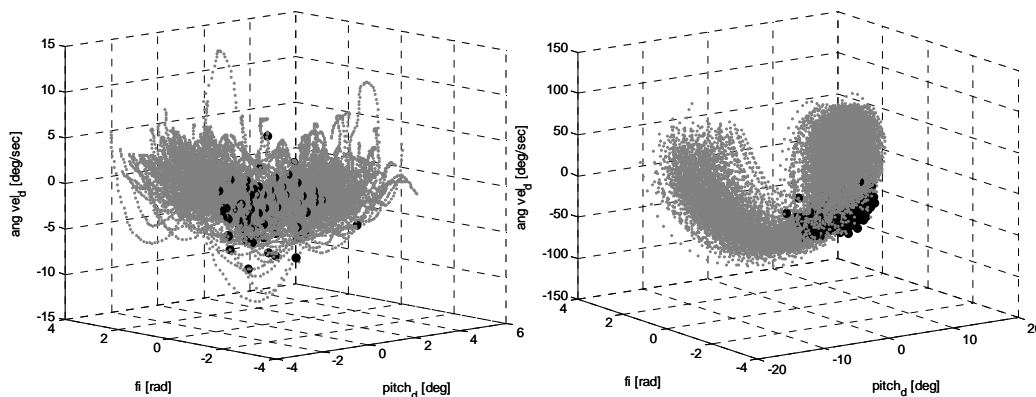


Figure 2. (Left) Head angular position (pitch) and velocity data from one subject with a 0.81 Hz and 15 mm peak amplitude input is presented in 3D phase space ($\dot{\theta}_h$ is the phase angle, refer to Figure 1 for explanation). The number of data points used to construct the phase space is 18000. Phase points at Poincare sections are shown as circles filled in black on system trajectories in 3D phase space. (Right) Head angular position (pitch) and velocity data from the same subject with a 2.25 Hz and 25 mm peak amplitude input is presented in 3D phase space.

Angular displacement and angular velocity of the head in the sagittal plane is used to plot the 3D phase space representation of the head dynamics. Figure 2 (left) shows the data of a representative subject for a 0.81 Hz and 15 mm peak displacement amplitude stimulation in 3D phase space (low frequency, low amplitude), while Figure 2 (right) presents the data for the same subject for a high frequency and higher peak displacement amplitude (2.25 Hz, 25 mm) perturbation. The head response of the subject in Figure 2 (left) demonstrates an irregular and diffused pattern of dynamics with the Poincaré section occupying some voids in

its plane of section. Correlation dimension (D_k) computed at the Poincaré section has been found to be 1.69 for this trial of the subject with the sign of the largest Lyapunov exponent being positive ($LLE=0.82 \text{ s}^{-1}$). The non-integer dimension value of the attractor related to the head dynamics at the low frequency and low amplitude stimulation points out to chaotic dynamics having a fractal structure. However, the same subject behaved in a different manner (Figure 2, right) when high frequency and higher amplitude sled perturbation has been delivered. The head response represented in 3D phase space presented a highly ordered pattern with a much more regular geometry compared to the previous case. The diffused pattern observed in the head response to 0.81 Hz perturbation (Figure 2, left) has been lost; on the contrary, the phase points in the Poincaré section of Figure 2 (right) demonstrates a highly dense and compact pattern with involving less voids in the plane of section. Accordingly, the correlation dimension value was higher ($D_k=1.76$) in this case and the sign of the LLE was slightly negative (-0.06 s^{-1}). Yet, there existed inter-subject and intra-subject variability in the head responses to the stimulations. Further analysis presents the correlation dimension and the largest Lyapunov exponent values for twelve subjects at three different perturbation frequencies with two different peak displacement amplitudes (Table 1).

Table 1. The correlation dimension (D_k) and the largest Lyapunov exponent (LLE) values for twelve subjects at three different perturbation frequencies with two different peak displacement amplitudes

Subjects ^a	Peak displacement amplitude: 15 mm			Peak displacement amplitude: 25 mm**		
	Perturbation frequency [†] [Hz]			Perturbation frequency [Hz]		
	0.81 ^{*,°,***}	1.76 [*]	2.25 ^{°,***}	0.81	1.76	2.25
1 (F)	1.69 ^c /0.82 ^b	1.76/1.00	1.85/0.80	1.73/0.15	1.74/0.20	1.76/-0.06
2 (M)	1.63/0.40	1.80/-1.00	1.73/-0.30	1.71/-0.15	1.81/-0.07	1.80/-0.08
3 (M)	1.75/-0.05	1.85/0.25	1.80/-0.45	1.77/-0.10	1.77/-0.95	1.82/-0.20
4 (F)	1.70/0.20	1.78/-1.15	1.77/-0.65	1.68/0.30	1.79/-0.40	1.72/-0.85
5 (F)	1.74/0.35	1.79/0.15	1.75/-0.30	1.70/0.18	1.74/0.97	1.76/-0.20
6 (F)	1.76/0.95	1.66/-1.40	1.70/-0.23	1.64/-0.37	1.67/-2.90	1.71/-1.70
7 (F)	1.66/-1.27	1.81/-0.14	1.64/0.44	1.81/-0.14	1.78/-0.90	1.70/0.04
8 (M)	1.61/0.70	1.76/0.67	1.80/-1.80	1.64/-0.25	1.84/-1.84	1.81/-1.00
9 (M)	1.83/-0.02	1.81/-3.00	1.79/-2.90	1.73/0.34	1.76/-2.10	1.77/-0.50
10 (F)	1.62/1.10	1.72 ^d	1.67/0.25	1.61/0.57	1.67 ^d	1.70/-0.75
11 (M)	1.61/-0.30	1.79/0.80	1.79/-1.50	1.82/-0.14	1.76/-0.60	1.73/-0.40
12 (F)	1.65/1.00	1.77/2.75	1.76/-2.30	1.71/-0.18	1.73/0.20	1.67/0.67

(F) = female and (M) = male subjects.

^aInter-subject variability was significant ($p < 0.0037$) for correlation dimension values (D_k) computed for each subject across frequencies and displacements

[†]Three perturbation frequencies were found to be significantly different ($p < 0.0001$) for correlation dimension values (D_k)

^bLargest Lyapunov exponent (LLE) values in [1/sec] computed at the Poincaré section [1]

^cCorrelation dimension values (D_k) computed at the Poincaré section

^dLLE couldn't be computed at the Poincaré section for this trial because the initial part of the data was missing.

^{*,°}Correlation dimension (D_k) values computed at 0.81 Hz were significantly different ($p < 0.002$) than D_k values at 1.76 and 2.25 Hz for 15 mm peak displacement amplitude.

^{***}Largest Lyapunov exponents (LLE) in [1/sec] present significant differences with respect to the frequency of perturbation ($p < 0.006$).

^{**}Significantly greater negative LLE in [1/sec] across frequencies ($p < 0.01$).

A 3-way ANOVA statistical test applied to the correlation dimension (D_k) data computed at Poincaré sections for twelve subjects at two different peak amplitudes (15 and 25 mm) and three different frequencies (0.81, 1.76, and 2.25 Hz) of perturbation revealed that the subjects behaved in a significantly different manner ($p < 0.0037$). For example, the ninth subject's correlation dimension values are comparatively larger at three frequencies and two peak amplitudes of stimulation, which points to an attractor with a relatively more regular structure. In contrast, the tenth subject's head responses to perturbations at all frequencies and amplitudes presented low correlation dimension values showing much more diffused patterns at the Poincaré sections. Furthermore, the head responses observed in three different

frequencies of perturbation presented significant differences ($p < 0.0001$) in the correlation dimension values (D_k). The correlation dimension of the chaotic attractor observed at the small amplitude perturbations of the head increased significantly with increasing perturbation frequency from 0.81 Hz to 2.25 Hz. We observed that the phase points on the attractor in 3D phase space became much more compact and densely packed at the plane of Poincaré section when the perturbation frequency increased. But the correlation dimension values did not show any significant differences with respect to the two different peak amplitudes of displacements. Further analysis by using multiple comparison tests demonstrated that the attractor dimension at 0.81 Hz perturbation is significantly lower ($p < 0.002$) than the attractor dimensions at 1.76 and 2.25 Hz stimulations at 15 mm peak displacement amplitude. However, any significant differences in the attractor dimensions at three different frequencies for 25 mm peak displacement amplitude could not be diagnosed.

Simulation of the experimental data

In order to gain insight in the nonlinear dynamics causing the observed chaotic attractor, an inverted pendulum with position and velocity threshold non-linearity was adopted as a simplistic model of the head and neck. Simulations with the model using position sensor threshold only ($f(\theta, \dot{\theta}) = f(\theta)$ in Equation 1 and Figure 1) resulted in features similar to those observed in the experimental data for low frequency low amplitude perturbation (referring to Figure 1a and Figure 2, left) with comparable attractor size (D_k) and LLE value. However, the simulation results (referring to Figure 1b and Figure 2, right) did not fit to the variability observed in the experimental data for high frequencies and higher amplitude perturbation. We didn't observe that much negative LLE values in the experimental data, rather the LLE values for high frequencies (and also for higher amplitude) were slightly negative; although there was considerable variability between the responses of the subjects. The size of the attractor in the experimental data for higher frequencies at higher amplitude was not that different from the size of the attractor observed in the trials at 0.81 Hz and 15 mm amplitude. Furthermore, the geometry of the attractor in the experimental data for higher frequencies and high amplitude stimulation didn't imitate a limit cycle closely, rather demonstrated a scatter of phase points in the plane of Poincaré section. It is worth to note the discrepancy between the characteristics of the attractor in simulated case (Figure 1b; $D_k = 0$ and $LLE = -6 \text{ s}^{-1}$) with the attractor observed in experimental data (Figure 2, right; $D_k = 1.76$

and $LLE = -0.06 \text{ s}^{-1}$). The dynamics simulated in Figure 1b is a limit cycle which is mapped to a point in the Poincaré section, while the dynamics presented in the experimental data (Figure 2, right) shows a solid bundle of trajectories in 3D phase space, which is mapped to a plane in the Poincaré section with a scatter of phase points. Further, LLEs derived from the experimental data indicate that the system exhibited varied levels of stability (Table 1). Thus, a velocity/position sensory function was then incorporated into the model (i.e, $f(\theta, \dot{\theta}) = f(\theta, \dot{\theta})$ in Equation 1).

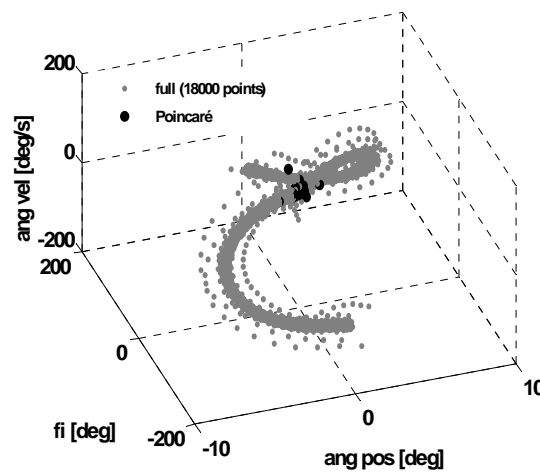


Figure 3 Output of the model simulation with both of the thresholds having nonzero values for high frequency and high amplitude case is presented. Input parameters: driving frequency $\omega_d = 2.25 \text{ Hz}$; input torque $T = 0.8 \text{ Nm}$, $m = 4.5 \text{ kg}$, $k = 20 \text{ Nm/rad}$, $b = 0.2 \text{ Nmsec/rad}$, $\theta_{th} = 1^\circ$, $\dot{\theta}_{th} = 80^\circ/\text{sec}$.

Figure 3 presents the results when both of the sensor thresholds have nonzero values with $D_k = 1.6$ and $LLE = -0.01 \text{ s}^{-1}$. Hence, the inclusion of the velocity threshold component produced a better match to the experimental data in the sense that the size of the attractor is comparable to those observed at the trials of high frequency high amplitude stimulation and LLE value is slightly negative. Still, the diffused pattern at the Poincaré section (Figure 1a and Figure 2, left) has been changed to a relatively dense pattern with an ordered geometry at the plane of Poincaré section (Figure 3).

DISCUSSION

The head-neck system has multiple degrees of freedom in both its control and response characteristics, but is often modeled as single joint mechanical system [4,24,6]. Linear system identification techniques associated with small amplitude perturbations are most often employed to understand the nature of the dynamics and control strategies that the central nervous system uses even with complex sensory-motor systems. However, it has been shown that the head-neck system does not behave in a linear fashion even around its equilibrium point by computing its largest Lyapunov exponent and the correlation dimension (D_k) of the attractor observed at the head responses to small amplitude perturbations [1].

The principal result of this study is that an attractor which has a correlation dimension of 1.74 ± 0.06 has been identified at the 3D phase space representation of twelve subjects' head responses to three different frequencies (0.81, 1.76, and 2.25 Hz) and two different peak amplitude displacements (15 and 25 mm). Although the correlation dimension of the identified attractor increased significantly with increasing perturbation frequency, the increase in the peak displacement amplitude of the perturbations did not change the size of the attractor significantly. However, the size of the attractor computed for 0.81 Hz and 15 mm amplitude stimulation was significantly different than the size of the attractors at the other two frequencies for 15 mm peak amplitude, while there was not any significant change in the size of the attractors found for three frequencies at 25 mm amplitude of perturbation. The general outcome of the statistical analysis of the previous study [1] based on the sign of the largest Lyapunov exponent of the system demonstrated that although there is variability within each amplitude across frequencies and across subjects, the general direction of the LLEs was to decrease toward a more stable behavior (more negative values) as a function of increased amplitude. This finding may be one possible explanation of the attractor size (D_k) being significantly lower at 0.81 Hz compared to 1.76 and 2.25 Hz frequencies at 15 mm amplitude but not indicating any significant change in attractor size with respect to the perturbation frequencies at 25 mm amplitude stimulation. Furthermore, the significant difference in the correlation dimension value of the attractor observed at 0.81 Hz compared to 1.76 and 2.25 Hz at 15 mm amplitude stimulation has also been verified by the statistical analysis performed on the sign of LLEs at 15 mm amplitude perturbation [1]. In other words, within the 15 mm peak displacement there was a significant shift toward increased stability of the head when the perturbation frequency increased from 0.81 to 2.25 Hz. This result points to an increasing

order in the structure of the attractor with increasing perturbation frequencies at 15 mm amplitude.

Although an attractor demonstrating fractal structure characteristics has been identified at the head responses given to the small amplitude perturbations, intra-subject and inter-subjects variability existed in the experimental data. The variability observed in the responses of the subjects may be due to the nonlinear frequency dependent behavior of the head-neck sensory-motor system [7,10,28]. We know that different sensory modalities respond to different frequency bandwidths. Specifically, the head-neck sensory-motor control system utilizes information coming from at least three different senses; i.e., vestibular, proprioceptive, and visual senses [4,9,29,30]. Time-varying spectral characteristics in the head stabilization imply that adaptation to an external perturbation can continuously shift between several control mechanisms [1]. Our simulations suggest that the deterministic element in this paradigm was the neural component of the head-neck system, specifically the position and velocity thresholds of system receptors [4,5,30,31,32,33]. When only a position threshold was included in our model, the low frequency responses were described, but variability in the higher frequency effects could not be explained. When a velocity threshold was also incorporated, the model simulation more closely matched the overall pattern of behavior with a similar size of the attractor and comparable value for the largest Lyapunov exponent computed for the system over the frequency spectrum. The problem of identifying the correct threshold for the different sensory modalities remains, however. To examine if changing the sensory modalities would elicit a significant change in the nonlinear behaviors observed here, further experiments that target to control the senses involved in the control process as well as a patient population with some sort of sensory deficit are warranted. It is believed that nonlinear system identification methods will enable us with a much more complete understanding of head control and stabilization.

Acknowledgements

Supported by NIH - NIDCD grant DC01125 (Keshner, E.A.) and NIH – NINDS grant NS38286 (Hain, T.C.)

REFERENCES

1. Gurses S, Dhaher Y, Hain TC, Keshner EA *Chaos* **15**: 23905 (2005).
2. Lackner JR, DiZio PA *Trends Cogn Sci* **4** (7), 279-288 (2000).
3. Peterson BW *Prog Brain Res* **143**, 369-381 (2004).
4. Keshner EA, Peterson BW *J Neurophysiol* **73** (6), 2293-2301 (1995).
5. Keshner EA, Cromwell RL, Peterson BW *J Neurophysiol* **73** (6), 2302-2312 (1995).
6. Chen KJ, Keshner EA, Peterson BW, Hain TC *J Vestib Res* **12** (1), 25-33 (2002).
7. Berthoz A, Vidal PP, Graf W Editors, *The head-neck sensory motor system*, (Oxford University Press, NY, 1992)
8. Viviani P, Berthoz A *Biological Cybernetics* **19** (1), 19-37 (1975).
9. Guitton D, Kearney RE, Wereley N, Peterson BW *Exp Brain Res* **64** (1), 59-69 (1986).
10. Fard MA, Ishihara T, Inooka H *J Biomech Eng* **125** (4), 533-539 (2003).
11. Eckmann JP, Ruelle D *Rev of Modern Physics* **57**(3), 617-656 (1985).
12. Nayfeh AH, Balachandran B *Applied Nonlinear Dynamics*, (John Wiley & Sons, Inc., New York, NY, 1995).
13. Farmer JD, Ott E, Yorke JA *Physica* **7D**, 153-180 (1983).
14. Baker GL, Gollub JP *Chaotic dynamics* (Cambridge University Press, NY, 1990).
15. Hentschel HGE, Procaccia I *Physica D* **8** 435-444 (1983)
16. Argyris J, Faust G, Haase M, *An Exploration of Chaos* (Elsevier Science, Amsterdam, 1994).
17. Robinson C, *Dynamical systems* (CRC, Boca Raton, Florida, 1999).
18. Grassberger P, Procaccia I *Phys Rev Lett* **50** 346-349 (1983a).
19. Grassberger P, Procaccia I *Phys Rev A* **28** 2591-2593 (1983b).

20. Takens F *Detecting strange attractors in turbulence, in: Dynamical systems and turbulence*, Rand DA, Young LS (eds.), Lecture Notes in Mathematics **898** Springer, Berlin, 1981
21. Wolf A, Swift JB, Swinney HL, Vastano JA *Physica D* **16**, 285-317 (1985).
22. Gurses S, *PhD Dissertation*, Middle East Tech University, (2002).
23. Gurses S, Platin BE, Akkas N *Sci and Eng J of Istanbul Kültür Univ*, **4(4)**, 121-137 (2006)
24. Peng GCY, Hain TC, Peterson BW *Biological Cybernetics* **75**, 309-319 (1996).
25. Keshner EA, Hain TC, Chen KJ, *J Vestib Res* **9 (6)**, 423-434 (1999).
26. Peterson BW, Baker JF, Goldberg J, Banovetz J *Prog Brain Res* **76**, 163-172 (1988).
27. Peng GCY, *PhD Dissertation*, Northwestern University, (1996).
28. Gresty M, *Mov Disord* **2 (3)**, 165-185 (1987).
29. Mergner T, *Current Psychology of Cognition* **21**, 129-212 (2002).
30. Goldberg J, Peterson BW, *J. Neurophysiology*, **56 (3)**, 857-75 (1986)
31. Proske U, Wise AK, Gregory JE *Progress in Neurobiology*, **60**, 85-96 (2000).
32. Keshner EA, Peterson BW, *Prog Brain Res*, **76**, 329-39 (1988)
33. Peterson BW, Goldberg J, Bilotto G, Fuller JH, *J Neurophysiology*, **54 (1)**, 90-109 (1985)
34. Bilotto G, Schor RH, Uchino Y, Wilson VJ, *Brain Res*, **238 (1)**, 217-21 (1982)

On the approximate explicit solution of linear and non-linear non-homogeneous dissipative wave equations

S.HA.Hashemi.K¹, N.Tolou², A. Barari¹, A. J.Choobbasti¹

¹ Mazandaran University of technology, Departments of civil and Mechanical Engineering, P.O. Box 484, Babol, Iran

² Islamic Azad University, Ayatollah Amoli Branch, Amol, Iran

Abstract

In this paper, the solution of the two types of wave equations consist of linear and non-linear non-homogeneous dissipative wave equations is obtained by means of variational iteration method (VIM). These equations describe the propagation of a wave (disturbance), and it arises in a wide variety of physical problems. The results reveal that the variational iteration method (VIM) is very effective, convenient and quite accurate to systems of partial differential equations.

Keywords: wave equations; variational iteration method; exact solution

1. Introduction

In this paper, we consider the linear and non-linear wave equation [1]:

$$u_{tt} = u_{xx} - \varphi(u, u_t, u_x, uu_x, u^2) + F(x, t) \quad (1)$$

On the finite x-interval $[0, \pi]$ with Dirichlet boundary condition:

$$u(x, 0) = 0 = u(t, \pi), \quad -\infty < t < \infty \quad (2)$$

and $F(x, t)$ is a given function of x and t .

These equations describe the propagation of a wave (or disturbance), and it arises in a wide variety of physical problems. Some of these problems include a vibrating string, vibrating membrane, longitudinal vibrations of an elastic rod or beam, shallow water waves, acoustic problems for the velocity potential for a fluid flow through which sound can be transmitted, transmission of electric signals along a cable, shock waves, chemical exchange processes in chromatography, sediment transport in rivers and waves in plasmas, and both electric and magnetic fields in the absence of charge and dielectric [2]. We will apply the variational iteration method (VIM) [3-8] for the two types of partial differential wave equations.

Variational iteration method (VIM) is the most effective and convenient ones for both linear and nonlinear equations. The VIM is to construct correction functional using general Lagrange multipliers identified optimally via the variational theory, and the initial approximation can be freely chosen with unknown constants.

2. Basic idea of Variational iteration method

To clarify the basic ideas of VIM, we consider the following differential equation:

$$Lu + Nu = g(t), \quad (3)$$

Where L is a linear operator, N is a nonlinear operator and $g(t)$ is a homogeneous term.

According to VIM, we can write down a correction functional as follows:

$$u_{n+1}(t) = u_n(t) + \int_0^t \lambda (Lu_n(\tau) + N\tilde{u}_n(\tau) - g(\tau)) d\tau \quad (4)$$

Where λ is a general lagrangian multiplier which can be identified optimally via the variational theory. The subscript n indicates the n th approximation and u_n is considered as a restricted variation, i.e., $\delta \tilde{u}_n = 0$

3. Examples

Example 1. We consider the following linear non-homogeneous dissipative wave equation:

$$\frac{\partial^2}{\partial t^2} u(x, t) = \frac{\partial^2}{\partial x^2} u(x, t) + \frac{\partial}{\partial t} u(x, t) - \frac{\partial}{\partial x} u(x, t) + 2(t - x), \quad 0 \leq x \leq 1, \quad t > 0, \quad (5)$$

The initial and boundary conditions posed are:

$$u(x, 0) = x^2, \quad 0 < x < 1, \quad u_t(x, 0) = 0, \quad u(0, t) = t^2, \quad t \geq 0, \quad (6)$$

Exact solution of this equation is:

$$u(x, t) = x^2 + t^2 \quad (7)$$

The variational iteration formula is obtained in the form:

$$u_{n+1}(x, t) = u_n(x, t) + \int_0^t \lambda \left(\frac{\partial^2 u_n(x, \tau)}{\partial \tau^2} - \frac{\partial u_n(x, \tau)}{\partial \tau} + \frac{\partial u_n(x, \tau)}{\partial x} - \frac{\partial^2 u_n(x, \tau)}{\partial x^2} - 2\tau + 2x \right) d\tau. \quad (8)$$

The lagrangian multiplier can there be identified as:

$$\lambda = e^{(\tau-t)} - 1 \quad (9)$$

As a result, we obtain the following iteration formula:

$$u_{n+1}(x, t) = u_n(x, t) + \int_0^t (e^{(\tau-t)} - 1) \left(\frac{\partial^2 u_n(x, \tau)}{\partial \tau^2} - \frac{\partial u_n(x, \tau)}{\partial \tau} + \frac{\partial u_n(x, \tau)}{\partial x} - \frac{\partial^2 u_n(x, \tau)}{\partial x^2} - 2\tau + 2x \right) d\tau \quad (10)$$

Now we start with an arbitrary initial approximation that satisfies the initial condition:

$$u_0(x, t) = x^2 \quad (11)$$

Using the above variational formula (10), we have:

$$u_1(x, t) = u_0(x, t) + \int_0^t (e^{(\tau-t)} - 1) \left(\frac{\partial^2 u_0(x, \tau)}{\partial \tau^2} - \frac{\partial u_0(x, \tau)}{\partial \tau} + \frac{\partial u_0(x, \tau)}{\partial x} - \frac{\partial^2 u_0(x, \tau)}{\partial x^2} - 2\tau + 2x \right) d\tau \quad (12)$$

Substituting Eq. (11) in to Eq. (12) and after simplification, we have:

$$u_1(x, t) = x^2 - 2e^{(-t)}x + t^2 - 2xt + 2x \quad (13)$$

In the same way, we obtain $u_2(x, t)$ as follows:

$$u_2(x, t) = x^2 - 10e^{-t}x + 3t^2 - 6xt + 10x - 4e^{-t} - 4xte^{-t} - 4t + 4 \quad (14)$$

And so on. In the same way the rest of the components of the iteration formula can be obtained.

Table 1. Shows comparison between results of exact solution and variational iteration method (VIM).

Table 1. Comparison between results of exact solution and (VIM).

X	t	Exact solution	VIM
X=0.1	T=0.1	0.02	0.01961941300
	T=0.2	0.05	0.05084777400
	T=0.3	0.1	0.1070107100
	T=0.4	0.17	0.1911485630
	T=0.5	0.26	0.3060405700
X=0.2	T=0.1	0.05	0.04858849900
	T=0.2	0.08	0.07661856100
	T=0.3	0.13	0.1272943030
	T=0.4	0.2	0.2035773090
	T=0.5	0.29	0.3082037780
X=0.3	T=0.1	0.1	0.097557584
	T=0.2	0.13	0.122389348
	T=0.3	0.18	0.1675778960
	T=0.4	0.25	0.2360060560
	T=0.5	0.34	0.3303669860
X=0.4	T=0.1	0.17	0.166526669
	T=0.2	0.2	0.1881601340
	T=0.3	0.25	0.2278614880
	T=0.4	0.32	0.2884348030
	T=0.5	0.41	0.372530195
X=0.5	T=0.1	0.26	0.255495754
	T=0.2	0.29	0.273930921
	T=0.3	0.34	0.308145081
	T=0.4	0.41	0.360863549
	T=0.5	0.5	0.4346934030

Example 2. We consider non-linear non-homogeneous dissipative wave equation described by:

$$u_{tt} = u_{xx} - \left(\frac{\partial}{\partial t}\right)uu_x + 2e^{-t} \sin x - 2e^{-t} \sin x \cos x, \quad (15)$$

The initial and boundary conditions posed are:

$$u(x, 0) = \sin x, \quad u_t(x, 0) = -\sin x, \quad u(0, t) = u(\pi, t) = 0. \quad (16)$$

Exact solution of this equation is:

$$u(x, t) = e^{-t} \sin x, \quad (17)$$

The variational iteration formula is obtained in the form:

$$u_{n+1}(x, t) = u_n(x, t) + \int_0^t \lambda \left(\begin{aligned} &\left(\frac{\partial^2 u_n(x, \tau)}{\partial \tau^2} - \frac{\partial^2 u_n(x, \tau)}{\partial x^2} + \left(\frac{\partial u_n(x, \tau)}{\partial \tau} \right) \right) \\ &\left(\frac{\partial u_n(x, \tau)}{\partial x} \right) + \left(\frac{\partial^2 u_n(x, \tau)}{\partial x \partial \tau} \right) u_n(x, \tau) - \\ &2e^{-\tau} \sin x + 2e^{-\tau} \sin x \cos x \end{aligned} \right) d\tau, \quad (18)$$

Its stationary conditions can be obtained as follows:

$$\begin{aligned} 1 - \lambda' \Big|_{\tau=t} &= 0, \\ \lambda \Big|_{\tau=t} &= 0, \\ \lambda'' \Big|_{\tau=t} &= 0, \end{aligned} \quad (19)$$

The lagrangian multiplier can there be identified as:

$$\lambda = \tau - t, \quad (20)$$

As a result, we obtain the following iteration formula:

$$u_{n+1}(x, t) = u_n(x, t) + \int_0^t (\tau - t) \left(\begin{aligned} & \left(\frac{\partial^2 u_n(x, \tau)}{\partial \tau^2} - \frac{\partial^2 u_n(x, \tau)}{\partial x^2} + \left(\frac{\partial u_n(x, \tau)}{\partial \tau} \right) \right) \\ & \left(\frac{\partial u_n(x, \tau)}{\partial x} \right) + \left(\frac{\partial^2 u_n(x, \tau)}{\partial x \partial \tau} \right) u_n(x, \tau) - \\ & 2e^{-\tau} \sin x + 2e^{-\tau} \sin x \cos x \end{aligned} \right) d\tau, \quad (21)$$

Now we start with an arbitrary initial approximation:

$$u_0(x, t) = x(1 - t), \quad (22)$$

Using the above variational formula (21), we have:

$$u_1(x, t) = u_0(x, t) + \int_0^t (\tau - t) \left(\begin{aligned} & \left(\frac{\partial^2 u_0(x, \tau)}{\partial \tau^2} - \frac{\partial^2 u_0(x, \tau)}{\partial x^2} + \left(\frac{\partial u_0(x, \tau)}{\partial \tau} \right) \right) \\ & \left(\frac{\partial u_0(x, \tau)}{\partial x} \right) + \left(\frac{\partial^2 u_0(x, \tau)}{\partial x \partial \tau} \right) u_0(x, \tau) - \\ & 2e^{-\tau} \sin x + 2e^{-\tau} \sin x \cos x \end{aligned} \right) d\tau, \quad (23)$$

Substituting Eq. (22) in to Eq. (23) and after simplification, we have:

$$u_1(x, t) = x - xt - \frac{1}{3}xt^3 + t^2x + t^2e^{-t} \sin x - t^2e^{-t} \sin x \cos x, \quad (24)$$

In the same way, we obtain $u_2(x, t)$ as follows

$$\begin{aligned}
u_2(x, t) = & -\frac{2}{3}t^4e^{-t}\sin x - 2t\sin x - \frac{1}{63}t^7x - \frac{1}{3}t^5xe^{-t} - \frac{11}{3}e^{-t}t^3x - \frac{2}{3}e^{-t}t^4x + \\
& \frac{3}{4}e^{-2t}\sin x - \frac{3}{2}\sin x(\cos x)^3 + t^2x + 40e^{-t}x(\cos x)^2 + 13t^2e^{-t}\sin x\cos x - tx + \\
& \frac{2}{3}t^4x + t^2x + 8t\sin x\cos x - 20e^{-t}tx - \frac{1}{3}xt^5 - 10e^{-t}t^2x + 21x - 40x\cos^2 x - \\
& 20e^{-t}tx\cos x - 20e^{-t}x\cos x - \frac{1}{3}e^{-t}t^5\sin x + 20x\cos(x) - 24t\sin xe^{-t} + \frac{2}{3}e^{-t} \\
& t^4\sin x\cos x + 40e^{-t}xt\cos^2 x + \frac{2}{3}e^{-t}xt^5\cos^2 x - \frac{2}{3}e^{-t}t^4x\cos x + \frac{1}{3}e^{-t}t^5\sin x \\
& \cos x - \frac{11}{3}t^3e^{-t}x\cos x + \frac{11}{3}e^{-t}t^3\sin x\cos x + 36te^{-t}\sin x\cos x - \frac{1}{3}e^{-t}t^5x\cos x \\
& + \frac{4}{3}xe^{-t}t^4\cos^2 x - 44\sin x\cos x - 10e^{-t}t^2x\cos x + 20e^{-t}xt^2\cos^2 x + 44e^{-t}\sin x \\
& \cos x - 26e^{-t}\sin x + \frac{1}{9}xt^6 - xt^3 - 10t^2e^{-t}\sin x - \frac{11}{3}t^3\sin xe^{-t}\sin x + \frac{101}{4}\sin x + \\
& \frac{22}{3}e^{-t}xt^3\cos^2 x - 20xe^{-t} + e^{-2t}t^4\sin x\cos^3 x + 3e^{-2t}t\sin x\cos^3 x - \frac{9}{2}t^2e^{-2t}\sin x \\
& \cos^2 x + 3t^2e^{-2t}\sin x\cos^3 x + 2e^{-2t}t^3\sin x\cos^3 x - 3e^{-2t}t^3\sin x\cos^2 x - \frac{9}{2}te^{-2t}\sin x \\
& \cos^2 x - \frac{3}{2}t^4e^{-2t}\sin x\cos^2 x + \frac{9}{4}\sin x\cos^2 x + \frac{1}{2}t^4e^{-2t}\sin x + \frac{3}{2}t^2e^{-2t}\sin x + \frac{3}{2}te^{-2t} \\
& \sin x - \frac{9}{4}e^{-2t}\sin x\cos^2 x + \frac{3}{2}e^{-2t}\sin x\cos^3 x + e^{-2t}t^3\sin x
\end{aligned} \tag{25}$$

And so on. In the same way the rest of the components of the iteration formula can be obtained.

Table 2. Shows comparison between results of exact solution and variational iteration method (VIM).

Table 2. Comparison between results of exact solution and (VIM)

X	t	Exact solution	VIM
X=0.1	T=0.1	0.09033301095	0.09091261900
	T=0.2	0.08173668840	0.08334423500
	T=0.3	0.07395841409	0.07695618500
	T=0.4	0.06692034044	0.07153768200
	T=0.5	0.06055202806	0.06697202800
X=0.2	T=0.1	0.1797634443	0.1818485400
	T=0.2	0.1626566908	0.1667600960
	T=0.3	0.1471778602	0.1540313700
	T=0.4	0.1331720350	0.1432206530
	T=0.5	0.1204990403	0.1340780640
X=0.3	T=0.1	0.2673977408	0.2728299730
	T=0.2	0.2419514814	0.2503161610
	T=0.3	0.2189267537	0.2313400430
	T=0.4	0.1980931185	0.2151895550
	T=0.5	0.1792420659	0.2014491160
X=0.4	T=0.1	0.3523602874	0.3638770150
	T=0.2	0.3188287727	0.3340750530
	T=0.3	0.2884882035	0.3089878810
	T=0.4	0.2610349211	0.2875759940
	T=0.5	0.2361941641	0.2692106280
X=0.5	T=0.1	0.4338021665	0.4550067140
	T=0.2	0.3925204323	0.4180907590
	T=0.3	0.3551671745	0.3870677880
	T=0.4	0.3213685491	0.3604986620
	T=0.5	0.2907862882	0.3374806420

4. Conclusion

The variational iteration method has been successfully used to study different types of wave equations. These equations describe the propagation of a wave (disturbance), and it arises in a wide variety of physical problems.

The results obtained from proposed method have been compared and verified with those obtained by the exact solution. The results revealed that variational iteration method is powerful mathematical tool for solutions of linear and nonlinear partial differential equations in the terms of accuracy and efficiency while systems of partial differential equations having wide applications in engineering.

References

- [1] M.Inc, Y. Cherruault, K.Abbasoui, A computational approach to the wave equations, *Kybernetes*, (2004) 80-97.
- [2] L.Debnath, *Nonlinear partial differential equations for scientists and engineering*, Birkhauser, Boston, (1997).
- [3] Ganji,D.D, M. Jannatabadi, E. Mohseni, Application of He's variational iteration method to nonlinear Jaulent–Miodek equations and comparing it with ADM, *J. Comput. Appl. Math*, 207(2007), 35-45.
- [4] Ganji,D.D, A. Sadighi, Application of homotopy–perturbation and variational iteration methods to nonlinear heat transfer and porous media equations, *J.comput. Appl. Math*, 207 (2007), 24-34.
- [5] J.H. He, Variational iteration method: a kind of nonlinear analytical technique: some examples, *Internat Nonlinear Mech.* 344 (1999), 699–708.
- [6] J.H. He, Variational iteration method for autonomous ordinary differential systems, *Applied Mathematics and Computation*, 114 (2000), 115–123.
- [7] J.H. He, Some asymptotic methods for strongly nonlinear equations, *Int. J. Mod. Phys. B* 20, 10(2006), 1141–1199.
- [8] J.H. He, Wu X.H, Construction of solitary solution and compacton–like solution by variational iteration method, *Chaos Soliton Fract*, 29 (2006), 108–113.

ECOLOGICAL COMPLEXITY: A heuristic explanation of fourth dimension of life

Ji-Huan He

Modern Textile Institute, Donghua University, Shanghai 200051, China

Email: jhhe@dhu.edu.cn

1. What is Dimension ?

In the theory of n dimensional spaces, what we mean by n dimensional is simply that we need n numbers representing n coordinates to fix the position of a point in this space.

1.1. Three dimensional space

Newton's universe is a God's eye view of the world; it looks the same to every observer, wherever he is and however he travels. Newton's law can be expressed in the form

$$F = ma \quad (1)$$

where time is a mere flying parameter.

1.2 Four dimensional spacetime

Einstein's clock is a man's eye view of the world, in which what you see and what I see is only relative to one another. Within such a space, Newton's law becomes only approximately true. The famous Einstein's mass-energy relation is written in the form

$$E = mc^2 \quad (2)$$

In 4 dimensional spacetime, the distance is defined as

$$ds = \sqrt{(dx)^2 + (dy)^2 + (dz)^2 + (idt)^2} \quad (3)$$

1.3. E-infinity spacetime[1-8]

By contrast, El-Naschie's spacetime is a fractal eye view, which differs considerably from the spacetime of our sensual experience, and models the world at quantum scales. At such a deep level of observation, Einstein's spacetime must resemble a stormy ocean and his original Riemannian smooth manifold is only an approximation.

First let us make a careful inspection of Einstein's field equation

$$R_{ij} - \frac{1}{2} g_{ij} R = -KT_{ij} \quad (4)$$

where R_{ij} is the Ricci tensor, T_{ij} the energy-momentum tensor, K a coupling constant and g_{ij} the metric tensor.

On the right hand side of Eq.(4) we have the mass tensor. According to Einstein's famous formula $E = mc^2$, matter and energy are by virtue of the special relative equivalent. However, energy on a fundamental level obeys Planck's quantum, so at quantum scale, the right hand side of Eq.(4) becomes *quantized discrete*, while the left hand side of the equation is still *continuous*. Thus at quantum scale, Einstein's spacetime must become discrete in the sense of quantum mechanics, resembling a stormy ocean due to quantum fluctuation or the equation would be extremely limited.

As stated by Gerardus 't Hooft[9,10] *discrete space time* may be the most radical and logical viewpoint of reality. Unfortunately most mainstream physicists are unwilling to adopt the picture that space and time consist of a collection of isolated points, where particles can be only on those

points, but not in between. E-Infinity theory extends this notion to a transfinite setting where a collection of points can mimic the continuum. Such a collection of unaccountably infinite set of points is said to possess the cardinality of the continuum and as such it is a compromise between the discrete and the continuum.

In view of E-Infinity theory, quantum space-time is in reality a collection of transfinite discrete set of points, which appears when observed at a distance to be a nowhere disjointed continuum. This geometry which is best described by its Hausdorff dimension leads us ultimately to a radical change of some of our most basic mathematical assumptions in string theory.

The formal dimension in *E*-infinity theory is

$$D_F = \infty \quad (5)$$

The topological dimension in *E*-infinity theory reads

$$D_T = 4 \quad (6)$$

Now we write down the Hausdorff dimension in *E*-infinity theory

$$D_H = \{\text{Dim}_H^{(\infty)}\} = 4 + \phi^3 = 4 + \frac{1}{4 + \frac{1}{4 + \frac{1}{4 + \dots}}} = 4.23606\dots \quad (7)$$

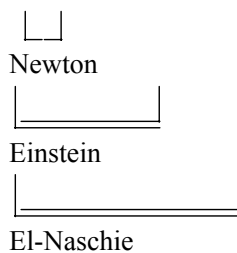
where $\phi = (\sqrt{5} - 1)/2$ is the golden mean.

This means that the formally infinite dimensional but hierarchical E-infinity spacetime looks from a distance as if it were four-dimensional $D_T = 4$, with a corresponding Hausdorff dimension which is equal to 4 plus the golden mean to the third power.

Despite of the great success and undeniable brilliance of the standard model of high-energy elementary particles, it is fair to say that it is by no means perfect. Now E-infinity theory has changed the situation radically. El Naschie actually built a bridge between high-energy particle physics on the one side and nonlinear dynamics, complex theory, chaos, and fractals on the other, and he benefits tremendously from this scientific cross-fertilization.

The space dimension formula is schematically shown as follows:

$$\text{Dimension} = 3 + 1 + \phi^3 = 4.236\dots$$



2. Ecological Complexity -From Simplicity to Complexity: A Historical Remark

2.1. Geometrical Complexity

Let us begin with N-dimensional cubes[11]. Fig.1 is a four dimensional cube, while Fig.2 is an eleven dimensional cube. Pondering Fig. 1 and 2 the reader must be intrigued by the quasi-fuzziness of the appearance of for higher dimensional polytopes. In fact Fig.2 shows a space filling global chaos-like behavior.

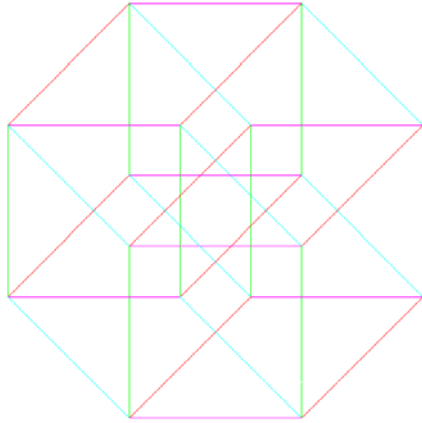


Fig.1 The four dimensional cube[11].

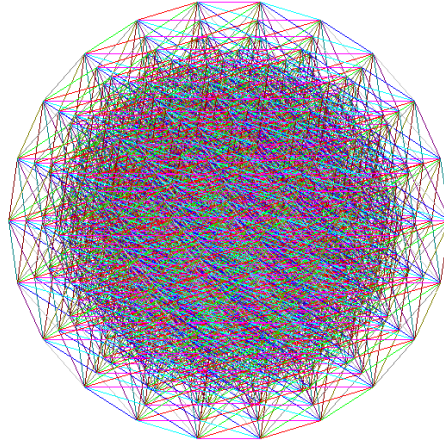


Fig.2 The 11dimensional cube[11].

From a simple geometrical rule, we can produce chaos-like complexity. Similar phenomena appear also in life.

2.2 Rubner 2/3 law[12]

In 1883, Rubner[12] obtained that the metabolic rate depended on the body's surface-to-volume ratio, or $M^{2/3}$, where M is the whole-body mass. The Rubner law can be obtained by a simple geometry analysis. This law was misunderstood as a “surface law”, which correlates the metabolic rate with the body surface. Actually the metabolic cost does not depend upon only the heat exchange through the body surface. So the Rubner 2/3-law, resulting in a Euclidean surface-to-volume relationship, was rebutted by many researchers due to its theory pitfall, but a thorough re-examination of large data sets has concluded that the null hypothesis of a 2/3 power relation can not be rejected.

Rubner's law is very similar to the well-known Kepler's 3rd law, which says

The squares of the periods of revolution around the Sun are proportional to the cubes of the distances.

In allometric form, the Kepler's 3rd law can be expressed in the form

$$R \propto T^{2/3} \quad (8)$$

where R is the distance from the planet to the Sun, T is the period.

2.3 Kleiber 3/4 law[13]

In 1932, Max Kleiber[13] claimed that the oxygen consumption of a resting body scaled instead with $M^{3/4}$. There is no obvious reason for the exponent to have this value, and dueling theories aim at explaining the mystery of how an animal's metabolic rate is related to its size, but no convincing result is so far obtained, so the allometric scaling in biology still keeps an intriguing and enduring problem. The contention throughout this body of literature focuses on the arguments for and against the Rubner 2/3 law or Kleiber 3/4 law.

West *et al.*[14] proposed a general model that describes how essential materials are transported through space-filling fractal networks of branching tubes. The theory, as pointed out by Weibel[15], is indeed an attractive model, a simple unified theory as the solution for a complex system—almost too good to be true. This theory has been questioned by many authors. Dawson[16] points out that the assumption that the capillary dimensions do not vary with mammal size is contrary to his early work and to the basic cardiovascular design and physiological processes of mammals. The most pitfall of the theory is to apply the well-known Poiseuille formula to the calculation of the viscous resistance of a capillary, which is not valid for blood flow in capillary, the viscosity depends strongly upon the radius of the capillary. And the

assumed steady laminar flow of a Newtonian fluid in capillary does not lead to a minimal viscous resistance, this is contrary to their second assumption that energy dissipated is minimized. Dodds *et al.* also pointed out the contradiction existed in West *et al.*'s theory, and the optimization procedure based on Poiseuille formula is seen to yield $a \approx 1$ rather than $a=3/4$ [17].

He and Chen[18] tried to explain the allometry by taking into account the pH value, and they predicted 1/2-law, 2/3-law, and 3/4-law for, respectively, one-dimensional, two-dimensional, and three-dimensional organisms

$$B \propto M^{D/(D+1)}, \quad (9)$$

where D is the dimension of space, B is the basal metabolic rate of an organism, M is the mass of the organism.

Using E-infinity theory, we predict that

$$B \propto M^{(D_H-1)/D_H}, \quad (10)$$

where $D_H = 4.236\cdots$.

Taylor *et al.* found that the maximal metabolic rate induced by exercise scales with $M^{0.86}$ rather than $M^{0.75}$ [19]. Darveau *et al.*[20] gave an explanation that metabolic rate is a complex feature that results from a combination of functions, and they apply the notion of distributed control that is being used in relation to biochemical pathways. Wang *et al.*[21] reconstructed Kleiber's law at the organ-tissue level, and they found that 4 metabolically active organs, brain, liver, kidneys and heart, have high specific resting metabolic rates when compared with the remaining less-active tissues, such as skeletal muscle, adipose tissue, bone and skin. Brain, liver, kidneys and heart together account for ~60% of resting energy expenditure in humans, even though the 4 organs represent <6% of body mass.

It is still a conundrum of why different organs in mammals have different allometric cascades, and how basal metabolic rate and maximal metabolic rate take different scaling forms continues to exercise biologists. Our theory now can successfully explain these mysterious phenomena[22-28].

3. The Fourth Dimension of Life

In 1997, Blum[29] suggested that the 3/4-law can be understood by a four dimensional approach. In $D+1$ dimensions, the "area" A of the hypersurface enclosing a $D+1$ dimensional hypervolume scales like $A \propto V^{D/(D+1)}$, where D is the spatial dimension of the organism. When $D=3$, we have $A \propto V^{3/4}$, a four dimensional construction.

The fourth dimension of life have caught much attention since West *et al.*'s work[26]. But so far no physical explanation is given for the fourth dimension of life. We have proved that[27]

$$n \propto r \quad (11)$$

for three dimensional organisms, so the fourth dimension of life exists only in three dimension organs, such as heart and kidneys. If a cell is isolated from a heart of a rat, no 4th dimension is endowed. However, if enough number of heart cells are cultivated and accumulated together in three dimensions, the isolated cardiac cell begins to beat[30], and the 4th dimension of life is endowed.

Diversity of motion patterns in nature suggests different scaling patters in biology by constraints. Constraining a particle motion will naturally change its motion patterns, similarly artificial or natural energetic constraint of cell growth may alter expected scaling patters. If heart cells are cultivated on a plane, the isolated cardiac cells can not beat[30].

The scaling relationship between metabolic rate, B , and body mass, M , can be generally expressed as $B \propto M^{3/4}$. The height of an animal scales as $L \propto M^{1/4} \propto V^{1/4}$, where V is the total volume of the animal, implying a fourth dimension of life, see "The Fourth Dimension of Life: Fractal Geometry and Allometric Scaling of Organisms" by West, Brown, and Enquist[31].

4. Fifth-dimension of Brain

Consider a mammal brain, and assume that there are N brain cells, we have[28]

$$N \propto r^2 \quad (12)$$

$$r \propto V^{1/5} \quad (13)$$

$$B_{brain} \propto M_{brain}^{4/5} \quad (14)$$

Eq.(13) endows a fifth dimension of mammal brains and we call it thought-dimension. Eq.(12) elucidates that a mammal brain works functionally depending upon its net construction.

5 . Memory and Thought

A brain cell is of fractal construction, and a cell can produce various fractal images by stimulation. The fractal picture corresponds to the information memorized in the brain, so a brain cell is a repository of information. Memory and the acquired immunity in humans are the very ability to re-collect the past fractal pictures in brain cells, thought in humans is capable of re-arranging the past known fractal pictures in such a way to draw a new fractal image in the brain.

$$B_{memory} \propto M_{memory}^{D/(D+1)} \quad D \rightarrow \infty \quad (15)$$

Why more complex viruses (for examples, influenza virus, HIV-virus, SARS-virus) tend to be more fatal? The paper concludes that the fractal geometry of viruses is the key.

The brain cells are not of sphere as other body cells in humans do. The brain is made up of many cells, including neurons and glial cells. The branching dendrites and the axon of a neuron make the brain cell more complex than the usual spherical cells do, see the picture of a brain cell in the web

The fractal geometry of a brain cell might be slightly changed by stimulation, the original fractal geometry recovers after the stimulation is eliminated. When a mosquito bites you on your arm, your another hand will be instructed to hit it. The procedure reflects the fractal picture of the cell. So a fractal picture is a repository of information, when we “read” the fractal picture, the same conduct is done according to the instructions just as a mosquito attack you.

In case simulation is too strong for brain cells to recover their original forms, the nerve system will be injured, leading to, for examples, reduction of retentive faculty , aphasia, or most seriously, neuropathy. This procedure is just as same as the deformation of an elastic solid under the action of a given system of forces.

5. Of Kleiber’s Law in Biology and Newton’s Second Law[28]

We find a linking of Kleiber’s law in biology to Newton’s law of motion.

We consider first a single particle of mass m , moving subject to a force field. The potential energy and kinetic energy will change, but the total energy is conserved in the procedure:

$$T + U = \text{constant}, \quad (16)$$

where U is the kinetic energy, and T is the potential energy, $T = m\dot{\mathbf{r}}^2 / 2$.

The equation for the motion can be derived in view of calculus of variations, i.e.,

$$\int_0^t (U - T) dt \rightarrow \max., \quad (17)$$

from which we obtain the well-known Newton’s law of motion in the form:

$$m\ddot{\mathbf{r}} + \mathbf{F} = 0, \quad (18)$$

where the force vector is defined as

$$\mathbf{F} = -\frac{\partial U}{\partial \mathbf{r}} + \frac{d}{dt} \left(\frac{\partial U}{\partial \dot{\mathbf{r}}} \right). \quad (19)$$

Now we study the metabolic procedure in biology. Nature selection has tended to maximize metabolic capacity, by maximizing its exchange surface area for absorbing enough resources from the environment.

$$B \rightarrow \max., \quad (20)$$

where B is metabolic rate. But the metabolic procedure is constrained by the fixed energy supply and fixed body mass.

$$B_0 = \text{constant}, \quad (21)$$

$$M = \text{constant}, \quad (22)$$

where B_0 is the total energy supply, and M is the body mass.

Assume that there are n basal cells with characteristic (or typical) radius r in the organism, we have the following scaling relations:

$$B_0 \propto nB \propto M, \quad (23)$$

$$nr^3 \propto M. \quad (24)$$

Note that in the above relations (23) and (24), M is an invariant.

The metabolic rate B of the organ scales linearly with respect to its total surface:

$$B \propto nr^2. \quad (25)$$

From (24) and (25), we can easily obtain the following relation:

$$B \propto n \left(\frac{M}{n} \right)^{2/3} = n^{1/3} M^{2/3}. \quad (26)$$

In view of (23), we have

$$nB \propto n^{4/3} M^{2/3} \propto M, \quad (27)$$

which leads to the result:

$$n \propto M^{1/4}. \quad (28)$$

and

$$r \propto M^{1/4} \propto V^{1/4}. \quad (29)$$

Substituting (28) into (27) results in the Kleiber's law, which reads

$$B \propto M^{3/4}. \quad (30)$$

The Kleiber's law is considered as a ubiquitous law in biology, but this is not the fact. He and Chen[18] pointed out that the Kleiber's law holds only for three dimensional organisms.

The Kleiber 3/4 law implies a fourth dimension of life as pointed out by West et al.[31]. In Ref.[28] we discussed the fifth dimension of brain. It is interesting to image a kind of 2-dimensional beings who live in a plane as illustrated in Fig.1, where the line between A and B cells ban the beings in A and B from seeing each other. The 2-dimensional beings can never understand what 3-dimensional beings do. But in a three dimension view, we can see simultaneously the beings at different cells. Similarly we could not see what my colleagues in a

neighbor office were doing, however, a four dimension eye could see what happened in all offices simultaneously. Maybe an UFO is a projection of higher dimension beings into our real three dimensional world? We can not detect its motion and its communication in a dimension higher than 3. So the most effective encryption technique is of higher dimensions.

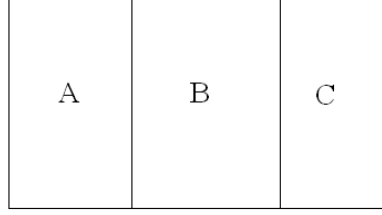


Fig.3 2-dimeninal beings. 2-dimensional life ? Super dimensional life?

Temperature and life

The scaling relationship between metabolic rate, B , and body mass, M , can be generally expressed as

$$B \propto M^a, \quad (31)$$

where a is the scaling exponent, it is a temperature-related function. Early studies proposed, and found in preliminary data, that if home range size is directly proportional to resource needs, then $a \approx 3/4$. Later studies with more data, however, found that, for all tropical groups combined, $a \approx 1$. The scaling exponent is an important biological parameter. For example, the life span, L , scales as

$$L \propto M^{1-a} \quad (32)$$

Gilloly *et al.* suggested the following model[32]

$$B \propto M^{3/4} e^{-E_i/kT}, \quad (33)$$

where E_i represents an average activation energy for the rate-limiting enzyme-catalyzed biochemical reactions of metabolism, T is the absolute temperature(in degrees K), k is Boltzmann's constant.

White *et al.* gave a correction for temperature difference in the form[33]

$$M_C = M 10^{(T_c - T_b) \log Q_{10} / 10}, \quad (34)$$

where M_C is the temperature-corrected basal metabolic rate, T_c is the temperature to which all observations corrected ($36.2^\circ C$), and Q_{10} is the factorial increase in BMR associated with a temperature increase of $10^\circ C$.

Hereby we suggest another modified scaling relationship in the form

$$B \sim M^{\frac{3}{4} + \frac{T-30}{40}} \quad (35)$$

The prediction (35) is valid within the limited range of “biologically relevant” temperatures between approximately $0^\circ C$ and $40^\circ C$. This is the range that organisms commonly operate within under natural conditions. Near $0^\circ C$, metabolic reactions cease due to the phase transition associated with freezing water, and above approximately $40^\circ C$, metabolic reaction rates reduced by the increasing influence of catabolism.

The life span, is, therefore, predicted as

$$L \propto M^{1-T/40} \quad (36)$$

The increase of temperature leads to the increase of metabolic rate, decrease of life span[23].

Effects of CO₂ and Temperature on Biomass of Parasitic Plants

Global warming has attracted considerable attention in recent years. The increase of global mean surface temperature and atmospheric CO₂ concentration lead to the increase of metabolic rate of plants. This might lead to an unexpected threat from parasite plants for plants, and *Cryptomeria fortunei* with more than a millennium millennia year old in Mount Tian-Mu, Zhejiang province, People's Republic of China, seemingly the most vulnerable. The Mountain Tianmu Nature Reserve is an ancient rare plant treasure-house and is called an "ancient tree kingdom" of 2,160 species of plants including 37 species of what are named as "Tianmu" plants. There are totally 2,150 *Cryptomeria fortunei* in the area, the height of which can reach as high as 54 meters, and its diameter can arrive at 3.6 meters. Parasite plants, which first appeared in early 1990s, and now almost all *Cryptomeria fortunei* in this area are infected, triggers serious disease and death in a very short time. Climate change and carbon dioxide emissions have already been causing in the region of 585 deaths of the ancient trees and 335 *Cryptomeria fortunei* in serious danger of death, see Fig.1.



Fig.2 Parasitic Plant and its Host-*Cryptomeria fortunei* in Mountain Tainmu Nature Reserve.

The 2/3-law for plants reads:

$$B \propto M^{2/3}, \quad (37)$$

where M is the total inner bark mass.

The 2/3-law is valid for predicting maximal plant height[34]

$$L \propto D^{2/3} \quad (38)$$

where D - maximal basal stem diameter, L - maximal plant height

$$M \propto DL \propto D^{5/3} \quad (39)$$

where M is the total mass

$$B \propto D^{10/9} \quad (40)$$

Elevation of CO₂ concentration enhances photosynthesis. Considering the effect of CO₂ on plant's metabolic rate, the scaling law, Eq.(6), can be modified as follows

$$B \propto M^{2/3+\beta(C-C_0)} \quad (41)$$

where C_0 is the normal ambient CO₂ concentration, β is a constant. The maximal scaling exponent can never exceed 1, i.e.,

$$\left[\beta(C - C_0) \right]_{\max} = 1/3 \quad (42)$$

In case of sufficient CO₂, we have approximately

$$B_{co_2} \propto M \quad (43)$$

Considering the effects of CO₂ and temperature on plant's metabolic rate, the scaling law, Eq.(6), can be modified as follows

$$B \sim M^{2/3+\alpha(T-T_0)+\beta(C-C_0)} \quad (44)$$

where

$$\left[\alpha(T - T_0) + \beta(C - C_0) \right]_{\max} = 1/3 \quad (45)$$

Similarly the basal metabolic rate of the parasite, b_p , scales as

$$b_p \propto m^{3/4} \quad (46)$$

where m is the parasite biomass supported by the host body.

Parasitic plants are a group of exploitative organisms that have evolved to utilize another plant's resources (for reviews, see Phoenix and Press, 2005; Press and Phoenix, 2005). They tap into the xylem or phloem stream of their host and withdraw water, mineral nutrients and carbohydrates through the haustorium, a structure which provides vascular continuity from parasite to host.

The maximal basal metabolic rate of a parasite should not be larger than the basal metabolic rate of its host body, or the host will die of malnutrition, we call it consistence of metabolic rates of a parasitic plant and its host. Under such an assumption, we have[22]

$$b_{p\max} \propto B \quad (47)$$

leading the scaling relationship between the maximal parasite biomass and its host body mass, which reads

$$M^{2/3+\alpha(T-T_0)+\beta(C-C_0)} \propto m^{3/4} \quad (48)$$

or

$$m \propto M^{8/9+4\alpha(T-T_0)/3+4\beta(C-C_0)/3} \quad (49)$$

Under normal conditions, we have

$$m_0 \propto M^{8/9} \quad (50)$$

Affecting by CO₂ or temperature, the maximal parasite biomass scales as

$$m_{co_2} \propto M^{4/3} \quad (51)$$

That means increase of CO₂ or temperature leads to more biomass of parasitic plant.

Climate change is a far greater threat to the world than terrorism. The Reserve is one of famous sightseeing places in China and then is an ideal place for scientific survey, education practice, sightseeing and tour.

A boom in world tourism is posing a huge threat to some of the planet's most sensitive ecosystems, according to a study released last week.

Acknowledgement: The project is supported by National Natural Science Foundation of China under grand No.10772054 and the Program for New Century Excellent Talents in University under grand No. NCET-05-0417.

References

- [1] MS El Naschie. The cosmic Da Vinci code for the big bang - a mathematical toy model, *Int. J. Nonlinear Sci.*, 8 (2007): 191-194
- [2] MS El Naschie. Quantum probability without a phase and a topological resolution of the two-slit experiment, *Int. J. Nonlinear Sci.*, 8 (2007): 195-198
- [3] MS El Naschie. Deterministic quantum mechanics versus classical mechanical indeterminism, *Int. J. Nonlinear Sci.*, 8 (2007): 5-10
- [4] MS El Naschie. A review of applications and results of E-infinity theory, *Int. J. Nonlinear Sci.*, 8 (2007): 11-20
- [5] MS El Naschie. Probability set particles, *Int. J. Nonlinear Sci.*, 8 (2007): 117-119
- [6] MS El Naschie. On an eleven dimensional E-infinity fractal spacetime theory, *Int. J. Nonlinear Sci.*, 7 (2006): 407-409
- [7] MS El Naschie. The brain and E-Infinity, *Int. J. Nonlinear Sci.*, 7 (2006): 129-132
- [8] MS El Naschie. A review of E infinity theory and the mass spectrum of high energy particle physics, *Chaos Solitons & Fractals* 19 (2004): 209-236
- [9] 't Hooft, G. In search of the ultimate building blocks. Cambridge University Press, 1997
- [10] 't Hooft, G. A confrontation with infinity, Nobel Lecture, Dec. 8, 1999.
- [11] He JH, Xu L, et al. *Chaos Solitons & Fractals*,
- [12] Rubner, M. *Zeitschrift fur Biologie*, 19, 1883, 536-562
- [13] Kleiber M. Body size and metabolism, *Hilgardia*, 6, 1932, 315-353
- [14] West GB, Brown JH, Enquist BJ. A general model for origin of allometric scaling laws in biology, *Science*, 276(5309), 1997, 122-126
- [15] Weibel ER. Physiology: the pitfalls of power laws, *Nature*, 417, 2002, 131-132
- [16] Dawson TH. Allometric scaling in biology, *Science*, 281(5378), 1998, 751
- [17] Dodds PS, Rothman DH, Weitz JS. Re-examination of the 3/4-law of metabolism, *Journal of Theoretical Biology*, 209(1), 2001, 9-27
- [18] He JH, Chen H. Effects of size and pH on metabolic rate, *Int. J. Nonlinear Sci.*, 4(2003): 429-432
- [19] Taylor CR et al. *Respir. Physiol.* 44, 1981, 25-37
- [20] Darveau CA, Suarez RK, Andrews RD, Hochachka PW. Allometric cascade as a unifying principle of body mass effects on metabolism, *Nature*, 417, 2002, 166-170
- [21] Wang ZM, O'Connort TP, Heshka S, Heymsfield SB. The reconstruction of Kleiber's law at organ-tissue level, *Journal of Nutrition*, 131, 2001, 2967-2970
- [22] He JH, Mo LF, Xu L. On body size of infected mice, *Acta Tropica*, 104(2007) 140-141
- [23] He JH. Shrinkage of body size of small insects: A possible link to global warming? *Chaos Soliton. Fract.*, 34(2007) 727-729
- [24] He JH. Cell size and cell number as links between noncoding DNA and metabolic rate scaling, *Chaos Soliton. Fract.*, 28(2006) 1026-1028
- [25] He JH. An allometric scaling law between gray matter and white matter of cerebral cortex, *Chaos Soliton. Fract.*, 27(2006) 864-867

- [26] He JH, Huang ZD. A novel model for allometric scaling laws for different organs, *Chaos Soliton. Fract.*, 27(2006) 1108-1114
- [27] He JH. The allometry of leaf form in early plant ontogeny, *Bullet. Math. Biol.*, 67(2005): 1333-1337
- [28] He JH, Zhang J. Fifth dimension of life and the 4/5 allometric scaling law for human brain, *Cell Biol. Int.*, 28(2004) 809-815
- [29] Blum JJ. On the geometry of four-dimensions and the relationship between metabolism and body mass. *J. Theor. Biol.*, 64, 1997, 599-601
- [30] NASA microgravity research highlights, Advancing heart research, reprinted from the Spring 2000 issue of *Microgravity News*. Detailed information is published in *American Journal of Physiology*, 277(Heart Circ. Physiol.46), 1999, H433-H444 and *Biotechnology and Bioengineering*, 64, 1999, 580-589
- [31] West GB, Brown JH, Enquist BJ. The Fourth Dimension of Life: Fractal Geometry and Allometric Scaling of Organisms, *Science*, 284, 1999, 1677-1679
- [32] Gillooly, J.F., Brown, J.H., West, G.B., Savage, V.B., Charnov, E.L., Effects of size and temperature on metabolic rate, *Science*, 293, 2248-2251 (2001)
- [33] White, C.R. & Seymour, R.S. Mammalian basal metabolic rate is proportional to body mass $2/3$. *Proc. Natl. Acad. Sci., USA* 100(7), 4046-4049 (2003)
- [34] McMahon TA. 1973. The mechanical design of trees. *Science* 233: 92–102.

Futalognkosaurus dukei: cost and benefit of being the biggest

Ji-Huan He¹, Qin Yang¹, Lu-Feng Mo²

1. Modern Textile Institute, Donghua University, 1882 Yan'an Xilu Road, Shanghai 200051, China Email: jhhe@dhu.edu.cn

2. School of Information Engineering, Zhejiang Forestry College, Lin'an 311300, Zhejiang, China

Abstract

A giant herbivore called *Futalognkosaurus dukei* measured between 32 and 34 meters from head to tail was uncovered in Argentina. An allometric approach is suggested to estimate its mass and its life-span, predicting its mass between 200 and 400 tons, and its maximal life-span of about 500 years. The rocketing population and no prey and limited food source during the late Cretaceous period might be the main forces pushing the biggest animals to be extinct.

Keywords: metabolic rate; Dinosaurs, allometry, weight-length relationship

1. Introduction

The skeleton of what is believed to be a new dinosaur species called *Futalognkosaurus dukei* - a 32 meters plant-eater that is among the largest dinosaurs ever found - has been uncovered in Argentina (Calvo, et al. 2007). Our question is how heavy the gigantic herbivorous *F. dukei* is. Body mass is a major selective force in evolution and a key structuring force in ecosystems. Various theories have been arisen recently to explain various biological phenomena, such as allometrical

method(West et al., 1997; Kuikka 2006), statistical method(Al-Suwaiyel et al., 2006)) and E-infinity theory(El Naschie, 2006; El Naschie 2007). In particular, using a blend of the methodology of allometrical scaling and E-infinity theory it was possible to solve various basic problems in biology(He 2006a, He 2006b, He 2006c, He 2007).

2. The Fourth Dimension of Life

The simplest way to estimate the weight of an animal is to calculate its volume. By simple geometric analysis, we have

$$H \propto V^{1/3} \quad (1)$$

where H is the length or height of the animal, V is the estimated volume. The volume is proportional to body mass, M , so we have

$$H \propto M^{1/3} \quad (2)$$

If Eq.(2) were valid, life and nonlife were not so different. Actually nature endows life an additional dimension (West et al., 1999).

Allometric laws in biology enable us to estimate the mass of such a gigantic herbivorous *F. dukei*. A biological variable Y is related allometrically to the mass M of the organism by a power law(West et al., 1997):

$$Y \propto M^b \quad (3)$$

where b is the so-called allometric exponent, and Y can be, for example, the length of an animal from head to tail, H , which scales as (West et al., 1997)

$$H \propto M^{1/4} \quad (4)$$

From this scaling relationship, we can, for example, from a polar bear with mass of 0.5 ton and length of 2.5 meters to predict the mass of an elephant with length of 5 meters:

$$M_{elephant} = k 0.5 \times \left(\frac{7.5}{2.5}\right)^4 = 40k \quad (5)$$

where k is a constant, $0 < k < 1$. The value of k depends upon the ratio of the masses of the compared animals. For this problem, we can write $k = (2.5/7.5)^\delta$, which tends to 1 when the two compared species are very much closed. In case $\delta = 1$, we can obtain $H \propto M^{1/3}$ which is valid for non-life solids. Here we choose $k = 0.15$, and predict $M_{elephant} = 6$ tons. We choose $k = 1$ for inter-species estimation. If a man and a woman live together at exactly same conditions, and we know the woman has weight of 60 kilograms and height of 165 mm, and the man is 175 mm high, we can predict the mass of the man as $M_{man} = 60 \times (175/165)^4 = 76kg$.

Accordingly the mass of this biggest animal can be estimated from an elephant with mass of 6 tons and length of 7.5 meters:

$$M_F = k 6 \times \left(\frac{32}{7.5}\right)^4 = 1988k \quad (6)$$

In case $k = 0.15$, the mass of *F. dukei* is estimated to be 300 tons. It needs eat about 9-12 tons of grasses, 3-4% of its weight.

The allometric scaling relationship between life-span, L , and body mass can be expressed as (West et al., 1997; 1999)

$$L \propto M^{1/4} \quad (7)$$

They could live on the Earth without prey, and shared natural life peacefully just as human beings are doing now. Accordingly we can predict its maximal life-span with the data of human beings: mass 70kg, life-span 70 years

$$L_{max} = 70 * \left(\frac{300}{0.07}\right)^{1/4} = 500 \text{ years} \quad (8)$$

This biggest animal could live as long as half century !

Now let's consider hypothetical *F. dukei*. Let's say we start with two *F. dukeis*. After a time, they produce two new *F. dukeis*. The final number follows the well-known Fibonacci sequence, that is exponential growth.

3. Discussion and Conclusions

We give a very simple allometric method for predicting the mass of *F. dukei*. The rocketing population and no prey and limited energy source might be the main forces pushing the biggest animals to be extinct.

Our approach is very simple but rigorous, the obtained result might be of importance, and the theory would be easily extended to other animals or plants.

Acknowledgement: The project is supported by National Natural Science Foundation of China under grand No.10772054 and the Program for New Century Excellent Talents in University under grand No. NCET-05-0417.

References

- Al-Suwaiyel, M.I., Alani, A., Al-Swailem, A., 2006. An investigation of Fibonacci-like sequences in biology and mathematics, *Int. J. Nonlinear Sci.*, 7, 133-136
- Calvo JO, Porfiri JD, Gonzalez-Riga BJ, Kellner AWA, 2007. A new Cretaceous terrestrial ecosystem from Gondwana with the description of a new sauropod dinosaur, *ANAIS DA ACADEMIA BRASILEIRA DE CIENCIAS* 79 (3): 529-541
- El Naschie, M.S., 2006. The brain and E-Infinity, *Int. J. Nonlinear Sci.*, 7, 129-132
- El Naschie, M.S., 2007. A review of applications and results of E-infinity theory, *Int. J. Nonlinear Sci.* 8, 11-20
- He, J.H., Zhang, J., 2004. Fifth dimension of life and the 4/5 allometric scaling law for human brain, *Cell Biol. Int.*, 28, 809-815
- He, J.H., 2005. The allometry of leaf form in early plant ontogeny, *B. Math. Biol.*, 67, 1333-1337
- He, J.H., 2006. Cell size and cell number as links between noncoding DNA and metabolic rate scaling, *Chaos Soliton. Fract.*, 28, 1026-1028

- He, J.H.,2006. An allometric scaling law between gray matter and white matter of cerebral cortex, *Chaos Soliton. Fract.*, 27,864-867
- He, J.H., 2006. Application of E-infinity theory to biology, *Chaos Soliton. Fract.*, 28, 285-289
- He, J.H., Huang Z.D.,2006. A novel model for allometric scaling laws for different organs, *Chaos Soliton. Fract.*, 27, 1108-1114
- He,J.H., 2007. Shrinkage of body size of small insects: A possible link to global warming? *Chaos Soliton. Fract.*, 34, 727-729
- Kuikka, J.T.,2006. Fractal analysis of organ structure, function and interactions, *Int. J. Nonlinear Sci.*, 7, 239-243
- He, J.H., Mo, L.F., Xu, L. , 2008. On body size of infected mice, *Acta Trop*, in press
- West, G.B., Brown, J.H., Enquist, B.J.,1997. A general model for origin of allometric scaling laws in biology, *Science*, 276, 122-126
- West, G.B., Brown, J.H., Enquist, B.J., 1999, The Fourth Dimension of Life: Fractal Geometry and Allometric Scaling of Organisms , *Science*,284, 1677-1679

COMPLEX EVOLUTION OF BUILT ENVIRONMENT

H. Serdar KAYA, Fulin BÖLEN

Abstract

Urban transformation process is consists of several changes in space and time. These changes include, social, economic, physical, political, ecologic and some other factors which constitute the city as a complex system. As the spatial organisation of the cities is a kind of reflection of that factors, this research focused on understanding the transformation rules of the built environment as a complex system which is constituted by simple and complex sub systems.

The main question of this research is what are the transformation rules which lead the continuity or discontinuity of built environment and how the changes in built environment can be formulated to contribute the urban planning and urban design processes.

Keywords: urban morphology, chaos, fractal, space syntax

Introduction

Urban system is a complex system and consists of many subsystems. Physical organisation is one of these subsystems and it is strongly correlated with activities and quality of urban life.

As an urban planner, designer or architect, we are planning urban life by organising some subsystems and relationships. The decision making process is being done on mainly three areas. Three phases of design and evaluating urban space can be summarise as follows:

1. Organisation of movement (Most Flexible)
2. Organisation of Usage (Medium Flexibility)
3. Organisation of Space (Most Stable)

Also there is an interrelationship between them and there are some approaches about this interrelationship which try to explain the strength of correlation between urban activities and physical environment:

- “1. Environmental Determinism: The view that the physical environment determines human behaviour
2. Possibilism: The view that the physical environment provides possibilities and constraints within which people make choices based on other, mainly cultural, criteria.
3. Probabilism: The physical environment does, in fact, provide possibilities for choice and is not determining, but some choices are more probable than others in given physical settings” [48].

There are many researches from the point of view of environmental determinism, possibilism and probabilism for evaluating urban system and several methods for analysing urban spatial structure to

[* hserdarkaya@itu.edu.tr](mailto:hserdarkaya@itu.edu.tr), İ.T.Ü Mimarlık Fakültesi, Şehir ve Bölge Planlaması Bölümü, Taşkışla Binası, 34437 Taksim, Beyoğlu/İstanbul

[**bolen@itu.edu.tr](mailto:bolen@itu.edu.tr), İ.T.Ü Mimarlık Fakültesi, Şehir ve Bölge Planlaması Bölümü, Taşkışla Binası, 34437 Taksim, Beyoğlu/İstanbul

understand and explain the features of built environment. The main procedure of these methods is simplifying the complex urban system and some of them use computers for simulating and measuring. Traditional maps, axial or network maps and cellular maps are main methods for simulating. These researches can be grouped into three perspectives:

1. Researches related interrelationships: These researches concentrated on hierarchical organisations, topological properties rather than geometrical measures and system properties. Agricultural land use model with concentric rings developed by Johann Heinrich von Thünen, in 1820s, Concentric zone model developed in 1920s by Ernest W. Burgess, Harris and Ullman's multiple nuclei model, Christaller's Central places theory are some models related urban form and location of functions.

"The Principle of Least Effort" and "Rank Size Rule" are two approaches based on several researches in urban planning and other disciplines to explain the hierarchical distribution of system components [19, 24, 29, 45, and 46].

The contemporary methods of urban analysis such as fractal geometry [22, 28, 49, 50], cellular automata [4, 26, 31], fuzzy logic [6, 7, 8, 9, 10, 11, 12, 13, 14, 17, 18], and rule definition methods [1, 2, 3, 20, 21, 37, 38] representing the more realistic simulation of urban environment by using advanced mathematical models and computer software. Urban system is simplified as nodes, cells or networks in the simulation models.

2. Researches related physical and geometric properties: Urban texture can be evaluated as a whole spatial organization [20, 47], or divided to components such as streets and squares [41, 44] with their features in detail.

Geometrical properties such as dimensions, repetition of some specific ratios or numbers which have mystical meanings, as golden section, Fibonacci numbers, are used to analyze architectural form and spatial orientation of urban elements. [27, 35, 39] Furthermore, these geometric features evaluated as a language which represents socio-cultural environment and some shape grammars were produced.

Added to these, the contribution of interdisciplinary researches based on analogies between urban structure and thermodynamics and entropy in physics are beneficial. [16, 38]

3. Researches related perception, behaviour: the effects of geometry, colour, texture on human perception; human behaviour and choice in built environment and cognitive maps are main interests of these researches. [20, 23, 25, 30, 32, 33, 34, 36, 40, 42, 43, 51, 52, 53]
4. Researches related transformation in urban structure: these researches can be classified in two group, one of them are interested in the evolution of specific city or cities, the others tries to explain evolution of cities from general perspective as urban history or general principles of evolution. Publications of Trancik, Penarai, Gebauer and Samuels shows the lost values through the changes of urban history and searching the way of regaining that values. [54, 55, 56, 57]. On the other hand, Bacon analysed mass-space, movement, time-space, geometrical features and perception through the time to understand the mechanisms underlying the spatial evolution. [40]

With the improvement in mathematics and computer technology, especially chaos and complexity theories and computer simulation techniques, evolution of cities can be analysed from the different

point of view which proposes an essentially new approach of urban space based on chaos theory and fractal geometry. [15, 58, 59, 60, 61]

According to this approach, cities are fractal and their evolution is strictly dependent to the initial conditions which it can be called as sustainability and continuity of cultural values. Especially in traditional cities, the continuity of spatial organisation and built environment in time, is one of the dominant features which gives the unique character to the cities.

Methodology

In this research, changes in physical environment have been searched. There are several parameters defined which contribute to understand the geometrical, topological and complex features of spatial organisation of urban space. Distribution of road segment lengths gives clue about geometrical features of physical environment and spatial integration values shows the changes of topological structure of transformation system. On the other hand the complex properties of built environment need to be analysed by using the more comprehensive method such as fractal analysis.

Study examined on the some squares in İstanbul. The criterion for selecting the squares are having a historical background and serving the whole city not for local groups. Taksim square was selected as one sample area and 1km X 1km square drawn around the Taksim square in İstanbul to measure the changes in spatial arrangement through the time (Figure 1).

When we look at the historical maps, the continuity of taxim square can be seen easily as an open space through the history. (Figure 2) Topography is the one of dominant factor to be chosen at this location. As in shown in figure 1, Taksim square settled at the top of hilly topography. (Figure 2)



Figure 1: Location of Taksim area

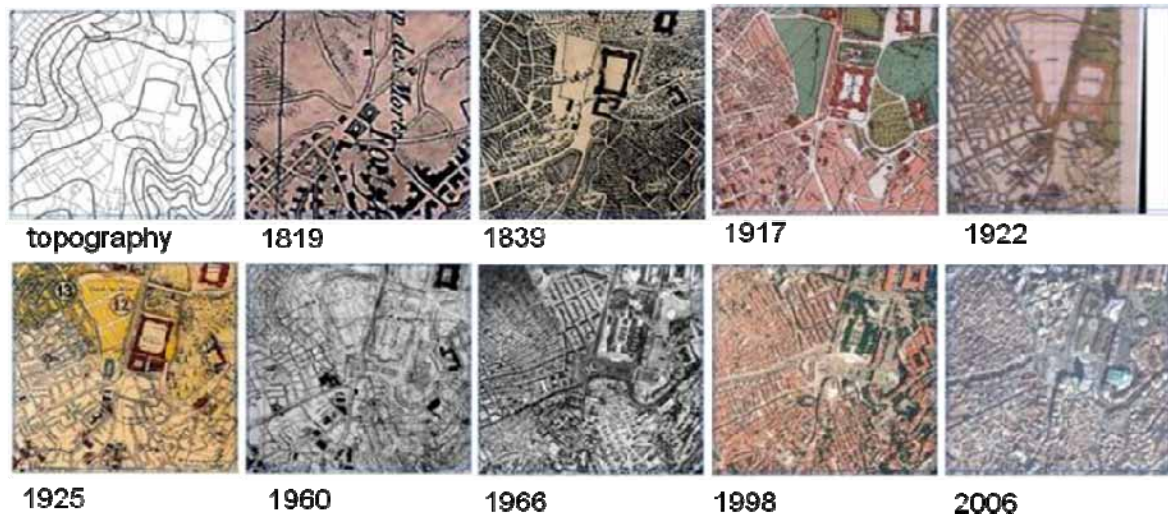


Figure 2: Transformation of built environment in Taksim Square

The comparison of two maps of 1925 and 2006 reflects the changes and continuity of built space. On the other hand, study area is differentiated and there are four main sub regions can be seen from the maps which show the building blocks and transportation systems (Figures 3-4). The building blocks getting smaller and becomes more regular rectangular blocks from the sub region 1 to region 4.

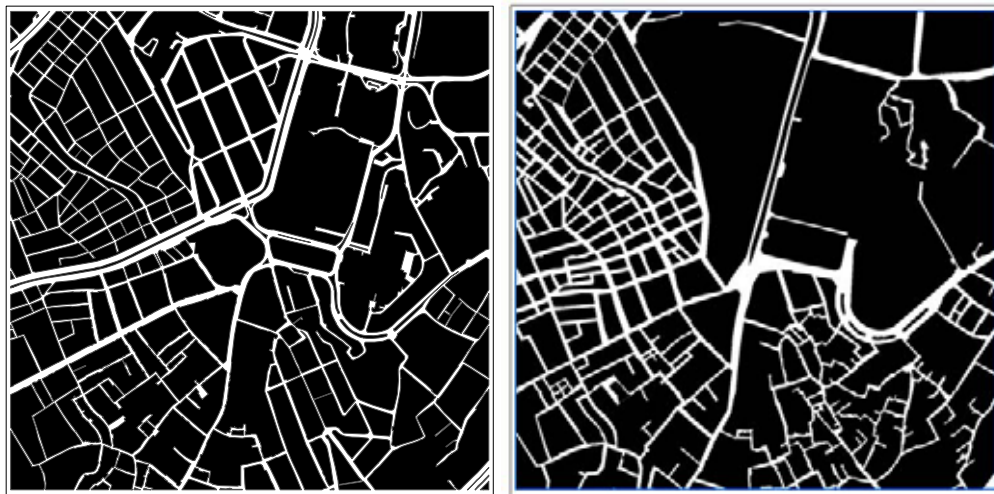


Figure 3: Taksim Square 2006 (left) and 1925 (right)

Geometrical features: Distribution of road segments

These features mainly related with urban morphology, dimensions of urban elements such as roads and streets. The distribution of geometrical differences is another method to understand the built environment.



Figure 4: Four sub regions in Taksim

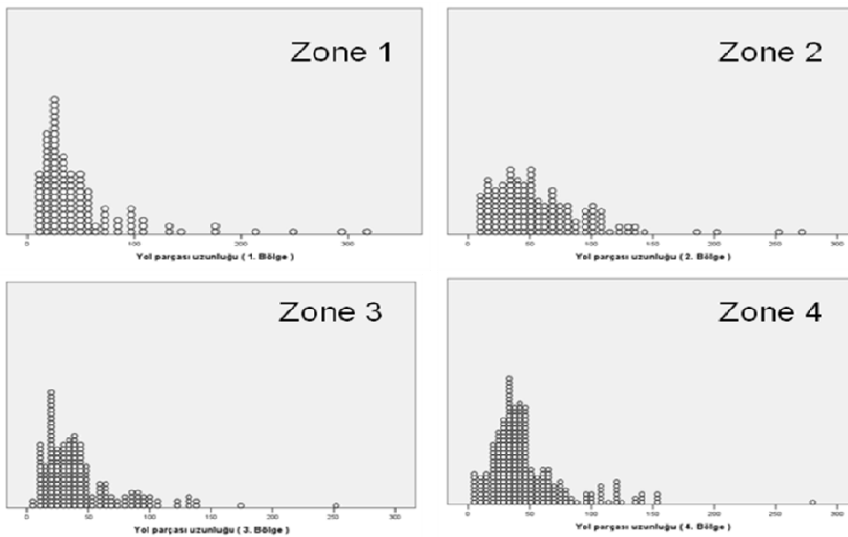


Figure 5: Distribution of road segments for sub regions.

Figure 5 shows the difference of road segment distribution of each sub regions. The bigger building blocks and grid structures causes less dispersed distribution than the organic structure.

Topological features: syntactic values

Not only distribution but also measuring their spatial configuration will contribute to understanding city structure. Syntactic analysis examined to evaluate the changes in two time segments, 1925 and 2006 and there are some differences between them. (Figure 6)

Space syntax is a technique for measuring the relative accessibility of different locations in a spatial system. Space syntax method is interested in movement and especially “natural movement” which means the movement in urban spaces that is determined by the structure of the urban grid itself, rather than by specific attractors or generators.

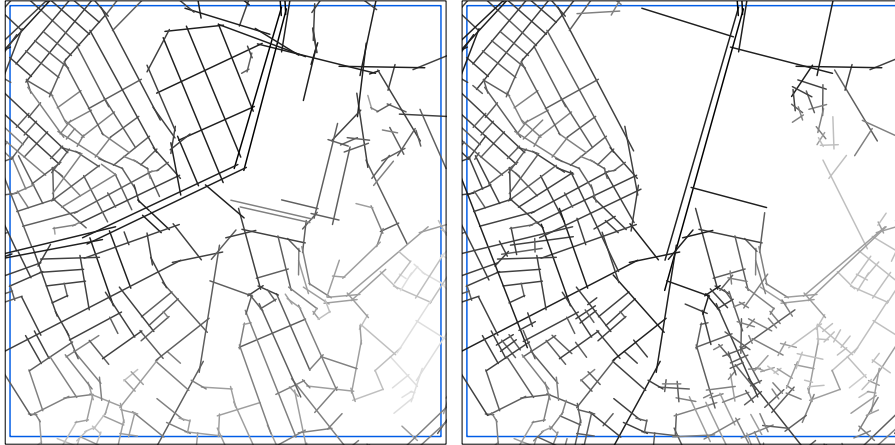


Figure 6: Global integration maps of Taksim Square in 2006 (left) and 1925 (right)

The two maps shows the changing importance of roads. After the widening the Tarlabası street, the new distribution of high global integration values moves north left of the area (figure 7). The two graphs shows the increasing integration values on few roads and decreasing the range of values which reflects the loss of balance and increasing dominance of Tarlabası street in time.

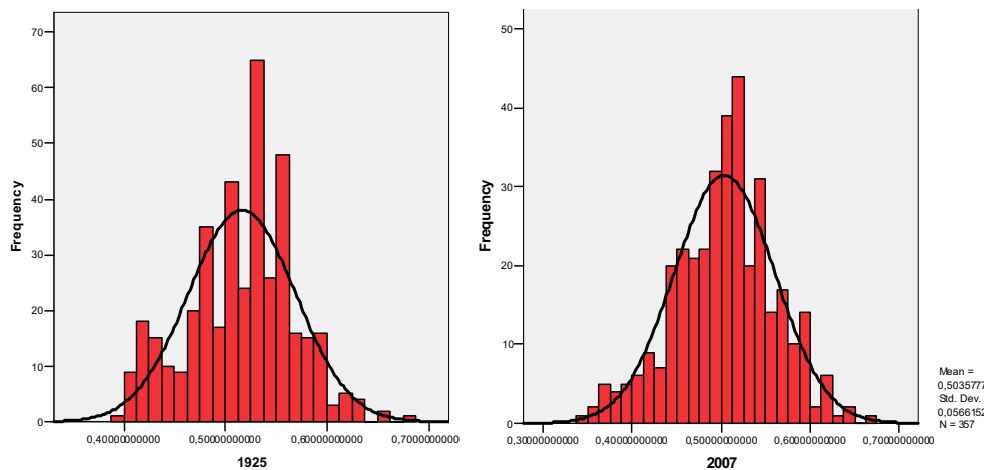


Figure 7: Changes in the distribution of global integration values.

While, the maximum value of global integration is 0,682 and minimum 0,397 in 1925, the maximum value decreased to the 0,667, and minimum value is 0,341 and this shows us Tarlabası street change the balance in the network of study area as increasing the accessibility on few roads but not all the road network.

Complex features: Fractal dimension (Figure 8)

Fractal dimension has three main components:

1. Initial Object: Basic Geometry
2. Generator: Transformation rule, Scaling
3. Fractal Object: Complex Geometry

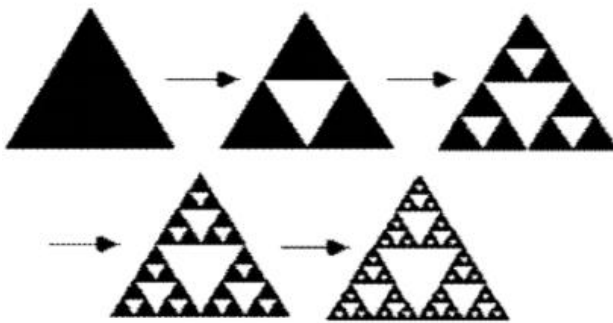


Figure 8 Fractal object: Sierpinsky gasket

Urban space is a kind of fractal object which has similar properties with fractals (Figure 9)

1. Initial Object: Topography, natural nevironment
2. Generator: Buildings, roads, city blocks, restrictions, laws
3. Fractal Object: Urban texture

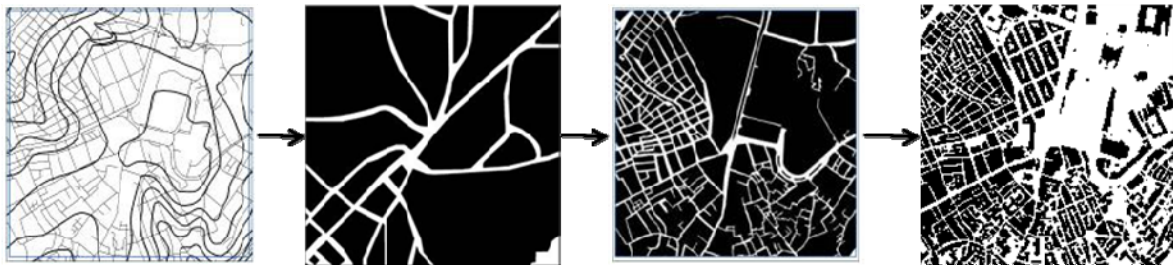


Figure 9 Urban spaces as fractal object

The built environment consists of three main components as city blocks, roads and buildings. These three components give the main character to the settlements.

Although the built environment is fractal, there is a difference between artificial fractals produced by computers and spatial organisation of settlements. Spatial organisation is not pure fractals and they have different fractal dimensions in different scales. Other features of artificial fractal objects is self similar structure in all scales which are not applicable to the built environment.

Although there are several methods for calculating fractal dimension, the box counting method is the most suitable to analyse urban environment (Figure 10).

The formula of box counting dimension is as follows:

$$\text{Fractal Dimension, } D = [\log N(2^{-(k+1)}) - \log N(2^{-k})] / [\log 2^{k+1} - \log 2^k] = \log_2 [N(2^{-(k+1)}) / N(2^{-k})]$$

N is representing the count of boxes intersecting the objects such as city blocks, buildings or roads

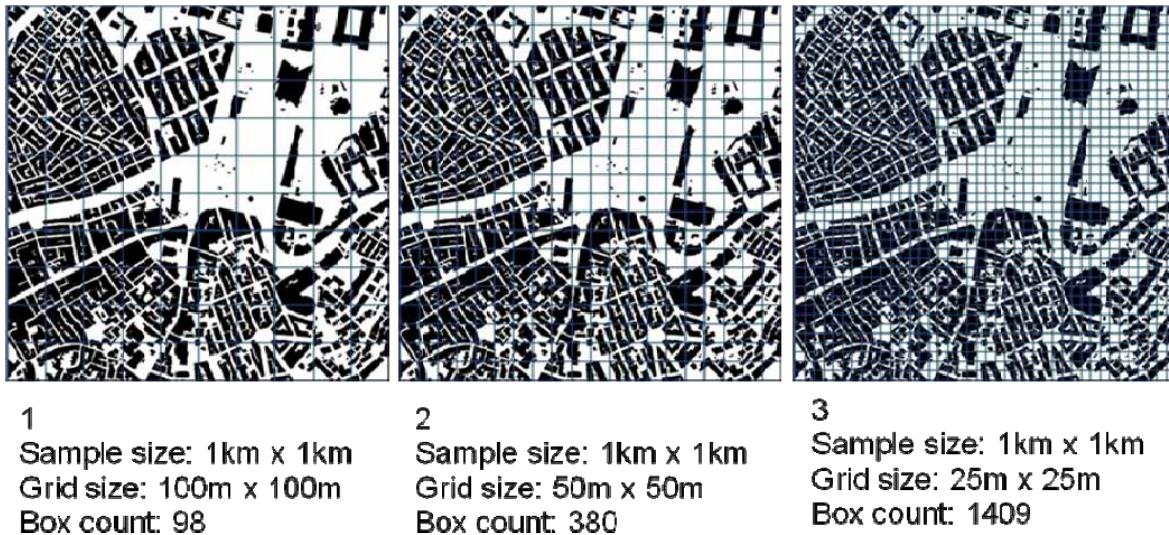


Figure 10: calculating box counting dimension

$$D1 = [\log 380 - \log 98] / [\log 20 - \log 10] = 1,955$$

$$D2 = [\log 1409 - \log 380] / [\log 40 - \log 20] = 1,891$$

Fractal dimension of built environment changes depends on the grid size. Because of this reason, in this research the one fractal analysis program “HarFa” have been used to calculate fractal dimension over 400 times. [62]

The fractal analysis of three components of built space during the time is as follows:

1. Fractal dimension of buildings

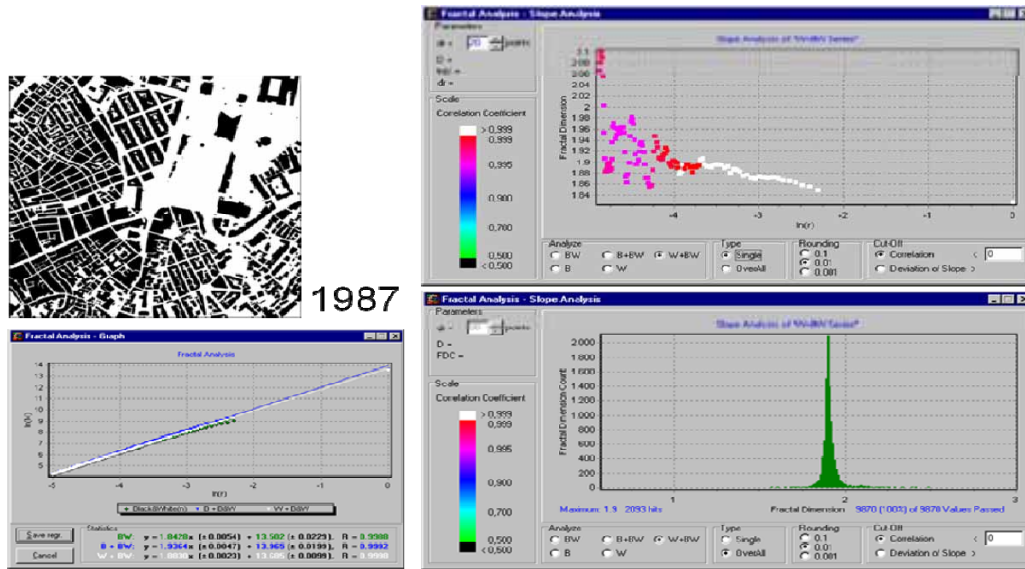


Figure 11: Fractal dimension of Buildings in 1987

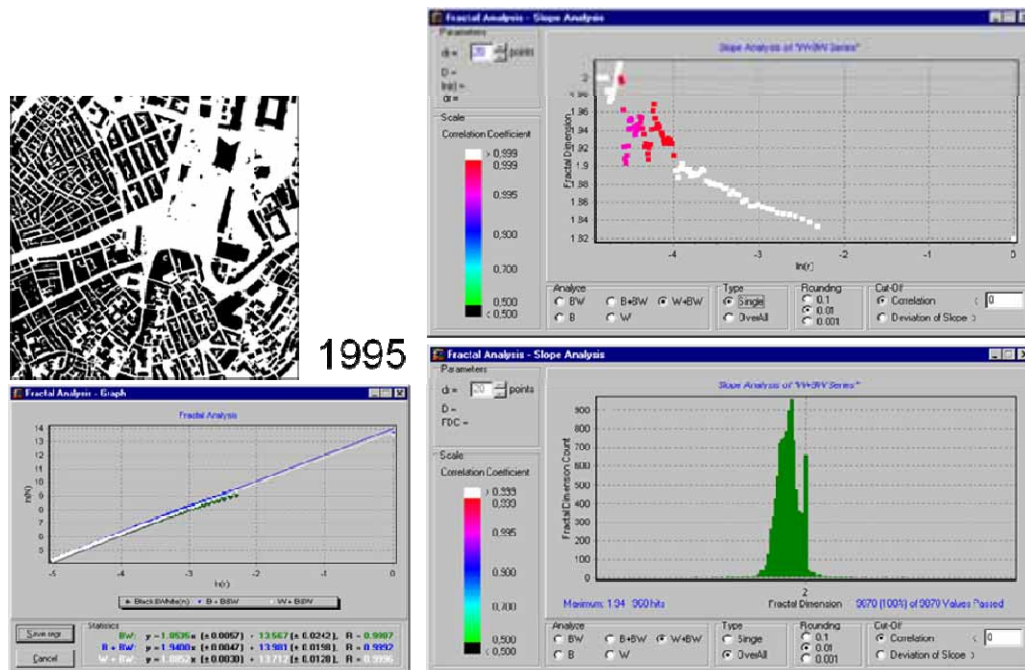


Figure 12: Fractal dimension of Buildings in 1995

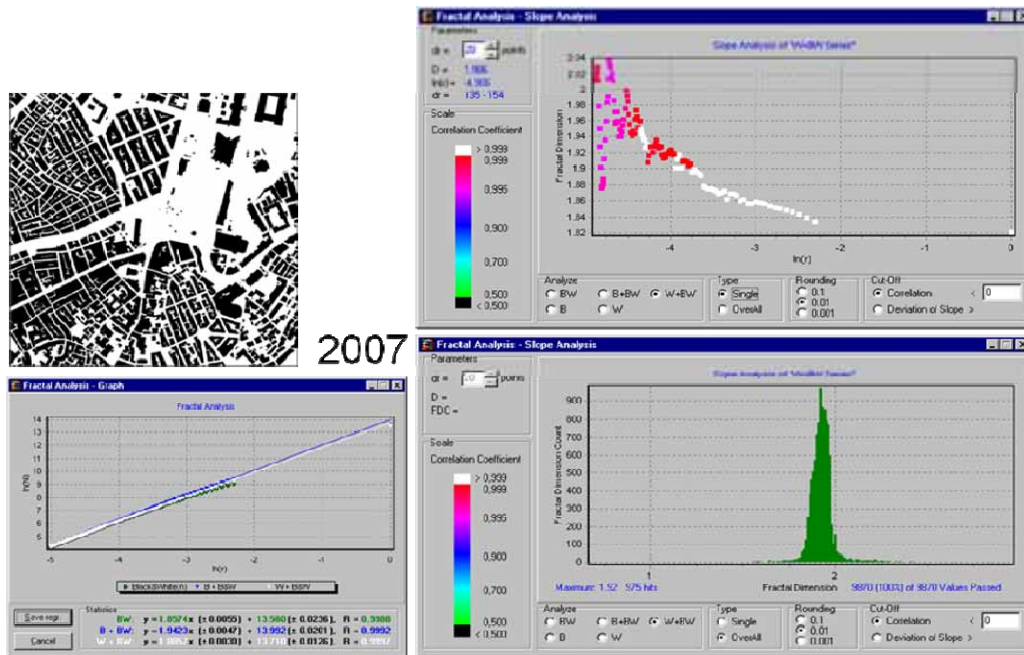


Figure 13: Fractal dimension of Buildings in 2007

Fractal dimension of buildings 1,9 and there is not big change over the time (Figures 11-13).

2. Fractal dimension of City Blocks

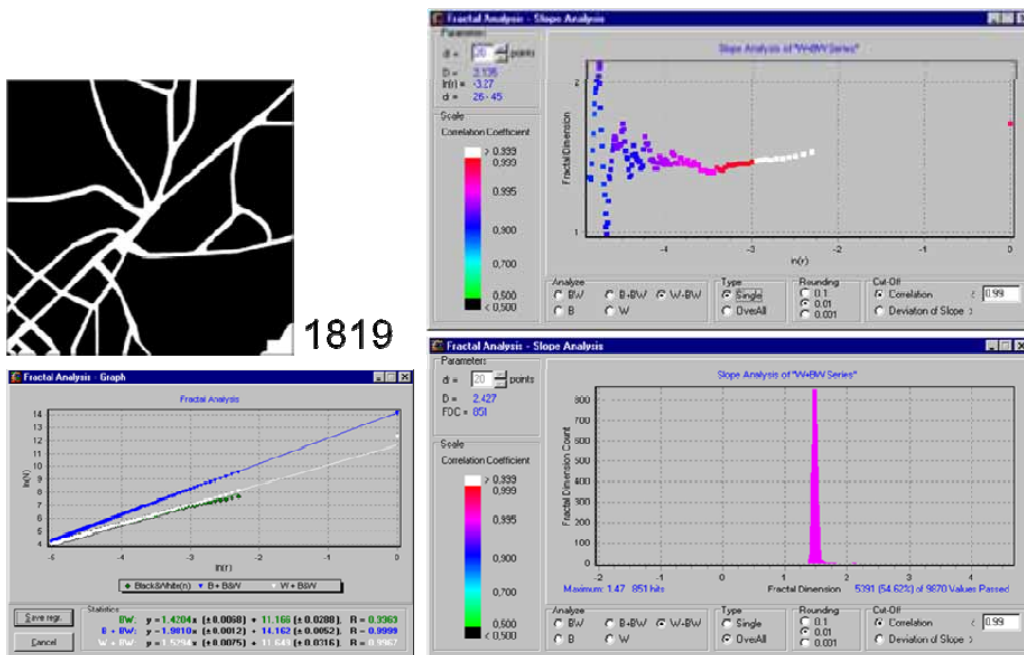


Figure 14: Fractal dimension of City Blocks in 1819

In 1819, the building blocks are bigger than that in 1925 and this affects the fractal dimension of building blocks. The fractal dimension is 1, 47 and it increased to the value of 1,83 in the year of 1925 and reaches 1,96 in 2007. The small size and complex geometry of city blocks is the main reason for this increase (Figures 14-17).

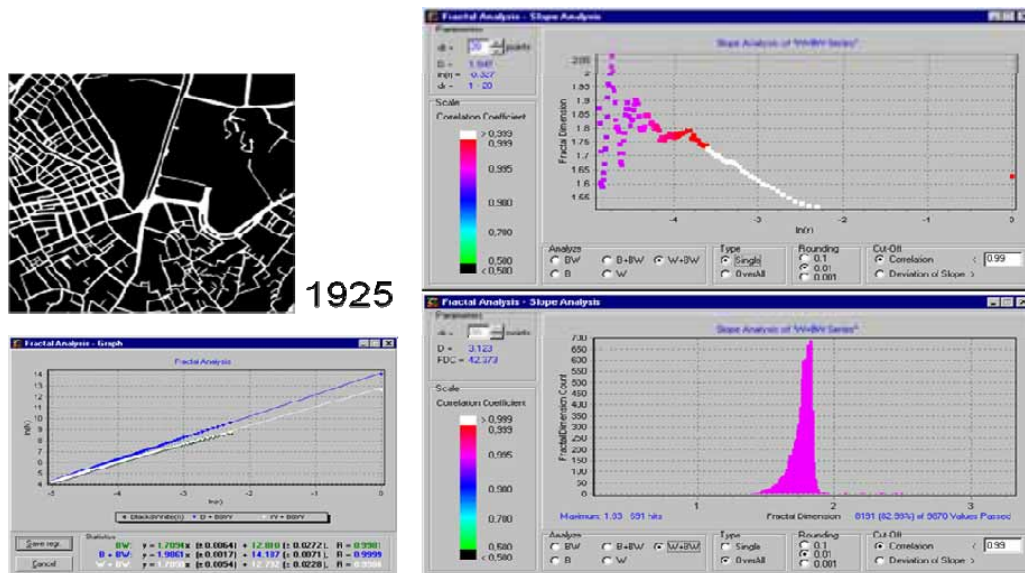


Figure 15: Fractal dimension of City Blocks in 1925

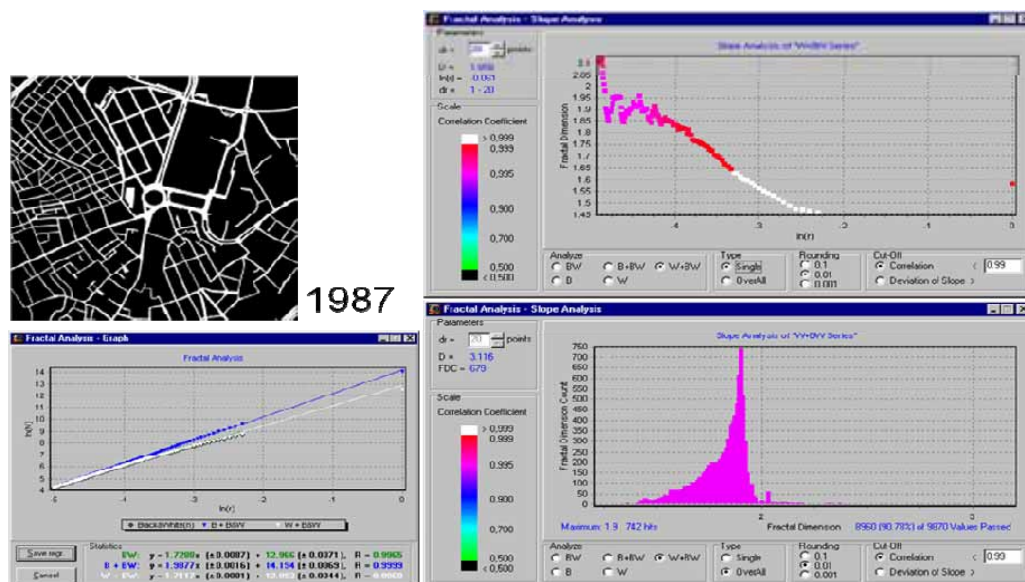


Figure 16: Fractal dimension of City Blocks in 1987

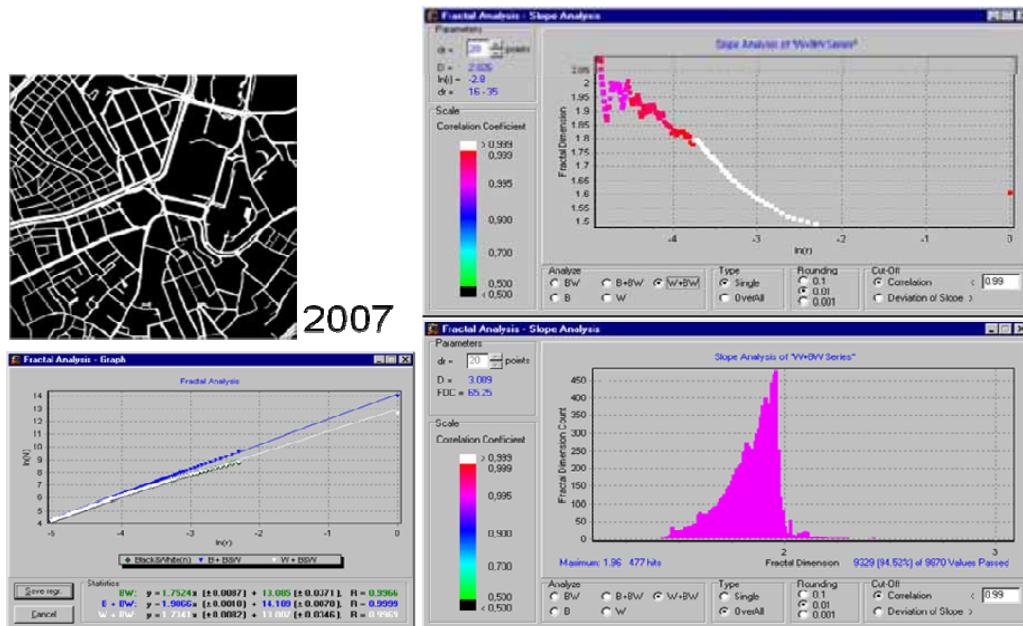


Figure 17: Fractal dimension of City Blocks in 2007

3. Fractal dimension of roads

The change in fractal dimensions of roads during the time is similar with the city blocks. In 1819 there are only main arterials existed. The fractal dimension in this year is, 1,46 (Figure 18).

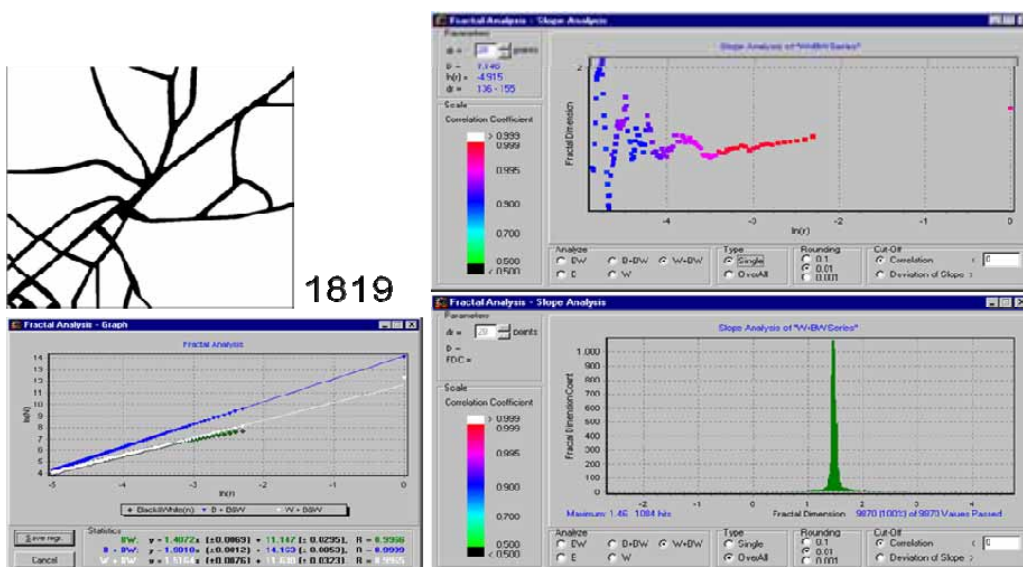


Figure 18: Fractal dimension of Roads in 1819

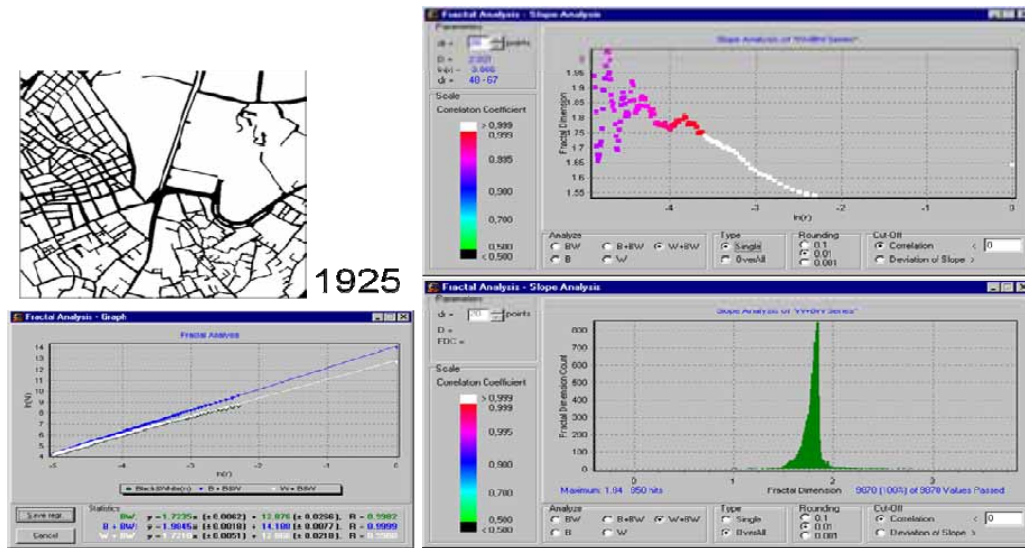


Figure 19: Fractal dimension of Roads in 1925

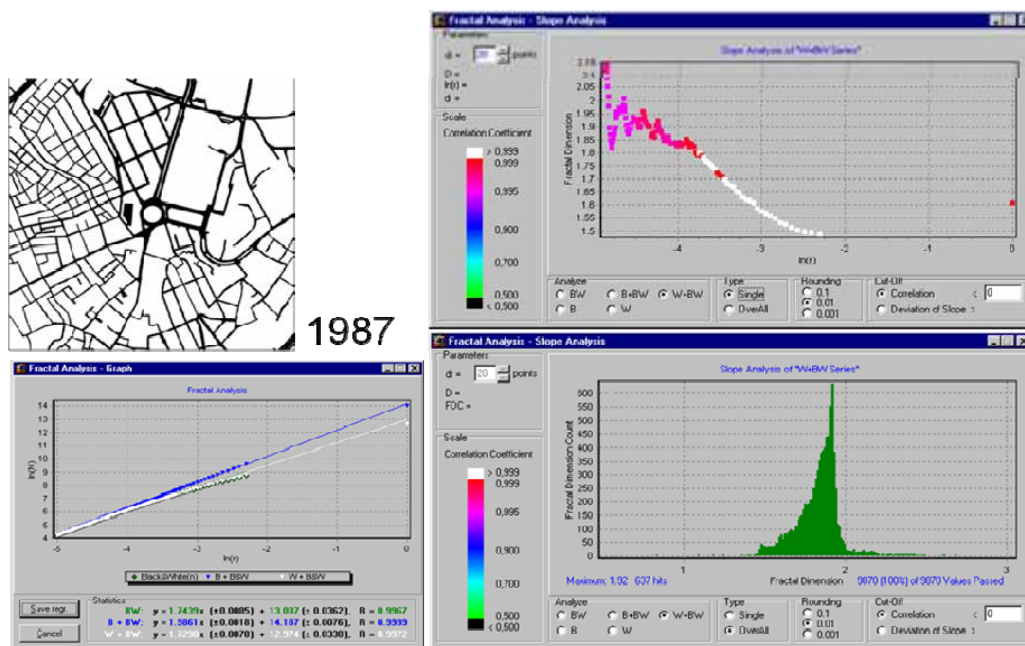


Figure 20: Fractal dimension of Roads in 1987

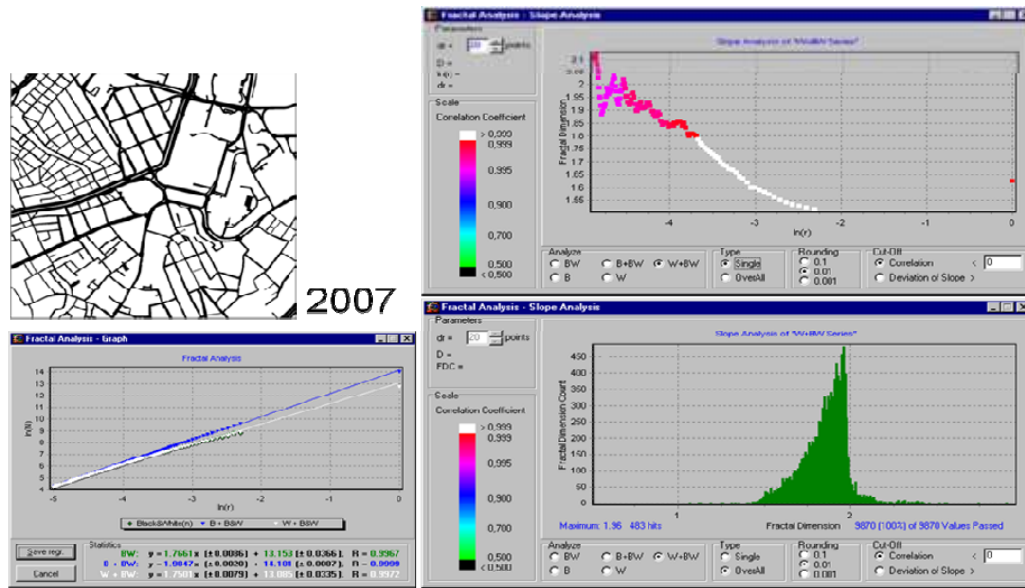


Figure 21: Fractal dimension of Roads in 2007

TAKSİM	Year	Fractal Dimension
Buildings	1987	1,9
	1995	1,94
	2007	1,92
City Blocks	1819	1,47
	1925	1,83
	1987	1,90
Roads	2007	1,96
	1819	1,46
	1925	1,84
	1987	1,92
	2007	1,96

Conclusion

As a conclusion it can be said that the urban texture is a kind of fractal object and measuring fractal dimension is one of the effective methods for analysing urban texture.

Measurement results shows that Taksim has high fractal dimension which means it has high complexity level of spatial organisation of urban texture which is increasing in time by adding new buildings, roads or dividing the city

blocks into small parts. Similar values of fractal dimension in different years can be evaluated as a continuity of spatial organization of built environment in time.

This research lead us to search more to find a regularity of the change of spatial organisation. Although some findings shows us that it is possible to measure the changes in physical organisation, this area need to be searched more such as fractality of transportation network and buildings.

ACKNOWLEDGEMENT

This study was supported by the Turkish Scientific and Technological Research Council of Turkey (TUBITAK) under the 2214 - Fellowship Program.

REFERENCES

- [1] Alexander, C. , (1966), Notes on The Synthesis of Form, Harvard University Press,Cambridge, Massaschusetts
- [2] Alexander, C. , (1977), A Pattern Language, Oxford University Press, New York
- [3] Alexander, C. , ve diğ.,(1987), A New Theory of Urban Design, Oxford University Press, New York ve Oxford
- [4] Batty, M., Hutchinson, B., (1983), Sytems Analysis In Urban Policy-Making and Planning, Plenum press, New York and London
- [5] Forrester, J. W., (1969), Urban Dynamics, The M.I.T. Press, Cambridge, Massachusetts
- [6] Akkerman, A., (1992), "Fuzzy targeting of population niches in urban planning and the fractal dimension of demographic change," *Urban Studies* 29(7): 1093-1114
- [7] Albrecht, J.,Guesgen, H. , A Combinatorial Fuzzy Set-Theoretic Approach to the Mapping Between Quantitative and Qualitative Data,
http://divcom.otago.ac.nz/SIRC/GeoComp/GeoComp98/49/gc_49.htm
- [8] Altman, D. A., (1994), ``Fuzzy set theoretic approaches for handling imprecision in spatial analysis" *International Journal of GIS* 8 271-289
- [9] Banai, R., (1993), ``Fuzziness in geographical information systems: contributions from the analytic hierarchy process" *International Journal of GIS* 7 315 -329
- [10] Bezdek, J. C., (1981), Pattern Recognition with Fuzzy Objective Function Algorithms. New York: Plenum Press.
- [11] Bezdek, J.C., Sankar, P. K., (1992), Fuzzy Models For Pattern Recognition: Methods That Search for Structures in Data. New York: IEEE Press.
- [12] Dragicevic, S., (2001), Space, time, and dynamics modeling in historical GIS databases: a fuzzy logic approach, *Environment and Planning B: Planning and Design* 2001, volume 28, pp. 545-562
- [13] Heikkila, E. J., (2003), Fuzzy urban sets: theory and application to desakota regions in China, *Environment and Planning B: Planning and Design* 2003, vol.30, p.239-254
- [14] Kosko, B. , (1994), Fuzzy Thinking, Harper Collins Manufacturing, Glasgow, UK
- [15] Rodin, V. A. , Rodina, E. V. ,(2003), Typology and Conformity to Natural Laws of "Chaotic City" Development, http://www.urbanchaosresearch.com/article_japan.doc
- [16] Stamps, A.E, (2003), Advances in visual diversity and entropy, *Environment and Planning B: Planning and Design* 2003, volume 30, pages 449-463
- [17] Sui, D.Z., (1992), A fuzzy GIS modelling approach for urban land evaluation, *Comput., Environ. and Urban Systems*, Vol. 16, pp. 101-115,1992
- [18] Şen, Z. , (2001), Bulanık Mantık ve Modelleme ilkeleri, Bilge Kültür Sanat yay. , İstanbul

- [19] Zipf, G. K., (1972), Human behavior and the principle of least effort, Hafner Publishing Company, New York
- [20] Lynch, K. , (1960), The Image of the City, M. I. T. Presss, Cambridge, Mass.
- [21] Lynch, K. , (1984), Good City Form, MIT. Press., Cambridge, Mass
- [22] Wurster, C. B. , (1969), Cities and Space; The Future Use of Urban Land:The Book is based on 1962 RFF(Resources For The Future). Forum on The Future Use of Urban Space, The Johns Hopkins Presss, Baltimore and London
- [23] Kwan, M.P., (2000), Analysis of human spatial behavior in a GIS environment: Recent developments and future prospects, Journal of geographical Systems, Springer-verlag
- [24] Gabaix, X., (1999), Zipf's law for cities: An explanation, The quarterly Journal of Economics, August
- [25] Guy, B., (2002), Mental Morphology, AESOP, Volos
- [26] Batty, M., Xie, Y., Sun, Z., (1999), Modeling urban dynamics through GIS-based cellular automata, Computers, Environment and Urban Systems, 23, s.205-233
- [27] Teller, J., (2003), A spherical metric for the field-oriented analysis of complex urban open spaces, Environment and Planning B: Planning and Design, vol. 30, s. 339-356
- [28] Salingaros, N. A., (2003), Connecting the Fractal City, <http://www.math.utsa.edu/sphere/salingar/connecting.html>
- [29] Chen, Y., Zhou, Y., (2003), The rank-size rule and fractal hierarchies of cities: mathematical models and empirical analyses, Environment and Planning B: Planning and Design, 2003, vol. 30, s. 799 – 818
- [30] Jiang, B., (1999), SimPed: Simulating Pedestrian Flows in a Virtual Urban Environment, Journal of Geographic Information and Decision Analysis, vol.3, no.1, s. 21-29
- [31] Dietzel, C., ve Clarke, K. C., (2004), Spatial Differences in Multi-Resolution Urban Automata Modeling, Transactions in GIS, (2004), 8(4): 479–492
- [32] Helbing, D., (1998), Models for Pedestrian Behavior, <http://www.theo2.physik.uni-stuttgart.de/helbing.html>
- [33] Helbing, D., Molnar, P., (1998), Self-Organization Phenomena in Pedestrian Crowds, <http://www.theo2.physik.uni-stuttgart.de/helbing.html>
- [34] Helbing, D., (1998b), A Mathematical Model for the Behavior of Pedestrians, <http://www.theo2.physik.uni-stuttgart.de/helbing.html>
- [35] March, L., Steadman, P., (1974), The Geometry of Environment: an introduction to spatial organization in design, Methuen and Co Ltd., London, UK.
- [36] Giritlioğlu, C. , (1998), Şehirselsel mekan öğeleri ve tasarımı 1, İ.T.Ü Mimarlık fakültesi Baskı atölyesi, İstanbul
- [37] Salingaros, N. A. , (1997), Life and Complexity in Architecture From a Thermodynamic Analogy, www.math.utsa.edu/sphere/salingar
- [38] Klinger, A. ,Salingaros, N. A. , 2000. A Pattern Measure, Environment and Planning B; Planning and Design, Vol. 27, s. 537-547
- [39] Steadman J.P., (1983), Architectural Morphology: An introduction to the geometry of building plans, Pion Ltd., London
- [40] Bacon, E. N., 1982, Design Of Cities, M.I.T Press, U.S.A
- [41] Çelik, Z., Favro, D., Ingersoll, R., (1994), Streets: Critical Perspectives on Public Space, Univ. Of California Press, California
- [42] Hillier, B., (1997), "The Hidden Geometry of Deformed Grids", SSS1, London, UK
- [43] Hillier B., (1996), "Space is the Machine", Cambridge Univ. Press, Cambridge, UK
- [44] Moughtin, C., (1992), Urban Design: Street and Square, Butterworth-Heinemann Ltd., Oxford
- [45] Newton, J. Moura, Jr., Ribeiro, M. B., (2006), Zipf law for Brazilian cities, Physica A 367, s. 441–448

- [46] Pietronero, L., Tosatti, E., Tosatti, V., Vespignani, A, (2001), Explaining the uneven distribution of numbers in nature: the laws of Benford and Zipf, *Physica A* 293, s. 297–304
- [47] Wingo Jr., L. (Ed), (1969), *Cities and Space: The future use of urban land*, John hopkins Press, Baltimore and London
- [48] Rapoport, A. , (1977) *Human Aspects of Urban Form*, Pergamon Presss, Oxford
- [49] Trippet, J. ,(2007), *A Pattern Language of Sustainability Ecological Design and Permaculture*, www.holocene.net/dissertation.htm
- [50] Gleick, J. , (1997) *Kaos*, Tübitak yayınları, Ankara
- [51] Appleyard, D ve diğ. (1964), *The View from the Road*, M. I. T, Presss, Cambridge, Mass.
- [52] Cullen, G. , (1961,) *Townscape*, The Architectural Presss, London
- [53] Ünlü, A. , (1998), *Çevresel Tasarımda İlk Kavramlar*, İ. T. Ü Mimarlık Fakültesi Yayınları, İstanbul
- [54] Kostof, S. , (1991), *The city Shaped, Urban Patterns and Meanings Throughout History*, Little, Brown and Company, Boston
- [55] Trancik, Roger, (1986), *Finding Lost Space*, Van Nostrand Reinhold, New York
- [56] Gebauer, M. A. ,(1983), *Samuels, Urban Morphology*; Oxford, *A Place for A Forum*, Oxford Polytechnic, JCUD, Oxford
- [57] Rossi, A. , (1985), *The Architecture of the City*, MIT Presss, Massachusetts
- [58] Peitgen, H. O. / Jürgens, H. / Saupe, D. , (1993), *Chaos and Fractals, New frontiers of Science*, Springer-Verlag Presss, New York
- [59] Tippet, Joanne, (1994), *A Pattern Language of Sustainability Ecological Design and Permaculture*, www.holocene.net/dissertation.htm
- [60] Cramer, F. , (1998), *Kaos ve Düzen*, Alan yayıncılık,
- [61] Gleick, J. , (1997), *Kaos*, Tübitak yayınları, Ankara
- [62] <http://www.fch.vutbr.cz/lectures/imagesci>

The new class of super-implicit second derivative multistep methods for stiff systems

M. Mehdizadeh Khalsarayi *, M.Y. Rahimi Ardabili, G. Hojjati

Faculty of Mathematical Science, University of Tabriz, Tabriz, Iran

Abstract

In this paper we present details of a new class of implicit formulas of second derivative linear multistep methods to integrate ordinary differential equations (IVPs) numerically. The formulas, which we call it super-implicit, are of more implicitness than the so-called implicit formulas in the sense that they require the knowledge of functions not only at the past and present step-point, but also at the two future ones. In order to obtain higher order A -stable, $A(\alpha)$ -stable multistep methods, we have used second derivatives of the solutions, additional stages and two super future points, which give the class of general linear methods. The stability analysis is discussed and an improvement is obtained in stability region. More numerical experiments and comparison with several popular codes are given, showing strong superiority of this new class of methods.

Keywords : Stiff ODEs, Super Implicit, Multistep and Multiderivative Methods, stability aspects.

1 Introduction

In recent years the problems of deriving more advanced and efficient methods for stiff problems has received a great deal of attention, and as a result a wide variety of approaches have been proposed. A potentially good numerical method for the solution of stiff systems of ODEs must have good accuracy and some reasonably wide region of absolute stability^[5]. One of the first and most important stability requirement particularly for linear multistep method, is that A -stability which proposed in^[6]. However, the requirement of A -stability puts some limitations on the choice of suitable linear multistep methods. Dahlquist proved that the order of an A -stable linear multistep method must be ≤ 2 and that an A -stable multistep method must be implicit. This pessimistic result has encouraged researches to seek other classes of numerical methods for solving stiff equations.

The search for higher order A -stable multistep methods is carried out in the two main directions :

- use higher derivatives of the solutions,
- throw in additional stages, off-step points, super-future points and like. This leads into the large field general linear methods^[7].

One successful proposal in this direction was introduced by Enright^[6] that used second derivative of solution in his algorithm, Cash^[3] and Ismail^[10] and Hojjati^[9] introduced second derivative multistep methods that have good stability properties. These methods are A -stable of high orders. The new class of second derivative multistep methods that we introduce requiring not just past and present but also two future values and they have good stability and accuracy properties.

*Corresponding Author, e-mail : m-mehdizadeh@tabrizu.ac.ir

Here, we construct A -stable super-implicit methods for the numerical solution of the stiff initial value problems. The superiority of this new class of methods is A -stability of order 8.

This study is arranged as follows :

In the second section, second derivative multistep method (SDMM) is described . In the third section, the new class of super-implicit second derivative multistep methods (SISDMM) is introduced. In the forth section, the stability behavior of our approaches is analyzed and a comparison is made with existing methods for A -stability orders. The numerical results and advantages of the method are discussed in the final section.

2 Second derivative multistep methods (SDMM)

Let us consider the stiff initial value problem

$$y'(x) = f(x, y(x)) \quad , \quad y(x_0) = y_0$$

on the finite interval $I = [x_0, x_N]$ where $y : I \rightarrow R^m$ and $f : I \times R^m \rightarrow R^n$ is continuous and differentiable.

SDMM can written in the form

$$\sum_{j=0}^k \alpha_j y_{n+j} = h \sum_{j=0}^k \beta_j f_{n+j} + h^2 \sum_{j=0}^k \gamma_j g_{n+j} \quad (1)$$

where α_j, β_j and γ_j are parameters to be determined $g_{n+j} = f_{n+j}^{(1)}$. If either β_k or γ_k is nonzero, the formula is implicit.

Taylor expansion shows that method (1) is of order p if and only if

$$\sum_{j=0}^k \alpha_j j^q = q \sum_{j=0}^k \beta_j j^{q-1} + q(q+1) \sum_{j=0}^k \gamma_j j^{q-2}, \quad 0 \leq p \leq q$$

some known important SDMM schemes that will be used for comparison are as follows :

- The Enright^[6] k -step formulas of order $k+2$ which takes the following form :

$$y_{n+1} - y_n = h \sum_{j=0}^k \beta_j f_{n+j-k+1} + h^2 \gamma_k g_{n+1}$$

- Second derivative extended backward differentiation formulas (E2BD), that was introduced by Cash^[3] with the following form :

class 1 :

$$\text{Predictor :} \quad y_{n+k} - y_{n+k-1} = h \sum_{j=0}^k \beta_j f_{n+j} + h^2 \gamma_k g_{n+k}$$

$$\text{Corrector :} \quad y_{n+k} - y_{n+k-1} = h \sum_{j=0}^{k+1} \bar{\beta}_j f_{n+j} + h^2 (\bar{\gamma}_k g_{n+k} + \bar{\gamma}_{k+1} g_{n+k+1})$$

and

class 2 :

$$\text{Predictor :} \quad y_{n+k} - y_{n+k-1} = h \sum_{j=0}^k \beta_j f_{n+j} + h^2 \gamma_k g_{n+k}$$

$$\text{Corrector :} \quad y_{n+k} - y_{n+k-1} = h \sum_{j=0}^{k+1} \bar{\beta}_j f_{n+j} + h^2 \bar{\gamma}_k g_{n+k}$$

- Hojjati^[9] introduced second derivative multistep method as follows :

$$\sum_{j=0}^k \alpha_j y_{n+j} = h\beta_k f_{n+k} + h^2(\gamma_k g_{n+k} - \gamma_{k+1} g_{n+k+1})$$

3 Two super-implicit second derivative multistep methods (SISDMM)

We are going to introduce a special class of super-implicit secondary derivative multistep methods with the following general form :

$$\sum_{j=0}^k \hat{\alpha}_j y_{n+j} = h(\hat{\beta}_k f_{n+k} + \hat{\beta}_{k+1} f_{n+k+1} + \hat{\beta}_{k+2} f_{n+k+2}) + h^2(\hat{\gamma}_k g_{n+k} - \hat{\gamma}_{k+1} g_{n+k+1}) \quad (2)$$

Assuming that the solution values $y_n, y_{n+1}, \dots, y_{n+k-1}$ are available, the way in which (2) is used in practice is by carry out the following computations:

stage 1 : Compute \bar{y}_{n+k} as the solution of

$$\sum_{j=0}^k \alpha_j y_{n+j} = h\beta_k f_{n+k} + h^2\gamma_k g_{n+k} \quad (3)$$

stage 2 : Compute \bar{y}_{n+k+1} as the solution of

$$\sum_{j=0}^k \alpha_j y_{n+j+1} = h\beta_k f_{n+k+1} + h^2\gamma_k g_{n+k+1} \quad (4)$$

stage 3 : Evaluate

$$\bar{g}_{n+k+1} = g(x_{n+k+1}, \bar{y}_{n+k+1}) \quad (5)$$

stage 4 : Compute \bar{y}_{n+k+2} as the solution of

$$\sum_{j=0}^k \alpha_j y_{n+j+2} = h\beta_k f_{n+k+2} + h^2\gamma_k g_{n+k+2} \quad (6)$$

stage 5 : Compute y_{n+k} as the solution of

$$\sum_{j=0}^k \hat{\alpha}_j y_{n+j} = h(\hat{\beta}_k f_{n+k} + \hat{\beta}_{k+1} f_{n+k+1} + \hat{\beta}_{k+2} f_{n+k+2}) + h^2(\hat{\gamma}_k g_{n+k} - \hat{\gamma}_{k+1} g_{n+k+1}) \quad (7)$$

Table 1: Coefficient in (2)

[illegible]

Table 2: Coefficient in (3)

[illegible]

Lemma 1. Let

- (i) formula (3) is of order $k+1$,
 - (ii) formula (2) is of order $k+4$,
 - (iii) the implicit algebra equations defining \bar{y}_{n+k} , \bar{y}_{n+k+1} and \bar{y}_{n+k+2} are solved exactly,
- then scheme (2) has order $k+2$.

Proof : Suppose the values $y_n, y_{n+1}, \dots, y_{n+k-1}$ be exact. From (3) we have

$$y(x_{n+k}) - \bar{y}_{n+k} = C_1 h^{k+2} y^{(k+2)}(x_{n+k}) + \mathbf{O}(h^{k+3}),$$

and for one super-future point we have

$$\begin{aligned} y(x_{n+k+1}) - \bar{y}_{n+k+1} &= C_1 h^{k+2} y^{(k+2)}(x_{n+k+1}) + \mathbf{O}(h^{k+3}) \\ &= C_1 h^{k+2} (y^{(k+2)}(x_{n+k}) + h y^{(k+3)}(x_{n+k}) + \frac{h^2}{2} y^{(k+4)}(x_{n+k}) + \dots) + \mathbf{O}(h^{k+3}) \\ &= C_1 h^{k+2} y^{(k+2)}(x_{n+k}) + C_1 h^{k+3} y^{(k+3)}(x_{n+k}) + \mathbf{O}(h^{k+3}). \end{aligned}$$

But since in (4) we apply \bar{y}_{n+k} , we must add the error of $\alpha_{k-1}(y(x_{n+k}) - \bar{y}_{n+k})$ to the above expression. Hence

$$\begin{aligned} y(x_{n+k+1}) - \bar{y}_{n+k+1} &= C_1 h^{k+2} y^{(k+2)}(x_{n+k}) + \mathbf{O}(h^{k+3}) - \alpha_{k-1} C_1 h^{k+2} y^{(k+2)}(x_{n+k}) \\ &= C_1 (1 - \alpha_{k-1}) h^{k+2} y^{(k+2)}(x_{n+k}) + \mathbf{O}(h^{k+3}), \end{aligned} \quad (8)$$

and for two super-future point we have

$$\begin{aligned} y(x_{n+k+2}) - \bar{y}_{n+k+2} &= C_1 h^{k+2} y^{(k+2)}(x_{n+k+2}) + \mathbf{O}(h^{k+3}) \\ &= C_1 h^{k+2} (y^{(k+2)}(x_{n+k}) + 2h y^{(k+3)}(x_{n+k}) + \dots + \mathbf{O}(h^{k+3})) + \mathbf{O}(h^{k+3}) \\ &= C_1 h^{k+2} y^{(k+2)}(x_{n+k}) + 2C_1 h^{k+3} y^{(k+3)}(x_{n+k}) + \mathbf{O}(h^{k+3}) \\ &= C_1 h^{k+2} y^{(k+2)}(x_{n+k}) + \mathbf{O}(h^{k+3}). \end{aligned}$$

But since in (5) we apply \bar{y}_{n+k} and \bar{y}_{n+k+1} , we must add the error of $\alpha_{k-2}(y(x_{n+k}) - \bar{y}_{n+k})$ and $\alpha_{k-1}(y(x_{n+k+1}) - \bar{y}_{n+k+1})$ to the above expression. Hence

$$\begin{aligned} y(x_{n+k+2}) - \bar{y}_{n+k+2} &= C_1 h^{k+2} y^{(k+2)}(x_{n+k}) + \mathbf{O}(h^{k+3}) - \alpha_{k-2} C_1 h^{k+2} y^{(k+2)}(x_{n+k}) - \alpha_{k-1} C_1 h^{k+2} y^{(k+2)}(x_{n+k}) \\ &= C_1 (1 - \alpha_{k-2} - \alpha_{k-1}) h^{k+2} y^{(k+2)}(x_{n+k}) + \mathbf{O}(h^{k+3}). \end{aligned} \quad (9)$$

If now $C_2 h^{k+5} y^{(k+5)}(x_{n+k}) + \mathbf{O}(h^{k+6})$ is the defect of formula (2), replacing $f(x_{n+k+1}, y_{n+k+1})$ by $f(x_{n+k+1}, \bar{y}_{n+k+1})$ and $g(x_{n+k+1}, y_{n+k+1})$ by $g(x_{n+k+1}, \bar{y}_{n+k+1})$ we obtain

$$\begin{aligned} y(x_{n+k}) - y_{n+k} &= C_2 h^{k+5} y^{(k+5)}(x_{n+k}) - \hat{\beta}_{k+1} h (f(x_{n+k+1}, y(x_{n+k+1})) - f(x_{n+k+1}, \bar{y}_{n+k+1})) \\ &\quad - \hat{\beta}_{k+2} h (f(x_{n+k+2}, y(x_{n+k+2})) - f(x_{n+k+2}, \bar{y}_{n+k+2})) \\ &\quad - \hat{\gamma}_{k+1} h^2 (g(x_{n+k+1}, y(x_{n+k+1})) - g(x_{n+k+1}, \bar{y}_{n+k+1})) \end{aligned}$$

From (8) and (9)

$$\begin{aligned} f(x_{n+k+1}, y(x_{n+k+1})) - f(x_{n+k+1}, \bar{y}_{n+k+1}) &= \frac{\partial f}{\partial y}(\eta_1)(y(x_{n+k+1}) - \bar{y}_{n+k+1}) \\ &= \frac{\partial f}{\partial y}(\eta_1)C_1(1 - \alpha_{k-1})h^{k+2}y^{(k+2)}(x_{n+k}) + \mathbf{O}(h^{k+3}) \end{aligned}$$

$$\begin{aligned} f(x_{n+k+2}, y(x_{n+k+2})) - f(x_{n+k+2}, \bar{y}_{n+k+2}) &= \frac{\partial f}{\partial y}(\eta_2)(y(x_{n+k+2}) - \bar{y}_{n+k+2}) \\ &= \frac{\partial f}{\partial y}(\eta_2)C_1(1 - \alpha_{k-2} - \alpha_{k-1})h^{k+2}y^{(k+2)}(x_{n+k}) + \mathbf{O}(h^{k+3}) \end{aligned}$$

$$\begin{aligned} g(x_{n+k+1}, y(x_{n+k+1})) - g(x_{n+k+1}, \bar{y}_{n+k+1}) &= \frac{\partial g}{\partial y}(\eta_3)(y(x_{n+k+1}) - \bar{y}_{n+k+1}) \\ &= \frac{\partial g}{\partial y}(\eta_3)C_1(1 - \alpha_{k-1})h^{k+2}y^{(k+2)}(x_{n+k}) + \mathbf{O}(h^{k+3}) \end{aligned}$$

This yields

$$\begin{aligned} y(x_{n+k}) - \bar{y}_{n+k} &= C_2h^{k+5}y^{(k+5)}(x_{n+k}) \\ &\quad - \hat{\beta}_{k+1}h\left(\frac{\partial f}{\partial y}(\eta_1)C_1(1 - \alpha_{k-1})h^{k+2}y^{(k+2)}(x_{n+k}) + \mathbf{O}(h^{k+3})\right) \\ &\quad - \hat{\beta}_{k+2}h\left(\frac{\partial f}{\partial y}(\eta_2)C_1(1 - \alpha_{k-2} - \alpha_{k-1})h^{k+2}y^{(k+2)}(x_{n+k}) + \mathbf{O}(h^{k+3})\right) \\ &\quad - \hat{\gamma}_{k+1}h^2\left(\frac{\partial g}{\partial y}(\eta_3)C_1(1 - \alpha_{k-1})h^{k+2}y^{(k+2)}(x_{n+k}) + \mathbf{O}(h^{k+3})\right) \\ &= h^{k+3}(C_2h^2y^{(k+5)}(x_{n+k}) - \frac{\partial f}{\partial y}(\eta_1)C_1(1 - \alpha_{k-1})\hat{\beta}_{k+1}y^{(k+2)}(x_{n+k}) \\ &\quad - \frac{\partial f}{\partial y}(\eta_2)C_1(1 - \alpha_{k-2} - \alpha_{k-1})\hat{\beta}_{k+2}y^{(k+2)}(x_{n+k}) \\ &\quad - \frac{\partial g}{\partial y}(\eta_3)C_1(1 - \alpha_{k-1})hy^{(k+2)}(x_{n+k})) + \mathbf{O}(h^{k+3}) \end{aligned}$$

which shows that the order of scheme (2) is $k+2$.

4 Stability analysis

We now examine the stability behavior of our approach. If we apply (3) and (7) to the test problem $y' = \lambda y$ for which $y'' = \lambda^2 y$, we get

$$\sum_{j=0}^k C_j(\bar{h})y_{n+j} = 0 \quad (10)$$

where

$$\begin{aligned} C_k &= 1 - \bar{h}\hat{\beta}_k + \bar{h}\hat{\beta}_{k+2}s_k - \bar{h}^2\hat{\gamma}_k \\ C_j &= \hat{\alpha}_j - \bar{h}\hat{\beta}_{k+1}d_j + \bar{h}\hat{\beta}_{k+2}s_j + \bar{h}^2\hat{\gamma}_{k+1}d_j, \quad j = 0, 1, \dots, k-1 \\ s_0 &= \frac{\alpha_{k-1}d_0}{A}, \quad s_1 = \frac{\alpha_{k-1}d_1}{A}, \quad s_k = \frac{\alpha_{k-2}}{A} \\ s_j &= \frac{\alpha_{j-2} + \alpha_{k-1}d_j}{A}, \quad j = 2, 3, \dots, k-1 \\ d_0 &= \frac{\alpha_0\alpha_{k-1}}{A^2}, \quad d_j = \frac{\alpha_j\alpha_{k-1}}{A^2} - \frac{\alpha_{j-1}}{A}, \quad j = 1, 3, \dots, k-1 \end{aligned}$$

and

$$\bar{h} = \lambda h, \quad A = 1 - \bar{h}\beta_k - \bar{h}^2\gamma_k$$

Therefore, the corresponding characteristic equation of k th order difference equation of the method is

$$\pi(\xi, \bar{h}) = \sum_{j=0}^k C_j \xi^j = 0 \quad (11)$$

To see the zero-stability of this new method, one can easily show that by substituting $\bar{h} = \lambda h = 0$ in (11) the resulting characteristic polynomial satisfies the root condition and so the method is zero-stable, for example see^[11].

To obtain the region of absolute stability we use the boundary locus method. By collecting coefficients of different powers of \bar{h} in (11), we obtain

$$A_8\bar{h}^8 + A_7\bar{h}^7 + A_6\bar{h}^6 + A_5\bar{h}^5 + A_4\bar{h}^4 + A_3\bar{h}^3 + A_2\bar{h}^2 + A_1\bar{h} + A_0 = 0 \quad (12)$$

where A_0, A_1, \dots, A_8 are functions of ξ . Inserting $\xi = e^{i\theta}$, Eq. (12) gives us eight roots $\bar{h}(\theta), i = 1, 2, \dots, 8$ which describe the stability domain. The corresponding (approximation) regions of $A(\alpha)$ -stability found using a numerical approach are given in Table 3.

Comparison of Table 3 and Table 4 show that our method is high order of A -stability and the region of $A(\alpha)$ -stability for our method is larger than those of the other mentioned methods.

L-stability : From (10) the characteristic equation takes the form :

$$c_0 y_n + c_1 y_{n+1} + \dots + c_k y_{n+k} = 0.$$

That is

$$y_{n+k} = -\frac{c_{k-1}}{c_k} y_{n+k-1} - \frac{c_{k-2}}{c_k} y_{n+k-2} - \dots - \frac{c_1}{c_k} y_{n+1} - \frac{c_0}{c_k} y_n.$$

We observe that $y_{n+k} \rightarrow 0$ as $\bar{h} \rightarrow \infty$ that means the method is L -stable or $L(\alpha)$ -stable according to whether the method is A -stable or $A(\alpha)$ -stable, respectively.

5 Numerical Results

In this section, we present some numerical results to compare our new class of methods SISDMM with that of other second derivative multistep methods.

Table 3: The $A(\alpha)$ -stability of some mentioned methods

Enright method			E2BDF Class 1		E2BDF Class 2		Ismail method		Hojjati method	
k	p	$\alpha(^{\circ})$	p	$\alpha(^{\circ})$	p	$\alpha(^{\circ})$	p	$\alpha(^{\circ})$	p	$\alpha_{max} (^{\circ})$
1	3	90	4	90	4	90	2	90	3	90
2	4	90	5	90	5	90	3	90	4	90
3	5	87.88	6	90	6	90	4	90	5	90
4	6	82.03	7	90	7	89	5	89.9	6	90
5	7	73.10	8	90	8	87	6	87.3	7	89.8
6	8	59.95	9	89	9	83	7	84.2	8	88.3

Table 4: The $A(\alpha)$ -stability of SISDMM methods

k	p	$\alpha(^{\circ})$	k	p	$\alpha(^{\circ})$
1	3	90	7	9	89.77
2	4	90	8	10	87.8
3	5	90	9	11	84.5
4	6	90	10	12	80.06
5	7	90	11	13	74.25
6	8	90	12	14	66.9

References

- [1] Cash J.R., On the integration of stiff systems of ODEs using extended backward differentiation formula, *Numer. Math.*, 34(1980) 235-246.
- [2] Cash J.R., The integration of stiff initial value problems in ODEs using extended backward differential formula, *Computers Math. Applic.* 9(1983)645-657.
- [3] Cash J.R., Second derivative extended backward differentiation formula for the numerical integration of stiff systems, *SIAM J. Numer. Anal.*,18(1981),21-36.
- [4] Cash J.R. A comparison of some codes for the stiff oscillatory problem, *Journal of computational and applied mathematics*, 36(1998)51-57.
- [5] Dahlquist G., A special stability problem for linear multistep methods, *BIT*, 3(1963) 27-43.
- [6] Enright W.H., Second derivative multistep methods for stiff ordinary differential equation, *SIAM J. Numer. Anal.*,11(1974)321-331.
- [7] Hairer E. and Wanner G., *Solving ordinary differential equation II: Stiff and Differential-Algebraic problems*, Springer, Berlin,(1996).
- [8] Hojjati G., Rahimi Ardabili M.Y. and Hosseini S.M., A-EBDF: An adaptive method for numerical solution of stiff systems of ODEs, *Mathematics and Computers in Simulation* 66(2004) 33-41.
- [9] Hojjati G., Rahimi Ardabili M.Y. and Hosseini S.M., New second derivative multistep methods for stiff system, *Applied Mathematical Modelling* 30(2006) 466-476.
- [10] Ismail G. and Ibrahim I., New efficient second derivative multistep methods for stiff systems, *Applied Mathematical Modelling*, 23(1999)279-288.
- [11] Lambert J. D., *Computational methods in ordinary differential equation*, John Wiley Sons,(1972).

Solving System of Non-linear Volterra Integro-Differential Equations by Using an Operational Method

Ali Khani*

*Faculty of science, Department of Mathematics,
Azarbaijan University of Tarbiat Moallem, Tabriz, IRAN
E-mail: khani@azaruniv.edu*

Sedaghat Shahmorad

*Department of Applied Mathematics, University of Tabriz, Tabriz, IRAN
E-mail: shahmorad@tabrizu.ac.ir*

Abstract

In this paper we will develop an operational method to find a numerical solution for the System of Non-linear Volterra integro-differential Equations (SNVE). To this end, we will present our method based on the matrix form of the (SNVE). The corresponding unknowns of our method are determined by using computational aspects of matrices. Finally the accuracy of the method has been verified by presenting some numerical computations.

Keywords: Volterra Integro-Differential Equations, Matrix Forms, Numerical Solutions.
American Mathematical Subject Classification (AMSC): 65R20

1 Introduction

In recent years the operational technique of the Tau method and Adomian decomposition method have developed to cover the numerical solution of differential, integral and integro-differential equations [1, 2, 3, 4, 6, 7, 8, 9, 10]. Liu and Pan [5] presented extension of the operational approach to the Tau method for the numerical solution of mixed-order systems of linear ordinary differential equations with polynomial or rational polynomial coefficients, together with initial or boundary conditions. In this paper, we use the Ortiz and Samara's operational approach [7] for the differential parts and the Adomian method for the non-linear parts of a system of non-linear Volterra integro-differential equations. This approach leads to linear system to find coefficients of the unknown functions.

$$\sum_{j=1}^m \{D_{ij}u_j(x) - \int_0^x k_{ij}(x,t)F_{ij}(u_1(t), \dots, u_m(t))dt\} = f_i(x), \quad x \in [0, a], \quad i = 1, \dots, m \quad (1.1)$$

with the initial conditions

$$u_j^{(i)}(0) = d_{ij}, \quad j = 1, \dots, m, \quad i = 0, \dots, \omega_j - 1, \quad (1.2)$$

*corresponding Author(Ali Khani)

we have taken $\omega_j = \max\{\alpha_{1j}, \dots, \alpha_{mj}\}$ where α_{ij} denotes the order of differential operator D_{ij}

$$D_{ij} = \sum_{r=0}^{\alpha_{ij}} P_{ijr}(x) \frac{d^r}{dx^r} \quad (1.3)$$

with

$$P_{ijr}(x) = \sum_{s=0}^{\beta_{ijr}} p_{ijrs} x^s.$$

We assume that $k_{ij}(x, t) \in C([0, a] \times [0, a])$ and $f_i(x) \in C[0, a]$ for $i, j = 1, \dots, m$. We also assume that $F_i(u_1(x), \dots, u_m(x))$ is sufficiently differentiable with respect to $u_i(x)$ for $i = 1, \dots, m$ and $u_i(x)$ is sufficiently differentiable with respect to x .

This paper is organized as follows. In section 2 and 3, we develop a combination of the operational approach to the Tau method and the Adomian technique to obtain a useful method for the numerical solution of SNVE (1.1). Some numerical results are provided to illustrate the efficiency of the presented method. Closing section includes some useful remarks and conclusion.

2 Operational Tau method

The Tau method describes converting of a given linear integral, integro-differential equation or system of these equations to a system of linear algebraic equations based on two simple matrices:

$$\mu = \begin{bmatrix} 0 & 1 & 0 & 0 \\ & 0 & 1 & 0 \\ & & 0 & 1 & \vdots \\ & & & 0 \\ \dots & & & & \ddots \end{bmatrix}, \quad \eta = \begin{bmatrix} 0 \\ 1 & 0 \\ 0 & 2 & 0 & \vdots \\ 0 & 0 & 3 & 0 & \\ \dots & & & & \ddots \end{bmatrix}.$$

We recall the following results from [7] and [2].

Let

$$P_n(x) = \sum_{i=0}^n a_i x^i = \sum_{i=0}^{\infty} a_i x^i = \underline{\mathbf{a}}_n \mathbf{X}$$

where $\underline{\mathbf{a}}_n = (a_0, a_1, \dots, a_n, 0, \dots)$ and $\mathbf{X} = [1, x, x^2, \dots]$ are constant coefficients and basis vectors respectively. So that

$$xP_n(x) = \sum_{i=0}^{\infty} a_i x^{i+1} = \underline{\mathbf{a}}_n \mu \mathbf{X}$$

$$\frac{d}{dx} P_n(x) = \sum_{i=1}^{\infty} i a_i x^{i-1} = \underline{\mathbf{a}}_n \eta \mathbf{X}$$

Theorem 2.1 Let $P_n(x) = \underline{\mathbf{a}}_n \mathbf{X} \in C^{(\alpha)}[0, a]$ ($C^{(\alpha)}[0, a]$ be the space of α -times continuously differentiable functions defined on $[0, a]$) and

$$D = \sum_{i=0}^{\alpha} \sum_{j=0}^{\beta_i} p_{ij} x^i \frac{d^j}{dx^j} \in \mathcal{D}$$

β_i is the degree of i th coefficient polynomial. (\mathcal{D} is a class of linear differential operators of order α with polynomial coefficients). Then

$$DP_n(x) = \underline{\mathbf{a}}_n \Pi \mathbf{X} \quad (2.1)$$

where

$$\Pi = \sum_{i=0}^{\alpha} \eta^i p_i(\mu).$$

Proposition 2.2 The structure of Π is as follows

$$\Pi = \begin{bmatrix} \pi_{1,1} & \pi_{1,2} & \pi_{1,3} & \dots & \pi_{1,m_1} & 0 & & \\ \vdots & & & \ddots & & & \ddots & \\ \pi_{\alpha+1,1} & \pi_{\alpha+1,2} & \pi_{\alpha+1,3} & \dots & & \pi_{\alpha+1,m_{\alpha+1}} & 0 & \\ 0 & \pi_{\alpha+2,2} & \pi_{\alpha+2,3} & \dots & & & \pi_{\alpha+2,m_{\alpha+2}} & 0 \\ & \ddots & & & & & & \ddots \end{bmatrix} \quad (2.2)$$

where

$$m_i = \begin{cases} \max\{\beta_0 + i, \beta_1 + i - 1, \dots, \beta_{i-1} + 1\} & \text{if } i = 1, 2, \dots, \alpha + 1 \\ m_{\alpha+1} + i - \alpha + 1 & \text{if } i = \alpha + 2, \alpha + 3, \dots \end{cases} \quad (2.3)$$

and

$$\pi_{i,j} = \sum_{k=0}^{\min\{i-1, \alpha+1\}} \frac{(i-1)!}{(i-1-k)!} \hat{p}_{k,j-i+k} \quad i = 1, 2, \dots \quad j = 1, 2, \dots, m_i \quad (2.4)$$

$$\hat{p}_{i,j} = \begin{cases} p_{i,j} & \text{if } j = 0, 1, \dots, \beta_i \\ 0 & \text{if } j < 0 \text{ or } j > \beta_i. \end{cases} \quad (2.5)$$

Thus, Π is a band matrix which gives the coefficients of $DP_n(x)$ in terms of those of $P_n(x)$.

Theorem 2.3 Let $u_n(x)$ and $k(x, t)$ be continuous functions defined on $[0, a]$ and $[0, a] \times [0, a]$ by

$$u_n(x) = \sum_{i=0}^n a_i x^i$$

and

$$k(x, t) = \sum_{i=0}^{\infty} \sum_{j=0}^{\infty} \hat{k}_{ij} x^i t^j$$

then

$$\int_0^x k(x, t) F(u_n(t)) dt = \mathcal{F}_n \underline{K} \mathbf{X} \quad (2.6)$$

where $\mathcal{F}_n = [\mathcal{F}_0, \mathcal{F}_1, \dots]$ with $\mathcal{F}_j = \mathcal{F}(a_0, a_1, \dots, a_j) = \frac{1}{j!} \left\{ \frac{d^j}{dx^j} F\left(\sum_{l=0}^n a_l x^l\right) \right\}_{x=0}$ for $j = 0, 1, 2, \dots$ and

$$\underline{K} = \begin{bmatrix} 0 & \hat{k}_{0,0} & \hat{k}_{1,0} + \frac{1}{2}\hat{k}_{0,1} & \hat{k}_{2,0} + \frac{1}{2}\hat{k}_{1,1} + \frac{1}{3}\hat{k}_{0,2} & \hat{k}_{3,0} + \frac{1}{2}\hat{k}_{2,1} + \frac{1}{3}\hat{k}_{1,2} + \frac{1}{4}\hat{k}_{0,3} & \cdots \\ & 0 & \frac{1}{2}\hat{k}_{0,0} & \frac{1}{2}\hat{k}_{1,0} + \frac{1}{3}\hat{k}_{0,1} & \frac{1}{2}\hat{k}_{2,0} + \frac{1}{3}\hat{k}_{1,1} + \frac{1}{4}\hat{k}_{0,2} & \cdots \\ & & 0 & \frac{1}{3}\hat{k}_{0,0} & \frac{1}{3}\hat{k}_{1,0} + \frac{1}{4}\hat{k}_{0,1} & \cdots \\ & & & 0 & \frac{1}{4}\hat{k}_{0,0} & \cdots \\ & & & \vdots & & \ddots \end{bmatrix}. \quad (2.7)$$

Proof: The equation (2.6) obtains by using the Adomian technique for $F(u_n(x))$ (see [8].)

3 system of non-linear Volterra integro-differential equations

Let

$$u_{in}(x) = \mathbf{a}_i \mathbf{X} \\ \mathbf{a}_i = (a_{i0}, a_{i1}, \dots, a_{in}, 0, 0, \dots) \quad i = 1, 2, \dots, m$$

be the Tau approximations of $u_i(x)$ for $i = 1, 2, \dots, m$, of the exact solution of problem (1.1) with the initial conditions (1.2). By substituting $u_{in}(x)$ in (1.1), (1.2) and applying (2.1) and (2.6) to the differential and integral parts of each equation of the system (1.1), we obtain

$$D_{ij} u_{in}(x) = \mathbf{a}_i \Pi_{ij} \mathbf{X}, \quad i, j = 1, 2, \dots, m \quad (3.1)$$

$$\int_0^x k_{ij}(x, t) F_{ij}(u_{1n}(t), \dots, u_{mn}(t)) dt = \mathcal{F}_{ij} \underline{K}_{ij} \mathbf{X}, \quad i = 1, 2, \dots, m \quad (3.2)$$

where

$$\mathcal{F}_{ij} = (\mathcal{F}_{ij0}, \mathcal{F}_{ij1}, \mathcal{F}_{ij2}, \dots)$$

Let

$$\begin{aligned} g_{ij}(x) &= F_{ij}(u_{1n}(x), \dots, u_{mn}(x)) \\ &= F_{ij}(\sum_{r=0}^{\infty} a_{1r}x^r, \dots, \sum_{r=0}^{\infty} a_{mr}x^r) \\ &= \sum_{s=0}^{\infty} A_{ijs}x^s \end{aligned}$$

and

$$A_{ijs} = \frac{1}{s!} \left\{ \frac{d^s}{dx^s} F \left(\sum_{r=0}^{\infty} a_{1r}x^r, \dots, \sum_{r=0}^{\infty} a_{mr}x^r \right) \right\}_{x=0} = \frac{g_{ij}^{(s)}(0)}{s!} \quad (3.3)$$

which is dependent on $a_{10}, \dots, a_{m0}, \dots, a_{1s}, \dots, a_{ms}$ for $i, j = 1, 2, \dots, m, \quad s = 0, 1, \dots$ and for $i, j = 1, 2, \dots, m$, Π_{ij} is a band matrix associated by Theorem 2.1 with D_{ij} , as defined by (1.3), and \underline{K}_{ij} is the upper triangular matrix associated by Theorem 2.3 with $k_{ij}(x, t)$. We assume that

$$\begin{aligned} f_i(x) &= \sum_{j=0}^{n_i} f_{ij}x^j = \underline{\mathbf{f}}_i \mathbf{X} \\ \text{with} & \\ \underline{\mathbf{f}}_i &= (f_{i0}, f_{i1}, \dots, f_{in_i}, 0, 0, \dots). \end{aligned} \quad (3.4)$$

where n_i denotes the estimation degree of $f_i(x)$.

Since $\underline{\mathcal{F}}_{ij} = (\mathcal{F}_{ij0}, \mathcal{F}_{ij1}, \dots) = (A_{ij0}, A_{ij1}, \dots)$ for $i, j = 1, \dots, m$, by using (3.1), (3.2) and (3.4) we have

$$\check{\Pi} = \begin{bmatrix} \Pi_{11} & \Pi_{21} & \cdots & \Pi_{m1} \\ \Pi_{12} & \Pi_{22} & \cdots & \Pi_{m2} \\ \vdots & \vdots & \ddots & \vdots \\ \Pi_{1m} & \Pi_{2m} & \cdots & \Pi_{mm} \end{bmatrix}. \quad (3.5)$$

Let $\check{V}_i = \sum_{j=1}^m \underline{\mathcal{F}}_{ij} \underline{K}_{ij}$ for $i = 1, \dots, m$, $\check{\mathbf{a}} = (\underline{\mathbf{a}}_1, \dots, \underline{\mathbf{a}}_m)$ and $\check{\mathbf{f}} = (\underline{\mathbf{f}}_1, \dots, \underline{\mathbf{f}}_m)$ then we can rewrite matrix form of (1.1) as

$$\check{\mathbf{a}} \check{\Pi} = \check{V} + \check{\mathbf{f}}.$$

By using (1.2) we obtain

$$a_{ij} = \frac{d_{ij}}{j!}, \quad i = 1, \dots, m, \quad j = 0, \dots, \omega_i - 1$$

and determine other coefficients by forward substituting from the following systems

$$\left\{ \begin{array}{l} (\Pi_{11})_{\omega_1+1,1} a_{1,\omega_1} + (\Pi_{12})_{\omega_2+1,1} a_{2,\omega_2} + \dots + (\Pi_{1m})_{\omega_m+1,1} a_{m,\omega_m} = h_{11} \\ (\Pi_{21})_{\omega_1+1,1} a_{1,\omega_1} + (\Pi_{22})_{\omega_2+1,1} a_{2,\omega_2} + \dots + (\Pi_{2m})_{\omega_m+1,1} a_{m,\omega_m} = h_{21} \\ \vdots \\ (\Pi_{m1})_{\omega_1+1,1} a_{1,\omega_1} + (\Pi_{m2})_{\omega_2+1,1} a_{2,\omega_2} + \dots + (\Pi_{mm})_{\omega_m+1,1} a_{m,\omega_m} = h_{m1} \end{array} \right. \quad (3.6)$$

where

$$h_{i1} = f_{i0} - \sum_{r=1}^m \sum_{s=1}^{\omega_r} (\Pi_{ir})_{s1} a_{r,s-1}, \quad i = 1, \dots, m.$$

$$\begin{cases} (\Pi_{11})_{\omega_1+j,j}a_{1,\omega_1+j-1} + (\Pi_{12})_{\omega_2+j,j}a_{2,\omega_2+j-1} + \dots + (\Pi_{1m})_{\omega_m+j,j}a_{m,\omega_m+j-1} = h_{1j} \\ (\Pi_{21})_{\omega_1+j,j}a_{1,\omega_1+j-1} + (\Pi_{22})_{\omega_2+j,j}a_{2,\omega_2+j-1} + \dots + (\Pi_{2m})_{\omega_m+j,j}a_{m,\omega_m+j-1} = h_{2j} \\ \vdots \\ (\Pi_{m1})_{\omega_1+j,j}a_{1,\omega_1+j-1} + (\Pi_{m2})_{\omega_2+j,j}a_{2,\omega_2+j-1} + \dots + (\Pi_{mm})_{\omega_m+j,j}a_{m,\omega_m+j-1} = h_{mj} \end{cases} \quad (3.7)$$

for $j = 2, 3, \dots, \tilde{\omega}$ where $\tilde{\omega} = n - \min\{\omega_1, \omega_2, \dots, \omega_m\}$,

$$\begin{aligned} h_{ij} &= f_{i,j-1} + \sum_{r=1}^m \sum_{s=1}^{j-1} (\mathcal{F}_{ir})_{s-1} (\underline{K}_{ir})_{sj} - \sum_{r=1}^m \sum_{s=1}^{\omega_r+j-1} (\Pi_{ir})_{sj} a_{r,s-1} \\ &= f_{i,j-1} + \sum_{r=1}^m \sum_{s=1}^{j-1} A_{ir,s-1} (\underline{K}_{ir})_{sj} - \sum_{r=1}^m \sum_{s=1}^{\omega_r+j-1} (\Pi_{ir})_{sj} a_{r,s-1}, \end{aligned}$$

for $i = 1, \dots, m$, $j = 2, 3, \dots, \tilde{\omega}$.

Remark 3.1 Note that, this method failed in solving (1.1)-(1.2), whenever all coefficients of differential parts $(p_{ijr}(x))$ in (1.3) are zero at $x = 0$.

4 Algorithm

The following algorithm is used for solving required linear system

Step 1 Compute the elements of the matrix $\tilde{\Pi}$ by using the formulas (2.2)-(2.5) and (3.5)

Step 2 Compute the elements of the matrix K by using the formulas (2.7)

Step 3 Compute the elements of the vector $\check{V} + \check{f}$ by using the formulas (3.3), (3.4)

Step 4 Form the linear system by (3.6)

use the result of step 4 in system (3.7) to determine other unknown coefficients.

5 Numerical examples

The following examples are given to clarify accuracy of the presented method.

Example 1:

$$\begin{cases} (x + x^2)u_1(x) + 2u_2(x) + \int_0^x (u_1(t) - u_2(t))dt = 2x - \frac{1}{2}x^2 + \frac{4}{3}x^3 + x^4 \\ u_1(x) - xu_2(x) - \int_0^x (2xu_1(t) + 2u_2(t))dt = -x^2 - \frac{2}{3}x^4, \quad 0 \leq x \leq 1. \end{cases}$$

The exact solution is given by $u_1(x) = x^2$, $u_2(x) = x$. For the numerical results with $n = 2$ see Table 1.

Example 2:

$$\begin{cases} (\cos^2 x - 2)u_1(x) + (x - 1)u_2(x) - \int_0^x e^{t-x}(u_1(t) - u_2(t)) + 8\sin(t - x)u_1(t)u_2^2(t)dt = -e^{-x} \\ e^{2x}u_1'(x) - 4x\cos(x)u_2(x) - \int_0^x e^{t+x}(u_1(t) + u_2(t)) + 4(t + x)u_1(t)u_2(t)dt = -3x - \frac{1}{2}\sin(2x), \\ 0 \leq x \leq \frac{\pi}{2}. \end{cases}$$

The exact solution is given by $u_1(x) = \sin(x)$, $u_2(x) = \cos(x)$. For the numerical results with $n = 5, 10, 15$ see Table 2.

Example 3:

$$\begin{cases} -e^x u_1'(x) + xu_2(x) - \int_0^x e^{x+t}u_1(t)u_2(t)dt = xe^{-x} \\ u_1'(x) + u_2(x) + \int_0^x (u_1(t) + u_2(t))dt = 1, \quad u_1(0) = 1, \quad 0 \leq x \leq \frac{\pi}{2}. \end{cases}$$

The exact solution is given by $u_1(x) = \cos(x)$, $u_2(x) = e^{-x}$. For the numerical results with $n = 5, 10, 15$ see Table 3.

Remark 5.1 Note that in the following tables, the notations $Exactu_i$, $App.u_i$ and $Abs.Err.u_i$, for $i = 1, 2$ have been used for exact solution, approximate solution obtained by our method and absolute error of approximate solution respectively.

Table 1: example(1)

x	$Exactu_1$	$App.u_1$	$Abs.Err.u_1$	$Exactu_2$	$App.u_2$	$Abs.Err.u_2$
$n = 2$						
0.00	0.000000	0.000000	0	0.000000	0.000000	0
0.20	0.040000	0.040000	0	0.200000	0.200000	0
0.40	0.160000	0.160000	0	0.400000	0.400000	0
0.60	0.360000	0.360000	0	0.600000	0.600000	0
0.80	0.640000	0.640000	0	0.800000	0.800000	0
1.00	1.000000	1.000000	0	1.000000	1.000000	0

Table 2: example(2)

x	$Exactu_1$	$App.u_1$	$Abs.Err.u_1$	$Exactu_2$	$App.u_2$	$Abs.Err.u_2$
$n = 5$						
0.00	0.000000	0.000000	0	1.000000	1.000000	0
0.31	0.309017	0.309017	$5.98444e-08$	0.951057	0.951058	$1.33291e-06$
0.63	0.587785	0.587793	$7.62868e-06$	0.809017	0.809102	$8.48570e-05$
0.94	0.809017	0.809146	$1.29455e-04$	0.587785	0.588743	$9.58118e-04$
1.26	0.951057	0.952017	$9.60607e-04$	0.309017	0.314335	$5.31768e-03$
1.57	1.000000	1.004525	$4.52486e-03$	0.000000	0.019969	$1.99690e-02$
$n = 10$						
0.00	0.000000	0.000000	0	1.000000	1.000000	0
0.31	0.309017	0.309017	$7.36577e-14$	0.951057	0.951057	$1.92853e-15$
0.63	0.587785	0.587785	$1.50565e-10$	0.809017	0.809017	$7.88642e-12$
0.94	0.809017	0.809017	$1.29825e-08$	0.587785	0.587785	$1.02047e-09$
1.26	0.951057	0.951057	$3.06032e-07$	0.309017	0.309017	$3.20938e-08$
1.57	1.000000	1.000004	$3.54258e-06$	0.000000	0.000000	$4.64766e-07$
$n = 15$						
0.00	0.000000	0.000000	0	1.000000	1.000000	0
0.31	0.309017	0.309017	$7.94976e-24$	0.951057	0.951057	$4.30168e-22$
0.63	0.587785	0.587785	$1.04109e-18$	0.809017	0.809017	$2.81643e-17$
0.94	0.809017	0.809017	$1.02427e-15$	0.587785	0.587785	$1.84697e-14$
1.26	0.951057	0.951057	$1.35987e-13$	0.309017	0.309017	$1.83866e-12$
1.57	1.000000	1.000000	$6.02342e-12$	0.000000	0.000000	$6.51336e-11$

Table 3: example(3)

x	$Exactu_1$	$App.u_1$	$Abs.Err.u_1$	$Exactu_2$	$App.u_2$	$Abs.Err.u_2$
$n = 5$						
0.00	1.000000	1.000000	0	1.000000	1.000000	0
0.31	0.951057	0.951058	$1.33291e-06$	0.730403	0.730401	$1.27761e-06$
0.63	0.809017	0.809102	$8.48570e-05$	0.533488	0.533410	$7.83491e-05$
0.94	0.587785	0.588743	$9.58118e-04$	0.389661	0.388805	$8.56311e-04$
1.26	0.309017	0.314335	$5.31768e-03$	0.284610	0.279987	$4.62252e-03$
1.57	0.000000	0.019969	$1.99690e-02$	0.207880	0.190917	$1.69626e-02$
$n = 10$						
0.00	1.000000	1.000000	0	1.000000	1.000000	0
0.31	0.951057	0.951057	$1.92853e-15$	0.730403	0.730403	$7.18203e-14$
0.63	0.809017	0.809017	$7.88642e-12$	0.533488	0.533488	$1.43408e-10$
0.94	0.587785	0.587785	$1.02047e-09$	0.389661	0.389661	$1.21007e-08$
0.26	0.309017	0.309017	$3.20938e-08$	0.284610	0.284610	$2.79636e-07$
1.57	0.000000	0.000000	$4.64766e-07$	0.207880	0.207883	$3.17890e-06$
$n = 15$						
0.00	1.000000	1.000000	0	1.000000	1.000000	0
0.31	0.951057	0.951057	$4.30168e-22$	0.730403	0.730403	$4.22491e-22$
0.63	0.809017	0.809017	$2.81643e-17$	0.533488	0.533488	$2.71935e-17$
0.94	0.587785	0.587785	$1.84697e-14$	0.389661	0.389661	$1.75476e-14$
1.26	0.309017	0.309017	$1.83866e-12$	0.284610	0.284610	$1.72048e-12$
1.57	0.000000	0.000000	$6.51336e-11$	0.207880	0.207880	$6.00816e-11$

6 Conclusions

As we showed in section 2, the operational Tau method combined with Adomian's technique makes a linear system with simple structure for solving (SNVE), which is solved directly by forward substituting.

We also showed the high accuracy of this method by numerical results for various type of problems (see tables 1, 2, 3).

References

- [1] E. Babolian and J. Biazar, A.R. Vahidi, The decomposition method applied to system of Fredholm integral equations of the second kind, *Applied Mathematics and Computation*, 148, 443-452 (2004).
- [2] S.M. Hosseini and S. Shahmorad, A matrix formulation of the Tau for Fredholm and Volterra linear integro - differential equations, *the Korean J. Comput. & Appl. Math.* Vol. 9, NO.2, 497-507 (2002).
- [3] S.M. Hosseini and S. Shahmorad, Numerical solution of a Class of integro-differential equations by the Tau method with an error estimation, *Appl. Math. Comput*, 136, 559-570 (2003).
- [4] S.M. Hosseini and S. Shahmorad, Tau numerical solution of Fredholm integro-differential equations with arbitrary polynomial bases, *J. Appl. Math. Modelling*, 27, 145-154 (2003).
- [5] K.M. Liu and C.K. Pan, The automatic solution to systems of Ordinary differential equations by the Tau method, *Computers Math. Applic.*, 38, 197-210 (1999).
- [6] E.L. Ortiz, The Tau method. *Siam J. Numer. Anal.* Vol. 6, No. 3, 480 - 492 (1969).
- [7] E.L. Ortiz and H. Samara, An operational approach to the Tau method for the numerical solution of non linear differential equations. *Computing* 27, 15 - 25 (1981).
- [8] T. Badredine, K. Abbaoui and Y. Cherruault, Convergence of Adomian's method applied to integral equations, *Kybernetes*, Vol. 28, No. 5, 557-564 (1999).
- [9] J. Biazar, E. Babolian, R. Islam, Solution of a system of Volterra integral equations of the first kind by Adomian method, *Appl. Math. and Comput*, 139, 249258 (2003).
- [10] N.M. Madbouly, D.F. Mcghee, G.F. Roach, Adomian's method for Hammerstein integral equations arising from chemical reactor theory, *Appl. Math. Comput*, 117, 241-249, (2001).

Modeling of Multilane highway Traffic with an Auxiliary lane

M. Levent KURNAZ, A. Nihan IMREM and Hunter T. KING

Department of Physics, Bogazici University 34342 Bebek Istanbul TURKIYE

In this paper, we use the Nagel-Schreckenberg (NaSch) model to simulate the traffic flowing from the European side to Asian side over the Bosphorus on the Fatih Sultan Mehmet Bridge. We investigate the effects of the auxiliary lane and its position on the traffic flow. Traffic research still cannot fully predict under which conditions a traffic jam may suddenly occur. The aim of our project is to define what causes such traffic jams. Another important question is the effect of the auxiliary lane which is supposed to decrease the traffic congestion. To test the psychological aspects of the driver behavior and cultural side of the traffic flow problem, two scientists from different ethnic background approach this problem using different parameters related to their traffic cultures.

Introduction

Have you ever wondered how many hours you have spent sitting in a bumper-to-bumper traffic? We live in a city whose population is more than 10 million people and western side of Istanbul is considered as a business centre. People generally work on the western side and live on the eastern side of Istanbul. The traffic therefore flows at the direction of the western side in the morning, and at the direction of the eastern side in the evening along the two bridges. Due to the fact that when 25 lanes come from the western side after the toll booths and the number of lanes is decreased to 4, traffic jams become a huge problem. The transportation authority makes an arrangement in order to decrease the traffic jam, by taking one lane from the direction from eastern side to western side and adds this lane to the crowded side as an auxiliary lane at the rush hours. We investigate the effect of this auxiliary lane and its position on the traffic flow. The possible reasons for the jam formation can be the frequent lane changing or less headway. Density is an important parameter that we investigate. Even when drivers obey all the rules, jams can be formed at roads with a high density of traffic. These parameters are changed and analyzed for their effect on the traffic flow. Local rules are decided by the programmers according to their perception of the traffic rules. The difference and similarities between the two approaches can be seen clearly at the graphics of the simulations. The results are given as a comparative study of these two simulations.

Cellular automata (CA) are often used to model traffic flow with the intent to both better understand the internal dynamics of traffic from a statistical physics point of view, and to create virtual experiments which cannot be normally performed on real roads. Statistical Physics is commonly used in traffic theories [8]. In general, one can distinguish microscopic and macroscopic approach. While in macroscopic approach, traffic is treated as a gas of interacting particles like “Kinetic theory of vehicular traffic model” [4], in microscopic approach individual vehicles are distinguished like “Nagel-Schreckenberg (NaSch) model” [9]. Many such models in the recent past have had success in these areas, including the Nagel-Schreckenberg (NaSch) model we use as a generic example. Based on the NaSch we have written our simulation with the aim of acquiring physically significant and realistic data for a simple virtual highway consisting of four lanes, an onramp, an off-ramp, and an auxiliary lane running from the beginning of the road to after the off-ramp. As we travel daily through this traffic jam, we have the opportunity of observing the short-comings of the auxiliary lane in easing the traffic burden. In analyzing our results, we have studied space-time diagrams showing the position of all vehicles in each time step, and “fundamental diagrams” showing the relationship between flow and density.

The Nagel Schrenkenberg Model

Nagel-Schreckenberg(NaSch) model is a minimal model in that all the components of its characteristic local rule are necessary (in the order applied) to reproduce the basic features of realistic traffic. In NaSch model, a one dimensional array is used and they perceive the road as one lane as defined at Ref.[9]. A cell may be occupied or unoccupied. Occupied cells may have integer state values between 0 and maximum speed value (5). The local rule, which is applied to occupied cells, consists of four parts, which are applied in the following order:



Fig.1 The picture of the road of our simulation

Acceleration: if n^{th} vehicle (occupied cell) has a velocity less than the given speed limit, its speed is increased by one.

$$V(n) = \min(V(n)+1, V_{\max})$$

Deceleration: where $V(n)$ is the velocity of the n^{th} car and $V(\max)$ is the speed limit. If the car in front is at a distance within the range of the next movement of the n^{th} car, its speed is decreased accordingly.

$$V(n) = \min(V(n), d(n) - 1)$$

where $d(n)$ is the gap between the n^{th} car and its predecessor $(x(n+1)-x(n))$

Randomization: If n^{th} car's speed is greater than zero, it may decrease its speed by one with some probability p .

$$V(n) = \max(V(n)-1, 0)$$

Movement: Once the new velocities are determined by the above rules, the cars are moved simultaneously.

$$X(n) = X(n) + V(n)$$

Our Models

We use a five dimensional array together with our own lane changing, exiting and entering rules. In this simulation, there are 500 cells and 4 lanes on the main road. Cars move by adding their speed to their position. The maximum speed is 5, speed of one speed translates to 22.5 km/h and one cell length is 7.5 m, which agrees with [5]. The density of the main road is measured for 4 lane and auxiliary lane from the beginning of the road to the off-ramp at 300th cell. The entrance probability of a new car and its type are regulated with the use of this density.

The densities of the onramp and auxiliary lane can be changed and are identified initially. Onramp begins at the 300th cell and ends at the 330th cell. Auxiliary lane begins at the beginning of the road and it merges into the main road at 350th cell. The density of cars that exit from the off-ramp is identified initially and the cars are named as being of second type. The cars of first type cars do not exit from the off-ramp. Due to the position of the auxiliary lane entrance to the main road, cars of second type are not allowed in the auxiliary lane. The densities of the first and second type cars stay constant.

Model I

In this simulation, the exit sign is placed onto the road at the 200th cell. With this exit sign, drivers now know the entrance of the off-ramp and its position and they shift towards right as soon as possible. Cars know about the location of the preceding car, and not the cars behind. However, cars have no knowledge of the speed of the preceding car.

Acceleration: the same as NaSch model [9].

Randomization: the same as NaSch model [9].

Movement: $X(n) = \min(x(n)+V(n) , x(n+1)-1)$

Deceleration (if movement influenced car in front): $V(n) = x(n+1) - x(n) - 1$

Overdeceleration: The overreaction in breaking to avoid collision (with r probability).

$V(n) = x(n+1) - x(n) - 2$

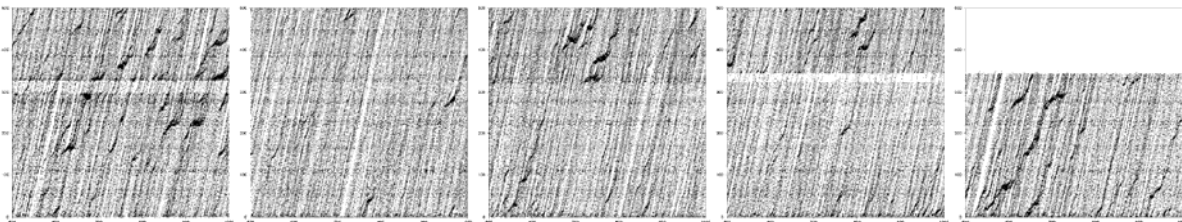
Lane Changing Rules: If the speed is going to be higher by changing lanes, and when you look behind to the lane you are going to change to, there are no cars for n places, you can move left or right.

Exiting (Off-ramp) Rules: Exiting cars are determined from the start of the simulation. When these cars can see the exit sign, they are moving right. When they are close to the exit, they do not obey the lane changing rules to change lanes towards right.

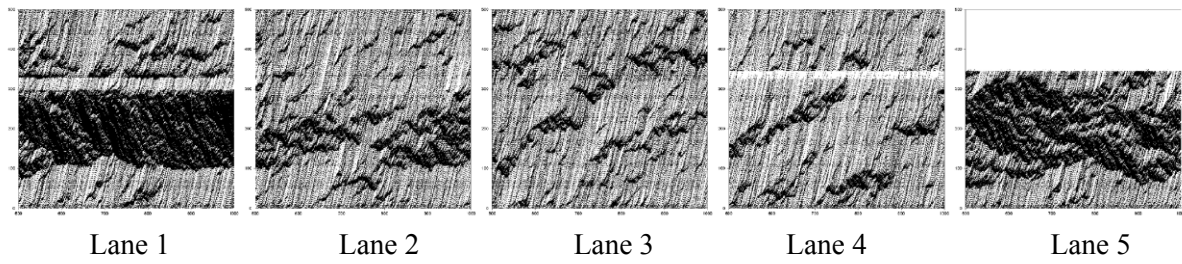
Auxiliary Lane Rules: Auxiliary lane joins the main road unperturbed; therefore 4th lane must be emptied before auxiliary lane joins the main road. When cars on the 4th lane must evacuate to 3th lane because of this juncture, they do not obey the lane changing rules.

Onramp Rules: The density of the onramp lane is identified at the start. If there is a car waiting to enter the main road, that car finds the first empty space on the 1st lane and adjusts its speed to the preceding car instantaneously.

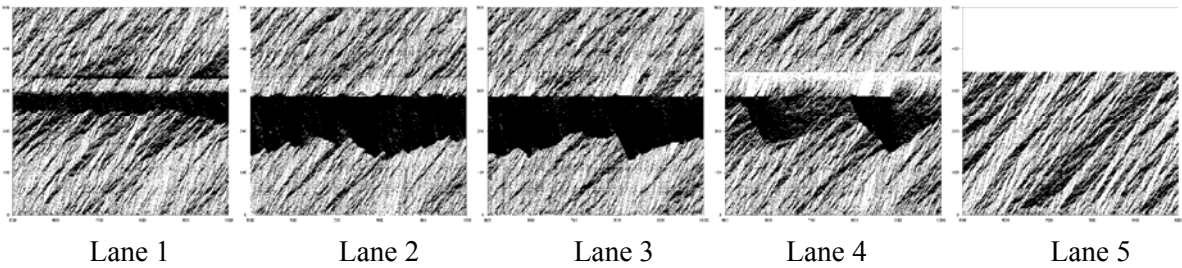
Adding Cars to the Road: The cars are added to the road from the beginning. The place to add is randomly chosen, and its speed is adjusted so that the incoming car does not collide with other cars in the present or next step.



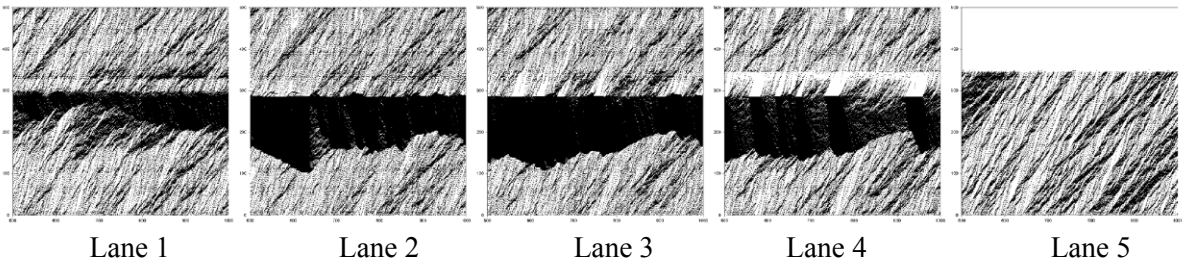
Case A: Density: %30, random slowing probability: %10, lane change gap: 2 units, change probability: %30, exit sign: yes.



Case B: Density: %50, random slowing probability: %10, lane change gap: 2 units, change probability: %30, exit sign: yes



Case C: Density: %50, random slowing probability: % 30, lane change gap: 2 units, change probability: %100, exit sign: no.



Case D: Density: %50, random slowing probability: %30, lane change gap: 1 unit, change probability: %100, exit sign: no.

Fig. 2 Simulation results for model I

Model II

This simulation is based on the cars rather than the road and hence we can follow each vehicle's motion. Each car knows the other's number, speed and the distance between any cars and both the preceding and the following cars are also known. Cars are placed on road, on auxiliary lane and on onramp randomly and with random speed as an initial condition. As Turkish drivers do not care much about street signs, we do not place the exit sign, so drivers are not forced to shift right as soon as possible. Even they can wait until they come to 290 cells to shift right. This situation is observed as the main cause of the jam formation. The difference from the first model is the deceleration step. Driver behavior in second model is more aggressive than the first's. Drivers go fast as soon as possible and they can stop or decrease their speed more than one level instantly. This behavior model is placed to the code to simulate the general Turkish driver behavior.

Acceleration: The same with the NaSch model [9].

Motion: If the car cannot change lane, it follows the preceding car just behind it. Aggressive behavior causes more braking and acceleration.

Deceleration: This step is different than the first model. The car can decrease its speed to 0 in one step. We investigate the relation between the braking and jam formation. Deceleration probability is used for driver's unexpected braking one level. Random deceleration is used for the decrease of the car with reason, not based on the flow, (e.g. based on watching an accident on the other side of the road while passing, attention disorder, and aggressiveness).

Lane Changing Rules: If the distance between the car and its preceding car is less than the speed of the car or if the speed of the preceding car is the same or less than the speed of the car, the car looks for the opportunity to go faster. If the distance to the preceding car on the target lane is larger than the distance to the preceding car on the current lane, or if the position on the target lane (new position after lane changing) is not exactly behind the preceding car on the current lane (which gives the opportunity to go faster in the next iteration), the car accelerates by one. If the prospect position on the target lane is just behind the preceding car, car decelerates for lane changing. This search procedure is valid for both sides and with equal chance the car moves to the left or to the right. This randomization is put into the simulation for showing various drivers' behavior such as not to change lane even it is to their advantage or to change lane even it is to their disadvantage. The deterministic CA Model in single lane highway becomes stochastic in multilane highway model which agrees with Ref.[2].

Extra lane changing rule: Sometimes, although all cars have max speed around, the car can change lane if there is more unoccupied cells on the right or left lane. The car looks to the right and to the left. If the distance to the preceding car on the current lane is less than the distance to the preceding car on the right or left lane, it moves to the lane which allows for more spacing. This step is not used in the earlier model. If the preceding car on the right lane and the left lane is at the same distance, the car decides to change lanes with 50% probability.

Exiting (Off-ramp) Rules: Type 2 cars exit automatically from the off-ramp when they come to the off-ramp. For the cars on the second lane less than 15 cells before the off-ramp, for the cars on the third lane less than 25 cells before the off-ramp, and for the cars on the fourth lane less than 35 cells before the off-ramp, cars begin to move towards right if condition 1 is satisfied, so that they do not miss the off-ramp. The exit sign is not placed on the road. If a type 2 car cannot move to the right with condition 1, then the car looks for the condition 2.

Condition 1: The car that wants to move towards right looks at the right lane, if there is a car within 5 cells, we calculate the distance between them. If $v+x$ is less than (the position of the preceding car - 1) at the target lane and v is less than 5, the car increases its speed ($v+1$) and moves right just behind the preceding car at the target lane. If $v+x$ is more than (the position of the preceding car - 1) at the target lane (collision), to avoid collision the speed is decreased to the distance between them. If $v+x$ is the same as (the position of the preceding car - 1) at the target lane, car continues with its speed, the new speed becomes the same with the preceding car's speed. If there is no car at the target lane and v is less than 5, speed is increased by one and continues.

Condition 2: For the cars on second lane, 7 cells before the off-ramp, for the cars on third lane, 9 cells before the off-ramp, and for the cars on fourth lane 11 cells before the off-ramp, cars cut the other car on the right lane off for last chance to exit from the main road. The other car has to stop at this condition. If there is no car at the just front cell of the car at both the current lane and the target lane, car shifts to just front cell at the right lane.

Auxiliary Lane Rules: The car on the fourth lane and between cell 335 and cell 360 is forced to shift to right lanes in order to allow the cars on the auxiliary lane enter the road. Otherwise, auxiliary lane is jammed. These cars look both at the preceding and at the trailing car on the target lane. If the car can exit from auxiliary lane, it looks the position of the preceding car on the target lane not to collide. If it will collide with its current speed, it adapts its speed to avoid collision at the entrance.

Onramp Rules: If the car can exit from onramp, it looks to the position of the preceding car on the target lane not to collide. If the car can enter the road by accelerating one level, accelerates and enters with accelerated speed. If it will collide with its speed, it adapts its speed to avoid collision at the entrance and it slides to the cell just behind the preceding car on the target lane. After entering, the car adapts speed to the speed of the preceding car. If it cannot enter the main road, it adapts speed to the preceding car. If it comes to the end of the onramp, it stops and waits for entering. The car number at onramp is decreased by one and added one car from the beginning of the onramp if possible.

Adding Cars to the Road: As we are keeping the density of the cars constant, we look at the number of cars leaving the road at the off-ramp and the cars crossing the line of the off-ramp on the main road. We add the sum of these two values to the beginning of the road. This way the concentration between the beginning of the road and the first exit is kept constant. The cars are added to the beginning of the road with the following conditions, true for each lane:

If there is a car on any of the first 5 cells on the lane, the new car is placed just behind the first car on the road, and new car's speed becomes the same with the first car on that lane.

If there are no cars on the first 5 cells on the lane, we look at the total number of cars exiting (by how much the density decreases):

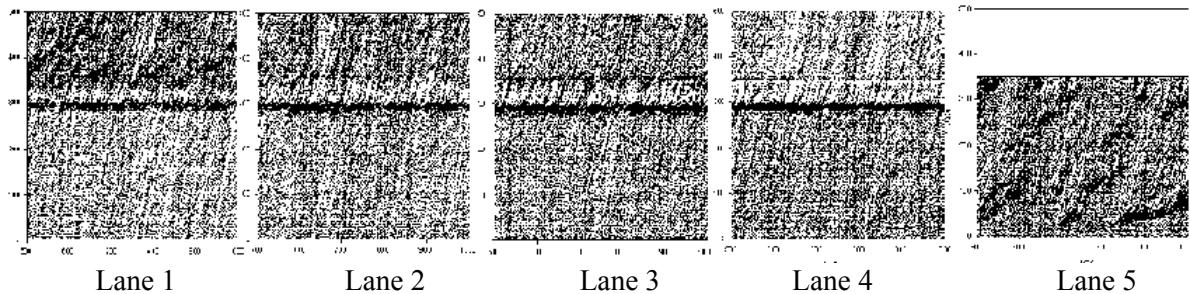
If the total number of cars exiting is 5 or less than 5, the car can be randomly placed on any of the first five cells.

If the total number of cars exiting is between 5 and 7, the car can be randomly placed on cells 2-5.

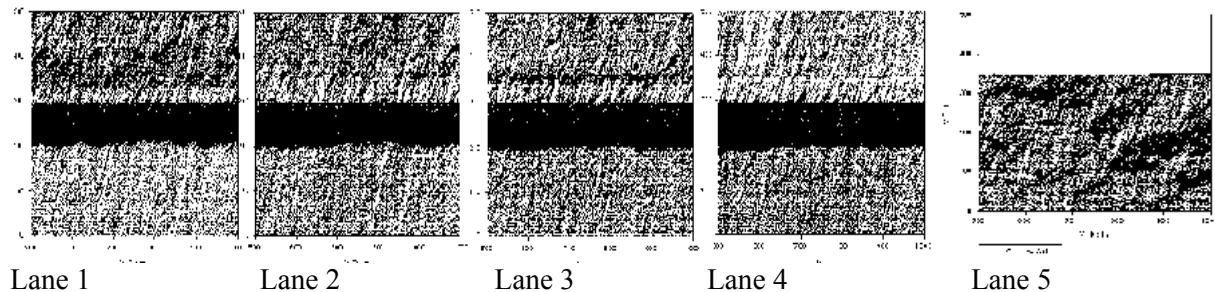
If the total number of cars exiting is between 7 and 10, the car can be randomly placed on cells 3-5.

If the total number of cars exiting is between 10 and 15, the car can be randomly placed on cells 4-5.

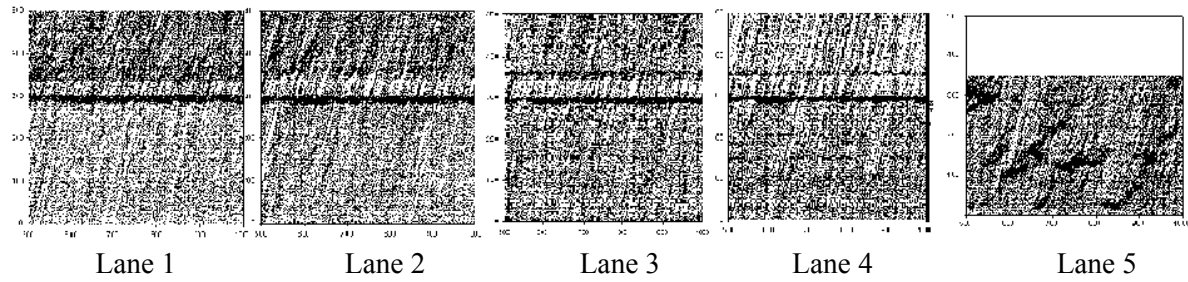
If the total number of cars exiting is larger than 15, the car must be randomly placed on cell 5.



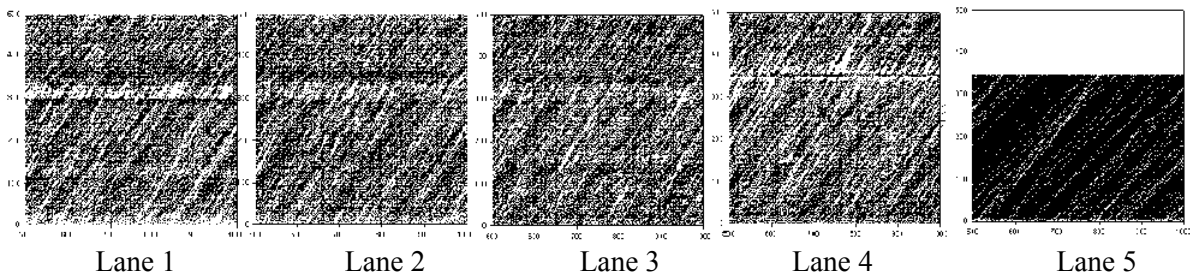
Case A: Density: %30, Random deceleration probability: %10, Exit sign: No



Case B: Density: %50, random deceleration probability: %10, Exit sign: No



Case C: Density: %30, random deceleration probability: %50, Exit sign: No.



Case D: Density: %50, random deceleration probability: %50, Exit sign: No.

Fig. 3 Simulation results for model II

Conclusion

A traffic jam occurs when cars slow down, and the slowing trend continues backward like a domino effect. As long as there are more cars approaching from behind, the traffic congestion travels in a wave. Traffic congestion travels backwards on the road. As the first car stops, the following cars must also stop. Even when the first car begins to move again, additional approaching cars have to stop farther down the road, and so the congested area travels backward in a wave until traffic is light enough for it to dissipate.

It has been found that individual incidents (such as accidents or even a single car braking heavily in a previously smooth flow) may cause ripple effects which then spread out and create a sustained traffic jam when otherwise, normal flow might have continued for some time longer. Jams can arise spontaneously, triggered by minor events (butterfly effects) such as an abrupt steering maneuver by a single motorist.

We have observed two distinct phases in unobstructed flow caused by the formation of spontaneous jams.[12] We observe that allowing lane changing in multilane highways increases total flow by preventing spontaneous jams to some extent. The congestion at MODEL I / CASE C and CASE D with respect to CASE A and CASE B show the efficiency of the exit sign. In MODEL II the heavy congestion is caused by not placing the exit sign and not forcing cars to move right in advance. For multilane highways with off ramps, we conclude that placing a sign well ahead of the exit is crucial in preventing large scale congestion in that it allows for exiting cars to change lanes without decelerating and for onward moving cars to move away from the right lane.

Simple and logical rules seem to have a better result in terms of the traffic flow, whereas driver's disrespect for common traffic rules can result in serious traffic jams. Random slowing down in our model is basically due to frequent and abrupt lane changing behavior commonly seen in our traffic. The difference between MODEL I CASE B and CASE C shows us that this random slowing can have

adverse effects on all of the freeway lanes. With logical rules of exiting cars trying to move to the right lane as early as possible, only the traffic on the rightmost lane slows down somewhat. However if the drivers wait until the last moment to move towards right, then the rightmost lane is less crowded, but the traffic can come to a standstill on other lanes. Even though keeping a very small lane change gap is looked upon as one of the major sources of traffic problems, we observe that the traffic chaos is not caused by this behavior, only slightly enhanced by it.

Using Nagel-Schrenkenberg model, it is possible to model complex traffic patterns including careless drivers. Especially MODEL I CASE C, CASE D and MODEL II simulate the daily traffic conditions experienced by the authors every evening quite accurately.

However, in MODEL I CASE A and CASE B only first lane and auxiliary lane are congested, in MODEL II all lanes are congested, the reason being more aggressive behavior. In MODEL II cars change lanes with less care and they accelerate and decelerate more. The difference on the speed is the source of the jam formation. The congestion is shared by all lanes. In MODEL I, if the lane changing probability becomes %100, the pattern becomes similar to MODEL II.

In MODEL II, the congestion after off-ramp should be taken into consideration, the possible cause of the heavy congestion at near the off-ramp is the congestion after off-ramp. The congestion at onramp entrance can travel backwards and contribute to the jam formation. The bottleneck at cell 330 (entering onramp) causes congestion, according to Kerner's three phase traffic theory, the pattern can be the wide moving jam formation at the bottleneck. In both Ref.[10] and Ref.[6], wide moving jam can not occur in free flow, and the transition from synchronized flow to wide moving jam only can be seen on traffic. The line formation with respect to time around the bottleneck is the empirical feature of the wide moving jam and is named as the breakdown phenomenon. The other important result of distance-time graphics is the curvature on the line around bottleneck due to car accumulation, as shown in Fig 10 at Ref.[3].

MODEL I is designed by an American scholar and MODEL II is designed by a Turkish scholar. The exit sign and less aggressive and more organized behavior for entering from off-ramp (characteristics of the American style of driving) decrease the jam formation explicitly. MODEL II clearly explains the reason of the jam formation on the direction from the bridge to Kavac k in the evening. The important difference between MODEL I and MODEL II is that at the same density, MODEL II is more congested than MODEL I due to the high braking probability in MODEL II. For different braking probabilities, flow-density graphics can be drawn.[1] The comparison between MODEL II CASE A – CASE C and CASE B – CASE D show the effect of the random deceleration probability. Due to the abrupt deceleration (braking) caused the variant gap distribution and the behavior of the gap distribution shows that the traffic can exhibit a self organized criticality for high values of random deceleration probability as found at Ref.[7].

In MODEL II, when we increase the deceleration probability from 10% to 50%, the critical behavior is explicitly seen, lines become less congested and the relation between the self organized criticality defined at Ref.[11] and this pattern can be investigated in future research. The congestion on the auxiliary lane at CASE D, based on the lack of changing lanes, is more than other four lanes.

References

- [1] M. Schrenkenberg, A. Schadschneider , K. Nagel , and N. Ito, "Discrete Stochastic Models for Traffic Flow," Physical Review Letters E 51 (1995) 2939.
- [2] S. Benjaafar et al, 1997 "Cellular Automata for Traffic Flow Modeling", University of Minnesota, Minneapolis.

- [3] M. J. Lighthill, G. B. Whitham, Proc. Roy. Soc. Lond. A 229 (1955) 281.
- [4] L. Priogine, R. Herman, Kinetic Theory of Vehicular Traffic, Elsevier, Amsterdam, 1971.
- [5] A. Schadschneider “Statistical Physics of Traffic Flow” Physica A 285 (2000), 101-120
- [6] C.F. Daganzo, M. J. Cassidy, and R.L. Bertini “Causes and Effects of Phase Transitions in Highway Traffic” Institute of Transportation Studies Research Report UCB-ITS-RR-1997-8
- [7] K. Fourrate and M. Loulidi, “Disordered Cellular Automata Traffic Flow Models” 5, 151, (2004) The Moroccan Statistical and Condensed Matter Society.
- [8] D. Chowdhury, L. Santen, A. Schadschneider “Statistical Physics of Vehicular Traffic and Some Related Systems” Phys Rep. 329 199-329(2000)
- [9] K. Nagel, and M. Schreckenberg, “A Cellular Automaton Model for Freeway Traffic”, J. Phys. I France (1992) 2221-2229
- [10] B. S. Kerner, “The physics of Traffic”
- [11] Per Bak, How Nature Works”
- [12] A. Schadschneider, Physica A 372,142(2006)

BIFURCATION SCENARIOS OF SOME MODIFIED PREDATOR – PREY NONLINEAR SYSTEMS

İlknur Kuşbeyzi, Avadis Hacınlıyan

Department of Information Systems and Technologies, Yeditepe University, Istanbul, Turkey

ABSTRACT

Bifurcation scenarios in predator prey models are studied with particular emphasis on a form including a cubic interaction. The instability introduced by this term and the subsequent Hopf bifurcation are numerically studied. The behavior is comparable to the fractional nonmonotonic forms customarily used in the literature.

1. INTRODUCTION

The predator prey problem attempts to model the relationship in the populations of different species that share the same environment and some of the species (predators) prey on the others. The prey is assumed to exhibit linear growth given by a positive parameter. Predator species consume preys with a nonlinear interaction with another set of parameters that determine the rate of competition between predators. The natural death rate of the predator is assumed to be linear and given by a negative parameter. One of the earliest implementations, the Lotka-Volterra model serves as a starting point of more advanced models in the analysis of population dynamics. Because of its stability problems^[1], the model and its generalizations serve as a popular object of stability analysis that has recently gained much attention. To understand the behavior of a nonlinear system one has to also analyze the existence and stability of equilibrium points which change. Changes in the number and stability of equilibrium points as parameters are varied lead to *bifurcation*. Numerical methods are usually employed to perform this analysis.^[2] A semi-perturbative analytic approach is provided by the normal form method.^[3]

Well known generalizations of the Lotka-Volterra model include the addition of polynomial interactions^[4], non monotonic response functions^{[5] [6]}, time delayed^[7] and diffusion effected time delayed^[8] non monotonic interactions. Bifurcation properties of some of these and a generalization of the model with a cubic interaction term that is shown to introduce additional stability in a simple way are studied in this work.

2. THE LOTKA-VOLTERRA MODEL

The classic mathematical model of predator – prey systems was first developed in 1925 by the American biophysicist Alfred Lotka (1880 – 1949) and Italian mathematician Vito Volterra (1860 – 1940) to analyze the cyclic changes in the populations of sharks and the fish eaten by sharks in the Adriatic Sea. It is given by

$$\begin{aligned}\frac{dx}{dt} &= ax - bxy \\ \frac{dy}{dt} &= -cy + dxy\end{aligned}$$

Here, $a, b, c, d > 0$ are parameters described above, x and y are the prey and predator populations. The equilibrium points are $(x_0, y_0) = (0, 0)$ and $(\frac{c}{d}, \frac{a}{b})$. Eigenvalues associated with the equilibrium point $(x_0, y_0) = (0, 0)$ is $\{a, -c\}$ and eigenvalues associated with the equilibrium point $(\frac{c}{d}, \frac{a}{b})$ are $\{-i\sqrt{ac}, i\sqrt{ac}\}$. Since a and c are always greater than zero, the origin is a saddle point. The eigenvalues for the equilibrium point $(\frac{c}{d}, \frac{a}{b})$ are purely imaginary, hence all the solutions are periodic which means the predator and prey populations cycle and oscillate around this equilibrium.

This model is popular as a simple predator-prey system since it shows cycling of predator-prey populations^[9]. However, the model has significant problems. Its equilibrium points are not stable; the model does not exhibit structural stability, the simulated populations cycle endlessly without settling down. Thus, it fails to describe realistic predator and prey populations which typically reach characteristic steady state values. Hence, realistic models should predict a single closed orbit, or perhaps finitely many, but not a continuous family of neutrally stable cycles. For this reason, the model is generalized by adding additional information.

3. GENERALIZED QUADRATIC LOTKA-VOLTERRA MODEL WITH POLYNOMIAL INTERACTION

The simplest polynomial generalization involves the addition of a quadratic term^[4] and the model becomes

$$\begin{aligned}\frac{dx}{dt} &= a(x - x^2) - bxy \\ \frac{dy}{dt} &= -c(y + y^2) + dxy\end{aligned}$$

Two additional equilibrium points are introduced by this change. The equilibrium points are $(x_0, y_0) = (0, 0), (1, 0), (\frac{(a+b)c}{ac+bd}, \frac{a(-c+d)}{ac+bd})$ and $(0, -1)$. Eigenvalues associated with the equilibrium point $(x_0, y_0) = (0, 0)$ are $\{a, -c\}$ so that this is a saddle node. Eigenvalues associated with the equilibrium point $(1, 0)$ are $\{-a, -c+d\}$. If $d > c$ this equilibrium is a saddle node, otherwise it is a stable equilibrium. The eigenvalues associated with the equilibrium point $(\frac{(a+b)c}{ac+bd}, \frac{a(-c+d)}{ac+bd})$ form a complex conjugates pair and the corresponding

eigenvectors are complex conjugates of one another. If $\frac{a^2c + abc - ac^2 + acd}{2(-ac - bd)} < 0$ then this equilibrium is stable.

Eigenvalues associated equilibrium $(0, -1)$ are $\{a+b, c\}$. This equilibrium is unstable. Hence, this generalization can introduce one or two stable equilibrium points in the linearized approximation for appropriate values of the parameters. Since the stability of the equilibrium points can change with the parameter values, bifurcation may, in principle, occur.

4. GENERALIZED QUADRATIC LOTKA-VOLTERRA MODEL WITH NONPOLYNOMIAL INTERACTION

As we add more parameters we add to a nonlinear system, we will get additional bifurcation points. Thus, the model becomes closer to the real life problem. For this reason, modified Predator – Prey multi parameter systems with non monotonic response functions are studied. Here is the simplest generalization of the quadratic model.

$$\begin{aligned}\frac{dx}{dt} &= x(a - \lambda x) - yP(x) \\ \frac{dy}{dt} &= -\delta y - \mu y^2 + yQ(x) \\ P(x) &= \frac{mx}{1 + \beta x + \alpha x^2}, \alpha \geq 0, \delta > 0, \mu \geq 0, \beta > -2\sqrt{\alpha} \\ Q(x) &= cP(x), c > 0\end{aligned}$$

The equilibrium points are $(x_0, y_0) = (0, 0), (\frac{a}{\lambda}, 0), (0, -\frac{\delta}{\mu})$ and there are further 5 nontrivial equilibrium points. Eigenvalues associated with the equilibrium point $(x_0, y_0) = (0, 0)$ are $\{a, -\delta\}$, the origin is a saddle point since a and δ are nonnegative. Eigenvalues associated with the equilibrium point $(\frac{a}{\lambda}, 0)$ are $\{-a, -\delta + \frac{acm}{(1 + \frac{a^2\alpha}{\lambda^2} + \frac{a\beta}{\lambda})\lambda}\}$, if $\delta > \frac{acm}{(1 + \frac{a^2\alpha}{\lambda^2} + \frac{a\beta}{\lambda})\lambda}$ this equilibrium is a stable node. Eigenvalues associated to equilibrium point $(0, -\frac{\delta}{\mu})$ are $\{\delta, a + \frac{\delta m}{\mu}\}$. This equilibrium is clearly unstable.

5. GENERALIZED CUBIC LOTKA-VOLTERRA MODEL WITH POLYNOMIAL INTERACTION

Nutku has proposed a generalization where a cubic rather than a quadratic interaction is involved. This is an interaction that has not been studied before. It is of interest, since the non interacting parts for both the prey and the predator would undergo pitchfork bifurcation rather than transcritical bifurcation along opposite directions for the predator and prey.

$$\begin{aligned}\frac{dx}{dt} &= a(x - x^3) - bxy \\ \frac{dy}{dt} &= -c(y + y^3) + dxy\end{aligned}$$

The equilibrium points are $(x_0, y_0) = (0,0), (1,0), (-1,0), (0,i), (0,-i)$ and additionally roots of two cubic equations that produce two real and two complex conjugate pairs of equations. Eigenvalues associated with the equilibrium point $(x_0, y_0) = (0,0)$ are $\{a, -c\}$ and this is again a saddle point. Eigenvalues associated with the equilibrium point $(0, -i)$ are $\{a+bi, 2c\}$ and it is unstable. The eigenvalues associated with the equilibrium point $(0,i)$ are $\{a-bi, 2c\}$ and it is either a saddle node or unstable. The linearized stability of the eigenvalues associated to those equilibrium points that correspond to the roots of the cubic equations depend on the parameter values. However the equilibrium points $(1, 0)$ and $(-1, 0)$ have the eigenvalues $\{-2a, -c-d\}$ and $\{-2a, -c+d\}$. One of them is always stable, the other one is stable if $d < c$. We also note that the normal form expansion may or may not have resonant terms, depending on the values of the parameters.

6. GENERALIZED CUBIC LOTKA-VOLTERRA MODEL WITH NONPOLYNOMIAL INTERACTION

The cubic model suggested by Nutku can also be generalized in like fashion.

$$\begin{aligned}\frac{dx}{dt} &= x(a - \lambda x^2) - yP(x) \\ \frac{dy}{dt} &= -\delta y - \mu y^3 + yQ(x) \\ P(x) &= \frac{mx}{1 + \beta x + \alpha x^2}, \alpha \geq 0, \delta > 0, \mu \geq 0, \beta > -2\sqrt{\alpha} \\ Q(x) &= cP(x), c > 0\end{aligned}$$

Equilibrium points are $(x_0, y_0) = (0,0), (-\frac{\sqrt{a}}{\sqrt{\lambda}}, 0), (\frac{\sqrt{a}}{\sqrt{\lambda}}, 0), (0, -i\frac{\sqrt{\delta}}{\sqrt{\mu}}), (0, i\frac{\sqrt{\delta}}{\sqrt{\mu}})$ and there are other 10 nontrivial equilibrium points. Eigenvalues associated with the equilibrium point $(x_0, y_0) = (0,0)$ are $\{a, -\delta\}$. Hence the origin is again a saddle point. Eigenvalues associated with the equilibrium point $(-\frac{\sqrt{a}}{\sqrt{\lambda}}, 0)$ are $\{-2a, -\delta - \frac{\sqrt{acm}}{(1 + \frac{a\alpha}{\lambda} - \frac{\sqrt{a\beta}}{\sqrt{\lambda}})\sqrt{\lambda}}\}$ and this equilibrium

is clearly stable. Eigenvalues associated with the equilibrium point $(\frac{\sqrt{a}}{\sqrt{\lambda}}, 0)$ are $\{-2a, -\delta + \frac{\sqrt{acm}}{(1 + \frac{a\alpha}{\lambda} + \frac{\sqrt{a\beta}}{\sqrt{\lambda}})\sqrt{\lambda}}\}$. If $\delta > \frac{\sqrt{acm}}{(1 + \frac{a\alpha}{\lambda} + \frac{\sqrt{a\beta}}{\sqrt{\lambda}})\sqrt{\lambda}}$, this equilibrium is stable.

Eigenvalues associated with the equilibrium point $(0, -i\frac{\sqrt{\delta}}{\sqrt{\mu}})$ are $\{2\delta, a + \frac{i\sqrt{\delta}m}{\sqrt{\mu}}\}$ and this equilibrium is unstable. Eigenvalues associated with the equilibrium point $(0, i\frac{\sqrt{\delta}}{\sqrt{\mu}})$ are $\{2\delta, a - \frac{i\sqrt{\delta}m}{\sqrt{\mu}}\}$. If $a < \frac{i\sqrt{\delta}m}{\sqrt{\mu}}$ then this equilibrium is a saddle point, otherwise it is unstable.

It is clear that the cubic generalization has stable equilibrium points in the linear approximation with or without additional non monotonic terms.

7. NUMERICAL STUDY OF BIFURCATION IN THE CUBIC MODEL

We perform the bifurcation analysis of the following example of the cubic predator – prey model suggested by Nutku.

$$\begin{aligned}\frac{dx}{dt} &= a(x - x^3) - bxy \\ \frac{dy}{dt} &= -c(y + y^3) + bxy\end{aligned}$$

For simplicity we fix the parameters as follows: $a=1, b=2, c=\sqrt{2}$. There are nine equilibrium points for this choice and we choose the starting value $(x, y) = (\sqrt{2} - 1, \sqrt{2} - 1)$ which is the only equilibrium points of our system that gives rise to Hopf bifurcation, since the linearized eigenvalues are $\pm 2i\sqrt{2(-7 + 5\sqrt{2})}$. This also implies a resonant normal form. Four of the other equilibrium points also give rise to resonant normal forms but no Hopf bifurcation. With the help of the Matlab package MATCONT^[10], we can start to visualize the bifurcation scenario of this system by choosing the parameters a, b, c and d as free parameters. We have the following Hopf and branch points shown in the Table below for a as free parameter.

Table 6. Positions in Fig.6

x	y	a	Lyapunov Coefficient	Eigenvalues	Point
0.707106	0	0	7.987319e+000	$\{-1.26192e - 009 \pm 4.10442e - 005\}$	Hopf

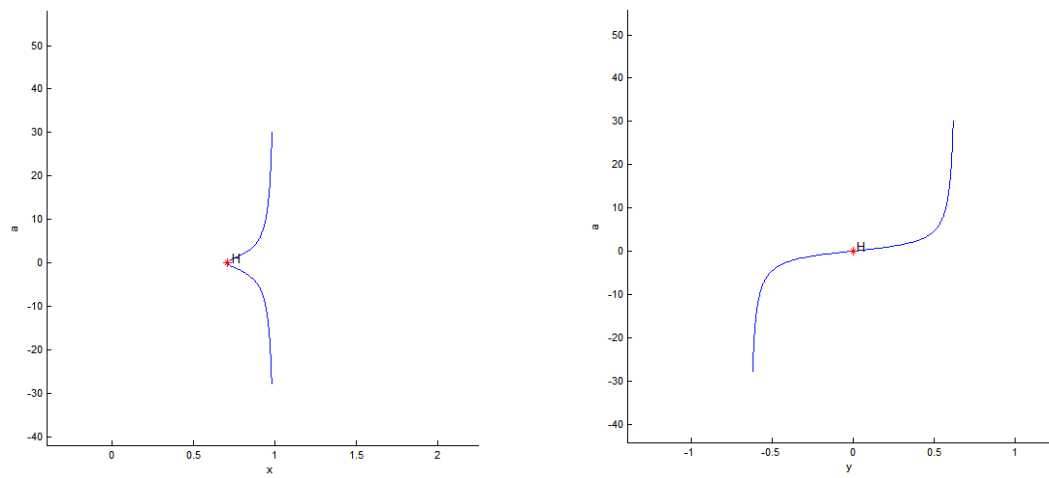


Table 7. Positions in Fig.

x	y	b	Eigenvalues	Point
1	0	1.414213	$\{-2, -1.69407e-016\}$	Branch Point
1.157251	-0.260013	1.304664	$\{-2.86968, -5.32657e-009\}$	Limit Point

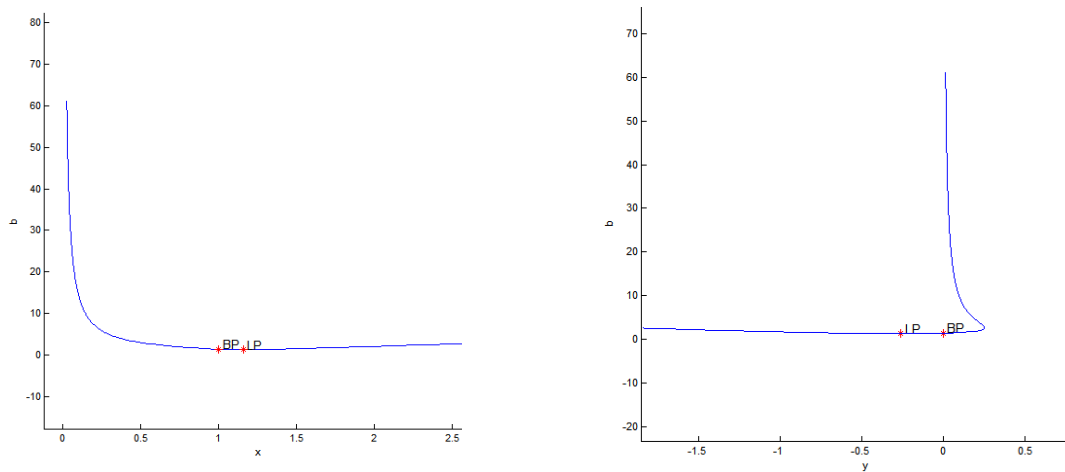
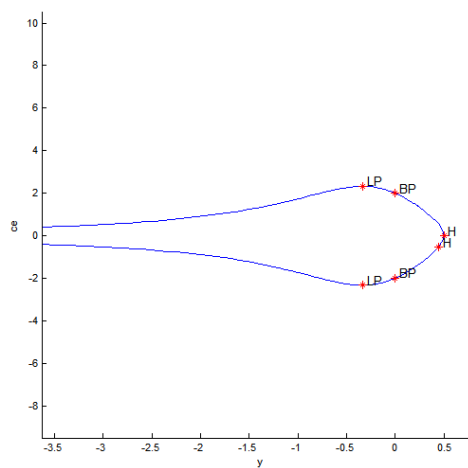
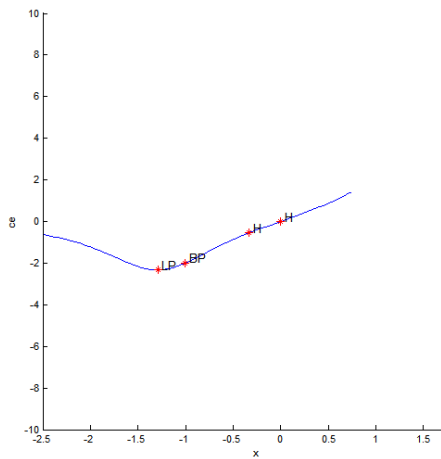


Table 7. Positions in Fig.

x	y	c	Lyapunov Coefficient	Eigenvalues	Point
1	0	2		$\{-2, -4.66925e-015\}$	Branch Point
1.29099	-0.33333	2.32379		$\{-3.84973, -2.82834e-009\}$	Limit Point
0	0.5	0	$2.230560e+000$	$\{-3.78123e-009 \pm 0.000136588\}$	Hopf Point
-	0.445253	-		$\{\pm 0.798305\}$	Neutral Saddle
0.33089		0.552304			
-1	0	-2		$\{-2, -5.08537e-015\}$	Branch Point
-1.2909	-0.33333	2.3237		$\{-3.84973, -2.82834e-009\}$	Limit Point



8. LYAPUNOV FUNCTION STUDY OF BIFURCATION IN THE CUBIC MODEL

We define the following scalar function $V : \mathfrak{R} \times \mathfrak{R} \rightarrow \mathfrak{R}$ which is a positive definite function satisfying $V(0,0) = 0, V(x, y) > 0$.

$$V(x, y) = \alpha x^2 + \beta y^2$$

Taking time derivate we have

$$\begin{aligned}
 \frac{dV}{dt} &= 2\alpha x(a(x - x^3) - bxy) + 2\beta y(c(-y - y^3) + dxy) \\
 &= \alpha(2ax^2 - 2ax^4 - 2bx^2y) + \beta(-2cy^2 - 2cy^4 + 2dxy^2) \\
 &\rightarrow -2a\alpha x^4 - 2c\beta y^4
 \end{aligned}$$

This approaches to a negative number when time goes to infinity, so we conclude that generalized cubic model is asymptotically stable.

9. INTEGRABILITY OF LOTKA VOLTERRA MODELS

According to Nutku^[12] the simple Lotka Volterra Model is defined as

$$\begin{aligned}\frac{dx}{dt} &= ax - bxy \\ \frac{dy}{dt} &= -cy + dxy\end{aligned}$$

and has the first integral

$$dx + by - c \log(x) - a \log(y)$$

The generalized quadratic model is

$$\begin{aligned}\frac{dx}{dt} &= a(x - x^2) - bxy \\ \frac{dy}{dt} &= -c(y + y^2) + dxy\end{aligned}$$

and has the first integral

$$x^{c_1} y^{c_2} (1 + c_3 x + c_4 y)$$

where

$$\begin{aligned}c_1 &= \frac{-ac - cd}{ac + bd}, c_2 = \frac{ab - ac}{ac + bd}, c_3 = \frac{ac + bd}{bc - bd - c^2 + cd}, \\ c_4 &= (a^2 c^2 x + 2abcdx - ac^3 + ac^2 d + b^2 d^2 x - bc^2 d + bcd^2) / \\ & (a^2 c^2 x - a^2 c^2 - a^2 cdx + a^2 cd - abc^2 + abcdx + abcd - abd^2 x + ac^2 dx - ac^2 d - acd^2 x + acd^2 \\ & - bc^2 d + bcd^2 x + bcd^2 - bd^3 x)\end{aligned}$$

$$\text{provided } \frac{ac(-a - b + c - d)}{ac + bd} = 0$$

An algebraic integral has not been found for the cubic Lotka Volterra Model.

10. CONCLUSIONS:

In this work, we have confirmed that quadratically self coupled two dimensional Lotka Volterra systems do not possess inherent stability and require the addition of non polynomial, non monotonic terms to induce the stability and more realistic bifurcation schemes. As suggested by Nutku, a simpler way of inducing non monotonicity and stability is changing the self coupling from quadratic to cubic. This introduces stability at least in the linearized approximation. The normal form method or numerical simulation could be invoked to study the behavior of the system near these equilibrium points.

The authors thank Professor Yavuz Nutku for suggesting this problem.

REFERENCES

- [1] Gleria, I.M., Figueiredo, A., Rocha Filho, T. M., “Stability Properties of a General Class of Nonlinear Dynamical Systems” J.Phys. A: Math. Gen. 34 3561-3575, 2001.
- [2] Ghosh, D. and Chowdhury, A.R., “On the Bifurcation Pattern and Normal Form in a Modified Predator – Prey Nonlinear System” Journal of Computational and Nonlinear Dynamics 2 267 – 273,2007.
- [3] Chen, J., “Bifurcations, Normal Forms and their Applications”, PHD Thesis, 2005.
- [4] Cairo, L and Feix, M. R. “On the Hamiltonian structure of 2D ODE possessing an invariant” J. Phys. A Math. Gen. 25, L1287-LI293, 1992.
- [5] Zhu, H., Campbell, S. A., Wolkowicz, G. S. K., “Bifurcation Analysis of a Predator – Prey System with Nonmonotonic Functional Response” SIAM J. Appl. Math. Vol.63 No.2 636-682, 2002.
- [6] Broer, H.W., Naudot, V., Roussarie, R., Saleh, K., “Bifurcations of a Predator – Prey Model With Non-monotonic Response Function” C. R. Acad. Sci. Paris, Ser. I 341 601 – 604, 2005.
- [7] Xiao, D., “Multiple Bifurcations in a Delayed Predator – Prey System with Nonmonotonic Functional Response” Journal of Differential Equations 176 494 – 510, 2001.
- [8] Yan, X.P., Li, W.T., “Hopf Bifurcation and Global Periodic Solutions in a Delayed Predator – Prey System”, Applied Mathematics and Computation 177 427-445, 2006.
- [9] Pankovic, V., Banjac, D., Glavatovic, R., Predojevic, M., “A Simple Solution of the Lotka – Volterra Equations”, <http://arxiv.org/abs/q-bio/0607042v1>, 2006.
- [10] Dhooge, A., Sautois, B., Govaerts, W., Kuznetsov, Y.A., “MATCONT: Matlab software for bifurcation study of dynamical systems”, ICNAAM Extended Abstracts, 1-4, 2005.
- [11] Kuznetsov, Yu. A., “Elements of Applied Bifurcation Theory” Springer New York – 1995.
- [12] Nutku, Y. “Hamiltonian structure of the Lotka-Volterra equations” Phys. Lett A 145 (1990) 27

Solution of Strongly nonlinear oscillation systems using Variational approach

SHA. Hashemi. Kachapi¹, A. Barari^{*1}, N. Tolou², D.D.Ganji¹

¹*Departments of Civil and Mechanical Engineering, Babol University of Technology, Babol, Iran.*

²*Department of Engineering, Islamic Azad University, Ayatollah Amoly Branch, Amol, Iran.*

Abstract

In this paper, we use the variational approach proposed by Ji-Huan He for strongly nonlinear oscillators. Two examples are given to illustrate the effectiveness and convenience of the method.

The mentioned approach can be expressed as a Ritz-like method and this approach is an explicit method with highly valid for resolution of strong nonlinear oscillation systems. In short, this approach yields extended scope of applicability, simplicity, flexibility in application, and avoidance of complicated numerical and analytical integration as compared to other of the previous approaches such as the perturbation methods. The obtained results are valid for the whole solution domain with high accuracy. The method can be easily extended to other nonlinear oscillations and so can be found widely applicable in engineering and science.

Keywords: *Variational Approach; Nonlinear Oscillation; Discontinuity.*

1. Introduction

Nonlinear oscillations systems are such phenomena that mostly occur nonlinearly; hence solving of governing equations have been one of the most time-consuming and difficult affairs among researchers of vibrations. Therefore, many researchers and scientist of both vibrations and mathematics have recently paid much attention to find and develop approximate solutions. If there is no small parameter in the equation, the traditional perturbation methods cannot be applied directly. Recently, considerable attention has been directed towards the analytical solutions for nonlinear equations without possible small parameters. The traditional perturbation methods have many shortcomings, and they are not valid for strongly nonlinear equations. To overcome the shortcomings, many new techniques have appeared in open literature [1–8].

Variational methods have been, and continue to be, popular tools for nonlinear analysis. When contrasted with other approximate analytical methods, variational methods combine the following two advantages: (1) they provide physical insight into the nature of the solution of the problem; (2) the obtained solutions are the best among all the possible trial-functions. Recently, some approximate variational methods, including approximate energy method [9–12] and variational iteration method [13–19], to soliton solution, bifurcation, limit cycle and period solutions of nonlinear equations have been given much attention. The approximate energy approach [9, 10] can

* corresponding author: amin78404@yahoo.com

be applied not only to weakly nonlinear equations, but also to strongly nonlinear ones. The so obtained results are valid for the whole solution domain [11, 12]. Variational iteration method is based on a general Lagrange multiplier, and it can be applied to various nonlinear equations [20, 21]. Recently new couple variational approach proposed by SHA. Hashemi. K [22].

In the present paper, we use a variational method (VM) for nonlinear oscillators which proposed by He JH [23] and recently, this method used in nonlinear oscillation system and other engineering usages (such as [24]), which leads to a very rapid convergence of the solution and can be easily extended to other nonlinear oscillations and so can be found widely applicable in engineering and science.

2. Variational approach

In this Section, a brief introduction to He's variational approach [23] is illustrated below. Consider a general nonlinear oscillator in the form [23]

$$u''(t) + f(u(t)) = 0 \quad (1)$$

Its variational principle can be easily established using the semi-inverse method [4]

$$J(u) = \int_0^{T/4} \left(-\frac{1}{2} u'^2 + F(u) \right) dt \quad (2)$$

where $T = 2\pi / \omega$ is period of the nonlinear oscillator, $F(u) = \int f(u) du$.

Non-linear oscillations systems are independent upon initial conditions. In general, oscillations systems contain two important physical parameters, i.e. the frequency ω and the amplitude A of oscillation. So, without loss of any generality, consider such initial conditions:

$$u(0) = A, \quad u'(0) = 0, \quad (3)$$

Assume that its solution can be expressed as

$$u(t) = A \cos \omega t \quad (4)$$

Substituting (4) into (2) results in

$$\begin{aligned} J(A, \omega) &= \int_0^{T/4} \left(-\frac{1}{2} A^2 \omega^2 \sin^2 \omega t + F(A \cos \omega t) \right) dt \\ &= -\frac{1}{2} A^2 \omega \int_0^{\pi/2} \sin^2 t dt + \frac{1}{\omega} \int_0^{\pi/2} F(A \cos t) dt \end{aligned} \quad (5)$$

Applying the Ritz method, we require

$$\partial J / \partial A = 0 \quad (6)$$

$$\partial J / \partial \omega = 0 \quad (7)$$

But by a careful inspection, for most cases we find that

$$\partial J / \partial \omega = \left(-\frac{1}{2} A^2 \int_0^{\pi/2} \sin^2 t dt - \frac{1}{\omega^2} \int_0^{\pi/2} F(A \cos t) dt \right) < 0 \quad (8)$$

Thus, we modify the conditions (6) and (7) into a more simply form:

$$\partial J / \partial A = 0 \quad (9)$$

3. Applications

In order to assess the advantages and the accuracy of the variational approach, we will consider the following examples.

Example 1. The first example let us consider a family of nonlinear differential equations [25]

$$u'' + \alpha u + \gamma u^{2m+1} = 0, \quad \alpha \geq 0, \quad \gamma > 0, \quad m = 1, 2, 3, \dots \quad (10)$$

With the initial conditions

$$u(0) = A, \quad u'(0) = 0 \quad (11)$$

For this problem, $f(u) = \alpha u + \gamma u^{2m+1}$ and $F(u) = \frac{1}{2} \alpha u^2 + \frac{\gamma u^{2m+2}}{2m+2}$.

Its variational formulation can be readily obtained as follows:

$$J(u) = \int_0^{T/4} \left(-\frac{1}{2} u'^2 + \frac{1}{2} \alpha u^2 + \frac{\gamma u^{2m+2}}{2m+2} \right) dt \quad (12)$$

Substituting (4) into (12), we obtain

$$J(A) = \int_0^{T/4} \left(-\frac{1}{2} A^2 \omega^2 \sin^2 \omega t + \frac{1}{2} \alpha A^2 \cos^2 \omega t + \frac{\gamma (A \cos \omega t)^{2m+2}}{2m+2} \right) dt \quad (13)$$

The stationary condition with respect to A reads

$$\begin{aligned} \partial J / \partial A &= \int_0^{T/4} \left(-A \omega^2 \sin^2 \omega t + \alpha A \cos^2 \omega t + \frac{\gamma (A \cos \omega t)^{2m+2}}{A} \right) dt \\ &= \int_0^{\pi/2} \left(-A \omega^2 \sin^2 t + \alpha A \cos^2 t + \frac{\gamma (A \cos t)^{2m+2}}{A} \right) dt = 0 \end{aligned} \quad (14)$$

This leads to the following result;

$$\omega = \frac{\sqrt{A \pi \Gamma(m+2) \left(\alpha A \pi \Gamma(m+2) + 2 \gamma A^{2m+1} \Gamma\left(\frac{3}{2} + m\right) \sqrt{\pi} \right)}}{A \pi \Gamma(m+2)}, \quad (15)$$

Γ Function is proved in Appendix A. With $T = 2\pi / \omega$, yield;

$$T = \frac{2A\pi^2\Gamma(m+2)}{\sqrt{A\pi\Gamma(m+2)\left(\alpha A\pi\Gamma(m+2)+2\gamma A^{2m+1}\Gamma\left(\frac{3}{2}+m\right)\sqrt{\pi}\right)}} \quad (16)$$

The corresponding exact period T is

$$T_{ex} = 4 \int_0^{\pi/2} \frac{dt}{\sqrt{\alpha + \frac{\gamma}{m+1} A^{2m} (1 + \sin^2 t + \sin^4 t + \dots + \sin^{2m} t)}}. \quad (17)$$

For $m = 1, 3$ and $m = 4, 6$ with $\alpha = \gamma = 1$ and $A = 1, 10, 100, 200$, comparisons of the approximate periods (VM) T with exact periods T_{ex} are tabulated in Tables 1 and 2, respectively.

According to Eq. (15) and substituted in Eq. (4), we can obtain the following approximate solution

$$u(t) = A \cos\left(\frac{\sqrt{A\pi\Gamma(m+2)\left(\alpha A\pi\Gamma(m+2)+2\gamma A^{2m+1}\Gamma\left(\frac{3}{2}+m\right)\sqrt{\pi}\right)}}{A\pi\Gamma(m+2)} t\right). \quad (18)$$

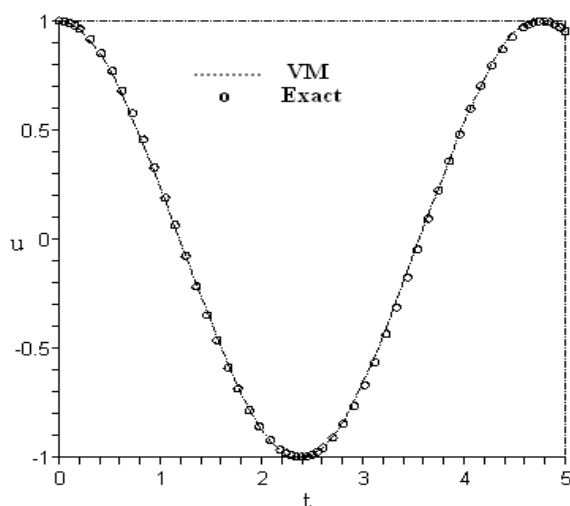
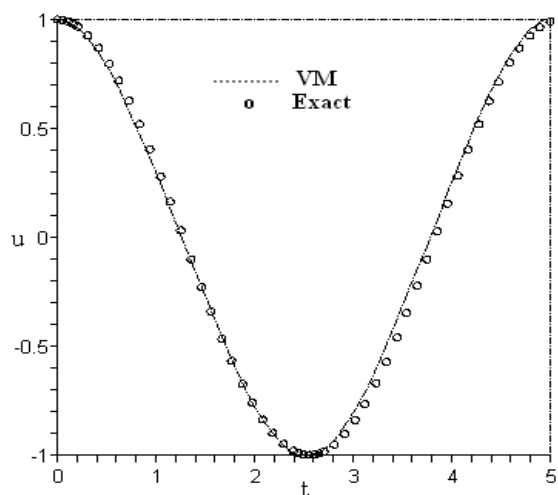
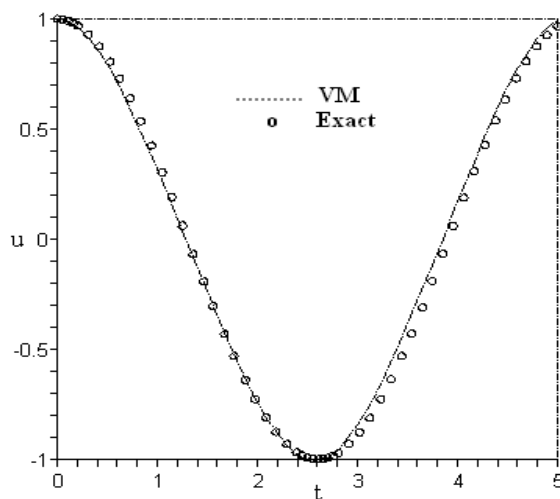
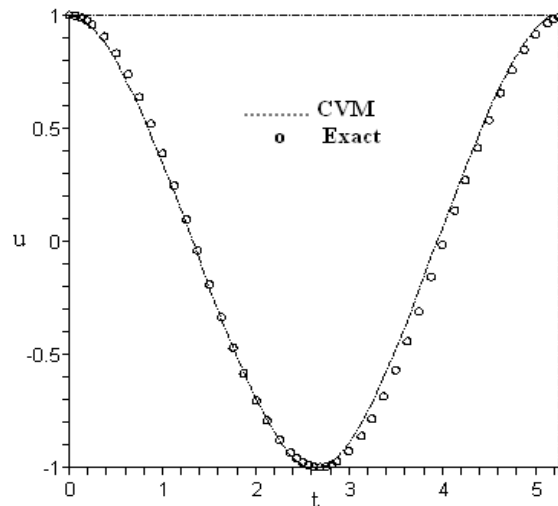
The above results are in good agreement with the results obtained by the exact solution in [25] as illustrated in Fig. 1(a–d).

Table 1. Comparison of the approximate period with exact period when $m = 1, 3$ and $\alpha = \gamma = 1$

A	$m = 1$			$m = 3$		
	T	T_{ex}	Percentage error	T	T_{ex}	Percentage error
1	4.7497	4.7682	0.39 %	5.0520	5.1060	1.05 %
10	0.72077	0.73628	2.1 %	0.84964E–02	0.93088E–02	8.7 %
100	0.072550	0.074153	2.16 %	0.84964E–05	0.93088E–05	8.7 %
200	0.36275E–01	0.37081E–01	2.17 %	0.10621E–05	0.11636E–05	8.7 %

Table 2. Comparison of the approximate period with exact period when $m = 4, 6$ and $\alpha = \gamma = 1$

A	$m = 4$			$m = 6$		
	T	T_{ex}	Percentage error	T	T_{ex}	Percentage error
1	5.1436	5.2080	1.24 %	5.2749	5.1480	2.46 %
10	0.89558E–03	0.10128E–02	11.5 %	0.97079E–05	0.11758E–04	17.4 %
100	0.89558E–07	0.10128E–06	11.5 %	0.97079E–11	0.11758E–10	17.4 %
200	0.55976E–08	0.63296E–08	11.5 %	0.15168E–12	0.18373E–12	17.4 %

Fig.1—a. $\alpha = \gamma = A = m = 1$ Fig.1—b. $\alpha = \gamma = A = 1, m = 3$ Fig.1—c. $\alpha = \gamma = A = 1, m = 4$ Fig.1—d. $\alpha = \gamma = A = 1, m = 6$ **Fig. 1(a–d).** Comparison of the approximate solution (VM) with the exact solution.

Example 2. In this example, consider the following nonlinear oscillators with discontinuities [26]:

$$u'' + u + \varepsilon u|u| = 0, \quad (19)$$

With the initial conditions $u(0) = A$ and $u'(0) = 0$. Here the discontinuous function is $f(u) = u + \varepsilon u|u|$. From Eq. (2), the variational formulation is yields;

$$J(u) = \int_0^{T/4} \left(-\frac{1}{2} u'^2 + \frac{1}{2} u^2 + F(\varepsilon u|u|) \right) dt \quad (20)$$

Using Eq. (4) and noting that $|\cos \omega t| = \cos \omega t$ when $-\pi/2 \leq \omega t \leq \pi/2$ and $|\cos \omega t| = -\cos \omega t$ when $\pi/2 \leq \omega t \leq 3\pi/2$, so we write Eq. (20) in the following form:

$$J(u) = \int_{-T/4}^{T/4} \left(-\frac{1}{2} u'^2 + \frac{1}{2} u^2 + F(\varepsilon u^2) \right) dt + \int_{T/4}^{3T/4} \left(-\frac{1}{2} u'^2 + \frac{1}{2} u^2 - F(\varepsilon u^2) \right) dt \quad (21)$$

Now we using Eq. (5) and (9), results;

$$J(A) = \int_{-T/4}^{T/4} \left(-\frac{1}{2} A^2 \omega^2 \sin^2 \omega t + \frac{1}{2} A^2 \cos^2 \omega t + \frac{1}{3} \varepsilon A^2 \cos^2 \omega t \right) dt + \int_{T/4}^{3T/4} \left(-\frac{1}{2} A^2 \omega^2 \sin^2 \omega t + \frac{1}{2} A^2 \cos^2 \omega t - \frac{1}{3} \varepsilon A^2 \cos^2 \omega t \right) dt \quad (22)$$

$$\partial J / \partial A = \int_{-\pi/2}^{\pi/2} \left(\omega^2 \sin^2 t + \cos^2 t + \varepsilon A \cos^3 t \right) dt + \int_{\pi/2}^{3\pi/2} \left(\omega^2 \sin^2 t + \cos^2 t - \varepsilon A \cos^3 t \right) dt = 0 \quad (23)$$

From the above equation, one can easily conclude that

$$\omega = \frac{\sqrt{3} \sqrt{\pi(8\varepsilon A + 3\pi)}}{3\pi} \quad (24)$$

According to Eq. (24), we can obtain the first-order following approximate solution

$$u(t) = A \cos\left(\frac{\sqrt{3} \sqrt{\pi(8\varepsilon A + 3\pi)}}{3\pi} t\right) \quad (25)$$

The above results are in good agreement with the results obtained by the homotopy perturbation reported in [27].

In order to compare with traditional perturbation solution, we write Nayfeh's result:

$$u(t) = A \cos\left(1 + \frac{4}{3\pi} \varepsilon A\right)t + \dots, \quad (26)$$

Where is valid only for small parameter.

4. Conclusions

We used a very simple but effective method for nonlinear oscillators. The first-order approximate solutions are of a high accuracy. Of course the accuracy can be improved upon using a higher order approximate solution. These examples have shown that the approximate analytical solutions are in excellent agreement with the corresponding exact solutions. The method can be easily extended to any nonlinear oscillator without any difficulty. Moreover, the present paper can

be used as paradigms for many other applications in searching for periodic solutions of nonlinear oscillations.

Appendix A

$$\Gamma(m) = \int_0^\infty e^{-t} t^{m-1} dt, \quad m > 0 \quad (\text{A.1})$$

$$\Gamma(m+1) = m\Gamma(m), \quad m > 0 \quad (\text{A.2})$$

$$\Gamma(m+1) = m(m-1)(m-2)\cdots 2\Gamma(1) = m! \quad (\text{A.3})$$

$$m! = \int_0^\infty e^{-t} t^n dt, \quad n \in N \quad (\text{A.4})$$

References

- [1] He JH. Homotopy perturbation technique, computer methods in applied mechanics and engineering, 178 (1999) 257–262.
- [2] He JH. A coupling method of a homotopy technique and a perturbation technique for non-linear problems, international journal of non-linear mechanics, 35 (2000) 37–43.
- [3] S.H. Hashemi.K, H.R.M. Daniali, D.D. Ganji, Numerical simulation of the generalized Huxley equation by He's homotopy perturbation method, Appl. Math. Comput, 192 (2007) 157–161.
- [4] Liu HM. Generalized variational principles for ion acoustic plasma waves by He's semi-inverse method. Chaos, Solitons & Fractals, 23 (2005) 573–579.
- [5] Wu Y. Variational approach to higher-order water-wave equations. Chaos, Solitons & Fractals, 32 (2007) 195–203.
- [6] Xu L. Variational approach to solitons of nonlinear dispersive K (m, n) equations, Chaos, Solitons & Fractals, 37(2008)137-143.
- [7] He JH. Some asymptotic methods for strongly nonlinear equations. Int J Mod Phys B, 20 (2006) 1141–99.
- [8] He JH. Non-perturbative methods for strongly nonlinear problems. Dissertation, de-Verlag im Internet GmbH, Berlin; 2006.
- [9] He JH. Preliminary report on the energy balance for nonlinear oscillations. Mech Res Commun, 29 (2002) 107–118.
- [10] He JH. Determination of limit cycles for strongly nonlinear oscillators. Phys Rev Lett, 90 (2003) [Art. No. 174301].
- [11] D'Acunto M. Determination of limit cycles for a modified van der Pol oscillator. Mech Res Commun, 33 (2006) 93–102.
- [12] D'Acunto M. Self-excited systems: analytical determination of limit cycles. Chaos, Solitons & Fractals, 30 (2006) 719–743.

- [13] He JH. Variational iteration method—a kind of non-linear analytical technique: some examples. *Int J Nonlinear Mech*, 34 (1999) 699–708.
- [14] He JH. Approximate solution of nonlinear differential equations with convolution product nonlinearities. *Comp Meth Appl Mech Eng*, 167 (1998) 69–73.
- [15] M. Rafei, D.D. Ganji, H. Daniali, H. Pashaei, The variational iteration method for nonlinear oscillators with discontinuities, *Journal of Sound and Vibration*, 305 (2007) 614–620.
- [16] D.D. Ganji, A. Sadighi, *Int. J. Nonlinear Sci. Numer. Simul*, 7 (4) (2006) 411.
- [17] M. Rafei, D.D. Ganji, *Int. J. Nonlinear Sci. Numer. Simul*, 7 (3) (2006) 321.
- [18] He JH, Wu XH. Construction of solitary solution and compacton-like solution by variational iteration method. *Chaos, Solitons & Fractals*, 29 (2006) 108–121.
- [19] Barari A, Omidvar M, Ganji, D.D, Tahmasebi poor A. An Approximate Solution for Boundary Value Problems in Structural Engineering and Fluid Mechanics. *Journal of Mathematical Problems in Engineering*, 2008, In press.
- [20] Odibat ZM, Momani S. Application of variational iteration method to nonlinear differential equations of fractional order. *Int J Nonlinear Sci Numer Simulat*, 7 (2006) 27–34.
- [21] Bildik N, Konuralp A. The use of Variational Iteration Method, Differential Transform Method and Adomian Decomposition Method for solving different types of nonlinear partial differential equations. *Int J Nonlinear Sci Numer Simulat*, 7 (2006) 65–70.
- [22] SHA. Hashemi. K, S. M. Varedi, D. D. Ganji, Periodic Solution for Strongly Nonlinear Vibration Systems by New Couple Variational Approach, *Communications in Nonlinear Science and Numerical Simulations*, 2008, in press.
- [23] He JH, Variational approach for nonlinear oscillators, *Chaos, Solitons and Fractals*, 34 (2007) 1430–1439.
- [24] M. Naghipour, D.D. Ganji, SHA. Hashemi. K, Jafari, Analysis of non-linear oscillations systems using Analytical approach, *Journal of physics*, 96(2007) 012077.
- [25] V. Marinca, N. Herisanu. A modified iteration perturbation method for some nonlinear oscillation problems, *Acta Mech*, 184 (2006) 231–242.
- [26] A.H. Nayfeh, *Introduction to Perturbation Techniques*, Wiley, New York, 1981.
- [27] J.H. He, the homotopy perturbation method for nonlinear oscillators with discontinuities, *Applied Mathematics and Computation*, 151 (2004) 287–292.

ONE BIQUATERNION MODEL OF ELECTRO-GRAVYMAGNETIC FIELD

Alexeyeva Lyudmila A.

Institute of Mathematics, Pushkin str.125, Almaty, Kazakhstan, 050010

alexeeva@math.kz

Abstract. One biquaternion model for electro-gravymagnetic field (EGM) is considered, which is named as A-field. There is one hypothesis in the base of this model on equivalence of magnetic charge to the gravitational mass, which has allowed to use the Hamilton form of Maxwell's equations for building field analogues of three Newton's laws for material points. Tensions tensor for charges-currents field is built and equations of moving an electro-gravymagnetic medium which is like to equations of mechanics of continuous medium. The law of energy conservation is obtained like to the first thermodynamics beginning. With introduction the energy-pulse biquaternion of interaction, the conditions of separation, absorbing and conservations of energy at the interaction of masses, charges and currents are constructed.

Keywords: *Maxwell's equations, Newton's laws, mass, charge, currents, interaction, tensions tensor, conservation laws*

1. Algebra of biquaternions on Minkovskiy space. On the space $M = \{(\tau, x) : \tau \in R^1, x \in R^3\}$ one functional space of biquaternions is considered: $\mathbf{K}(M) = \{\mathbf{F} = f(x, \tau) + F(x, \tau)\}$, where f is complex function, F is three dimensional vector-function with complex components, f and F are locally integrable and differentiable on M . \mathbf{K} is linear space: for any complex numbers a and b

$$a\mathbf{F} + b\mathbf{G} = a(f + F) + b(g + G) = (af + bg) + (aF + bG), \quad (1.1)$$

with known operation of quaternions multiplying (\circ)

$$\mathbf{F} \circ \mathbf{G} = (f + F) \circ (g + G) = (fg - (F, G)) + (fG + gF + [F, G]). \quad (1.2)$$

Here (F, G) is usual scalar production of vectors F and G (without complex conjugation for second vector), $[F, G]$ is their vector production. \mathbf{K} is associative algebra but not commutative.

We enter *complex conjugate* biquaternion $\overline{\mathbf{F}} = \bar{f} + \overline{F}$ and *conjugate* biquaternion $\mathbf{F}^* = \bar{f} - \overline{F}$. If

$\mathbf{F} \circ \overline{\mathbf{F}} = \overline{\mathbf{F}} \circ \mathbf{F} = 1$, then it is *unitary* biquaternion. , if $\mathbf{F}^* = \mathbf{F}$, then quaternion is *self conjugate*.

Scalar production of $\mathbf{F}_1, \mathbf{F}_2$ is $(\mathbf{F}_1, \mathbf{F}_2) = f_1 \bar{f}_2 + (F_1, \overline{F_2})$. *Norma* of \mathbf{F} is

$\|\mathbf{F}\| = \sqrt{(\mathbf{F}, \overline{\mathbf{F}})} = \sqrt{f \cdot \bar{f} + (F, \overline{F})} = \sqrt{|f|^2 + \|F\|^2}$, *pseudonorma* of \mathbf{F} is defined as

$\langle \mathbf{F} \rangle = \sqrt{f \cdot \bar{f} - (F, \bar{F})} = \sqrt{|f|^2 - \|F\|^2}$. For example, the biquaternions $\mathbf{Z} = \tau + ix$, $\bar{\mathbf{Z}} = \tau - ix$ are self conjugate, $\mathbf{Z} = \mathbf{Z}^*$, $\bar{\mathbf{Z}} = \bar{\mathbf{Z}}^*$ and $\|\mathbf{Z}\| = \|\bar{\mathbf{Z}}\| = \sqrt{(\mathbf{Z}, \bar{\mathbf{Z}})}$, $\langle \mathbf{Z} \rangle^2 = \langle \bar{\mathbf{Z}} \rangle^2 = \mathbf{Z} \circ \bar{\mathbf{Z}}$.

We introduced the differential biquaternion operators of such type: $\mathbf{D}^+ = \partial_\tau + i\nabla$, $\mathbf{D}^- = \partial_\tau - i\nabla$, where $\nabla = grad = (\partial_1, \partial_2, \partial_3)$, $\partial_\tau = \frac{\partial}{\partial \tau}$. We named them as *mutual complex gradients*. By definition

$$\mathbf{D}^+ \mathbf{F} = (\partial_\tau + i\nabla) \circ (f + F) = (\partial_\tau f - i(\nabla, F) + \partial_\tau F + i\nabla f + i[\nabla, F]), \quad (1.3)$$

$$\mathbf{D}^- \mathbf{F} = (\partial_\tau - i\nabla) \circ (f + F) = (\partial_\tau f + i \operatorname{div} F) + \partial_\tau F - i \operatorname{grad} f - i \operatorname{rot} F.$$

Note, in the sense of above given determinations, $(\mathbf{D}^-)^* = \mathbf{D}^+$, $(\mathbf{D}^+)^* = \mathbf{D}^-$. Their superposition has the useful property: $\mathbf{D}^- (\mathbf{D}^+ \mathbf{F}) = \mathbf{D}^+ (\mathbf{D}^- \mathbf{F}) = (\mathbf{D}^- \circ \mathbf{D}^+) \mathbf{F} = \square \mathbf{F}$, where \square is the wave operator:

$\square = \frac{\partial^2}{\partial \tau^2} - \Delta$. Using this, it is possible to construct some solutions of differential equations on

$\mathbf{K}(M)$: $\mathbf{D}^\pm \mathbf{K} = \mathbf{G} \Rightarrow \square \mathbf{K} = \mathbf{D}^\mp \mathbf{G} \Rightarrow \mathbf{K} = \mathbf{D}^\mp \mathbf{G} * \psi$, where $\psi(\tau, x)$ is fundamental solution of wave equation: $\square \psi = \delta(\tau, x)$. Really, using property of convolution differentiation it is easy to see that

$$\mathbf{D}^\pm \mathbf{K} = \mathbf{D}^\pm \mathbf{D}^\mp (\mathbf{G} * \psi) = \square (\mathbf{G} * \psi) = (\mathbf{G} * \square \psi) = \mathbf{G} * \delta(\tau) \delta(x) = \mathbf{G}.$$

Here sign "*" is operation of convolution. Generalized function $\psi(\tau, x)$ is the simple layer on light cone $(\tau = \|x\|)$: $\psi = (4\pi\|x\|)^{-1} \delta(\tau - \|x\|)$.

2. Biquaternions of A-field. For description of EGM-field the such biquaternions are introduces [1,2]: the potential $\Phi = i\phi - \Phi$, tension $\mathbf{A} = 0 + A$, charge - current $\Theta = i\rho + J$. Here A is complex vector of tensions of EGM-field:

$$A = A^E + iA^H = \sqrt{\varepsilon} E + i\sqrt{\mu} H, \quad (2.1)$$

E, H are the tension of electric and gravymagnetic fields; ε, μ are the constants of electric conductivity and magnetic penetrable. Potential part H^P of vector H describes the tension of gravitational field, torsional (solenoidal) part H^t defines the tension of magnetic field: $H = H^P + H^t$, $\operatorname{div} H^t = 0$, $\operatorname{rot} H^P = 0$. Density of charge ρ is expressed through the density of electrical charge ρ^E and density of gravitational mass ρ^H : $\hat{\rho} = \operatorname{div} A = \varepsilon^{-1/2} \rho^E - i\mu^{-1/2} \rho^H$,

$$\rho^E = \varepsilon \operatorname{div} E, \quad \rho^H = -\mu \operatorname{div} H. \quad (2.2)$$

J - current is expressed through electrical (j^E) and gravymagnetic (j^H) currents with formula: $J = \sqrt{\mu} j^E - i\sqrt{\varepsilon} j^H$. Using the Hamilton form of Maxwell's equations [3], the equation of A-field may be written as one biquaternion equation [1]:

$$\mathbf{D}^+ \mathbf{A} + \mathbf{\Theta} = 0. \quad (2.4)$$

Note, in Maxwell's equations $\operatorname{div} H = 0$, but here we refuse from this condition and suppose second condition (2.2). It means that magnetic charge is equivalent to gravitational mass. Then potential part H^P defines gravitational field, but torsional part H^t defines magnetic field. This hypothesis has plausible effects, which we hereinafter show.

If potential Φ satisfies to Lorenz calibration: $\partial_\tau \phi - \operatorname{div} \Phi = 0$, then $\mathbf{D}^- \Phi = \operatorname{grad} \phi - \partial_\tau \Phi + i \operatorname{rot} \Phi = \mathbf{A}$ then $\square \Phi + \mathbf{\Theta} = 0$ and $\square \mathbf{A} = -\mathbf{D}^- \mathbf{\Theta} = -i(\partial_\tau \rho + \operatorname{div} J) - \nabla \rho - \partial_\tau J + i \operatorname{rot} J$. From scalar part of last equation we get the conservation law of charges:

$$\partial_\tau \rho + \operatorname{div} J = 0. \quad (2.5)$$

From vectorial part of it we get known equation for A [3]:

$$\square A = i \operatorname{rot} J - \nabla \rho - \partial_\tau J \quad (2.6)$$

We enter $\Xi = 0,5 \mathbf{A} \circ \mathbf{A}^* = W + iP$, named *energy-pulse* biquaternion, because $W = \varepsilon \|E\|^2 + \mu \|H\|^2$ is density of A-field energy, $P = c^{-1} [E, H]$ is Poynting vector, $c = 1/\sqrt{\varepsilon\mu}$ is light velocity.

Maxwell's equation (2.4) allows to define charges and currents of A-field, if its tension is known and other wise, on given charges and currents to find a tension of A-field as a solution of some Cauchy problem. I.e. it describes a system "material-field", mutually generating each other.

3. Equations of charges-currents interaction. Fields analogues of Newton's laws. Let consider two fields of charges-currents $\mathbf{\Theta}, \mathbf{\Theta}'$ and corresponding two fields \mathbf{A} и \mathbf{A}' . For their interaction description we introduced the biquaternion of *power-force*, which describes the action of one field on charges-currents of other:

$$\mathbf{F} = M - iF = -\mathbf{\Theta} \circ \mathbf{A}' = (A', J) - i\rho A' + [A', J], \quad (3.1)$$

$$\mathbf{F}' = M' - iF' = -\mathbf{\Theta}' \circ \mathbf{A} = -(i\rho' + J') \circ A = (A, J') - i\rho' A + [A, J']. \quad (3.2)$$

Here M is the power of acting force F :

$$M = (A', J) = c^{-1} ((E', j^E) + (H', j^H)) + i((B', j^E) - (D', j^H)), \quad (3.3)$$

where $B = \mu H$ is magnetic displacement vector, $D = \varepsilon E$ is electrical displacement vector. Calculating real and imaginary part of $F = F^H + iF^E$ we obtain:

$$F^H = \rho^E E' + \rho^H H' + j^E \times B' - j^H \times D'$$

$$F^E = c \left(\rho^E B' - \rho^H D' \right) + c^{-1} \left(E' \times j^E + H' \times j^H \right)$$

According to accepted hypothesis, at right part (3.3) we see all well known forces: first summand is electric Coulon's force, acting on electric charges; second summand is *gravymagnetic* force, acting on mass, it contains Newton's gravitational force in potential part of H ; third one is Laurence force, acting on electric currents in magnetic field. Last forth force we name *gravyelectric* force, which describes the action of electric field on moving masses and magnetic currents. It is interesting that power of Laurence force does not enter in real part (3.2), since, as is well known, it does not work at moving a mass. But in real part there are the powers of Coulon's and gravymagnetic forces as must be.

Naturally, on the strength of third Newton's law on acting and counteracting forces, we suppose that for (3.1) and (3.2) must fulfilled:

$$\mathbf{F}' = -\mathbf{F} \quad \text{i.e.} \quad \Theta \circ \mathbf{A}' = -\Theta' \circ \mathbf{A} \quad (3.4)$$

Interesting that in scalar part this equation requires equalities of powers of corresponding forces, acting on charges and currents of other field, i.e. befitted to known in mechanics identity of Betty reciprocity, which is usually written for work of forces.

For the determination of changing the charges-currents the equations system is offered, in the base of which there is one hypothesis, that changing the charges-currents, which is described by their complex gradient, occurs in power-force "direction", acting from the EGM-field generated by other charges-currents. It has following type:

$$\kappa \mathbf{D}^+ \Theta + \Theta \circ \mathbf{A}' = 0, \quad \kappa \mathbf{D}^+ \Theta' + \Theta' \circ \mathbf{A} = 0, \quad (3.5)$$

where interaction constant κ is incorporated. These equations correspond to the second Newton's law. Together with biquaternion form of Maxwell's equations for A-field

$$\mathbf{D}^+ \mathbf{A} + \Theta = 0, \quad \mathbf{D}^+ \mathbf{A}' + \Theta' = 0, \quad (3.6)$$

Eqs (3.4), (3.5) give the closed nonlinear system of differential equations for determinations of EGM-fields, their charges and currents.

Scalar and vector part of equations (3.5) give equations, which we name *the equation of charge-currents transformation* under the action of external field. So the first equation (3.5) is equivalence to the following two ones

$$i\kappa(\partial_\tau \rho - \text{div} J) = M, \quad i\kappa(\partial_\tau J + i \text{rot} J + \nabla \rho) = F. \quad (3.7)$$

Whence we obtain for imaginary and real part F two equations:

$$\kappa \left(\sqrt{\varepsilon} \partial_\tau j^H - \sqrt{\mu} \operatorname{rot} j^E - \frac{1}{\sqrt{\mu}} \nabla \rho^H \right) = \rho^E E' + \rho^H H' + j^E \times B' - j^H \times D' \quad (3.8)$$

$$\kappa \left(\sqrt{\mu} \partial_\tau j^E + \sqrt{\varepsilon} \operatorname{rot} j^H - \frac{1}{\sqrt{\varepsilon}} \nabla \rho^E \right) = c \left(\rho^E B' - \rho^H D' \right) + c^{-1} \left(E' \times j^E + H' \times j^H \right) \quad (3.9)$$

First Eq.(3.8) is the field analogue of second Newton's law. Eq.(3.9) describes transformation of electric currents under action of external EGM-field. If external A'-field is known they allow to find charges-currents of A-field. For instance, if one of the field is much more powerful then other ($\|A'\| \gg \|A\|$), its from-changing possible to neglect and consider A' as given.

Notice that own interaction of charges and currents of A-field is defined by the Maxwell's equations, which is unclosed. In absence of external field ($A' = 0$), it is closed by the equation free charges-currents (*free field*): $D^+ \Theta = 0$. It is field analogue of first Newton's law.

4. Conservation law of Θ -field energy. Similarly as density of energy of A-field [2] we enter density of energy-pulse of charges-currents, which is characterized by the value:

$$\Xi_\Theta = W_\Theta + iP_\Theta = 0,5 \Theta \circ \Theta^* = (i\rho + J) \circ (-i\bar{\rho} - \bar{J}) = 0,5 \left(|\rho|^2 + \|J\|^2 \right) - i \left\{ \operatorname{Re}(\rho \bar{J}) - 0,5i [J, \bar{J}] \right\},$$

$$W_\Theta = Q_\rho + Q_J = 0,5 \left(|\rho|^2 + \|J\|^2 \right) = 0,5 \left(|\rho^E|^2 / \varepsilon + |\rho^H|^2 / \mu + \mu \|j^E\|^2 + \varepsilon \|j^H\|^2 \right),$$

$$P_\Theta = P_J - \sqrt{\frac{\mu}{\varepsilon}} \rho^E j^E - \sqrt{\frac{\varepsilon}{\mu}} \rho^H j^H.$$

Here the scalar part W_Θ is strictly density of energy of charges-currents, where Q_J includes Joule heat $\|j^E\|^2$ and density of kinetic energy of mass currents $\|j^H\|^2$. Vector $P_J = 0,5c^{-1} [j^H, j^E]$ is similar to Pointing vector of A-field. Notice, if gravymagnetic and electrical currents are parallel and possible to enter velocity vector V then

$$\Xi_\Theta = 0,5 \Theta \circ \Theta^* = W_\Theta - iV \left(\sqrt{\frac{\mu}{\varepsilon}} (\rho^E)^2 + \sqrt{\frac{\varepsilon}{\mu}} (\rho^H)^2 \right) = W_\Theta - i \frac{V}{c} \left((\rho^E)^2 / \varepsilon + (\rho^H)^2 / \mu \right).$$

If to multiply scalar equation (3.5) on $(-i\bar{J})$, to take then the sum with corresponding complex-associate equation and divide on 2, we obtain

The law of energy conservation:

$$\kappa \left(\partial_\tau Q_J + \operatorname{div} P_J + \operatorname{Re}(\nabla \rho, \bar{J}) \right) = \sqrt{\mu} (F^E, j^E) - \sqrt{\varepsilon} (F^H, j^H), \quad (4.1)$$

which is similar to the law of conservation of energy for A-field [2,3]. However, a third summand with the gradient of density has appeared in the left part. This law is like to the first beginning of thermodynamics. Here first summand characterizes the velocity of heat changing. Two following summands

$$-U = \left(\operatorname{div} P_J + \sqrt{\varepsilon/\mu} \left(\nabla \rho^E, j^E \right) + \sqrt{\mu/\varepsilon} \left(\nabla \rho^H, j^H \right) \right)$$

characterize the velocity of changing density of internal energy U. Right part (5.1) describes power of acting forces.

5. Tensions pseudotensor. Equations of EGM medium. From formula (3.8) follows, that, using Levy-Chivita pseudotensor e_{ikl} we can introduce stress pseudotensor

$$\sigma_{ik}^H = -\kappa \left(\frac{\rho^H}{\sqrt{\mu}} \delta_{ik} + \sqrt{\mu} j_l^E e_{ikl} \right), \quad i, k, l = 1, 2, 3, \quad (5.1)$$

which is analogue of *stress tensor* (σ_{ik}) in liquid. Really, with its using Eq. (3.8) is similar to equations of liquid mechanics:

$$\begin{aligned} \partial_k \sigma_{ik}^H + F_i^H &= \kappa \varepsilon \sqrt{\mu} \partial_t j_i^H, \\ F_i^H &= \rho^E E_i' + \rho^H H_i' + j^E \times B_i' - j^H \times D_i'. \end{aligned} \quad (5.2)$$

The first summand in (5.2) is divergence of stress tensor, second one is the density of volume forces, and on the right part we see the analogue of derivative on time from density of motion quantity. But, as you see, usual symmetry property does not fulfilled: $\sigma_{ik} \neq \sigma_{ki}$.

In analogy, to write equations for changing the electrical currents (3.9), in similar type we enter *pseudotensor of electrical tensions*:

$$\sigma_{ik}^E = -\kappa \left(\frac{\rho^E}{\sqrt{\varepsilon}} \delta_{ik} - \sqrt{\varepsilon} j_l^H e_{ikl} \right) \quad (5.3)$$

With its help Eq.(3.9) is written as

$$\begin{aligned} \partial_k \sigma_{ik}^E + F_i^E &= \kappa \mu \sqrt{\varepsilon} \partial_t j_i^E, \\ F_i^E &= c \left(\rho^E B_i' - \rho^H D_i' \right) + c^{-1} \left(E_i' \times j^E + H_i' \times j^H \right) \end{aligned} \quad (5.5)$$

The analogue of this formula is unknown for us.

6. Energy-pulse of charges-currents interaction. If there are several (M) interacting fields, the equations (3.2) - (3.4) will be such

$$\kappa \mathbf{D}^- \Theta^k + \Theta^k \circ \sum_{m \neq k} \mathbf{A}^m = \mathbf{0}, \quad \mathbf{D}^+ \mathbf{A}^k + \Theta^k = \mathbf{0}, \quad k = 1, \dots, M \quad (6.1)$$

$$\mathbf{D}^+ \mathbf{A}^m \circ \mathbf{A}^k + \mathbf{D}^+ \mathbf{A}^k \circ \mathbf{A}^m = \mathbf{0}, \quad k \neq m \quad (6.2)$$

United field is generated by all charges and currents field. On the strength of the third law of Newton (3.4), as easy to see, it is free, as far as, similarly mechanics of interacting bodies, all forces are internal:

$$\kappa \mathbf{D}^- \Theta = \mathbf{D}^- \sum_{m=1}^M \Theta^m \equiv \mathbf{0}. \text{ I.e. united field is free.}$$

Transformation of energy of A-fields at the charges-currents interaction is considered in [2]. Let consider a transformation of energy of charges-currents at the interaction. Energy-pulse for united field is

$$\begin{aligned} \Xi_{\Theta} &= 0,5 \Theta \circ \Theta^* = 0,5 \sum_{k=1}^N \Theta^k \circ \sum_{l=1}^N \Theta^{*l} = 0,5 \left(\sum_{k=1}^N \Theta^k \circ \Theta^{*k} + \sum_{k \neq l} \Theta^k \circ \Theta^{*l} \right) = \\ &= \sum_{k=1}^N W_{\Theta}^{(k)} + i \sum_{k=1}^N P_{\Theta}^{(k)} + \delta \Xi_{\Theta} \end{aligned}$$

Here first summands are an amount of energy-pulses of acting charges-currents. We introduce the biquaternion of *energy-pulse of charges-currents interaction* $\delta \Xi_{\Theta} = \delta W_{\Theta} + i \delta P_{\Theta}$. Real scalar δQ_{Θ} describes energy of interactions of the same name charges and currents; real vector δP_{Θ} describes the pulse of interaction of different name charges and currents:

$$\begin{aligned} \delta \Xi_{\Theta} &= \delta W_{\Theta} + i \delta P_{\Theta} = \sum_{k \neq l} \Xi_{\Theta}^{kl}, \quad \Xi_{\Theta}^{kl} = 0,5 \left(\Theta^k \circ \Theta^{*l} + \Theta^l \circ \Theta^{*k} \right) \\ \Xi_{\Theta}^{kl} &= \text{Re} \left(\rho^k \rho^{*l} + (J^k, J^{*l}) \right) - i \left\{ \text{Re} \left(\rho^k J^{*l} + \rho^{*l} J^k \right) + \text{Im} [J^k, J^{*l}] \right\} \end{aligned}$$

or in initial indications

$$\begin{aligned} \Xi_{\Theta}^{kl} &= \frac{\rho^{E(k)} \rho^{E(l)}}{\sqrt{\varepsilon_k \varepsilon_l}} + \frac{\rho^{(k)H} \rho^{H(l)}}{\sqrt{\mu_k \mu_l}} + \sqrt{\mu_k \mu_l} \left(j^{(k)E}, j^{(l)E} \right) + \sqrt{\varepsilon_k \varepsilon_l} \left(j^{(k)H}, j^{(l)H} \right) - \\ &- i \left\{ \sqrt{\frac{\mu_l}{\varepsilon_k}} \rho^{(k)E} j^{(l)E} + \sqrt{\frac{\varepsilon_l}{\mu_k}} \rho^{(k)H} j^{(l)H} + \sqrt{\frac{\mu_k}{\varepsilon_l}} \rho^{(l)E} j^{(k)E} + \sqrt{\frac{\varepsilon_k}{\mu_l}} \rho^{(l)H} j^{(k)H} - \right. \\ &\quad \left. - \sqrt{\varepsilon_k \mu_l} [j^{(l)E}, j^{(k)H}] + \sqrt{\varepsilon_l \mu_k} [j^{(k)E}, j^{(l)H}] \right\} \end{aligned}$$

As a result we get conditions on transformation of energy at interaction of charges-currents:

separation of energy, if $\delta W_{\Theta} > 0$;

absorption of energy, if $\delta W_{\Theta} < 0$;

conservation of energy-pulse, if $\delta \Xi_{\Theta} = 0$.

Notice that equation of A-field does not contain universal constants. Equations of interaction of charges-currents contain only one universal dimensioned constant κ . That allows to unite tensions, charges and currents and enter united EGM-field.

Conclusion

Equations of A-fields interaction are based on the hypothesis on equivalence of the magnetic charge to gravitational mass. We have shown that for gravymagnetic charge-currents they are similar to Newton's laws for material bodies. On their base it's possible to explain many observed physical phenomena. For instance, well known that constant revolving electrical currents generate solenoidal magnetic fields. From the present theory similarly follows that revolving masses create solenoidal electrical fields (this possible to check experimentally). This explains, for instance, presence of electrical axis in the Earth, electrical field of the Earth in consequence of its rotating, and beside other planets.

Other example. According to this theory it should take into account that electrical field of Sun generates gravelectric force, displacing orbits of planets. Interesting that in paper [4] for the determination of Mercury perihelion displacement, what is unexplained within the framework of the classical gravitational theory, in Newton's equations for two bodies the one additional power was incorporated, what was named by authors "cogravity ". On the form it's like to gravelectric force, which was considered here. Presented theory gives also earlier unknown equations of changing electrical charges and currents under the action of the EGM-fields.

References

- [1] Alexeyeva L.A., (2004), "On the one model of electro-gravymagnetic field. Interaction equations and conservation laws". *Mathematical Journal*. V.4. #2. P.23-34.
- [2] Alexeyeva L.A., (2004), "Interaction equations of A-fields and Newton's laws". *News of National Ac. of Sci. of Rep. Kazakhstan. Physical and mathematical series*. #3. P.45-53.
- [3] Alexeyeva L.A., (2003), "Hamilton form of Maxwell's equation and its generalized solutions". *Differential equations*. V.39. #6. P.769-776.
- [4] Matos C.J., Tajmar M., (2003), "Advance of Mercury Perihelion Explained by Cogravity".
<http://arxiv.org/ftp/gr-qc/papers/0304/0304104.pdf>

On the gravitational collapse of relativistic binary pulsars

K. Mamehrashi*
Payame Noor University(PNU)

April 18, 2008

Abstract

In the study of Long term Nonlinear evolution of Keplerian binary system under the combined action of perturbations due to the emission and absorption of gravitational radiation averaging is usually employed.we studied the perturbation of gravitational radiation in binary system with two order and analyzed it by numerical method with Lie transforms.

1 Introduction

The Dynamical evolution of a binary orbit under perturbations due to the absorption as well as the emission of gravitational radiation is the subject of this paper.we consider the traditional Kepler problem except that post-Newtonian effect of gravitational radiation damping is taken into account in the quadruple approximation.we use the Lie transformations to extend the order of equations into 2 and express the orbit of motion in configuration space.we compare the orbits of motion in ϵ and ϵ^2 orders.we show that the system remain planar and loses energy and angular momentum such that eventually $L \rightarrow 0, G \rightarrow 0$ and the system collapses.

2 The Fundamental Algorithm

In this section we explain two prepositions of Lie transforms which are applied in our survey.

*The author is supported in part by Payame Noor university of Boukan.

proposition 1:given a differential system

$$(1) \quad \frac{dx}{dt} = f(x, \epsilon) = \sum_{i \geq 0} \frac{\epsilon^i}{i!} f_i^{(0)}(x)$$

such that $x = (q, p)$ represents a set of canonical variables of coordinates q and momenta p . Moreover the function $f_i^0, i \geq 0$ are decomposed in two different parts

$$f_i^{(0)}(x) = f_{H_i}^{(0)}(x) + f_{NH_i}^{(0)}(x)$$

, such that $f_{H_i}^{(0)}$ come from a Hamiltonian function $H_i^{(0)}$, then equation (1) is transformed, though the generating function

$$W(x, \epsilon) = \sum_{i \geq 1} \frac{\epsilon^i}{i!} (W_i^H(x) + W_i^{NH}(x))$$

into another differential equation

$$\frac{dy}{dt} = f^*(y, \epsilon) = \sum_{i \geq 0} \frac{\epsilon^i}{i!} (f_{H_0}^{(i)}(y) + f_{NH_0}^{(i)}(y)),$$

which the terms of $f_{H_0}^{(i)}, i \geq 0$ are obtained by calculating $f_{H_j}^{(i)} = \wp \cdot \text{grad}_x H_j^{(i)}$, with the symplectic matrix \wp , and $H_j^{(i)}$ by using the algorithm of Lie transforms for Hamiltonians

$$H_j^{(i)} = H_{j+1}^{(i-1)} + \sum_{0 \leq k \leq j} \binom{j}{k} \{H_{j-k}^{(i-1)}; \nu_{k+1}\}, \quad \text{for } j \geq 0, i \geq 1.$$

Finally, the terms $f_{NH_0}^{(i)}, i \geq 1$ are calculated with

$$f_{NH_j}^{(i)} = f_{NH_{j+1}}^{(i-1)} + \sum_{0 \leq k \leq j} \binom{j}{k} [(L_{k+1}^H + L_{k+1}^{NH})f_{NH_{j-k}}^{(i-1)} + L_{k+1}^{NH}f_{H_{j-k}}^{(i-1)}]$$

also for $j \geq 0, i \geq 1$. The Lie operators L^H and L^{NH} are defined by

$$L_j^\circ S = \frac{\partial S}{\partial x} \cdot W_j^\circ - \frac{\partial W_j^\circ}{\partial x} \cdot S, \quad \text{with } \circ = H \text{ or } NH$$

proposition 2: The direct transformation $x = \sum \frac{\epsilon^i}{i!} y_0^{(i)}(y)$ is given by

$$y_j^{(i)} = y_{j+1}^{(i-1)} + \sum_{0 \leq k \leq j} \binom{j}{k} L_{k+1} y_{j-k}^{(i-1)}(y),$$

where $L_j S = \frac{\partial S}{\partial y} . W_j$ with $y_0^{(0)} = y, y_j^{(0)} (j > 0)$, and the inverse transformation $y = \sum \frac{\epsilon^i}{j!} x_j^{(0)}(x)$

$$x_j^{(i)} = x_{j-1}^{(i+1)} - \sum_{0 \leq k \leq j-1} \binom{j-1}{k} L_{k+1} x_{j-k-1}^{(i)}(x),$$

where $L_j S = \frac{\partial S}{\partial y} . W_j$ with $x_0^{(0)} = x, x_0^{(i)} (i > 0)$

3 Collapsing relativistic binaries with gravitational radiation

In the quadruple approximation under consideration here, gravitational waves carry energy and angular momentum away from the system but not linear momentum. Similarly, in absorption the orbit exchanges energy and angular momentum with the incident gravitational wave but not linear momentum.

The state of relative motion is specified by $(r, \theta, p_r, p_\theta)$ in polar coordinates; therefore using the standard formulae for elliptic motion we have $p_r p_\theta = e \sin \hat{\nu}$ and $p_\theta^2 / r = 1 + e \cos \hat{\nu}$, which uniquely specify the eccentricity e and the true anomaly $\hat{\nu}$ of the osculating ellipse.

The action-angle variables appropriate to the Kepler problem are the Delaunay elements that are given for the planar problem under consideration by

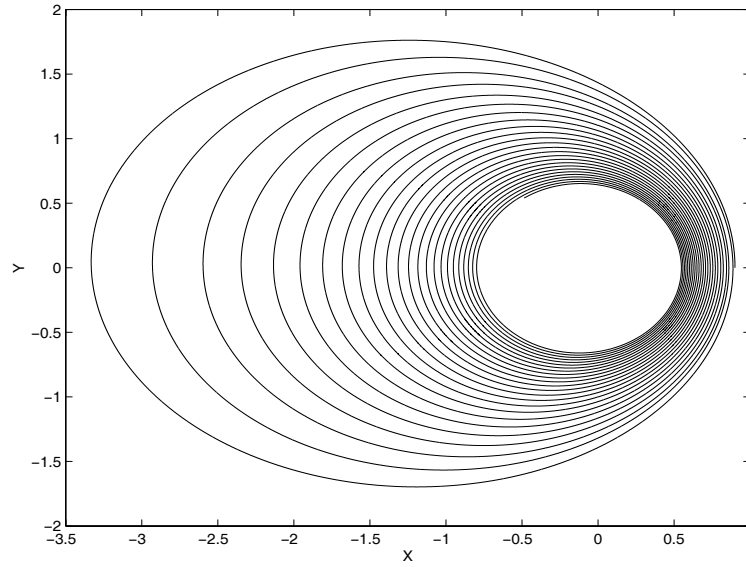
$$(2) \quad \begin{aligned} L : &= (ka)^{\frac{1}{2}}, & G := p_\theta &= L(1 - e^2)^{\frac{1}{2}}, \\ \ell : &= \hat{u} - e \sin \hat{u}, & g := \theta - \hat{\nu}. \end{aligned}$$

Our equation in this case are:

$$(3) \quad \begin{aligned} \frac{dL}{dt} &= \epsilon f_L, \\ \frac{dG}{dt} &= \epsilon f_G, \\ \frac{d\ell}{dt} &= \omega + \epsilon f_\ell, \\ \frac{dg}{dt} &= \epsilon f_g, \end{aligned}$$

Where

$$\begin{aligned} f_L &= \frac{4}{Lr^3} \left[1 - \frac{16}{3} \frac{L^2}{r} + \left(\frac{20}{3} L^2 - \frac{17}{2} G^2 \right) \frac{L^2}{r^2} + \frac{50}{3} \frac{L^4 G^2}{r^3} - \frac{25}{2} \frac{L^4 G^4}{r^4} \right], \\ f_G &= -\frac{18G}{L^2 r^3} \left(1 - \frac{20}{9} \frac{L^2}{r} + \frac{5}{3} \frac{L^2 G^2}{r^2} \right), \end{aligned}$$

Figure 1: The graph of motion in averaged system with ϵ order

$$\begin{aligned}
 f_\ell &= \frac{2 \sin \hat{\nu}}{e L^2 r^3} \left[4e^2 + \frac{1}{3} (73G^2 - 40L^2) \frac{1}{r} - 2 \left(1 + \frac{70}{3} L^2 - \frac{29}{2} G^2 \right) \frac{G^2}{r^2} \right. \\
 (4) \quad &- \left. \frac{25}{3} \frac{L^2 G^4}{r^3} + 25 \frac{L^2 G^6}{r^4} \right], \\
 f_g &= -\frac{2 \sin \hat{\nu}}{e L^2 r^3} \left[11 + \left(7G^2 - \frac{80}{3} L^2 \right) \frac{1}{r} - \frac{25}{3} \frac{L^2 G^2}{r^2} + 25 \frac{L^2 G^4}{r^3} \right],
 \end{aligned}$$

and

$$\omega = \frac{k^2}{L^3}$$

The eccentric anomaly \hat{u} can be determined from

$$\cos \hat{\nu} = \frac{\cos \hat{u} - e}{1 - e \cos \hat{u}}, \quad \sin \hat{\nu} = \frac{\sqrt{1 - e^2} \sin \hat{u}}{1 - e \cos \hat{u}}.$$

By the averaging theorem and integration on true anomaly we get

$$\begin{aligned}
 \dot{\ell} &= \frac{k^2}{L^3}, \\
 \dot{g} &= 0, \\
 (5) \quad \dot{L} &= -\epsilon \left(\frac{37}{12 L^4 G^3} - \frac{61}{2 L^2 G^5} + \frac{425}{12 G^7} \right), \\
 \dot{G} &= -\epsilon \left(\frac{15}{L^3 G^4} - \frac{7}{L^5 G^2} \right),
 \end{aligned}$$

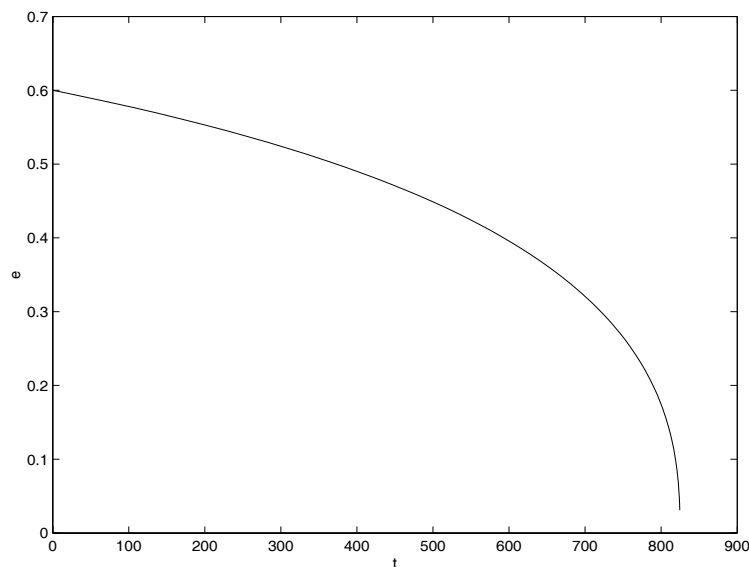


Figure 2: The graph of e with respect to time in averaged system

We apply the Runge-Kutta method for solving of equations (5).
indeed we use the Keplerian equations and

$$\begin{aligned} X &= a \cos E \cos g - ae \cos g - a\sqrt{1-e^2} \sin E \sin g, \\ Y &= a \cos E \sin g - ae \sin g + a\sqrt{1-e^2} \sin E \cos g. \end{aligned}$$

Where the orbit of motion is shown in Figure(1).

In order to get a good impression from our system we take into account the changes of e in a long time.

Figure(2) describes the changes of e respect to time,as gradually because of system dissipative, the elliptic orbit changes to circle orbit.

Now we extend the statements of equations (5) to order ϵ^2 .this system able to describe the long behaviour of relativistic binaries.

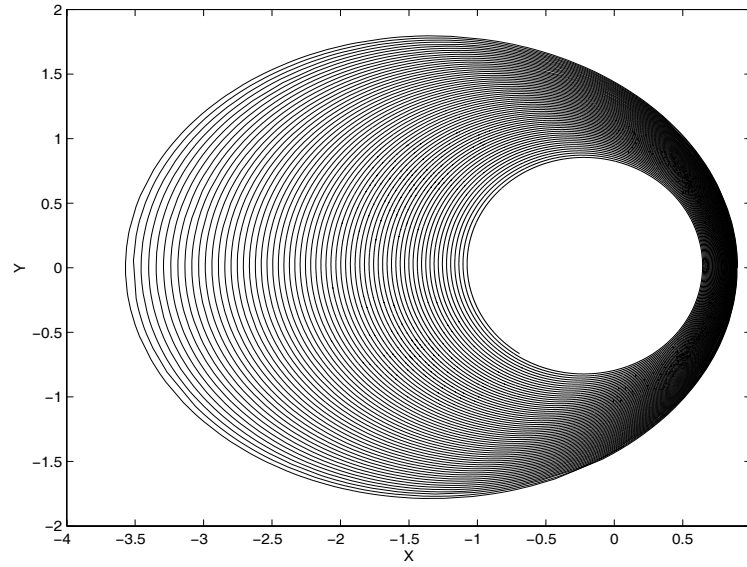
Referring to preposition (1) we have

$$f_{NH_0}^{(1)} = f_{NH_1}^{(0)} + L_1^{II} f_{H_0}^{(0)}$$

where, by substitution and preposition (2) we can obtain W_1^{II} , the coefficient of ϵ in generating function.

The coefficient of ϵ^2 in object function is

$$f_{NH_0}^{(2)} = f_{NH_1}^{(1)} + (L_1^I + L_1^{II}) f_{NH_0}^{(1)} + L_1^{II} f_{H_0}^{(1)}$$

Figure 3: The motion graph of equations (6) with $\epsilon = 10^{-4}$

on the other hand,

$$\begin{aligned} f_{NH_1}^{(1)} &= f_{NH_2}^{(0)} + [(L_1^I + L_1^{II})f_{NH_1}^{(0)} + L_1^{II}f_{H_1}^{(0)}] + (L_2^I + L_2^{II})f_{NH_0}^{(0)} + L_2^{II}f_{H_0}^{(0)} \\ &= L_1^{II}f_{NH_1}^{(0)} + L_2^{II}f_{H_0}^{(0)} \end{aligned}$$

Therefore,

$$f_{NH_0}^{(2)} = L_1^{II}f_{NH_0}^{(1)} + L_1^{II}f_{NH_1}^{(0)} + L_2^{II}f_{H_0}^{(0)}$$

so we apply the averaging theorem for statements

$$L_1^{II}f_{NH_1}^{(0)} + L_2^{II}f_{H_0}^{(0)}$$

Which Lie operators are introduced in preposition (1).

The final equations will be

$$\begin{aligned} \dot{\ell} &= \frac{k^2}{L^3} + \epsilon^2 D_1, \\ \dot{g} &= \epsilon^2 D_2, \\ (6) \quad \dot{L} &= -\epsilon \left(\frac{37}{12L^4G^3} - \frac{61}{2L^2G^5} + \frac{425}{12G^7} \right) + \epsilon^2 D_3, \\ \dot{G} &= -\epsilon \left(\frac{15}{L^3G^4} - \frac{7}{L^5G^2} \right) + \epsilon^2 D_4, \end{aligned}$$

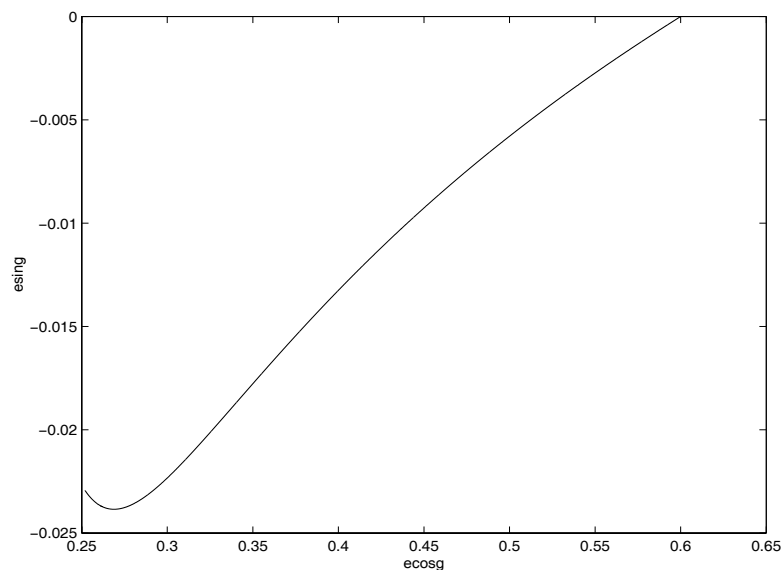


Figure 4: The components graph of $e \cos g$ and $e \sin g$

Where the coefficients D_1, D_2, D_3 and D_4 are calculated in terms of Delaunay elements, L and G .

Figure(3) explains the orbit which has obtained from equations(6) as it accentuates the previous results and exactly shows the long behaviour of system, losses energy and finally collapses.

As well as, Figure(4) is the dynamic of e and g . In fact it shows the changing both of e and g in that case.

We studied the perturbation of gravitational radiation in binary system with two order and analyzed it. Also we showed that the effects of gravitational radiation make the system collapses. of course this property is studied in two order but we would like to survey and compare our result by another method. We use Poncare mapping algorithm which have tried to eliminate complicating of system.

In this case we only concentrate our concerns on the changes of e with respect to time.

Figure(5) is the view of e changing respect to time in Poncare mapping which verifies and completes our numerical results in lie method.

ACKNOWLEDGMENT. we would like to express our gratitude to Professors R. Bario and J. Palacian for their valuable comments and suggestions.

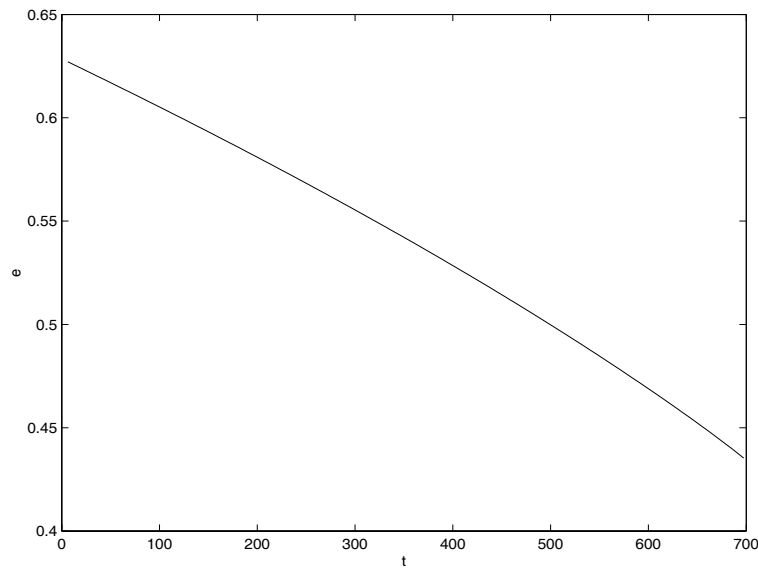


Figure 5: The graph of e in time in Poncare mapping

REFERENCES

1. A.Deprit, "Canonical Transformations Depending on a small Parameter", *Celestial Mechanics 1* (1969) 12-30
2. R.Barrio, and J.Palacian, "Lie Transformations for ordinary differential equations: Taking Advantage of the hamiltonian form of terms of the perturbation", *International Journal for numerical methods in engineering* Vol.40,(1997) 2289-2300
3. K.R.Meyer, "Perturbation analysis of nonlinear systems" in E Tournier (ed), *Computer Algebra and Differential Equations*, Combridge University Press, Cambridge , 1994, pp. 103-139
4. J.Henrard, "on a perturbation theory using lie transforms", *Celestial Mechanics 3* (1970) 107-120
5. A.A.Kamel, "Perturbation Method in the theory of nonlinear oscilations, *Celestial Mechanics 3* (1970) 90-106
6. R.Barrio, "Construction of seminumerical schemes:applications to the artificial satellite problem", *Appeared in L.Vulkov, J.Wasniewski, and P.Yalamov*

(Eds.): *NNA 2000*, *LNCS 1988*, Springer-Verlag Berlin Heidelberg, pp.42-50, (2001).

7. D.Boccaletti, and G.Pucacco, "Theory of orbits", 1: Integrable System and Non-perturbative Methods, Springer (1996) 125-156
8. C.Chiconet, B.Mashhoon and D.G.Retzloff, "Gravitational ionization: a chaotic net in the kepler system", *Class Quantum Gravitational* 14 (1997) 699-723
9. J.Guckenheimer, and P.Holmes, "Nonlinear Oscillations, Dynamical Systems and Bifurcations of vector fields", springer (1983) 167-168

Instructions to Contributors

Journal of Applied Functional Analysis

A quarterly international publication of Eudoxus Press, LLC of TN.

Editor in Chief: George Anastassiou

Department of Mathematical Sciences
University of Memphis
Memphis, TN 38152-3240, U.S.A.

1. Manuscripts, hard copies in quadruplicate and in English, should be submitted by regular, unregistered mail, to the Editor in Chief.

Authors may want to recommend an associate editor most related to the submission to possibly handle it. In addition, to assist the Editor and speed the decision process, authors may include a PDF file of the paper on disk with the submitted copies of the manuscript.

Also authors may want to submit a list of six possible referees, to be used in case we cannot find related referees by ourselves.

2. Manuscripts should be typed using any of TEX, LaTeX, AMS-TEX, or AMS-LaTeX and according to EUDOXUS PRESS, LLC. LATEX STYLE FILE. (Click [HERE](#) to save a copy of the style file.) They should be carefully prepared in all respects. Submitted copies should be brightly printed (not dot-matrix), double spaced, in ten point type size, on one side high quality paper 8(1/2)x11 inch. Manuscripts should have generous margins on all sides and should not exceed 24 pages.

3. Submission is a representation that the manuscript has not been published previously in this or any other similar form and is not currently under consideration for publication elsewhere. A statement transferring from the authors (or their employers, if they hold the copyright) to Eudoxus Press, LLC, will be required before the manuscript can be accepted for publication. The Editor-in-Chief will supply the necessary forms for this transfer. Such a written transfer of copyright, which previously was assumed to be implicit in the act of submitting a manuscript, is necessary under the U.S. Copyright Law in order for the publisher to carry through the dissemination of research results and reviews as widely and effectively as possible.

4. The paper starts with the title of the article, author's name(s) (no titles or degrees), author's affiliation(s) and e-mail addresses. The affiliation should comprise the department, institution (usually university or company), city, state (and/or nation) and mail code.

The following items, 5 and 6, should be on page no. 1 of the paper.

5. An abstract is to be provided, preferably no longer than 150 words.
6. A list of 5 key words is to be provided directly below the abstract. Key words should express the precise content of the manuscript, as they are used for indexing purposes.

The main body of the paper should begin on page no. 1, if possible.

7. All sections should be numbered with Arabic numerals (such as: 1. INTRODUCTION) .

Subsections should be identified with section and subsection numbers (such as 6.1. Second-Value Subheading).

If applicable, an independent single-number system (one for each category) should be used to label all theorems, lemmas, propositions, corollaries, definitions, remarks, examples, etc. The label (such as Lemma 7) should be typed with paragraph indentation, followed by a period and the lemma itself.

8. Mathematical notation must be typeset. Equations should be numbered consecutively with Arabic numerals in parentheses placed flush right, and should be thusly referred to in the text [such as Eqs.(2) and (5)]. The running title must be placed at the top of even numbered pages and the first author's name, et al., must be placed at the top of the odd numbered pages.

9. Illustrations (photographs, drawings, diagrams, and charts) are to be numbered in one consecutive series of Arabic numerals. The captions for illustrations should be typed double space. All illustrations, charts, tables, etc., must be embedded in the body of the manuscript in proper, final, print position. In particular, manuscript, source, and PDF file version must be at camera ready stage for publication or they cannot be considered.

Tables are to be numbered (with Roman numerals) and referred to by number in the text. Center the title above the table, and type explanatory footnotes (indicated by superscript lowercase letters) below the table.

10. List references alphabetically at the end of the paper and number them consecutively. Each must be cited in the text by the appropriate Arabic numeral in square brackets on the baseline.

References should include (in the following order):
 initials of first and middle name, last name of author(s)
 title of article,
 name of publication, volume number, inclusive pages, and year of publication.

Authors should follow these examples:

Journal Article

1. H.H.Gonska, Degree of simultaneous approximation of bivariate functions by Gordon operators, (journal name in italics) *J. Approx. Theory*, 62,170-191(1990).

Book

2. G.G.Lorentz, (title of book in italics) *Bernstein Polynomials* (2nd ed.), Chelsea, New York, 1986.

Contribution to a Book

3. M.K.Khan, Approximation properties of beta operators, in (title of book in italics) *Progress in Approximation Theory* (P.Nevai and A.Pinkus, eds.), Academic Press, New York, 1991, pp.483-495.

11. All acknowledgements (including those for a grant and financial support) should occur in one paragraph that directly precedes the References section.

12. Footnotes should be avoided. When their use is absolutely necessary, footnotes should be numbered consecutively using Arabic numerals and should be typed at the bottom of the page to which they refer. Place a line above the footnote, so that it is set off from the text. Use the appropriate superscript numeral for citation in the text.

13. After each revision is made please again submit four hard copies of the revised manuscript. And after a manuscript has been accepted for publication submit four hard copies of the final revised manuscript. Additionally, two copies of the final version of the TEX/LaTeX source file and a PDF file, are to be submitted to the Editor's Office on personal 3.5 inch computer disks. Label the disks individually with clearly written identifying information, e.g. :

Your name, title of article, kind of computer used, kind of software and version number, disk format and files names of article, as well as abbreviated journal name.

Package the disks in a disk mailer or protective cardboard. Make sure contents of disks are identical with the ones of final hard copies submitted!

Note: The Editor's Office cannot accept the disks without the accompanying matching hard copies of manuscript. No e-mail final submissions are allowed! File submission on disk must be used.

14. Effective 1 Jan. 2009 the journal's page charges are \$15.00 per PDF file page, plus \$40.00 for electronic publication of each article. Upon acceptance of the paper an invoice will be sent to the contact author. The fee payment will be due one month from the invoice date. The article will proceed to publication only after the fee is paid. The charges are to be sent, by money order or certified check, in US dollars, payable to Eudoxus Press, LLC, to the address shown on the Eudoxus [homepage](#).

No galleys will be sent and the contact author will receive one(1) electronic copy of the journal issue in which the article appears.

15. This journal will consider for publication only papers that contain proofs for their listed results.

TABLE OF CONTENTS, JOURNAL OF APPLIED FUNCTIONAL ANALYSIS,
VOLUME 4, NO.3, 2009

PREFACE,	372
A VISUAL BASIC SOFTWARE FOR COMPUTING OF THE ONE-DIMENSIONAL HEAT EQUATION BY USING B-SPLINE SOLUTION, H.CAGLAR, L.CUHACI, N.CAGLAR, M.OZER,	373
SOLUTION OF BEAM DEFORMATION EQUATION USING PERTURBATION AND HOMOTOPY PERTURBATION METHODS, A.J.CHOOBASTI, F.FARROKHZAD, A.K.MOOSAVI, A.BARARI, D.D.GANJI,	392
THE ‘CHAOSMOTIC’ AND ENTROPIC SITUATIONS OF CONTEMPORARY ART MUSEUMS, D.BALIK,	400
GENERATION OF CHAOTIC OSCILLATIONS IN DYNAMICAL SYSTEM WITH FIELD-EFFECT TRANSISTOR AS AN ACTIVE ELEMENT, A.S.DMITRIEV, E.V.EFREMOVA, L.V.KUZMIN, A.N.MILIOU, S.G.STAVRINIDES,	409
ANALYSIS OF WAVE EQUATION IN PILES DURING IMPACT DRIVING USING APPROXIMATE METHODS , F.FARROKHZAD, A.J.CHOOBASTI, A.BARARI, D.D.GANJI,	417
ERGODICITY OF NONLINEAR TRANSFORMATIONS, N.N.GANIKHODJAEV,	430
IDENTIFICATION OF AN ATTRACTOR IN THE NONLINEAR RESPONSES OF THE HEAD AT SMALL AMPLITUDES, S.GURSES,	434
ON THE APPROXIMATE EXPLICIT SOLUTION OF LINEAR AND NON-LINEAR NON-HOMOGENEOUS DISSIPATIVE WAVE EQUATIONS, S.HA.HASHEMI.K., N.TOLOU, A. BARARI,A.J.CHOOBASTI,	449
ECOLOGICAL COMPLEXITY: A HEURISTIC EXPLANATION OF FOURTH DIMENSION OF LIFE, J.H.HE,	459

TABLE OF CONTENTS, JOURNAL OF APPLIED FUNCTIONAL ANALYSIS,
VOLUME 4, NO.3, 2009, continued from inside back cover

FUTALOGNKOSAURUS DUKEI: COST AND BENEFIT OF BEING THE BIGGEST, J.H.HE, Q.YANG, L.F. MO,.....	470
COMPLEX EVOLUTION OF BUILT ENVIRONMENT, H.S.KAYA, F.BOLEN,.....	475
THE NEW CLASS OF SUPER-IMPLICIT SECOND DERIVATIVE MULTISTEP METHODS FOR STIFF SYSTEMS, M.M.KHALSARAYI, M.Y.R.ARDABILI, G.HOJJATI,.....	492
SOLVING SYSTEMS OF NON-LINEAR VOLTERRA INTEGRO-DIFFERENTIAL EQUATIONS BY USING AN OPERATIONAL METHOD, A.KHANI, S.SHAHMORAD,.....	501
MODELING OF MULTILANE HIGHWAY TRAFFIC WITH AN AUXILIARY LANE, M.L.KURNAZ, A.N.IMREM, H.T. KING,.....	510
BIFURCATION SCENARIOS OF SOME MODIFIED PREDATOR – PREY NONLINEAR SYSTEMS, I.KUSBeyZI, A.HACINLIYAN,.....	519
SOLUTION OF STRONGLY NONLINEAR OSCILLATION SYSTEMS USING VARIATIONAL APPROACH, S.HA.HASHEMI.K., A.BARARI, N.TOLOU, D.D.GANJI,.....	528
ONE BIQUATERNION MODEL OF ELECTRO-GRAVYMAGNETIC FIELD, A.LYUDMILA A.,.....	536
ON THE GRAVITATIONAL COLLAPSE OF RELATIVISTIC BINARY PULSARS, K.MAMEHRASHI.,.....	544

Volume 4, Number 4

October 2009

ISSN:1559-1948 (PRINT), 1559-1956 (ONLINE)

EUDOXUS PRESS,LLC



JOURNAL OF APPLIED FUNCTIONAL ANALYSIS

GUEST EDITORS: HIKMET CAGLAR and MEHMET OZER

SPECIAL ISSUE III: "CHAOS and COMPLEX SYSTEMS 2008"

SCOPE AND PRICES OF
JOURNAL OF APPLIED FUNCTIONAL ANALYSIS
A quarterly international publication of **EUDOXUS PRESS,LLC**
ISSN:1559-1948(PRINT),1559-1956(ONLINE)

Editor in Chief: George Anastassiou
Department of Mathematical Sciences
The University of Memphis
Memphis, TN 38152,USA
E mail: ganastss@memphis.edu

The purpose of the "Journal of Applied Functional Analysis"(JAFA) is to publish high quality original research articles, survey articles and book reviews from all subareas of Applied Functional Analysis in the broadest form plus from its applications and its connections to other topics of Mathematical Sciences. A sample list of connected mathematical areas with this publication includes but is not restricted to: Approximation Theory, Inequalities, Probability in Analysis, Wavelet Theory, Neural Networks, Fractional Analysis, Applied Functional Analysis and Applications, Signal Theory, Computational Real and Complex Analysis and Measure Theory, Sampling Theory, Semigroups of Operators, Positive Operators, ODEs, PDEs, Difference Equations, Rearrangements, Numerical Functional Analysis, Integral equations, Optimization Theory of all kinds, Operator Theory, Control Theory, Banach Spaces, Evolution Equations, Information Theory, Numerical Analysis, Stochastics, Applied Fourier Analysis, Matrix Theory, Mathematical Physics, Mathematical Geophysics, Fluid Dynamics, Quantum Theory. Interpolation in all forms, Computer Aided Geometric Design, Algorithms, Fuzzyness, Learning Theory, Splines, Mathematical Biology, Nonlinear Functional Analysis, Variational Inequalities, Nonlinear Ergodic Theory, Functional Equations, Function Spaces, Harmonic Analysis, Extrapolation Theory, Fourier Analysis, Inverse Problems, Operator Equations, Image Processing, Nonlinear Operators, Stochastic Processes, Mathematical Finance and Economics, Special Functions, Quadrature, Orthogonal Polynomials, Asymptotics, Symbolic and Umbral Calculus, Integral and Discrete Transforms, Chaos and Bifurcation, Nonlinear Dynamics, Solid Mechanics, Functional Calculus, Chebyshev Systems. Also are included combinations of the above topics.

Working with Applied Functional Analysis Methods has become a main trend in recent years, so we can understand better and deeper and solve important problems of our real and scientific world.

JAFA is a peer-reviewed International Quarterly Journal published by Eudoxus Press,LLC.

We are calling for high quality papers for possible publication. The contributor should send four copies of the contribution to the EDITOR in CHIEF in TEX,LATEX double spaced,in ten point type size. They should be sent BY REGULAR MAIL ONLY, NOT REGISTERED MAIL, AND NO E-MAIL SUBMISSIONS [See: Instructions to Contributors]

Journal of Applied Functional Analysis(JAFA)
is published in January, April, July and October of each year by

EUDOXUS PRESS,LLC,

1424 Beaver Trail Drive,Cordova,TN38016,USA,

Tel.001-901-751-3553

anastassioug@yahoo.com

<http://www.EudoxusPress.com> visit also <http://www.msci.memphis.edu/~ganastss/jafa>.

Webmaster:Ray Clapsadle

Annual Subscription Current Prices:For USA and Canada,Institutional:Print \$280,Electronic \$220,Print and Electronic \$350.Individual:Print \$ 100, Electronic \$60,Print &Electronic \$150.For any other part of the world add \$40 more to the above prices for Print.
Single article PDF file for individual \$10.Single issue in PDF form for individual \$40.

The journal carries page charges \$15 per page of the pdf file of an article, plus \$40 for the electronic publication of all article, both payable upon acceptance of the article within one month and before publication.

No credit card payments.Only certified check,money order or international check in US dollars are acceptable.

Combination orders of any two from JoCAAA,JCAAM,JAFa receive 25% discount,all three receive 30% discount.

Copyright©2009 by Eudoxus Press,LLC all rights reserved.JAFa is printed in USA.

JAFa is reviewed and abstracted by AMS Mathematical Reviews,MATHSCI,and Zentralblatt MATH.

It is strictly prohibited the reproduction and transmission of any part of JAFa and in any form and by any means without the written permission of the publisher.It is only allowed to educators to Xerox articles for educational purposes.The publisher assumes no responsibility for the content of published papers.

JAFa IS A JOURNAL OF RAPID PUBLICATION

Journal of Applied Functional Analysis

Editorial Board

Associate Editors

Editor in-Chief:

George A. Anastassiou
Department of Mathematical Sciences
The University of Memphis
Memphis, TN 38152, USA
901-678-3144 office
901-678-2482 secretary
901-751-3553 home
901-678-2480 Fax
ganastss@memphis.edu
Approximation
Theory, Inequalities, Probability,
Wavelet, Neural Networks, Fractional Calculus

Associate Editors:

1) Francesco Altomare
Dipartimento di Matematica
Universita' di Bari
Via E. Orabona, 4
70125 Bari, ITALY
Tel+39-080-5442690 office
+39-080-3944046 home
+39-080-5963612 Fax
altomare@dm.uniba.it
Approximation Theory, Functional Analysis,
Semigroups and Partial Differential
Equations,
Positive Operators.

2) Angelo Alvino
Dipartimento di Matematica e Applicazioni
"R. Caccioppoli" Complesso
Universitario Monte S. Angelo
Via Cintia
80126 Napoli, ITALY
+39(0)81 675680
angelo.alvino@unina.it,
angelo.alvino@dma.unina.it
Rearrangements, Partial Differential
Equations.

3) Catalin Badea
UFR Mathematiques, Bat. M2,
Universite de Lille1
Cite Scientifique
F-59655 Villeneuve d'Ascq, France

23) Nikolaos B. Karayiannis
Department of Electrical and
Computer Engineering
N308 Engineering Building 1
University of Houston
Houston, Texas 77204-4005
USA
Tel (713) 743-4436
Fax (713) 743-4444
Karayiannis@UH.EDU
Karayiannis@mail.gr
Neural Network Models, Learning
Neuro-Fuzzy Systems.

24) Theodore Kilgore
Department of Mathematics
Auburn University
221 Parker Hall,
Auburn University
Alabama 36849, USA
Tel (334) 844-4620
Fax (334) 844-6555
Kilgota@auburn.edu
Real Analysis, Approximation Theory,
Computational Algorithms.

25) Jong Kyu Kim
Department of Mathematics
Kyungnam University
Masan Kyungnam, 631-701, Korea
Tel 82-(55)-249-2211
Fax 82-(55)-243-8609
jongkyuk@kyungnam.ac.kr
Nonlinear Functional Analysis, Variational
Inequalities, Nonlinear Ergodic Theory,
ODE, PDE, Functional Equations.

26) Miroslav Krbeč
Mathematical Institute
Academy of Sciences of Czech Republic
Žitná 25
CZ-115 67 Praha 1
Czech Republic
Tel +420 222 090 743
Fax +420 222 211 638
krbecm@matsrv.math.cas.cz
Function spaces, Real Analysis, Harmonic

Tel. (+33)(0)3.20.43.42.18
Fax (+33)(0)3.20.43.43.02
Catalin.Badea@math.univ-lille1.fr
Approximation Theory, Functional
Analysis, Operator Theory.

4) Erik J. Balder
Mathematical Institute
Universiteit Utrecht
P.O. Box 80 010
3508 TA UTRECHT
The Netherlands
Tel. +31 30 2531458
Fax +31 30 2518394
balder@math.uu.nl
Control Theory, Optimization,
Convex Analysis, Measure Theory,
Applications to Mathematical
Economics and Decision Theory.

5) Carlo Bardaro
Dipartimento di Matematica e Informatica
Universita di Perugia
Via Vanvitelli 1
06123 Perugia, ITALY
TEL +390755853822
+390755855034
FAX +390755855024
E-mail bardaro@unipg.it
Web site: <http://www.unipg.it/~bardaro/>
Functional Analysis and Approximation
Theory,
Signal Analysis, Measure Theory, Real
Analysis.

6) Heinrich Begehr
Freie Universitaet Berlin
I. Mathematisches Institut, FU Berlin,
Arnimallee 3, D 14195 Berlin
Germany,
Tel. +49-30-83875436, office
+49-30-83875374, Secretary
Fax +49-30-83875403
begehr@math.fu-berlin.de
Complex and Functional Analytic
Methods in PDEs, Complex Analysis,
History of Mathematics.

7) Fernando Bombal
Departamento de Analisis Matematico
Universidad Complutense
Plaza de Ciencias, 3
28040 Madrid, SPAIN
Tel. +34 91 394 5020
Fax +34 91 394 4726
fernando_bombal@mat.ucm.es

Analysis, Interpolation and
Extrapolation Theory, Fourier Analysis.

27) V. Lakshmikantham
Department of Mathematical Sciences
Florida Institute of Technology
Melbourne, FL 32901
e-mail: lakshmik@fit.edu
Ordinary and Partial Differential Equations,
Hybrid Systems, Nonlinear Analysis

28) Peter M. Maass
Center for Industrial Mathematics
Universitaet Bremen
Bibliotheksstr. 1,
MZH 2250,
28359 Bremen
Germany
Tel +49 421 218 9497
Fax +49 421 218 9562
pmaass@math.uni-bremen.de
Inverse problems, Wavelet Analysis and
Operator Equations, Signal and Image
Processing.

29) Julian Musielak
Faculty of Mathematics and Computer Science
Adam Mickiewicz University
Ul. Umultowska 87
61-614 Poznan
Poland
Tel (48-61) 829 54 71
Fax (48-61) 829 53 15
Grzegorz.Musielak@put.poznan.pl
Functional Analysis, Function Spaces,
Approximation Theory, Nonlinear Operators.

30) Vassilis Papanicolaou
Department of Mathematics
National Technical University of Athens
Zografou campus, 157 80
Athens, Greece
tel.: +30(210) 772 1722
Fax +30(210) 772 1775
papanico@math.ntua.gr
Partial Differential Equations,
Probability.

31) Pier Luigi Papini
Dipartimento di Matematica
Piazza di Porta S. Donato 5
40126 Bologna
ITALY
Fax +39(0)51 582528
papini@dm.unibo.it
Functional Analysis, Banach spaces,

Operators on Banach spaces,
Tensor products of Banach spaces,
Polymeasures, Function spaces.

8) Michele Campiti
Department of Mathematics "E.De Giorgi"
University of Lecce
P.O. Box 193
Lecce, ITALY
Tel. +39 0832 297 432
Fax +39 0832 297 594
michele.campiti@unile.it
Approximation Theory,
Semigroup Theory, Evolution problems,
Differential Operators.

9) Domenico Candeloro
Dipartimento di Matematica e Informatica
Universita degli Studi di Perugia
Via Vanvitelli 1
06123 Perugia
ITALY
Tel +39(0)75 5855038
+39(0)75 5853822,
+39(0)744 492936
Fax +39(0)75 5855024
candelor@dipmat.unipg.it
Functional Analysis, Function spaces,
Measure and Integration Theory in
Riesz spaces.

10) Pietro Cerone
School of Computer Science and
Mathematics, Faculty of Science,
Engineering and Technology,
Victoria University
P.O.14428,MCMC
Melbourne,VIC 8001,AUSTRALIA
Tel +613 9688 4689
Fax +613 9688 4050
Pietro.cerone@vu.edu.au
Approximations, Inequalities,
Measure/Information Theory,
Numerical Analysis, Special Functions.

11) Michael Maurice Dodson
Department of Mathematics
University of York,
York YO10 5DD, UK
Tel +44 1904 433098
Fax +44 1904 433071
Mmd1@york.ac.uk
Harmonic Analysis and Applications to
Signal Theory, Number Theory and
Dynamical Systems.

Approximation Theory.

32) Svetlozar T. Rachev
Chair of Econometrics, Statistics
and Mathematical Finance
School of Economics and
Business Engineering
University of Karlsruhe
Kollegium am Schloss, Bau II, 20.12, R210
Postfach 6980, D-76128,
Karlsruhe, GERMANY.
Tel +49-721-608-7535,
+49-721-608-2042(s)
Fax +49-721-608-3811
Zari.Rachev@wiwi.uni-karlsruhe.de
Second Affiliation:
Dept. of Statistics and Applied Probability
University of California at Santa Barbara
rachev@pstat.ucsb.edu
Probability, Stochastic Processes and
Statistics, Financial Mathematics,
Mathematical Economics.

33) Paolo Emilio Ricci
Department of Mathematics
Rome University "La Sapienza"
P.le A.Moro, 2-00185
Rome, ITALY
Tel ++3906-49913201 office
++3906-87136448 home
Fax ++3906-44701007
Paoloemilio.Ricci@uniroma1.it
riccip@uniroma1.it
Special Functions, Integral and Discrete
Transforms, Symbolic and Umbral Calculus,
ODE, PDE, Asymptotics, Quadrature,
Matrix Analysis.

34) Silvia Romanelli
Dipartimento di Matematica
Universita' di Bari
Via E.Orabona 4
70125 Bari, ITALY.
Tel (INT 0039)-080-544-2668 office
080-524-4476 home
340-6644186 mobile
Fax -080-596-3612 Dept.
romans@dm.uniba.it
PDEs and Applications to Biology and
Finance, Semigroups of Operators.

35) Boris Shekhtman
Department of Mathematics
University of South Florida
Tampa, FL 33620, USA
Tel 813-974-9710

12) Sever S.Dragomir
School of Computer Science and
Mathematics, Victoria University,
PO Box 14428,
Melbourne City,
MC 8001,AUSTRALIA
Tel. +61 3 9688 4437
Fax +61 3 9688 4050
sever@csm.vu.edu.au
Inequalities,Functional Analysis,
Numerical Analysis, Approximations,
Information Theory, Stochastics.

13) Paulo J.S.G.Ferreira
Department of Electronica e
Telecomunicacoes/IEETA
Universidade de Aveiro
3810-193 Aveiro
PORTUGAL
Tel +351-234-370-503
Fax +351-234-370-545
pjf@ieeta.pt
Sampling and Signal Theory,
Approximations, Applied Fourier Analysis,
Wavelet, Matrix Theory.

14) Gisele Ruiz Goldstein
Department of Mathematical Sciences
The University of Memphis
Memphis,TN 38152,USA.
Tel 901-678-2513
Fax 901-678-2480
ggoldste@memphis.edu
PDEs, Mathematical Physics,
Mathematical Geophysics.

15) Jerome A.Goldstein
Department of Mathematical Sciences
The University of Memphis
Memphis,TN 38152,USA
Tel 901-678-2484
Fax 901-678-2480
jgoldste@memphis.edu
PDEs,Semigroups of Operators,
Fluid Dynamics,Quantum Theory.

16) Heiner Gonska
Institute of Mathematics
University of Duisburg-Essen
Lotharstrasse 65
D-47048 Duisburg
Germany
Tel +49 203 379 3542
Fax +49 203 379 1845
gonska@math.uni-duisburg.de
Approximation and Interpolation Theory,

boris@math.usf.edu
Approximation Theory, Banach spaces,
Classical Analysis.

36) Panayiotis Siafarikas
Department of Mathematics
University of Patras
26500 Patras
Greece
Tel/Fax +302 610 997169
panos@math.upatras.gr
ODE,Difference Equations, Special
Functions, Orthogonal Polynomials,
Applied Functional Analysis.

37) Rudolf Stens
Lehrstuhl A fur Mathematik
RWTH Aachen
52056 Aachen
Germany
Tel ++49 241 8094532
Fax ++49 241 8092212
stens@mathA.rwth-aachen.de
Approximation Theory, Fourier Analysis,
Harmonic Analysis, Sampling Theory.

38) Juan J.Trujillo
University of La Laguna
Departamento de Analisis Matematico
C/Astr.Fco.Sanchez s/n
38271.LaLaguna.Tenerife.
SPAIN
Tel/Fax 34-922-318209
Juan.Trujillo@ull.es
Fractional: Differential Equations-
Operators-
Fourier Transforms, Special functions,
Approximations,and Applications.

39) Tamaz Vashakmadze
I.Vekua Institute of Applied Mathematics
Tbilisi State University,
2 University St. , 380043,Tbilisi, 43,
GEORGIA.
Tel (+99532) 30 30 40 office
(+99532) 30 47 84 office
(+99532) 23 09 18 home
Vasha@viam.hepi.edu.ge
tamazvashakmadze@yahoo.com
Applied Functional Analysis, Numerical
Analysis, Splines, Solid Mechanics.

40) Ram Verma
International Publications
5066 Jamieson Drive, Suite B-9,
Toledo, Ohio 43613,USA.

Computer Aided Geometric Design,
Algorithms.

17) Karlheinz Groechenig
Institute of Biomathematics and Biometry,
GSF-National Research Center
for Environment and Health
Ingolstaedter Landstrasse 1
D-85764 Neuherberg, Germany.
Tel 49-(0)-89-3187-2333
Fax 49-(0)-89-3187-3369
Karlheinz.groechenig@gsf.de
Time-Frequency Analysis, Sampling Theory,
Banach spaces and Applications,
Frame Theory.

18) Vijay Gupta
School of Applied Sciences
Netaji Subhas Institute of Technology
Sector 3 Dwarka
New Delhi 110075, India
e-mail: vijay@nsit.ac.in;
vijaygupta2001@hotmail.com
Approximation Theory

19) Weimin Han
Department of Mathematics
University of Iowa
Iowa City, IA 52242-1419
319-335-0770
e-mail: whan@math.uiowa.edu
Numerical analysis, Finite element method,
Numerical PDE, Variational inequalities,
Computational mechanics

20) Tian-Xiao He
Department of Mathematics and
Computer Science
P.O.Box 2900, Illinois Wesleyan University
Bloomington, IL 61702-2900, USA
Tel (309)556-3089
Fax (309)556-3864
the@iwu.edu
Approximations, Wavelet, Integration Theory,
Numerical Analysis, Analytic Combinatorics.

21) Don Hong
Department of Mathematical Sciences
Middle Tennessee State University
1301 East Main St.
Room 0269, Bldg KOM
Murfreesboro, TN 37132-0001
Tel (615) 904-8339
dhong@mtsu.edu
Approximation Theory, Splines, Wavelet,
Stochastics, Mathematical Biology Theory.

Verma99@msn.com
rverma@internationalpubls.com
Applied Nonlinear Analysis, Numerical
Analysis, Variational Inequalities,
Optimization Theory, Computational
Mathematics, Operator Theory.

41) Gianluca Vinti
Dipartimento di Matematica e Informatica
Universita di Perugia
Via Vanvitelli 1
06123 Perugia
ITALY
Tel +39(0) 75 585 3822,
+39(0) 75 585 5032
Fax +39 (0) 75 585 3822
mategian@unipg.it
Integral Operators, Function Spaces,
Approximation Theory, Signal Analysis.

42) Ursula Westphal
Institut fuer Mathematik B
Universitaet Hannover
Welfengarten 1
30167 Hannover, GERMANY
Tel (+49) 511 762 3225
Fax (+49) 511 762 3518
westphal@math.uni-hannover.de
Semigroups and Groups of Operators,
Functional Calculus, Fractional Calculus,
Abstract and Classical Approximation
Theory, Interpolation of Normed spaces.

43) Ronald R. Yager
Machine Intelligence Institute
Iona College
New Rochelle, NY 10801, USA
Tel (212) 249-2047
Fax (212) 249-1689
Yager@Panix.Com
ryager@iona.edu
Fuzzy Mathematics, Neural Networks,
Reasoning,
Artificial Intelligence, Computer Science.

44) Richard A. Zalik
Department of Mathematics
Auburn University
Auburn University, AL 36849-5310
USA.
Tel 334-844-6557 office
678-642-8703 home
Fax 334-844-6555
zalik@auburn.edu
Approximation Theory, Chebychev Systems,
Wavelet Theory.

22) Hubertus Th. Jongen
Department of Mathematics
RWTH Aachen
Templergraben 55
52056 Aachen
Germany
Tel +49 241 8094540
Fax +49 241 8092390
jongen@rwth-aachen.de
Parametric Optimization, Nonconvex
Optimization, Global Optimization.

Preface

These three special issues, which constitute the proceedings of the symposium CCS2008 – Second International Interdisciplinary Chaos Symposium on “CHAOS and COMPLEX SYSTEMS”, have tried to create a forum for the exchange of information and experience in the exciting interdisciplinary field of Chaos. However the conference was more in the Applied Mathematics direction centered.

The expectation of the organizers concerning international resonance of the conference has been fulfilled: 150 scientists from 15 different countries (China, France, Greece, Iran, Japan, Kazakhstan, Lebanon, Lithuania, Malaysia, Mexico, Pakistan, Romania, Russia, Turkey, and Uzbekistan) have participated. Good relations to research institutes of these countries might be of great importance for science and applications.

On behalf of the Organizing Committee we would like to express our thanks to the Scientific Committee, the Program Committee and to all who have contributed to this conference for their support and advice. We are also grateful to the invited lecturers Prof. George A. Anastassiou, Prof. Amir Atiya, Prof. Mohamed Saladin El Naschie, Prof. Ramazan Gencay, Prof. Ji-Huan He, Prof. Robert Kozma, Prof. V. Lakshmikantham, and Prof. Paul Refenes.

Special thanks are due to Rector Prof. Tamer Kocel, Vice Rector Prof. Cetin Bolcal and Dean Prof. Dursun Kocer for their support, advice and encouragement.

Our thanks are also due to the Istanbul Kultur University, which was hosting this symposium and provided all of its facilities.

We are grateful to the Editor-in-Chief, Prof. George A. Anastassiou for accepting this volume for publication in Journal of Applied Functional Analysis.

Hikmet Caglar

On behalf of the Organizing Committee

Istanbul Kultur University, Department of Mathematics-Computer, Istanbul, Turkey

Tel.: +90-212-4984367; Fax: +90-212-4658310; E-mail: s.caglar@iku.edu.tr

Mehmet Ozer

On behalf of the Organizing Committee

Istanbul Kultur University, Department of Physics, Istanbul, Turkey

Tel.: +90-212-4984317; Fax: +90-212-4658310; E-mail: m.ozel@iku.edu.tr

The application of fractal analysis and spatial technologies for urban analysis

Michael A. McAdams¹

Abstract

Urban areas and their built form are the result of complex cultural, social, economic, and technological agents/processes and their physical environment. Traditional forms of analysis (i.e., linear modeling, statistics) have wrestled with the chaotic nature of urban systems and the urban built form with an increasing amount of apparent sophistication (i.e. additional algorithms, new models) often with no significant increase in accuracy or understanding. Fractal analysis, which is firmly grounded in chaos theory, allied with spatial technologies (i.e., Geographic Information Systems, Remote Sensing, spatial modeling) is proving to be an innovative technique to study urban form/structure. This paper discusses how fractal analysis can be used to evaluate urban form. The findings of those that have applied fractal analysis to study urban form, including the author, have concluded that the fractal dimensions of urban form are not infinite, but settle in a defined fuzzy range of values based on the distinct characteristics of urban processes. The amalgamation of fractal analysis and other chaotic analytical tools (i.e., neural networks, agent based modeling) with spatial technologies to study urban form and dynamic forces represents a major paradigm shift that is just beginning to be observed in urban analysis and urban planning.

Keywords: *chaos theory, fractal analysis, built environment, spatial analysis, urban geography, urban planning, spatial technologies*

¹ Geography Department, Fatih University, 34500 Büyükçekmece / İstanbul, Türkiye. E-mail: mcadams@fatih.edu.tr

Introduction

To a growing number in the scientific community, chaos and complexity theories represent a major paradigm shift in understanding numerous phenomena [8] [25] [13]. In the field of urban geography, these developing areas could have a major impact on its direction. Michael Batty in his seminal book, Fractal Cities [3] revealed the promise of using fractal analysis in studying cities. Recently, he explored agent based modeling and cellular automata in Cities and Complexity [1]. The combination of these methods are ‘unraveling the urban fabric’ and giving urban geographers, urban planners and others interested in urban development greater insights. Fractal analysis has revealed that urban areas have patterns which can be distinguished, measured and dissected quantitatively, revealing the simplicity and complexity of their geometric formation. Spatial metrics is also contributing to our knowledge of the geometry of urban areas and integrating with cellular automata and fractal analysis [1] [9]. The analysis of urban areas combining chaos related tools and spatial analysis software is proliferating such that there is a growing number of urban geographers which are utilizing them to study different aspects of urban development.

Urban processes are naturally chaotic. Urban analysis have traditionally used linear and standard statistical techniques. These techniques have been found to be significantly flawed for the study of different aspects of urbanization such as growth, transportation, economic development. Chaos theory and other ‘new’ methods of analysis such as cellular automata, agent based modeling, spatial metrics, artificial intelligence, neural networks, non-linear simulation and fractal generation represent means to study urban phenomenon from the ‘bottom up’. These new developing methods of analysis are challenging the tenets of logical-positivism and associated methods of analysis such as statistics and aggregate linear modeling techniques. The ability to analyze the processes of urbanization has been greatly enhanced by the increasing ability to collect and process geographic information that is now found in the spatial technologies such as GIS and Remote Sensing.

Fractal Analysis and Urban Analysis

How did fractal analysis become a part of urban analysis? Fractal analysis, grounded in mathematical theory, developed independently of traditional urban analytical techniques. Urban geographers, being involved in a discipline which is inherently inter-disciplinary, began to realise that the attributes of abstract fractals and fractal generation were complementary in the investigation of urban form. Michael Batty [3] was the first to comprehensively examine the use of fractal analysis to investigate urban structure. Batty further developed these ideas in his book Complexity and Cities [1], incorporating complexity theory and related fields such as cellular automata and agent-based modeling. These areas have been facilitated by Geographic Information Systems, Remote Sensing, the development of advanced spatial analysis tools and increased computer processing capacities. The areas of complexity and chaos theory along with related spatial analysis techniques such as agent-based modeling, simulation, and cellular automata have a rapidly developing literature in urban geography and spatial analysis, carrying with them the potential to transform the traditional areas of examining cities such as applications of regression analysis, econometric models etc. Although some may disagree, this author perceives that this is beginning of a major paradigm shift that is not only apparent in Urban Geography, but in other disciplines. To introduce the basis for fractal analysis, the next

paragraphs will discuss its development and some of the major tenets. However, it should not be considered a comprehensive analysis of this subject, but an overview.

Some of the elements of fractal analysis were first introduced by D'Arcy Wentworth Thompson in his book On Growth and Form [22], indicating that although Mandelbrot [12] is credited with developing fractal mathematics, the roots are obviously stretching back much further. Mandelbrot [12] introduced the basic concepts of fractals and fractal analysis such as self-similarity, multiple iterations of simple formulas, and scaling and dimensions. Now, fractals and their analysis are robust areas of study in mathematics, but a still developing sub-field.

The basic elements related to fractal creation/generation and analysis are: 1) an object; 2) a generator (initiator); 3) iteration and 4) the emerged form. Fractal analysis is concerned with the study of the emerged form. For example, the object may be a line. This line may be subject to different rules or a generator (i.e., divide the line by a third) and iterated for an established amount of times. At the conclusion of those iterations, which theoretically could be infinite, an emergent form would appear. The resulting form/object will not be the same as the original object as it is not a replication but a mutation. However, the paradox is that the abstract fractal actually has self-similarity and scalelessness so in essence it is a replication, but, is mysteriously different. The best example in nature would be a tree whose structure was initiated by the bifurcation (dividing by 2) of a single twig and repeated numerous times. Cell development or mutation is similar. Another definition of a fractal is that it is an object which is less than a plane and more than a line possessing self similar elements. It would follow that fractal analysis is the study of the characteristics of fractals. Theories of simplicity, complexity, chaos theory and analysis techniques such as agent-based modeling and cellular automata are intrinsically coupled with fractal analysis. The 'butterfly effect' is the most simple explanation of the chaos theory. This is the concept which states that the single action of a butterfly flapping its wings in South America might result in a hurricane developing in the Atlantic Ocean. This concept of one action repeating and mutating is also one of the basic tenets of fractal generation and chaos theory. James Gleick, himself a mathematician, gives a more detailed explanation of the history of the development of chaos theory and also fractals in his entertaining book, Chaos: Making a New Science [8].

Fractals can be analyzed in a number of manners. One of the most common is to examine its dimension, lacunarity, and scaling [6]. Dimension refers to the fractal variation or how the fractal fills the space. The dimension for a fractal is always between 1 and 2 with 1 being a line and 2 being a plane. Dimension for a point would be 0 and for a cube, 3.

The formula for calculating a fractal dimension is as follows:

$$\text{Dimension (Dim)} = \log(\text{number of self-similar pieces}) / \log(\text{magnification factor})$$

[5]

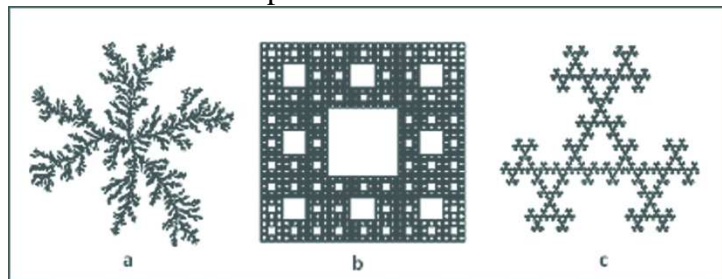
Or $\text{Dim} = -(\log N_k / \log r_k) = \log N_k / \log (1/r_k)$
[3]

Whereas the negative of the logarithm of the number (N) of self similar objects (vector or raster) is divided by the log of the scaling ratio (r_k).

Therefore, for a square which is divided into 4 equal parts and a scaling dimension of 2, the dimension would be 2.

Fractal dimension can be better analyzed when combined with lacunarity. Lacunarity refers to the texture of a fractal. A fractal with more gaps, bays or tears has a higher lacunarity. Tolle et al. [22] state, 'Fractal dimension only measures how much space is filled. Lacunarity complements fractal dimension by measuring how the data fills the space.' Tolle et al. [23] further state that multiple fractals may have the same dimension, but will have different lacunarity.

While there are multiple types of fractals that can be generated, only a few can be used as models for the city (i.e., Seripenski Carpet, diffusion.) This demonstrates that although the city is complex, there are limited forms that are being manifested in the evolution of urban areas. 'Real life' urban fractal dimensions can be compared against abstract fractal objects (see following figure) as a standard to determine the similarity or difference of different urban forms. Abstract fractal objects which could be seen as the basis for examining cities are the Dendritic Pattern (a), Sierpensi Carpet (b) and Sierpensi Triangle Variation (c) [21]. The Sierpensi Carpet is similar to a regular gridded city. Its fractal dimension is 1.77 and luncanrity is 292.08 This indicates a pattern that is highly regular, but containing a large amount gaps or 'bays'. The Dendritic Pattern, similar to the growth of urban development along transportation lines, has a fractal demenison of 1.60 and a luncanrity of 29.91. The Sierpensi Triangle Variation has a fractal dimension of 1.65 and lacunarity of 17.35. This also indicates a dendritic type pattern and small bays. The closer to a the dimension to linear demenison indicates more hierarchy and the small luncanrity means smaller gaps or 'bays'. These dimension and lacunarity of abstract fractal can useful as a means to compare the different fractal of cities.



Abstract Fractals—a- Dendritic Pattern b- Sierpensi Carpet
and c-Sierpensi Triangle Variation

In the urban environment, as opposed to a theoretical one, 'real' urban fractals are also subject to the influence of physical topography in limited and shaping its direction and sometimes form. The fractal formation in an urbanized area is not equal in the way it develops over time. The economic and technological agents effect the manner in which the fractal grows or diffuses. In addition, there are entropy factors based on economic functioning of the city. In a polycentric city, the distance from the core is related to the ability of commercial and industrial

concentrations to form on the periphery of the urban agglomeration [16]. Some of these issues are being taken up in the application of agent based and cellular automata modeling of cities.

Comparative Fractal Analysis of Cities

There are two objectives when analyzing the fractal dimension and lacunarity of urbanized areas. One is to examine the characteristics of a particular city and the other is to compare it with that of other cities. There have been several studies which examined the fractal aspects of urbanized areas. Batty [3] conjectured that all cities have fractal dimensions between 1 and 2. In this spectrum, there are high amounts of variability depending on the time period of the analysis. Batty [3] stated that most of the values were greater than 1.4 and most between 1.6 and 1.8 with a mean of 1.7. However, this was for a global analysis of the entire urban area. Frankhauser [7] took a different approach and compared cities with idealized geometric structures. He stated that, 'the value of the fractal dimension of the occupied sites is directly linked to the parameters of the generator, in particular to the number of N of elements and the reduction factor..' [7].

In examining French and other European cities, Frankhauser [7] found that city centers were between 1.8 to 1.95, regular estates without public space were between 1.8 and 1.99, new town between 1.6 and 1.77 and irregular or less controlled growth between 1.64 and 1.85. It should be noted that these measurements are not mutually exclusive, having a significant amount of overlap in some cases. In a study of Milan [4], a global analysis indicated a low fractal dimension of 1.075. Near the periphery of the urban area, the fractal value was 1.601, but near the center it was close to 1.804. This is consistent with other values found by Frankhauser [7]. In a study by Lagarias [10] of Thessaloniki, Greece the dimension of a selected suburban area was 1.741. McAdams [14] in his analysis of Istanbul found that its fractal dimensions when compared to European cities were similar but slightly higher at 1.83. In North America, the fractal dimensions of city were investigated by Shen [19]. He stated, concerning past studies using fractal analysis of cities, that 'While these studies have provided some interesting theoretical formulations and empirical results revealing the fractal nature of urban form and growth, they are not systematic in the sense that cities were not selected according to a spatial scheme (e.g., city or population size hierarchy) and a common set of parameters (i.e. map coverage, resolution, scale.) Thus, the results are incomplete and less useful for purpose of inter-city comparison from the urban system perspective.' Shen [19] selected 40 cities ranked by 1992 population and examined the relationship between population and fractal dimension. In this study, it is concluded that overall population size when regressed against dimension does reveal a good fit. In the study, if one inspects the highest populated city, New York City and the lowest populated city, Omaha, Nebraska it was found that their fractal dimensions are 1.701 and 1.277 respectively. Shen [19] did not inspect the fractal dimensions of sub-areas such as central city versus suburban areas in these urbanized areas, nor did he analyze the lacunarity of these cities. Shen [19] emphasizes that fractal dimensions do not appear to be related to density and that other factors are influencing the fractal nature of a city.

Despite some irregularity in fractal dimensions, there appears to be some guidelines as to the fractal dimensions of cities. In the center, if a city is occupied with buildings and little open space, the fractal dimension would be approximately 1.8 or above. This would appear to be particularly true of large metropolitan areas. There could be some indication from some of the

author's preliminary studies using remote sensing images that this could be lower for smaller cities, perhaps in the range of 1.75. As the city diffuses outward, there is a tendency for less concentration and more dendricity due to uneven development and also more space devoted toward highways, which occupy a large amount of space in modern cities. The tendency is for the dimension of approximately to be near to 1.8 in the center to rapidly change to one of about 1.75. This seems to indicate that cities are being fragmented by the forces of modern urbanization processes.

Linking fractal analysis with spatial technologies/modeling

Fractal analysis for urban analysis and linking it to spatial technologies is still in the developmental stage. There are still major issues that need to be addressed in this area. The sampling of cities at various levels under controlled circumstances and the relationship to other spatial metrics measurements need to be better defined to improve the reliability and interpretation. At the base of understanding fractal analysis is the rules that are forming the fractals. Although the generation of fractals to approximate different urban forms has been done for sample cities [3], more research is necessary to understand why certain rules in fractal generation produce certain urban forms. These rules and fractal generation linkages to spatial technologies and spatial modeling would greatly increase the knowledge of urban systems.

Another unexplored area is the application of fractal analysis in the measurement of modeling urban growth using agent-based modeling. The fractal dimensions and lacunarity of the actual and the modeled urban areas could serve as calibration measurements. This possibility occurred to the author during a special course that he offered during Fall of 2007 on the use of agent-based modeling and GIS [15]. One of the group projects used the Dynamic Urban Evolutionary Model (DUEM) a cellular automata model as a basis for their project [26]. The students delineated the area of Istanbul, placed 'seeds' at growth points and then let the model proceed on its own. The model allows for growth to follow roads. The pattern that developed was very similar to the actual growth patterns of Istanbul. The fractal pattern dimensions would be similar, but naturally not identical to that of Istanbul. The use of fractal measurements has not been used, to the author's knowledge for calibration of agent based urban models.

Spatial technologies, particularly GIS and Remote Sensing are able presently able to collect and analyze static spatial data. The problems lie in 'hard coupling' time series and dynamic processes such as those that are modeled in fractal generation and agent-based modeling. There are programs such as Fractalyse [24] which can take images that are generated from geographic data and examine their fractal dimensions and lacunarity. However, the program would be much more useful if it was linked directly with a GIS or Remote Sensing program. Agent-based and fractal generation models have inherent problems with display due to the graphic limitations of GIS programs because they were primarily constructed to display static images. The improved ability of coupling of these different programs would make fractal analysis and GIS more robust tools for urban spatial analysis.

Implication of Fractal Analysis and Related Methods of Analysis for Urban Planning

At this period, fractal analysis, space syntax, agent based modeling and other other forms of urban analysis are in their infancy for use as tools for urban planning. While the use of spatial technologies by most urban and regional planning agencies is widespread in high and middle

income economies, the use of fractal analysis for urban analysis appears to be concentrated in the academic sphere. Salingaros [18], a mathematics professor at University of Texas at San Antonio, is one of a few academicians who is attempting to bridge the gap between fractal analysis theory and urban planning practice. He considers chaos theory and fractal analysis as overall philosophies which are challenging the concepts of urban planning which were based on rationalism and logical-positivism, elitism and top-down decision-making. However, just as logical-positivism, linear modeling and Newtonian physics is an outcome of a philosophy connected with industrialization, modernism and Fordism, chaos theory and fractal analysis is a product of post-modernism [20]. As such, chaos theory represents a philosophical break from the ideas that dominated much of the 19th and 20th Century. While the proponents' of chaos theory claim that it represents a scientific paradigm shift, the root may more have its basis in Post-Modern concepts with science backing it up [20].

Consider these two references related to urban planning:

Urban planning involves forecasting future population growth and planning for possible changes. Planners consider: rate of growth, rates of natural increases and migration, age profile of the forecasted population and housing types, employment services required [17].

Planning under the modernist approach uses grand plans and the "big broom" or "clean sweep" approach to development. This implies that planning serves the interests capitalists and developers as opposed to those with less power as only a select few can participate in the "major" schemes involved. Large-scale plans, development, and redevelopment activities can hardly be construed as being conducive to promoting the interests and wellbeing of those with less power as they are not in a position to participate in the planning process and gain the benefits of the outcomes of modernist planning. The accommodation of a small-scale approach of post-modern planning, with its sensitivity to local interests and context human scale demands that planning encompass a wider range of interests [11].

The statement by the City of Prince Albert (Canada) implies that planning is a linear rational process which is based on making the best projections and then accommodating growth. The latter is a criticism of modernist urban planning depicting it as a process that is controlled by a small group of individuals for their own benefit. Implied is that the methods of justification are linear models and linear long range planning. In reality, most planners are still operating with planning methods based on logical-positivism and regard any discussion concerning Post-Modern planning theory and concepts as purely academic and philosophical. Some of these criticisms of Post-Modern planning theory are well-grounded as it is still developing [11]. Also, Post-Modernistic planning is the antithesis of the concepts that most planners were taught in urban planning schools which are firmly situated within the elitist logical positivism philosophy from the latter part of the 19th and early 20th Century.

Fractal analysis and other related chaos based tools such as agent-based modeling and cellular automata are associated with the developing area of Post-Modern scientific thought. To incorporate chaotic methods into urban planning requires an overall change in the concept of urban planning-being one of not one future but numerous futures involving not just a few people and forces but a unknowable amount within and outside of an urban area with an indefinite amount of goals and objectives. As such, this concept leads an urban planning to

enter a new realm—one of uncertainty and non-conclusiveness where future outcomes are unknown. The illusion of long-range rational planning was that urban areas could plan 20 years in advance and arrive at some future state. Examining fractal analysis and cellular automata, one realizes that there is not one outcome, but an infinite amount based on different forces at a variety of scales. In fractal analysis and agent-based modeling, the outcomes—however varied—are determined by the rules and environment. If one changes the rules (sometimes only slightly) and/or the environment, the outcomes can be significantly different. This very premise changes the way one views urban development and planning.

Conclusion

Fractal analysis is a diverse and promising method to examine the built form of cities. While examining fractals in a theoretical manner is considerably advanced, its methods when examining actual urbanization is complex and sometime results in conflicting measurements. The interpretation of fractal analysis is not an easy task as there appears to be differences in measurements based on resolution and other factors. There is a developing literature concerning measurements from different cities. The application of fractal analysis of Istanbul by the author [14] further demonstrates that fractal analysis can prove to be a worthy technique to study urban structure but raised a multitude of questions that can not be adequately addressed within the scope of this article.

What is evident is that there needs to be more research into this area as to standardizing the methods and interpretation. While there is ample evidence that fractal analysis and related analysis methods such as cellular automata/agent based modeling are promising, they are remaining as theoretical tools and have not entered the mainstream of urban analysis and planning. The developing area of urban syntax hints at additional new tools that can further examine the city with unique tools. At this time, research into fractal analysis, agent based modeling and other analytical tools that seek to probe further into the composition of the urban environment are being conducted in a limited number of locations around the world. It is anticipated that this field will become even more diverse yielding a whole set of tools that those who are working in the field of urban geography and planning will utilize to better understand cities and discover new ways of managing them.

The use of fractal analysis for urban analysis opens up more questions than it answers. This is somewhat disconcerting to those attached to the general paradigm of urban planning which is based on using linear models and incorporating them within a process of rational decision making. However, it should be self-evident that the current methods of urban planning and likewise the role of planners are ineffective and do not mesh with the present realities of the urban environment. The ability of urban planning theory and methods of analysis to address Post-Modern scientific thought which includes chaos theory and their methods could bring new life into urban planning making it a powerful player in transforming urban environments. How those developing urban theory and methods of analysis address these issues could greatly effect the health of the profession and its effectiveness and role in shaping the urban environment.

References

- [1] Batty, M., (2005), *Cities and Complexity: Understanding Cities with Cellular Automata, Agent based Models, and Fractals*, Boston, MIT Press.
- [2] Batty, M., (2004), “A New Theory of Space Syntax (CASA Working Paper 75)”, Center for Advanced Spatial Analysis (CASA);
<http://www.casa.ucl.ac.uk/publications/workingPaperDetail.asp?ID=75>. Accessed 7 May 2008.
- [3] Batty, M. and Longley, P., (1996), *Fractal Cities: a Geometry of Form and Function*, London and San Diego, Academic Press.
- [4] Cagliani, M. And Giovanni, R., (2007), “Contribution to Fractal Analysis of Cities: a Study of the Metropolitan Area of Milan”, *Cybergeo*, article 269;
<http://www.cybergeo.eu/index3634.html>. Accessed 7 May 2008.
- [5] Devaney, R., (1995), “Chaos in the classroom: fractal dimension”;
<http://math.bu.edu/DYSYS/chaos-game/node6.html#SECTION00060000000000000000>. Accessed 7 May 2008.
- [6] Falconer, K., (2003), *Fractal geometry: mathematical foundations and applications, 2nd edition*, Chichester, New York. John Wiley and Sons Ltd.
- [7] Frankhauser, P., (2004), “Comparing the morphology of urban patterns in Europe a fractal approach. European Cities – Insights on outskirts”, Report COST Action 10 *Urban Civil Engineering*, Vol. 2, Structures, edited by A. Borsdorf and P., Zembri, Brussels, pp. 79-105;
<http://thema.univ-fcomte.fr/IMG/pdf/Cost10fractales.pdf> . Accessed 7 May 2008.
- [8] Gleick, J., (1987), *Chaos: Making a New Science*, London. Penguin Books.
- [9] Hillier, B., (2007), *Space is the Machine*. London. University College of London;
<http://eprints.ucl.ac.uk/3848/>. (originally published by Press Syndicate of the University of Cambridge in hardback and softback, 1996 and 1999 respectively.) Accessed on 7 May 2008.
- [10] Langarias, A., (2007), “Fractal analysis of the Urbanization at the Outskirts of the City, Measurement and Explanation, *Cybergeo*, article 391, 16 July 2007;
<http://www.cybergeo.eu/index8902.html>. Accessed on 7 May 2008.
- [11] MacLeod, D., (2008), “Post Modernism and Urban Planning”;
<http://www3.sympatico.ca/david.macleod/POMO.HTM#POMO7> . Accessed on 7 May 2008.

- [12] Mandelbrot, B. , (1983), *The Fractal Geometry of Nature, 3rd Edition*, San Francisco. W.H. Freeman.
- [13] Merali, Y. and McKelvey, B. , (2006), ‘ ‘ Using Complexity Science to Effect a Paradigm Shift in Information Systems for the 21st Century ’ ’, *Journal of Information Technology*, 21, 4, 211–215; <http://www.palgrave-journals.com/jit/journal/v22/n3/index.html>. Accessed on 7 May 2008.
- [14] McAdams, M., (2007), ‘ ‘Fractal Analysis and the Urban Morphology of a City in a Developing Country: A Case Study of Istanbul’ ’, *Marmara Coğrafya Dercisi (Marmara Geographical Review)*, 15, 147-170.
- [15] McAdams, M., (2007). ‘ ‘Course webpage for agent based modeling and GIS’ ’; <http://www.fatih.edu.tr/~mcadams/geo391/>. Accessed on 7 May 2008.
- [16] McAdams, M., (1995), *The Land Use Impact of an Airport and Urban Structure : a Case Study in Milwaukee, Wisconsin (dissertation)*, Milwaukee: University of Wisconsin-Milwaukee.
- [17] City of Prince Albert (Saskatchewan, Canada), (2007), ‘ ‘ Urban Growth and Urban Form Managing Urban Growth.’ ’; <http://www.citypa.ca/TheCity/Departments/EconomicDevelopmentandPlanning/ThePrinceAlbertDevelopmentPlanProcess/tabid/347/Default>. Accessed on 7 May 2008
- [18] Salinger, N., (2003). ‘ ‘Connecting the Fractal City (keynote speech)’ ’, *5th Biennial of towns and town planners in Europe*, Barcelona, April 2003.; <http://www.math.utsa.edu/sphere/salinger/connecting.html> . Accessed on 7 May 2008.
- [19] Shen, G. (2002), Fractal Dimension and Fractal Growth of Urbanized Areas, *International Journal of Geographical Information Science*, 16, 5, 419-437. Accessed on 7 May 2008.
- [20] Smith, W. , and Higgins, M., (2003), ‘ ‘Postmodernism and Popularisation: The Cultural Life of Chaos Theory ’ ’, *Culture and Organization* 9, 2 , 93-104.
- [21] Tannier C. and Pumain D., (2005), ‘ ‘ Fractals in Urban Geography: a Theoretical Outline and an Empirical Example, *Cybergeo* , 307, 20 ; <http://193.55.107.45/articles/307res.htm>. Accessed on 7 May 2008.
- [22] Thompson, D.W., (1992 [c1917]), *On Growth and Form*, Cambridge. Cambridge University Press.
- [23] Tolle, C., McJunkin, T., Rohrbaugh, D. , and LaViolette, R., (2004), ‘ ‘Lacunarity definition for ramified data sets based on optimal cover’ ’, *Physica D* ,179, 129–152; http://www.inl.gov/physics/d/lacunarity_physicad2003.pdf. Accessed on 7 May 2008

- [24] University of Franche-Comté, France, ThéMA Research Group, (2007) , ‘Documentation for Fractalyse’; <http://www.fractalyse.org/>. Accessed on 7 May 2008.
- [25] Wolfram, S., (2002), A New Kind of Science, Champaign, Illinois. Wolfram Media.
- [26] Xie, Y and Batty, M., (2003), ‘‘Integrated Urban Evolutionary Modeling, CASA Working Paper 75, Center for Advanced Spatial Analysis (CASA); <http://www.casa.ucl.ac.uk/publications/workingPaperDetail.asp?ID=68> . Accessed 7 May 2008.

On infinite dimensional Volterra type operators

FARRUKH MUKHAMEDOV

*Department of Computational & Theoretical Sciences
Faculty of Sciences, International Islamic University Malaysia
P.O. Box, 141, 25710, Kuantan
Pahang, Malaysia*

MANSOOR SABUROV

*Department of Mechanics & Mathematics
National University of Uzbekistan
Vuzgorodok, 100174 Tashkent, Uzbekistan*

Abstract

In this paper we study Volterra type operators on infinite dimensional simplex. It is provided a sufficient condition for Volterra type operators to be bijective. Furthermore it is proved that the condition is not necessary.

Mathematics Subject Classification: 15A51, 47H60, 46T05, 92B99.

Key words: Infinite dimensional simplex, Volterra type operators, cubic stochastic operators.

1. INTRODUCTION

Since Lotka and Volterra's seminal and pioneering works (see [10]) many decades ago, modeling of interacting, competing species have received considerable attention in the fields of biology, ecology, mathematics (for example, see [3, 9]). In their remarkably simple deterministic model, Lotka and Volterra considered two coupled nonlinear differential equations that mimic the temporal evolution of a two-species system of competing predator and prey populations. They demonstrated that coexistence of both species was not only possible but inevitable in their model. Moreover, similar to observations in real populations, both predator and prey densities in this deterministic system display regular oscillations in time, with both the amplitude and the period determined by the prescribed initial conditions. Note that in [1, 2, 4, 5] finite dimensional Volterra and more general quadratic operators were studied.

When a system is large enough, it is interesting to investigate quadratic Volterra operators define on an infinite dimensional simplex. First studies in this direction were considered in [6]. Iterations of such operators define more complicated nonlinear operators. To better understanding the dynamics of such operators, it is important to study such nonlinear operators. The aim of this paper is to study more general class of nonlinear operators which contains a particular case of that quadratic Volterra operators. It is provided a sufficient condition for Volterra type operators to be bijective

2. VOLTERRA TYPE OPERATORS

In this section we give definition of Volterra type operators and study its basic properties. We prove that such operators are bijective under certain condition.

Let

$$\ell_1 = \{x = (x_n) : \|x\|_1 = \sum_{k=1}^{\infty} |x_k| < \infty\}$$

be the space of all absolutely convergent sequences. The set

$$S = \{x = (x_n) \in \ell_1 : x_i \geq 0, \sum_{n=1}^{\infty} x_n = 1\}$$

is called *an infinite dimensional simplex*.

It is known [7] that $S = \overline{\text{convh}(\text{Extr}(S))}$ form a convex closed set, here

$$\text{Extr}(S) = \{e^{(n)} = (\underbrace{0, 0, \dots, 0}_n, 1, 0, \dots)\}$$

is the extremal points of the S and $\text{conv}(A)$ is the convex hull of a set A .

Let $\alpha \subset \mathbb{N}$ be an arbitrary set. The set

$$S_\alpha = \{x \in S : x_k = 0, \forall k \in \mathbb{N} \setminus \alpha\}$$

is called a *face* of the simplex. It is clear that S_α is also will be the simplex.

A *relatively interior* of a face S_α is defined by

$$\text{ri}S_\alpha = \{x \in S_\alpha : x_k > 0, \forall k \in \alpha\}.$$

In what follows we are interested in the following operator $V : S \rightarrow \ell_1$ defined by

$$(Vx)_k = x_k(1 + f_k(x)), \quad k \in \mathbb{N}, \quad x \in S, \quad (1)$$

where a mapping $\mathbf{f} : x \in S \rightarrow (f_1(x), f_2(x), \dots, f_n(x), \dots) \in \ell_1$.

One can see that

$$\left| \sum_{k=1}^{\infty} x_k f_k(x) \right| \leq \sum_{k=1}^{\infty} |x_k f_k(x)| \leq \sum_{k=1}^{\infty} |f_k(x)| < \infty$$

for any $x \in S$, that means that the operator V is well defined.

Theorem 2.1. *Let an operator V be given defined by (1). The following conditions are equivalent:*

- (i) *The operator V is continuous in ℓ_1 and $V(S) \subset S$. Moreover, $V(\text{ri}S_\alpha) \subset \text{ri}S_\alpha$ for every $\alpha \subsetneq \mathbb{N}$.*
- (ii) *The mapping \mathbf{f} satisfies the following conditions:*
 - 1⁰ *\mathbf{f} is continuous on ℓ_1 topology.*
 - 2⁰ *For every $k \in \mathbb{N}$ one holds $f_k(x) \geq -1$ for all $x \in S$.*
 - 3⁰ *For any $x \in S$ one has $\sum_{k=1}^{\infty} x_k f_k(x) = 0$.*

4⁰ For any $\alpha \subsetneq \mathbb{N}$ one has $f_k(x) > -1$ for all $x \in riS_\alpha$ and $k \in \alpha$.

Proof. (i) \Rightarrow (ii). The continuity of V implies 1⁰. Take $x \in S$, then $V(x) \in S$ yields that

- (a) $(V(x))_k \geq 0$,
- (b) $\sum_{k=1}^{\infty} (V(x))_k = 1$.

Hence, from (a) it follows that $x_k(1 + f_k(x)) \geq 0$, which implies 2⁰. From (b) one has

$$\sum_{k=1}^{\infty} x_k + \sum_{k=1}^{\infty} x_k f_k(x) = 1,$$

which immediately yields 3⁰.

Let $x \in riS_\alpha$, then $V(x) \in riS_\alpha$, which with (1) and $x_k > 0$ for all $k \in \alpha$ implies that $f_k(x) > -1$ for all $k \in \alpha$.

The implication (ii) \Rightarrow (i) is evident. □

We say that an operator $V : S \rightarrow S$ defined by (1) is *Volterra type* if one of the conditions of Theorem 2.1 is satisfied. The corresponding mapping \mathbf{f} is called *generating* for V . By \mathcal{V} we denote the set of all Volterra type operators.

From Theorem 2.1 we have

Corollary 2.2. *The set \mathcal{V} is convex, and for any $V_1, V_2 \in \mathcal{V}$ one has $V_1 \circ V_2 \in \mathcal{V}$, here \circ means composition of operators.*

Recall that the point $x \in S$ is called *fixed point* of V , if $Vx = x$. The set of all fixed points of V is denoted by $Fix(V)$. From Theorem 2.1 we immediately get the following

Corollary 2.3. *For any Volterra type operator V one holds*

- (i) $Extr(S) \subset Fix(V)$;
- (ii) *Restriction of V to any face of the simplex is again Volterra type operator.*

Let us consider more particular case of a mapping \mathbf{f} . Namely one has the following

Theorem 2.4. *Let $f_k : \ell_1 \rightarrow \mathbb{R}$ ($k \in \mathbb{N}$) be linear functionals. Then a mapping $\mathbf{f} : S \rightarrow \ell_1$ defined by $\mathbf{f}(x) = (f_1(x), f_2(x), \dots, f_n(x), \dots)$ satisfies the conditions 1⁰ – 4⁰ iff one has*

$$f_k(x) = \sum_{i=1}^{\infty} a_{ki}x_i, \quad k \in \mathbb{N} \tag{2}$$

with

$$a_{ki} = -a_{ik}, \quad |a_{ki}| \leq 1 \quad \text{for every } k, i \in \mathbb{N}$$

Note that Volterra type operators with generating mappings given by (2) are called *quadratic Volterra operators*. In [?] such quadratic Volterra operators have been studied, and it was shown that any such kind of operator is a bijection of S . In the case under consideration, i.e. for Volterra type operators we could not state an analogous result.

Example 2.1. Let us consider 1-dimensional simplex, i.e. $S^1 = [0, 1]$. Define a Volterra type operator $V : [0, 1] \rightarrow [0, 1]$ by

$$V(x) = x(1 - \sin \pi x), \quad x \in [0, 1].$$

A direct inspection shows that the defined operator is not bijection.

Now we are interested in finding some sufficient conditions for Volterra type operators to be bijective.

Theorem 2.5. *Let V be a Volterra type operator given by (1). Let*

$$\sum_{k=1}^{\infty} x_k f_k(y) + \sum_{k=1}^{\infty} y_k f_k(x) \leq 0 \quad \text{for every } x, y \in S. \quad (3)$$

be satisfied. Then V is a bijection of S

Proof. First let us prove that the V is an injection. Suppose that there are two distinct elements x, y such that

$$V(x) = V(y). \quad (4)$$

Without loss of generality we may assume that $x_i > 0, y_i > 0, \forall i \in \mathbb{N}$. If it is not true, then there is a face S_α , for some subset $\alpha \subset \mathbb{N}$ of S such that $x, y \in \text{ri} S_\alpha$ that is $x_i > 0, y_i > 0, \forall i \in \alpha$. According to Theorem 2.1 we have $V(S_\alpha) \subset S_\alpha$ therefore, due to Corollary 2.3 we can restrict V to S_α which is Volterra type too.

Now from (4) one gets

$$x_k(1 + f_k(x)) = y_k(1 + f_k(y)), \quad \forall k \in \mathbb{N}$$

or

$$x_k - y_k + x_k f_k(x) - y_k f_k(x) = y_k f_k(y) - y_k f_k(x), \quad \forall k \in \mathbb{N}$$

$$(x_k - y_k)(1 + f_k(x)) = -y_k(f_k(x) - f_k(y)), \quad \forall k \in \mathbb{N}.$$

Since $1 + f_k(x) > 0, \forall x \in \text{ri} S$ and $y_k > 0, \forall k \in \mathbb{N}$, then

$$\text{sgn}(x_k - y_k) = -\text{sgn}(f_k(x) - f_k(y)), \quad \forall k \in \mathbb{N}. \quad (5)$$

Hence

$$(x_k - y_k)(f_k(x) - f_k(y)) \leq 0, \quad \forall k \in \mathbb{N} \quad (6)$$

whence

$$\sum_{k=1}^{\infty} (x_k - y_k)(f_k(x) - f_k(y)) \leq 0. \quad (7)$$

Note that the last series absolutely converges, since

$$\begin{aligned} \left| \sum_{k=1}^{\infty} (x_k - y_k)(f_k(x) - f_k(y)) \right| &\leq \sum_{k=1}^{\infty} |x_k - y_k| |f_k(x) - f_k(y)| \\ &\leq \sum_{k=1}^{\infty} (x_k + y_k) (|f_k(x)| + |f_k(y)|) \\ &\leq 2 \left(\sum_{k=1}^{\infty} |f_k(x)| + \sum_{k=1}^{\infty} |f_k(y)| \right) < \infty \end{aligned}$$

From (7) one finds

$$\sum_{k=1}^{\infty} x_k f_k(x) - \sum_{k=1}^{\infty} x_k f_k(y) - \sum_{k=1}^{\infty} y_k f_k(x) + \sum_{k=1}^{\infty} y_k f_k(y) \leq 0. \quad (8)$$

By means of condition 3⁰, (8) can be rewritten by

$$\sum_{k=1}^{\infty} x_k f_k(y) + \sum_{k=1}^{\infty} y_k f_k(x) \geq 0. \quad (9)$$

From (3) and (9) we conclude that (6) is true if and only if

$$(x_k - y_k)(f_k(x) - f_k(y)) = 0, \quad \forall k \in \mathbb{N}.$$

The equality (5) with the last equality implies that $x = y$. Thus, $V : S \rightarrow S$ is injective.

Now let us show that V is onto. Denote

$$\begin{aligned} A_1 &= \{[1, n] \subset \mathbb{N} : n \in \mathbb{N}\}, \\ A_2 &= \{a \subset [1, n] : |[1, n] \setminus a| \geq 2, n \in \mathbb{N}\}, \\ A_3 &= \{b \subset \mathbb{N} : a \subset b, a \in A_1 \cup A_2, |\mathbb{N} \setminus b| < \infty\}, \\ A &= A_1 \cup A_2 \cup A_3. \end{aligned}$$

In A define an order by inclusion, i.e. $a \leq b$ means that $a \subset b$ for $a, b \in A$. It is evident that A is a completely ordering set. We will prove surjection of V by using transfer induction method with respect to the set A . Clearly that operator V is a surjection on $S_{\{1\}}$. Suppose that for an element $a \in A$ the operator V is a surjective on S_b for every $b < a$. Let us show that the V is a surjection on S_a as well. Assume that $V(S_a) \neq S_a$. For the boundary ∂S_a of S_a we have $\partial S_a = \bigcup_{c \in A: c < a} S_c$. According to the assumption of the induction we get

$$V(\partial S_a) = \partial S_a. \quad (10)$$

On the other hand, there exist $x, y \in riS_a$ such that $x \in V(S_a)$, $y \notin V(S_a)$. The segment $[x, y]$ contains at least one boundary point z of the set $V(S_a)$. Since $V : S_a \rightarrow V(S_a)$ is continuous and bijection, then the boundary point goes to boundary one. Therefore, for $z \in riS_a$, $V^{-1}(z) \in \partial S_a$, which contradicts to (10). \square

Remark 2.1. Note that the functionals (2) described in Theorem 2.4 satisfy the condition (3).

3. CUBIC VOLTERRA OPERATORS

From the previous section one arises a question: is there non-trivial (except for linear functionals f_k) examples of Volterra type operators for which condition (3) is satisfied. In this section we introduce so called cubic Volterra operators, and provide an examples of such operators which satisfy condition (3). Moreover, we establish that that condition is indeed sufficient, i.e. an example of bijective cubic Volterra operator will be given, which does not satisfy (3).

Recall that a mapping $V : S \rightarrow S$ is called *cubic stochastic operator* (shortly *c.s.o.*) if it is defined by

$$(Vx)_k = \sum_{i,j,l=1}^{\infty} p_{ijl,k} x_i x_j x_l, \quad \forall k \in \mathbb{N} \quad (11)$$

for all $x \in S$, here

$$\sum_{k=1}^{\infty} p_{ijl,k} = 1, \quad \text{and} \quad p_{ijl,k} = p_{\pi(i)\pi(j)\pi(l)} \geq 0, \quad (12)$$

where π is any permutation of the index set $\{i, j, l\}$.

Note that cubic stochastic operators were studied in [3],[8].

We say that a c.s.o. V is called *cubic Volterra operator* (*c.V.o.*) if any face of the simplex is invariant with respect to V . One can prove the following

Theorem 3.1. *A c.s.o. V is cubic Volterra operator if and only if $p_{ijl,k} = 0$ whenever $k \notin \{i, j, l\}$. Moreover, any cubic Volterra operator is Volterra type, and it can be represented by*

$$(Vx)_k = x_k \left(x_k^2 + 3x_k \sum_{i \in \mathbb{N}_k} p_{ikk,k} x_i + 3 \sum_{i \in \mathbb{N}_k} p_{iik,k} x_i^2 + 6 \sum_{i,j \in \mathbb{N}_k, i < j} p_{ijk,k} x_i x_j \right), \quad \forall k \in \mathbb{N} \quad (13)$$

where $\mathbb{N}_k = \mathbb{N} \setminus \{k\}$.

From this Theorem we immediately get the following

Corollary 3.2. *If for a c.V.o. V the coefficients $\{p_{ijl,k}\}$ do not depend one of indexes $\{i, j, l\}$, then V becomes a quadratic Volterra operator.*

Now we are going to provide an example of c.V.o. which satisfies (3).

Example 3.1. Let us consider c.V.o. $V_0 : S \rightarrow S$ defined by

$$p_{ikk,k} = 1, \quad p_{iik,k} = 0, \quad p_{ijk,k} = \frac{1}{3}$$

here i, j, k are pairwise distinct. Then V has the following form

$$(V_0 x)_k = x_k \left(x_k^2 + 3x_k \sum_{i \in \mathbb{N}_k} x_i + 2 \sum_{i,j \in \mathbb{N}_k, i < j} x_i x_j \right), \quad (14)$$

here, as before, $\mathbb{N}_k = \mathbb{N} \setminus \{k\}$.

Now let us check (3). One can see that

$$f_k(x) = x_k - \sum_{i=1}^{\infty} x_i^2.$$

Therefore, one gets

$$\sum_{k=1}^{\infty} y_k f_k(x) + \sum_{k=1}^{\infty} x_k f_k(y) = 2 \sum_{k=1}^{\infty} x_k y_k - \sum_{i=1}^{\infty} x_i^2 - \sum_{i=1}^{\infty} y_i^2 \leq 0,$$

which implies (3).

We are going to show that the condition (3) is sufficient. Next we give an example of bijective c.V.o. which doesn't satisfy that condition.

Example 3.2. Let us consider an operator $V : S \rightarrow S$ defined by

$$\left\{ \begin{array}{l} (Vx)_1 = x_1^3 \\ (Vx)_2 = x_2(x_2^2 + 3x_1) \\ (Vx)_3 = x_3(x_3^2 + 3(x_1 + x_2) - 3x_1x_2) \\ \dots\dots\dots \\ (Vx)_k = x_k \left(x_k^2 + 3 \sum_{i=1}^{k-1} x_i - 3 \sum_{i,j=1, i < j}^{k-1} x_i x_j \right) \\ \dots\dots\dots \end{array} \right. \quad (15)$$

Let us show that V maps the simplex into itself.

The relations

$$\sum_{i=1}^n x_i - \sum_{i,j=1, i < j}^n x_i x_j = \sum_{k=1}^{n-1} x_k \left(1 - \sum_{i=k+1}^n x_i \right) + x_n \geq 0 \quad (16)$$

imply that $(Vx)_k \geq 0$ for all $k \in \mathbb{N}$.

Lemma 3.3. *Let*

$$W_k(x) = \left(\sum_{i=k}^{\infty} x_i \right)^3 + 3 \sum_{i=1}^{k-1} x_i \left(\sum_{i=k}^{\infty} x_i \right)^2 + 3 \sum_{i,j=1, i \leq j}^{k-1} x_i x_j \sum_{i=k}^{\infty} x_i, \quad k \in \mathbb{N}.$$

Then for all $k \in \mathbb{N}$ one has

$$W_k(x) = (Vx)_k + W_{k+1}(x).$$

Proof.

$$\begin{aligned} W_k(x) &= \left(x_k + \sum_{i=k+1}^{\infty} x_i \right)^3 + 3 \sum_{i=1}^{k-1} x_i \left(x_k + \sum_{i=k+1}^{\infty} x_i \right)^2 \\ &\quad + 3 \sum_{i,j=1, i \leq j}^{k-1} x_i x_j \left(x_k + \sum_{i=k+1}^{\infty} x_i \right) \\ &= x_k^3 + 3x_k^2 \sum_{i=1}^{k-1} x_i + 3x_k \sum_{i=1}^{k-1} x_i \sum_{i=k+1}^{\infty} x_i + 3x_k \sum_{i,j=1, i \leq j}^{k-1} x_i x_j \\ &\quad + \left(\sum_{i=k+1}^{\infty} x_i \right)^3 + 3 \left(x_k + \sum_{i=1}^{k-1} x_i \right) \left(\sum_{i=k+1}^{\infty} x_i \right)^2 \\ &\quad + 3 \left(\sum_{i,j=1, i \leq j}^{k-1} x_i x_j + x_k \sum_{i=1}^{k-1} x_i + x_k^2 \right) \sum_{i=k+1}^{\infty} x_i \\ &= x_k \left(x_k^2 + 3 \sum_{i=1}^{k-1} x_i \sum_{i=k}^{\infty} x_i + 3 \sum_{i,j=1, i \leq j}^{k-1} x_i x_j \right) + W_{k+1}(x) \\ &= (Vx)_k + W_{k+1}(x). \end{aligned}$$

□

From Lemma 3.3 we obtain

$$1 = \left(\sum_{i=1}^{\infty} x_i \right)^3 = (Vx)_1 + W_2(x) = (Vx)_1 + (Vx)_2 + W_3(x) = \cdots = \sum_{i=1}^{\infty} (Vx)_i$$

Now we show that the operator (15) is bijective. To this end, first we prove that the operator is injective. Indeed, let $x, y \in S$ and $x \neq y$. Then there exists $k_0 \in \mathbb{N}$ such that

$$x_{k_0} \neq y_{k_0}, \quad x_i = y_i, \quad \forall i = \overline{1, k_0 - 1}.$$

From (15) we find that

$$(Vx)_i = (Vy)_i, \quad \forall i = \overline{1, k_0 - 1}.$$

From (16) and $x_i = y_i \forall i = \overline{1, k_0 - 1}$ it follows that

$$C := \sum_{i=1}^{k_0-1} x_i - \sum_{i,j=1, i < j}^{k_0-1} x_i x_j = \sum_{i=1}^{k_0-1} y_i - \sum_{i,j=1, i < j}^{k_0-1} y_i y_j \geq 0.$$

Consider a function $g(t) = t^3 + 3C \cdot t$, which is strictly increasing on the segment $[0, 1]$. Therefore, for $x_{k_0} \neq y_{k_0}$ we get

$$(Vx)_{k_0} = g(x_{k_0}) \neq g(y_{k_0}) = (Vy)_{k_0},$$

which means $Vx \neq Vy$.

Since the restriction of the operator (15) to any face of S is again of type (15), then by similar argument used in the proof of Theorem 2.5, one can establish that the operator (15) is surjective.

Let us show that (3) is not satisfied. From (15) one sees that

$$f_k(x) = x_k^2 + 3 \sum_{i=1}^{k-1} x_i - 3 \sum_{i,j=1, i < j}^{k-1} x_i x_j - 1.$$

The inequality (3) is not satisfied if we put $x = e^{(1)}, y = e^{(2)}$, indeed

$$\sum_{k=1}^{\infty} e_k^{(1)} f_k(e^{(2)}) + \sum_{k=1}^{\infty} e_k^{(2)} f_k(e^{(1)}) = -1 + 2 = 1 > 0.$$

ACKNOWLEDGEMENT

The F.M. thanks Research Endowment Grant B of International Islamic University Malaysia.

REFERENCES

- [1] Bernstein S.N. The solution of a mathematical problem concerning the theory of heredity. *Ucheniye-Zapiski N.-I. Kaf.Ukr.Otd.Mat.*, **1**(1924), 83–115 (Russian) .
- [2] Ganikhodzhaev.R.N. Quadratic stochastic operators, Lyapunov functions and tournaments. *Russian Acad.Sci. Sbornik.Math.*, **76**(1993), 489–506.
- [3] Hofbauer J., Sigmund K., *Evolutionary Games and Population Dynamics*, Cambridge University Press, Cambridge, 1998.
- [4] Kesten H. Quadratic transformations: a model for population growth. I,II *Adv.Appl.Prob.*, **2**(1970), 1–82; 179–228
- [5] Lyubich Yu.I. *Mathematical structures in population genetics*, Springer-Verlag, Berlin,1992.
- [6] Mukhamedov, F. Akin H., Temir S. On infinite dimensional quadratic Volterra operators, *Jour. Math. Anal. Appl.* **310**(2005), 533–556.
- [7] Roy N. Extreme points and $l_1(\Gamma)$ – spaces. *Proc. Amer. Math. Soc.* **86** (1982), 216–218.
- [8] Rozikov U A. Hamraev A.Yu. On Cubic operators defined on finite dimensional simplex. *Ukr.Mat. Jour.*, 56(2004), 1424-1433.
- [9] Takeuchi Y., *Global dynamical properties of Lotka–Volterra systems*, World Scientific, 1996.
- [10] Volterra V., Lois de fluctuation de la population de plusieurs espèces coexistant dans le même milieu, *Association Franc. Lyon* **1926** (1927), 96–98 .

FORCED VIBRATIONS OF A GENERAL CUBIC NONLINEAR CONTINUOUS SYSTEM

B. Burak ÖZHAN and Mehmet PAKDEMİRLİ*

Celal Bayar University, Department of Mechanical Engineering
45140, Muradiye, MANİSA, TÜRKİYE

ABSTRACT

A new generalized mathematical model encountered in nonlinear vibrations of continuous system is developed. Linear and cubic nonlinear parts of the model are represented by arbitrary operators. The equation of motion is solved in its general form by using the method of multiple scales (a perturbation technique). The primary resonances of excitation are investigated. Amplitude and phase modulation equations are found in their general form. Frequency response relation is also obtained in general sense. The general solution algorithm is applied to the nonlinear vibrations of an axially moving viscoelastic beam. Natural frequencies and frequency response relations of viscoelastic beam are derived.

Keywords: *Nonlinear Vibrations, Continuous Media, Primary Resonances, Perturbation Methods, Axially Moving Viscoelastic Beam*

* Corresponding author. Tel.: +90-236-241 21 44 (218); fax: +90-236-241 21 43
E-mail address: mpak@bayar.edu.tr (M. Pakdemirli)

1. INTRODUCTION

Vibrations of continuous systems are modelled by partial differential equations. Nonlinear models better represent the real behaviour of such systems. In the modelling of nonlinear vibration problems, quadratic and cubic nonlinearities frequently arise. These type of nonlinearities possess some common features. A new notation of expressing those nonlinearities has been first proposed by Pakdemirli[1]. In that study a general model including quadratic and cubic nonlinearities was developed by using arbitrary spatial operators. Free vibrations with linear damping were considered. That analyze involved only one mode. The analysis was generalized to infinite modes by Pakdemirli and Boyacı[2]. The authors considered primary resonances with forced vibrations. After that, the same authors treated subharmonic, superharmonic and combination resonances of a general model [3]. To comparing different versions of the method of multiple scales, the general notation was also used [4]. In that study the solution procedure was applied to the spesific problem of a beam resting on a nonliear elastic foundation. Pakdemirli [5] was investigated the general solution procedure to analyze primary resonances and one-to-one internal resonances of nonlinear vibrations of continuous system. And the algorithm was applied to nonlinear cable vibration problem. Pakdemirli was used the algorithm to solve coupled differential equations which presents also the nonlinear vibration of continuous systems. [6]. Pakdemirli and Özkaya was developed the general solution algorithm to cosider 3:1 internal resonances of cubic nonlinear system[7].The authors was applied the algorithm to simply supported Euler-Bernoulli beam resting on a nonlinear foundation. They were obtained frequency-response and force-response curves of a spesific problem. The generalized operator notation, which developed and used firstly by Pakdemirli (and co-workers), was also used by other authors [8],[9].

In this study a new cubic nonlinear vibration model is developed. This model covers many practical vibration problems of continuous systems such as axially moving Euler-Bernoulli beam-string, axially moving viscoelastic beam- string, fluid conveying pipe vibrations (see [12-15]). The cubic nonlinearity is inserted into the model in the form of arbitrary spatial operators. The method of multiple scales (a perturbation method) is used to solve the general model. Amplitude and phase modulation equations is found in general sense. Than the solution algorithm is applied an axially moving viscoelastic beam vibrations.

2. EQUATION OF MOTION

A general model which covers many cubic nonlinear vibration problems in continuous systems is

$$\ddot{w} + \mathbf{L}_1(w) + \mathbf{L}_2(\dot{w}) + \varepsilon \mu \dot{w} = \varepsilon F \cos \Omega t + \varepsilon \{ \mathbf{C}_1(w, w, w) + \mathbf{C}_2(\dot{w}, w, w) \} \quad (1)$$

$$\mathbf{B}_1(w) = 0 \quad x = 0 \quad \mathbf{B}_2(w) = 0 \quad x = 1 \quad (2)$$

where $w(x, t)$ is deflection, x and t are the spatial and time variables respectively. \mathbf{L}_1 and \mathbf{L}_2 are linear self- adjoint operators. \mathbf{C}_1 and \mathbf{C}_2 are nonlinear cubic operators. μ is the viscous damping coefficient. F and Ω are the external excitation amplitude and external excitation frequency respectively. \mathbf{B}_1 and \mathbf{B}_2 presents linear operators for boundary conditions. ε is a small dimensionless physical parameter. $(\dot{})$ denotes differentiation with respect to time.

The cubic operator possesses the property of being multilinear such that,

$$\begin{aligned} \mathbf{C}(c_1 w_1 + c_2 w_2, c_3 w_3 + c_4 w_4, c_5 w_5 + c_6 w_6) = & c_1 c_3 c_5 \mathbf{C}(w_1, w_3, w_5) + c_1 c_3 c_6 \mathbf{C}(w_1, w_3, w_6) \\ & + c_1 c_4 c_5 \mathbf{C}(w_1, w_4, w_5) + c_1 c_4 c_6 \mathbf{C}(w_1, w_4, w_6) + c_2 c_3 c_5 \mathbf{C}(w_2, w_3, w_5) + c_2 c_3 c_6 \mathbf{C}(w_2, w_3, w_6) \\ & + c_2 c_4 c_5 \mathbf{C}(w_2, w_4, w_5) + c_2 c_4 c_6 \mathbf{C}(w_2, w_4, w_6) \end{aligned} \quad (3)$$

In general,

$$\mathbf{C}(w_1, w_2, w_3) \neq \mathbf{C}(w_1, w_3, w_2) \neq \mathbf{C}(w_2, w_1, w_3) \neq \mathbf{C}(w_2, w_3, w_1) \neq \mathbf{C}(w_3, w_1, w_2) \neq \mathbf{C}(w_3, w_2, w_1) \quad (4)$$

3. PERTURBATION SOLUTION

To find the solution of Eq.(1) and Eq.(2), we apply the method of multiple scales [10-11] directly to the general model. We assume the expansion for $w(x, t)$ of the form,

$$w(x, T_0, T_1; \varepsilon) = w_0(x, T_0, T_1) + \varepsilon w_1(x, T_0, T_1) + \dots \quad (5)$$

where $T_0 = t$ is the usual fast time scale and $T_1 = \varepsilon t$ is the slow time scale. In terms of the new time variables, the derivatives become,

$$\frac{d}{dt} = D_0 + \varepsilon D_1 + \dots \quad \text{and} \quad \frac{d^2}{dt^2} = D_0^2 + 2\varepsilon D_0 D_1 + \dots \quad (6)$$

where $D_k = \frac{\partial}{\partial T_k}$. Substituting all into Eq.(1) and separating at each order of ε , one finally obtains,

$O(\varepsilon^0)$

$$D_0^2 w_0 + \mathbf{L}_1(w_0) + \mathbf{L}_2(D_0 w_0) = 0 \quad (7)$$

$$\mathbf{B}_1(w_0) = 0 \quad x = 0 \quad \mathbf{B}_2(w_0) = 0 \quad x = 1 \quad (8)$$

$O(\varepsilon^1)$

$$D_0^2 w_1 + \mathbf{L}_1(w_1) + \mathbf{L}_2(D_0 w_1) = -2D_0 D_1 w_0 - \mu D_0 w_0 - \mathbf{L}_2(D_1 w_0) + \mathbf{C}_1(w_0, w_0, w_0) + \mathbf{C}_2(D_0 w_0, w_0, w_0) + F \cos \Omega T_0 \quad (9)$$

$$\mathbf{B}_1(w_1) = 0 \quad x = 0 \quad \mathbf{B}_2(w_1) = 0 \quad x = 1 \quad (10)$$

At order 1, the solutions are,

$$w_0(x, T_0, T_1) = \sum_{n=1}^{\infty} A_n(T_1) e^{i\omega_n T_0} Y_n(x) + \bar{A}_n(T_1) e^{-i\omega_n T_0} \bar{Y}_n(x) \quad (11)$$

where A_n and \bar{A}_n are complex amplitudes and their conjugates respectively. $Y_n(x)$ satisfy the following equation and boundary conditions,

$$\mathbf{L}_1(Y_n) - \omega_n^2 Y_n + i\omega_n \mathbf{L}_2(Y_n) = 0 \quad n=1,2,\dots \quad (12)$$

$$\mathbf{B}_1(Y_n) = 0 \quad x = 0 \quad \mathbf{B}_2(Y_n) = 0 \quad x = 1 \quad (13)$$

Equation (12) with the associated boundary conditions is an eigenvalue-eigenfunction problem. ω_n are the eigenvalues and $Y_n(x)$ are eigenfunctions of the system. There are infinite number of eigenvalues for continuous systems.

Substituting Eq.(11) to the right hand side of Eq.(9), we obtain,

$$\begin{aligned} D_0^2 w_1 + \mathbf{L}_1(w_1) + \mathbf{L}_2(D_0 w_1) = & \sum_{n=1}^{\infty} \left\{ (-2i\omega_n D_1 A_n - i\mu\omega_n A_n) Y_n - D_1 A_n \mathbf{L}_2(Y_n) \right\} e^{i\omega_n T_0} \\ & + \sum_{m,p,q=1}^{\infty} \left\{ \left(A_m A_p A_q e^{i(\omega_m + \omega_p + \omega_q)T_0} \mathbf{C}_1(Y_m, Y_p, Y_q) + A_m A_p \bar{A}_q e^{i(\omega_m + \omega_p - \omega_q)T_0} \mathbf{C}_1(Y_m, Y_p, \bar{Y}_q) \right. \right. \\ & + A_m \bar{A}_p \bar{A}_q e^{i(\omega_m - \omega_p - \omega_q)T_0} \mathbf{C}_1(Y_m, \bar{Y}_p, \bar{Y}_q) + A_m \bar{A}_p A_q e^{i(\omega_m - \omega_p + \omega_q)T_0} \mathbf{C}_1(Y_m, \bar{Y}_p, Y_q) \left. \right) \\ & + i\omega_m \left(A_m A_p A_q e^{i(\omega_m + \omega_p + \omega_q)T_0} \mathbf{C}_2(Y_m, Y_p, Y_q) + A_m A_p \bar{A}_q e^{i(\omega_m + \omega_p - \omega_q)T_0} \mathbf{C}_2(Y_m, Y_p, \bar{Y}_q) \right. \\ & + A_m \bar{A}_p \bar{A}_q e^{i(\omega_m - \omega_p - \omega_q)T_0} \mathbf{C}_2(Y_m, \bar{Y}_p, \bar{Y}_q) + A_m \bar{A}_p A_q e^{i(\omega_m - \omega_p + \omega_q)T_0} \mathbf{C}_2(Y_m, \bar{Y}_p, Y_q) \left. \right) \left. \right\} + \frac{1}{2} F e^{i\Omega T_0} + cc \quad (14) \end{aligned}$$

where c.c stands complex conjugates of the proceeding terms. The boundary conditions for Eq.(14) are,

$$\mathbf{B}_1(w_1) = 0 \quad x = 0 \quad \mathbf{B}_2(w_1) = 0 \quad x = 1 \quad (15)$$

At order ε we assume that no interactions occur between the natural frequencies of the system and we express the nearness of external excitation frequency to one of the natural frequencies of the system,

$$\Omega = \omega_n + \varepsilon \sigma \quad (16)$$

where σ is a detuning parameter of $O(1)$. Now substituting Eq.(16) into Eq.(14). after rearranging yields,

$$\begin{aligned} D_0^2 w_1 + \mathbf{L}_1(w_1) + \mathbf{L}_2(D_0 w_1) = & -i\omega_n (2D_1 A_n + \mu A_n) e^{i\omega_n T_0} Y_1 - D_1 A_n e^{i\omega_n T_0} \mathbf{L}_2(Y_1) \\ & + A_n^2 \bar{A}_n e^{i\omega_n T_0} \{ \mathbf{C}_1(Y_1, Y_1, \bar{Y}_1) + \mathbf{C}_1(Y_1, \bar{Y}_1, Y_1) + \mathbf{C}_1(\bar{Y}_1, Y_1, Y_1) + i\omega_n [\mathbf{C}_2(Y_1, Y_1, \bar{Y}_1) \\ & + \mathbf{C}_2(Y_1, \bar{Y}_1, Y_1) - \mathbf{C}_2(\bar{Y}_1, Y_1, Y_1)] \} + \frac{1}{2} F e^{i\omega_n T_0} e^{i\sigma T_1} + \text{c.c} + \text{N.S.T} \end{aligned} \quad (17)$$

where N.S.T stands for non-secular terms. We assume a solution for w_1 of the form,

$$w_1(x, T_0, T_1) = \phi_1(x, T_1) e^{i\omega_n T_0} + \text{c.c} + W(x, T_0, T_1) \quad (18)$$

where $W(x, T_0, T_1)$ corresponds to the solution of non secular terms. Substituting Eq(18) into Eq.(17), using Eq.(16) yields for secular terms,

$$\begin{aligned} \mathbf{L}_1(\phi_1) - \omega_n^2 \phi_1 + i\omega_n \mathbf{L}_2(\phi_1) = & -i\omega_n (2D_1 A_n + \mu A_n) Y_1 - D_1 A_n \mathbf{L}_2(Y_1) \\ & + A_n^2 \bar{A}_n \{ \mathbf{C}_1(Y_1, Y_1, \bar{Y}_1) + \mathbf{C}_1(Y_1, \bar{Y}_1, Y_1) + \mathbf{C}_1(\bar{Y}_1, Y_1, Y_1) + i\omega_n [\mathbf{C}_2(Y_1, Y_1, \bar{Y}_1) \\ & + \mathbf{C}_2(Y_1, \bar{Y}_1, Y_1) - \mathbf{C}_2(\bar{Y}_1, Y_1, Y_1)] \} + \frac{1}{2} F e^{i\sigma T_1} \end{aligned} \quad (19)$$

$$\mathbf{B}_1(\phi_1) = 0 \quad x = 0 \quad \mathbf{B}_2(\phi_1) = 0 \quad x = 1 \quad (20)$$

The homegenous part of Eq.(19) possesses non-trivial solutions. The non-homogeneous equations have a solution only if a solvability condition is satisfied [11]. For the present model the solvability condition is

$$D_1 A_n + \mu k_1 A_n - k_2 A_n^2 \bar{A}_n - \frac{1}{2} f e^{i\sigma T_1} = 0 \quad (21)$$

The coefficients of Eq.(21) are ,

$$k_1 = \frac{i\omega_n \int_0^1 Y_1 \bar{Y}_1 dx}{2i\omega_n \int_0^1 Y_1 \bar{Y}_1 dx + \int_0^1 \mathbf{L}_2(Y_1) \bar{Y}_1 dx} \quad (22)$$

$$k_2 = \left\{ \int_0^1 \bar{Y}_1 \{ C_1(Y_1, Y_1, \bar{Y}_1) + C_1(Y_1, \bar{Y}_1, Y_1) + C_1(\bar{Y}_1, Y_1, Y_1) + i\omega_n [C_2(Y_1, Y_1, \bar{Y}_1) + C_2(Y_1, \bar{Y}_1, Y_1) - C_2(\bar{Y}_1, Y_1, Y_1)] \} dx \right\} / \left\{ 2i\omega_n \int_0^1 Y_1 \bar{Y}_1 dx + \int_0^1 L_2(Y_1) \bar{Y}_1 dx \right\} \quad (23)$$

$$f = \frac{\int_0^1 F \bar{Y}_1 dx}{2i\omega_n \int_0^1 Y_1 \bar{Y}_1 dx + \int_0^1 L_2(Y_1) \bar{Y}_1 dx} \quad (24)$$

The coefficients include real and imaginary parts,

$$k_1 = k_{1R} + i k_{1I}, \quad k_2 = k_{2R} + i k_{2I}, \quad f = f_R + i f_I$$

Now we will obtain amplitude and phase modulation equations. Polar form of complex amplitude is represented in polar form,

$$A_n = \frac{1}{2} a_n(T_1) e^{i\beta_n(T_1)} \quad (25)$$

Substituting Eq.(25) into Eq.(21) and seperating real and imaginary parts, we finally obtain the amplitude and phase modulation equations as follows,

$$a'_n = -\mu k_{1R} a_n + \frac{1}{4} k_{2R} a_n^3 + f_R \cos \gamma - f_I \sin \gamma \quad (26)$$

$$a_n \gamma' = a_n \sigma + \mu k_{1I} a_n - \frac{1}{4} k_{2I} a_n^3 - f_R \sin \gamma - f_I \cos \gamma$$

$$\text{where } \gamma = \sigma T_1 - \beta_n \quad (27)$$

To obtain steady-state solutions,

$$a'_n = \gamma' = 0 \quad (28)$$

should be taken. Substituting Eqs.(28), one has,

$$\mu k_{1R} a_n - \frac{1}{4} k_{2R} a_n^3 - f_R \cos \gamma + f_I \sin \gamma = 0 \quad (29)$$

$$\sigma a_n + \mu k_{1I} a_n - \frac{1}{4} k_{2I} a_n^3 - f_R \sin \gamma - f_I \cos \gamma = 0$$

Elimination of γ between the equations yield,

$$\sigma = -\mu k_{1I} + \frac{1}{4} k_{2I} a_n^2 \mp \sqrt{\frac{f_R^2 + f_I^2}{a_n^2} - \left(\mu k_{1R} - \frac{1}{4} k_{2R} a_n^2 \right)^2}$$

For analyzing the stability of the system, Eqs.(26) are rewritten as follows

$$\begin{aligned}
 a_n' &= -\mu k_{1R} a_n + \frac{1}{4} k_{2R} a_n^3 + f_R \cos \gamma - f_I \sin \gamma = F_1(a_n, \gamma) \\
 \gamma' &= \sigma + \mu k_{1I} - \frac{1}{4} k_{2I} a_n^2 - \frac{1}{a_n} f_R \sin \gamma - \frac{1}{a_1} f_I \cos \gamma = F_2(a_n, \gamma)
 \end{aligned}
 \tag{30}$$

Determination the stability of fixed points, the Jacobian matrix should be written,

$$\begin{bmatrix} \frac{\partial F_1}{\partial a_n} & \frac{\partial F_1}{\partial \gamma} \\ \frac{\partial F_2}{\partial a_n} & \frac{\partial F_2}{\partial \gamma} \end{bmatrix}_{\substack{a_n = a_{n0} \\ \gamma = \gamma_0}}
 \tag{31}$$

Eigenvalues of Jacobian matrix should not have positive real parts for stability. The response (or the approximate solution) of the system is,

$$w(x, t; \varepsilon) = a_n \cos(\Omega t - \gamma) Y_{1R} - a_n \sin(\Omega t - \gamma) Y_{1I} + O(\varepsilon)
 \tag{32}$$

Where Y_n can be expressed into its real and imaginary parts,

$$Y_n = Y_{nR} + i Y_{nI}
 \tag{33}$$

a_n and γ in the approximate solution are governed by Eqs.(30).

4. APPLICATION TO THE PROBLEM OF A MOVING VISCOELASTIC BEAM

In this section, the algorithm developed in previous sections is applied to a specific problem. Example model presents nonlinear vibrations of axially moving viscoelastic beam[13-15],

$$\ddot{w} + (v_0^2 - 1) w'' + 2v_0 \dot{w}' + v_f^2 w^{IV} + \alpha \dot{w}^{IV} = \varepsilon F \cos \Omega t + \varepsilon \left\{ \frac{3}{2} v_\ell^2 w'' w'^2 + 2\alpha k w' \dot{w} w'' + \alpha k w'^2 \dot{w}'' \right\}
 \tag{34}$$

$$w(0, t) = w(1, t) = w''(0, t) = w''(1, t) = 0
 \tag{35}$$

In the Eq.(34), v_f is the dimensionless flexural stiffness, v_ℓ is the dimensionless longitudinal stiffness, v_0 is dimensionless axially moving speed, α represents viscosity coefficient and k represents a dimensionless parameter including dynamical viscosity.

The general operators are defined for this specific problem first,

$$\mathbf{L}_1(w) = (v_0^2 - 1) w'' + v_f^2 w^{IV}
 \tag{36}$$

$$\mathbf{L}_2(\dot{w}) = 2v_0 \dot{w}' + \alpha \dot{w}^{IV}
 \tag{37}$$

$$C_1(w, w, w) = \frac{3}{2} v_\ell^2 w'' w'^2 \quad (38)$$

$$C_2(\dot{w}, w, w) = 2\alpha k w' \dot{w}' w'' + \alpha k w'^2 \dot{w}'' \quad (39)$$

The general eigenvalue-eigenfunction problem defined in Eq.(12) and Eq.(13) now reads

$$(v_f^2 + i\omega_n \alpha) Y_n^{IV} - \omega_n^2 Y_n + (v_0^2 - 1) Y_n'' + 2v_0 i\omega_n Y_n' = 0 \quad (40)$$

$$Y_n(0) = Y_n(1) = Y_n''(0) = Y_n''(1) = 0 \quad (41)$$

Solution of Eq.(40) is assumed as follows,

$$Y_n(x) = c_1 e^{i\beta_{1n}x} + c_2 e^{i\beta_{2n}x} + c_3 e^{i\beta_{3n}x} + c_4 e^{i\beta_{4n}x} \quad (42)$$

β_{in} satisfies the dispersive relation [12],

$$(v_f^2 + i\alpha \omega_n) \beta_{in}^4 + (1 - v_0^2) \beta_{in}^2 - 2v_0 \omega_n \beta_{in} - \omega_n^2 = 0 \quad (43)$$

Applying the boundary conditions to the solution, one obtains the mode shape equation,

$$Y_n(x) = c_1 \left\{ e^{i\beta_{1n}x} - \frac{(\beta_{4n}^2 - \beta_{1n}^2)(e^{i\beta_{3n}} - e^{i\beta_{1n}})}{(\beta_{4n}^2 - \beta_{2n}^2)(e^{i\beta_{3n}} - e^{i\beta_{2n}})} e^{i\beta_{2n}x} - \frac{(\beta_{4n}^2 - \beta_{1n}^2)(e^{i\beta_{2n}} - e^{i\beta_{1n}})}{(\beta_{4n}^2 - \beta_{3n}^2)(e^{i\beta_{2n}} - e^{i\beta_{3n}})} e^{i\beta_{3n}x} \right. \\ \left. + \left[-1 + \frac{(\beta_{4n}^2 - \beta_{1n}^2)(e^{i\beta_{3n}} - e^{i\beta_{1n}})}{(\beta_{4n}^2 - \beta_{2n}^2)(e^{i\beta_{3n}} - e^{i\beta_{2n}})} + \frac{(\beta_{4n}^2 - \beta_{1n}^2)(e^{i\beta_{2n}} - e^{i\beta_{1n}})}{(\beta_{4n}^2 - \beta_{3n}^2)(e^{i\beta_{2n}} - e^{i\beta_{3n}})} \right] e^{i\beta_{4n}x} \right\} \quad (44)$$

Natural frequencies and β_{in} values can be calculated numerically by using Eq.(43) and support condition [12] together. For a specific choice for $\alpha = 0.001$, $v_f = 0.2$ and $v_0 = 1$, the natural frequency $\omega_1 = 1.61785$ and β_{in} values are $\beta_{11} = 4.56488 - 0.05857i$, $\beta_{21} = -1.83063 + 3.80787i$, $\beta_{31} = -1.93048 - 3.74951i$, $\beta_{41} = -0.80376 + 0.0002i$.

Figure 1 shows the variation of natural frequencies with mean velocity of viscoelastic beam for three different flexural stiffness values for the first mode. Frequencies decreased by increasing the mean velocity values for each flexural stiffness. Figure 2 shows the first five natural frequencies versus axial moving speed. Figure 3 shows the frequency-response curves for three flexural stiffness values. It is clear that non-linear effects increased by increasing the flexural rigidity.

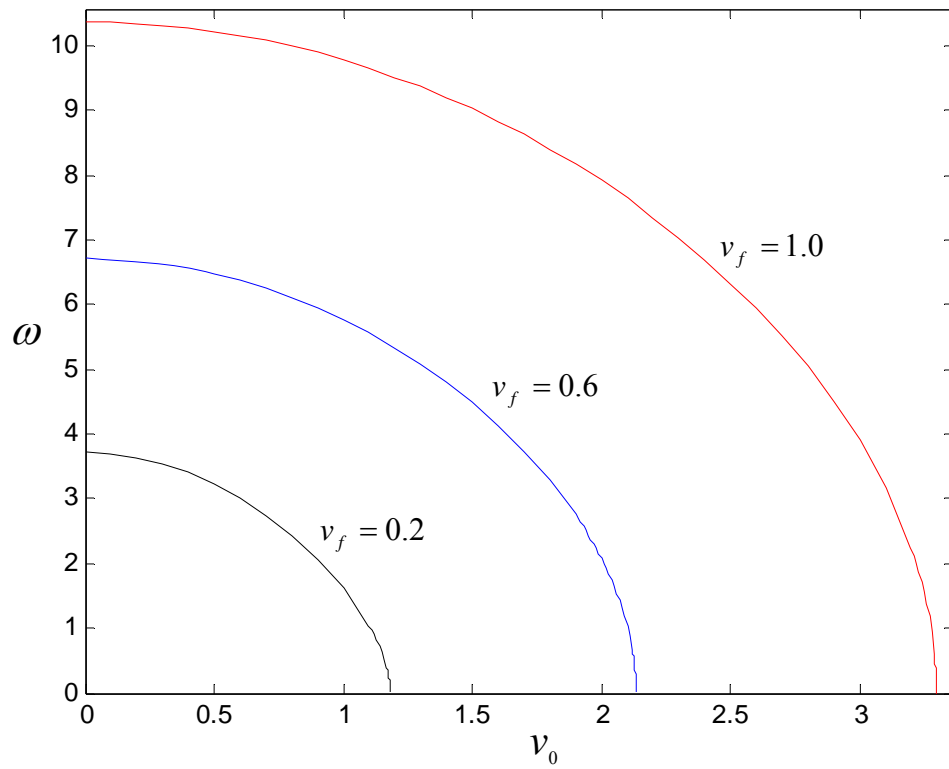


Figure1.Axial moving speed versus natural frequencies
 $\alpha = 0.001$. $k = 1$

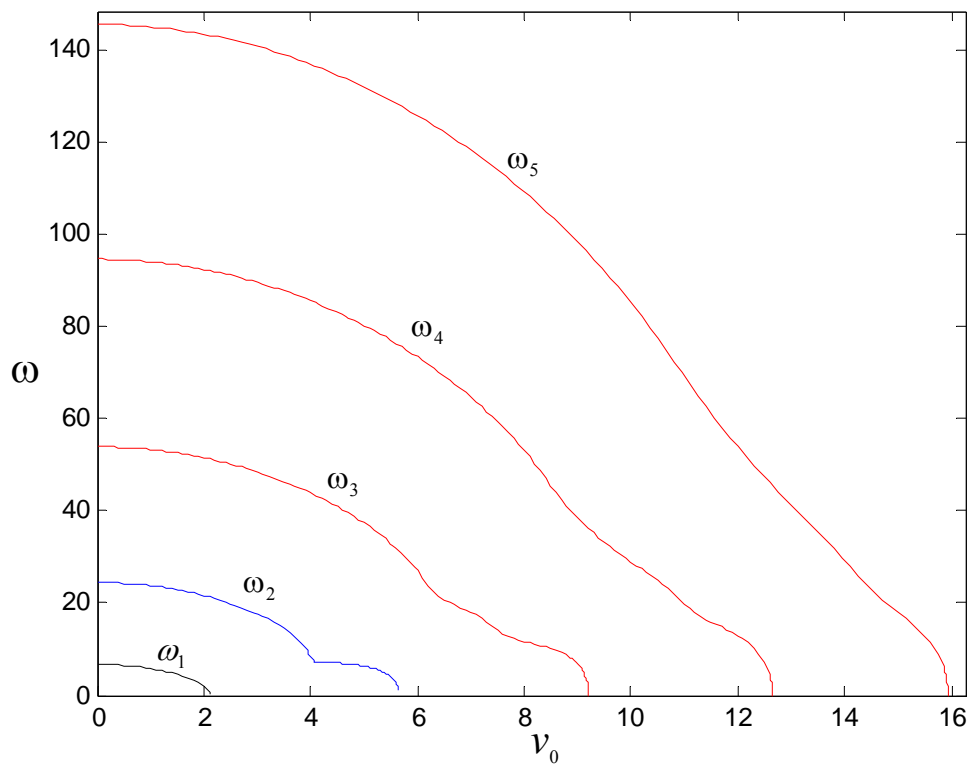


Figure 2. First five natural frequencies versus axial moving speed
 $\alpha = 0.001, v_f = 0.6, v_\ell = 0.6, k = 1$

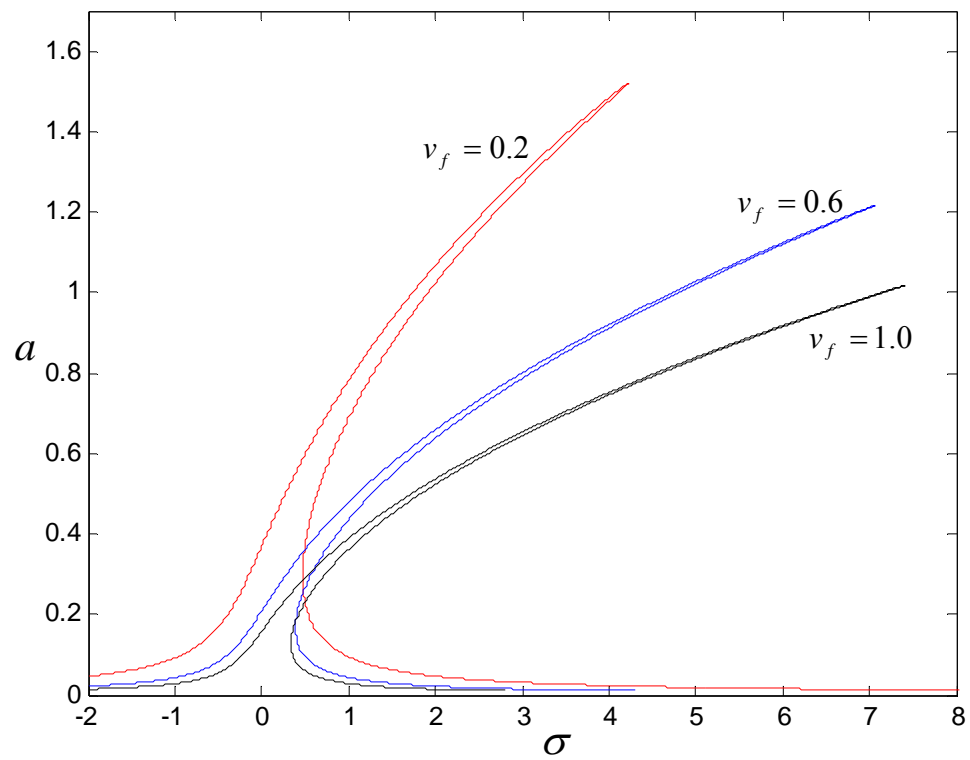


Figure 3. Frequency-Response curves
 $\alpha = 0.001$, $k = 1$

REFERENCES

- [1] Pakdemirli, M.,(1994) "A comparison of two perturbation methods for vibrations of systems with quadratic and cubic nonlinearities", *Mechanics Research Communications*, Volume 21, Issue 2, March-April, 203-208
- [2] Pakdemirli, M., and Boyacı, H.,(1995) "Comparision of direct- perturbation methods with discretization-perturbation methods for nonlinear vibrations", *Journal of Sound and Vibration*,186, 837-845,
- [3] Pakdemirli, M., and Boyacı, H., (1996) "Vibrations of continuous systems having arbitrary quadratic and cubic nonlinearities",*Applied Mechanics and Engineering*,1,3,445-463
- [4] Boyacı, H. and Pakdemirli, M., (1997) "A comparison of different versions of the method of multiple scales for partial differential equations", *Journal of Sound and Vibration* , 204(4),595-607
- [5] Pakdemirli, M., (2001) "Vibrations of continuous systems with a general operator notation suitable for perturbative calculations" , *Journal of Sound and Vibration* 246(5), 841}851
- [6] Pakdemirli, M., (2001) "A general solution procedure for coupled systems with arbitrary internal resonances", *Mechanics Research Communications*, Vol. 28. No. 6, pp. 617-522,
- [7] Pakdemirli, M. and Özkaya, E. , (2003) "Three-to-one internal resonances in a general cubic non-linear continuous system", *Journal of Sound and Vibration* 268 543–553
- [8] Nayfeh, A.H. , (1998) "Reduced order models of weakly nonlinear spatially continuous systems", *Nonlinear Dynamics* 16,105–125.
- [9] Lacarbonara, W., (1999)" Direct treatment and discretizations of non-linear spatially continuous systems", *Journal of Sound and Vibration* 221 849–866.
- [10]Nayfeh,A.H.and Mook,D.T.,(1979)"*Nonlinear Oscillations*".John Wiley&Sons,Inc, NY
- [11]Nayfeh,A.H.(1981)"*Introduction to Perturbation Techniques*"John Wiley&Sons, Inc,NY
- [12] Öz,H.R., Pakdemirli, M., Boyacı, H., (2001) "Non-linear vibrations and stability of an axially moving beam with time-dependent velocity", *International Journal of Non-Linear Mechanics* 36 107-115
- [13] Chen,L.Q., and Yang, X.D., (2005) "Stability in parametric resonance of axially moving viscoelastic beams with time-dependent speed", *Journal of Sound and Vibration* 284 879–891
- [14] Yang, X.D. and Chen,L.Q., (2005) "Bifurcation and chaos of an axially accelerating viscoelastic beam", *Chaos, Solitons and Fractals* 23 249–258
- [15] Chen,L.Q., ve Yang, X.D., (2006) " Transverse nonlinear dynamics of axially accelerating viscoelastic beams based on 4-term Galerkin truncation", *Chaos, Solitons and Fractals* 27 748–757

PRECURSORY SEISMIC QUIESCENCE BEFORE 1 MAY 2003 BİNGÖL (TURKEY) EARTHQUAKE: A STATISTICAL EVALUATION

Serkan ÖZTÜRK¹, Yusuf BAYRAK¹

¹ Karadeniz Technical University, Department of Geophysics, 61080 Trabzon, Turkey

Tel: +90 462 377 2783

e-mail: seko6134@hotmail.com

ABSTRACT

The variations of seismicity rate changes prior to the occurrence of 1 May 2003 Bingöl earthquake has been analyzed by statistical method, with the observation of pointing up precursory seismic sequence. We investigated the significance of seismic quiescence for the region 39.6°E-40.6°E and 38.2°N-39.6°N. The analysis was carried out on the instrumental catalogue of the Boğaziçi University, Kandilli Observatory and Earthquake Research Institute (KOERI), covering the period from 1970 to 2005. The catalogue is homogeneous for duration magnitude, M_D , including 1926 crustal earthquakes of magnitude equal and greater than 1.8, with depths less than 70 km. For the calculations, we used the completeness magnitude as 3.2 and the number of events exceeding this magnitude is 915. In the first step, we declustered the catalogue using the Reasenbergs algorithm. 43% of the events were removed and the number of these events was reduced to 522. The analysis was carried out making use of the *ZMAP* software package. The methodology we use involves the gridding method at the nodes of a 0.02° grid spacing. By *ZMAP*, the number of events associated with each grid point was selected as 50 after a few tests. The data are subdivided in bins of 28 days for each sample and we used a moving time window $T_W=5$ years for the imaging of space and time rate changes. Finally, using the declustered catalogue spatial variability of Z-values is mapped for every one year between 1990 and 1998. It is not observed any significant seismic quiescence in time interval 1990 and 1993 around the 2003 main shock. After 1993, we observed a clear quiescence in and around the main shock epicenter of 1 May 2003 Bingöl earthquake with Z level between 2 and 3. This quiescence period is best revealed between 1995 and 1998. To identify the starting time and duration of precursory quiescence it is plotted cumulative number of events corresponding LTA(t) function for a circle of 7.79 km radius centered on Bingöl main shock. A decrease of the seismicity rate is found with $Z_{max}=2.5$ level at 1997.6. Thus, we found that Bingöl earthquake on May 1, 2003 (2003.33) followed an outstanding seismic quiescence starting 5.73 years before main shock. Based on this result, an estimate of future seismic hazard of these areas is made by the detection of seismic quiescence.

Keywords: *Bingöl, earthquake prediction, seismic quiescence, precursors, decluster.*

1. INTRODUCTION

The seismicity rate changes have been used in a great number of studies as a significant tool in order to explain the stress distribution in a specific area of the Earth's crust. Many authors have reported that precursory seismic quiescence occurred in and around focal areas several years before earthquakes: Tokachi-Oki [1,2], Tonga-Kermadec [3], Morgan Hill [4], San Andreas [5,6], Izu-Oshima [7], Kurile [8], Colfiorito [9] and Kefalonia [10]. Some studies on precursors of past earthquakes suggest that particular space-time seismicity patterns, including the phenomenon of precursory quiescence, can be related to the seismo-tectonic processes that lead to earthquakes [6,11,12,13]. The quiescence hypothesis, as formulated by Wyss and Habermann [11], postulates that the quiet volume overlaps the main shock source volume. The seismic quiescence hypothesis assumes that some main shocks are preceded by seismic quiescence, which is a significant decrease of the mean seismicity rate (number of events of magnitude exceeding a given threshold, per unit time), as compared to the preceding declustered background rate in the same crustal volume [9]. As requisite for the quiescence to be positively correlated with an eventual subsequent main shock, the decrease of seismicity rate must be defined by objective criteria [14] and be observed in all or a part of the source volume of the main shock. In some cases, it has been observed that the quiescence lasts until the time of the main shock, but in others the quiescence is separated from the main shock by a period of increased seismicity. The possibility of comparing the seismicity rate in a relatively small time and space volume, with the background seismicity level, is based on the assumption that the average seismicity rate in large crustal volumes and long time intervals, is constant [7].

To detect the significant seismic quiescence, it is necessary to decluster the earthquake catalogue. For this process, it has been made use of the algorithm introduced by Reasenber [15]. The cluster analysis algorithm of Reasenber [15] "declusters" or decomposes a regional earthquake catalogue into main and secondary events [16]. It removes all the dependent events from each cluster, and substitutes them with a unique event, equivalent in energy to that of whole series. The declustering process introduces some artificial manipulations. In fact, the declustering algorithm contains some arbitrary parameters that allow the user to remove aftershocks in a smaller or larger time or space interval with respect to the main shock location [9].

Seismic quiescence as originally proposed by Wyss and Habermann [11] is investigated for crustal events. It can be recognized by the methodology introduced by Wiemer and Wyss [17] and implemented in the *ZMAP* software package [18]. The *ZMAP* technique allows the user to analyze and to obtain graphic displays of seismicity rate changes in both space and time, in selected magnitude ranges. It allows also the quantitative evaluation of the statistical significance of any rate change (quiescence), the percentage of space-time volume interested by anomalies and the conditions by which a quiescence episode can be put in relation with a main shock [9].

The purpose of this study is to evaluate the seismicity rate changes (quiescence episodes) occurred before 1 May 2003 Bingöl (Turkey) main shock. If such features could be recognized as a constant and reliable character of the seismicity, they could eventually contribute to the forecast of impending main shocks in future circumstances. Thus, we aimed to provide additional information regarding the future seismic hazard of Bingöl.

2. METHOD

A continuous image of space and time rate changes in seismicity is produced by *ZMAP*, creating a grid of geographical co-ordinates, and associating to each grid node a selected number of nearest events. The subset of events belonging to each grid node is sampled in short time windows (usually a few weeks), so that the average number of events occurred in a time period of several consecutive samples (foreground) can be compared with that of all the remaining samples (background) [9]. We applied the *ZMAP* method [17] for imaging the areas exhibiting a seismic quiescence. Wiemer and Wyss [17] described details of the method. In order to rank the significance of quiescence, we used the standard deviate *Z*-test, generating the *LTA(t)* (Log Term Average) function [5,17,19,20] for the statistical evaluation of the confidence level in units of standard deviations:

$$Z(t) = \frac{R_{all} - R_{wl}}{\sqrt{\frac{\sigma_{all}^2}{n_{all}} + \frac{\sigma_{wl}^2}{n_{wl}}}} \quad (1)$$

where R_{all} is the mean rate in the overall period including T_W (from t_0 to t_e), R_{wl} the mean rate in the considered time window (from t to $t+T_W$). σ_{all} and σ_{wl} are the standard deviations in these periods, and n_{all} and n_{wl} the number of samples. t is the "current time" ($t_0 < t < t_e$). The *Z*-value, calculated for all times t between t_0 and $t_e - T_W$

(Figure 1), by the equation is statistically appropriate for estimating seismicity rate change in a time window T_w in contrast with background seismicity. The Z-value computed as a function of time, letting the foreground window slide along the time duration of catalogue, is called $LTA(t)$. The shape of the $LTA(t)$ function strongly depends on the choice of the length of the foreground window (w_l). While the statistical robustness of the $LTA(t)$ function increases with the size of w_l , its shape becomes more and more smooth, if the w_l length exceeds the duration of the anomaly. Moreover, if one has to evaluate the statistical significance of an anomaly, it is not only necessary to decide the threshold level for the Z-value (in terms of standard deviations unit), but also the maximum time length allowed after the end of anomaly, before the occurrence of the main shock. The selection of the number of events at each point, and of the time bin, introduces two more free parameters in the procedure, and other three come from the choice of the geographical co-ordinates and the size of the sample. So, the geographical extension of the examined area must be sufficiently large in comparison with the presumable extension of the source area of an earthquake magnitude and the temporal extension of the catalog must be large enough [8].

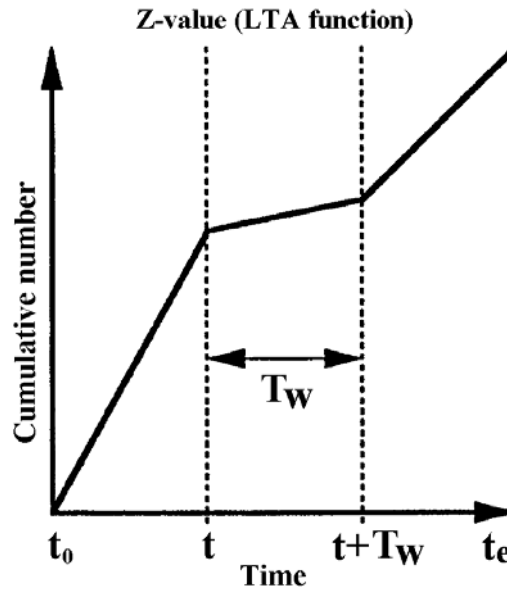


Figure 1. Schematic explanation of how to calculate Z-values. R_{all} is the average number of events in the whole background period, R_{wl} is the mean seismicity rate computed in the foreground window and T_w is the length of the time window in year. σ_{all} and σ_{wl} are the variances of the means, and n_{all} and n_{wl} the corresponding number of bins with a measured seismicity rate. t is the “current time” ($t_0 < t < t_e$).

The duration of quiescence is the important parameter to be determined and its significance is maximized when T_w is equal to that value and for meaningful results we demand that they do not depend on the choice of T_w . Since it is not known how long quiescence may last it is varied the window length from 1.5 to 5.5 years, because this is in the range of reported seismic quiescence prior to crustal main shocks [21,22].

3. DATA USED

The database we analyzed in this study is taken from the instrumental catalogue of Boğaziçi University, Kandilli Observatory and Earthquake Research Institute (KOERI), starting from 1970 up to 2005. The catalogue is homogeneous for duration magnitude (M_D). We carried out our analysis in the rectangular area limited by the co-ordinates 38.2°N and 39.6°N in latitude and by the co-ordinates 39.6°E and 40.6°E in longitude. Figure 2 shows the epicenter distribution of shallow earthquakes (depth < 70 km) in and around Bingöl occurred in time between 1970 and 2005 together with principal main shocks ($M_D \geq 5.0$). The catalogue includes 1926 events of magnitude $M \geq 1.8$. The completeness magnitude for Bingöl area is 3.2 and the number of earthquakes exceeding this magnitude range is 915. In this study, we proceed to decluster the appropriate catalogue using Reasenbergs [15] algorithm in order to remove aftershock sequences which can induce artificial quiescence. 43% of the events were removed and the number of events for Z-value analysis was reduced to 522. The cumulative number of earthquakes versus time for events with $M_D \geq 3.2$ (original catalog) and for declustered events (excluding aftershocks from original catalog) is shown in Figure 3.

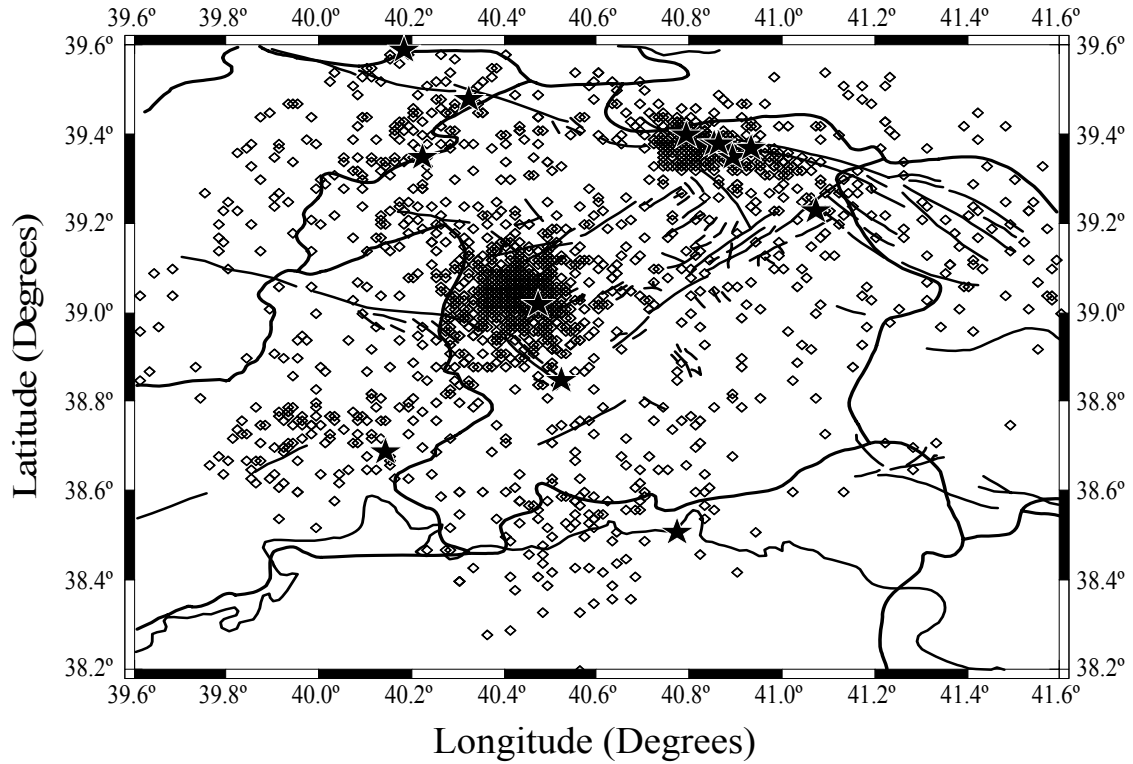


Figure 2. Epicentral map of the shallow seismicity ($M_D \geq 3.2$) between 1970 and 2005 in and around Bingöl. Stars show the principal main shocks with $M \geq 5.0$.

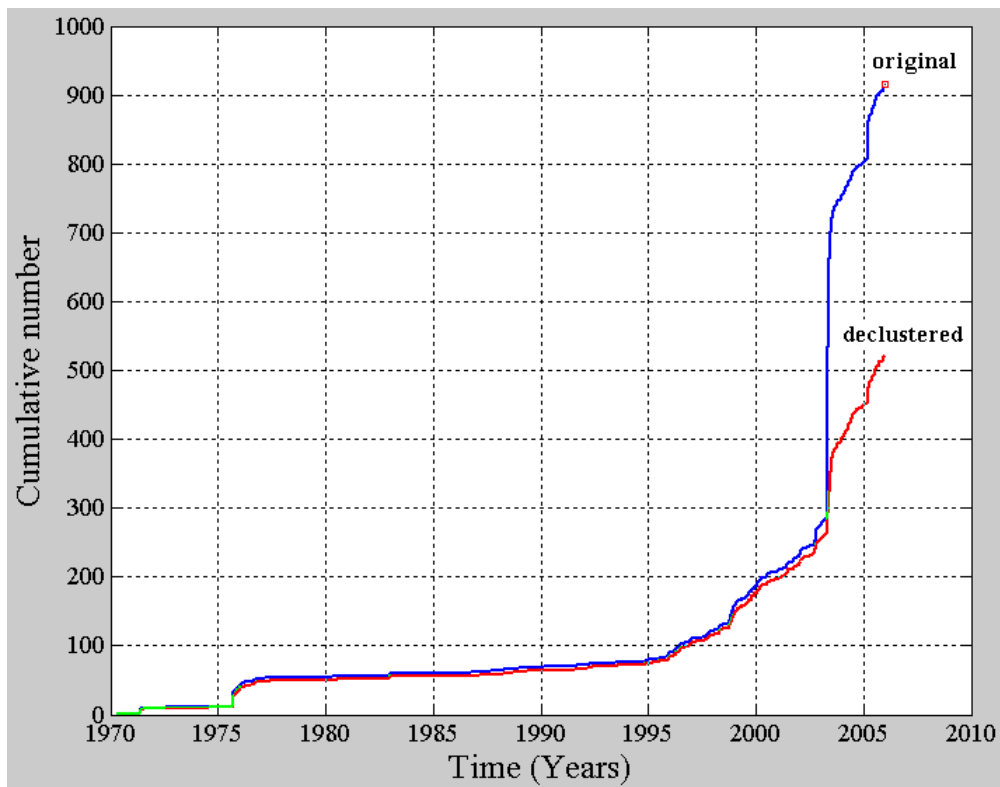


Figure 3. Cumulative number of earthquakes versus time for the original earthquake catalogue of KOERI containing 915 events and for the declustered catalogue containing 522 events, with $M_D \geq 3.2$ and depths less than 70 kilometers from 1970 until 2005.

4. ANALYSIS

Using *ZMAP*, we measured the significance of seismicity rate changes with a grid of points spacing 0.02° in longitude by 0.02° in latitude because this is related to the accuracy of epicentral determinations of the catalogue and it also provides a dense coverage in space. After some preliminary tests, we took the nearest earthquakes $N=50$ at each node and searched for rate changes by a moving time window T_w , stepping forward through the time series by a sampling interval as described by Wiemer and Wyss [17]. The sampling interval is selected as a time step of 28 days in order to have a continuous and dense coverage in time and N and T_w values are usually selected accordingly in order to enhance the quiescence signal and this choice does not influence the results in anyway. The total duration of the catalogue is 35.67 years.

The geographical distributions of Z -value for Bingöl and surrounding area are shown in Figure 4. The Z -maps of Figure 4 represents a choice obtained after numerous tests, carried out trying different values of T_w (indicated as *iwl* in the respective figure; 1.5, 2, 2.5, 3, 3.5, 4, 4.5 and 5 years) and different starting times for the foreground windows. Spatial variability of Z -values is presented for every one year between 1990 and 1998 based on the declustered catalogue. Each value of Z is represented by a different color: the scale spans from the lowest Z -values, indicating no significant changes in seismicity rate, shown in blue, and the highest ones (decrease in seismicity rate), shown in red. It should be recalled that in this representation each Z -value, computed in correspondence of a different grid point, comes from circular areas, the size of which is inversely proportional to the density of the spatial distribution of earthquakes. The time window, T_w , in which the mean rate is compared to the mean background rate, is 5 years. As shown in Z -value maps, there is no significant seismicity change in time interval 1990 and 1993. These maps show a clear area of quiescence after 1993, nearly overlapping the epicenter of the Bingöl, 2003 main shock with Z level between 2 and 3 (red areas). This quiescence is best revealed at the epicentral areas of the main shock of Bingöl earthquake between 1995 and 1998.

As stated before, in this study we are aiming to the recognition of a quiescence episode before the Bingöl 2003 earthquake. We want also to identify the beginning and duration of quiescence. For this purpose, we plotted cumulative number of events in a circular area including the epicenter of the 2003 Bingöl earthquake. Figure 5 shows the cumulative number curve versus time and the correspondent $LTA(t)$ function for a circle of 7.79 km radius centered on Bingöl main shock. The Z -value peaked with $Z_{max}=2.5$ at 1997.6. Thus, we observed that the duration of quiescence is 5.73 years before the 2003.33 (1 May 2003) Bingöl earthquake.

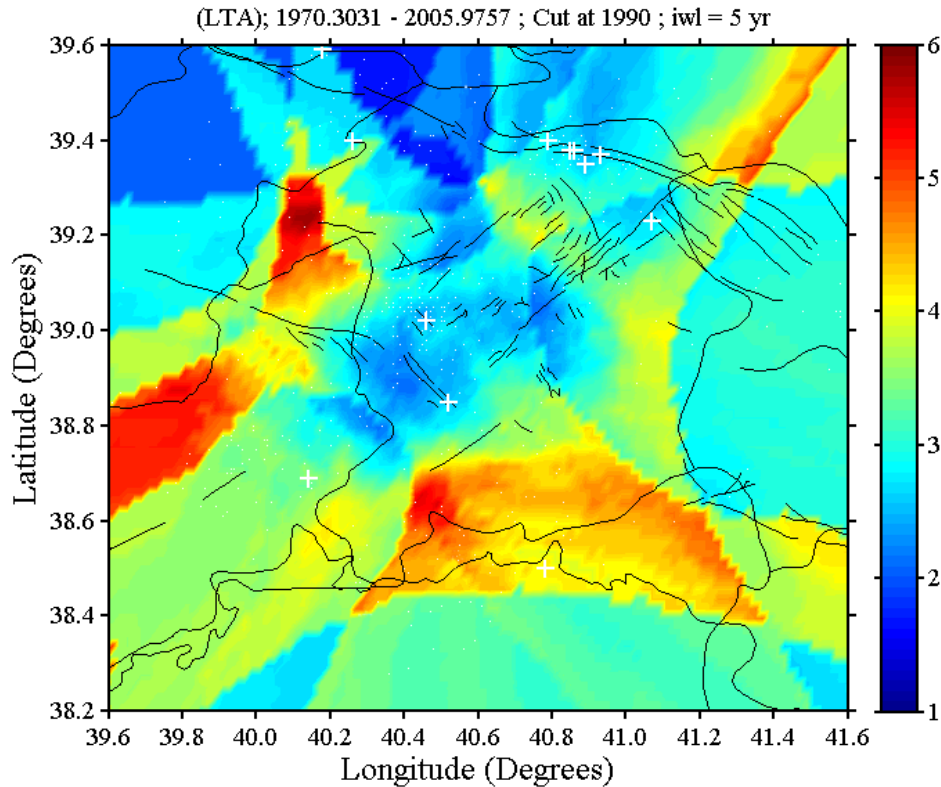


Figure 4. Geographical distribution of the statistical Z parameter every one year between 1990 and 1998 using declustered catalogue. The length of time window T_w is 5 years. The epicenter of main shocks with $M_D \geq 5.0$ is indicated by “+” symbol. Red color represents a decrease in seismicity rate.

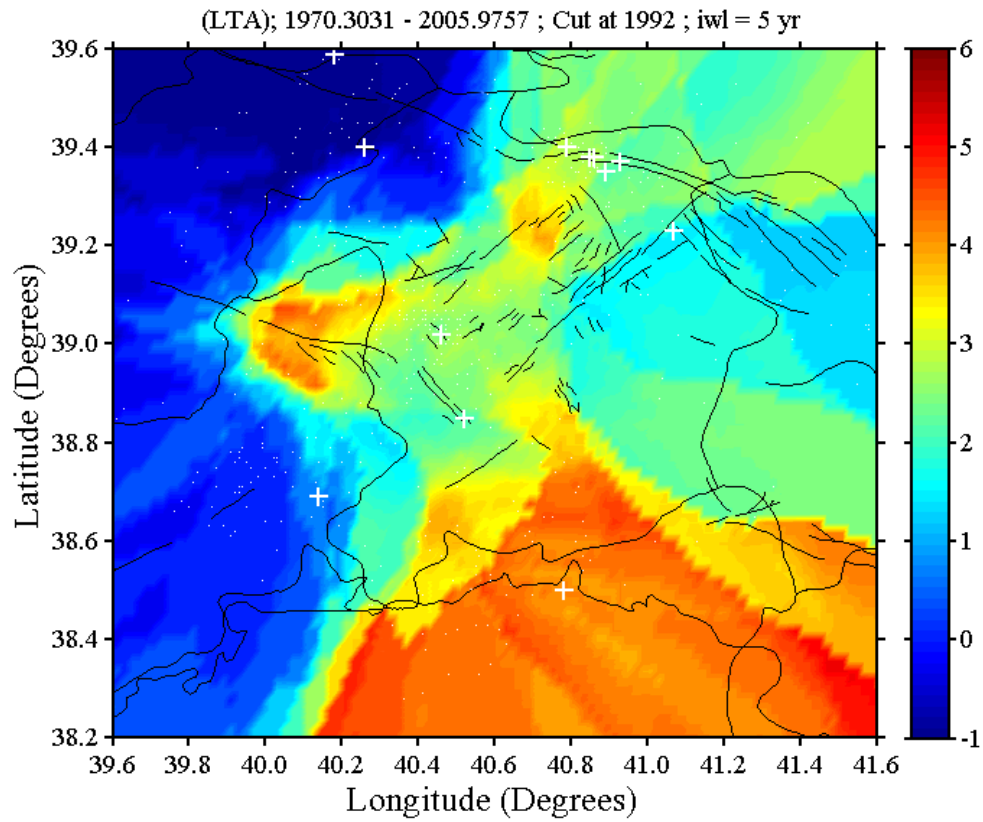
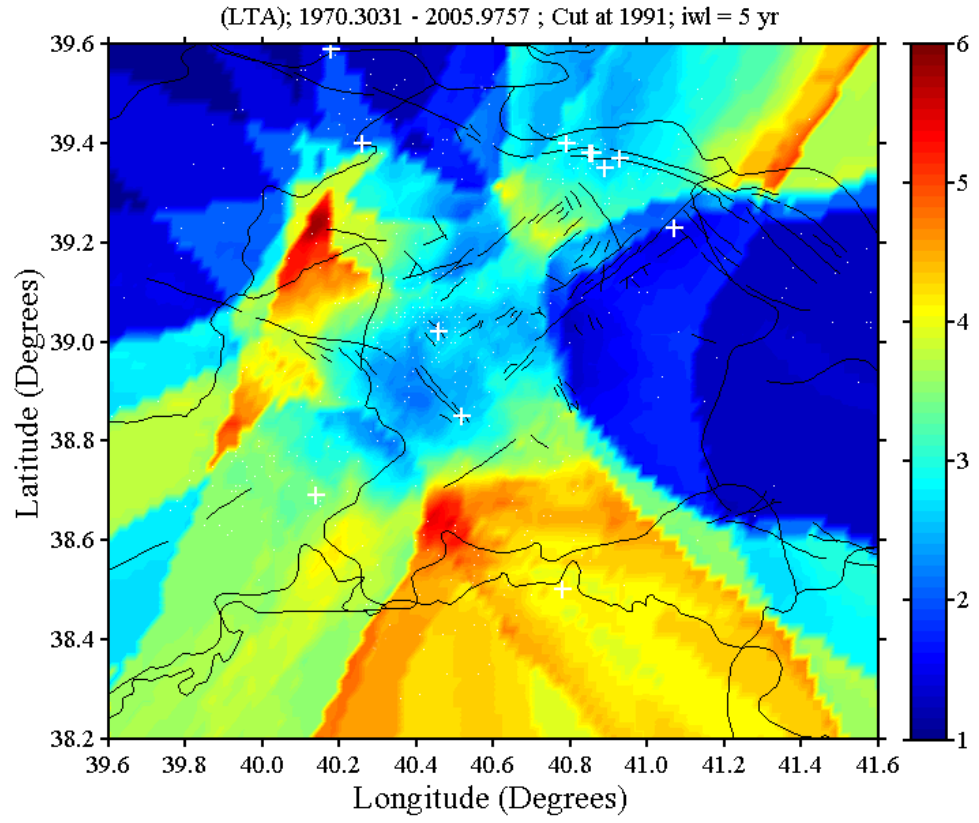


Figure 4 (continued)

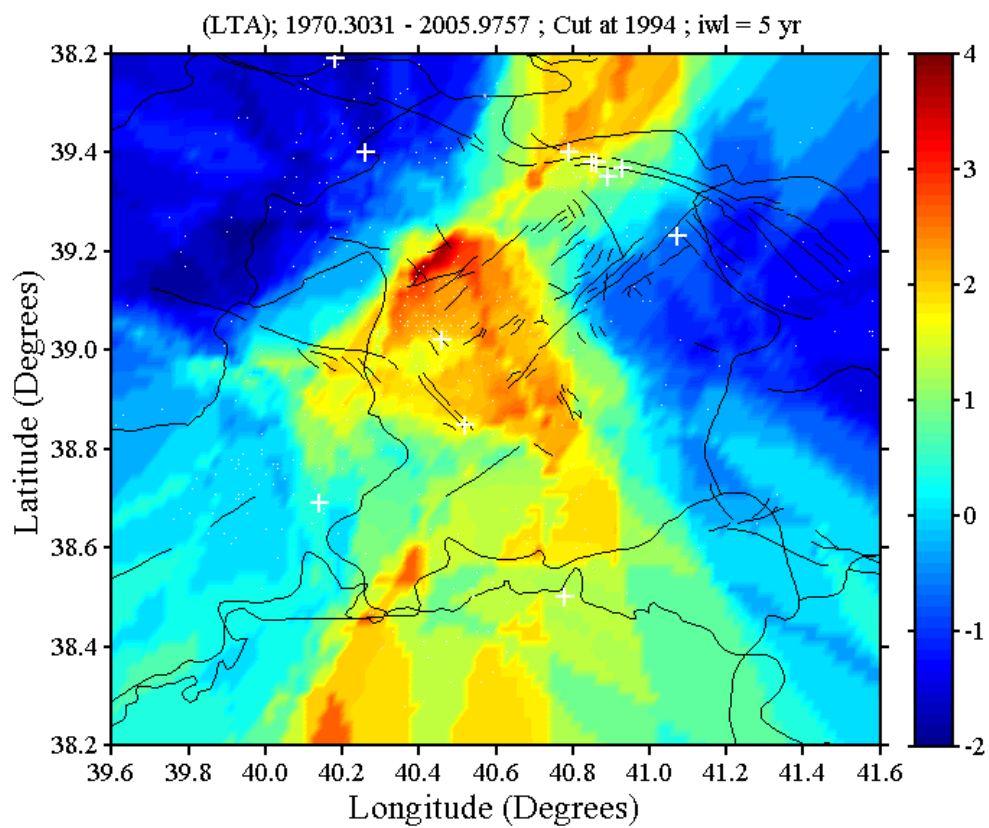
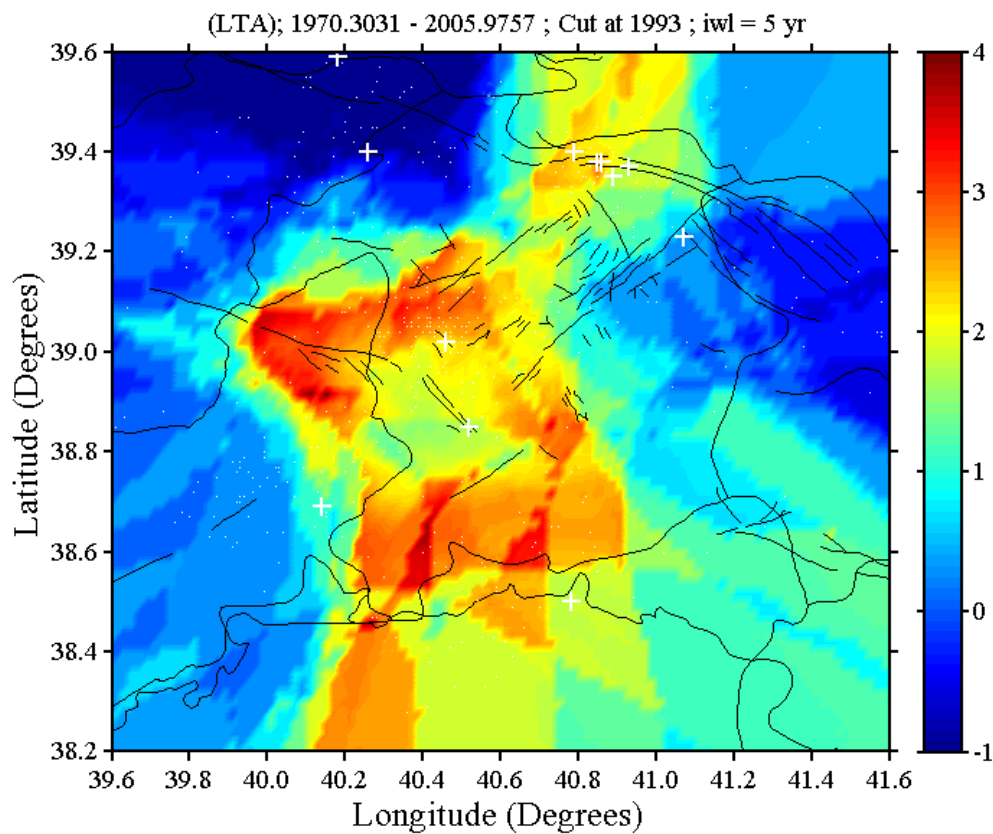


Figure 4 (continued)

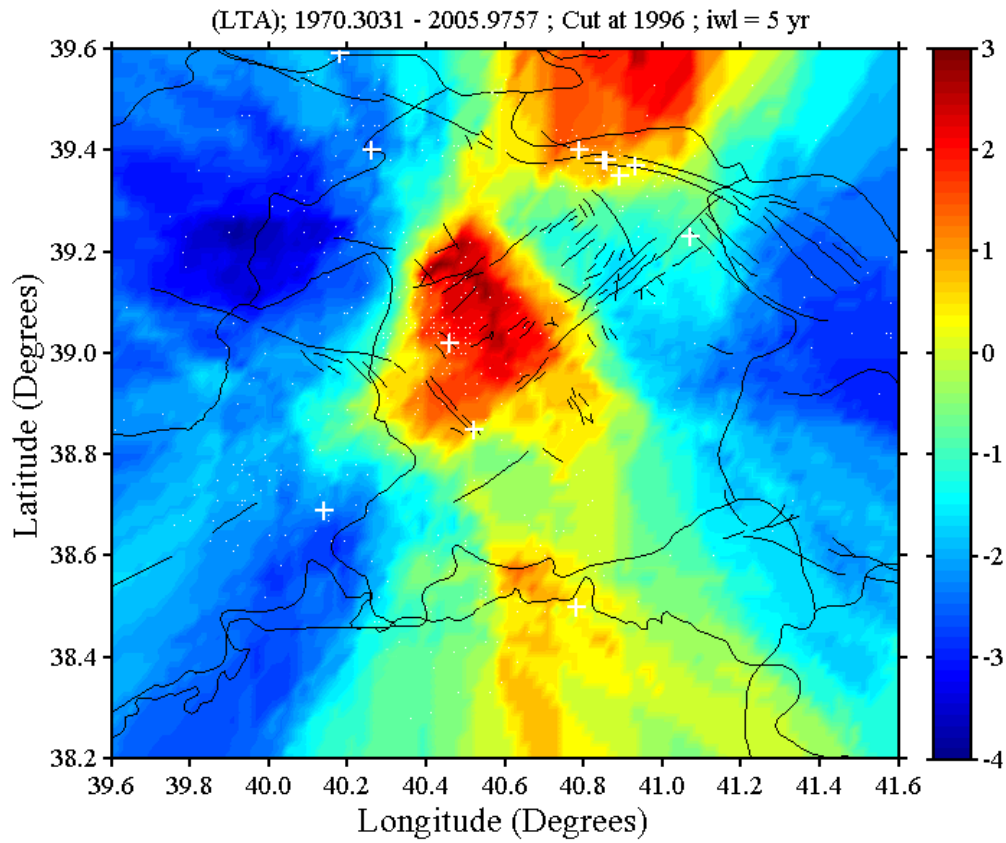
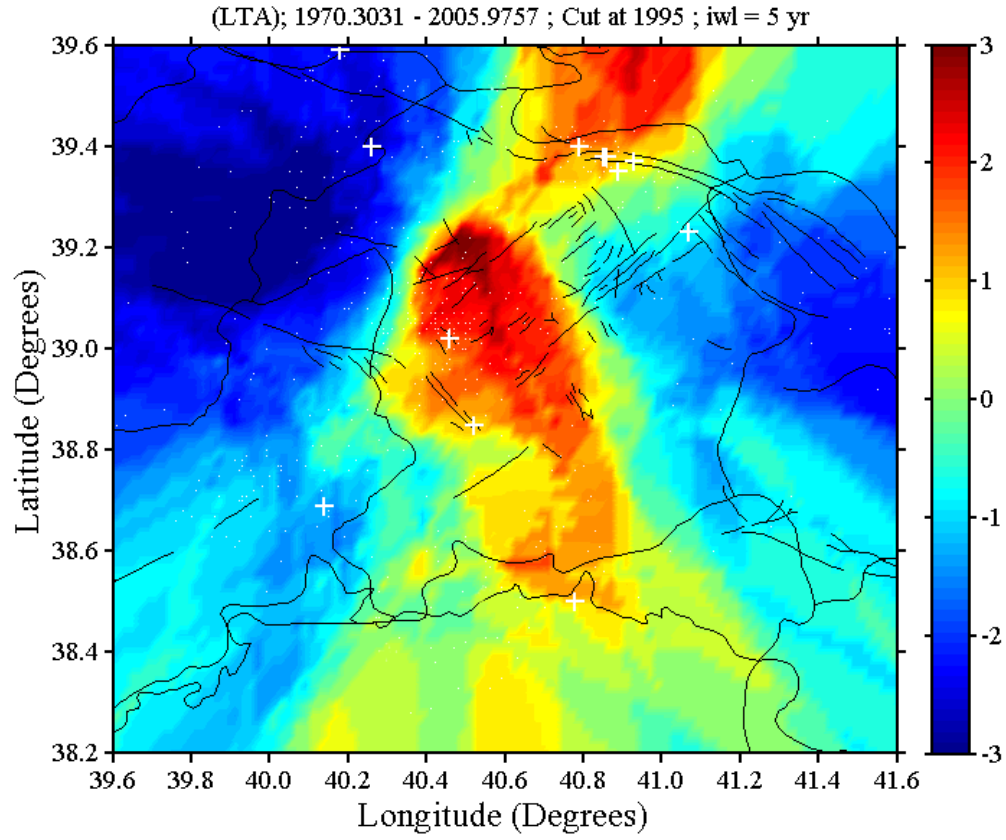


Figure 4 (continued)

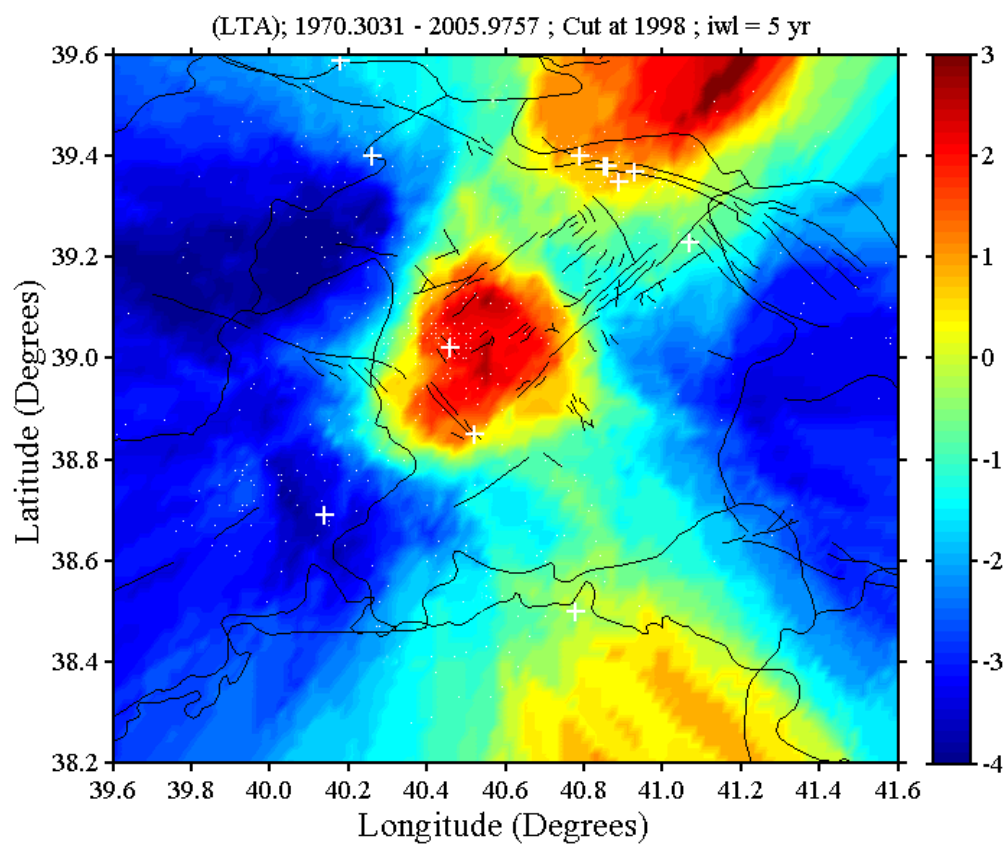
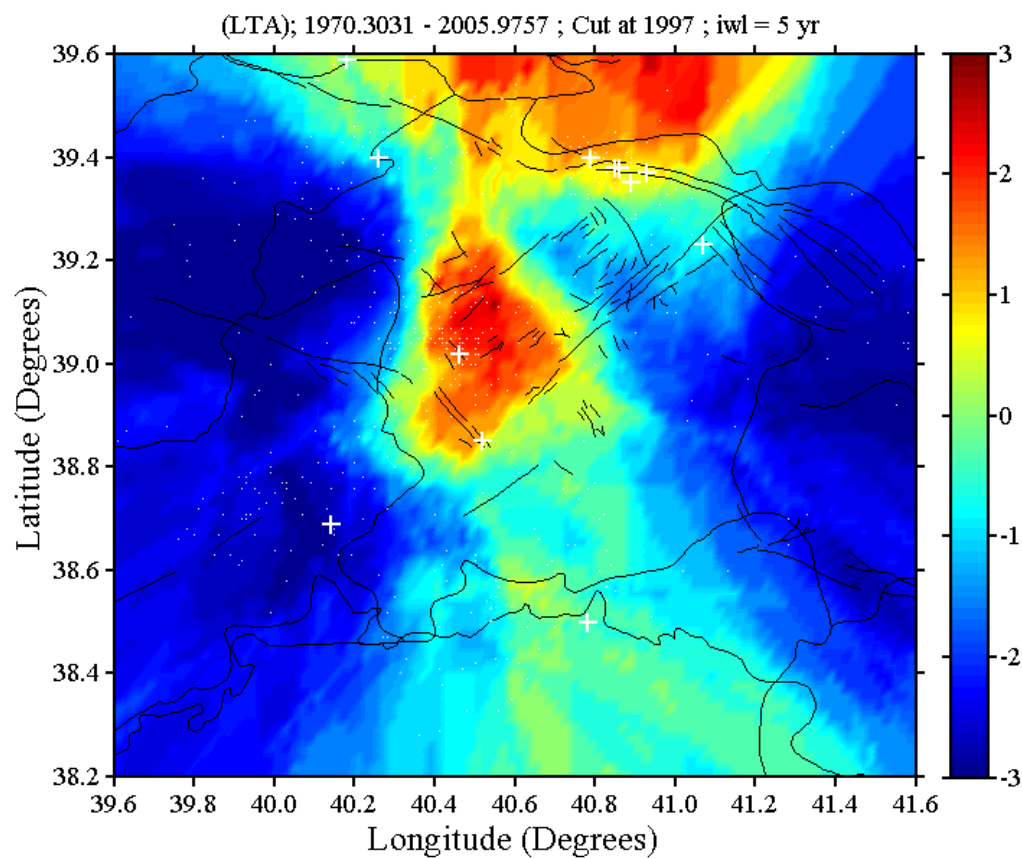


Figure 4 (continued)

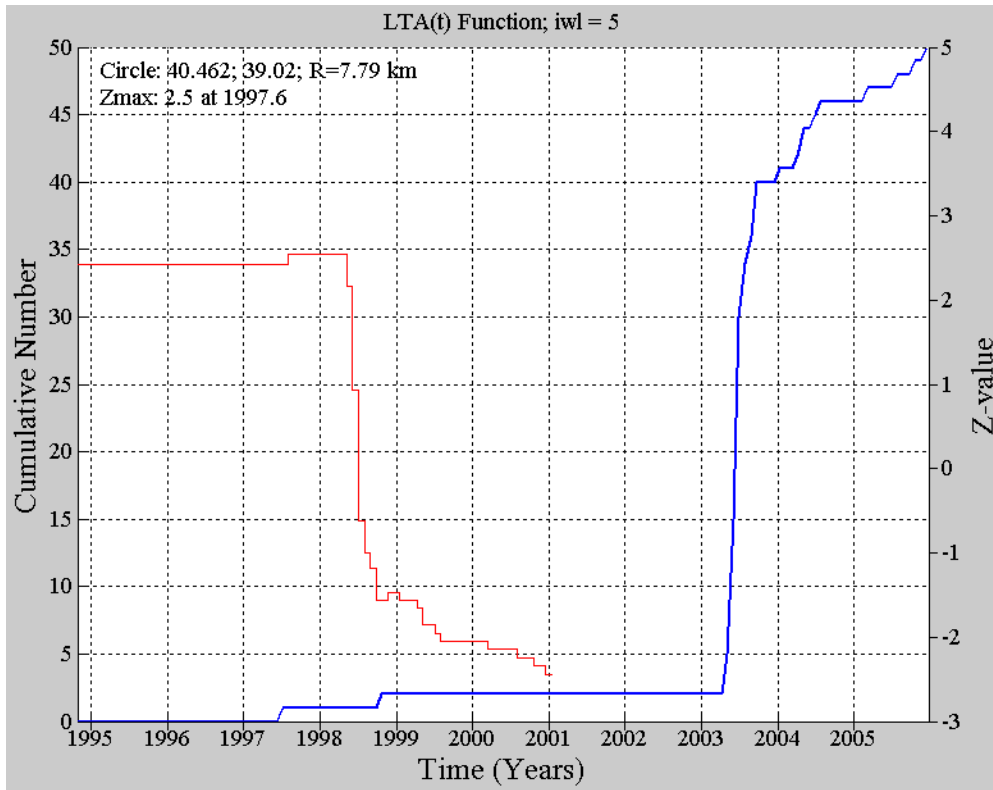


Figure 5. Cumulative number plots for the anomalous areas detected in Figure 4. Blue lines in cumulative number plots shows cumulative number and red lines Z-value as a function of time. Also, the center and radius of circle, Z_{max} value and the beginning time of the quiescence are given.

5. CONCLUSIONS

In this study we mapped the seismicity rate changes for future seismic hazard before May 1, 2003 Bingöl earthquake. The comparison is made by means of the standard deviate Z-test generating the LTA(t) function for the statistical evaluation of the confidence level in units of standard deviations. For this purpose, we used the instrumental earthquake catalog of the Boğaziçi University, Kandilli Observatory and Earthquake Research Institute (KOERI) from 1970 until 2005, for 1926 crustal earthquakes of magnitude equal and greater than 1.8, with depths less than 70 km. The catalogue is homogeneous for duration magnitude, M_D , and the completeness magnitude is 3.2. The number of events exceeding this magnitude is 915. We used the declustering algorithm in order to remove aftershock sequences from the catalogue. The process of declustering reduced the number of these events to 522 and 43% of the events were removed. We used the gridding method and the ZMAP software at each node of a grid spacing of 0.02° in order to investigate the significance of seismic quiescence pattern prior to the occurrence of 1 May 2003 Bingöl earthquake. We carried out our analysis in the rectangular area limited by the co-ordinates 38.2°N and 39.6°N in latitude and by the co-ordinates 39.6°E and 40.6°E in longitude. Using ZMAP software package, the number of events associated with each grid point was chosen, after several preliminary tests, equal to 50. For each sample, the data are subdivided in bins of 28 days. The total duration of the catalogue is 35.67 years. For the rate changes, it is used a moving time window $T_W=5$ years after a few different values from 1.5 to 5 years, and different starting times for the foreground windows. Finally, regional distribution of Z-values is mapped for every one year between 1990 and 1998 using the declustered catalogue. We could not observe any significant seismicity rate change in time interval 1990 and 1993. There is a clear area of quiescence after 1993, near the main shock epicenter of 1 May 2003 Bingöl earthquake with Z level between 2 and 3. This quiescence is best revealed at the epicentral areas of the main shock of Bingöl earthquake between 1995 and 1998. Also, we plotted cumulative number curve versus time in a circular area including the epicenter of the 2003 Bingöl earthquake in order to define the beginning and duration of quiescence. Corresponding LTA(t) function for a circle of 7.79 km radius centered on Bingöl main shock, a decrease of the seismicity rate is found at 1997.6 with $Z_{max}=2.5$ level. Thus, 5.73 years of seismic quiescence was clearly observed before 1 May 2003 Bingöl main shock. In conclusion, the detection of seismic quiescence is the key to the success of intermediate term earthquake prediction.

6. REFERENCES

- [1] Mogi, K., 1969, "Some features of recent seismic activity in and near Japan, {2}: Activity before and after great earthquakes", *Bull. Eq. Res. Inst. Univ.*, Tokyo, 47, 395-417.
- [2] Habermann, R. E., 1981, "Precursory seismicity patterns: Stalking the mature seismic gap", *In Earthquake Prediction* (Eds. D. W. Simpson And P. G. Richards), Maurice Ewing Series (Amer. Geophys. Union 4, 1981b) pp. 29-42.
- [3] Wyss, M., Habermann, R. E., and Griesser, J. C., 1984, "Seismic quiescence and asperities in the Tonga-Kermadec Arc", *J. Geophys. Res.*, 89, 9293-9304.
- [4] Habermann R. E., and Wyss, M., 1984, "Seismic quiescence and earthquake prediction on the Calaveras Fault, California", Abstract, *Eos*, 65, 988.
- [5] Wyss, M., and Burford, R.O., 1985, "Current episodes of seismic quiescence along the San Andreas Fault between San Juan Batista and Stone Canyon California; Possible precursors to local moderate main shocks", *U.S. Geol. Survey open-file report*, pp. 85-754.
- [6] Wyss, M., and Habermann, R. E., 1988b, "Precursory quiescence before the August 1982 Stone Canyon, San Andreas Fault, earthquakes", *Pageoph.*, 126, 333-356.
- [7] Wyss, M., Shimazaki, K., and Urabe, T., 1996, "Quantitative mapping of a precursory quiescence to the Izu-Oshima 1990 (M=6.5) Earthquake, Japan", *Geophys. J. Int.*, 127, 735-743.
- [8] Katsumata, K., and Kasahara, M., 1999, "Precursory seismic quiescence before the 1994 Kurile Earthquake (Mw=8.3) revealed by three independent seismic catalogs", *Pure Appl. Geophys.*, 155, 43-470.
- [9] Console, R., Montuori, C., and Murru, M., 2000, "Statistical assessment of seismicity patterns in Italy: Are they precursors of subsequent events?", *Journal of Seismology*, 4, 435-449.
- [10] Chouliaras, G., and Stavrakakis, G. N., 2001, "Current seismic quiescence in Greece: Implications for seismic hazard", *Journal of Seismology*, 5, 595-608.
- [11] Wyss, M., and Habermann, R. E., 1988a, "Precursory seismic quiescence", *Pageoph.*, 126, 319-332.
- [12] Wyss, M., Console, R., and Murru, M., 1997, "Seismicity rate change before the Irpinia (M=6.9) 1980 earthquake", *Bull. Seismol. Soc. Am.*, 87, 318-326.
- [13] Ogata, Y., 1992, "Detection of precursory relative quiescence before great earthquakes through a statistical model", *J. Geophys. Res.*, 97, 19845-19871.
- [14] Wyss, M., 1991, "Reporting history of the central Aleutians seismograph network and the quiescence preceding the 1986 Andreanof Island earthquake", *Bull. Seismol. Soc. Am.*, 81, 1231-1254.
- [15] Reasenber, P.A., 1985, "Second-order moment of Central California Seismicity, 1969-1982", *J. Geophys. Res.*, 90, 5479-5495.
- [16] Arabasz, W. J., and Hill, S. J., 1996, "Applying Reasenber's cluster analysis algorithm to regional earthquake catalogs outside California", *Seismol. Res. Lett.*, 67 (2), 30.
- [17] Wiemer, S., and Wyss, M., 1994, "Seismic quiescence before the Landers (M = 7.5) and Big Bear (6.5) 1992 earthquakes", *Bull. Seismol. Soc. Am.*, 84, 900-916.
- [18] Wiemer, S., 1996, "Analysis of seismicity: New techniques and case studies", dissertation Thesis (University of Alaska, Fairbanks, Alaska 1996) 151 pp.
- [19] Wyss, M., and Burford, R. O., 1987, "A predicted earthquake on the San Andreas fault, California", *Nature*, 329, 323-325.
- [20] Habermann, R. E., 1983, "Teleseismic detection in the Aleutian Island arc", *J. Geophys. Res.*, 88, 5056-5064.
- [21] Wyss, M., 1997a, "Second round of evaluations of proposed earthquake precursors", *Pageoph.*, 149(1), 3-16.
- [22] Wyss, M., 1997b, "Nomination of seismic quiescence as a significant precursor" *Pageoph.*, 149(1), 79-113.

CONSTRUCTION OF CRYPTOGRAPHIC HASH FUNCTIONS BASED ON TIME AVERAGE CHAOTIC MAP

M. Ragulskis¹, Z. Navickas², L. Saunoriene¹, K. Lukoseviciute¹

1 – Research Group for Mathematical and Numerical Analysis of Dynamical Systems

Kaunas University of Technology

Studentu 50-222, Kaunas LT-51638, Lithuania

2 – Department of Applied Mathematics

Kaunas University of Technology

Studentu 50-325C, Kaunas LT-51638, Lithuania

Abstract. An algorithm for the construction of cryptographic hash function based on optical time average geometric moiré, chaotic dynamics and digital image processing is proposed in this paper. This algorithm is based on the fact that inverse problem for identification of the original grayscale color function from its time averaged image is an ill-posed problem. The problem becomes even more complex if a chaotic map is incorporated into the process of time averaging. The algorithm is designed to cope with any type of digital data and efficiently compresses initial information into a smaller data set.

Keywords: *Chaotic map, Hash function, Time average moiré, Inverse problem.*

1. INTRODUCTION

A hash function is a transformation that takes a digital input and returns a fixed-size string, which is called the hash value. Hash functions with just this property have a variety of general computational uses, but when employed in cryptography, the hash functions are usually chosen to have some additional properties: it must be relatively easy to compute hash values for any given inputs; hash functions must be one-way and collision-free [1, 2]. A hash function is said to be one-way if it is hard to invert, where “hard to invert” means that given a hash value, it is computationally infeasible to find the input. A hash function is

said to be collision-free if it is computationally infeasible to find any two different digital inputs which hash values coincide.

We will construct a hash function exploiting physical principles of nonlinear dynamics and chaos embedded into optical digital image time averaging techniques. It must be noted that the considered optical methods are virtual optical methods and all digital algorithms can cope with any type of digital data. Recovery of original grayscale distribution from digital time averaged images is an ill-posed inverse problem. Incorporation of chaotic maps into time averaging makes the inverse problem even more complex. Nevertheless, the complexity of direct calculation of hash values is a straightforward and efficient digital procedure. The object of this paper is to propose an efficient numerical technique for implementation of a new class of hash algorithms.

2. OPTICAL BACKGROUND

Geometric moiré [3, 4] is a classical optical experimental technique based on the analysis of visual patterns produced by superposition of two regular gratings that geometrically interfere. Moiré patterns are used to measure variables such as displacements, rotations, curvature, and strain throughout the viewed area.

Moiré grating on the surface of a one-dimensional structure in the state of equilibrium can be interpreted as a harmonic function [3, 5]:

$$F(x) = \frac{1}{2} \cos\left(\frac{2\pi}{\lambda} x\right) + \frac{1}{2}, \quad (1)$$

where λ is the pitch of the grating. Such a continuous function is well applicable to digital image processing in virtual computational environments [5]. Numerical value 0 of the function in this equation corresponds to black color; 1 – to white color; all intermediate values – to grayscale color intensity levels. The grating of a one-dimensional structure in a deformed state can be interpreted as follows [6]:

$$F(x) = \frac{1}{2} \cos\left(\frac{2\pi}{\lambda}(x-s)\right) + \frac{1}{2}, \quad (2)$$

where s defines the deflection from the state of equilibrium.

Double exposure geometric moiré techniques can be extended to time average geometric moiré methods when the deflections from the state of equilibrium oscillate in time and long exposure times are used to average the grayscale levels [3]:

$$F(x) = \lim_{T \rightarrow \infty} \frac{1}{T} \int_0^T \left(\frac{1}{2} \cos\left(\frac{2\pi}{\lambda}(x - s \sin(\omega t + \varphi))\right) + \frac{1}{2} \right) dt = \frac{1}{2} \cos\left(\frac{2\pi}{\lambda}x\right) J_0\left(\frac{2\pi}{\lambda}s\right) + \frac{1}{2}, \quad (3)$$

where s now is the amplitude of dynamic deflections; ω and φ are the frequency and phase of harmonic oscillations; J_0 is zero order Bessel function of the first kind. Time averaged moiré fringes will form at such amplitudes of dynamic deflections where the argument of the Bessel function in eq. (3) becomes equal to a root of the Bessel function. Thus, an explicit relationship between the pitch of the grating, amplitude of harmonic oscillations and the order of the time averaged fringe takes the following form:

$$s_i = \frac{\lambda}{2\pi} r_i, \quad i = 1, 2, \dots, \quad (4)$$

where r_i is the i -th root of the zero order Bessel function of the first kind (Fig. 1).

Geometric moiré techniques have a general limitation associated with the fact that the displacements can be determined only in the direction orthogonal to the lines of the grating. Ability to exploit the natural microstructure of the surface as a stochastic grating eliminates this restraint. If the grayscale level of a non-deformable one-dimensional body is $F(x)$, then its time averaged grayscale intensity at a point x_0 is [7]:

$$\lim_{T \rightarrow \infty} \frac{1}{T} \int_0^T F(x_0 - s \sin(\omega t + \varphi)) dt = \frac{1}{\pi} \int_{-\frac{\pi}{2}}^{\frac{\pi}{2}} F(x_0 - s \sin t) dt = H_s(F(x)), \quad (5)$$

where H_s is a generalized operator of time averaging [8].

Inverse problems involving geometric moiré are characterized by the fact that the information of interest (e.g. the distribution of grayscale color intensity on the surface of a non-deformable body) is not directly available. The imaging device (the camera) provides measurements of a transformation of this information in the process of time averaging while the body performs harmonic or chaotic oscillations. In practice, these measurements are both incomplete (sampling) and inaccurate (statistical noise) [7]. This means that one must give up recovering the exact image. Indeed, aiming at full recovery of the information usually results in unstable solutions due to the fact that the reconstructed image is very sensitive to inevitable measurement errors. In other words, slightly different data would produce a significantly different image.

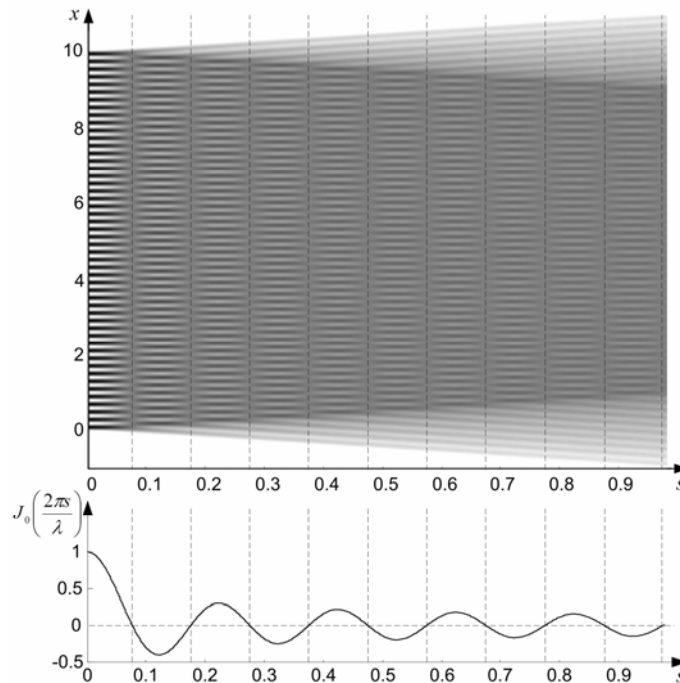


Figure 1. Time averaged moiré fringes produced by harmonic grating ($\lambda = 0.2$) at increasing amplitudes s . The graph of zero order Bessel function of the first kind is shown to illustrate the relationship between the centerlines of the fringes and roots of the Bessel function.

Solution of the inverse problem for identification of $F(x)$, when only time average image is known, is computationally infeasible and this fact is exploited for construction of hard to invert hash function.

3. TIME AVERAGING OF HARMONIC MOIRÉ GRATINGS

It is shown in [9] that it is possible to construct mathematical relationships in operator format between an original grayscale function $F(x)$ and its time average produced by harmonic oscillations around the state of equilibrium. First, function $\tilde{F}(x) = F(x) - \frac{1}{2}$ is constructed requiring that it must be square integrable and can be expressed in a Fourier series:

$$\int_{-\infty}^{+\infty} (\tilde{F}(x))^2 dx < +\infty; \quad \tilde{F}(x) = \sum_{n=-\infty}^{+\infty} c_n \exp\left(i \frac{n\pi}{l} x\right); \quad -l < x < l; \quad l > 0; \quad \text{where}$$

$$c_n = \frac{1}{2l} \int_{-l}^l \tilde{F}(u) \exp\left(-i \frac{n\pi}{l} u\right) du.$$

Then, time averaged image can be expressed in the following form [9]:

$$HF(x) = \Phi^{-1}\left(\hat{p}(sv)\Phi\tilde{F}(x)\right) + \frac{1}{2}, \quad (6)$$

where $p(x)$ is the distribution of the random variable which defines the displacements from the state of equilibrium during the process of time averaging; $\hat{p}(z)$ is the Fourier transform of $p(x)$. It is clear that $p(x)$ for harmonic oscillations is an arcsine distribution. As Fourier transform of arcsine distribution is zero order Bessel function of the first kind, the following equality holds true for harmonic oscillations:

$$H_s F(x) = \Phi^{-1}\left(J_0(sv)\Phi\tilde{F}(x)\right) + \frac{1}{2}. \quad (7)$$

Time averaging of a grayscale function (one-dimensional image which oscillates harmonically in time) produces grayscale blur. That blur can be characterized as a

convolution between the original image (function) and the point spread function which characterizes the distribution of deflections from the state of equilibrium in time.

Equation 7 is an important result which shows that the inverse problem of reconstruction of the original grayscale function is an ill-posed inverse problem.

Zero order Bessel function of the first kind has multiple roots (Fig. 1). Therefore there exists multiple divisions by zero in the kernel of the inverse problem (Eq. 7) what makes this inverse problem ill-posed. This property is illustrated by Fig. 1 where a number of time averaged interference fringes can be observed at increasing amplitude s .

4. DESCRIPTION OF THE ALGORITHM FOR CONSTRUCTION OF CRYPTOGRAPHIC HASH FUNCTION

The algorithm for construction of the one-dimensional hash function comprises three basic parts:

1. Acquisition of input data: amplitude s and grayscale function $F(x)$.
2. Production of the intermediate result: $H_s F(x)$.
3. Delivery of output data: time averaged grayscale function stretched to min-max levels.

There three basic parts are graphically illustrated in Fig. 2. The original grayscale function $F(x)$ is constructed as a set of random numbers evenly distributed in interval $[0,1]$. We plot the values of $H_s F(x)$ produced by harmonic oscillations at increasing s as s sweeps from 0 to 2. One can observe grayscale riddles in the upper and lower part of the digital image in Fig. 2(a) (similar to the riddles above and below time averaged fringes in Fig. 1). The hash value of the constructed hash function is the middle part of time averaged image (riddles are disregarded). Such approach enables to realize the compression of the original data into a smaller set what is a standard feature of existing hash functions. Finally, time averaged grayscale levels are stretched to min-max level range what eliminates even theoretical possibility to reconstruct the original $F(x)$ from its time averaged image.

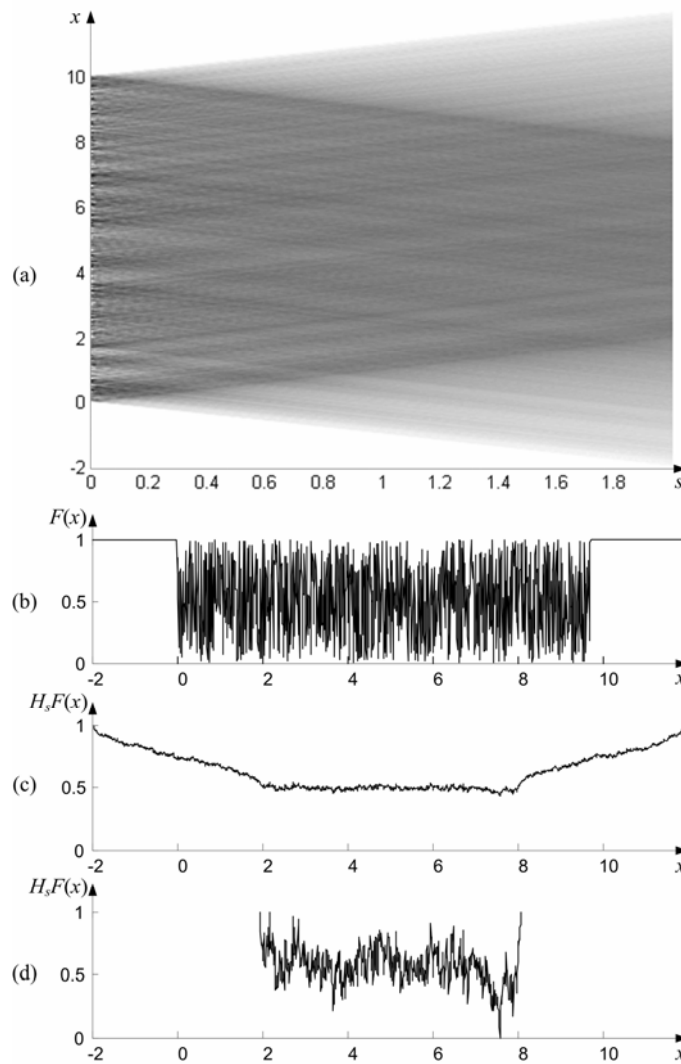


Figure 2. Graphical illustration of the three basic parts of the cryptographic algorithm:
 (a) $H_s F(x)$ at increasing amplitudes s ; (b) original grayscale function as a set of random numbers evenly distributed in interval $[0,1]$; (c) grayscale levels at $s=2$; (d) time averaged grayscale function stretched to min-max levels ($s=2$).

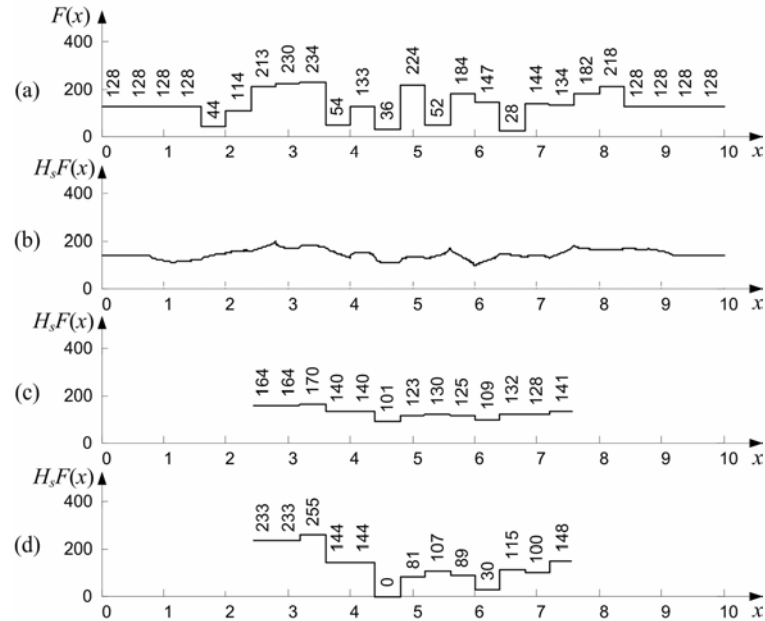


Figure 3. Illustration of the algorithm (harmonic motion): (a) original grayscale distribution (width of the virtual pixels is 0.4); (b) time averaged grayscale at $s=0.8$; (c) time averaged levels reconstructed at appropriate locations of virtual pixels; (d) hash value stretched to min-max levels.

As mentioned earlier, functionality of the proposed cryptographic hash function enables processing of any kind of data – not necessarily digital grayscale images. That fact is illustrated in Fig. 3 where an input set of natural numbers (Fig. 3(a)) is transformed to the output set (Fig. 3(d)); vertical integers denote virtual grayscale levels.

5. ALGORITHM FOR CONSTRUCTION OF HASH FUNCTION BASED ON THE CHAOTIC MAP

The theoretical result in eq. (6) enables use of any type of time function determining dynamic deflections from the state of equilibrium. As mentioned previously, the complexity of the problem would not decrease only if $\hat{p}(z)$ is not a trivial function (what may happen if the motion law is uni-directional motion with constant velocity). Thus we

incorporate state variable defining some sort of chaotic motion assuming that it describes dynamic deflection from the state of equilibrium.

The general structure of such a modified algorithm for construction of the two-dimensional hash function is illustrated in a schematic diagram in Fig. 4. Computations required to transform the digital input into a hash value are based on chaotic dynamics, geometric optics, and digital image processing. Data base holds a collection of virtual grayscale one-dimensional images which are represented as arrays of integers. Every integer must fit into grayscale range between 0 and 255. Control parameter is used to tune the shape of chaotic attractor. Preconditioning is required to fit the amplitudes of virtual dynamic deflections to a realistic computational scenario, what can be interpreted as an additional security parameter. Other steps in Fig. 4 are discussed in the previous Sections.

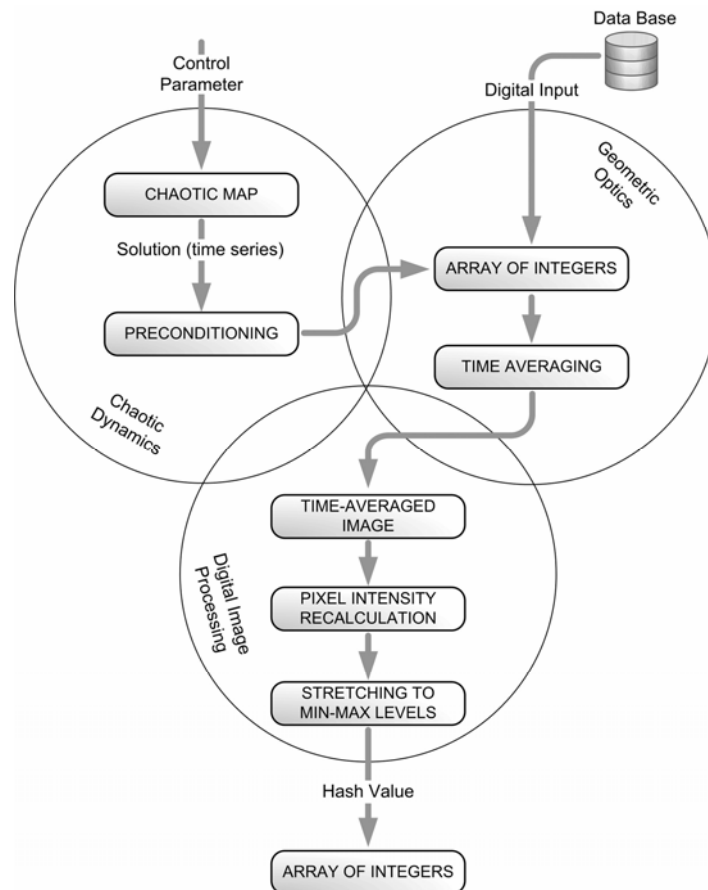


Figure 4. Schematic graphical representation of the algorithm for the construction of hash function.

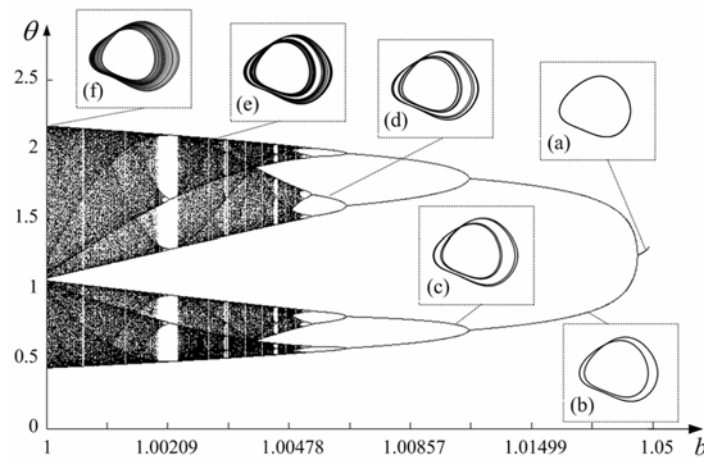


Figure 5. Bifurcation diagram for the driven damped nonlinear pendulum with parameter values $\omega=2/3$; $a=2.048$, with respect to the variation of the damping coefficient b . The insets show phase space diagrams with orbits corresponding to specific values of the parameters

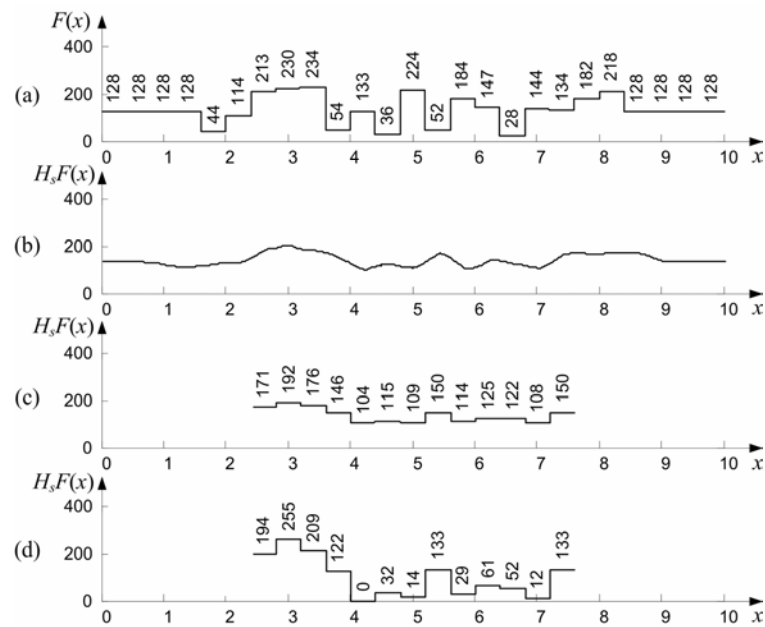


Figure 6. Illustration of the algorithm (chaotic motion): (a) original grayscale distribution (width of virtual pixels is 0.4); (b) time averaged grayscale distribution produced by chaotic oscillations; (c) time averaged grayscale distribution averaged at appropriate virtual pixels; (d) hash value stretched to min-max levels

As mentioned previously, we use a chaotic map for the construction of hash algorithm. We consider a nonlinear periodically driven damped pendulum, which is a paradigm model in the study of nonlinear dynamics. A dimensionless time evolution equation of such pendulum reads [10]:

$$\frac{d^2\theta}{dt^2} = -\sin\theta - b\frac{d\theta}{dt} + a\cos(\omega t), \quad (8)$$

where b is the damping coefficient; a is external forcing amplitude; and ω is the frequency. The driven damped pendulum with $\omega=2/3$, $b=1.0$, and $a=2.048$ yields chaotic behavior following a period-doubling sequence of bifurcations (Fig. 5).

Phase trajectories in the insets of Fig. 5 are plotted in frames $(\theta; \dot{\theta})$ at the following values of b : (a) $b=1.04$; (b) $b=1.025$; (c) $b=1.01$; (d) $b=1.0055$; (e) $b=1.003$; (f) $b=1.0002$.

Parameter b is varied following the rule $b_i = 1.05 - \frac{0.05}{\ln 201} \ln\left(1 + \frac{1000 - i + 1}{5}\right)$, $i=1, \dots, 1001$, what helps to expand the cascade of period-doubling bifurcations.

We use parameter value $b=1.0002$ for construction dynamic deflections which are used for time averaging of original grayscale function (Fig. 6(b)). Hash value is produced when the averaged grayscale levels are fitted to virtual pixels (Fig. 6(c)) and stretched to min-max levels (Fig. 6(d)).

6. CONCLUSIONS

A new class of hash functions is proposed in this paper. Chaotic map is incorporated into the process of virtual time averaging. Though the inverse problem is ill posed, algorithm for calculation of hash values is efficient and straightforward. Calculations are based on the principles of virtual geometric optics, nonlinear dynamics and digital image processing. Such an approach builds prerequisites of wide potential application of the proposed hash functions.

REFERENCES

- [1] Bicakci K., Tsudik G., Tung B., (2003), "How to Construct Optimal One-time Signatures", *Computer Networks*, 43, 339-349.
- [2] Xiao D., Liao X., Deng S., (2005), "One-way Hash Function Construction Based on the Chaotic Map with Changeable-parameter", *Chaos, Solitons & Fractals*, 24, 65-71.
- [3] Kobayashi A. S., (1993), *Handbook on Experimental Mechanics 2nd ed.*, Bethel, SEM.
- [4] Post D., Han B., Ifju P., (1997), *High Sensitivity Moiré: Experimental Analysis for Mechanics and Materials*, Berlin, Springer-Verlag.
- [5] Ragulskis M., Palevicius A., Ragulskis L., (2003), "Plotting Holographic Interferograms for Visualization of Dynamic Results from Finite-Element Calculations", *International Journal of Numerical Methods in Engineering*, 56, 1647-1659.
- [6] Ragulskis M., Ragulskis L., Maskeliunas R., (2003), "Applicability of Time Average Geometric Moiré for Vibrating Elastic Structures", *Experimental Techniques*, 28, 27-30.
- [7] Ragulskis M., Maskeliunas R., Saunoriene L., (2005), "Identification of In-plane vibrations Using Time Average Stochastic Moiré", *Experimental Techniques*, 29, 41-45.
- [8] Ragulskis M., Navickas Z., (2007), "Hash Function Construction Based on Time Average Moiré", *Discrete and Continuous Dynamical Systems-Series B, American Institute of Mathematical Sciences*, 8, 1007-1020.
- [9] Navickas Z., Ragulskis M., (2007), "Representation of the Time-averaged Vibrating Images in the Operator Format", *Journal of Vibroengineering*, 9, 1-8.
- [10] Hilborn R. C. (2000), *Chaos and Nonlinear Dynamics*, Norfolk, Oxford University Press.

Spatiotemporal Chaos and Break up of Spiral Waves due to Core Expansion in Excitable Media

Haidar Sabbagh^(*)

Department of Physics, Al-Manar University of Tripoli, Lebanon

We present a new type of meandering of spiral waves leading to spiral break up and spatiotemporal chaos. The end of the spiral follows itself an outward spiral-like trajectory as the core expands in time. This type of destabilization of simple rotation is attributed to curvature effects and wave-fronts interactions in the case of oscillatory damped recovery to the rest state in excitable media. The spiral wave is found to break up into smaller spirals near the centre of rotation when the spiral period falls below the minimal period allowed for plane wave propagation.

Keywords: spiral waves, spatiotemporal chaos, core expansion, meandering, breakup

1. Introduction

The transition from regular patterns to spatiotemporal chaos in spatially extended systems and in particular in excitable media remains a challenging problem in nonlinear science. Such wave patterns in excitable media include rotating spiral waves which have been observed in chemical reactive solutions [1, 2], in slime-mold aggregates [3] and most importantly in cardiac muscle [4].

For some values of the system control parameters, spiral waves undergo simple rigid rotation around a circular core. As the control parameter is varied, the spiral tip deviates from circular trajectories [5–11]. This non-steady rotation is known as meandering and it has been observed essentially in chemical systems such as in the Belousov-Zhabotinsky (BZ) reaction [12]. Experiments with this reaction have also demonstrated spiral breakup [13, 14]. Widely discussed in connection with the mechanisms of cardiac fibrillation [15, 16], spiral breakup has been shown to occur in models that show wave trains spatiotemporal instabilities [17, 18]. It is of particular interest in cardiology since it is the prelude to fibrillation, the commonest cause of sudden cardiac death.

2. Discussion

2.1. *New type of meandering due to curvature effects, wave interactions and oscillatory recovery*

In this paper, we investigate a new type of meandering followed by spiral breakup. The spiral tip follows an outward motion along spiraling trajectories as the core expands in time. This core

^{*}Email: Sabbaghhh@hcu.edu.lb

expansion was described by the theory of non-local effects [6, 9, 10] and it occurs due to wave-front interactions coupled to curvature effects. The interaction of wave-fronts propagating in an excitable medium is determined by the manner of recovery to the rest state. If the excitable medium recovers to in an oscillatory manner, the wave-fronts tend to lock up at fixed distances from the preceding ones. This can be shown by writing the solution of the basic reaction-diffusion system as a superposition of two solitary waves with a small perturbation term R which vanishes in the limit of infinite spacing between the two waves:

$$u(z) = u(z - z_1) + u(z - z_2) + R \quad (1),$$

where $z_1 = x_1 - ct$ and $z_2 = x_2 - ct$, x_1 and x_2 denote the waves positions. For large $|z_1|$ and $|z_2|$, the tail of the wave determines the manner in which the medium recovers to the resting state is: When the recovery is damped oscillatory, the tail of the wave $u(z) \propto e^{\eta z} \cos(\nu z + \psi)$; when it is monotonic, $u(z) \propto e^{\eta z}$. In both cases, the leading edge of the wave is assumed to be of the form $u(z) \propto e^{-\mu z}$. Equations for x_1 and x_2 are derived using the solvability conditions which remove singularities from R [19]:

$$\frac{\delta x_1}{\delta t} = c + a_R e^{-\mu(x_1 - x_2)} \quad (2)$$

$$\frac{\delta x_2}{\delta t} = c + a_L e^{-\eta(x_1 - x_2)} \cos(\nu(x_1 - x_2) + \psi) \quad (3),$$

where c is the propagation speed of a solitary wave. The second term on the right hand side of Eq. (2) represents the effect of the second wave on the propagation of the first one. It is usually negligible in excitable media. The second term on the right hand side of Eq. (3) represents the effect exerted on the second wave by the refractory wake of the first one. Using Eq. (2) and Eq. (3), the spacing between the two waves $\lambda = x_1 - x_2$ obeys the equation:

$$\frac{d\lambda}{dt} = a_L e^{-\eta \lambda} \cos(\nu \lambda + \psi) \quad (4).$$

If $\nu \neq 0$, the excitable medium recovers in an oscillatory way. Then, according to Eq. (4) an infinite number of steady state solutions exist. This means that the distance between the wave-fronts takes one of possible constant values.

This interaction of wave-fronts due to refractoriness is coupled to the effect of curvature on the normal velocity of propagation which is given by $v = v_0 - kD$, where k is the local curvature, D is the diffusion coefficient and v_0 is the plane wave velocity of propagation [11]. This gradient of the normal velocity of propagation plays a crucial role in sustaining the rotational motion of the spiral. It stabilizes wave propagation away from the spiral free end or tip as small wavelength perturbations on the segments away from the tip decay due to this dependence of the velocity on curvature. On the

contrary, upon straightening a small segment containing the tip, curvature is reduced, normal velocity is enhanced and further straightening is favored. Consequently, the gradient of the normal velocity becomes weaker. Consequently, the tip has a less tendency to curl, the wave would advance further, and the spiral tip undergoes an outward motion instead of simple rigid rotation. If the recovery is monotonic, wave-front interaction is repulsive due to the refractory period imposed on the medium after the passage of the preceding wave. This interaction counteracts the destabilizing effects of curvature and maintains circular rigid rotation. Actually, Ehud Meron proposed an approximate spiral wave solution of the reaction diffusion equations in the form of a superposition of curved solitary wave-fronts parallel to each other [6, 10]. Using a singular perturbation approach, an evolution equation for the spiral wave-front was then derived and solved numerically. For an oscillatory recovering excitable medium, the resulting numerical solution of the evolution equation was a spiral wave whose core expands in time and whose tip moves out along a spiraling trajectory.

2.2. New reaction-diffusion model

Here, we provide a new model showing for the first time the core expansion that was predicted by the theory of Meron. We use a modified Barkley's model [20, 21] given by:

$$\begin{aligned}\partial u / \partial t &= \frac{1}{\varepsilon} u(1-u)[u - ((b+v)/a)] + \nabla^2 u, \\ \partial v / \partial t &= u^3 - v,\end{aligned}\tag{5}$$

where u and v are the excitation and recovery variables respectively. The parameter b determines the excitation threshold. The inverse of the parameter ε specifies the recovery time and characterizes the abruptness of excitation. In the standard Barkley's model, the local kinetics in the second equation is given by $(u - v)$. Compared to the standard model where $\partial v / \partial t = u - v$, with increasing ε , propagation is maintained due to the delay in the production of the inhibitory variable v .

3. Results

Numerical simulations were performed on square grids using the explicit Euler integration method with a 9-point neighborhood of the Laplacian and no-flux boundary conditions. The space and time steps are respectively $dx = 0.51$ and $dt = 0.052$. Fig. 1(a) illustrates the nullclines and the profile of the PDE system. The time signals of the two variables are shown when the threshold of excitation is exceeded is shown in Fig. 1(b). It is seen here that the rate of recovery of the medium is made slower. Also, the production of the recovery or inhibitory variable v is delayed to allow the propagation of the wave for different and high values of ε .

A spiral wave was initiated by a coarse gradient cross-field: $u = 0$ in the left half of the medium and $u = 1$ in the right half; $v = a/2$ in the upper half and $v = 0$ in the lower half. In Fig. 2, snapshots show the evolution of the system at different times. As the value of the parameter ε is increased, the simple rigid rotation is destabilized, the tip starts meandering and upon increasing the parameter ε further, an interesting type of meandering arises (shown in Fig. 3(a)) as the spiral core expands in time. The spiral tip defined in Fig. 3 as the intersection of the two isolines $u = 0.5$ and $v = 0.5u - b$ follows an outward

motion along a spiraling path. This agrees with the prediction of the theory of non-local effects in the case of an oscillatory recovering excitable medium. The type of recovery then depends on the value of the control parameter ε . For low values of ε , perturbations near the spiral core are quenched by repulsive wave-fronts interactions in the monotonically recovering medium. Upon increasing the value of ε and for appropriate values for the other parameters, the tip undergoes this interesting outward motion along a spiraling trajectory while the core grows in size due to oscillatory recovery to the resting state. The distance between the tip segment and the one ahead of it is determined by one of the maxima of the oscillatory tail. This corresponds to one of the minima of the excitation threshold. The normal velocity of the wave-front segment containing the free end of the spiral increases as it gets flatter (i.e. as curvature decreases). Thus the waves that are generated by the tip segment move by a smaller distance than the ones generated by the segment ahead of it. In Fig. 3(a), the distance between parallel portions of the tip trajectory increases as the tip advances forward, implying that the tip motion is accelerated; note how the distance between the points denoting the tip positions increases as the tip moves outward. In Fig. 2, the spiral core expands until spiral breakup occurs as the spiral period and the minimum period compatible with plane wave propagation merge for this critical value of ε [22]. The spiral rotates more rapidly than plane waves can propagate, since the recovery rate is made slower by using $(u^3 - v)$ instead of the linear kinetics $(u - v)$. Conduction is then blocked, the spiral becomes unstable and breaks down into interacting spirals or wave breaks. The spiral period changes as the spiral drifts and meanders, until at some point within the excitable medium, it will reach the minimum period needed for plane waves propagation. This change in the spiral period as the tip moves outward and forward is due to Doppler shift since the core is seen as the source of waves. The newly born broken waves will soon evolve into spirals waves since they have broken ends leading to spatiotemporal chaos or irregularity as shown in Fig. 4 where the time variations of the excitatory and the recovery variables are recorded at point (10,10) in the excitable medium of size $L = 100$.

This phenomenon can be accounted for by considering a traveling wave solution of Eqs. (5), $u(z) = u(x + ct)$, where c is the wave speed. Substituting this solution into Eqs. (5) reduces the reaction-diffusion equations to the following ODE system:

$$\begin{aligned} dw/dt &= cw - (1/\varepsilon)u(1-u)[u - ((b+v)/a)] \\ du/dt &= w \\ dv/dt &= (1/c)(u^3 - v), \end{aligned} \quad (6)$$

Using parameter values $a=0.75$ and $b=0.06$, $\varepsilon^{-1} = 13.5$, the numerical solution shown in Fig. 5 approaches the resting state in an oscillatory manner. For those values of the parameter, the system can have complex eigenvalues implying that the fixed point $(0, 0, 0)$ is an unstable focus for $c^2 - 4.32 < 0$. This condition is satisfied for some range of the spiral period as seen below in the dispersion curve in Fig. 6. That justifies the oscillatory behavior of the solution. For other values of the parameter ε , it approaches the resting state $(0, 0, 0)$ in a non-oscillatory way if $\varepsilon^{-1} = 50.0$ for which the spiral rotates rigidly around a circular core. If $\varepsilon^{-1} = 20.0$, the recovery is also monotonic, but that does not necessarily imply rigid rotation. Actually, the spiral tip meanders following an epicycle-like orbit as shown in Fig. 3(b). On the other hand, if $\varepsilon^{-1} = 13.5$ or $\varepsilon^{-1} = 14.5$, the solution returns to the resting state in an oscillatory manner as seen in Fig. 4. However, unlike the case for $\varepsilon^{-1} = 13.5$ (shown in Fig. 3(a) and Fig. 2), the system does not undergo core expansion for $\varepsilon^{-1} = 14.5$ despite the oscillatory

type of recovery. Core expansion does not occur and the tip does not follow an outward spiraling trajectory. It undergoes meandering tracing loops like those of an epicycle as it rotates and drifts away. Actually, we found that the tip moves along a spiraling trajectory in the range $13.0 < \varepsilon^{-1} < 13.8$. For $\varepsilon^{-1} > 13.9$, it meanders but not along a spiraling path. Thus, oscillatory recovery does not necessarily lead to core expansion. For $\varepsilon^{-1} = 13.5$ and $\varepsilon^{-1} = 14.5$, the system undergoes a succession of super and subnormal periods until complete recovery is achieved as shown in Fig. 5.

Those oscillations in the excitation threshold and in the way of recovery to the resting state would imply oscillations in the dispersion. This can be shown by considering the times when wave-fronts pass through a given location x . The solution of Eqs. (5) is then approximated by widely spaced impulses:

$$u(x, t_i) = \sum_k u_k(t_i(x)) + R, \quad (7)$$

where $t_i(x)$ is the instant at which the i th impulse is at x , and R is a small perturbation term which vanishes in the limit of infinite spacing between the waves. Using Eq. (7) in Eqs. (5), we get

$$dt_i / dx = (1/c_0) + a' e^{\eta(t_i - t_{i-1})} \cos[v(t_i - t_{i-1}) + \psi] + b' e^{-\mu(t_{i+1} - t_i)} \quad (8)$$

where η is the rate at which the wave-fronts tail off. The second term on the right hand side of Eq. (8) represents the effect exerted on the i th impulse by the refractory wake of the preceding impulse. The last term represents the effect of the succeeding impulse and is negligible in excitable media. The coefficients a and b require the evaluation of certain integrals which are not shown here. Let $t_i(x) = (x/c) + (i-1)T$, where T is the period of a constant speed wavetrain. Then we get to leading order,

$$c = c_0 - c_0^2 a' e^{-\eta T} \cos[vT + \psi] \quad (9)$$

Thus for $v \neq 0$, i.e. for oscillatory recovery, damped oscillations occur in the dispersion curve. For monotonic recovery ($v = 0, a' > 0$), the wave speed is a monotonic increasing function of wave spacing. If $v = 0, a' < 0$, the recovery is said to be non-monotonic and could exhibit one supernormal period [10, 19]. In Fig. 6, the dispersion curve of the system exhibits a damped oscillatory character for $\varepsilon^{-1} = 13.5$ and $\varepsilon^{-1} = 14.5$. The first supernormal period during which the excitability is higher than that of the rest state is very pronounced. However, for $\varepsilon^{-1} = 50.0$, as expected, the monotonically recovering system is characterized by a dispersion curve with monotonic increase in the propagation velocity until the limit set by the solitary wave velocity is reached.

4. Conclusions

4.1. The first demonstration of core expansion

This oscillatory behavior and the occurrence of supernormal periods in the dispersion curve were observed in wave train solutions of the one-dimensional FitzHugh-Nagumo model [23]. But, no core expansion has ever been observed before. Also, the observation of expanding cores and spiraling tips here answers the query of Meron [6, 9, 10] and Winfree [24, 25] about the possible observation of core expansion when the dispersion curve is oscillatory. Using FitzHugh-Nagumo kinetics with parameters chosen such that the equilibrium point is nearly a center, Winfree showed that the medium can then support two stable rotors of different periods. The dispersion curve exhibited a damped oscillatory behavior which resulted in the coexistence of two rotors in the medium: the critical curve obtained by measurements of the spirals periods intersects the dispersion curve at more than one point. However, core expansion was not observed.

4.2. *Electrophysiological measurements*

This occurrence of 'supernormal' periods of excitability during which the threshold of excitation is diminished was reported in electrophysiological measurements in stimulated cardiac muscle [26]. The current that was needed to re-excite the Purkinje fibers was reduced. We can attribute it to the faster recovery of the threshold potential compared to the slower recovery of the action potential. It was seen that a smaller additional depolarization is needed to reach the threshold potential and it was brought about by a weaker depolarizing current.

4.3. *Possible defibrillation method*

This would lead us to conclude that if core expansion could be induced in cardiac systems, it would help to eliminate cardiac arrhythmias by causing spiral waves to move outward toward the unexcitable boundaries (non-cardiac tissue).

4.4. *New route to spiral breakup*

Our results would imply that core expansion could be one possible route leading to spiral breakup, through a unique meandering pattern, that depends on the wave interaction in the case of damped oscillatory recovery to the rest state.

Acknowledgments: This project has been supported by a grant from the CNRS (The National Council for Scientific Research), Lebanon.

- [1] Kapral R and Showalter K(eds) *Chemical Waves and Patterns* (Dordrecht: Kluwer), 1994
- [2] Imbuhl, R. and Ertl, G., *Chem. Rev.* **95**, 697 (1995)
- [3] Murray, J. *Mathematical Biology* (Berlin: Springer), 1989
- [4] Chaos Special Issue on Dynamics in Cardiac Tissue 2002 *Chaos* **12** 3
- [5] A. T. Winfree, *When Time Breaks Down* (Princeton Univ. Press, New Jersey, 1987)
- [6] E. Meron in: A.V. Holden et al. (Eds.), *Nonlinear Wave Processes in Excitable Media*, Plenum, 1991, pp. 145-153.
- [7] V. S. Zykov, *Biophysics* 31 (5) (1986) 940
- [8] V. S. Zykov, *Biophysics* 32 (2) (1987) 365
- [9] E. Meron, *Phys. Rev. Lett.* 63 (1989) 684
- [10] E. Meron, *Physica D* 49 (1991) 98
- [11] J. J. Tyson and J.P. Keener, *Physica D* 32 (1988) 327

- [12] V. S. Zykov, O. Steinbock and S.C. Muller, *Chaos* **4** (3), 509-518 (1994)
- [13] Nagy-Ungvarai, Zs. And Muller, S.C., *Int. J. Bifurc. Chaos* 4: 1257-1264 (1994)
- [14] Markus, M. and Stavridis, K., *Int. J. Bifurc. Chaos* 4: 1233-1243 (1994)
- [15] Panfilov, A. V. and Hogeweg, P., *Science* 270: 1223-1224 (1995)
- [16] Winfree, A. T., *Science* 266: 1003-1006 (1994)
- [17] Karma, A., *Chaos* 4: 461-472 (1994)
- [18] Courtemanche, M., Glass, L. and Kenner, J. P., *Phys. Rev. Lett.* 70: 2182-2185 (1993)
- [19] C. Elphick, E. Meron, J. Rinzel, and E. A. Spiegel, *J. Theor. Biol.* 146 (1990) 249.
- [20] D. Barkley, *Physica D* 49 (1991) 61.
- [21] D. Barkley, M. Kness, L.S. Tuckerman, *Phys. Rev. A* 42 (1990) 2489.
- [22] H. Sabbagh, *Chaos Solitons & Fractals* 11 (2000) 2141.
- [23] J. Rinzel, K. Maginu in: C. Vidal, A. Pacault (Eds.) *Nonequilibrium Dynamics in Chemical Systems*, Springer- Verlag, 1984, pp. 107-113.
- [24] A.T. Winfree, *Physica D* 49 (1991) 125.
- [25] A.T. Winfree, *Phys. Lett. A* 149 (1990) 203.
- [26] J.F. Spear, E.N. Moore, *Circ. Res.* 35 (1974) 782.

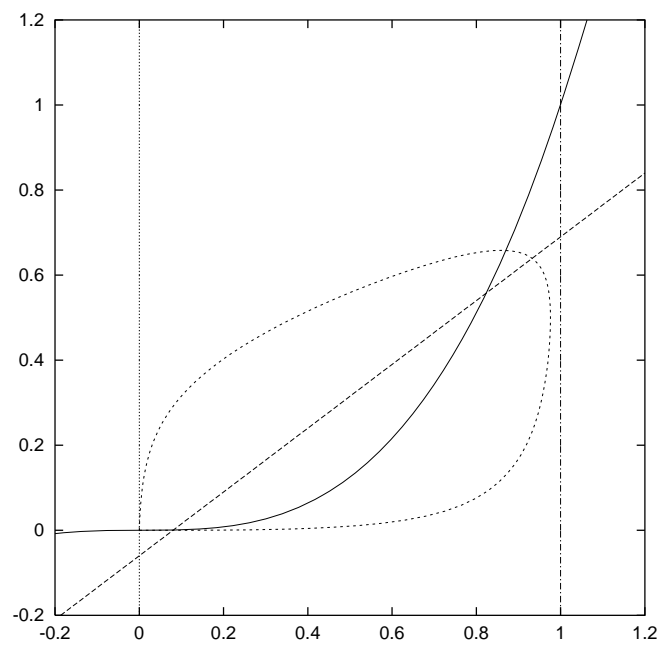


Fig. 1 (a)

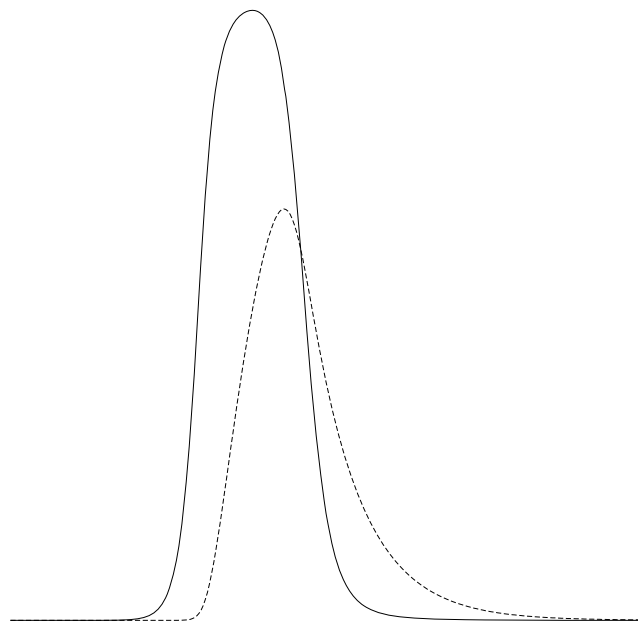


Fig. 1(b)

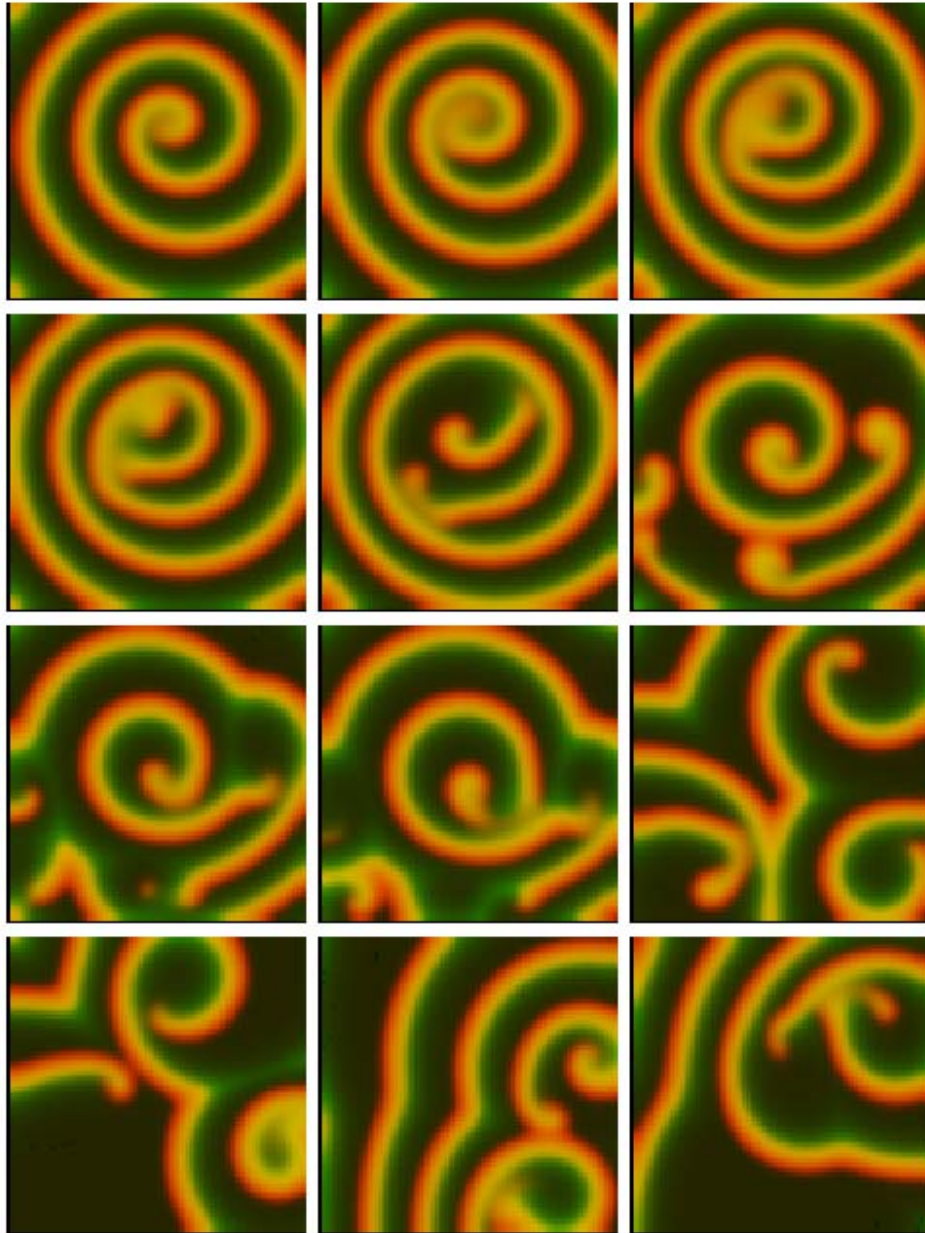


Fig. 2

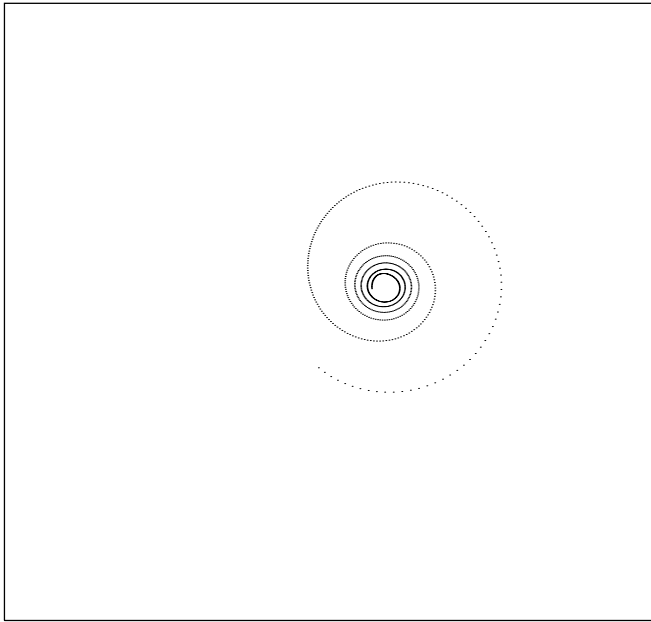


Fig.3 (a)

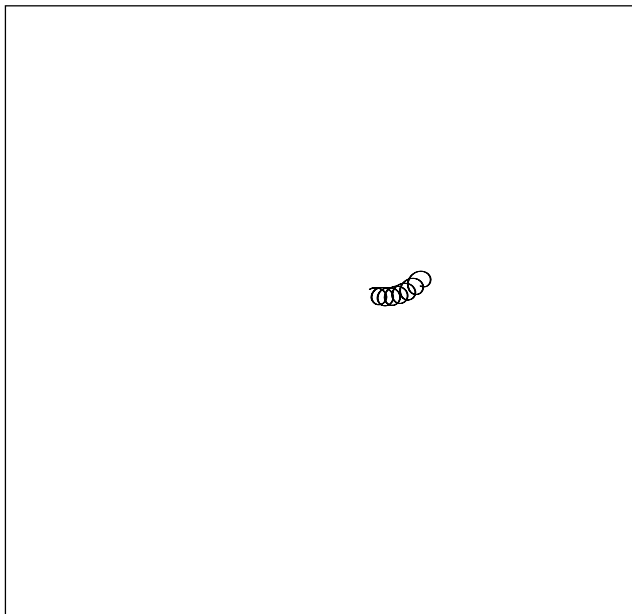


Fig. 3(b)

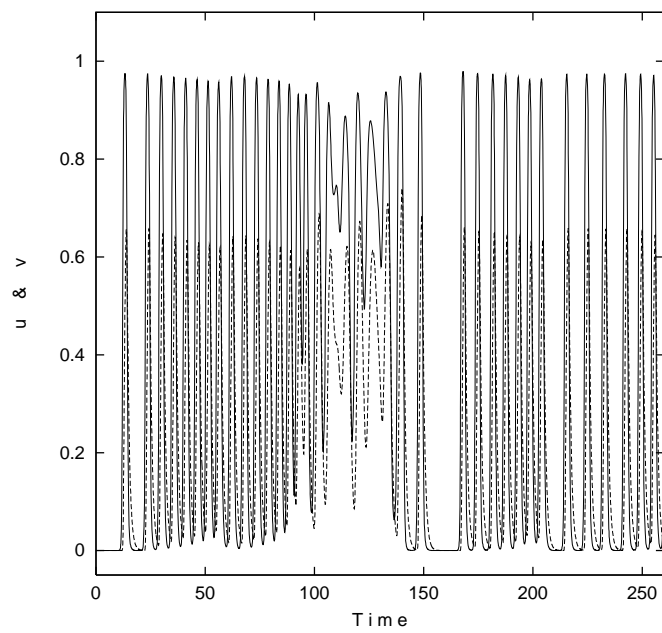


Fig.4

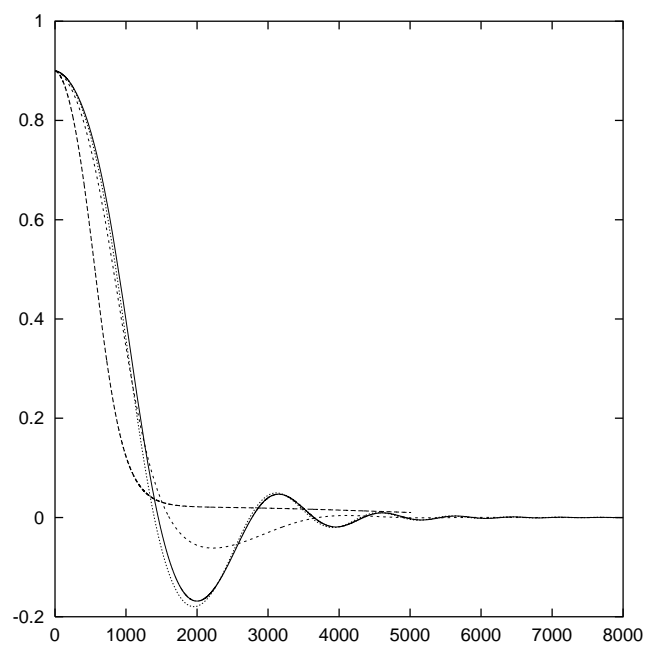


Fig. 5

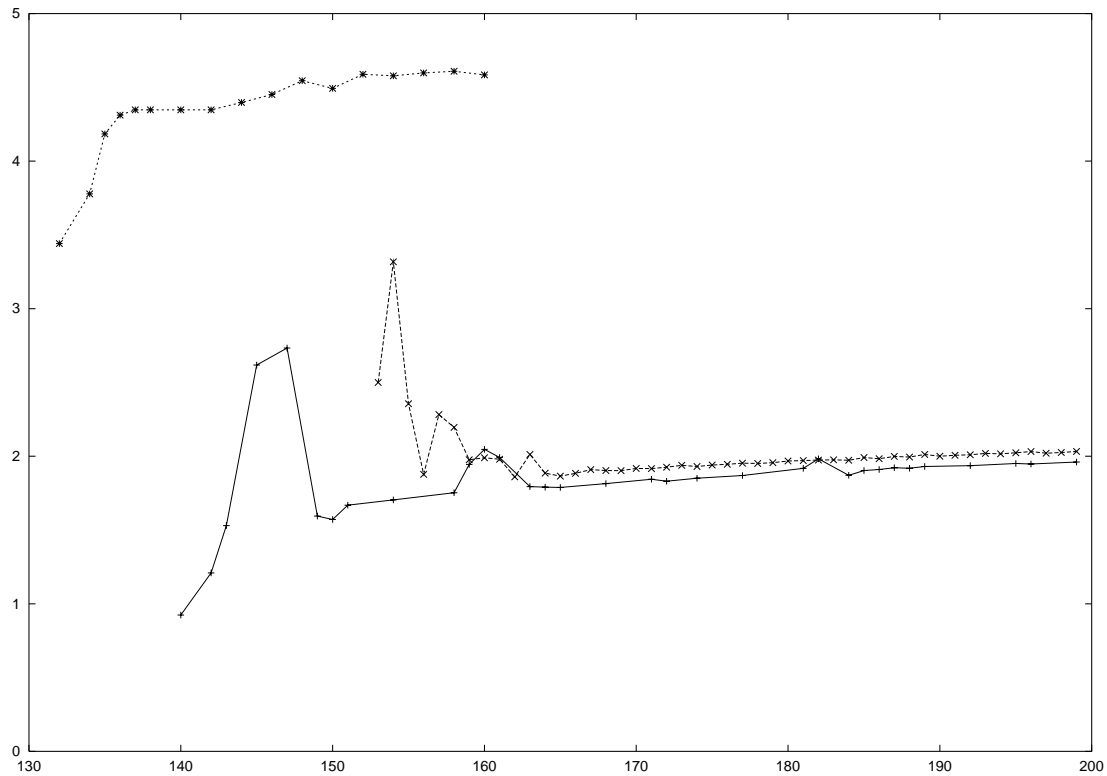


Fig. 6

Figure Captions

Fig. 1. (a) Phase diagram illustrating the dynamics of the PDE-system with u and v recorded at the point (40,40) in a grid size of 220. Parameters: $a = 0.75$, $b = 0.06$, $\varepsilon^{-1} = 13.5$. Shown are the nullclines: $v = u^3$, $u = u_{th}$, $u = 0$, and $u = 1$. (b) The time variation of u and v corresponding to one excursion along the phase diagram in (a).

Fig. 2. Snapshots showing the core expansion with $dt = 0.052$, $dx = 0.51$, $L = 48$, grid size: 95. (Time intervals between snapshots are not equal).

Fig. 3. Trajectory of the spiral tip defined as the intersection of the isolines $u = v = 0.5$, and following an outward spiral trajectory in (a) and meandering in (b). Parameters are the same as in Fig. 1 in (a) and in (b) $\varepsilon^{-1} = 18.0$.

Fig. 4 Time variation of the excitatory and the recovery variable recorded in the medium at the location (10,10). The dotted one is the variation of v .

Fig. 5. Recovering solitary travelling solution $u(z)=u(x+ct)$ of Eq.(5), illustrating damped oscillatory ($\varepsilon^{-1} = 13.5, 14.5$) and monotonic recovery ($\varepsilon^{-1} = 20.0, 50.0$).

Fig. 6. Dispersion curve: Instantaneous wave speed as a function of period for $\varepsilon^{-1} = 13.5, 14.5, 50.0$ respectively from bottom to top, computed by repetitively stimulating at one of the ends of an open line.

Non Corpus Parametrization for Studying Long-range Correlations in Natural Languages

Gökhan Şahin and O. Özgür Aybar

*Department of Information Systems and Technologies,
Yeditepe University, Kayisdagi Caddesi, 34755 Kadikoy, Istanbul, Turkey*

Avadis Hacinliyan

*Department of Physics and Department of Information Systems and Technologies,
Yeditepe University, Kayisdagi Caddesi, 34755 Kadikoy, Istanbul, Turkey*

Long-range correlation in a number of different languages have been reported by many authors including Montemurro et al. and Jaemi Bhan et al. This work proposes a non-corpus parametrization and uses it to extend this line of research to other languages, compares the differences between a meaningful and a randomly created English text by means of Detrended Fluctuation Analysis. The results imply a unique long-range correlation for each language analyzed, although similarities exist for languages of the same family.

I. INTRODUCTION

A natural language is a hierarchy of structures. The simplest structures consist of letters of the alphabet and the syllables; they will have a contribution to the sound but not to the meaning. Structures higher in the hierarchy such as words, sentences and paragraphs will also contribute to the meaning. A language must be patterned in order to constitute an effective communication medium. The patterns are expected to involve self similarity [1–3] and there should be a certain window of successive words that contribute to the meaning.[3]. Thus, a long range correlation in texts is implied. The existence of such long range correlations in English and Korean texts has been shown by Montemurro et al. and Jaemi Bhan et al. using Hurst's exponents [4, 5].

The first issue involved in an attempt to analyze a natural language as a time series is the need for a meaningful dependent variable that is to be used in the time series analysis. In this work a variable derived from values assigned to the letters constituting a given word is used. The resultant time series are analyzed via detrended fluctuation analysis (DFA) [6] .

DFA has become an important tool in analyzing long-term correlations in non stationary time series [6, 7] as illustrated in references involving molecular biology , medical science, econometrics, solid state meteorology and amorphous metarials [8–20]. DFA is reported to have advantages over conventional methods (e.g.,spectral analysis and Hurst analysis). It permits the detection of intrinsic self-similarity embedded in a seemingly non stationary time series, and also avoids the spurious detection of apparent self-similarity, which may be an artifact of extrinsic trends [21–25].

The parametrization used in this work is based on assigning values to the letters of a word has been introduced. This parametrization does not require a corpus, so that the quality of the corpus does not influence the results. Furthermore, one can study the dynamical properties of a text without having to use a collection based on several texts, since we have seen that languages evolve in time so that the period reflected by the corpus becomes significant.

Various types of text written in Turkish, English and translations of the same text in these and twelve additional languages were analyzed using detrended fluctuation analysis. Detrended fluctuation analysis permits the detection of intrinsic self-similarity embedded in a seemingly nonstationary time series, and also avoids the spurious detection of apparent self-similarity, which may be an artifact of extrinsic trends in the time series. The presence of two distinct scaling exponents indicate long range correlations. The progression from one word to the next implies a random walk model. Such a system would be relatively localized. The Detrended fluctuation analysis based on this new parametrization reveals differences with two regimes signalled by different correlation exponents that can serve as a means to distinguish between different languages. On the other hand, a universality is also signalled by the two regions with different correlation coefficients in spite of the grammatical differences between languages.

II. DETRENDED FLUCTUATION ANALYSIS

Detrended fluctuation analysis (DFA) is a scaling analysis method used to estimate long-range power-law correlation exponents [8]. One integrates the time series of length N , then divides the result into boxes of equal length, n . In each box of length n , a least squares line is fit to the data. The y coordinate of the straight line segments is denoted

by $y_n(k)$. Next, the integrated time series, $y(k)$, is detrended, by subtracting the local trend, $y_n(k)$, in each box. The root-mean-square fluctuation of this integrated and detrended time series is calculated by

$$F(n) = \sqrt{\frac{1}{N} \sum_{K=1}^N [y(k) - y_n(k)]^2} \quad 637 \quad (1)$$

This computation is repeated over all time scales (box sizes) to characterize the relationship between $F(n)$, the average fluctuation, as a function of box size, n . A linear relationship on a log-log plot indicates the presence of power law scaling. Under such conditions, the fluctuations can be characterized by a scaling exponent, α , such that $F(n) \sim n^\alpha$. A crossover in the scaling exponent, α , indicates a transition from one type to a different type of underlying correlation, due to a transition in the dynamical properties [6–9].

III. ANALYSIS OF TEXTS

As an example of the proposed analysis method, two Turkish and two English texts (these will be referred as Turkish text 1, Turkish text 2, English text 1, English text 2) were used. Turkish text 1 and English text 1 are independent of each other whereas Turkish text 2 and English text 2 are translations of each other. The time series is constructed using derived variable from values assigned to the letters constituting a given word. In the latter case DNA Random Walks [26] served as a main source of inspiration. The methodology is as follows: Each word is accepted as a single step in a random walk. The length of each step (word) is determined from the letters as

$$s(n) = \sum_{i=1}^N y(i) \quad (2)$$

Here N is the length of the word and $y(i)$ is the Unicode value of the corresponding letter. After the time series is constructed, the scaling exponent can be found.

The detrended fluctuation analysis of English text 2 and Turkish text 2 and Finnish text 2 (which are translations of each other) are presented in Fig. 1. A breakdown in the slope for both cases show the presence of two regions in which correlation properties are different. The slope of Turkish text is approximately 10% higher. Although the difference of correlation relations in the two regions for both languages are discernable, the break in slope is clearer for Turkish. Notice the resemblance of Finnish and Turkish texts which belong to the same language family. In order to further verify that the correlation properties are not due to the specific texts but the languages the same analysis is applied to two Turkish texts with different contexts. Fig. 2 is the result of analysis where the correlation properties of the different Turkish texts are the same. The same analysis applied to English (and Finnish) texts (of different context) and is presented in Fig 3 (4 for Finnish) which yield again the same correlation properties for the two texts.

As a last check, the correlation properties of a randomized text using Steganography ciphering [27] (in English) was checked. It is found that for the randomized text the correlation properties do not resemble the correlation properties of the English text (Fig. 6). This observation implies that a language has an inherent correlation property probably acquired during its development in order to achieve a meaning.

To detect the the extent of universality in the proposed parametrization we have also applied the same procedure to other languages using translations of the same text. The results are listed in the Table I. It can be observed that each language has its own correlation properties. The resemblance of the correlation properties of the languages of the same family should also be noted (with the exception of Spanish, whose correlation resembles Arabic more than the other Latin languages. The Arabic influence on Spanish is known, its influence on the correlation of Spanish is quite plausible.). A resemblance of the correlation properties can also be observed in Finnish and Turkish which belong to the same language family. On the other hand, the difference between English and German is more than what one would expect. This can be caused by the two different sentence structures (inversion) in the latter language. It is more interesting to note that if one looks at Medieval English as reflected by Chaucer, modern English and German, the curves that reflect German and Medieval English are very close. The differentiation is due to the evolution in the English language.

IV. CONCLUSION

The aim of this work has been to introduce a parametrization based on assigning values to the letters of a word and use it to analyze the similarities and differences between languages. This parametrization does not require a corpus,

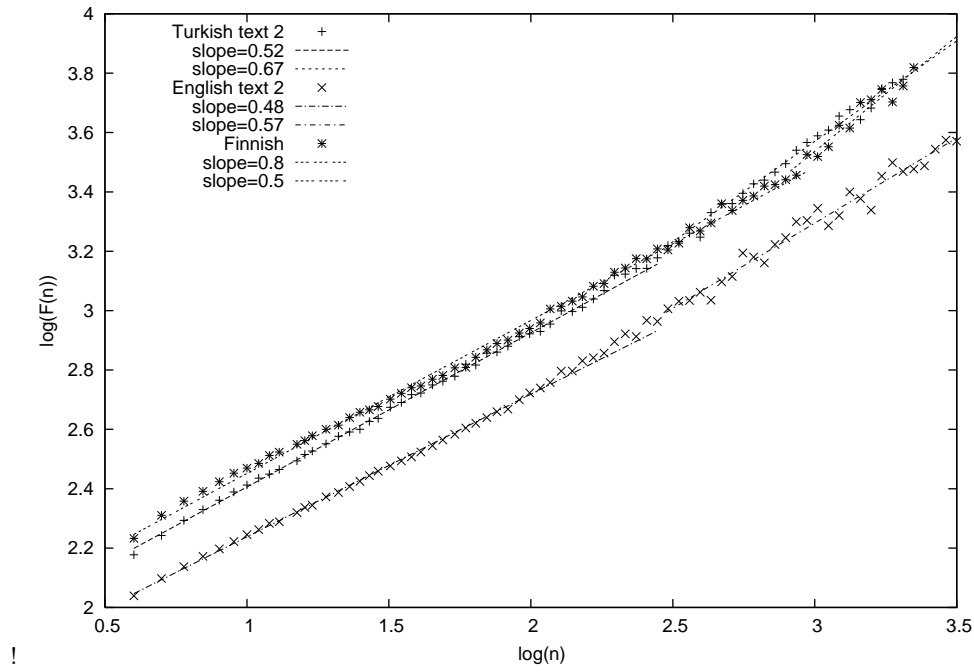


FIG. 1: $\log(F(n))$ vs $\log(n)$ for Turkish, English and Finnish texts .

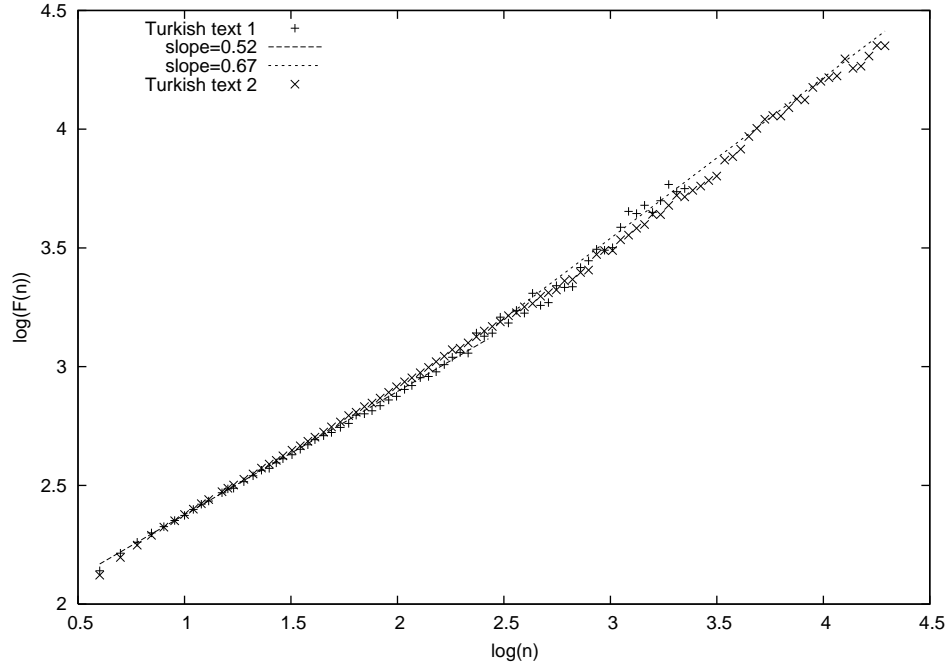
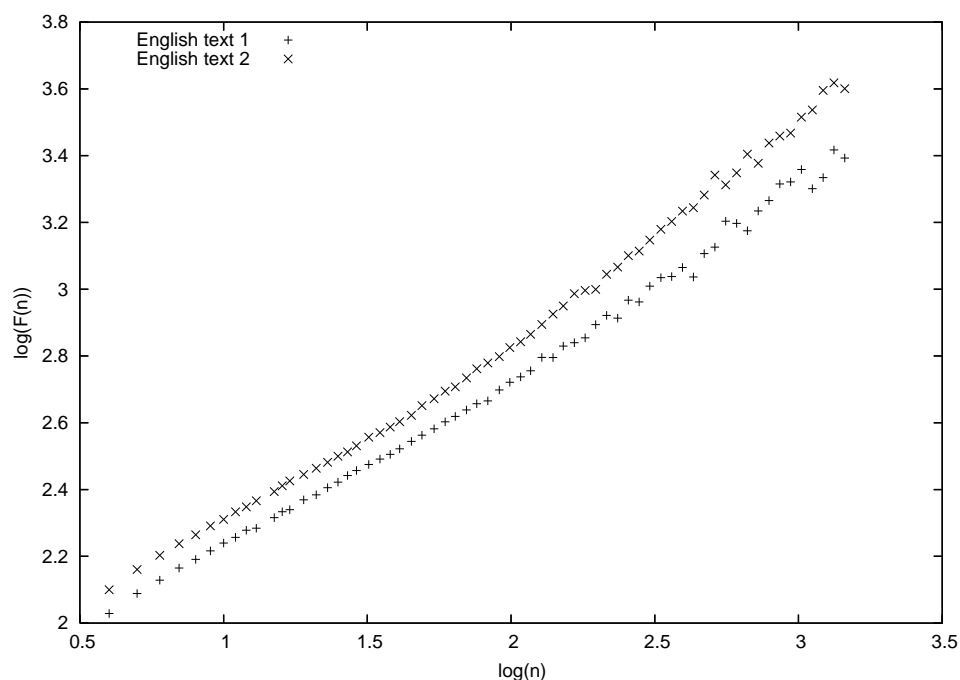
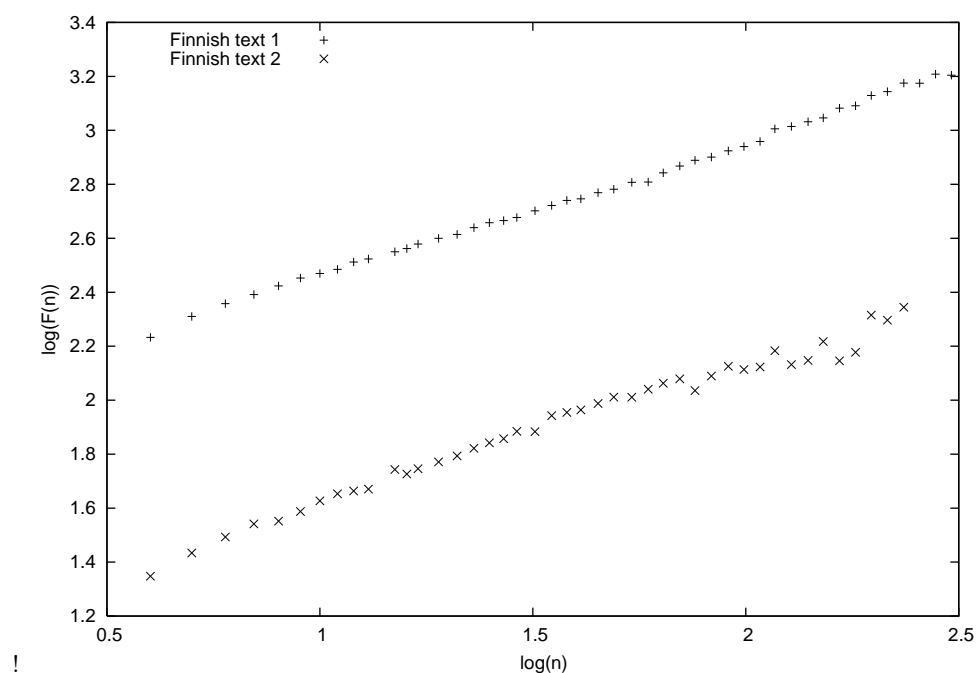


FIG. 2: $\log(F(n))$ vs $\log(n)$ for two Turkish texts.

hence the results are independent of the quality of the corpus. Furthermore, one can study the dynamical properties of a text without having to use a collection based on several corpora, since we have seen that languages evolve in time so that the period reflected by the corpus becomes significant.

Various types of text written in Turkish, English and translations of the same text in these and twelve additional languages were analyzed using detrended fluctuation analysis. Detrended fluctuation analysis has permitted the detection of intrinsic self-similarity embedded in a seemingly nonstationary time series, and also has avoided the spurious detection of apparent self-similarity, which may be an artifact of extrinsic trends in the time series. The

FIG. 3: $\log(F(n))$ vs $\log(n)$ two English texts .FIG. 4: $\log(F(n))$ vs $\log(n)$ two Finnish texts .

presence of two distinct scaling exponents indicate long range correlations. The progression from one word to the next implies a random walk model. Such a system would be relatively localized. The Detrended fluctuation analysis based on this new parametrization reveals differences with two regimes signalled by different correlation exponents that can serve as a means to distinguish between different languages. On the other hand, a universality is also signalled by the

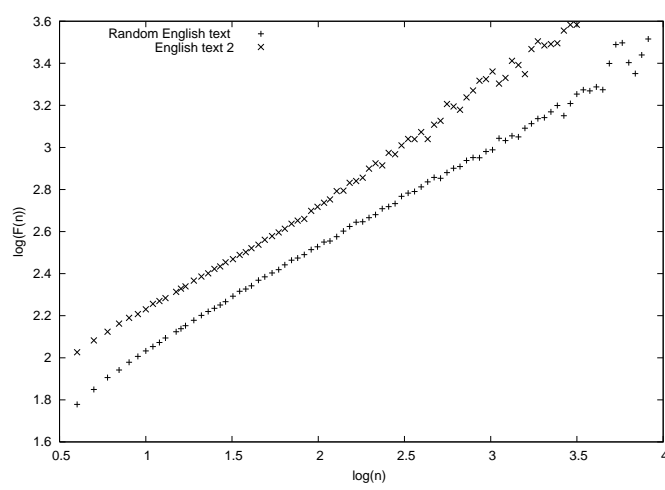


FIG. 5: $\log(F(n))$ vs $\log(n)$ for randomly created English text and regular English text.

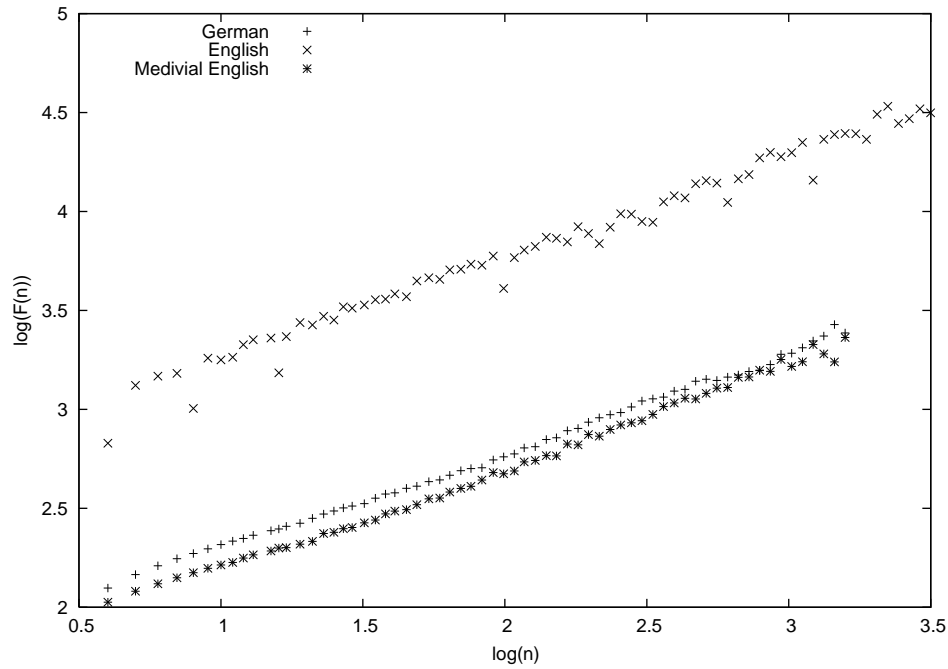


FIG. 6: $\log(F(n))$ vs $\log(n)$ for German, medieval English and modern English.

two regions with different correlation coefficients in spite of the grammatical differences between languages.

-
- [1] Hrebicek, Ludek, Universittsverlag Dr. N. Brockmeyer, Bochum, pp. 91-96, 1992.
 - [2] Hrebicek, Ludek, Quantitative Linguistics Vol. 566, Wissenschaftlicher Verlag Trier, 1995.
 - [3] Hrebicek, Ludek, Quantitative Linguistics Vol. 48, Universittsverlag Dr. N. Brockmeyer, Bochum, 1992,
 - [4] Montemurro MA, Pury PA. Long-range fractal correlations in literary corpora. 2002. Available from cond-mat/0201139.
 - [5] Bhan,J, S. Kim, J. Kim, Y. Kwon,Long-range correlations in Korean literary corpora,Chaos, Solitons and Fractals, 29, 6981, 2006.
 - [6] C.-K. Peng, S.V. Buldyrev, S. Havlin, M. Simons, H.E. Stanley, A.L. Goldberger, Phys. Rev. E 49, 1685,1994.
 - [7] J.W. Kantelhardt, E. Koscielny-Bunde, H.H.A. Rego, S. Havlin, and A. Bunde Physica A 295, 441 ,2001.
 - [8] Goldberger AL, Amaral LAN, Glass L, Hausdorff JM, Ivanov PCh, Mark RG, Mietus JE, Moody GB, Peng C-K, Stanley

Language	Region1	Region2
Arabic	0.47	0.54
Bosnian	0.48	0.47
Finnish	0.52	0.77
Turkish	0.52	0.67
Porteguese	0.48	0.7
French	0.51	0.82
Italian	0.45	0.8
Spanish	0.49	0.56
Polish	0.47	0.57
Indonesean	0.50	0.63
Malay	0.51	0.66
Swahili	0.49	0.41
German	0.48	0.7
Chaucer	0.49	0.6
English	0.48	0.56

TABLE I:

- HE, PhysioBank, PhysioToolkit, and PhysioNet: Components of a New Research Resource for Complex Physiologic Signals. Circulation 101(23): e215-e220 [Circulation Electronic Pages; <http://circ.ahajournals.org/cgi/content/full/101/23/e215>]; 2000 (June 13).
- [9] S.V. Buldyrev, A.L. Goldberger, S. Havlin, R.N. Mantegna, M.E. Matsu, C.-K. Peng, M. Simons, H.E. Stanley, Phys. Rev. E 51, 5084, 1995.
- [10] C.-K. Peng, S.V. Buldyrev, A.L. Goldberger, R.N. Mantegna, M. Simons, H.E. Stanley, Physica A 221 ,180, 1995.
- [11] S.V. Buldyrev, N.V. Dokholyan, A.L. Goldberger, S. Havlin, C.-K. Peng, H.E. Stanley, G.M. Viswanathan, Physica A 249, 430,1998.
- [12] C.-K. Peng, J. Mietus, J.M. Hausdorff, S. Havlin, H.E. Stanley, A.L. Goldberger, Phys. Rev. Lett. 70 ,1343, 1993.
- [13] C.-K. Peng, S. Havlin, H.E. Stanley, A.L. Goldberger, Chaos 5, 82, 1995.
- [14] K.K.L. Ho, G.B. Moody, C.-K. Peng, J.E. Mietus, M.G. Larson, D. Levy, A.L. Goldberger, Circulation 96, 842,1997.
- [15] G.M. Viswanatha, C.-K. Peng, H.E. Stanley, A.L. Goldberger, Phys. Rev. E 55 ,845, 1997.
- [16] C.K. Peng, J.M. Hausdorff, S. Havlin, J.E. Mietus, H.E. Stanley, A.L. Goldberger, Physica A 249 , 491, 1998.
- [17] Y.H. Liu, P. Cizeau, M. Meyer, C.-K. Peng, H.E. Stanley, Physica A 245, 437, 1997.
- [18] P. Cizeau, Y.H. Liu, M. Meyer, C.-K. Peng, H.E. Stanley, Physica A 245 , 441,1997.
- [19] M. Ausloos, N. Vandewalle, P. Boveroux, A. Minguet, K. Ivanova, Physica A 274, 229, 1999.
- [20] M. Ausloos, K. Ivanova, Physica A 286 , 353, 2000.
- [21] Buldyrev, S. V., A. L. Goldberger , S. Havlin, C. K. Peng , H. E. Stanley and M. Simons, Biophys. J., Vol.65, 2673,1993.
- [22] Ossadnik, S. M., S. V. Buldyrev, A. L. Goldberger, S. Havlin, R. N. Mantegna, C. K. Peng, M .Simons, H.E Stanley, Biophys. J., Vol. 67,64, 1994.
- [23] Hausdorff, J. M., C. K. Peng, Z. Ladin, J. Y. Wei, A. L. Goldberger, J. Appl. Physiol., Vol. 78, 349, 1995.
- [24] Hausdorff, J. M., P. Purdon, C. K. Peng, Z. Ladin, J. Y. Wei, A. L. Goldberger, J. Appl. Physiol., Vol. 80, 1448, 1996.
- [25] Hu, K., P.Ch. Ivanov, Z. Chen, P. Carpena, H. E. Stanley, "Effect of nonstationarities on detrended fluctuation analysis", Phys. Rev. E., Vol. 64, 011114, 2001.
- [26] Alexandre Rosas, Edvaldo Nogueira, Jr., and Jose F. Fontanari, PHYSICAL REVIEW E 66, 061906 , 2002.
- [27] <http://www.fourmilab.ch/javascript/stego.html>

TWO DIMENSIONAL PACKING OF GRANULAR RODS

S. SARIKAYA, Y. DEMIRAGAC* and M.L. KURNAZ**

Bogazici University, Istanbul, Turkey, saimesarikaya@gmail.com

*Istanbul University, Istanbul, Turkey, yesimdemiragac@gmail.com

**Bogazici University, Istanbul, Turkey, levent.kurnaz@boun.edu.tr

Abstract

We investigate the two-dimensional packing properties of prolate granular materials. As the dynamics of formation can be influenced by the method of delivery of the prolate particles to the surface, we experiment with different methods which include changing the viscosity of the medium as well. For an aspect ratio of Length/Diameter = 30 the average packing fraction for the rods is found to be 0.572 ± 0.033 . We measure the angular distribution of the rods and compare this with the previous experimental and computational results. We find that the peak value of the distribution function does not depend on the method of delivery of the prolate particles to the surface. We also measure the orientational order parameter of the rods as a function of the height within the pile. This order parameter is found to be dependent on the method of delivery and medium used during sedimentation.

I. Introduction

Packing of prolate granular materials is very important in many industrial applications in the sense that the networks formed by these materials can be quite extensive which can be a desirable or avoided outcome of the formation process. In applications like moving logs through rivers or production of LCD displays, these extensive networks are an undesired side effect whereas the quality of paper basically depends on the extent of these networks.

Most of the previous work on prolate particles is concentrated on non-spherical particles in 2D [1-6] or 3D [7] packing and an aspect ratio smaller than 5. Furthermore while looking for effective medium model elastic discs are studied [8]. In another work [9], interacting particles are investigated. The interaction between these particles is defined by a new parameter which is effective repulsive contact interaction between particles (q). The parameter q can be between 0 (which means uniformly random network) and 1 (which means overlapping is not allowed). The situation with perfectly rigid rods correspond to the situation where $q = 1$.

Stokely et al. [10] used such a system in their experimental and computational study. In their experiments 2D piles were formed by restricting and rotating acrylic rods with aspect ratio L (length) / D (diameter) = 12 between two vertical walls. In their simulations they studied on packing of particles with aspect ratio ranging from 10 to 1000. Especially with the angular distribution of the particles and the size of the voids formed by sedimentation, they have found that simulations and experiments have similar results for $L/D = 12$, the differences were due to the friction in the experiments which is not taken into account on the simulations. As many real life scenarios include the presence of a medium during the formation of the piles of prolate particles, we improved on their study by keeping their initial premise of forming a 2D pile between two vertical walls. However, in this study we have also allowed the cylindrical rods to sediment in a viscous environment.

II. Experiments

The particles in our study are cylindrical, rigid rods. The determining feature about these particles is the aspect ratio of the rods. We used the particles with high aspect ratio (L (length) / D (diameter) = 30). Compared to the sedimentation of the particles with small aspect ratio, they form lower packing fractions. By specifying the characteristics of the packing of these particles we can easily increase (or decrease when needed) the efficiency of sedimentation and this can increase the quality of, for example, paper which is made of fibres [11].

In our research, we have used an insulated copper cable with a diameter of 2.65 mm. We cut this cable into pieces of length 80 mm; hence we have an L/D ratio of about 30. We allow these particles to sediment between two glass sheets separated by a spacer nearly the diameter of the cable thick, giving us a cell width of 40 μm . This spacing between the glasses provides us 2 dimensional sedimentation and overlapping is prevented with this way. The separation between the glass sheets was filled with either nothing (air), or with distilled water, or with light paraffin oil. We primarily studied random delivery of the particles. Furthermore, we have studied on different methods of delivery such as vertical, horizontal and prearranged, the last one corresponding to the experimental setup used previously by Stokely et al. In vertical and horizontal methods, we let the particles sediment vertically and horizontally from random places over the sedimentation cell. To minimize the particle-particle interactions during sedimentation, we only allowed one particle to be in motion within the cell. In random delivery, we start the particles off with different random angles. In the prearranged method, we put all the particles in one of the glasses, put other glass on it and rotate the whole system slowly after putting spacers. During the sedimentation and after all the particles have settled down we took pictures (Fig. 1) and analyzed these pictures using ImageJ software.



Figure 1. A sample run with no water inside and the rods are dropped at random locations with random orientation.

III. Results

A. Average area fraction and angular distribution

To calculate the average area fraction of the packing we have neglected the top portion of the pile and counted only the areas which are bound either by other particles or the walls. As mentioned before, the area fraction of randomly delivered particles is 57.2 ± 3.3 %. This fraction is nearly same for horizontally (58.0 ± 2.5 %) and vertically (57.8 ± 3.5 %) delivered particle packing. However, while doing the experiments in water, for horizontally delivered particle packing this fraction decreases to 53.8 ± 5.1 %. On the other hand, for vertically delivered particles, average area fraction increases to 61.3 ± 1.2 %. Finally, as we expected, for prearranged packing the fraction is (53.6 ± 4.4 %) smaller compared to other techniques. We did not observe significant difference by increasing the viscosity of the sedimentation medium from water to light paraffin oil. The differences between the air and water experiments can be understood in terms of the forces of impact. In the case of vertical sedimentation in water, the particle gently rolls over after touching the surface hence making the structure rougher. In the case of horizontal sedimentation in water, the particle moves longer to the local minimum with the help of buoyancy, hence making the structure denser.

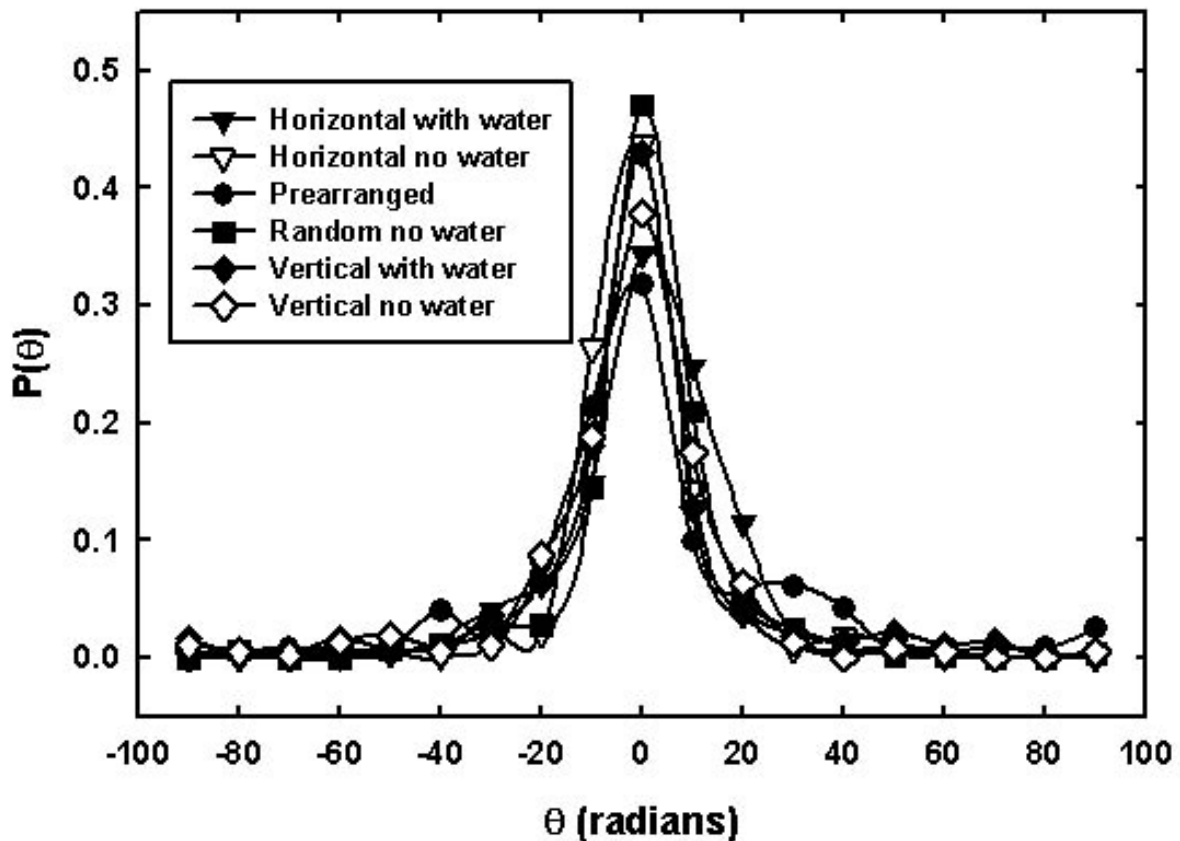


Figure 2. Angular distribution of the prolate particles with different experimental conditions.

Another analysis that we performed is the angular distribution of the particles. As seen in Figure 2, there is a sharp peak near zero. The shape of this distribution does not

significantly depend on the method of delivery and the medium. However, the height of the peak at the maximum changes significantly with the delivery method. The only difference between the distributions is the height of peak. Random deposition method in the absence of water has almost half of the particles nearly horizontal on the surface whereas this number drops to about 30% for the prearranged case.

B. Distribution of voids

As seen from Fig. 1, the morphology of the piles is dominated by large but rare voids. So we have analyzed the number of voids as a function of void area. In Fig.3 we can see the void distribution function as a function of void area / L^2 (which is dimensionless) for the waterless deposition of randomly oriented particles. By plotting the best fit line we can obtain a power law relation which fits to $A^{-0.25 \pm 0.08}$. In the previous study [10], larger values of this exponent were observed for a slightly different experimental setup. This clearly indicates that the results depend strongly on the experimental setup and initial conditions. It is hard to look at Fig.3 and claim a power law relationship as has been done in the previous study. The previous study, started with randomly distributed rods being slowly rotated. This kind of deposition clearly gives a more random surface, leading to a finer power law relationship between the size and the number of the void areas. However, as this problem is intrinsically not random, but strongly influenced by particle interactions and gravity, we cannot claim that we observe a power law relationship.

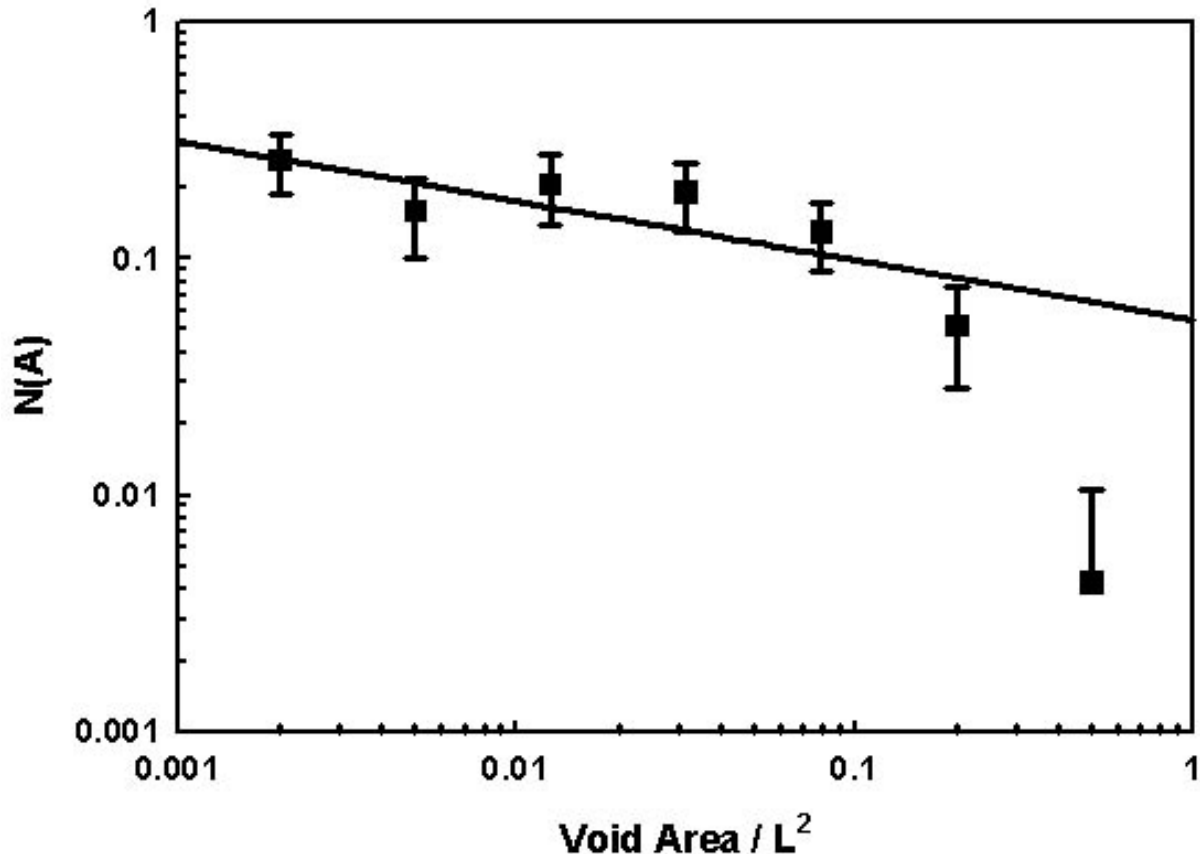


Figure 3. Void distribution function $N(A)$ as a function of dimensionless void area (area scaled by the particle length L^2)

C. Orientational order parameter as a function of height

We also analyzed is the orientational order parameter ($Q(h)$) as a function of height. For i^{th} particle is given by $Q(h) = \langle \cos(2\Theta_i) \rangle$ where Θ_i is the angle between the particle and base of the pile. If particle is horizontal $Q = +1$ and $Q = -1$ indicates that particle is vertical. For h near the base of the pile, particles are aligned more horizontally, as expected and as we can see from the Figure 4 below. Increasing the height leads us to a limit for Q . For the particles with aspect ratio 30 (for randomly delivered particles and medium of no water) this limiting value of $Q(h)$ is found to be 0.811 ± 0.049 , which roughly translates to an average inclination of $\pm 17^\circ$. Comparing this result to the previous study, we see that in the previous study $Q(h) = 0.33$ which leads to an average inclination of $\pm 35^\circ$. This difference can be attributed to the smaller aspect ratio of the particles in the previous study (therefore they can rotate easier). In our other trials with different deposition styles we found $Q(h)$ to be very close to the case described above for random no water method. However vertical deposition with water and the repetition of the previous study with our aspect ratio of 30 gave significantly different results. For vertical deposition with water this limit is 0.54 ± 0.37 and for the method of rotating randomly distributed rods we obtain 0.57 ± 0.19 , still much higher than the previous study of aspect ratio of 12.

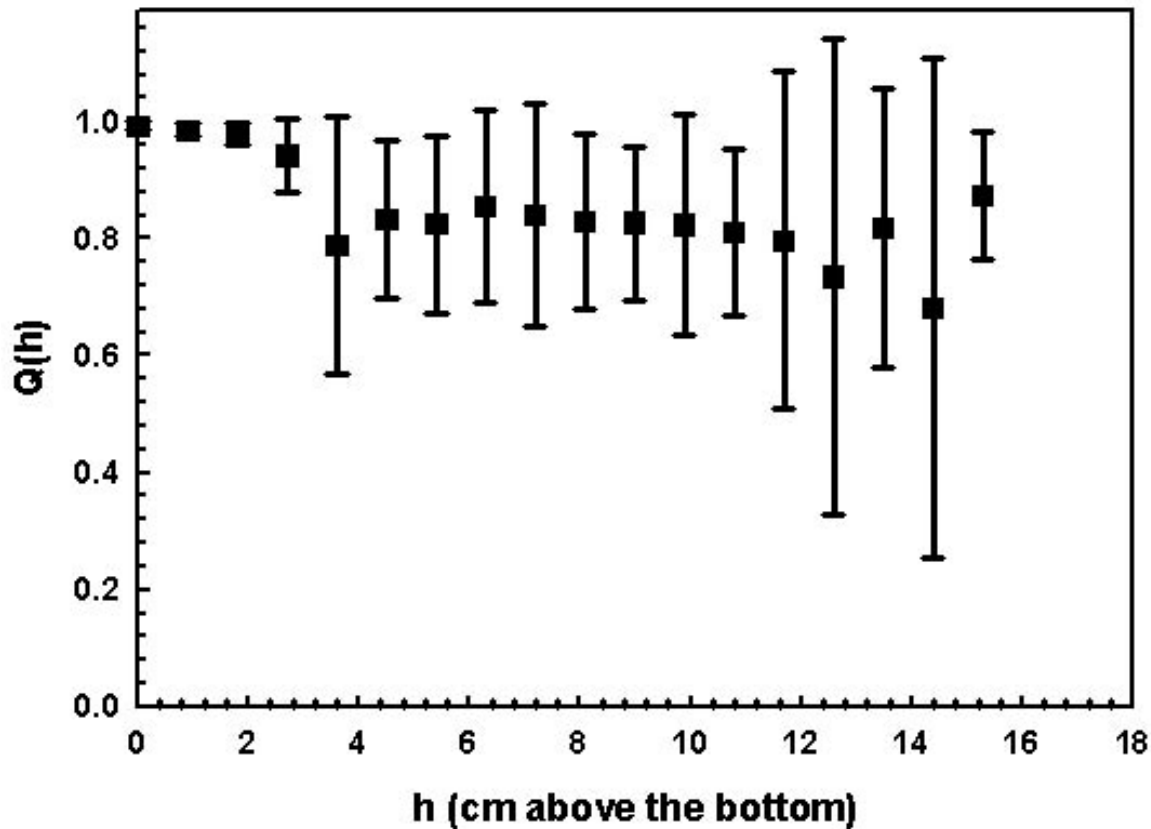


Figure 4. Orientational order parameter $Q(h)$ as a function of height within the 2D pile of deposited particles.

IV. Conclusion

We have presented the analysis of two dimensional packing of granular rods with an aspect ratio 30. For randomly delivered sedimentary particles, the packing fraction of these

particles is found to be $57.2 \pm 3.3\%$. We also analysed the effect of the method of the delivery (randomly, vertical, horizontal, prearranged) and the medium (water and no water). It is found that average area fraction and angular distribution is significantly effected by changing the medium and the delivery method. Therefore we conclude that the most efficient method (highest packing fraction) is the method of random no water and the least efficient method is prearranged which was the method of delivery in the previous study [10]. We also examined the distribution of the voids and orientational order parameter as a function of height. The distribution of voids cannot be simply explained by a power law relationship and different aspect ratios are needed to draw better conclusions. The orientational order parameter is however more readily explainable in the sense that higher aspect ratio rods tend to have an order parameter closer to unity especially deposited in viscous fluids.

V. References

- [1] B.J. Buchalter and R.M. Bradley, J. Phys. A **25**, L1219 (1992).
- [2] B.J. Buchalter and R.M. Bradley, Phys. Rev. A **46**, 3046 (1992).
- [3] J.R. Williams and G.W. Mustoe, in *Computers and Geotechnics* (Elsevier Applied Science, New York, 1990).
- [4] G.G.W. Mustoe, M. Miyata, and M. Nakagawa., in *Finite Elements: Techniques and Developments* (Civil-Comp Press, Stirling, United Kingdom, 2000).
- [5] P.W. Cleary and M.L. Sawley, Appl. Math. Model. **26**, 89 (2002).
- [6] I.C. Rankenburg and R.J. Zieve, Phys. Rev. E **63**, 061303 (2001).
- [7] F.X. Villarruel, B.E. Lauderdale, D.M. Mueth, and H.M. Jaeger, Phys. Rev. E **61**, 6914 (2000).
- [8] J. A. Aström, M. Latva-Kokko, J.P. Maekinen, J. Timonen, Granular Matter **5**, 99-103 (2003)
- [9] J. Asikainen, T. Ala-Nissila, Phys. Rev. E **61**, 5 (2000)
- [10] K. Stokely, A. Diacou, Scott V. Franklin, Phys. Rev. E **67**, 051302 (2003)
- [11] N. Provatas, M. J. Alavara, T. Ala-Nissila, Phys. Rev. E **54** 1 (1996)

TRANSVERSE VIBRATION CHARACTERISTICS OF EULER-BERNOULLI AND TIMOSHENKO BEAMS UNDER MOVING FORCES

A.Deniz Şenalp* Aytaç Arıkoğlu** İbrahim Özkol*** Vedat Z. Doğan****

Abstract

In this paper, dynamic response of homogeneous, isotropic Euler-Bernoulli and Timoshenko type beams under varying magnitude of moving forces is investigated considering different types of motion such as constant velocity, accelerated and decelerated cases. Effects of the velocity and magnitude of the force, shear deformation and rotary inertia to the vibration characteristics are examined. This work is a continuation of the authors' previous paper.[1]

1. Introduction

Because of the fact that, the moving force models that are constant and varying in time have a large application area in engineering, for instance, piping systems, bridges, beams subjected to pressure waves and high velocity machining operations, the investigation of these models has a great significance. By using the method of expansion of the eigenfunctions, transverse vibration of beams under moving forces was firstly examined by A.N.Kriloff[2]. Besides this, for the solution of the problem, Green's functions and integral equation methods are widely used in the works of S.P.Timoshenko[3], A.N.Lowen[4] and N.G.Bondar[5]. The textbook of Fryba[6] includes comprehensive studies about vibration of solids and structures under moving forces and loads. Mackertich's work[7] gives a solution to the problem with corrections for the rotary inertia and shear deformation. In recent years, studies of Abu-Hilal and Mohsen[8], Abu-Hilal and Zibdeh[9] offer a solution to the problem with general boundary conditions subjected to constant and harmonic moving forces.

In the present study, the transverse vibration characteristics of homogeneous, isotropic, simply-supported Euler-Bernoulli and Timoshenko beams, subjected to three different force cases, are studied by using the method of modal analysis. First, a constant magnitude force is acted upon the beam. Second, a linearly increasing force condition is considered. Third, a

*Research Assistant, Aeronautical Eng. Department, Istanbul Technical University, senalpa@itu.edu.tr

** Research Assistant, Aeronautical Eng. Department, Istanbul Technical University, arikoglu@itu.edu.tr

*** Professor, Aeronautical Eng. Department, Istanbul Technical University, ozkol@itu.edu.tr

**** Assistant Prof., Aeronautical Eng. Department, Istanbul Technical University, doganve@itu.edu.tr

linearly decreasing force is applied to the beams. For all three cases, accelerated, constant velocity and decelerated motion of the applied force are also investigated. Effects of the force velocity, rotary inertia and shear deformation on the dynamic responses are determined. Results are graphically displayed and compared to the static maximum deflections.

2. Theory and Formulation

In Figure 1, a simply-supported, homogeneous, isotropic and constant cross-section beam of length L , is shown. The beam is initially assumed to be at rest and undeformed. The beam damping ratio which is proportional to the velocity of the vibration is neglected. The force $f(x,t)$ is expressed as,

$$f(x,t) = \delta(x - g(t))P(t) \quad (1)$$

where $\delta(x-g(t))$ is Dirac-Delta function, $P(t)$ refers to the force for the considered case. $g(t)$ represents the kinematics of the moving force as follow,

$$g(t) = x_0 + vt + \frac{1}{2}at^2 \quad (2)$$

where x_0 is the starting point of the force ($x_0=0$), v is the initial speed and a is the constant acceleration. Dirac-Delta function $\delta(x)$ is thought of as a unit concentrated force acting at point $x=0$. Dirac-Delta function is defined as,

$$\int_a^b \delta(x - \xi)f(x)dx = f(\xi), \text{ for } a < \xi < b \quad (3)$$

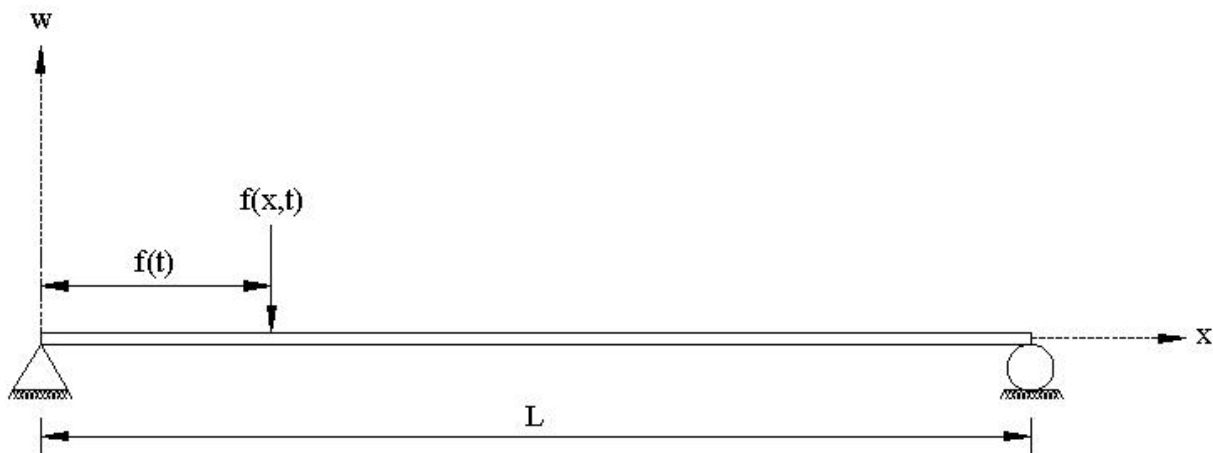


Figure 1 Simply-supported beam subjected to a concentrated moving force.

In this paper, three force cases are considered as follows,

- Constant Force: $P(t) = P_0$
- Linearly Increasing Force: $P(t) = P_0 \left(\frac{t}{\bar{t}} \right)$
- Linearly Decreasing Force: $P(t) = P_0 \left(1 - \frac{t}{\bar{t}} \right)$

where \bar{t} is traverse time of force over beam. Vibration characteristics for the Euler-Bernoulli and Timoshenko beam models will be investigated and graphically outlined in the following sections.

2.1. Vibration Characteristics of an Euler-Bernoulli Beam Under Moving Forces

The problem is governed by the following differential equation below:

$$EI \frac{\partial^4 w(x,t)}{\partial x^4} + \mu \frac{\partial^2 w(x,t)}{\partial t^2} + 2\mu\omega_b \frac{\partial w(x,t)}{\partial t} = f(x,t) \quad (4)$$

where EI , μ , ω_b and $w(x,t)$ are the flexural rigidity, the mass per unit length, the circular frequency of the damping, and the transverse deflection of the beam at point x and time t , respectively. Simply-supported beam boundary and initial conditions are,

$$w(0,t) = w(L,t) = \frac{\partial^2 w(0,t)}{\partial x^2} = \frac{\partial^2 w(L,t)}{\partial x^2} = 0 \quad (5)$$

$$w(x,0) = \frac{\partial^2 w(x,0)}{\partial t^2} = 0 \quad (6)$$

By using the method of modal analysis, transverse deflection $w(x,t)$ can be written as,

$$w(x,t) = \sum_{i=1}^{\infty} X_i(x) T_i(t) \quad (7)$$

where X_i is the i -th normal mode vibration of a uniform beam, expressed as,

$$X_i(x) = \sin\left(\frac{\lambda_i}{L} x\right) + A_i \cos\left(\frac{\lambda_i}{L} x\right) + B_i \sinh\left(\frac{\lambda_i}{L} x\right) + C_i \cosh\left(\frac{\lambda_i}{L} x\right) \quad (8)$$

For a simply-supported beam Eq.(8) reduces to the following form,

$$X_i(x) = \sin\left(\frac{\lambda_i}{L}x\right) \quad (9)$$

where $\lambda_i = i\pi$ (eigenvalues).

Substituting Eq.(9) into Eq.(7), and Eq.(7) into Eq.(4), then multiplying by $X_k(x)$ and integrating over the length of the beam, we have

$$\sum_{i=1}^{\infty} T_i(t) \int_0^L EI \left(\frac{\partial^4 X_i}{\partial x^4} \right) X_k dx + \sum_{i=1}^{\infty} \ddot{T}_i(t) \int_0^L \mu X_i X_k dx + 2\omega_b \sum_{i=1}^{\infty} \dot{T}_i(t) \int_0^L \mu X_i X_k dx = \int_0^L X_k f(x,t) dx \quad (10)$$

Orthogonality conditions are required that,

$$\int_0^L X_i X_k dx = 0, \quad i \neq k \quad (11)$$

Rearranging the terms in Eq.(10), we have

$$M_i = \int_0^L \mu X_i^2(x) dx; \quad H_i = \int_0^L EI \left(\frac{\partial^4 X_i}{\partial x^4} \right) X_i dx \quad (12)$$

By using these relations, we obtain the differential equation of the i -th mode of the generalized deflection as

$$\ddot{T}_i(t) + 2\omega_i \xi_i \dot{T}_i(t) + \omega_i^2 T_i(t) = Q_i(t) \quad (13)$$

where

$$\omega_i = \sqrt{\frac{H_i}{M_i}} = \left(\frac{\lambda_i}{L} \right)^2 \sqrt{\frac{EI}{\mu}}; \quad \xi_i = \frac{\omega_b}{\omega_i} \quad (14)$$

$$Q_i(t) = \frac{1}{M_i} \int_0^L X_i(x) f(x,t) dx \quad (15)$$

Solution of the Eq.(13) is,

$$T_i(t) = \frac{P_0 e^{-\xi_i \omega_i t}}{M_i \omega_i \sqrt{1 - \xi_i^2}} \int_0^t e^{-\xi_i \omega_i \tau} \sin(\omega_i \sqrt{1 - \xi_i^2} \tau) Q_i(\tau) d\tau \quad (16)$$

where $Q_i(t)$ is defined as for the three different force cases,

$$P(t) = P_0 \rightarrow Q_i = \frac{P_0}{M_i} X_i[g(t)] \quad (17)$$

$$P(t) = P_0 \left(\frac{t}{\tau} \right) \rightarrow Q_i = \frac{P_0}{M_i} X_i[g(t)] \left(\frac{t}{\tau} \right) \quad (18)$$

$$P(t) = P_0 \left(1 - \frac{t}{\tau} \right) \rightarrow Q_i = \frac{P_0}{M_i} X_i[g(t)] \left(1 - \frac{t}{\tau} \right) \quad (19)$$

2.2. Vibration Characteristics of a Timoshenko Beam Under Moving Forces

With the addition of shear deformation and rotary inertia effects, governing equation of the transverse vibration of the beam becomes[7],

$$EI \frac{\partial^4 w}{\partial x^4} - \left(f(x,t) - \mu \frac{\partial^2 w}{\partial t^2} - \eta \frac{\partial w}{\partial t} \right) - \mu r^2 \frac{\partial^4 w}{\partial x^2 \partial t^2} + \frac{EI}{\kappa AG} \frac{\partial^2}{\partial x^2} \left(f(x,t) - \mu \frac{\partial^2 w}{\partial t^2} - \eta \frac{\partial w}{\partial t} \right) - \frac{\mu r^2}{\kappa AG} \frac{\partial^2}{\partial t^2} \left(f(x,t) - \mu \frac{\partial^2 w}{\partial t^2} - \eta \frac{\partial w}{\partial t} \right) = 0 \quad (20)$$

where EI , μ , $w(x,t)$, κ , A , G , r , and η are the flexural rigidity, the mass per unit length, the transverse deflection, the cross-sectional area, the shear modulus, the radius of gyration, and the viscous damping per unit length of the beam, respectively.

Boundary conditions are the same as in Eq.(5), and initial conditions are as follows,

$$w(x,0) = \frac{\partial w(x,0)}{\partial t} = \frac{\partial^2 w(x,0)}{\partial t^2} = \frac{\partial^3 w(x,0)}{\partial t^3} = 0 \quad (21)$$

In the Timoshenko beam model, the method of modal expansion will be used as in the Euler-Bernoulli beam model. Substituting Eq.(7) into Eq.(20) by employing the orthogonality conditions, the differential equation for $T_i(t)$ is found as follows,

$$\begin{aligned} \frac{d^4 T_i(t)}{dx^4} + \sigma \frac{d^3 T_i(t)}{dx^3} + \beta \frac{d^2 T_i(t)}{dx^2} + \gamma \frac{dT_i(t)}{dx} + \phi T_i(t) &= \frac{2\kappa AG}{r^2 \mu^2 L} \int_0^L X_i(x) f(x,t) dx \\ - \frac{2EI}{r^2 \mu^2 L} \int_0^L X_i(x) \frac{\partial^2 f(x,t)}{\partial x^2} dx + \frac{2}{\mu^2 L} \int_0^L \mu X_i(x) \frac{\partial^2 f(x,t)}{\partial t^2} dx \end{aligned} \quad (22)$$

where

$$\sigma = \frac{\eta}{\mu} \quad (23)$$

$$\beta = \frac{\kappa AG}{r^2 \mu L^2} \left[L^2 + r^2 \lambda^2 \left(1 + \frac{E}{\kappa G} \right) \right] \quad (24)$$

$$\gamma = \frac{\kappa AG \eta}{r^2 \mu^2} \left[\frac{\lambda EI}{\kappa AG} + 1 \right] \quad (25)$$

$$\varphi = \frac{EI\kappa AG}{r^2\mu^2} \left(\frac{\lambda}{L} \right)^4 \quad (26)$$

The relationship with the damping coefficient, ξ in Eq.(14) and the viscous damping per unit length of the beam, η can be indicated by the equation below.

$$\eta = 2\mu\omega_b \quad (27)$$

Substituting Eq.(1) and Eq.(9) into the right side of the Eq.(22) yields to,

$$\begin{aligned} & \frac{d^4 T_i(t)}{dx^4} + \sigma \frac{d^3 T_i(t)}{dx^3} + \beta \frac{d^2 T_i(t)}{dx^2} + \gamma \frac{dT_i(t)}{dx} + \varphi T_i(t) \\ &= P(t) \sin\left(\frac{\lambda v}{L} t\right) \left[\frac{2\kappa AG}{r^2\mu^2 L} + \frac{2EI}{r^2\mu^2 L} \left(\frac{\lambda}{L}\right)^2 - \frac{2}{\mu L} \left(\frac{\lambda v}{L}\right)^2 \right] \\ & \text{for } 0 \leq t \leq \frac{L}{v} \end{aligned} \quad (28)$$

Solution of Eq. (28) provides the time part of Eq.(7) for the Timoshenko beam.

3. Results and Discussion

Results are found for the beam with $L=50$ m, $I=2.25$ m⁴, $E=33.4$ GPa, $\rho=2400$ kg/m³, and $\kappa=0.83$ as given in [7]. Both models are simply supported beams, and because of the symmetry, maximum deflections will occur at the mid-span of the beams, that is $L/2$.

To make a good comparison, dynamic deflections are nondimensionalized by static deflections which is $w_0 = \frac{P_0 L^3}{48EI}$ and time variable is nondimensionalized ($S = \frac{t}{\tau}$) by the total

time of the load(τ) in order to travel from the left-end to right-end of the beam. Non-dimensional speed parameter is $\alpha = \frac{v}{v_{cr}}$, where v_{cr} is the critical speed[6], $v_{cr} = \frac{\omega_i L}{\pi}$. Non-

dimensional damping coefficient is ξ_i , given in Eq.(14). For the accelerated motion, the force is assumed to be at rest at $x=0$ and reaches the speed v at $x=L$. For the constant velocity motion, the force is travelling at constant speed v along the beam. For the decelerated motion, the force is assumed to be at a speed v at $x=0$ and stops at $x=L$. Results are graphically displayed for all force and motion cases with several speed parameters and damping coefficients. Vertical axis represents the ratio of maximum dynamic deflection to static deflection, horizontal axis represents the non-dimensional time S .

3.1. Constant Velocity Motion with All Force Cases

3.1.1. Constant Load Case

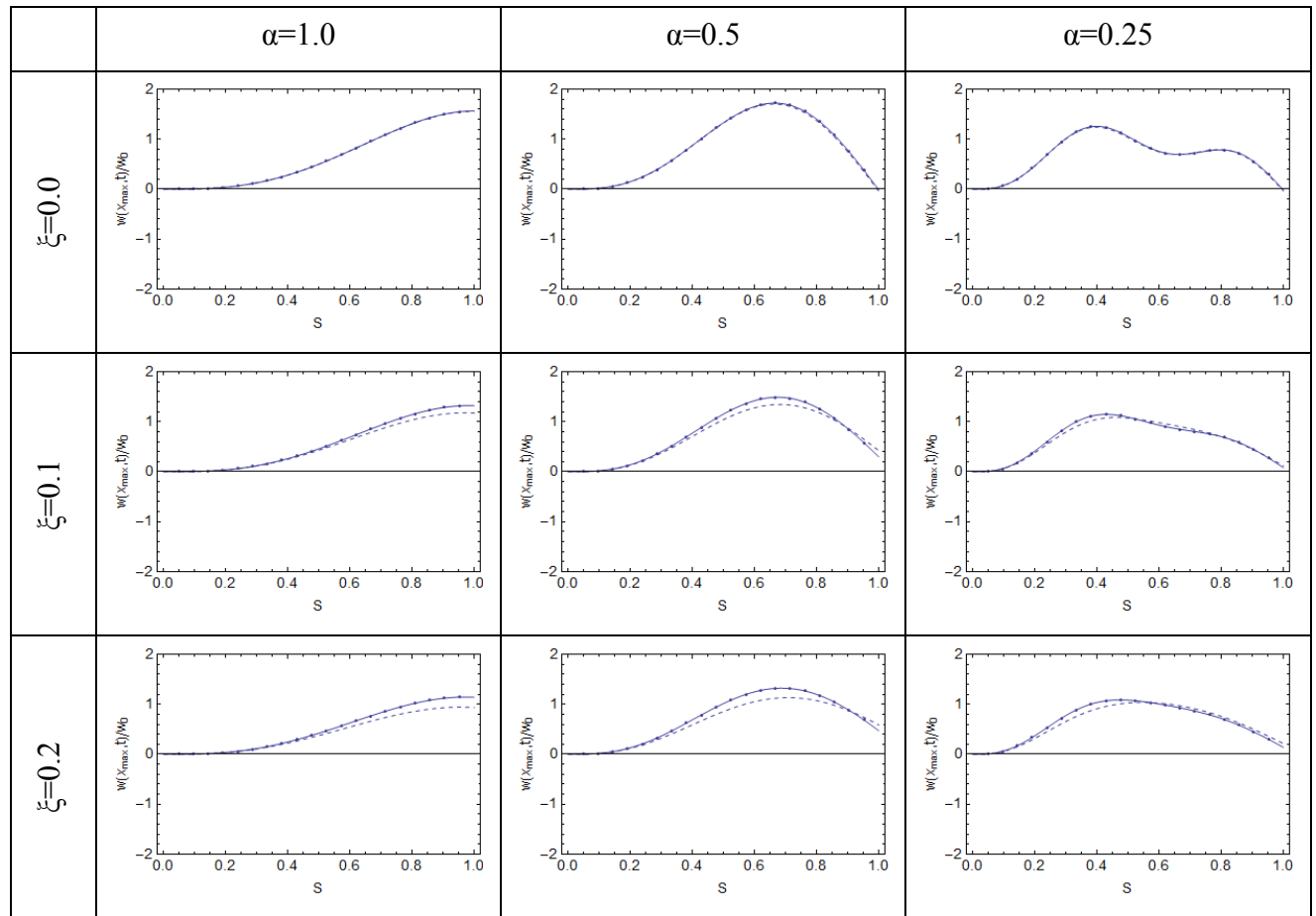


Figure 2: Dynamic response of the beam under moving constant magnitude load with constant velocity
 Ticked Line(Timoshenko Beam), Dashed Line(Euler-Bernoulli Beam)

3.1.2. Linearly Increasing Load Case

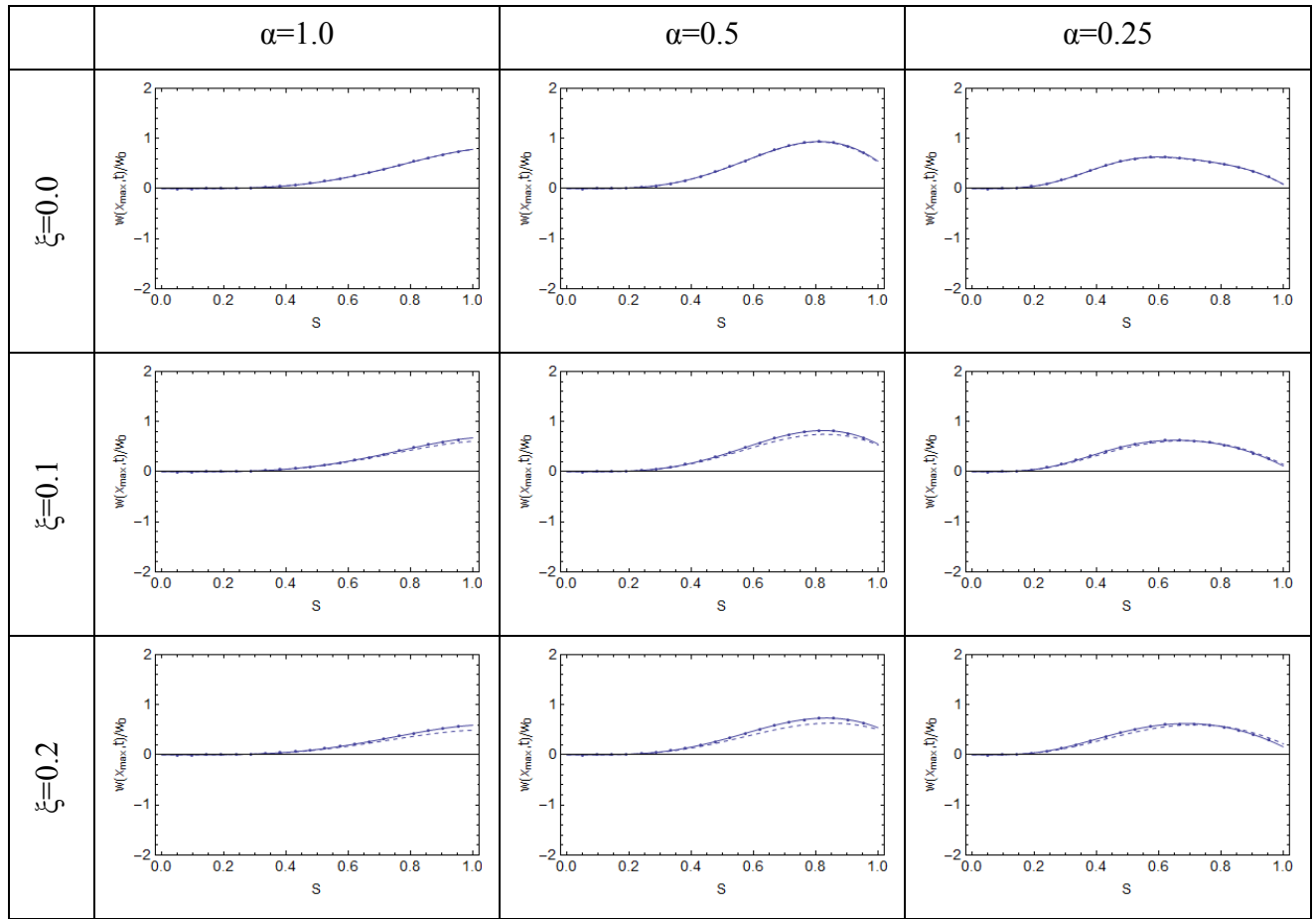
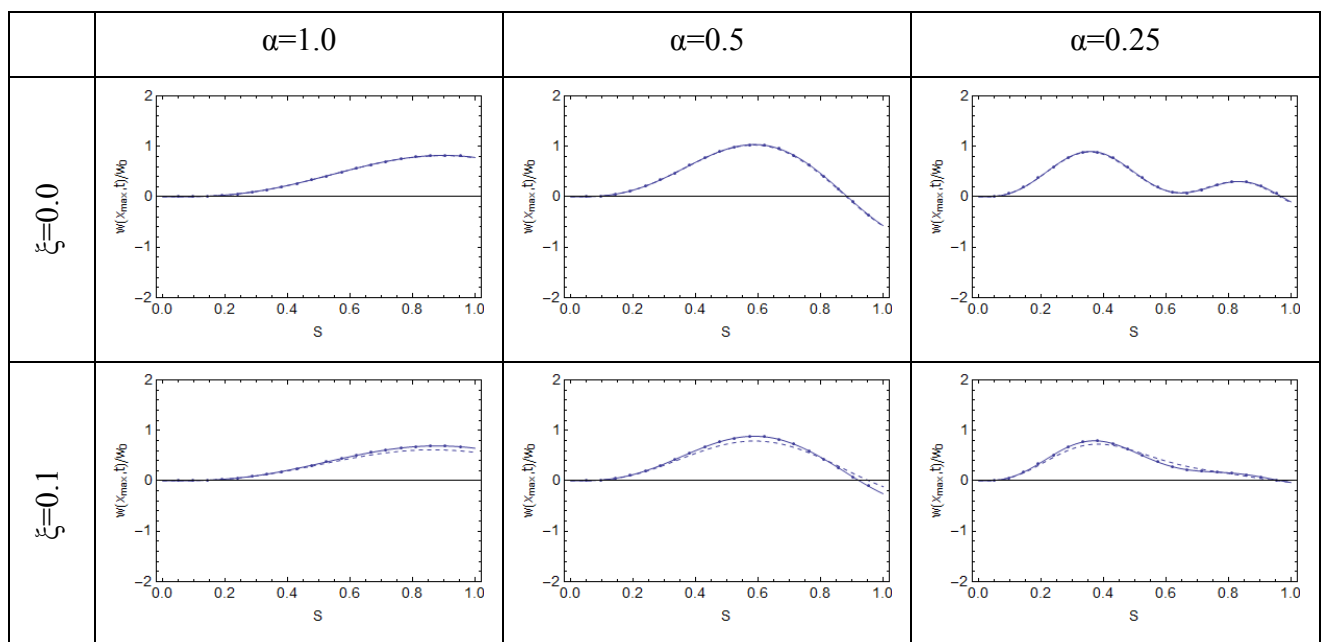


Figure 3: Dynamic response of the beam under moving linearly increasing magnitude load with constant velocity

Ticked Line(Timoshenko Beam), Dashed Line(Euler-Bernoulli Beam)

3.1.3. Linearly Decreasing Load Case



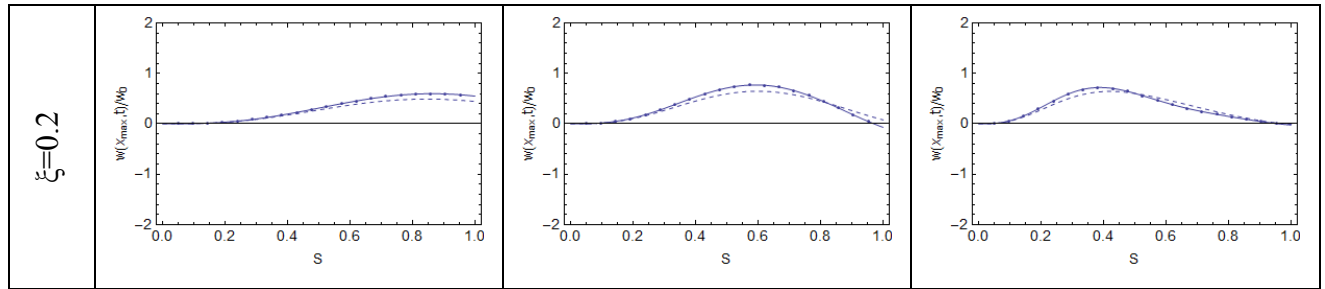


Figure 4: Dynamic response of the beam under moving linearly decreasing magnitude load with constant velocity

Ticked Line(Timoshenko Beam), Dashed Line(Euler-Bernoulli Beam)

3.2 Accelerated Motion with All Force Cases

3.2.1. Constant Load Case

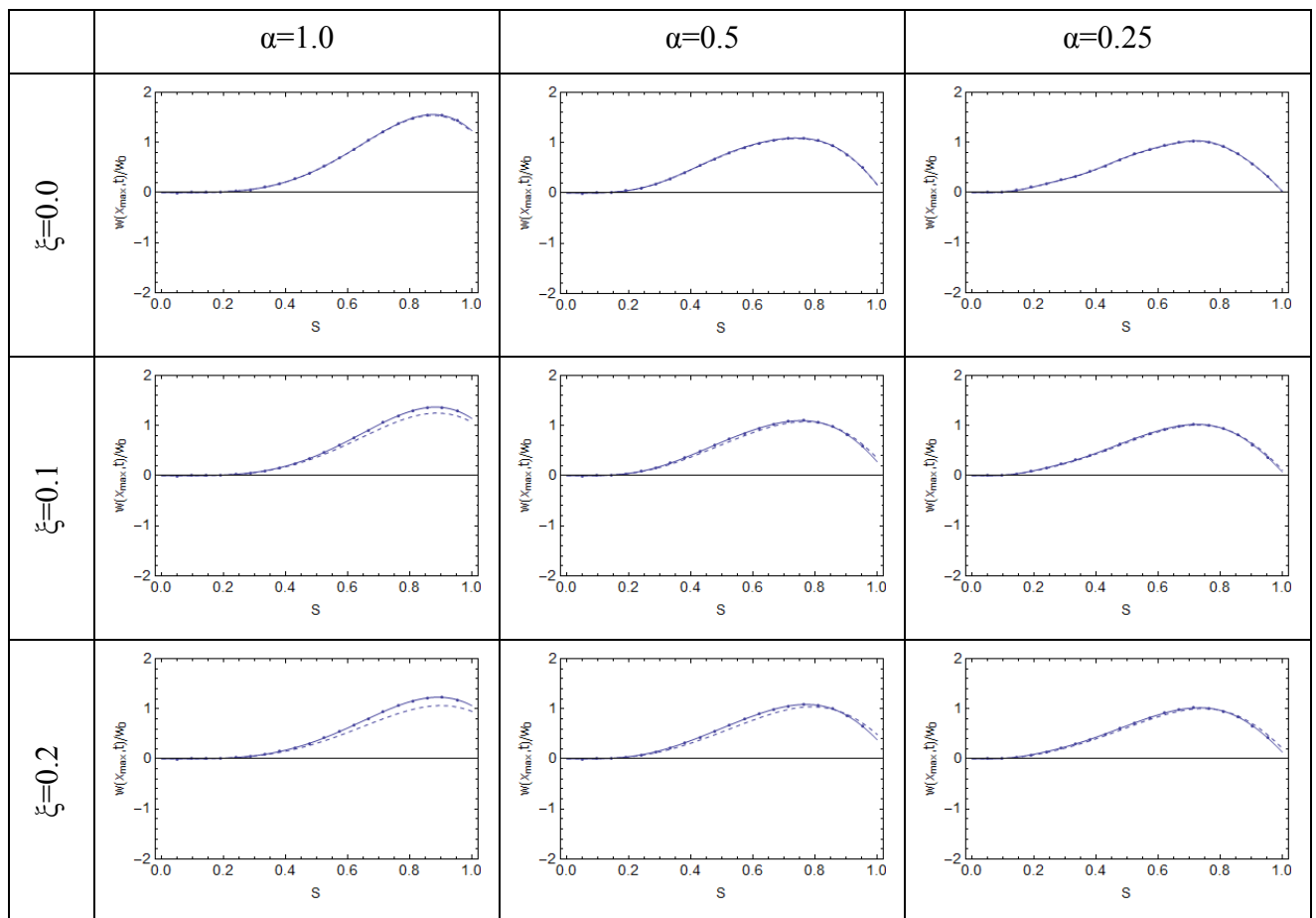


Figure 5: Dynamic response of the beam under moving constant magnitude load with accelerated motion case

Ticked Line(Timoshenko Beam), Dashed Line(Euler-Bernoulli Beam)

3.2.2. Linearly Increasing Load Case

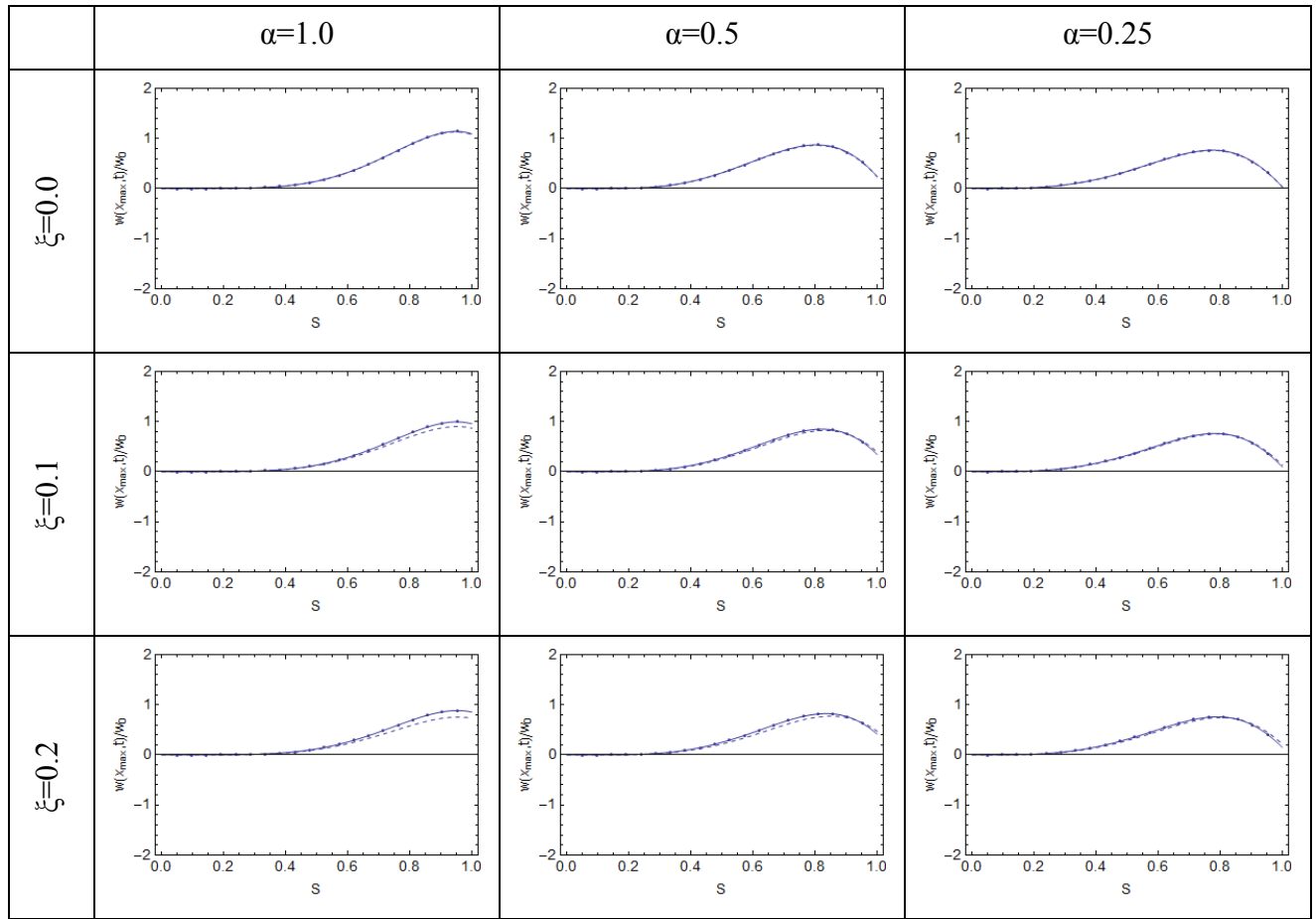
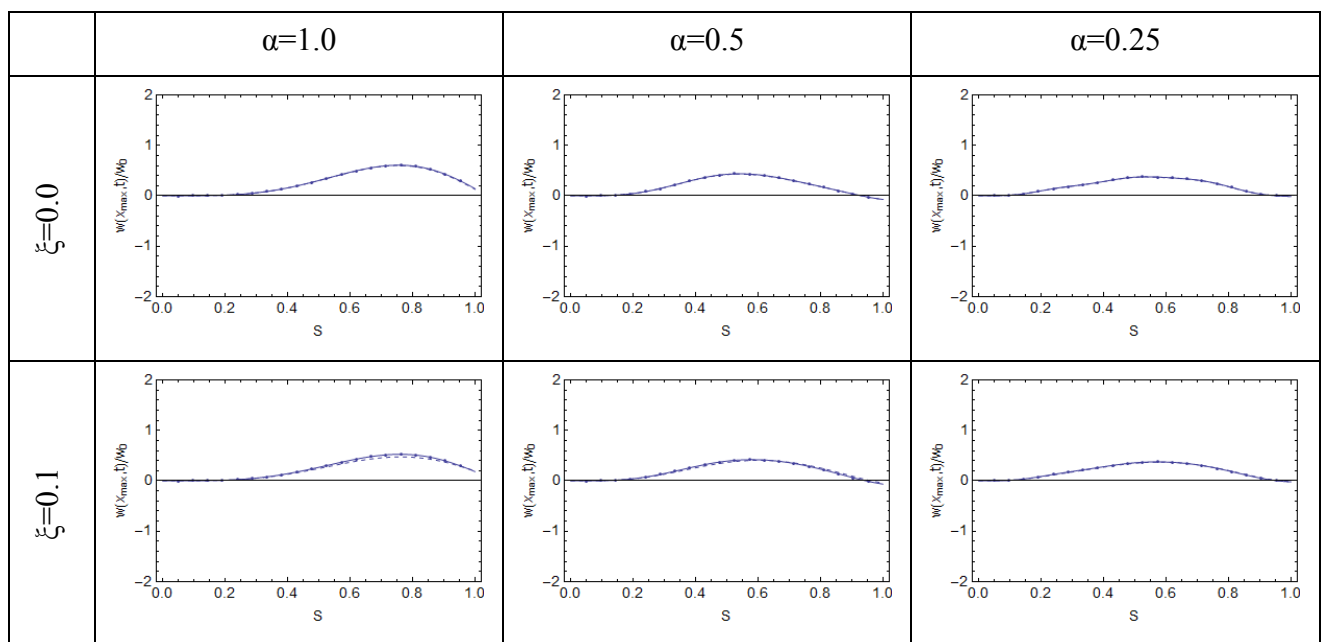


Figure 6: Dynamic response of the beam under moving linearly increasing magnitude load with accelerated motion case

Ticked Line(Timoshenko Beam), Dashed Line(Euler-Bernoulli Beam)

3.2.3. Linearly Decreasing Load Case



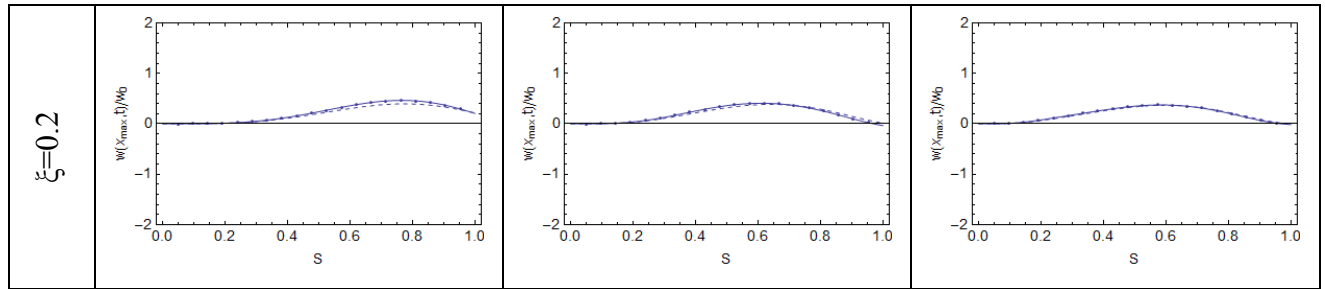


Figure 7: Dynamic response of the beam under moving linearly decreasing magnitude load with accelerated motion case

Ticked Line(Timoshenko Beam), Dashed Line(Euler-Bernoulli Beam)

3.3. Decelerated Motion with All Force Cases

3.3.1. Constant Load Case

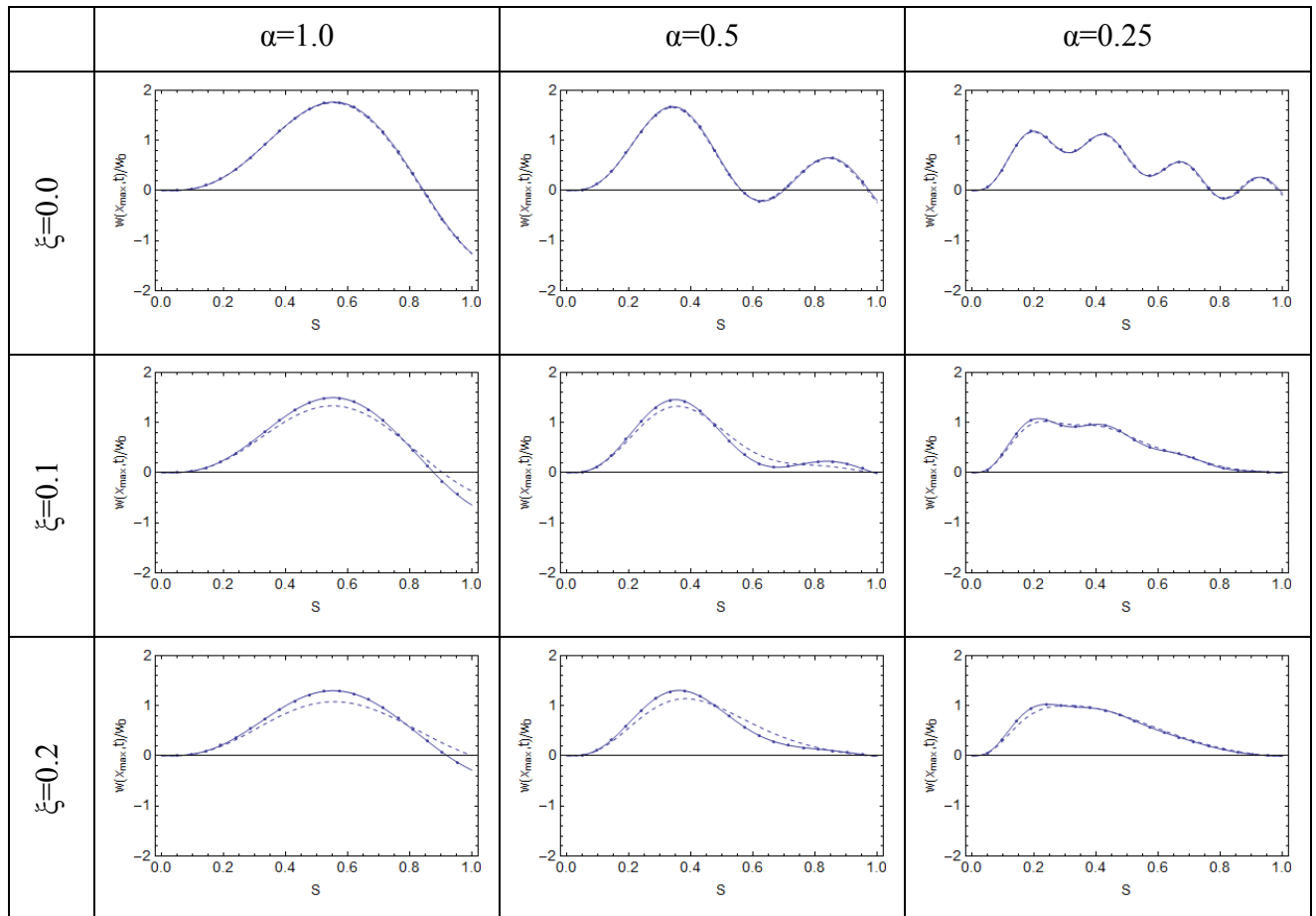


Figure 8: Dynamic response of the beam under moving constant magnitude load with decelerated motion case

Ticked Line(Timoshenko Beam), Dashed Line(Euler-Bernoulli Beam)

3.3.2. Linearly Increasing Load Case

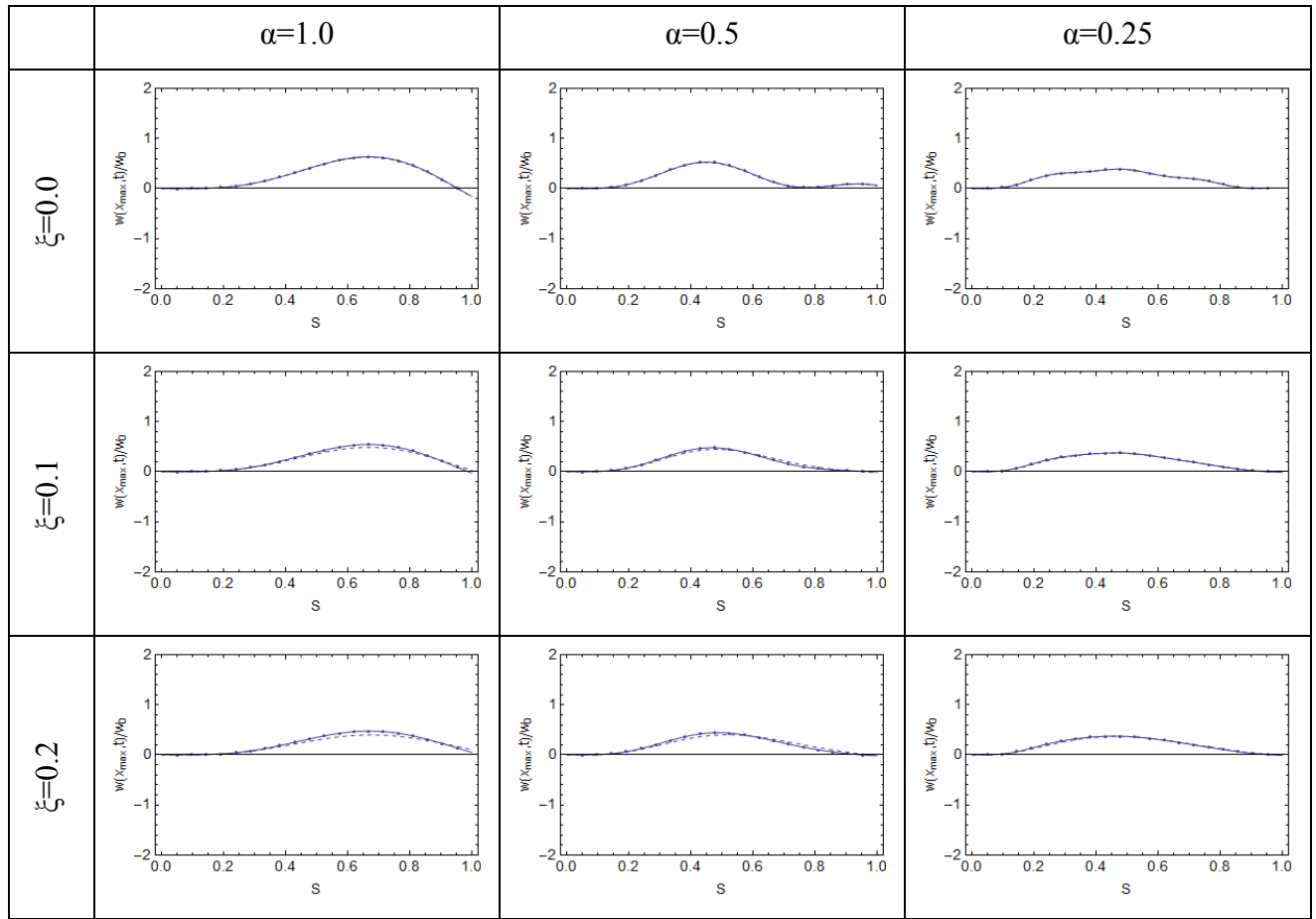
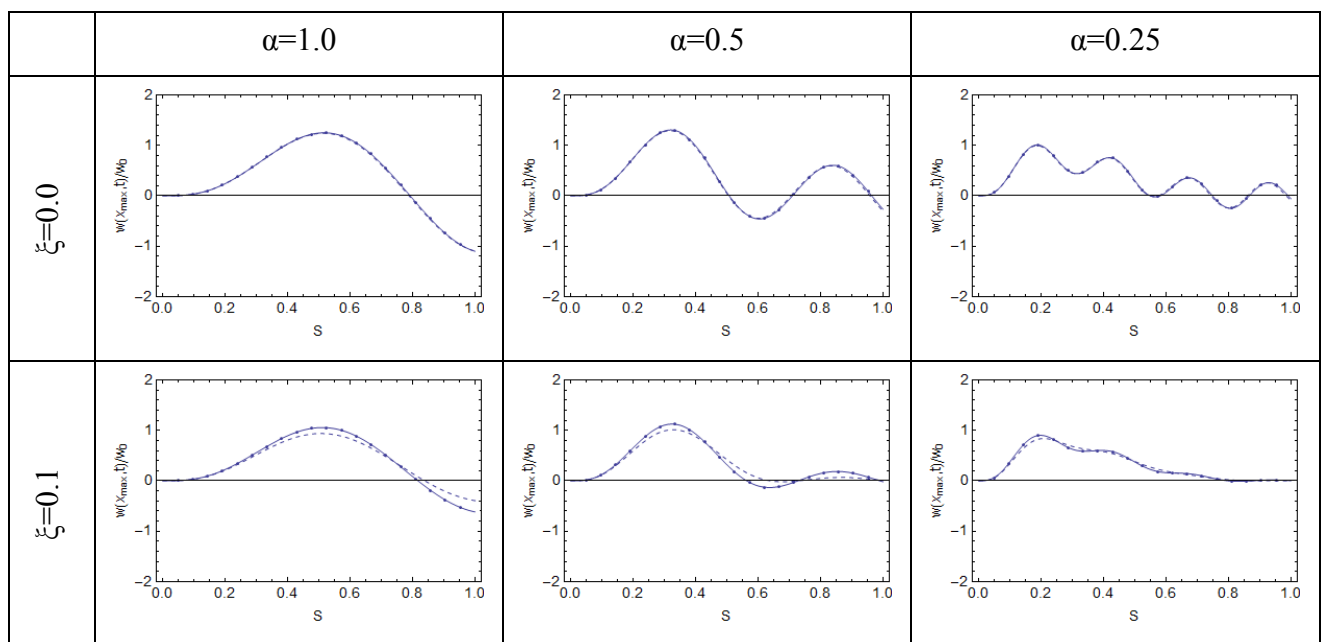


Figure 9: Dynamic response of the beam under moving linearly increasing magnitude load with decelerated motion case

Ticked Line(Timoshenko Beam), Dashed Line(Euler-Bernoulli Beam)

3.3.3. Linearly Decreasing Load Case



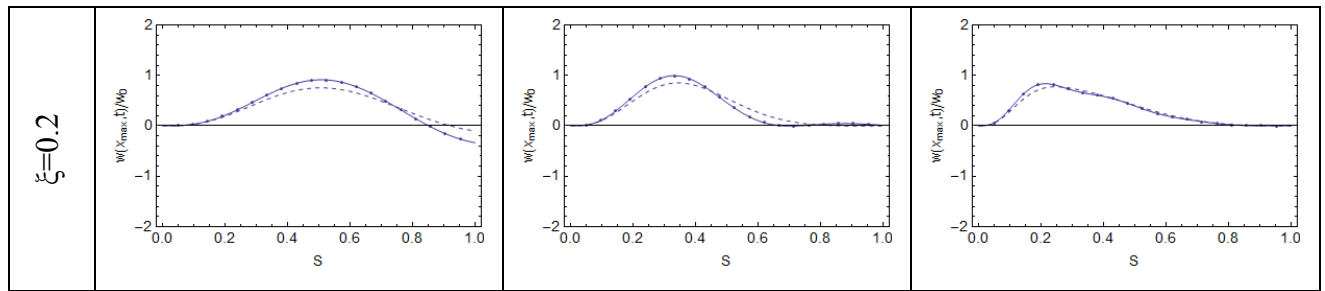


Figure 10: Dynamic response of the beam under moving linearly decreasing magnitude load with decelerated motion case

Ticked Line(Timoshenko Beam), Dashed Line(Euler-Bernoulli Beam)

4. Conclusions

In this study, the transverse vibration characteristics of Euler-Bernoulli and Timoshenko beams for constant, linearly varying magnitude moving force models with accelerating, constant velocity and decelerating motion cases are investigated. The effects of shear deformation, rotary inertia, damping and speed of the load on the vibration characteristics are presented. From the Figures 2-10, the conclusions below can be deduced:

- For all types of motion and all force cases including damping, the ratios of the maximum dynamic to maximum static deflections found by Timoshenko beam theory are higher than the ratios found by Euler-Bernoulli beam theory. This means that the moving load problem can be more critical when the shear deformation and rotary inertia effects are taken into account.
- It is verified that damping is inversely proportional to the dynamic response. On the other hand, when damping ratio is increased, the differences in the response of two models rise. It shows that Timoshenko beam theory based mathematical models are stiffer than Euler-Bernoulli based ones in terms of transverse vibration.
- The most critical situation for the moving load problem is decelerated motion with a constant magnitude load case shown in Figure 8. For $\alpha=1.0$ and $\xi=0.0$, the ratio of maximum dynamic deflection to maximum static deflection is approximately 1.8.
- It is observed that, increasing the speed of the load (increasing α) delays the time at which maximum response occurs.
- Both linearly increasing and linearly decreasing magnitude forces have an attenuating effect on the response of the beam compared to the constant magnitude force.

References

- [1] A.D. Senalp, A. Arikoglu, I. Ozkol, V.Z. Dogan “*Dynamic response of a simply-supported Euler-Bernoulli beam subjected to constant, linearly and exponentially varying moving forces*”, 4th Ankara International Aerospace Conference, Ankara, 2007
- [2] A. N. Krýlov, *Über die erzwungenen Schwingungen von gleichförmigen elastischen Stäben*, Mathematische Annalen, Vol. 61, p:211, 1905.
- [3] S. P. Timoshenko, *On the Forced Vibration of Bridges*, Philosophical Magazine, ser. 6., Vol. 43, p:1018, 1922.
- [4] A. N. Lowan, *On Transverse Oscillations of Beams under the Action of Moving Variable Loads*, Philosophical Magazine, ser. 7., Vol. 19, p:708-715, 1935.
- [5] N. G. Bondar’, *Dynamic Calculations of Beams Subjected to a Moving Load*. Issledovaniya po teorii sooruzhenii, Vol. 6, p:11-23, Stroizdat, Moscow 1954.
- [6] L. Frýba, *Vibration of Solids and Structures under Moving Loads*, ThomasTelford, 1999.
- [7] S. Mackertich, Moving load on a Timoshenko beam, Journal of Acoustical Society of America, Letters to the Editor, Vol. 88, Issue 2, 1990.
- [8] M. Abu-Hilal, and M. Mohsen, *Vibration of beams with general boundary conditions due to a moving harmonic load*, Journal of Sound and Vibration, Vol. 232, p:703-717, 2000.
- [9] M. Abu-Hilal, and H. S. Zibdeh, *Vibration analysis of beams with general boundary conditions traversed by a moving force*, Journal of Sound and Vibration, Vol. 229, p:377-388, 2000.

A New Method for Approximate Solution of Second Order Differential Equations in the Regular Singular Points

A. Salimi Shamloo ^{a, *}

^aDepartment of Mathematics, Islamic Azad University of Shabestar,
Shabestar, Iran.

Abstract

In this paper, we approximate solution of second order differential equations in the regular singular points. We first use operational matrices and then convert the problem to a system of linear equations. Numerical examples show that the approximate solutions have a good degree of accuracy.

Keywords: Piecewise constant orthogonal functions, Operational matrices, Regular singular point, Second order differential equation.

*E-Mail: ali-salimi@iaushab.ac.ir

1 Introduction

We consider the following differential equation

$$P(t)y'' + Q(t)y' + R(t)y = 0 \quad (1.1)$$

$$y'(0) = \alpha$$

$$y(0) = \beta.$$

Many different methods have been used to approximate the solution of second order differential equations in the regular singular points, such as Frobenius method and Newton method [1-2],[5-6]. In this paper, we first present the piecewise constant orthogonal functions, their properties and their operational matrices. Then we introduce second order differential equations in the regular singular points.

2 Piecewise constant orthogonal functions

Let I be the normal interval $[0, 1)$, the system of $\{\theta_i\}$ is called piecewise constant, if θ_i for $i = 1, 2, \dots, m$ be constant on each subinterval $[\frac{i-1}{m}, \frac{i}{m})$.

An m -set of Block-Pulse functions on $[0, 1)$ is defined as:

$$\beta_i(t) = \begin{cases} 1 & \frac{i-1}{m} \leq t < \frac{i}{m} \\ 0 & \text{otherwise} \end{cases} \quad (2.1)$$

for $i = 1, 2, \dots, m$.

Every function $f(t)$ which is square integrable in the interval $[0, 1)$ can be expanded in terms of Block-Pulse functions series as

$$\sum_{i=1}^m f_i \beta_i(t) \quad (2.2)$$

where, $f_i = \int_0^1 f(t) \beta_i(t) dt$. Equation (2.2), can be written as $\vec{f}^T = \vec{C}^T B_m$ where, \vec{f}^T is the discrete form of the continuous function, $f(t)$ and \vec{C}^T is called the wavelet coefficient. They are both column vectors, and B_m is the Block-Pulse matrix and is defined by

$$B_m = [\vec{b}_1^T, \vec{b}_2^T, \dots, \vec{b}_m^T] \quad (2.3)$$

where $\vec{b}_1^T, \vec{b}_2^T, \dots, \vec{b}_m^T$ are discrete form of the Block-Pulse bases; the discrete values are taken from the continuous curves $\beta_1(t), \beta_2(t), \dots, \beta_m(t)$, respectively (a one-to-one correspondence between piecewise constant orthogonal functions and vectors in R^m can be defined [4]).

Note: In the following sections we will not use the vector symbols for simplicity.

3 Operational matrices

3.1 Integral operational matrices

Consider $\int_0^t f(u)du$ and (2.2). This integral can be approximated as $\int_0^t f(u)du \simeq \int_0^t \underline{f}^T B_m(u)du$ with $\underline{f}^T = [f_1, f_2, \dots, f_m]$ and

$$B_m(t) = \begin{bmatrix} \beta_1(t) \\ \beta_2(t) \\ \vdots \\ \beta_m(t) \end{bmatrix}. \quad (3.1)$$

The first four Block-Pulse functions can be expressed as follows:

$$\beta_1(t) = [1 \quad 0 \quad 0 \quad 0]$$

$$\beta_2(t) = [0 \quad 1 \quad 0 \quad 0]$$

$$\beta_3(t) = [0 \quad 0 \quad 1 \quad 0]$$

$$\beta_4(t) = [0 \quad 0 \quad 0 \quad 1].$$

For example, if $f(t) = [5 \quad 1 \quad 7 \quad 2]$ is piecewise constant, then $f(t) = 5\beta_1(t) + 1\beta_2(t) + 7\beta_3(t) + 2\beta_4(t) = C^T B_4(t)$ where

$$B_4(t) = \begin{bmatrix} \beta_1(t) \\ \beta_2(t) \\ \beta_3(t) \\ \beta_4(t) \end{bmatrix} = \begin{bmatrix} 1 & 0 & 0 & 0 \\ 0 & 1 & 0 & 0 \\ 0 & 0 & 1 & 0 \\ 0 & 0 & 0 & 1 \end{bmatrix} = I.$$

In general

$$B_m(t) = \begin{bmatrix} \beta_1(t) \\ \beta_2(t) \\ \vdots \\ \beta_m(t) \end{bmatrix} = \begin{bmatrix} 1 & 0 & 0 & 0 \\ 0 & 1 & 0 & 0 \\ \vdots & \vdots & \vdots & \vdots \\ 0 & 0 & 0 & 1 \end{bmatrix} = I. \quad (3.2)$$

Since \underline{f}^T in $\int_0^t \underline{f}^T B_m(u)du$ is constant thus we only compute $\int_0^t B_m(u)du$. The integrals of the first four Block-Pulse functions can be expressed as:

$$\int_0^t \beta_1(u)du \simeq \frac{1}{4} \begin{bmatrix} 1 & 1 & 1 & 1 \\ 2 & & & \end{bmatrix}$$

$$\int_0^t \beta_2(u)du \simeq \frac{1}{4} \begin{bmatrix} 0 & 1 & 1 & 1 \\ 2 & & & \end{bmatrix}$$

$$\int_0^t \beta_3(u)du \simeq \frac{1}{4} \begin{bmatrix} 0 & 0 & 1 & 1 \\ 2 & & & \end{bmatrix}$$

$$\int_0^t \beta_4(u)du \simeq \frac{1}{4} \begin{bmatrix} 0 & 0 & 0 & 1 \\ 2 & & & \end{bmatrix}.$$

For example, consider

$$\int_0^t \beta_1(u) du = \begin{cases} t & 0 \leq t < \frac{1}{4} \\ 1/4 & \frac{1}{4} \leq t < 1 \end{cases}$$

with $m = 4$. If we expand solution of this integral by Block-Pulse functions, then we have

$$\int_0^t \beta_1(u) du \simeq \frac{1}{8}\beta_1(t) + \frac{1}{4}\beta_2(t) + \frac{1}{4}\beta_3(t) + \frac{1}{4}\beta_4(t).$$

Then we obtain

$$\int_0^t B_4(u) du \simeq \frac{1}{4} \begin{bmatrix} \frac{1}{2} & 1 & 1 & 1 \\ 0 & \frac{1}{2} & 1 & 1 \\ 0 & 0 & \frac{1}{2} & 1 \\ 0 & 0 & 0 & \frac{1}{2} \end{bmatrix} \begin{bmatrix} \beta_1(t) \\ \beta_2(t) \\ \beta_3(t) \\ \beta_4(t) \end{bmatrix} = E_\beta B_4. \quad (3.3)$$

E_β is integral operational matrix corresponding to Block-Pulse functions. In general

$$E_\beta = \frac{1}{m} \begin{bmatrix} \frac{1}{2} & 1 & \dots & 1 & 1 \\ 0 & \frac{1}{2} & \dots & 1 & 1 \\ \vdots & \vdots & \ddots & \vdots & \vdots \\ 0 & 0 & \dots & 0 & \frac{1}{2} \end{bmatrix}. \quad (3.4)$$

Note that we can also show every piecewise constant orthogonal functions by a diagonal matrix. For example, if $f(t) = [5 \ 1 \ 7 \ 2]$ is piecewise constant, then we can show it by

$$\begin{bmatrix} 5 & 0 & 0 & 0 \\ 0 & 1 & 0 & 0 \\ 0 & 0 & 7 & 0 \\ 0 & 0 & 0 & 2 \end{bmatrix}.$$

3.2 Differential operational matrices

We have $\int_0^t f'(\tau) d\tau = f(t) - f(0)$. Then

$$\underline{f}' = (E_\beta^{-1})^T (\underline{f} - f(0) \underline{u}_B^T) \quad (3.5)$$

where \underline{u}_B is the Block-Pulse functions spectrum of a unit step function. From (3.5) we have

$$\underline{f}'' = (E_\beta^{-1})^T (\underline{f}' - f'(0) \underline{u}_B^T) = (E_\beta^{-1})^T ((E_\beta^{-1})^T (\underline{f} - f(0) \underline{u}_B^T)) - f'(0) \underline{u}_B^T.$$

We suppose

$$N = (E_\beta^{-1})^T, \quad (3.6)$$

then we have

$$\underline{f}'' = N^2 \underline{f} - N^2 f(0) \underline{u}_B^T - N f'(0) \underline{u}_B^T. \quad (3.7)$$

4 Approximate Solution Of Second Order Differential Equations in the Regular Singular Points

Consider the following differential equation

$$P(t)y'' + Q(t)y' + R(t)y = 0 \quad (4.1)$$

$$y'(0) = \alpha$$

$$y(0) = \beta.$$

If in differential equation (4.1) $P(t)$ has a root t_0 and $\lim_{t \rightarrow t_0} (t - t_0) \frac{Q(t)}{P(t)} = p_0$ and $\lim_{t \rightarrow t_0} (t - t_0)^2 \frac{R(t)}{P(t)} = q_0$ exist, t_0 is called regular singular point.

Theorem 4.1. *If t_0 be an ordinary point of equation (4.1), that is $\frac{Q(t)}{P(t)}$ and $\frac{R(t)}{P(t)}$ be analytic at t_0 , then general solution of equation (4.1) has the form $y(t) = \sum_{n=0}^{\infty} a_n(t - t_0)^n$.*

Proof. See [1]. □

Theorem 4.2. *If $t_0 = 0$ be a regular singular point of equation $t^2y'' + t[tp(t)y'] + [t^2q(t)]y = 0$, that is $tp(t)$ and $t^2q(t)$ be analytic at t_0 , that is $tp(t) = \sum_{n=0}^{\infty} p_n t^n$, $t^2q(t) = \sum_{n=0}^{\infty} q_n t^n$ and $\lim_{t \rightarrow t_0} (t - t_0) \frac{Q(t)}{P(t)} = p_0$ and $\lim_{t \rightarrow t_0} (t - t_0)^2 \frac{R(t)}{P(t)} = q_0$ and r_1 and r_2 be the roots of equation*

$$r(r - 1) + p_0 r + q_0 = 0$$

then general solution of equation $t^2y'' + t[tp(t)y'] + [t^2q(t)]y = 0$ is one of the following forms:

1) *If $r_1 - r_2 \in \mathbb{Z}$ or $r_1 - r_2 \neq 0$, then $y_1 = |t|^{r_1} [1 + \sum_{n=1}^{\infty} a_n t^n]$ and $y_2 = |t|^{r_2} [1 + \sum_{n=1}^{\infty} b_n t^n]$*

2) *If $r_1 = r_2$, then $y_1 = |t|^{r_1} [1 + \sum_{n=1}^{\infty} a_n t^n]$ and $y_2 = y_1 \ln |t| + |t|^{r_2} \sum_{n=1}^{\infty} b_n t^n$*

3) *If $r_1 - r_2 \in \mathbb{N}$, then $y_1 = |t|^{r_1} [1 + \sum_{n=1}^{\infty} a_n t^n]$ and $y_2 = c y_1 \ln |t| + |t|^{r_2} [1 + \sum_{n=1}^{\infty} b_n t^n]$.*

Proof. See [1]. □

Theorem 4.3. *If y_1 be a solution of equation $y'' + P_1(t)y' + P_2(t)y = 0$, then other linear independent solution of equation comes from $y_2 = y_1 \int \frac{1}{y_1^2} e^{\int P_1(t) dt} dt$.*

Proof. See [1]. □

We approximate $y(t)$ by $y_m(x) = \sum_1^m y_i \beta_i(t) = \underline{y}^T B_m(t)$. We must determine y_i . Also, $P(x)$, $Q(x)$ and $R(x)$ can be show by the diagonal matrices of \underline{P} , \underline{Q} and \underline{R} . From equation (4.1) and $y_m(t) = \underline{y}^T B_m(t)$ we have:

$$\underline{P}\underline{y}'' + \underline{Q}\underline{y}' + \underline{R}\underline{y} = 0. \quad (4.2)$$

From (3.5) and (3.7) we have

$$\underline{P}(N^2 \underline{y} - \alpha N^2 \underline{u}_B^T - \beta N \underline{u}_B^T) + \underline{Q}(N \underline{y} - \alpha N \underline{u}_B^T) + \underline{R}\underline{y} = 0. \quad (4.3)$$

We suppose $A = \underline{P}N^2 + \underline{Q}N + \underline{R}$ and $b = (\alpha \underline{P}N^2 + \beta \underline{P}N + \alpha \underline{Q}N) \underline{u}_B^T$ then the coefficients $\{y_i\}$ are determined by solving the linear system

$$\underline{A}\underline{y} = b \quad (4.4)$$

where \underline{A} is an upper triangular matrix, so solving linear system (4.4) takes $O(m^3)$ operations.

4.1 Error estimation and the rate of convergence

If $y(t)$ is approximated by $y_m(t) = \sum_1^m y_i \beta_i(t)$ and we find \underline{y}_i (\underline{y}_i is approximation of y_i and $\underline{y} = \sum_1^m \underline{y}_i \beta_i(t)$), then for $t \in [\frac{i-1}{m}, \frac{i}{m}]$ we have

$$\begin{aligned} \|\underline{y}_i \beta_i - y(t)\| &= \|\underline{y}_i \beta_i - y(t) - y_i \beta_i + y_i \beta_i\| \\ &\leq \|y_i \beta_i - y(t)\| + \|\underline{y}_i \beta_i - y_i \beta_i\|. \end{aligned} \quad (4.5)$$

From [3] we have

$$\|y_i \beta_i - y(t)\| \leq \frac{1}{2\sqrt{3}m} \|y'\|_\infty, \quad t \in [\frac{i-1}{m}, \frac{i}{m}]. \quad (4.6)$$

We have

$$\begin{aligned} \|\underline{y}_i \beta_i - y_i \beta_i\| &= \left(\int_{\frac{i-1}{m}}^{\frac{i}{m}} (\underline{y}_i \beta_i - y_i \beta_i)^2 dt \right)^{1/2} \\ &= |\underline{y}_i - y_i| \left(\int_{\frac{i-1}{m}}^{\frac{i}{m}} (1)^2 dt \right)^{1/2} = \frac{|\underline{y}_i - y_i|}{\sqrt{m}} \leq \frac{\|\underline{y} - y\|_\infty}{\sqrt{m}} \end{aligned} \quad (4.7)$$

Then from (4.5), (4.6) and (4.7) we found following error bound

$$\|\underline{y}_i \beta_i - y(t)\| \leq \frac{1}{2\sqrt{3}m} \|y'\|_\infty + \frac{\|\underline{y} - y\|_\infty}{\sqrt{m}}, \quad t \in [\frac{i-1}{m}, \frac{i}{m}]. \quad (4.8)$$

We have from (4.8), $\lim_{m \rightarrow \infty} \underline{y}(t) = y(t)$. For the error estimation we consider

$$\underline{A}\underline{y} = b \quad (4.9)$$

where, y is the real wavelet coefficient of $y_m(t)$. Since \underline{A} is approximation of A , \underline{y} is approximation of y , we consider

$$\underline{A}\underline{y} = b \quad (4.10)$$

where, $\underline{A} = A + \delta A$, $\underline{y} = y + \delta y$. Then from (4.9) and (4.10) we have

$$(A + \delta A)\delta y = -\delta(A)y. \quad (4.11)$$

From (4.11) we have

$$\frac{\|y - \underline{y}\|}{\|y\|} \leq \frac{\|\delta A\|}{\|A\|} \quad (4.12)$$

5 Numerical examples

In the following examples we first find y_{m1} and then from theorem (4.3) other linear independent solution comes form $y_2 = y_{m1} \int \frac{1}{y_{m1}^2} e^{\int P_1(t)dt} dt$ where, $y_{m1}(t) = \sum_1^m \underline{y}_i \beta_i(t)$ and the real wavelet coefficient in the interval $[\frac{i-1}{m}, \frac{i}{m})$ is denoted by y_i and the estimation wavelet coefficient in the interval $[\frac{i-1}{m}, \frac{i}{m})$ is denoted by \underline{y}_i .

Example 1. Consider the differential equation

$$t^2 y'' - t^2 y' - ty = 0,$$

$$y_1(0) = 0, y_1'(0) = 1'$$

with exact solution $y_1(t) = te^t$. This problem was solved in [1]. In case $m = 16$, $\frac{\|\delta A\|}{\|A\|} = 0.0712$. Table 1 shows the numerical results for example 1 using $m = 16$.

Table 1: example(1) by m=16

i	\underline{y}_i	y_i	$ \underline{y}_i - y_i $
1	0.0331	0.0326	0.0005
2	0.1032	0.1033	0.0002
3	0.1819	0.1830	0.0011
4	0.2704	0.2726	0.0023
5	0.3695	0.3731	0.0037
6	0.4802	0.4853	0.0051
7	0.6038	0.6104	0.0066
8	0.7413	0.7498	0.0085
9	0.8940	0.9043	0.0103
10	1.0634	1.0758	0.0124
11	1.2509	1.2658	0.0148
12	1.4583	1.4757	0.0174
13	1.6871	1.7072	0.0201
14	1.9395	1.9632	0.0237
15	2.2174	2.2448	0.0274
16	2.5231	2.5536	0.0305

Example 2.

$$t^2 y'' + 2ty' + ty = 0,$$

$$y_1(0) = 1, y_1'(0) = -1/2,$$

with exact solution $y_1(t) = \sum_{n=0}^{\infty} \frac{(-t)^n}{n!(n+1)!}$. In case $m = 16$, $\frac{\|\delta A\|}{\|A\|} = 0.0711$. Table 2 shows the numerical results for example 2 .

Table 2: example(2) by m=16

i	\underline{y}_i	y_i	$ \underline{y}_i - y_i $
1	0.9845	0.9845	0.0000
2	0.9539	0.9539	0.0000
3	0.9239	0.9239	0.0000
4	0.8945	0.8946	0.0001
5	0.8658	0.8658	0.0001
6	0.8376	0.8377	0.0001
7	0.8101	0.8102	0.0001
8	0.7832	0.7832	0.0001
9	0.7568	0.7569	0.0001
10	0.7310	0.7311	0.0001
11	0.7058	0.7058	0.0000
12	0.6811	0.6811	0.0000
13	0.6570	0.6569	0.0000
14	0.6334	0.6333	0.0001
15	0.6103	0.6102	0.0001
16	0.5877	0.5875	0.0002

Example 3.

$$t^2 y'' + ty' - 2t^2 y = 0,$$

$$y_1(0) = 1, y_1'(0) = 0,$$

with exact solution $y_1(t) = \sum_{n=0}^{\infty} \frac{(\frac{t^2}{2})^n}{(n!)^2}$. In case $m = 16$, $\frac{\|\delta A\|}{\|A\|} = 0.0711$. Table 3 shows the numerical results for example 3 .

Table 3: example(3) by m=32

i	\underline{y}_i	y_i	$ \underline{y}_i - y_i $
1	0.9922	1.0007	0.0085
2	0.9858	1.0046	0.0188
3	0.9913	1.0124	0.0211
4	1.0016	1.0242	0.0227
5	1.0162	1.0401	0.0239
6	1.0351	1.0601	0.0250
7	1.0583	1.0844	0.0262
8	1.0858	1.1131	0.0273
9	1.1179	1.1464	0.0285
10	1.1547	1.1844	0.0297
11	1.1964	1.2274	0.0310
12	1.2432	1.2757	0.0325
13	1.2955	1.3295	0.0340
14	1.3535	1.3892	0.0357
15	1.4176	1.4550	0.0375
16	1.4881	1.5275	0.0394

References

1. W. E. Boyce and R. C. DiPrima, *Elementary Differential Equations and Boundary Value Problems*, John Wiley and Sons, 1977.
2. S. L. Ross, *Diferential equations* Xerox, 2d. Ed., 1974.
3. Canti Prasada Rao, *Piecewise Constant Orthogonal Functions and Their Application to Systems and Control*, Springer-Verlag, 1983.
4. E. Aboufadel and S. Schlicker, *Discovering Wavelets*, John Wiley and Sons, Inc, (1999).
5. J. Stoer and R. Bulirsch, *Introduction to Numerical Analysis*, Springer-Verlag New York, Inc, (2002).
6. D. Kincaid and W. E. Cheney, *Numerical Analysis Mathematics of Scientific Computing*, Published by Brooks/Cole Third Edition, 2002.

Finite Element Analysis of Disk Brake Squeal Phenomenon

N. Tolou, M. H. Hojjati¹

Mechanical Engineering Department, Mazandaran University, P. O. Box 484, Babol, Iran

Abstract

Friction-induced oscillations occur in many engineering systems, often resulting in noise, vibration, and excessive or uneven wear. This paper deals with a numerical modeling of such self excited oscillations in high frequency range, called squeal in the disk brake of a passenger vehicle. Nonlinear static and then modal analyses have been performed using a commercially available finite element package to study the squeal phenomenon occurring in disk brakes. The results illustrate that an increase in friction coefficient and hydraulic pressure will amplify the squeal propensity. An opposite effect was observed for angular velocity. Moreover, finite element modeling of only the disk and one pad is shown to be capable to analysis the brake squeal propensity instead of full disk brake system modeling.

Keywords: Friction-induced oscillations; Disk brake squeal; Finite element method (FEM)

1. Introduction

Disk brakes had been invented by F. W. Lanchester in 1902 in England, but it was only in 1961 that this type of brake was introduced by Teves in Germany in mass production in a passenger car and begun its triumphal march in passenger cars [1]. Today, disk brakes are standard in this type of automobile. Engine power has increased considerably during the last decades and since the power to be dissipated in a brake can be several times than that of the engine, so did the forces acting at the brake. The geometric space available for the brakes in a car is however rather limited and constrained by the dimensions of the wheel, so that new forms of brake design had to be developed and some of these new designs were more susceptible to generate unwanted noises.

Brake squealing noise is a key element of city environmental pollution in this decade. The main concern over the squeal problem is that it can cause discomfort to passengers and pedestrians and, hence, reduce the overall acceptability of the vehicle [2]. Customer complaints result in significant warranty costs yearly. Furthermore, customer dissatisfaction can cause a loss of future business. Thus, eliminating squeal becomes one of the top priorities in current brake development [2].

Brake squeal is commonly defined as a sustained, high frequency noise due to vibrations of the braking components of a vehicle during a braking action. There are three types of brake noise, depending on the frequency range [3-6]: brake “judder” (<100 Hz), brake “groan” (100 – 1000 Hz), and brake “squeal” (1 – 16 kHz), the latter being the focus of this work. From many experimental observations, it is known that squeal usually occurs at slow rotational speeds (around 0.1-1 Hz or 6-60 rev/min or 0-10 km/h) towards the end of a stop [3].

¹ Corresponding author, Associate Professor, hojjati@nit.ac.ir, Fax: +98 111 3234201

Physically, squeal noise occurs when the friction coupling between the rotor and pad creates a dynamic instability and this leads to vibration of the structure [2]. The phenomenon is also known to be associated with geometrically-induced instability where a small perturbation can grow exponentially into audible noise [2].

The different mechanisms of friction-induced vibration fall into four classes: stick-slip [4], variable dynamic friction coefficient [5], sprag-slip [6] and geometric coupling of degrees of freedom [7]. In this study, we will consider the latter two approaches that use modal coupling to develop instability when the friction coefficient is constant by the numerical method.

There are two main categories of numerical methods that are used to study this problem: (1) transient dynamic analysis and (2) complex eigenvalue analysis. Currently the complex eigenvalue method is preferred and widely used in predicting the squeal propensity of the brake system including damping and contact, since the transient dynamic analysis is computationally expensive [8–12]. The main idea of the complex eigenvalue method involves symmetry arguments of the stiffness matrix and the formulation of a friction coupling. This method is more efficient and provides more insight to the friction-induced dynamic instability of the disc brake system [12].

In the present study, an investigation of disc brake squeal is performed by using the new complex eigenvalue capability of a commercial finite element (FE) software [13]. This FE method uses nonlinear static analysis to calculate the friction coupling prior to the complex eigenvalue extraction, as opposed to the direct matrix input approach that requires the user to tailor the friction coupling to stiffness matrix. Thus, the effect of non uniform contact and other nonlinear effects are incorporated. Since the critical aspect in the generating disk brake squeal and other friction-induced oscillations system is the coupling between friction components, this paper deals with modeling of rotor and one pad, particularly the rotor/pad (frictional) interface. Then, some illustrating examples have been used in order to assess the effects of the friction coefficient, hydraulic pressure and angular velocity on the squeal propensity. The present method may also be applied to other complex nonlinear dynamics system.

2. Theoretical background

The method used in this work is in fact a procedure to determine the complex eigenvalues and corresponding eigenvectors of the systems. In order to incorporate the friction coupling into the dynamic analysis of the system, the presented method allows unsymmetrical $[K]$ and $[C]$ matrices to appear into the equation of the motion. Therefore, orthogonal coordinate transformation of the system matrices to reduce the eigen problem into the modal subspace is firstly applied. QR algorithm as described in [13] is then used to calculate eigenvalues of the resulting quadratic eigenvalue problem in the modal subspace.

The equations of elastic structural systems without external excitation can be written in the following abstract form:

$$[M]\{\ddot{u}\} + [C]\{\dot{u}\} + K\{u\} = \{0\} \quad (1)$$

It has been recognized that performing computations in the modal subspace is more efficient than in the full eigen space. The stiffness matrix $[K]$ can be symmetrized by rearranging the unsymmetric contributions; that is, the original stiffness matrix $[K]$ can be divided into symmetric and unsymmetric parts. By dropping the damping matrix $[C]$ and the unsymmetric

contributions of $[K]$, the symmetric eigenvalue problem is first solved to find real eigenvalues and the corresponding eigenvectors. In the present implementation, the unsymmetric element stiffness matrix is zeroed out for this eigenvalue extraction. The next step is the coordinate transformation as defined by the following equation used to transform the full eigen problem into modal subspace [14]:

$$\{u\} = \sum_{i=1}^n \{\Phi_i\} y_i \quad (2)$$

$$\{u\} = [\Phi] \{y\} \quad (3)$$

where $[\Phi]$ is the eigenvector matrix which is normalized with respect to the mass matrix $[M]$ and $\{y\}$ is vector of modal coordinates.

By using Eq (3) in Eq (1), we can write the differential equations of motion in the modal subspace as follows:

$$[I]\{\ddot{y}\} + [\Phi]^T [C] [\Phi] \{\dot{y}\} + ([\Lambda^2] + [\Phi]^T [K_{unsym}] [\Phi]) \{y\} = \{0\} \quad (4)$$

Where $[\Lambda^2]$ is a diagonal matrix containing the first n eigen frequencies ω_i .

For classically damped systems, the modal damping matrix $[\Phi]^T [C] [\Phi]$ is a diagonal matrix with the diagonal terms being $2\xi_i \omega_i$, where ξ_i is the damping ratio of the i -th mode. For non-classically damped systems, the modal damping matrix is either symmetric or unsymmetric. Unsymmetric stiffness contributions of the original stiffness are projected onto the modal subspace to compute the reduced unsymmetric modal stiffness matrix:

$$[\Phi]^T [K_{unsym}] [\Phi] \quad (5)$$

Introducing the $2n$ -dimensional state variable vector approach, Eq (4) can be written in reduced form as follows:

$$[I]\{\dot{Z}\} = [D]\{Z\} \quad (6)$$

where

$$\{Z\} = \begin{Bmatrix} \{y\} \\ \{\dot{y}\} \end{Bmatrix} \quad (7)$$

$$D = \begin{bmatrix} 0 & I \\ -[\Lambda^2] - [\Phi]^T [K_{unsym}] [\Phi] & -[\Phi]^T [C] [\Phi] \end{bmatrix} \quad (8)$$

The $2n$ eigenvalues of Eq (6) are calculated using the QR algorithm [15]. The inverse iteration method [16] is used to calculate the complex modal subspace eigenvectors. The full complex eigenvectors, $\{\psi\}$, of original system is recovered using the following equation:

$$\{\Psi\} = [\Phi][Z] \quad (9)$$

At last, the undamped eigenvalues and eigenvectors based on the symmetric $[K]$ matrix are calculated. Damping and the unsymmetric $[K]$ portion are then included in the modal equations. If one writes the equations in the modal subspace (using a reduced form), the following is obtained [13]:

$$\begin{bmatrix} 0 & I \\ I & \Phi^T C \Phi \end{bmatrix} \begin{Bmatrix} \ddot{y} \\ \dot{y} \end{Bmatrix} + \begin{bmatrix} -I & 0 \\ 0 & \Lambda^2 + \Phi^T K_{unsym} \Phi \end{bmatrix} \begin{Bmatrix} \dot{y} \\ y \end{Bmatrix} = \begin{Bmatrix} 0 \\ 0 \end{Bmatrix} \quad (12)$$

In order to see how friction coupling produce K_{unsym} and it influences Eq. (12), as an illustrating example, the simple case of two nodes, in element coordinates and separation of normal and sliding DOF is assumed. If $F_s < \mu F_n$, then the resulting stiffness matrix is as follows:

$$K = \begin{bmatrix} K_s & 0 & -K_s & 0 \\ 0 & K_s & 0 & -K_s \\ -K_s & 0 & K_s & 0 \\ 0 & -K_s & 0 & 0 \end{bmatrix} \quad (13)$$

One can see that this matrix is symmetric. However, if $F_s = \mu F_n$, then sliding occurs, and the stiffness matrix becomes unsymmetric:

$$K = \begin{bmatrix} 0 & -\mu K_n & 0 & \mu K_n \\ 0 & K_s & 0 & -K_s \\ 0 & \mu K_n & 0 & -\mu K_n \\ 0 & -K_s & 0 & 0 \end{bmatrix} \quad (14)$$

Hence, solving the actual unsymmetric $[K]$ matrix using Eq. (12) without symmetrizing the unsymmetric $[K]$ matrix, will result to better convergence behavior and fewer total equilibrium iterations.

Theoretically, when two modes of the system coalesce (mode lock-in), they begin to keep equal frequencies for a variation of the parameter, while the real part of the eigenvalues moves opposite with respect to the starting value. One of the two modes becomes unstable with a positive real part. A further variation of the parameter leads to the lockout between the two eigenvalues, the real parts return to the initial values and the imaginary parts split again with varying system parameter. Thus, if any of the eigenvalues resulting from Eq. (12) has a positive real part or damping ratio becomes negative, squeal is assumed to occur.

Note that the magnitude of the real part of the complex eigenvalue provide no insight into the magnitude of the squeal that arises. The magnitude of the real part only determines the rate of the squeal propensity. The theory may also be used to explain instabilities of other friction-induced oscillations systems.

3. Finite element modeling

A disc brake system consists of a disc that rotates about the axis of a wheel, a caliper-piston assembly where the piston slides inside the caliper which is mounted to the vehicle suspension system, and a pair of brake pads. When hydraulic pressure is applied, the piston is pushed forward to press the inner pad against the disc and simultaneously the outer pad is pressed by the calliper against the disc [17]. The brake model used in this study is a simplified model of a disc brake system that consists of a disc and a brake pad. The geometry properties of the model are assumed as Table 1. The brake pad is pressed against the disc in order to generate a friction torque to slow the disc rotation.

Table 1

Geometry and material properties and operation conditions for the finite element modeling.

Geometry properties	Pad	Rotor
Inner radius, a (m)	0.04	0.04
Outer radius, b (m)	0.17	0.17
Starting Angel (degrees)	0	0
Ending Angle (degrees)	60	360
Thickness, t (m)	0.005	0.005
Material properties		
Density, ρ (kgm ⁻³)	1400	7850
Poisson's ratio, ν	0.25	0.3
Elastic modulus, E (GPa)	1	200
Operation conditions		
Coefficient of friction, μ	0.5	0.5
Angular velocity, ω (rad/s)	-	1
Hydraulic Pressure, p (MPa)	0.5	-

The FE mesh of all the components of the system is generated using the ANSYS element, SOLID95. This kind of element is a three-dimensional (3D) brick element characterized by ten nodes, with three translational degrees of freedom per node to make continuum elements for the disc and pads as shown in Fig. 1, where a fine mesh is used in the contact regions. The friction contact interactions are defined for disk/pad interface. A constant friction coefficient and a constant angular velocity of the disc are used for simulation purposes. Figs. 2(a)–(b) illustrate the constraints and loadings for the pad and disc assembly. The disc is completely clamped centrally as shown in Fig. 2(a) and sides of the pads are constrained to allow only axial directional movements as shown in Figs. 2(b). The calliper–piston assembly is not defined in the simplified model of the disc brake system, hence the hydraulic pressure, which has a typical value of 0.5

MPa, is directly applied to the back of pad into nodes as shown in Figs. 2(b). The analysis procedure contains the following steps: (1) nonlinear static analysis for the application of brake pressure and impose a rotational velocity on the disc to make unsymmetric stiffness matrix; (2) QRDAMPED modal analysis for complex eigenvalue extraction to find unstable modes.

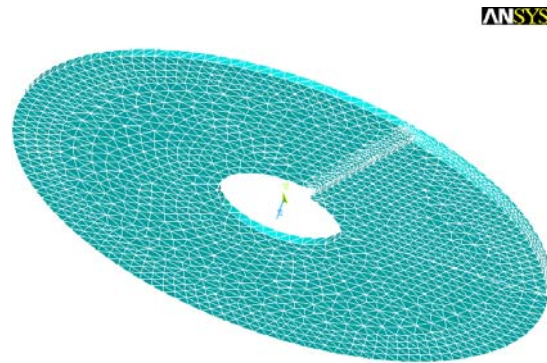


Fig. 1. Geometry and finite element mesh of the simplified disc brake system.

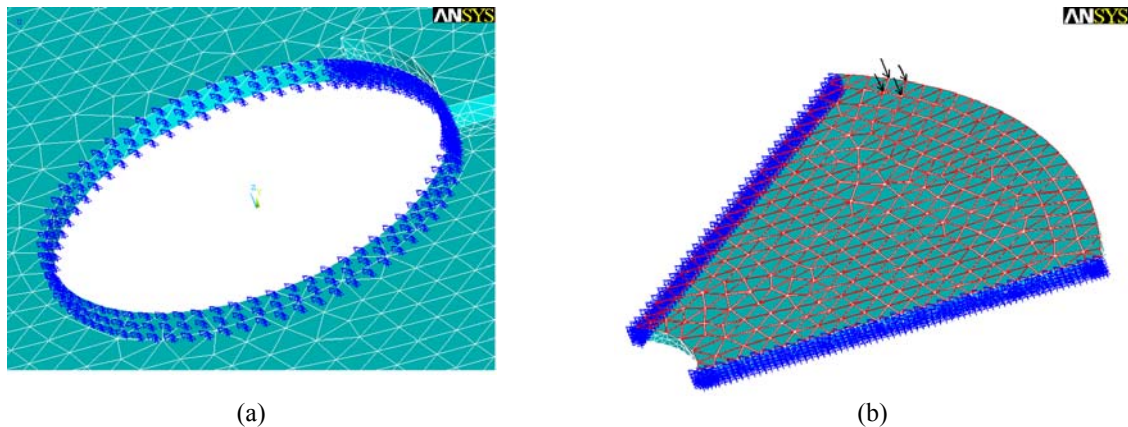


Fig. 2. Constraints and loadings of the disc brake system; (a) rotor; (b) pad.

4. Results and Discussions

The effects of the system parameters, such as the friction coefficient of the contact interactions between the pad and the disc, μ , the hydraulic pressure, P and the rotational velocity of the disc, ω on the disc squeal propensity are investigated by the simulation model. The complex eigenvalue analysis is performed up to 12 kHz which is the range of squeal occurrence for the presented disc model. As mentioned previously, if the real part of eigenvalues is positive, the system becomes unstable. When the disc system is unstable, the squeal propensity increases with an increased value of the real part (absolute values are used). For clarity, only positive values of the eigenvalue's real part are depicted. The typical values for the geometry and material properties and operation condition adopted in the computations have been previously shown in Table. 1 [10, 12]. Analysis is carried out by changing the values of each parameter while retaining the respective typical values for the others.

4.1. Unstable modes of disc brake system

The simulation results show that for all the cases with large real parts, the unstable frequencies are approximately 6.1 kHz as shown in Table. 2. There is a significant pad bending vibration for these cases. Figs. 3(a) and (b) give an example of the vibration mode of the disc brake system at a frequency of 6066 Hz, where all the system parameters are the typical values before and after instability. It can be seen that the disc has only slight out-of-plane modes of vibration but the pad have serious out-of-plane modes of vibration which occur mainly at the top and the bottom end parts of the pads as shown in Fig. 3(b), while it is not significance before instability as seen in Fig. 3(a). This suggests that the brake pad may be the source of the disc brake squeal. So, modifications aim to reduce the pad bending vibration may be used to eliminate the disc squeal.

Table 2
Eigenvalues of unstable modes

Real part	Imaginary part (Frequency)	Mode number
47.30	6066	52
42.29	6178	54
3.68	6314	56

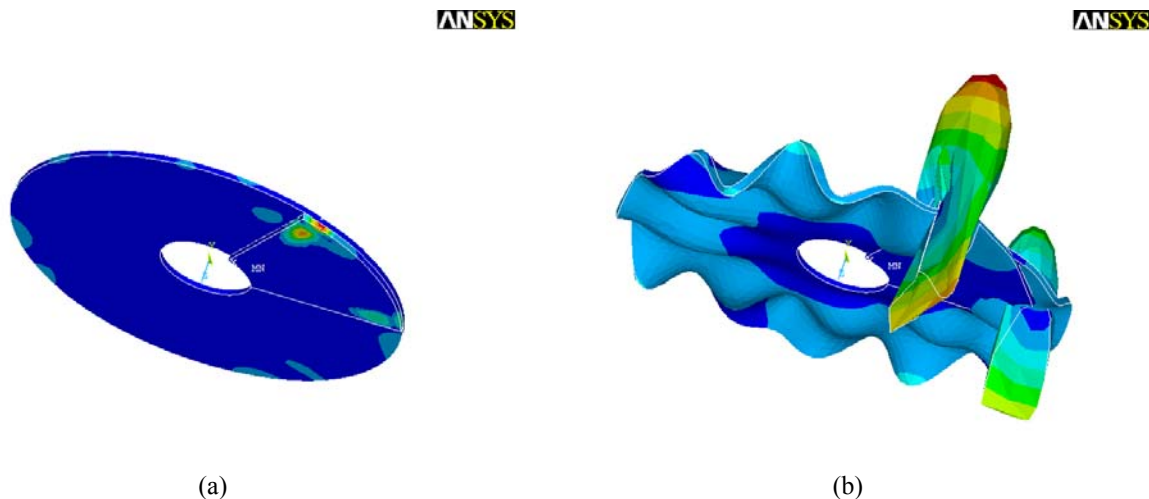


Fig. 3. Mode shape of the disc brake model at the frequency of 6.1 kHz; (a) before, (b) after instability.

4.2. Effects of friction coefficient

Disc squeal is believed to be caused mainly by friction-induced dynamic instability [4-6]. This section presents the effect of the friction coefficient of the contact interactions between the pad and the disc on the disc squeal propensity, in which the friction coefficient μ varies from 0.3 to 0.5. Fig. 4(a) shows the results in the form of the eigenvalue's real part as a function of frequency for different friction coefficients. It can be seen that the major squeal frequency is approximately 6.1 kHz. The value of the real part is decreased significantly with a decrease of the friction coefficient as shown in Fig. 4(b) for the frequency of 6066 Hz. It is clear that with an increase in the friction coefficient, there is an accompanying increase in the instability of the

system especially for $\mu = 0.4-0.5$, thus an increase in the real part of eigenvalue. This means that the most fundamental method of eliminating brake squeal is to reduce the friction between the pads and the disc. However, this obviously reduces braking performance and is not always a preferable method to employ or should need more consideration before selection. Table 3 clearly shows good agreement between the results from the presented finite element method with those of full disk brake FE model [10] and experimental results [18].

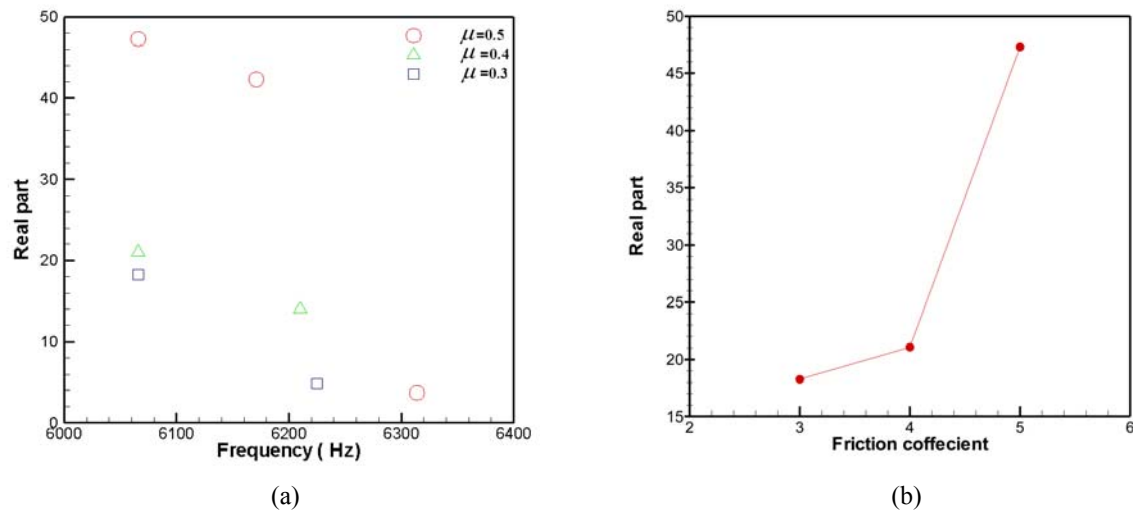


Fig. 4. (a) Variation of the real part of eigenvalue with frequency for different friction coefficient of contact region; (b) variation of the real part with friction coefficient of contact region at frequency 6.1 kHz.

Table 3

Comparison of variation of squeal propensity at different friction coefficients with respect to $\mu=0.3$ as the reference value.

Friction coefficient	0.35	0.4	0.45	0.5
Presented finite element method	16%	33%	77%	166%
Numerical results of full disk brake modeling [10]	18%	37%	63%	152%
Experimental results [18]	20%	45%	80%	160%

4.3. Effects of hydraulic pressure

The effect of the hydraulic pressure, P , on the squeal propensity is studied by varying P from 0.5 MPa to 1.5 MPa. Fig. 5(a) shows the change of the real part with respect to frequency for different hydraulic pressures. The major squeal frequency is approximately 6.1 kHz. It can be seen from Fig. 5(b) that with an increase in P , the value of the real part increases, so does the squeal propensity. This is due to the fact that a larger hydraulic pressure induces more friction

force between the pads and the disc. However, the simulation results also show that the effect of the hydraulic pressure on the disc brake squeal is not significant because the value of the real part only changes from 47.3 to 48.2 when P increases from 0.5 MPa to 1.5 MPa. As it is presented in Table 4, the obtained results are close to those of full disk brake FE model [10] and experimental results [18].

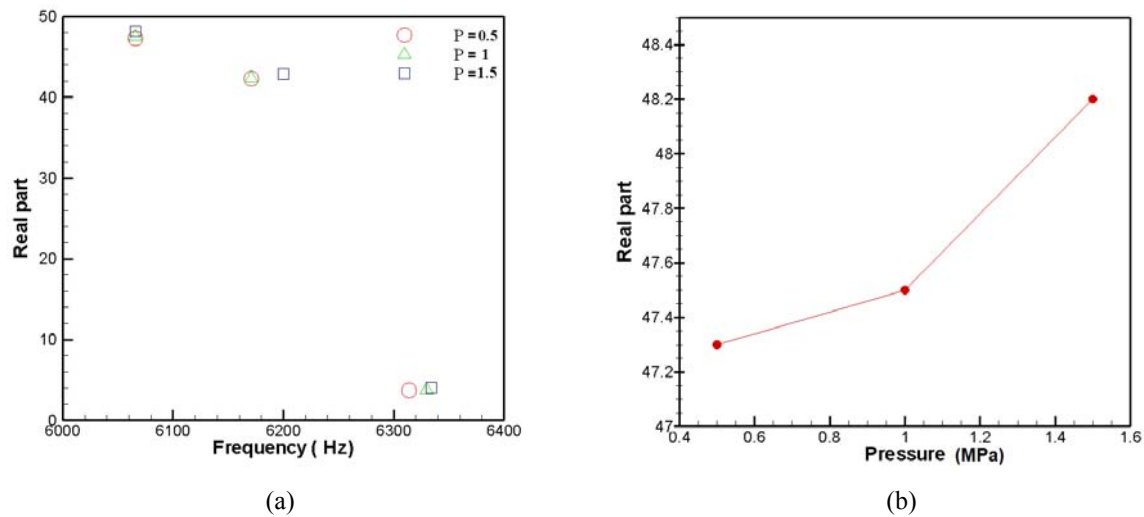


Fig. 5. (a) Variation of the real part with the frequency for different hydraulic pressure; (b) variation of the real part with the hydraulic pressure at the frequency of 6.1 kHz.

Table 4

Comparison of variation of squeal propensity at different hydraulic pressure with respect to $P=0.5$ MPa as the reference value.

Hydraulic pressure	0.7	0.9	1.1	1.3	1.5
Presented finite element method	0.17%	3.52%	5.3%	7.05%	8.82%
Numerical results of full disk brake modeling [10]	0.17%	3.52%	5.3%	7.05%	8.82%
Experimental results [18]	0.4%	4%	6%	8%	10%

4.4. Effects of rotational velocity of the disc

Fig. 6(a) presents the variation of the real part with the frequency at different disc angular velocities ω (1, 3, 6 rad/s). The dominant squeal frequency is approximately 6.1 kHz. As the angular velocity increases, the value of the real part decreases. However, as with the previous case, the effect of changing the angular velocity on the squeal propensity is also not obvious. This can be seen from Fig. 6(b) which shows that the value of the real part varies insignificantly with an increase in the rotational velocity of the disc. Table 5 shows the comparison of variation

of squeal propensity versus angular velocity for the presented finite element method, full disk brake model [10] and experimental results [18] with respect to $\omega=1 \text{ rads}^{-1}$ as the reference value. The agreement between the results is very good.

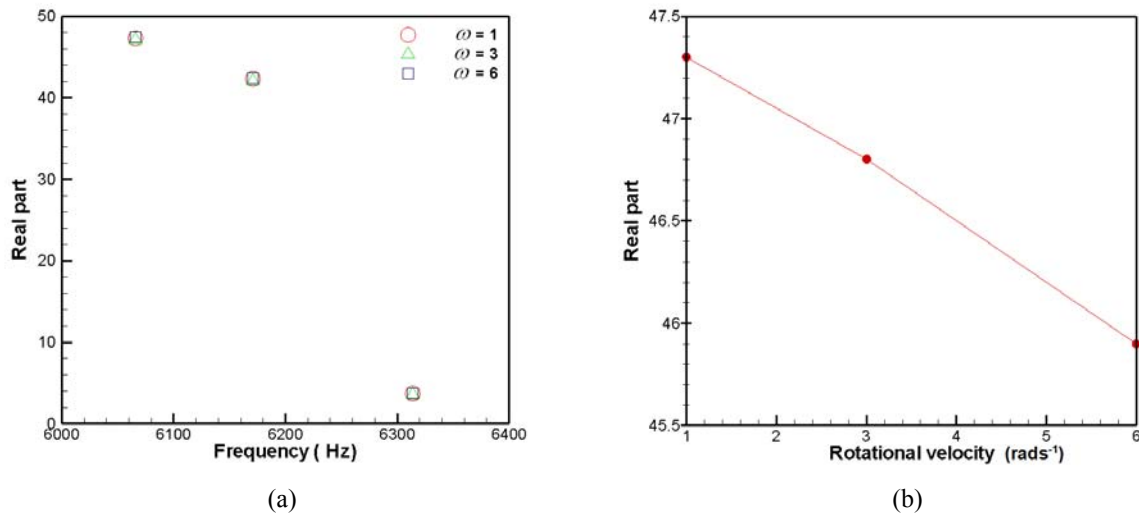


Fig. 6. (a) Variation of the real part with frequency for different rotation speeds of the disc; (b) variation of the real part with rotation speed of the disc at the frequency of 6.1 kHz.

Table 5

Comparison of variation of squeal propensity versus angular velocity for presented finite element method, full disk brake model and experimental results with respect to $\omega=1 \text{ rads}^{-1}$ as the reference value.

Angular velocity	2	3	4	5	6
Presented finite element method	-0.1%*	-1.4%	-1.9%	-2.9%	-4%
Numerical results of full disk brake modeling [10]	-0.13%	-2%	-3%	-4%	-5%
Experimental results [18]	-0.1%	-2%	-1%	-3%	-6%

* A negative value means reduction in squeal propensity

5. Conclusions

Finite element analysis of friction-induced disc brake squeal is investigated using the new function of commercially finite element (FE) software, the QRDAMPED method that allows using unsymmetrical matrix created in previous analysis by friction force to calculate the complex eigenvalue. The systematic analysis here shows that significant pad bending vibration may be responsible for causing the disc brake squeal and the major squeal frequency is approximately 6.1 kHz for the present disc brake system. An increase in friction coefficient

results to significant increase in instability and the effects of the friction between the pads and the disc on disc squeal is significant. Also, increase in pressure and decrease in angular velocity result in negligible increase of instability and therefore in squeal propensity. Therefore, the design of these components is the most crucial in order to reduce or eliminate squeal propensity. It can be concluded that, squeal can be reduced by decreasing the friction coefficient and also modifying the shape and material properties of the pads. On the other hand, the simplified model of disk brake was successful to analysis the brake squeal propensity versus variation of brake system conditions. Consequently, this can remarkably reduce the costs and CPU time.

References

- [1] P. Hagedorn, Modeling Disk Brakes With Respect To Squeal. TU Darmstadt, Germany. Report, 2003.
- [2] Antti Papinniemi, Brake squeal: a literature review. *Applied Acoustics*, 63, 391–400, 2002.
- [3] J.J. Sinou, Friction-induced vibration for an aircraft brake system—Part 1: Experimental approach and stability analysis. *International Journal of Mechanical Sciences* 48, 536–554, 2006.
- [4] H.R. Mills, Brake Squeak. Technical Report 9000 B, Institution of Mechanical Engineers, 1938.
- [5] M.R. North, A survey of published work on vibration in braking systems. The Motor Industry Research Association (M.I.R.A.) Report, Bulletin Number 4, 1969.
- [6] R.T. Spurr, A theory of brake squeal. In *The Institution of Mechanical Engineers(A.D.)*, number 1, pages 33–40, 1961-1962.
- [7] M.R. North, Disc brake squeal - a theoretical model. In *The Motor Industry Research Association (M.I.R.A.) Report*, number 1972/5, 1972.
- [8] Guillaume Fritz, Jean-Jacques Sinou, Effects of damping on brake squeal coalescence patterns—application on a finite element model, *Mechanics Research Communications* 34 , 181–190, 2007.
- [9] N.M. Kinkaid, O.M. O'Reilly, and P. Papadopoulos, Automotive disc brake squeal. *Journal of Sound and Vibration*, 267(1): 105-166, 2002.
- [10] Chung, Chih-Hung, and Steed, William, and Kobayashi, and Nakata, Hiroyuki, “A New Analysis Method For Brake Squeal Part I: Virtual Design of Brake Squeal ”, SAE paper 2003-01-1625.
- [11] Francesco Massi, Laurent Baillet, Oliviero Giannini and Aldo Sestieri, Brake squeal: Linear and nonlinear numerical approaches. *Mechanical Systems and Signal Processing*, In Press.
- [12] Q. Cao, H. Ouyang, Linear eigenvalue analysis of the disc-brake squeal problem, *International Journal For Numerical Methods In Engineering Int. J. Numer. Meth. Engng* 61:1546–1563, 2004.
- [13] ANSYS Inc., Manual of ANSYS 10, ANSYS Inc., 2006.
- [14] L. Meirovitch. Principles and techniques of vibrations. Virginia; Prentice-Hall International, Inc; 1997.
- [15] M. Gyimesi, D. Lavers, D. Ostergaard, and T. Pawlak, "Hybrid Finite Element - Trefftz Method for Open Boundary Analysis", *COMPUMAG*, Berlin 1995, *IEEE Transactions on Magnetic*, Vol. 32(3): 671-674, 1996.
- [16] J.H. Wilkinson, and C. Reinsch, “Linear Algebra”, Vol. II of “Handbook for Automatic Computation”, Springer-Verlag, New York, NY, pp. 418–439, 1971.
- [17] D. Marr. Automotive Brake Systems: Delmar Pub, 2001.
- [18] Private Communications, Iran Khodro Industrial Group.

Analytical Investigation of Strongly Nonlinear Normal Mode Using Homotopy perturbation method and He's Variational Method

N. Tolou*, SHA. Hashemi. Kachapi**, A. Barari^{1***}, D.D.Ganji**

Department of Engineering, Islamic Azad University, Ayatollah Amoly Branch, Amol, Iran.*

*Department of Mechanical Engineering**, Noushivani University of Technology, Babol, Iran.*

*Department of Civil Engineering***, Noushivani University of Technology, Babol, Iran.*

Abstract

Analytical solution for the Strongly Nonlinear Normal Mode (NNMs equations) is obtained. The analysis is based on the homotopy perturbation method (HPM) and He's variational method (VM). The obtained results from the proposed approximate solutions have been compared and verified with those obtained from the numerical method. It shows that the numerical results of these methods are the same; while VM can be much easier, HPM more convenient and more efficient to approach such problems in comparison to the traditional methods.

Keywords: *Homotopy Perturbation Method (HPM); Variational Method (VM); Nonlinear Normal Mode Equations (NNMs);*

1. Introduction

Most scientific phenomena occur nonlinearly. We know that except a limited number, most of them do not have exact analytical solutions. Therefore, these nonlinear equations are to be solved using other methods. Most scientists believe that the combination of numerical and semi-exact analytical methods can also end with remarkable results.

Perturbation method is one of the most well-known methods to solve nonlinear equations studied by a large number of researchers that have appeared in open literature [1–5]. Actually, these scientists had paid more attention to the mathematical aspects of the subject which included a loss of physical verification. Since, there are some limitations with the common perturbation method and also because the basis of the common perturbation method was upon the existence of a small parameter, developing the method for different applications is very difficult. Therefore, many different methods have recently introduced some ways to eliminate the small parameter, such as artificial parameter method introduced by Liu [6], recently new couple variational approach proposed by SHA. Hashemi. K [7]. The variational method (VM) and the Homotopy perturbation method (HPM) proposed by He JH [8, 9]. These methods used in nonlinear science and other engineering usages (such as [10–19]).

In this paper, the work of G. Recktenwald and R. Rand [20] is extended by applying HPM and VM. These methods are one of the latest analytical methods for solving linear and nonlinear equations. So, brief reviews of the proposed methods are firstly presented; those are applied to an

¹ Amin78404@yahoo.com

example of a non-linear dynamic equation (see equation 3) of a periodic system from the family of nonlinear normal modes (NNMs) [20]. Finally, a numerical example is given to demonstrate the validity of the proposed methods.

2. Governing Equation

To obtain the governing equation of a nonlinear normal mode (NNM) equation, we consider the periodic motions in multi degree of freedom conservative dynamical systems with kinetic energy T and potential energy V as below:

$$\begin{aligned} T &= \frac{1}{2} \dot{x}^2 + \frac{1}{2} \dot{y}^2 \\ V &= \frac{1}{2} (\omega^2 + x^2) y^2 + \frac{1}{4} x^4 + \frac{1}{5} x^5 \end{aligned} \quad (1)$$

This system is governed by the following equations of motion:

$$x'' + x^3 + x^4 + xy^2 = 0, \quad y'' + \omega^2 y + x^2 y = 0 \quad (2)$$

These equations possess an invariant manifold $y = 0$, on which lies a family of nonlinear normal modes (NNMs) which satisfy the following equation:

$$x'' + x^3 + x^4 = 0 \quad (3)$$

The initial conditions are defined as:

$$\begin{aligned} x(0) &= A \\ x'(0) &= 0 \end{aligned} \quad (4)$$

3. Methodology

3.1. Background of Homotopy Perturbation Method (HPM)

In this paper, we apply the homotopy perturbation method to solve the NNMs equation. In order to demonstrate how this method works, let us consider the following nonlinear differential equation [9]:

$$A(u) - f(r) = 0, \quad r \in \Omega, \quad (5)$$

With the boundary conditions of:

$$B(u, \partial u / \partial n) = 0, \quad r \in \Gamma, \quad (6)$$

where A is a general differential operator, B is a boundary operator, $f(r)$ is a known analytic functional and Γ is the boundary of the domain Ω .

The operator A can generally be divided into two parts L and N , where L is linear and N is nonlinear operator. Therefore Eq. (5) can be rewritten as:

$$L(u) + N(u) - f(r) = 0. \quad (7)$$

Homotopy-Perturbation structure is shown to be as the following equation [9]:

$$H(v, p) = (1 - p)[L(v) - L(u_0)] + p[L(v) + N(v) - f(r)] = 0 \quad (8)$$

Where:

$$v(r, p) : \Omega \times [0, 1] \rightarrow R \quad (9)$$

For $p = 0$ and $p = 1$, Eq. 8 reduces to the following equations respectively:

$$H(v, 0) = L(v) - L(u_0) = 0 \quad (10)$$

$$H(v, 1) = A(v) - f(r) = 0 \quad (11)$$

where $p \in [0, 1]$ is an embedding parameter and u_0 is the first approximation that satisfied the boundary condition.

The process of changes in p from zero to unity is that of $v(r, p)$ changing from u_0 to $u(r)$. We consider v , as the following:

$$v = v_0 + pv_1 + p^2v_2 \dots, \quad (12)$$

And the best approximation for solution is [10-19]:

$$u = \lim_{p \rightarrow 1} v = v_0 + v_1 + v_2 + \dots, \quad (13)$$

3.2. Background of He's Variational Method (VM)

To clarify the basic ideas of He's Variational Method [8], we consider the general governing differential equation of nonlinear oscillator in the following form [8]:

$$u''(t) + f(u) = 0 \quad (14)$$

Firstly, we use a variational approach (VM) for calculate of frequency. Its variational principle can be easily established using the semi-inverse method [21]

$$J(u) = \int_0^T \left(-\frac{1}{2} u'^2 + F(u) \right) dt \quad (15)$$

which $T = \frac{2\pi}{\omega}$ is period of the nonlinear oscillator and $\frac{\partial F}{\partial u} = f$.

Non-linear oscillations systems are independent upon initial conditions. In general, oscillations systems contain two important physical parameters, i.e. which A and ω are the amplitude and frequency of oscillator. So, without loss of any generality, consider such initial conditions:

$$\begin{aligned} u(0) &= A \\ u'(0) &= 0 \end{aligned} \quad (16)$$

Assume that its solution can be expressed as below:

$$u(t) = A \cos \omega t \quad (17)$$

Substituting (17) into (15) we have:

$$J(A, \omega) = \int_0^T \left(-\frac{1}{2} A^2 \omega^2 \sin^2 \omega t + F(A \cos \omega t) \right) dt =$$

$$\frac{1}{\omega} \int_0^{\frac{\pi}{2}} \left(-\frac{1}{2} A^2 \omega^2 \sin^2 t + F(A \cos t) \right) dt = -\frac{1}{2} A^2 \omega \int_0^{\frac{\pi}{2}} \sin^2(t) dt + \frac{1}{\omega} \int_0^{\frac{\pi}{2}} F(A \cos t) dt \quad (18)$$

Applying the Ritz method, we require

$$\frac{\partial J}{\partial A} = 0 \quad (19)$$

$$\frac{\partial J}{\partial \omega} = 0 \quad (20)$$

But by a careful inspection, for most cases we find that

$$\frac{\partial J}{\partial \omega} = -\frac{1}{2} A^2 \int_0^{\frac{\pi}{2}} \sin^2(t) dt - \frac{1}{\omega^2} \int_0^{\frac{\pi}{2}} F(A \cos t) dt < 0 \quad (21)$$

Thus, we modify the conditions (19) and (20) into a more simply form:

$$\frac{\partial J}{\partial A} = 0 \quad (22)$$

From the relationship between the amplitude and frequency of the oscillator can be obtained.

4. Applications

4.1. Implementation of HPM

To solve the Eq. (3) by means of the homotopy perturbation method, we construct homotopy functions in the following forms:

$$(1-p) \left[\frac{d^2 x}{dt^2} \right] + p \left[\frac{d^2 x}{dt^2} + x^3 + x^4 \right] = 0 \quad (23)$$

It is obvious that when $p = 0$, Eq. (23) becomes a linear equation; when $p = 1$ it becomes the original non-linear one. So the variation of p from zero to unity makes the equation to change to non-linear from linear one.

According to the homotopy-perturbation method, we assume that the solution of Eq. (23) can be expressed in a series of p as below:

$$u(t) = u_0(t) + p u_1(t) + p^2 u_2(t) + p^3 u_3(t) + \dots \quad (24)$$

According to Eq. (4) the initial approximations are:

$$u_0(t) = A \quad (25)$$

where A is amplitude of the oscillator. Substituting $u(t)$ from Eq. (24) into Eq. (23) and after some simplification and substitution and rearranging based on powers of p -terms we have:

$$p^0 : \frac{d^2 u_0(t)}{dt^2} \quad (26)$$

$$p^1 : \frac{d^2 u_1(t)}{dt^2} + u_0^3(t) + u_0^4(t) \quad (27)$$

$$p^2 : \frac{d^2 u_2(t)}{dt^2} + 3u_0^2(t)u_1(t) + 4u_0^3(t)u_1(t) \quad (28)$$

$$p^3 : \frac{d^2 u_3(t)}{dt^2} + u_0(t)(2u_0(t)u_2(t) + u_1^2(t)) + 2u_1^2(t)u_0(t) + \dots, \quad (29)$$

Then, solving Eq. (27-29) we have:

$$u_1(t) = \frac{1}{2}(-A^3 - A^4)t^2 \quad (30)$$

$$u_2(t) = \frac{1}{24}A^5 t^4 (A+1)(4A+3) \quad (31)$$

$$u_3(t) = -\frac{1}{720}A^7 t^6 (A+1)(52A^2 + 78A + 27) \quad (32)$$

Consequently, substitution of Eqs. (30-32) into Eq. (24), respectively gives the solution of $u(t)$ in the following closed forms:

$$\begin{aligned} u(t) = A + p^1 \left[\frac{1}{2}(-A^3 - A^4)t^2 \right] + p^2 \left[\frac{1}{24}A^5 t^4 (A+1)(4A+3) \right] \\ + p^3 \left[-\frac{1}{720}A^7 t^6 (A+1)(52A^2 + 78A + 27) \right] \end{aligned} \quad (33)$$

As $p = 0.89, A = 0.1, u(t) \rightarrow x(t)$ in Eq. (34), respectively gives the solution of $u(t)$ in the following form:

$$x(t) = 0.1 - 4.895 \times 10^{-4} t^2 + 1.234 \times 10^{-6} t^4 - 3.804 \times 10^{-9} t^6 \quad (34)$$

The solution for the nonlinear oscillator system which lies a family of nonlinear normal modes (NNMs) is given by Eq. (34).

4.2 Implementation of He's Variational Method

To solve the Eq. (3) by means of the VM, we construct its variational formulation according to Eq. (15) in the following form:

$$J(u) = \int_0^T \left\{ -\frac{1}{2} u'^2 + \frac{1}{4} u^4 + \frac{1}{5} u^5 \right\} dt \quad (35)$$

For this problem, $f(u) = u^3 + u^4$ and $F(u) = \frac{1}{4}u^4 + \frac{1}{5}u^5$. Substituting Eq. (17) into (35):

$$J(A) = \int_0^T \left\{ -0.5A^2 \sin^2(\omega t) \omega^2 + \frac{1}{4}A^4 \cos^4(\omega t) + \frac{1}{5}A^5 \cos^5(\omega t) \right\} dt \quad (36)$$

The stationary condition with respect to A reads:

$$\begin{aligned} \frac{\partial J}{\partial A} &= \int_0^T \left\{ -1A \sin^2(\omega t) \omega^2 + A^3 \cos^4(\omega t) + A^4 \cos^5(\omega t) \right\} dt = \\ \int_0^{\frac{\pi}{2}} \left\{ -1A \sin^2(\omega t) \omega^2 + A^3 \cos^4(\omega t) + A^4 \cos^5(\omega t) \right\} dt &= 0 \end{aligned} \quad (37)$$

After some simplification and substitution and rearranging following Eq. (37) we have:

$$\omega = 3.8197 \times 10^{-10} + \left(4.654 \times 10^{18} A + 5.1404 \times 10^{18} \right)^{\frac{1}{2}} A \quad (38)$$

As $A = 0.1$ in Eq. (38), the value of ω for this equation is given as below:

$$\omega = 9.0438 \times 10^{-2} \quad (39)$$

In Eq. 17 while $u(t) \rightarrow x(t)$ gives the solution of $u(t)$ in the following form:

$$x(t) = 0.1 \cos(9.0438 \times 10^{-2} t) \quad (40)$$

5. Results and Discussion

To demonstrate the validity of the proposed method a numerical example is given. The results obtained from HPM and VM were compared and verified with those obtained from the numerical methods such as Runge-Kutta's Method.

The result shown in figures (1) and (2) indicates that these methods experience a high accuracy. In addition, in comparison with traditional analytical methods, a considerable reduction in the volume of the calculations can be seen in the propose methods especially in VM. It can be approved that HPM and VM is a powerful and efficient technique in finding analytical solutions for such nonlinear problems.

Fig. 1 (a) and (b) illustrates the time history diagram of the displacement and velocity respectively. This figure confirms obviously the excellent agreement between HPM, VM and the Runge-Kutta method. For further verification, the accuracy of Fig. 1 is depicted in Fig. 2. This Figure shows that increasing the time give rise to reduce the accuracy of displacement as well as the velocity. It can be seen that for displacement, the VM shows more accurate results. While for velocity, HPM touches more accuracy. Fig. 1 as well as Fig. 2 is obtained for $A = 0.1$.

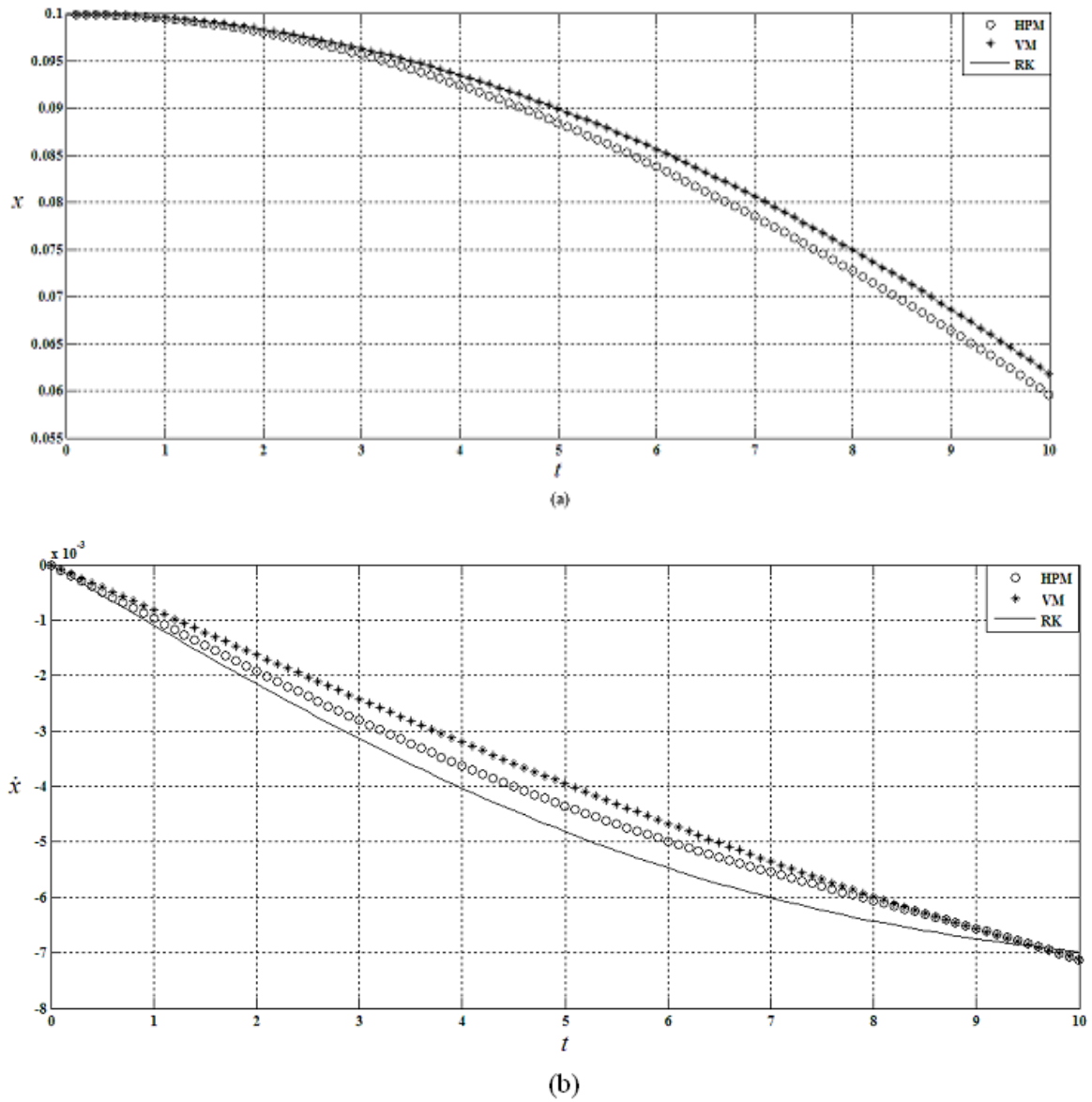


Fig. 1. Time history diagram at $x(0) = 0.1$, $\dot{x}(t) = 0$ and $A = 0.1$; (a) displacement $x(t)$, (b) velocity $\dot{x}(t)$.

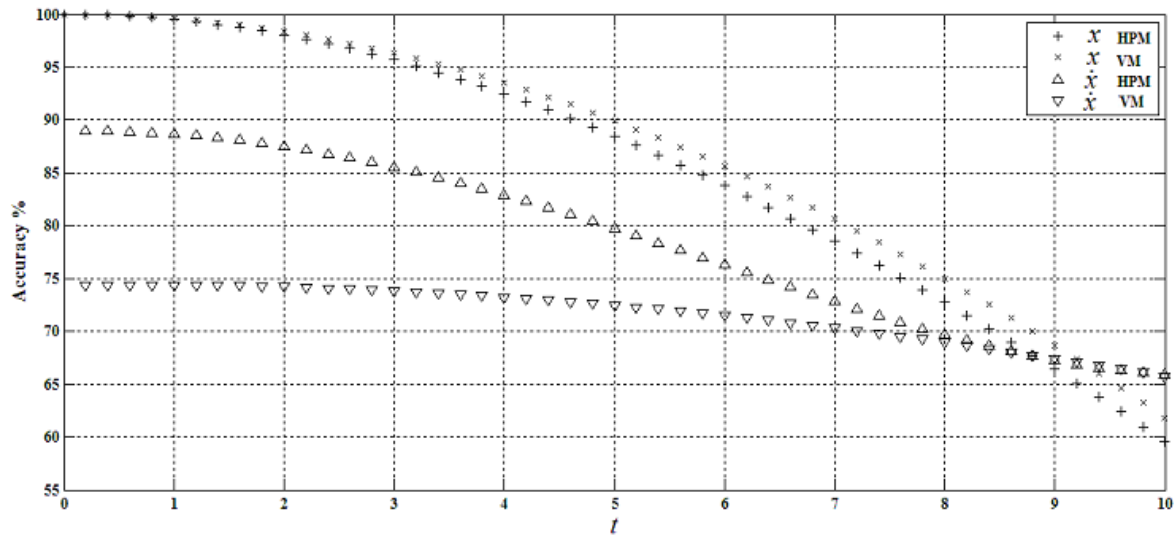


Fig. 2. Accuracy of the results shown in Fig. 1.

6. Conclusion

In this survey, the homotopy-perturbation method (HPM) and the variational method (VM) have been employed to analysis the nonlinear normal modes (NNMs) equations. The results obtained from these methods have been compared with those obtained from the numerical method, using Runge-Kutta's algorithm. This comparison shows excellent agreement between propose methods and the numerical method.

It is found clearly that the proposed methods have got more advantages than traditional analytical methods:

1. Those are convenient and efficient technique to overcome such problem.
2. Those overcome the difficulties arising in the calculation of other methods.

While

3. NVM is much easier than HPM.
4. HPM doesn't experience the limitation of VM to be restricted in oscillator systems.
5. HPM doesn't require small parameters in the equation. so, the limitations of the traditional perturbation method can be eliminated and thereby the calculations will be simple and straightforward.

Reference

- [1] R. Bellman, Perturbation Techniques in Mathematics, Physics and Engineering, Holt, inehart & Winston, New York, 1964.
- [2] J. D. Cole, Perturbation Methods in Applied Mathematics, Blaisedell, Waltham, MA, 1968.
- [3] R.E. O'Malley Jr., Introduction to Singular Perturbation, Academic, New York, 1974.
- [4] Nayfeh AH, perturbation Methods, Wiley, New York, 1973.
- [5] Van Dyke M, Perturbation Methods in Fluid Mechanics, Annotated Edition, parabolic press, Stanford, CA, 1975.

- [6] G.L. Liu, New research directions in singular perturbation theory: artificial parameter approach and inverse-perturbation technique, Conference of 7th Modern Mathematics and Mechanics, Shanghai, 1997.
- [7] SHA. Hashemi. K, S. M. Varedi, D. D. Ganji, Periodic Solution for Strongly Nonlinear Vibration Systems by New Couple Variational Approach, Communications in Nonlinear Science and Numerical Simulations, 2008, accepted.
- [8] He JH, Variational approach for nonlinear oscillators, Chaos, Solitons and Fractals 34 (2007) 1430–1439.
- [9] He JH. Homotopy perturbation technique, computer methods in applied mechanics and engineering, 178 (1999) 257–262.
- [10] M. Naghipour, D.D. Ganji, SHA. Hashemi. K, Jafari, Analysis of non-linear oscillations systems using Analytical approach, Journal of physics, 2007, in press.
- [11] Xu L. Variational approach to solitons of nonlinear dispersive K (m, n) equations, Chaos, Solitons & Fractals [in press].
- [12] Wu Y. Variational approach to higher-order water-wave equations. Chaos, Solitons & Fractals; 32 (2007) 195–203.
- [13] J.H. He, the homotopy perturbation method for nonlinear oscillators with discontinuities, Applied Mathematics and Computation, 151 (2004) 287–292.
- [14] S.H. Hashemi. K, H.R.M. Daniali, D.D. Ganji, Numerical simulation of the generalized Huxley equation by He's homotopy perturbation method, Appl. Math. Comput, 192 (2007) 157–161.
- [15] D.D. Ganji, The application of He's homotopy perturbation method to nonlinear equations arising in heat transfer, Physics Letters A, 355 (2006) 337–341.
- [16] N. Tolou, D.D. Ganji, M.J. Hosseini, Z.Z. Ganji, Application of Homotopy Perturbation Method in Nonlinear Heat Diffusion – Convection – Reaction Equations, The Open Mechanic Journal 1 (2007) 20–25.
- [17] D.D. Ganji, A. Sadighi, Application of homotopy-perturbation and variational iteration methods to nonlinear heat transfer and porous media equations, J. Comput. Appl. Math 207 (2007) 24–34.
- [18] H. Tari, D.D. Ganji, Approximate explicit solutions of nonlinear BBMB equations by He's methods and comparison with the exact solution, Physics Letters 367 (2007) 95–101.
- [19] A. Sadighi, D.D. Ganji, Exact solutions of Laplace equation by homotopy-perturbation and Adomian decomposition methods, Physics Letters 367 (2007) 83–87.
- [20] G. Recktenwald and R.Rand, Stability of strongly nonlinear normal modes, Nonlinear Science Numerical Simulation, 7(3) (2006) 321–328.

LONG MEMORY ANALYSIS OF TURKISH INFLATION SERIES

Nilgün ÇAĞLARIRMAK USLU* and Nesrin ALPTEKİN†

Abstract

In this paper, notion of inflation persistence is tested by long memory analysis. Long memory analysis is an active research area in financial economics in recent years. Fundamental aim of this study, it is examined the inflation persistence phenomena resulted by disinflation politics which applied in Turkey between 2002 and 2007. Long memory analysis is used to detect the persistence in Turkish inflation series. If a series exhibits long memory property, there is persistent temporal dependence among its observations at long lags. To test persistence of inflation series, modified R/S analysis, KPSS test and Modified variance (V/S) test are used. These tests are applied monthly CPI (consumer price index) series from January 1996 to December 2007 obtained from Central Bank Republic of Turkey, e-data service.

Keywords: Cause of inflation, Inflation persistence, Long memory analysis, Modified R/S Analysis, KPSS test, Rescaled Variance (V/S) test.

1. Introduction

This paper investigates long memory of Turkish inflation series. In our paper, we try to investigate the causes of inflation in Turkey and to determine that the inflation time series has long memory or not? The long-term behavior of discrete time dynamical systems in economics and finance has increased much attention in the recent literature. Inflation rate or inflation uncertainty is very important efficient resource of allocation for economy. The impact of inflation on growth, output and productivity has been one of the main issues examined in macroeconomics. Very high inflation adversely impacts economic performance, as evidence from cross-country studies shows. Likewise, moderate levels of inflation can distort investment and consumption decisions. Distortions in economic activity also may result from the uncertainty that arises about inflation's future course. When inflation is stable, people are more likely to have roughly the same anticipation of its future level. When inflation is highly volatile, however, people have different guesses. Most turn out to be wrong inflation uncertainty has much more negative effect on growth in comparison with inflation. In other words, while 1% increases in inflation rate decrease growth 0.56%, an 1% increase in inflation uncertainty diminishes growth 3.95%. (Artan 2006)

Turkey provides a unique environment to analyze the dynamics of inflation. Consider the inflation experienced in countries; generally accepted view is that something structural in

* Economics Department, Anadolu University, Eskişehir, TURKEY

† Business Department, Anadolu University, Eskişehir, TURKEY

economies causes inflation. The most causes are defined that money growth rates, high employment targets, budget deficit. In this study, for purpose of emphasizes in inflation persistence going to analyses long memory concept in Turkish inflation series which choosing as the indicator CPI series. The paper is organized as follows: In section two, we summarize literature review about inflation inertia and measuring inertial component in inflation series. In section three, we present cause of inflation and inflation persistence in Turkey. Section four and five of the paper examines characteristics of long memory processes and we introduces calculation of test statistics which are used modified R/S analysis; KPSS test and Modified variance (V/S) test. Section six asses result of calculating long memory test statistics and we are given descriptive analysis of CPI inflation series. These tests are applied monthly CPI (consumer price index) series from January 1996 to December 2007.

Finally, we conclude and discuss some suggest for applied test statistics long memory process in the last section.

2. Literature Review

Inflation is defined as the condition of a continually and rapidly rising price level. In macro economic theory and economic policy, the development of the general price level or of the inflation rate plays a prominent role. Many empirical and theoretical results on the long memory of inflation series can be found in the literature. Hassler and Wolters investigated inflation rates for The United Kingdom, France, Germany, Italy, The United States with monthly data from 1969 to 1992. They employ different approaches to investigate the stationary behavior of monthly inflation rates. These are more descriptive method by Tiao and Tsay (1983), Traditionally unit root test has the stationary assumption as null hypothesis. Second, they applied fractionally integrated ARFIMA models to describe the fluctuations of inflation rates. These class of models that allow for various degrees of long range dependence (long memory). For all countries both of the method in the study has indicates that choosing series has a long memory process. (Hassler and Walters 1995). The other research related the long memory analysis is persistence in international inflation rates (Baum, *et al.* 1999). In the research has investigated for fractional dynamics inflation rates based on consumer price index (CPI) 27 countries (include in Turkey) and inflation rates based on Whole sale Price index (WPI) for 22 countries (include in Turkey). The fractional differencing parameter is estimated using semi parametric and approximate maximum likelihood methods. Significant evidence fractional dynamics with long memory features is found in both CPI and WPI based

inflation rates for industrial as well as developing countries. The different research related the long memory or persistence is Ozcan *et al* 2004. In question paper is to explain the behavior of CPI inflation by looking at the dynamics of its determinants. This result of study indicates that strong inertia Turkish inflation. (Erlat 2001), using autoregressive fractionally integrated moving average (ARFIMA) models, showed that Turkish monthly CPI and WPI inflation rates are essentially stationary but have generally significant long memory components. It tests for long memory in CPI series and estimates the fractional differencing parameter using a number of approaches. The present study has different estimating methodology these researches. We are testing for persistence of inflation series; modified R/S analysis, KPSS test and Modified variance (V/S) test are used. The result of these test statistics is discussing next the section.

3. Cause of Inflation and Inflation Persistence in Turkey

Inflation in Turkey may have a highly persistent nature. Turkey is a high inflation country but, as opposed to other countries like Argentina, Brazil and Israel where periods of high inflation occurred, the inflation in Turkey is not hyper-inflation; in other words, it does not reach large three-digit levels annually but remains around a figure which is, consistently, greater than fifty percent but never goes beyond a hundred percent except for a couple of months in 1994. (Erlat, 2000).

The Turkish economy has been plagued by high and persistent inflation in the last two decades, although the economy grew at reasonable levels, economic growth has been volatile and macro economic instability became the hallmark of the post -1980 periods. Despite many attempts to stabilize the economy, these stabilization attempts have been unsuccessful. Common explanations of inflation since late 1970s include

- 1- High public sector deficit (due to, among other things, populist government expenditures, massive infrastructure projects, bankrupt social security intuitions, loses incurred by state own enterprises)
- 2- Monetization of public sector deficit
- 3- Increases in prices of mayor imported inputs (particularly, crude-oil prices)
- 4-Inflationary effects of rising exchange rates via increases in prices of imported goods
- 5- Persistence inflationary expectations of economic agents. (Diboglu, Kibritçioglu 2001)

In developing countries the inflation rate which admitted as price stability should be below %2 Central bank of Republic of Turkey (hereafter, CBRT) has been attempt various monetary policy controlling inflation during the between 1980-2007, if we want to categorized these period The evolution of inflation in Turkey can be divided into three sub-periods: (i) the period during which price developments were influenced by the financial liberalization and the deteriorating current account outlook (1989-1993); (ii) the 1994 currency crisis and worsening debt dynamics (1995-1999); and (iii) the exchange-rate based stabilization program and its collapse (2000-2001). (Bahmani, *et al* 2002).

To evaluation of inflation dynamics of the other period is called “*disinflation period.*” This period is cover 2002-2006 years. Especially, we have started inflation targeting regime strategies in 2006. Before evaluating inflation targeting strategies As such, at the beginning of 2002 the CBRT began implementing an implicit inflation targeting framework, which encompassed core attributes of an inflation targeting regime including, among other requirements, the announcement of a formal target for inflation. Coupled with fiscal discipline and economic reforms, the implicit inflation targeting framework helped to guide inflation from over 70% to below 10% in just twenty-nine months and to below 8% by year-end 2005 and 10% in 2006 while the CBT consistently outperformed its year-end point targets measured by the consumer price index (CPI) except for the year 2006. Given overall economic progress and improvements in fiscal conditions and the banking system in particular, the CBT introduced full-fledged inflation targeting at the beginning of 2006, which brought further transparency to the new framework and a change in IMF conditionality adding more flexibility to monetary policy. (Sıklar,Çağlarırnak Uslu 2007). Recent studies have displayed that there is very strong expectation of inflation in Turkey. Especially CBRT has been applied that oriented restricted expectation of inflation policy. Persistently high inflation rates have led many to believe that inflation in Turkey has become “inertial,” posing an obstacle to disinflation. We assess the empirical validity of this argument Turkey is ideal case study for the issues, because is has experienced persistently high inflation since the 1970’s. (Celasun 2003). Especially CBRT has started disinflation politics since 2001. The chart supporting of these arguments illustrates persistent of inflation series as follows.

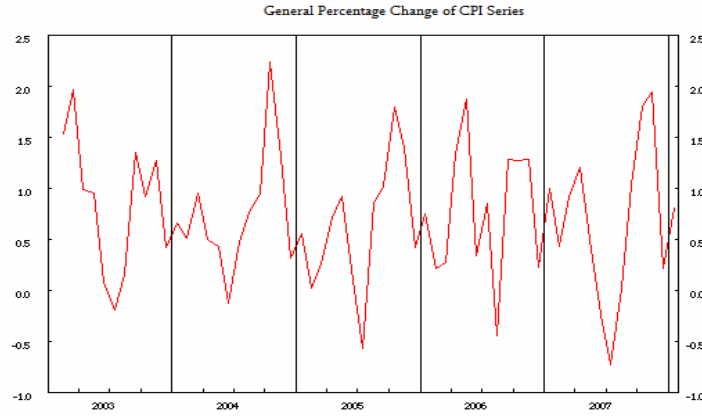


Figure 1. Annual Percentage Change of CPI Series

Source: CBRT

The Turkish economy has been plagued by high and persistent inflation in the last two decades. On the account this make government stabilizations attempts difficult given the unusual resistance these disinflation measures the face. One can conjecture that inflation inertia is a combined consequence both of persistent expectations related to lack of government credibility, and backward looking expectations in contracts for wages, sales, rents etc. in the economy (Diboglu, Kibritçioglu 2001)

High and sustained output growth in conjunction with low inflation is the central objective of macroeconomic policy. Inflation impedes efficient resource allocation by obscuring the signaling role of relative price changes, the most important guide to efficient economic decision making. (Khan, Senhadji 2001). On this account, not only shape of money indicator but also for the macro economic stability is evaluated that choosing inflation series of long memory process.

4. Characteristics of Long Memory Processes

Long memory property of time series is an active research area in economics and finance. Economists have been interested in long memory since the original work of Mandelbrot in the 1960's on price series. Since then attention has concentrated on long

memory in asset prices and foreign exchange rates, and within the last ten years, on real national output measures as well.

The long memory, or long term dependence, property describes the high-order correlation structure of a series. If a series exhibits long memory, there is persistent temporal dependence even between distant observations. Such series are characterized by distinct but non-periodic cyclical patterns.

A stationary stochastic process $\{Y_t\}$ is called a long memory process if there exist a real number H and a finite constant C such that the autocorrelation function $\rho(\tau)$ has the following rate of decay:

$$\rho(k) \sim C \tau^{2H-2} \text{ as } \tau \rightarrow \infty \quad (1)$$

The parameter H , Hurst Exponent, display the long memory property of the time series. The Hurst exponent takes values from 0 to 1 ($0 \leq H \leq 1$). If $H = 0.5$, the series is a random walk (a Brownian time series). In a random walk there is no correlation between any element and a future element.

If $0.5 < H < 1$, the series indicates persistent behavior or long memory. If there is an increase from time step t_{i-1} to t_i there will be probably be an increase from t_i to t_{i+1} . On the other hand, the same is true for decreases. A decrease will tend to follow a decrease.

If $0 < H < 0.5$, the series is called anti-persistent. In this case, an increase will tend to be followed by a decrease or a decrease will be followed by an increase. This behavior is sometimes called mean reversion.

Brownian walks can be generated from a defined Hurst exponent. If the Hurst exponent is $0.5 < H < 1$, the random walk will be a long memory process. The time series like this is sometimes referred to as fractional Brownian motion.

A long memory time series is also said fractionally integrated, where the fractional degree of integration d is related to the parameter H by the equality

$$d = H - 0.5 \quad (2)$$

There are many methods for estimating the Long memory parameter d , such as R/S (rescaled range analysis), Modified R/S analysis, KPSS, Rescaled Variance (V/S) Test, GPH (Log Periodogram Estimation) and so on.

In this paper, Modified R/S test, KPSS and Rescaled Variance (V/S) test are applied to Turkish Inflation rate series in determining for long memory.

5. Long Memory Tests

A long memory process with degree of d is said to be integrated order of d and is denoted by $I(d)$. A stochastic process is $I(d)$ if it needs to be differentiated d times in order to become $I(0)$.

5.1 Modified R/S Test (Lo's test)

The first test for long memory was used by the hydrologist Hurst (1951) for the design of an optimal reservoir for the Nile River, of where flow regimes were persistent. Hurst gave the following formula:

$$(R/S)_n = cn^H \quad (3)$$

$(R/S)_n$ is the rescaled range statistic measured over a time index n , c is a constant and H the Hurst exponent. This shows the how the R/S statistic is scaling in time. The aim of the R/S statistic is to estimate the Hurst exponent which can characterize a series. Estimation of Hurst exponent can be done by transforming (3) to:

$$\log(R/S)_n = \log(c) + H \log(n) \quad (4)$$

and H can be estimated as the slope of log/log plot of $(R/S)_n$ vs. n .

For a time series $\{X_t\}$ ($t = 1, \dots, N$), the R/S statistic can be defined as the range of cumulative deviations from the mean of the series, rescaled by the standard deviation.

The analytical procedure to estimate the $(R/S)_n$ values can be described as:

$$\left(\frac{R}{S}\right)_j = s_j^{-1} \left[\max_{1 \leq k \leq n} \sum_{i=1}^k (X_{ij} - \bar{X}_j) - \min_{1 \leq k \leq n} \sum_{i=1}^k (X_{ij} - \bar{X}_j) \right] \quad (5)$$

Although Mandelbrot (1972) gave a formal justification for the use of this test, Lo(1991) showed that this statistic was not robust to short memory dependence and modified this statistic.

Lo defined modified R/S statistic as:

$$Q_T = \frac{1}{\hat{\sigma}_T(q)} \left[\max_{1 \leq k \leq T} \sum_{j=1}^k (X_j - \bar{X}_T) - \min_{1 \leq k \leq T} \sum_{j=1}^k (X_j - \bar{X}_T) \right] \quad (6)$$

where,

$$\hat{\sigma}_T^2 = \hat{\gamma}_0 + 2 \sum_{j=1}^q \left(1 + \frac{j}{1+q} \right) \hat{\gamma}_j, \quad q < T. \quad (7)$$

$\hat{\gamma}_0$ is the variance of the series and the sequence $\{\hat{\gamma}_j\}_{j=1}^q$ denotes the autocovariances of the series up to order q .

If $q = 0$, Lo's statistic reduces to Hurst's R/S statistic. This statistic is highly sensitive to the order of truncation q but there is no a statistical criteria for choosing q in the framework of this statistic. If q is too small, this statistic does not account for the autocorrelation of the process, while if q is too large, it accounts for any form of autocorrelation and the power of this test tends to its size. Given that the power of a useful test should be greater than its size; this statistic is not very helpful. For that reason, (Teverovsky *et al.* 1999) suggest to use this statistic with other tests.

Since there is no data driven guidance for the choice of this parameter, the default values for $q = 5, 10, 25$ and 50 are considered. At 5% significance level, the null hypothesis of no long memory process is rejected if the modified R/S statistic does not fall within the confidence interval $[0.809, 1.862]$.

5.2 KPSS Test

The KPSS statistic (Kwiatkowski, Phillips, Schmidt and Shin) is often used for testing the null hypothesis of stationarity against the alternative of unit root. This test has a power equivalent to modified R/S statistic against to long memory processes and can therefore be used to distinguish between short and long memory processes. This test is similar to Lo's modified R/S statistic in power and construction.

The two KPSS statistics η_t and η_μ are respectively based on the residuals of two regression models. In these regression models, t is an intercept and a trend, and μ is a constant.

The partial sums $S_t = \sum_{i=1}^t \hat{e}_i$ is denoted by S_t , where \hat{e}_i are the residuals of these regressions, the KPSS statistic is defined by:

$$\eta = T^{-2} \sum S_t^2 / \hat{\sigma}_T^2(q) \quad (8)$$

$\hat{\sigma}_T^2(q)$ is the estimator of the variance of residuals defined in equation (7). The statistic η_t tests for trend-stationarity against a long memory alternative, while the statistic η_μ tests for stationarity against a long memory alternative. Critical values of KPSS test are as follow:

Table I
KPSS Test Critical Values

	%10	%5	%1
Constant	0.347	0.463	0.739
Trend	0.119	0.146	0.216

5.3 Rescaled variance (V/S) Test

Giraitis *et al.* (2003) have proposed a centering of the KPSS statistic is based on the partial sum of the deviations from the mean. They called it rescaled variance test V/S as its expression given by:

$$V/S = \frac{1}{T^2 \hat{\sigma}_T^2(q)} \left[\sum_{k=1}^T \left(\sum_{j=1}^k (Y_j - \bar{Y}_T) \right)^2 - \frac{1}{T} \left(\sum_{k=1}^T \sum_{j=1}^k (Y_j - \bar{Y}_T) \right)^2 \right] \quad (9)$$

can be equivalently be rewritten as

$$V/S = T^{-1} \frac{\hat{V}(S_1, \dots, S_T)}{\hat{\sigma}_T^2(q)} \quad (10)$$

where

$$S_k = \sum_{j=1}^k (Y_j - \bar{Y}_T) \quad (11)$$

are the partial sums of the observations. The V/S statistic is the sample variance of the series of partial sums. The limiting distribution of this statistic is a Brownian bridge of which the distribution is related to the Kolmogorov statistic.

This statistic has uniformly higher power than the KPSS, and is less sensitive than the Lo's statistic to the choice of the order q . For $2 \leq q \leq 10$, the V/S statistic can appropriately detect the existence of long memory in the level series, although, like most tests and estimators, this test may wrongly detect the existence of long memory in series with shifts in the levels.

This test is evaluated for lag of orders $q = 2, 4, 6$. The critical value for this test is 0.1869 at 5% significance level.

6. Data and Testing Long Memory of Inflation Series

Data covers monthly CPI (consumer price index) series from January 1996 to December 2007. It is below that descriptive statistics all series are given in figure 2. According to JB test, inflation series is not normal distributed.

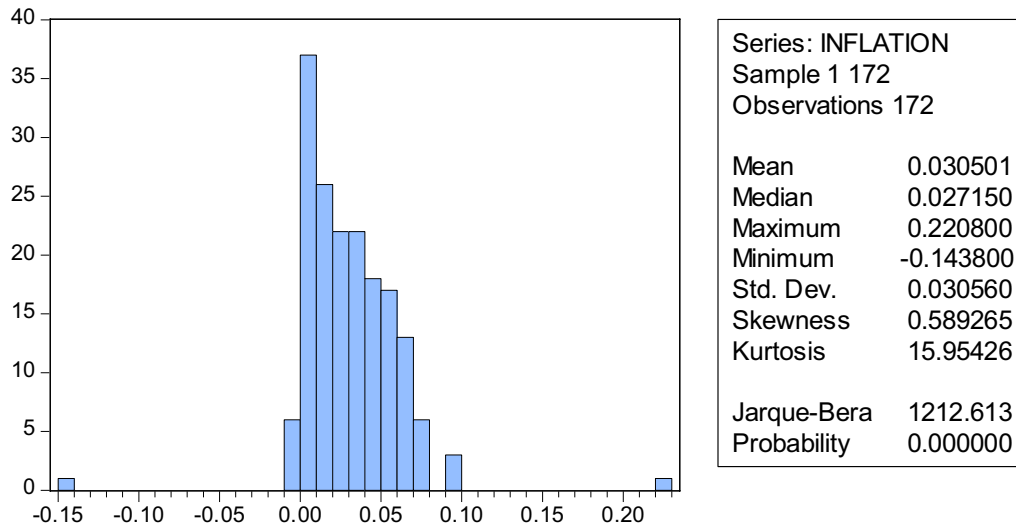


Figure 2. Descriptive statistics of Turkish inflation series

Table 2. Modified R/S Test Results of Inflation Series

Order(q)	Statistic
5	2.0780*
10	2.7190*
25	3.9142*
50	5.5937*

Modified R/S test is applied to daily Turkish inflation rate series. The test is evaluated for lag orders 5, 10, 25 and 50. At the 5% significance level, the null hypothesis of no long memory is rejected because the modified R/S statistics for all orders do not fall within the confidence interval [0.809, 1.862].

* indicates significance at the 5% level.

Table 3. Kpss Test Results

	Test Statistic	Critical Value		
		10%	5%	1%
Constant	9.4078*	0.347	0.463	0.739
Trend	2.1842*	0.119	0.146	0.216

KPSS test is performed on Turkish inflation rate series. The test is evaluated lag order of 0.

* indicates significance at 10%, 5% and 1% levels.

Table 4. V/S Test Results

Order	Statistic	Critical Value
2	0.6442*	0.1869
4	0.4768*	0.1869
6	0.3755*	0.1869

The V/S test which is performed on Turkish inflation rate series is evaluated for lag orders of $q = 2, 4, 6$. The critical value of this test is 0.1869 at 5% level.

* indicates significance at 5% level. Thus, null hypothesis of no long memory is rejected.

7. Conclusion

This study has investigated the long memory behavior of inflation series (CPI) over the period from January 1996 to December 2007. It is tested for the presence of long memory or fractional dynamics of the series. All test statistics are displayed that the Turkish inflation rate series has a long memory process or persistence process.

The method was used on the most recent test of long memory of a time series in the other countries. The result show that Turkish inflation series exhibit long memory by the three of test.

Our empirical analysis is related the persistence of Turkish inflation series in this paper differs from existing studies in the literature in methodology and methods which applied in Turkey.

Therefore when the construction of stabilization program for the economy; first the policy makers is tend to direct orientation of future expectation in economy. Because, the time series has a long memory indicates expectation related with from the past is determined future expectation. This is the best of example preconceived notion of about inflationary expectation.

References

- [1] Artan Seyfettin, “Türkiye’de Enflasyon, Enflasyon Belirsizliği ve Büyüme”, Türkiye Ekonomi Kurumu Tartışma Metni,2006/14, <http://www.tek.org.tr> ,pp.1-20
- [2] Bahmani –Oskooee, M., Domaç, İ. (2008). “On the Link between Dollarization and Inflation: Evidence from Turkey”, <http://www.tcmb.gov.tr/research/discus/dpaper59.pdf>.
- [3]] Baum F. Christopher , Barkoulas, John T, Çağlayan Mustafa , “ Persistence in International Inflation rates” , Southern Economic Journal, 1999 65(4) , 900-913
- [4] Celasun O., Gelos R. G., Alessandro Prati1 A. (2003) “Would Cold Turkey Work in Turkey?”, http://www.ecomod.net/conferences/ecomod2003/ecomod2003_papers/Celasun.pdf .
- [5] Diboglu S, Kibritritçioglu A, “Inflation, Output, and Satabilization In A High Inflation Economy; Turkey, 1980-2000”, Universty of Illinois at Urbana-Champaign, College of Commerce and Business Administration Office of Research, *Office of Research Working Paper Number 01-0112*, pp.1-33
- [6] Erlat, H. (2000). “Long Memory in Turkish Inflation Rates”, *Book of ABS of ERC/Metu Int. Conference on Economics IV*, paper 145
- [7] Hassler Uwe and Wolters Jürgen, “Long Memory in Inflation Rates: International Evidence”, *Journal of Business & Economic Statistics*, January 1995, Vol 13, no 1, pp 37-45
- [8] Lo, A. W., (1991), “Long-term memory in stock market prices”, *Econometrica*, 59, 1279-1313.
- [9] Mandelbrot B.B., (1972), “A statistical methodology for non-periodic cycles: From the covariance to R/S analysis”, *Annals of Economic and Social Measurement*, 1,259-290.
- [10] Khan Mohsin S. and Senhadji A.S. , IMF Staff Papers, Vol. 48, No. 1, 2001 International Monetary Fund,pp.1-2)
- [11] Peters, Edgar E., (1992), “R/S Analysis Using Logarithmic Returns”, *Financial Analysts Journal*, Nov.-Dec., 81-82.
- [12] Peters, E.E., (1996), *Chaos and Order in the Capital Markets*, New York, John Wiley and Sons.
- [13] Şıklar, İ., Çağlarırnak Uslu, N. (2007). “Exchange Rate Pass-Through to Domestic Prices:The Turkish Case (1994-2006)”, *The Business Review Cambridge*, 162-169.

EXPERIMENTAL STUDY OF THE DYNAMIC BEHAVIOR OF A DOUBLE SCROLL CIRCUIT

Christos K. Volos*, Ioannis M. Kyprianidis*, Ioannis N. Stouboulos*
and Antonios N. Anagnostopoulos*

Abstract

In this paper, we present an analytical study of the dynamic behavior of an electronic circuit, which generates double scroll attractors. The nonlinear resistor is a simple saturated circuit, based on operational amplifiers. The dynamical behavior of the proposed circuit is investigated both theoretically and experimentally. The tools of the theoretical approach are the bifurcation diagrams, the Lyapunov exponents and the phase portraits. Also, the circuit is investigated experimentally, by analyzing the phase portraits and the Poincaré maps, which we took with an oscilloscope.

Keywords: *Double Scroll, Saturated Function, Lyapunov Exponents, Coexistence of Attractors, Period doubling.*

1. Introduction

In the last decades the research activities in the field of systems with chaotic behavior have forced a lot of investigation on possible applications of such systems. Especially, the design and implementation of chaotic circuits became a very interesting subject due to their applications in secure communications [1], cryptography [2], random number generators [3] and so on.

From the beginning of this century, the research groups have focused their attempts in designing circuits, which generate n-scroll chaotic attractors using simple circuits, such as the generalized Chua's circuit. Suykens and Vandewalle [4]-[6] first proposed the so-called family of n-scroll attractors. Also, Yalcin, Suykens, Vandewalle and Ozoguz [7] proposed a step function method for generating n-scroll attractors. Tang, Zhong, Chen and Man [8] introduced a sine function approach and recently a saturated function series method was also introduced by Lu, Chen, Yu and Leung [9]. Elwakil and Kennedy [10] proposed some

*Physics Department, Aristotle University of Thessaloniki, Thessaloniki 54124, GREECE

hysteresis chaotic oscillators. It must be mentioned that the hysteresis circuit, the stair circuit and the saturated circuit are the three kind of basic circuits used for implementing the nonlinear function of the n-scroll chaos generators.

In the following, a simple electronic circuit, based on a saturated function, is presented. This circuit can create double scroll chaotic attractors. The dynamic mechanism of the saturated function is then further investigated by analyzing the system dynamical behavior. This happens by comparing the experimental results (phase portraits and Poincaré maps) with those from the simulation (bifurcation diagram, maximal Lyapunov exponents). Finally, the concluding part highlights the main points of this work.

2. The Double Scroll Circuit

The double scroll circuit, which we have studied, is shown in Fig. 1, while in Fig. 2, we can see the experimental characteristic curve of the saturated function. The state equations of the circuit are:

$$\begin{cases} \dot{x} = y \\ \dot{y} = z \\ \dot{z} = -\alpha \cdot x - \alpha \cdot y - b \cdot z + c \cdot f(x) \end{cases} \quad (1)$$

where $f(x)$ is the saturated function and defined by (2).

$$f(x) = \begin{cases} 1, & x > k \\ \frac{1}{k} \cdot x, & -k \leq x \leq k \\ -1, & x < -k \end{cases} \quad (2)$$

The saturated function has been modified in regard to that in [9]. Also, Lu, Chen, Yu and Leung [9], keep $\alpha = b = c = 0.7$, but in this work, the parameters a , b , and c are different. From (2) we conclude that the saturated plateaus are ± 1 and the saturated slope is $1/k$.

The circuit parameters are: $R_4 = R_5 = R_6 = R_7 = R_8 = R_9 = R_{10} = R_{11} = 20\text{k}\Omega$, and $C_1 = C_2 = C_3 = 1\text{nF}$. The saturated circuit is implemented with operational amplifiers 4 and 5, where, $R_{12} = 25\text{k}\Omega$, $R_{13} = R_{15} = 1\text{k}\Omega$, and $R_{14} = 14.3\text{k}\Omega$. Also, the operational amplifier 6 implements the function $-f(x)$, which is necessary at the procedure of solving the circuit of Fig. 1. So, if we use $R_{16} = R_{17} = 1\text{k}\Omega$, $R_1 = 20\text{k}\Omega$ and $R_x = 10\text{k}\Omega$, the system parameters

$$\alpha = \frac{1}{R_1 \cdot C_3}, \quad b = \frac{1}{R_3 \cdot C_3}, \quad c = \frac{1}{R_x \cdot C_3} \quad (3)$$

take the normalized values, $\alpha = 0.5$, $c = 1$, while b plays the role of the control parameter. The value of k is equal to 0.5. The voltages of the positive and negative electrical sources are $\pm 15\text{V}$. The outputs of the saturated voltages are $\pm 14.3\text{V}$. The signals x , y , and z , which we used, come from the outputs of the operational amplifiers 1, 2 and 3 respectively, as it is shown in Fig. 1.

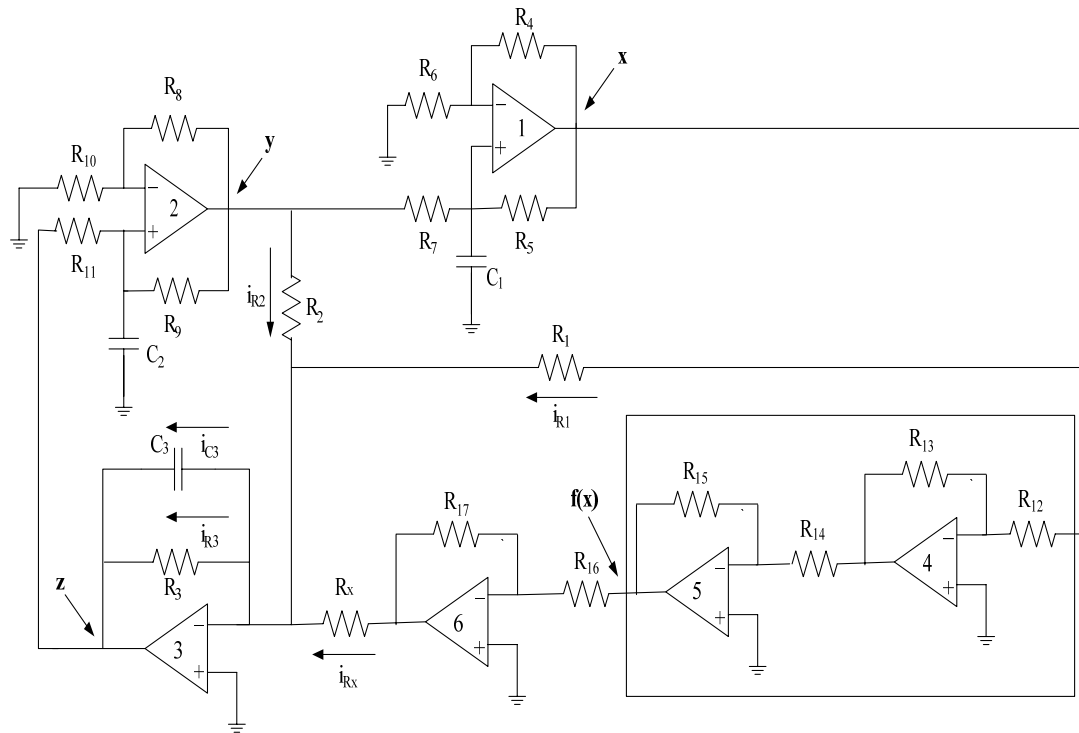


Figure 1. The proposed double scroll circuit.

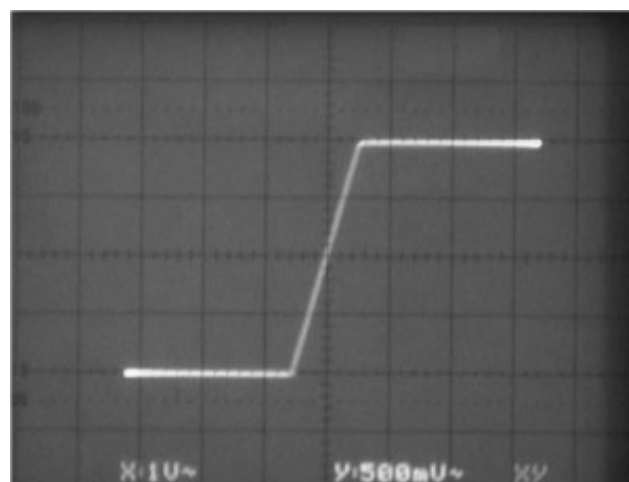


Figure 2. The characteristic curve of $f(x)$ vs. x , for the saturated circuit.
(Horizontal scale 1 V/div, Vertical scale 0.5 V/div).

3. Dynamics of the Double Scroll Circuit

The system (1) has three equilibria $S_1(0, 0, 0)$, $S_2(c/\alpha, 0, 0)$, $S_3(-c/\alpha, 0, 0)$, and eigenvalues of the form

$$\lambda_1 = \beta \text{ and } \lambda_2 = \gamma \pm \delta i. \quad (4)$$

If $\beta < 0$, $\gamma > 0$, and $\delta \neq 0$, the system appears chaotic behavior. Numerical computations show, that the system has a negative eigenvalue and one pair of complex conjugate with positive real part, when the control parameter $b < 1$. Moreover, the equilibrium point S_1 has the characteristic equation (5), while the equilibria points S_2 and S_3 have the characteristic equation (6).

$$\lambda^3 + b\lambda^2 + \alpha\lambda + \alpha = 0 \quad (5)$$

$$\lambda^3 + b\lambda^2 + \alpha\lambda + \alpha - c = 0 \quad (6)$$

For example, if $\alpha = 0.5$, $b=0.57$, and $c=1$, for which the system appears a chaotic behavior (Fig. 3), the equilibrium point S_1 , has eigenvalues, $\lambda_1 = 0.461805$, $\lambda_2 = 0.630903 - 0.827448i$, and $\lambda_3 = 0.630903 + 0.827448i$. So it is an unstable saddle. The equilibria S_2 and S_3 have eigenvalues $\lambda_1 = 0.878618$, $\lambda_2 = 0.0393091 - 0.753346i$, and $\lambda_3 = 0.0393091 + 0.753346i$, so they are called saddle points of index 2. These two equilibria correspond to the two saturated plateaus. Also, the equilibrium point S_1 is responsible for connecting the two symmetrical scrolls around the equilibria points S_2 and S_3 . Finally, for the above parameters, the Lyapunov exponents were calculated, $LE_1 = 0.16223$, $LE_2 = 0$, $LE_3 = -0.98121$. So, the numerical analysis of the proposed circuit confirmed the appearance of the chaotic attractor.

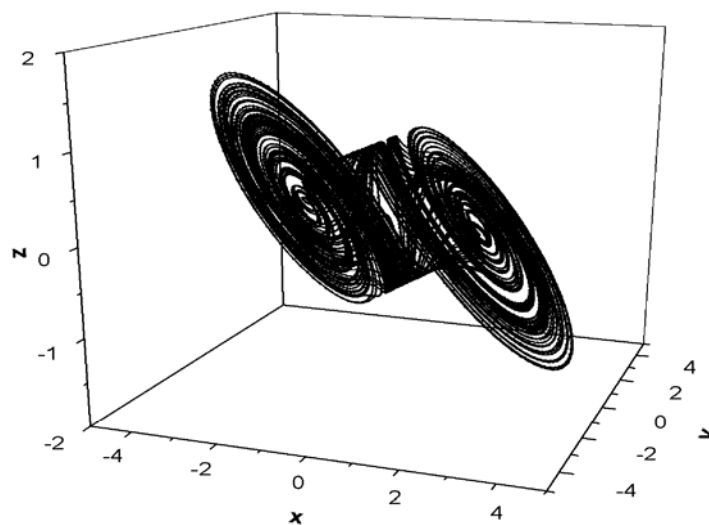
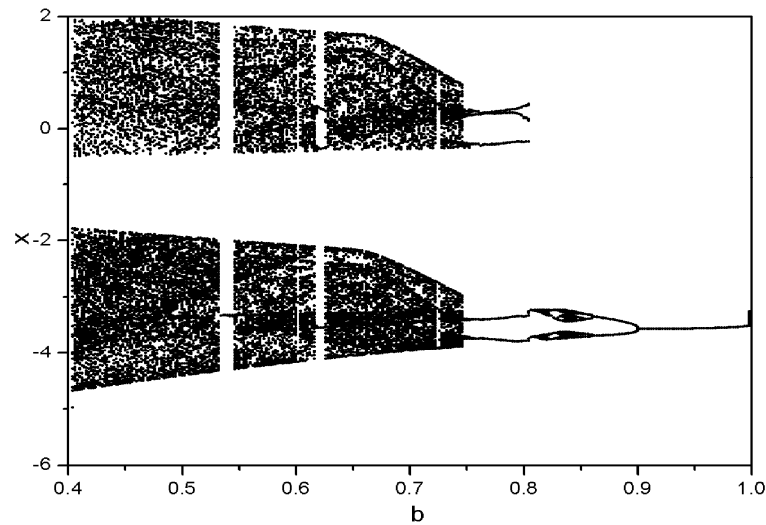


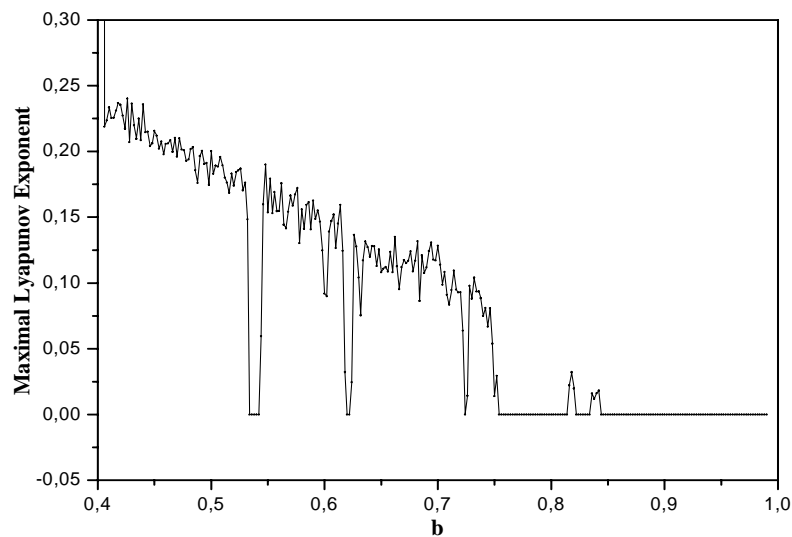
Figure 3. Double – scroll chaotic attractor, for $\alpha = 0.5$, $b=0.57$, $c = 1$, in $x - y - z$ space.

4. Experimental Results

In the beginning we retained the parameters $\alpha = b = c$ and we took the bifurcation diagram of x versus a . From this diagram, we obtained the value of α , for which the circuit shows chaotic behavior ($\alpha = 0.5$) and we took again the bifurcation diagram of x versus c of the saturation function. From the new bifurcation diagram we isolated a value of the parameter c , so that the system is in chaotic state ($c = 1$). Finally, for $\alpha = 0.5$ and $c = 1$, we took the bifurcation diagram of x versus b (Fig. 4(a)).



(a)



(b)

Figure 4. (a) Bifurcation diagram of x versus b , and (b) maximal Lyapunov exponents, for $\alpha = 0.5$ and $c = 1$.

From this diagram arises the appearance of phenomena, which are related the nonlinear dynamic and the chaos theory. The first phenomenon, which is obvious from Fig. 4(a) is the route to chaos, through the mechanism of period doubling (Fig. 5). This happens, while the value of b is decreasing, starting from the value $b = 1$. Next we observe, that after the bifurcation from period – 1 to period – 2 and specifically for $b = 0.862$ every branch creates one bubble of period – 1, that means we have a bubble of period – 2 or a ‘double’ bubble of period – 1 (Fig. 7(a)). For values of $b < 0.746$ the system goes in chaotic behavior area (Figs. 6 and 7(c)), which is interrupted from periodic windows (Fig. 7(b)). This conclusion also arises from Fig. 4(b), in which we can see the diagram of the maximal Lyapunov exponent versus the control parameter b . From the comparison of Figs. 4(a) and 4(b) we can deduct, that in chaotic areas, the maximal Lyapunov exponent has positive sign. For values $b < 0.4$, the circuit is in saturation (Fig. 7(d)), that’s why that area isn’t shown in the bifurcation diagram of Fig. 4(a).

A phenomenon, which was discovered both theoretically and experimentally, was the coexistence of attractors for various values of the initial conditions of the system. In Fig. 8 we can see the experimental phase portrait for $\alpha = 0.5$, $b = 0.95$, and $c = 1$, for which the circuit has different initial conditions. This results in limit cycles of period – 1, which appear around the equilibrium point S_3 , (Fig. 8(a)) in the first case and around the equilibrium point S_2 (Fig. 8(b)) in the second case.

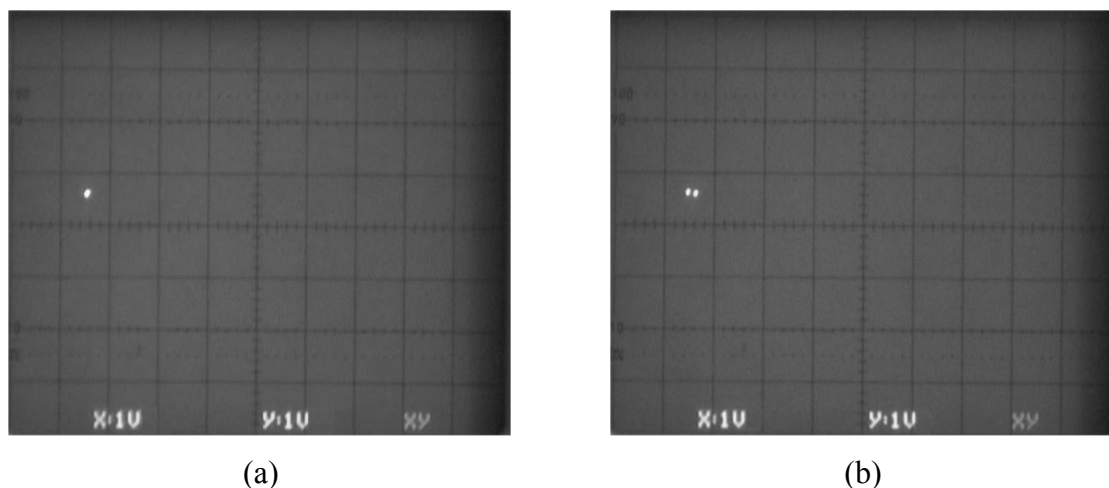


Figure 5. Experimental Poincaré maps on section $y = 0$, (a) for $\alpha = 0.5$, $b = 0.95$, and $c = 1$, the system is in period – 1 state, and (b) for $\alpha = 0.5$, $b = 0.88$, and $c = 1$, the system is in period -2 state. (Horizontal scale 1 V/div, Vertical scale 1 V/div)

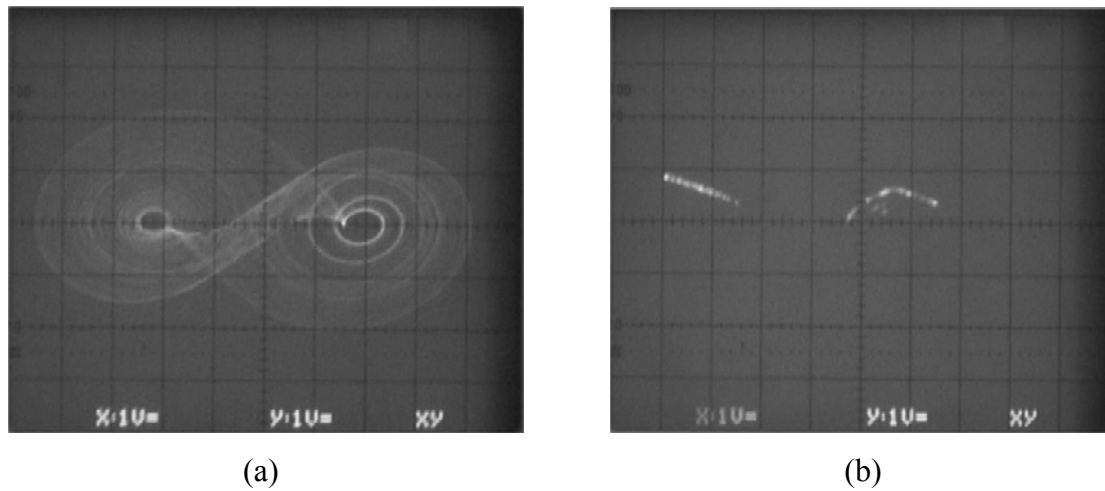


Figure 6. (a) Experimental $x - y$ plane projection, and (b) experimental Poincaré map on section $y = 0$, for $\alpha = 0.5$, $b = 0.57$, and $c = 1$. (Horizontal scale 1 V/div, Vertical scale 1 V/div)

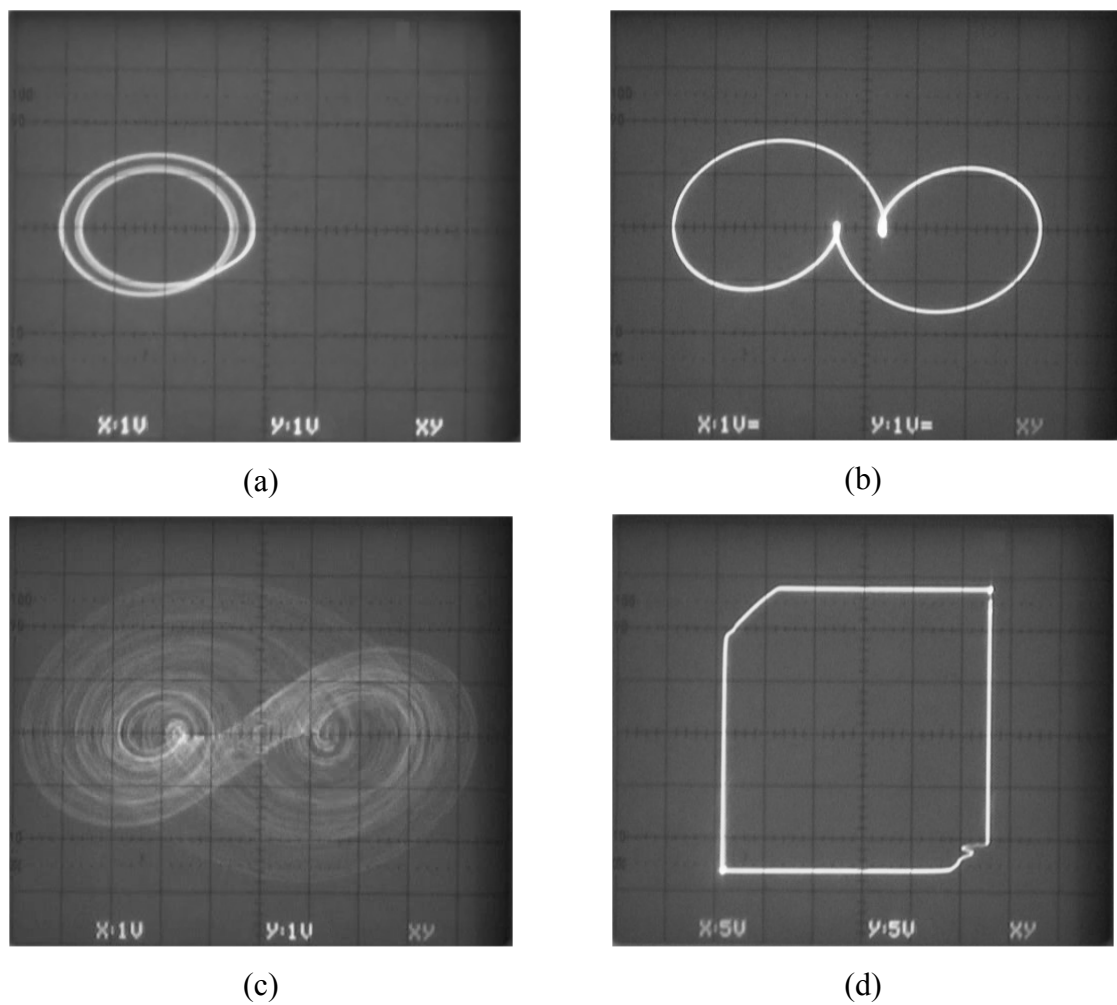


Figure 7. Experimental $x - y$ plane, (a) for $\alpha = 0.5$, $b = 0.862$, and $c = 1$, the system appear the bubble of period - 2, (b) for $\alpha = 0.5$, $b = 0.622$, and $c = 1$, the system is in

periodic state, (c) for $\alpha = 0.5$, $b = 0.862$, and $c = 1$, the system appear a double scroll attractor, and (d) for $\alpha = 0.5$, $b = 0.35$, and $c = 1$ the circuit is in a saturation region.

(Horizontal scale 1 V/div, Vertical scale 1 V/div)

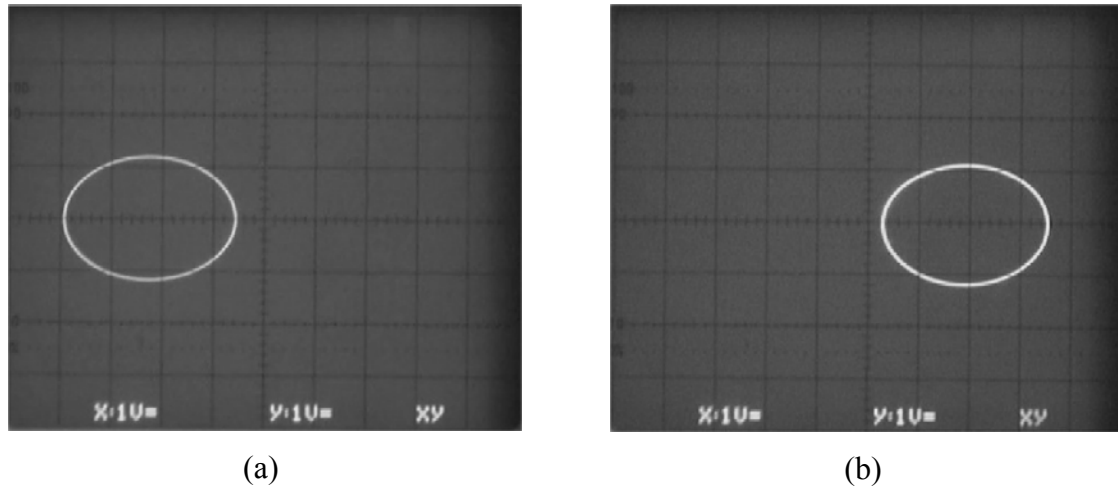


Figure 8. Experimental $x - y$ plane for $\alpha = 0.5$, $b = 0.95$, and $c = 1$, in two different sets of initial conditions. (Horizontal scale 1 V/div, Vertical scale 1 V/div)

5. CONCLUSION

This paper introduced a double scroll circuit, based on the saturated function, which was different from those in previous works. We analyzed the dynamic behavior of the proposed circuit theoretically and experimentally, and we found very interesting chaotic phenomena. Finally, the experimental results (phase portraits and Poincaré maps) confirmed the theoretical approach of the system (bifurcation diagram and Lyapunov exponents).

References

- [1] Tse C. K. and Lau F., (2003), "Chaos-based digital communication systems: operating principles," Analysis Methods, and Performance Evaluation, Berlin, New York: Springer Verlag.
- [2] Volos Ch. K., Kyprianidis I. M., and Stouboulos I. N., (2006), "Experimental demonstration of a chaotic cryptographic scheme," WSEAS Trans. Circuits Syst., 5, 1654-1661.
- [3] Stojanovski T. and Kocarev L., (2001), "Chaos-based random number generators-part I: Analysis," IEEE Trans. Circuits Syst. I, 48, 281-288.

- [4] Suykens J. A. K. and Vandewalle J., (1993) "Generation of n-double scrolls ($n = 1, 2, 3, 4, \dots$)," IEEE Trans. Circuits Syst. I, 40, no. 11, 861-867.
- [5] Suykens J. A. K., Huang A., and Chua L. O., (1997), "A family of n-scroll attractors from a generalized chua's circuit," Int. J. Electron. Commun., 51, no. 3, 131-138.
- [6] Suykens J. A. K. and Chua L. O., (1997), "n-double scroll hypercubes in 1-D CNNs," Int. J. Bifurcation Chaos, 7, no. 8, 1873-1885.
- [7] Yalcin M. E., Suykens J. A. K., Vandewalle J., and Ozoguz S., (2002), "Families of scroll grid attractors," Int. J. Bifurcation Chaos, 12, no. 1, 23-41.
- [8] Tang K. S., Zhong G. Q., Chen G., and Man K. F., (2001), "Generation of n- scroll attractors via sine function," IEEE Trans. Circuits Syst. I, 48, 1369-1372.
- [9] Lü J., Chen G., Yu X., and Leung H., (2004), "Design and analysis of multi-scroll chaotic attractors from saturated function series," IEEE Trans. Circuits Syst. I, 51, no. 2, 2476-2490.
- [10] Elwakil A. S. and Kennedy M. P., (2000), "Systematic realization of a class of hysteresis chaotic oscillators," Int. J. Circuit Theor. Appl., 28, 319-334.

Discontinuous Nanofibers by Electrospinning

Lan Xu, Ji-Huan He

Modern Textile Institute, Donghua University, 1882 Yan'an Xilu Road, Shanghai 200051, China

Email: xlmail@21cn.com

Because of ultra high specific surface, nanoporous structures, which are potentially of great technological interest for the development of electronic, catalytic and hydrogen-storage systems, invisibility device (e.g. stealth plane, stealth clothes), and others, have been caught much attention recently. Pore structure and connectivity determine how microstructured materials perform in applications such as adsorption, separation, filtering, catalysis, fluid storage and transport, electrode materials or as reactors. Far-reaching implications are emerging for applications including medical implants, cell supports, materials that can be used as instructive three-dimensional environments for tissue regeneration and others.

Nanoporous materials can be prepared by leaching the purified montmorillonite clay with sulfuric acid (H_2SO_4) solution with varying concentrations and other methods, nanoporous membranes can also be widely produced by electrospinning.

In this paper we will apply electrospinning to prepare for nanoporous microspheres. We use a kind of Chinese traditional drugs called 'Yunnan Baiyo' as an additive for possible application in drug carrier. The chosen drug 'Yunnan Baiyo' is a kind of fawn powder mixture composed of several kinds of drugs. In the field of tissue engineering, 'Yunnan Baiyo' can be added to scaffolding materials so that the material can restrain an inflammatory response. The base material for electrospun fibrous is poly(butylene succinate) (PBS), a kind of biodegradable materials. The mixture of iso-propylalcohol and chloroform with the weight ratio 1:9 was used as solvent. A control amount of PBS particles and 'Yunnan Baiyo' powder were dissolved in the mixed solvent with the weight ratio 1:6:43 ('Yunnan Baiyo': PBS: mixed solvent). All electrospinning processes were carried out under room temperature in a vertical spinning configuration.

Our experiment reveals that the numbers and sizes of electrospun nanoporous microspheres could be controlled by tunable voltage and flow rate applied in the electrospinning process. With the increase of voltage and the decrease of flow rate, there had appeared ever-increasing numbers and ever-decreasing sizes of the nanoporous microspheres. Furthermore, 'Yunnan Baiyo' can be used as an additive to control the number and size of micro spheres with nanoporosity. The mechanism is worth further studying.

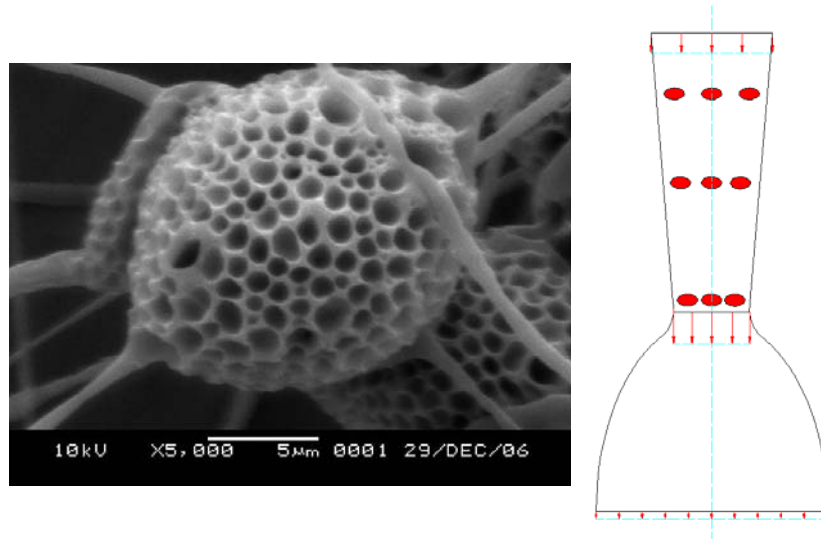


Figure 1 Macromolecular chains are compacted during the electrospinning

During the electrospinning process, the charged jet is accelerated by a constant external electric field, and the spinning velocity probably reached maximum and perhaps exceeded the velocity of sound in air in a very short time before the spinning became instability. According to the mass conservation equation $\pi r^2 \rho u = Q$, the radius of the jet decreases with the increase of the velocity of the incompressible charged jet. Macromolecules of the polymers are compacted together tighter and tighter during the electrospinning process as illustrated in Figure 1. There must exist a critical minimal radius r_{cr} for all electrospun jet $r \leq r_{cr}$ for continuous ultrafine fibers, and the critical maximal velocity is $u_{cr} = Q / \pi \rho r_{cr}^2$. However, the velocity can exceed this critical value u_{cr} if a higher voltage is applied and the distance between the needle and the collecting plate is infinite long.

In case when the radius of the jet reaches the value of the critical value $r = r_{cr}$, and the jet speed exceeds its critical value $u > u_{cr}$, in order to keep conservation of mass equation, the jet dilates by decreasing its density, leading to porosity of the electrospun fibers, we call this phenomenon as electrospinning-dilation.

In conclusion we suggested a general strategy for the synthesis of microspheres with nanoporosity by electrospinning, the porous sizes having uniform but tunable diameters can be controlled by voltage applied or flow rate in the electrospinning process. The flexibility and adaptation provided by the method have made the method a strong candidate for producing nanoporous materials.

Acknowledgement

The work is supported by National Natural Science Foundation of China under Grant No. 10372021, the 111 Project under Grant No. B07024 and Program for New Century Excellent Talents in University.

Further Generalization of Quasilinearization Method with Initial Time Difference

Coskun YAKAR and Ali YAKAR

Gebze Institute of Technology Department of Mathematics

Gebze-Kocaeli 141-41400 TURKEY

E-mail: cyakar@gyte.edu.tr and ayakar@gyte.edu.tr

01/29/2008

Abstract. In this paper, the method of the quasilinearization technique is applied to obtain upper and lower sequences with initial time difference in terms of the solutions of the linear differential equations that start at different initial times. It is also shown that these sequences converge to the unique solution of the nonlinear equation uniformly and quadratically, and uniformly and semi-quadratically. Keywords. initial time difference, quasilinearization, semi-quadratic convergence, quadratic convergence.

AMS (MOS) subject classification: 34A12, 34A45, 34C11

1 Introduction

The most important applications of the quasilinearization method has been to obtain a sequence of lower bounds which are the solutions of linear differential equations that converge quadratically. As a result, the method has been popular in applied areas. However, the convexity assumption that is demanded by the method of quasilinearization has been a stumbling block for further development of the theory. Recently, this method has been generalized, refined and extended in several directions so as to be applicable to a much larger class of nonlinear problems by not demanding convexity property. Moreover, other possibilities that have been explored make the method of generalized quasilinearization universally useful in applications [6, 9]. In the investigation of initial value problems of differential equations, we have been partial to initial time all along in the sense that we only perturb the space variable and keep the initial time unchanged. However, it appears important to vary the initial time as well because it is impossible not to make errors in the starting time [4, 5, 7, 8, 9, 10, 11]. The investigations of initial value problems of differential equations where the initial time changes with each solution in addition to the change of spatial variable have been initiated and some results on the comparison theorems, global existence, the method of variation of parameters, the method of lower and upper solutions and the method of monotone iterative techniques [3, 4, 5, 7, 10] have been obtained.

Let $\alpha_0, \beta_0 \in C^1[J, \mathbb{R}]$ with $\alpha_0(t) \leq \beta_0(t)$ on $J = [t_0, t_0 + T]$ and $\Omega = \{(t, u) : \alpha_0(t) \leq u \leq \beta_0(t), t \in J\}$.

Consider the following initial value problems

$$x' = f(t, x), \quad x(t_0) = x_0, \quad t \in J \quad (1.1)$$

$$u' = N(t, u), \quad u(t_0) = u_0, \quad t \in J \quad (1.2)$$

where $f, N \in C[\Omega, \mathbb{R}]$ and $N(t, x) = f(t, x) + g(t, x) + h(t, x)$.

That the result of generalized quasilinearization method is employed to obtain upper and lower bounds for the solution of (1.1) have been obtained in [9], when $f(t, x)$ is not convex, however $f(t, x) + \phi(t, x)$ is convex function where $\phi(t, x)$ is a convex function in x on Ω . These bounds are the sequences that have been constructed by the

solutions of linear differential equations starting at different initial times. It is also shown that these sequences converge to the unique solution of the given problem uniformly and quadratically.

We have investigated that the case [11] when the function $N(t, x)$ in (1.2) can be decomposed into a difference of two convex and concave functions on Ω and developed several result in that frame work of initial value problems of differential equations when the initial time and the position in upper and lower solutions are of natural form or of coupled form changed. We have the main result in [11] is a new initial time difference generalized quasilinearization this method provide an approximation for the solutions of (1.2), when $h(t, x) = 0$, $f(t, x)$ is convex function in x on Ω and $g(t, x)$ is concave function in x on Ω , by means of lower and upper solutions with initial time difference this technique is that generalized quasilinearization produces rapid convergence that is of great interest in applications.

In main result, we first consider the situation when the function $N(t, x)$ in (1.2) can be split as the sum of three functions $f(t, x), g(t, x), h(t, x)$. Here $f(t, x) + \phi(t, x)$ is convex function where $\phi(t, x)$ is a convex function in x on $\tilde{\Omega}$, $g(t, x) + \psi(t, x)$ is concave function where $\psi(t, x)$ is a concave function in x on $\tilde{\Omega}$ and $h(t, x)$ is only Lipschitzian in x on $\tilde{\Omega}$, and we have upper and lower solutions with initial time difference where $\tilde{\Omega}$ is $\tilde{\Omega} = \{(t, u) : t_0 \leq t \leq t_0 + T, \tilde{\alpha}_0(t) \leq u \leq \tilde{\beta}_0(t)\}$ and $\tilde{\alpha}_0(t) = \alpha_0(t), \tilde{\beta}_0(t) = \beta_0(t + \eta_1), \eta_1 = \tau_0 - t_0$. We have two new results in this set up. The first result provides nonlinear iterates due to the Lipschitzian term and gives quadratic convergence with initial time difference. In the second result, we have linear iterates and obtain semi-quadratic convergence with initial time difference. Some of the results in [5, 6, 7, 9, 11] will be special case of these results.

2 Preliminaries

In this section, we will give two useful theorems for the future reference that will be needed to prove the main results. First one is existence result in terms of the upper and lower solutions with initial time difference, the second one is comparison result.

Consider the following initial value problem

$$u' = N(t, u) = f(t, u) + g(t, u) + h(t, u), \quad u(t_0) = u_0 \quad (2.1)$$

for $t \geq t_0, t_0 \in \mathbb{R}^+$ where $f, g, h \in C[\mathbb{R}^+ \times \mathbb{R}, \mathbb{R}]$. Let $\alpha_0, \beta_0 \in C^1[J, \mathbb{R}]$ be the lower and upper solutions of (2.1) satisfying the following inequalities (2.2) and (2.3) respectively

$$\alpha'_0 \leq N(t, \alpha_0) = f(t, \alpha_0) + g(t, \alpha_0) + h(t, \alpha_0), \quad \alpha_0(t_0) \leq u_0 \quad \text{for } t \geq t_0 \quad (2.2)$$

$$\beta'_0 \geq N(t, \beta_0) = f(t, \beta_0) + g(t, \beta_0) + h(t, \alpha_0), \quad \beta_0(t_0) \geq u_0 \quad \text{for } t \geq t_0 \quad (2.3)$$

such that $\alpha_0(t) \leq \beta_0(t)$ on J . It is obvious that when the lower and upper solutions do not start the same point we need the following existence result.

Theorem 2.1: Assume that

(i) Let $\alpha_0 \in C^1[[t_0, t_0 + T], \mathbb{R}]$, $t_0, T > 0$, $\beta_0 \in C^1[[\tau_0, \tau_0 + T], \mathbb{R}]$, $\tau_0 > 0$ and $f, g, h \in C[\mathbb{R}^+ \times \mathbb{R}, \mathbb{R}]$, $\alpha'_0(t) \leq f(t, \alpha_0) + g(t, \alpha_0) + h(t, \alpha_0)$, $t_0 \leq t \leq t_0 + T$ and $\beta'_0(t) \geq f(t, \beta_0) + g(t, \beta_0) + h(t, \beta_0)$, $\tau_0 \leq t \leq \tau_0 + T$ with $\alpha_0(t_0) \leq \beta_0(\tau_0)$;

(ii) $t_0 < \tau_0$, $f(t, u), g(t, u)$ and $h(t, u)$ are nondecreasing in t for each u and $\alpha_0(t) \leq \beta_0(t + \eta)$ for $t_0 \leq t \leq t_0 + T$ where $\eta = \tau_0 - t_0$.

Then there exist a solution $u(t)$ of (2.1) with $u(t_0) = u_0$, satisfying $\alpha_0(t) \leq u(t) \leq \beta_0(t + \eta)$ for $t_0 \leq t \leq t_0 + T$.

Proof 2.1: For the proof, we let $\beta(t) = \beta_0(t + \eta)$, and proceed the Theorem 1.1.4, page 4 in [3] for $\alpha_0(t)$ and $\beta(t)$. We omit the detail.

Now we will give the following comparison result.

Theorem 2.2: Let $x, y \in C^1[[0, T], \mathbb{R}]$ be lower and upper solutions of (2.1) respectively and $f, g, h \in C[[0, T] \times \mathbb{R}, \mathbb{R}]$. Suppose that

$$[f(t, w_1) - f(t, w_2)] + [g(t, w_1) - g(t, w_2)] + [h(t, w_1) - h(t, w_2)] \leq L(w_1 - w_2)$$

whenever $w_1 \geq w_2$ for some $L > 0$. Then $x(0) \leq y(0)$ implies that $x(t) \leq y(t)$ for $t \in [0, T]$.

Proof 2.2: For the proof, let $\tilde{f} = f + g + h$. First, one can prove the theorem very easily for strict inequalities by using proof by contradiction.. That is $x(t) < y(t)$ for $t \in [0, T]$ if $\frac{dy(t)}{dt} > \tilde{f}(t, y(t))$, $\frac{dx(t)}{dt} \leq \tilde{f}(t, x(t))$, $t \in [0, T]$ and $x(0) < y(0)$. Define $\tilde{y}(t) = y(t) + \epsilon e^{2Lt}$, where ϵ is sufficiently small. Then we obtain $\frac{d\tilde{y}(t)}{dt} > \tilde{f}(t, \tilde{y}(t))$. We have $x(0) \leq y(0) < \tilde{y}(0)$. Therefore it follows from the previous argument that $x(t) < \tilde{y}(t)$ for $t \in [0, T]$. Letting $\epsilon \rightarrow 0$, we have the desired result. The details (Theorem 1.1.1, page 2 in [3]) are omitted.

3 Main Results

In this section, we will prove two theorems that give several different conditions to apply the method of generalized quasilinearization to the nonlinear differential equations with initial time difference and state corollaries for special cases.

Theorem 3.1: Assume that

(A₁) $\alpha_0 \in C^1[[t_0, t_0 + T], \mathbb{R}]$ and $\beta_0 \in C^1[[\tau_0, \tau_0 + T], \mathbb{R}]$ for $\tau_0 > t_0 > 0$ and $T > 0$,

$$\begin{aligned} \alpha'_0 &\leq N(t, \alpha_0) = f(t, \alpha_0) + g(t, \alpha_0) + h(t, \alpha_0) \text{ for } t_0 \leq t \leq t_0 + T \\ \beta'_0 &\geq N(t, \beta_0) = f(t, \beta_0) + g(t, \beta_0) + h(t, \beta_0) \text{ for } \tau_0 \leq t \leq \tau_0 + T, \end{aligned}$$

where $f, g, h \in C[[t_0, \tau_0 + T] \times \mathbb{R}, \mathbb{R}]$ and $\alpha_0(t_0) \leq \beta_0(\tau_0)$;

(A₂) $t_0 < s_0 < \tau_0$, $f(t, x), g(t, x), h(t, x)$ are nondecreasing in t for each x ;

(A₃) $N \in C[\tilde{\Omega}, \mathbb{R}]$, $N(t, x) = f(t, x) + g(t, x) + h(t, x)$, f_x, g_x, f_{xx}, g_{xx} exist and are continuous functions

satisfying $F = f + \phi, G = g + \psi, F_{xx} = f_{xx} + \phi_{xx} \geq 0, G_{xx} = g_{xx} + \psi_{xx} \leq 0$ on $\tilde{\Omega}$ and $\phi, \psi \in C^{0,2}[\tilde{\Omega}, \mathbb{R}]$ such that $\phi_{xx} \geq 0, \psi_{xx} \leq 0$ on $\tilde{\Omega}$ and $h(t, x)$ satisfies $h(t, x_1) - h(t, x_2) \leq k(x_1 - x_2)$ whenever $x_1 \geq x_2, x_1, x_2 \in \tilde{\Omega}$, where $k > 0$ is the Lipschitz constant. Further more, $\tilde{x}(t)$ is the unique solution of $\tilde{x}'(t) = N(t + \eta_2, \tilde{x}), \eta_2 = s_0 - t_0$.

Then there exist monotone sequences $\{\tilde{\alpha}_n(t)\}$ and $\{\tilde{\beta}_n(t)\}$ which converge uniformly to the unique solution of (2.1) with $x(s_0) = x_0$ where s_0 is the initial time of the transformed initial value problem of (3.10) on $[s_0, s_0 + T]$, and the convergence is quadratic.

Proof: Since $\tilde{\beta}_0(t) = \beta_0(t + \eta_1)$, we get $\tilde{\beta}_0(t_0) = \beta_0(\tau_0) \geq \alpha_0(t_0) = \tilde{\alpha}_0(t_0)$ and

$\tilde{\beta}'_0(t) \geq N(t + \eta_1, \tilde{\beta}_0)$ for $t_0 \leq t \leq t_0 + T$. Using the assumptions $F_{xx} \geq 0, G_{xx} \leq 0$ yield the following inequalities

$$f(t, x) \geq f(t, y) + F_x(t, y)(x - y) + \phi(t, y) - \phi(t, x) \quad (3.1)$$

$$g(t, x) \geq g(t, y) + G_x(t, y)(x - y) + \psi(t, y) - \psi(t, x)$$

and also by using (A₃) we see that whenever $\tilde{\alpha}_0(t) \leq y \leq x \leq \tilde{\beta}_0(t)$

$$N(t, x) - N(t, y) \leq L(x - y) \quad (3.2)$$

for some $L > 0$.

Consider the Initial Value Problems

$$\begin{aligned} u' &= M(t + \eta_2, \tilde{\alpha}_0, \tilde{\beta}_0; u), \quad u(t_0) = x_0 \\ &= f(t + \eta_2, \tilde{\alpha}_0) + g(t + \eta_2, \tilde{\alpha}_0) + h(t + \eta_2, u) \\ &\quad + [F_x(t + \eta_2, \tilde{\alpha}_0) + G_x(t + \eta_2, \tilde{\beta}_0) - \phi_x(t + \eta_2, \tilde{\beta}_0) - \psi_x(t + \eta_2, \tilde{\alpha}_0)](u - \tilde{\alpha}_0) \end{aligned} \quad (3.3)$$

$$\begin{aligned}
v' &= K \left(t + \eta_2, \tilde{\alpha}_0, \tilde{\beta}_0; v \right), \quad v(t_0) = x_0 \\
&= f \left(t + \eta_2, \tilde{\beta}_0 \right) + g \left(t + \eta_2, \tilde{\beta}_0 \right) + h \left(t + \eta_2, v \right) \\
&\quad + \left[F_x \left(t + \eta_2, \tilde{\alpha}_0 \right) + G_x \left(t + \eta_2, \tilde{\beta}_0 \right) - \phi_x \left(t + \eta_2, \tilde{\beta}_0 \right) - \psi_x \left(t + \eta_2, \tilde{\alpha}_0 \right) \right] \left(v - \tilde{\beta}_0 \right)
\end{aligned} \tag{3.4}$$

Note that these equations are nonlinear in u and v respectively.

The inequality (3.1) and (A_1) imply

$$\begin{aligned}
\tilde{\alpha}'_0 &\leq N(t + \eta_2, \tilde{\alpha}_0) \\
&= f(t + \eta_2, \tilde{\alpha}_0) + g(t + \eta_2, \tilde{\alpha}_0) + h(t + \eta_2, \tilde{\alpha}_0) \equiv M(t + \eta_2, \tilde{\alpha}_0, \tilde{\beta}_0; \tilde{\alpha}_0) \\
\tilde{\beta}'_0 &\geq N(t + \eta_2, \tilde{\beta}_0) \\
&\geq f(t + \eta_2, \tilde{\alpha}_0) + F_x(t + \eta_2, \tilde{\alpha}_0)(\tilde{\beta}_0 - \tilde{\alpha}_0) + \phi(t + \eta_2, \tilde{\alpha}_0) - \phi(t + \eta_2, \tilde{\beta}_0) \\
&\quad + g(t + \eta_2, \tilde{\alpha}_0) + G_x(t + \eta_2, \tilde{\beta}_0)(\tilde{\beta}_0 - \tilde{\alpha}_0) + \psi(t + \eta_2, \tilde{\alpha}_0) - \psi(t + \eta_2, \tilde{\beta}_0) + h(t + \eta_2, \tilde{\beta}_0) \\
&\geq f(t + \eta_2, \tilde{\alpha}_0) + g(t + \eta_2, \tilde{\alpha}_0) + h(t + \eta_2, \tilde{\beta}_0) \\
&\quad + \left[F_x(t + \eta_2, \tilde{\alpha}_0) + G_x(t + \eta_2, \tilde{\beta}_0) - \phi_x(t + \eta_2, \tilde{\beta}_0) - \psi_x(t + \eta_2, \tilde{\alpha}_0) \right] (\tilde{\beta}_0 - \tilde{\alpha}_0) \\
&\equiv M(t + \eta_2, \tilde{\alpha}_0, \tilde{\beta}_0; \tilde{\beta}_0)
\end{aligned}$$

Therefore, we see that $\tilde{\alpha}_0$ and $\tilde{\beta}_0$ are lower and upper solutions of (3.3) respectively. Hence by Theorem 2.1, it follows that there exist a solution $\tilde{\alpha}_1(t)$ of (3.3) such that $\tilde{\alpha}_0(t) \leq \tilde{\alpha}_1(t) \leq \tilde{\beta}_0(t)$, $t \in J = [t_0, t_0 + T]$. Since M satisfies a Lipschitz condition, it follows that $\tilde{\alpha}_1(t)$ is a unique on J .

We now show that $\tilde{\alpha}_0$ is a lower solution of (3.4) and $\tilde{\beta}_0$ is an upper solution of (3.4). Using (3.1) and (A_1) and ϕ_x is increasing ψ_x is decreasing on $\tilde{\Omega}$, we have

$$\begin{aligned}
\alpha'_0(t) &\leq N(t + \eta_2, \tilde{\alpha}_0) \\
&\leq f(t + \eta_2, \tilde{\beta}_0) - F_x(t + \eta_2, \tilde{\alpha}_0)(\tilde{\beta}_0 - \tilde{\alpha}_0) - \phi(t + \eta_2, \tilde{\alpha}_0) + \phi(t + \eta_2, \tilde{\beta}_0) \\
&\quad + g(t + \eta_2, \tilde{\beta}_0) + G_x(t + \eta_2, \tilde{\beta}_0)(\tilde{\alpha}_0 - \tilde{\beta}_0) + \psi(t + \eta_2, \tilde{\beta}_0) - \psi(t + \eta_2, \tilde{\alpha}_0) + h(t + \eta_2, \tilde{\alpha}_0) \\
&\leq f(t + \eta_2, \tilde{\beta}_0) + g(t + \eta_2, \tilde{\beta}_0) + h(t + \eta_2, \tilde{\alpha}_0) \\
&\quad + \left[F_x(t + \eta_2, \tilde{\alpha}_0) + G_x(t + \eta_2, \tilde{\beta}_0) - \phi_x(t + \eta_2, \tilde{\beta}_0) - \psi_x(t + \eta_2, \tilde{\alpha}_0) \right] (\tilde{\alpha}_0 - \tilde{\beta}_0) \\
&\equiv K(t + \eta_2, \tilde{\alpha}_0, \tilde{\beta}_0; \tilde{\alpha}_0) \\
\beta'_0(t) &\geq N(t + \eta_2, \tilde{\beta}_0) \\
&= f(t + \eta_2, \tilde{\beta}_0) + g(t + \eta_2, \tilde{\beta}_0) + h(t + \eta_2, \tilde{\beta}_0) \\
&\equiv K(t + \eta_2, \tilde{\alpha}_0, \tilde{\beta}_0; \tilde{\beta}_0)
\end{aligned}$$

Therefore by using Theorem 2.1, as before, there exist a solution $\tilde{\beta}_1(t)$ of (3.4) such that $\tilde{\alpha}_0(t) \leq \tilde{\beta}_1(t) \leq \tilde{\beta}_0(t)$, $t \in [t_0, t_0 + T]$. Since K satisfies the Lipschitz condition, it follows that $\tilde{\beta}_1(t)$ is a unique on J .

We must show that $\tilde{\alpha}_1$ and $\tilde{\beta}_1$ are lower and upper solutions of (2.1); respectively. Thus

$$\tilde{\alpha}'_1(t) = M(t + \eta_2, \tilde{\alpha}_0, \tilde{\beta}_0; \tilde{\alpha}_1), \quad \tilde{\alpha}_1(t_0) = x_0$$

we get

$$\begin{aligned}
\tilde{\alpha}'_1(t) &= f(t + \eta_2, \tilde{\alpha}_0) + g(t + \eta_2, \tilde{\alpha}_0) + h(t + \eta_2, \tilde{\alpha}_1) \\
&\quad + \left[F_x(t + \eta_2, \tilde{\alpha}_0) + G_x(t + \eta_2, \tilde{\beta}_0) - \phi_x(t + \eta_2, \tilde{\beta}_0) - \psi_x(t + \eta_2, \tilde{\alpha}_0) \right] (\tilde{\alpha}_1 - \tilde{\alpha}_0) \\
&\leq f(t + \eta_2, \tilde{\alpha}_1) - F_x(t + \eta_2, \tilde{\alpha}_0) (\tilde{\alpha}_1 - \tilde{\alpha}_0) - \phi(t + \eta_2, \tilde{\alpha}_0) + \phi(t + \eta_2, \tilde{\alpha}_1) \\
&\quad + g(t + \eta_2, \tilde{\alpha}_1) - G_x(t + \eta_2, \tilde{\alpha}_1) (\tilde{\alpha}_1 - \tilde{\alpha}_0) + \psi(t + \eta_2, \tilde{\alpha}_1) - \psi(t + \eta_2, \tilde{\alpha}_0) \\
&\quad + \left[F_x(t + \eta_2, \tilde{\alpha}_0) + G_x(t + \eta_2, \tilde{\beta}_0) - \phi_x(t + \eta_2, \tilde{\beta}_0) - \psi_x(t + \eta_2, \tilde{\alpha}_0) \right] (\tilde{\alpha}_1 - \tilde{\alpha}_0) + h(t + \eta_2, \tilde{\alpha}_1) \\
&\leq f(t + \eta_2, \tilde{\alpha}_1) + \phi_x(t + \eta_2, \tilde{\beta}_0) (\tilde{\alpha}_1 - \tilde{\alpha}_0) - G_x(t + \eta_2, \tilde{\beta}_0) (\tilde{\alpha}_1 - \tilde{\alpha}_0) + g(t + \eta_2, \tilde{\alpha}_1) \\
&\quad + \psi_x(t + \eta_2, \tilde{\alpha}_0) (\tilde{\alpha}_1 - \tilde{\alpha}_0) + \left[G_x(t + \eta_2, \tilde{\beta}_0) - \phi_x(t + \eta_2, \tilde{\beta}_0) - \psi_x(t + \eta_2, \tilde{\alpha}_0) \right] (\tilde{\alpha}_1 - \tilde{\alpha}_0) + h(t + \eta_2, \tilde{\alpha}_1) \\
&= N(t + \eta_2, \tilde{\alpha}_1)
\end{aligned}$$

because of the fact that G_x and ψ_x are nonincreasing, ϕ_x is nondecreasing on $\tilde{\Omega}$ and $\tilde{\alpha}_0(t) \leq \tilde{\alpha}_1(t) \leq \tilde{\beta}_0(t)$. Similarly we get using (3.4)

$$\begin{aligned}
\tilde{\beta}'_1(t) &\equiv K(t + \eta_2, \tilde{\alpha}_0, \tilde{\beta}_0; \tilde{\beta}_1), \quad \tilde{\beta}_1(t_0) = x_0 \\
&\geq f(t + \eta_2, \tilde{\beta}_1) - F_x(t + \eta_2, \tilde{\beta}_1) (\tilde{\beta}_1 - \tilde{\beta}_0) + \phi(t + \eta_2, \tilde{\beta}_1) - \phi(t + \eta_2, \tilde{\beta}_0) \\
&\quad + g(t + \eta_2, \tilde{\beta}_1) - G_x(t + \eta_2, \tilde{\beta}_0) (\tilde{\beta}_1 - \tilde{\beta}_0) + \psi(t + \eta_2, \tilde{\beta}_1) - \psi(t + \eta_2, \tilde{\beta}_0) \\
&\quad + h(t + \eta_2, \tilde{\beta}_1) + \left[F_x(t + \eta_2, \tilde{\alpha}_0) + G_x(t + \eta_2, \tilde{\beta}_0) - \phi_x(t + \eta_2, \tilde{\beta}_0) - \psi_x(t + \eta_2, \tilde{\alpha}_0) \right] (\tilde{\beta}_1 - \tilde{\beta}_0) \\
&\geq f(t + \eta_2, \tilde{\beta}_1) + g(t + \eta_2, \tilde{\beta}_1) + h(t + \eta_2, \tilde{\beta}_1) - F_x(t + \eta_2, \tilde{\beta}_1) (\tilde{\beta}_1 - \tilde{\beta}_0) - \phi_x(t + \eta_2, \tilde{\beta}_0) (\tilde{\beta}_0 - \tilde{\beta}_1) \\
&\quad - \psi_x(t + \eta_2, \tilde{\beta}_1) (\tilde{\beta}_0 - \tilde{\beta}_1) + \left[F_x(t + \eta_2, \tilde{\alpha}_0) - \phi_x(t + \eta_2, \tilde{\beta}_0) - \psi_x(t + \eta_2, \tilde{\beta}_1) \right] (\tilde{\beta}_1 - \tilde{\beta}_0) \\
&\geq N(t + \eta_2, \tilde{\beta}_1)
\end{aligned}$$

because of the fact that F_x is nondecreasing in x on $\tilde{\Omega}$ and $\tilde{\alpha}_0 \leq \tilde{\beta}_1 \leq \tilde{\beta}_0$. Also from (A_3) , N satisfies the Lipschitz condition, it then follows from Theorem 2.2 that $\tilde{\alpha}_1 \leq \tilde{\beta}_1$ on J . Thus we obtain

$$\tilde{\alpha}_0 \leq \tilde{\alpha}_1 \leq \tilde{\beta}_1 \leq \tilde{\beta}_0 \text{ on } J.$$

We now prove by induction that $\tilde{\alpha}_0 \leq \tilde{\alpha}_1 \leq \tilde{\alpha}_2 \leq \dots \leq \tilde{\alpha}_n \leq \tilde{\alpha}_{n+1} \leq \tilde{\beta}_{n+1} \leq \tilde{\beta}_n \leq \dots \leq \tilde{\beta}_2 \leq \tilde{\beta}_1 \leq \tilde{\beta}_0$ on J . Consider the following IVP

$$\begin{aligned}
u' &= M(t + \eta_2, \tilde{\alpha}_n, \tilde{\beta}_n; u), \quad u(t_0) = x_0 \\
&= f(t + \eta_2, \tilde{\alpha}_n) + g(t + \eta_2, \tilde{\alpha}_n) + h(t + \eta_2, u) \\
&\quad + \left[F_x(t + \eta_2, \tilde{\alpha}_n) + G_x(t + \eta_2, \tilde{\beta}_n) - \phi_x(t + \eta_2, \tilde{\beta}_n) - \psi_x(t + \eta_2, \tilde{\alpha}_n) \right] (u - \tilde{\alpha}_n)
\end{aligned} \tag{3.5}$$

Assume that for some $n > 1$, $\tilde{\alpha}_0 \leq \tilde{\alpha}_n \leq \tilde{\beta}_n \leq \tilde{\beta}_0$ on J . We must show that $\tilde{\alpha}_0 \leq \tilde{\alpha}_{n+1} \leq \tilde{\beta}_{n+1} \leq \tilde{\beta}_0$ on J . For that, consider

$$\begin{aligned}
\tilde{\alpha}'_n &= f(t + \eta_2, \tilde{\alpha}_{n-1}) + g(t + \eta_2, \tilde{\alpha}_{n-1}) + h(t + \eta_2, \tilde{\alpha}_n) \\
&\quad + \left[F_x(t + \eta_2, \tilde{\alpha}_{n-1}) + G_x(t + \eta_2, \tilde{\beta}_{n-1}) - \phi_x(t + \eta_2, \tilde{\beta}_{n-1}) - \psi_x(t + \eta_2, \tilde{\alpha}_{n-1}) \right] (\tilde{\alpha}_n - \tilde{\alpha}_{n-1}) \\
&\leq f(t + \eta_2, \tilde{\alpha}_n) - F_x(t + \eta_2, \tilde{\alpha}_{n-1}) (\tilde{\alpha}_n - \tilde{\alpha}_{n-1}) - \phi(t + \eta_2, \tilde{\alpha}_{n-1}) + \phi(t + \eta_2, \tilde{\alpha}_n) \\
&\quad + g(t + \eta_2, \tilde{\alpha}_n) - G_x(t + \eta_2, \tilde{\alpha}_n) (\tilde{\alpha}_n - \tilde{\alpha}_{n-1}) + \psi(t + \eta_2, \tilde{\alpha}_n) - \psi(t + \eta_2, \tilde{\alpha}_{n-1}) + h(t + \eta_2, \tilde{\alpha}_n) \\
&\quad + \left[F_x(t + \eta_2, \tilde{\alpha}_{n-1}) + G_x(t + \eta_2, \tilde{\beta}_{n-1}) - \phi_x(t + \eta_2, \tilde{\beta}_{n-1}) - \psi_x(t + \eta_2, \tilde{\alpha}_{n-1}) \right] (\tilde{\alpha}_n - \tilde{\alpha}_{n-1}) \\
&\leq f(t + \eta_2, \tilde{\alpha}_n) + g(t + \eta_2, \tilde{\alpha}_n) + h(t + \eta_2, \tilde{\alpha}_n) - G_x(t + \eta_2, \tilde{\alpha}_n) (\tilde{\alpha}_n - \tilde{\alpha}_{n-1}) \\
&\quad + G_x(t + \eta_2, \tilde{\alpha}_n) (\tilde{\alpha}_n - \tilde{\alpha}_{n-1}) + \phi_x(t + \eta_2, \tilde{\beta}_{n-1}) (\tilde{\alpha}_n - \tilde{\alpha}_{n-1}) - \phi_x(t + \eta_2, \tilde{\beta}_{n-1}) (\tilde{\alpha}_n - \tilde{\alpha}_{n-1}) \\
&\quad + \psi_x(t + \eta_2, \tilde{\alpha}_{n-1}) (\tilde{\alpha}_n - \tilde{\alpha}_{n-1}) - \psi_x(t + \eta_2, \tilde{\alpha}_{n-1}) (\tilde{\alpha}_n - \tilde{\alpha}_{n-1}) \\
&= f(t + \eta_2, \tilde{\alpha}_n) + g(t + \eta_2, \tilde{\alpha}_n) + h(t + \eta_2, \tilde{\alpha}_n) \\
&\equiv M(t + \eta_2, \tilde{\alpha}_n, \tilde{\beta}_n; \tilde{\alpha}_n)
\end{aligned}$$

from (3.1) and the fact that ϕ_x is increasing ψ_x and G_x are decreasing on $\tilde{\Omega}$. This implies that $\tilde{\alpha}_n(t)$ is a lower solution of (3.5). Similarly we will prove that $\tilde{\beta}_n$ is an upper solution of (3.5) on J .

$$\begin{aligned}
\tilde{\beta}'_n &= f(t + \eta_2, \tilde{\beta}_{n-1}) + g(t + \eta_2, \tilde{\beta}_{n-1}) + h(t + \eta_2, \tilde{\beta}_n) \\
&\quad + \left[F_x(t + \eta_2, \tilde{\alpha}_{n-1}) + G_x(t + \eta_2, \tilde{\beta}_{n-1}) - \phi_x(t + \eta_2, \tilde{\beta}_{n-1}) - \psi_x(t + \eta_2, \tilde{\alpha}_{n-1}) \right] (\tilde{\beta}_n - \tilde{\beta}_{n-1}) \\
&\geq f(t + \eta_2, \tilde{\alpha}_n) + F_x(t + \eta_2, \tilde{\alpha}_n) (\tilde{\beta}_{n-1} - \tilde{\alpha}_n) + \phi(t + \eta_2, \tilde{\alpha}_n) - \phi(t + \eta_2, \tilde{\beta}_{n-1}) + g(t + \eta_2, \tilde{\alpha}_n) \\
&\quad + G_x(t + \eta_2, \tilde{\beta}_{n-1}) (\tilde{\beta}_{n-1} - \tilde{\alpha}_n) - \psi(t + \eta_2, \tilde{\beta}_{n-1}) + \psi(t + \eta_2, \tilde{\alpha}_n) + h(t + \eta_2, \tilde{\beta}_n) \\
&\quad + \left[F_x(t + \eta_2, \tilde{\alpha}_{n-1}) + G_x(t + \eta_2, \tilde{\beta}_{n-1}) - \phi_x(t + \eta_2, \tilde{\beta}_{n-1}) - \psi_x(t + \eta_2, \tilde{\alpha}_{n-1}) \right] (\tilde{\beta}_n - \tilde{\beta}_{n-1}) \\
&\geq f(t + \eta_2, \tilde{\alpha}_n) + g(t + \eta_2, \tilde{\alpha}_n) + h(t + \eta_2, \tilde{\beta}_n) + F_x(t + \eta_2, \tilde{\alpha}_n) (\tilde{\beta}_{n-1} - \tilde{\alpha}_n) + F_x(t + \eta_2, \tilde{\alpha}_{n-1}) (\tilde{\beta}_n - \tilde{\beta}_{n-1}) \\
&\quad - \phi_x(t + \eta_2, \tilde{\beta}_{n-1}) (\tilde{\beta}_{n-1} - \tilde{\alpha}_n) + G_x(t + \eta_2, \tilde{\beta}_{n-1}) (\tilde{\beta}_{n-1} - \tilde{\alpha}_n) + G_x(t + \eta_2, \tilde{\beta}_{n-1}) (\tilde{\beta}_n - \tilde{\beta}_{n-1}) \\
&\quad - \psi_x(t + \eta_2, \tilde{\alpha}_{n-1}) (\tilde{\beta}_{n-1} - \tilde{\alpha}_n) - \psi_x(t + \eta_2, \tilde{\alpha}_{n-1}) (\tilde{\beta}_n - \tilde{\beta}_{n-1}) - \phi_x(t + \eta_2, \tilde{\beta}_{n-1}) (\tilde{\beta}_n - \tilde{\beta}_{n-1}) \\
&\geq f(t + \eta_2, \tilde{\alpha}_n) + g(t + \eta_2, \tilde{\alpha}_n) + h(t + \eta_2, \tilde{\beta}_n) - F_x(t + \eta_2, \tilde{\alpha}_n) (\tilde{\alpha}_n - \tilde{\beta}_n) + \phi_x(t + \eta_2, \tilde{\beta}_{n-1}) (\tilde{\alpha}_n - \tilde{\beta}_n) \\
&\quad - G_x(t + \eta_2, \tilde{\beta}_{n-1}) (\tilde{\alpha}_n - \tilde{\beta}_n) + \psi_x(t + \eta_2, \tilde{\alpha}_{n-1}) (\tilde{\alpha}_n - \tilde{\beta}_n) \\
&\geq f(t + \eta_2, \tilde{\alpha}_n) + g(t + \eta_2, \tilde{\alpha}_n) + h(t + \eta_2, \tilde{\beta}_n) \\
&\quad + \left[F_x(t + \eta_2, \tilde{\alpha}_n) + G_x(t + \eta_2, \tilde{\beta}_n) - \phi_x(t + \eta_2, \tilde{\beta}_n) - \psi_x(t + \eta_2, \tilde{\alpha}_n) \right] (\tilde{\beta}_n - \tilde{\alpha}_n) \\
&\equiv M(t + \eta_2, \tilde{\alpha}_n, \tilde{\beta}_n; \tilde{\beta}_n)
\end{aligned}$$

where we have used (3.1) and the fact that ϕ_x and F_x are increasing on $\tilde{\Omega}$ and ψ_x and G_x are decreasing on $\tilde{\Omega}$. Thus, employing Theorem 2.1 gives a solution $\tilde{\alpha}_{n+1}$ of (3.5) such that $\tilde{\alpha}_n \leq \tilde{\alpha}_{n+1} \leq \tilde{\beta}_n$ on J . Since M satisfies the Lipschitz condition, it follows that $\tilde{\alpha}_{n+1}(t)$ is a unique on J . In a similar way we can prove that $\tilde{\alpha}_n \leq \tilde{\beta}_{n+1} \leq \tilde{\beta}_n$ on J . Next we must prove that $\tilde{\alpha}_{n+1} \leq \tilde{\beta}_{n+1}$ on J . For that purpose, consider

$$\begin{aligned}
\tilde{\alpha}'_{n+1} &= f(t + \eta_2, \tilde{\alpha}_n) + g(t + \eta_2, \tilde{\alpha}_n) + h(t + \eta_2, \tilde{\alpha}_{n+1}) \\
&\quad + \left[F_x(t + \eta_2, \tilde{\alpha}_n) + G_x(t + \eta_2, \tilde{\beta}_n) - \phi_x(t + \eta_2, \tilde{\beta}_n) - \psi_x(t + \eta_2, \tilde{\alpha}_n) \right] (\tilde{\alpha}_{n+1} - \tilde{\alpha}_n) \\
&\leq f(t + \eta_2, \tilde{\alpha}_{n+1}) - F_x(t + \eta_2, \tilde{\alpha}_n) (\tilde{\alpha}_{n+1} - \tilde{\alpha}_n) - \phi(t + \eta_2, \tilde{\alpha}_n) + \phi(t + \eta_2, \tilde{\alpha}_{n+1}) \\
&\quad + g(t + \eta_2, \tilde{\alpha}_{n+1}) + G_x(t + \eta_2, \tilde{\alpha}_{n+1}) (\tilde{\alpha}_n - \tilde{\alpha}_{n+1}) - \psi(t + \eta_2, \tilde{\alpha}_n) + \psi(t + \eta_2, \tilde{\alpha}_{n+1}) \\
&\quad + h(t + \eta_2, \tilde{\alpha}_{n+1}) + \left[F_x(t + \eta_2, \tilde{\alpha}_n) + G_x(t + \eta_2, \tilde{\beta}_n) - \phi_x(t + \eta_2, \tilde{\beta}_n) - \psi_x(t + \eta_2, \tilde{\alpha}_n) \right] (\tilde{\alpha}_{n+1} - \tilde{\alpha}_n) \\
&\leq f(t + \eta_2, \tilde{\alpha}_{n+1}) + \phi_x(t + \eta_2, \tilde{\beta}_n) (\tilde{\alpha}_{n+1} - \tilde{\alpha}_n) + \psi_x(t + \eta_2, \tilde{\alpha}_n) (\tilde{\alpha}_{n+1} - \tilde{\alpha}_n) + g(t + \eta_2, \tilde{\alpha}_{n+1}) - G_x(t + \eta_2, \tilde{\beta}_n) (\tilde{\alpha}_n - \tilde{\alpha}_{n+1}) \\
&\quad + h(t + \eta_2, \tilde{\alpha}_{n+1}) + G_x(t + \eta_2, \tilde{\beta}_n) (\tilde{\alpha}_{n+1} - \tilde{\alpha}_n) - \phi_x(t + \eta_2, \tilde{\beta}_n) (\tilde{\alpha}_{n+1} - \tilde{\alpha}_n) - \psi_x(t + \eta_2, \tilde{\alpha}_n) (\tilde{\alpha}_{n+1} - \tilde{\alpha}_n) \\
&= N(t + \eta_2, \tilde{\alpha}_{n+1})
\end{aligned}$$

Therefore, $\tilde{\alpha}_{n+1}$ is a lower solution of (1.2) on J . In a similar manner, it can be showed that $\tilde{\beta}_{n+1}$ is an upper solution of (1.2) on J . Thus from Theorem 2.1, as before, it follows that $\tilde{\alpha}_{n+1} \leq \tilde{\beta}_{n+1}$ on J . Consequently, by induction, we get that for all n ,

$$\tilde{\alpha}_0 \leq \tilde{\alpha}_1 \leq \dots \leq \tilde{\alpha}_n \leq \tilde{\alpha}_{n+1} \leq \tilde{\beta}_{n+1} \leq \tilde{\beta}_n \leq \dots \leq \tilde{\beta}_1 \leq \tilde{\beta}_0 \text{ on } J.$$

Employing the Standard techniques (see [1]) it can be shown that the sequences $\{\tilde{\alpha}_n(t)\}$ and $\{\tilde{\beta}_n(t)\}$ converge uniformly and monotonically to the unique solution of $x(t)$ of

$$\tilde{x}'(t) = N(t + \eta_2, \tilde{x}(t)), \quad \tilde{x}(t_0) = x_0 \quad (3.6)$$

But letting $s = t + \eta_2$ and changing the variable, we can show that (3.6) is equivalent to

$$x'(s) = N(s, x(s)), \quad x(s_0) = x_0.$$

Next we prove the quadratic convergence. For this purpose, consider

$$p_{n+1}(t) = \tilde{x}(t) - \tilde{\alpha}_{n+1}(t) \geq 0 \text{ and } q_{n+1}(t) = \tilde{\beta}_{n+1}(t) - \tilde{x}(t) \geq 0.$$

Note that $p_{n+1}(t_0) = q_{n+1}(t_0) = 0$.

$$\begin{aligned}
p'_{n+1}(t) &= \tilde{x}'(t) - \tilde{\alpha}'_{n+1}(t) \\
&= f(t + \eta_2, \tilde{x}) + g(t + \eta_2, \tilde{x}) + h(t + \eta_2, \tilde{x}) - f(t + \eta_2, \tilde{\alpha}_n) - g(t + \eta_2, \tilde{\alpha}_n) - h(t + \eta_2, \tilde{\alpha}_{n+1}) \\
&\quad - \left[F_x(t + \eta_2, \tilde{\alpha}_n) + G_x(t + \eta_2, \tilde{\beta}_n) - \phi_x(t + \eta_2, \tilde{\beta}_n) - \psi_x(t + \eta_2, \tilde{\alpha}_n) \right] (\tilde{\alpha}_{n+1} - \tilde{\alpha}_n) \\
&\leq F_x(t + \eta_2, \tilde{x}) (\tilde{x} - \tilde{\alpha}_n) - \phi(t + \eta_2, \tilde{x}) + \phi(t + \eta_2, \tilde{\alpha}_n) + G_x(t + \eta_2, \tilde{\alpha}_n) (\tilde{x} - \tilde{\alpha}_n) \\
&\quad + \psi(t + \eta_2, \tilde{\alpha}_n) - \psi(t + \eta_2, \tilde{x}) + k(\tilde{x} - \tilde{\alpha}_{n+1}) - F_x(t + \eta_2, \tilde{\alpha}_n) (\tilde{\alpha}_{n+1} - \tilde{\alpha}_n) \\
&\quad - G_x(\tilde{\alpha}_{n+1} - \tilde{\alpha}_n) + \phi_x(t + \eta_2, \tilde{\beta}_n) (\tilde{\alpha}_{n+1} - \tilde{\alpha}_n) + \psi_x(t + \eta_2, \tilde{\alpha}_n) (\tilde{\alpha}_{n+1} - \tilde{\alpha}_n) \\
&\leq F_{xx}(t + \eta_2, \sigma) p_n^2 - G_{xx}(t + \eta_2, \gamma) p_n (p_n + q_n) + F_x(t + \eta_2, \tilde{\alpha}_n) p_{n+1} \\
&\quad + G_x(t + \eta_2, \tilde{\beta}_n) p_{n+1} + \phi_{xx}(t + \eta_2, \xi) p_n (p_n + q_n) - \psi_{xx}(t + \eta_2, \zeta) p_n^2 \\
&\quad + k p_{n+1} - \left[\phi_x(t + \eta_2, \tilde{\beta}_n) + \psi_x(t + \eta_2, \tilde{\alpha}_n) \right] p_{n+1}
\end{aligned}$$

where $\sigma, \zeta \in (\tilde{\alpha}_n, \tilde{x})$ and $\xi, \gamma \in (\tilde{\alpha}_n, \tilde{\beta}_n)$. Letting $|f_{xx}| < A$, $|\phi_{xx}| < B$, $|g_{xx}| < C$, $|\psi_{xx}| < D$, $|f_x| < E$, $|g_x| < T$, $|\phi_x| < R$, $|\psi_x| < S$, we get

$$\begin{aligned}
p'_{n+1} &\leq (A + B + D) p_n^2 + \frac{1}{2} (B + C + D) (3p_n^2 + q_n^2) + (k + E + T + 2R + 2S) p_{n+1} \\
&= V p_n^2 + U q_n^2 + W p_{n+1}
\end{aligned}$$

where $V = A + \frac{5}{2}B + \frac{3}{2}C + \frac{5}{2}D$, $U = \frac{1}{2}(B + C + D)$ and $W = k + E + T + 2R + 2S$. Gronwall's inequality with $p_{n+1}(t_0) = 0$ yields

$$p_{n+1}(t) \leq \int_{t_0}^t e^{W(t-s)} [Vp_n^2(s) + Uq_n^2(s)] ds$$

this gives the desired result,

$$\max_{t \in J} |\tilde{x}(t) - \tilde{\alpha}_{n+1}(t)| \leq \frac{e^{WT}}{W} \left[V \max_{t \in J} |\tilde{x}(t) - \tilde{\alpha}_n(t)|^2 + U \max_{t \in J} |\tilde{\beta}_n(t) - \tilde{x}(t)|^2 \right]$$

Similarly,

$$q_{n+1}(t) \leq \int_{t_0}^t e^{S_1(t-s)} [R_1 p_n^2(s) + Q_1 q_n^2(s)] ds$$

$$\max_{t \in J} |\tilde{\beta}_{n+1}(t) - \tilde{x}(t)| \leq \frac{e^{S_1 T}}{S_1} \left[R_1 \max_{t \in J} |\tilde{x}(t) - \tilde{\alpha}_n(t)|^2 + Q_1 \max_{t \in J} |\tilde{\beta}_n(t) - \tilde{x}(t)|^2 \right]$$

where $Q_1 = \frac{3}{2}A + \frac{5}{2}B + C + \frac{5}{2}D$, $R_1 = \frac{1}{2}(A + B + D)$, $S_1 = k + E + T + 2R + 2S$.

The next theorem demonstrates that if we try linearizing the previous iterates (3.3) and (3.4), then quadratic convergence is lost.

Theorem 3.2: Assume that together with (A_1) , (A_2) , (A_3) of Theorem 3.1, following assumption hold.

(A_4) $h(t, x) - h(t, y) \geq -k(x - y)$, where $x \geq y$, $x, y \in \tilde{\Omega}$.

Then there exist monotone sequences $\{\tilde{\alpha}_n(t)\}$ and $\{\tilde{\beta}_n(t)\}$, where $\{\tilde{\alpha}_n(t)\}$, $\{\tilde{\beta}_n(t)\}$ are solutions of linear differential equations, which converge uniformly and monotonically to the unique solution of (2.1) with $x(s_0) = x_0$ on $[s_0, s_0 + T]$, and the convergence is semi-quadratic.

Proof: Since $\tilde{\beta}_0(t) = \beta_0(t + \eta_1)$, we get $\tilde{\beta}_0(t_0) \geq \tilde{\alpha}_0(t_0)$ and $\tilde{\beta}'_0(t) \geq N(t + \eta_1, \tilde{\beta}_0)$ for $t_0 \leq t \leq t_0 + T$. Using the assumptions $F_{xx} \geq 0$, $G_{xx} \leq 0$ yield the inequalities of (3.1) and (3.2) respectively and also by using (A_3) we see that whenever $\tilde{\alpha}_0(t) \leq y \leq x \leq \tilde{\beta}_0(t)$

$$N(t, x) - N(t, y) \leq L(x - y)$$

for some $L > 0$.

Consider following IVPs

$$\begin{aligned} \tilde{\alpha}'_1(t) &= N(t + \eta_2, \tilde{\alpha}_0) + \left[F_x(t + \eta_2, \tilde{\alpha}_0) + G_x(t + \eta_2, \tilde{\beta}_0) - \phi_x(t + \eta_2, \tilde{\beta}_0) - \psi_x(t + \eta_2, \tilde{\alpha}_0) - k \right] (\tilde{\alpha}_1 - \tilde{\alpha}_0) \\ \tilde{\alpha}_1(t_0) &= x_0 \end{aligned} \quad (3.7)$$

$$\begin{aligned} \tilde{\beta}'_1(t) &= N(t + \eta_2, \tilde{\beta}_0) + \left[F_x(t + \eta_2, \tilde{\alpha}_0) + G_x(t + \eta_2, \tilde{\beta}_0) - \phi_x(t + \eta_2, \tilde{\beta}_0) - \psi_x(t + \eta_2, \tilde{\alpha}_0) - k \right] (\tilde{\beta}_1 - \tilde{\beta}_0) \\ \tilde{\beta}_1(t_0) &= x_0 \end{aligned} \quad (3.8)$$

We shall show that $\tilde{\alpha}_0(t) \leq \tilde{\alpha}_1(t)$ on J . Let us set $p = \tilde{\alpha}_0(t) - \tilde{\alpha}_1(t)$, then $p(0) \leq 0$,

$$\begin{aligned} p' &= \tilde{\alpha}'_0(t) - \tilde{\alpha}'_1(t) \\ &\leq N(t + \eta_2, \tilde{\alpha}_0) - N(t + \eta_2, \tilde{\alpha}_0) \\ &\quad - \left[F_x(t + \eta_2, \tilde{\alpha}_0) + G_x(t + \eta_2, \tilde{\beta}_0) - \phi_x(t + \eta_2, \tilde{\beta}_0) - \psi_x(t + \eta_2, \tilde{\alpha}_0) - k \right] (\tilde{\alpha}_1 - \tilde{\alpha}_0) \\ &= \left[F_x(t + \eta_2, \tilde{\alpha}_0) + G_x(t + \eta_2, \tilde{\beta}_0) - \phi_x(t + \eta_2, \tilde{\beta}_0) - \psi_x(t + \eta_2, \tilde{\alpha}_0) - k \right] p \end{aligned}$$

which yields $p(t) \leq 0$ on J . This proves that $\tilde{\alpha}_0(t) \leq \tilde{\alpha}_1(t)$ on J . Let $p(t) = \tilde{\alpha}_1(t) - \tilde{\beta}_0(t)$, then $p(0) \leq 0$ and we get

$$\begin{aligned}
 p'(t) &= \tilde{\alpha}'_1(t) - \tilde{\beta}'_0(t) \\
 &\leq N(t + \eta_2, \tilde{\alpha}_0) + \left[F_x(t + \eta_2, \tilde{\alpha}_0) + G_x(t + \eta_2, \tilde{\beta}_0) - \phi_x(t + \eta_2, \tilde{\beta}_0) - \psi_x(t + \eta_2, \tilde{\alpha}_0) - k \right] (\tilde{\alpha}_1 - \tilde{\alpha}_0) \\
 &\quad - N(t + \eta_2, \tilde{\beta}_0) \\
 &\leq N(t + \eta_2, \tilde{\alpha}_0) + \left[F_x(t + \eta_2, \tilde{\alpha}_0) + G_x(t + \eta_2, \tilde{\beta}_0) - \phi_x(t + \eta_2, \tilde{\beta}_0) - \psi_x(t + \eta_2, \tilde{\alpha}_0) - k \right] (\tilde{\alpha}_1 - \tilde{\alpha}_0) \\
 &\quad - f(t + \eta_2, \tilde{\alpha}_0) - \left[F_x(t + \eta_2, \tilde{\alpha}_0) - \phi_x(t + \eta_2, \tilde{\beta}_0) \right] (\tilde{\beta}_0 - \tilde{\alpha}_0) - h(t + \eta_2, \tilde{\alpha}_0) + k(\tilde{\beta}_0 - \tilde{\alpha}_0) \\
 &\quad - g(t + \eta_2, \tilde{\alpha}_0) - \left[G_x(t + \eta_2, \tilde{\beta}_0) - \psi_x(t + \eta_2, \tilde{\alpha}_0) \right] (\tilde{\beta}_0 - \tilde{\alpha}_0) \\
 &= \left[F_x(t + \eta_2, \tilde{\alpha}_0) + G_x(t + \eta_2, \tilde{\beta}_0) - \phi_x(t + \eta_2, \tilde{\beta}_0) - \psi_x(t + \eta_2, \tilde{\alpha}_0) - k \right] p
 \end{aligned}$$

This implies that $p(t) \leq 0$. Thus, $\tilde{\alpha}_1(t) \leq \tilde{\beta}_0(t)$. Similarly, one can prove that $\tilde{\alpha}_0(t) \leq \tilde{\beta}_1(t) \leq \tilde{\beta}_0(t)$ on J . We now prove that $\tilde{\alpha}_1(t) \leq \tilde{\beta}_1$ by showing that $\tilde{\alpha}_1(t)$ and $\tilde{\beta}_1(t)$ are lower and upper solutions of (2.1), respectively. Using (3.7), we have

$$\begin{aligned}
 \tilde{\alpha}'_1(t) &= N(t + \eta_2, \tilde{\alpha}_0) + \left[F_x(t + \eta_2, \tilde{\alpha}_0) + G_x(t + \eta_2, \tilde{\beta}_0) - \phi_x(t + \eta_2, \tilde{\beta}_0) - \psi_x(t + \eta_2, \tilde{\alpha}_0) - k \right] (\tilde{\alpha}_1 - \tilde{\alpha}_0) \\
 &= [f(t + \eta_2, \tilde{\alpha}_0) + F_x(t + \eta_2, \tilde{\alpha}_0) (\tilde{\alpha}_1 - \tilde{\alpha}_0)] + \left[g(t + \eta_2, \tilde{\alpha}_0) + G_x(t + \eta_2, \tilde{\beta}_0) (\tilde{\alpha}_1 - \tilde{\alpha}_0) \right] \\
 &\quad - k(\tilde{\alpha}_1 - \tilde{\alpha}_0) - \phi_x(t + \eta_2, \tilde{\beta}_0) (\tilde{\alpha}_1 - \tilde{\alpha}_0) - \psi_x(t + \eta_2, \tilde{\alpha}_0) (\tilde{\alpha}_1 - \tilde{\alpha}_0) + h(t + \eta_2, \tilde{\alpha}_0) \\
 &\leq [f(t + \eta_2, \tilde{\alpha}_0) + F_x(t + \eta_2, \tilde{\alpha}_0) (\tilde{\alpha}_1 - \tilde{\alpha}_0)] + [g(t + \eta_2, \tilde{\alpha}_0) + G_x(t + \eta_2, \tilde{\alpha}_1) (\tilde{\alpha}_1 - \tilde{\alpha}_0)] \\
 &\quad - k(\tilde{\alpha}_1 - \tilde{\alpha}_0) - \phi_x(t + \eta_2, \tilde{\beta}_0) (\tilde{\alpha}_1 - \tilde{\alpha}_0) - \psi_x(t + \eta_2, \tilde{\alpha}_0) (\tilde{\alpha}_1 - \tilde{\alpha}_0) + h(t + \eta_2, \tilde{\alpha}_0) \\
 &\leq [f(t + \eta_2, \tilde{\alpha}_1) + \phi(t + \eta_2, \tilde{\alpha}_1) - \phi(t + \eta_2, \tilde{\alpha}_0)] + [g(t + \eta_2, \tilde{\alpha}_1) + \psi(t + \eta_2, \tilde{\alpha}_1) - \psi(t + \eta_2, \tilde{\alpha}_0)] \\
 &\quad - \phi_x(t + \eta_2, \tilde{\beta}_0) (\tilde{\alpha}_1 - \tilde{\alpha}_0) - \psi_x(t + \eta_2, \tilde{\alpha}_0) (\tilde{\alpha}_1 - \tilde{\alpha}_0) + h(t + \eta_2, \tilde{\alpha}_1) \\
 &\leq N(t + \eta_2, \tilde{\alpha}_1) + \phi_x(t + \eta_2, \tilde{\beta}_0) (\tilde{\alpha}_1 - \tilde{\alpha}_0) - \phi_x(t + \eta_2, \tilde{\beta}_0) (\tilde{\alpha}_1 - \tilde{\alpha}_0) \\
 &\quad + \psi_x(t + \eta_2, \tilde{\alpha}_0) (\tilde{\alpha}_1 - \tilde{\alpha}_0) - \psi_x(t + \eta_2, \tilde{\alpha}_0) (\tilde{\alpha}_1 - \tilde{\alpha}_0) \\
 &= N(t + \eta_2, \tilde{\alpha}_1)
 \end{aligned}$$

where we have used the inequalities of (3.1) and (3.2) and the fact that ϕ_x is nondecreasing on $\tilde{\Omega}$ and ψ_x is non-increasing on $\tilde{\Omega}$. Similarly we can show that $\tilde{\beta}'_1 \geq N(t, \tilde{\beta}_1)$, $\tilde{\beta}_1(t_0) = x_0$. Hence using Theorem 2.2 gives that $\tilde{\alpha}_1 \leq \tilde{\beta}_1$ on J . Consequently, we get $\tilde{\alpha}_0 \leq \tilde{\alpha}_1 \leq \tilde{\beta}_1 \leq \tilde{\beta}_0$ on J . Following the same pattern as in Theorem 3.1, using

induction with $n > 1$ we can show that $\tilde{\alpha}_0 \leq \tilde{\alpha}_n \leq \tilde{\beta}_n \leq \tilde{\beta}_0$ on J . Let $p_n(t) = \tilde{\alpha}_n - \tilde{\alpha}_{n+1}$, then, $p_n(0) = 0$ and

$$\begin{aligned}
 p'_n(t) &= \tilde{\alpha}'_n(t) - \tilde{\alpha}'_{n+1}(t) \\
 &= N(t + \eta_2, \tilde{\alpha}_{n-1}) + \left[F_x(t + \eta_2, \tilde{\alpha}_{n-1}) + G_x(t + \eta_2, \tilde{\beta}_{n-1}) - \phi_x(t + \eta_2, \tilde{\beta}_{n-1}) - \psi_x(t + \eta_2, \tilde{\alpha}_{n-1}) - k \right] (\tilde{\alpha}_n - \tilde{\alpha}_{n-1}) \\
 &\quad - N(t + \eta_2, \tilde{\alpha}_n) - \left[F_x(t + \eta_2, \tilde{\alpha}_n) + G_x(t + \eta_2, \tilde{\beta}_n) - \phi_x(t + \eta_2, \tilde{\beta}_n) - \psi_x(t + \eta_2, \tilde{\alpha}_n) - k \right] (\tilde{\alpha}_{n+1} - \tilde{\alpha}_n) \\
 &\leq -[F_x(t + \eta_2, \tilde{\alpha}_{n-1}) - \phi_x(t + \eta_2, \tilde{\alpha}_n) + G_x(t + \eta_2, \tilde{\alpha}_n) - \psi_x(t + \eta_2, \tilde{\alpha}_{n-1}) - k] (\tilde{\alpha}_n - \tilde{\alpha}_{n-1}) \\
 &\quad + \left[F_x(t + \eta_2, \tilde{\alpha}_{n-1}) + G_x(t + \eta_2, \tilde{\beta}_{n-1}) - \phi_x(t + \eta_2, \tilde{\beta}_{n-1}) - \psi_x(t + \eta_2, \tilde{\alpha}_{n-1}) - k \right] (\tilde{\alpha}_n - \tilde{\alpha}_{n-1}) \\
 &\quad - \left[F_x(t + \eta_2, \tilde{\alpha}_n) + G_x(t + \eta_2, \tilde{\beta}_n) - \phi_x(t + \eta_2, \tilde{\beta}_n) - \psi_x(t + \eta_2, \tilde{\alpha}_n) - k \right] (\tilde{\alpha}_{n+1} - \tilde{\alpha}_n) \\
 &\leq -[F_x(t + \eta_2, \tilde{\alpha}_{n-1}) - \phi_x(t + \eta_2, \tilde{\alpha}_n) + G_x(t + \eta_2, \tilde{\alpha}_n) - \psi_x(t + \eta_2, \tilde{\alpha}_{n-1}) - k] (\tilde{\alpha}_n - \tilde{\alpha}_{n-1}) \\
 &\quad + [F_x(t + \eta_2, \tilde{\alpha}_{n-1}) - \phi_x(t + \eta_2, \tilde{\alpha}_n) + G_x(t + \eta_2, \tilde{\alpha}_n) - \psi_x(t + \eta_2, \tilde{\alpha}_{n-1}) - k] (\tilde{\alpha}_n - \tilde{\alpha}_{n-1}) \\
 &\quad + \left[F_x(t + \eta_2, \tilde{\alpha}_n) + G_x(t + \eta_2, \tilde{\beta}_n) - \phi_x(t + \eta_2, \tilde{\beta}_n) - \psi_x(t + \eta_2, \tilde{\alpha}_n) - k \right] (\tilde{\alpha}_n - \tilde{\alpha}_{n+1}) \\
 &= \left[F_x(t + \eta_2, \tilde{\alpha}_n) + G_x(t + \eta_2, \tilde{\beta}_n) - \phi_x(t + \eta_2, \tilde{\beta}_n) - \psi_x(t + \eta_2, \tilde{\alpha}_n) - k \right] p
 \end{aligned}$$

using (3.1)-(3.2) and the fact that ϕ_x is increasing on $\tilde{\Omega}$ and G_x is decreasing on $\tilde{\Omega}$. This gives $p_n(t) \leq 0$, then we have $\tilde{\alpha}_n \leq \tilde{\alpha}_{n+1}$ on J . Next we show that $\tilde{\alpha}_{n+1} \leq \tilde{\beta}_{n+1}$ on J . Using the inequalities of (3.1) and (3.2)

$$\begin{aligned}
 \tilde{\alpha}'_{n+1}(t) &= N(t + \eta_2, \tilde{\alpha}_n) + \left[F_x(t + \eta_2, \tilde{\alpha}_n) + G_x(t + \eta_2, \tilde{\beta}_n) - \phi_x(t + \eta_2, \tilde{\beta}_n) - \psi_x(t + \eta_2, \tilde{\alpha}_n) - k \right] (\tilde{\alpha}_{n+1} - \tilde{\alpha}_n) \\
 &= [f(t + \eta_2, \tilde{\alpha}_n) + F_x(t + \eta_2, \tilde{\alpha}_n) (\tilde{\alpha}_{n+1} - \tilde{\alpha}_n)] + \left[g(t + \eta_2, \tilde{\alpha}_n) + G_x(t + \eta_2, \tilde{\beta}_n) (\tilde{\alpha}_{n+1} - \tilde{\alpha}_n) \right] \\
 &\quad - \left[\phi_x(t + \eta_2, \tilde{\beta}_n) + \psi_x(t + \eta_2, \tilde{\alpha}_n) \right] (\tilde{\alpha}_{n+1} - \tilde{\alpha}_n) - k (\tilde{\alpha}_{n+1} - \tilde{\alpha}_n) + h(t + \eta_2, \tilde{\alpha}_n) \\
 &\leq [f(t + \eta_2, \tilde{\alpha}_{n+1}) + \phi(t + \eta_2, \tilde{\alpha}_{n+1}) - \phi(t + \eta_2, \tilde{\alpha}_n)] + [g(t + \eta_2, \tilde{\alpha}_{n+1}) + \psi(t + \eta_2, \tilde{\alpha}_{n+1}) - \psi(t + \eta_2, \tilde{\alpha}_n)] \\
 &\quad - \left[\phi_x(t + \eta_2, \tilde{\beta}_n) + \psi_x(t + \eta_2, \tilde{\alpha}_n) \right] (\tilde{\alpha}_{n+1} - \tilde{\alpha}_n) + h(t + \eta_2, \tilde{\alpha}_{n+1}) \\
 &\leq f(t + \eta_2, \tilde{\alpha}_{n+1}) + \phi_x(t + \eta_2, \tilde{\beta}_n) (\tilde{\alpha}_{n+1} - \tilde{\alpha}_n) - \phi_x(t + \eta_2, \tilde{\beta}_n) (\tilde{\alpha}_{n+1} - \tilde{\alpha}_n) \\
 &\quad + g(t + \eta_2, \tilde{\alpha}_{n+1}) + \psi_x(t + \eta_2, \tilde{\alpha}_n) (\tilde{\alpha}_{n+1} - \tilde{\alpha}_n) - \psi_x(t + \eta_2, \tilde{\alpha}_n) (\tilde{\alpha}_{n+1} - \tilde{\alpha}_n) + h(t + \eta_2, \tilde{\alpha}_{n+1}) \\
 &= N(t + \eta_2, \tilde{\alpha}_{n+1}), \quad \tilde{\alpha}_{n+1}(t_0) = x_0
 \end{aligned}$$

because of the fact that ϕ_x is increasing on $\tilde{\Omega}$ and ψ_x is decreasing on $\tilde{\Omega}$. Therefore $\tilde{\alpha}_{n+1}(t)$ is a lower solution of (2.1). Also it can be shown that is an upper solution of (2.1), that is, $\tilde{\beta}'_{n+1}(t) \geq N(t + \eta_2, \tilde{\beta}_{n+1}(t))$, $\tilde{\beta}_{n+1}(t_0) = x_0$. Consequently, as before, it follows from the comparison result, we get $\tilde{\alpha}_{n+1}(t) \leq \tilde{\beta}_{n+1}(t)$ on J . By induction, we obtain

$$\tilde{\alpha}_0(t) \leq \tilde{\alpha}_1(t) \leq \cdots \leq \tilde{\alpha}_n(t) \leq \tilde{\alpha}_{n+1}(t) \leq \tilde{\beta}_{n+1}(t) \leq \tilde{\beta}_n(t) \leq \cdots \leq \tilde{\beta}_1(t) \leq \tilde{\beta}_0(t) \text{ on } J.$$

Employing the standard techniques (see[1]), it is easy to show that the sequences $\{\tilde{\alpha}_n(t)\}$ and $\{\tilde{\beta}_n(t)\}$ converge uniformly and monotonically to the unique solution of $x(t)$ of

$$\tilde{x}'(t) = N(t + \eta_2, \tilde{x}(t)), \quad \tilde{x}(t_0) = x_0 \quad (3.9)$$

But letting $s = t + \eta_2$ and changing the variable, we can show that (3.9) is equivalent to

$$x'(s) = N(s, x(s)), \quad x(s_0) = x_0 \quad (3.10)$$

Next we prove that the convergence is semi-quadratic. For this purpose, consider

$$p_{n+1}(t) = \tilde{x}(t) - \tilde{\alpha}_{n+1}(t) \geq 0 \text{ and } q_{n+1}(t) = \tilde{\beta}_{n+1}(t) - \tilde{x}(t) \geq 0$$

Note that $p_{n+1}(t_0) = q_{n+1}(t_0) = 0$.

$$\begin{aligned} p'_{n+1}(t) &= \tilde{x}'(t) - \tilde{\alpha}'_{n+1}(t) \\ &= N(t + \eta_2, \tilde{x}) - N(t + \eta_2, \tilde{\alpha}_n) - \left[F_x(t + \eta_2, \tilde{\alpha}_n) + G_x(t + \eta_2, \tilde{\beta}_n) - \phi_x(t + \eta_2, \tilde{\beta}_n) - \psi_x(t + \eta_2, \tilde{\alpha}_n) - k \right] (\tilde{\alpha}_{n+1} - \tilde{\alpha}_n) \\ &= f(t + \eta_2, \tilde{x}) + g(t + \eta_2, \tilde{x}) + h(t + \eta_2, \tilde{x}) - f(t + \eta_2, \tilde{\alpha}_n) - g(t + \eta_2, \tilde{\alpha}_n) - h(t + \eta_2, \tilde{\alpha}_n) + \phi(t + \eta_2, \tilde{x}) + \psi(t + \eta_2, \tilde{x}) \\ &\quad - \phi(t + \eta_2, \tilde{\alpha}_n) - \psi(t + \eta_2, \tilde{\alpha}_n) - \phi(t + \eta_2, \tilde{x}) - \psi(t + \eta_2, \tilde{x}) + \phi(t + \eta_2, \tilde{\alpha}_n) + \psi(t + \eta_2, \tilde{\alpha}_n) \\ &\quad - \left[F_x(t + \eta_2, \tilde{\alpha}_n) + G_x(t + \eta_2, \tilde{\beta}_n) - \phi_x(t + \eta_2, \tilde{\beta}_n) - \psi_x(t + \eta_2, \tilde{\alpha}_n) - k \right] (\tilde{\alpha}_{n+1} - \tilde{\alpha}_n) \\ &\leq [F(t + \eta_2, \tilde{x}) - F(t + \eta_2, \tilde{\alpha}_n)] + [G(t + \eta_2, \tilde{x}) - G(t + \eta_2, \tilde{\alpha}_n)] + k(\tilde{x} - \tilde{\alpha}_n) - \phi_x(t + \eta_2, \tilde{\alpha}_n)(\tilde{x} - \tilde{\alpha}_n) \\ &\quad - \psi_x(t + \eta_2, \tilde{x})(\tilde{x} - \tilde{\alpha}_n) - \left[F_x(t + \eta_2, \tilde{\alpha}_n) + G_x(t + \eta_2, \tilde{\beta}_n) - \phi_x(t + \eta_2, \tilde{\beta}_n) - \psi_x(t + \eta_2, \tilde{\alpha}_n) - k \right] (\tilde{\alpha}_{n+1} - \tilde{\alpha}_n) \\ &\leq F_x(t + \eta_2, \tilde{x})(\tilde{x} - \tilde{\alpha}_n) + G_x(t + \eta_2, \tilde{\alpha}_n)(\tilde{x} - \tilde{\alpha}_n) + \phi_{xx}(t + \eta_2, \delta)(\tilde{x} - \tilde{\alpha}_n)(\tilde{\beta}_n - \tilde{\alpha}_n) - \psi_{xx}(t + \eta_2, \mu)(\tilde{x} - \tilde{\alpha}_n)^2 \\ &\quad - \left[F_x(t + \eta_2, \tilde{\alpha}_n) + G_x(t + \eta_2, \tilde{\beta}_n) - \phi_x(t + \eta_2, \tilde{\beta}_n) - \psi_x(t + \eta_2, \tilde{\alpha}_n) - k \right] (\tilde{\alpha}_{n+1} - \tilde{x}) \\ &\quad - \left[F_x(t + \eta_2, \tilde{\alpha}_n) + G_x(t + \eta_2, \tilde{\beta}_n) \right] (\tilde{x} - \tilde{\alpha}_n) + 2k(\tilde{x} - \tilde{\alpha}_n) \\ &= F_{xx}(t + \eta_2, \gamma)(\tilde{x} - \tilde{\alpha}_n)^2 - \psi_{xx}(t + \eta_2, \mu)(\tilde{x} - \tilde{\alpha}_n)^2 - G_{xx}(t + \eta_2, \sigma)(\tilde{x} - \tilde{\alpha}_n)(\tilde{\beta}_n - \tilde{\alpha}_n) + \phi_{xx}(t + \eta_2, \delta)(\tilde{x} - \tilde{\alpha}_n) \\ &\quad - \left[F_x(t + \eta_2, \tilde{\alpha}_n) + G_x(t + \eta_2, \tilde{\beta}_n) - \phi_x(t + \eta_2, \tilde{\beta}_n) - \psi_x(t + \eta_2, \tilde{\alpha}_n) - k \right] (\tilde{\alpha}_{n+1} - \tilde{x}) + 2k(\tilde{x} - \tilde{\alpha}_n) \\ &= [F_{xx}(t + \eta_2, \gamma) - \psi_{xx}(t + \eta_2, \mu)](\tilde{x} - \tilde{\alpha}_n)^2 + [-G_{xx}(t + \eta_2, \sigma) + \phi_{xx}(t + \eta_2, \delta)](\tilde{x} - \tilde{\alpha}_n)(\tilde{\beta}_n - \tilde{\alpha}_n) \\ &\quad + \left[F_x(t + \eta_2, \tilde{\alpha}_n) + G_x(t + \eta_2, \tilde{\beta}_n) - \phi_x(t + \eta_2, \tilde{\beta}_n) - \psi_x(t + \eta_2, \tilde{\alpha}_n) - k \right] (\tilde{x} - \tilde{\alpha}_{n+1}) + 2k(\tilde{x} - \tilde{\alpha}_n) \end{aligned}$$

where $\mu, \gamma \in (\tilde{\alpha}_n, \tilde{x})$ and $\sigma, \delta \in (\tilde{\alpha}_n, \tilde{\beta}_n)$. Letting $|f_{xx}| < A$, $|\phi_{xx}| < B$, $|g_{xx}| < C$, $|\psi_{xx}| < D$, $|f_x| < E$, $|g_x| < T$, $|\phi_x| < R$, $|\psi_x| < S$, we get

$$\begin{aligned} p'_{n+1} &\leq (A + B + D)p_n^2 + \frac{1}{2}(B + C + D)(3p_n^2 + q_n^2) + (E + T + 2R + 2S)p_{n+1} + 2kp_n \\ &= Vp_n^2 + Uq_n^2 + Wp_{n+1} + 2kp_n \end{aligned}$$

where $V = A + \frac{5}{2}B + \frac{3}{2}C + \frac{5}{2}D$, $U = \frac{1}{2}(B + C + D)$ and $W = E + T + 2R + 2S$. Gronwall's inequality with $p_{n+1}(t_0) = 0$ yields

$$p_{n+1}(t) \leq \int_{t_0}^t e^{W(t-s)} [2Vp_n^2(s) + Uq_n^2(s) + 2kp_n] ds$$

this gives the desired result,

$$\max_{t \in J=[t_0, t_0+T]} |\tilde{x}(t) - \tilde{\alpha}_{n+1}(t)| \leq \frac{e^{WT}}{W} \left[2V \max_{t \in J} |\tilde{x}(t) - \tilde{\alpha}_n(t)|^2 + U \max_{t \in J} |\tilde{\beta}_n(t) - \tilde{x}(t)|^2 + 2k \max_{t \in J} |\tilde{x}(t) - \tilde{\alpha}_n(t)| \right]$$

Similarly,

$$q'_{n+1}(t) \leq P.q_n^2 + R.p_n^2 + 2kq_n + Qq_{n+1}, \quad q_{n+1}(t_0) = 0$$

$$\max_{t \in J=[t_0, t_0+T]} |\tilde{\beta}_{n+1}(t) - \tilde{x}(t)| \leq \frac{e^{QT}}{T} \left[2P \max_{t \in J} |\tilde{\beta}_n(t) - \tilde{x}(t)|^2 + R \max_{t \in J} |\tilde{x}(t) - \tilde{\alpha}_n(t)|^2 + 2k \max_{t \in J} |\tilde{\beta}_n(t) - \tilde{x}(t)| \right]$$

where $P = \frac{3}{2}A + \frac{5}{2}B + C + \frac{5}{2}D$, $R = \frac{1}{2}(A + B + D)$, $Q = E + T + 2R + 2S$. The convergence is semi-quadratic. This completes the proof.

Next we give the following corollaries for special cases.

Corollary 3.1: If the assumptions of the Theorem 3.1 hold with $s_0 = t_0$, then the conclusion of the theorem remains valid.

Proof: For the proof, we let $\tilde{\beta}_0(t) = \beta(t + \eta_1)$, $\tilde{\alpha}_0(t) = \alpha(t)$ and $\tilde{u}(t) = u(t)$ and proceed, as we did in Theorem 3.1.

Corollary 3.2: If the assumptions of the Theorem 3.1 hold with $s_0 = \tau_0$, then the conclusion of the theorem remains valid.

Proof: Similarly, we let $\tilde{\alpha}_0(t) = \alpha(t - \eta_1)$, $\tilde{\beta}_0(t) = \beta(t)$ and $\tilde{u}(t) = u(t)$ and proceed, as we did in Theorem 3.1.

Corollary 3.3: If the assumption (A_4) of the Theorem 3.2 holds with $h(t, x) \equiv 0$, then the conclusion of the theorem remains valid with quadratic convergence.

Proof: The proof is very much similar to the proof of Theorem 3.1. The details are omitted.

Corollary 3.4: If the assumption of the Theorem 3.2 holds with $f(t, x) + g(t, x) \equiv 0$, then we have the monotone iterative techniques, and the conclusion of the theorem remains valid with linear convergence.

Proof: The details of the proof is similar to monotone iterative technique for nonlinear differential equations in [3].

Corollary 3.5: If the assumption of the Theorem 3.2 holds with $h(t, x) \equiv 0$ and $g(x, t)$ is continuous on $\tilde{\Omega} = \{(t, u) : t_0 \leq t \leq t_0 + T, \tilde{\alpha}_0(t) \leq u \leq \tilde{\beta}_0(t)\}$ and assume that one of the inequalities (A_1) in Theorem 3.1 to be strict, then we have only weakly quadratic convergence.

Proof: The details of the proof is similar to quasilinearization for nonlinear problems in [6].

4 Examples

The following examples illustrate some of the theorems above.

Example 4.1: Consider the nonlinear initial value problem

$$\frac{dx}{dt} = N(t, x) = f(t, x) + g(t, x) + h(t, x) = 1 + x^2, x(t_0) = x_0 \text{ for } x_0 > 0 \text{ and } t \geq t_0 > 0 \quad (4.1)$$

where $f(t, x) = -\sin(x) - \frac{3}{2}x^2 - \exp(t) + \sinh(t)$, $g(t, x) = -\cos(x) + \frac{5}{2}x^2 + \cosh(t)$, $h(t, x) = \cos(x) + \sin(x) + 1 \in C[[t_0, \tau_0 + T] \times \mathbb{R}, \mathbb{R}]$.

(E_1) $\alpha_0(t) = \frac{1}{2} \tan(t - t_0 + \arctan(x_0))$ for $t \geq t_0$, $\alpha_0 \in C^1[[t_0, t_0 + T], \mathbb{R}]$ and $\beta_0(t) = 2 \tan(t - \tau_0 + \arctan(x_0))$ for $t \geq \tau_0$ and $\beta_0 \in C^1[[\tau_0, \tau_0 + T], \mathbb{R}]$ for $\tau_0 > t_0 > 0$ and $T > 0$,

$$\begin{aligned} \alpha'_0 &\leq N(t, \alpha_0) = f(t, \alpha_0) + g(t, \alpha_0) + h(t, \alpha_0) = 1 + \frac{1}{4} \tan^2(t - t_0 + \arctan(x_0)) \text{ for } t_0 \leq t \leq t_0 + T \\ \beta'_0 &\geq N(t, \beta_0) = f(t, \beta_0) + g(t, \beta_0) + h(t, \beta_0) = 1 + 4 \tan^2(t - \tau_0 + \arctan(x_0)) \text{ for } \tau_0 \leq t \leq \tau_0 + T, \end{aligned}$$

where $f, g, h \in C[[t_0, \tau_0 + T] \times \mathbb{R}, \mathbb{R}]$ and $\alpha_0(t_0) = \frac{1}{2}x_0 < x_0 < 2x_0 = \beta_0(\tau_0)$;

(E_2) $t_0 < s_0 < \tau_0$, $f(t, x) = -\sin(x) - \frac{3}{2}x^2 - \exp(t) + \sinh(t)$, $g(t, x) = -\cos(x) + \frac{3}{2}x^2 + \cosh(t)$ and $h(t, x) = \cos(x) + \sin(x) + 1$ are nondecreasing in t for each x ;

(E₃) $N \in C\left[\tilde{\Omega}, \mathbb{R}\right]$, $N(t, x) = f(t, x) + g(t, x) + h(t, x) = 1 + x^2$, $f_x = -\cos(x) - 3x$, $g_x = \sin(x) + 5x$, $f_{xx} = \sin(x) - 3 < 0$, $g_{xx} = \cos(x) + 5 > 0$ exist and are continuous functions satisfying $F = f + \phi = -\sin(x) - \frac{3}{2}x^2 - \exp(t) + \sinh(t) + \frac{5}{2}(x^2 + t^2)$, $G = g + \psi = -\cos(x) + \frac{5}{2}x^2 + \cosh(t) - \frac{9}{2}(x^2 - t^2)$, $F_{xx} = f_{xx} + \phi_{xx} = \sin(x) + 2 > 0$, $G_{xx} = g_{xx} + \psi_{xx} = \cos(x) - 2 < 0$ on $\tilde{\Omega}$ where

$$\tilde{\Omega} = \left\{ (t, u) : t_0 \leq t \leq t_0 + T, \tilde{\alpha}_0(t) = \frac{1}{2} \tan(t - t_0 + \arctan(x_0)) \leq u \leq \tilde{\beta}_0(t) = 2 \tan(t - \tau_0 + \arctan(x_0)) \right\}$$

and $\phi = \frac{5}{2}(x^2 + t^2)$, $\psi = -\frac{9}{2}(x^2 - t^2) \in C^{0,2}\left[\tilde{\Omega}, \mathbb{R}\right]$ such that $\phi_{xx} = 5 > 0$, $\psi_{xx} = -9 < 0$ on $\tilde{\Omega}$ and $h(t, x)$ satisfies $h(t, x_1) - h(t, x_2) \leq 2(x_1 - x_2)$ whenever $x_1 \geq x_2, x_1, x_2 \in \tilde{\Omega}$, where $k = 2 > 0$ is the Lipschitz constant on $\tilde{\Omega}$. Also $\tilde{\alpha}_0(t) = \alpha_0(t) = \frac{1}{2} \tan(t - t_0 + \arctan(x_0))$ and $\tilde{\beta}_0(t) = \beta_0(t + \eta_1) = 2 \tan(t + \eta_1 - \tau_0 + \arctan(x_0))$, $\eta_1 = \tau_0 - t_0$ for $t \geq t_0$.

Therefore, $\tilde{\alpha}_{n+1}$ is a lower solution and $\tilde{\beta}_{n+1}$ is an upper solutions of (4.1) on J . Thus $\tilde{\alpha}_{n+1} \leq \tilde{\beta}_{n+1}$ on J . Consequently, we have for all n ,

$$\tilde{\alpha}_0 \leq \tilde{\alpha}_1 \leq \dots \leq \tilde{\alpha}_n \leq \tilde{\alpha}_{n+1} \leq \tilde{\beta}_{n+1} \leq \tilde{\beta}_n \leq \dots \leq \tilde{\beta}_1 \leq \tilde{\beta}_0 \text{ on } J.$$

Employing the Standard techniques (see [1]) it can be shown that the sequences $\{\tilde{\alpha}_n(t)\}$ and $\{\tilde{\beta}_n(t)\}$ converge uniformly and monotonically to the unique solution $\tilde{x}(t)$ of $\tilde{x}'(t) = N(t + \eta_2, \tilde{x}) = 1 + \tilde{x}^2$, $\eta_2 = s_0 - t_0$ and it is equivalent to $x'(s) = N(s, x(s)) = 1 + x^2(s)$, $x(s_0) = x_0$, $s = t + \eta_2 \geq s_0$ that has the unique solution $x(s) = \tan(s - s_0 + \arctan(x_0))$ for $s \geq s_0$ and the convergence is quadratic.

Example 4.2: Consider the Riccati's differential equation

$$\frac{dx}{dt} = N(t, x) = f(t, x) + g(t, x) + h(t, x) = t^2 + x^2, x(t_0) = x_0 \text{ for } t \geq t_0 > 0 \quad (4.2)$$

where $f(t, x) = -\sin(x) - \frac{3}{2}x^2 + \frac{1}{6}t^2$, $g(t, x) = -\cos(x) + \frac{3}{2}x^2 + \frac{1}{2}t^2$, $h(t, x) = \cos(x) + \sin(x) + \frac{1}{3}t^2 + x^2 \in C[[t_0, \tau_0 + T] \times \mathbb{R}, \mathbb{R}]$.

(E₁^{*}) $\alpha_0 \in C^1[[t_0, t_0 + T], \mathbb{R}]$ and $\beta_0 \in C^1[[\tau_0, \tau_0 + T], \mathbb{R}]$ for $\tau_0 > t_0 > 0$ and $T > 0$,

$$\begin{aligned} \alpha'_0 &\leq N(t, \alpha_0) = f(t, \alpha_0) + g(t, \alpha_0) + h(t, \alpha_0) = t^2 + \alpha_0^2 \text{ for } t_0 \leq t \leq t_0 + T \\ \beta'_0 &\geq N(t, \beta_0) = f(t, \beta_0) + g(t, \beta_0) + h(t, \beta_0) = t^2 + \beta_0^2 \text{ for } \tau_0 \leq t \leq \tau_0 + T, \end{aligned}$$

where $f, g, h \in C[[t_0, \tau_0 + T] \times \mathbb{R}, \mathbb{R}]$ and $\alpha_0(t_0) \leq x_0 \leq \beta_0(\tau_0)$;

(E₂^{*}) $t_0 < s_0 < \tau_0$, $f(t, x) = -\sin(x) - \frac{3}{2}x^2 + \frac{1}{6}t^2$, $g(t, x) = -\cos(x) + \frac{3}{2}x^2 + \frac{1}{2}t^2$, $h(t, x) = \cos(x) + \sin(x) + \frac{1}{3}t^2 + x^2$ are nondecreasing in t for each x ;

(E₃^{*}) $N \in C\left[\tilde{\Omega}, \mathbb{R}\right]$, $N(t, x) = f(t, x) + g(t, x) + h(t, x) = t^2 + x^2$, $f_x = -\cos(x) - 3x$, $g_x = \sin(x) + 3x$, $f_{xx} = \sin(x) - 3 < 0$, $g_{xx} = \cos(x) + 3 > 0$ exist and are continuous functions satisfying $F = f + \phi = -\sin(x) - \frac{3}{2}x^2 + \frac{1}{6}t^2 + \frac{5}{2}(x^2 + t^2)$, $G = g + \psi = -\cos(x) + \frac{3}{2}x^2 + \frac{1}{2}t^2 - \frac{5}{2}(x^2 - t^2)$, $F_{xx} = f_{xx} + \phi_{xx} = -\sin(x) + 2 > 0$, $G_{xx} = g_{xx} + \psi_{xx} = \cos(x) - 2 < 0$ on $\tilde{\Omega}$ where $\tilde{\Omega} = \left\{ (t, u) : t_0 \leq t \leq t_0 + T, \tilde{\alpha}_0(t) \leq u \leq \tilde{\beta}_0(t) \right\}$ and $\phi = \frac{5}{2}(x^2 + t^2)$, $\psi = -\frac{5}{2}(x^2 - t^2) \in C^{0,2}\left[\tilde{\Omega}, \mathbb{R}\right]$ such that $\phi_{xx} = 5 > 0$, $\psi_{xx} = -5 < 0$ on $\tilde{\Omega}$ and $h(t, x)$ satisfies $h(t, x_1) - h(t, x_2) \leq k(x_1 - x_2)$ whenever $x_1 \geq x_2, x_1, x_2 \in \tilde{\Omega}$, where $k \geq 2 > 0$ is the Lipschitz constant on $\tilde{\Omega}$ since $h(t, x) = \cos(x) + \sin(x) + \frac{1}{3}t^2 + x^2 \in C^{0,1}\left[\tilde{\Omega}, \mathbb{R}\right]$. Also $\tilde{\beta}_0(t) = \beta_0(t + \eta_1)$, $\eta_1 = \tau_0 - t_0$, $\tilde{\alpha}_0(t) = \alpha_0(t)$. Therefore,

$\tilde{\alpha}_{n+1}$ is a lower solution and $\tilde{\beta}_{n+1}$ is an upper solution of (4.2) on J . Thus $\tilde{\alpha}_{n+1} \leq \tilde{\beta}_{n+1}$ on J . Consequently, we have monotone sequences for all n ,

$$\tilde{\alpha}_0 \leq \tilde{\alpha}_1 \leq \cdots \leq \tilde{\alpha}_n \leq \tilde{\alpha}_{n+1} \leq \tilde{\beta}_{n+1} \leq \tilde{\beta}_n \leq \cdots \leq \tilde{\beta}_1 \leq \tilde{\beta}_0 \text{ on } J.$$

The sequences $\{\tilde{\alpha}_n(t)\}$ and $\{\tilde{\beta}_n(t)\}$ converge uniformly and monotonically to the unique solution $\tilde{x}(t)$ of $\tilde{x}'(t) = N(t + \eta_2, \tilde{x}) = t^2 + \tilde{x}^2$, $\eta_2 = s_0 - t_0$ and it is equivalent to $x'(s) = N(s, x(s)) = t^2 + x^2(s)$, $x(s_0) = x_0$, $s = t + \eta_2 \geq s_0$ that has the unique solution $x(s) = x(s, s_0, x_0) = s \frac{\left[x_0 J_{-\frac{1}{4}}(s_0^2/2) - s_0 J_{\frac{3}{4}}(s_0^2/2) \right] J_{-\frac{3}{4}}(s^2/2) + \left[x_0 J_{\frac{1}{4}}(s_0^2/2) + s_0 J_{-\frac{3}{4}}(s_0^2/2) \right] J_{\frac{3}{4}}(s^2/2)}{\left[x_0 J_{\frac{1}{4}}(s_0^2/2) + s_0 J_{-\frac{3}{4}}(s_0^2/2) \right] J_{-\frac{1}{4}}(s^2/2) - \left[x_0 J_{-\frac{1}{4}}(s_0^2/2) - s_0 J_{\frac{3}{4}}(s_0^2/2) \right] J_{\frac{1}{4}}(s^2/2)}$ for $s \geq s_0 > 0$ in terms of Bessel functions and the convergence is quadratic.

Acknowledgements

The authors wish to express their sincere gratitude to Prof. V. Lakshmikantham and Prof. S. Köksal for their helpful suggestion in improving the paper.

References

- [1] Ahmad, B., Integro-differential equations with initial time difference. *Dynamic Systems and Applications*. 16 (2007) Pages 497-506.
- [2] Jankowski, T., Quadratic Convergence of monotone iterations for differential equations with initial time difference. *Dynamic Systems and Applications* 14 (2005) Pages 245-252.
- [3] Ladde, G.S, Lakshmikantham, V. and Vatsala, A.S., *Monotone Iterative Technique for Nonlinear Differential Equations*, Pitman Publishing Inc., Boston 1985.
- [4] Lakshmikantham, V. and Leela, S. and Vasundhara Devi, J., Another Approach to the Theory of Differential Inequalities Relative to Changes in the Initial Times. *Journal of Inequalities and Applications* Volume 4 (1999), Issue 2, Pages 163-174.
- [5] Lakshmikantham, V. and Vatsala, A.S., Differential Inequalities with Initial Time Difference and Applications. *Journal of Inequalities and Applications*.1999, Vol. 3, pp. 233-244
- [6] Lakshmikantham, V. and Vatsala, A.S., *Generalized Quasilinearization for Nonlinear Problems*, Kluwer Academic Publisher, The Netherlands 1998.
- [7] Lakshmikantham, V. and Vatsala, A.S., Theory of Differential and Integral Inequalities with Initial Time Difference and Applications". *Analytic and Geometric Inequalities and Applications* Kluwer Academic Publishers, (1999), pp 191-203.
- [8] Shaw, M.D. and Yakar C., Generalized Variation of Parameters with Initial Time Difference and A Comparison Result in terms of Lyapunov-like Functions. *International Journal Nonlinear Differential Equations Theory-Methods and Applications*. Volume5, Numbers 1&2, Jan-Dec. 1999. (89-108).
- [9] Köksal, S. and Yakar, C., "Generalized Quasilinearization Method with Initial Time Difference," *Simulation, an International Journal of Electrical, Electronic and other Physical Systems*, 24(5), 2002.
- [10] Yakar, C. and S.G., Deo. Variation of Parameters Formulae with Initial Time Difference for Linear Integrodifferential Equations. *Journal of Applicable Analysis*. Taylor & Francis. Vol. 85, No. 4, April 2006, 333-343
- [11] Yakar, C. and Yakar, A., An Extension of the Quasilinearization Method with Initial Time Difference. *Dynamics of Continuous, Discrete and Impulsive Systems*. Series A: Mathematical Analysis. Watam Press. Waterloo. Page: 275-279. DCDIS 14 (S2) 1-305 (2007). ISSN 1201-3390. Editors: Zhaosheng Feng, Xinzhi Liu, Lokenath Debnath.

Determination of Chaotic Behaviour in Aortic Doppler Signal Dynamics using Correlation Dimension Analysis

Derya Yılmaz, N. Fatma Güler^{*}, N. Kürşad Tokel^{**}

Abstract

The chaotic analysis methods have been frequently used in the physiological signal analysis to determine the pathological cases of various physiological systems in recent years. In this study, the correlation dimension (CD) analysis has been applied to the aortic Doppler signals to investigate the complexity of the Doppler signal dynamics for healthy and aortic disorder groups. In this research, the aortic Doppler signals obtained from healthy, aortic stenosis (AS) and aortic insufficiency (AI) cases have been analyzed for children subjects. The Doppler signals were acquired via the Doppler echocardiography system that is a reliable and noninvasive technique to determine the blood flow dynamics from subjects of Başkent University hospital. The CD analysis has been performed by using the Grassberger-Procaccia (GP) algorithm. The CD of healthy group has been found significantly lower those found in AS disorder group. Although no significant difference was found between the CDs of healthy and AI groups, the CD of AS group has also been found higher than those found in AI group, fortunately. The results of this study have indicated that the aortic valve Doppler signal dynamics have high level chaotic behaviour for aortic valve disorders with respect to healthy case. As a result, the CD can be used as an efficient method to determine the pathological cases of aortic valve.

Keywords: *Chaos, Nonlinear Analysis, Aortic Valve Disorders, Children Aortic patients*

1. Introduction

The Doppler signals have non-stationary characteristics and have been considered as chaotic signals since they are obtained from the blood flow under the influence of cardiovascular system's complex behaviour [1, 2]. The chaos theory methods are used to analyse the

Department of Biomedical Equipment Technology, Vocational School of Technology, Başkent University, Ankara, Turkey, e-mail: derya@baskent.edu.tr.

^{}Department of Electronics and Computer Education, Faculty of Technical Education, Gazi University, Ankara, Turkey.*

*^{**}Department of Pediatric Cardiology, Başkent University, Ankara Hospital, Ankara, Turkey.*

physiological signals such as Doppler signal and give useful results for studying the physiological system and evaluating the system functions [1, 3, 4]. Therefore, the effects of the pathological case on the physiological system dynamics can be determined and contributions can be obtained for making a medical decision by using the chaotic analysis. In this study, the CD analysis which is most commonly used method in chaotic analysis of physiological signals as an chaotic indicator have been performed to evaluate the aortic valve Doppler signal dynamics in healthy and, AS and AI pathological cases of the heart.

For children, AS and AI which are two types of heart diseases occur such that congenital heart defect and also can be the result of infection of the heart due to rheumatic fever happened in childhood. The aortic valve is between the left ventricle of heart and the aorta. AS is an obstructive defect in the heart namely the aortic valve opening is narrow. AI is leaking of the aortic valve, occurring when the aortic valve does not close properly [5]. The early detection of AS and AI diseases is very important for children. For diagnosis these heart diseases, the Doppler echocardiography primarily used by cardiologist as a noninvasive technique [6, 7]. Doppler echocardiography technique provides an assessment of heart structure, function and blood flow dynamics by use of ultrasound waves. Because of the blood flow hemodynamics, the Doppler signals observed at various disorders of heart valves, demonstrate different flow characteristics with respect to normal ones [8]. Both of these aortic disorders cause turbulent blood flow. When the blood flow comes to turbulence, velocities and directions of fluid molecules rapidly vary, therefore the local and instantaneous fluctuations occur in blood velocity and blood flow becomes irregular and unsteady. In this case, the blood flow dynamics demonstrate chaotic behaviour [9, 10]. Therefore, the Doppler signals have been used to investigate the chaotic behaviour of blood flow in healthy and pathological cases of aortic valve by using CD analysis in this study.

The chaotic analysis of Doppler blood flow signals have been performed for several arteries [11-13]. Usually, the Doppler signals, obtained from various heart diseases, have been analyzed using the conventional spectral analysis methods [14-18]. In these analyses, the power spectral densities of the Doppler signal (that gives the velocity histogram of blood cells and commonly referred as the Doppler spectrum) and the Doppler sonograms (which is time-frequency representation of Doppler signal) have been obtained. Various spectral analysis methods such as Fourier technique, autoregressive moving average, moving average and wavelet method have been suggested for classification of heart diseases in adults [14-18].

In this study, the CD analysis has been applied to the aortic valve Doppler signals obtained from healthy, AS and AI disorders assessed by Doppler echocardiography in children. The CD

describes the chaotic behaviour of Doppler signals and gives the minimum number of independent variables the cardiovascular system needs to generate the blood flow dynamics. The CD calculation was performed after the phase space reconstruction of the Doppler signals using the GP algorithm [19]. The student-t test has been applied to the CD values calculated for healthy and, AS and AI disorders of aortic valve to diagnose.

2. Material and Methods

2.1. Doppler Signals and Noise Reduction

The aortic valve Doppler signals are gathered from 23 healthy children subjects (mean age: 6.22 ± 4.92 years; 10 male and 13 female) and 24 children patients (mean age: 8.40 ± 4.95 years; 17 male and 7 female), 12 of them are suffered from AS (mean age: 7.21 ± 4.77 years) and 12 of them are suffered from AI (mean age: 9.58 ± 5.04 years). The Doppler signals have been collected from Pediatric Cardiology Department of the Başkent University Ankara Hospital between 2004 to 2006 years.

Doppler echocardiography is frequently used as a noninvasive, inexpensive method for evaluating of the nature of heart and blood flow characteristics through heart valves [8].

The aortic valve Doppler signal measurements are performed utilizing Acuson Sequoia 256 echocardiography system with 2 MHz ultrasonic transducer. The Doppler signals were recorded from audible output of echocardiography device by sampling at 22050 Hz and digitizing with 16 bit resolution. During the records of Doppler signal, Doppler angle was mostly hold at 0 degree and rarely changed between 0-20 degrees.

DC value was removed from the data and high frequency noisy components on the Doppler signals were filtered using wavelet analysis in order to improve the quality of the Doppler signal and to increase the reliability of the nonlinear analysis. Because, the high frequency noise components can significantly increase the CD of the Doppler signal [20, 21]. For reduction of the high frequency noise, the soft thresholding technique was applied using discrete wavelet transform with Db8 wavelet [22, 23].

In Figure 1, the sonograms before and after pre-processing of a healthy (subject no: 1) and an AS (subject no: 26) Doppler signals were calculated using the short-time Fourier transform.

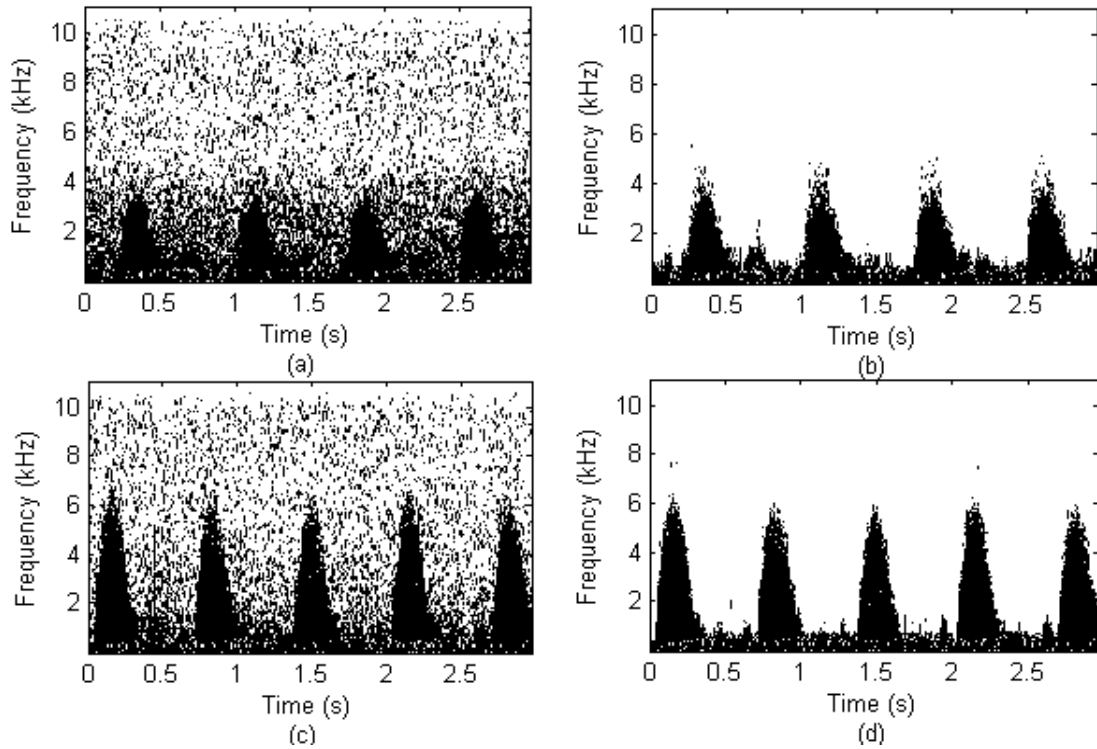


Figure 1. The sonograms before (a, c) and after filtering (b, d) of a healthy (a, b) and an AS (c, d) Doppler signals

2.2. Correlation Dimension (CD) Analysis

To study the physiological time series with chaotic analysis methods, at first, the phase space of the physiological system is reconstructed using observed scalar measurement [25]. This process is called phase space reconstruction and the form occurring in the phase space using an embedding dimension and a time delay is called attractor. The chaotic measures of the system are calculated on this attractor [25]. A property of chaotic systems is that their attractor has a fractal geometry and dimension. On the attractor, more than one dimension calculations can be performed (box counting, information, correlation) [26]. The CD is a measure of the complexity of a dynamic system.

The aortic valve Doppler signal ($x(n) = x(n\Delta t)$, $n = 1, 2, \dots, N$) is a scalar time series of recorded values at constant discrete time intervals (Δt) from cardiovascular system and reconstructed in the m dimensional phase space with delay coordinate τ by using Takens' embedding method [27]. According to Takens' theorem, time-delay vectors in m dimensional phase space are formed below:

$$X_i = (x_i, x_{i+\tau}, x_{i+2\tau}, x_{i+3\tau}, \dots, x_{i+(m-1)\tau}) \quad (1)$$

where, X_i is the i th point on the attractor ($i = N-(m-1)\tau$), x_i is the i th value of the time series, m is the dimension of the phase space, τ is the time delay or lag ($\tau = k\Delta t$, k is an integer multiplier of Δt).

The average mutual information (AMI) function is used for determining the time delay τ as given in Eq. 2 [25, 28]. The AMI is a quantity that measures the average amount of information shared by the two measurements. According to Fraser and Swinney [28], the proper time delay τ is the first minimum value of the AMI function because the measurements are somewhat independent, but not statistically independent. In Eq. 2, the probabilities come from a histogram of the data points and point pairs of data.

$$I(\tau) = \sum_{n=1}^N P(x(n), x(n+\tau)) \log_2 \left[\frac{P(x(n), x(n+\tau))}{P(x(n))P(x(n+\tau))} \right] \quad (2)$$

The dimension of phase space which is called as embedding dimension m , has to be $m \geq 2D+1$ or $m \geq D_2$ is sufficient to estimate the CD from the embedding (D : box-counting dimension, D_2 : correlation dimension) according to Takens [27] and Sauer et al. [29], respectively. In this study, 15 dimensional phase space was used for reconstructing of the Doppler signals.

The CD was estimated using the GP algorithm using correlation integrals on the reconstructed Doppler signal [19]. This algorithm is based on the following idea: The probability of the two points (X_i, X_j and $i \neq j$) of the set to be in the same cell with size r is nearly equal to the probability of two points of the set, to be separated with a distance equal to r or less than r .

$$C(m, r) = \lim_{N \rightarrow \infty} \frac{1}{N^2} \sum_{i,j} \Theta(r - \|X_i - X_j\|) \quad (3)$$

Where, N is the number of considered points in the reconstructed phase space, $\|X_i - X_j\|$ is the distance between the points in the phase space and calculated as Euclidean norm and $\Theta(\rho)$ is the Heaviside step function.

The correlation integral $C(m, r)$ is estimated for the range of r . The CD (D_2) of the attractor is estimated by assuming the power dependence $C(m, r) \propto r^{D_2}$. The CD is the slope of the linear scaling region of the plot of $\ln C(m, r)$ versus $\ln(m, r)$ and is defined as:

$$D_2(m) = \lim_{r \rightarrow 0} \frac{\ln C(m, r)}{\ln r} \quad (4)$$

The slopes (D_2) are calculated by using the least squares fit and plotted as a function of embedding dimension m . These D_2 values go to saturation for as increasing m and this value was taken as the CD of the system [30].

3. Results and Discussion

The time delay which is determined by the number of samples has been found using the AMI function. The AMI analysis has been performed by TSTool program packet [31]. The optimal time delay values (τ) have been determined from the first minimum of AMI function in this study. The mean \pm standard deviation of time delay values for healthy, AS and AI groups have been found as 8.04 ± 3.53 , 8.42 ± 1.44 and 7.08 ± 0.74 , respectively. For comparing the time delay values of three groups, the student-t test was applied between these groups. No statistical differences were found between healthy and AS and, healthy and AI groups ($p > 0.05$). The time delay values between AS and AI groups were found statistically different ($p < 0.05$). Therefore, their own time delay values of each Doppler signal were used in the CD calculation.

The CD analyses of the aortic valve Doppler signals have been performed by using the GP algorithm by Matlab routine [19]. For an AI Doppler signal (subject no: 45), the estimated correlation integrals for each embedding dimension (from 1 to 15) have been presented in Figure 2 with respect to r and scaling region used in CD calculation is also indicated.

The D_2 was calculated as slope of the linear part of $\ln C(m, r)$ versus $\ln(r)$ plots for each embedding dimensions. The slopes were estimated by using a simple least square linear fitting of scaling region that is over a certain range of r . These D_2 values were plotted as a function of embedding dimension. The D_2 values go to saturation for as increasing embedding dimension m from 1 to 15, and this value was taken as the CD of the signal [30]. The CDs of a healthy (subject no: 14), an AI (subject no: 45) and an AS (subject no: 25) Doppler signals were obtained as 6.5987, 8.2194 and 9.6491, respectively (Figure 3).

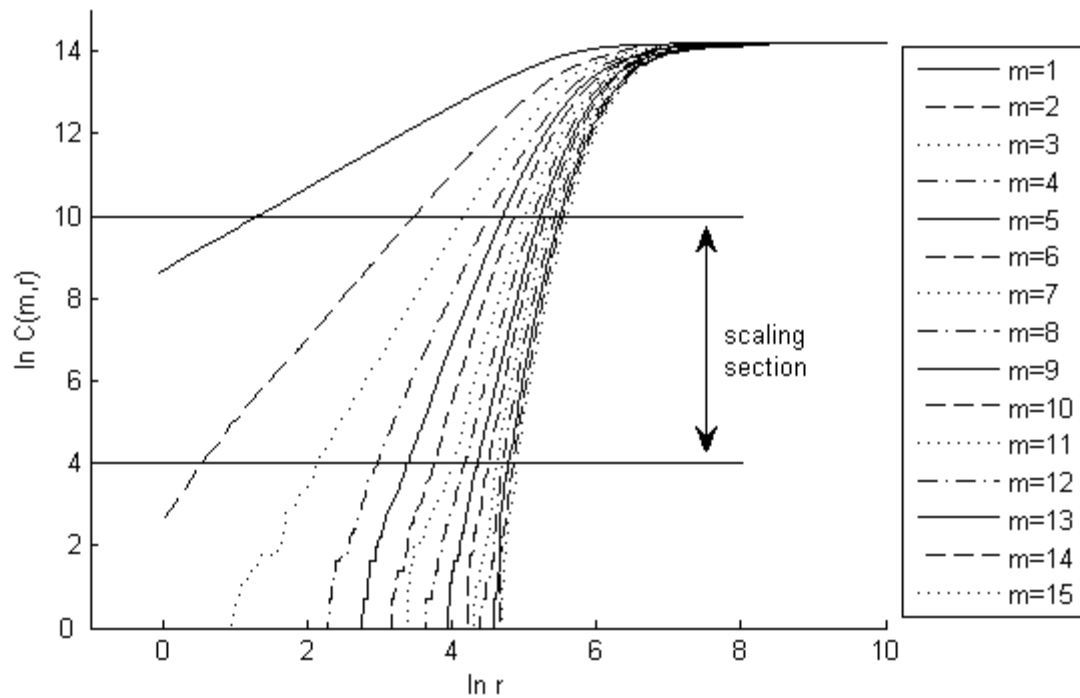


Figure 2. The correlation integrals of an AI Doppler signal

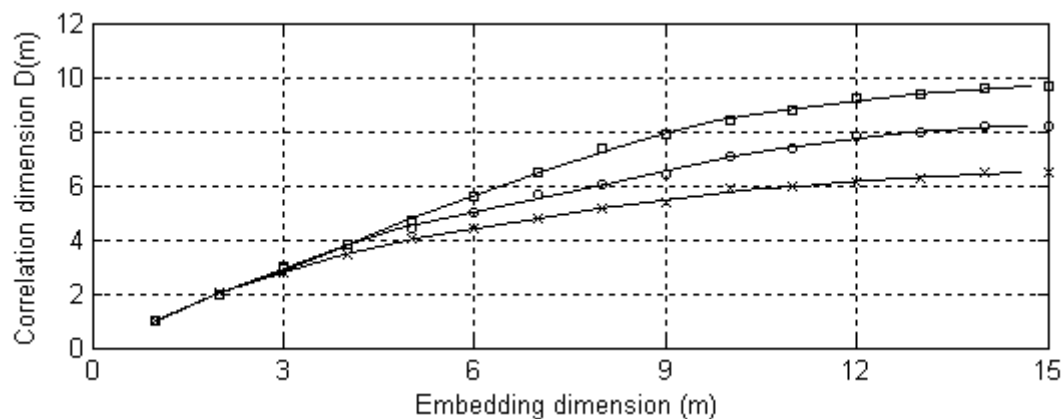


Figure 3. The CD estimation as a function of the embedding dimension m for a healthy (-x-), an AI (-o-) and an AS (-□-) Doppler signals

The results obtained from the CD analyses on healthy, AS and AI Doppler signals have been expressed as means \pm SD in Table 1 and Figure 4. The student-t test has been applied to compare the CD values of healthy, AI and AS groups, after normality tests, by using Matlab. The p values have been found statistically significant as shown in Table 1. The CD values for AS group is found higher than CD values of healthy group. Additionally, CD value is also higher for AS group than AI group, but CDs are not significantly different between healthy and AI groups ($p > 0.05$). CD of total diseased group (AS and AI groups) have significant difference with respect to CD of healthy group.

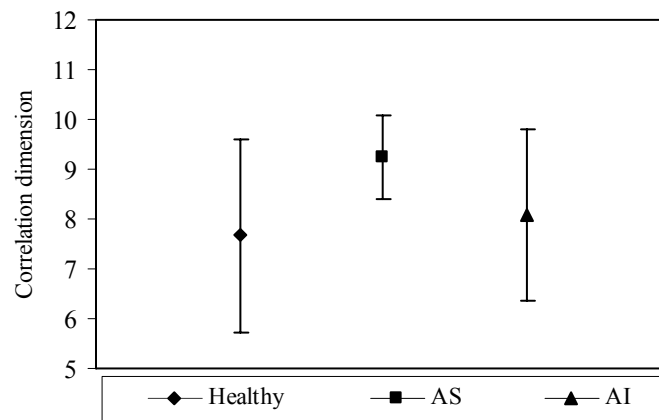
Table 1. The estimated CDs for healthy, AI and AS groups and results of student-t test

	Healthy group	AS group	AI group	Total diseased group
CD	7.6749±1.941	9.2546±0.844	8.0700±1.739	8.6623±1.467
p value		p<0.005 ^a	p=0.27 ^a p<0.05 ^b	p<0.05 ^a

^a: student-t test p value for comparing with healthy group.

^b: student-t test p value for comparing between AS and AI groups.

In this study, the CDs of all groups have shown that aortic blood flow is chaotic. The CD of healthy aortic Doppler signals has been found lower than aortic valve disorder groups, statistically in general (Table 1). In AS and AI diseases, since the blood flow regimes turn into turbulence, the behaviour of aortic flow is more complex than healthy case. Therefore, the degree of chaotic behaviour of aortic flow increases for AI and AS disorders and the increment of CD is an indicator of instability of aortic flow.

**Figure 4.** The CD values estimated for healthy, AS and AI groups (mean ± SD)

In the CD calculation, selection of optimal embedding dimension is important. In practical applications, the GP algorithm can be applied to calculate the CD for various embedding dimensions. Then minimum embedding dimension of the attractor is $m+1$, where m is the embedding dimension above which the CD value remains constant [30]. In this study, the CD estimation was performed for a range of embedding dimension from 1 to 15 and the selection of 15 dimensional phase space is sufficient.

The number of data points is an important parameter for CD calculation. In this study, 65536 data points were used and sufficiently high [10-13, 32]. Additionally, in order to minimize the statistical errors and reduce the computation time, randomly selected reference points are used in the CD calculation [33, 35]. The numbers of reference points have been selected sufficiently

high that will allow the CD go to saturate. Moreover, the Theiler correction [33] procedure was taken into account in CD calculation to eliminate the influence of autocorrelation effects.

Several blood flow studies were performed on various arteries (transcranial, carotid, peripheral) using the chaotic analysis techniques [10-13, 35, 36]. A few studies were found in nonlinear analysis of cardiac Doppler signals in the literature insofar as our knowledge [37, 38] but they were made for animals. These studies showed that the signals (aortic flow, pressure, left ventricular pressure etc.) are chaotic [37, 38].

The results of this study are consistent with study of May et al. [10] and Yılmaz et al. [39, 40]. May et al. [10] used nonlinear measures to characterize the level of turbulence occurred in blood flow through normal and graded stenosed rat carotid artery by in-vivo technique. They found that the CD values in the stenosis case are higher than normal case and correlated with the stenosis degree. Yılmaz et al. [40, 41] used largest Lyapunov exponent and CD to investigate the blood flow dynamics in healthy and various degree stenosed human carotid artery. They also found that the CDs in case of stenosis are higher than healthy case and correlated with the stenosis degree. In this study, the CDs also increased by reason of blood flow disturbances in AS and AI diseases with respect to healthy case.

4. Conclusions

In this study, CD analysis of Doppler signals which are obtained from healthy children subjects and AI and AS children patients have been performed by using the GP algorithm. The results have shown that CD is significantly lower for healthy group than aortic valve disorder group, AS. And CD of AS group is also significantly higher than AI group. The increment of the CD in the cases of AI and AS indicate that the blood flow dynamics of aortic valve disorders have high level chaotic behaviour and are more complex with respect to healthy case.

Consequently, CD calculation gives useful information for diagnosing the aortic valve Doppler signals with healthy and aortic disorders in children. The results have indicated that the CD analysis can be used as efficient tools to detect the disorder of aortic valve. In future, this analysis can be repeated for different time delays and embedding dimensions.

References

- [1] Wagner, C.D., Persson, P.B., (1998), "Chaos in the Cardiovascular System: An Update", *Cardiovascular Research*, 40(2), 257.
- [2] Stefanovska, A., Bracic, M., (1999), "Reconstructing Cardiovascular Dynamics", *Cont. Eng. Prac.*, 7, 161.

- [3] Glass, L., Kaplan, D.T., (1993), "Time Series Analysis of Complex Dynamics in Physiology and Medicine", *Med. Prog. Technol.*, 19, 115.
- [4] Yilmaz D., Güler, N.F., (2006), "A Study on the Chaotic Time Series Analysis", *J. Fac. Eng. Arch. Gazi Univ.*, 21(4), 759.
- [5] Otto, C.M., (1999), "*Valvular Heart Disease*", W.B. Saunders Company, Pennsylvania.
- [6] ACC/AHA Practice guidelines for the management of patients with valvular heart disease: Executive Summary. "A report of the American College of Cardiology/American Heart Association Task Force on Practice Guidelines", (2006), *J Am Coll Cardiol* 48, 598.
- [7] DeGroff, C.G., (2002), "Doppler Echocardiography", *Pediatr. Cardiol.*, 23, 307.
- [8] Hatle, L., Angelsen, B., (1982), "*Doppler Ultrasound in Cardiology Physical Principles and Clinical Applications*", Lea & Febiger, Philadelphia, USA.
- [9] Ruelle, D., Takens, F., (1971), "On the Nature of Turbulence", *Communications in Mathematical Physics*, 20, 167 and 23, 343.
- [10] May, P., Arrouvel, C., Revol, M., Servant J.M., Vicaut, E., (2002), "Detection of Hemodynamic Turbulence in Experimental Stenosis: an in Vivo Study in the Rat Carotid Artery", *J. Vascular Research*, 39, 21.
- [11] Keunen, R.W.M., Vliegen, J.H.R., Stam, C.J., Tavy, D.L.J., (1996), "Nonlinear Transcranial Doppler Analysis Demonstrates Age-Related Changes of Cerebral Hemodynamics", *Ultrasound Med. & Biol.*, 22(4), 383-390.
- [12] Güler, İ., Übeyli, E.D., (2004), "Detecting Variability of Internal Carotid Arterial Doppler Signals by Lyapunov Exponents", *Med. Eng. Phys.*, 26, 763.
- [13] Ozturk, A., Arslan, A., (2007), "Classification of Transcranial Doppler Signals Using Their Chaotic Invariant Measures", *Comput. Meth. Prog. Biomed.*, 86, 171.
- [14] Güler, İ., Kara, S., Güler, N.F., Kıymık, M.K., (1996), "Application of Autoregressive and Fast Fourier Transform Spectral Analysis to Tricuspid and Mitral Valve Stenosis", *Comput. Meth. Prog. Biomed.*, 49, 29.
- [15] Güler, İ., Hardalaç, F., Müldür, S., (2001), "Determination of Aorta Failure with the Application of FFT, AR, and Wavelet Methods to Doppler Technique", *Comput. Biol. Med.*, 32, 435.
- [16] Turkoglu, I., Arslan, A., Ilkay, E., (2005), "An Intelligent System for Diagnosis of the Heart Valve Diseases with Wavelet Packet Neural Networks", *Comput. Biol. Med.*, 33, 319.
- [17] Barışçi, N., Topal, E., Hardalaç, F., Güler, İ., (2005), "Classification of Aorta Insufficiency and Stenosis Using Neuro-Fuzzy System", *J. Med. Sys.*, 29, 155.
- [18] Kara, S., (2007), "Classification of Mitral Stenosis from Doppler Signals Using Short Time Fourier Transform and Artificial Neural Networks", *Expert Sys. Appl.*, 31, 229.
- [19] Grassberger, P., Procaccia, I., (1983), "Measuring the Strangeness of Strange Attractors", *Physica D*, 9, 189.
- [20] Papadimitriou, S., Bezerianos, A., (1999), "Nonlinear Analysis of the Performance and Reliability of Wavelet Singularity Detection Based Denoising for Doppler Ultrasound Fetal Heart Rate Signals", *Int. J. Med. Inf.*, 53, 43.
- [21] Zhang, Y., Wang, Y., Wang, W., Liu, B., (2001), "Doppler Ultrasound Signal Denoising Based on Wavelet Frames", *IEEE Trans. Ultrason Ferroelec Freq. Contr.*, 48(3), 709-716.
- [22] Donoho, D.L., (1995), "De-noising by Soft-Thresholding", *IEEE Trans. Inf. Theory*, 41, 613.
- [23] Daubechies, I., (1992), "*Ten Lectures on Wavelets*", SIAM, Philadelphia, PA.
- [24] Donoho, D.L., Johnstone, I.M., (1994), "Ideal Spatial Adaptation via Wavelet Shrinkage" *Biometrika*, 81, 425.
- [25] Abarbanel, H.D.I., Brown R., Sidorowich J.J., Tsimring L.S., (1993), "The Analysis of Observed Chaotic Data in Physical Systems", *Reviews of Modern Physics*, 65(4), 1331.
- [26] Hentschel H. G. E., Procaccia, I., (1983), "The Infinite Number of Generalized Dimensions of Fractals and Strange Attractors", *Physica D*, 8, 435.

- [27] Takens, F., (1981), "Detecting Strange Attractors in Turbulence", *Lecture Notes in Mathematics*, 898, 366.
- [28] Fraser, A.M., Swinney, H.L., (1986), "Independent Coordinates for Strange Attractors from Mutual Information", *Phys. Rev. A*, 33, 1134.
- [29] Sauer, T., Yorke, J., Casdagli, M., (1994), "Embedology", *J. Stat. Phys.*, 65, 579.
- [30] Ding, M., Grebogi, C., Ott, E., Sauer, T., Yorke, J.A., (1993), "Estimating Correlation Dimension from Chaotic Time Series: When Does Plateau Occur?", *Physica D*, 69, 404.
- [31] Merkwirth, C., Partliz, U., Lauterborn, W., (1998), "TSTOOL - A Software Package for Nonlinear Time Series Analysis", *Proc. Int. Workshop on Advanced Black-Box Techniques for Nonlinear Modelling*, Katholieke Universiteit, Leuven, Belgium, July 8-10, p. 144.
- [32] Almog, Y., Oz, O., Akselrod, S., (1999), "Correlation Dimension Estimation: Can This Nonlinear Description Contribute to the Characterization of Blood Pressure Control in Rats?", *IEEE Trans. Biomed. Eng.*, 46, 535.
- [33] Theiler, J., (1990), "Estimating fractal dimension", *J. Opt. Soc. Am. A*, 7, 1055.
- [34] Theiler, J., (1990), "Statistical Precision of Dimension Estimators", *Phys. Rev. A*, 41, 3038.
- [35] Barclay, K.D., Klassen, G.A., Young, C., (2000), "A Method for Detecting Chaos in Canine Myocardial Microcirculatory Red Cell Flux", *Microcirculation*, 7, 335.
- [36] Parthimos, D., Osterloh, K., Pires, A.R., Griffith, T.M., (2004), "Deterministic Nonlinear Characteristics of in Vivo Blood Flow Velocity and Arteriolar Diameter Fluctuations", *Phys. Med. Biol.*, 49, 1789.
- [37] Barclay, K.D., Klassen, G.A., Young, C., (2000), "A Method for Detecting Chaos in Canine Myocardial Microcirculatory Red Cell Flux", *Microcirculation*, 7, 335.
- [38] Schulz, S., Bauernschmitt, R., Schwarzhaupt, A., Vahl, C.F., Kiencke, U., (1999), "Nonlinear Dynamic Analysis of Hemodynamic Signals for Identifying Transitions Between Ventriculoarterial Coupling States", *Computers in Cardiology*, 26, 507.
- [39] Yılmaz, D., Musapaşaoğlu, H., Kırbaş, İ., Güler, N.F., (2006), "Karotid Atardamar Doppler Sinyalleri Üzerinde En Büyük Lyapunov Üsteli ve İlinti Boyutu Hesabı", *J. İstanbul Kültür University, Science and Engineering*, 4(2), 61.
- [40] Yılmaz, D., Güler, N.F., Musapaşaoğlu, H., Kırbaş, İ., (2006), "Correlation Dimension Analysis of the Healthy and Stenosed Carotid Artery Doppler Signals", *Proceedings of IEEE, 14th Signal Processing and Communications Application Conf., Antalya, Türkiye*.

Instructions to Contributors

Journal of Applied Functional Analysis

A quarterly international publication of Eudoxus Press, LLC of TN.

Editor in Chief: George Anastassiou

Department of Mathematical Sciences
University of Memphis
Memphis, TN 38152-3240, U.S.A.

1. Manuscripts, hard copies in quadruplicate and in English, should be submitted by regular, unregistered mail, to the Editor in Chief.

Authors may want to recommend an associate editor most related to the submission to possibly handle it. In addition, to assist the Editor and speed the decision process, authors may include a PDF file of the paper on disk with the submitted copies of the manuscript.

Also authors may want to submit a list of six possible referees, to be used in case we cannot find related referees by ourselves.

2. Manuscripts should be typed using any of TEX, LaTeX, AMS-TEX, or AMS-LaTeX and according to EUDOXUS PRESS, LLC. LATEX STYLE FILE. (Click [HERE](#) to save a copy of the style file.) They should be carefully prepared in all respects. Submitted copies should be brightly printed (not dot-matrix), double spaced, in ten point type size, on one side high quality paper 8(1/2)x11 inch. Manuscripts should have generous margins on all sides and should not exceed 24 pages.

3. Submission is a representation that the manuscript has not been published previously in this or any other similar form and is not currently under consideration for publication elsewhere. A statement transferring from the authors (or their employers, if they hold the copyright) to Eudoxus Press, LLC, will be required before the manuscript can be accepted for publication. The Editor-in-Chief will supply the necessary forms for this transfer. Such a written transfer of copyright, which previously was assumed to be implicit in the act of submitting a manuscript, is necessary under the U.S. Copyright Law in order for the publisher to carry through the dissemination of research results and reviews as widely and effectively as possible.

4. The paper starts with the title of the article, author's name(s) (no titles or degrees), author's affiliation(s) and e-mail addresses. The affiliation should comprise the department, institution (usually university or company), city, state (and/or nation) and mail code.

The following items, 5 and 6, should be on page no. 1 of the paper.

5. An abstract is to be provided, preferably no longer than 150 words.
6. A list of 5 key words is to be provided directly below the abstract. Key words should express the precise content of the manuscript, as they are used for indexing purposes.

The main body of the paper should begin on page no. 1, if possible.

7. All sections should be numbered with Arabic numerals (such as: 1. INTRODUCTION) .

Subsections should be identified with section and subsection numbers (such as 6.1. Second-Value Subheading).

If applicable, an independent single-number system (one for each category) should be used to label all theorems, lemmas, propositions, corollaries, definitions, remarks, examples, etc. The label (such as Lemma 7) should be typed with paragraph indentation, followed by a period and the lemma itself.

8. Mathematical notation must be typeset. Equations should be numbered consecutively with Arabic numerals in parentheses placed flush right, and should be thusly referred to in the text [such as Eqs.(2) and (5)]. The running title must be placed at the top of even numbered pages and the first author's name, et al., must be placed at the top of the odd numbered pages.

9. Illustrations (photographs, drawings, diagrams, and charts) are to be numbered in one consecutive series of Arabic numerals. The captions for illustrations should be typed double space. All illustrations, charts, tables, etc., must be embedded in the body of the manuscript in proper, final, print position. In particular, manuscript, source, and PDF file version must be at camera ready stage for publication or they cannot be considered.

Tables are to be numbered (with Roman numerals) and referred to by number in the text. Center the title above the table, and type explanatory footnotes (indicated by superscript lowercase letters) below the table.

10. List references alphabetically at the end of the paper and number them consecutively. Each must be cited in the text by the appropriate Arabic numeral in square brackets on the baseline.

References should include (in the following order):
 initials of first and middle name, last name of author(s)
 title of article,
 name of publication, volume number, inclusive pages, and year of publication.

Authors should follow these examples:

Journal Article

1. H.H.Gonska, Degree of simultaneous approximation of bivariate functions by Gordon operators, (journal name in italics) *J. Approx. Theory*, 62,170-191(1990).

Book

2. G.G.Lorentz, (title of book in italics) *Bernstein Polynomials* (2nd ed.), Chelsea, New York, 1986.

Contribution to a Book

3. M.K.Khan, Approximation properties of beta operators, in (title of book in italics) *Progress in Approximation Theory* (P.Nevai and A.Pinkus, eds.), Academic Press, New York, 1991, pp.483-495.

11. All acknowledgements (including those for a grant and financial support) should occur in one paragraph that directly precedes the References section.

12. Footnotes should be avoided. When their use is absolutely necessary, footnotes should be numbered consecutively using Arabic numerals and should be typed at the bottom of the page to which they refer. Place a line above the footnote, so that it is set off from the text. Use the appropriate superscript numeral for citation in the text.

13. After each revision is made please again submit four hard copies of the revised manuscript. And after a manuscript has been accepted for publication submit four hard copies of the final revised manuscript. Additionally, two copies of the final version of the TEX/LaTeX source file and a PDF file, are to be submitted to the Editor's Office on personal 3.5 inch computer disks. Label the disks individually with clearly written identifying information, e.g. :

Your name, title of article, kind of computer used, kind of software and version number, disk format and files names of article, as well as abbreviated journal name.

Package the disks in a disk mailer or protective cardboard. Make sure contents of disks are identical with the ones of final hard copies submitted!

Note: The Editor's Office cannot accept the disks without the accompanying matching hard copies of manuscript. No e-mail final submissions are allowed! File submission on disk must be used.

14. Effective 1 Jan. 2009 the journal's page charges are \$15.00 per PDF file page, plus \$40.00 for electronic publication of each article. Upon acceptance of the paper an invoice will be sent to the contact author. The fee payment will be due one month from the invoice date. The article will proceed to publication only after the fee is paid. The charges are to be sent, by money order or certified check, in US dollars, payable to Eudoxus Press, LLC, to the address shown on the Eudoxus [homepage](#).

No galleys will be sent and the contact author will receive one(1) electronic copy of the journal issue in which the article appears.

15. This journal will consider for publication only papers that contain proofs for their listed results.

TABLE OF CONTENTS, JOURNAL OF APPLIED FUNCTIONAL ANALYSIS,
VOLUME 4, NO.4, 2009

PREFACE,.....	568
THE APPLICATION OF FRACTAL ANALYSIS AND SPATIAL TECHNOLOGIES FOR URBAN ANALYSIS, M.A. MCADAMS,.....	569
ON INFINITE DIMENSIONAL VOLTERRA TYPE OPERATORS, F.MUKHAMEDOV, M.SABUROV,.....	580
FORCED VIBRATIONS OF A GENERAL CUBIC NONLINEAR CONTINUOUS SYSTEM, B.B.OZHAN, M.PAKDEMIRLI,.....	589
PRECURSORY SEISMIC QUIESCENCE BEFORE 1 MAY 2003 BINGOL (TURKEY) EARTHQUAKE: A STATISTICAL EVALUATION, S.OZTURK, Y.BAYRAK,.....	600
CONSTRUCTION OF CRYPTOGRAPHIC HASH FUNCTIONS BASED ON TIME AVERAGE CHAOTIC MAP, M.RAGULSKIS, Z.NAVICKAS, L.SAUNORIENE, K.LUKOSEVICIUTE,.....	611
SPATIOTEMPORAL CHAOS AND BREAK UP OF SPIRAL WAVES DUE TO CORE EXPANSION IN EXCITABLE MEDIA, H.SABBAGH,.....	623
NON CORPUS PARAMETRIZATION FOR STUDYING LONG-RANGE CORRELATIONS IN NATURAL LANGUAGES, G.SAHIN, O.O.AYBAR, A.HACINLIYAN,.....	636
TWO DIMENSIONAL PACKING OF GRANULAR RODS, S. SARIKAYA, Y. DEMIRAGAC, M.L. KURNAZ,.....	642
TRANSVERSE VIBRATION CHARACTERISTICS OF EULER-BERNOULLI AND TIMOSHENKO BEAMS UNDER MOVING FORCES, A.D.SENALP, A.ARIKOGLU, I.OZKOL, V.Z. DOGAN,.....	648

TABLE OF CONTENTS, JOURNAL OF APPLIED FUNCTIONAL ANALYSIS,
VOLUME 4, NO.4, 2009, continued from inside back cover

A NEW METHOD FOR APPROXIMATE SOLUTION OF SECOND ORDER DIFFERENTIAL EQUATIONS IN THE REGULAR SINGULAR POINTS, A.S.SHAMLOO,.....	662
FINITE ELEMENT ANALYSIS OF DISK BRAKE SQUEAL PHENOMENON, N.TOLOU, M.H.HOJJATI,.....	671
ANALYTICAL INVESTIGATION OF STRONGLY NONLINEAR NORMAL MODE USING HOMOTOPY PERTURBATION METHOD AND HE'S VARIATIONAL METHOD, N.TOLOU, S.HA.HASHEMI.K., A.BARARI, D.D.GANJI,.....	682
LONG MEMORY ANALYSIS OF TURKISH INFLATION SERIES, N.CAGLARIRMAK USLU, N.ALPTEKIN,.....	691
EXPERIMENTAL STUDY OF THE DYNAMIC BEHAVIOR OF A DOUBLE SCROLL CIRCUIT, C.K.VOLOS, I.M.KYPRIANIDIS, I.N.STOUBOULOS, A.N.ANAGNOSTOPOULOS.....	703
DISCONTINUOUS NANOFIBERS BY ELECTROSPINNING, L.XU, J.H.HE,.....	712
FURTHER GENERALIZATION OF QUASILINEARIZATION METHOD WITH INITIAL TIME DIFFERENCE, C.YAKAR, A.YAKAR,.....	714
DETERMINATION OF CHAOTIC BEHAVIOUR IN AORTIC DOPPLER SIGNAL DYNAMICS USING CORRELATION DIMENSION ANALYSIS, D.YILMAZ, N.F.GULER, N.K.TOKEL,.....	728